A METHODOLOGY TO DESCRIBE SPATIAL SURFACE FLUX BOUNDARY CONDITIONS FOR SOLVING TAILINGS IMPOUNDMENT CLOSURE WATER BALANCE PROBLEMS

A Thesis Submitted to the College of
Graduate Studies and Research
in Partial Fulfillment of the Requirements
for the Degree of Doctor of Philosophy
in the Department of Civil Engineering
University of Saskatchewan
Saskatoon, Canada

by
E. Maritz Rykaart
January, 2002

PERMISSION TO USE

In presenting this thesis in partial fulfillment of the requirements for a Postgraduate degree from the University of Saskatchewan, the author agrees that the Libraries of this University may make it freely available for inspection. The author further agrees that permission for copying of this thesis in any manner, in whole or in part, for scholarly purposes may be granted by the professor who supervised this research, Professor G. Ward Wilson, or, in his absence, by the Head of the Department of Civil Engineering or the Dean of the College of Engineering. It is understood that any copying or publication or use of this thesis or parts thereof for financial gain shall not be allowed without the written permission of the author and the University of Saskatchewan. It is also understood that due recognition shall be given to the author and to the University of Saskatchewan in any scholarly use which may be made of any material contained herein.

Requests for permission to copy or to make other use of material in this thesis in whole or part should be addressed to:

Head of the Department of Civil Engineering
University of Saskatchewan
57 Campus Drive
Saskatoon, Saskatchewan, S7N 5A9
Canada

ABSTRACT

This study deals with the closure water balance of a low-tonnage tailings impoundment in an arid climate that hosts a permanent pond on a portion of its surface. The calculation of surface fluxes from such an unsaturated tailings impoundment surface is difficult due to the fact that there is a spatially varying phreatic surface which determines the thickness of the vadose zone. This study presents a spatial flux hypothesis, which states that spatial flux boundary conditions on a generalized tailings impoundment cross-section (of this tailings facility) follow a characteristic shape that is governed by the depth to the phreatic surface. The hypothesis states that evaporation will be a minimum close to the tailings impoundment embankment wall where the depth to the phreatic surface is the greatest, and will increase to a maximum close to the pool. Inversely infiltration will be a maximum at the embankment and will decrease to a minimum close to the pool.

This study presents methodology to calculate the spatial flux boundary functions proposed in the hypothesis, and shows how these flux boundary functions can be used as a direct input for surface flux boundary conditions in multidimensional saturated/unsaturated flow seepage analysis models. This method effectively bridges the gap that currently exists between rigorous coupled soil/atmosphere one-dimensional surface flux boundary numerical models and multidimensional saturated/unsaturated flow seepage analysis models. The effective use of the calculated spatial flux boundary functions is proven through detailed evaluation modeling. The calculation of the flux boundary function stems from the development of a technique whereby the one-dimensional SoilCover surface flux boundary model can be used to solve a two-dimensional cross section. The technique consists of a generalized non-dimensionalized tailings impoundment cross-section that comprises a beach profile and a phreatic level function. Material properties and the shape functions have been tested and calibrated through an extensive laboratory and field characterization program of the tailings. The generalized cross-section is divided into a number of equal zones and a SoilCover simulation is performed for each zone before being integrated to give a cumulative result. The cumulative result is tested and calibrated against a detailed transient tailings impoundment water balance. This cumulative result represents the spatial flux boundary function that is consistent with the spatial flux

hypothesis. Effectively, what is presented in this thesis is a quasi-three-dimensional model for calculation of surface flux boundary conditions.

ACKNOWLEDGEMENTS

This thesis took three years to complete, and during this time a great number of people assisted me on various aspects of my work, and I would like to express my deepest gratitude towards everyone. Specifically I would like to acknowledge the assistance and support of the various professors, support staff, and graduate students with whom I had the pleasure of dealing with, and who made my time at the University enjoyable.

Firstly I would like to thank Placer Dome Pacific and Kidston Gold Mine for the financial support that allowed me to conduct this research. The additional funding I received from the University of Saskatchewan in the form of a Scholarship is also greatly appreciated.

I am especially grateful for the assistance and guidance provided by my supervisor, Professor Ward Wilson over the course of this thesis work. The suggestions and recommendations provided by my Advisory Committee Professors Del Fredlund, Bill Stolte, Charles Maule, Dennis Pufahl and Dr Garth van der Kamp is appreciated and surely improved the quality of the final thesis. A special word of thanks is due to Professor Del Fredlund who came on-board as co-supervisor midway through the program. The constructive comments by my external examiner, Dr Michael Davies are greatly appreciated. His comments added great value and made the final manuscript more valuable.

During my two site visits to Kidston Gold Mines, Nick Currey, Paul Ritchie and George Ryan went out of their way to assist me, and their continued assistance over the three years in terms of data collection and maintenance of my equipment definitely played a crucial role in the successful outcome of the work. I would also like to thank Professor David Williams for all his help in the materials testing that he did for me.

Most importantly I would like to express my deepest love and gratitude towards my wife Beulah, who shared my dream to complete this thesis and sacrificed a great deal in order for me to be able to complete it. Thanks also to our little girl Camille, whom happily adjusted to our crazy schedules, and helped in making this dream come true.

This page was left blank intentionally.

TABLE OF CONTENTS

LIST OF TABLES

LIST OF FIGURES

This page was left blank intentionally.

CHAPTER 1
Introduction

1.1 Mining and the Need to Solve the Surface Flux Boundary Condition

Mining, whether opencast or underground, produces large volumes of solid waste material. The waste consists of two distinct types; waste rock or tailings. Waste rock is the overburden material (or that material from which minerals cannot economically be extracted), that is excavated (often by means of drill-and-blast operation) in order to reach the ore body. This overburden, which by the nature of the excavation has great heterogeneity with regard to particle size distribution, is dumped in huge piles in demarcated areas around the mine site. The waste rock is not necessarily inert with regard to potential for becoming an environmental hazard, as the exposed rock can contain minerals that could oxidize and result in acidic drainage to name but one potential hazard (Williams *et al.*, 1997).

Tailings is the second waste stream that is produced when the ore containing the target minerals are crushed and ground fine in the ore processing plants. Chemicals and water are added to the ground ore mixture to extract the minerals, and the remaining slurry is called the tailings (Vick, 1983; Morgenstern and Kupper, 1988). The tailings are often pumped to an engineered impoundment, called a tailings impoundment (also called tailings pond or tailings dam), where the slurry is allowed to settle such that the water therein can be recovered for use in the processing plant. Tailings tend to hold an inherently higher environmental risk, both with regard to water pollution and instability.

The tailings impoundment water balance is of great importance to the successful operation during the life of a mine. The amount of water sent to the impoundment and the subsequent recovery volume often has a significant impact on how the mine processing is scheduled. During this time the impoundment leakage rate and stability issues are addressed only insofar as insuring compliance and safe operating conditions. However, upon mine closure the water balance changes dramatically. Seepage rates, especially long-term impoundment seepage,

become the most important aspect and govern whether the mine can successfully obtain closure for the impoundment (Portfors, 1980).

The accurate calculation of the seepage rates upon closure is dependent on defining the surface flux boundary condition for the water balance (i.e. infiltration, evaporation and runoff) on the tailings impoundment. Since long-term predictive seepage is the question, accurate numerical modeling of the water balance is most often required as a minimum (EPA, 1995).

1.2 Tailings Impoundment Types

There are a great variety of tailings impoundments, and they are characterized by factors such as the type of mineral that is being mined, the regional climate, and the volume of material being mined. Tailings can be hydraulically placed, can be thickened, can be formed into a paste, and can even be co-disposed with the waste rock.

The work described in this thesis has been performed on a low tonnage gold tailings impoundment in a semi-arid climate. The tailings were hydraulically placed by spigotting from an engineered embankment. Throughout this thesis reference will be made to typical and/or generalized tailings impoundments; however the reader is reminded that these statements are applicable only to low tonnage impoundments in a semi-arid climate.

Another important distinction must be made between operating tailings impoundments and impoundments that are under closure conditions. The water balance for a tailings impoundment during these two stages is significantly different. The tailings impoundment on which the research covered in this thesis has been done was under closure conditions, and as such the water balance is a closure water balance.

1.3 Determining the Magnitude of Surface Flux Boundary Conditions

The amount of seepage that a tailings impoundment produces depends on a multitude of factors. Key factors include the tailings impoundment geometry, tailings properties, subsurface hydrogeology and surface fluxes (Kealy and Busch, 1971). Conventional tailings impoundments have a pool of water on top due to the hydraulic deposition technique adopted for placing the tailings (Boldt, 1989). The tailings settle out and the decant water is ponded on top of the

impoundment either for reuse in the mill (Vick, 1983), or is allowed to seep and evaporate as a rehabilitation method (Blight and Lufu, 2000; Blight and Kreuiter, 2000). The presence of the pond (or pool) results in the formation of a phreatic surface within the tailings impoundment. The position of this phreatic surface is dependant on the tailings properties as well as the presence (if any) of any toe or blanket drains in the impoundment embankment walls or the impoundment base. Irrespective of where the phreatic line is established, there is thus a zone of saturated tailings below this line and a zone of unsaturated tailings above the line.

The seepage rate from tailings impoundments during closure conditions is dependent on the head of water in the pond (Mittal and Morgenstern, 1976; van Zyl and Harr, 1988), the tailings physical and hydraulic properties, as well as the amount of recharge to the phreatic surface via surface flux boundary conditions, i.e. precipitation and evapotranspiration. If the net annual infiltration for a specific site is positive, recharge occurs, and seepage will be produced. However, the inverse is true if the net annual climatic water balance for a specific site is negative. In such a case more water will leave the profile (i.e. via evapotranspiration) than enters it (i.e. via infiltration), and subsequently the amount of seepage should decrease to zero.

The calculation of the magnitude of surface flux boundary conditions from an unsaturated soil surface is not simple, and researchers have been actively working on the various surface flux boundary components for the last 30 years. Some of the earlier work on surface flux boundary calculations is found in the soil science discipline (Horton and Hawkins, 1965; Fuchs and Tanner, 1967; Mein and Larson, 1973; Klute and Heerman, 1978; Hino *et al.*, 1987). Their primary concern is the better understanding of surface flux boundary conditions to be able to produce and manage better crops, and as a result all of their advances are not directly applicable to solving engineering problems. As engineers started to move into unsaturated soil technology in an attempt to better understand engineering problems, surface flux boundary issues were again highlighted as probably the crucial aspect with regard to solving engineering problems in the vadose zone. This has led to a lot of research into understanding infiltration, evaporation and transpiration. Most research attempts have led to the development of numerical models to simulate the water movement as impacted by these processes. The major stumbling block in this research is however the high degree of non-linearity associated with the material properties of unsaturated soils, which makes numerical solutions inherently unstable, and as such prone to simplifications via assumptions. Notwithstanding these problems, numerous numerical models capable of calculating the surface flux boundary components are available and used by

engineers to solve tailings impoundment closure water balance problems. These models include codes such as SoilCover (SoilCover, 1997), HELP (Schroeder *et al.*, 1994), UNSAT-H (Fayer and Jones, 1990), SWACROP (Feddes *et al.*, 1984), HYDRUS (Simunek *et al.*, 1998), and SWIM (Ross, 1990), to name but the few most well known.

These models all attempt to calculate the surface flux boundary components using a multitude of methods and assumptions. The most important single component to consider is suitable calculation of evaporation. Numerous empirical and semi-empirical methods for calculating actual evaporation are available (Monteith, 1965; Shuttleworth and Wallace, 1985; Choudhury and Monteith, 1988; Passerat De Silans *et al.*, 1989). One mechanistic method for calculating actual evaporation is using the modified Penman formulation as proposed by Wilson *et al.* (1994). A mechanistic approach is considered essential for the present study. The only known model that currently uses the modified Penman formulation is SoilCover, and that makes it an appropriate tool to use.

Due to the detailed field data required for use of a model such as SoilCover, and the fact that it is only a 1-Dimensional (1-D) model, modeling unsaturated zones of varying thickness is difficult and the best solutions are obtained running multiple model runs and interpolating the results somehow to give a spatial distribution of surface flux boundary conditions. Since the actual concern that the engineer must address is the seepage from the tailings impoundment, and application of a code such as SoilCover cannot be used to provide the answer in multi dimensions. As a result the surface flux boundary condition is often oversimplified using coarse recharge numbers. It is common practice to solve these water balance problems using multidimensional saturated/unsaturated seepage analysis models like SEEP/W (GEO-SLOPE, 1991), MODFLOW (McDonald and Harbaugh, 1988), FEMWATER (Lin *et al.*, 1997) or SVFlux™ (SoilVision Systems, 2001). These models however do not allow for the actual calculation of the surface flux boundary conditions, but require the specification of a surface flux boundary condition as a surface boundary condition. In most cases, the recharge value is back calculated by using a known parameter, generally being a phreatic surface, and as such the most suitable recharge value might not represent the surface flux boundary situation as it is (Woyshner and St-Arnaud, 1994). In other words, the use of back calculated recharge numbers is conducive to calibration manipulation, due to the inherent uncertainty of the values.

The thesis proposes a conceptual model that allows for the spatial surface flux boundary distribution to be calculated using rigorous coupled soil/atmosphere surface flux boundary codes such as SoilCover, and these resulting functions can be used as direct input to the multidimensional saturated/unsaturated seepage analysis models, effectively bridging the current gap between the two modeling systems.

1.4 Spatial Surface Flux Hypothesis

The hydraulic deposition of the tailings can result in the tailings surface being a characteristic shape (Vick, 1983; Blight, 1987; Morris and Williams, 1997), and the presence of a pool of water on the tailings impoundment results in a phreatic surface in the impoundment (Vick, 1983) that is independent of the position of the regional water table. A large saturated zone exists in the tailings impoundment due to the presence of the pool. The established phreatic surface has a characteristic shape that is governed by the tailings properties, and the exit condition is determined by the presence of drains in the embankment walls. If one consider a typical cross-section at any location through the tailings impoundment (a low-tonnage impoundment in an arid climate), as shown in Figure 1.1(a) it can be seen an unsaturated zone in the tailings forms that varies in thickness from the embankment end to the pool end.

During closure conditions the surface of the tailings impoundment (i.e. the beach profile) along this typical cross-section would be subject to the usual water balance components of precipitation (P), evapotranspiration (ET), Infiltration (I), runoff (R), recharge (R_e), and seepage (S). It can however be expected that there would be a spatial variation in the magnitude of these components shown in Figure 1.1(b) as one move between the embankment and the pool. The reason for this is the availability of moisture in the profile, which is governed by the presence of the phreatic surface (Staley, 1957; Blight, 1997; Chu, 1997). Therefore, at a point close to the embankment evaporation is expected to be a minimum, and should increase moving in a direction towards the pool where it reaches a maximum (i.e. potential evaporation) at the pool edge. Similarly infiltration is expected to be a maximum close to the embankment and decrease towards the pool.

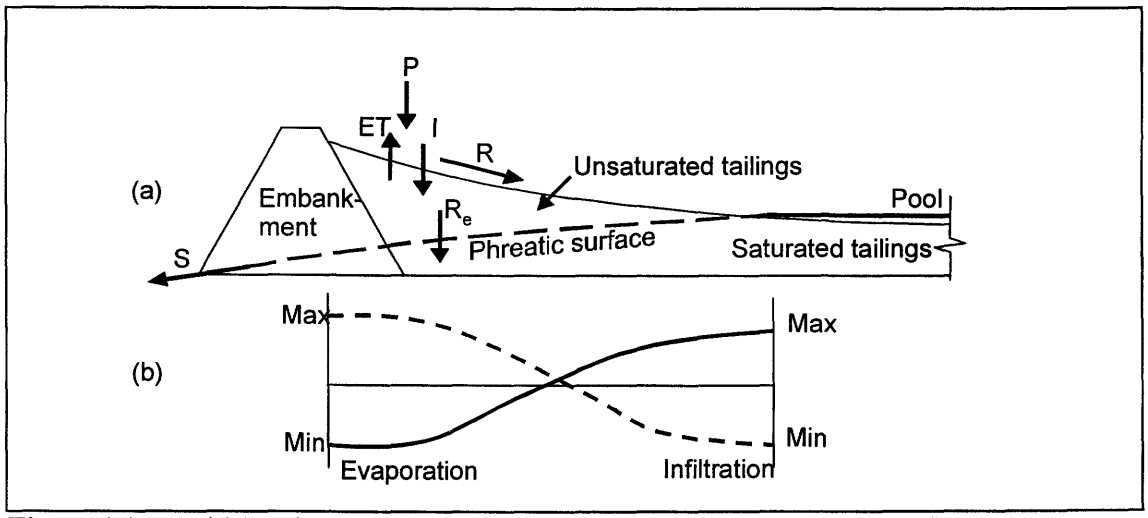

Figure 1.1: **(a) Typical cross-section through a tailings impoundment (low-tonnage impoundment in an arid climate), and**
(b) Spatial distribution of surface fluxes of infiltration and evaporation.

1.5 Objectives of the Research

The general discussion outlined in the previous section provides the backdrop for the research that is being reported in this thesis. Current commercially available products (i.e. numerical models) does not permit suitable prediction of the combined saturated/unsaturated flow regime in tailings impoundments that is directly impacted on by surface flux boundary conditions. As a result closure water balance problems (i.e. seepage volumes emanating from tailings impoundments) are solved by deducing infiltration rates from calculated seepage rates, as opposed to using infiltration rates to calculate seepage rates. The general objective of this thesis was to develop an analytical tool that would bridge this gap, and thereby allow for easier and more suitable tailings impoundment water balance calculations.

The problem lies in the fact that rigorous coupled soil/atmosphere surface flux boundary numerical models are only available for one-dimensional problem solving. On the other hand the multidimensional saturated/unsaturated seepage analysis models cannot calculate coupled soil/atmosphere surface flux boundary conditions at all. It is thus not possible to solve the closure water balance for a problem where the surface flux boundary conditions vary spatially as is found in a tailings impoundment. This gap between the two modeling systems defines the need for the research documented in this thesis.

The specific objective of this thesis is to develop a methodology to calculate spatial flux boundary functions for a tailings impoundment during closure conditions that would represent how surface flux boundary conditions (i.e. evaporation, runoff and infiltration) varies spatially across the tailings impoundment surface. The spatial variance is as a result of the variable tailings physical and hydraulic properties, and the depth to the phreatic surface in the tailings impoundment. The determination of such a function would be dependent on using detailed field measurements in combination with rigorous coupled soil/atmosphere surface flux boundary numerical modeling tools, thus minimizing modeling assumptions. In essence the objective is to verify that the spatial surface flux hypothesis is reasonably correct, and show how calculating it could be used as a valuable tool towards finding a better solution technique for solving tailings impoundment water balance problems (i.e. overcoming the problem associated with the spatially varying surface flux boundary conditions).

It is important to note that the objective was not to develop a new numerical code, or to investigate alternative individual surface flux boundary component calculation methods. The general objective is to develop a methodology that would allow the use of existing rigorous numerical models to solve the tailings impoundment closure water balance. Although the proposed methodology could likely be extended for use on other types of tailings impoundments, the research program did not extend beyond testing for any other impoundment than the Kidston tailings impoundment.

A secondary objective of this thesis was to determine, using the developed spatial flux boundary function, what the surface flux boundary condition to the tailings impoundment would be for a tailings impoundment surface void of any vegetation, and for the tailings impoundment surface covered with vegetation. Further, each of the previous two cases had to be solved for a mean-, extremely wet-, and extremely dry climatic year. The purpose of modeling these six cases was to determine what the long-term impact of the Kidston tailings impoundment rehabilitation approach would be with respect to overall tailings seepage rates during closure conditions. The secondary objective was not to compile and calibrate a detailed 3-D numerical model of the tailings impoundment to predict the long-term impacts, but was restricted to what effect the unsaturated zone would have on the overall closure water balance, based on typical and extreme climatic conditions.

1.6 Methodology for Achieving the Research Objectives

A holistic study approach was adopted in order to achieve the stated objectives. Specific tasks were identified that had to be completed in order to meet the objectives. These tasks are listed below.

1.6.1 Literature Review

A review of the literature with a view to establishing the current state-of-the-art with respect to solving tailings impoundment closure water balance problems, specifically taking into account unsaturated zone surface flux boundary conditions was undertaken. This paved the way for defining the direction that the research had to go, in order to fill knowledge gaps. Secondly a review of all the Kidston Gold Mines Limited records was undertaken with a view to obtain a complete understanding of the site under investigation.

1.6.2 Basic Surface Flux Boundary Condition Theory

The basic theory describing the surface flux boundary components, i.e. infiltration, runoff, evaporation and evapotranspiration had to be investigated. This was further expanded to allow for an understanding of the theory for coupled soil/atmosphere surface flux boundary numerical solutions. This basic theory paved the way for understanding the need for the research documented in this thesis.

1.6.3 Site Characterization

Prior to conducting any research work on a site it is crucial to understand the site and its surrounds. By developing a database of information that describe the site it is possible to start make sense of how all the physical components interact. The first task was thus to establish such a database of all relevant mine records containing data pertinent too physically describing the Kidston Gold Mine tailings impoundment.

The second step in characterizing the site was to instrument the site to physically measure all the aspects that are of concern. The primary objective in understanding the site was to understand the tailings impoundment closure water balance. The parameter that delineates the

transition between the saturated and unsaturated zones in the tailings dam is the phreatic surface, and subsequently piezometers were installed in the impoundment to measure this. The next obvious component of the closure water balance is seepage collected around the impoundment perimeter. Field monitoring equipment were designed and installed to measure seepage rates. Since both the phreatic surface location and the seepage volumes from the tailings impoundment is dependant on the tailings pond level, instrumentation was installed to monitor the tailings pond level.

The next level of field instrumentation involved measurement climatic parameters, which are required to perform surface flux boundary calculations that are driven by atmospheric conditions. These installations included a continuous weather station, as well as, evaporation pans to measure potential evaporation on and around the tailings impoundment. Rigorous numerical modeling of surface flux boundary conditions are dependant on suitable model calibration. Two field monitoring stations were installed to provide this data. The first was a Bowen ratio station which measured continuous actual evapotranspiration from the tailings impoundment surface, and the second was the measurement of continuous in-situ tailings response to moisture content and temperature via matric suction sensors.

1.6.4 Tailings Characterization

Solving water balance problems in unsaturated soils can only be done if the physical and hydraulic properties of the soils in question are adequately described. A crucial part of this research program was thus to identify and collect representative tailings samples. These samples were then subjected to laboratory testing to measure their physical and hydraulic properties.

Laboratory testing alone is not sufficient and extensive in-situ testing was done to completely understand the behavior of the tailings. The final step in characterizing the tailings was to develop a database of tailings physical and hydraulic properties from work completed by other researchers and consultants over the life of the mine. By integrating this work with the testing done specifically for this research program, the tailings could be characterized with an unprecedented level of confidence.

1.6.5 Numerical Surface Flux Boundary Modeling

The successful use of rigorous coupled soil/atmosphere surface flux boundary numerical modeling tools to predict surface flux boundary conditions are dependent on first calibrating the model with field data. The SoilCover (SoilCover, 1997) model was used in this research program, which implied that a detailed calibration of the SoilCover model had to be conducted.

Any modeling must be done within a framework of modeling guidelines (goals) that would ensure representative and relevant numerical modeling, and these guidelines were fixed early on in the research program. Since the primary objective of this research program was to develop a spatial flux boundary function, which essentially implies solving the flux boundary condition problem in two dimensions (2-D), a methodology had to be developed whereby SoilCover could be used to solve this problem. A conceptual model was developed which allows for the SoilCover model to be applied to a 2-D generalized cross-section through the Kidston tailings impoundment that produces a spatial flux boundary function as an output.

The modeling was further extended to solve for six different case studies; a vegetated and a non-vegetated tailings surface, governed by mean-, wet- and dry climatic seasons. The results of these case studies were used to determine whether Kidston Gold Mine would have long-term impacts associated with their tailings impoundment rehabilitation option.

1.6.6 Evaluation of the Suitability of the Spatial Surface Flux Boundary Functions

The research suggests that the spatial flux boundary functions can be used as surface flux boundary inputs into multidimensional saturated/unsaturated seepage analysis models. To test the validity of this assumption, as well as to test the applicability of the spatial flux boundary functions, rigorous two- and three-dimensional seepage analysis was done. Finally some recommendations as to the value of the research with respect to the current knowledge are made.

1.7 Organization of Thesis

The organization of this thesis is set out in such a fashion to logically lead towards the solving of the objectives. A specific chapter describing the literature review is not provided.

Alternatively references to related literature are included in each chapter or appendix as required. A detailed overview of the theory associated with the basic principles of the surface flux boundary components (i.e. infiltration, runoff and evapotranspiration) is provided in Chapter 2. This chapter further contains the theoretical formulation for rigorous coupled soil/atmosphere surface flux boundary calculations as it is applied in the SoilCover code. The chapter concludes with a discussion on the limitations of SoilCover and clearly defines the need for the research documented in this thesis.

Chapter 3 describes the Kidston mine site with regard to its location, environment, climate, geology etc., as well as providing specific detail with regard to the tailings impoundment under investigation. This chapter serves as the backdrop for the common physical aspects of the mine site that has relevance throughout the thesis.

Physical and hydraulic properties of the tailing are described in Chapter 4. This includes both in-situ field testing as well as laboratory test results. Data summaries and descriptions of the data are provided with more detailed individual data included in the referenced appendixes. Chapter 5 describes the general water balance of the tailings impoundment as a whole, without detailed analysis for the actual surface flux boundary functions. The purpose of this approach is to describe the elements that affect the tailings impoundment closure water balance, as well as to make some first order estimates as to how much runoff would enter the tailings pond. The generalized approach is subsequently used to provide guideline boundaries, against which, the later numerical modeling can be compared and evaluated.

The SoilCover (SoilCover, 1997) numerical model was used to perform the one-dimensional surface flux boundary calculations, and Chapter 6 documents the calibration of the numerical model. Chapter 7 contains the main element of this thesis, which is the development of a conceptual model that would allow spatial surface flux boundary functions to be developed for the tailings impoundment. This chapter describes how the conceptual model was developed as well as how it is used to calculate spatial surface flux boundary conditions using the SoilCover numerical model. Chapter 8 documents the actual SoilCover modeling for the generalized tailings dam cross-section for all the different cases. The modeling results allow for comparison of vegetated and non-vegetated tailings surfaces for each of the three selected climatic periods of a mean-, wet- or dry season. The analysis and discussion allows for conclusions to be reached regarding the suitability of the rehabilitation approach that Kidston Gold Mine has adopted.

The development of the spatial flux boundary functions are documented in Chapter 9, before proceeding to Chapter 10 which documents the evaluation of these functions. The evaluation was carried out at various levels, stepping up from one-dimensional numerical modeling through to three-dimensional numerical modeling using commercially available software. Chapter 11 concludes the thesis describing the relevant insights gained throughout the research program. Specific conclusions as to the application and applicability of the spatial surface flux boundary functions are presented. Recommendations for further research into the issue of solving mine waste water balance problems are also provided.

Appendixes containing detailed data and information of relevance to the study but too voluminous for the main body of the thesis are included in order of their first reference in the main body of the text. Specific reference lists are included after each chapter or appendix.

1.8 References

Blight, G.E. (1987). The concept of the master profile for tailings dam beaches. Proceedings of the International Symposium on Prediction and Performance in Geotechnical Engineering, Calgary, Alberta, Canada, 17-19 June, pp. 361-365.

Blight, G.E. (1997). Interactions between the atmosphere and the Earth. Geotechnique, Vol. 47(4), pp. 715-767.

Blight, G.E., Kreuiter, A. (2000). Disposal of industrial waste liquids by evaporation and capillary storage in waste dumps. Proceedings of Tailings and Mine Waste 2000, Fort Collins, Colorado, pp. 141-148.

Blight, G.E., Lufu, L. (2000). Principles of tailings dewatering by solar evaporation. Proceedings of Tailings and Mine Waste 2000, Fort Collins, Colorado, pp. 55-63.

Boldt, C.M.K. (1989). Beach Characteristics of Mine Waste Tailings. Report of investigations 9171, United States Department of the Interior, Bureau of Mines, 24 pp.

Choudhury, B.J., Monteith, J.L. (1988). A four-layer model for the heat budget of homogeneous land surfaces. Quarterly Journal of the Royal Meteorology Society, Vol. 114, pp. 373-398.

Chu, S.T. (1997). Infiltration Model for Soil Profiles with a Water Table. American Society of Agricultural Engineers, Vol. 40, No. 4, pp. 1041-1046.

Environment Protection Agency (EPA). (1995). Rehabilitation and Revegetation. Module in series on: Best Practice Environmental Management in Mining. Australian Federal Environment Department, June 1995.

Fayer, M.L., Jones, T.L. (1990). UNSAT-H version 2: Unsaturated soil water and heat flow model, PNL-6779, Pacific Northwest Laboratory, Richland, Washington, U.S.A.

Feddes, R.A., Wesseling, J.G., Wiebing, R. (1984). Simulation of Transpiration and Yield of Potatoes with the SWACROP-model. 9th Tri-annual Conference of the European Association of Potato Research (EAPR), Interlaken, Switzerland, July 2-6.

Fuchs, M., Tanner, C.B. (1967). Evaporation from a Drying Soil. Journal of Applied Meteorology, Vol. 6, October, pp. 852-857.

GEO-SLOPE International Ltd. (1991). SEEP/W for finite element seepage analysis, Version 4 for Windows 95 and NT, Getting Started Guide, Calgary, Alberta, Canada.

Hino, M., Fujita, K., Shutto, H. (1987). A laboratory experiment on the role of grass for infiltration and runoff processes. Journal of Hydrology, Vol. 90, pp. 303-325.

Horton, J.H., Hawkins, R.H. (1965). Flow path of rain from the soil surface to the water table. Soil Science, Vol. 100, No. 6, pp. 377-383.

Kealy, C.D., Busch, R.A. (1971). Determining Seepage Characteristics of Mill-Tailings Dams by the Finite-Element Method. Report of Investigations 7477, United States Department of the Interior, Bureau of Mines, January, 51 pp.

Klute, A., Heerman, D.F. (1978). Water Movement in Uranium Mill Tailings Profiles. Technical Note ORP/LV-78-8. U.S. Environmental Protection Agency Research Report, 78 pp.

Lin, H.J., Richards, D.R., Talbot, C.A., Yeh, G., Cheng, J., Cheng, H., Jones, N.L. (1997). FEMWATER: A Three-Dimensional Finite Element Computer Model for Simulating Density-Dependent Flow and Transport in Variably Saturated Media. Technical Report CHL-97-12, July.

McDonald, M.C., Harbaugh, A.W. (1988). MODFLOW, a Modular Three-Dimensional Finite Difference Groundwater Flow Model. U.S. Geological Survey, Open-File Report 91-536, Denver.

Mein, R.G., Larson, C.L. (1973). Modeling Infiltration during a Steady Rain. Water Resources Research, Vol. 9, No. 2, April, pp. 384-394.

Mittal, H.K., Morgenstern, N.R. (1976). Seepage control in tailings dams. Canadian Geotechnical Journal, Vol. 13, pp. 277-293.

Monteith, J.L. (1965). Evaporation and environment. In The State and Movement of Water in Living Organisms, Symposium: Society of Experimental Biology. Vol. 19, Edited by G.E. Fogg. Academic Press, San Diego, California, pp. 205-234.

Morgenstern, N.R., Kupper, A.A.G. (1988). Hydraulic Fill Structures – A Perspective. Hydraulic Fill Structures; geotechnical special publication No. 21. Edited by DJA van Zyl and SG Vick, New York, 1988, pp. 1-31.

Morris, P.H., Williams, D.J. (1997). Hydraulic conditions leading to exponential mine tailings delta profiles. Transactions of the Institution of Mining and Metallurgy (Section A: Min. Industry), Volume 106, January-April, pp. A34-A37.

Passerat De Silans, A, Bruckler, L, Thory, J.L., Vauclin, M. (1989). Numerical modeling of coupled heat and water flows during drying in a stratified bare soil – comparison with field observations. Journal of Hydrology, Vol. 105, pp. 109-138.

Portfors, E.A. (1980). Environmental Aspects and Surface Water Control. Proceedings of Seminar: Design and Construction of Tailings Dams. Colorado School of Mines, Golden, Colorado, 6-7 November.

Ross, P.J. (1990). SWIM – a Simulation Model for Soil Water Infiltration and Movement. CSIRO Division of Soils, Davies Laboratory, Townsville, Queensland, Australia.

Schroeder, P.R., Lloyd, C.M., Zappi, P.A. (1994). The Hydrological Evaluation of Landfill Performance (HELP) Model User's Guide for Version 3, EPA/600/R-94/168a, U.S.A.

Shuttleworth, W.J., Wallace, J.S. (1985). Evaporation from sparse crops – an energy combination theory. Quarterly Journal of the Royal Meteorology Society. Vol., 111, pp. 839-855.

Simunek, J., Huang, K., van Genuchten, M.Th. (1998). The HYDRUS code for simulating the one-dimensional movement of water, heat, and multiple solutes in variably-saturated media, Version 6.0. Research Report No. 144, U.S.A. Salinity Laboratory, USDA, ARS, Riverside, California, 164 pp.

SoilCover. (1997). SoilCover User's Manual. Unsaturated Soils Group, Department of Civil Engineering, University of Saskatchewan, Saskatoon, Saskatchewan, Canada.

Staley, R.W. (1957). Effect of depth of water table on Evaporation from fine sand. Master of Science Thesis, Colorado State University, Fort Collins, Colorado, U.S.A.

SoilVision Systems (2001). SVFlux™ : Saturated/Unsaturated Automated 3D Seepage Modeling. SoilVision Systems Ltd.

van Zyl, D.J.A, Harr, M.E. (1988). Modeling of Seepage Through Mine Tailings Dams. Hydraulic Fill Structures; geotechnical special publication No. 21. Edited by DJA van Zyl and SG Vick, New York, 1988, pp. 727-743.

Vick, S.G. (1983). Planning Design and Analysis of Tailings Dams. A Wiley-Interscience Publication, John Wiley & Sons, New York, 369 pages.

Williams, D.J, Wilson, G.W., Currey, N.A. (1997). A cover system for a potentially acid forming waste rock dump in a dry climate. Proceedings of the Fourth International Conference on Tailings and Mine Waste '97, Fort Collins, Colorado, USA, 13-17 January. pp. 231-235.

Wilson, G.W., Fredlund, D.G., Barbour, S.L. (1994). Coupled soil-atmosphere modeling for soil evaporation. Canadian Geotechnical Journal, Vol. 31, pp. 151-161.

Woyshner, M.R., St-Arnaud, L. (1994). Hydrogeological evaluation and water balance of a thickened tailings deposit near Timmins, ON, Canada. Proceedings of the International Land Reclamation and Mine Drainage Conference and the Third International Conference on the Abatement of Acidic Drainage, Pittsburg, PA, April 24-29, pp. 198-207.

CHAPTER 2

Theory on Calculation of Surface Flux Boundary Conditions

2.1 Introduction

Unsaturated soil profiles develop as a result of surface flux boundary conditions. Atmospheric forcing associated with the local microclimate together with the hydrologic properties of the ground surface determines the surface flux boundary condition. Precipitation is delivered to the ground surface as rainfall and/or snow. The partitioning of this precipitation into runoff, evapotranspiration, soil moisture storage and infiltration is a function of soil properties, vegetation, and potential evaporation. The sum of these surface fluxes determines the net infiltration rate or flux boundary condition at the soil surface. Soil suction values, pore water pressures and groundwater flow in the soil profile below the surface respond directly to the imposed flux boundary condition at the soil surface.

The primary objective of this study is to establish a methodology to determine the spatial variation of the surface flux boundary conditions for the case where the depth to the water table is variable as is often found in tailings impoundments (this study only focuses on the closure conditions for a tailings impoundment). This chapter provides the basic theoretical framework and establishes the need for the research. The first section describes the basic concepts with respect to the surface flux boundary components (i.e. precipitation, evaporation, transpiration, infiltration, and runoff). This section is concluded with a discussion regarding the spatial variation of surface flux boundary conditions.

The second section of this chapter describes how the surface flux boundary components can be coupled to the soil profile to allow prediction of the fluxes through this highly non-linear system. The soil-atmosphere coupling is described in terms of the SoilCover (SoilCover, 1997) model that is used as a tool to develop the spatial surface flux boundary conditions in subsequent chapters of this thesis.

A statement regarding the limitations of SoilCover and the need to develop the methodology for determining spatial flux boundary functions is provided. This is described in relation to the gap that exists between one-dimensional mechanistic coupled soil-atmosphere numerical models such as SoilCover, and multidimensional models for saturated/unsaturated seepage analysis.

2.2 The Surface Water Balance

Freeze and Cherry (1979) provide the following simple expression for the surface water balance:

$$P = I + ET + R \qquad [2.1]$$

Where, P = precipitation (mm),
I = infiltration (mm),
ET = evapotranspiration (mm),
= (E + T)
E = evaporation (mm),
T = transpiration (mm), and
R = runoff (mm).

Precipitation is the primary input to the surface water balance and can easily be quantified. Precipitation most often consists of rainfall, but can be in the form of snow, or even irrigation. The processes of infiltration and evapotranspiration govern the exchange of water between the soil surface and the atmosphere; these processes are described in detail in subsequent sections. Runoff is a complex process that is closely related to infiltration, and is controlled by many factors such as precipitation intensities and durations, surface topography, vegetation and soil properties.

The quantity of water that enters the ground surface and flows to the unsaturated zone of a natural soil system may be defined as the net infiltrative water flux, NI. This net infiltrative flux is controlled by the surface water balance and determines the quantity of groundwater recharge to natural soil systems. The net infiltrative water flux through a specified depth and time period may be computed as follows (Farquhar, 1989; Benson *et al.*, 1994):

$$NI = P - ET - R - D_r \pm \Delta S \qquad [2.2]$$

Where, D_r = lateral drainage (mm), and

ΔS = change in moisture storage (mm).

The various components of the water balance for a natural soil system are illustrated in Figure 2.1. The quantity of ΔS, determined from the measurement of changes in volumetric water content within the soil profile approaches zero when averaged over many years (Freeze and Cherry, 1979); however the magnitude of ΔS can be significant when short durations of time are being considered (i.e. seasonal storage). The quantity of lateral drainage is primarily a function of the ground surface slope and is negligible in most water balance evaluations (Benson *et al.*, 1994).

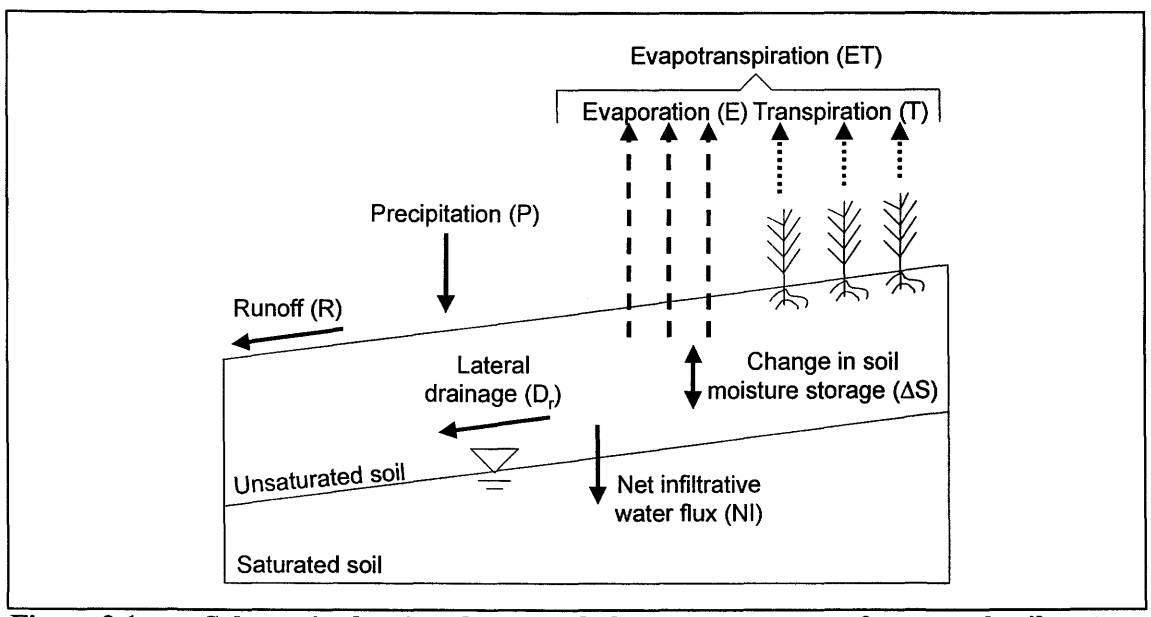

Figure 2.1: Schematic showing the water balance components of a natural soil system, as described in Equations 2.1 and 2.2.

2.2.1 Infiltration

Infiltration is the flow of liquid water into the surface of a soil due to a hydraulic gradient associated with soil water potential and gravity. Mein and Larson (1973) used the well-known Richard's equation to compute infiltration rates into unsaturated soil. The equation may be written as follows:

$$\frac{\delta\theta}{\delta t} = \frac{\delta}{\delta z}\left[k_w \frac{\delta h_w}{\delta z}\right] \qquad [2.3]$$

Where, θ = volumetric water content as a function of matric suction (%),

h_w = hydraulic head (m),

k_w = hydraulic conductivity as a function of matric suction (m/s),

z = vertical position (m), and

t = time (s).

The Richard's equation shown in Equation 2.3 describes transient one-dimensional flow. Mein and Larson (1973) showed the infiltration rate into an unsaturated soil surface to be a function of time. Figure 2.2 shows typical functional relationships for infiltration rates into unsaturated soil. Various boundary conditions are imposed on an initially dry soil surface. The infiltration rate shown as line A corresponds to a constant applied flux or rainfall intensity less than the saturated hydraulic conductivity of the soil. The infiltration rate equals the rainfall intensity since the minimum infiltration capacity of the soil is equal to the saturated hydraulic conductivity under a hydraulic gradient of one.

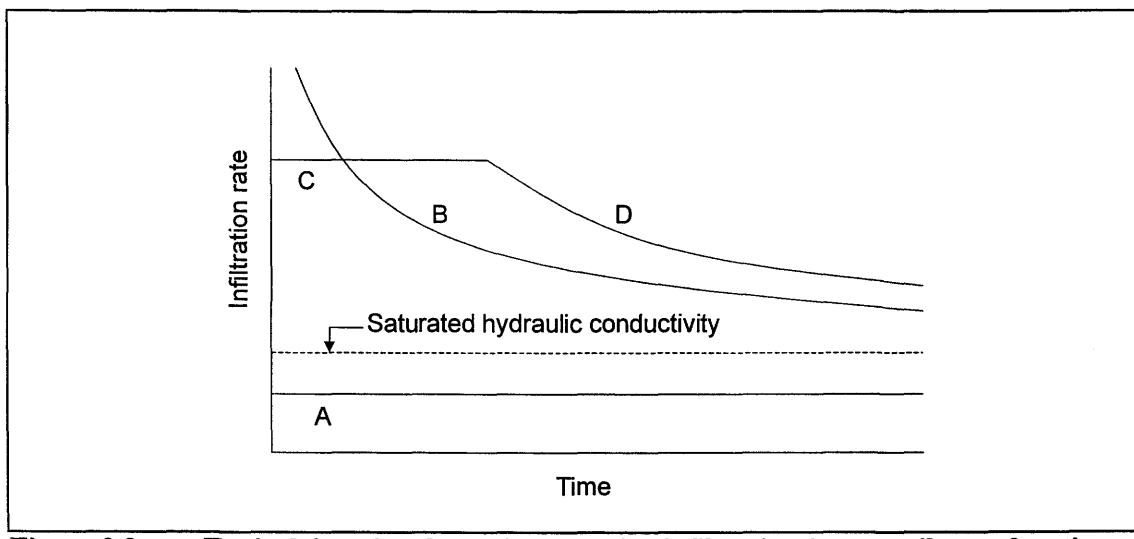

Figure 2.2: Typical functional relationships for infiltration into a soil as a function of time (after Mein and Larson, 1973).

Line B shows the infiltration rate into the same unsaturated soil profile under a ponding condition or with the pressure head set equal to zero at the surface. The initial infiltration rate greatly exceeds the saturated hydraulic conductivity. This occurs as a result of the strong downward hydraulic gradient associated with the high value of matric suction at the soil surface

suddenly set equal to zero. The infiltration rate decreases with time as water continues to infiltrate into the soil profile, which dissipates the initially large values of matric suction. In other words, the advancing wetting front results in the progressive reduction of matric suction values and associated pressure head gradients as shown in Figure 2.3. The downward vertical hydraulic gradient continues to decrease with time together with the resulting infiltration rate. The infiltration rate continues to decay with time until it reaches the minimum value equal to the saturated hydraulic conductivity of the soil.

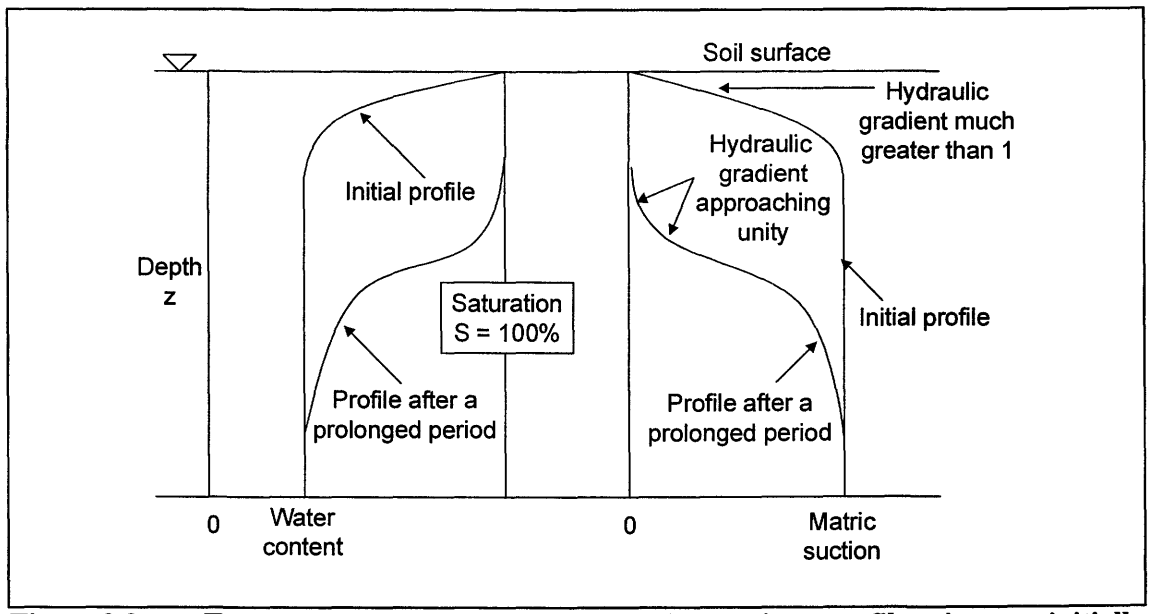

Figure 2.3: Typical water content and matric suction profiles in an initially unsaturated soil profile after time, t, after surface ponding (after Mein and Larson, 1973).

The curve shown as segments C and D in Figure 2.2 illustrates the case for a constant rainfall event where the rainfall intensity exceeds the saturated hydraulic conductivity of the soil. The infiltration rate is equal to the rainfall intensity during the earlier stages of the event resulting in all rainfall entering the soil surface. As water continues to enter, the soil suction and hydraulic gradients continue to decline, the infiltration rate begins to decay at some time "t" in the same fashion as described for the case ponding at the soil surface. The time required for the decline in infiltration from line C to curve D correspond to ponding at the surface. Runoff develops at this point in time if free topographic drainage is provided and the quantity of runoff is simply computed as the difference between rainfall intensity and infiltration rate.

In summary, the infiltration rate into a soil surface is computed using a saturated/unsaturated flow equation such as the Richard's equation. The surface flux boundary condition during

precipitation events is the quantity of rainfall specified over a period of time. Alternately, it may be given as a depth of snow that melts over a specified time period. Solving the flow equation determines the actual rate of infiltration and the quantity of runoff if the specified flux of precipitation exceeds the infiltrating capacity of the soil. This method of analysis shows that the actual infiltration rate into the soil is a function of both the climatic fluxes, soil properties, initial conditions such as matric suction values and soil water content, and the surface topography.

2.2.2 Evaporation

Soil water exfiltrates or leaves the soil surface of a soil, which may or may not be saturated, through the process of evaporation. Root water uptake and plant transpiration also occurs if vegetation is present and is considered as a combined process known as evapotranspiration. This section deals with the first concept of soil evaporation.

Hillel (1980) presents typical functional relationships for evaporation from soil with respect to various applied fluxes of potential evaporation as shown in Figure 2.4. Potential evaporation can be defined as the maximum rate of evaporation that would occur from a free water surface under the given climatic conditions of net radiation, temperature, relative humidity and wind speed. Numerous methods for determining potential evaporation are available such as the Thornthwaite (1948), Penman (1948) and Priestly and Taylor (1972) methods.

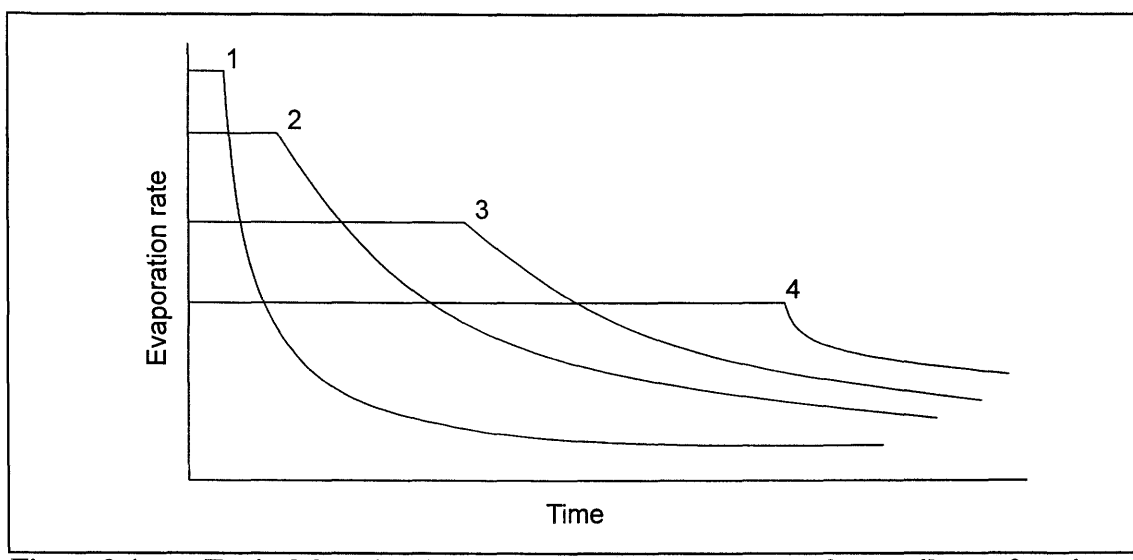

Figure 2.4: Typical functional relationships for evaporation from soil as a function of time (after Hillel, 1980).

The curves for evaporation with respect to time are similar to those shown in Figure 2.2 for infiltration. The primary difference is the soil is initially saturated at time zero and progressively dries with time instead of progressive wetting as was the case for infiltration. Curve 1 represents a high potential evaporation rate (i.e. hot, sun filled arid day) applied to a saturated soil. The maximum potential rate of evaporation is maintained for a short period of time and the actual rate of evaporation rapidly declines to a low residual value. Curves 2, 3 and 4 show similar trends for reduced potential rates of evaporation. In general terms, lower potential rates of evaporation can be maintained over longer periods of time. However, a restriction or decay in actual evaporation eventually occurs as some function of soil drying.

Holmes (1961) suggested that the actual evaporation rate, AE, as a function of potential evaporation, PE, controlled by soil moisture availability as shown in Figure 2.5. Figure 2.5 shows the ratio of AE/PE as a function of moisture availability for a reference sand and clay, and with different drying rates for the sand. The units for moisture availability were not specifically stated by Holmes (1961) but the range of wet to dry is implied as the range of field capacity (i.e. low suction $\approx$ 30 kPa) to the permanent wilting point (i.e. suction $\approx$ 1500 kPa). The field capacity and wilting point of a soil refers to moisture availability for vegetative root uptake. The wilting point refers to the suction at which the plant can no longer extract water. The curves shown in Figure 2.5 help explain the factors that influence soil evaporation such as soil moisture availability; however, they also indicate texture and drying rate as controlling factors.

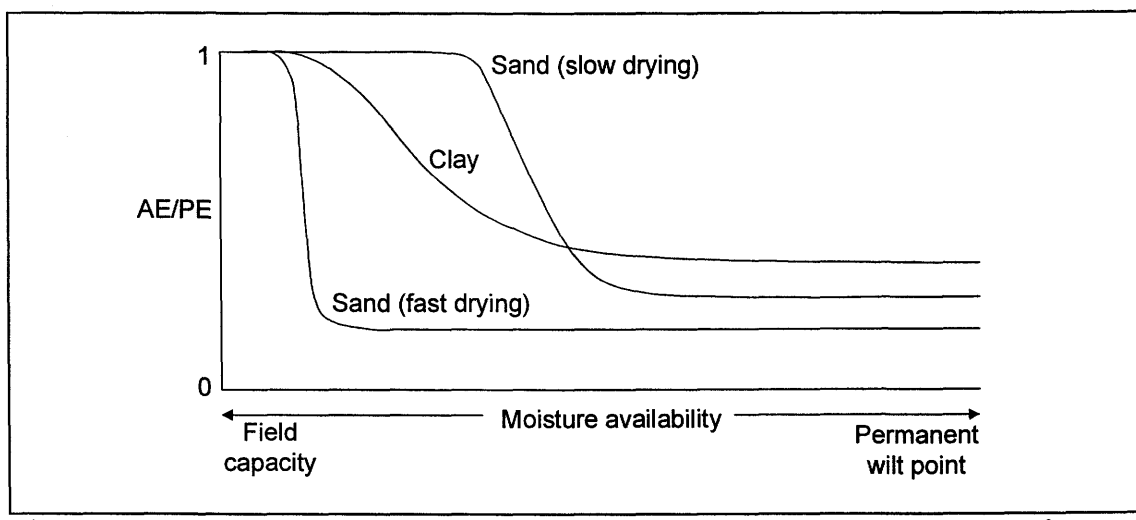

Figure 2.5: Typical drying curves for sand and clay showing actual evaporation as a fraction of potential evaporation versus soil moisture availability (after Holmes, 1961).

The shape of the drying curves in Figure 2.5 is described as having three stages of drying, as illustrated in Figure 2.6. Stage I drying is the maximum or potential rate of drying that occurs when the soil surface is at or near saturation, and is determined by climatic conditions. Stage II drying begins when the conductive properties of the soil no longer permit a sufficient flow of water to the surface to maintain the maximum potential rate of evaporation. The rate of evaporation progressively declines during stage II drying as the surface continues to desiccate and reaches a slow residual value defined as stage III drying. Hillel (1980) states that the slow rate of evaporation during stage III drying occurs after the soil surface becomes sufficiently desiccated to cause the liquid-water phase to become discontinuous. The flow of liquid water to the surface ceases and water molecules may only migrate to the surface through the process of vapour diffusion. In summary, it can be seen that the rate of actual evaporation from a soil surface is controlled by both climatic conditions, which define the potential rate of evaporation, and soil properties such as hydraulic conductivity and vapour diffusivity.

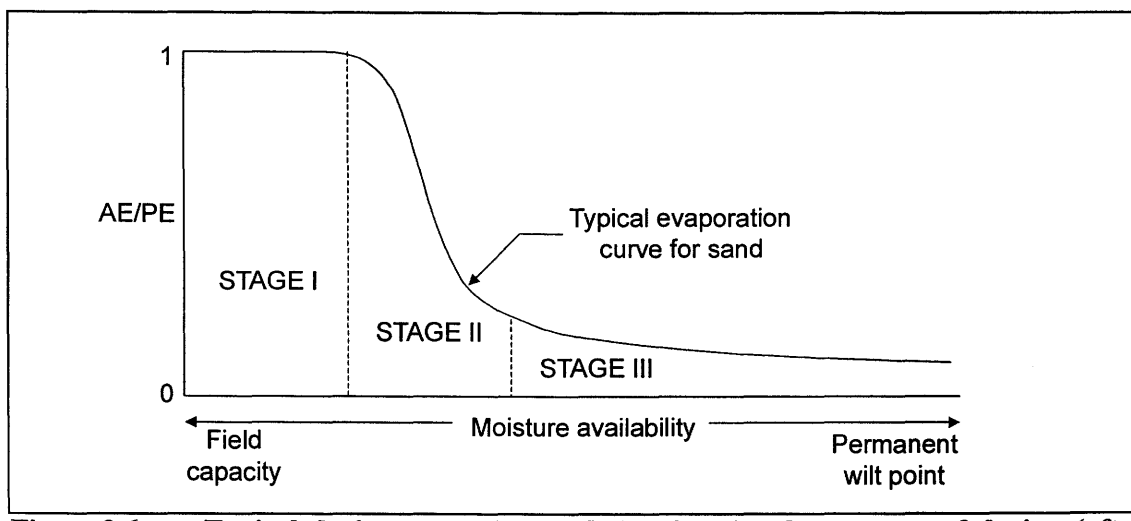

Figure 2.6: Typical drying curve for sand showing the three stages of drying (after Hillel, 1980).

Wilson *et al.* (1997) investigated the factors that influence soil evaporation including soil texture, drying time and water content. Drying tests were carried out for three principal classes of soil; clay, silt and sand. The laboratory drying tests demonstrated that the actual rate of soil evaporation is a function of soil suction at the surface as shown in Figure 2.7. Actual soil evaporation is nearly equal to the potential rate of evaporation until the value of matric suction reaches approximately 3000 kPa where it progressively declines with increasing suction. The reason for the decline in evaporation is attributed to depression of the vapour pressure in the soil with increasing suction. The relationship between relative humidity and suction is given by Edlefsen and Anderson (1943) as follows:

$$h_r = e^{\left(\frac{\varphi W_v}{RT}\right)} \qquad [2.4]$$

Where, h_r = relative humidity of soil surface as a function of total suction (%),

ψ = total suction in the soil (kPa),

W_v = molecular weight of water (0.018 kg/mole),

R = universal gas constant (8.314 J/mole/°K),

T = absolute temperature (°K).

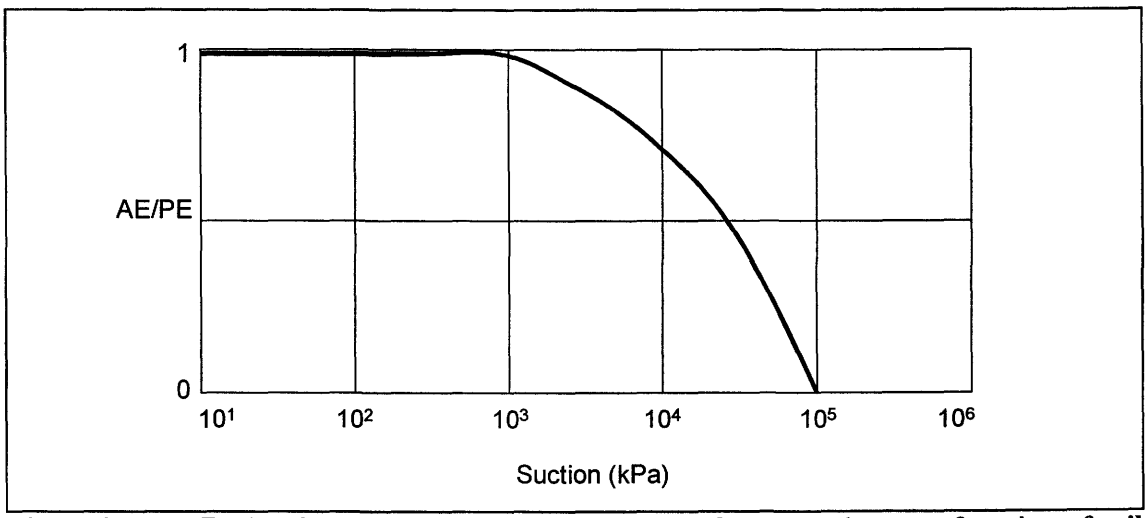

Figure 2.7: Ratio of actual evaporation and potential evaporation as a function of soil suction (after Wilson *et al.*, 1997).

Figure 2.8 shows a plot of the relationship described by Equation 2.4. The reason for the suppression in evaporation at 3000 kPa can be seen in Figure 2.8 as the point at which the relative humidity in the soil begins to fall below 100%. The relative humidity continues to decrease with increasing suctions and approaches zero at approximately 1 million kPa. The maximum value corresponds approximately to oven dryness at 105°C. In summary, actual evaporation from a soil is increasingly suppressed as soil suction increases with continual drying.

The depth to the phreatic surface affects the evaporation rate. Gardner and Fireman (1958) concluded that there are two maximum evaporation rates to consider when considering evaporation from a soil profile where a phreatic surface is present. The first is the potential evaporation rate that is determined by external conditions (i.e. the evaporation rate from a free-water surface), and the maximum rate that the soil can transmit upward through the soil column

from the phreatic surface to the soil surface. They state that actual evaporation will be limited to the lesser of these two maximas. Staley (1957) conducted column evaporation experiments with fine sand and concluded that there is a critical depth for the phreatic level that results in a rapid decline of surface evaporation. This critical depth is associated with the air entry value of the soil. Staley (1957) observed that at phreatic surface depths of less than the equivalent air entry value suction head for the soil, the actual evaporation from the soil profile matched the evaporation rate in a soil profile where the phreatic level was at the surface. As soon as the phreatic surface was lowered below this point, the evaporation rate was found to decline rapidly. This finding was supported by similar work by Gardner (1958) who stated that the evaporation rate depends on the moisture profile of the unsaturated soil. Wilson *et al.* (1994) provides a general theory for coupled soil/atmosphere modeling to predict AE/PE as a function of suction. Wilson *et al.* (1994) demonstrated that it is possible to predict the drying curve shown in Figure 2.6 and verified the model with column drying experiments for sand profiles with a fixed lower boundary condition. This method will be discussed in detail in a subsequent section.

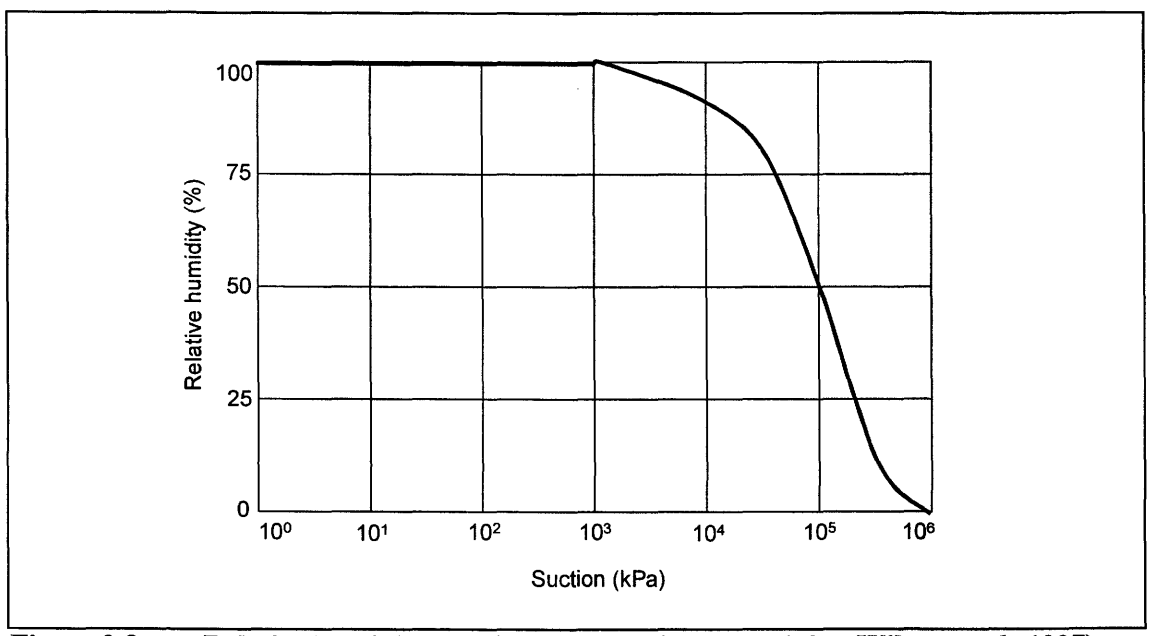

Figure 2.8: Relative humidity as a function of soil suction (after Wilson *et al.*, 1997).

Wilson *et al.* (1997) provides an expression to compute actual evaporation, AE as a function of potential evaporation and soil suction as follows:

$$AE = PE\left(\frac{1-e^{\frac{\varphi W_v}{RT}}}{1-RH}\right) \qquad [2.5]$$

Where, AE = actual soil evaporation (mm/day),
PE = potential evaporation (mm/day), and
RH = relative humidity of the air above the soil surface (%).

The value of potential evaporation, PE may be determined using any conventional method such as the measured rate of pan evaporation or the climate based methods above. Wilson (1990) and Wilson *et al.* (1994) also provides a modified form of the Penman (1948) method to compute actual soil evaporation as follows:

$$E = \frac{\Delta Q_n + \gamma E_a}{\Delta + A} \qquad [2.6]$$

Where, E = evaporative flux (mm/day),
Δ = slope of the saturation vapour pressure versus temperature curve at the mean temperature of the air (mmHg/°C),
Q_n = net radiant energy available at the surface (mm/day),
γ = psychrometric constant,
E_a = $f(u)e_a(B - A)$ where,
- $f(u)$ = $0.35(1 + 0.146\ W_a)$,
- W_a = wind speed (km/hr),
- e_a = water vapour pressure of the air above the soil surface (mmHg),
- B = inverse of the relative humidity of the air, and
- A = inverse of the relative humidity at the soil surface.

Machibroda *et al.* (1993) verified the use of the modified Penman formulation for the prediction of actual evaporation from a tailings surface. The use of the modified Penman equation is useful since the value of soil evaporation is computed on the basis of routinely obtained climatic parameters such as net radiation, temperature, relative humidity and wind speed. In addition, Equation 2.6 transforms to the conventional Penman (1948) equation when the soil is saturated

(i.e. A = unity) and the rate of the actual evaporation is equal to the potential rate of evaporation.

The methods for the computation of soil evaporative fluxes given in Equations 2.5 and 2.6 are useful provided the relative humidity at the soil surface is known. The actual rate of soil evaporation depends on the imposed climatic flux (i.e. PE) and is controlled in the same way that the imposed climatic flux (i.e. rainfall intensity) and the suction at the surface control the rate of infiltration. Therefore, a method for computing the relative humidity or value of suction at the soil surface is required. The Richard's equation given in Equation 2.3 is suitable for solving infiltrative fluxes for the entry of liquid water into the soil surface but is not suitable for computing the exfiltration of water from the soil surface due to evaporation. The primary reason for this is water exits the soil as vapour and not liquid. In fact, the residual evaporation rates that occur after prolonged drying as shown in Figures 2.4 and 2.5 is controlled by the diffusion rate of water vapour through the layer of dry soil that forms at the surface. A more general flow equation is required in place of the Richard's equation for saturated/unsaturated soils and will be described in a subsequent section.

2.2.3 Evapotranspiration

Transpiration refers to the loss of water vapour by plants (Meidner and Sheriff, 1976). Plant transpiration is a physical process that occurs concurrently with the biological processes involving plant growth and reproduction. Engineers are however primarily concerned with transpiration in terms of its mechanistic behavior. The pathway of transpiring water originates from the movement of water within the soil matrix towards the root surface. The roots absorb the soil water and transport it upward into the plant stem, into the leaves and up to the leaf surfaces. The moisture then vaporizes and diffuses into the atmosphere through tiny openings in the leaf surfaces, known as stomata.

Tratch (1995) presents a mechanistic methodology to predict transpiration based upon a method proposed by Feddes *et al.* (1978). This semi-empirical method to evaluate the transpiration flux was selected due to its ability to be adapted to bare soil and partitioned cover evaporation and evapotranspiration.

The first step in evaluating the transpiration flux involves determination of the potential evaporation rate. Details for the determination of this parameter have been described in the previous section. The second step involves determination of the potential transpiration flux. Because the evaporation and transpiration components must be evaluated individually, the potential evaporation flux must be distributed into its evaporation and transpiration components. Ritchie (1972) observed the transpiration component was dependent upon the leaf area index (LAI) values of the plant canopy. Three degrees of vegetative cover were identified with the resulting influence upon the potential transpiration flux presented in Equations 2.7, 2.8 and 2.9:

If, $LAI < 0.1$: $E_p = 0.0$ [2.7]

If, $0.1 < LAI < 2.7$: $E_p = E_o (-0.21 + 0.70^{1/2})$ [2.8]

If, $2.7 < LAI$: $E_p = E_o$ [2.9]

Where, E_p = potential transpiration rate (mm/day),

LAI = leaf area index for vegetative cover

$= \left(\frac{surface\_area_{leaf}}{surface\_area_{soil}} \right)$, and

E_o = potential evaporation rate (mm/day).

Depending on the ratio of the surface area of the leaves to the soil surface area they cover, the surface flux condition described by either Equations 2.7, 2.8 and 2.9 assume either: evaporation only, a combined evaporation and transpiration flux or solely transpiration flux conditions. The three phases of vegetative cover are identified as bare soil, partial cover and full cover conditions respectively. Ritchie (1972) describes the leaf area index values that define lower and upper limits of the partial cover conditions as 0.1 and 2.7 respectively. Vegetation effectively intercepts incoming radiation that will reduce actual evaporation rates. The net radiation is modified on the basis of the LAI.

The mass flux due to transpiration must be distributed through the soil that is occupied by the vegetative root structure. The proposed method of distributing the potential transpiration is presented in Figure 2.9 as a decreasing root uptake rate with depth (Prasad, 1988).

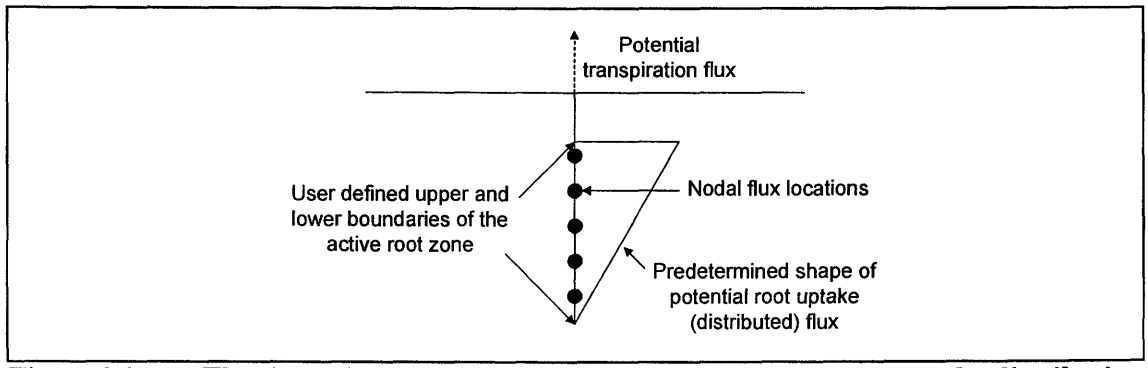

Figure 2.9: The shape function used to calculate the potential root uptake distribution through the active root zone (after Prasad, 1988).

The potential transpiration flux, defined in Figure 2.9 is distributed into nodal fluxes. The potential nodal flux rates are then dependant upon the potential transpiration flux, the location of the node with respect to the top and bottom of the active root zone and the node spacing. The potential nodal fluxes are then modified to determine the actual nodal root uptake flux as required in Equation 2.11 (Tratch, 1995; Wilson *et al.* 1994). The potential root uptake flux is modified by a reducing term given in Equation 2.10, which is in turn based upon the matric suction at the nodal locations by the relationship presented in Figure 2.10.

$$S = PRU \cdot PLF \qquad [2.10]$$

Where, S = actual nodal root uptake sink term (m/s),
PRU = potential root uptake flux (m/s), and
PLF = plant limiting factor, dependant upon the nodal matric suction as defined in Figure 2.2.

2.3 Spatially Varying Surface Flux Boundary Conditions

The basic water balance components discussed in the previous sections are easily understood and applied when considering the process in one-dimension. The reality is that the vadoze zone thickness varies spatially, and as a result the water balance components are expected to vary spatially (Tyler *et al.*, 1996; Heuvelman and McInnes, 1997; Shevenell, 1999; Cerda, 1999). Regional vadoze zone variations associated with groundwater tables are not what provides the cause for concern for the present study but rather engineered systems such as some tailings impoundments where the depth to the phreatic level can change significantly within a limited space. Figure 2.11 (a) presents a generalized cross-section through a tailings impoundment that

has a spatially varying phreatic surface that extends from a pool on top of the impoundment to seepage drains in the toe of the impoundment embankment (this is only typical of a low-tonnage tailings impoundment in an arid climate, such as the Kidston tailings impoundment investigated in this study.

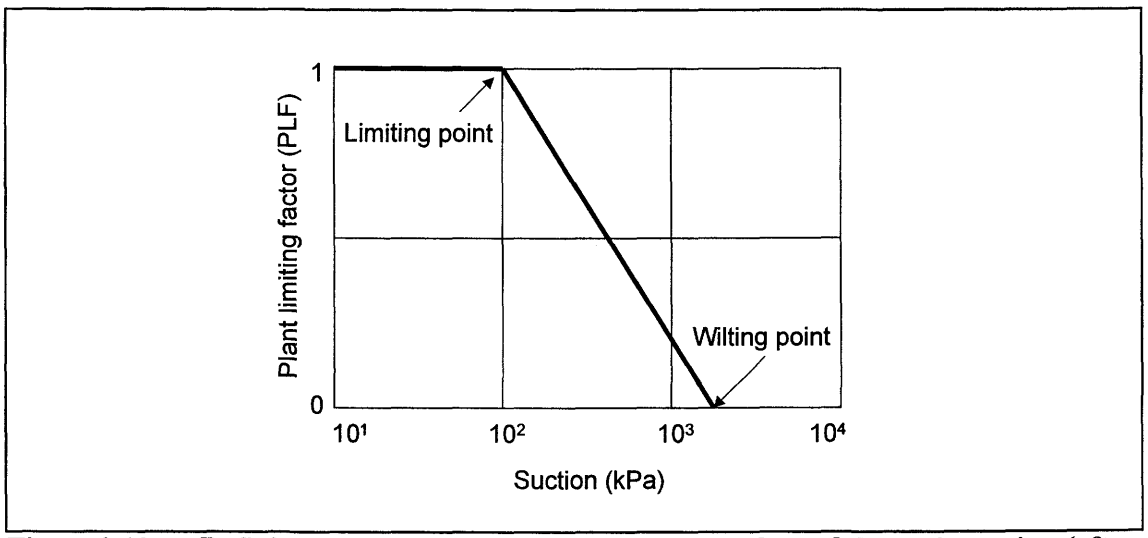

Figure 2.10: Definition of the plant limiting factor from the nodal matric suction (after, Tratch, 1995). Generally accepted values for the limiting and wilting points range from 50 to 100 kPa and 1500 to 2000 kPa respectively (Feddes *et al.*, 1978).

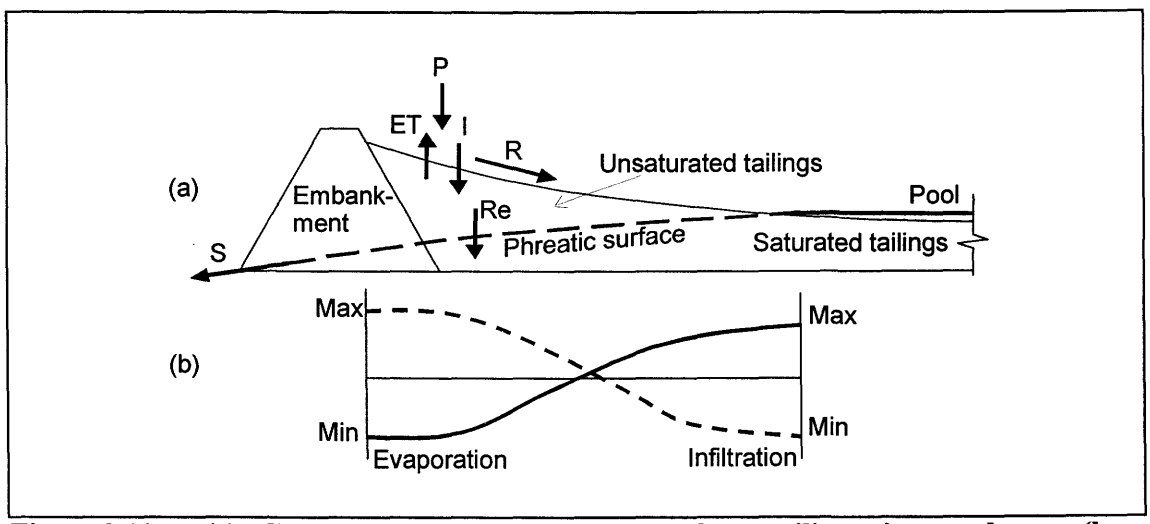

Figure 2.11: (a) Generalized cross-section through a tailings impoundment (low-tonnage impoundment in an arid climate, such as the Kidston tailings impoundment, (b) Spatial distribution of surface fluxes of infiltration and evaporation.

The surface of the tailings impoundment along this generalized cross-section would be subject to the usual water balance components of precipitation (P), evapotranspiration (ET), Infiltration

(I), runoff (R), recharge (R_e), and seepage (S). We would however expect that there would be a spatial variation in the magnitude of these components shown in Figure 2.11(b) as we move between the embankment and the pool. The reason for this is the availability of moisture in the profile, which is governed by the presence of the phreatic surface (Staley, 1957; Blight, 1997; Chu, 1997). Therefore, at a point close to the embankment evaporation is expected to be a minimum, and should increase moving in a direction towards the pool where it reaches a maximum (potential evaporation) at the pool edge. Similarly infiltration is expected to be a maximum close to the embankment and decrease towards the pool. The ability to calculate these spatial surface flux boundary conditions is crucial with respect to solving water balance calculations for engineered systems such as tailings impoundments. This hypothesis naturally only holds true for tailings impoundments such as the one at Kidston Gold Mine, i.e. a low-tonnage impoundment in an arid climate.

2.4 General Theory for Modeling Soil/Atmosphere Interaction

The previous sections described the principles for infiltration, runoff and evapotranspiration for soils. The actual rates of infiltration and evaporation were shown to be a function of both atmospheric forcing (i.e. precipitation and potential evaporation) and the properties of the soil surface. The fluxes across the soil/atmosphere continuum are fully coupled in terms of mass transfer and heat transfer. Figure 2.12 (after Wilson, 1990) shows a one-dimensional view of these fluxes. The mass transfer fluxes are liquid water for precipitation and saturated/unsaturated groundwater flow together with water vapour flow for evaporation and vapour diffusion in the unsaturated zone. The heat transfer components consist of conductive and latent heat flow within the saturated/unsaturated soil profile and net radiation, sensible heat and latent heat in the overlying atmosphere.

Wilson *et al.* (1994) provides the equation for the flow of liquid water and water vapour. This equation in its modified form include the transpiratory root uptake flux (Tratch, 1995) and is defined as follows:

$$\frac{\delta h_w}{\delta t} = C_w^1 \frac{\delta}{\delta y}\left(k_w \frac{\delta h_w}{\delta y}\right) + C_w^2 \frac{\delta}{\delta y}\left(D_v \frac{\delta P_v}{\delta y}\right) + S \qquad [2.11]$$

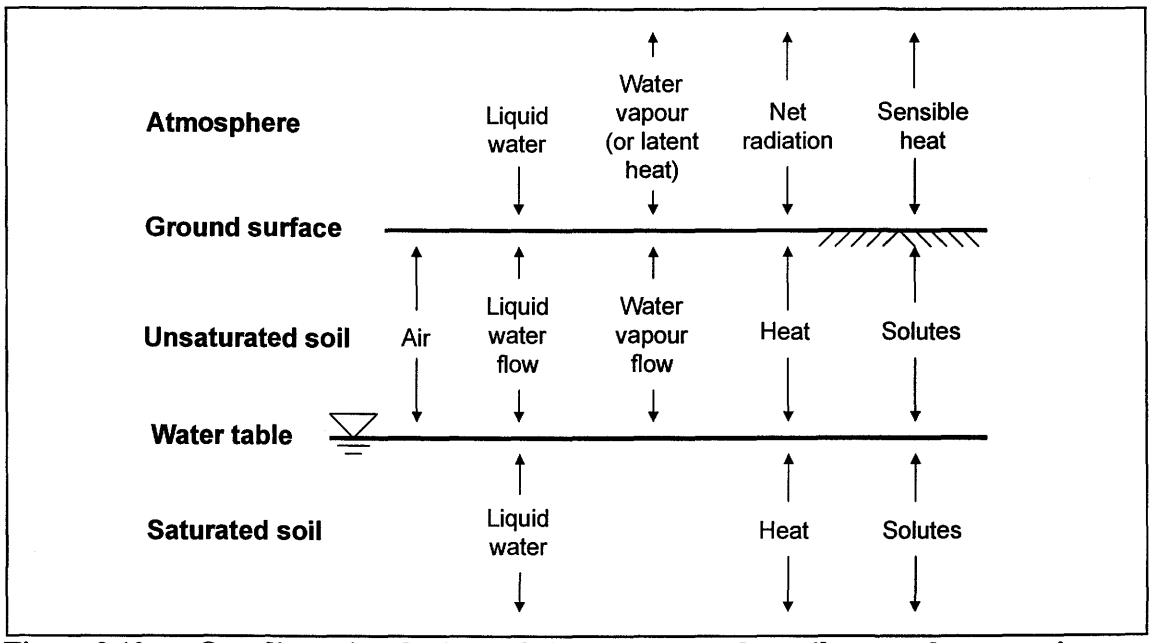

Figure 2.12: One-dimensional view of fluxes across the soil-atmosphere continuum (after Wilson, 1990).

Where, C_w^1 = modulus of volume change with respect to the liquid water phase

$$= \frac{1}{\rho_w g m_w^2},$$

C_w^2 = modulus of volume change with respect to the water vapour phase

$$= \frac{(P + P_v)}{P(\rho_w)^2 g m_2^w},$$

D_v = coefficient of diffusion for water vapour through soil (kg.m/kN.s),

ρ_w = density of liquid water (kg/m^3),

g = acceleration due to gravity (m/s^2),

m_2^w = slope of the soil water characteristic curve (1/kPa),

P = total atmospheric pressure (kPa),

P_v = partial pressure in the soil due to water vapour (kPa), and

S = root uptake sink term (m/s).

The heat transfer equation is given as:

$$C_h \frac{\delta T}{\delta t} = \frac{\delta}{\delta y}\left(\lambda \frac{\delta T}{\delta y}\right) - L_v\left(\frac{P + P_v}{P}\right)\frac{\delta}{\delta y}\left(D_v \frac{\delta P_v}{\delta y}\right) \qquad [2.12]$$

Where, C_h = volumetric specific heat ($J/m^3.^oC$),

T = temperature (^oC),

λ = thermal conductivity ($W/m.^oC$), and

L_v = latent heat of vaporization (J/kg).

Equations 2.11 and 2.12 are coupled through the vapour transfer terms related to P_v and therefore, must be solved simultaneously. In addition, soil suction (or pressure head), and hydraulic head are related to vapour pressure through Equation 2.13:

$$P_v = P_{sv} \cdot h_r \qquad [2.13]$$

Where, P_{sv} = saturation vapour pressure of the soil at the soil temperature, T.

The surface flux boundary condition is determined by solving Equations 2.11, 2.12 and 2.13 simultaneously using atmospheric forcing conditions such as rainfall intensity for the infiltration of liquid water and Equation 2.6 for the vapour flux due to evaporation.

The solution for the coupled heat and mass transfer equations requires a surface boundary condition for temperature which is computed as follows (Wilson, 1990; Wilson *et al.* 1994):

$$T_s = T_a + \frac{1}{\gamma(f(u))}(Q_n - E) \qquad [2.14]$$

Where, T_s = surface temperature (^oC),

T_a = air temperature above the soil surface (^oC).

In summary, the general soil/atmosphere model is formed by solving the system of Equations 2.6, 2.11, 2.12, 2.13 and 2.14 simultaneously for transient conditions of precipitation (i.e. rainfall) and evaporation events (i.e. net radiation, temperature, relative humidity and wind speed) for the period of interest (i.e. hours, days or years).

The inherent assumptions included in the Wilson (1990) and Wilson *et al.* (1994) formulation for coupling the soil/atmosphere are as follows; (1) The soil particles, water and air form a continuum, the behavior of which may be represented by a representative elementary volume, (2) The flow of liquid water in the soil due to osmotic pressure gradients is neglected, (3) The coefficients of hydraulic conductivity for the water and air phases respectively, are functions of the water content, degree of saturation or matric suction of the soil, (4) Hysteresis in the relationship between hydraulic conductivity and the matric suction is neglected, i.e. only the drying curves are used in the analysis, (5) Local thermodynamic equilibrium between the liquid water and water vapor phases prevails at all times at any point in the soil, (6) The temperature of the soil remains above the freezing point and below the boiling point of water at all times, (7) The effect of the double diffuse layer or the adsorbed fluid hull around the soil particles is not accounted for, and (8) The dissolving of air into the fluid phase is not considered.

2.5 The SoilCover Model

SoilCover is a mechanistic one-dimensional, transient, finite element, heat and water transfer (liquid and vapour) model that implements the physically based method described by Wilson *et al.* (1994) for predicting the exchange of moisture between the atmosphere and a soil surface. The coupling of the soil profile to the atmosphere is accomplished using a modified Penman formulation developed by Wilson (1990) and Wilson *et al.* (1994) that allows for the calculation of evaporation from a saturated or an unsaturated surface.

2.5.1 History of SoilCover

SoilCover was developed as a research tool by the Unsaturated Soils Group at the Department of Civil Engineering, University of Saskatchewan, Saskatoon, Saskatchewan, Canada (MEND, 1993). The initial research that ultimately resulted in the development of the present form of SoilCover (SoilCover, 1997), began with the soil-atmosphere coupling work by Wilson (1990) and Wilson *et al.* (1994). Wilson (1990) developed a rigorous formulation for heat and mass transfer through a soil profile that was numerically solved with an explicit finite difference model called "Flux". This model was capable of using either Dalton's mass transfer equation or the modified Penman equation to couple the soil to the atmosphere. The finite difference method used was proven successful, however was inefficient due to the small time step increments needed to achieve numerical stability (Machibroda, 1994).

A more effective formulation was achieved using a finite element method of solution under the name "VAPI" (Joshi, *et al.*, 1993). The Dalton mass transfer equation was used to couple the soil surface to the atmosphere. Cook (1994) converted the formulation by Joshi (1993) for use on a personal computer. Machibroda (1994) used the Joshi (1993) finite element formulation and in incorporated the modified Penman formulation proposed by Wilson (1990) and Wilson *et al.* (1994).

Tratch (1995) expanded the SoilCover model to allow for moisture loss from the soil profile due to transpiration, and Swanson (1995) improved SoilCover with respect to accuracy and efficiency and included a subroutine for the calculation of the daily oxygen flux through a soil profile. A freezing and thawing formulation was developed by Newman (1995) and Newman and Wilson (1997) and included into SoilCover.

2.5.2 The Finite Element Formulation

The finite element formulation for the SoilCover model was developed by Joshi (1993) and is based on the Galerkin weighted residual approach. The finite element formulation required replacing vapour pressure terms in the heat flow and moisture flow equations with equivalent water pressures. The result is two equations with two dependant variables; namely, pressure and temperature.

An adaptive time stepping scheme is used by SoilCover to automatically calculate the size of the time step during each day. Time step control parameters implemented by Joshi (1993) are used to calculate the initial size if the time step for the beginning of each day. Cook (1994) modified the original time stepping scheme to provide improved numerical stability. In the new scheme, suctions and temperatures from the previous time step are used to back calculate what the time step should have been based on the Crank Nicholson marching forward in time method.

SoilCover utilizes a relative convergence scheme for the dependant variables of suction and temperature that is evaluated at every node in the system (Cook, 1994). The original Joshi (1993) formulation utilized a relative convergence scheme that was evaluated for the norm of nodal head and temperature vectors (i.e. essentially evaluated for averaged nodal conditions). This modified method provided a more stringent control over system convergence.

2.5.3 Verification of SoilCover

Components of the SoilCover model have been extensively tested and verified. The mathematical formulation for coupling the soil and atmosphere as well as the calculation of actual evaporation was verified by Wilson (1990). The finite element code itself was verified by Joshi (1993) using direct laboratory measurements provided by Wilson (1990). The application of the modified Penman formulation to calculate actual evaporation in SoilCover was verified by Machibroda (1994) and Machibroda *et al.* (1993). Newman and Wilson (1997) verified the soil-freezing module in SoilCover and Tratch (1995) verified the plant transpiration module. The only component that has not been directly verified for the SoilCover model is the infiltration module and the implications of this is discussed later on in this chapter.

2.5.3.1 Verification of Atmospheric Coupling/Actual Evaporation

Wilson (1990) performed a series of column tests on a sandy material. Two columns of sand, initially close to saturation, were allowed to dry over a 42 day period in an environmental chamber. To determine the actual evaporation from the columns, the change in mass was monitored. The columns were 300 mm in height. The bottom was a no flow boundary and the top was exposed to the air in the environmental chamber. The air temperature was kept at 38°C. The relative humidity of the air chamber, and the temperature and relative humidity of the soil columns were measured continually. Good agreement between measured and computed values of actual evaporation was observed for the 42 day period.

2.5.3.2 Verification of Soil Freezing Theory

Newman and Wilson (1997) modified the SoilCover model by adding a soil-freezing module. The research covered in this thesis does not require the use of this module, and the theory for this module is not presented. It should however be pointed out that Newman and Wilson (1997) verified the soil freezing module by simulating 72 hour freezing tests carried out using silica flour (similar to fine silt). The results confirmed that the freezing module does in fact produce accurate results.

2.5.3.3 Verification of the Vegetation Algorithm

Tratch (1995) verified the SoilCover vegetation algorithm by modeling an evapotranspiration experiment that was carried out in a carefully controlled environmental chamber. The experiment was similar to the Wilson (1990) column study except, in this case, plants were allowed to grow and the leaf area index and root depth were monitored. The findings of the verification simulations confirmed that the vegetation algorithm does produce accurate results.

2.5.3.4 Verification of the Finite Element Formulation

A number of numerical simulations were performed by Joshi (1993) to verify the finite element formulation. Analytical solutions for fully coupled non-linear moisture and heat flow do not exist. However, solutions for simpler cases such as uncoupled liquid, vapour or heat flow are available. Comparison of the analytical solutions for these simple systems with the results from the Joshi (1993) formulation demonstrated that the finite element formulation was valid for both uncoupled liquid water and heat flow. Joshi (1993) also verified the finite element formulation under fully non-linear coupled conditions using the column experiment of Wilson (1990). The findings of Joshi (1993) was that the finite element formulation accurately simulate the flow of moisture both in the liquid and vapour phases as well as the transfer of sensible and latent heat under laboratory conditions. Only Dalton's simple mass transfer equation, using an experimentally determined mass transfer coefficient has been used to evaluate the evaporative flux at the surface. Essentially this meant that the numerical model presented by Joshi (1993) is not suitable for practical field scale applications.

Machibroda (1994) modified the Joshi (1993) finite element formulation to allow atmospheric coupling by means of the modified Penman method proposed by Wilson *et al.* (1994). Field measurements on the non-vegetated Kidd Creek tailings impoundment near Timmins, Ontario, Canada, were conducted to measure the actual evaporation rates from the profile. Predictive modeling with the revised finite element formulation confirmed that the modified Penman method was a suitable method for predicting evaporative fluxes.

2.5.4 Field Application of SoilCover

The SoilCover model has been applied successfully at a number of field sites. Machibroda *et al.* (1993) documents how SoilCover was applied towards predicting the net infiltrative fluxes across non-vegetated tailings at Kidd Creek, near Timmins, Ontario, Canada. The work consisted of detailed meteorological measurements that allowed for calculation of actual evaporation rates using the Bowen ratio energy balance method (Bowen, 1926), and potential evaporation rates using evaporation pans. The SoilCover predicted evaporation rates were compared to the measured rates and good matches were found using the modified Penman formulation.

Wilson *et al.* (1997b) demonstrated the application of SoilCover for the waste rock cover systems installed at Equity Silver Mine in British Columbia, Canada, and Durham *et al.* (2000) documents the application of SoilCover at the Kidston Gold Mine in Queensland, Australia. The work by Durham *et al.* (2000) comprised of evaluating the performance of various cover alternatives for waste rock dumps. Extensive field response monitoring equipment was installed including measurement of matric suction and water content in the cover profile, Bowen ratio equipment and detailed meteorological instrumentation. Calibration of the SoilCover model for predictive modeling of the cover system found excellent matches between the field response data and the modeled results.

2.5.5 SoilCover Limitations

The coupled soil and atmosphere numerical model SoilCover has been shown to effectively calculate the actual evaporation from a soil profile. The model does however have some limitations that should be mentioned. Highlighting these limitations does not diminish the value of the model, but are intended to allow for a more thorough understanding of the complexity of calculating surface flux boundary conditions.

2.5.5.1 SoilCover Infiltration/Runoff Calculations

SoilCover assumes that any precipitation that does not infiltrate according to the flow equation for liquid water given in Equation 2.11 (or the Richards equation given in Equation 2.3) will run

off. This is handled within the finite element program on every iteration and for every time step as follows (after SoilCover, 1997):

1. If the surface is not saturated the user specified precipitation minus any internally calculated actual evaporation will be applied at the top node as a liquid flux boundary condition. For small precipitation with high evaporation, this boundary flux can be negative (i.e. leaving the soil profile).
2. If the surface has a zero pore pressure (i.e. saturated), then the finite element routine applies a pressure equal to 0 kPa boundary condition at the surface. The runoff equals precipitation minus actual evaporation minus Darcy flux infiltration across the first two gauss points between the top and the second node in the mesh. This procedure implies no ponding is allowed at the surface.
3. If runoff is calculated as a negative number, then, according to the mass balance equation in step 2, the top node is passing enough Darcy liquid flux to desaturate the surface. When this occurs, the top boundary condition is applied as in step 1, above.

This method has some small inherent error because in step 2 the runoff depends on the Darcy flux between two points just below the soil surface, not at the surface. It is possible, to have a small water balance error when there is a very steep hydraulic gradient between the first and the second nodes in the mesh. This happens, for example, when the surface is very dry and a rainfall event occurs (clean sandy soils with steep soil water characteristic curves that desaturate rapidly are more susceptible to this problem). The first node wets up faster than the Darcy flux below the surface can respond. The result is a low suction at the top node and a very high suction at the second node. The Darcy flux used in step 2 above is based on average material properties in the region between the top two nodes and this approximation looses accuracy when the gradient is large.

SoilCover is a one-dimensional model and cannot differentiate runoff from surface slopes of varying degrees. Differences in runoff for flat surfaces and sloping surfaces can be accounted for by considering the duration of the rainfall event. In the case of flat surfaces, the total amount of rainfall is distributed evenly over the entire day (i.e. 24 hours). The reasoning behind this methodology is based on the local surface retention that occurs over a regional flat surface. Few surfaces are completely flat, but rather have local topographic lows and highs. These highs and lows are capable of retaining shallow volumes of water from rainfall events that would

otherwise be lost to runoff. This ponded water is then allowed to infiltrate throughout the day. Distributing the rainfall evenly throughout the day simulates the condition of ponding without having to know topographic details of the flat surface to average surface retention. Field verification of the SoilCover model at the Kidd Creek, Equity Silver and Kidston Mines has been conducted on the basis of this assumption.

Runoff for slopes can be accounted for in a general way by considering the actual intensity of the rainfall event. For sloping surfaces, any infiltration excess will be lost immediately to runoff. This is opposite to the flat surface that can store the infiltration excess until complete infiltration can occur. By specifying the amount and duration of a rainfall event, runoff for a sloping surface can be adequately described. This description does not however, account for varying degrees of slope. In general, both the methods adopted for flat and sloping surfaces have significant limitations. However, a more rigorous physical account of runoff would require a detailed two-dimensional analysis. This would require solution of a two-dimensional head distribution along the slope face while accounting for runoff from the upper slope regions which could become potential infiltration for the lower slope regions. The effect of vegetation on the sloping surface is not taken into account.

2.5.5.2 Spatial Limitations

SoilCover is a one-dimensional model and as such spatial variations of surface flux boundary conditions associated with spatially varying unsaturated zone thickness as illustrated in Figures 2.11 (a) and (b), cannot be directly calculated. The methodology for using SoilCover to calculate these spatial variances would be to run individual SoilCover simulations for representative profiles and interpolate between locations to provide some indication as to the spatial surface flux boundary conditions variations. What this means in practical terms is that a system like a tailings impoundment that has a spatially varying phreatic surface cannot readily be modeled using SoilCover.

2.6 Multidimensional Saturated/Unsaturated Seepage Analysis Models

Multidimensional saturated/unsaturated seepage analysis models have a distinct advantage over 1-D models in that they provide a fully mechanistic description of flow in multi dimensions. The chief disadvantage of present multidimensional seepage analysis models is that they are not

coupled to the atmosphere. Such models require a surface flux boundary condition for input into the multidimensional models. Using the calculated surface flux boundary conditions of a coupled 1-D model as a surface flux boundary for the multidimensional models is commonly done, and has been shown to provide accurate results (Yanful and Aube, 1993; Bews *et al.*, 1994, and Woyshner and Yanful, 1993). A problem is however again introduced as soon as the vadoze zone thickness varies spatially, since the coupled surface flux boundary models cannot calculate these spatial surface flux boundary conditions readily.

2.7 Conclusions

The calculation of spatially varying surface flux boundaries are not easily done due to the fact that mechanistic soil/atmosphere coupled numerical models capable of rigorously calculating the surface flux boundary conditions are one-dimensional, and mechanistic multidimensional saturated/unsaturated seepage analysis models are not coupled. Using the output of the 1-D surface flux boundary model as a surface flux boundary condition in multidimensional seepage analysis modeling is not where the limitation lies, but rather determining the actual multidimensional spatial variations of the surface flux boundary conditions. There is thus a definite need to develop a methodology that would allow for the calculation of multidimensional spatial surface flux boundary conditions using the mechanistic soil/atmosphere coupled models available.

The research documented in the subsequent chapters will describe a methodology to calculate these spatial surface flux boundary functions using the coupled soil/atmosphere surface flux boundary model SoilCover, for use as surface flux boundary conditions in multidimensional saturated/unsaturated flow seepage analysis models.

2.8 References

Benson, C.H., Bosscher, P.J, Lane, D.T., Pliska, R.J. (1994). Monitoring system for hydrologic evaluation of landfill covers. Geotechnical Testing Journal, Vol. 17, pp. 855-974.

Bews, B, Barbour, S.L., Wilson, G.W. (1994). SEEP/W and SoilCover Modeling for the Dona Lake Mine Site, Final Report. Geotechnical Engineering Group, University of Saskatchewan, Saskatoon, Saskatchewan, Canada.

Blight, G.E. (1997). Interactions between the atmosphere and the Earth. Geotechnique, Vol. 47(4), pp. 715-767.

Bowen, I.S. (1926). The ration of heat losses by conduction and by evaporation from any water surface. Physical Review, Vol. 27, pp. 779-787.

Cerda, A. (1999). Seasonal and spatial variations in infiltration rates in badland surfaces under Mediterranean climatic conditions. Water Resources Research, Vol. 35, No. 1, pp. 319-328.

Chu, S.T. (1997). Infiltration Model for Soil Profiles with a Water Table. American Society of Agricultural Engineers, Vol. 40, No. 4, pp. 1041-1046.

Cook, D. (1994). Modification of a Finite Element Soil-Atmosphere Model. B.Sc. Undergraduate Thesis, Department of Civil Engineering, University of Saskatchewan, Saskatoon, Saskatchewan, Canada.

Durham, A.J.P., Wilson, G.W., Currey, N. (2000). Field Performance of Two Low Infiltration Cover Systems in a Semi Arid Environment. Proceedings of the Fifth international conference on Acid Rock Drainage, Denver, Colorado, USA. May, pp. 1319-1326.

Edlefsen, N.E., Anderson, A.B.C. (1943). Thermodynamics of Soil Moisture. Hilgardia, Vol. 15, No. 2, pp. 31-298.

Farquhar, G.J. (1989). Leachate: production and characterization. Canadian Journal of Civil Engineering, Vol. 16, pp. 317-325.

Feddes, R.A., Kowaklik, P.J., Zaradny, H. (1978). Simulation of Filed Water Use and Crop Yield. John Wiley & Sons, Toronto, Canada. 188 pp.

Freeze, R.A., Cherry, J.A. (1979). Groundwater. Prentice Hall, Englewood Cliffs, NJ, USA.

Gardner, W.R. (1958). Some steady state solutions of the unsaturated moisture flow equation with application to evaporation from a water table. Soil.

Gardner, W.R., Fireman, W. (1958). Laboratory studies of evaporation from soil columns in the presence of a water table. Soil Science Society Journal of America, Vol. 85, No. 4, pp. 244-249.

Heuvelman, W.J., McInnes, K.J. (1997). Spatial Variability of Water Fluxes in Soil: A Field Study. Soil Science Society of America Journal, Vol. 61, pp. 1037-1041.

Hillel, D. (1980). Application to Soil Physics. Academic Press, New York, USA.

Holmes, R.M. (1961). Estimation of Soil Moisture Content Using Evaporation Data. Proceedings of Hydrology Symposium, No. 2 Evaporation. Queen's Printer, Ottawa, pp. 184-196.

Joshi, B. (1993). A finite element model for the coupled flow of moisture and heat in soils under atmospheric forcing. M.Sc. Thesis, University of Saskatchewan, Saskatoon, Saskatchewan, Canada.

Joshi, B., Barbour, S.L., Krause, A.E., Wilson, G.W. (1993). A finite element model for the coupled flow of heat and moisture in soils under atmospheric forcing. Finite Elements in Analysis and Design, Vol. 15, pp. 57-68.

Machibroda, R.M. (1994). Soil evaporative flux modeling of layered cover systems. M.Sc. Thesis, University of Saskatchewan, Saskatoon, Saskatchewan, Canada.

Machibroda, R.L., Wilson, G.W., Barbour, S.L. (1993). Evaluation of Net Infiltrative Fluxes Across the Surface of Exposed Mine Tailings. Proceedings of the 46th Canadian Geotechnical Conference, Saskatoon, Saskatchewan, Canada, 27-19 Sep, pp. 167-175.

MEND (1993). SoilCover: User's Manual for an Evaporative Flux Model. University of Saskatchewan, Saskatoon, Saskatchewan, Canada.

Meidner, H., Sheriff, D.W. (1976). Water and Plants. Halsted Press, John Wiley and Sons, New York, USA.

Mein, R.G., Larson, C.L. (1973). Modeling Infiltration during a Steady Rain. Water Resources Research, Vol. 9, No. 2, April, pp. 384-394.

Newman, G.P. (1995). Heat and mass transfer in unsaturated soils during freezing. M.Sc. Thesis, University of Saskatchewan, Saskatoon, Saskatchewan, Canada.

Newman, G.P., Wilson, G.W. (1997). Heat and mass transfer in unsaturated soils during freezing. Canadian Geotechnical Journal, Vol. 34, pp. 63-70.

Penman, H.L. (1948). Natural evapotranspiration from openwater, bare soil and grass. Proc. R. Soc. London Ser. A, Vol.193, pp. 120-145.

Prasad, R. (1988). A Linear Root Uptake Model. Journal of Hydrology, Vol. 99, pp. 297-306.

Priestly, C.H.B., Taylor, R.J. (1972). On the Assessment of the Surface and Heat Flux and Evaporation Using Large Scale Parameters. Monthly Water Review, Vol. 100, pp. 81-92.

Ritchie, J.T. (1972). Model for Predicting Evaporation from a Row Crop with Incomplete Cover. Water Resources Research, Vol. 8, No.5, pp. 1204-1213.

Shevenell, L. (1999). Regional potential evapotranspiration in arid climates based on temperature, topography and calculated solar radiation. Hydrological Processes, Vol. 13, pp. 577-596.

Swanson, D.A. (1995). Predictive modeling of moisture movement in engineered soil covers for acid generating mine waste. M.Sc. Thesis, Department of Civil Engineering, University of Saskatchewan, Saskatoon, Saskatchewan, Canada.

Thornthwaite, C.W. (1948). An Approach Toward a Rational Classification of Climate. Geographical Review, Vol. 38, pp. 55-94.

Tratch, D. (1995). Moisture uptake within the root zone. M.Sc. Thesis, Department of Civil Engineering, University of Saskatchewan, Saskatoon, Saskatchewan, Canada.

Tyler, S.W., Chapman, J.B, Conrad, S.H., Hammermeister, D.P., Blout, D.O., Miller, J.J., Sully, M.J., Ginanni, J.M. (1996). Soil-water flux in the southern great Basin, United Sates: Temporal and spatial variations in the last 120,000 years. Water Resources Research, Vol. 32, No. 6, pp. 1481-1499.

SoilCover. (1997). SoilCover User's Manual. Unsaturated Soils Group, Department of Civil Engineering, University of Saskatchewan, Saskatoon, Saskatchewan, Canada.

Staley, R.W. (1957). Effect of depth of water table on Evaporation from fine sand. Master of Science Thesis, Colorado State University, Fort Collins, Colorado, U.S.A.

Wilson, G.W. (1990). Soil Evaporative Fluxes for Geotechnical Engineering Problems. Ph.D. Thesis, University of Saskatchewan, Saskatoon, Saskatchewan, Canada.

Wilson, G.W., Fredlund, D.G., Barbour, S.L. (1994). Coupled soil-atmosphere modeling for soil evaporation. Canadian Geotechnical Journal, Vol. 31, pp. 151-161.

Wilson, G.W., Fredlund, D.G., Barbour, S.L. (1997). The effect of soil suction on evaporative fluxes from soil surfaces. Canadian Geotechnical Journal, Vol. 34, No. 1, pp. 145-155.

Wilson, G.W., Newman, L.L., Barbour, S.L., O'Kane, M., Swanson, D.A. (1997). The cover research program at Equity Silver Mine Limited. Proceedings of the 4th International Conference on Acid Mine Drainage, Vancouver, British Columbia, Canada. Vol. 1, pp. 197-210. 31 May – 6 June.

Woyshner, M.R., Yanful, E.K. (1993). Hydrological Analysis and Prediction in a Soil Cover. 1993 Joint CSCE – ASCE National Conference on Environmental Engineering, Montreal, Quebec, Canada, July, pp. 289-296.

Yanful, E.K., Aube, B.C. (1993). Modeling Moisture Retaining Soil Covers. 1993 Joint CSCE – ASCE National Conference on Environmental Engineering, Montreal, Quebec, Canada, July, pp. 273-280.

CHAPTER 3

Kidston Gold Mine Site and Tailings Impoundment Description

3.1 Introduction

This chapter provides a general overview of the Kidston Mine Site and the tailings impoundment, and it places the work described in this thesis in context with the mining operation. Most of the topics discussed in this chapter are not detailed, since they do not play a crucial role in the development of the thesis. Where topics are of crucial importance, the reader is referred to the relevant chapters in the thesis.

3.2 Kidston Gold Mine History

Gold was first discovered in the Kidston area in the 1880s, but the alluvial field was only publicly opened in 1907. The field proved to be rich and over the next three years an estimated 622,000 g (2,194 oz) of gold were mined. The field was originally operated as a number of individual holdings, which by 1915 had amalgamated to form larger companies. By the early 1920s, Kidston had its own battery, which was built by the Queensland government, and this structure still remains on site today.

In 1921 the mine was converted to an open cut operation, and mining continued to 1945 when it was shut down. During the 1960s there was some interest in reopening the mine, but it was not until 1979 that Kidston Gold Mines Limited applied to the Queensland government to start full production again. The Kidston Gold Mine, as it stands today, was opened in 1985 and mining is conducted 24 hours a day, 7 days a week. There is no longer a township at the mine site, only a permanent motel-style camp for the workers who work 4 or 7 day on/off shifts and are generally flown to site from the nearest city, Cairns.

Placer Dome Asia Pacific (PDAP) is a wholly owned subsidiary of Placer Dome Inc (PDI) and manages and operates the Kidston Gold Mine, in which it holds a 70% share. Kidston Gold

Mines Limited own the remainder of the shares. Annual mill feed for the mine averaged around 5 million tones, with an average ore grade of 1.1 g/t at a recovery rate of approximately 80% (Placer Dome Inc, 1999). The resultant average annual gold production is between 150,000 and 250,000 oz, with an estimated total production of 3.2 million oz up to the end of 1999 (Placer Dome Asia Pacific, 2000).

Gold ore is reduced to passing 300 mm in the primary crusher then to passing 25 mm in a secondary crusher, before it is fed to a semi-autogeneous grinding (SAG) mill with recycle crushing and ball milling. In the SAG mill the ore is ground to 80% passing 0.2 mm. Crushing and milling is followed by conventional cyanide leaching. Precious metals are recovered using carbon-in-pulp (CIP) and carbon column technology and subsequent carbon stripping, electrowinning and smelting.

The mine is scheduled for final closure by mid 2001 due to the depletion of economic reserves. The total area disturbed during the life of the mine (all pits, dumps, roads, building sites, access roads, power lines etc.) is estimated at 835 ha (Placer Dome Asia Pacific, 2000), which includes the 310 ha tailings impoundment under investigation in this thesis. Since 1997, Kidston Gold Mine has been actively working towards rehabilitation of the disturbed areas with the ultimate goal of achieving closure of the mine site and returning the land to the care of the Queensland government.

3.3 Kidston Mine Site Location

The Kidston Mine is located in the north-east portion of Australia, in the state of Queensland, approximately 280 km west-north-west of the city of Townsville and 260 km south-west of the city of Cairns (latitude 18°52'S, longitude 144°09'E). Both Cairns and Townsville lies on the Pacific Ocean coastline as illustrated in Figure 3.1.

The mine is located on the catchment divide of the Copperfield River to the east and the Charles Creek to the west (Gutteridge, Haskins and Davey, 1984). These two rivers coalesce about 16 km downstream from the mine. Butchers Creek is a small tributary of the Copperfield River, and the tailings impoundment is constructed within its catchment of 4.5 km^2. The general landscape is rolling terrain, with the mine pits located under rocky knolls (now mined out) which were up to 40 m above the surrounding hills. The predominant land use of the area is

cattle grazing on the largely unimproved native pastures. The predominant vegetation associations are typical of inland North Queensland, being open savanna woodlands or low woodlands. Tall, open scrubland is generally associated with the Copperfield River floodplain (AGE Consultants, 2001). Iron Bark Eucalyptus and Box trees are the most predominant species of the area.

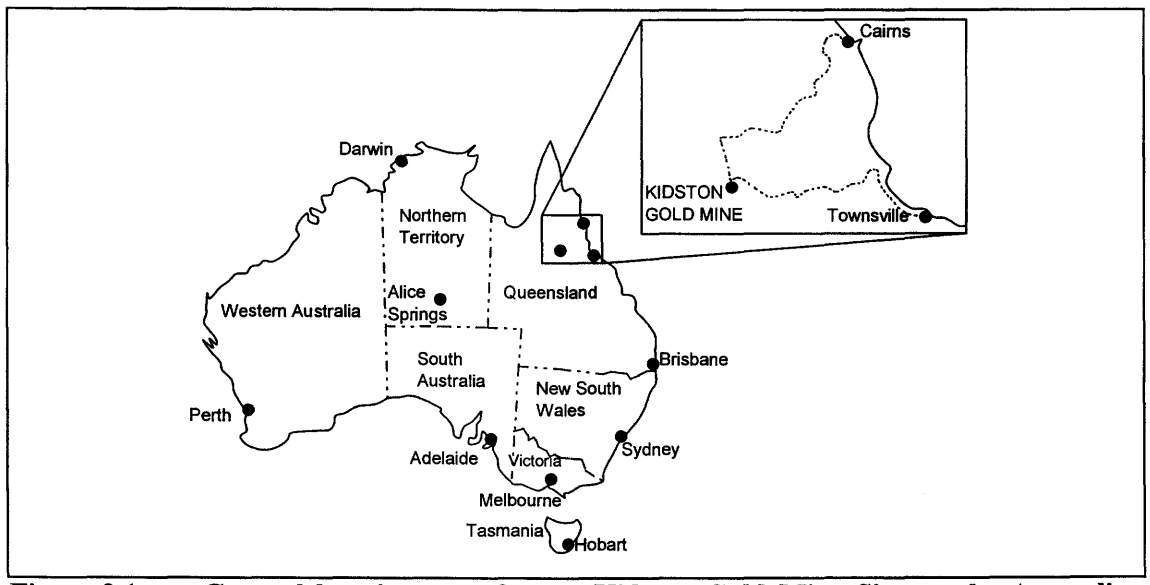

Figure 3.1: General location map for the Kidston Gold Mine Site on the Australian continent.

3.4 General Site Climate

The climate is dry and sub-tropical with pronounced wet and dry seasons. Approximately 80% of the 702 mm average rainfall occur between the summer months of November and April. The average annual potential evaporation of 1651 mm far exceeds the rainfall, resulting in a net-negative annual climatic water balance for the area.

Annual maximum and minimum average daily temperatures for the Kidston area is 29.7°C and 17.5°C respectively, with typical maximum and minimum temperatures around 41.3°C and 2.7°C. Freezing conditions is extremely uncommon, and when occasionally temperatures does drop below freezing overnight, frost will disappear within hours of daylight. A detailed discussion of the Kidston climate is presented in Chapter 5 and Appendixes H, I and J.

3.5 Mine Site Geology

The regional geology underlying the tailings impoundment area include part of the Einasleigh Metapmorphics formation of the Precambrian (Archaen) age, intruded to the east by Forsayth granodiorite of Upper Precambrian (Proterozoic) age. The Einasleigh Metamorphics are typically isoclinally folded with steep dips trending in a north-westerly direction. The two principal rock types exposed consist of fine-grained mica schist and amphibolite. The contact zone with the Forsayth granodiorite consists of a zone of banded gneiss forming a gradational margin. Immediately to the east of the tailings impoundment location a substantial dyke of quartz feldspar porphyry, also with a north-westerly trend is found (Wood Geotechnical Consultants, 1981; Gutteridge Haskins and Davey, 1984).

The Butchers Creek channel, over which the tailings impoundment has been constructed, had a flat sandy base between 15 and 25 m wide, with the sand fairly coarse, angular and granitic of origin. Alluvium depths are between 5.7 and 5.5 m deep, with some interbedded gravel and boulder layers. Erosion from this channel has removed almost all the weathered material, and the alluvium is resting mainly on fresh jointed bedrock in the stream channel. The soil cover overlaying the parent rock within the tailings impoundment area consists of between 1 and 2 m of weathered material with soil properties forming a mantle over highly weathered gneiss with weak rock properties. Further downstream, between the embankment and the Copperfield River, there is a layered colluvial and alluvial fill from 1 to 2 m thick resting on a highly weathered layer, which in turn passes into slightly weathered rock (Wood Geotechnical Consultants, 1981).

Open drill hole permeability testing by means of a combination of constant head and falling head permeability testing, as well as Packer Tests was performed on the base geology beneath the tailings impoundment and the results are summarized in Table 3.1 (Gutteridge, Haskins and Davey, 1984). The permeabilities listed in Table 3.1 indicate that the potential for deep groundwater leakage from the tailings impoundment is limited by the relative impervious nature of the base geology. This is further supported by the fact that no large-scale regional faults have been detected in the tailings dam area. The area is also in a zone known to have minimal seismic activity (Wood Geotechical Consultants, 1981).

Table 3.1 Summary of field permeability tests for the Kidston base geology (Gutteridge Haskins and Davey, 1984).

Test type	# Tests	Permeability range (m/s)	Average permeability (m/s)
Falling Head	7	1.0×10^{-10} to 3.1×10^{-8}	1.2×10^{-8}
Constant Head	3	1.0×10^{-8} to 2.5×10^{-8}	2.0×10^{-8}
Packer Test*	9	0 to 1.3×10^{-8}	2.5×10^{-9}
Combined Results	19	0 to 3.1×10^{-8}	9.6×10^{-9}

* Two Packer Test results of 9×10^{-7} m/s and 1.1×10^{-7} m/s were excluded due to suggestions by Gutteridge Haskins and Davey (1984) that these were not representative of the base geology permeability.

3.6 Kidston Mine Site Layout

Mining at Kidston is from two open pits, Wises Hill and Eldridge. Mining started in Wises Hill Pit and was completed in 1996, leaving a final void 200 m deep and with an exposed surface area of 55 ha. Eldridge Pit was opened in 1995 and will be approximately 300 m deep when mining ceases, with an exposed surface area of 52 ha. Various waste rock dumps (260 ha total surface area) surround the two pits, as can be seen on Figure 3.2, which is a schematic of the mine layout. The waste rock dump locations were selected for haul convenience alone, and no site preparation was carried out prior to the commencement of dumping. Construction of the waste rock dumps were by means of haul truck end tipping in layers, where each layer is flattened with a dozer to allow access by the haul trucks. Only surface compaction due to haul truck traffic (fleet of 7 to 13, 200 t, pneumatic tire haul trucks) occurred at the top of each bench. Side slope angle was determined by the natural angle of repose of the waste rock.

The tailings impoundment was built in the Butchers Creek valley, and details of the tailings impoundment construction is described in a subsequent section. Tailings deposition started in January 1985 and the impoundment was decommissioned in October 1997. The decommissioned impoundment holds 68 million tons of tailings.

Further surface features of the mine site are water dams, seepage collection drains, haul roads, access roads, scrap yards, stock yards, workshops, mill and offices. The total disturbed surface area of the mine is 835 ha (Placer Dome Asia Pacific, 2000).

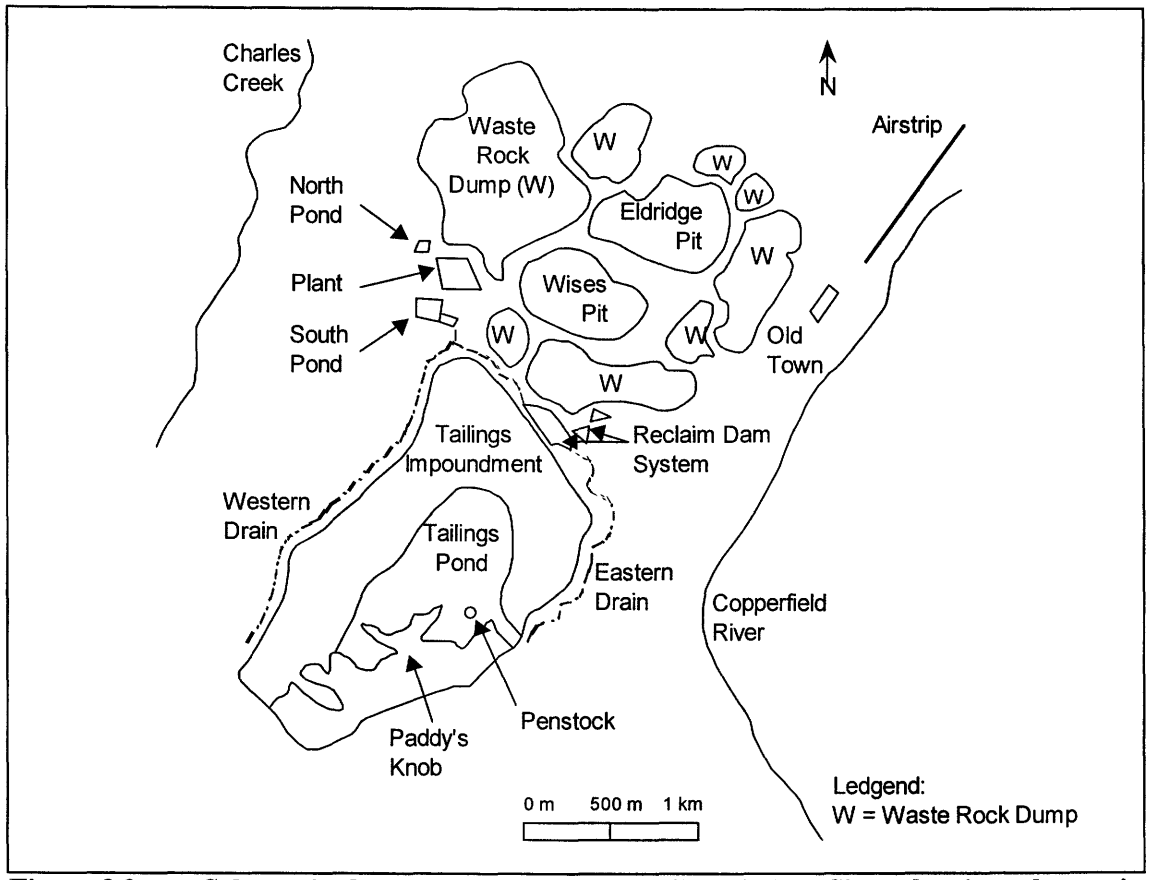

Figure 3.2: Schematic layout of the Kidston Gold Mine Site, showing the main components of the site (scale approximate).

3.7 Tailings Impoundment Design and Construction

The 5.8 km long tailings impoundment wall, which encircles about 70% of the perimeter of the tailings storage, was progressively raised with five lifts to the outer wall during operation. At the southern end of the dam, the dam wall was adjoined to the local hill, Paddy's Knob. The height of the wall varies between almost 32 m at its highest point at the northern end, to less than 1 m where it joins Paddy's Knob.

The first wall section (stage I) was constructed in 1984 to an initial crest level of 535.0 m. The bulk of the starter embankment was constructed from semi-pervious waste rock and river drainage material. The embankment was raised (stage II) to a level of 540.0 m in 1986 using the downstream raising technique, using compacted mine waste material with finger drains constructed beneath the downstream side of the embankment. In 1989 the crest level was raised (stage III) to 552.0 m at the northern end, whilst the extended western side of the embankment

was raised higher to accommodate for the increasing beach height resulting from the single point depositional method. The stage II lift was also constructed using the downstream raising technique, using run-of-mine waste material. As part of stage II and III construction, a filter chimney drain was constructed through the embankment to the compacted river gravel zone in the starter embankment (AGC Woodward-Clyde, 1994). These drains were constructed using river sand protected by a geotextile and a wrap of fresh barren waste rock (Williams, 1998b).

The stage IV embankment lift was completed early in 1993 to a level of 555.5 m and a final crest width of 19.5 m. This lift was constructed by a combination of downstream and centerline techniques, using a low permeability oxide waste upstream/downstream rockfill (barren waste) shoulder embankment section. The embankment chimney drain was terminated below the stage IV lift (AGC Woodward-Clyde, 1994). The embankment was finally raised (stage V) to a level of 557.6 m in 1996, again using the centerline technique, with a final crest width of 6 m. Fresh barren waste rock was used for this construction (AGC Woodward-Clyde, 1996).

Prior to construction of the stage I, embankment the topsoil was stripped and a full-width cut-off key was excavated to a depth of 1.0 m to ensure a stable foundation (Williams, 1998b). None of the subsequent embankments along the eastern or western boundaries were keyed into the ground surface, with the design only calling for clearing of vegetation and removal of the topsoil (Ritchie and Currey, 2000). The embankment walls were designed to leak and the seepage is collected in 2 to 3 m deep interception trenches cut down through the decomposed granitic layer.

Typical sections of the tailings impoundment embankment wall are the higher eastern section, and the lower western section. The eastern section is approximately 23.5 m high, with an upstream slope of 1.35H:1.00V (35.5°), a downstream slope of 1.40H:1.00V (36.5°), and a 6 m wide crest. The western section is about 12.6 m high, with upstream and downstream slopes of 1.35H:1.00V (35.5°), and a 7 m wide crest. The assumed (designed for but not consistent in practice) free-board from the crest to the tailings surface is 1 m. Both sections have internal drains comprising blanket base drains and vertical chimney drains (Williams, 1998b). Figure 3.3 is a schematic of the typical cross-section of the embankment wall at any location.

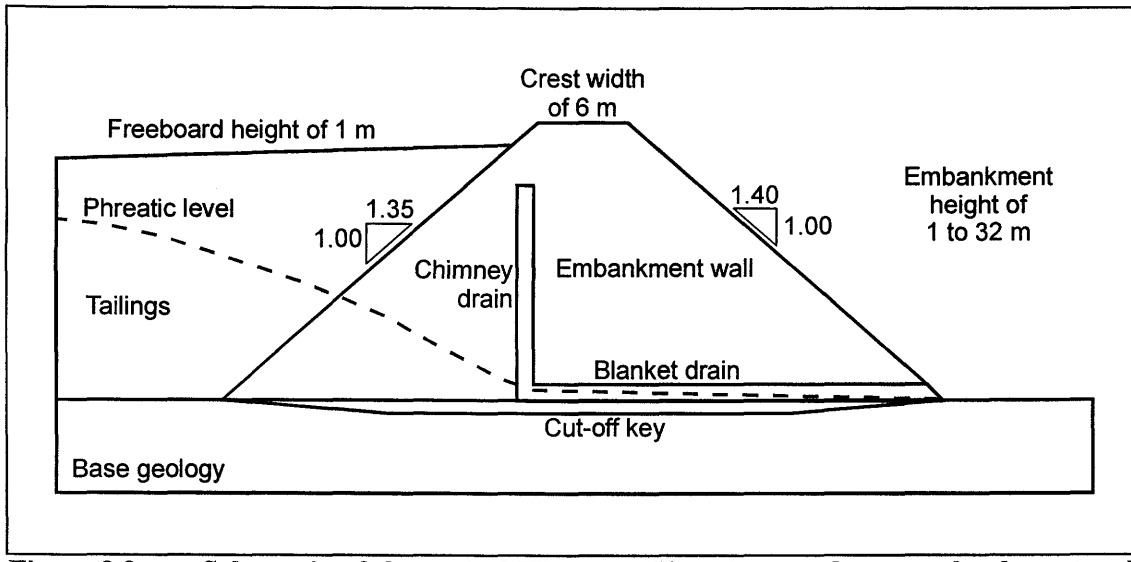

Figure 3.3: Schematic of the typical Kidston tailings impoundment embankment wall cross-section at any location along the impoundment perimeter.

3.8 Tailings Impoundment Operational History

Initially, the tailings impoundment design called for single point spigot discharge (so called long-beach deposition) at the southwestern and southeastern end of the impoundment, with the decant (4 towers) located along the main wall at the northern end of the impoundment. After 1990 the strategy was changed (and the 4 towers was sealed with concrete plugs) to one of sub-aerial deposition around the periphery of the impoundment (this was only implemented in 1991). Tailings were discharged from twin 300 mm pipes at flow rates up to 800 tph at 45% solids. The solids settled relatively quickly due to the coarse grain size (80% passing 200 μm) against the wall and the residual water was ponded against Paddy's Knob to the south. The single decant tower in the back south-east corner of the impoundment was used to recycle ponded water to the plant site for processing operations.

In October 1997, after the decommissioning of the tailings impoundment, a 36 m diameter High Compression Thickener was commissioned on the rim of Wises Pit and backfilling of the void (43.5 million m^3) commenced with thickened (70% solids) tailings and barren waste rock from the Eldridge Pit operations. Not only was the backfilling of Wises Pit an economic advantage, but allowed the early decommissioning of the tailing impoundment whilst the mine was still operating.

3.9 Tailings Characterization

An understanding of the physical, hydraulic, chemical and mineralogical characteristics of the tailings are of utmost importance in characterizing the behavior of the tailings impoundment in terms of stability, seepage rates and volumes, and the potential for poor quality leachate. The sections that follow provide sufficient information to understand the Kidston tailings.

3.9.1 Physical and Hydraulic Properties

Three different ores are processed at the mine, namely oxide ore, fresh ore and a transition between the two. Each ore type has different grinding characteristics and will produce tailings with slightly differing physical properties (Gutteridge Haskins and Davey, 1984). The specific gravity of the ore particles range from 2.63 for fresh ore to 2.38 for oxide with an overall weighted average of 2.60.

The particle size distribution of the tailings will impact on the water retention characteristics and the unsaturated and saturated shear strengths. Historical testing of the whole tailings indicates a median particle size (D_{50}) of 0.05 mm. They can be described as being 51% silt-sized, 47% sand-sized and 2% clay-sized (Rassam and Williams, 1997) which results in a relatively free draining mass. Soil moisture testing indicates that the tailings have a low air entry value, indicative of the large pores in their structure. Upon open pipe discharge, the particles undergo hydraulic sorting whereby the coarser particles are deposited near the discharge (against the impoundment wall) and the finer particles are carried out into the pond. The coarser particles include pyrite, which has a higher specific gravity, and settles close to the discharge outlet. Chapter 4 and Appendixes A, B, C, D and E contain detailed information on the tailings testing and the measured properties.

3.9.2 Chemical Properties

Tailings samples at Kidston to determine the potential for Acid Rock Drainage (ARD) and heavy metal concentrations were analyzed four times during the life of the mine. The first test involved collection of seventy-two cores (to a depth of 600 mm) in December 1994. These cores were split into 4 fractions (0 - 150 mm, 150 - 300 mm, 300 - 450 mm, and 450 - 600 mm). Thirty samples were collected for testing in May 1996. The completed tailings surface was

sampled in August 1998 along 5 transect lines and 5 composite samples were tested for ARD potential. The final test was in July 1999 when an additional 5 samples from the tailings impoundment surface were tested (Currey, 1999; Kidston Gold Mine, 1998). Table 3.2 presents a summary of the ARD potential results, while Table 3.3 lists the heavy metal concentrations, as tested in 1998, together with the relevant Queensland testing guideline.

Table 3.2: Geochemical testing of the Kidston tailings to determine ARD potential (Currey, 1999; Kidston Gold Mine, 1998).

Component	1994 (280 samples) Mean (range)	1996 (30 samples) Mean (range)	1998 (5 samples) Mean (range)	1999 (5 samples) Mean (range)
pH	8.1 (2.8-8.6)	8.4 (8.4-8.5)	7.9 (7.9-8.0)	No analysis
Electrical Conductivity (mS/cm)	1.0 (up to 8.5)	1.3 (0.7-1.8)	2.9 (1.9-3.7)	No analysis
Total Sulfur (%)	1.3 (1.1-1.6)	1.6	1.4 (1.3-1.7)	1.8 (0.8-3.1)
MPA (kg H_2SO_4/t)	No analysis	No analysis	42 (38-52)	55 (25-93)
ANC (kg H_2SO_4/t)	33 (31-37)	40	45 (37-54)	21 (14-32)
NAPP (kg H_2SO_4/t)	5	-5	-3 (-13-5)	-38 (-80-(-8))
NAG pH	8.4 (6.8-9.0)	NA	7.6 (7.1-7.9)	4.7 (0.1-51.6)
ANC:MPA	No analysis	No analysis	1.1 (0.9-1.3)	0.4 (0.2-0.7)

MPA = Maximum Potential Acidity; ANC = Acid Neutralizing Capacity; NAPP = Net Acid Producing Potential; NAG = Net Acid Generation.

Table 3.3: August 1998 composite tailings surface samples total metal analysis results (Currey, 1999; Kidston Gold Mines, 1998).

Parameter	Range	Average	Queensland CLA*
Arsenic [As] (mg/kg)	220 – 384	287	200
Cadmium [Cd] (mg/kg)	6 – 14	10	40
Copper [Cu] (mg/kg)	100 – 212	143	2000
Manganese [Mn] (mg/kg)	591 – 804	657	3000
Nickel [Ni] (mg/kg)	16 – 25	19	600
Lead [Pb] (mg/kg)	80 – 190	140	600
Zinc [Zn] (mg/kg)	800 – 1450	1036	14000
Beryllium [Be] (mg/kg)	0.2 – 0.3	0.3	40
Mercury [Hg] (mg/kg)	< 0.1 – 0.1	0.1	30
Chromium-IV [Cr](mg/kg)	< 1	< 1	No Criteria
Cyanide [Cn] (mg/kg)	15 – 46	28	1000

*Queensland Department of Environment Contaminated Lands Act Guidelines for health based investigation levels, suitable for parks, recreation areas and playing fields, including secondary schools.

3.9.3 Tailings Mineralogy

X-ray diffraction of three selected samples form the 11 ha trial site was performed prior to 1997 (Kidston Gold Mines, 1998). The samples were crushed to less than 100 micron size prior to analysis in the spectrometer. Table 3.4 lists the results of these tests.

Table 3.4: Mineralogy of the Kidston tailings (Kidston Gold Mine, 1998).

Sample number	Mineral identified in sample*
1	Quartz, Na-Plagioclase Feldspar, Muscovite, Chlorite, Chalcopyrite**
2	Quartz, Muscovite, Plagioclase Feldspar, Chlorite, Gypsum
3	Quartz, Muscovite, Na-Plagioclase Feldspar, Chlorite, Magnetite**

*Minerals are listed in decreasing order of abundance; **Minerals are possibly present, in amounts <5%.

3.10 Tailings Pond Water Quality

Ponded water and seepage water emanating from the tailings impoundment generally are of good quality with sulfate being the only determinant lying outside the Australian Water Quality Guidelines for Fresh and Marine Waters (ANZEEC) cattle watering guidelines as illustrated in Tables 3.5 and 3.6. All metal concentrations meet the ANZEEC guideline, including cyanide concentrations since 1998. Sulfate (SO_4) in the seepage water is similar in concentration to the ponded water, suggesting minimal enrichment due to oxidation processes (Currey, 1999; Ritchie and Currey, 2000).

Table 3.5: Tailings pond water quality data summary for the period ranging from 1985 to 2000.

Element	Range	Average	Comment
Dissolved SO_4 (mg/l)	170 – 4100	1486	Trend shows increasing concentrations
pH	6.1 – 11.5	8.3	Trend shows decreasing pH
Dissolved Cu (mg/l)	0.01 – 420	34.5	Concentration averages at 0.6 mg/l since 1998
Total Cyanide (mg/l)	< 0.05 – 800	84.2	Below detection limit since 1998

Table 3.6: Tailings impoundment western drain seepage pond water quality data summary for the period ranging from 1992 to 2000.

Element	Range	Average	Comment
Dissolved SO_4 (mg/l)	480 – 4000	2308	Trend indicates constant concentration
pH	5.5 – 8.3	7.5	Trend indicates constant pH
Dissolved Cu (mg/l)	< 0.05 – 3.35	0.07	Single peak, mostly below detection limit
Total Cyanide (mg/l)	< 0.01 – 38	1.1	Single peak, mostly below detection limit

Three deep monitoring boreholes, intersecting the regional groundwater table, downstream of the tailings impoundment show minimal impact of the deep groundwater, with the exception of slightly elevated sulfate concentrations in two boreholes as documented in Table 3.7.

Table 3.7: Deep groundwater quality from three boreholes located downstream of the tailings impoundment for the period 1990 to 2000.

Element	Bore #1	Bore #2	Bore #3	Comment
pH	7.5	6.8	7.3	The pH has remained fairly constant
SO_4 (mg/l)	838	133	1181	Bore #1,#2 concentrations increase from 1995
Cyanide (mg/l)	< 0.05	< 0.05	< 0.05	Concentrations always below detection limit

3.11 Tailings Impoundment Water Balance

Total water usage at the Kidston Gold Mine varied, but the 1999 total usage of 8,234 Ml/yr is a fair reflection of the average annual demand. The total water usage is made up of 4,320 Ml/yr of fresh water pumped in from the Copperfield Dam, and 3,914 Ml/yr of recycled water (Placer Dome Asia Pacific, 1999). The tailings impoundment was designed for zero discharge, with all decant water and rainfall within its catchment to be recycled to the plant. Whilst the tailings impoundment was in full operation this recycled water accounted for 40% of the mill process water.

The tailings impoundment has its own unique water balance, and is described in detail in Chapter 5, but the following paragraphs summarizes the system. Even though the tailings surface area is 310 ha, the active catchment of the impoundment is 414 ha, due to its proximity to Paddy's Knob. Whilst the impoundment was in operation, water was introduced to the impoundment surface via tailings deposition (at 45% solids) and rainfall. The water was ponded and recycled via a penstock arrangement. Since the impoundment has been decommissioned, the primary source of water to the pond is rainfall, with the exception of water pumped from the recycle dam, the western drain pond, and on occasion tailings slurry from the south pond (refer to Figure 3.2 and Chapter 5 for details regarding the location of these ponds).

During operation, and after decommissioning, the decant water, seepage through the northern and eastern portions of the embankment wall, and surface runoff between these wall sections and the interception drains were collected in the reclaim dam, from where it was either pumped to the mill, or back onto the tailings impoundment. Seepage from the western embankment is

collected in a pond adjacent to the embankment and pumped back to the impoundment manually. Seepage from the north western portions of the embankment wall is directed towards the south pond.

The south- and north ponds are the main active water supply for the plant and the levels in these ponds are kept within tight tolerances. Any excesses or shortfall are compensated for from water pumped to/from the reclaim dam, which in turn governs additional decants/tailings pump back. Further, water from the South Dump seepage pond is pumped to the reclaim dam seepage dam, which collects any seepage from the reclaim dam, and all that water is in turn returned to the reclaim dam (Gutteridge Haskins and Davey, 1987).

Of course the tailings pond, as well as the tailings surface, provides a pathway for water loss via evaporation and evapotranspiration. Getting an accurate estimate of this quantity has been difficult, and the primary objective of the research conducted is to develop a methodology to predict evaporation and evapotranspiration. Deep groundwater seepage is not considered to be a significant source of water loss from the system, and this statement is supported by the bedrock integrity and permeability as well as water quality monitoring of deep boreholes downstream of the tailings impoundment.

3.12 Tailings Impoundment Rehabilitation Strategy

The aim of the decommissioning for the tailings impoundment is to create a sustainable vegetation cover that meets the Australian Department of Mines and Energy (DME) key closure criteria (EPA, 1995). These include creating a stable landform, not only for the impoundment wall structure but also of low surface erodability. The final landuse for the area will be native bushland that will support low intensity cattle grazing, provided the contaminants meet Contaminated Lands Act Guidelines or are similar to natural mineralized zones. The strategy also aims to maintain downstream water quality by controlling poor quality seepage from the toe of the impoundment.

A 1994 study of the various rehabilitation strategies for the tailings impoundment indicated the "preferred" option of direct vegetation of native species on the tailings impoundment surface. The "fallback " option was a 0.5 m soil cover ("B" horizon, oxide waste rock) on top of the tailings in order to provide a suitable media for vegetation establishment. The soil cover design

was solely to establish vegetation and not to provide a physical barrier for water or oxygen infiltration (AGC Woodward-Clyde, 1994).

3.13 Tailings Impoundment Revegetation Program

Planning for rehabilitation of the impoundment commenced in the 1989/90 wet season when the earliest trials of in situ revegetation of the impoundment surface were initiated. The first large-scale trial (11 ha) located at the southern end of the tailing impoundment commenced in March 1994 when 1,778 native tree and shrub species were planted directly into tailings sediment. An additional 40 ha trial was established in 1998, which was expanded by another 50 ha in 1999. This combined 103 ha is covered with grass and trees. A further 100 ha were covered with grass only in 1999, to control dust erosion prior to establishing trees over the entire impoundment surface (Ritchie and Currey, 2000; Placer Dome Asia Pacific, 1999).

The research for the sustainability of the vegetative cover on the impoundment indicates that a stable mix of species can be applied. The implications of a successful vegetative cover are seen to be critical to the successful outcome of the surface stability and overall hydrology of the impoundment. The value of healthy grass and native tree and shrub cover are important to the interception of surface seepage into the impoundment from incident rainfall via the process of evapotranspiration. It is anticipated that if the vegetation can successfully intercept most of the incident rainfall in the future and release it back into the atmosphere via evapotranspiration then the long term seepage from the impoundment will eventually cease (Ritchie and Currey, 2000).

Water use rates from native tree species (Eucalyptus, Melaleuca, Casuarina, Acacia and Callistemon) on the tailings impoundment were directly measured using heat pulse techniques. On dry surface tailings (dry plot) the water use (assumed to be via transpiration) by five year old specimens were 0.64 mm/day and 0.96 mm/day during the dry season and wet season respectively. These rates declined on a site where the tailings were flooded, and the trees were thus waterlogged (wet plots). The rates of transpiration were then 0.38 mm/day and 0.55 mm/day for the dry- and wet seasons respectively. The estimated grass understorey (Sabi, Rhodes, Speedy Couch, Seca Stylo, Black Spear, Jap Millet, Red Natal, Indian Blue, Queensland Blue and Acacia holosericea) evapotranspiration rate, as measured by the neutron moisture meter was 0.200 and 0.014 mm/day during the wet season (for the dry and wet plots). The Biomass method (dry biomass/water use efficiency of Buffel grass) gave the water usage

from the grass community during the wet season as 0.67 mm/day for the dry plot and 0.26 mm/day for the wet plot. During the dry season, grasses are unable to continue using water at the same rate as in the wet season due to depletion of plant available water in the upper parts of the soil profile (Ritchie and Currey, 2000).

In order to evaluate the impact of metal toxicity's in grazing cattle on the rehabilitated tailings impoundment, a grazing trial was established in 2000 on the pasture covering the surface sediments of the tailings impoundment (Ritchie and Currey, 2000).

3.14 Conclusions

The Kidston Gold Mine is fairly typical of an open cast gold mine in this part of the world. The rehabilitation program suggested for the tailings impoundment is however not that common. Direct vegetation of tailings is often done in South Africa for the purposes of dust suppression or erosion protection (Blight, 1989), but the establishment of vegetation on the hostile tailings environment is not generally attempted as a final closure alternative. Mason *et al.* (1995) describes one such application in New Zealand, where the climate is of course more forgiving, and allows vegetation a better chance to establish.

It is clear that the Kidston tailings impoundment is impacting on the environment, and therefore rehabilitation is needed. The magnitude of the tailings impoundment impact on the receiving environment is however relatively small and therefore Kidston's goals of minimizing the impact by controlling seepage as opposed to preventing it altogether seems both viable and responsible.

3.15 References

AGE Consultants (2001). Kidston Tailings Dam Rehabilitation Numerical Model and Water Balance. Consultants report prepared for Kidston Gold Mines Limited, Project No. G1036/A. Edited by I.P. Callow & E.H. Briese, Brisbane, Queensland, Australia, January, 26 pp.

AGC Woodward-Clyde (1994). Kidston Gold Mine – Tailings Dam Evaluation. Consultants report prepared for Kidston Gold Mines Limited, Job Number 4508-2. Brisbane, Queensland, Australia, February, 11pp.

AGC Woodward-Clyde (1996). Kidston Gold Mine Tailings Storage – Stage V Raising, Construction Report. Consultants report prepared for Kidston Gold Mines Limited, Project Number 4184-12, Document Number R001-A. Brisbane, Queensland, Australia, December.

Blight, G.E. (1989). Erosion losses from the surfaces of gold-tailings dams. Journal of the South African Institute of Mining & Metallurgy, Vol. 89(1), January 1989, pp. 23-29.

Currey N.A. (1999). Tailings Revegetation at Kidston Gold Mine. Proceedings of the 2nd Annual Summit of Mine Tailings Disposal Systems. Brisbane, Queensland, Australia, November.

Environment Protection Agency (EPA) (1995). Rehabilitation and Revegetation. Module in series on: Best Practice Environmental Management in Mining. Australian Federal Environment Department, June 1995.

Gutteridge Haskins and Davey (1984). Kidston Project – Tailings Dam Study. Consultants report prepared for Kidston Gold Mines Limited. Brisbane, Queensland, Australia, November 1983, Amended July, 19 pp.

Gutteridge Haskins and Davey (1987). Review of Water Management System. Consultants report prepared for Kidston Gold Mines Limited. Brisbane, Queenlsand, Australia, September.

Kidston Gold Mine (1998). Summary of Soil Studies Undertaken on KGM Tailings. Internal report, August, 10 pp.

Mason, K.A, Gregg, P.E.H., Stewart, R.B. (1995). Land reclamation trials and practices at Martha Hill Gold Mine, Waihi, New Zealand. Proceedings of the 1995 PACRIM Congress: Exploring the Rim, Auckland, New Zealand.

Placer Dome Inc. (1999). Unlocking Value – Annual Report 99. Placer Dome Publication, 68 pp.

Placer Dome Asia Pacific (1999). Kidston mine – 1999 sustainability report. Placer Dome Asia Pacific Publication, 17 pp.

Placer Dome Asia Pacific (2000). Placer Dome Asia Pacific Limited – 2000 sustainability report update. Placer Dome Asia Pacific Publication, 13 pp.

Rassam, D.W., Williams, D.J. (1997). Geotechnical characterization of mine waste. Proceedings of the 1st Australia-New Zealand Conference on Environmental Geotechnics – GeoEnvironment 97. Melbourne, Victoria, Australia, 26-28 November, pp. 459-464.

Ritchie, P.J., Currey, N.A. (2000) Tailing Dam Rehabilitation at Kidston Gold Mines. Proceedings of ANCOLD 2000, Australian National Committee on Large Dams Conference. Cairns, Queensland, Australia. 21 –27 October.

Williams, D.J. (1998a). Tailings Dam Research Project Report. Consultants report to Kidston Gold Mines Limited. Department of Civil Engineering, The University of Queensland, Brisbane, Queensland, Australia. 30 April, 14 pp.

Williams, D.J. (1998b). Report on Tailings Dam Stability Audit. Consultants report to Kidston Gold Mines Limited. Department of Civil Engineering, The University of Queensland, Brisbane, Queensland, Australia. 10 December, 14 pp.

Wood Geotechnical Consultants (1981). Kidston Project: Tailings Dam Site Investigation – Results of Diamond Drilling Program. Consultants report to Gutteridge Haskins & Davey. Edited by C.C. Wood, Brisbane, Queensland, Australia, 7 April, 9 pp.

CHAPTER 4

Physical and Hydraulic Characterization of the Kidston Tailings

4.1 Introduction

A laboratory and field test program was carried out in order to characterize the physical and hydraulic properties for use in predictive numerical modeling. The laboratory test program consisted of the measurement of grain size distribution, specific gravity, Atterberg limits, consolidation (this data was not used, and is subsequently not reported), saturated and unsaturated vertical hydraulic conductivity, soil water characteristic curves (SWCC) and shrinkage tests. The field test program consisted of in-situ infiltration tests and in-situ horizontal saturated hydraulic conductivity tests. Methods and procedures used in the testing programs are briefly referenced in this chapter, and where they deviated from standard methods, detailed descriptions are provided in the relevant appendixes. The chapter also includes laboratory and field-testing performed on the Kidston tailings by other researchers, consultants and organizations throughout the history of the tailings operation. This is included in order to reduce the level of uncertainty when entering the numerical modeling phase.

4.2 Laboratory Tailings Testing Program

Characterization of the tailings material is one of the important aspects that should be clearly defined in a study such as this. Since there are so many unknown factors that affect the final outcome, it is imperative that all those parameters that can readily be identified be measured. One form of measurement is laboratory testing, and the following sections highlight laboratory testing by the author as well as testing by other institutions.

4.2.1 Tests Completed by the Author Specifically for this Study

The detailed laboratory program was conducted using tailings samples collected from Kidston in 1995, 1997 & 1999 as described in Appendix A. All tests were done using standard American

Society for Testing Materials (ATSM) test methods, and where these were not available, the appropriate test method is described briefly in this chapter (and in greater detail in appendixes). Table 4.1 below lists the details of laboratory tests completed specifically for this study by the author.

Table 4.1: Laboratory tests conducted on the Kidston tailings material by the author specifically for this study.

Test type	Test method	# Tests	# Samples
Sieve test	ASTM D 422-63 (ASTM, 1996a)	11	7
Hydrometer test	ASTM D 422-63 (ASTM, 1996a)	11	7
Specific gravity	ASTM D 854-92 (ASTM, 1996d)	6	2
Atterberg limits	ASTM D 4318-84 (ASTM, 1996b)	2	2
Consolidation test*	ASTM D 2435-90 (ASTM, 1996f)	8	2
Saturated hydraulic conductivity	Consolidation – Hydraulic Conductivity Test, Modified Odoemeter (O'Kane, 1995)	8	2
SWCC	Modified Pressure Plate Test (O'Kane, 1995)	9	2
Shrinkage	ASTM D4943-95(wax method) (ASTM, 1996c)	4	2

* The consolidation test data was not used for any analysis in this thesis and subsequently no data is reported.

4.2.2 Tests on Kidston Tailings by Other Institutions

The Kidston tailings material has been tested by various other researchers, organizations and consultants since 1987, and every effort was made to gather all the available laboratory data, such that a database of the tailings properties can be built up to allow for a clearer understanding of the physical properties. Table 4.2 below lists all laboratory tests undertaken by these other institutions. The testing done by Wog (2000) and Williams (2000a,b,c) was conducted on samples collected by the author, and were tested specifically for the purpose of this study (see Appendix A for details of the samples).

Table 4.2: Laboratory tests conducted on the Kidston tailings material by other institutions.

Test type	Test method	# Tests	# Samples	Source
SWCC	Modified Pressure Plate Test (O'Kane, 1995)	2	2	O'Kane (1997)
	Dynamic Method, Pressure Plate Method & Static Method	5	2	Rassam (1998)
	Modified Pressure Plate Test (O'Kane, 1995)	3	3	Wog (2000)
	Tempe Cells	6	6	Williams (2000a)
Sieve & Hydrometer	ASTM D 422-63	2	2	O'Kane (1997)
	AS1289.C6.1-1977 & AS1289.C6.3-1977	8	8	Rassam (1998)

Table 4.2: Laboratory tests conducted on the Kidston tailings material by other institutions.

Test type	Test method	# Tests	# Samples	Source
Sieve & Hydrometer	AS1289.C6.1 & AS1289.C6.3	17 sieve, 3 hydrometer	17	Gutteridge Haskins & Davey (1987)
	AS1289.C6.1-1977 & AS1289.C6.3-1977	6	6	Williams (2000c)
	ASTM D 422-63	5	5	Wog (2000)
Sieve, Hydrometer & Laser sizing	AS1289.1-1977 Method C6.1 & AS1289.1-1994 Method 3.6.3 & Malvern Mastersizer/E	6 sieve, 4 hydrometer, 6 laser	6	Williams (2000a)
Specific Gravity	Pycnometer (no standard mentioned)	2	2	Rassam (1998)
Consolidation*	ASTM D2435-1990	2	2	O'Kane (1997)
	Not mentioned	2	2	Gutteridge Haskins & Davey (1987)
Saturated Hydraulic Conductivity	Consolidation – Hydraulic Conductivity Test, Modified Odoemeter (O'Kane, 1995)	2	2	O'Kane (1997)
	Steady State Head Control Method – Saturated Hydraulic Conductivity	1	1	Rassam (1998)
	Steady State Head Control Method – Saturated Hydraulic Conductivity	6	6	Williams (2000b)
Unsaturated Hydraulic Conductivity	Steady State Flux Control Method – Unsaturated Hydraulic Conductivity	1	1	Rassam (1998)
	Steady State Flux Control Method – Unsaturated Hydraulic Conductivity	6	6	Williams (2000b)

* The consolidation test data was not used for any analysis in this thesis and subsequently no data will be reported.

4.3 Field (In-Situ) Testing Program

Laboratory testing alone is not sufficient to clearly classify the tailings, and therefore in-situ field-testing was done. The following sections describe the in-situ testing done on the Kidston tailings impoundment by the author as well as tests reported by other institutions.

4.3.1 Specific Tests Completed for this Study

A field program comprising of double-ring infiltrometer (DR) and Guelph permeameter (GP) tests were carried out in order to measure the in-situ saturated surface hydraulic conductivity of the tailings. The first set of tests were performed in September 1999 and concentrated on tailings close to the embankment wall and approximately midway between the embankment and

the pool. An additional set of Guelph permeameter tests was completed in December 2000, in the zone immediately adjacent to the pool. A summary of the tests completed is provided in Table 4.3.

Table 4.3: Field (In-situ) tests conducted on the Kidston tailings material specifically for this study by the author.

Test type	Test method	# Tests
Double-ring infiltrometer	ASTM D3385-94 (ASTM, 1996e)	12
Guelph permeameter	Standard Method (SoilMoisture, 1986)	62

4.3.2 Tests on Tailings by Other Institutions

A number of different institutions have completed in-situ testing on the tailings impoundment throughout the life of the mine, and where relevant, the data from these tests have been gathered to enhance the database of tailings properties. These tests are all summarized in Table 4.4.

Table 4.4: Field (in-situ) tests conducted on the Kidston tailings material by other institutions.

Test type	Test method	# Tests	Source
Rainfall simulator	CMLR specific procedure	4	Horn *et al.* (1998)
Rainfall simulator	CMLR specific procedure	13	Horn (1999)
Saturated hydraulic conductivity	Piezometer pumping test	9	Edraki (1999)
Saturated hydraulic conductivity	Piezometer constant head test	10	Edraki (1999)
Horizontal permeability	Piezocone penetration test	10	Douglas Partners (1997)
Horizontal permeability	Piezocone penetration test (AS1726-1993)	41	Earthtech Consultants (1999)

4.4 Tailings Physical Properties

A thorough understanding of the basic physical properties of the tailings material is required as a minimum, as these properties allows for judgements to be made as to the performance of the tailings under various conditions. The sections that follow summarize the findings of the physical laboratory tailings testing program undertaken for this study. The tailings were deposited hydraulically, and as a result the tailings properties is expected to change in coarseness with respect to the distance from the wall. The coarser fraction settles out first,

leaving the coarse tailings fraction close to the wall and the finest particles only settle out in the pool, or close to the edge of the pool. Throughout this chapter and the rest of the thesis this particle size variance comes into play, and three classes of tailings have been selected to group the tailings into certain zones. The first class of tailings is the coarse fraction, which is tailings located close to the wall. The second class is intermediate tailings, which constitutes tailings located midway between the wall and the pool. The final class of tailings is the fine tailings that generally consist of the finest tailings that are located close to the edge of the tailings impoundment pool. When mention is made of the tailings type in this chapter it often refers to a visual observation of the tailings size fraction, combined with an indication of where along the tailings dam beach the sample has been collected. All tested samples are surface samples, unless specified otherwise.

4.4.1 Specific Gravity

The specific gravity tests were done in accordance with the standard test method ASTM Designation: D 854 – 92 (ASTM, 1996d). The measured specific gravity is for the whole sample fraction, i.e. no separation of the minus 75 micron (#200 sieve) fraction. The results of 6 tests conducted by the author, including 3 tests by Rassam (1998), are summarized in Tables 4.5 and 4.6. Appendix A provides for details regarding the samples used, and the approximate sample locations are indicated in Figure 4.1. The location of the samples tested by Rassam (1998) is not reported, and therefore the location of these samples on Figure 4.1 is only indicative.

Table 4.5: Results of all the individual specific gravity tests performed on the Kidston tailings.

Sample detail	Sample distance from wall (m)	Tailings type*	Specific gravity, G_s
Kidston #1/7A**	500	Fine	2.72
Kidston #1/7B**	500	Fine	2.73
Kidston #1/7C**	500	Fine	2.71
-0.075 mm (Rassam, 1998)	not specified	Fine	2.89
Kidston #2/7A**	20	Coarse	2.71
Kidston #2/7B**	20	Coarse	2.73
Kidston #2/7C**	20	Coarse	2.71
+0.075 mm (Rassam, 1998)	not specified	Coarse	2.75
Fresh waste rock (Rassam, 1998)	-	Fresh waste rock	2.70

* The tailings type is a relative judgement based on a visual observation when the sample was collected (see Appendix A for sample descriptions). ** Samples tested by the author.

Table 4.6: Statistical summary of all the specific gravity tests performed on the Kidston tailings.

Tailings type*	Average, G_s	Maximum, G_s	Minimum, G_s	Standard deviation, G_s
Fine	2.76	2.89	2.71	0.09
Coarse	2.73	2.75	2.71	0.02
Overall	2.74	2.89	2.71	0.06

* The tailings type is a relative judgement based on a visual observation when the sample was collected (see Appendix A for sample descriptions).

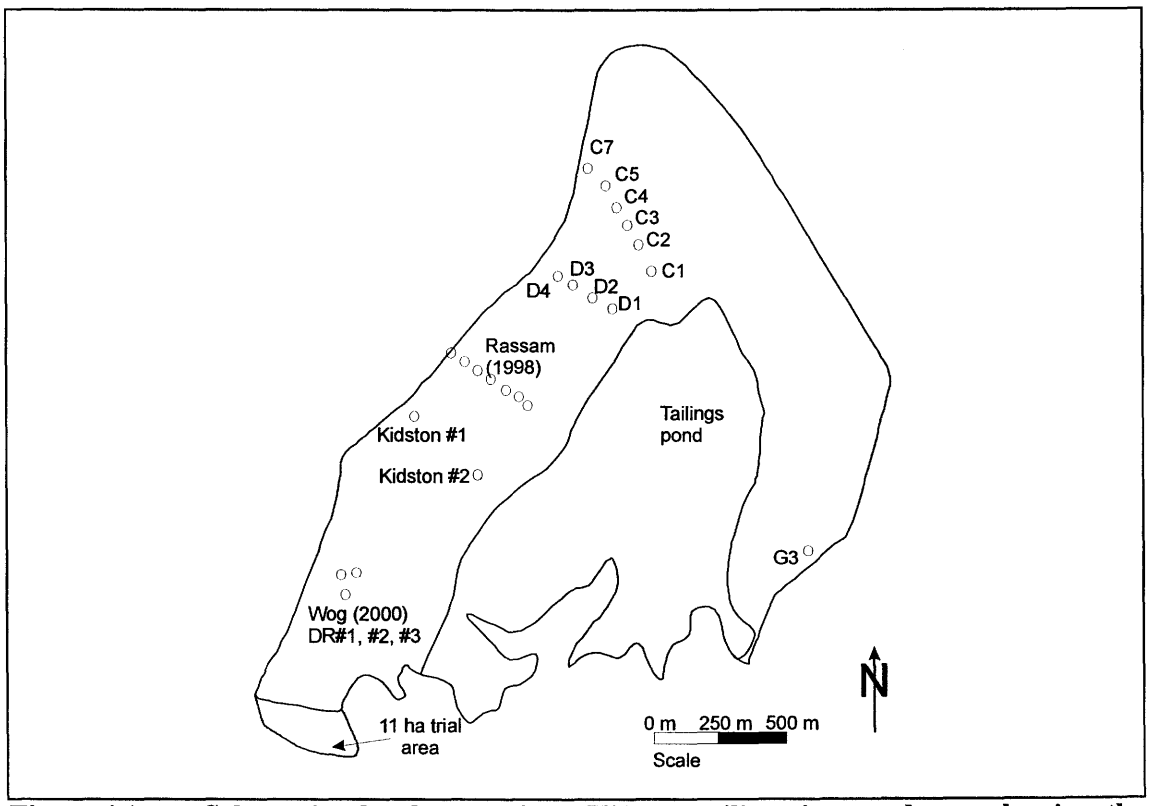

Figure 4.1: Schematic plan layout of the Kidston tailings impoundment showing the sample locations for all the physical and hydraulic tailings property laboratory testing conducted.

4.4.2 Grain Size Distribution

The 11 grain size distribution tests performed by the author were determined by sieve analysis and hydrometer tests according to the standard testing method ASTM Designation: D 422 – 63 (ASTM, 1996a). Complete samples were split and mixed prior testing to ensure that a representative fraction was taken for testing. The details of the samples used for these tests are documented in Appendix A. The complete grain size distribution test envelope for all 11 tests

by the author plus 55 tests conducted by others for a total number of 66 tests are listed in Tables 4.1 and 4.2 are presented in Figure 4.2.

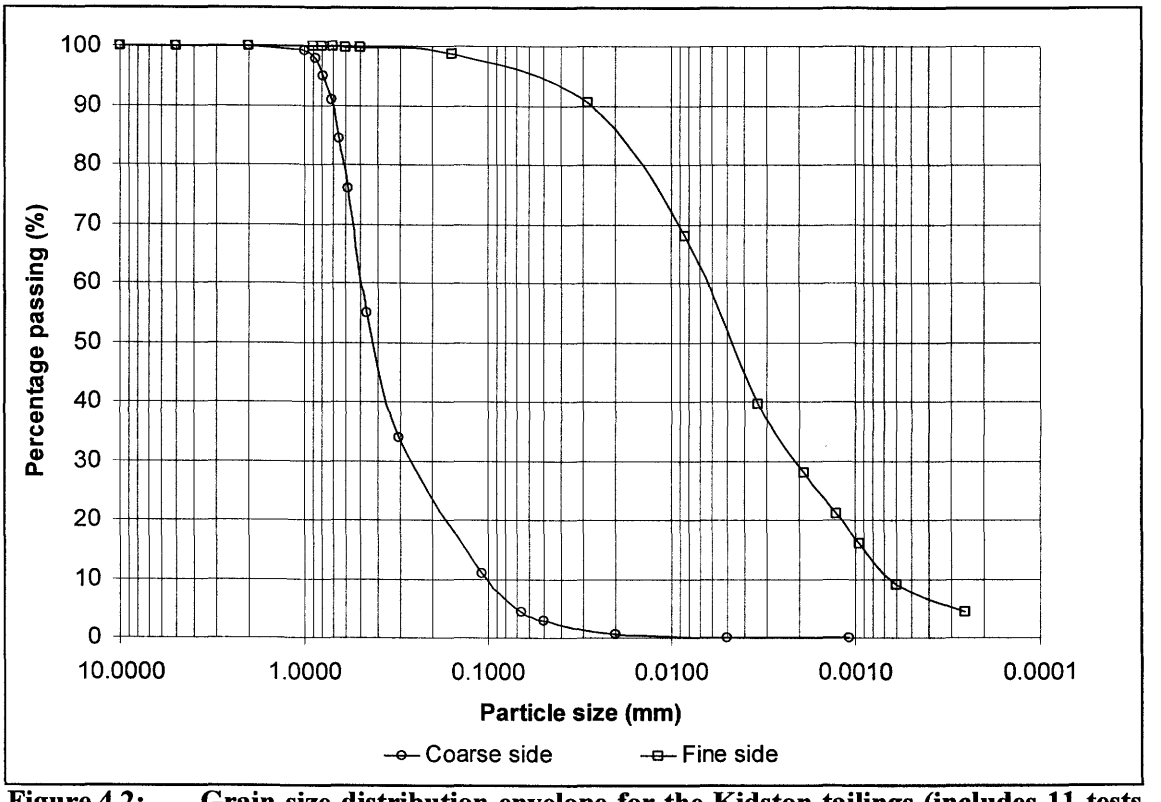

Figure 4.2: Grain size distribution envelope for the Kidston tailings (includes 11 tests by the author and 55 tests by others).

The individual data sets and grain size distribution curves are presented in Appendix B. The classification method used for identifying the tailings is the Unified Soil Classification System (USCS) (Holtz and Kovacs, 1981). There are no tailings retained on the U.S. standard sieve no. 4 (4.75 mm), which means no gravel material is present. The percentage sand (% sand) is the percentage of material not passing the U.S. standard sieve no. 200 (0.075 mm) sieve. The percentage silt (% silt) is the percentage of material passing the no. 200 sieve but larger than 0.002 mm, and the percentage clay (% clay) is that percentage of material smaller than 0.002 mm.

Two shape factors, the coefficient of uniformity, C_u, and the coefficient of curvature, C_c are used to further classify the tailings, and are defined by the following expressions (Holtz and Kovacs, 1981):

$$C_u = \frac{D_{60}}{D_{10}} \quad [4.1]$$

$$C_c = \frac{(D_{30})^2}{(D_{10})(D_{60})} \quad [4.2]$$

Where D_{10}, D_{30}, and D_{60} are the grain diameters (mm) corresponding to 10%, 30% and 60% passing by weight. Similarly D_{15}, D_{50}, D_{85}, D_{90} and D_{95} are the grain diameters corresponding to 15%, 50%, 85%, 90% and 95% passing by weight.

Any tailings sample with a percentage sand greater than 50% was classified as sand, while all other tailings was classified as silt (ML). Any tailings classified as sand, were considered well-graded sand (SW) if the C_c was between 1 and 3 and the C_u was also greater than 6. If the C_c was between 1 and 3, but the C_u was less than 6, and the amount of fines (% silt + % clay) was less than 10%, the tailings is considered to be a poorly graded sand (SP). Tailings with a C_c between 1 and 3, and a C_u between 4 and 6, with a fines total greater than 10% is considered to be silty sand (SM). Since the tailings samples have no plasticity, there are no samples classified as clays, even though they might be clay sized. Tables 4.7 and 4.8 summarizes the results of all the grain size distribution tests completed for the Kidston tailings, which includes 11 tests by the author and 55 by other institutions.

The Kidston tailings varies from well graded sand (SW) with an average D_{50} of 0.16 mm through to fine sand (ML) with an average D_{50} of 0.03 mm. Overall the tailings can be classified as a silty sand (SM) with an average D_{50} of 0.15 mm. A detailed statistical breakdown of the grain size distribution data can be found in Appendix B.

Table 4.7: Summary table of the average sand, silt and clay content of the Kidston tailings, the coefficients of uniformity and curvature of all the identified tailings classes tested.

Tailings type	# Tests	% Sand	% Silt	% Clay	C_u	C_c
Well graded sand (SW)	21	71.0	27.5	1.6	12.90	1.90
Poorly graded sand (SP)	7	91.3	6.7	1.9	3.45	1.18
Silty sand (SM)	26	73.4	23.3	3.4	14.30	2.44
Fine sand (ML)	12	19.4	69.4	11.3	12.47	0.99
All tailings (SM)	66	64.7	31.2	4.1	12.37	1.87

Table 4.8: Summary of the average tailings size fractions for all the identified Kidston tailings classes tested.

Tailings type	D_{10} (mm)	D_{15} (mm)	D_{30} (mm)	D_{50} (mm)	D_{60} (mm)	D_{85} (mm)	D_{90} (mm)	D_{95} (mm)
Well graded sand (SW)	0.019	0.032	0.082	0.156	0.198	0.349	0.408	0.465
Poorly graded sand (SP)	0.081	0.099	0.162	0.238	0.276	0.443	0.524	0.615
Silty sand (SM)	0.025	0.044	0.097	0.173	0.212	0.355	0.403	0.497
Fine sand (ML)	0.013	0.014	0.018	0.030	0.041	0.089	0.117	0.160
All tailings (SM)	0.027	0.041	0.085	0.149	0.183	0.314	0.366	0.438

The hydraulic deposition of the tailings results in particle segregation as the coarser particles settle out first close to the embankment wall, while the finest tailings settle out closer to the tailings pond (Kealy and Busch, 1971; Vick, 1983; Fourie, 1988). Table 4.9 and Figure 4.3 presents data by Rassam (1998) and Williams (2000c) (see also Appendix B) indicating how the grain size distribution varies down the beach profile of the tailings impoundment. Figure 4.3 also contains data from Blight and Steffen (1979) for the grain size distribution variation along a gold tailings beach profile in South Africa. The sample locations for the tests by Rassam (1998) and Williams (2000c) are indicated on Figure 4.1.

Grain size distribution is a good indication for saturated hydraulic conductivity, and calculations of the saturated hydraulic conductivity (k_s) can be made using the D_{10} and D_{15} values and an applying the empirical Hazen (Hazen, 1911) and Sherard (Sherard *et al.*, 1984) equations. Results of the application of these equations to the data of Rassam (1998) and Williams (2000c) are listed in Table 4.9. The Hazen equation is expressed as follows:

$$k_s = \frac{CD_{10}^2}{100} \qquad [4.3]$$

The Sherard equation is expressed as:

$$k_s = \frac{0.35D_{15}^2}{100} \qquad [4.4]$$

Where k_s = saturated hydraulic conductivity (m/s),
C = constant, assumed to be 1 for silty sands (Holtz and Kovacs, 1981),
D_{10} = grain size diameter passing 10% by weight (mm), and
D_{15} = grain size diameter passing 15% by weight (mm).

Table 4.9: **Grain size distribution data and calculated saturated hydraulic conductivity indicating how the grain size distribution varies from the embankment wall towards the tailings pond.**

Sample no.	Distance from wall (m)	% retained on #200 sieve	D_{10} (mm)	D_{15} (mm)	D_{50} (mm)	Saturated hydraulic conductivity (m/s)	
						Hazen	Sherard
Data for 0 m*	0	76.1	0.018	0.031	0.164	3.24E-06	3.36E-06
Data for 50 m*	50	89.1	0.056	0.086	0.255	3.14E-05	2.59E-05
Data for 75 m*	75	83.3	0.035	0.060	0.199	1.23E-05	1.26E-05
Data for 100 m*	100	88.4	0.053	0.092	0.249	2.81E-05	2.96E-05
Data for 125 m*	125	86.6	0.038	0.079	0.247	1.44E-05	2.18E-05
Data for 150 m*	150	71.8	0.019	0.029	0.137	3.61E-06	2.94E-06
Data for 200 m*	200	70.1	0.015	0.020	0.121	2.25E-06	1.40E-06
Sieve C1**	500	28.2	0.001	0.001	0.010	1.00E-08	3.50E-09
Sieve C2**	400	63.0	0.006	0.018	0.108	3.60E-07	1.13E-06
Sieve C3**	300	68.9	0.011	0.025	0.139	1.21E-06	2.19E-06
Sieve C4**	200	60.1	0.005	0.011	0.112	2.50E-07	4.24E-07
Sieve C5**	150	54.8	0.003	0.008	0.092	9.00E-08	2.24E-07
Sieve D1**	300	3.0	0.001	0.001	0.005	1.00E-08	3.50E-09
Sieve D2**	200	11.5	0.001	0.001	0.011	1.00E-08	3.50E-09
Sieve D3**	150	69.2	0.006	0.014	0.165	3.60E-07	6.86E-07
Sieve D4**	100	58.3	0.007	0.014	0.100	4.90E-07	6.86E-07

* Testing by Rassam (1998); ** Testing by Williams (2000c).

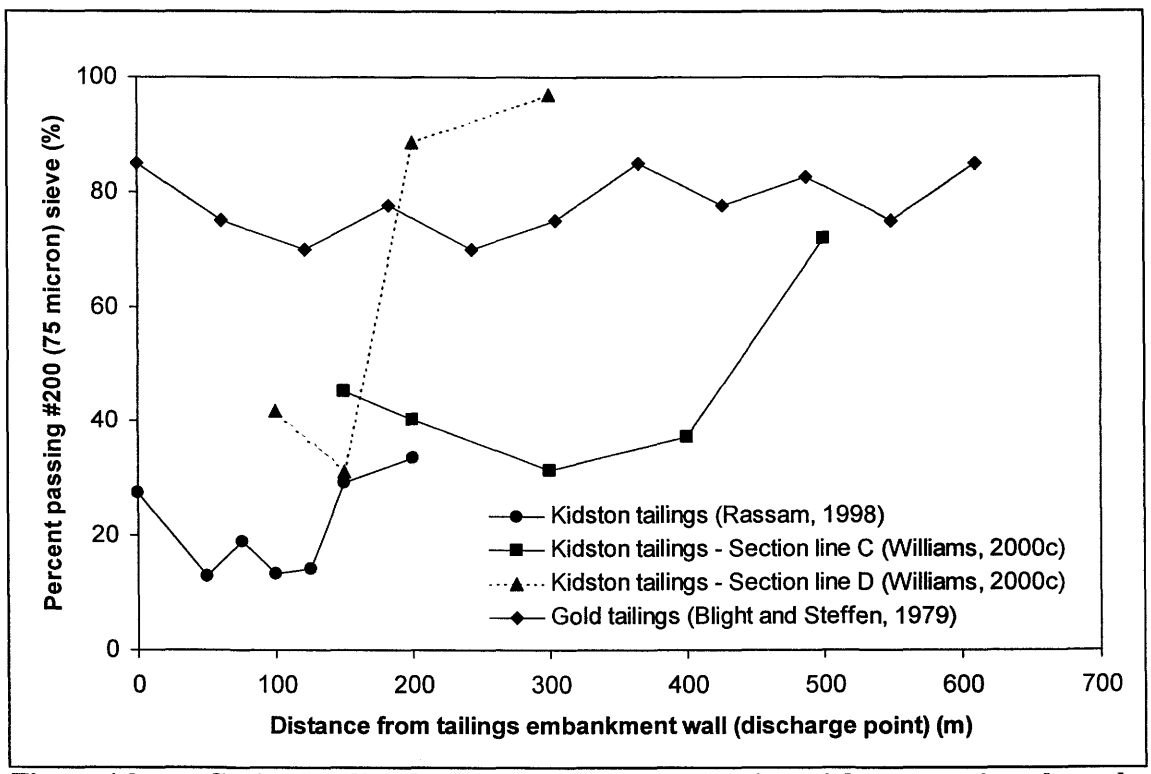

Figure 4.3: **Grain size distribution spread as a result of particle segregation along the Kidston beach profile.**

4.4.3 Atterberg Limits and Shrinkage Tests

Atterberg limits testing using standard test method ASTM Designation: D 4318 – 84 (ASTM, 1996b) was completed and the tailings were found to be non-plastic. Shrinkage testing using standard test method ASTM Designation: D 4843 – 95 (Wax Method) (ASTM, 1995) was attempted, but the tailings were found to be non-shrinking.

4.5 Tailings Hydraulic Properties

Understanding the tailings hydraulic properties is essential in describing the unsaturated flow through the tailings profile in the vadose zone. The sections that follow describe these properties from both laboratory and in-situ testing programs. The results are summaries of tests performed by the author as well as data from other institutions. The reader is reminded that all data are expressed in terms of a tailings type that varies between coarse, intermediate and fine. The distinction between these material types are based on a visual observation of the tested sample as well as a statement as to how far away from the wall the sample has been collected.

4.5.1 Laboratory Testing of Tailings Hydraulic Properties

Three basic tailings hydraulic properties were tested in laboratory testing. Saturated hydraulic conductivity was determined using a falling head hydraulic conductivity test. The next level of testing was unsaturated hydraulic conductivity testing to determine the relationship between matric suction and the degree of hydraulic conductivity of the tailings. The final hydraulic tailings testing consisted of conducting soil water characteristic curves. The summarized results of all these tests are documented in the sections that follow.

4.5.1.1 Falling Head Saturated Hydraulic Conductivity Tests

The Modified Odoemeter apparatus was used in combination with a falling head hydraulic conductivity test (O'Kane, 1995). The samples used in the falling head saturated hydraulic conductivity testing were prepared by slurrying the samples using distilled water. Porous brass stones were placed above and below the slurried sample separated by a #200 filter paper cut to size within a stainless steel ring. Details of the falling head permeability's measured in 8 tests by the author as well as one by O'Kane (1997) are listed in Appendix C. The samples used for

the testing were identical to those for the consolidation testing (data not reported in this thesis). The sample locations are illustrated on Figure 4.1. Table 4.10 summarize the resultant saturated hydraulic conductivity's from these tests performed on the Kidston tailings.

Table 4.10: Average saturated hydraulic conductivity's as measured using the falling head saturated hydraulic conductivity test portion of the Modified Odoemeter apparatus (O'Kane, 1995) (see Appendix C for details).

Sample detail	Tailings type*	Saturated hydraulic conductivity (m/s)	
		Individual**	Average
Kidston #1A	Fine	5.39E-06	4.98E-06
Kidston #1B	Fine	5.24E-06	
Kidston #1C	Fine	3.57E-06	
Kidston #1D	Fine	5.46E-06	
Kidston #1 (O'Kane, 1997)	Fine	5.23E-06	
Kidston #2A	Coarse	4.03E-06	5.92E-06
Kidston #2B	Coarse	2.88E-06	
Kidston #2C	Coarse	5.16E-06	
Kidston #2D	Coarse	5.80E-06	
Kidston #2 (O'Kane, 1997)	Coarse	1.17E-05	

* The tailings type is a relative judgement based on a visual observation when the sample was collected (see Appendix A for sample descriptions); ** These are the average saturated hydraulic conductivity for all the loading stresses of each consolidation test. The maximum stress in each case was approximately 1250 kPa

4.5.1.2 Soil Water Characteristic Tests

The 9 soil water characteristic curves (SWCC) determined by the author were determined using the axis translation technique, using the modified pressure plate apparatus (O'Kane, 1995). The two samples tested were similar to the samples tested in the consolidation tests, i.e. Kidston #1 and Kidston #2 (see Figure 4.1 for the sample locations). Since the residual suction of the tailings material is in the region of 100 kPa, there was no need to conduct vapour equilibrium testing on the samples to obtain the higher end matric suction versus moisture content range (greater than 500 kPa). This is further supported by results of vapour equilibrium testing on the Kidston tailings by Rassam (1998). The individual results for all 25 of the SWCC tests are reported in Appendix D. The 2 tests conducted by O'Kane (1997) were also on the Kidston #1 and Kidston #2 samples. The 5 tests by Rassam (1998) were done on samples 50 m and 150 m from the embankment. Williams (2000a) conducted his 6 tests on samples collected from piezometer boreholes C7 and G3. These samples are thus not surface samples but are from specific depths as indicated in Table 4.11. The 3 tests by Wog (2000) were from samples taken during the double-ring infiltrometer testing. The locations of all these samples are indicated on

Figure 4.1. Samples for testing by Wog (2000) and Williams (2000a) were taken by the author, specifically for the purpose of this study (further details on these samples are documented in Appendix A). Rassam (1998) also completed hysteresis testing on two samples of the Kidston tailings. Due to the fact that the numerical modeling used in the later phase of this research does not use any data other than the drying curve, no further hysteresis testing as part of this study was not done.

Table 4.11 Soil water characteristic curve properties for all the tests performed on the Kidston tailings (both by the author and other researchers).

Test no (reference)	Saturated volumetric water content, θ_s (%)	Air entry value, AEV, (kPa)	Residual suction, ψ_r, (kPa)	Residual volumetric water content, θ_r, (%)
Kidston #1A*	42.6%	7.0	11.0	4.0%
Kidston #1B*	44.6%	3.2	7.2	4.0%
Kidston #1C*	44.4%	3.2	9.0	7.5%
New #1A*	43.9%	4.0	8.0	5.0%
New #1B*	43.6%	3.2	10.0	3.0%
Kidston #2A*	43.1%	1.5	8.0	3.0%
Kidston #2B*	43.8%	2.0	6.2	3.0%
New #2A*	38.4%	3.0	8.0	5.0%
New #2B*	38.2%	3.2	8.5	2.5%
Kidston #1 (O'Kane, 1997)	56.4%	3.2	8.5	3.0%
Kidston #2 (O'Kane, 1997)	49.1%	2.5	10.0	3.0%
50 m 1st drying (Rassam, 1998)	39.0%	2.5	11.0	7.0%
50 m wetting (Rassam, 1998)	37.0%	1.5	7.5	8.0%
150 m 1st drying (Rassam, 1998)	39.1%	7.0	70.0	7.0%
150 m wetting (Rassam, 1998)	34.0%	3.5	23.0	12.5%
150 m redrying (Rassam, 1998)	34.0%	6.5	30.0	12.5%
C7: (2-4 m) (Williams, 2000a)	39.1%	9.0	500.0	5.0%
C7: (4-7 m) (Williams, 2000a)	42.2%	12.0	700.0	3.0%
C7: (13-15 m) (Williams, 2000a)	38.5%	1.8	70.0	2.5%
G3: (4-6 m) (Williams, 2000a)	37.3%	6.0	300.0	6.0%
G3: (12-13.5 m) (Williams, 2000a)	43.5%	8.0	100.0	3.0%
G3: (0-1.5 m) (Williams, 2000a)	37.3%	2.1	150.0	2.5%
DR#1 (Wog, 2000)	42.5%	2.0	3.5	7.5%
DR#2 (Wog, 2000)	51.5%	3.0	20.0	15.0%
DR#3 (Wog, 2000)	41.5%	6.0	8.5	6.0%

* Samples tested by the author for the current study.

The determination of the saturated volumetric water content, θ_s, for each test was a direct outcome of the test. The determination of the air entry value, AEV, the residual matric suction, ψ_r, and the residual moisture content, θ_r, for each test was carried out using the construction technique proposed by Fredlund and Xing (1994). Table 4.11 lists the properties of each test,

and Table 4.12 presents a statistical summary of all the Kidston tailings SWCC data. The overall SWCC envelope containing all the data are presented in Figure 4.4.

Table 4.12 **Statistical summary of soil water characteristic curve properties for all the tests performed on the Kidston tailings, both by the author and other researchers.**

Parameter	Saturated volumetric water content, θ_s (%)	Air entry value, AEV, (kPa)	Residual suction, ψ_r, (kPa)	Residual volumetric water content, θ_r, (%)
Number of samples	25	25	25	25
Mean value	42.2	3.2	10.0	5.0
Average value	41.8	4.3	83.5	5.6
Minimum value	34.0	1.5	3.5	2.5
Maximum value	56.4	12.0	700.0	15.0
Standard deviation	0.05	2.7	170.9	0.03
25-percentile value	38.4	2.5	8.0	3.0
50-percentile value	42.2	3.2	10.0	5.0
75-percentile value	43.8	6.0	70.0	7.0

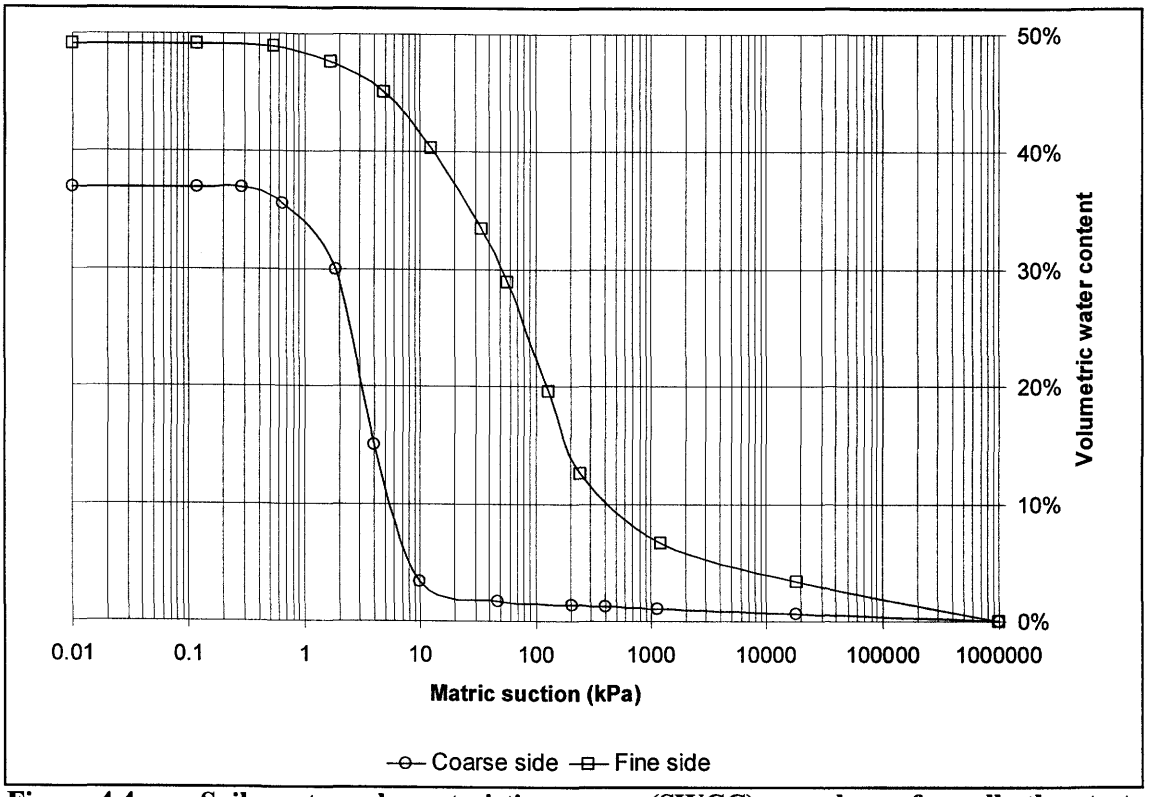

Figure 4.4: **Soil water characteristic curve (SWCC) envelope for all the tests performed on the Kidston tailings.**

4.5.1.3 Unsaturated Hydraulic Conductivity Testing

Williams (2000b) performed saturated and unsaturated hydraulic conductivity tests on six tailings samples collected by the author during the installation of the piezometers on the tailings impoundment as described in Appendix A. These tests were specifically completed for the purpose of this study under instruction from the author. The test procedure was the steady state head control method, as described by Rassam (1998). Table 4.13 list the results of the saturated permeability tests on each sample and Figures 4.5 and 4.6 present the saturated and unsaturated hydraulic conductivity as a function of the tailings matric suction respectively.

Each sample was made up as a slurry and tested in an oedometer at applied stresses of 2 kPa, 20 kPa, 50 kPa and 150 kPa. These applied stress increments correspond to a tailings depth of up to about 10 m, typical of the depth of tailings in the Kidston tailings dam. Each applied stress increment was maintained for 24 hours to ensure full consolidation of the sample. From the oedometer results, the coefficients of consolidation and volume decrease were calculated, from which the saturated hydraulic conductivity was determined as a function of applied stress. The average saturated hydraulic conductivity over the applied stress range was used as the basis for calculating the unsaturated hydraulic conductivity.

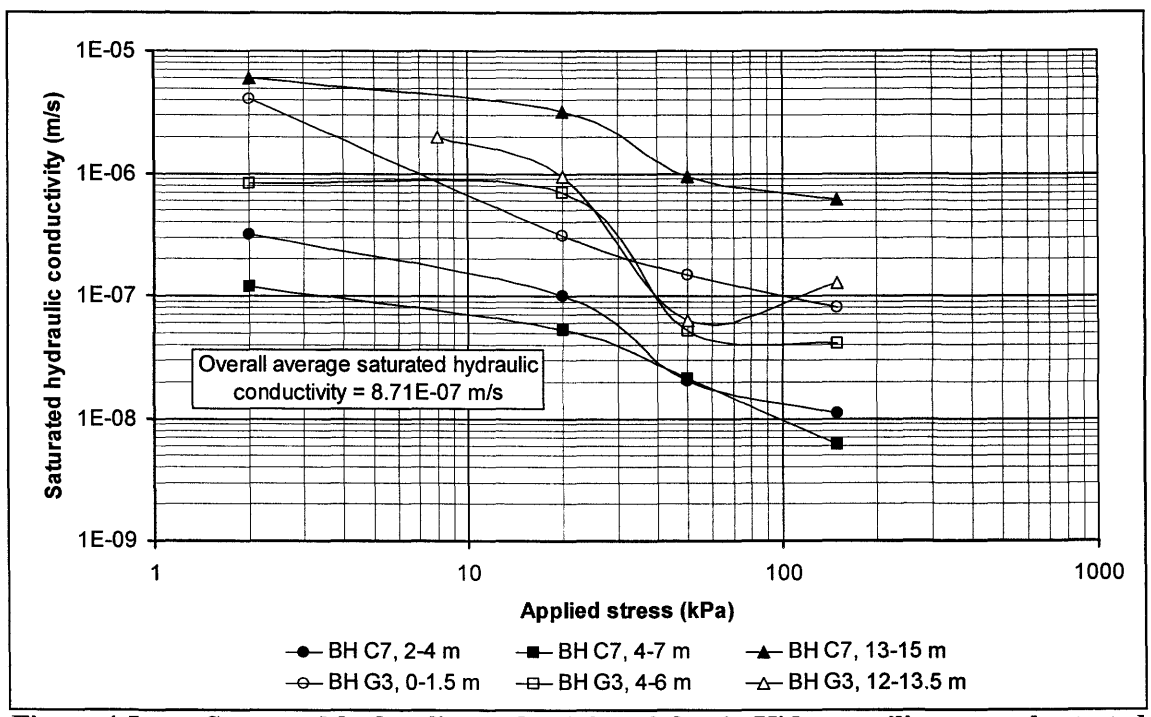

Figure 4.5: Saturated hydraulic conductivity of the six Kidston tailings samples tested by Williams (2000b).

Fredlund *et al.* (1994) combined the equation representing the SWCC after Fredlund and Xing (1994) with the hydraulic conductivity model of Childs and Collis-George (1950) to estimate the relative hydraulic conductivity function of soils. This function was calibrated against the average saturated hydraulic conductivity over the range of applied stresses to yield the unsaturated hydraulic conductivity as a function of matrix suction for each of the combined tailings samples tested as shown on Figure 4.6.

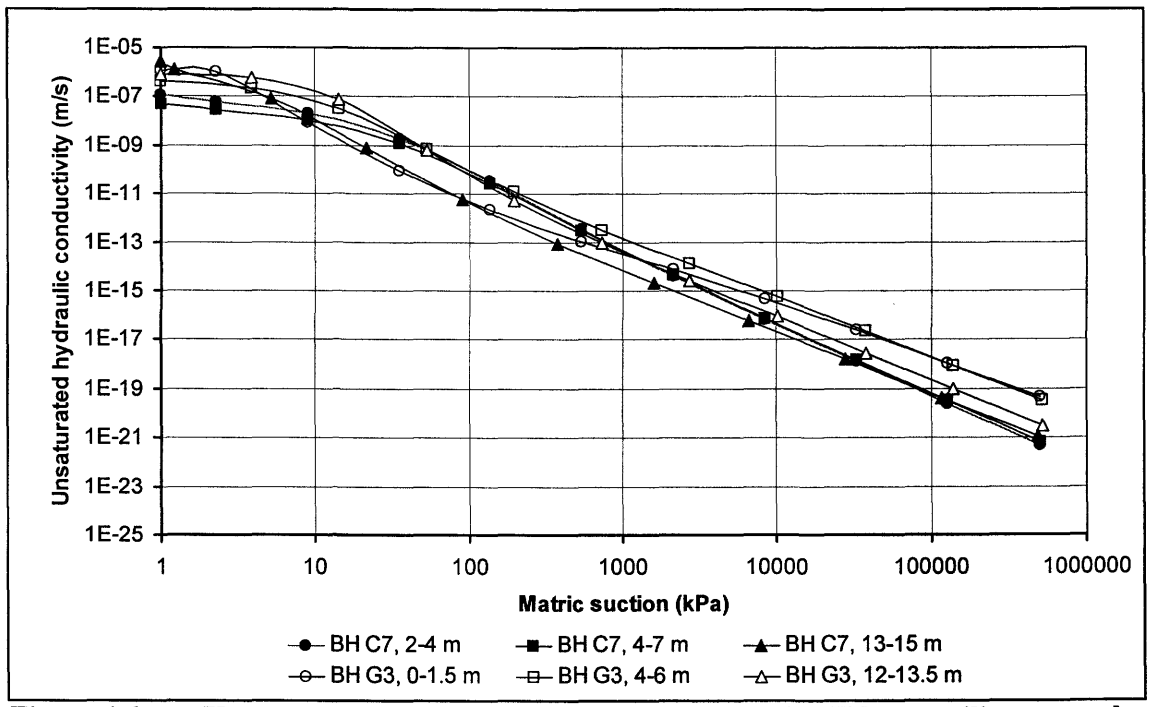

Figure 4.6: Unsaturated hydraulic conductivity of the six Kidston tailings samples tested by Williams (2000b).

Table 4.13 Saturated hydraulic conductivity of six Kidston tailings samples as measured by Williams (2000b) using the steady state head control method (Rassam, 1998).

Test number (see Appendix A)	Saturated hydraulic conductivity (m/s)
C7: 2-4 m	1.13E-07
C7: 4-7 m	5.02E-08
C7: 13-15 m	2.72E-06
G7: 0-1.5 m	1.16E-06
G3: 4-6 m	4.07E-07
G3: 12-13.5 m	7.82E-07

4.5.2 In-Situ Testing of Tailings Hydraulic Properties

Laboratory testing of the tailings hydraulic properties is important, however the best indicator of actual behavior is in-situ testing. 12 Double-ring infiltrometer and 62 Guelph permeameter tests were conducted by the author to test the saturated hydraulic conductivity of the tailings surface. This data was further enhanced by recalculating data from 17 rainfall simulator tests performed by the Center for Mined Land Reclamation (CMLR) (Horn *et al*, 1998; Horn, 1999). The sections that follows also contains data from 19 down-hole piezometer saturated hydraulic conductivity tests (Edraki, 1999) as well as 51 horizontal permeability tests by means of piezocone testing in piezometer holes (Douglas Partners, 1997; Earthtech Consultants, 1999).

Just as with the laboratory testing phase the tailings have been characterized into 3 types based on the distance from the wall and visual observation. These three types are coarse (closest to wall), intermediate (midway between wall and pool), and fine (closest to pool) tailings.

4.5.2.1 Double-Ring Infiltrometer Tests

These 12 tests were conducted according to the ASTM D3385-94 Standard (ASTM, 1996e), and the relevant data analysis procedure and detailed test methodology is presented in Appendix E. The sites selected for infiltration testing was chosen to correspond to the sites where the Center for Mined Land Reclamation (CMLR), conducted their rainfall simulator tests (Horn, 1999). Where soil conditions allowed, the double-ring infiltrometer was in fact installed on the actual test plot where the rainfall simulator test was conducted. In some cases however there was evidence of piping or erosion from the rainfall simulator test sites, and subsequently a close, but representative site was chosen.

Figure 4.7 is an overall plan layout of the tailings impoundment indicating the approximate position of the 12 double-ring infiltration tests, while Figure 4.8 is a more detailed sketch of the double ring infiltrometer locations, together with the CMLR rainfall simulator test sites on the beach tailings (beach tailings constitutes the coarsest tailings material type). The CMLR selected to test three separate conditions at this site, depicting the presence and abundance of vegetation. The sites were classified as; bare, poorly vegetated, or well vegetated. Poorly vegetated corresponds to a visual observation that vegetation was present, but the majority of the area was exposed bare tailings (10% vegetation cover). Well vegetated on the other hand

was evaluated by visual observation that the majority of the tailings was in fact covered by vegetation (80% - 90% vegetation cover).

A second set of double-ring infiltrometer tests was conducted on finer tailings located midway between the tailings impoundment outer wall and the pool (Figures 4.7 and 4.9). The tailings in this region of the impoundment were classed as intermediate tailings. This site had only bare tailings (i.e. non-vegetated tailings) and well vegetated tailings. Two double-ring infiltrometer tests were conducted in the vicinity of the weather-, and Bowen ratio station (as illustrated on Figures 4.7 and 4.10). This was specifically done for calibration of the flux data collected by the data logger to be described in Chapter 6. Table 4.14 list details of all the double ring infiltrometer test locations.

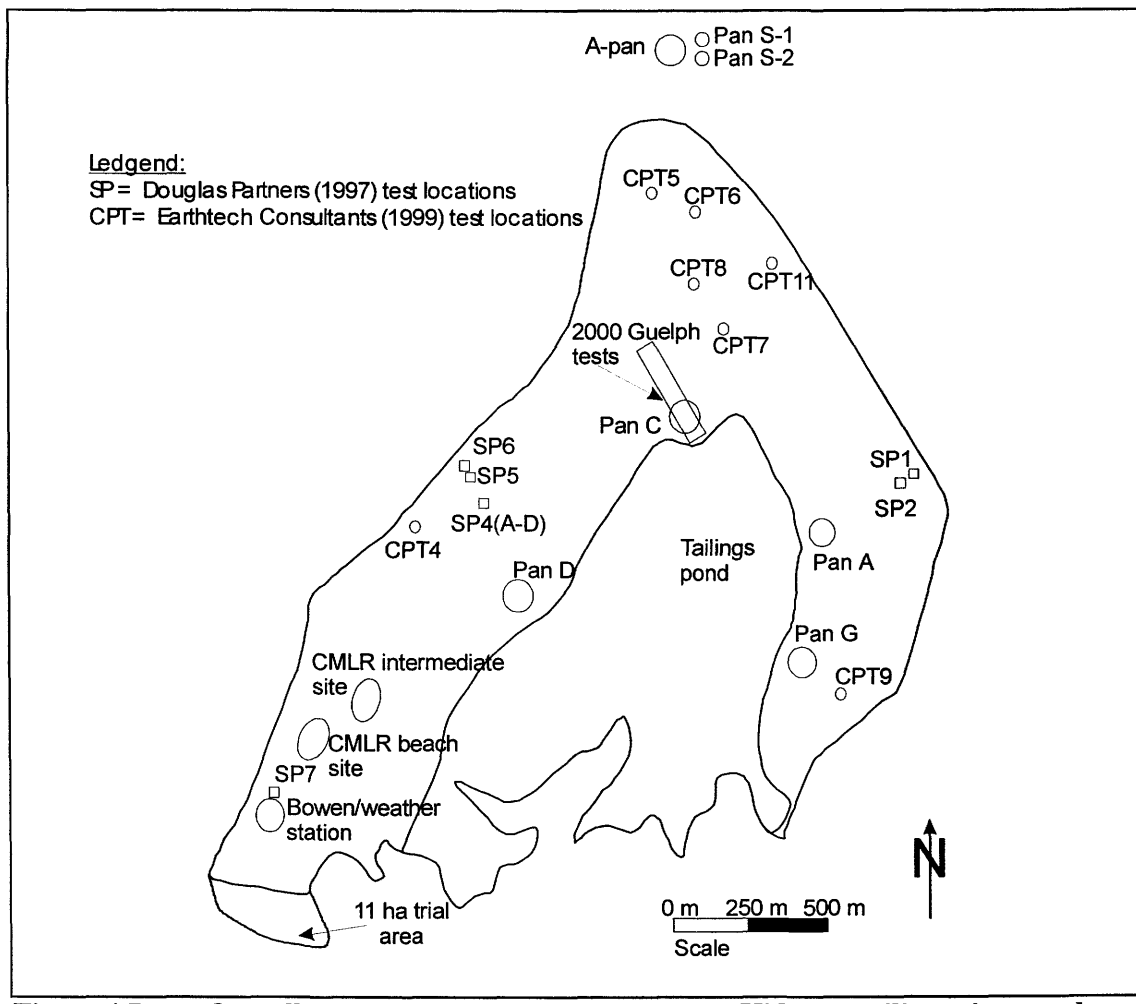

Figure 4.7: Overall schematic plan layout of the Kidston tailings impoundment showing the field infiltration testing locations, the piezometer locations and the evaporation pan locations.

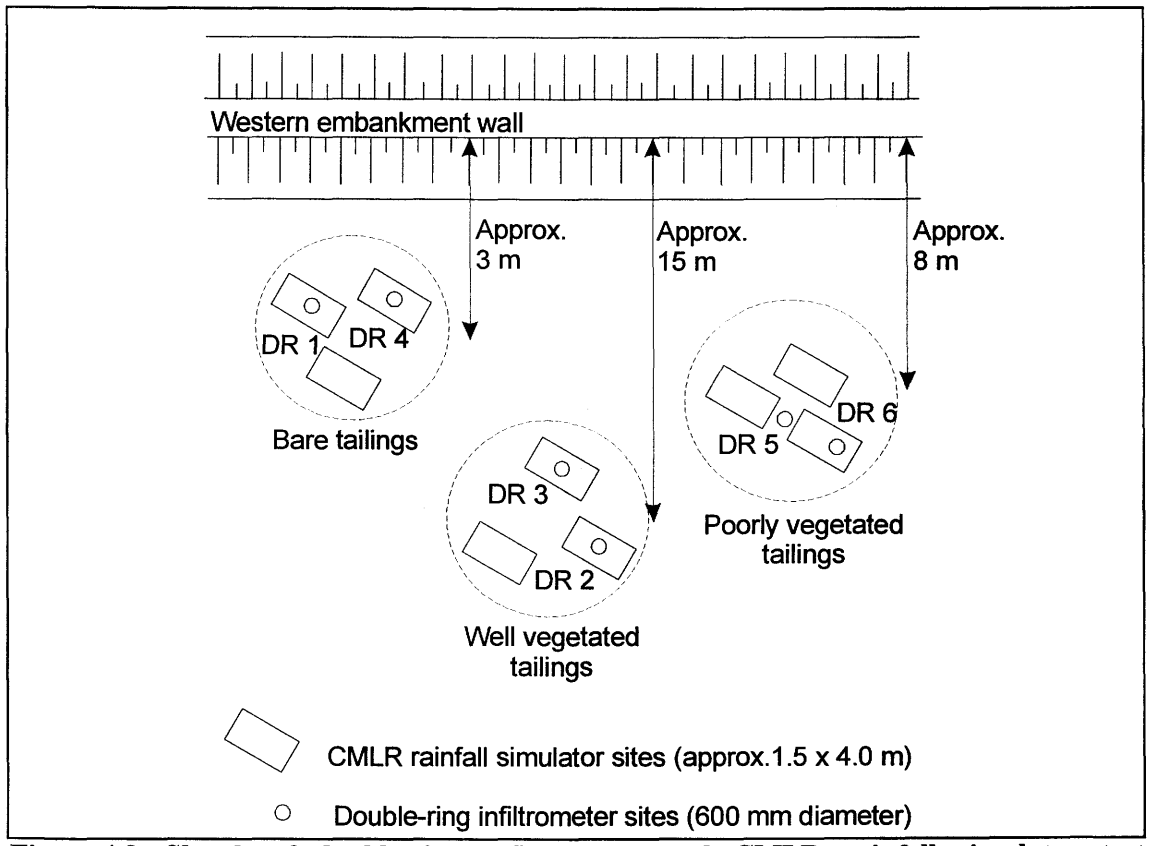

Figure 4.8: Sketch of double-ring infiltrometer and CMLR rainfall simulator test locations on the beach (coarsest) tailings.

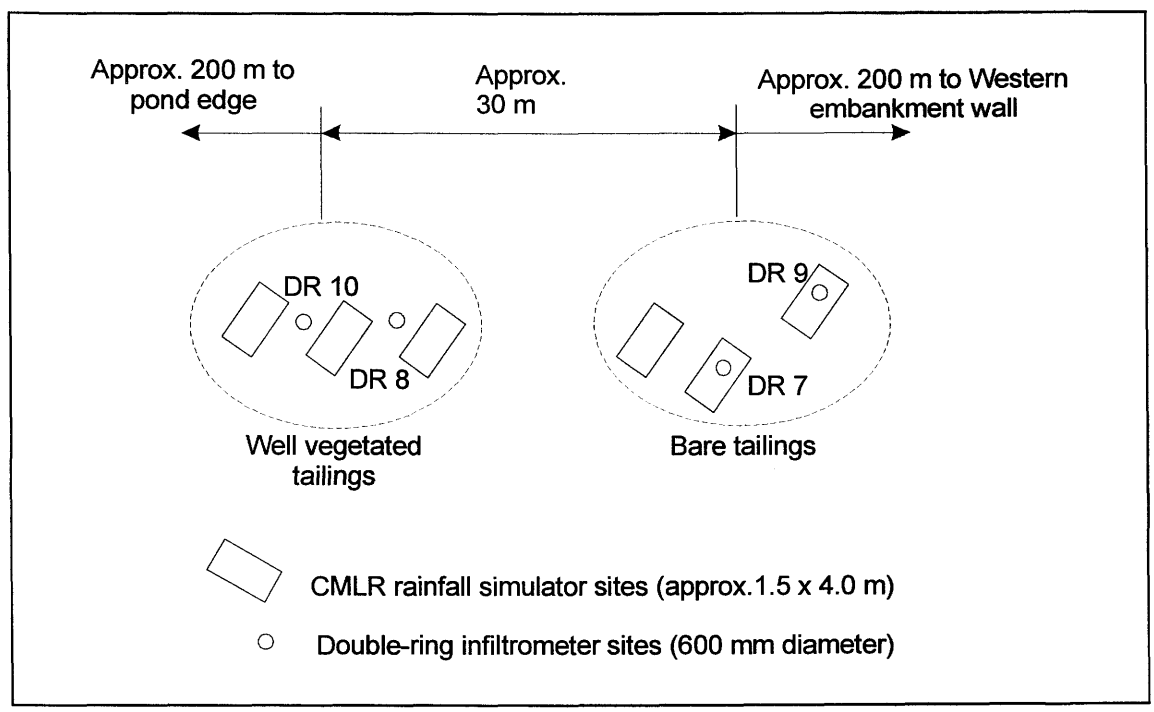

Figure 4.9: Sketch of double-ring infiltrometer and CMLR rainfall simulator test locations on the intermediate tailings.

Table 4.14 Details of the double-ring infiltrometer test locations.

Test no.*	Location (distance from wall)	Tailings type	Corresponding CMLR rainfall simulator site+
DR1	Non-vegetated tailings adjacent wall (3 m)	Coarse	Kidtailings, 0% veg.
DR2	Poorly vegetated tailings adjacent wall (15 m)	Coarse	Kidtailings, 20% veg.
DR3	Well vegetated tailings adjacent wall (15 m)	Coarse	Kidtailings, 80-90% veg.
DR4	Non-vegetated tailings adjacent wall (3 m)	Coarse	None
DR5	Poorly vegetated tailings adjacent wall (8 m)	Coarse	None
DR6	Poorly vegetated tailings adjacent wall (8 m)	Coarse	None
DR7	Well vegetated tailings midway through dam 200 m)	Intermediate	None
DR8	Non-vegetated tailings midway through dam (230 m)	Intermediate	Kidtailings, 0% veg.
DR9	Well vegetated tailings midway through dam (200 m)	Intermediate	Kidtailings, 90% veg.
DR10	Non-vegetated tailings midway through dam (230 m)	Intermediate	Kidtailings, 10% veg.
DR11	Poorly vegetated tailings at Bowen station (90 m)	Coarse	None
DR12	Poorly vegetated tailings at Bowen station (90 m)	Coarse	None

*These test no's correspond to the Guelph permeameter test no's, and are based on the same locations, i.e. Guelph tests DR1A, DR1B & DR1C are at double-ring infiltrometer location DR1; +The infiltration tests were done on the rainfall simulator sites except where undue erosion prevented it, in which case the closest available adjacent location was used.

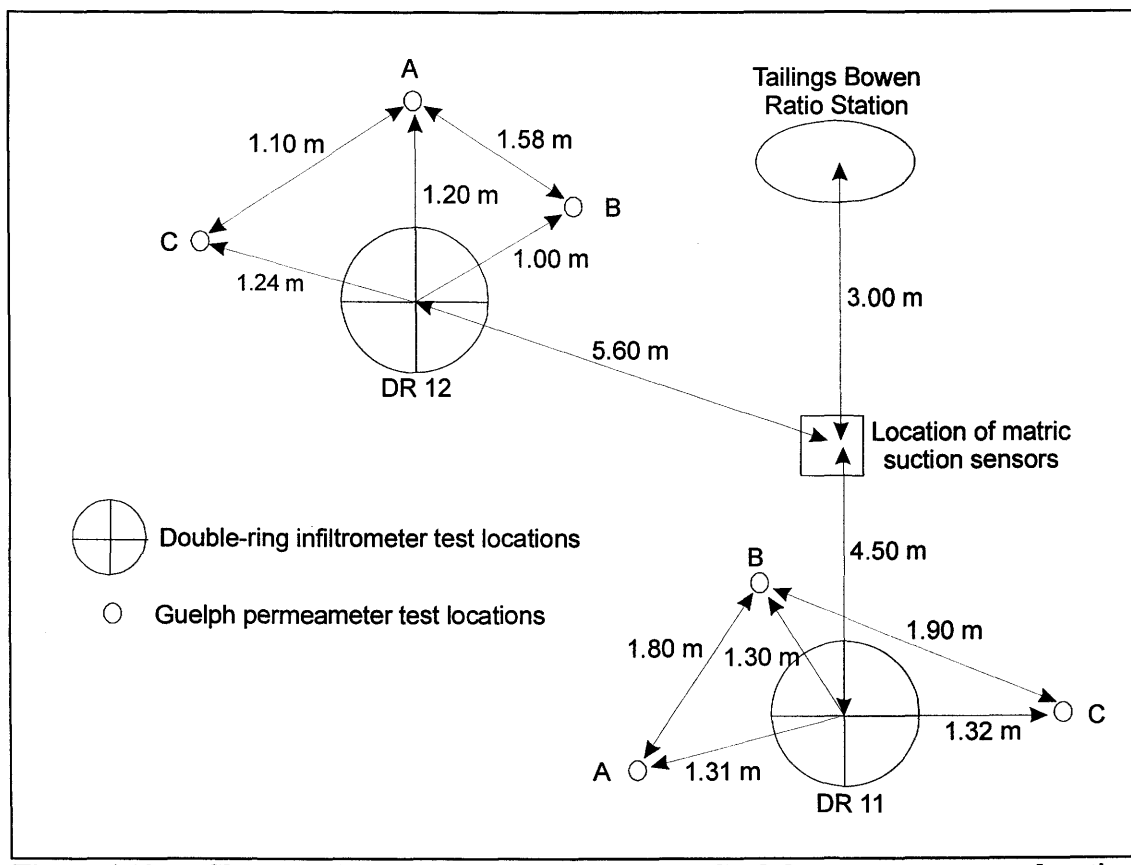

Figure 4.10: Sketch of double-ring infiltrometer and Guelph permeameter test locations in the proximity of the Bowen ratio station.

The resultant saturated hydraulic conductivity's associated with each of the double-ring infiltrometer tests are listed Table 4.15.

Table 4.15: Results of the double-ring infiltrometer tests performed on the Kidston tailings impoundment.

Test no.	Distance from wall (m)	Tailings type	Saturated hydraulic conductivity (m/s)	
			Individual	Average
DR1	3	Non-vegetated coarse	1.72E-05	2.18E-05
DR4	3	Non-vegetated coarse	2.63E-05	
DR8	230	Non-vegetated intermediate	1.63E-06	1.49E-06
DR10	230	Non-vegetated intermediate	1.34E-06	
DR5	8	Poorly vegetated coarse	9.25E-06	1.41E-05
DR6	8	Poorly vegetated coarse	1.17E-05	
DR11	90	Poorly vegetated coarse	1.98E-05	
DR12	90	Poorly vegetated coarse	1.56E-05	
DR2	15	Well vegetated coarse	1.96E-06	3.61E-06
DR3	15	Well vegetated coarse	5.25E-06	
DR7	200	Well vegetated intermediate	1.56E-06	6.28E-06
DR9	200	Well vegetated intermediate	1.10E-05	

4.5.2.2 Guelph Permeameter Tests

The Guelph permeameter is a well known apparatus to measure in-situ permeability, and the 66 tests conducted as part of this research was done as per the standard method described in the apparatus manual (SoilMoisture, 1986). A description of the apparatus and an overview of the measurement protocol is presented in Appendix E. Deviations from the standard method as well as details of the tests specific to this research are presented in Appendix E. Two separate sets of tests were conducted. The first coincided with the double-ring infiltrometer tests (27 September to 5 October 1999), and the second set was completed between 27 November, and 7 December 2000.

The first series of Guelph permeameter tests were carried out in conjunction with the double-ring infiltrometer tests. As a measure of quality control it was decided to do three Guelph permeameter tests in close proximity to each of the double-ring infiltrometer tests. The positions for these tests were chosen arbitrarily, although where possible they were also on the CMLR rainfall simulator plots (Horn, 1999), but always at least 1.2 m away from the double-ring infiltrometer to avoid test interference. Appendix E provides sketches of all individual test sites indicating the placement of the Guelph tests in relation to the double-ring tests. Table 4.16 list the details of the locations where Guelph permeameter tests were conducted during the 1999 test period, and Table 4.17 list details of the second series testing in 2000. The 2000 testing was

conducted on the piezometer section line C, illustrated on Figure 4.7, from the edge of the pool outwards. At each of the locations listed in Table 4.17, three Guelph tests were performed, no more than 1.0 m apart. This was done for quality control purposes. The tailings tested as part of these tests were classed as fine tailings.

Table 4.16: Details of the first series Guelph permeameter test locations (27 September to 5 October 1999).

Test no.	Location (distance to wall)	Tailings type	Corresponding double ring test
DR1A	Non-vegetated tailings adjacent wall (3 m)	Coarse	DR1
DR1B	Non-vegetated tailings adjacent wall (3 m)	Coarse	DR1
DR1C	Non-vegetated tailings adjacent wall (3 m)	Coarse	DR1
DR2A	Poorly vegetated tailings adjacent wall (15 m)	Coarse	DR2
DR2B	Poorly vegetated tailings adjacent wall (15 m)	Coarse	DR2
DR2C	Poorly vegetated tailings adjacent wall (15 m)	Coarse	DR2
DR3A	Well vegetated tailings adjacent wall (15 m)	Coarse	DR3
DR3B	Well vegetated tailings adjacent wall (15 m)	Coarse	DR3
DR3C	Well vegetated tailings adjacent wall (15 m)	Coarse	DR3
DR4A	Non-vegetated tailings adjacent wall (3 m)	Coarse	DR4
DR4B	Non-vegetated tailings adjacent wall (3 m)	Coarse	DR4
DR4C	Non-vegetated tailings adjacent wall (3 m)	Coarse	DR4
DR5A	Poorly vegetated tailings adjacent wall (8 m)	Coarse	DR5
DR5B	Poorly vegetated tailings adjacent wall (8 m)	Coarse	DR5
DR5C	Poorly vegetated tailings adjacent wall (8 m)	Coarse	DR5
DR6A	Poorly vegetated tailings adjacent wall (8 m)	Coarse	DR6
DR6B	Poorly vegetated tailings adjacent wall (8 m)	Coarse	DR6
DR6C	Poorly vegetated tailings adjacent wall (8 m)	Coarse	DR6
DR7A	Well vegetated tailings midway through dam (200 m)	Intermediate	DR7
DR7B	Well vegetated tailings midway through dam (200 m)	Intermediate	DR7
DR7C	Well vegetated tailings midway through dam (200 m)	Intermediate	DR7
DR8A	Non-vegetated tailings midway through dam (230 m)	Intermediate	DR8
DR8B	Non-vegetated tailings midway through dam (230 m)	Intermediate	DR8
DR8C	Non-vegetated tailings midway through dam (230 m)	Intermediate	DR8
DR9A	Well vegetated tailings midway through dam (200 m)	Intermediate	DR9
DR9B	Well vegetated tailings midway through dam (200 m)	Intermediate	DR9
DR9C	Well vegetated tailings midway through dam (200 m)	Intermediate	DR9
DR10A	Non-vegetated tailings midway through dam (230 m)	Intermediate	DR10
DR10B	Non-vegetated tailings midway through dam (230 m)	Intermediate	DR10
DR10C	Non-vegetated tailings midway through dam (230 m)	Intermediate	DR10
DR11A	Poorly vegetated tailings at Bowen ratio station (90 m)	Coarse	DR11
DR11B	Poorly vegetated tailings at Bowen ratio station (90 m)	Coarse	DR11
DR11C	Poorly vegetated tailings at Bowen ratio station (90 m)	Coarse	DR11
DR12A	Poorly vegetated tailings at Bowen ratio station (90 m)	Coarse	DR12
DR12B	Poorly vegetated tailings at Bowen ratio station (90 m)	Coarse	DR12
DR12C	Poorly vegetated tailings at Bowen ratio station (90 m)	Coarse	DR12

Table 4.17: Details of the second series Guelph permeameter test locations (27 November to 5 December 2000).

Test no's.	Location	Main tailings type
#1, #2, #3	550 m from dam wall on section line C	Fine tailings
#25, #26, #27	575 m from dam wall on section line C	Fine tailings
#4, #5, #6	584 m from dam wall on section line C	Fine tailings
#22, #23, #24	600 m from dam wall on section line C	Fine tailings
#7, #8	617 m from dam wall on section line C	Fine tailings
#19, #29, #21	634 m from dam wall on section line C	Fine tailings
#10, #11, #12	650 m from dam wall on section line C	Fine tailings
#13, #14, #15	667 m from dam wall on section line C	Fine tailings
#16, #17, #18	675 m from dam wall on section line C	Fine tailings

The results of the two series of Guelph permeameter testing are presented in Tables 4.18 and 4.19. The set average value for each set of three Guelph permeameter test results can be compared to the corresponding double-ring infiltrometer test.

Table 4.18: Results of the first series of Guelph permeameter tests performed on the Kidston tailings impoundment (27 September to 5 October 1999).

Test no.	Tailings type	Distance from wall (m)	Saturated hydraulic conductivity (m/s)		
			Individual	Set average	Type average
DR1A	Non-vegetated coarse	3	8.09E-06	1.27E-05	2.17E-05
DR1B	Non-vegetated coarse	3	1.94E-05		
DR1C	Non-vegetated coarse	3	1.05E-05		
DR4A	Non-vegetated coarse	3	1.38E-05	3.08E-05	
DR4B	Non-vegetated coarse	3	7.65E-05		
DR4C	Non-vegetated coarse	3	2.06E-06		
DR8A	Non-vegetated intermediate	230	1.81E-06	3.44E-06	6.12E-06
DR8B	Non-vegetated intermediate	230	2.70E-06		
DR8C	Non-vegetated intermediate	230	5.81E-06		
DR10A	Non-vegetated intermediate	230	6.09E-06	8.80E-06	
DR10B	Non-vegetated intermediate	230	1.01E-05		
DR10C	Non-vegetated intermediate	230	1.02E-05		
DR5A	Poorly vegetated coarse	8	4.20E-06	4.97E-06	1.18E-05
DR5B	Poorly vegetated coarse	8	3.09E-06		
DR5C	Poorly vegetated coarse	8	7.61E-06		
DR6A	Poorly vegetated coarse	8	1.19E-05	6.61E-06	
DR6B	Poorly vegetated coarse	8	2.38E-06		
DR6C	Poorly vegetated coarse	8	5.55E-06		
DR11A	Poorly vegetated coarse	90	1.08E-05	1.55E-05	
DR11B	Poorly vegetated coarse	90	2.75E-05		
DR11C	Poorly vegetated coarse	90	8.33E-06		
DR12A	Poorly vegetated coarse	90	1.49E-05	2.00E-05	
DR12B	Poorly vegetated coarse	90	2.74E-05		
DR12C	Poorly vegetated coarse	90	1.76E-05		
DR2A	Well vegetated coarse	15	6.50E-06	1.60E-05	1.64E-05
DR2B	Well vegetated coarse	15	1.90E-05		
DR2C	Well vegetated coarse	15	2.25E-05		
DR3A	Well vegetated coarse	15	4.92E-06	1.68E-05	

Table 4.18: Results of the first series of Guelph permeameter tests performed on the Kidston tailings impoundment (27 September to 5 October 1999).

Test no.	Tailings type	Distance from wall (m)	Saturated hydraulic conductivity (m/s)		
			Individual	Set average	Type average
DR3B	Well vegetated coarse	15	1.49E-05		
DR3C	Well vegetated coarse	15	3.06E-05		
DR7A	Well vegetated intermediate	200	5.50E-06		
DR7B	Well vegetated intermediate	200	5.31E-06	1.18E-05	
DR7C	Well vegetated intermediate	200	2.47E-05		1.02E-05
DR9A	Well vegetated intermediate	200	1.21E-05		
DR9B	Well vegetated intermediate	200	3.73E-06	8.61E-06	
DR9C	Well vegetated intermediate	200	9.99E-06		

Table 4.19: Results of the second series of Guelph permeameter tests performed on the Kidston tailings impoundment (27 November to 5 December 2000).

Test no.	Tailings type	Distance from wall (m)	Saturated hydraulic conductivity, k_s (m/s)		
			Individual	Set average	Type average
1	Non-vegetated fine	550	3.90E-09		
2	Non-vegetated fine	550	9.53E-09	7.70E-09	
3	Non-vegetated fine	550	9.66E-09		
25	Non-vegetated fine	575	3.26E-07		
26	Non-vegetated fine	575	1.75E-07	2.98E-07	
27	Non-vegetated fine	575	3.92E-07		
4	Non-vegetated fine	584	1.40E-08		
5	Non-vegetated fine	584	3.66E-08	2.75E-08	
6	Non-vegetated fine	584	3.19E-08		
22	Non-vegetated fine	600	5.83E-07		
23	Non-vegetated fine	600	7.88E-07	7.83E-07	
24	Non-vegetated fine	600	9.79E-07		
7	Non-vegetated fine	617	2.86E-06	1.50E-06	
8	Non-vegetated fine	617	1.43E-06		
19	Non-vegetated fine	634	2.81E-09		
20	Non-vegetated fine	634	2.75E-08	1.42E-08	
21	Non-vegetated fine	634	1.24E-08		
10	Non-vegetated fine	650	1.90E-07		
11	Non-vegetated fine	650	2.38E-08	1.56E-07	
12	Non-vegetated fine	650	2.55E-07		
13	Non-vegetated fine	667	2.82E-06		
14	Non-vegetated fine	667	3.09E-07	1.88E-06	
15	Non-vegetated fine	667	2.50E-06		
16	Non-vegetated fine	675	6.66E-08		
17	Non-vegetated fine	675	7.45E-07	3.92E-07	
18	Non-vegetated fine	675	3.63E-07		

4.5.2.3 Rainfall Simulator Tests

The Center for Mined Land Rehabilitation (CMLR) at the University of Queensland, Brisbane, Australia was contracted to conduct rainfall simulator tests on the tailings impoundment with a

view to determining the erosion susceptibility of the tailings under varying vegetation conditions and for various slopes (Horn *et al.*, 1998; Horn, 1999). Two rounds of testing were conducted. The first set of tests (Horn *et al.*, 1998) was conducted on the 11 ha trial section of the tailings impoundment during the period April to June 1998, and the second set of tests was conducted on the main tailings impoundment in August 1999 (Horn, 1999). The test locations are illustrated on Figure 4.6.

The tests were carried out using a portable rainfall simulator that was developed at the CMLR, and comprised of a combined two nozzle and three nozzle unit raining over a plot area measuring 4.0 m x 1.5 m (Horn *et al.*, 1998). The simulator produces rain from flat Veejet 80100 nozzles, with oscillation of a manifold causing the fan sprays to sweep to and fro across the plot. The sites selected for the first round of testing (Horn *et al.*, 1998) on the 11 ha trial plot of the tailings impoundment, were chosen based on a request from the mine to test the tailings susceptibility to erosion and is documented in Table 4.20. The sites were selected based on two factors; (1) it had to have a slope of between 1-5%, and (2) it had to have varying degrees of vegetative covers.

Table 4.20: Test sites for first round rainfall simulator testing by the CMLR (Horn *et al.*, 1998).

Site	Vegetative cover	Slope	No. of tests
#1	0 – 10 %	1 – 5 %	Not reported
#2	10 - 20 %	1 – 5 %	Not reported
#3	25 - 35 %	1 – 5 %	Not reported
#4	40+ %	1 – 5 %	Not reported

The second round of testing (Horn, 1999) on the main tailings impoundment was done with the additional goal of selecting sites with different particle size distributions. To this effect three sites were selected on beach tailings, located close to the dam wall, and another three sites were selected midway between the wall and the pool, on intermediate tailings. Table 4.21 lists the tested sites for the second round of testing. These locations are also depicted in Figures 4.7, 4.8 and 4.9.

Table 4.21: Test sites for second round rainfall simulator testing by the CMLR (Horn, 1999).

Site	Vegetative cover	Slope	Tailings type	No. of tests
#1	0 %	2.3 – 3.8 %	Coarse	3
#2	20 %	2.2 - 20 %	Coarse	3
#3	80 – 90 %	0 – 3.6 %	Coarse	3

Table 4.21: Test sites for second round rainfall simulator testing by the CMLR (Horn, 1999).

Site	Vegetative cover	Slope	Tailings type	No. of tests
#4	0 %	3.6 %	Intermediate	1
#5	10 %	3.8 - 10 %	Intermediate	2
#6	90 %	20 %	Intermediate	1

Since the rainfall simulator tests was not conducted with a view to measuring the infiltration rate into the tailings, the data gathered by the CMLR had to be computed as part of this research program in order to make use of the inferred infiltration rate. The resultant infiltration rates, which are in fact equivalent to saturated hydraulic conductivity's, are listed in Table 4.22.

Table 4.22: Inferred saturated hydraulic conductivity's from the results of the rainfall simulator tests by Horn (1999).

Test no.	Test site	Tailings type	Dist. from wall (m)	Infil. rate (mm/h)	Saturated hydraulic conductivity (m/s)	
					Ind.	Average
Rep 1	Kidtailings, 0% veg	Intermediate	230	40.4	1.12E-05	2.13E-05
Rep 2	Kidtailings, 0% veg	Intermediate	230	88.9	2.47E-05	
Rep 3	Kidtailings, 0% veg	Intermediate	230	101.2	2.81E-05	
Rep 1	Kidtailings, 10% veg	Intermediate	90	78.9	2.19E-05	2.19E-05
Rep 1	Kidtailings, 90% veg	Intermediate	200	76.2	2.12E-05	2.12E-05
Rep 1	Kidtailings, 0% veg	Coarse	3	88.7	2.46E-05	2.39E-05
Rep 2	Kidtailings, 0% veg	Coarse	3	82.6	2.29E-05	
Rep 3	Kidtailings, 0% veg	Coarse	3	86.3	2.40E-05	
Rep 1	Kidtailings, 20% veg	Coarse	8	58.9	1.64E-05	1.51E-05
Rep 2	Kidtailings, 20% veg	Coarse	8	62.9	1.75E-05	
Rep 3	Kidtailings, 20% veg	Coarse	8	41.3	1.15E-05	
Rep 1	Kidtailings, 80-90% veg	Coarse	15	110.3	3.06E-05	2.10E-05
Rep 2	Kidtailings, 80-90% veg	Coarse	15	66.5	1.85E-05	
Rep 3	Kidtailings, 80-90% veg	Coarse	15	49.9	1.39E-05	

4.5.2.4 Pump and Constant Head Saturated Hydraulic Conductivity (Edraki, 1999)

Edraki (1999) reports on a study on the 11 ha trial plot illustrated on Figure 4.7, of the tailings impoundment to estimate the direction and magnitude of groundwater flow. Numerous shallow piezometers were installed in the impoundment as part of this work and the researchers proceeded to measure the saturated hydraulic conductivity of the tailings using one of two independent methods. The first method, piezometer pumping tests, were used in piezometers, which showed an appreciable amount of standing water. The water was pumped out using a small submersible pump and the rate of recharge to the well was measured by recording the depth to water at different intervals of time.

For the remainder of the piezometers, the second test method of constant head permeability, was used. Water was poured into the well using a measuring cylinder to contain a constant level in the slotted portion of the piezometer and this was continued until a steady rate of flow to the surrounding well was reached. Addition of water was then stopped and the drawdown of water in the well was recorded at different time intervals. Tables 4.23 and 4.24 list the results of these tests. The depth of the tests was not reported, although it is inferred that it's approximately 2 m deep. The location of each piezometer with respect to the distance to the wall is not given.

Table 4.23: Results of the saturated hydraulic conductivity testing in piezometer holes on the Kidston tailings impoundment using the piezometer pumping method (Edraki, 1999).

Test number	Saturated hydraulic conductivity (m/s)	
	Individual	Average
A1	8.75E-07	6.94E-06
B1	1.91E-06	
F1	8.42E-06	
B1 (rep)	2.09E-06	
E1	6.12E-06	
A1 (rep)	4.90E-06	
C1	2.43E-05	
F2	6.46E-06	
C2	7.40E-06	

Table 4.24: Results of the saturated hydraulic conductivity testing in piezometer holes on the Kidston tailings impoundment using the constant head method (Edraki, 1999).

Test number	Saturated hydraulic conductivity (m/s)	
	Individual	Average
D2 (1)	1.29E-05	8.06E-06
D2 (2)	2.19E-05	
D2 (3)	1.58E-05	
D3 (1)	3.98E-06	
D3 (2)	2.74E-06	
E2 (1)	5.06E-06	
E2 (2)	5.06E-06	
E3 (1)	9.44E-06	
E3 (2)	3.25E-06	
B2	5.39E-07	

4.5.2.5 Horizontal Saturated Hydraulic Conductivity

All of the saturated hydraulic conductivity tests reported in the previous sections are for the vertical hydraulic conductivity. Many authors have shown that the hydraulic conductivity is anisotropic (Vick, 1983). The anisotropy is caused by the deltaic deposition of the tailings when spiggoting from a moving endpipe. Some indirect testing results of the horizontal hydraulic conductivity for the Kidston tailings impoundment is described in the following sections.

4.5.2.5.1 Testing by Douglas Partners (1997)

Ten piezometers were installed on the tailings impoundment between 2-5 June 1997, as part of a tailings stability study by the University of Queensland, Brisbane, Australia. Douglas Partners Pty Ltd, a local consulting engineering firm undertook the installations of the piezometers, as well as geotechnical testing by means of seven piezocone penetration tests (CPTUs), and eight conductivity cone penetration tests (CCPTs) (Douglas Partners, 1997).

Both a CPTU and a CCPT was undertaken at each location followed by the installation of a standpipe piezometer. Test locations were chosen by Professor David Williams of the University of Queensland, and are shown on Figure 4.7.

The CPTUs were undertaken using a 0.035 m diameter cone with a following 0.13 m long friction sleeve attached to rods of the same diameter, and pushed continuously into the tailings by hydraulic thrust from a ballasted, truck mounted test rig. Strain gauges in the cone and sleeve measure resistance to penetration and a saturated porous filter mounted behind the cone tip connected to a pressure diaphragm measures pore pressure response to cone penetration. Pore pressure dissipation tests were carried out during the CPTUs at selected depths within the tailings. In these tests the penetration of the piezocone is halted and the decay of excess pore pressure generated during penetration is measured with time.

Horizontal permeability cannot be measured directly. It is deduced from time taken to achieve 50% dissipation of excess pore pressure (t_{50}) in the CPTU. This is used to calculate the coefficient of consolidation in the horizontal direction (C_h) using the modified time factor (T^*). Table 4.25 lists the details and results of the CPTU tests that were reported by Douglas Partners (1997).

Table 4.25: Details of the saturated horizontal hydraulic conductivity measured in the piezometer holes using CPTU tests (Douglas Partners, 1997)*.

Test number	t_{50}	Coeff. of consol., C_h	k_h/a_v	Saturated horizontal hydraulic conductivity, k_h (m/s)	
				Individual	Average
SP4: CPTU 4a (3.0 m depth)	0.6	6.34E-09	3.48E-05	1.08E-08	4.49E-08
SP4: CPTU 4b (3.0 m depth)	0.6	1.90E-08	1.04E-04	3.24E-08	
SP5: CPTU 5a (13.0 m depth)	0.3	9.51E-09	5.22E-05	1.62E-08	
SP5: CPTU 5b (13.0 m depth)	0.3	3.49E-08	1.91E-04	5.93E-08	
SP6: CPTU 6a (11.5 m depth)	0.1	3.17E-08	1.74E-04	5.39E-08	
SP6: CPTU 6b (11.5 m depth)	0.1	1.08E-07	5.91E-04	1.83E-07	
SP7: CPTU 7a (8.0 m depth)	1.6	6.34E-10	3.48E-06	1.08E-09	
Sp7: CPTU 7b (8.0 m depth)	1.6	1.27E-09	6.96E-06	2.16E-09	

* For calculations in Table 4.26 the following has been assumed: ρ_w = 1000 kg/m^3; g = 9.81 m/s^2; e_0 = 0.788; a_v = 2.10E-4 m^2/N.

These results indicate that there is a degree of anisotropy evident in the Kidston tailings impoundment.

4.5.2.5.2 Testing by Earthtech Consultants (1999)

Earthtech Consultants Pty Ltd, a specialist consulting engineering firm performed a geotechnical investigation, by means of piezocone penetration tests (CPTUs) as part of a contract of Australian Groundwater Consultants Pty Ltd (AGE) (Earthtech Consultants, 1999). Piezometers were installed at the test locations after completion of the CPTU tests.

The test locations were selected by the author, and were selected primarily to enhance the data set from the shallow piezometers previously installed. Figure 4.6 depicts the test locations.

The testing was done between 2-4 November 1999 in accordance with AS1726-1993 "Geotechnical Site Investigations". The 12 CPTUs was conducted by pushing the instrumented probe into the ground at an approximate rate of 0.020 m/s using a truck mounted drilling rig. Readings of tip resistance sleeve friction and pore pressure were taken and digitally recorded at 0.025 m intervals. A number of dissipation tests whereby the decay of excess pore pressures at the probe is monitored, were undertaken at regular intervals during each CPTU. Each test was terminated when natural material (i.e. bedrock) was encountered.

An artificial neural network was used to infer horizontal permeability's based on the measured CPTU data. An artificial neural network is a form of artificial intelligence whereby software can be "trained" to produce a result from a given set of input values. Table 4.26 lists the values of

specific horizontal saturated hydraulic conductivity reported by Earthtech Consultants (1999). From the inferred strata and permeability datasheets in their report, the horizontal saturated hydraulic conductivity ranges consistently between 1.0E-09 m/s and 1.0E-03 m/s (6 orders of magnitude), and most changes are rapid and random indicating layering of the tailings. Most often the changes are only for slight tailings thickness, indicating thinly banded tailings. This is consistent with visual observations that were made of the tailings profile when the double-ring infiltrometer tests were conducted. Another consistent observation from the detailed piezocone logs are that the top 1.5 to 6.0 m of the tailings profile in every hole has a constant horizontal saturated hydraulic conductivity of approximately 1.0E-4 m/s, indicating a fairly coarse homogeneous material overlying the thinly banded slimes.

Table 4.26: Results of the specific saturated horizontal hydraulic conductivity testing done in piezometer holes using CPTU tests (Earthtech Consultants, 1999).

Test no.	Test depth (m)	Saturated horizontal hydraulic conductivity, k_h (m/s)
CPTU No. 4	13.565	9.70E-08
CPTU No. 5	13.820	2.00E-06
CPTU No. 6	9.970	1.60E-07
CPTU No. 6	8.500	2.80E-07
CPTU No. 6	15.945	2.30E-07
CPTU No. 7	7.925	1.10E-06
CPTU No. 7	11.920	3.40E-07
CPTU No. 7	13.935	1.70E-07
CPTU No. 7	15.910	1.00E-07
CPTU No. 7	17.910	1.80E-07
CPTU No. 7	19.915	6.10E-07
CPTU No. 8	16.955	5.50E-07
CPTU No. 8	19.070	1.40E-07
CPTU No. 8	21.060	1.70E-07
CPTU No. 8	24.050	4.10E-08
CPTU No. 9	13.850	2.80E-07
CPTU No. 11	6.905	4.00E-07
CPTU No. 11	11.905	1.70E-07
CPTU No. 11	19.895	2.90E-07

4.5.3 Summary of all Saturated Hydraulic Conductivity Testing (Laboratory and In-Situ)

The saturated hydraulic conductivity data in the preceding sections are summarized in the following section for ease of use of the data. The average saturated hydraulic conductivity of

each tested tailings type and laboratory and in-situ test method is listed in Tables 4.27 and 4.28 respectively, and a statistical summary of all these tests are presented in Table 4.29.

Table 4.27: Average saturated hydraulic conductivity of each tested tailings type and laboratory test method.

Source	Test method	Tailings type	#	k_s (m/s)
Author	Consolidation*	Coarse	4	6.82E-09
Author	Consolidation*	Fine	4	5.82E-09
Author	Falling head	Coarse	4	4.47E-06
Author	Falling head	Fine	4	4.91E-06
Gutteridge Haskins & Davey (1987)	Consolidation*	Unspecified	1	8.62E-09
O'Kane (1997)	Consolidation*	Fine	1	4.88E-09
O'Kane (1997)	Falling head	Coarse	1	1.17E-05
O'Kane (1997)	Falling head	Fine	1	5.23E-06
Rassam (1998)	Head control method	Unspecified	6	8.30E-07
Williams (2000c)	Head control method	Unspecified	6	8.72E-07

* Since the consolidation testing data is not used for any analysis in this thesis, no explanation or discussion of the reported measurements will be made.

Table 4.28: Average saturated hydraulic conductivity of each tested tailings type and in-situ test method.

Source	Test method	Tailings type	#	k_s or k_h (m/s)
Author	Double-ring	Non-vegetated coarse	2	2.18E-05
Author	Double-ring	Non-vegetated intermediate	2	1.49E-06
Author	Double-ring	Poorly vegetated coarse	4	1.41E-05
Author	Double-ring	Well vegetated coarse	2	3.61E-06
Author	Double-ring	Well vegetated intermediate	2	6.28E-06
Author	Guelph	Non-vegetated coarse	6	2.17E-05
Author	Guelph	Non-vegetated intermediate	6	6.12E-06
Author	Guelph	Poorly vegetated coarse	12	1.18E-05
Author	Guelph	Well vegetated coarse	6	1.64E-05
Author	Guelph	Well vegetated intermediate	6	1.02E-05
Author	Guelph	Average non-vegetated fine	26	5.26E-07
Douglas Partners (1997)	Piezocone	Unspecified	8	4.49E-08
Horn et al. (1998)	Rainfall simulator	0% Cover, unspecified	na	6.67E-06
Horn et al. (1998)	Rainfall simulator	10% Cover, unspecified	na	7.33E-06
Horn et al. (1998)	Rainfall simulator	25% Cover, unspecified	na	8.36E-06
Horn et al. (1998)	Rainfall simulator	44% Cover, unspecified	na	1.04E-05
Horn (1999)	Rainfall simulator	Non-vegetated coarse	3	2.39E-05
Horn (1999)	Rainfall simulator	Non-vegetated intermediate	3	2.13E-05
Horn (1999)	Rainfall simulator	Poorly vegetated coarse	3	1.51E-05
Horn (1999)	Rainfall simulator	Intermediate	1	2.19E-05
Horn (1999)	Rainfall simulator	Well vegetated coarse	3	2.10E-05
Horn (1999)	Rainfall simulator	Well vegetated intermediate	1	2.12E-05
Edraki (1999)	Constant head	Unspecified	10	8.06E-06
Edraki (1999)	Piezometer pumping	Unspecified	9	6.94E-06
Earthtech Consultants (1999)	Piezocone	Top zone (1.5-6.0 m)	19	1.00E-04
Earthtech Consultants (1999)	Piezocone	Unspecified	19	3.85E-07

na = no numbers are reported

Table 4.29: Summary table of all the Kidston saturated hydraulic conductivity testing (laboratory and in-situ).

Test grouping	# Tests	Mean	Average	Maximum	Minimum
All tests (excl. k_h)	143	2.72E-06	9.79E-06	5.26E-05	4.88E-09
All laboratory tests	32		2.26E-06	1.17E-05	4.88E-09
All field tests (excl. k_h)	111		1.47E-05	5.26E-05	1.49E-06
All horizontal permeability tests	46	1.20E-06	3.35E-05	1.0E-04	1.08E-09
All fine tailings (excl. k_h)	31	2.13E-06	8.98E-06	2.19E-05	4.88E-09
All coarse tailings (excl. k_h)	50	1.39E-05	7.11E-06	2.39E-05	6.82E-09
All unspecified tailings (excl. k_h)	62	1.52E-06	7.09E-06	5.26E-05	8.62E-09

As explained in the section on grain size distribution, the hydraulic deposition of the tailings results in particle segregation along the tailings beach. This means that the coarse tailings settle out first and finally the slimes settle out in the pond base. Since saturated hydraulic conductivity is a function of grain size distribution, we would thus expect the saturated hydraulic conductivity to vary in a similar fashion down the beach slope. The highest permeability is expected close to the wall, and closer to the pool the surface tailings should become less permeable. Figure 4.11 presents empirically calculated saturated hydraulic conductivity from particle size data testing by Rassam (1998) and Williams (2000b).

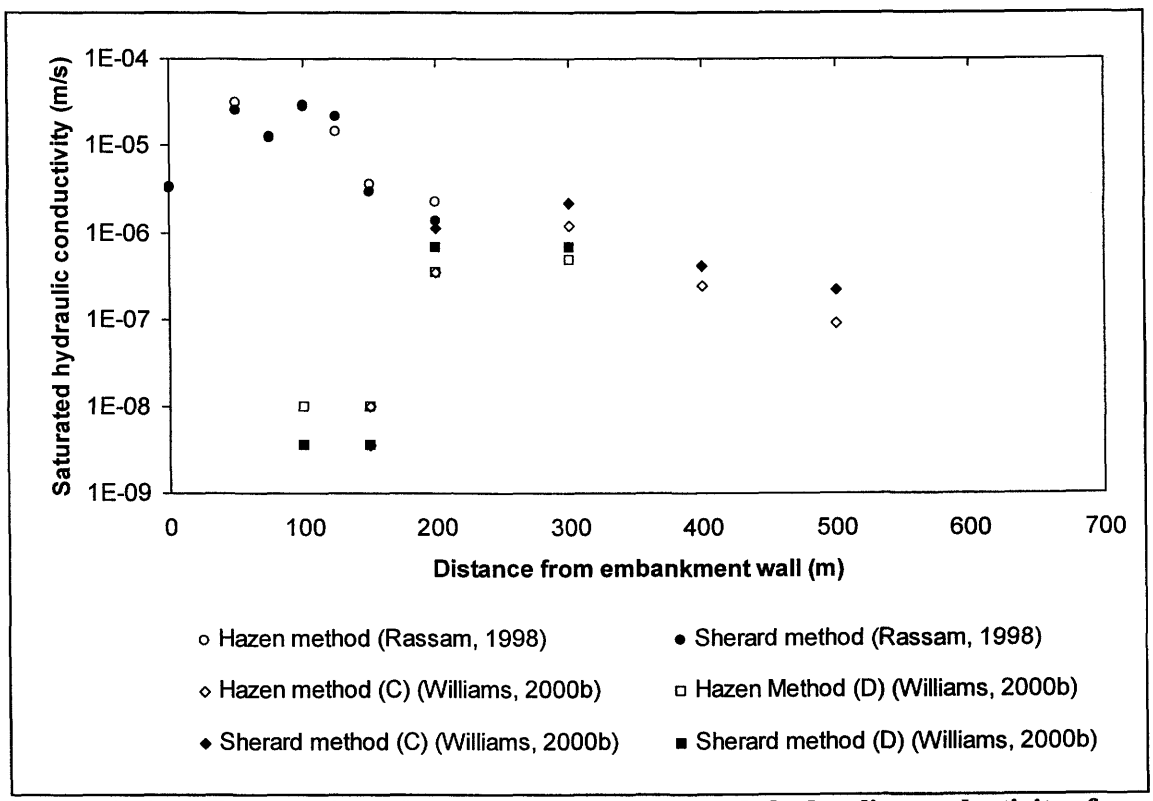

Figure 4.11: Empirically calculated surface saturated hydraulic conductivity from particle size data for the Kidston tailings impoundment.

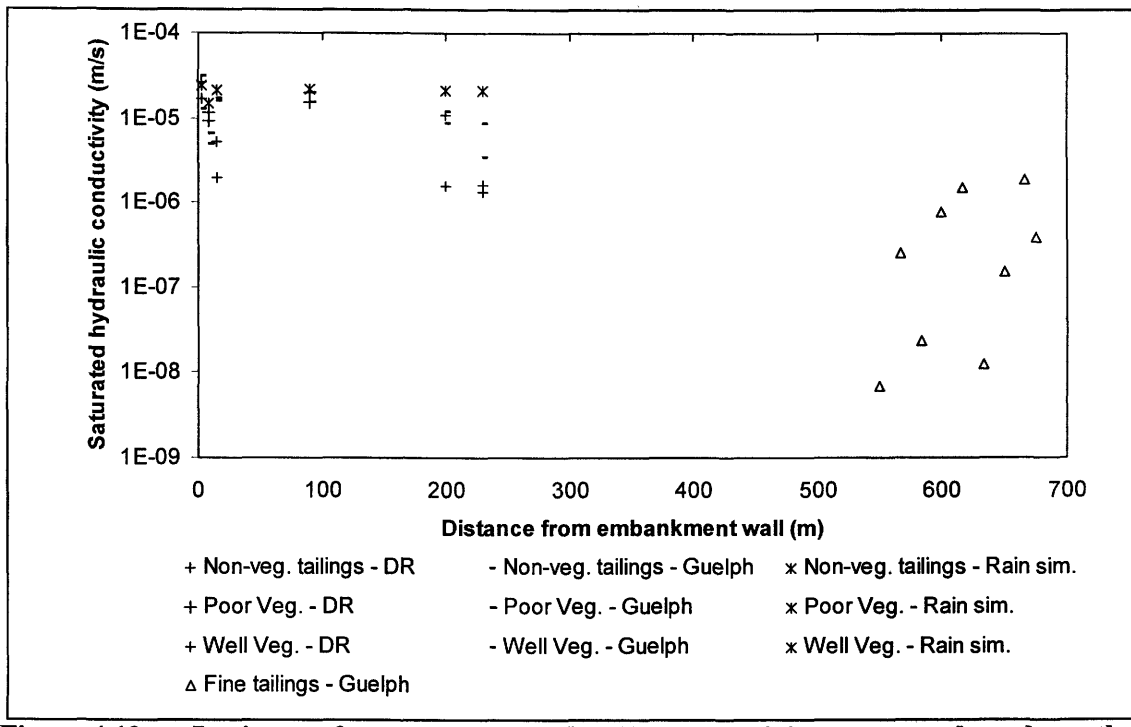

Figure 4.12: In-situ surface saturated hydraulic conductivity tests conducted on the Kidston tailings impoundment.

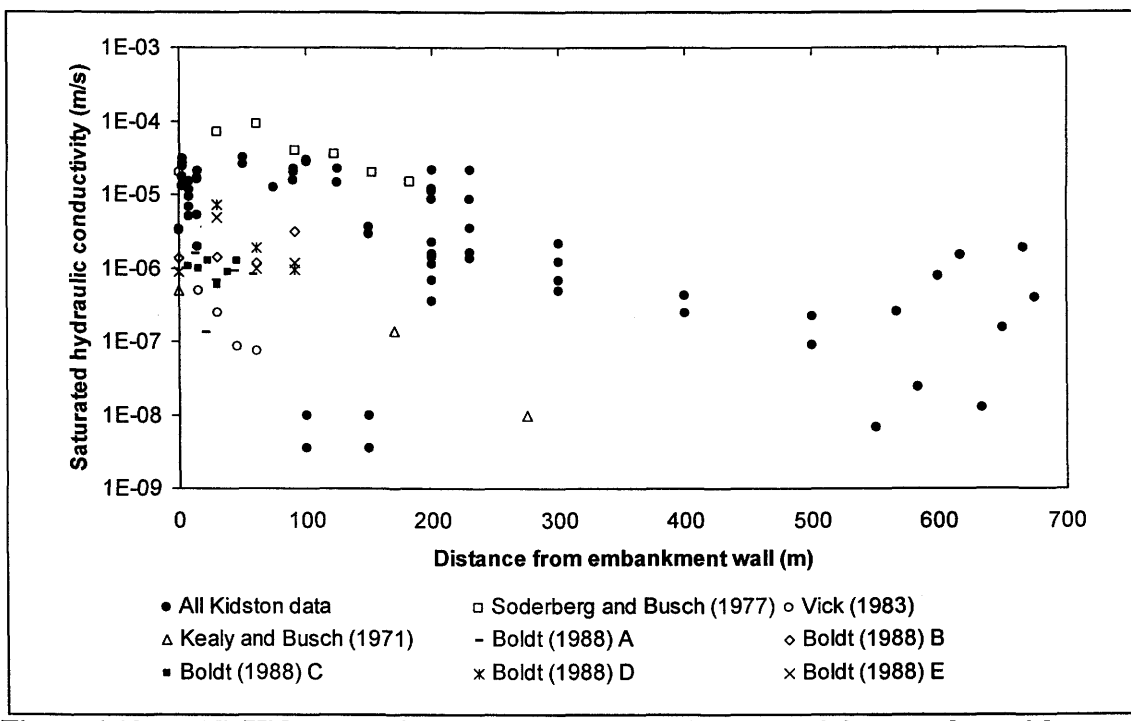

Figure 4.13: All Kidston surface saturated hydraulic conductivity together with some results reported in the literature for tailings segregation.

Figure 4.12 summarizes all the in-situ saturated hydraulic conductivity testing conducted on the tailings impoundment surface. Finally, Figure 4.13 presents all the laboratory and in-situ saturated hydraulic conductivity data for the Kidston tailings impoundment together with data reported by Vick (1983), Boldt (1989), Soderberg and Busch (1977) and Kealy and Busch (1971) on tailings surface permeability versus position along the beach.

4.6 Conclusions

The detailed physical and hydraulic testing program undertaken for this study, together with the gathering of all the historic data provides a significant database of material properties for application to the numerical modeling that follow in Chapter 6. The success on numerical modeling rest on many assumptions, of which the appropriate choice of material properties is one of the more important ones. By reducing the uncertainty in the choices, or by at least completely understanding the properties, the errors with selecting appropriate properties are substantially reduced.

4.7 References

American Society for Testing and Materials (ASTM). (1996a). Standard test method for particle size analysis of soils (D422-63; reapproved 1990). *In* 1996 Annual Book of ASTM Standards, Volume 4.08. ASTM, Philadelphia, PA, USA, pp. 10-16.

American Society for Testing and Materials (ASTM). (1996b). Standard test method for ATTERBERG (D4318-84). *In* 1996 Annual Book of ASTM Standards, Volume 4.08. ASTM, Philadelphia, PA, USA.

American Society for Testing and Materials (ASTM). (1996c). Standard test method for Shrinkage (D4943-95 (Wax Method)). *In* 1996 Annual Book of ASTM Standards, Volume 4.08. ASTM, Philadelphia, PA, USA.

American Society for Testing and Materials (ASTM). (1996d). Standard test method for specific gravity of soils (D854-92). *In* 1996 Annual Book of ASTM Standards, Volume 4.08. ASTM, Philadelphia, PA, USA, pp. 80-83.

American Society for Testing and Materials (ASTM). (1996e). Standard test method for infiltration rate of soil in field using double-ring infiltrometer. (D3385-94). *In* 1996 Annual Book of ASTM Standards, Volume 4.08. ASTM, Philadelphia, PA, USA, pp. 331-337.

American Society for Testing and Materials (ASTM). (1996f). Standard test method for one-dimensional consolidation properties of soils (D2435-90). *In* 1996 Annual Book of ASTM Standards, Volume 4.08. ASTM, Philadelphia, PA, USA, pp. 207-216.

Blight, G., Steffen, D. (1979). Geotechnics of Gold Mine Waste Disposal. Current Geotechnical Practice in Mine Waste Disposal, ASCE, pp. 1-52.

Boldt, C.M.K. (1989). Beach Characteristics of Mine Waste Tailings. Report of investigations 9171, United States Department of the Interior, Bureau of Mines, 24 pp.

Childs, E.C. and Collis-George, G.N. (1950). The permeability of porous materials. Proceedings of the Royal Society of London, Series A, Vol. 201, pp. 392-405.

Douglas Partners. (1997). Factual Report on Tailings Dam Insitu Testing at Kidston Gold Mine. Consultants report to Kidston Gold Mines, Project No. 21712, July, 5 pages.

Earthtech Consultants. (1999). Report on Piezocone Testing, Kidston Tailings Storage Facility. Consultants report to Australasian Groundwater & Environmental Consultants Pty Ltd., Project No. MF 1367, December, 3 pages.

Edraki, M. (1999). Groundwater Survey and Hydraulic Conductivity of the Tailings in the Rehabilitation Area of Kidston Gold Mine Site. Interim research report by the University of Queensland, Brisbane, Queensland, Australia. September, 9 pages.

Fourie, A. (1988). Beaching and Permeability Properties of Tailings. Hydraulic Fill Structures, Geotechnical Special Publication No. 21, pp. 142-154.

Fredlund, D.G., Xing, A. (1994). Equations for the soil-water characteristic curve. Canadian Geotechnical Journal, Vol. 31, No. 3, pp. 521-532.

Fredlund, D.G., Xing, A. and Huang, S. (1994). Predicting the permeability function for unsaturated soils using the soil water characteristic curve. Canadian Geotechnical Journal, Vol. 31, pp. 533-546.

Gutteridge, Haskins and Davey Pty Ltd. (1987). Kidston Project; Interim Report on Tailings Disposal. Consultants Report to Kidston Gold Mines Limited. Brisbane, Queensland, Australia. July, 9 pages.

Hazen, A. (1911). Discussion of "Dams on Sand Foundations", by A.C. Koenig, Transactions, ASCE, Vol. 73, pp. 199-203.

Holtz, R.D., Kovacs, W.D. (1981). An Introduction to Geotechnical Engineering. Prentice-Hall Civil Engineering and Engineering Mechanics Series, N.M. Newmark and W.J. Hall, Editors, Prentice-Hall, Englewood Cliffs, New Jersey, U.S.A.

Horn, C.P., So, H.B., Mulligan, D.R. (1998). Waste Rock Dump Rehabilitation Research Project, Stability of Outer Dump Surfaces. Report by Center for Mined Land Reclamation to Kidston Gold Mines Limited. September, 40 pages.

Horn, C.P. (1999). Datasheets of Rainfall Simulator Tests on Kidston Tailings Dam, Verbal Discussion.

Kealy, DC, Busch, RA. (1971). Determining Seepage Characteristics of Mill-Tailings Dams by the Finite-Element Method. Report of Investigations 7477, United States Department of the Interior, Bureau of Mines. January, 113 pages.

O'Kane, M. (1995). Instrumentation and Monitoring of an Engineered Soil Cover System for Acid Generating Mine Waste. M.Sc. Thesis, department of Civil Engineering, University of Saskatchewan, Saskatoon, Canada. 303 pages.

O'Kane, M. (1997). Laboratory characterization of Kidston tailing samples #1/7 & #2/7. Unpublished data in Kidston file, Unsaturated Soils Group, Department of Civil Engineering, University of Saskatchewan, Saskatoon, Canada.

Rassam, D.W. (1998). Engineering Behavior of Metalliferous Tailings and Waste Rock Relevant to their Disposal and Rehabilitation. P.hD. dissertation, Department of Civil Engineering, University of Queensland, Brisbane, Australia.

Sherard, J.L., Dunnigan, L.P., Talbot, J.R. (1984). Basic properties of sand and gravel filters. Journal of Geotechnical Engineering, Vol. 110, No. 6, pp. 684-700.

Soderberg, R., Busch, R. (1977). Design Guide for Metal and Nonmetal Tailings Disposal. U.S. Bureau of Mines, IC 8755.

SoilMoisture Equipment Corp. (1986). Guelph Permeameter 2800KI Operating Instructions. Revision 8/86, 26 pages.

Vick, SG. (1983). Planning Design and Analysis of Tailings Dams. A Wiley-Interscience Publication, John Wiley & Sons, New York, 369 pages.

Williams, D.J. (2000a). Tailings Dam Research Project; Report on Preliminary Testing. Report to Mr. Nick Currey, Kidston Gold Mines Limited. Department of Civil Engineering, University of Queensland, Brisbane, Australia. 20 January, 10 pages.

Williams, D.J. (2000b). Tailings Dam Research Project; Unpublished Report on Saturated/Unsaturated Tailings Testing. Report to Mr. Nick Currey, Kidston Gold Mines Limited. Department of Civil Engineering, University of Queensland, Brisbane, Australia.

Williams, D.J. (2000c). Tailings Dam Research Project; Unpublished Report on Further Grains Size Distribution Testing. Report to Mr. Nick Currey, Kidston Gold Mines Limited. Department of Civil Engineering, University of Queensland, Brisbane, Australia.

Wog, K. (2000). Laboratory characterization of Kidston tailings samples. Unpublished data, Department of Civil Engineering, University of Saskatchewan, Saskatoon, Canada.

CHAPTER 5

Basic Tailings Impoundment Closure Water Balance

5.1 Introduction

This chapter describes the basic Kidston tailings impoundment closure water balance that is used to estimate the quantity of runoff that will flow to the tailings pond from the exposed tailings impoundment surface. It is vitally important to obtain a number against which subsequent numerical model calibration of the surface flux boundary condition can be carried out. The water balance calculation discussed in this chapter does not include detailed calculations for evapotranspiration and infiltration rates into the exposed tailings, but makes use of simplified assumptions regarding these parameters to allow for a first order estimate to be made of the runoff volume.

The reader is reminded that the primary objective of this research is to develop a spatial flux boundary function for the tailings impoundment as a whole. This is done by solving the flux boundary condition problem using the 1-D SoilCover (SoilCover, 1997) numerical model. In order to apply the SoilCover model to the two-dimensional problem of a spatially varying phreatic table, a conceptual model of the generalized tailings impoundment cross-section is developed and a methodology to solve this problem using the SoilCover model is developed (the details of this methodology is documented in Chapter 7). It is however vitally important to have a number against which the numerical modeling can be calibrated in order to ensure that the modeling provides the correct answer. Runoff was identified as the most appropriate number to use in this study, and the tailings impoundment water balance described in this chapter shows how the runoff number is calculated.

This chapter starts off by describing the entire Kidston tailings impoundment closure water balance via a set of equations. The second part of this chapter describes how each individual water balance component is calculated. The chapter is then concluded with the results of the actual water balance calculation, which consist of a runoff for the tailings impoundment surface.

5.2 Kidston Tailings Impoundment as Part of the Mine Site Water Balance

The logical place to start is to describe where the Kidston tailings impoundment fit into the mine site water balance. The tailings impoundment was not merely a waste disposal site. Water pumped to the tailings impoundment during operation with the tailings was recovered for plant water use. Since this study deals with the tailings impoundment water after the impoundment has been decommissioned, tailings are no longer being pumped to the impoundment and the decant water is no longer the primary plant water source. However, the impoundment is still very much part of the mine water system and will be dealt with as such.

Figure 5.1 presents a simple block diagram of the tailings impoundment water balance and how it fits into the general mine site water balance. There are five water containment sites; (1) North pond, (2) South pond, (3) Reclaim dam, (4) Reclaim dam seepage dam, and (5) tailings impoundment. Each water containment site has losses and gains associated with it, and they interact upon each other via either controlled pumping, or uncontrolled seepage. Each of these containment systems will be described in detail in the following sections.

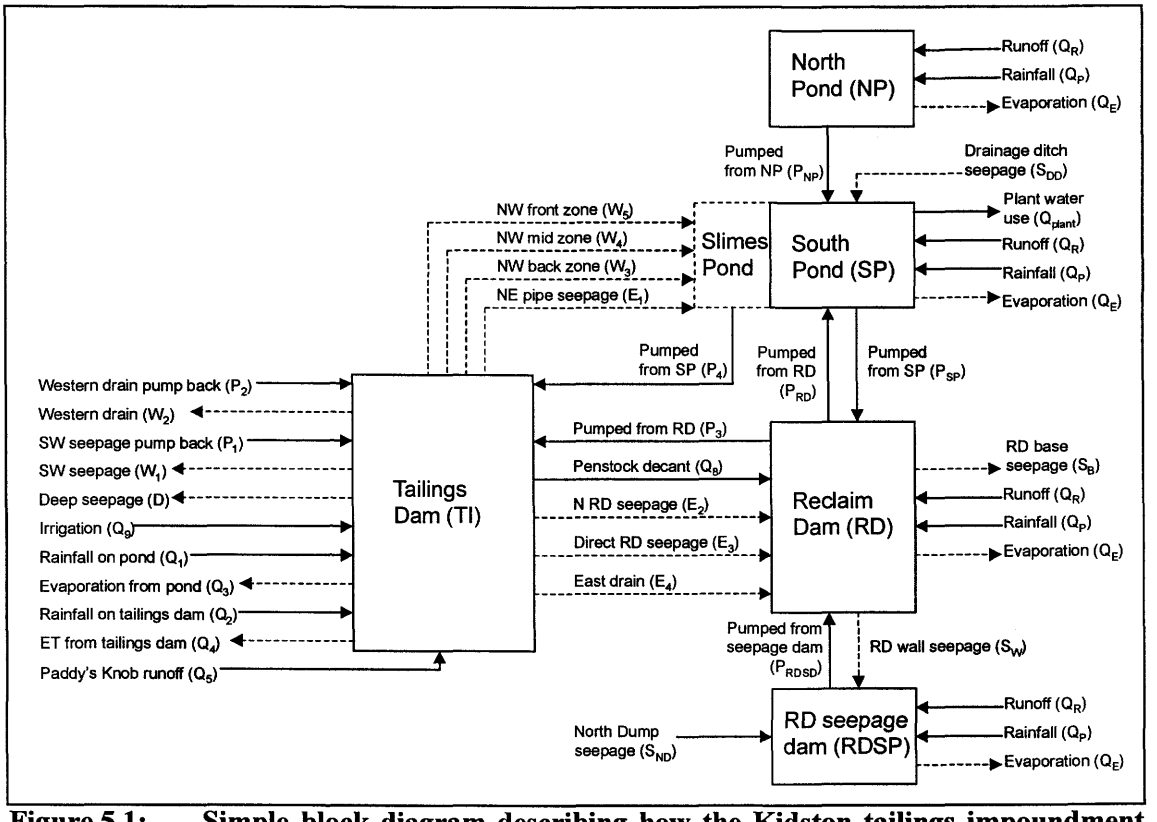

Figure 5.1: Simple block diagram describing how the Kidston tailings impoundment fits into the overall Kidston mine site water balance.

5.2.1 North Pond

The north pond (NP) is an anti-pollution pond that collects runoff from the plant area including stockpiles and lime/cyanide storage and handling areas. When the water depth in the pond rises above 0.5 m (507.5 mRL), a manually activated pump is used to pump water to the south pond (SP). The estimated capacity of this pump is 50 l/s. The design capacity of the pond was 7700 m^3, however siltation during mine construction in the first 2.5 years of the mine operation, reduced the capacity to 4600 m^3 (Gutteridge Haskins and Davey, 1987). Gutteridge Haskins and Davey (1987) estimated that the rate of siltation for the life of the mine would be 20 t/ha/yr., effectively reducing the pond capacity to 3600 m^3 by 1996. For the purpose of the water balance calculations in this thesis the north pond was assumed to be constant at 85 m x 85 m, giving it a surface area of 7225 m^2, with an operational storage volume of 3613 m^3. The catchment area for the pond is 8.2 ha and a runoff factor of 0.4 (Gray, 1970; Gutteridge Haskins and Davey, 1984) was used to calculate the runoff volume. The north pond base level is at 507 mRL and its full supply level (FSL) is at 509.5 mRL. This additional storage volume is to reduce the load on the south pond during storm events. Standard safe practice further required the dam to be designed with 0.5 m freeboard for a final crest level of 510.0 mRL. Appendix L contains details of the north pond water balance calculations, based on the following water balance expression:

$$V_{NP} = Q_P - Q_E + Q_R - P_{NP} \qquad [5.1]$$

Where V_{NP} = volume of retained water in north pond (m^3),

Q_P = volume of precipitation on the water surface area (m^3),

Q_E = volume of potential evaporation from the water surface area (m^3),

Q_R = volume of runoff water entering from the catchment (m^3), and

P_{NP} = volume of water pumped from the north pond to the south pond (m^3).

5.2.2 South Pond

The south pond (SP) is an anti-pollution pond that collects runoff from the plant area including low grade and waste stockpile areas. Dewatering and runoff from the mine pit are pumped to a drainage ditch which connects with the south pond (assumed to be constant at 15 l/s; Gutteridge Haskins and Davey, 1987). Other inflows to the south pond include pumping from north pond and mill overflows which occur in small volumes (mill overflows have been assumed to be

insignificant for these calculations). Make-up water is pumped from the reclaim dam (RD) as required for recycling in the plant. Automated pumps kick in to supply the water when the water level in the south pond drops below 536.05 mRL. All plant runoff, inflows from the mine pit and mill overflows are directed to a settling pond next to the south pond before overflowing into the south pond.

Process water required for plant operation is pumped from the south pond to an internal reclaim tank at the plant. Two 90 l/s pumps are used to provide the required flow rate and are automatically controlled by the water level in the reclaim tank. While the tailings impoundment was operational, water from the south pond provided up to 90% of the process water requirements with freshwater from the Copperfield dam making up the difference. Since the decommissioning of the tailings impoundment, the south pond provides less than 25% (estimated at a constant rate of 22 l/s) of the process water with fresh water making up the rest. The overall water requirement for the mine has lowered by about 50% since the thickened tailings plant has been in use. Water is also pumped to the tailings impoundment from the south pond when the south pond low operating level 535.8 mRL is reached. The dam base is at a level of 533.0 mRL, with the full supply level (FSL) and spillway at 537.1 mRL. The freeboard on this dam is only 0.25 m with the final crest at 537.35 m. The settling dam is often dredged and the sludge is pumped to the tailings impoundment, on an ad-hoc basis.

The design capacity of the south pond was 54200 m^3, but as with the north pond, siltation has reduced its capacity to approximately 33000 m^3 by 1996 (Gutteridge Haskins and Davey, 1987). Existing mine survey maps were used to determine a stage curve for the south pond as described in Appendix L and the following best fit equations was used in the water balance calculations for the south pond:

$$A_{SP} = 3.17\times10^{1}\cdot h_{SP}^{6} - 1.02\times10^{5}\cdot h_{SP}^{5} + 1.36\times10^{8}\cdot h_{SP}^{4} - 9.72\times10^{10}\cdot h_{SP}^{3} + 3.90\times10^{13}\cdot h_{SP}^{2} - 8.35\times10^{15}\cdot h_{SP} + 7.45\times10^{17} \quad [5.2]$$

$$V_{SP} = 3.97\times10^{1}\cdot h_{SP}^{6} - 1.27\times10^{5}\cdot h_{SP}^{5} + 1.70\times10^{8}\cdot h_{SP}^{4} - 1.22\times10^{11}\cdot h_{SP}^{3} + 4.88\times10^{13}\cdot h_{SP}^{2} - 1.04\times10^{16}\cdot h_{SP} + 9.31\times10^{17} \quad [5.3]$$

Where A_{SP} = south pond water surface area (m^2),

V_{SP} = south pond water storage volume (m^3), and

h_{SP} = south pond water level (m).

The catchment area for the pond is 21.9 ha and a runoff factor of 0.4 (Gray, 1970; Gutteridge Haskins and Davey, 1984) was used to calculate the runoff volume. Appendix L contains details of the water balance calculations based on the following water balance expression for the south pond:

$$V_{SP} = Q_P - Q_E + Q_R + P_{NP} + S_{DD} - Q_{plant} - P_{SP} - P_4 + P_{RD} + W_3 + W_4 + W_5 + E_1 \quad [5.4]$$

Where S_{DD} = volume of drainage ditch seepage (m^3),

Q_{plant} = volume of water required by plant (m^3),

P_{SP} = volume of water pumped from south pond to reclaim dam (m^3),

P_4 = volume of water pumped from south pond to tailings impoundment (m^3),

P_{RD} = volume of water pumped from reclaim dam to south pond (m^3),

W_3 = seepage volume from NW back section (m^3),

W_4 = seepage volume from NW mid section (m^3),

W_5 = seepage volume from NW front section (m^3), and

E_1 = seepage volume from NE pipe section (m^3).

5.2.3 Reclaim Dam

The reclaim dam (RD) is located downstream of the tailings impoundment embankment and stores decant water from the tailings impoundment for recycling in the plant. Pumps with capacity of 180 l/s pump water from the reclaim dam to the south pond and are automatically controlled by the water level in the south pond (see the previous section).

The inflow of decant (penstock) water from the tailings impoundment is controlled by a float valve in the reclaim dam. Decant water inflow only occurs when the water level in the reclaim dam is less than the float valve level (523.10 mRL). The storage available between the float valve level and the dam full supply level (527.5 mRL) is used for containment of runoff from the reclaim dam catchment area. A pump has also been installed to return water to the tailings

impoundment should levels in the reclaim dam become too high (523.7 mRL). The base elevation of the dam is at 519.0 mRL and the crest level, which allows for a freeboard of 0.5 m is at 528.0 mRL. Existing mine survey maps were used to determine a stage curve for the reclaim dam described in Appendix L and the following best fit solutions was used in the water balance calculations for the reclaim dam:

$$A_{RD} = 6.52 \times 10^{3} \cdot h_{RD} - 3.39 \times 10^{6} \quad [5.5]$$

$$V_{RD} = 2.13 \times 10^{3} \cdot h_{RD}^{2} - 2.21 \times 10^{6} \cdot h_{RD} + 5.75 \times 10^{8} \quad [5.6]$$

Where A_{RD} = reclaim dam water surface area (m^2),
V_{RD} = reclaim dam water storage volume (m^3), and
h_{RD} = reclaim dam water level (m).

The catchment area for the reclaim dam is 17.0 ha and a runoff factor of 0.4 (Gray, 1970; Gutteridge Haskins and Davey, 1984) was used to calculate the runoff volume. Appendix L contains details of the water balance calculations based on the following water balance expression for the reclaim dam:

$$V_{RD} = Q_P - Q_E + Q_R - S_B - S_W + P_{RDSD} + P_{SP} - P_{RD} - P_3 + Q_8 + E_2 + E_3 + E_4 \quad [5.7]$$

Where S_B = volume of seepage from reclaim dam base (m^3),
S_W = volume of seepage through reclaim dam wall (m^3),
P_{RDSD} = volume of water pumped from seepage dam to reclaim dam (m^3),
P_3 = volume of water pumped from reclaim dam to tailings impoundment (m^3),
Q_8 = volume of water from penstock decant (m^3),
E_2 = seepage volume from N RD section (m^3),
E_3 = seepage volume directly into reclaim dam from tailings impoundment (m^3), and
E_4 = seepage volume from eastern drain (m^3).

For the purpose calculating seepage through the dam wall and through the dam base foundation a permeability of 1 x 10^{-11} m/s was used (Gutteridge Haskins and Davey, 1984).

5.2.4 Reclaim Dam Seepage Dam

The reclaim dam seepage dam is located downstream of the reclaim dam to contain any seepage from either the tailings impoundment or reclaim dam. A manually activated pump with a capacity of 16 l/s has been installed to return any seepage or runoff from the seepage dam catchment to the reclaim dam. This occurs when the pond reaches a level of 519.9 mRL. This allows for an operational dam depth of 0.9 m since the dam base is at of level of 519.0 mRL. The dam crest is at 521.0 mRL, which includes a design freeboard of 0.5 m. Seepage from the North Dump (assumed to be constant at 2 l/s) also flows into this dam for return to the reclaim dam circuit. A storage curve for the seepage dam was established from survey data as described in Appendix L and the following best fit expressions are used in the water balance calculations for the seepage dam:

$$A_{RDSD} = 1.52 \times 10^{3} \cdot h_{RDSD} - 7.89 \times 10^{5} \qquad [5.8]$$

$$V_{RDSD} = -6.72 \times 10^{2} \cdot h_{RDSD}^{3} + 1.05 \times 10^{6} \cdot h_{RDSD}^{2} - 5.47 \times 10^{8} \cdot h_{RDSD} + 9.49 \times 10^{10} \qquad [5.9]$$

Where A_{RDSD} = seepage dam water surface area (m^2),
V_{RDSD} = seepage dam water storage volume (m^3), and
h_{RDSD} = seepage dam water level (m).

The catchment area for the seepage dam is 2.5 ha and a runoff factor of 0.4 (Gray, 1970; Gutteridge Haskins and Davey, 1984) was used to calculate the runoff volume. Appendix L contains details of the water balance calculations based on the following water balance expression for the seepage dam:

$$V_{RDSD} = Q_P - Q_E + Q_R + S_{ND} - P_{RDSD} + S_W \qquad [5.10]$$

Where S_{ND} = volume of seepage from the North Dump (m^3).

5.2.5 Tailings Impoundment

The components of the Kidston tailings impoundment closure water balance are shown in Figure 5.1. Figure 5.2(a) presents a more descriptive schematic of where these components lie with respect to the tailings impoundment layout. Figure 5.2(b) is s schematic showing the zones of the tailings impoundment seepage water balance components. The tailings impoundment itself has a closed surface catchment area of 310 ha, however an additional surface runoff catchment area of 104 ha is introduced due to the fact that the impoundment is constructed adjacent Paddy's Knob. In addition to the standard water balance components of precipitation, runoff and evapotranspiration that impacts on the catchment, the tailings impoundment loses water due to seepage. Most of the seepage is collected via interception drains around the impoundment perimeter, and subsequently returned to the water circuit. Deep seepage through the impoundment foundation is also expected, resulting in an additional loss of pond water.

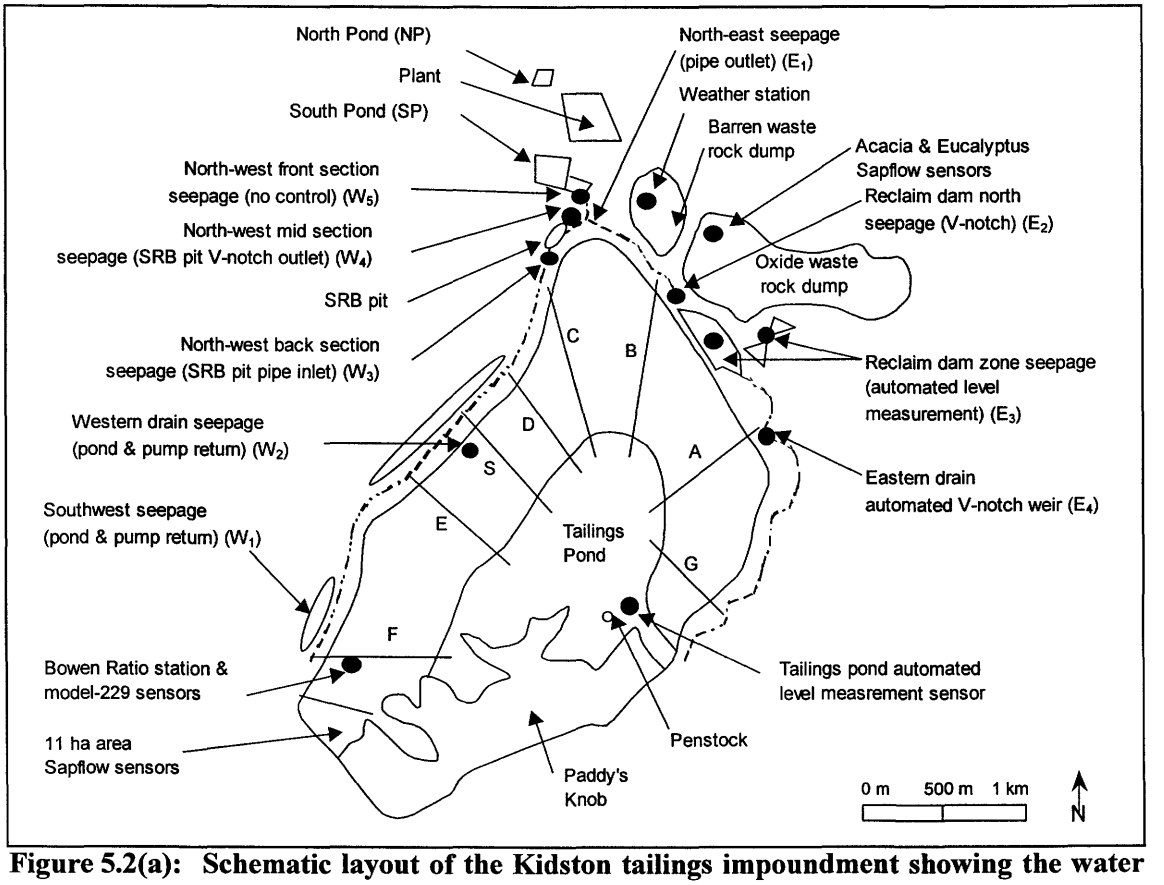

Figure 5.2(a): Schematic layout of the Kidston tailings impoundment showing the water balance components.

Although the tailings impoundment has not been in operation since October 1997, the pond water is still used as part of the mine water circuit. This means that when mill process water is

required penstock decants still occur, and when excess reclaim dam and south pond dam levels are reached, water is pumped to the tailings impoundment. On occasion the silt dam upstream of the south pond had to be dredged cleaned and the resulting slimes and water was also pumped onto the tailings impoundment. There are no records indicating when and how much water has been pumped onto or decanted from the tailings impoundment, which makes any water balance calculations subject to some interpretation. A further source of water to the tailings impoundment is irrigation water to support the establishment of vegetation on the tailings impoundment. The water balance for the tailings impoundment is complicated by the fact that infiltration and evapotranspiration into the exposed tailings play a vital role in the understanding of the system, and as such cannot be ignored or simply dealt with by means of runoff coefficients.

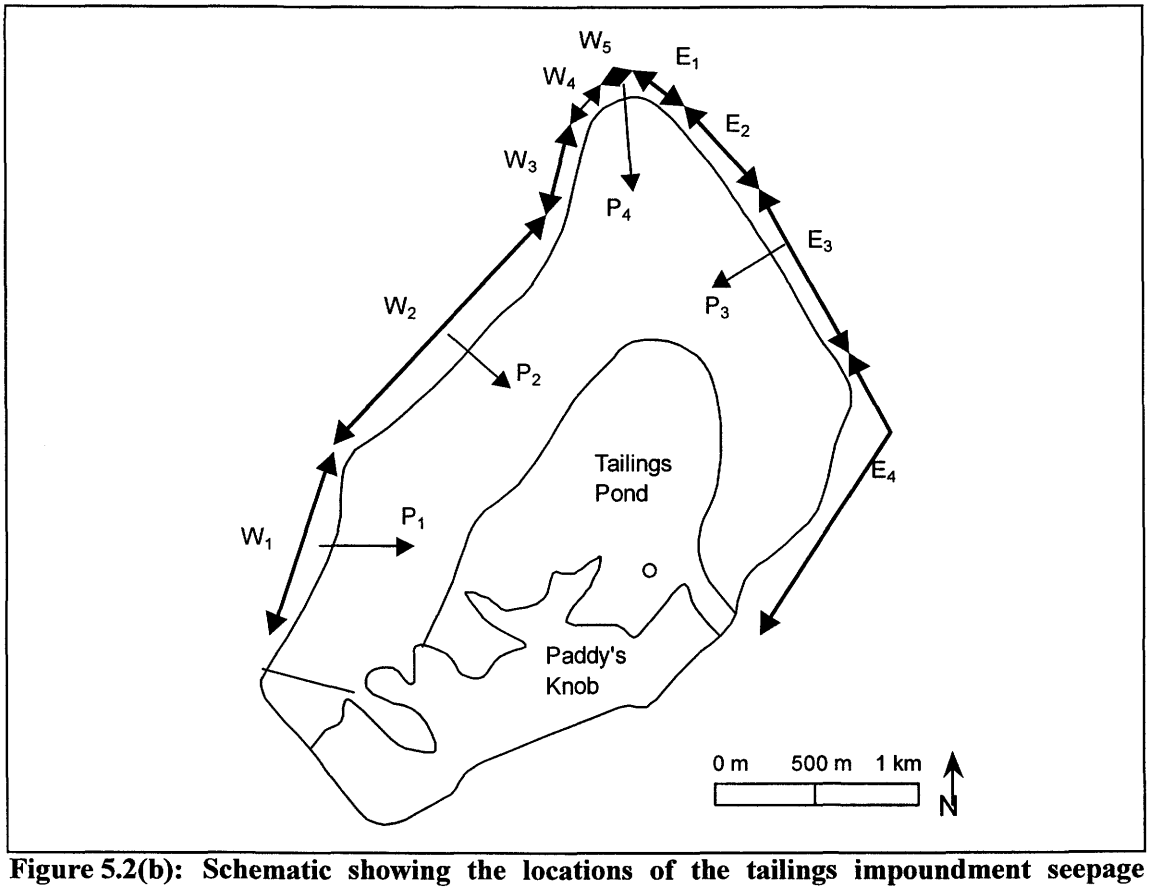

Figure 5.2(b): Schematic showing the locations of the tailings impoundment seepage components on the Kidston tailings impoundment.

Annual aerial surveys were obtained for the mine, including the tailings impoundment, and from this data a stage curve for the tailings impoundment pond has been developed as described in Appendix L. Survey data is only available for a pond level up to an elevation of 554.0 mRL, and therefore best fit expressions for the stage curve have been produced to make estimations

on the pond level and size beyond the range of measured data. The best-fit mathematical expressions for the Kidston tailings impoundment storage volume, and pond surface area, are respectively given as:

$$A = 1.21 \cdot h^2 - 1321.18 \cdot h + 359230 \qquad [5.11]$$

$$V = 5.68 \times 10^4 \cdot h^2 - 6.21 \times 10^7 \cdot h + 1.70 \times 10^{10} \qquad [5.12]$$

Where V = tailings impoundment pond storage volume (m^3),
A = tailings impoundment pond surface area (m^3), and
h = tailings pond elevation (m).

Monitoring the tailings pond level allows calculation of the tailings pond area, as well as the exposed dry tailings area and thus computation of the water balance components shown in Figure 5.3. The tailings dam water balance is determined using the following equation:

$$\Delta S = Q_1 - Q_3 + Q_5 - Q_6 - Q_8 + Q_9 + Q_{10} + \Delta Q_{12} - Q_{13} \qquad [5.13]$$

Where ΔS = change in tailings pond storage volume (m^3),
Q_1 = volume of precipitation falling on pond area (m^3),
Q_3 = volume of potential evaporation from pond area (m^3),
Q_5 = volume of runoff water from Paddy's Knob (m^3),
Q_6 = volume of seepage loss from tailings impoundment (m^3),
Q_8 = volume of penstock decant (m^3),
Q_9 = volume of irrigation water (m^3),
Q_{10} = volume of water pumped back to tailings impoundment (m^3),
ΔQ_{12} = volume of moisture retained by unsaturated tailings zone (m^3), and
Q_{13} = volume of water released as the tailings consolidate (m^3).

The tailings consolidation takes place over an extremely long period of time (often 100 years or more). The volume of water associated with this component can be substantial soon after deposition, but after a number of years the release of water via this route becomes less prominent. There is no evidence at Kidston that consolidation water is a significant contributor

towards the seepage volume and as such it has been considered to be negligible for the purpose of these calculations.

The tailings storage component, ΔQ_{12}, is the exposed tailings surface flux, and is calculated as follows:

$$\Delta Q_{12} = Q_2 - Q_4 = Q_7 + Q_{11} - Q_4 \qquad [5.14]$$

Where Q_2 = volume of precipitation falling on exposed tailings impoundment (m^3),

Q_4 = volume of actual evapotranspiration from exposed tailings impoundment (m^3),

Q_7 = volume of runoff from exposed tailings impoundment into pond (m^3), and

Q_{11} = volume of rainfall infiltrating into the exposed tailings surface (m^3).

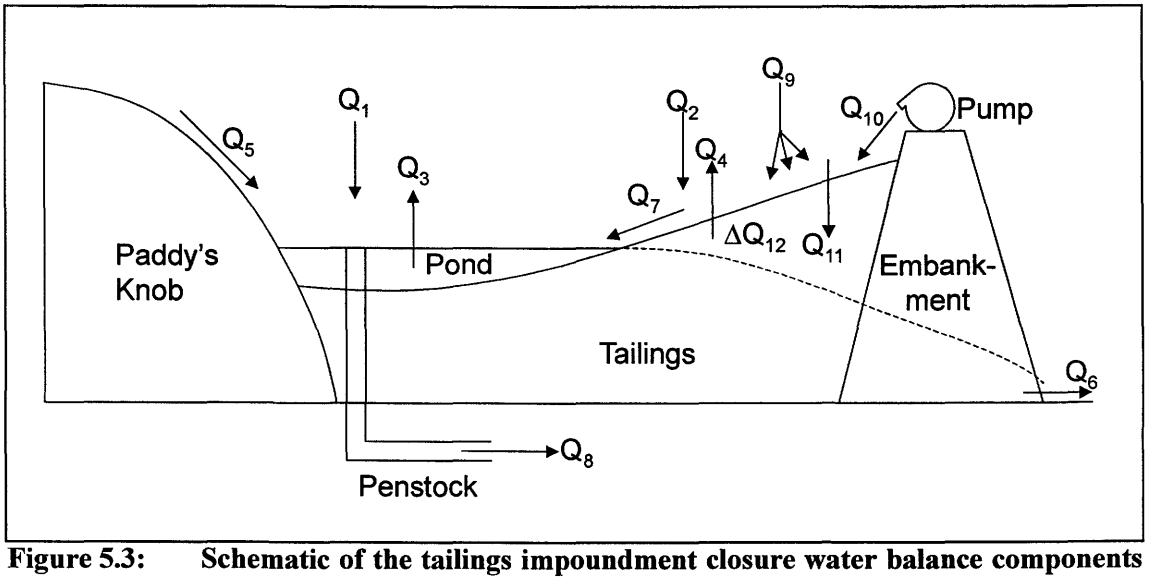

Figure 5.3: Schematic of the tailings impoundment closure water balance components required for solving Equation 5.13.

The individual components Q_1, Q_2, Q_3, Q_4 and Q_5 are calculated as follows:

$$Q_1 = (A_{pond})P \qquad [5.15]$$

$$Q_2 = (A_{dam} - A_{pond})P \qquad [5.16]$$

$$Q_3 = (A_{pond})PE \quad [5.17]$$

$$Q_4 = (A_{dam} - A_{pond})AE \quad [5.18]$$

$$Q_5 = A_{paddy}(P \cdot R_f) \quad [5.19]$$

Where A_{pond} = area of the tailings pond (m^2),
A_{dam} = total area of the tailings impoundment (m^2),
A_{paddy} = catchment area for Paddy's Knob impacting on the tailings impoundment (m^2),
P = precipitation (m),
PE = potential evaporation (m),
AE = actual evaporation (m), and
R_f = Paddy's Knob runoff factor (-).

The tailings impoundment seepage volume, Q_6, is calculated as follows:

$$Q_6 = W + E + D \quad [5.20]$$

Where W = total western seepage drain volume (m^3),
E = total eastern seepage drain volume (m^3), and
D = total tailings dam deep seepage volume (m^3).

The seepage components, W and E are calculated as follows:

$$W = W_1 + W_2 + W_3 + W_4 + W_5 \quad [5.21]$$

$$E = E_1 + E_2 + E_3 + E_4 \quad [5.22]$$

Where W_1 = seepage volume from the Southwest section (m^3),
W_2 = seepage volume from the Western drain (m^3),
W_3 = seepage volume from the NW back section (m^3),
W_4 = seepage volume from the NW mid section (m^3),

W_5 = seepage volume from the NW front section (m^3),

E_1 = seepage volume from the NE pipe section (m^3),

E_2 = seepage volume from the North reclaim dam section (m^3),

E_3 = seepage volume directly into the reclaim dam (m^3), and

E_4 = seepage volume from the Eastern drain (m^3).

The pump back volume Q_{10} are calculated as follows:

$$Q_{10} = P_1 + P_2 + P_3 + P_4 \qquad [5.23]$$

Where P_1 = volume of seepage pumped back from the Southwest section (m^3),

P_2 = volume of seepage pumped back from the Western drain (m^3),

P_3 = volume of water pumped from the reclaim dam (m^3), and

P_4 = volume of water pumped from the south pond (m^3).

Equation 5.13 can thus be rewritten in terms of the runoff volume, Q_7, and Equations 5.14 through 5.23 can be substituted, to allow an expression that could be used to calculate the tailings impoundment surface runoff. This expression is:

$$\begin{aligned} Q_7 = {} & \Delta S - (A_{pond})P + (A_{pond})PE + (A_{dam} - A_{pond})AE - A_{paddy}(P \cdot R_f) \\ & + W_1 + W_2 + W_3 + W_4 + W_5 + E_1 + E_2 + E_3 + E_4 + D + Q_8 - Q_9 - P_1 - P_2 \\ & - P_3 - P_4 - Q_{11} \end{aligned} \qquad [5.24]$$

5.3 Tailings Impoundment Water Balance Data Set

The preceding sections describe all the water balance components and the equations and conditions required to calculate a water balance for the Kidston tailings impoundment. It was necessary to extend the water balance to this level, since accurate records do not exist for the decant and pumping volumes to the tailings impoundment. A total water balance is the only way to estimate these volumes and thus reduce the uncertainty of the calculations. The entire water balance discussed in this chapter required direct measurement of the water levels in the tailings pond. Water balance calculations presented in the following sections are done in batch calculations based on spot water level readings with a frequency varying between one week to a

couple of months. A complete water balance calculation corresponding to the period between readings was performed for each day that a pond level measurement was available.

The solution of Equation 5.24 rest on the water balance components of precipitation (Q_P, Q_1, Q_2), evaporation/evapotranspiration (Q_E, Q_3, Q_4), runoff (Q_R, Q_5, Q_7), irrigation (Q_9), seepage (Q_6), penstock decant (Q_8), and pumping to the tailings impoundment (Q_{10}). The following sections describe how each of the data sets was generated and applied for use in the water balance calculations.

5.3.1 Tailings Pond Levels

The pond level has been manually measured by Kidston mine site personnel since 8 September 1997, at intervals ranging between weekly and monthly increments. In December 2000, the author installed an automated water level sensor to continuously log the tailings impoundment pond level. Figure 5.4 presents the recorded pond levels together with some spot manual measurements for the period between December 2000 and April 2001.

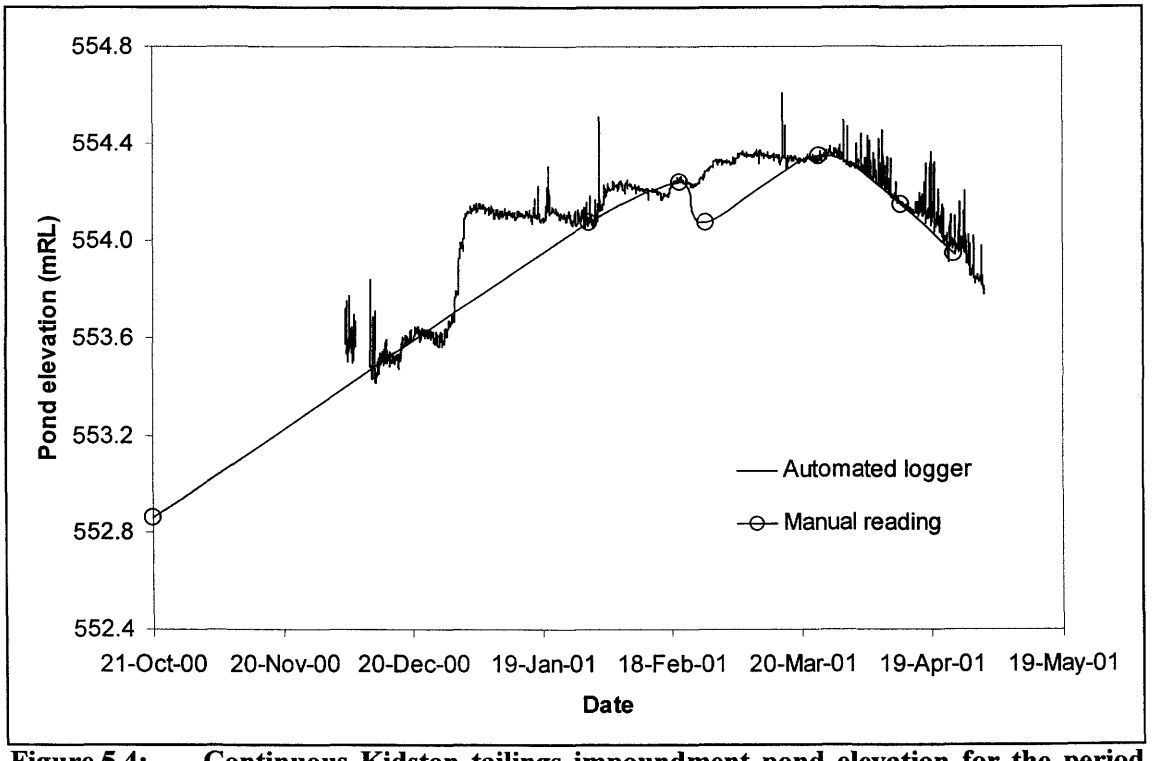

Figure 5.4: Continuous Kidston tailings impoundment pond elevation for the period between December 2000 and April 2001.

The pond level fluctuated seasonally approximately one meter in elevation, with a recorded maximum pond elevation of 554.35 mRL and a recorded minimum elevation of 552.53 mRL (1.82 m range). The complete pond elevation versus time data set is presented in Appendix F, with the details for the automated level sensor installation described in Appendix G. Appendix L contains the detailed data for each date that the pond level was recorded and subsequently used in the water balance calculations. The measured pond levels were used to estimate the change in the pond storage volume, ΔS as shown in Equation 5.13.

5.3.2 Precipitation

The daily total precipitation as measured with an automated tipping bucket raingauge is described in Appendix H. The cumulative precipitation for the period between 8 September 1997, and 30 April 2001 is presented in Figure 5.5. The cumulative precipitation for this period amounts to 2293.6 mm (Appendix J provides the complete set of precipitation data). This precipitation was measured on the adjacent Barren waste rock dump as shown in Figure 5.2(a).

The cumulative precipitation volumes together with pond level measurement dates are summarized in tabular form in Appendix L. This includes Q_1 and Q_2 for the tailings impoundment, and Q_P for all the other dams and ponds of the system.

5.3.3 Evaporation/Evapotranspiration

Daily pan evaporation (Class A-pan) rate was measured at the main security gate on the Kidston Gold Mine and is summarized in Appendix I. Unfortunately the pan is not well placed to be able to provide representative evaporation numbers for the tailings impoundment surface. The pan is situated less than 100 m north-east of the tailings impoundment, and as a result the tailings impoundment acts as a windbreak, effectively altering the evaporation regime at the pan as opposed to that on the tailings impoundment surface. Subsequently a field experiment was undertaken to measure the pan evaporation from the top of the tailings impoundment surface over short periods of time, between December 2000 and April 2001. The data from this experiment was used in an attempt to adjust the A-pan data such that it would be representative of the evaporation regime on the tailings impoundment surface. The details of this analysis are documented in Appendix I.

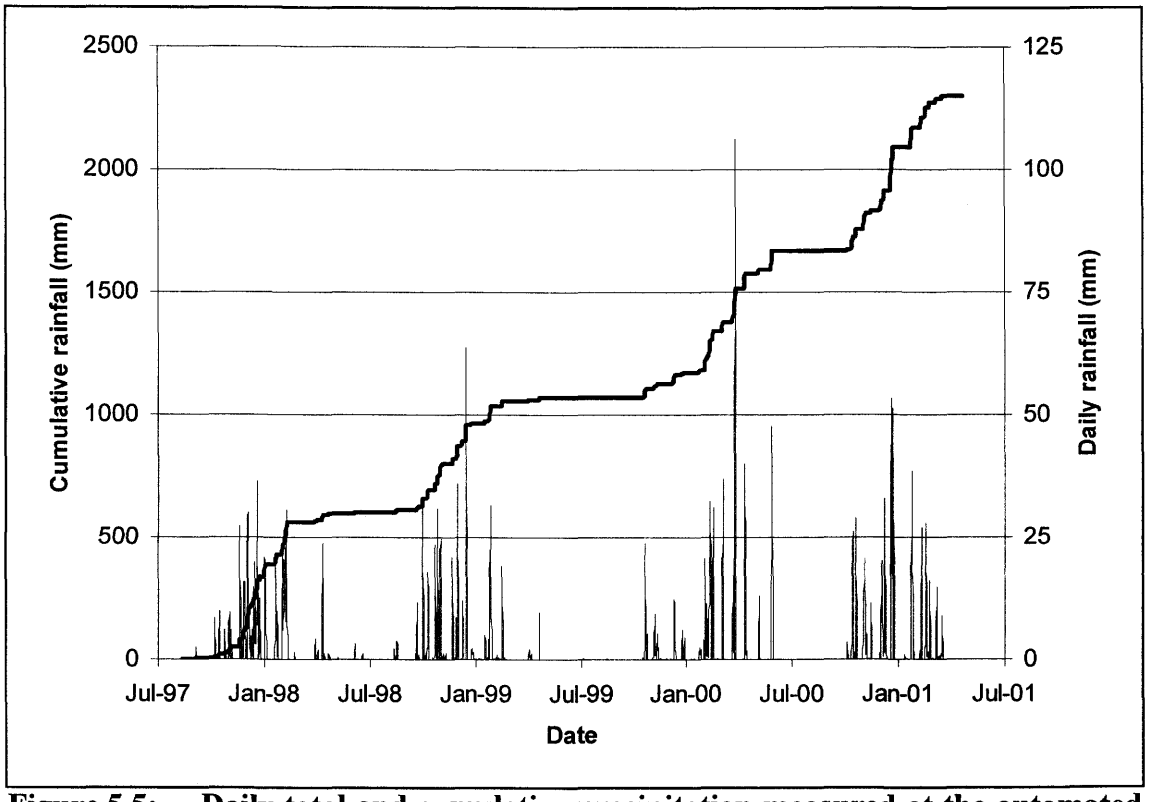

Figure 5.5: Daily total and cumulative precipitation measured at the automated tipping bucket raingauge for the period 8 September 1997 to 30 April 2001.

The evaporation experiment was not entirely successful, as the amount of collected data was not sufficient to conclusively establish a relationship between the evaporation rate on the tailings impoundment surface and at the security gate. The data does however suggest a tendency for the evaporation rate on the tailings impoundment surface to be approximately 10% higher than at the security gate. This is entirely feasible, especially if one considers the possible oasis effect that the tailings impoundment pond would have in this otherwise arid climate (Oke, 1987).

It was subsequently decided that daily potential evaporation from the pond surface would be calculated from the daily weather station data presented in Appendix H. The Penman method (Penman, 1948) was used to calculate the potential evaporation, and this choice was based on the fact that the SoilCover (SoilCover, 1997) numerical model could be used to verify this data. The total cumulative daily potential evaporation between each pond level measurement period is tabled in Appendix L. The total cumulative potential evaporation for the period between 8 September 1997 and 30 April 2000, was computed to be 6009.0 mm, which is almost 3 times greater than the rainfall.

The evapotranspiration rate from the exposed tailings surface had to be estimated somehow, and for the purpose of the calculations in this thesis is was done by applying an actual evaporation/potential evaporation (AE/PE) ratio of 0.2. The choice of this number was based on a number of trial SoilCover (SoilCover, 1997) numerical model runs for simple one-dimensional tailings profiles with varying depths to the phreatic level. These data are not presented in the thesis, as the runs were simplistic and served only to find some guideline as to an appropriate AE/PE ratio.

5.3.4 Runoff Coefficients

For the calculation of the runoff volume from Paddy's Knob, Q_5, and all other runoff volumes in the ponds and dams, Q_R, a runoff factor of 0.4 was used. Data reported by Gutteridge Haskins and Davey (1984) suggested a runoff factor between 0.18 and 0.42 for the natural catchments of the Kidston surrounding areas. The lower runoff factors were obtained from the nearby Einasleigh and Narrawa catchments, which closely resembles the topography and soils of the Butchers Creek catchment that the Kidston Mine falls into. However, higher runoff factors were recorded in the Middle Creek Gap catchment, which consist of rocky knolls, not unlike Paddy's Knob. Therefore a runoff factor of 0.4 was chosen for Paddy's Knob. Since the catchments of the other ponds and dams have been disturbed due to the mining operations, using the lower runoff factor for them would not be reasonable as higher runoff rates would be expected, and thus a runoff factor of 0.4 was selected for all the other catchments in this study.

Further investigation to determine the runoff coefficients for natural and disturbed catchments was carried out based on the hydrology principles reported by Gray (1970). Based on this work, a runoff coefficient factor for the topography, $C_t = 0.1$ was determined. The runoff coefficient factor for the soil type, C_s was set equal to 0.3 and a runoff coefficient for the cover type, $C_c = 0.2$ was selected. These give a combined runoff coefficient of $C = 0.6$, and the runoff factor is then calculated by subtracting C from 1.0, for $R_f = 0.4$. This value is in good agreement with the empirical method reported by Gutteridge Haskins and Davey (1984).

5.3.5 Irrigation

Irrigation was done periodically on the tailings impoundment surface to allow the establishment of the tree stock that had been planted as part of the vegetation trials. The irrigation was carried

out by means of individual drip feed to each tree, with an equivalent application rate of 3 l/hr per 50 m^2. At any time the irrigation is only applied to a maximum surface area of 55 ha, and irrigation is only done in 3 month continuous increments, normally during the early dry part of the growth season, (August onwards). For the purpose of the water balance calculation the constant irrigation rate over the entire 55 ha area during the months of irrigation was computed as 9.2 l/s.

5.3.6 Seepage Volumes

Seepage from the tailings impoundment is collected in a drainage ditch around the impoundment perimeter. Portions of this can be physically measured and the sections below describe how and where these seepage rates are monitored. The results of two periods of seepage monitoring is presented, allowing for good judgements to be made regarding actual seepage rates from the tailings impoundment. This section is concluded with a simplified theoretical methodology to calculate the seepage rates from the tailings impoundment. This calculation is necessary since field measurements cannot physically be made everywhere due to practical constraints. The simplified theoretical seepage calculation is used to calculate Q_6 in Equation 5.24.

5.3.6.1 Seepage Measuring Devices

The tailings embankment wall were designed with chimney and blanket drains that would allow the seepage to exit at controlled points at the base of the embankment walls. The Kidston Gold Mine constructed a deep collection ditch around the perimeter of the tailings impoundment to intercept seepage for containment within the polluted water circuit of the mine. Measurement of the seepage rates along portions of the drainage ditches have been done by Kidston on intermitted occasions, consisting mainly of manual spot readings at V-notch weirs and overflows.

As part of this study, the seepage regime of the dam was investigated for the 2000/2001 wet season based on a detailed field measurement program to accurately measure seepage rates. This program, which ran from December 2000 to April 2001, included continuous flow measurements using automated water level sensors and data acquisition systems. Table 5.1 describes the identified seepage zones of the tailings impoundment along with the seepage

monitoring history and the seepage measuring components installed for this study. The locations of these components are indicated on Figures 5.2(a) and (b). The flow measuring equipment and the installation thereof are described in detail in Appendix G.

Table 5.1: Components of the Kidston tailings impoundment field seepage measurement for the study period December 2000 to April 2001.

Seepage component	Historical measurement	Revised measurement
Southwest seepage (pond & pump return)	Not detected	Manual recording of pump return volume.
Western drain seepage (pond & pump return)	Intermitted flow monitoring on tailings dam using flow wheel	Manual measurement of pump flow volume and rate over V-notch on dam surface and noting recharge timing for seepage pond.
Northwest back section seepage (SRB pond pipe inlet)	Not detected	Regular manual flow rate measurement from pipe inlet.
Northwest mid section seepage (SRB pond outlet V-notch weir)	Not detected	Regular manual flow rate measurement over V-notch weir.
Northwest front section seepage (no control)	Not detected	Manual flow estimation based on Northwest mid section seepage volume.
Eastern drain seepage (V-notch weir)	Intermitted manual flow rate measurement	Continuous flow rate measurement over V-notch weir using a pressure sensor and data acquisition system.
Reclaim dam north seepage	Once-off manual flow rate measurement	Regular manual flow rate measurement over V-notch weir.
Direct seepage into Reclaim dam	Not detected	None, reclaim dam level monitored continuously with automated level pressure sensor and data acquisition system.
Northeast seepage (pipe outlet)	Not detected	Regular manual flow rate measurement from pipe outlet.
Deep foundation seepage	Not detected	None.

5.3.6.2 Measured Seepage Rates

Kidston Gold Mine undertook a yearlong seepage-monitoring program between October 1998 and November 1999. During this period some of the seepage rates emanating from the tailings impoundment seepage drains were manually measured. The results of this are listed in Table 5.2. It should be noted that these flow rates include surface runoff that have entered the seepage drains, and are thus an overestimation of the actual seepage rate from the tailings impoundment.

The surface runoff eluded to here are runoff from the area between the outer tailings impoundment embankment and the seepage collection ditch as shown in Figure 5.6.

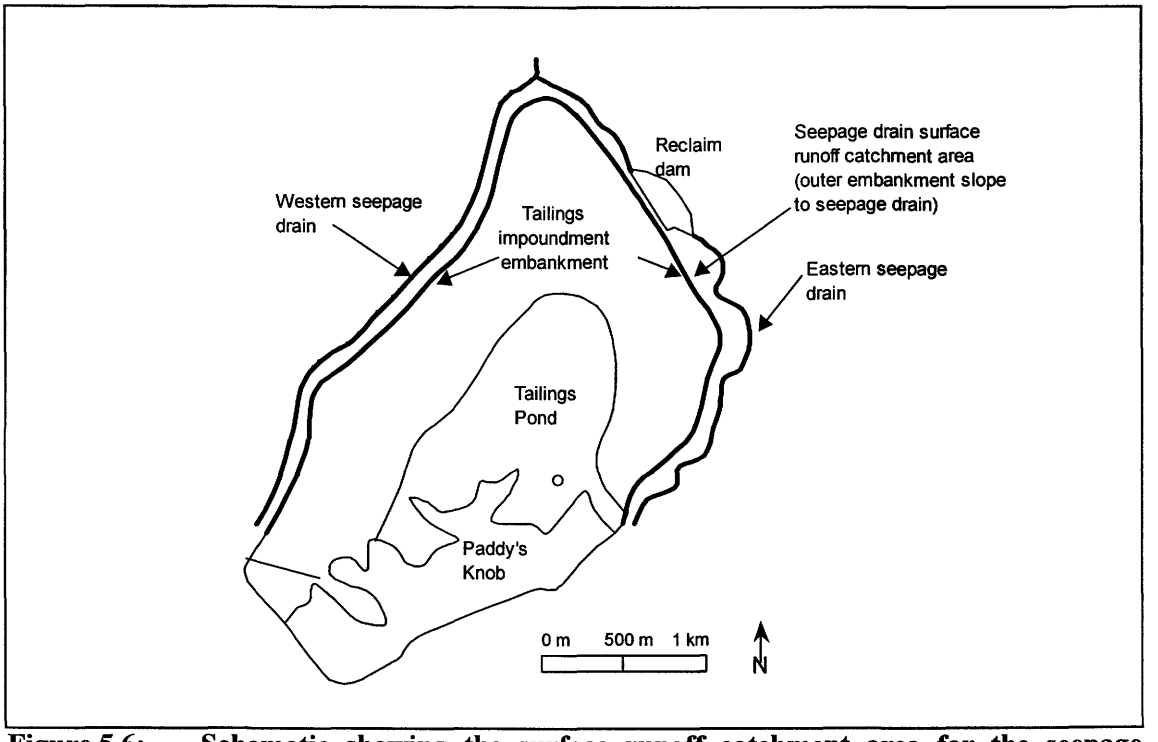

Figure 5.6: Schematic showing the surface runoff catchment area for the seepage collection ditch.

Table 5.2: Seepage rates (l/s) from the Kidston tailings impoundment seepage drains as manually measured by Kidston Gold Mines between October 1998 and November 1999.

Sample date	North reclaim dam (E_2)	Eastern drain (E_4)	Total eastern seepage (E)	NW back, mid, & front ($W_3+W_4+W_5$)	Western drain (W_2)	Total Western seepage (W)	Overall total seepage (E+W)
8-Oct-98	nd	4.00	4.00	nd	nd	nd	4.00
12-Oct-98	1.90	5.00	6.90	2.14	nd	2.14	9.04
19-Oct-98	1.20	5.30	6.50	1.70	nd	1.70	8.20
26-Oct-98	0.99	4.00	4.99	1.60	nd	1.60	6.59
1-Nov-98	nd	6.00	6.00	nd	nd	nd	6.00
2-Nov-98	1.50	5.00	6.50	3.00	nd	3.00	9.50
10-Nov-98	1.50	6.00	7.50	2.50	nd	2.50	10.00
16-Nov-98	1.23	6.00	7.23	1.30	2.72	4.02	11.25
24-Nov-98	1.50	9.00	10.50	1.40	nd	1.40	11.90
30-Nov-98	1.50	6.00	7.50	1.10	1.83	2.93	10.43
11-Jan-99	nd	6.00	6.00	0.95	2.61	3.56	9.56
1-Feb-99	nd	nd	Nd	nd	3.22	3.22	3.22
18-Feb-99	0.78	11.30	12.08	3.60	2.62	6.22	18.30
28-Jul-99	0.45	7.10	7.55	0.67	1.81	2.48	10.03
9-Sep-99	0.40	5.23	5.63	0.40	0.74	1.14	6.76

Table 5.2: Seepage rates (l/s) from the Kidston tailings impoundment seepage drains as manually measured by Kidston Gold Mines between October 1998 and November 1999.

Sample date	North reclaim dam (E_2)	Eastern drain (E_4)	Total eastern seepage (E)	NW back, mid, & front (W_3 +W_4+W_5)	Western drain (W_2)	Total Western seepage (W)	Overall total seepage (E+W)
10-Oct-99	0.99	7.06	8.05	1.00	nd	1.00	9.05
3-Nov-99	1.04	6.75	7.79	0.83	0.33	1.16	8.95
Average	1.15	6.23	7.17	1.59	1.98	2.54	9.71

nd = no data available, not measured by Kidston Gold Mine.

In December 2000 additional seepage flow rate measuring devices were installed as described in Appendix G and the seepage flow rates was measured until April 2001. The results of this monitoring period are summarized in Tables 5.3 through 5.5. Again the seepage rates reported includes surface runoff that enters the open seepage drains. The flow rate reported in Table 5.3 for the Eastern drain is an average flow rate for the period between measurements, based on the continuous flow record available from the automated measuring station.

Table 5.3: Seepage rates from the Kidston tailings impoundment eastern seepage drains as manually or automatically measured by Kidston Gold Mines between December 2000 and April 2001.

Sample date	NE pipe, E_1 (l/s)	North reclaim dam, E_2 (l/s)	Eastern drain, E_4 (l/s)	Total Eastern seepage, E (l/s)
1-Dec-00	nd	nd	nd	nd
20-Dec-00	nd	nd	4.12	4.12
12-Jan-01	0.439	nd	10.21	10.65
16-Jan-01	1.270	5.50	4.08	10.85
9-Feb-01	0.582	3.90	6.00	10.48
19-Feb-01	nd	nd	12.11	12.11
27-Feb-01	1.000	3.15	nd	4.15
14-Mar-01	0.950	2.14	5.41	8.50
20-Mar-01	0.869	2.72	5.02	8.61
19-Apr-01	0.540	1.80	nd	2.34
Average	0.807	3.20	6.71	7.98

nd = no data available, not measured by Kidston Gold Mine.

Table 5.4: Seepage rates from the Kidston tailings impoundment western seepage drains as manually measured by Kidston Gold Mines between December 2000 and April 2001.

Sample date	NW back, W_3 (l/s)	NW mid, W_4 (l/s)	NW front, W_5 (l/s)	Western drain, W_2 (l/s)	Total Western seepage, W (l/s)
1-Dec-00	nd	0.39	nd	nd	0.39
20-Dec-00	nd	0.81	nd	nd	0.81

Table 5.4: Seepage rates from the Kidston tailings impoundment western seepage drains as manually measured by Kidston Gold Mines between December 2000 and April 2001.

Sample date	NW back, W_3 (l/s)	NW mid, W_4 (l/s)	NW front, W_5 (l/s)	Western drain, W_2 (l/s)	Total Western seepage, W (l/s)
12-Jan-01	nd	0.83	nd	nd	0.83
16-Jan-01	nd	0.88	0.31	0.57	1.75
9-Feb-01	nd	0.98	0.23	0.76	1.97
19-Feb-01	nd	2.00	0.40	1.60	4.00
27-Feb-01	3.92	2.36	1.10	1.27	8.64
14-Mar-01	nd	1.18	0.58	0.60	2.35
20-Mar-01	0.92	1.18	0.45	0.73	3.27
19-Apr-01	1.50	1.18	0.56	0.62	3.86
Average	2.11	1.18	0.52	0.88	2.79

nd = no data available, not measured by Kidston Gold Mine.

Table 5.5: Summary of the seepage rates from the Kidston tailings impoundment seepage drains as manually and automatically measured by Kidston Gold Mines between December 2000 and April 2001.

Sample date	Total Western seepage, W (l/s)	Total Eastern seepage, E (l/s)	Total overall seepage, W+E (l/s)
1-Dec-00	0.385	nd	0.39
20-Dec-00	0.812	4.12	4.93
12-Jan-01	0.825	10.65	11.48
16-Jan-01	1.750	10.85	11.68
9-Feb-01	1.968	10.48	12.45
19-Feb-01	4.000	12.11	16.11
27-Feb-01	8.640	4.15	12.79
14-Mar-01	2.352	8.50	10.85
20-Mar-01	3.272	8.61	11.88
19-Apr-01	3.860	2.34	6.20
Average	2.786	7.98	10.77

nd = no data available, not measured by Kidston Gold Mine.

The results in Table 5.2 state that for the period between October 1998 through November 1999 the average seepage rate from the seepage collection ditch ranged between 3.2 and 18.3 l/s with an average number of 9.7 l/s. Similarly the data in Table 5.5 state that for the period between December 2000 and April 2001 the seepage rate ranged between 0.4 and 16.1 l/s with an average rate of 10.8 l/s.

5.3.6.3 Simplified Theoretical Seepage Rate Calculation

Since the seepage rates at every point along the tailings impoundment perimeter cannot practically be physically measured, a simple method was implemented to theoretically estimate the seepage rates for all the sections of the seepage drain indicated on Figure 5.2 (a) and (b), and described by Equations 5.20 through 5.22. A first order calculation of the seepage through the tailings dam reporting to each of the seepage sections in Figure 5.2(b) can be made using the Darcy equation (Holtz and Kovacs, 1981), and the components of Equation 5.25 below are presented in Figure 5.7:

$$q = kiA = k\frac{\Delta h}{L}A \qquad [5.25]$$

Where, q = seepage flow rate (m^3/s),
k = tailings permeability (m/s),
i = hydraulic gradient (-),
A = seepage area (m^2),
Δh = change in headloss (m), and
L = Length of seepage zone (m).

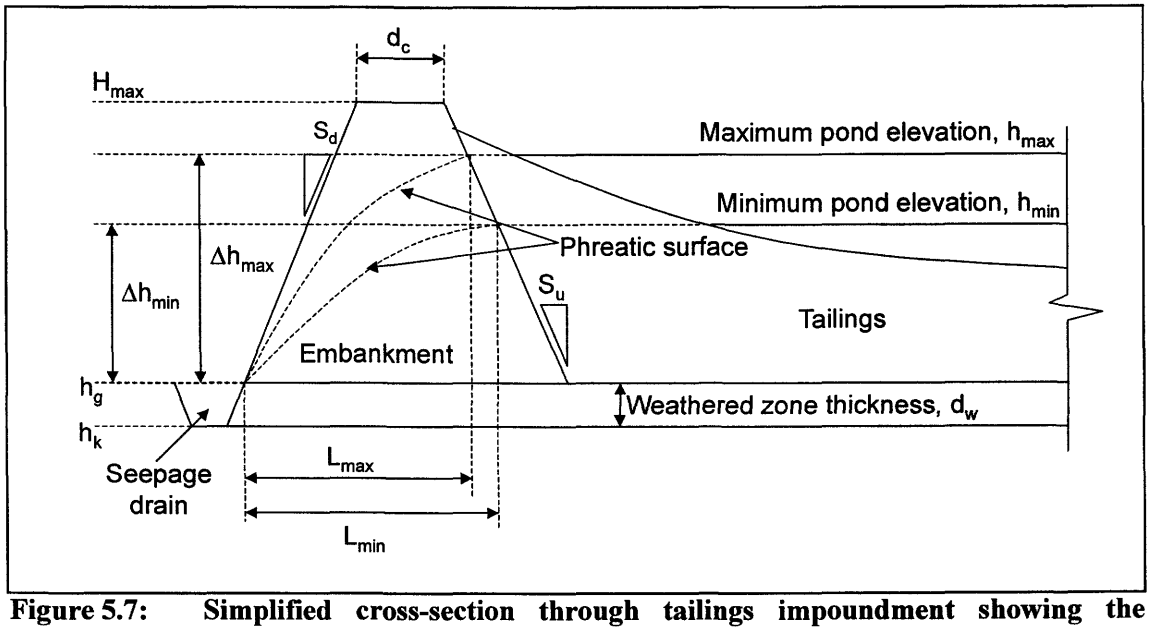

Figure 5.7: Simplified cross-section through tailings impoundment showing the components of Equation 5.25.

Table 5.6 lists the assumed constants for the theoretical seepage calculations while Tables 5.7 and 5.9 summarize the physical tailings impoundment dimensions that is relevant to each seepage zone of the tailings impoundment for which a theoretical calculation has been made. The resultant seepage rates for each seepage zone is listed in Tables 5.8 and 5.10 for the western and eastern seepage zones of the tailings impoundment respectively. The permeability used for the calculation in Tables 5.8 and 5.10 are an average, maximum or minimum value to provide a range of seepage results. These permeability values are based on the laboratory and in-situ testing as reported in Chapter 4. The maximum and minimum head reported in Tables 5.8 and 5.10 correspond to conditions associated with a maximum and a minimum measured tailings pond level respectively as indicated in Figure 5.7.

Table 5.6: Assumed constants used in the simplified seepage calculations for the Kidston tailings impoundment.

Parameter	Symbol	Value
Maximum tailings pond level	h_{max}	554.35 mRL
Minimum tailings pond level	h_{min}	552.53 mRL
Maximum tailings impoundment wall height	H_{max}	559.50 mRL
Assumed thickness of weathered layer	d_w	0.5 m
Wall crest width	d_c	6.0 m
Upstream wall slope	$1:S_u$	1:1.35
Downstream wall slope	$1:S_d$	1:1.35
Minimum tailings permeability	$k_{s(min)}$	4.88E-09
Maximum tailings permeability	$k_{s(max)}$	5.26E-05
Average tailings permeability	$k_{s(avg)}$	9.79E-06

Table 5.7: Physical Kidston tailings impoundment dimensions relevant to the western seepage drains.

Component	SW (W_1)	Western drain (W_2)	NW back (W_3)	NW mid (W_4)	NW front (W_5)
Ground level at wall base, h_g (mRL)	555.0	539.1	546.3	542.9	539.5
Cut-off key base elevation, h_k (mRL)	554.5	538.6	545.8	542.4	539.0
Length of seepage front, L_s (m)	875.0	1300.0	650.0	50.0	125.0
Seepage area, A (m^2)	437.5	650.0	325.0	25.0	62.5

The application of Equation 5.25 to the SW seepage zone, W_1 results in a negative seepage rate being calculated. The reason for this is due to the fact that the pond level drops below the embankment wall key level. Physically this means that the seepage from this zone is zero, and this fact is proven by the piezometer level measurements taken along section line F of the tailings impoundment as described in Appendix F. This is further supported by visual

observations by the mine personnel that no seepage had to be pumped back to the impoundment since 1996.

Table 5.8: Theoretical seepage rates (l/s) for the Kidston tailings impoundment western seepage drains.

Seepage component	Average k_s		Minimum k_s		Maximum k_s		Overall average
	Max head	Min head	Max head	Min head	Max head	Min head	
SW section (W_1)	0.00	0.00	0.00000	0.00000	0.00	0.00	0.00
Western drain (W_2)	2.40	1.99	0.00119	0.00099	12.88	10.69	4.66
NW back (W_3)	0.84	0.60	0.00042	0.00030	4.49	3.22	1.53
NW mid (W_4)	0.08	0.06	0.00004	0.00003	0.43	0.34	0.15
NW front (W_5)	0.23	0.19	0.00011	0.00009	1.22	1.01	0.44
Western total (W)	3.54	2.84	0.00176	0.00142	19.01	15.26	6.78

Table 5.9: Physical Kidston tailings impoundment dimensions relevant to the eastern seepage drains.

Component	NE Pipe (E_1)	North reclaim dam (E_2)	Reclaim dam direct (E_3)	Eastern Drain (E_4)
Ground level at wall base, h_g (mRL)	544.0	528.1	533.6	540.4
Cut-off key elevation, h_k (mRL)	544.0	528.1	533.6	540.4
Length of seepage front, L_s (m)	350.0	475.0	450.0	1600.0
Seepage area, A (m^2)	175.0	237.5	225.0	800.0

Table 5.10: Theoretical seepage rates (l/s) for the Kidston tailings impoundment eastern seepage drains.

Seepage component	Average k_s		Minimum k_s		Maximum k_s		Overall average
	Max head	Min head	Max head	Min head	Max head	Min head	
NE pipe (E_1)	0.52	0.40	0.00026	0.00020	2.81	2.16	0.98
N reclaim dam (E_2)	1.10	0.98	0.00055	0.00049	5.92	5.28	2.21
Reclaim dam (E_3)	0.95	0.83	0.00048	0.00041	5.13	4.45	1.89
Eastern drain (E_4)	2.82	2.31	0.00141	0.00115	15.17	12.41	5.45
Eastern total (E)	5.40	4.52	0.00269	0.00225	29.03	24.30	10.54

The deep seepage component refers to the potential for deep recharge via the foundation materials of the tailings impoundment. The intact permeability of these foundation materials was measured by Gutteridge Haskins and Davey (1984) and has been reported in Chapter 3. In calculating the deep seepage an assumption has been made that the pool size is constant at 100 ha, the hydraulic gradient is constant at 1, and foundation permeability's are as follows; average = 9.6×10^{-9} m/s; minimum = 1.0×10^{-10} m/s; maximum = 3.1×10^{-8} m/s. The resultant deep seepage rates are listed in Table 5.11.

Table 5.11: Summary of the theoretical seepage rates (l/s) for the entire Kidston tailings impoundment.

Seepage component	Average k_s		Minimum k_s		Maximum k_s		Overall average
	Max head	Min head	Max head	Min head	Max head	Min head	
Western seepage total	3.54	2.84	0.00176	0.00142	19.01	15.26	6.78
Eastern seepage total	5.40	4.52	0.00269	0.00225	29.03	24.30	10.54
Total Drain seepage	8.94	7.36	0.00446	0.00367	48.05	39.56	17.32
Deep seepage	9.56		0.10		31.00		13.55
Overall Seepage	18.50	16.92	0.105	0.103	79.05	70.56	30.87

The theoretical seepage calculations described in the preceding sections have been used in the tailings impoundment water balance, as documented in Appendix L. Due to the limited amount of actual seepage data available, it was deemed to provide the best overall solution. A comparison between the actual cumulative actual seepage volume for each of the two monitored periods listed in Tables 5.2 and 5.5 with the theoretical calculated cumulative volumes indicated that the theoretical seepage volumes are approximately 10-15% lower than the actual measured rates. A simple comparison shows that this difference is reasonable considering the fact that the actual measured rates include some runoff during storm events, especially the eastern drain.

5.3.7 Penstock Decant Volumes

Kidston Gold Mines did not measure the penstock decant volumes with flowmeters, as the discharge was generally associated with automated level switching on the reclaim dam. The reclaim dam stage curve is known, so Kidston knew what the decant volume is based on the reclaim dam level prior to and after a decant episode. The tailings pond held more water than the mill ever required, which allowed Kidston mine site personnel to operate the decant system without keeping detailed records.

For the purpose of this study it was imperative to quantify the penstock decant volumes, and therefore the reclaim dam, seepage dam, south- and north ponds were included in the water balance calculations. The penstock decant volume was calculated in two ways. Firstly as part of the tailings impoundment water balance, the penstock decant was allowed to occur when after the balance was calculated, there was still an excess of water, i.e. the excess were assumed to be unaccounted for decant. Secondly the decant was calculated based on the demands of the mine site from the secondary dam system, i.e. reclaim dam to north pond. A plot of the cumulative penstock decants for these two calculations are presented in Figure 5.8, showing a close match,

suggesting that the calculated penstock decant volume is a good representation of the actual conditions.

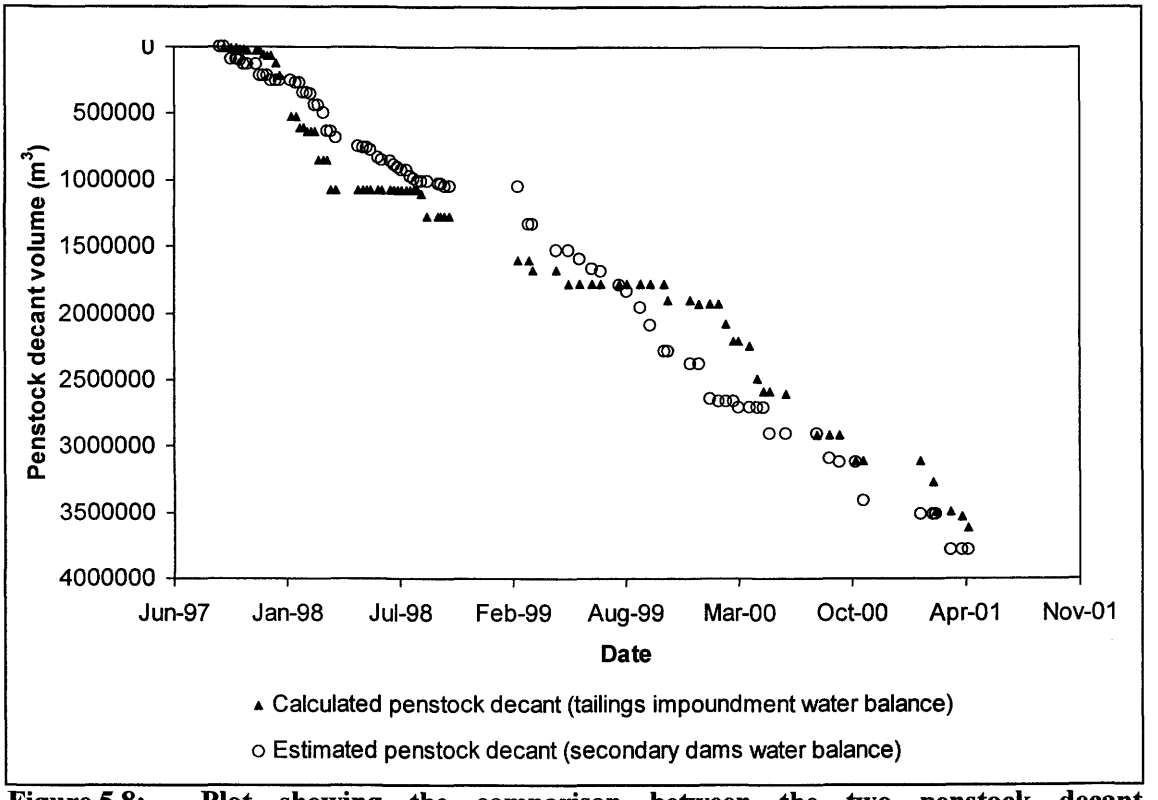

Figure 5.8: Plot showing the comparison between the two penstock decant calculations.

5.3.8 Volumes of Water Pumped on Tailings Impoundment Surface

As with the penstock decant volume, Kidston kept limited records of the volumes of water that were pumped to the tailings impoundment form the various sources mentioned in Equation 5.23. It was however possible to make good judgements of these volumes based on physical data and interviews with the mine operating personnel. The pump-back volume from the SW seepage zone (P_1) had been zero for the entire period observed in this study. Mr. Paul Ritchie, the Kidston Environmental Officer, verbally communicated this fact to the author. This is supported by the previously mentioned theoretical seepage calculation which suggests a negative seepage, as well as the piezometer readings along section line F (Appendix F) which shows that seepage from this zone was negligible.

The pump-back from the western drain seepage zone (P_2) was measured periodically with the intent of establishing what the seepage rate would be. The actual pumping is done via one of two methods; an automated level sensor in the pond switches the pump on when a high water level has been reached, and a low water sensor switches the pump off; secondly the pump is often started manually in anticipation of rainfall events to avoid spillage. In actual fact the seepage water thus ponds and some evaporation occurs before it is pumped to the dam. However, surface runoff from this small catchment can also flow into this pond, increasing the potential pump volume. For the purpose of this calculation it was assumed that the seepage water would be returned to the tailings impoundment surface at the same rate and volume as it exits.

After the tailings impoundment was decommissioned in 1997 the records of the volumes pumped to the tailings impoundment from the reclaim dam or the south pond, either due to storm water control or from dredging operations is incomplete. However, personal discussions with the relevant operators of the pump systems lead the author to believe that these pumpings occurred relatively frequently, and a reasonable reconstruction of events could be determined. This fact was supported by observing various aerial photographs of the impoundment over the period under investigation, as well as actual inspection of the tailings impoundment during two site visits. Pumping was regularly observed and the site investigation and aerial photographs show distinct drainage channels eroded into the tailings impoundment surface where regular high volume pumping was done.

The actual pumping volumes used were based on trial-and-error calculations of the overall water balance as discussed in previous sections. Once the runoff was assumed to be reasonable the appropriate corrections were made to the water balance which included allowing pumping to occur if there was a shortfall of surface water. Figure 5.9 is a simplistic flow diagram indicating how the water balance calculation is done. The calculation is done in the following sequence (a) north pond (NP), (b) reclaim dam seepage dam (RDSD), (c) south pond (SP), (d) reclaim dam (RD), and (e) tailings impoundment (TI). If after one sequence of calculations the tailings impoundment water balance does not equate to the measured pond volume increase/decrease, the appropriate adjustment is made to decant (Q_8) and pump volumes (P_3), and the process is repeated.

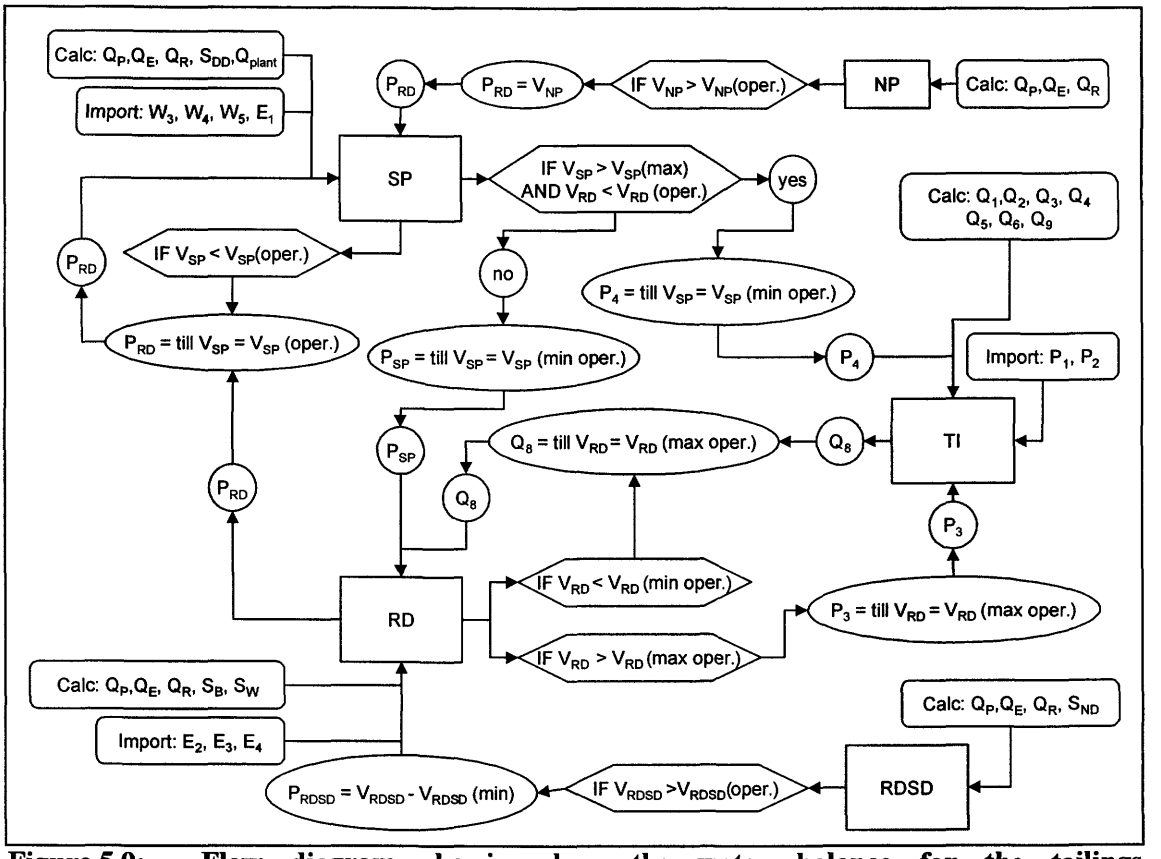

Figure 5.9: Flow diagram showing how the water balance for the tailings impoundment is calculated.

5.4 Water Balance Results

This section presents the final results of the water balance calculations presented in this chapter. The results are presented for two specific time periods. The first time period corresponds to a 5 year span and provides a value for the overall average runoff from the Kidston tailings. The second time period corresponds to the 2000/2001 wet season at the Kidston mine site and has been specifically calculated to provide a runoff number that can be used for subsequent evaluation modeling.

5.4.1 Runoff from Tailings Impoundment Surface For The Periods 1997 Through 2001

As explained previously, the purpose of this water balance calculation was to estimate runoff from the tailings impoundment surface to the pond for the study period. Knowing the magnitude of runoff allows subsequent numerical model calibration. The previous sections of this chapter

describe the mathematical formulation for the water balance problem, as well as the methodologies and assumptions used in deriving the tailings surface runoff. The calculation results are tabled in Appendix L with the final results shown here. The calculation of the runoff volume involved a number of iterations and corrections had to be made for pumping rates to the impoundment, as well as penstock decant rates, as explained in the previous section and Figure 5.9. The subsequent overall annual runoff percentages (expressed as a fraction of the total rainfall volume on the exposed tailings) are presented in Table 5.12.

Table 5.12: Overall annual runoff volumes into the pond, calculated for the Kidston tailings impoundment using the water balance equations.

Period (approximate year)	Rainfall volume, Q_2 (m^3)	Runoff volume, Q_7 (m^3)	Runoff (%)
8 Sep 1997 – 12 Jan 1998 (1997)	605854	303329	50%
12 Jan 1998 – 18 Feb 1999 (1998)	1606399	668050	42%
18 Feb 1999 – 4 Jan 2000 (1999)	298482	83896	28%
4 Jan 2000 – 30 Jan 2001 (2000)	1993879	849242	43%
30 Jan 2001 – 24 April 2001 (2001)	396015	173604	44%
8 Sep 1997 – 24 April 2001 (Overall)	4900630	2078122	42%

The data in Table 5.12 suggests that the overall annual runoff from the exposed tailings is 42% of incident rainfall. The 1997 data shows the highest runoff of 50%, but it should be noted that the investigation period corresponds only to the rainy season and excludes the dry season. The lowest runoff of 28% is computed for 1999, which corresponds with the fact that this year was an exceptionally dry year, showing far less than average annual precipitation. The runoff for 1998 and 2000, at 42% and 43% respectively, corresponds well with the overall value of 42%. The 2001 data set is not for a complete calendar year since it includes only a short portion of the annual wet season, excluding the dry season entirely.

Close inspection of the water balance data in Appendix L shows that 44% of the water loss on the tailings impoundment is associated with direct evaporation of water from the pond. The next largest loss is the penstock decant at 28%. Evapotranspiration (at the assumed AE/PE ratio of 0.2) results in 21% of the water loss and the seepage loss of 8% is the smallest.

The largest gain of water to the system is due to the rainfall on the exposed tailings and equals 38%. The contribution of the rainfall may be broken down into two separate gains with runoff equal to 16% and infiltration equal to 22%. The next largest gain is the water pumped to the tailings impoundment, at 34%. This equates to pumping at full capacity from both the south

pond (180 l/s) and the reclaim dam (180 l/s) for 10% of the time, which is entirely reasonable based on interviews with the mine operating personnel. Runoff from Paddy's Knob constitutes 8% of the gains with the irrigation volume completing the gains at 2%.

The cumulative volumes of each of the systems gains and losses for the entire period under investigation are presented in Figures 5.10 and 5.11 respectively.

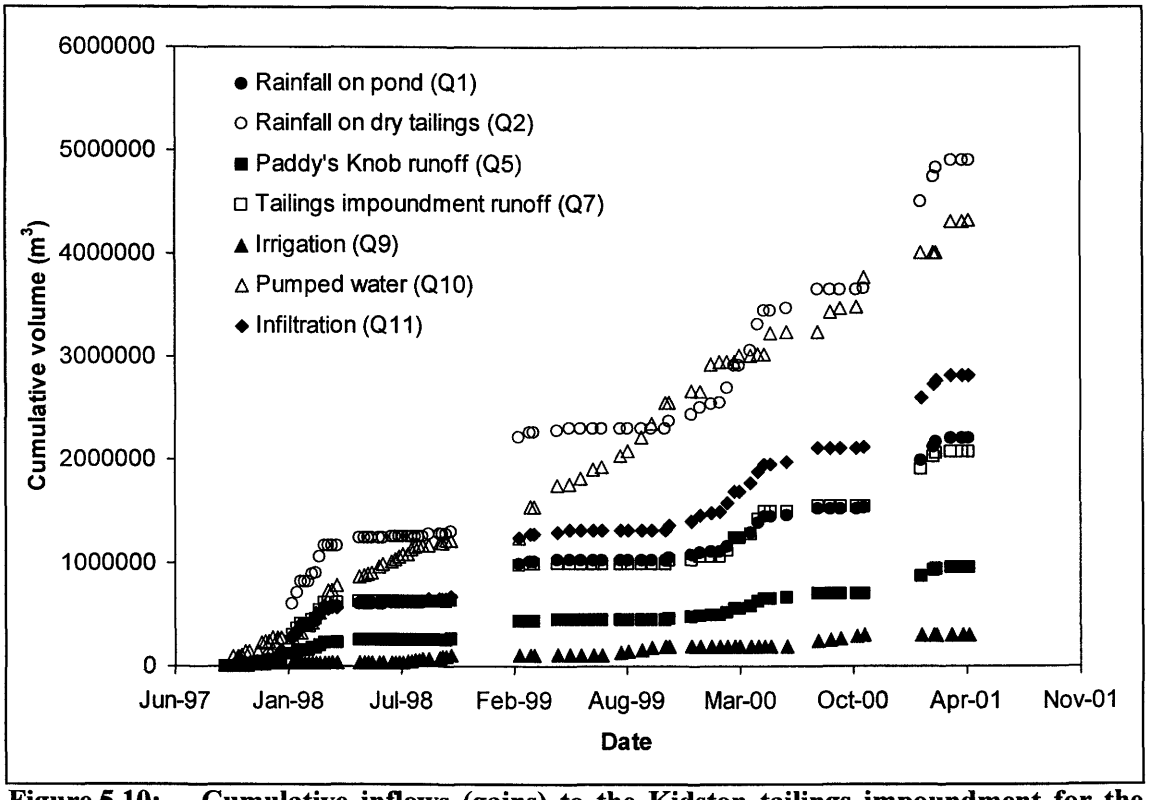

Figure 5.10: Cumulative inflows (gains) to the Kidston tailings impoundment for the period of the water balance calculations.

5.4.2 Runoff from Tailings Impoundment Surface For the Period December 2000 to March 2001

A separate water balance was performed for the period 1 December 2000 through 31 March 2001. This corresponds to the period for which detailed tailings seepage rates were measured and subsequently used for an evaluation data set to be used with subsequent numerical modeling. The calculation of the water balance for this period was carried out in the same way as described in this chapter, with the only difference being that more refined pond levels and

seepage rates were available for the calculation. Table 5.13 contains specific parameters of importance for the verification water balance calculation.

Table 5.13: Constant parameters for the calculation of the tailings impoundment water balance for the period 1 December 2000 to 31 March 2001.

Constant	Value	Comment
Pond level on 1 December 2000	553.40 mRL	Manual pond level measurement
Pond level on 31 March 2001	554.35 mRL	Automated pond level measurement
Total precipitation	469.00 mm	From automated tipping bucket raingauge
Total potential evaporation	583.20 mm	Calculated with Penman method
Total number of days	121 days	

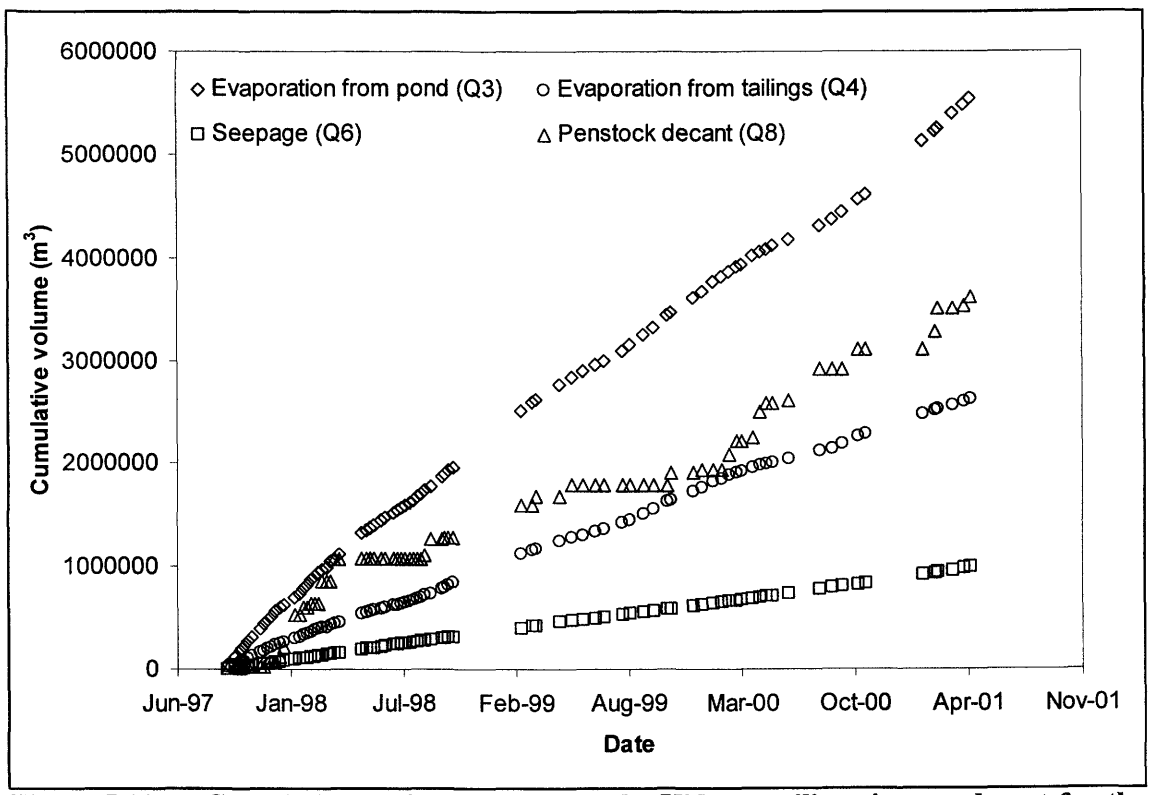

Figure 5.11: Cumulative outflows (losses) to the Kidston tailings impoundment for the period of the water balance calculations.

Using the theoretical seepage rates for the period mentioned, the total surface runoff is calculated to be 55%. However when the actual measured seepage rates are used, the surface runoff increases to 58%. This is reasonable since the loss of additional water via seepage could result in more surface water required to reach the pond via runoff. The runoff quantity of 55% will be used for subsequent evaluation modeling presented in Chapter 10.

5.5 Conclusions

The water balance calculation documented in this chapter indicates that on average, the surface runoff from the Kidston tailings impoundment is approximately 42%. This number does vary according to actual annual precipitation but for the almost five years of data, an overall average of 42% seems reasonable. The water balance calculation does of course not produce an exact result, as a lot of assumptions had to be made along the way. The author however believes that all the assumptions are based on sound engineering judgement and are justified. In conclusion this runoff number will be used as a guideline with regard to finding optimal solutions in the numerical modeling phase presented in the subsequent chapters.

5.6 References

Gray, D.M. (1970). Handbook on the principles of Hydrology. A Water Information Center Publication, ISBN. 0-912394-07-2.

Gutteridge Haskins and Davey Pty Ltd (1984). Kidston Project – Tailings Dam Study. Consultants Report to Kidston Gold Mines Limited, November 1983 – Amended July 1984, 19 Pages.

Gutteridge, Haskins and Davey Pty Ltd (1987). Kidston Project; Interim Report on Tailings Disposal. Consultants Report to Kidston Gold Mines Limited. Brisbane, Queensland, Australia. July, 9 pages.

Holtz, R.D., Kovacs, W.D. (1981). An Introduction to Geotechnical Engineering. Prentice-Hall Civil Engineering and Engineering Mechanics Series, N.M. Newmark and W.J. Hall, Editors, Prentice-Hall, Englewood Cliffs, New Jersey, U.S.A.

Oke, T.R. (1987). Boundary Layer Climates. Second Edition, Methuen: London, 435 pp.

Penman, H.L. (1948). Natural evapotranspiration from openwater, bare soil and grass. Proc. R. Soc. London Ser. A, Vol.193, pp. 120-145.

SoilCover (1997). SoilCover User's Manual. Unsaturated Soils Group, Department of Civil Engineering, University of Saskatchewan, Saskatoon, Saskatchewan, Canada.

This page was intentionally left blank.

CHAPTER 6
SoilCover Calibration

6.1 Introduction

This chapter describes the selection of a numerical model for surface flux boundary calculations, as well as calibration of the model. The SoilCover model (SoilCover, 1997), was selected to be the most appropriate model for accurately calculating surface flux boundary conditions. However, in order to substantiate this selection, calibration of the model using real-time in-situ matric suction data measured in the tailings profile was carried out.

6.2 Selection of Surface Flux Boundary Numerical Model

There are a number of saturated/unsaturated flow numerical models available that report the ability to accurately calculate the surface flux boundary conditions through the modeled profile. These models include SoilCover (SoilCover, 1997), HELP (Schroeder *et al.*, 1994), UNSAT-H (Fayer and Jones, 1990), SWACROP (Feddes *et al.*, 1984), HYDRUS (Simunek *et al.*, 1998), and SWIM (Ross, 1990). Some investigators have reported comparisons between these various models (Baca and Magnuson, 1990; McCord and Goodrich, 1994; Link *et al.*, 1993; Webb, 1996), however there appears to be little direct comparative information available in the literature.

These models all attempt to calculate the surface flux boundary components using various methods and assumptions. Many of the models were developed for crop management purposes and as such, their degree of detail is not adequate for cover systems for mine closure purposes. In the case of mine closure in arid climates the single most important issue is accurate calculation of evaporation. One method available to calculate actual evaporation is the modified Penman formulation as proposed by Wilson *et al.* (1994). The only known model that currently uses the modified Penman formulation is SoilCover and is considered to be the most appropriate tool for the current study.

Machibroda *et al.*, (1993) and Machibroda (1994) show how the modified Penman formulation can be used to accurately predict actual evaporation from non-vegetated exposed tailings. SoilCover is a research tool developed and verified by the Unsaturated Soils Group at the Department of Civil Engineering, University of Saskatchewan, Saskatoon, Saskatchewan, Canada (Wilson, 1990; Joshi, 1993; Machibroda, 1994; Newman, 1995; Swanson, 1995; Tratch, 1995).

6.3 Calibration Purpose

The purpose of calibrating SoilCover is twofold. Firstly, and most importantly, the calibration was done in order to gain confidence that SoilCover could accurately model the transient unsaturated zone surface fluxes in the Kidston tailings impoundment. Secondly, the calibration exercise allows for a sensitivity analysis to be performed for identification of potential modeling difficulties related to the material properties and the boundary conditions used in the Kidston tailings impoundment.

The calibration was done by setting up all SoilCover simulations to run over the same time period for which detailed in-situ matric suction measurements have been obtained within the tailings impoundment profile. A comparison of the field data with the model prediction allows for conclusions to be drawn with respect to the accuracy of the SoilCover model.

6.4 Calibration Data

Real time data required for calibration of the model was measured on-site to ensure that accurate response monitoring could be achieved. A single automatic data logging station was installed on the tailings impoundment to specifically measure atmospheric forcing events and the soil profile response required for accurate model calibration.

6.4.1 Calibration Instrumentation

The instrumentation consisted of a Campbell Scientific Bowen ratio station (CSI, 1997) described in Appendix H that measured continuous evapotranspiration (one reading every 20 minutes) from the tailings profile based on the Bowen ratio method (Bowen, 1926). Nine Campbell Scientific model-229 matric suction sensors (CSI, 1993) were installed at depths of

50, 150, 300, 500, 750, 1000, 1250, 1500 and 2000 mm respectively as described in Appendix K. These sensors measured the matric suction in the tailings profile at each depth twice a day, at noon and at midnight. Figures 4.7 and 4.10 in Chapter 4 indicate the location of these installations. Complete details regarding the instrumentation, installation thereof, as well as all the measured data, are presented in Appendixes H and K, and will not be repeated here.

The Bowen ratio station and the model-229 matric suction sensors were connected to a single power supply and data logger. Numerous lightning strikes resulted in a discontinuous data set reported in Appendix K. Three periods of reliable continuous data have been recorded since the instruments were installed in 1997. These periods range between 69 and 218 days. The most continuous data set for both the Bowen ratio and the matric suction data corresponds to the period between 22 October 1998 and 8 January 1999 (79 days). There were 31 days of missing or rejected data (39%) for the Bowen ratio data during this period, and six (8%) days of missing data for the matric suction data.

The detailed daily climate data required for the SoilCover runs were obtained from the Campbell Scientific weather station (CSI, 1994) installed on the barren waste rock dump adjacent to the tailings impoundment as described in Appendixes H and J. The daily climate data comprised of minimum and maximum air temperatures, minimum and maximum relative humidity, average net radiation, average wind speed, and actual rainfall volume and intensity. The format in which the daily rainfall was distributed was modeled in two ways for each case. The first method consisted of using actual measured rainfall intensities, and the second method consisted of distributing the total daily rainfall equally over 24 hours.

6.5 Calibration Modeling

The following section describes the calibration procedure. The sections are started with a description of the input requirements for the SoilCover model before proceeding to the actual modeling results. The calibration results are presented in terms of evaporation, matric suction and soil temperature.

6.5.1 SoilCover Setup

The calibration modeling was done using a non-vegetated tailings surface. Some areas of the tailings impoundment near where the calibration instrumentation were installed, were vegetated during the period under investigation, but the actual instrumentation site was fenced off and vegetation had not yet established in the immediate area of concern. The calibration period spanned over two calendar years (1998/1999). For convenience of the SoilCover simulations the first run day (22 October 1998, Julian day 295) was given a Julian day value of 1, and the last run day (8 January 1999, Julian day 8) was thus Julian day 79.

6.5.1.1 Convergence, Time Step and Mesh

The convergence and time step parameters (SoilCover 1997) for the SoilCover calibration runs, were adjusted for efficient convergence. The primary criteria for setting convergence parameters was to obtain a water balance within acceptable limits of less than 5% of the total surface water budget. The maximum number of iterations allowed were 50, while the maximum change in matric suction and soil temperature was set to 1%. The matric suction and soil temperature damping was set at 0%. The minimum time step was set equal to five seconds with the maximum time step equal to 3000 seconds. The maximum allowable change in matric suction and temperature during any given time step was fixed at 1%.

The mesh for the tailings profile consisted of a single homogeneous layer with a base elevation of 0 mm. The top mesh elevation was set at 3410 mm. This gave a profile depth of 3410 mm between the surface and the phreatic level that was determined by a piezometer reading on 19 October 1998 as describe in Appendix F. The minimum mesh space allowed was 0.5 mm, the maximum space was 300 mm and the expansion factor was set at 2. This configuration gave rise to a mesh with 28 nodes.

6.5.1.2 Material Properties

Five tailings samples were collected during the installation of the model-229 matric suction sensors. Particle size distribution analysis were done on these samples as described in Chapter 4 and Appendix B. These samples obtained at depths of 50, 500, 1000, 1500 and 2000 mm were all very similar, and consisted of silty to well graded sands (according to the USCS soil

classification system, Holtz and Kovacs (1981)). The sand content of these samples varied between 70.8 % and 85.2 %, the silt content varied between 12.6 % and 24.6 % and the clay content varied between 2.2 % and 6.0 %. The median particle size for these samples varied between 0.142 and 0.272 mm. Soil water characteristic curve tests were not measured for these samples, however a number of tests were performed on samples with similar particle size distribution as reported in Chapter 4 and Appendix D. The soil water characteristic curve used for the calibration modeling represented one of the soil water characteristic curves measured for a coarse tailings. Minor modification to the selected soil water characteristic curve was required to give satisfactory results. The resultant curve is presented in Figure 6.1.

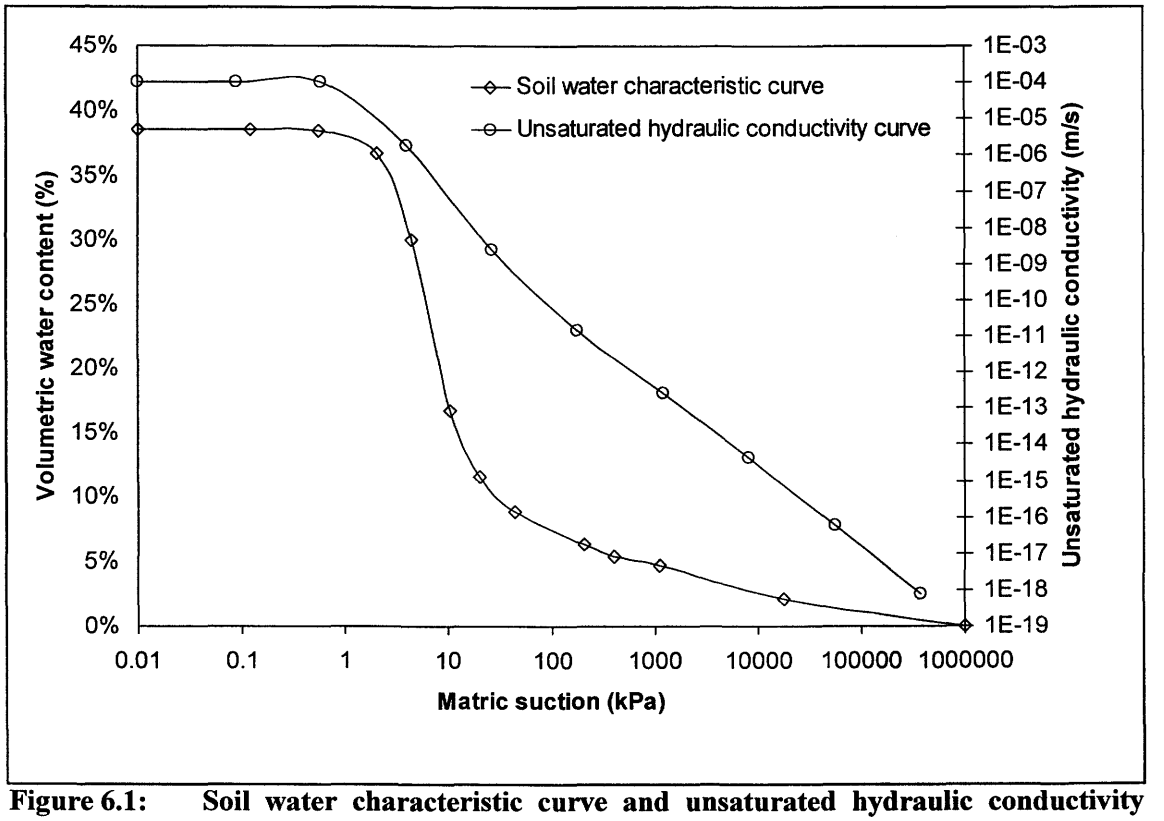

Figure 6.1: Soil water characteristic curve and unsaturated hydraulic conductivity curve used in the SoilCover calibration modeling.

SoilCover uses the Fredlund and Xing (1994) curve fitting technique to produce a smooth curve for the soil water characteristic curve. The associated calibration coefficients a, n and m were computed to be 3.97, 3.09 and 0.73 respectively. The tailings porosity at saturation was set equal to 0.385 with the specific gravity equal to 2.77. The coefficient of volume change was 1.90×10^{-3}/kPa.

SoilCover uses a function proposed by Fredlund *et al.* (1994) to produce a relative unsaturated hydraulic conductivity function. This function uses the curve fitting coefficients a, n and m corresponding to the soil water characteristic curve. The unsaturated hydraulic conductivity function is then calculated by multiplying the saturated hydraulic conductivity of the soil with the relative unsaturated hydraulic conductivity. The saturated hydraulic conductivity for the tailings at the calibration instrumentation site was measured using a double ring infiltrometer (2 tests together with 6 Guelph permeameter tests as described in Chapter 4 and Appendix E). The measured results for the tests varied between 1.55×10^{-5} m/s and 2.00×10^{-5} m/s, with an average value of 1.77×10^{-5} m/s. This value was initially used for calibration, however it was modified to achieve an optimum solution. The final saturated hydraulic conductivity value selected for the calibration modeling was 1.03×10^{-4} m/s, and the unsaturated hydraulic conductivity curve is presented in Figure 6.1.

Finally, SoilCover requires functions for thermal conductivity and volumetric specific heat (SoilCover, 1997). SoilCover generates these functions automatically, however the user must specify the quartz content of the soil, as well as the mass specific heat of the soil. For the calibration runs these values were set at 90% and 792 $J/kg^3.^oC$ respectively (Holtz and Kovacs, 1981; de Vries, 1963). The corresponding curves are presented in Figure 6.2.

Although, the five tailings samples tested at the calibration site were similar when their particle size distributions were compared, they still do differ, and this was observed when the trenching for the installation was done. Attempts were made to divide the 3410 mm calibration profile into layers, to simulate the effect of the different layers on the calibration modeling outcome, however these attempts were abandoned. It will be noticed in the sections that follow that excellent match between the simulated homogeneous profile and the measured profile with regard to matric suction and temperature is achieved. The layering in the tailings impoundment is random of nature due to the deltaic deposition of the tailings and as a result it would not be viable to generalize this aspect. For the purpose of this study a homogeneous profile of the tailings is thus considered to be a good representation.

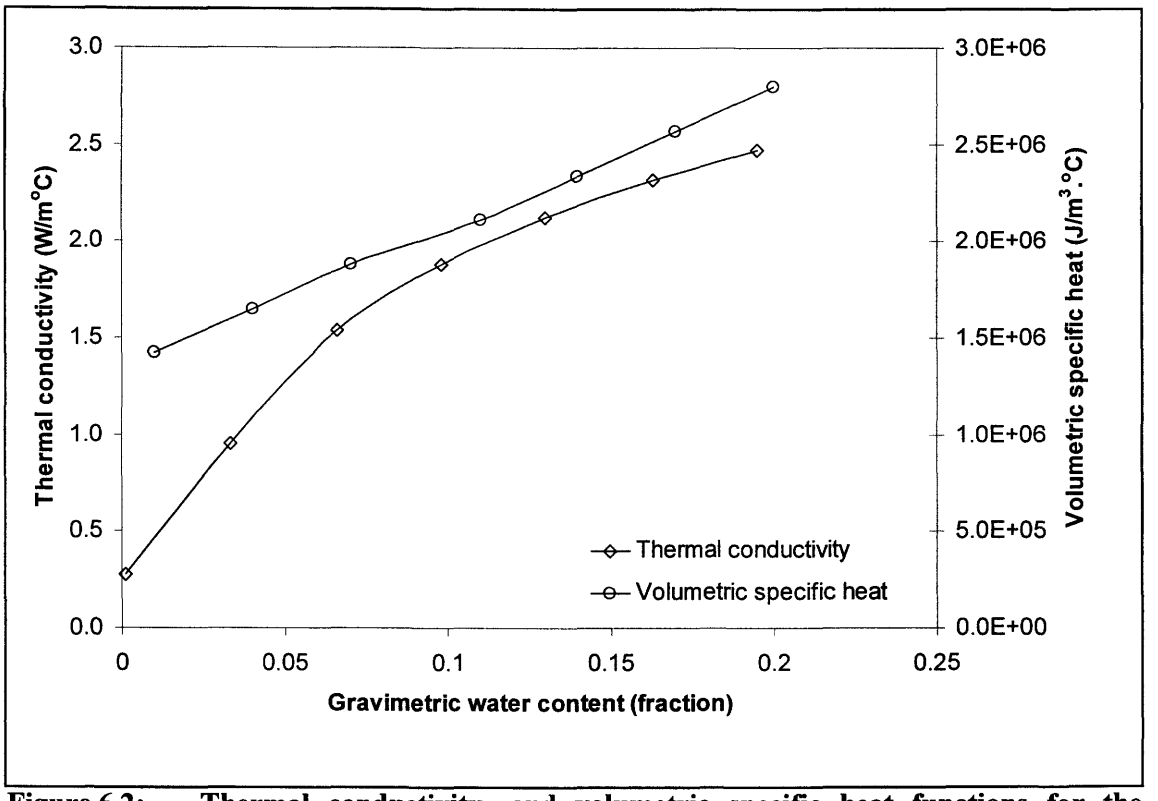

Figure 6.2: Thermal conductivity- and volumetric specific heat functions for the SoilCover calibration data set.

6.5.1.3 Surface Flux Boundary Conditions

The site latitude was set equal to -18°, denoting the fact that the site is in the Southern Hemisphere. The daily climatic data for the site was obtained from the continuous weather station installed on the barren waste rock dump adjacent to the tailings impoundment. Figure 6.3 presents both the daily rainfall and the cumulative rainfall for the calibration period. The complete data sets including rainfall intensity is listed in Appendixes H and J.

6.5.1.4 Initial (Starting) Conditions

The actual measured matric suction profile corresponding to midnight on 21 October 1998 was assigned as the initial matric suction profile for the SoilCover calibration run. This profile is presented in Figure 6.4. The measured data suggest that the water table is at a depth of 2 m below ground surface, however the water table is known to be at a depth of 3.41 m through a piezometer reading taken on 19 October 1998. The anomaly is ascribed to the inaccuracy of the matric suction sensors as described in Appendix K.

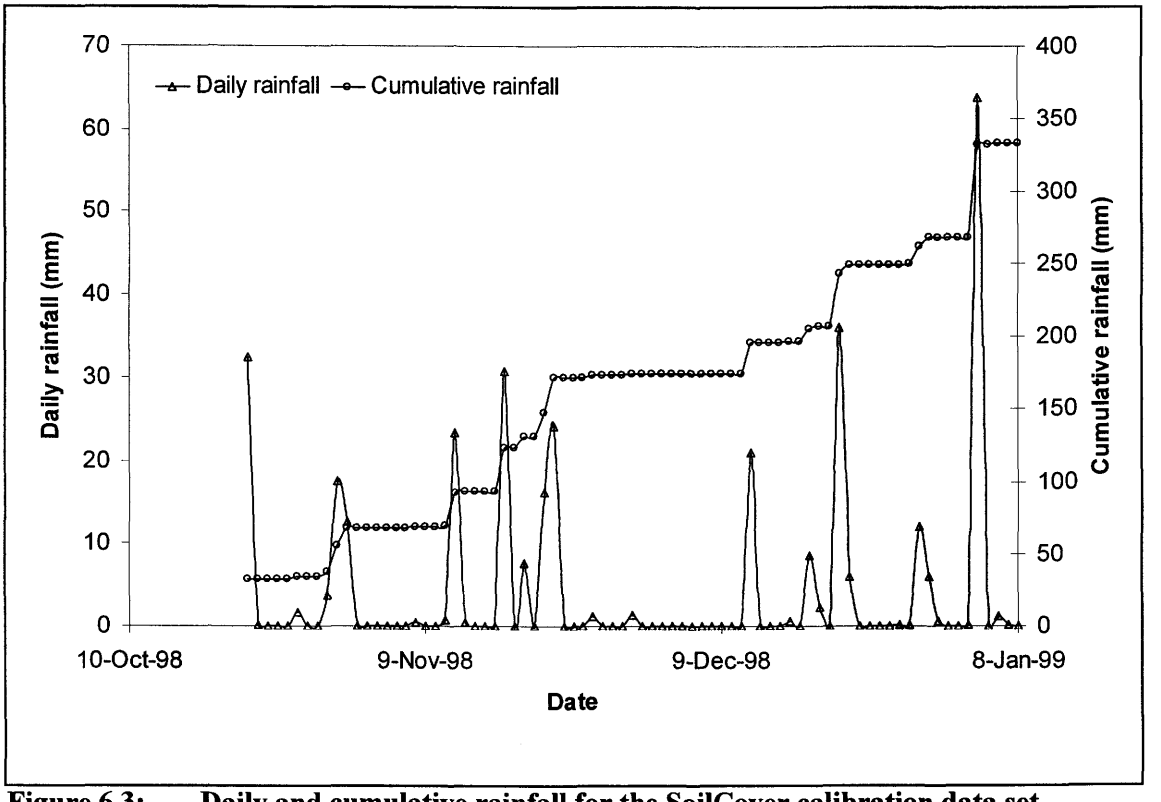

Figure 6.3: Daily and cumulative rainfall for the SoilCover calibration data set.

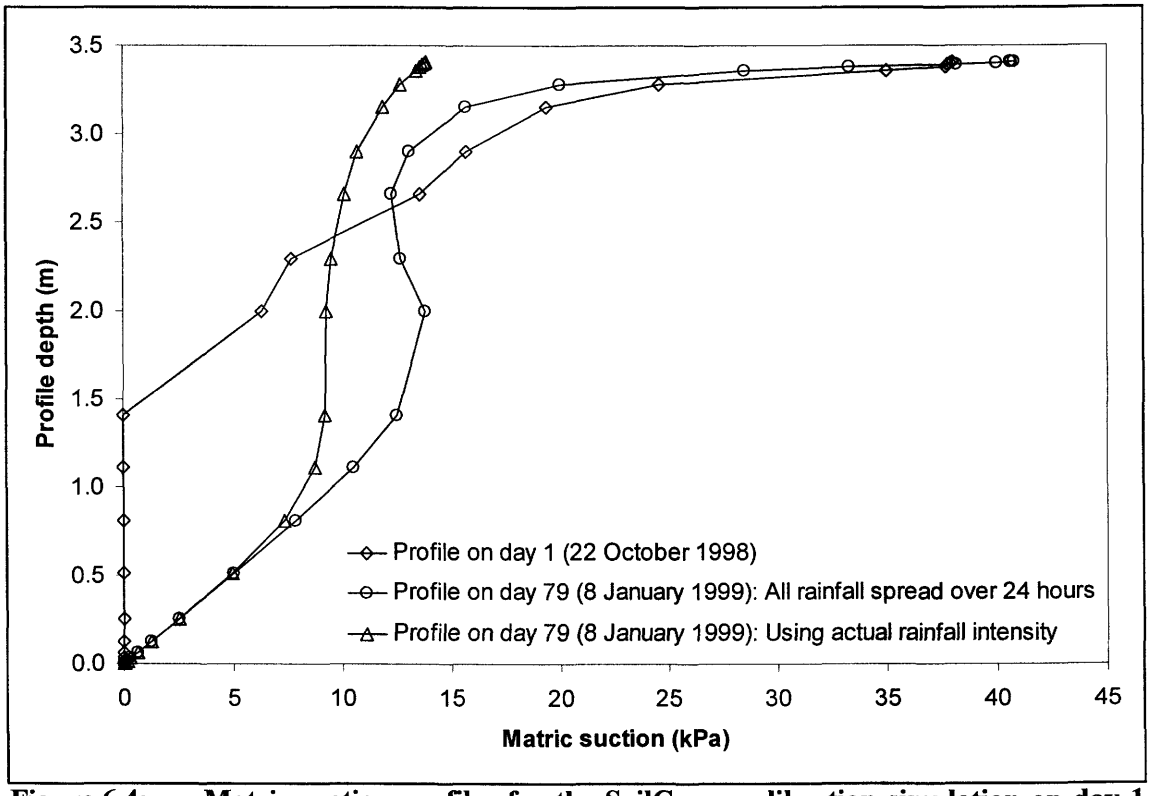

Figure 6.4: Matric suction profiles for the SoilCover calibration simulation on day 1 and day 79.

The initial surface temperature of the tailings was based on actual measured soil temperatures at midnight on 21 October 1998 equal to 31°C. The base soil temperature was kept constant at 25°C, and the initial temperature profile was assumed to be a linear distribution between these temperatures as shown in Figure 6.5.

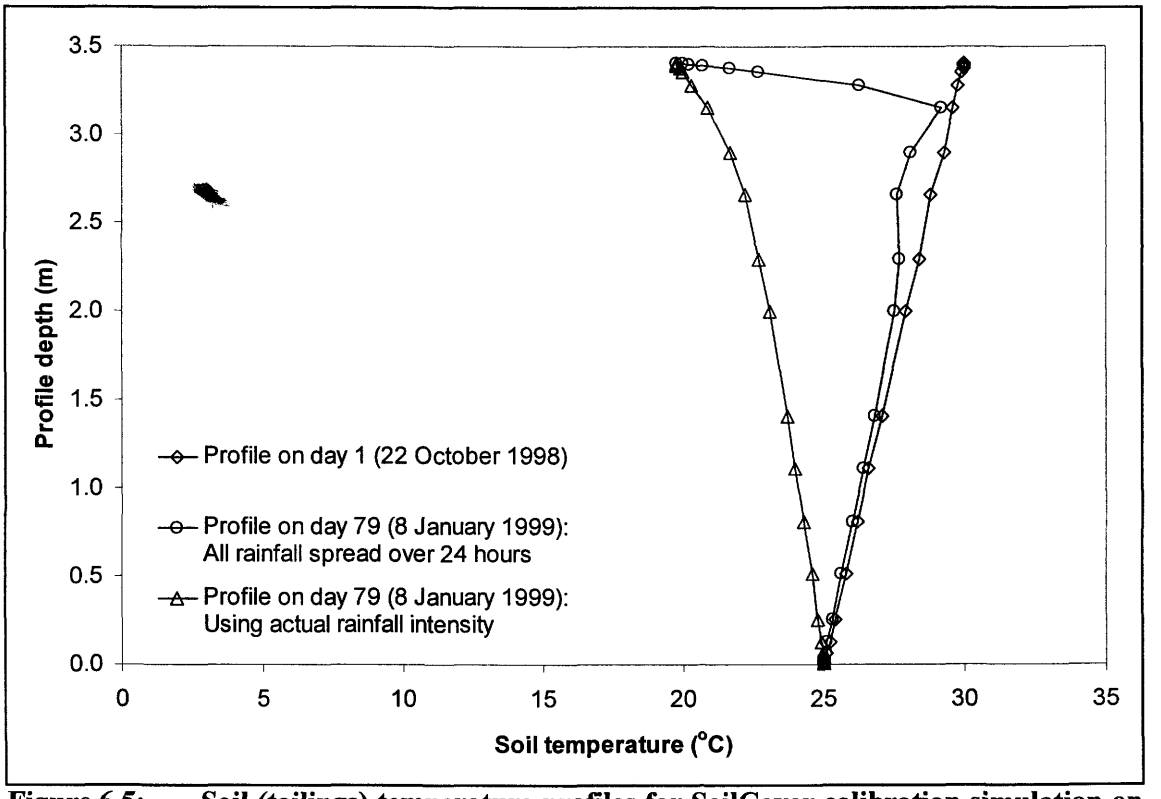

Figure 6.5: Soil (tailings) temperature profiles for SoilCover calibration simulation on day 1 and day 79.

6.5.2 SoilCover Calibration Results

The sections that follow document the results of the calibration modeling. The first results are the evaporation calibration that indicate how well the SoilCover model predicts actual evaporation rates as measured with the Bowen ratio station. The calibration results for the matric suction and temperature profiles in the tailings are presented for two depths within the tailings profile. These depths of 50 mm and 750 mm below surface.

For the given time and convergence criteria, the calibration simulation resulted in an overall water balance error of 1.2% when rainfall was equally spread over 24 hours. This is well within the recommended water balance criteria of 5% (SoilCover, 1997).

6.5.3 Evaporation

The results of the SoilCover calibration modeling are presented for two cases. Firstly the case, where the actual rainfall intensity was used is presented. The second case is for all rainfall events to be distributed equally over a 24-hour period. Figure 6.6 presents the results of the evaporation modeling. In this case there is no result reported for the case where the actual rainfall intensity was used. The large water balance error that occur for that run due to the instability created by the combination of the steep soil water characteristic curve and the rapid soil wetting and drying resulted in incorrect evaporation rates being calculated. The match between the measured data and the modeled results for rainfall distributed equally over 24 hours appear to be in good agreement. For all subsequent SoilCover modeling simulations in this study, rainfall was distributed equally over 24 hours to achieve numerical stability and a satisfactory water balance.

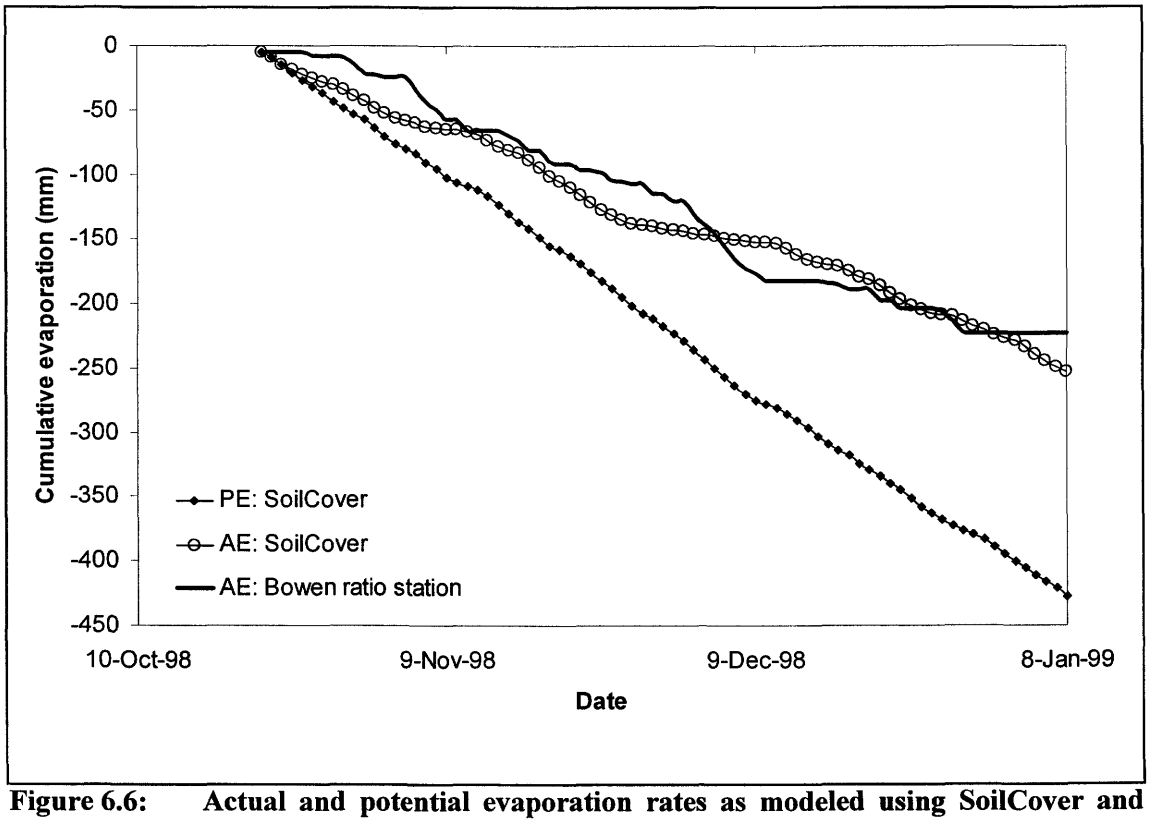

Figure 6.6: Actual and potential evaporation rates as modeled using SoilCover and measured using the Bowen ratio equipment.

6.5.4 Matric suction

Comparisons of the field matric suction data and the SoilCover calibration modeling results at two depths, 50 mm and 750 mm are presented in Figures 6.7 and 6.8 respectively. These results correspond to the field data measured at midnight every day, which correspond to the output generated by SoilCover. The results for spreading the rainfall events over 24 hours show a good match with the field data at both depths. The trends are a definite match, with only the peaks and lows, differing somewhat. These differing peaks and lows can be ascribed to the inherent inaccuracies in the matric suction sensors described in Appendix K.

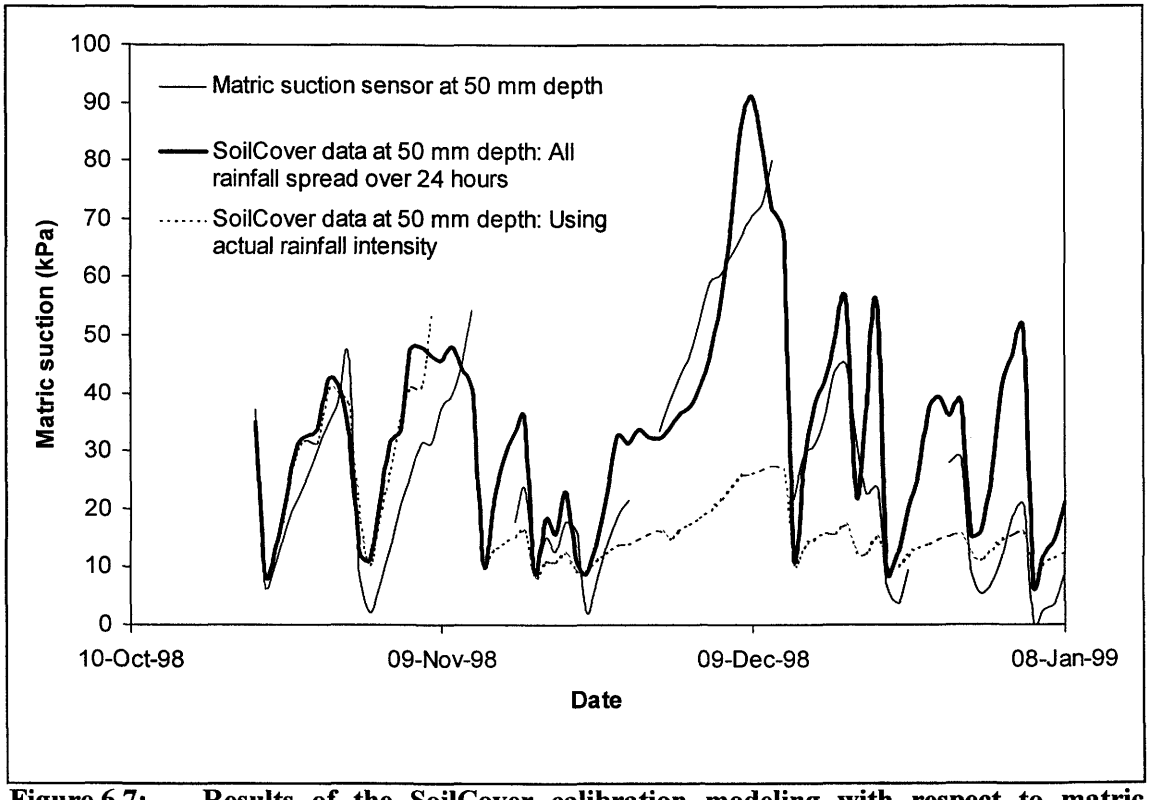

Figure 6.7: Results of the SoilCover calibration modeling with respect to matric suction at a depth of 50 mm below surface.

The poor performance of the model run using actual rainfall intensity is again as a result of the numerical instability that occurs when the rainfall event is forced over a shorter time period. The rapid wetting of the dry surface of the tailings with a steep soil water characteristic curves cause the numerical errors. The only way to prevent these errors is to lengthen the precipitation event or change the material properties, which was not considered to be a viable solution to the problem.

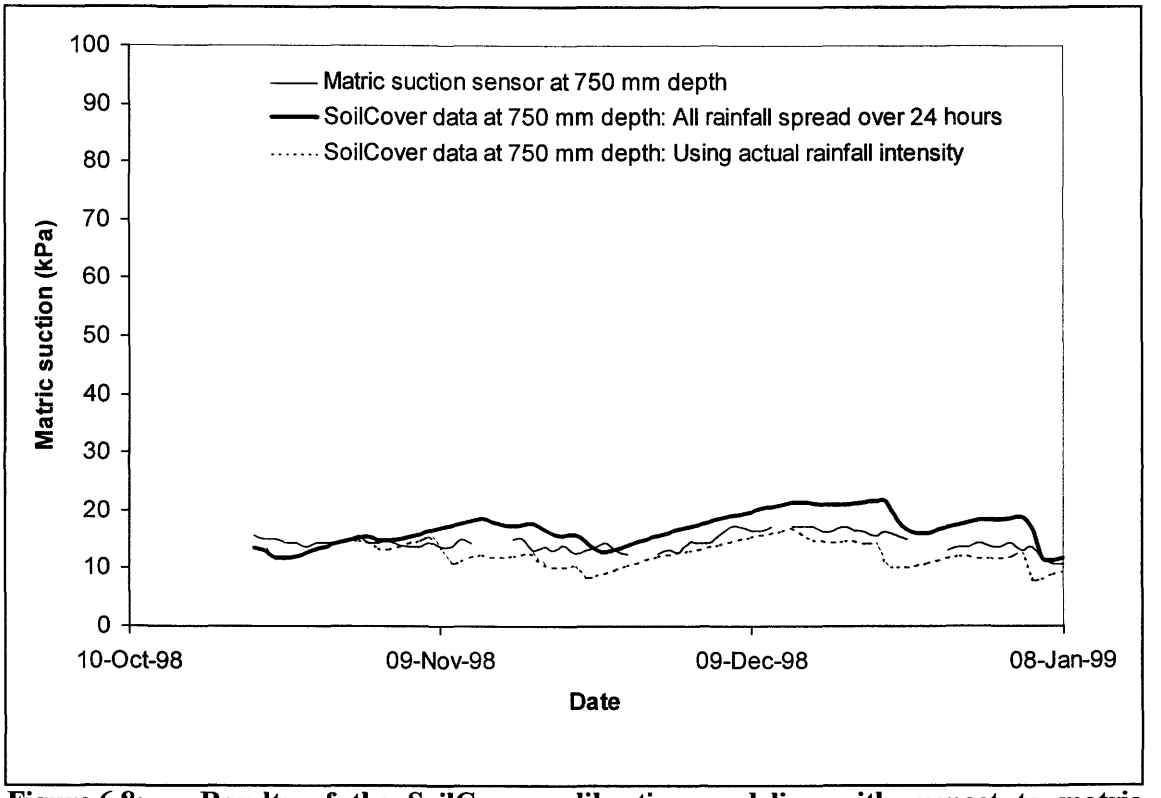

Figure 6.8: Results of the SoilCover calibration modeling with respect to matric suction at a depth of 750 mm below surface.

Figure 6.4 shows the matric suction profile for the last day of the simulation (day 79). The simulated profile suggest that the water table would be at 3.41 m, however a piezometer reading on 5 January 1999 measures the water table at 3.37 m. This 40 mm difference is considered negligible, due to the matric suction sensor accuracy limits, and the overall match between the measured and simulated profiles is considered excellent.

6.5.5 Tailings Temperature

The tailings temperatures in the field were not measured directly using an dependant instrument, but was a by-product of the model-229 matric suction sensors (CSI, 1994). Figures 6.9 and 6.10 presents the results of the SoilCover calibration modeling with respect to the tailings temperatures at depths of 50 mm and 750 mm below ground surface.

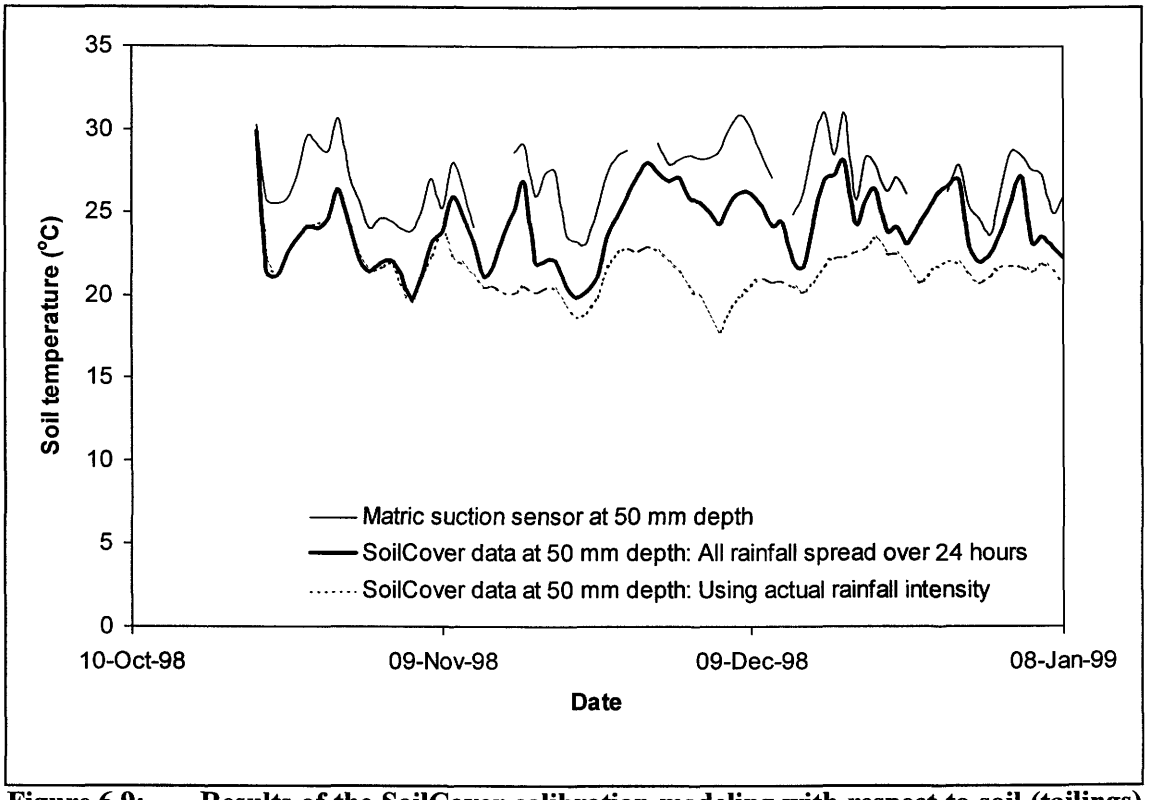

Figure 6.9: Results of the SoilCover calibration modeling with respect to soil (tailings) temperature at a depth of 50 mm below surface.

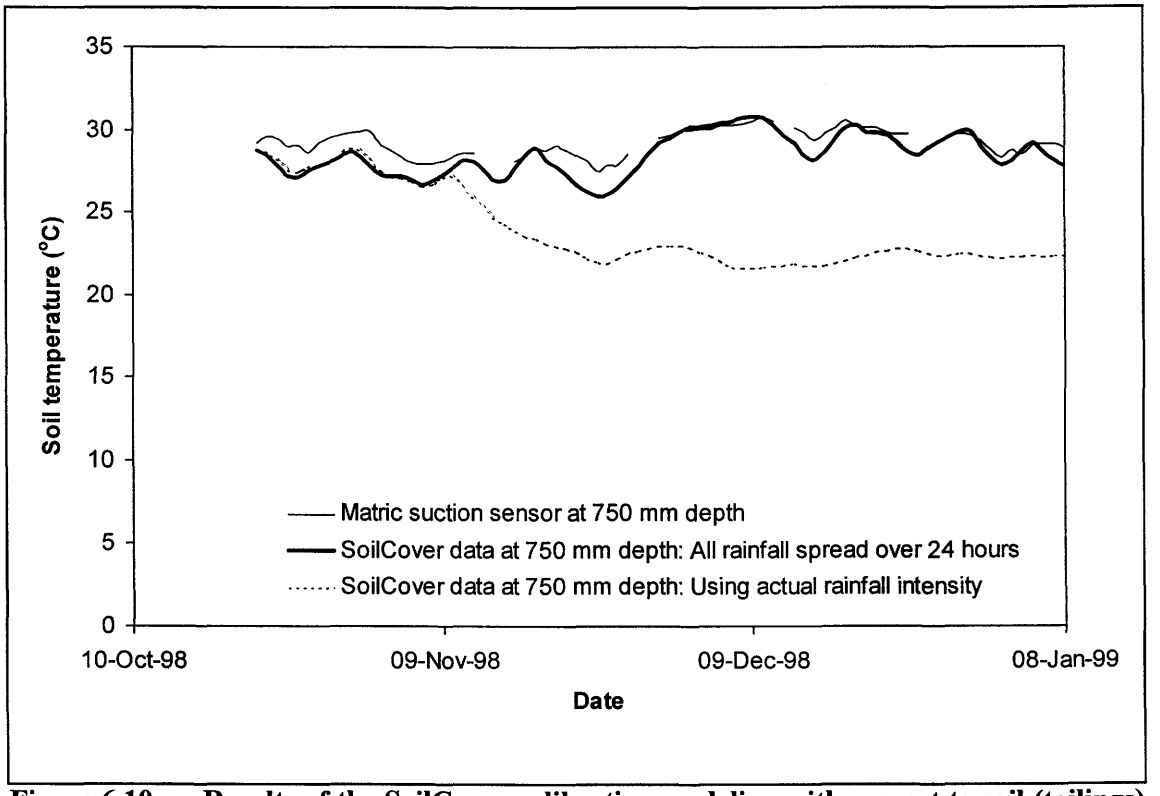

Figure 6.10: Results of the SoilCover calibration modeling with respect to soil (tailings) temperature at a depth of 750 mm below surface.

At both depths the trends for the case when rainfall is spread over 24 hours are excellent, however the field data appear to be consistently higher than the modeled data. The reason for this variance is not clear, however it could be suggested that perhaps the constants used for determining the thermal conductivity and the volumetric specific heat functions were not accurate enough. Another possible reason is that there is an inherent higher temperature measured by the suction sensor, due to the heating of the sensor when the reading is taken.

The inconsistent trend associated with the runs using actual rainfall intensities were discussed in the previous section and will not be repeated. The temperature profile on the last day of the model run is presented in Figure 6.5 and shows a similar linear trend, except for the top surface layer where there is a cooling that can be ascribed due to the large rainfall event 5 days prior.

6.6 Conclusions

The results presented in this chapter proves that the SoilCover numerical model is capable of accurately predicting the surface flux boundary components within the Kidston tailings material, provided the precipitation is distributed equally over 24 hours. The excellent matches between simulated and measured matric suction and temperature profiles at two depths in the tailings impoundment confirm that SoilCover is capable of accurately predicting the unsaturated flow of moisture and heat through the tailings. This observation is further supported by the excellent match between simulated and measured actual evaporation rates obtained from the Bowen ration station on the tailings impoundment. SoilCover can thus be used with confidence for all the subsequent modeling in this research study.

6.7 References

Baca, R.G., Magnuson, S.O. (1990). Independent Verification and Benchmark Testing of the UNSAT-H Computer Code, Version 2.0. EGG-BEG-8811, Idaho National Engineering Laboratory.

Bowen, I.S. (1926). The ration of heat losses by conduction and by evaporation from any water surface. Physical Review, Vol. 27, pp. 779-787.

Campbell Scientific, Inc. (CSI) (1993). 229 Matrix Water Potential Sensor Operator's Manual.

Campbell Scientific, Inc. (CSI) (1994). Tripod-Based Weather Station Installation Manual.

Campbell Scientific, Inc. (CSI). (1997). Bowen Ratio Instrumentation Instruction Manual. Revision 1/97.

de Vries, D.A. (1963). Thermal Properties of Soils. Physics of Plant Environment, W.R van Wihk (ed.), North Holland Pub. Co., pp. 382.

Fayer, M.L., Jones, T.L. (1990). UNSAT-H version 2: Unsaturated soil water and heat flow model, PNL-6779, Pacific Northwest Laboratory, Richland, Washington, U.S.A.

Feddes, R.A., Wesseling, J.G., Wiebing, R. (1984). Simulation of Transpiration and Yield of Potatoes with the SWACROP-model. 9th Tri-annual Conference of the European Association of Potato Research (EAPR), Interlaken, Switzerland, July 2-6.

Fredlund, DG., Xing, A. (1994). Equations for the soil-water characteristic curve. Canadian Geotechnical Journal, Vol. 31, No. 3, pp. 521-532.

Fredlund, D.G., Xing, A., Huang, S. (1994). Predicting the Permeability Function for Unsaturated Soils Using the Soil-Water Characteristic Curve. Canadian Geotechnical Journal, vol. 31, pp. 533-546.

Holtz, R.D., Kovacs, W.D. (1981). An Introduction to Geotechnical Engineering. Prentice-Hall Civil Engineering and Engineering Mechanics Series, N.M. Newmark and W.J. Hall, Editors, Prentice-Hall, Englewood Cliffs, New Jersey, U.S.A.

Joshi, B. (1993). A finite element model for the coupled flow of moisture and heat in soils under atmospheric forcing. M.Sc. Thesis, University of Saskatchewan, Saskatoon, Saskatchewan, Canada.

Link, S.O., Kickett, R.N., Fayer, M.J., Gee, G.W. (1993). A Comparison of Simulation Models for Predicting Soil Water Dynamics in Bare and Vegetated Lysimeters. Report no, PNL-8675, UC-702, Report prepared for the U.S. Department of Energy by Pacific Northwest Laboratories, Battelle Memorial Institute, June, 33 pp.

Machibroda, R.M. (1994). Soil evaporative flux modeling of layered cover systems. M.Sc. Thesis, University of Saskatchewan, Saskatoon, Saskatchewan, Canada.

Machibroda, R.L., Wilson, G.W., Barbour, S.L. (1993). Evaluation of Net Infiltrative Fluxes Across the Surface of Exposed Mine Tailings. Proceedings of the 46th Canadian Geotechnical Conference, Saskatoon, Saskatchewan, Canada, 27-19 Sep, pp. 167-175.

McCord, J.T., Goodrich, M.T. (1994). Benchmark Testing and Independent Verification of the VS2DT Computer Code. SAND91-1526, Sandia National Laboratories.

Newman, G.P. (1995). Heat and mass transfer in unsaturated soils during freezing. M.Sc. Thesis, University of Saskatchewan, Saskatoon, Saskatchewan, Canada.

Ross, P.J. (1990). SWIM – a Simulation Model for Soil Water Infiltration and Movement. CSIRO Division of Soils, Davies Laboratory, Townsville, Queensland, Australia.

Schroeder, P.R., Lloyd, C.M., Zappi, P.A. (1994). The Hydrological Evaluation of Landfill Performance (HELP) Model User's Guide for Version 3, EPA/600/R-94/168a, U.S.A.

Simunek, J., Huang, K., van Genuchten, M.Th. (1998). The HYDRUS code for simulating the one-dimensional movement of water, heat, and multiple solutes in variably-saturated media, Version 6.0. Research Report No. 144, U.S.A. Salinity Laboratory, USDA, ARS, Riverside, California, 164 pp.

SoilCover. (1997). SoilCover User's Manual. Unsaturated Soils Group, Department of Civil Engineering, University of Saskatchewan, Saskatoon, Saskatchewan, Canada.

Swanson, D.A. (1995). Predictive modeling of moisture movement in engineered soil covers for acid generating mine waste. M.Sc. Thesis, Department of Civil Engineering, University of Saskatchewan, Saskatoon, Saskatchewan, Canada.

Tratch, D. (1995). Moisture uptake within the root zone. M.Sc. Thesis, Department of Civil Engineering, University of Saskatchewan, Saskatoon, Saskatchewan, Canada.

Webb, S.W. (1996). Selection of a Numerical Unsaturated Flow Code for Tilted Capillary Barrier Performance Evaluation. SAND96-2271, UC-2040, Sandia National Laboratories, September, pp. 23.

Wilson, G.W. (1990). Soil Evaporative Fluxes for Geotechnical Engineering Problems. Ph.D. Thesis, University of Saskatchewan, Saskatoon, Saskatchewan, Canada.

Wilson, G.W., Fredlund, D.G., Barbour, S.L. (1994). Coupled soil-atmosphere modeling for soil evaporation. Canadian Geotechnical Journal, Vol. 31, pp. 151-161.

This page was intentionally left blank.

CHAPTER 7

Conceptual Model for Flux Boundary Conditions

7.1 Introduction

This chapter presents the crucial aspects of this thesis. The conceptual model described here shows how the SoilCover (SoilCover, 1997) model can be used to develop a spatial surface flux boundary function for the Kidston tailings impoundment as described in Chapter 9. The details of the physical site described in the previous chapters explain the complexity of the problem, which makes conventional water balance solution techniques difficult to apply. The development of the conceptual model, together with the solution technique presented in this chapter allows the problem at hand to be simplified using a set of validated engineering assumptions, which are clearly understood, and as such allows for a good understanding of the subsequent numerical modeling results as described in Chapter 8.

Solving surface flux boundary problems at tailings impoundments is complex. The position of the phreatic level in tailings directly impacts the surface fluxes when using rigorous methods such as those adopted in numerical models such as SoilCover. The only recourse is to set up numerous simulations with variable boundary conditions, each representing a different profile and depth to the water table. The selection of appropriate profiles and interpolation over the surface of the tailings becomes difficult. The successful outcome is dependent on the experience of the modeler to make appropriate assumptions. Although this is not uncommon in engineering practice, improvement are required. The conceptual model proposed here provides a rational basis for the solution of this problem.

A methodology is presented to define a generalized tailings impoundment cross-section using continuous mathematical functions that defines the top (beach) and bottom (phreatic line) geometry's. Together these functions define the unsaturated profile at any point along the generalized section. The generalized cross-section is expanded by assigning material properties

to it that allow the profile to be completely defined. Finally a methodology is presented to solve this 2-D generalized cross-section numerically using the 1-D SoilCover model.

It must be emphasized that the generalized cross-section and methodology is only directly applicable to tailings impoundments similar to the Kidston tailings impoundment, i.e. low-tonnage impoundments in arid climates.

7.2 Generalized Tailings Impoundment Cross-Section Concept

Chapter 3 provided a detailed description of the Kidston tailings impoundment layout. The tailings impoundment is a highly irregular three dimensional object (3-D) that requires a solution for the closure water balance (i.e. what the long-term seepage from the impoundment will be). The tailings thickness varies from less than 1 m to more than 32 m deep at places. The dam has been founded on natural topography and the top shape of the dam has been shaped by hydraulic placement of the tailings. The geometry of the perimeter embankment was governed by the ground topography, combined with engineered design requirements for storage volume of tailings required. The tailings placed in the dam are not homogeneous as defined in Chapter 4 due to variations in operations, changes in the milling rate, hydraulic placement technique, depositional location as well as depositional segregation and pond water recycling methodology. The tailings thus appear in stratifications of varying tailings types in a quasi-random pattern. Following the history of the tailings deposition, it is possible to make adequate estimates of what the tailings layering should look like, but mine records are not adequate enough to provide the exact details.

In addition to the limits described above, the tailings pond covers roughly 30% of the impoundment surface area. The associated position of the phreatic level varies greatly as it exits at the impoundment perimeter though toe and blanket drains installed in the embankment walls. This causes both a saturated and unsaturated zone of varying thickness to exist throughout the tailings impoundment. At first glance, it would appear that any form of generalization of the tailings impoundment in order to simplify modeling of the water balance is difficult. However, by applying good engineering judgement, making appropriate assumptions based on measurable data, it is possible to simplify the problem. A decision was made to use the available physical data and produce a generalized conceptual cross-section through the tailings impoundment that could represent the impoundment at any location. This generalized cross-section could then be

extrapolated further to a 3-D environment that would allow for accurate numerical modeling of the three-dimensional groundwater regime within the tailings impoundment.

In order to generate the generalized tailings impoundment cross-section, the top (beach) and bottom (phreatic line) geometry had to be defined in such a way that they would be representative of the profile of any location within the tailings impoundment. The cross-section can then be further expanded by defining material properties assigned to it, before providing a solution methodology for applying the one-dimensional (1-D) SoilCover code to this two- and three-dimensional problem.

7.3 Description of the Surface Geometry (Beach Shape)

The top boundary shape of the generalized tailings impoundment cross-section is formed by the tailings impoundment surface, or beach as it is commonly known (Vick, 1983). Blight (1987) reported on a procedure to calculate a master profile for a tailings impoundment beach in arid climates, similar to the Kidston tailings impoundment. The profile of a hydraulic fill beach is unique. Blight (1987) showed that it could be non-dimensionalized such that the profile would be the same for all beaches with specific material deposited at a specific solids concentration, deposition rate and in a arid climate. The master profile applies regardless of the length of the beach or the difference in elevation between the point of deposition and the pond. The profile is said to be generated by the gravitational sorting of particle sizes as the tailings slurry moves down the beach. Figure 7.1 presents beach profiles measured at 14 different locations on the Kidston tailings impoundment. It can be seen that each profile has a different length H_b, and a difference in elevation y_b between the point of deposition (adjacent to the embankment wall) and the pool. In Figure 7.2 these profiles have been non-dimensionalized by normalizing the elevation and distance down the beach of each point on the profile. The result is a single master beach profile that can be described by the following equation (Blight, 1987):

$$\frac{h_b}{y_b} = \left(1 - \frac{H_b}{X}\right)^n \qquad [7.1]$$

Where h_b = beach height at any point between the embankment wall and the pool (m),

y_b = maximum beach height between the embankment wall and the pool (m),

H_b = distance from the embankment wall (m),

X = overall distance between the embankment wall and the pool (m), and

n = exponent characterizing the beach profile (-).

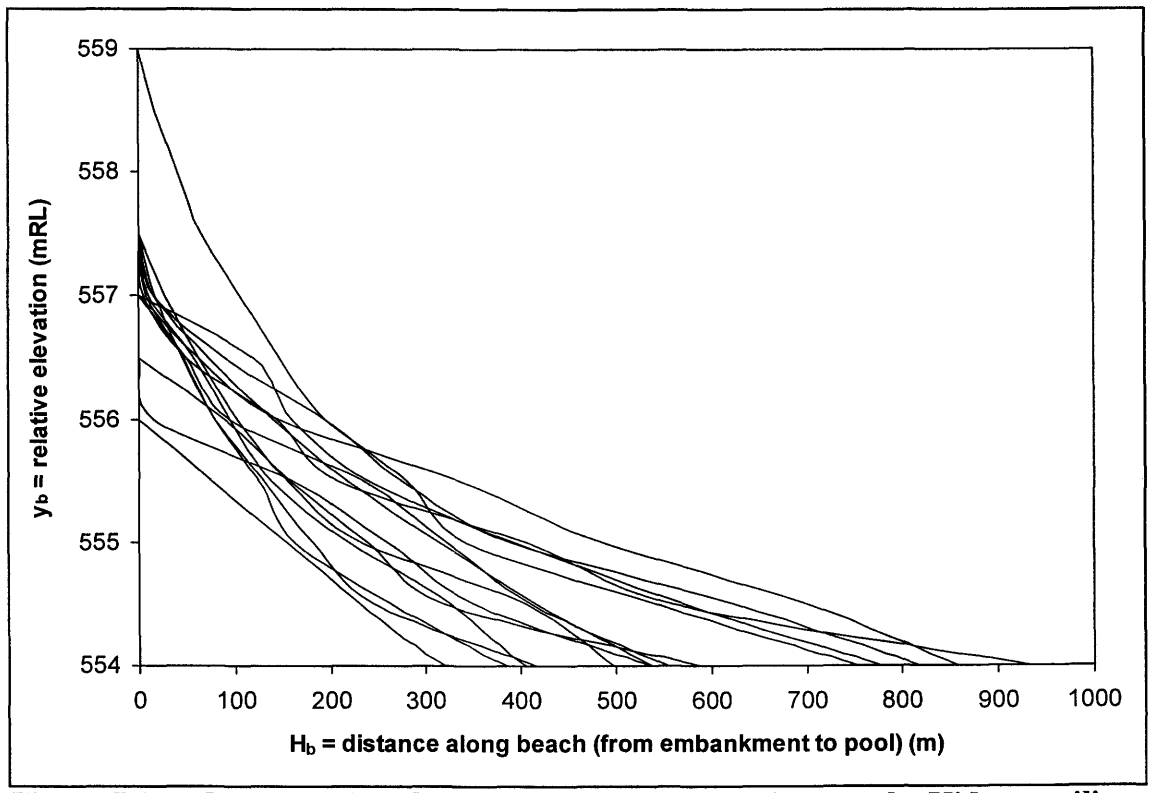

Figure 7.1: Measured beach profiles for 14 cross-sections on the Kidston tailings impoundment.

The components listed in Equation 7.1 are defined in Figure 7.3. The exponent, n characterizes the type of tailings used, as can be seen from the curves reported in Figure 7.2 (Blight, 1987). The exponent that best describes the Kidston tailings beach was determined to have a value of 1.85, with an overall beach distance, X = 650 m, and the maximum beach height, y_b = 3.4 m. The selection of these constants was made based on the detailed tailings impoundment surface survey data. The use of the non-dimensionalized beach function for the Kidston tailings impoundment, can thus now be used to describe the beach shape anywhere along the tailings impoundment surface.

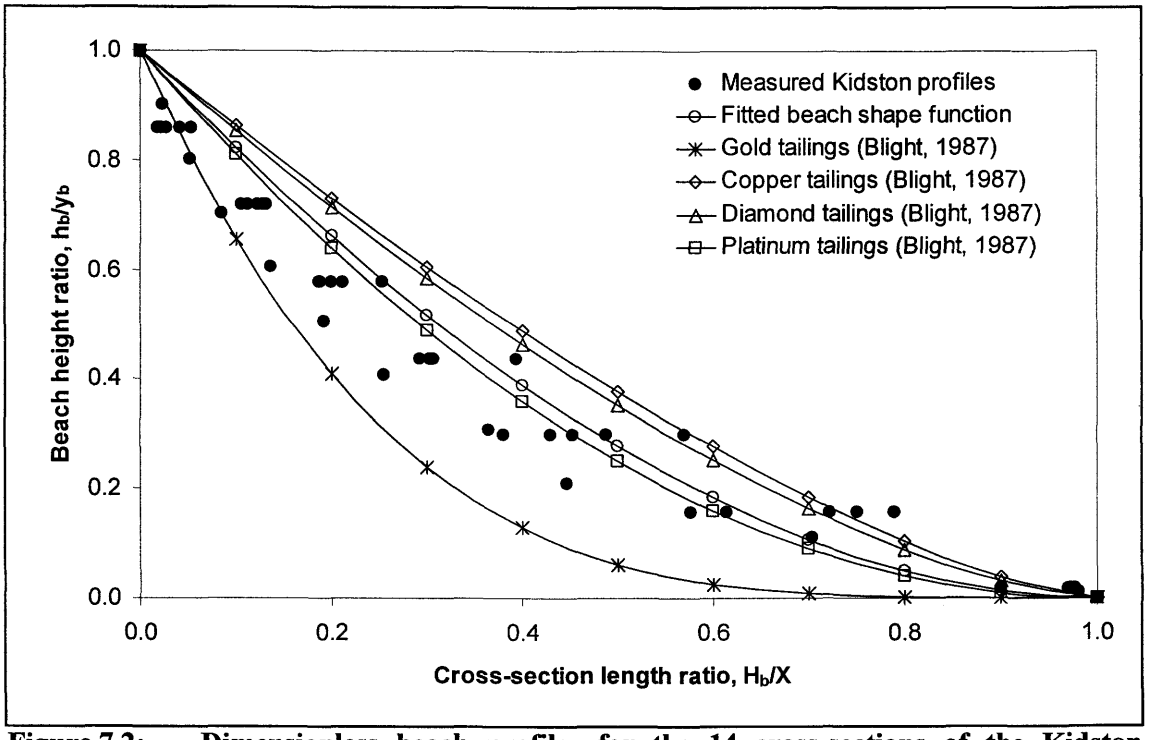

Figure 7.2: **Dimensionless beach profiles for the 14 cross-sections of the Kidston tailings impoundment.**

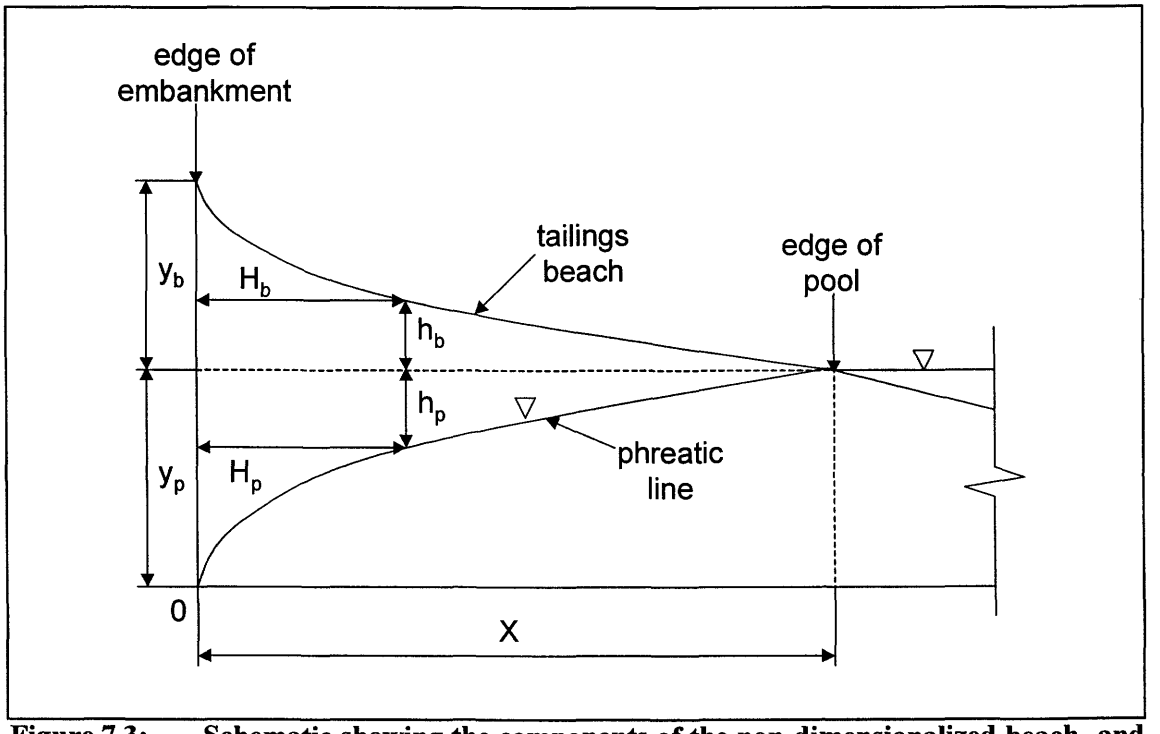

Figure 7.3: **Schematic showing the components of the non-dimensionalized beach- and phreatic line profiles.**

7.4 Description of the Position of the Phreatic Line

The bottom boundary for the generalized tailings impoundment cross-section is the phreatic line since it defines where the unsaturated zone ends, and therefore the zone where complex numerical unsaturated zone flux calculations cease. Figure 7.4 presents the four-year averaged results of nine piezometer section lines on the Kidston tailings impoundment summarized in Appendix F. It can be seen that each profile has a different length H_p, and a difference in elevation y_p, between the embankment wall and the pool. The factors that determine the shape of the phreatic line are the tailings properties, the pool location, as well as the presence of any toe or blanket drains in the embankment wall. Many researchers attempt to characterize the seepage pattern through a tailings impoundment (Abadjiev, 1976; Mittal and Morgenstern, 1976; Volpe, 1975), van Zyl and Harr (1988) provide an excellent summary of these efforts. A more simplistic approach was required for the purpose of this study, since none of the reported methods were suitable for describing a generic phreatic line function.

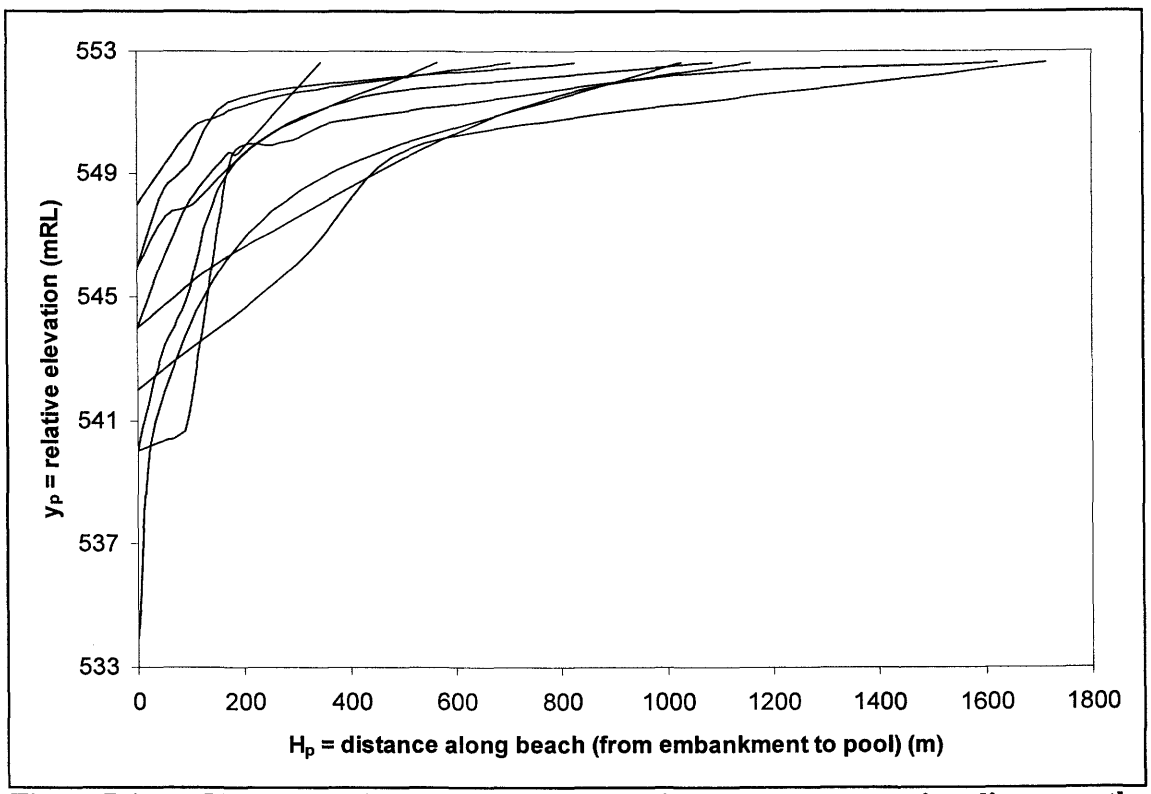

Figure 7.4: Measured phreatic levels along nine piezometer section lines on the Kidston tailings impoundment (four-year averaged data set).

It was found that by non-dimensionalizing the profiles in Figure 7.4, and replotting them in dimensionless form as described in Figure 7.5, a master phreatic line profile could be fitted to describe the position of the phreatic line at any location within the Kidston tailings dam.

The phreatic line master profile can be described by the following equation:

$$\frac{h_p}{y_p} = \left(1 - \frac{H_p}{X}\right)^{-n} \qquad [7.2]$$

Where h_p = phreatic level depth at any point between the embankment wall and the pool (m),

y_p = maximum phreatic level depth between the embankment wall and the pool (m),

H_p = distance from the embankment wall (m),

X = overall distance between the embankment wall and the pool (m), and

n = exponent characterizing the phreatic line profile (-).

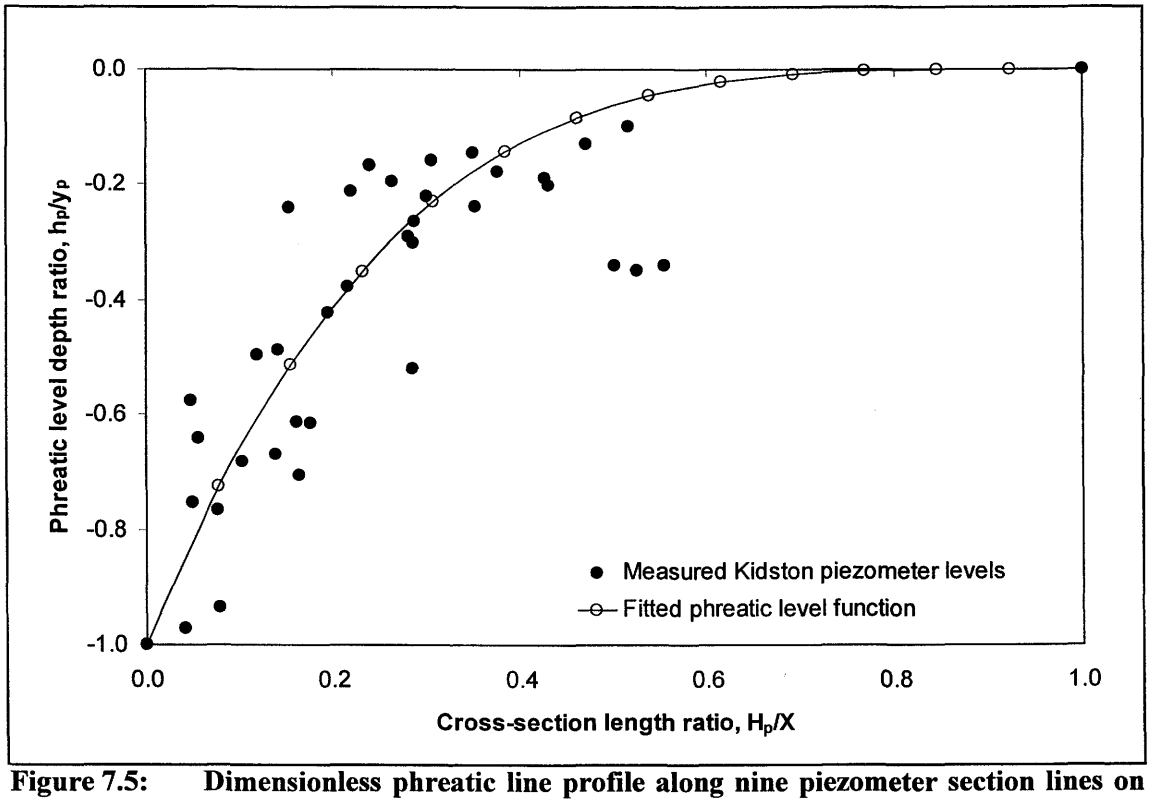

Figure 7.5: Dimensionless phreatic line profile along nine piezometer section lines on the Kidston tailings impoundment (four-year averaged data set).

Equation 7.2 is the same basic form as Equation 7.1 that is the master profile equation for a tailings impoundment beach as presented by Blight (1987). The phreatic line master profile was found to follow the same basic geometry, and as such was the appropriate function to use.

All the components listed in Equation 7.2 are defined in Figure 7.3. The exponent, n characterizes the type of tailings used. The exponent that best describes the Kidston tailings phreatic level was determined to be 4.0, while the overall beach distance, X = 650 m, and the maximum phreatic level depth, y_p = 10.0 m. The choice of these constants have been made using the record of piezometer readings on the Kidston tailings impoundment since 1997 as described in Appendix F. The use of the non-dimensionalized phreatic line function for the Kidston tailings impoundment, can thus now be used to describe the position of the phreatic surface anywhere within the cross-section of the tailings impoundment.

7.5 Overall Generalized Tailings Impoundment Cross-Section Shape

The zone of unsaturated tailings along any Kidston tailings impoundment cross-section is known by combining the shape functions for the tailings surface and phreatic line presented in Figures 7.2 and 7.5, and defined by Equations 7.1and 7.2. This zone is presented in Figure 7.6. This can be referred to as the generalized Kidston tailings impoundment cross-section.

From Figures 7.2 and 7.5 it is evident that there is a significant amount of scatter in the data, and it might be argued that the shape functions are not truly representative of the physical conditions in the impoundment. The scatter is however judged to be reasonable, given the complex geometry of the tailings impoundment. When one considers the value of using a generalized cross-section that can be described by a continuous mathematical function, it becomes reasonable to accept the shape functions as the best alternative.

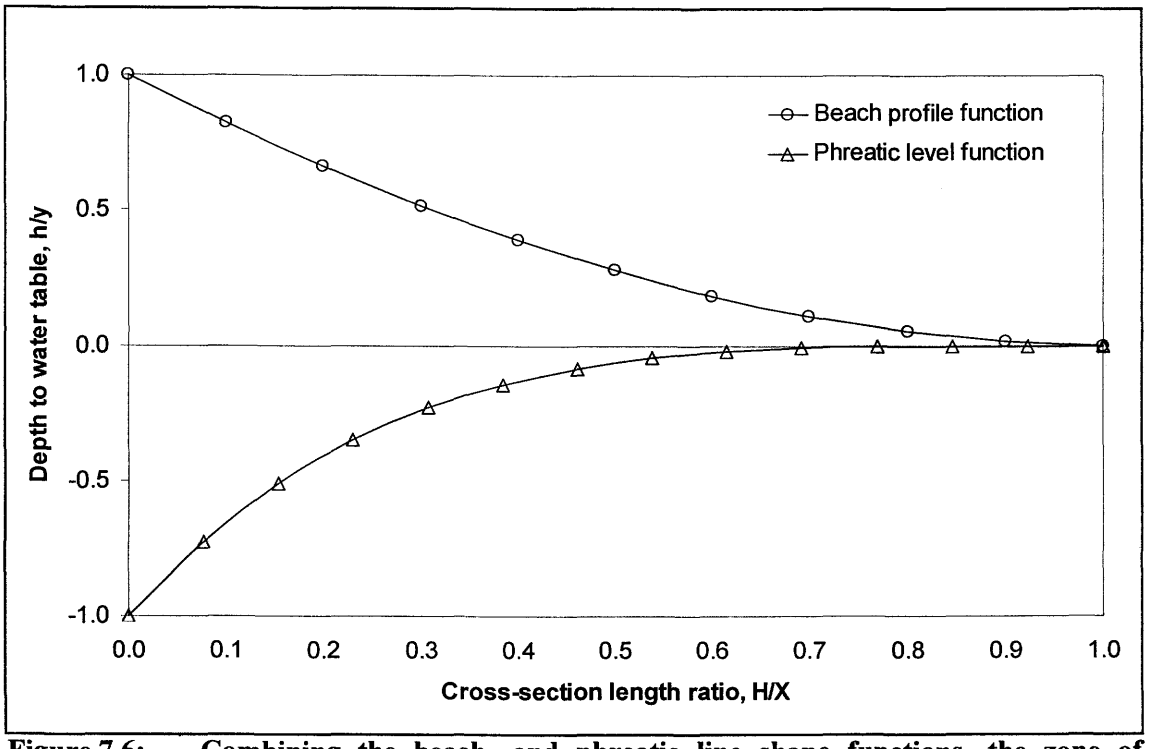

Figure 7.6: Combining the beach- and phreatic line shape functions, the zone of unsaturated tailings along any Kidston tailings impoundment cross-section is known.

7.6 Surface Hydraulic Conductivity

Since, the analysis depends on the SoilCover model to numerically calculate the surface flux boundary conditions through the generalized tailings impoundment cross-section presented in Figure 7.6, it is necessary to develop the appropriate material properties. One of the most crucial elements in calculating surface flux boundary conditions through unsaturated soils, is the hydraulic conductivity of the tailings surface, since it is the parameter that governs the infiltrability at the surface. In hydraulically placed tailings there is a tendency for the tailings particles to gravitate to the bottom of the slurry stream and deposit out. According to the laws of gravitational settling, larger particles will settle out higher up the beach (closer to the embankment) while finer particles will travel further towards the pool. This phenomena is true in natural streams (Morris and Williams, 1997a), as well as in hydraulically placed mine waste. Morris and Williams (1997b) reports on particle segregation of co-disposed coal wastes, Fourie (1988) documents characteristics of bauxite, nickel and coal tailings, Boldt (1989) documents results of 18 metal- and non metal mine wastes, and Blight (1987) documents the case of a

diamond tailings, to name but a few prominent studies. In Chapter 4 it was shown that this trend is true for the Kidston tailings impoundment as well, with 16 individual grain size distribution tests along three section lines on the tailings impoundment showing decreasing particle sizes as one move closer to the pool.

The most important consequence of the particle size sorting is that the saturated hydraulic conductivity of the tailings mass will decrease continuously from the embankment wall to the pond. The variation of permeability will follow a relationship such given by Blight (1987) for his master profile studies. The mathematical relationship is defined as:

$$k_s = ae^{-bH_b} \qquad [7.3]$$

Where k_s = saturated hydraulic conductivity (m/s),
a,b = characteristics of the tailings (-), and
H_b = distance down the beach from the embankment wall (m).

The saturated hydraulic conductivity along the tailings impoundment beach can be calculated using the particle size distribution data mentioned using empirical formulas such as Hazen (Hazen, 1911) or the more recent method by Sherard *et al.* (1984), however a multitude of field infiltration tests was conducted on the Kidston tailings impoundment to directly measure the saturated hydraulic conductivity as described in Chapter 4. These tests included 12 double-ring infiltrometer tests, 62 Guelph permeameter tests, and 17 rainfall simulator tests.

Figure 7.7 presents all the measured saturated hydraulic conductivities for the Kidston tailings impoundment together with a best-fit exponential function. A critical evaluation of the data allows for the elimination of some of the data (outlyers), which gives rise to a new exponential-best fit function for the saturated hydraulic conductivity. A detailed analysis of various tailings types to be used for the SoilCover modeling (see following section), as well as some sensitivity analysis (not documented), resulted in the selection of the following function to describe the saturated hydraulic conductivity at any point along the generalized Kidston tailings impoundment cross-section:

$$k_s = 1.94 \times 10^{-5} . e^{-0.00977 H_b} \qquad [7.4]$$

This function is presented in Figure 7.7, as well as Figure 7.8, which is the dimensionless presentation of the saturated hydraulic conductivity function for the Kidston tailings impoundment. Equation 7.4 is identical to Equation 7.3, except for the values given to constants a and b.

7.7 Tailings Properties

The generalized Kidston tailings impoundment cross-section must have tailings properties assigned to it in order to perform the numerical modeling. The tailings properties define the soil water characteristic curve of the profile, which determines how the surface flux boundary conditions are calculated. The concept of particle segregation along the tailings beach, resulting in coarser tailings close to the embankment wall and finer tailings close to the pool have been discussed in detail in the previous section. This concept, however suggests that varying tailings properties should be selected for the generalized cross-section to represent this phenomena. Kealy and Busch (1971) document a study for determining seepage characteristics for tailings impoundments. They report that the optimum solutions were found using three tailings types for a tailings impoundment cross-section. Their cross-section consisted of a beach length of approximately 152 m long. The first 79 m from the embankment wall end consisted of the coarsest tailings, the next 49 m was somewhat finer tailings and the last 24 m consisted of the finest tailings (which extended to underneath the pool). Their choice of three tailings types was based on model calibration and extensive property testing.

Due to the extensive material property testing completed for the tailings for this study, which included 25 soil water characteristic tests presented in Chapter 4 and Appendix D, a decision was made to select three tailings types. (i.e. as per the work by Kealy and Busch (1971)). These three tailings types are named coarse, intermediate and fine, and comprise the 25-, 50- and 75-percentile values of the 25 soil water characteristic curves measured as part of this study. These soil water characteristic curves are presented in Figure 7.9, and the main properties are listed in Table 7.1.

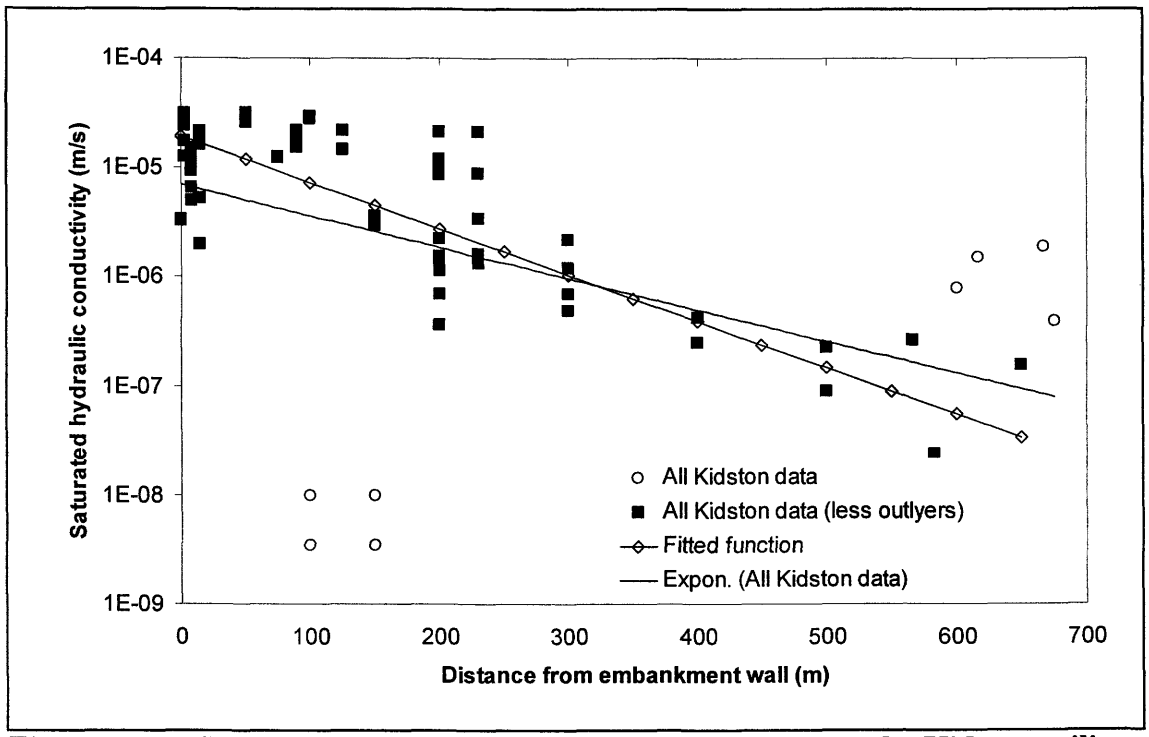

Figure 7.7: Measured saturated hydraulic conductivities on the Kidston tailings impoundment beach.

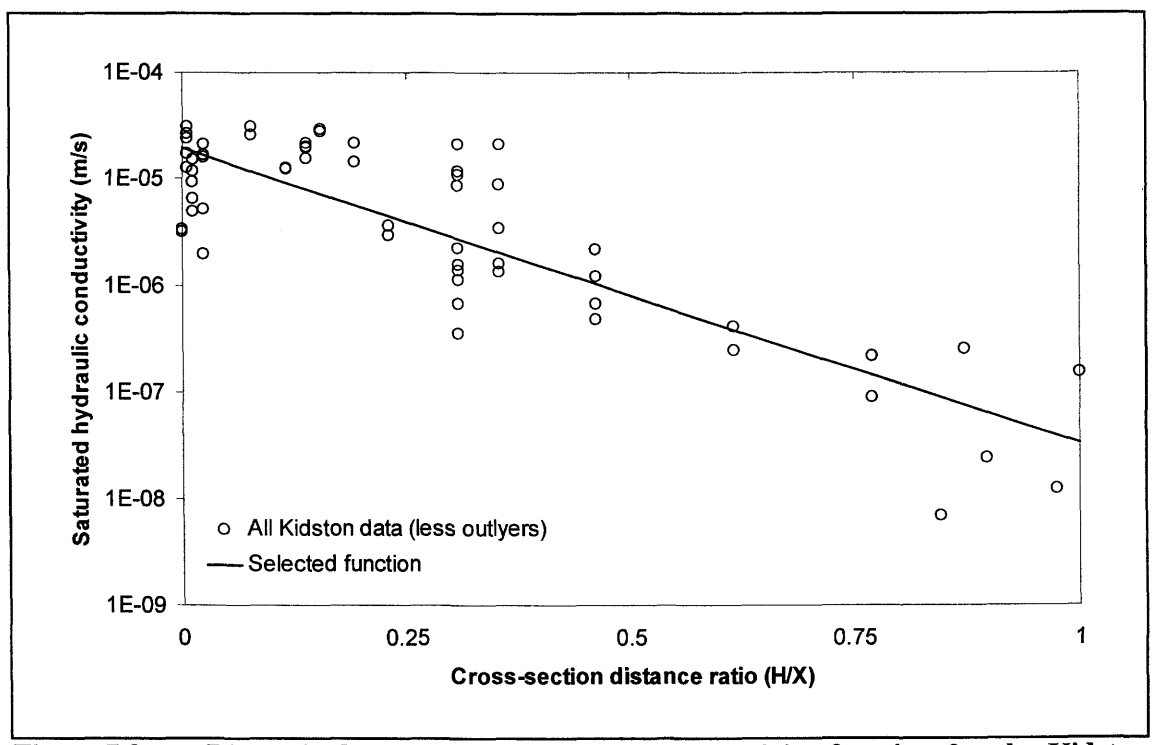

Figure 7.8: Dimensionless saturated hydraulic conductivity function for the Kidston tailings impoundment, based on measured data.

Table 7.1: **Soil water characteristic curve properties for the three tailings types to be used in numerical modeling of the typical Kidston tailings impoundment cross-section.**

Tailings type	Saturated volumetric water content, θ_s (%)	Air entry value, AEV, (kPa)	Residual suction, ψ_r, (kPa)	Residual volumetric water content, θ_r, (%)
Coarse	38.4	2.5	8.0	3.0
Intermediate	42.2	3.2	10.0	5.0
Fine	43.8	6.0	70.0	7.0

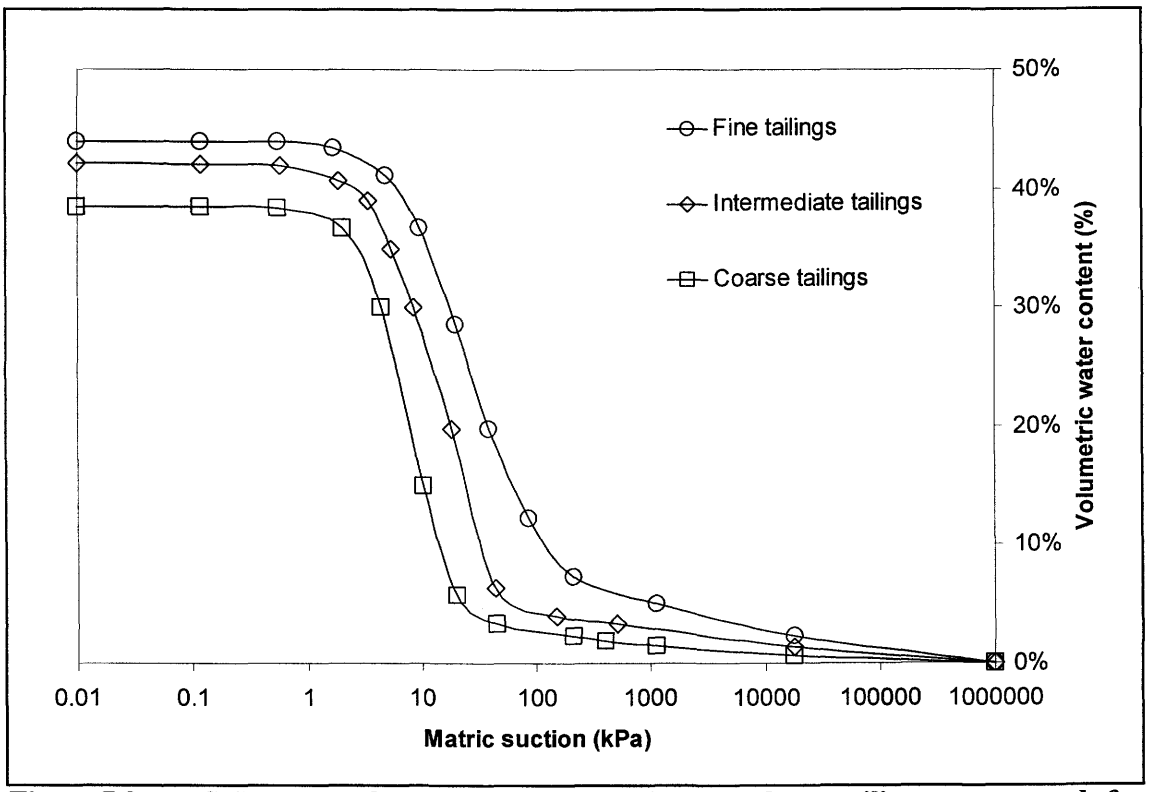

Figure 7.9: **Soil water characteristic curves for the three tailings types used for numerical modeling of the generalized tailings impoundment cross-section.**

The exact transition between the coarse, intermediate and fine tailings will be determined by the outcome of the SoilCover modeling, however the ratios suggested by Kealy and Busch (1971) were used to provide a guideline for definition as described in the following section.

The next important issue to consider was the influence of tailings layering. Due to the depositional technique, homogeneous vertical tailings profiles are usually rare, and test-pits excavated in the Kidston tailings impoundment, confirmed that there is significant layering. This means that there are fine, low permeability slimes interbedded with highly permeable coarse tailings (Vick, 1983). This has also been observed in the horizontal hydraulic

conductivity testing performed on the Kidston tailings impoundment, as reported in Chapter 4 (Douglas Partners, 1997; Earthtech Consultants, 1999). The deposition of the tailings at Kidston has always been via an open-ended pipe, which was located on the embankment wall. When the tailings deposition delta reached a certain height, the discharge pipe was relocated further up or down the wall, which resulted in a new deposition delta forming, inevitably overlapping the previous one. This leads to the conclusion, that although there are bands of varying tailings, no bands extend continuously from the embankment wall to the pond. This thus implies that these bands of tailings are unlikely to act as conduits which would short-circuit subsurface seepage flows.

Furthermore the tailings layering is completely random, and therefore would be extremely difficult to make some form of generalized statement as to the tailings layering for incorporation in the typical tailings impoundment cross-section. It is for these reasons that a decision was made that the generalized tailings impoundment cross-section be defined as homogeneous vertical profiles of coarse, intermediate or fine tailings. In other words, the values of the hydraulic conductivity assigned to each profile are considered to be the bulk hydraulic conductivity.

The calibration modeling documented in Chapter 6, used a bulk profile, and the results show favorable comparisons with measured values of matric suction profiles in the tailings. This thus supports the approach for homogeneous bulk profiles, and provides confidence that the errors so incorporated are small.

7.8 Solution Technique

The entire chapter up to this point described how a generalized Kidston tailings impoundment cross-section can be defined. The idea is that this 2-D cross-section can now be numerically solved using SoilCover in order to obtain the correct surface flux boundary condition along the beach profile. SoilCover is however a 1-D model, and can only solve profiles with a fixed depth. To overcome this problem the generalized tailings impoundment is divided into a number of equally sized zones, as illustrated in Figure 7.10. For the generalized Kidston cross-section 13 zones, each measuring 50 m wide were selected. Based on the geometry, this was deemed to be a reasonable breakdown of the problem.

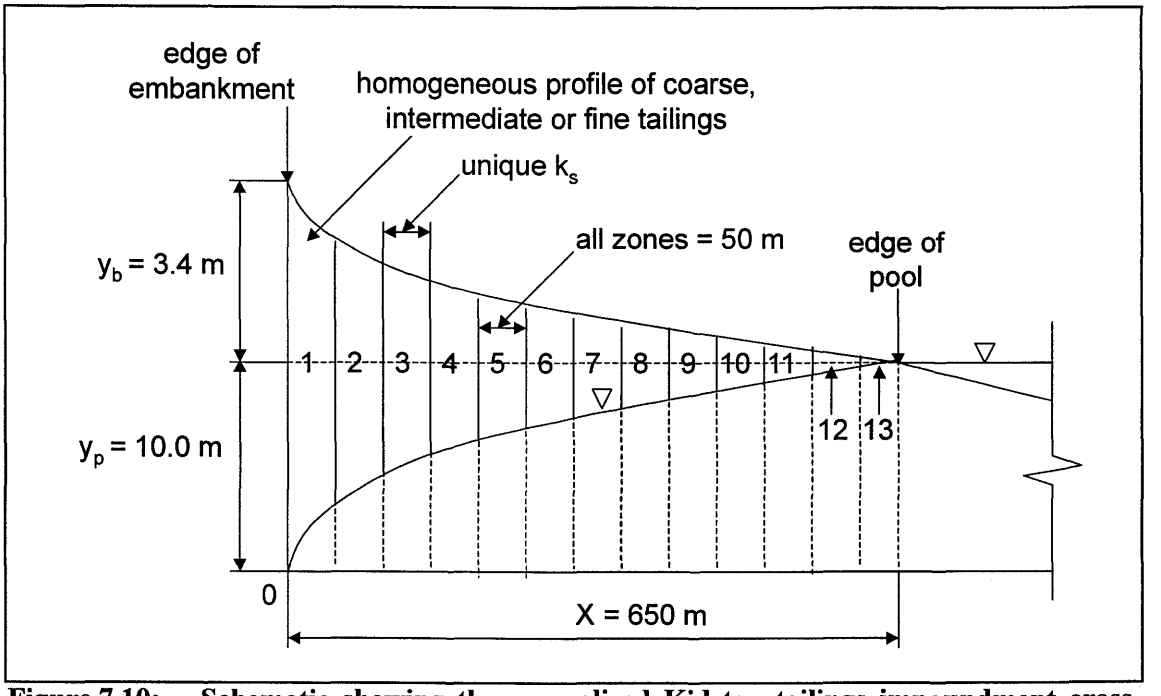

Figure 7.10: Schematic showing the generalized Kidston tailings impoundment cross-section, divided in to 13 equal zones.

A SoilCover model run are performed for each of these zones, with the profile depth defined by the sum of the maximum beach height, h_b, and the maximum phreatic level depth, h_p along the zone. These profile depths are documented in Chapter 8. Each zone is modeled three times, using a coarse, intermediate and fine tailings profile respectively.

The SoilCover model produces a result for surface fluxes that consist of runoff (R), evaporation (E) (or evapotranspiration (ET) if vegetation is present), bottom flux (BF) and net infiltration (NI) for each zone. After the model has been run for all 13 zones, the cumulative flux result for all water balance components are calculated by integration (the trapezoidal rule (Bird, 1997)). An assumption was made that any runoff emanating from a zone report to the pond (i.e. implying that it flows over the other regions). No allowance is made for runoff loss to infiltration downstream.

The parameter that was used to calibrate the SoilCover results for the 13 composite profiles was the total integrated runoff number. Chapter 5 describes the water balance for the Kidston tailings impoundment, from which it was estimated that the average runoff to the tailings pond is approximately 42%. Since each zone has been modeled using each tailings type, these zones of varying tailings types could be varied to find the optimum solution where the runoff most

closely matches the value of 42%. It was determined that using coarse tailings in the first five zones (i.e. 5 x 50 m = 250 m from embankment wall), intermediate tailings in the next five zones (i.e. 5 x 50 m = 250 m further), and fine tailings in the last three zones (i.e. 3 x 50 m = 150 m), provided the optimal solution with runoff calculated at 40.4% as described in Chapter 8. This is illustrated in Figure 7.11. The tailings type transition ratio for the generalized Kidston tailings impoundment cross-section is thus 250 m of coarse tailings (of a possible 650 m section), 250 m of intermediate tailings and 150 m of fine tailings (i.e. 250 m/650 m: 250 m/650 m: 150 m/650 m). The transition ratio can also be expressed in terms of the number of zones of a specific tailings type (i.e. 5 of 13 zones are coarse tailings, 5 of 13 zones are intermediate tailings and 3 of 13 zones are fine tailings, or 5:5:3).

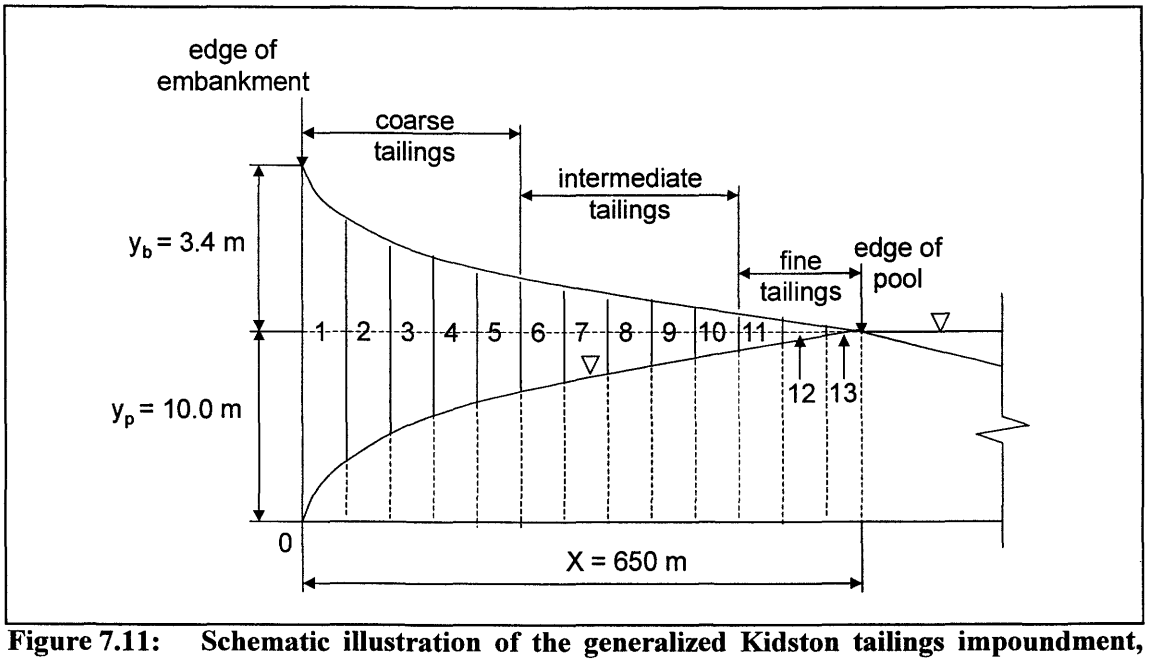

Figure 7.11: Schematic illustration of the generalized Kidston tailings impoundment, and the transition locations of the three tailings types.

Setting of the tailings type transition zones, and calibration of the integrated runoff number was done solely for a non-vegetated tailings impoundment surface, using a mean climatic year (see Chapter 8 for complete results). For all other cases modeled, including the evaluation data set reported in Chapter 10, these transition zones were used, and the subsequent runoff number was deemed correct. The transition zone ratio for the tailings types in the generalized Kidston tailings impoundment cross-section of 5:5:3 closely resembles the 7:4:2 ratio documented by Kealy and Busch (1971) (i.e. 79 m/152 m: 49 m/152 m: 24 m/152 m).

7.9 Conclusions

This chapter develops a procedure to use the 1-D SoilCover numerical model to solve a 2-D generalized tailings impoundment cross section, in order to obtain surface flux boundary conditions for a profile geometry that vary spatially due to the surface geometry, depth to the phreatic line and change in hydraulic conductivity. The complex problem is simplified by developing and describing the generalized tailings impoundment cross-section, non-dimensionalizing it, and thereby making the cross-section representative of any location on the tailings impoundment. The boundary conditions for the top (beach) and bottom (phreatic line) surface are fixed using continuous mathematical functions founded on the actual measured beach and phreatic level profiles. The tailings properties used in the cross-section is based on extensive laboratory and field-testing data, and is representative of the actual materials in the impoundment.

7.10 References

Abadjiev, Ch.B. (1976). Seepage Through Mill Tailings Dams. Transactions of the 12th International Congress on Large Dams, Mexico City, Vol. 1, pp. 381-393.

Bird, J.O. (1997). Mathematics Pocket Book for Engineers, 2nd Edition. Newnes, Oxford, England.

Blight, G.E. (1987). The concept of the master profile for tailings dam beaches. Proceedings of the International Symposium on Prediction and Performance in Geotechnical Engineering. Calgary, Alberta, Canada, 17-19 June, pp. 361-365.

Boldt, C.M.K. (1989). Beach Characteristics of Mine Waste Tailings. Report of investigations 9171, United States Department of the Interior, Bureau of Mines, 24 pp.

Douglas Partners. (1997). Factual Report on Tailings Dam Insitu Testing at Kidston Gold Mine. Consultants report to Kidston Gold Mines, Project No. 21712, July, 5 pages.

Earthtech Consultants. (1999). Report on Piezocone Testing, Kidston Tailings Storage Facility. Consultants report to Australasian Groundwater & Environmental Consultants Pty Ltd., Project No. MF 1367, December, 3 pages.

Fourie, A. (1988). Beaching and Permeability Properties of Tailings. Hydraulic Fill Structures, Geotechnical Special Publication No. 21, pp. 142-154.

Hazen, A. (1911). Discussion of "Dams on Sand Foundations", by A.C. Koenig, Transactions, ASCE, Vol. 73, pp. 199-203.

Kealy, DC, Busch, RA. (1971). Determining Seepage Characteristics of Mill-Tailings Dams by the Finite-Element Method. Report of Investigations 7477, United States Department of the Interior, Bureau of Mines. January, 113 pages.

Mittal, H.K., Morgenstern, N.R. (1976). Seepage control in tailings dams. Canadian Geotechnical Journal, Vol. 13, pp. 277-293.

Morris, P.H., Williams, D.J. (1997a). Hydraulic conditions leading to exponential mine tailings delta profiles. Transactions of the Institution of Mining and Metallurgy (Section A: Min. Industry), Volume 106, January-April, pp. A34-A37.

Morris, P.H., Williams, D.J. (1997b). Hydraulic sorting of co-disposed coarse and fine coal wastes. Transactions of the Institution of Mining and Metallurgy (Section C: Mineral Process. Extr. Metall.), Volume 106, January-April, pp. C21-C26.

Sherard, J.L., Dunnigan, L.P., Talbot, J.R. (1984). Basic properties of sand and gravel filters. Journal of Geotechnical Engineering, Vol. 110, No. 6, pp. 684-700.

SoilCover. (1997). SoilCover User's Manual. Unsaturated Soils Group, Department of Civil Engineering, University of Saskatchewan, Saskatoon, Saskatchewan, Canada.

van Zyl, D.J.A, Harr, M.E. (1988). Modeling of Seepage Through Mine Tailings Dams. Hydraulic Fill Structures; geotechnical special publication No. 21. Edited by DJA van Zyl and SG Vick, New York, 1988, pp. 727-743.

Vick, SG. (1983). Planning Design and Analysis of Tailings Dams. A Wiley-Interscience Publication, John Wiley & Sons, New York, 369 pages.

Volpe, R.L. (1975). Geotechnical Engineering Aspects of Copper Tailings Dams. ASCE National Convention, Denver, Meeting Reprint No. 2629, 30 pp.

CHAPTER 8
SoilCover Modeling

8.1 Introduction

This chapter documents the application of the SoilCover (SoilCover, 1997) model, as well as the model results as described in Chapter 7. The SoilCover model setup, boundary conditions and material properties are documented as well as a summary of results for the annual and monthly composite cross-section simulations. Detailed results for the individual model simulations are documented in Appendix M, together with summarized results for all cases not specifically discussed in this chapter.

8.2 General SoilCover Modeling Approach

The methodology of how to use individual SoilCover runs, in order to calculate the surface fluxes along the generalized tailings impoundment cross-section have been described in Chapter 7. This chapter focuses on the actual SoilCover simulations. The general modeling approach was to perform a SoilCover (SoilCover, 1997) simulation for each of the 234 individual case profiles to be evaluated. These consist of 13 individual simulations for each composite cross-section, for three material types, for three climatic types and for both vegetated and non-vegetated tailings impoundment surfaces (13 x 3 x 3 x 2 = 234). The numbering protocol and a detailed list of all these models are presented in Appendix M. Each model simulation was for a full year of 365 days. The year started on 1 July (Julian day 182) and ended 30 June (Julian day 181). Since SoilCover does not allow modeling across calendar years, the Julian days for the model simulations documented here were transposed such that 1 July was day 1, and 30 June was day 365. The model simulations were carried out using generic climate data sets, and were not representative of any specific actual calendar year. The production of the generic climate data sets is detailed in Appendix H.

8.3 Model Setup

This section describes the input requirements for the SoilCover modeling. These inputs cover the convergence and time intervals for the numerical solution, setting of the mesh representing the modeled profile, assigning material properties to the profile and finally assigning boundary conditions to the profile.

8.3.1 Convergence

The convergence parameters of the individual model (SoilCover, 1997) simulations were constant for all model simulations, and were initially determined on the basis of a sensitivity analysis (not documented). The maximum number of iterations allowed were 100, the maximum change in matric suction and soil temperature was for individual time steps was set equal to 1%, and the matric suction and soil temperature damping was set equal to 0%.

8.3.2 Time Steps

The time steps used in the SoilCover (SoilCover, 1997) models were kept constant for all simulations based on a sensitivity analysis at the outset of the modeling stage (not documented). The time sequence starts at one second, the minimum time step is one second and the maximum time step is 3600 seconds. The maximum matric suction and soil temperature change was set equal to 1%.

8.3.3 Mesh Generation

The mesh was generated and kept constant for each of the 13 individual profile depths analyzed. The mesh always consisted of a single layer, with either coarse, intermediate or fine tailings present. The base elevation of the mesh (the phreatic table) was set at 0.0 m. The mesh components (SoilCover, 1997) are listed in Table 8.1.

Table 8.1: Mesh components for each of the individual SoilCover simulations of different profile depths.

Simulation no.	Top elevation (m)	Minimum space (mm)	Maximum space (mm)	Expansion factor	No. of nodes
1	13.400	0.5	1000	2.0	34
2	10.192	0.5	1000	2.0	32

Table 8.1: Mesh components for each of the individual SoilCover simulations of different profile depths.

Simulation no.	Top elevation (m)	Minimum space (mm)	Maximum space (mm)	Expansion factor	No. of nodes
3	7.622	0.5	700	2.0	30
4	5.594	0.5	600	2.0	28
5	4.019	0.5	400	2.0	28
6	2.819	0.5	250	2.0	28
7	1.922	0.5	200	2.0	26
8	1.267	0.5	110	2.0	26
9	0.799	0.5	80	1.5	32
10	0.474	0.5	50	1.5	30
11	0.254	0.5	20	1.5	28
12	0.112	0.5	10	1.5	24
13	0.030	0.1	3	1.3	30

The base temperature was kept constant at 15°C, while the initial surface temperature was set equal to 25°C for all the simulations. These temperatures were selected based on the sensitivity analysis that was carried out prior to the final modeling (not documented). The algorithms in SoilCover was used to calculate the daily ground temperatures for all simulations (SoilCover, 1997). Initial moisture conditions for each profile was set by means of matric suction and is discussed in a subsequent section of this chapter.

8.3.4 Material Properties

The material properties required defining the SoilCover model is presented in this section. These properties are tailings soil water characteristic curves, unsaturated hydraulic conductivity functions, saturated hydraulic conductivity, thermal conductivity- and volumetric specific heat functions. The material properties are for the three tailings classes defined i.e. coarse, intermediate and fine.

8.3.4.1 Soil Water Characteristic Curves

All the SoilCover simulations were performed with a homogeneous vertical profile, however three different tailings types were used in the different simulations. These tailings types were classified as coarse, intermediate and fine tailings, and were based on the extensive laboratory and field characterization of the tailings undertaken as part of this study as described in Chapter 4. The soil water characteristic curves of the three tailings types were based on the 25, 50 and 75%-tile values of all the tests performed. Due to the steepness of these curves, significant

numerical instability occurred, and to reduce this the curves were smoothed slightly. The actual matric suction versus volumetric water content data together with the modified data for numerical stability in SoilCover (SoilCover, 1997) are presented in Table 8.2 and illustrated in Figure 8.1.

Table 8.2: Actual and modified soil water characteristic curve data for the three tailings types used in the SoilCover modeling.

Fine tailings			Intermediate tailings			Coarse tailings		
Matric suction, ψ (kPa)	Volumetric moisture content, θ (fraction)		Matric suction, ψ (kPa)	Volumetric moisture content, θ (fraction)		Matric suction, ψ (kPa)	Volumetric moisture content, θ (fraction)	
	Actual	Modified		Actual	Modified		Actual	Modified
0.01	0.439	0.439	0.01	0.422	0.422	0.01	0.385	0.385
0.12	0.439	0.439	0.12	0.420	0.422	0.12	0.385	0.385
0.55	0.439	0.439	0.59	0.419	0.419	0.55	0.384	0.384
1.70	0.434	0.434	1.91	0.407	0.407	2.04	0.367	0.367
4.90	0.411	0.411	3.47	0.390	0.390	4.47	0.300	0.300
9.55	0.367	0.367	5.38	0.349	0.349	10.35	0.150	0.167
19.95	0.286	0.286	8.51	0.300	0.300	20.23	0.058	0.116
38.90	0.198	0.198	18.24	0.198	0.198	44.67	0.033	0.089
87.10	0.122	0.122	43.85	0.064	0.117	208.93	0.023	0.064
208.93	0.073	0.073	147.91	0.040	0.070	407.38	0.019	0.054
1122.02	0.050	0.050	512.86	0.033	0.054	1122.02	0.015	0.047
18197.01	0.023	0.023	18197.01	0.014	0.024	18197.01	0.006	0.021
1000000	0.000	0.000	1000000	0.000	0.000	1000000	0.000	0.000

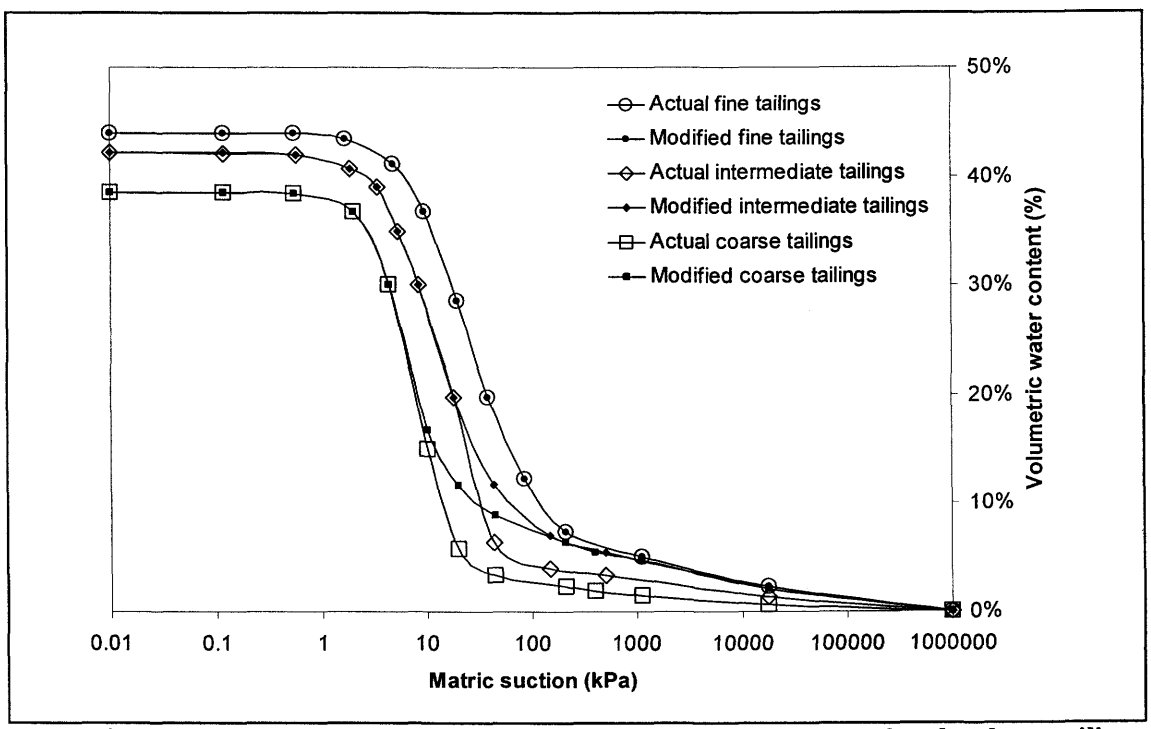

Figure 8.1: Actual and modified soil water characteristic curves for the three tailings types used in the SoilCover modeling.

Table 8.3 provides a summary of the material properties input data required by SoilCover for each tailings type, in addition to the soil water characteristic curve data. This data is based on the modified soil water characteristic curve data presented in Table 8.2. The curve fit parameters are based on the Fredlund and Xing (1994) curve fitting technique used by SoilCover to define the soil water characteristic curve.

Table 8.3: Summary of the material property constants for the three tailings types required for the SoilCover modeling.

Parameter	Fine tailings	Intermediate tailings	Coarse tailings
Porosity, n	0.439	0.422	0.385
Specific gravity, G_s	2.767		
Coefficient of volume change, m_v (1/kPa)	3.00E-03	5.20E-03	1.90E-03
Fredlund and Xing (1994), a	14.94	7.12	3.97
Fredlund and Xing (1994), n	1.64	1.89	3.09
Fredlund and Xing (1994), m	1.14	1.00	0.73

8.3.4.2 Unsaturated Hydraulic Conductivity Functions

Only a limited amount of unsaturated hydraulic conductivity testing was done as described in Chapter 4, and as a result hydraulic conductivity functions for the three tailings types were predicted using the Fredlund and Xing (1994) curve fitted data for the soil water characteristic curves in SoilCover (SoilCover, 1997). The curve fitting technique for the unsaturated hydraulic conductivity function used by SoilCover are those proposed by Fredlund *et al.* (1994). SoilCover produces relative unsaturated hydraulic conductivity functions, which means that the predicted unsaturated hydraulic conductivity of a soil for any given suction is the relative unsaturated hydraulic conductivity multiplied by the saturated hydraulic conductivity. Numerical instability again resulted in these functions being modified in the high suction range. Table 8.4 contains the relative unsaturated hydraulic conductivity function data for both the predicted- and the modified curves. These curves are presented in Figure 8.2.

Table 8.4: Predicted and modified relative unsaturated hydraulic conductivity curve data for the three tailings types used in the SoilCover modeling.

Matric suction, ψ (kPa)	Predicted data			Modified fine tailings		Modified intermediate tailings		Modified coarse tailings	
	Fine	Interm.	Coarse						
	Hydraulic conductivity, k (m/s)			ψ (kPa)	k (m/s)	ψ (kPa)	k (m/s)	ψ (kPa)	k (m/s)
0.01	1.00E-02	1.00E-02	1.00E-02	0.01	1.00E-02	0.01	1.00E-02	0.01	1.00E-02
0.09	9.99E-03	9.96E-03	1.00E-02	0.09	9.90E-03	0.09	9.96E-03	0.09	1.00E-02
0.59	9.18E-03	9.26E-03	9.95E-03	0.59	9.18E-03	0.59	9.26E-03	0.59	9.95E-03

Table 8.4: Predicted and modified relative unsaturated hydraulic conductivity curve data for the three tailings types used in the SoilCover modeling.

Matric suction, ψ (kPa)	Predicted data			Modified fine tailings		Modified intermediate tailings		Modified coarse tailings	
	Fine	Interm.	Coarse						
	Hydraulic conductivity, k (m/s)			ψ (kPa)	k (m/s)	ψ (kPa)	k (m/s)	ψ (kPa)	k (m/s)
4.02	4.09E-03	1.12E-03	1.68E-04	6.00	4.09E-03	3.50	5.13E-03	2.50	5.62E-03
27.19	2.22E-05	2.33E-06	2.37E-07	38.90	2.22E-05	27.19	2.33E-06	27.19	2.37E-07
183.88	4.74E-08	7.61E-09	1.48E-09	183.88	4.74E-08	183.88	7.61E-09	183.88	1.48E-09
1243.48	2.91E-10	7.41E-11	2.50E-11	1243.48	2.91E-10	1243.48	7.41E-11	1243.48	2.50E-11
8408.96	2.60E-12	8.80E-13	4.25E-13	8408.96	2.60E-12	8408.96	8.80E-13	8408.96	4.25E-13
56865.06	2.31E-14	9.37E-15	5.78E-15	56865.06	2.75E-13	56865.06	1.02E-13	56865.06	3.55E-14
384546	2.04E-16	9.98E-17	7.87E-17	384546	1.00E-13	384546	5.00E-14	384546	1.00E-14

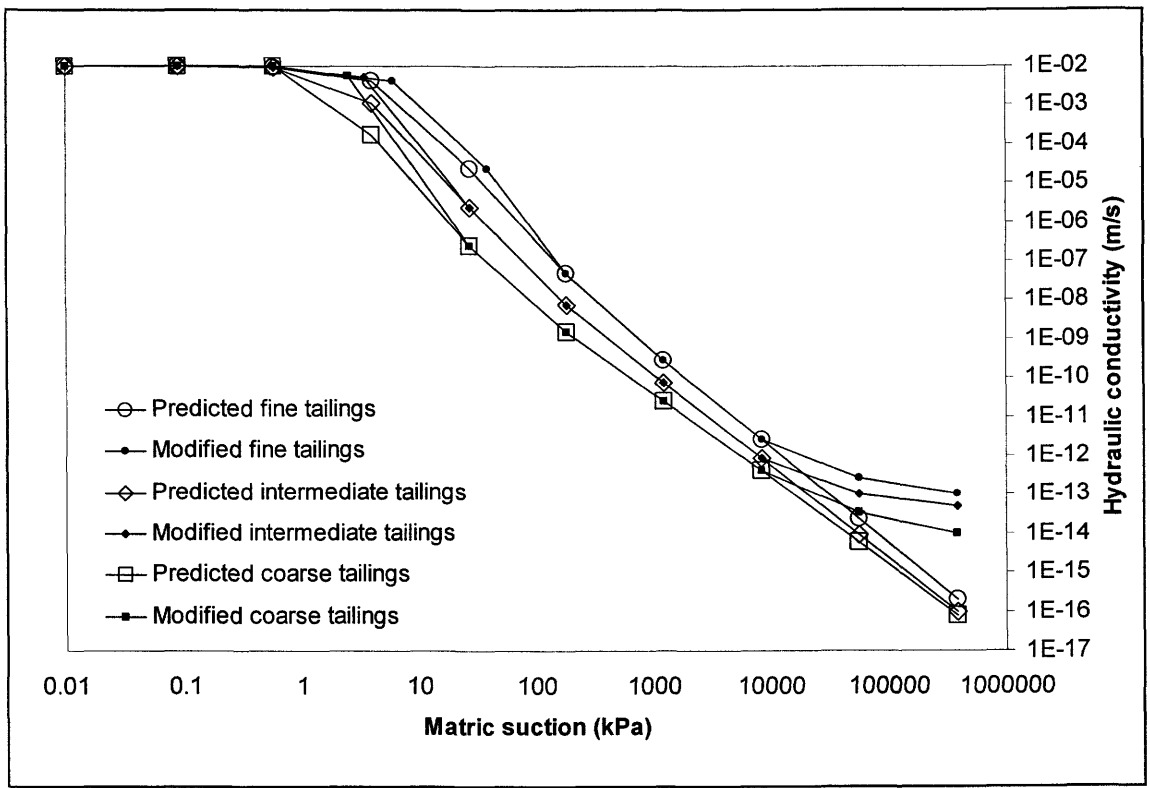

Figure 8.2: Predicted and modified relative unsaturated hydraulic conductivity functions for the three tailings types used in the SoilCover modeling.

8.3.4.3 Saturated Hydraulic Conductivity

The surface saturated hydraulic conductivity has been defined by means of a function described in Chapter 7 based on intensive field data. The resultant surface saturated hydraulic conductivity for each of the 13 model runs in the generalized cross-section is presented in Table 8.5. These

values are used to convert the relative unsaturated hydraulic conductivity functions to their true values.

Table 8.5: Surface saturated hydraulic conductivity for each SoilCover profile.

Simulation no.	Top elevation (m)	Surface saturated hydraulic conductivity, k_s (m/s)
1	1.3400	1.94E-05
2	1.0192	1.19E-05
3	7.622	7.30E-06
4	5.594	4.48E-06
5	4.019	2.75E-06
6	2.819	1.69E-06
7	1.922	1.03E-06
8	1.267	6.35E-07
9	0.799	3.90E-07
10	0.474	2.39E-07
11	0.254	1.47E-07
12	0.112	9.00E-08
13	0.030	5.52E-08

8.3.4.4 Thermal Conductivity Function

The thermal conductivity reflects the ability of the soil (or in this case, the tailings) to transmit heat just as the hydraulic conductivity reflects the soils ability to transmit water. The rate at which heat is transferred depends on the temperature gradient and the thermal conductivity of the soil. The thermal conductivity of a soil can be defined as the amount of heat which flows through a unit area of soil in a unit time, under a unit gradient (SoilCover, 1997). Since no experimental data to measure this function was available, the function in SoilCover to generate a function using a method proposed by Johansen (1975) was used. The percentage quartz had to be specified in order to determine this function, and a value of 90% was selected (Holtz and Kovacs, 1981). The resultant thermal conductivity functions are presented in Figure 8.3.

8.3.4.5 Volumetric Specific Heat Function

The volumetric specific heat of a soil is defined as the amount of stored heat required to change the temperature of a unit volume (1 m^3) of the soil by 1°C (Jumikis, 1977). The volumetric specific heat of the soil can then be calculated by multiplying the mass specific heat of the soil with the mass density of the soil. SoilCover can generate the specific heat function if the mass specific heat of the soil is specified using the de Vries (1963) method. For this study a value of 792 $J/kg^3.°C$ was selected. The resultant functions are presented in Figure 8.4.

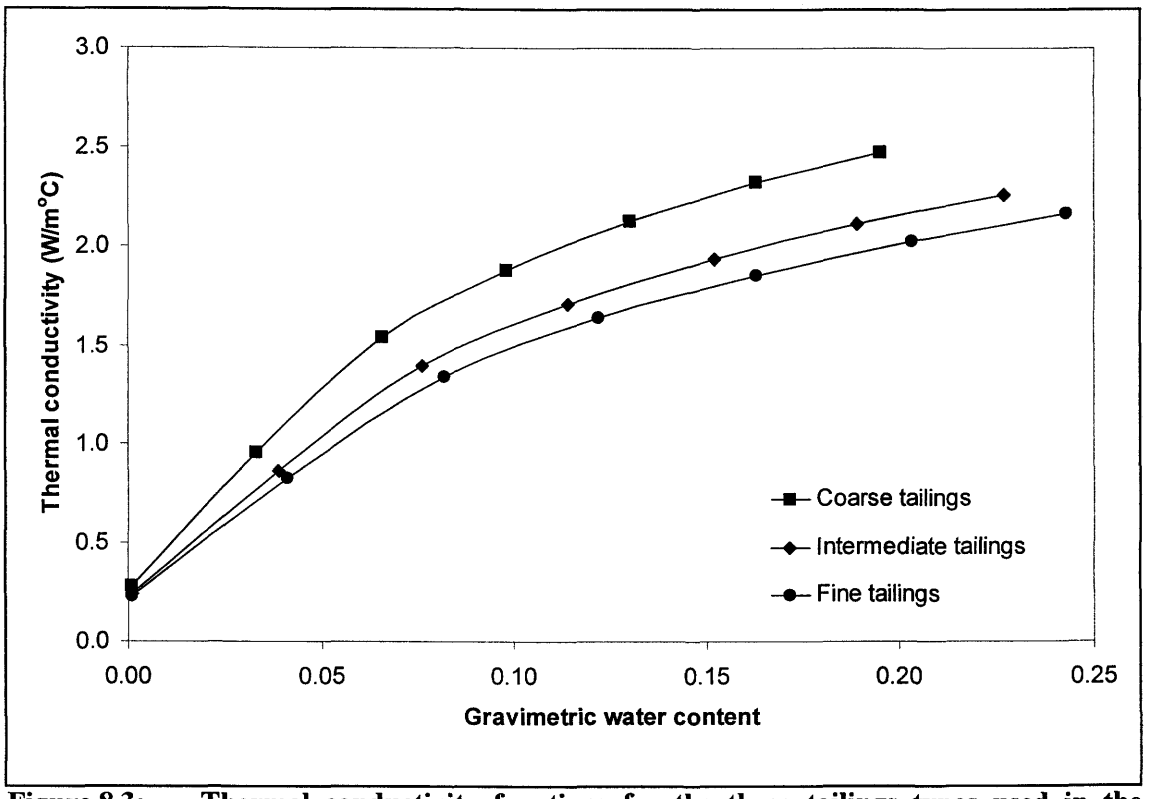

Figure 8.3: **Thermal conductivity functions for the three tailings types used in the SoilCover modeling.**

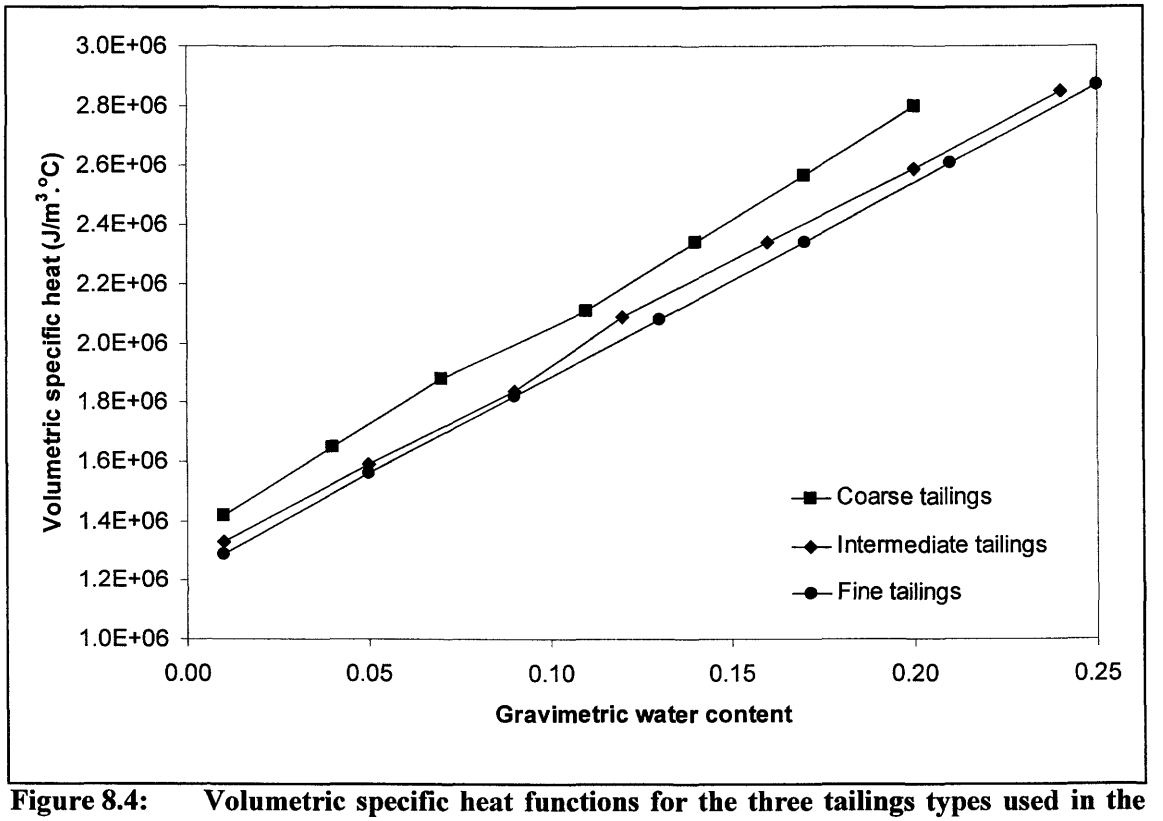

Figure 8.4: **Volumetric specific heat functions for the three tailings types used in the SoilCover modeling.**

The SoilCover manual states that the numerical solutions are not very sensitive to the thermal conductivity and specific heat properties (SoilCover, 1997). This was tested by varying the quartz content and the soil specific heat value, with no significant impact on the results.

8.3.5 Boundary Conditions

The boundary conditions for the SoilCover model consist of climate data that causes the atmospheric forcing, vegetation data that defines root extraction of soil moisture, and initial conditions, i.e. the moisture profile prior to starting the simulation. The sections below describe all these components.

8.3.5.1 Site Data

SoilCover requires site-specific data to define the top surface boundary conditions. In the event that the site under investigation lies in the shadow of a mountain range allowance can be made for delayed sunshine hours and temperature changes. For the Kidston tailings impoundment this does not apply and the temperature and relative humidity lag was set to zero. The site latitude was input as -18°, with the negative sign denoting the fact that the site is in the Southern Hemisphere.

8.3.5.2 Climate Data

The detailed weather data used for the model simulations consisted of daily maximum and minimum air temperatures, maximum and minimum relative humidity, wind speed, net radiation and precipitation. The data used for the SoilCover (SoilCover, 1997) simulations were not specific to any calendar year, but were a generic data set created specifically for the purpose of the modeling. The generic data set represents a typical mean, an extremely wet, or an extremely dry year respectively. The methodology for creating these generic climate data sets are presented in Appendix J, together with the detailed daily precipitation data used in the modeling. The detailed daily air temperature, relative humidity, wind speed and net radiation data for each generic climate data set is presented in Appendix H. In all instances daily precipitation events were spread evenly over 24 hours. This was done due to the increased numerical instability, which was introduced when actual storm intensities were used. This

assumption has been validated by the SoilCover calibration reported in Chapter 6. An analysis of actual storm intensities for Kidston is presented in Appendix J.

8.3.5.3 Vegetation Data

All the model simulations were conducted with and without a vegetative cover. When vegetation was present the growth season started on 18 May (Julian day 138) and ended on 15 November (Julian day 318). These are of course the transposed dates to accommodate for the July/June year that was modeled. The actual growth season starts on 15 November and ends on 15 May, based on visual observation by Mr. Paul Ritchie, the Kidston Environmental Officer.

The potential evaporation is the maximum evaporative flux for bare soil conditions (i.e. non-vegetated tailings) and a saturated soil surface, however when a full vegetative cover is present, the potential evaporation is the maximum transpiration flux (Ritchie, 1972). The leaf area index is defined as the leaf surface area divided by the soil surface area. SoilCover gives a choice of a poor grass cover, a good grass cover or an excellent grass cover. The excellent cover LAI was used for these simulations is presented in Figure 8.5.

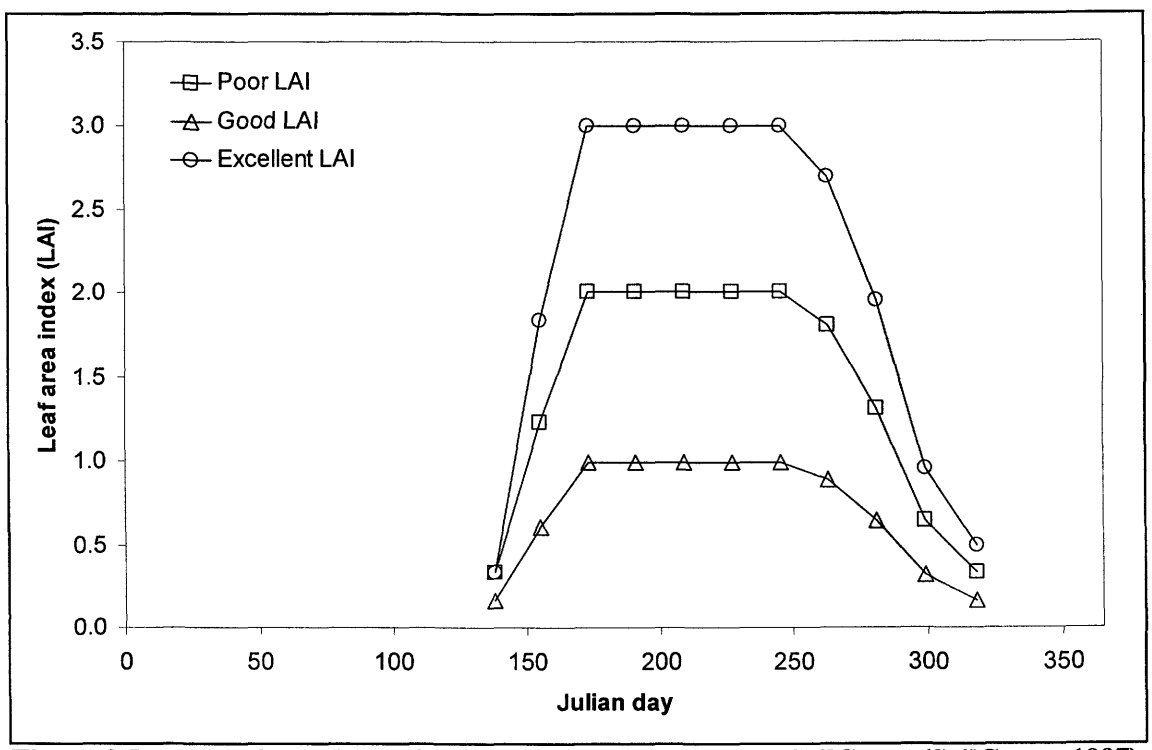

Figure 8.5: Leaf area index functions as recommended in SoilCover (SoilCover, 1997). The excellent LAI was used in the Kidston tailings impoundment modeling.

The potential transpiration (PT) is a function of the plant rooting depth, and in particular the active root zone. SoilCover uses the predetermined shape factor method, and in particular a triangular constant decreasing root uptake rate with depth distributions. This means that two rooting depths must be specified at any time during the growth season. The first is the top active rooting depth, while the second depth is the bottom rooting depth at which time the root uptake is at its minimum (Tratch, 1995). The actual vegetation cover on the tailings impoundment upon closure will be Eucalyptus and Acacia trees with a natural grass understorey. SoilCover's vegetation algorithm is very simplistic (Tratch, 1995) and cannot simulate such a complex vegetation system (i.e. a root system with distinctly different rooting profiles for the different species), and as a result the model simulations were conducted assuming only a grass cover. The rooting depths were considered to be constant throughout the growing season, being between 60 and 400 mm deep for the first 10 simulations in each set, i.e. zone No. 1 through zone No. 10. For zone No. 11 the rooting depth varied between 60 and 200 mm, for zone No. 12 it varied between 30 and 80 mm and finally for zone No. 13 it varied between 5 and 25 mm. These changes were necessary to ensure that the rooting depths were not below the phreatic level at the starting condition of each simulation, as SoilCover does not allow for that case. The rooting depths were chosen based on visual observations and measurements during on-site test pitting as well as communications with Mr. Paul Ritchie, the Kidston Environmental Officer.

For all model simulations the moisture wilting point was set at 1500 kPa with a moisture limiting point of 100 kPa. Durham *et al.* (2000) found these values to be suitable based on field observations and predictive modeling for the waste rock cover system at Kidston Gold Mine. These numbers are typical of grass species and since no actual data for the species on the Kidston tailings impoundment were available, these were deemed to be acceptable. The moisture limiting point is the soil suction at which the plants would begin to be stressed and reduce transpiration, while the moisture wilting point is the suction whereby the plant can no longer uptake moisture from the soil and transpiration shuts down and tissue death occurs. SoilCover uses a straight-line function between the moisture limiting and wilting point to calculate the actual transpiration (AT) rate. At suctions lower than the limiting point the plant-limiting factor (PLF) is zero and the actual transpiration equals potential transpiration. When the suction exceeds the wilting point suction, actual transpiration is zero. Between these points the actual transpiration varies according to the straight-line function.

A simplistic sensitivity analysis was performed to test the sensitivity of the rooting depths and the LAI on the outcome of the SoilCover results. A standard profile was selected, which was identical in all aspects except for the LAI and the rooting depths. These model simulations together with the subsequent evapotranspiration results are listed in Table 8.6.

Table 8.6: Results of simplistic sensitivity analysis regarding the LAI and rooting depths for the typical Kidston tailings profile.

LAI	Minimum root depth	Maximum root depth	PE (mm)	AE (mm)	PT (mm)	AT (mm)	AET (mm)
Excellent	60 mm	400 mm	1639	152	695	386	538
Excellent	60 mm	750 mm	1639	157	695	354	511
Poor	60 mm	400 mm	1639	412	326	184	595
Poor	60 mm	750 mm	1639	413	326	145	559

As expected the actual evaporation for the runs using an excellent LAI is significantly less than for those runs with a poor LAI, due to the variance in net radiation reaching the ground surface. In both cases the actual transpiration is less when the maximum rooting depth is increased, which might seem contra to what one would expect. However, an analysis of the moisture profiles in the tailings revealed that the active wet zone is typically 100 mm deep, due to the infrequent, and high intensity precipitation events experienced at Kidston. Since the SoilCover algorithm distributes the root uptake via a constant shape function, a deeper root zone lessens the area over which active root uptake can occur. Analysis of the active area show that for the shallow root zones, the active area of the shape function is 45%, while for the deep root zone the active area is only 27%. This phenomena shows that perhaps the SoilCover vegetation algorithm is not sensitive enough to solve the problem of deep-rooted vegetation in extremely dry moisture regimes.

8.3.5.4 Initial Matric Suction Profiles (Steady State)

The initial or starting matric suction profile for each model simulation was required, and to obtain this, each model was run once, using the mean year climate data and an assumed starting profile (very dry, since the simulation was started mid dry season, i.e. 1 July). The output matric suction profile for each of these simulations at the last day (transposed Julian day 365) were used as input profiles for the final simulations. This method resulted in the assumption that all runs followed a year of mean climatic conditions, including the extreme wet and dry years. Due

to the fact that all model simulations started in July, midway through the dry season, the impact of the initial assumed starting conditions were found not to be significant.

8.3.6 Output Frequency

The SoilCover model produces daily outputs of all the detailed data that it generates. For the purpose of this project only the data at the end of each month was saved, as a decision was made that monthly data increments would be the finest resolution of the data. The saved data corresponds to Julian days 1, 31, 62, 92, 123, 153, 184, 215, 243, 274, 304, 335 and 365.

8.4 Modeling Results

The following sections contain a discussion for the modeling results. The data will be discussed in two main categories, annual data and monthly data. These categories attempt to explain the same data but at different resolutions. For the annual data there are 234 individual model simulations that make up the data, and naturally all the individual results cannot be presented in detail. Data has been documented in Appendix M where necessary. The same is true for the monthly data, which in actual fact represents 2808 individual SoilCover simulations.

Chapter 7 describes how for each profile case, 13 individual SoilCover simulations are performed and the results thereof are integrated together to provide a two-dimensional (2-D) result representing a generalized Kidston tailings impoundment cross-section. In the discussions that follow the results reported are those composite 2-D results, as opposed to individual SoilCover simulations.

All the SoilCover results are presented in terms of five individual water balance components. The first component is runoff (R), and represents that portion of the precipitation that does not infiltrate during storm events. This value is always expressed as a positive value. The steep gradients caused by the tailings property functions often caused numerical instability and associated large water balance errors in the SoilCover simulations. Most often these errors were instantaneous large jumps associated with days of large precipitation volumes following long dry periods. These situations were manually modified by checking each file and adjusting the runoff volume to be in line with the precipitation event.

The second SoilCover water balance component is evaporation (E). This value, which is always expressed as a positive value and represents the amount of actual evaporation from the exposed tailings surface. The transpiration (T), presents the amount of actual transpiration lost through the vegetation and is always expressed as a positive number. The sum of the evaporation and transpiration is the evapotranspiration (ET) and presents the actual total loss of moisture through the tailings system via evaporation and transpiration. Note that for non-vegetated surfaces the evapotranspiration is equal to the evaporation. The net infiltration (NI) is calculated with the following equation:

$$NI = P - R - ET \qquad [8.1]$$

Where P, is the precipitation for the given climatic year. The net infiltration can thus be positive or negative, depending of the respective water balance in play. A positive NI implies an overall gain of water to the tailings surface, while a negative NI implies the opposite. All five the components R, E, T, ET and NI are presented in terms of a value in mm as well as a percentage of annual precipitation. Runoff can thus never exceed a value of 100%, while all the other components can theoretically exceed 100%. Equation 8.2 explains how these components are calculated:

$$X_c = \frac{x_c}{P} \cdot 100\% \qquad [8.2]$$

Where X_c = R, E, T, ET or NI (%),
x_c = R, E, T, ET or NI (mm), and
P_c = precipitation for specific climatic year (mm).

The three climatic years used were mean, wet and dry, and their respective annual precipitation totals are 702.2 mm, 1535.0 mm and 270.0 mm. The final component discussed in this chapter is the net infiltration flux (q). This number is equal to the net infiltration (NI), but expressed in terms of an infiltration/exfiltration rate (mm/d):

$$q = \frac{NI}{t} \qquad [8.3]$$

Where NI = net infiltration (mm), and

t = time period for NI value (d).

8.4.1 Annual Results

The results of the SoilCover simulations for each profile case, whether non-vegetated or vegetated are listed in Tables 8.7 to 8.12. Since comparisons of the results of the different case profiles are of specific interest, these will be made according to each component of the water balance listed in these tables. The variances between the vegetated and non-vegetated modeling results for the composite cross-section cases have been presented in Table 8.13.

Table 8.7: SoilCover modeling results for the non-vegetated tailings impoundment surface, using the mean climatic year data (702.2 mm precipitation).

Tailings profile	R		NI		E		T		ET	
	(mm)	(%)	(mm)	(%)	(mm)	(%)	(mm)	(%)	(mm)	(%)
Coarse	357	50.9	-260	-37.0	605	86.1	0	0.0	605	86.1
Intermediate	222	31.6	-318	-45.3	798	113.7	0	0.0	798	113.7
Fine	138	19.7	-435	-62.0	999	142.3	0	0.0	999	142.3
Composite	284	40.4	-385	-54.8	803	114.4	0	0.0	803	114.4

Table 8.8: SoilCover modeling results for the non-vegetated tailings impoundment surface, using the wet climatic year data (1535.0 mm precipitation).

Tailings profile	R		NI		E		T		ET	
	(mm)	(%)	(mm)	(%)	(mm)	(%)	(mm)	(%)	(mm)	(%)
Coarse	1087	70.8	-213	-13.9	661	43.1	0	0.0	661	43.1
Intermediate	812	52.9	-173	-11.3	896	58.4	0	0.0	896	58.4
Fine	519	33.8	-102	-6.6	1118	72.8	0	0.0	1118	72.8
Composite	956	62.3	-281	-18.3	860	56.0	0	0.0	860	56.0

Table 8.9: SoilCover modeling results for the non-vegetated tailings impoundment surface, using the dry climatic year data (270.0 mm precipitation).

Tailings profile	R		NI		E		T		ET	
	(mm)	(%)	(mm)	(%)	(mm)	(%)	(mm)	(%)	(mm)	(%)
Coarse	66	24.5	-285	-105.7	489	181.2	0	0.0	489	181.2
Intermediate	28	10.5	-353	-130.7	595	220.2	0	0.0	595	220.2
Fine	14	5.3	-460	-170.2	715	264.9	0	0.0	715	264.9
Composite	45	16.8	-421	-155.9	646	239.1	0	0.0	646	239.1

Table 8.10: SoilCover modeling results for the vegetated tailings impoundment surface, using the mean climatic year data (702.2 mm precipitation).

Tailings profile	R		NI		E		T		ET	
	(mm)	(%)	(mm)	(%)	(mm)	(%)	(mm)	(%)	(mm)	(%)
Coarse	358	51.1	-301	-42.9	288	41.0	357	50.9	645	91.9
Intermediate	209	29.8	-362	-51.5	377	53.8	477	67.9	854	121.7
Fine	119	17.0	-485	-69.1	502	71.5	566	80.6	1068	152.1
Composite	257	36.6	-404	-57.5	417	59.4	431	61.5	849	120.9

Table 8.11: SoilCover modeling results for the vegetated tailings impoundment surface, using the wet climatic year data (1535.0 mm precipitation).

Tailings profile	R		NI		E		T		ET	
	(mm)	(%)	(mm)	(%)	(mm)	(%)	(mm)	(%)	(mm)	(%)
Coarse	1069	69.7	-212	-13.8	308	20.1	369	24.1	678	44.2
Intermediate	799	52.0	-190	-12.4	426	27.8	500	32.6	926	60.3
Fine	488	31.8	-129	-8.4	565	36.8	611	39.8	1176	76.6
Composite	927	60.4	-286	-18.6	446	29.0	448	29.2	894	58.2

Table 8.12: SoilCover modeling results for the vegetated tailings impoundment surface, using the dry climatic year data (270.0 mm precipitation).

Tailings profile	R		NI		E		T		ET	
	(mm)	(%)	(mm)	(%)	(mm)	(%)	(mm)	(%)	(mm)	(%)
Coarse	61	22.4	-358	-132.6	245	90.8	322	119.3	567	210.1
Intermediate	17	6.2	-444	-164.6	312	115.5	386	142.9	698	258.4
Fine	10	3.9	-562	-208.0	397	147.2	424	156.9	821	304.1
Composite	21	7.7	-492	-182.3	362	134.2	379	140.4	741	274.6

Table 8.13: Differences between SoilCover modeling results for the non-vegetated and vegetated composite tailings impoundment surface (a negative value suggests the non-vegetated value exceed the vegetated value).

Climatic year (precipitation)	R		NI		E		T		ET	
	(mm)	(%)	(mm)	(%)	(mm)	(%)	(mm)	(%)	(mm)	(%)
Mean (702.2 mm)	-27	-3.8	19	2.7	-386	-54.9	431	61.5	46	6.5
Wet (1535.0 mm)	-29	-1.9	5	0.3	-415	-27.0	448	29.2	34	2.2
Dry (270.0 mm)	-24	-9.1	71	26.4	-283	-104.9	379	140.4	96	35.5

8.4.1.1 Runoff

Irrespective of what climatic data set is used, the runoff is always the greatest number for a cross-section containing only coarse tailings, and runoff is the least for a profile with fine

tailings. At first glance this might seem contradictory, as one would assume that coarse material would promote infiltration, and thus reduce the amount of runoff. However, by investigating the matric suction profiles in the tailings surface prior to precipitation events, it becomes evident that due to the sporadic nature of the precipitation events the profile tends to dry out significantly between precipitation events. When the precipitation events do occur, they tend to be high intensity, short duration showers, and consistent with unsaturated soils theory, the dry surface profile is in actual fact extremely impermeable, making it less susceptible to infiltration. The finer tailings has a greater ability to retain its moisture between precipitation events, and thus has a higher surface permeability, which in turn results in a higher infiltrability.

This is illustrated in Figure 8.6. The soil water characteristic curves and hydraulic conductivity functions for the fine and coarse tailings are presented. If one considers a relatively dry tailings profile at a suction of say 50 kPa, it is clear that the hydraulic conductivity of the fine tailings is higher than for the coarse tailings. At 50 kPa this difference is two orders of magnitude, which is significant.

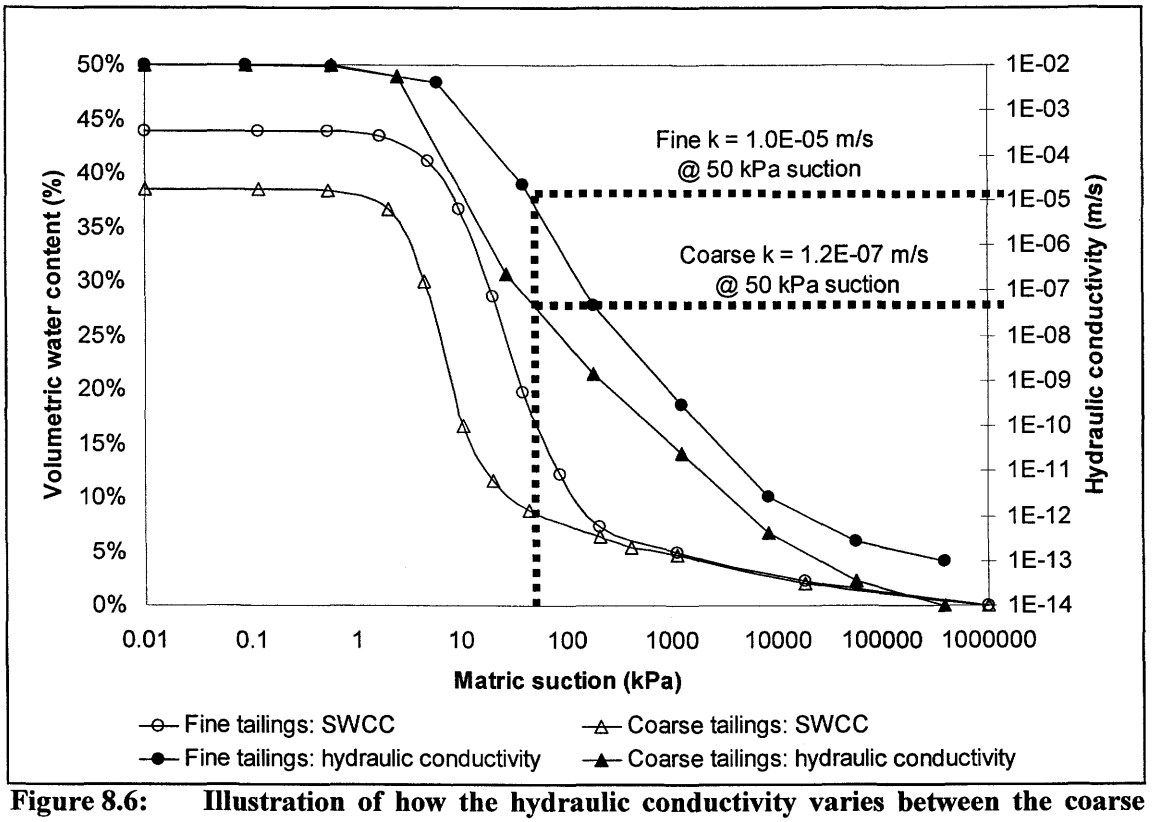

Figure 8.6: Illustration of how the hydraulic conductivity varies between the coarse and fine tailings for any given matric suction.

The next observation is that runoff is the most during a wet year, and the least during a dry year (relative to the precipitation totals). Intuitively this sounds correct, as the soil profile is expected to become wetter in the wet year, and if the storm events exceed the infiltrability of the profile, runoff will be generated. Inversely if the profile is extremely dry, there is more potential for water uptake. If it is assumed that the storm events that give rise to runoff during a mean year are the same events that result in runoff in the extreme years, then during the wet year the infiltration rate has already been peaked by the average year storm magnitude, and as a result the additional precipitation merely adds to the runoff. Inversely, during a dry year, some infiltration is allowed to occur during the period that runoff would occur in a mean year because the storm magnitude is less intense. Naturally the additional drying out of the dry year surface profile could result in some storm events to cause runoff due to additional surface drying, however the impact of that seems to be less significant.

The same is true for the composite runoff results, where the mean climatic year value of 40.4% is consistent with the annual water climatic balance calculation value described in Chapter 5 of 42%. During the wet year the runoff is increased by approximately 50% to 62.3% and in a dry year it is reduced to 16.8%.

The runoff value of 40.4% for the mean year with a non-vegetated tailings surface is 3.8% greater than for a vegetated surface. This trend is consistent for the wet and dry years with variances of 1.9% and 9.1% respectively. This result is consistent with theory that suggests that runoff can be reduced by the presence of vegetation (Hino, *et al.*, 1987). The relative trends are presented in Figure 8.7. It is important to note that SoilCover does not take into account interception of water via vegetation, which has been shown to effectively reduce not only the runoff volume, but decrease overall infiltration into the soil profile (Doorenbos and Pruitt, 1977; Penman, 1963). Another factor that SoilCover does not account for is the change in soil structure due to the presence of roots, which has been shown to increase the effective coefficient of permeability of the bulk soil (Hino *et al.*, 1987). Hino *et al.* (1987) showed that adding vegetation could change the permeability by one order of magnitude. This would of course alter the infiltrability of the tailings surface and thus affect the runoff magnitude. It would therefore be reasonable to suggest that the relatively small effect that adding vegetation to the tailings has shown to have might very well be overly conservative, and had canopy interception and permeability changes been taken into account the vegetated surface might have shown to have significantly less runoff.

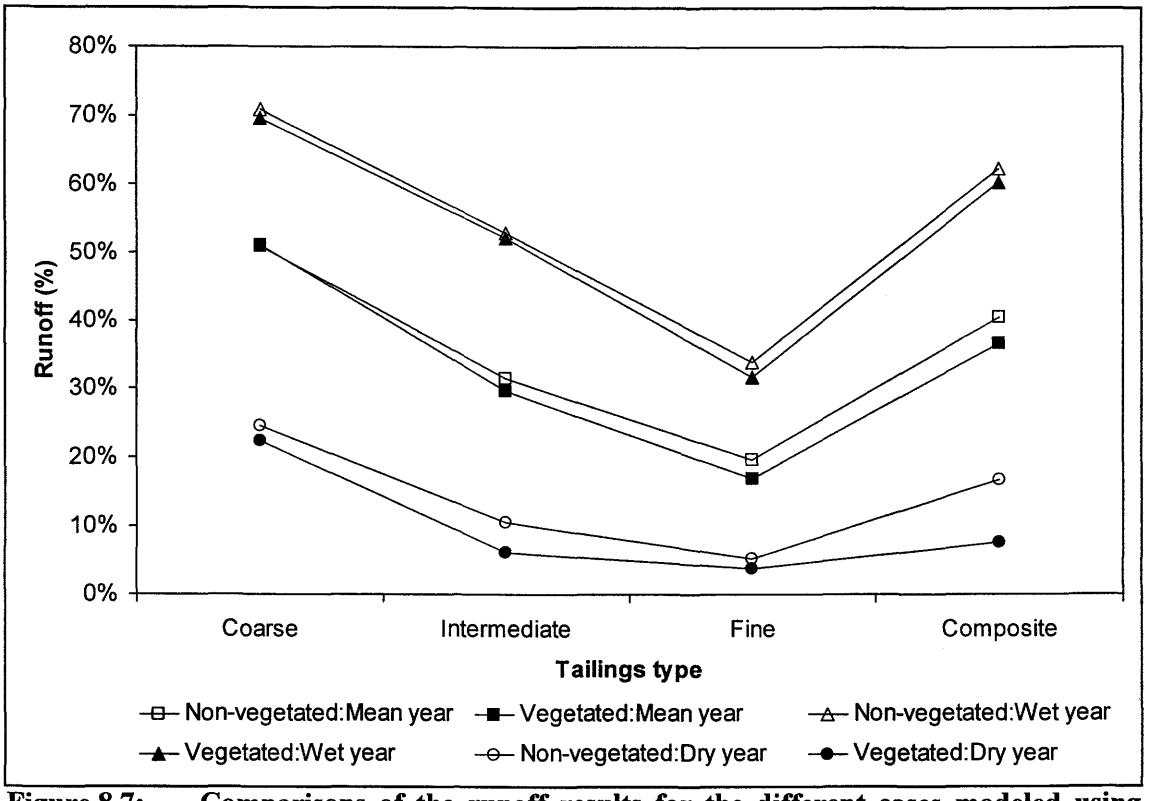

Figure 8.7: Comparisons of the runoff results for the different cases modeled using SoilCover.

8.4.1.2 Evaporation

For the non-vegetated tailings dam surface transpiration is zero. Therefore the evaporation equals the evapotranspiration. Irrespective of what climatic year was modeled, the evaporation is always the least for a cross-section containing only coarse tailings and the most for one with only fine tailings. This is consistent with the theory that suggests that finer grained materials can transmit more moisture via evaporation (Buckingham, 1907; Harris and Robinson, 1916). The finer tailings have a greater air entry value and can thus access moisture from deeper within the profile. This of course assumes that the depth of the water table is shallow enough to allow constant replenishment of the moisture lost via evaporation (Staley, 1957; Gardner, 1958).

The wet year data shows evaporation rates far less than for the mean year and similarly the dry year indicates evaporation rates that far exceed those for a mean year. These numbers are a bit misleading, since they are expressed in terms of the annual precipitation. If one considers the actual evaporation rates in according to volume, the wet year shows about 10% increase above

the average year, while the dry year is approximately 20% less than the average year. This can be ascribed due to the increased wetted area during the wet season making more water available for evaporation, while the lower precipitation, with subsequent deeper dryer profiles, resulting in less available moisture for evaporation in the dry year. This trend is carried through in the composite cross-section results.

The evaporation numbers show that the non-vegetated tailings experienced between 27% and 104% more evaporation than the vegetated tailings as illustrated in Figure 8.8. This is to be expected, since the presence of vegetation reduces the exposed tailings area, which in turn reduces the evaporation capacity. In SoilCover this is governed by the leaf area index (LAI), which had been set as "excellent", to simulate a very good coverage. The vegetation tends to lower the wind speed, net radiation and vapor pressure gradient at the soil surface, and therefore significantly impact on the evaporation (Penman, 1963; Ritchie, 1972). SoilCover used the LAI index to reduce the amount of net radiation that reaches the soil surface (Tratch, 1995), however no corrections for wind speed or vapor pressure gradient is made. It is important to note that the most of the evaporation observed for the vegetated tailings surface is in fact during the period of time when vegetation growth has not yet started, or after the vegetation has died off. The vegetation cover has thus been very effective in reducing bare soil evaporation.

8.4.1.3 Transpiration

Irrespective of what climatic year has been modeled, the transpiration rate increases as the tailings become increasingly finer as illustrated in Figure 8.9, with the greatest transpiration rate calculated for a fine tailings cross-section. The wet year transpiration rates indicate transpiration rates of approximately 4% higher than for the mean year when one considers actual transpiration volumes. Similarly the dry year results in approximately 12% less transpiration than the mean year. Since actual transpiration rates is a function of potential evaporation (Tratch, 1995), the principles that govern evaporation form the profile will directly influence the transpiration.

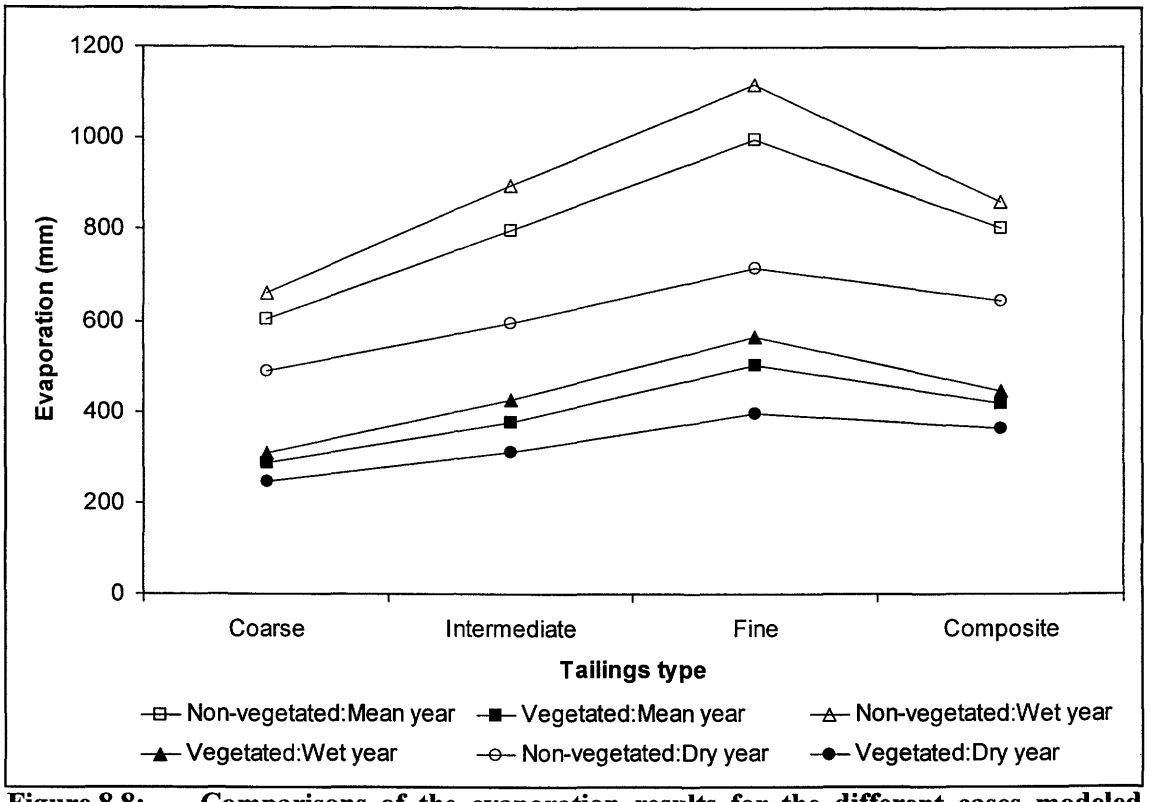

Figure 8.8: **Comparisons of the evaporation results for the different cases modeled using SoilCover.**

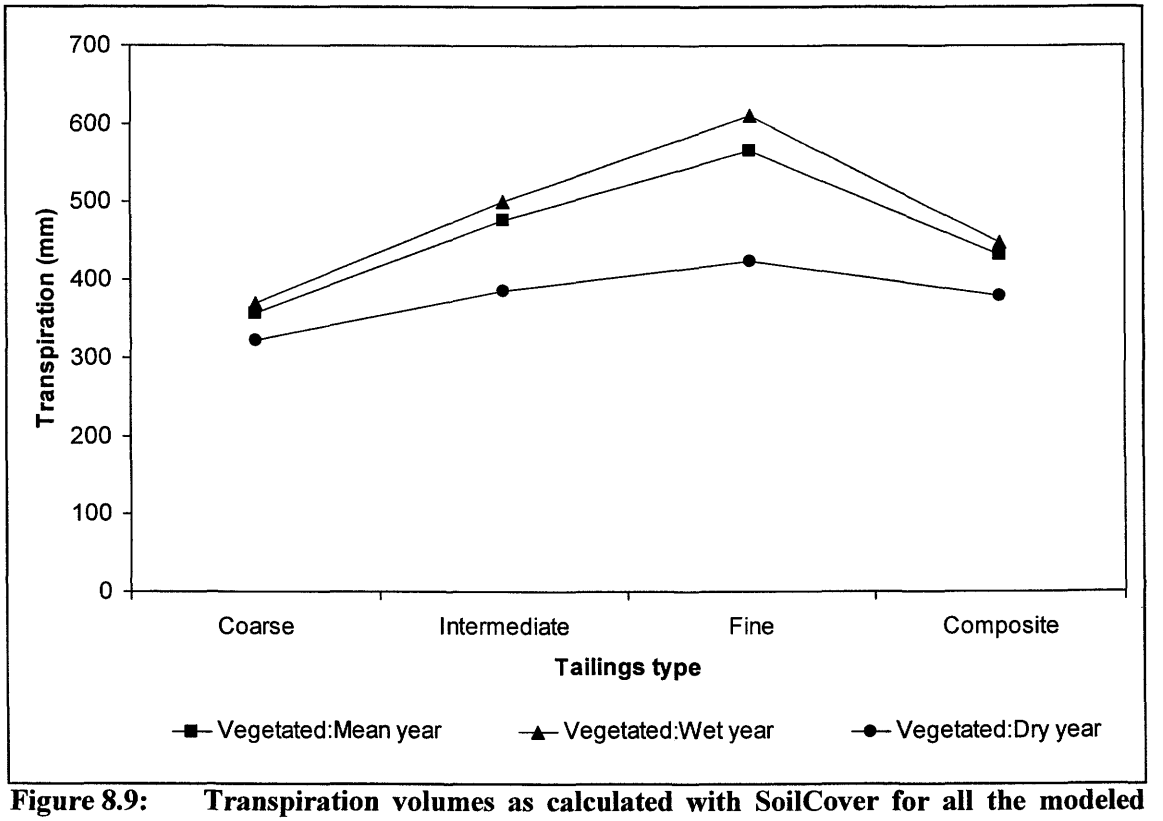

Figure 8.9: **Transpiration volumes as calculated with SoilCover for all the modeled cases.**

8.4.1.4 Evapotranspiration

The evapotranspiration numbers are merely the summation of the evaporation and transpiration values, and as a result the trends previously mentioned are applicable. This number is the single most important number in determining how effective the vegetation is in reducing the surface net infiltration. For the mean year the benefit is 6.5%, only 2.2% for the wet year and a dramatic 35.5% for the dry year. This thus suggests that in an unusually dry year the vegetation can significantly contribute towards water loss from the system, while in extremely wet years the impact is less severe. The main reason for this is the fact that in wet years increased evaporation can occur due to the availability of moisture in the non-vegetated profile. In the vegetated profile, the LAI prevents this evaporation, and the uptake of water by the roots is only as good as the rooting depth allows. More moisture is thus retained in the profile, than would actually be expected. These trends are presented in Figure 8.10.

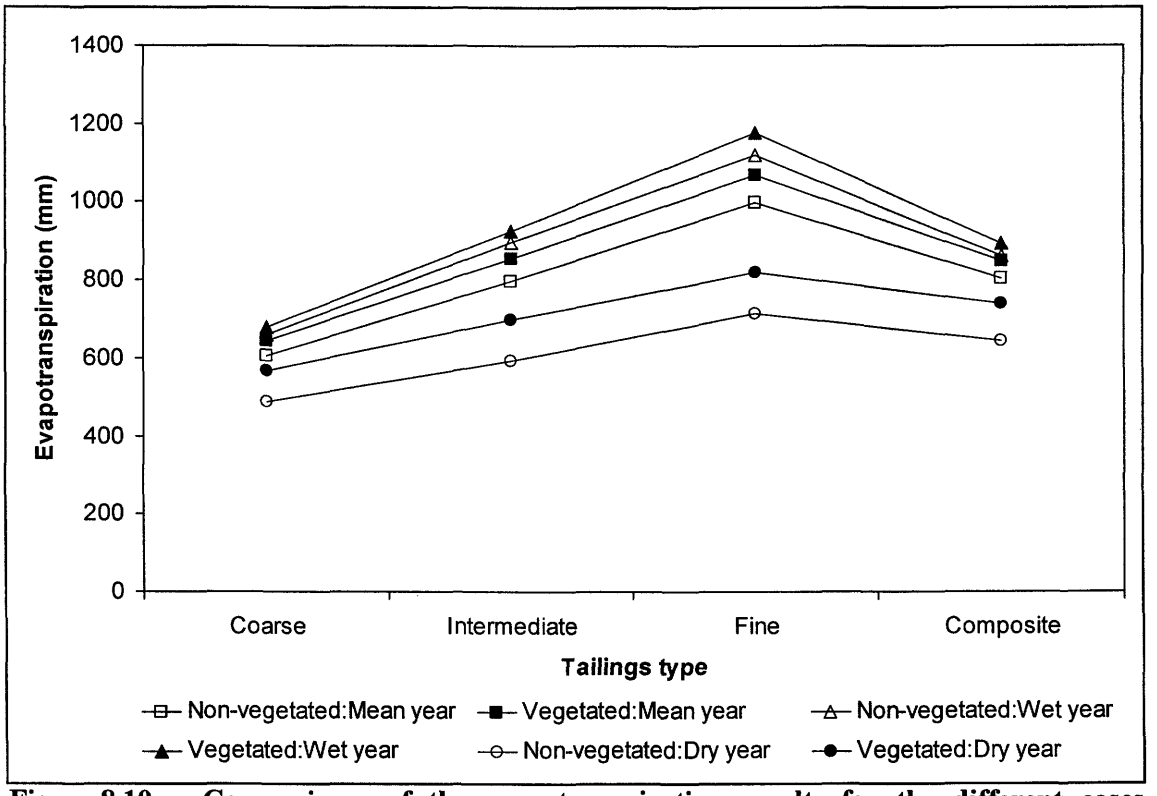

Figure 8.10: Comparisons of the evapotranspiration results for the different cases modeled using SoilCover.

8.4.1.5 Net Infiltration

The first and most obvious observation is that the net infiltration for all case profiles is negative as illustrated in Figure 8.11, meaning an overall loss of water from the profile. This is consistent with the net negative climatic water balance for the site, which suggests a mean precipitation:evaporation ratio of 1:3. For the mean and dry years, the greatest net infiltration loss occurs in cross-sections containing only fine tailings, whilst the least loss occurs in coarse tailings profiles. The inverse in true for the wet climatic year. The reason for these results is the relative magnitudes of the runoff and evaporation numbers for each case. Overall for the composite cross-sections the dry year results in the greatest loss of water from the profile, while the wet year results in the least. This suggests that in a dry year the impact on the phreatic level will be the most significant. For all climatic conditions however, the impact on the phreatic level should be an annual lowering. As the phreatic level moves down and the profiles become deeper the rate of the lowering of the water table will decrease due to less moisture being able to escape via evaporation (Staley, 1957; Gardner, 1958).

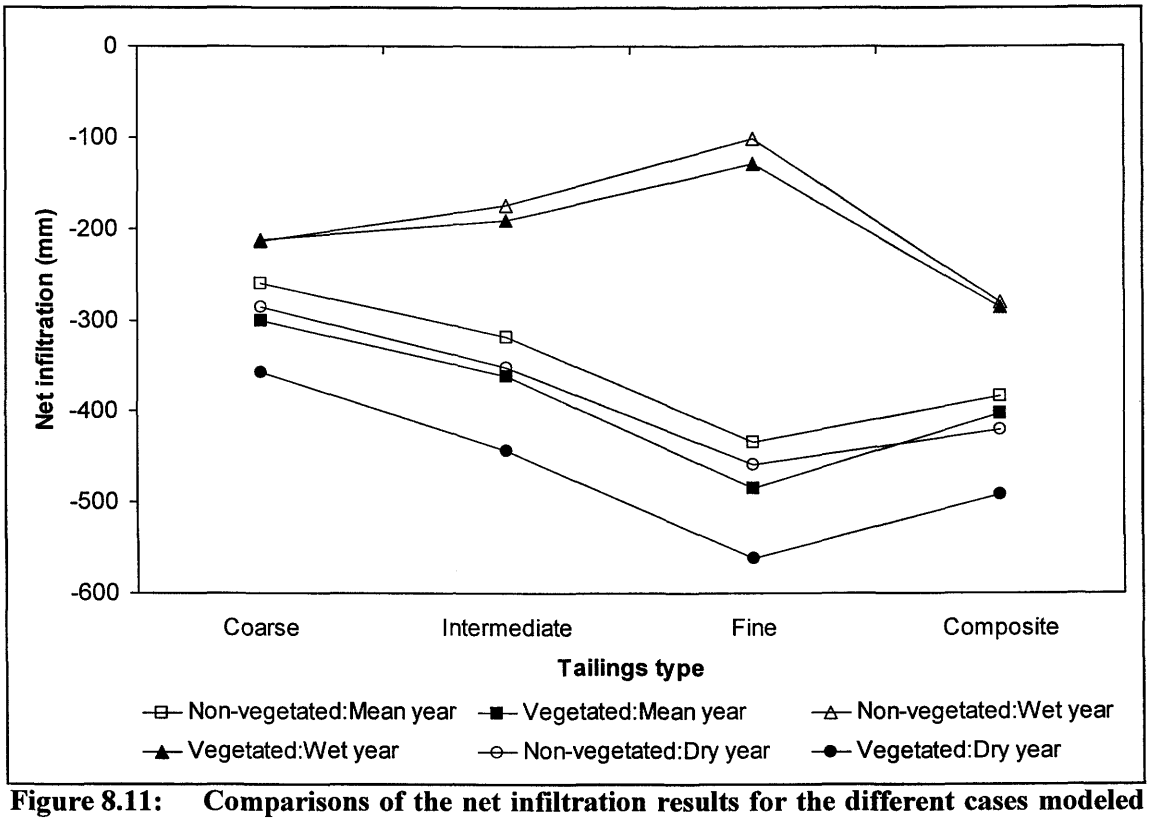

Figure 8.11: Comparisons of the net infiltration results for the different cases modeled using SoilCover.

Overall, for a composite cross-section, the wet year results in 40% less water loss than the mean year, while for a dry year the water loss is 18% greater than for a mean year.

The net infiltration results suggest a 2.7% increased water loss between the unvegetated and the vegetated surfaces for a mean climatic year. This number is only 0.3% for a wet year and 26.4% during a dry year. The benefit of adding vegetation to the profile for a mean or wet year is thus marginal, whilst great improvements is predicted during dry years.

8.4.2 Monthly Results

The annualized results explained in the previous section are suitable for presenting overall findings, however, breaking this data down into monthly increments provides better resolution, especially if the data is to be used as input for multidimensional saturated/unsaturated flow seepage analysis modeling. This section describes the monthly breakdown of two profile cases, i.e. a mean year with and without vegetation. The monthly data for these two profile cases are listed in Tables 8.14 and 8.15 respectively, and Figure 8.12 presents the data graphically.

Table 8.14: Monthly SoilCover water balance results for a mean year and a composite tailings surface without vegetation.

Month	P (mm)	R	NI	E	T	ET	Days	NI (mm)	q (mm/d)
July	7.3	0.0%	-3.9%	5.0%	0.0%	5.0%	31	-27.57	-0.889
August	8.8	0.7%	-4.3%	4.8%	0.0%	4.8%	62	-30.21	-0.974
September	6.8	0.0%	-7.4%	8.4%	0.0%	8.4%	92	-51.99	-1.733
October	17.5	1.5%	-7.5%	8.5%	0.0%	8.5%	123	-52.45	-1.692
November	45.6	0.3%	-5.0%	11.2%	0.0%	11.2%	153	-35.04	-1.168
December	103.0	8.7%	-6.1%	12.1%	0.0%	12.1%	184	-43.03	-1.388
January	184.9	10.9%	-2.3%	17.8%	0.0%	17.8%	215	-16.19	-0.522
February	181.8	9.1%	3.1%	13.7%	0.0%	13.7%	243	22.05	0.787
March	102.8	6.9%	-4.2%	11.9%	0.0%	11.9%	274	-29.81	-0.961
April	20.6	1.3%	-7.5%	9.1%	0.0%	9.1%	304	-52.87	-1.762
May	12.7	0.9%	-5.0%	6.0%	0.0%	6.0%	335	-35.34	-1.140
June	10.4	0.2%	-4.6%	5.9%	0.0%	5.9%	365	-32.39	-1.080
Year	702.2	40.4%	-54.8%	114.4%	0.0%	114.4%	365	-384.83	

Table 8.15: Monthly SoilCover water balance results for a mean year and a tailings surface with vegetation.

Month	P	R	NI	E	T	ET	Days	NI (mm)	q (mm/d)
July	7.3	0.0%	-3.9%	5.0%	0.0%	5.0%	31	-27.57	-0.889
August	8.8	0.4%	-3.9%	4.8%	0.0%	4.8%	62	-27.65	-0.892
September	6.8	0.0%	-7.4%	8.4%	0.0%	8.4%	92	-52.19	-1.740
October	17.5	1.2%	-7.2%	8.5%	0.0%	8.5%	123	-50.50	-1.629
November	45.6	0.2%	-5.7%	9.9%	2.1%	12.0%	153	-40.03	-1.334
December	103.0	8.2%	-5.5%	2.4%	9.5%	11.9%	184	-38.30	-1.236
January	184.9	9.7%	-1.2%	0.8%	17.0%	17.8%	215	-8.51	-0.275
February	181.8	7.8%	3.3%	0.7%	14.0%	14.7%	243	23.50	0.839
March	102.8	7.1%	-7.3%	2.1%	12.7%	14.8%	274	-51.00	-1.645
April	20.6	1.2%	-9.3%	5.7%	5.2%	11.0%	304	-65.22	-2.174
May	12.7	0.6%	-5.0%	5.3%	0.9%	6.2%	335	-35.08	-1.132
June	10.4	0.1%	-4.5%	5.9%	0.0%	5.9%	365	-31.38	-1.046
Year	702.2	36.6%	-57.5%	59.4%	61.5%	120.9%	365	-403.94	

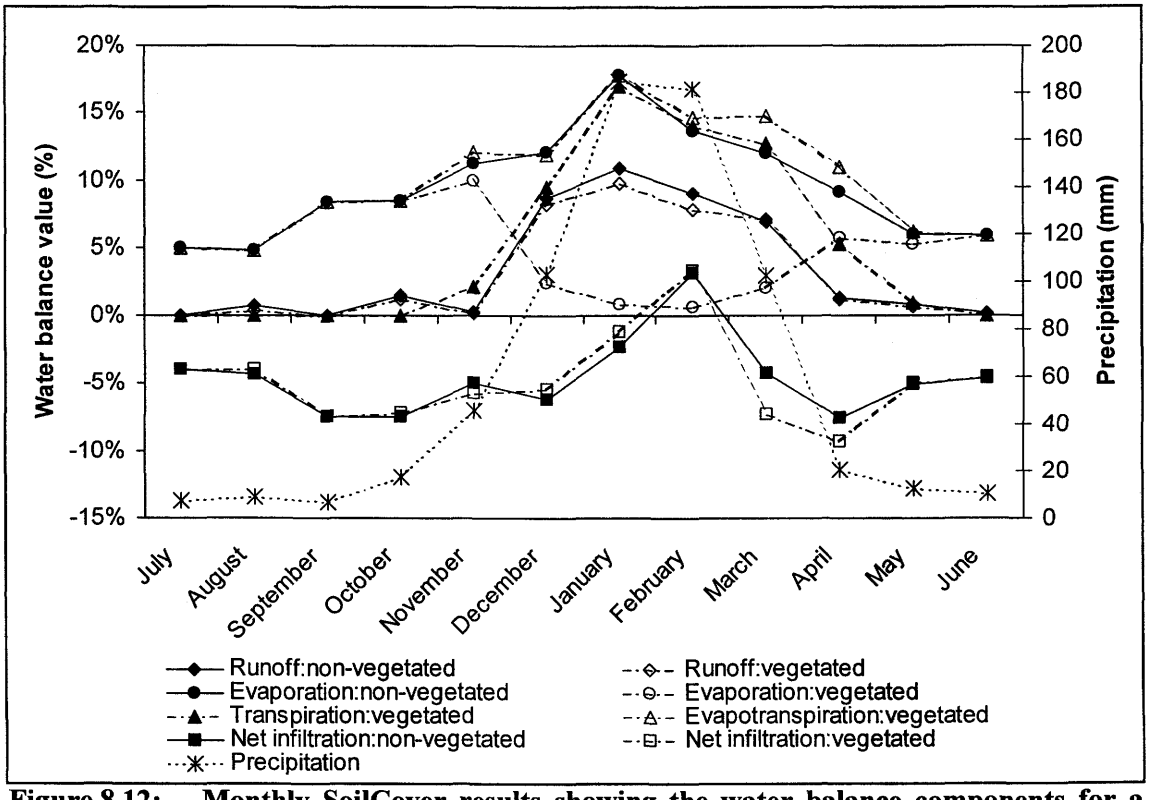

Figure 8.12: Monthly SoilCover results showing the water balance components for a mean year and a tailings surface with or without vegetation.

8.4.2.1 Runoff

The monthly runoff closely mimics the precipitation data, with the runoff increasing dramatically as the precipitation increases between November and March. For the months where the rainfall is less the runoff diminishes to zero. The difference between the vegetated and non-vegetated runoff numbers is not significant, except that during the rainy season the vegetated tailings produces slightly less runoff.

8.4.2.2 Evaporation

The evaporation for the vegetated and non-vegetated tailings surfaces are similar up to 15 November when the growth season starts, and after 15 May when it stops. During the growth season the evaporation from the non-vegetated surface increases to a peak value of 17.8% in January before starting to decrease steadily to a value of 6% at the end of the growth season. The vegetated surface evaporation decreases to a minimum value of 0.7% in February after the growth season starts, before starting to increase as the growth season ends. This is indicative of how the LAI changes as the plants grow bigger, and ultimately die off.

8.4.2.3 Transpiration

The transpiration of the vegetated surface starts in mid November and increases rapidly to a peak value of 17.8% in January. After that it gradually decreases to zero by mid June when the growth seasons ends. This trend is consistent with how the LAI changes.

8.4.2.4 Evapotranspiration

The evapotranspiration of the vegetated surface closely mimics the evaporation of the non-vegetated surface, with the exception of the month November and the period February to April, where the increased transpiration results in 5.8% more moisture loss from the tailings surface.

8.4.2.5 Net Infiltration

During the dry season the net infiltration remains fairly constant, however, as the rainy season starts, the net infiltration starts to increase to a peak in February. February is also the only

month when the net infiltration is a positive number, suggesting that more water infiltrate the profile than exits it. The peak value of net infiltration decreases rapidly to the dry season value. Figure 8.13 presents the net infiltration flux step functions for the two cases described above. These step functions suggest that up to the peak in the growing season for the non-vegetated cover appears to perform better with respect to achieving a smaller net infiltration. However during the months of March and April the vegetation consumes significant amounts of water and far the net infiltration for the vegetated surface is greater than for the non-vegetated surface.

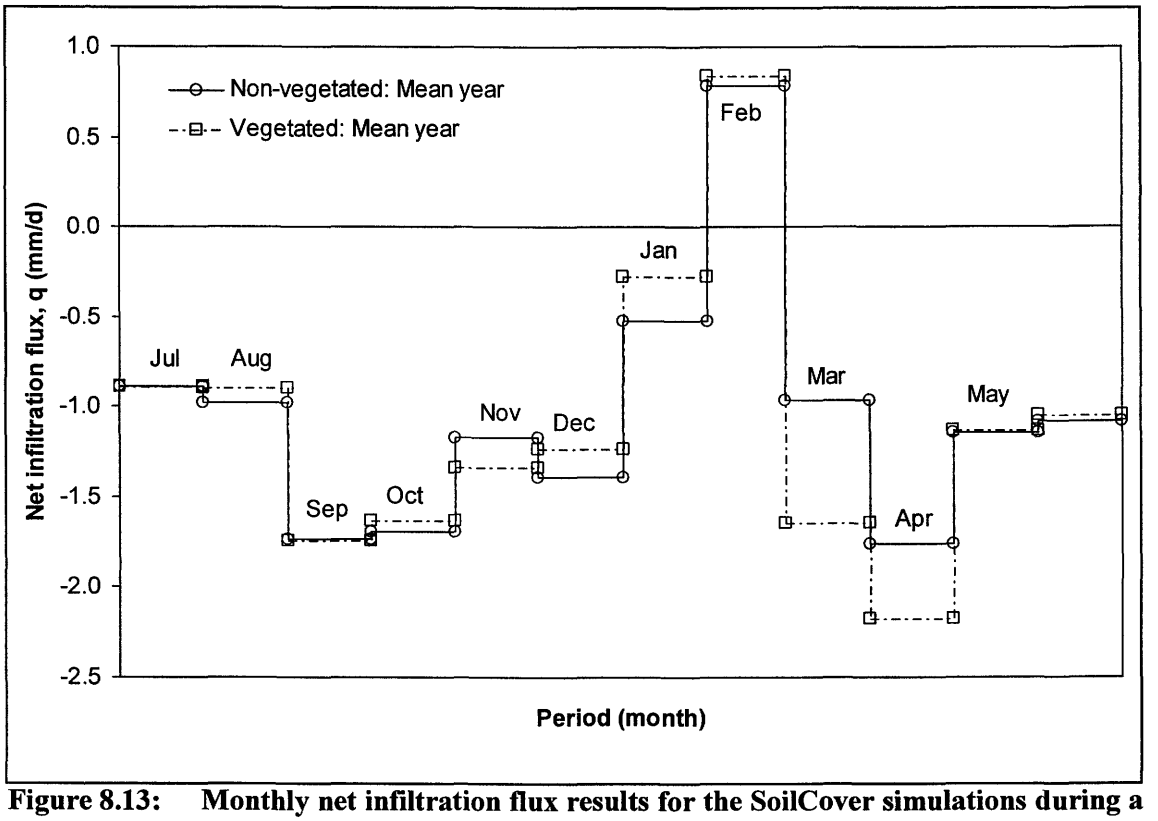

Figure 8.13: Monthly net infiltration flux results for the SoilCover simulations during a mean climatic year.

8.5 Conclusions

The results presented in this chapter, together with the remaining data documented in Appendix M suggest that the overall tailings impoundment water balance will be negative, consistent with the climatic water balance. For the profile case modeling a non-vegetated tailings surface, the reported fluxes are probably a fairly good estimate of what would happen at the site. Confidence in the results are boosted by the fact that the models have been based on actual material

properties, and the method used by SoilCover in the flux boundary calculations are based on coupled soil/atmosphere heat and mass transfer theory as described in Chapter 2. The same can however not be said for the profile case where vegetation is introduced. The algorithm used by SoilCover to calculate the transpiration fluxes are too simplistic to provide a high degree of confidence in the reported results. At best the results for the vegetated tailings are a conservative estimate of the fluxes, which implies that even greater negative net infiltration fluxes might be expected; this is especially true for the wet climatic year. The impact of evapotranspiration is expected to be much greater than reported, effectively increasing the overall water loss from the tailings profile. The discrepancy is due to two main concerns; (1) SoilCover's predetermined shape factor method to calculate root extraction does not allow accurate modeling of deep rooted vegetation in dry soil profiles (i.e. the shallow regime is satisfied, but deep rooted water availability by the phreatic table is ignored), and (2) SoilCover does not allow for intercepted water by the vegetation canopy.

Irrespective of these concerns, it can be said with confidence that the long-term water balance of the tailings impoundment, would be such that in time the presence of the pond will be seasonal, with an associated overall lowering of the phreatic table. This would result in a reduction in the amount of seepage emanating from the toe drains, and as a result a reduction of the environmental impact. Further, if it is assumed that adding vegetation to the tailings surface would increase the rate at which this water loss would occur, it can only benefit the system as a whole. One factor that cannot be answered however, is the long-term impact of the vegetation on the bulk permeability of the tailings that could increase the infiltrability and perhaps negate the beneficial effects of the vegetation.

8.6 References

Buckingham, E. (1907). Studies on the movement of soil moisture. Washington, U.S. Government Printing Office, U.S. Department of Agriculture, Bureau of Soils, Bulletin, no. 38, pp. 61.

de Vries, D.A. (1963). Thermal Properties of Soils. Physics of Plant Environment, W.R van Wihk (ed.), North Holland Pub. Co., pp. 382.

Doorenbos, J., Pruitt, W.O. (1977). Guidelines for Predicting Crop Water Requirements. FAO Irrigation and Drainage Paper 24, FAO, Rome, 114 pp. (Revised Version of the 1975 edition).

Durham, A.J.P., Wilson, G.W., Currey, N. (2000). Field Performance of Two Low Infiltration Cover Systems in a Semi Arid Environment. Proceedings of the Fifth international conference on Acid Rock Drainage, Denver, Colorado, USA. May, pp. 1319-1326.

Fredlund, DG., Xing, A. (1994). Equations for the soil-water characteristic curve. Canadian Geotechnical Journal, Vol. 31, No. 3, pp. 521-532.

Fredlund, D.G., Xing, A., Huang, S. (1994). Predicting the Permeability Function for Unsaturated Soils Using the Soil-Water Characteristic Curve. Canadian Geotechnical Journal, vol. 31, pp. 533-546.

Gardner, W.R. (1958). Some steady state solutions of the unsaturated moisture flow equation with application to evaporation from a water table. Soil Science, Vol. 85, No.4.

Harris, F.S., Robinson, J.S. (1916). Factors affecting the evaporation of moisture from the soil. U.S. Department of Agriculture. Journal of Agriculture Research, 7(10): 439-461.

Holtz, R.D., Kovacs, W.D. (1981). An Introduction to Geotechnical Engineering. Prentice-Hall Civil Engineering and Engineering Mechanics Series, N.M. Newmark and W.J. Hall, Editors, Prentice-Hall, Englewood Cliffs, New Jersey, U.S.A.

Hino, M., Fujita, K., Shutto, H. (1987). A laboratory experiment on the role of grass for infiltration and runoff processes. Journal of Hydrology, Vol. 90, pp. 303-325.

Jumikus, A.R. (1977). Thermal Geotechnics. Rutger University Press. New Brunswick, N.J.

Penman, H.L. (1963). Vegetation and Hydrology. Technical Communication No. 53, Commonwealth Bureau of Soils, Harpenden, England, pp. 124.

Ritchie, J.T. (1972). Model for Predicting Evaporation from a Row Crop with Incomplete Cover. Water Resources Research, 8 (5): pp. 1204-1213.

SoilCover. (1997). SoilCover User's Manual. Unsaturated Soils Group, Department of Civil Engineering, University of Saskatchewan, Saskatoon, Saskatchewan, Canada.

Staley, R.W. (1957). Effect of depth of water table on Evaporation from fine sand. Master of Science Thesis, Colorado State University, Fort Collins, Colorado, U.S.A.

Tratch, D. (1995). Moisture uptake within the root zone. M.Sc. Thesis, Department of Civil Engineering, University of Saskatchewan, Saskatoon, Saskatchewan, Canada.

This page was intentionally left blank.

CHAPTER 9

Spatial Flux Boundary Functions

9.1 Introduction

One of the driving factors for this study is to develop a method to determine the spatial variability of the water balance components that impact the tailings impoundment surface. The conceptual model developed and described in Chapter 7 provided the tool for actually measuring these fluxes. The SoilCover (SoilCover, 1997) modeling results documented in Chapter 8 described the cumulative results of all case profiles integrated over the generalized tailings impoundment cross-section. The cumulative fluxes are actually the result of 13 individual SoilCover runs, each representing a different spatial location along the generalized tailings impoundment cross-section. These spatial variations of the water balance components will be described in this chapter.

9.2 Spatial Flux Boundary Function Concept

The spatial flux boundary hypothesis described in Chapter 1 essentially stated that surface flux boundary conditions vary spatially along a generalized tailings impoundment cross-section, in response to the position of the phreatic surface. The conceptual model developed and described in Chapter 7 presents a novel way to calculate these spatially varying surface flux boundary conditions, using the most appropriate numerical techniques. In Chapter 8 the results of numerous modeled profile cases using the SoilCover model are presented, allowing for the prediction of the long-term water balance of the tailings impoundment. Irrespective of the case, all these results are the cumulative solution of 13 individual SoilCover simulations, which together form a generalized tailings impoundment cross-section. Each of the individual simulations represents a separate and distinctly different spatial portion of that cross-section, which allows for the spatial determination of the surface flux boundary conditions.

These spatial surface flux boundary conditions are vitally important in bridging the gap between conventional surface flux boundary numerical modeling and multidimensional saturated/unsaturated seepage analysis modeling (GEOSLOPE, 1991; Lin *et al.*, 1997; McDonald and Harbaugh, 1988; SoilVision Sytems, 2001) as described in Chapter 1. It is now possible to use these spatial surface flux boundary conditions as direct inputs to these models; which could allow for more accurate predictive modeling, since these flux boundary conditions are based on actual mechanisms for infiltration, runoff and evaporation, as opposed to user assumptions.

In this study the term "spatial flux boundary function" is used. The reader should not be confused with the expectation of a mathematical equation, but rather a conceptual and/or graphical representation of how the surface flux boundary components vary along the generalized tailings impoundment cross-section. Throughout this chapter each of the regions covered by the 13 individual SoilCover simulations will be referred to as zones, with zone 1 being the region neighboring the tailings impoundment embankment wall, and zone 13 neighboring the tailings impoundment pond. Although, these zones represent a portion of the 2-D tailings impoundment cross-section, it can be extrapolated to the third dimension, by considering each zone to represent a 3-D zone which lies in equally spread rings around the tailings impoundment pond. These are presented schematically in Figure 9.1.

9.3 Spatial Flux Boundary Functions

Due to the large number of case profiles evaluated in Chapter 8 it is not possible to present all flux boundary functions individually. This chapter will thus focus solely on the three main closure water balance components, i.e., runoff, evapotranspiration and net infiltration. Furthermore only the annualized results for a non-vegetated tailings surface during a mean climatic year will be discussed in detail. Results of the other case profiles are presented in Appendix N. Summarized plots for the other annualized case profiles will be presented in this chapter for completeness. In reporting the monthly flux boundary functions only composite results for non-vegetated tailings during a mean year will be presented (i.e. no discussion of the individual tailings types). All other monthly case profiles are documented in Appendix N. The sections that follow will describe how the flux boundary functions have been determined, and how they can be used to enhance multidimensional saturated/unsaturated seepage analysis modeling.

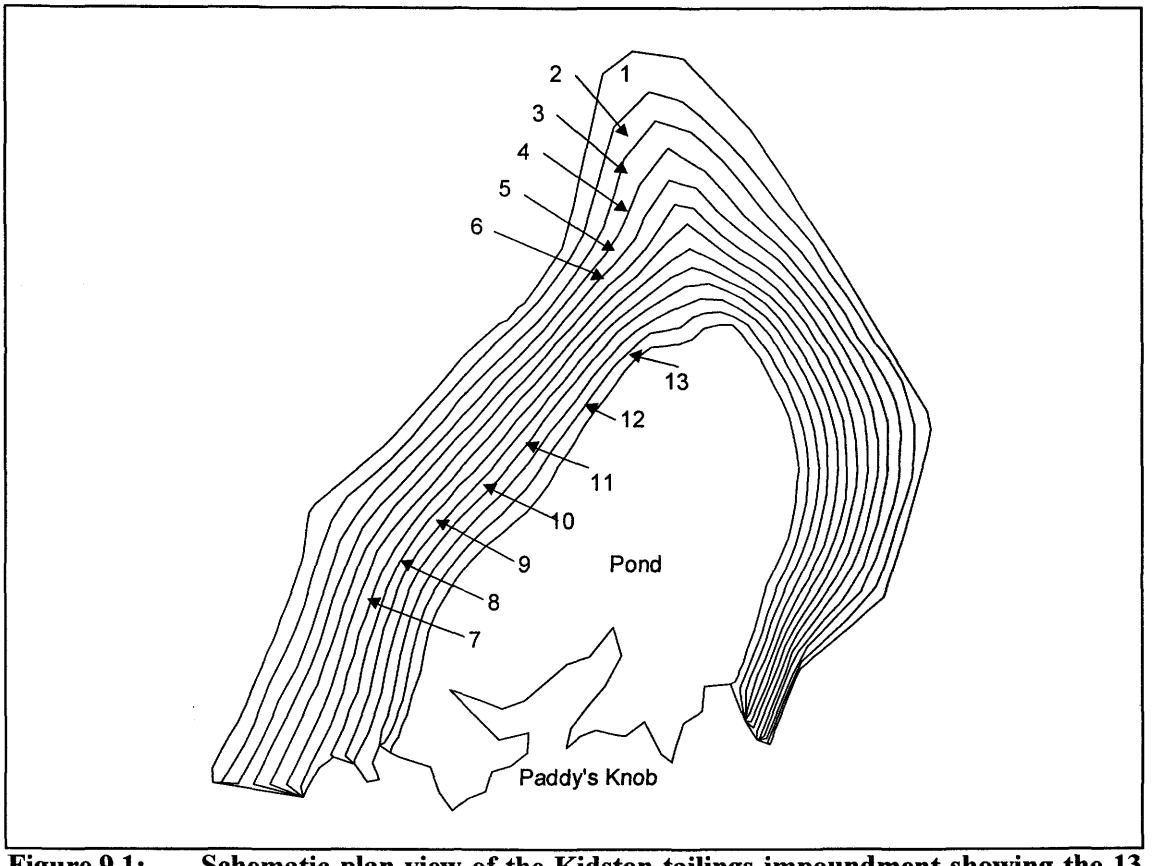

Figure 9.1: Schematic plan view of the Kidston tailings impoundment showing the 13 spatial surface flux boundary zones, applied with respect to multidimensional saturated/unsaturated seepage analysis modeling.

Plots of the spatial flux boundary functions will be for the non-dimensionalized generalized cross-section of the Kidston tailings impoundment. Spatial location along the tailings impoundment beach is thus presented as a cross-section distance ratio, H/X as described in Chapter 7. The embankment is located at H/X = 0, and the pool is located at H/X = 1. The spatial flux boundary functions for runoff, evapotranspiration and net infiltration will be expressed in terms of non-dimensionalized flux ratios, which will be defined in the sections below. This allows for direct comparison of all the spatial flux boundary functions.

9.3.1 Annualized Results

As explained in Chapter 8, all case profiles were modeled in two levels of detail. The first, and usually the most common in long-term water balance predictions, were annualized calculations. The results discussed in this section represent the overall results for the 365 days over which the model simulations were conducted.

The flux boundary functions for runoff, evaporation and net infiltration is presented. Every flux boundary function is presented for 4 composite case profiles. The first three composite case profiles consist of all 13 zones in the generalized cross-section comprising homogeneous profiles of coarse, intermediate or fine tailings. The final composite case profile consist of the generalized cross-section comprising all three tailings types as discussed in Chapter 7. Zone 1 through 5 consists of coarse tailings, zone 6 through 10 consists of intermediate tailings and zone 11 through 13 is fine tailings.

9.3.1.1 Runoff

The first spatial flux boundary function to consider is the runoff. Runoff was used as the determinant in selecting the transition between coarse, intermediate and fine tailings along the generalized tailings impoundment cross-section, based on the overall runoff from the cross-section as described in Chapter 7. The material zoning was deemed correct when the total runoff from the tailings impoundment cross-section matched the number of 42% calculated in the tailings impoundment water balance documented in Chapter 5. For the non-vegetated tailings surface during a mean climatic year, the change in runoff can be plotted such that its variance along the tailings impoundment beach can be observed. For ease in understanding the data runoff is plotted as a runoff ratio defined as follows:

$$R_r = \frac{R_z}{R_T} \qquad [9.1]$$

Where R_r = runoff ratio (-),
R_z = total incremental zonal runoff (mm), and
R_T = total runoff from tailings cross-section (mm).

The runoff ratio for the non-vegetated tailings during a mean climatic year is presented in Figure 9.2. Appendix N presents similar plots for the other case profiles. The runoff ratio shown in Figure 9.2 is a cumulative ratio, and thus dampens some of the effects for the individual runs. Since evaporation and net infiltration are critical aspects of the spatial flux hypothesis, the runoff results must be viewed in an appropriate context. The coarse tailings profile shows the most linear pattern, suggesting near constant increase in runoff as you move towards the pool. The curve corresponding to the tailings profile with only fine tailings shows a steady but

significantly reduced runoff rate up to 75% (H/X = 0.75) from the beach, however the runoff rate increases dramatically for H/X > 0.75. Irrespective of the tailings type, it may be expected that the runoff would increase as the depth to the phreatic surface decreases. This is due to the fact that the profile is almost completely saturated close to the pool and all precipitation is shed as runoff (assuming no ponding is allowed). If the difference between coarse and fine tailings is considered, the depth of the phreatic surface where the profile is saturated is deeper for the fine tailings, due to its higher air entry value. Therefore increased runoff is likely to occur further from the pool in fine tailings as compared to coarse tailings. If one however considers the runoff ratio as an individual zone ratio as opposed to the cumulative ratio presented in Figure 9.2, it can be seen that there is another factor that must be considered as illustrated in Figure 9.3.

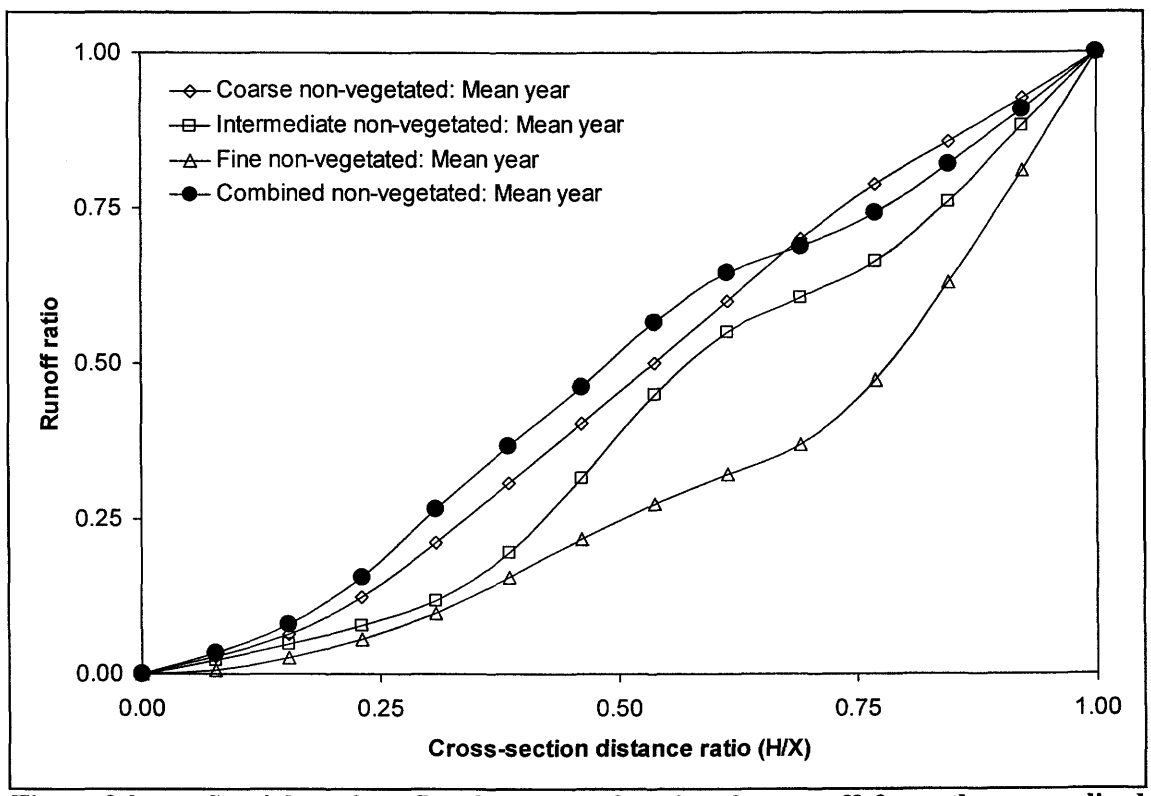

Figure 9.2: Spatial surface flux boundary function for runoff from the generalized tailings impoundment cross section; non-vegetated tailings and mean climatic year.

For the coarse and intermediate tailings profiles, the runoff peaks at some point midway through the cross-section and actually reduces as one moves closer to the pond. This can be attributed to the decreased infiltrability associated with the unsaturated condition and reduced hydraulic conductivity of the surface tailings; causing a usually high runoff value in the zones where the depth to the phreatic table is deep. When the depth to the phreatic table is reduced, such that

there is a consistent interaction between the wetting front in the profile and the phreatic surface, the runoff pattern returns to a more expected pattern. For the coarse tailings this point is at H/X = 0.65, for the intermediate tailings this is at H/X = 0.45, and for the fine tailings it is at H/X = 0.30.

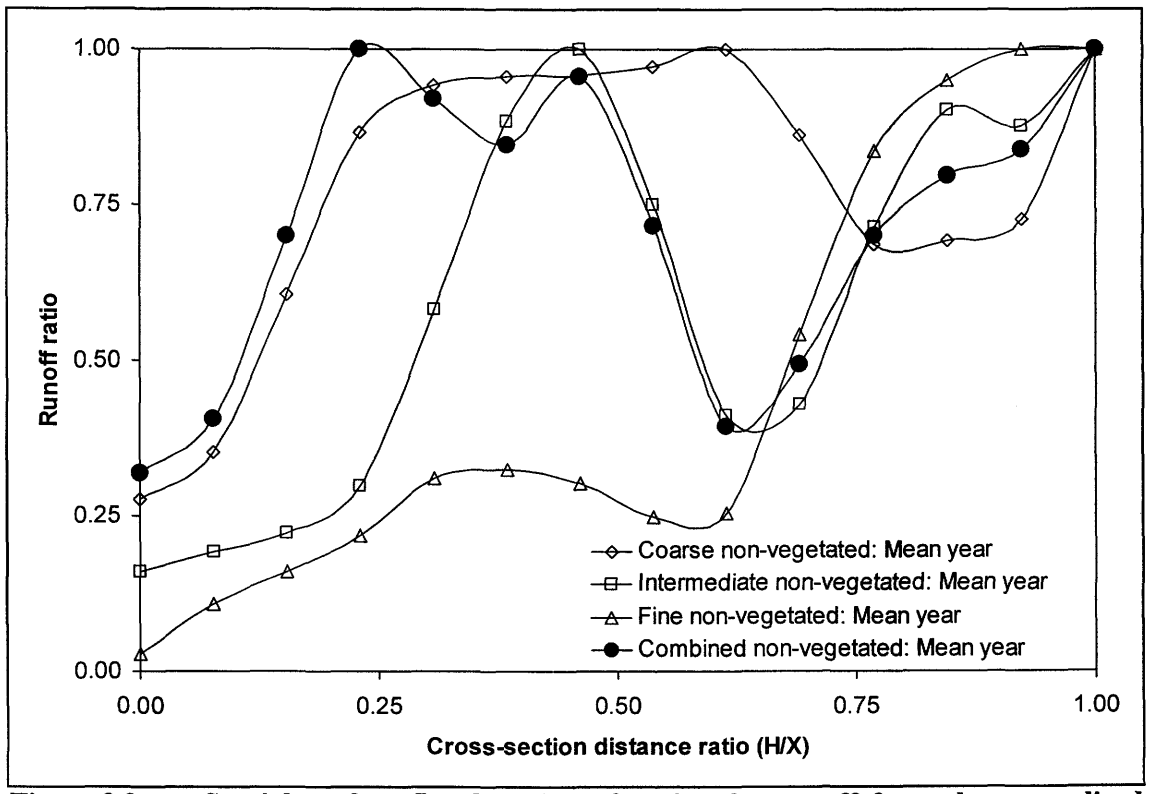

Figure 9.3: Spatial surface flux boundary function for runoff from the generalized tailings impoundment cross section; non-vegetated tailings and mean climatic year (individual zone runoff ratio).

Since the composite generalized cross-section represents a 5:5:3 ratio of coarse, intermediate and fine tailings as described in Chapter 7, the cumulative runoff ratio more closely represents the linearly increasing runoff suggested by the coarser tailings, and the individual runoff ratio seems to peak twice. These peaks can be attributed to the modeling technique as opposed to having a true physical meaning.

For comparison purposes the cumulative runoff ratio for the six primary case profiles modeled are presented in Figure 9.4. The primary case profiles refer to the composite generalized tailings impoundment cross-section simulations for both vegetated and non-vegetated tailings surfaces during each of the three climatic periods (i.e. wet, mean and dry years). It can be seen that there

is not much difference, except to say that there is a slightly increased runoff drop for the vegetated profiles, especially for the dry climatic year.

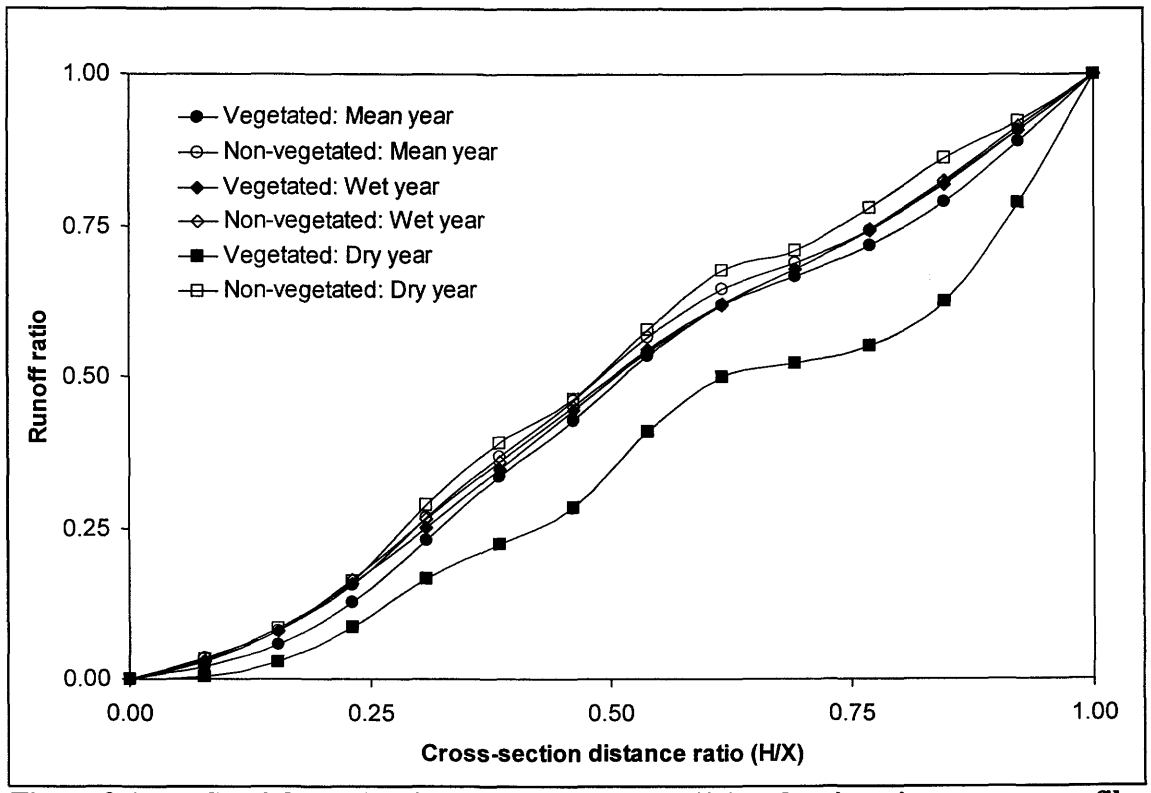

Figure 9.4: Spatial distribution summary of runoff for the six primary case profiles modeled (vegetated and non-vegetated tailings surface for each of the three climatic seasons).

9.3.1.2 Evapotranspiration

Evapotranspiration is one of the two primary water balance components that we are interested in with respect to the spatial flux hypothesis presented in Chapter 1. We can present the evapotranspiration spatial distribution in terms of the actual evapotranspiration ratio, which is defined as follows:

$$AET_r = \frac{AET_z}{AET_{max}} \qquad [9.2]$$

Where AET_r = evapotranspiration ratio (-),

AET_z = individual zonal actual evapotranspiration (mm), and

AET_{max} = maximum individual zonal actual evapotranspiration (mm).

This ratio is in actual fact almost the same as the AET/PET ratio for each individual SoilCover simulation, since the AET_{max} is equal to the PET. Naturally when analyzing results where no vegetation was present, the evapotranspiration equals evaporation, but for simplicity and to avoid confusion, all discussion will be in terms of evapotranspiration ratio. Figure 9.5 presents the evapotranspiration ratio for the non-vegetated tailings surface during a mean climatic year.

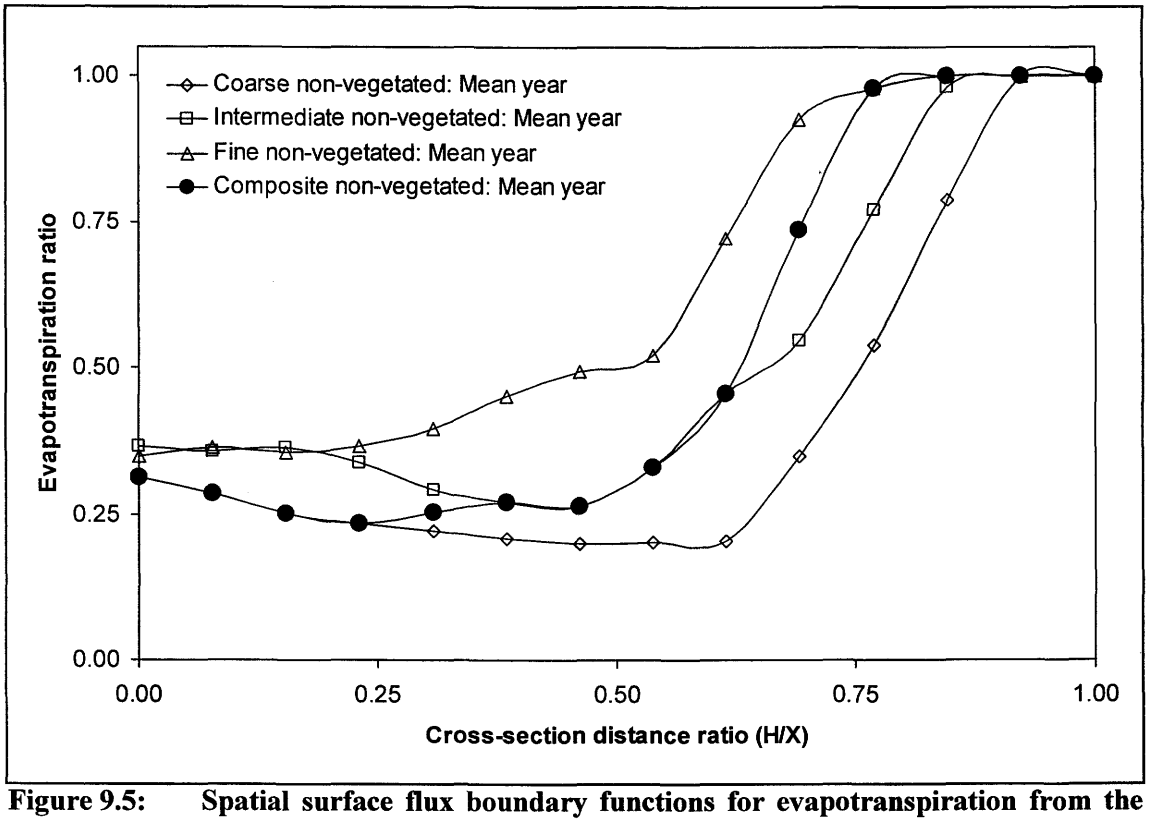

Figure 9.5: Spatial surface flux boundary functions for evapotranspiration from the generalized tailings impoundment cross-section; non-vegetated tailings and mean climatic year.

For all three runs where homogeneous tailings materials were used, the pattern is the same. Initially, the evapotranspiration ratio stays almost constant, before increasing rapidly, and finally leveling out at the maximum. The coarse tailings starts at a ratio of approximately 0.25 and starts rising at H/X = 0.65, before leveling out at approximately H/X = 0.90. The intermediate tailings starts of at around 0.28 before increasing at H/X = 0.45 and leveling out at H/X around 0.80. The fine tailings shows a more gradual rise from H/X = 0.25 to leveling off at H/X = 0.65, after starting at an evapotranspiration ratio of around 0.30. The initial section of each curve suggests that high matric suction values are present at the surface of the tailings

profiles most of the time. It has been shown that the actual evaporation rates decreases as the suctions of the soil exceed 3000 kPa (Wilson *et al.*, 1997). The slight differences are a result of precipitation driven events with temporary increase in evaporation, due to shallow wetted zones that vary with each tailings type. The point where the evapotranspiration ratio starts to increase is a function of the depth to the water table, and suggests that there is a definite interaction between the wetting front and the phreatic level. It is therefore the reason why the increase starts first for the fine tailings and last for the coarse tailings.

The point, at which the evapotranspiration reaches a maximum (i.e. a value of 1 corresponds to AE = PE) is that point at which the phreatic table is so close to the surface that it acts as an unlimited supply of water to the surface for evapotranspiration (Staley, 1957). It is therefore reasonable that this point is further from the tailings pond for the finer tailings, which has a greater air entry value and thus a greater potential to saturate a deeper profile. The composite model thus integrates the properties of the three material types. In the deep dry portions of the cross-section where the coarse material is present, the evapotranspiration ratio is equal to 0.25. The rise in the ratio is governed by the intermediate tailings properties, while the fine tailings properties govern where the profile will be saturated.

Figure 9.6 presents summary graphs for all the evapotranspiration ratios for the six primary case profiles modeled (i.e. vegetated and non-vegetated tailings surface for the three climatic years; wet, dry and mean). These graphs are for the composite models only (see Appendix N for the individual results). The trends for the non-vegetated climatic years are similar, with the exception of the initial evapotranspiration ratio, which is highest for the wet year at about 0.30, while for the dry year its at about 0.18 compared to 0.25 for the mean year. This can be simply explained by the fact that the precipitation events during the wet year, wets a deeper portion of the profile, which in turn allows for greater evaporative fluxes. The inverse is true for the dry climatic year, even when less of the profile is wetted and thus less evaporation is expected.

The trends for the evapotranspiration ratio for the vegetated surface are identical to the non-vegetated surfaces, with the exception of the apparent inconsistency after the evapotranspiration ratio appears to have leveled out. This is however due to the fact that when vegetation is present, the maximum value of actual evaporation is less than potential evaporation, even when the phreatic level is at ground surface. This is due to the reduced net radiation as a result of the leaf area index (LAI) (i.e. refer to Chapter 8 for a discussion of this aspect). For the purpose of

these discussions, it can however be assumed that once the point of leveling off has been reached, the actual evapotranspiration maximum has been reached.

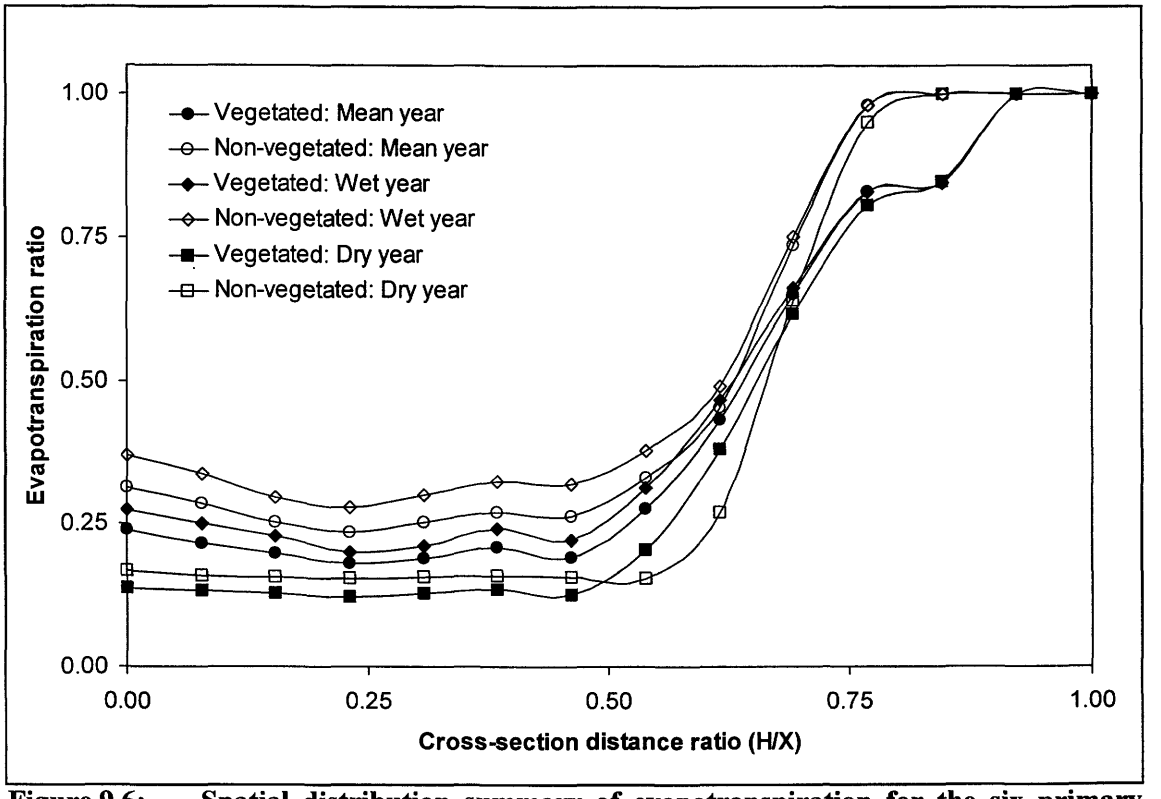

Figure 9.6: Spatial distribution summary of evapotranspiration for the six primary case profiles modeled (vegetated and non-vegetated tailings for the three climatic seasons).

9.3.1.3 Net Infiltration

Throughout this thesis the term net infiltration has been used as opposed to "infiltration". The reason for this difference is intentional, due to the meaning of the two terms. Normally infiltration (I) is defined as that volume of water that does not run off (R) during a precipitation (P) event:

$$I = P - R \qquad [9.3]$$

This implies that the infiltration is merely the inverse of the runoff; but more importantly it does not mean that the water infiltrate would actually penetrate the deeper profile of the tailings. Evapotranspiration often intercepts some of this water, effectively removing it from the profile

before it can contribute to recharge. When multidimensional saturated/unsaturated seepage analysis modeling is done, the surface flux boundary conditions must be in terms of a recharge value, which means that the net flux through the surface is required. In summary, the results are presented in terms of a net infiltration (NI), as previously defined in Equation 8.1, and correspond to the flux boundary or recharge values to be used for multidimensional saturated/unsaturated seepage analysis modeling:

$$NI = P - R - ET \qquad [8.1]$$

Equation 8.1 thus indicates that the net infiltration is the overall flux through the top surface, after all the water balance components have been taken into account (assuming the storage component of the profile is catered for by the evapotranspiration calculations). Since evapotranspiration can exceed the precipitation on any given day, the net infiltration can be a negative number, which implies that the system has an overall loss of water. Inversely, if the net infiltration is a positive number, there is a gain of moisture, which would contribute towards deep recharge. The fact that net infiltration can be either positive or negative complicates generating a spatial flux boundary function, and therefore the spatial flux boundary function is presented in terms of the net infiltration ratio, defined as follows:

$$NI_r = 1 - \frac{(NI_z - NI_{max})}{-1(|NI_{min}| + |NI_{max}|)} \qquad [9.4]$$

Where NI_r = net infiltration ratio (-),
NI_z = individual zonal net infiltration (mm),
NI_{max} = maximum individual zonal net infiltration (mm), and
NI_{min} = minimum individual zonal net infiltration (mm).

Presenting the spatial flux boundary function for evapotranspiration in terms of the net infiltration ratio allows for easy comparison of the relative magnitude of the net infiltration at any point along the generalized tailings impoundment cross-section. Further, the net infiltration ratio places the flux function in the same format as the evapotranspiration- and runoff ratios. Essentially a net infiltration ratio of 1 implies maximum net infiltration, while a value of zero means the net infiltration is at a minimum.

Figure 9.7 presents the spatial flux boundary function for net infiltration for the non-vegetated tailings during a mean climatic year.

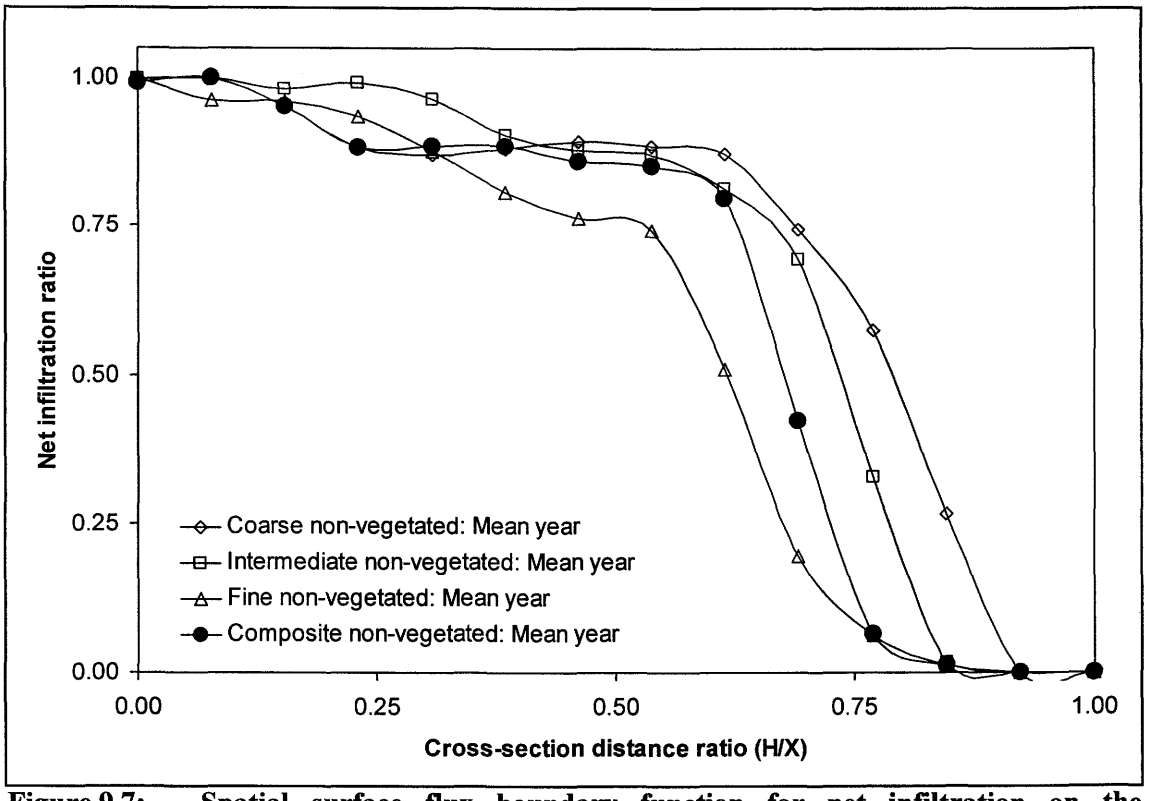

Figure 9.7: Spatial surface flux boundary function for net infiltration on the generalized tailings impoundment cross section; non-vegetated tailings and mean climatic year.

For the tailings cross-section using only coarse tailings, the net infiltration ratio is at a maximum close to the embankment wall, and drops off only marginally, until it reaches a H/W = 0.65, after which it drops dramatically to a minimum at H/X = 0.9. The same trend is true for the intermediate and fine tailings profiles with the drop starting at H/X = 0.55 and 0.50 respectively, before reading a minimum value at H/X = 0.80. It can be seen that the features of the curves shown in Figure 9.7 are consistent with evapotranspiration patterns shown in Figure 9.5. Since evapotranspiration becomes the major component of the net infiltration calculation, as the depth to the phreatic surface becomes shallower, the net infiltration starts to decline rapidly.

Examination of the actual water balance fluxes for each of the model simulations as shown in Appendix M, shows that the net infiltration is positive at the embankment (H/X = 0) but as the position move towards the pond, the net infiltration becomes negative, and increasingly

negative right at the edge of the pool (i.e. H/X = 1). The composite tailings cross-section closely resembles that for the coarse tailings profile in the region of the embankment, but at the pool edge it reflects the properties of the finer tailings; this is consistent with tailings type transition zone ratios used in the composite generalized tailings impoundment cross-section. Figure 9.8 presents the net infiltration ratio flux boundary functions for all six the primary case profiles modeled (i.e. vegetated and non-vegetated tailings surface for each climatic period; wet, mean and dry year).

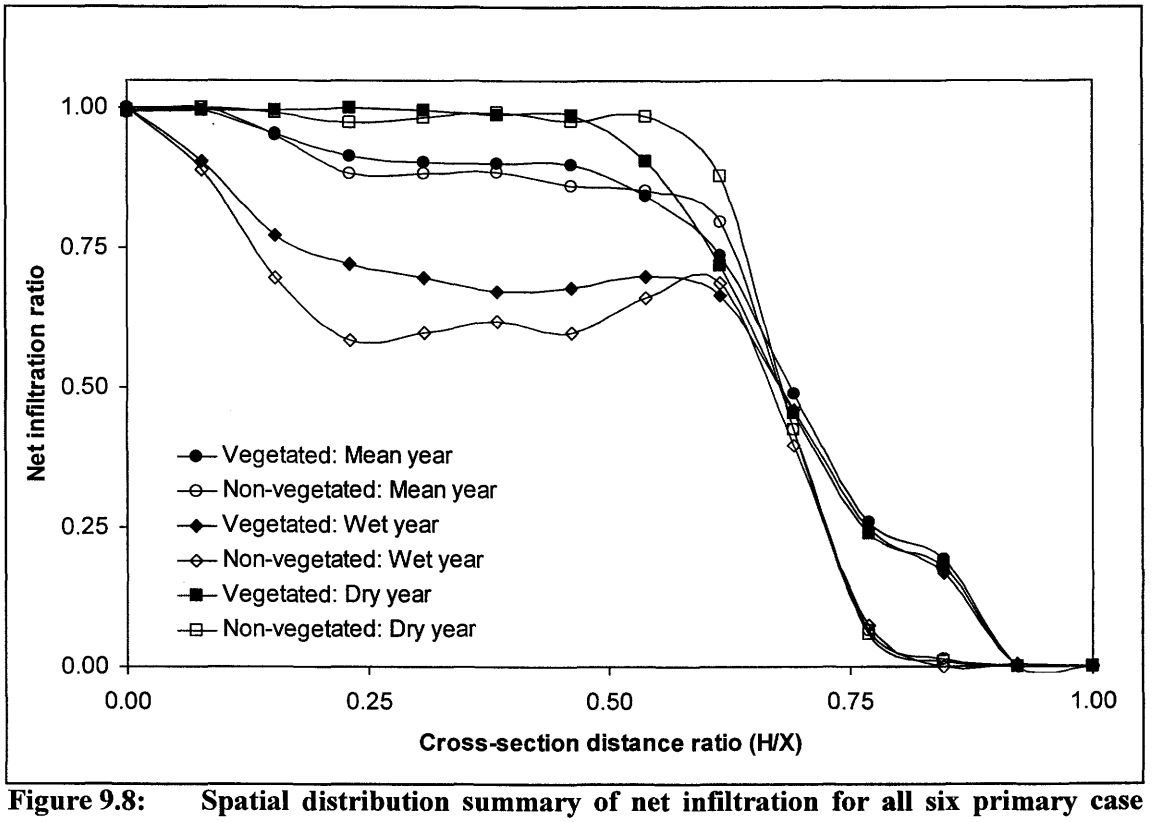

Figure 9.8: Spatial distribution summary of net infiltration for all six primary case profiles modeled (vegetated and non-vegetated tailings for the three climatic years).

The trends observed in Figure 9.8 are similar to those observed in Figure 9.6 for the evapotranspiration ratio. The differences in the initial net infiltration ratios before the rapid slope difference between the different cases can be ascribed to the relative increased evapotranspiration rates for each case. The increased evapotranspiration results in a reduced zone of positive net infiltration, or in more negative net infiltration numbers, which thus drops the ratio. The apparent anomaly in the zone close to the pool for the vegetated cases, are again as a result of the reduction in potential evaporation associated with the leaf area index (i.e. the

maximum value of actual evaporation cannot reach potential evaporation at the pools edge). The anomaly is thus not correct, but a product of the SoilCover modeling.

9.3.1.4 Spatial Flux Hypothesis

Throughout this chapter mention has been made of the spatial flux hypothesis described in Chapter 1. Figure 9.9 presents the evapotranspiration and net infiltration flux boundary functions for the non-vegetated tailings surface, during a mean climatic year on the same graph. These functions are for the composite tailings cross-sections. It can clearly be seen that the spatial flux boundary functions bear a resemblance to the spatial flux hypothesis.

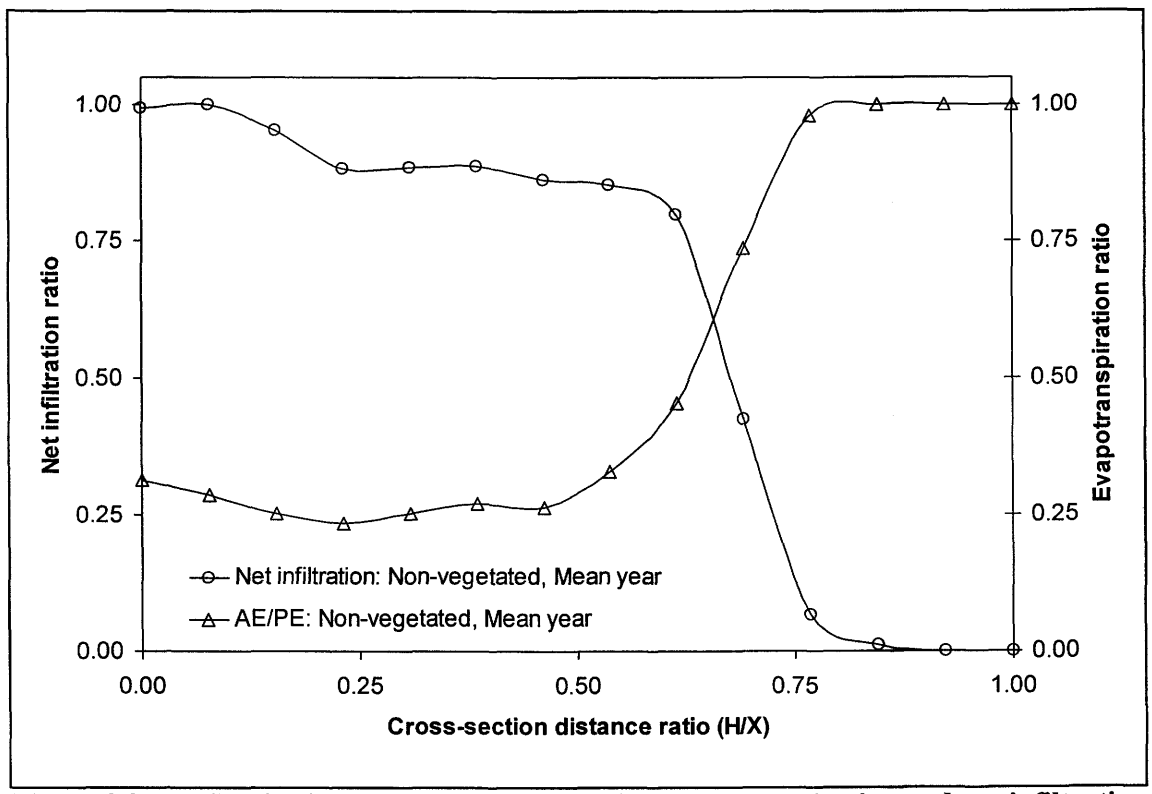

Figure 9.9: Spatial flux boundary functions for evapotranspiration and net infiltration for the non-vegetated case during a mean climatic year.

It would thus appear that for the generalized cross-section through a tailings impoundment, where there is a phreatic surface present, there is a characteristic function describing how evaporation and infiltration vary spatially. Essentially evaporation is at a minimum close to the embankment wall and increases towards a maximum at the pool edge. The infiltration is at a maximum close to the embankment wall and reduces to a minimum at the pool edge. Similar graphs for the remaining 5 case profiles modeled can be found in Appendix N.

9.3.1.5 Net Infiltration Flux

A primary aim of the present study is to develop spatial flux boundary conditions, which may be used as a direct input in multidimensional saturated/unsaturated seepage analysis modeling. This can be achieved using the net infiltration value computed in the previous section. To allow for use in multidimensional saturated/unsaturated seepage analysis the net infiltration is rewritten in terms of a net infiltration flux (q), as described in Chapter 8, Equation 8.3:

$$q = \frac{NI}{t} \qquad [8.3]$$

Where the net infiltration is expressed in mm, the time period (t) is expressed in terms of days, and the net infiltration flux (q) is expressed in terms of mm/d. Figures 9.10 and 9.11 presents the annual net infiltration fluxes for each zone, for each of the six primary case profiles modeled (i.e. vegetated and non-vegetated tailings for the three climatic periods; wet, mean and dry year).

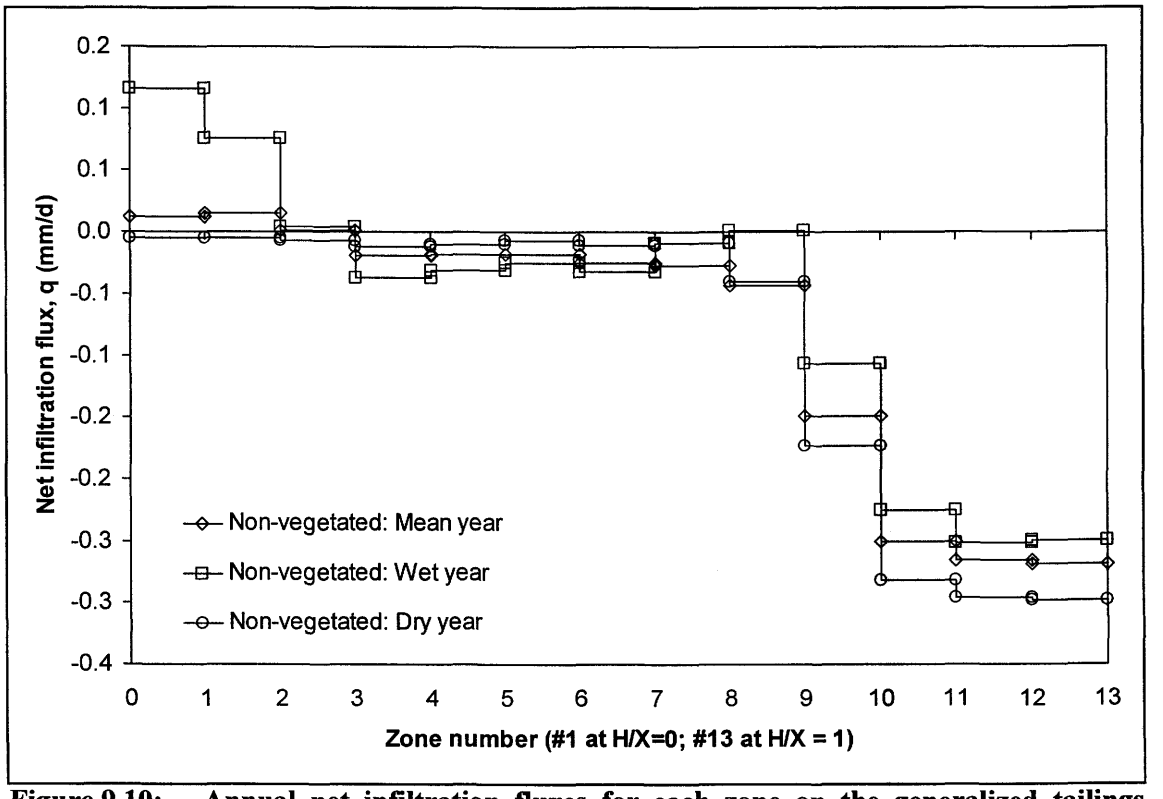

Figure 9.10: Annual net infiltration fluxes for each zone on the generalized tailings impoundment cross-section; for mean, wet and dry climatic year on non-vegetated tailings.

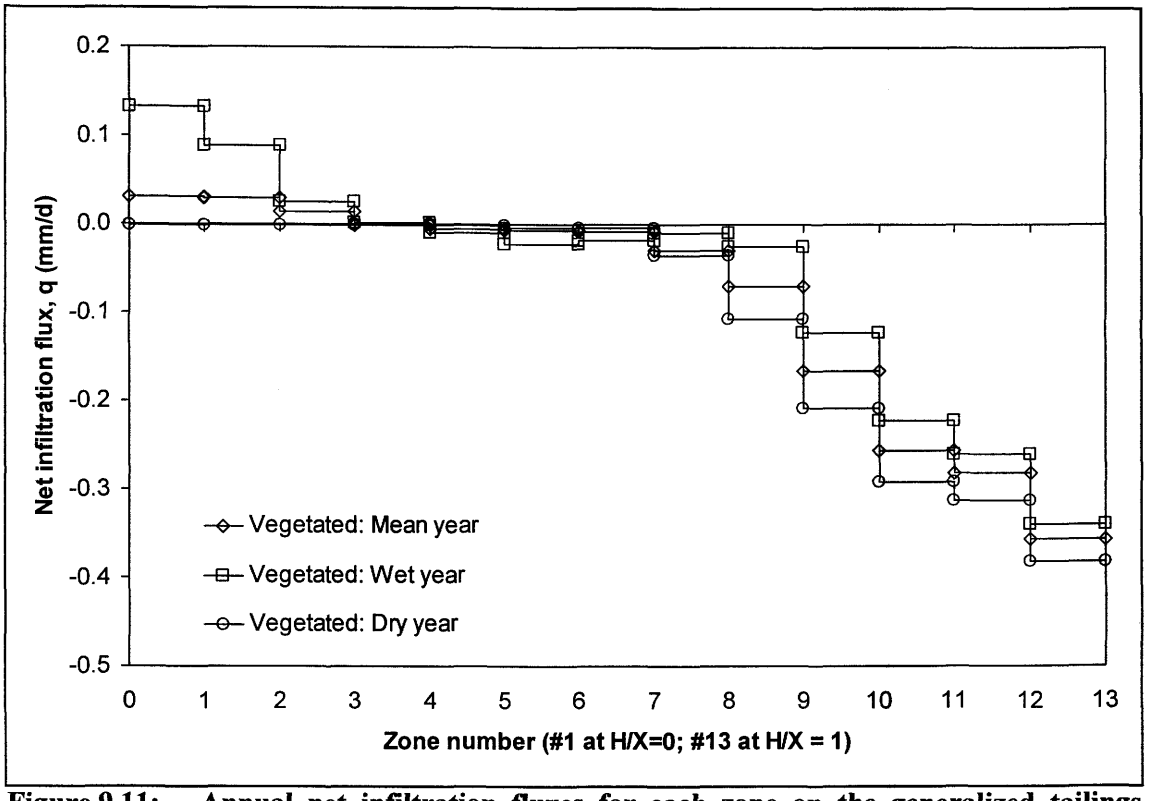

Figure 9.11: Annual net infiltration fluxes for each zone on the generalized tailings impoundment cross-section; for mean, wet and dry climatic year on non-vegetated tailings.

A multi-dimensional saturated/unsaturated seepage analysis model can thus be set up with the flux zones as presented in Figure 9.1. The predicted net infiltration fluxes can be used as recharge input. Since these fluxes have been calculated using a rigorous mechanistic approach, they should result in a more appropriate solution.

9.3.2 Monthly Results

An annual time scale of the system performance is often most appropriate for overall water balance calculations and long-term predictions. However, a more rigorous approach would be to look at seasonal changes. For this reason the annualized data presented in the previous section has been subdivided into monthly time increments, and the spatial flux boundary functions will be evaluated in terms of the increased resolution. Since the general trends presented here are similar to those previously discussed, the focus will be directed at seasonal changes. Furthermore only the non-vegetated tailings during a mean climatic year will be presented here, however Appendix N provides for details of the case profiles.

9.3.2.1 Runoff Ratio

Figures 9.12 and 9.13 present the monthly spatial flux boundary functions for runoff. The only seasonal impacts worth noting for the runoff ratio is that during the normally dry months (May to September), the patterns are highly irregular, which is a function of the highly desiccated tailings surface. Precipitation events occur every month and when the profile is sufficiently dry runoff is high, even when the precipitation event is small. This phenomenon is attributed due to the unsaturated hydraulic conductivity of the tailings.

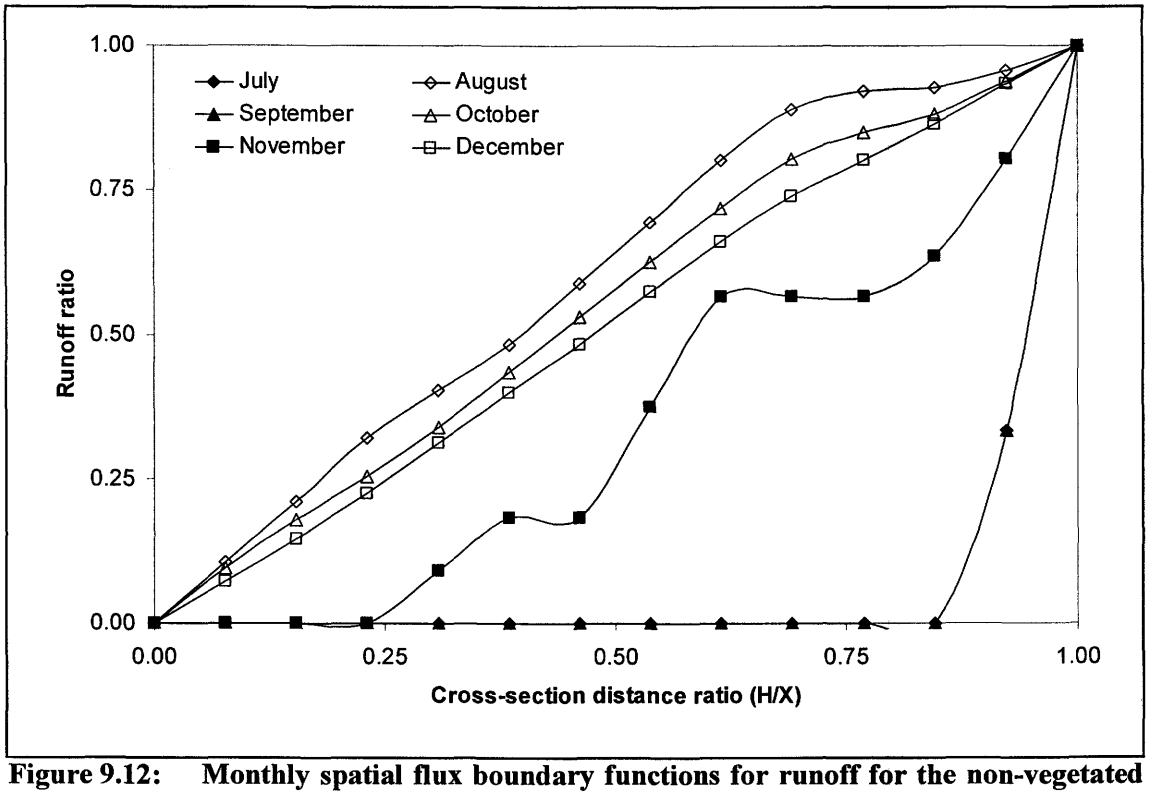

Figure 9.12: Monthly spatial flux boundary functions for runoff for the non-vegetated tailings during a mean climatic year (July to December).

9.3.2.2 Evapotranspiration Ratio

The spatial flux functions for evapotranspiration are presented in Figures 9.14 and 9.15. The most significant seasonal trend that can be noted here is the evapotranspiration increases dramatically during the wet months (November to March). The reason for this increase is the shallow wetted front, which makes moisture readily available for evaporation and root uptake. Precipitation events are frequent enough to allow a shallow zone in the top potion of the deeper, normally dry profiles close to the embankment to establish. This results in greater

evapotranspiration rates, but as the precipitation decreases this wetted zone dries up and the evapotranspiration rate returns to a reduced constant rate.

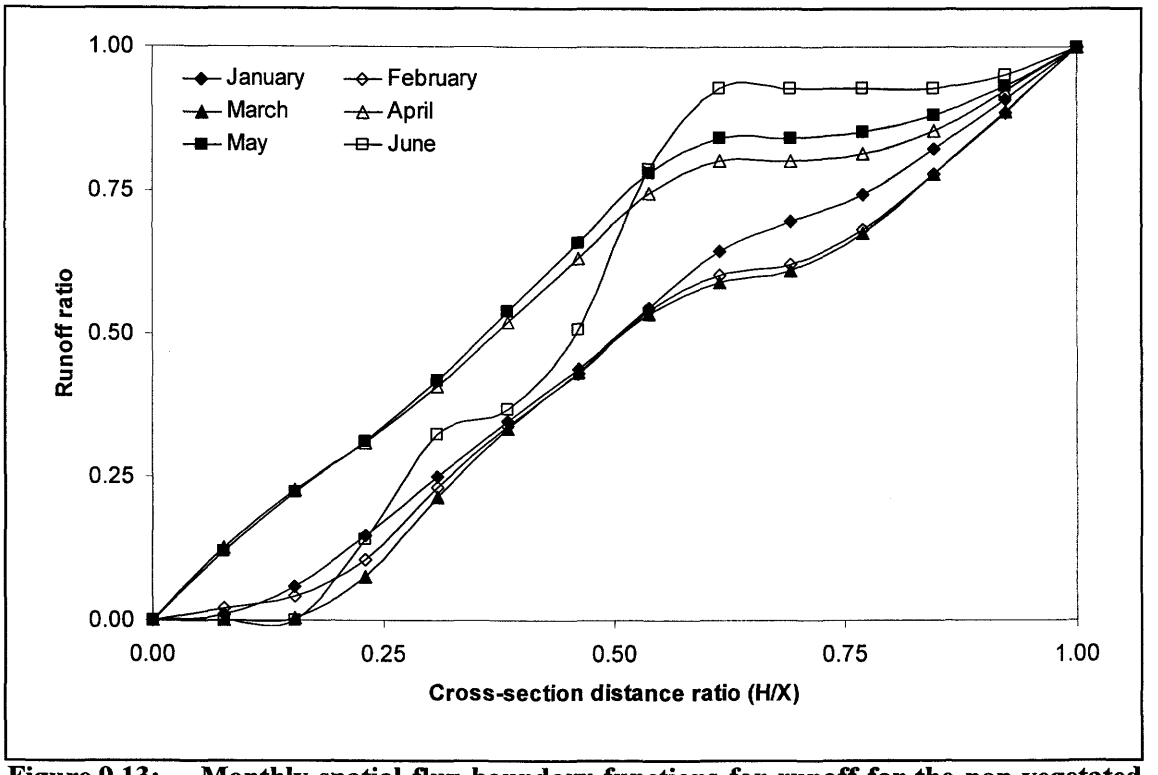

Figure 9.13: Monthly spatial flux boundary functions for runoff for the non-vegetated tailings during a mean climatic year (January to June).

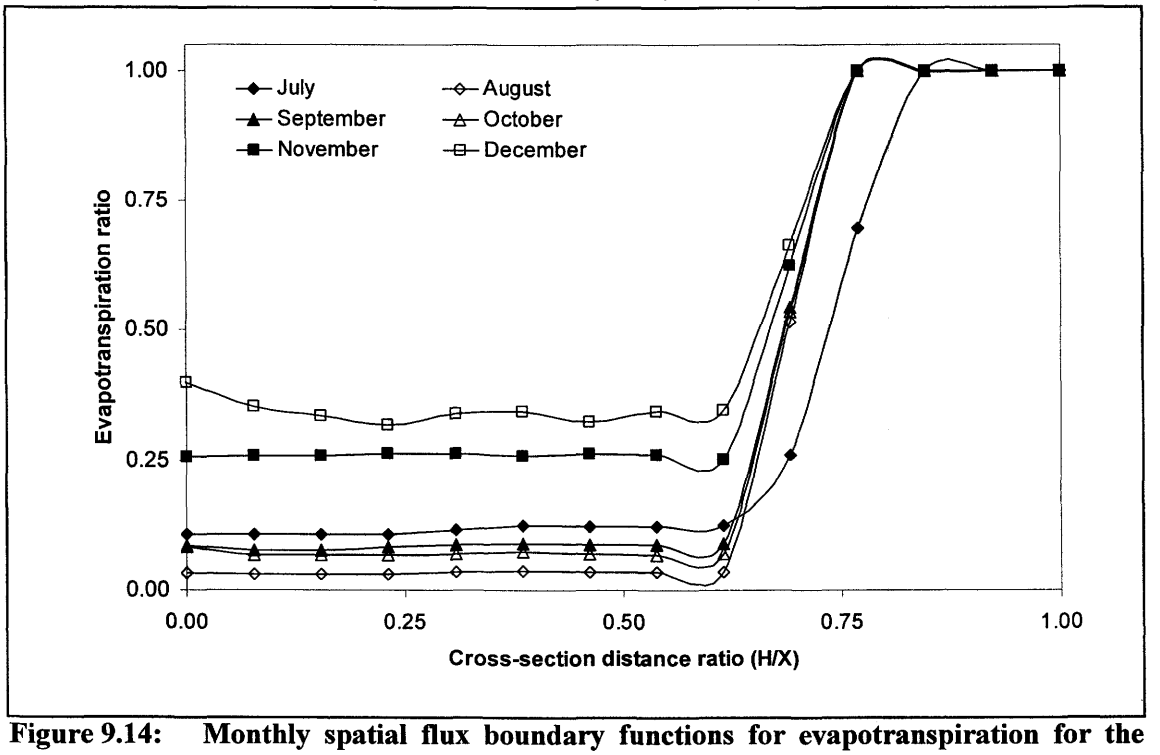

Figure 9.14: Monthly spatial flux boundary functions for evapotranspiration for the non-vegetated tailings during a mean climatic year (July to December).

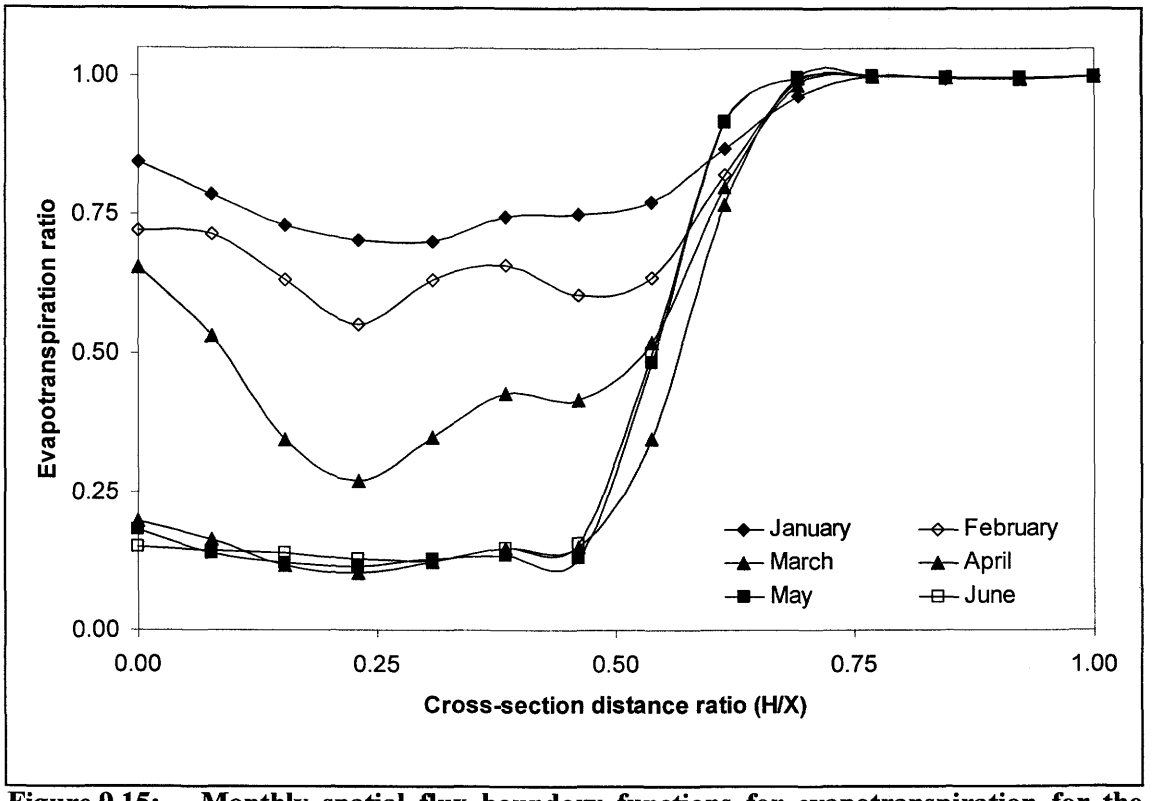

Figure 9.15: Monthly spatial flux boundary functions for evapotranspiration for the non-vegetated tailings during a mean climatic year (January to June).

9.3.2.3 Net Infiltration Ratio

The monthly net infiltration flux functions are presented in Figures 9.16 ad 9.17. The seasonal trends are very similar to those observed for the monthly evapotranspiration spatial fluxes, with the wet season dominating the variances. The most marked deviation in the trend is for the months January to March, when the precipitation is at maximum. The increased evapotranspiration results in a reduction in the net infiltration (i.e. making it more negative, in the region close to the embankment). However there appears to be a reversal of the net infiltration flux between the mid-section and the pool, which implies there is a zone where more actual net infiltration occurs. The reason for this is due to the fact that this is the region where there are finer tailings, and the precipitation has wetted the profile sufficiently to allow for a marked reduction in the runoff volume, which increases the overall infiltration to the profile.

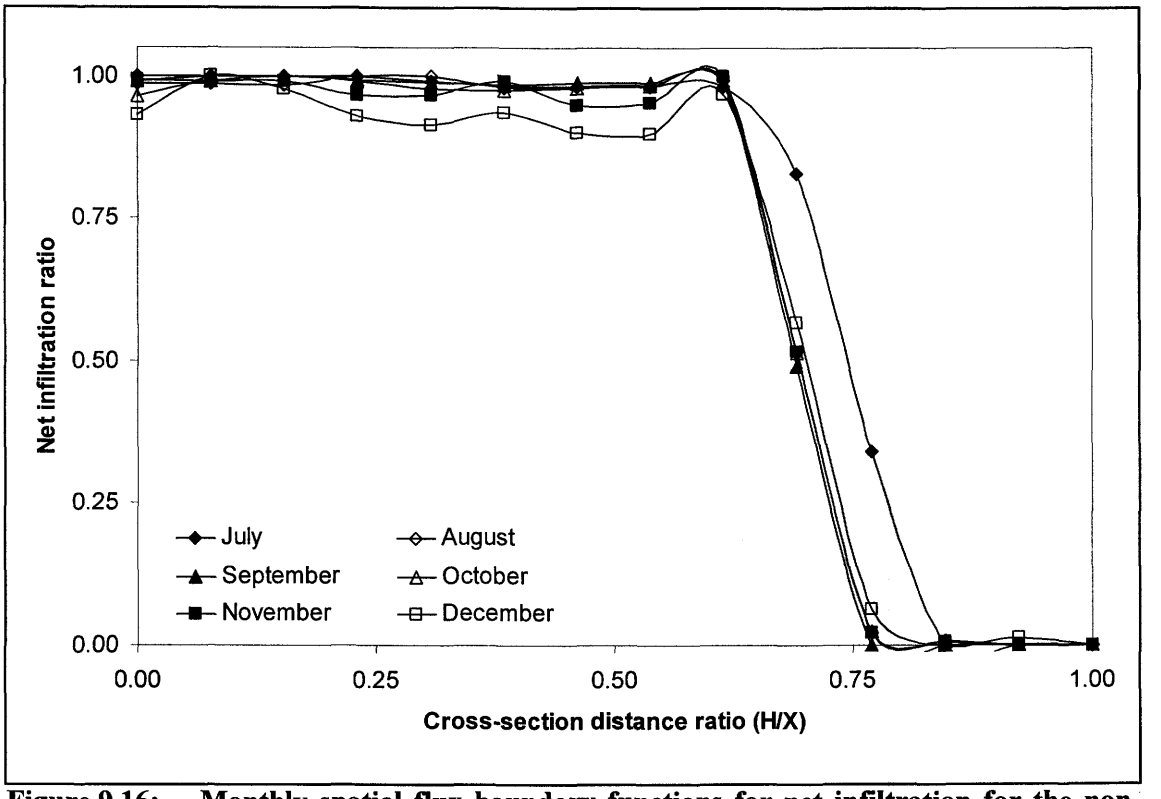

Figure 9.16: **Monthly spatial flux boundary functions for net infiltration for the non-vegetated tailings during a mean climatic year (July to December).**

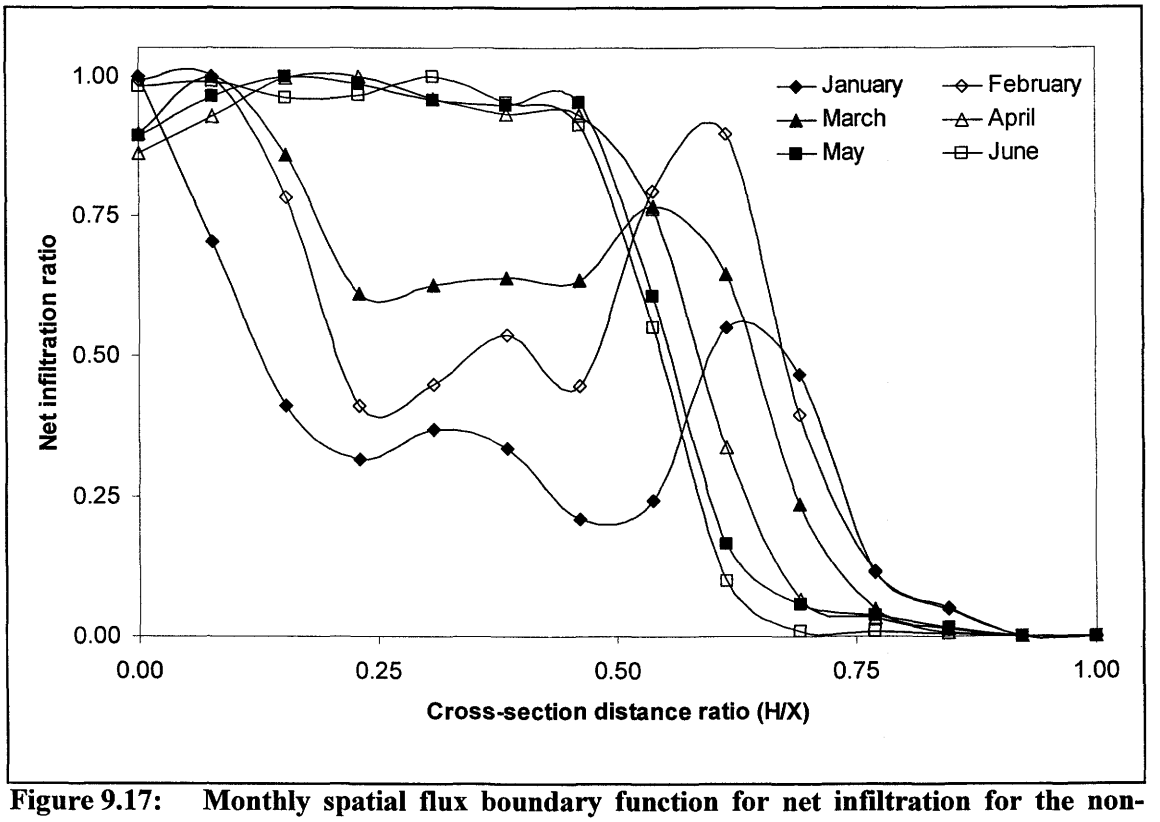

Figure 9.17: **Monthly spatial flux boundary function for net infiltration for the non-vegetated tailings during a mean climatic year (July to December).**

9.3.2.4 Net Infiltration Flux

Just as for the annualized case, monthly net infiltration fluxes can be calculated for each zone for use in multidimensional saturated/unsaturated seepage analysis modeling. These monthly fluxes for the non-vegetated tailings during a mean year are presented in Figures 9.18 and 9.19.

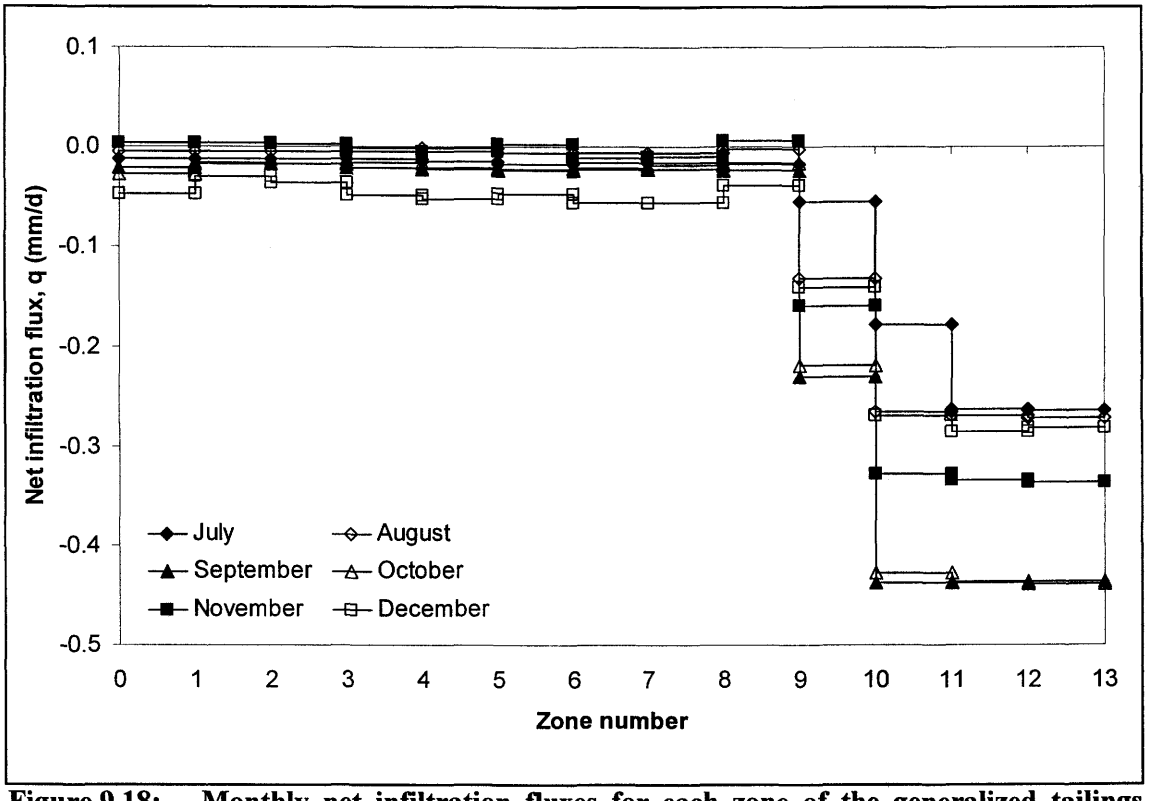

Figure 9.18: Monthly net infiltration fluxes for each zone of the generalized tailings impoundment cross-section; for the non-vegetated tailings during a mean climatic year (July to December).

For most of the year the net infiltration flux for zone 9 onwards is negative, which shows that the impact of evapotranspiration is the dominant water balance component. During the wet months there is positive net infiltration across zones 1 to 9, which suggests there is some deep recharge. The most predominant positive net infiltration occurs during February, which is after the tailings have been well wetted due to precipitation in the preceding months. The wetted front has progressed far enough down the profile to escape evapotranspiration and deep recharge occurs.

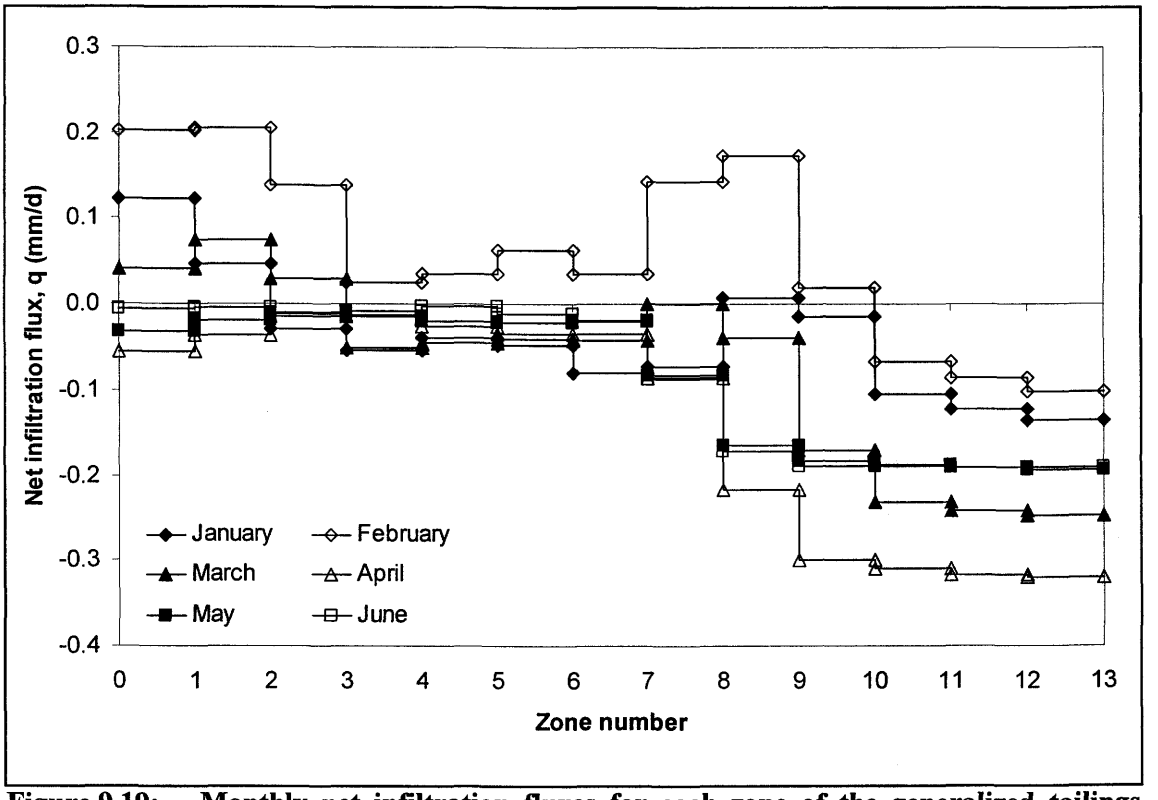

Figure 9.19: Monthly net infiltration fluxes for each zone of the generalized tailings impoundment cross-section for the non-vegetated tailings during a mean climatic year (January to June).

9.4 Conclusions

The spatial flux boundary functions presented and discussed in this chapter shows that there is a distinct pattern of spatial surface flux distributions, when the depth to the phreatic surface is variable. The spatial flux hypothesis presented in Chapter 1 has shown to exist for the Kidston tailings impoundment.

The true benefit of the spatial flux boundary function is that spatial infiltration fluxes for each zone can be generated for direct input in 2-D and 3-D saturated/unsaturated seepage analysis models. These fluxes are representative of the actual surface fluxes at any point along the generalized tailings impoundment cross section, and are based on mechanistic soil/atmosphere flux boundary modeling.

The overall net infiltration to the Kidston tailings impoundment appears to be negative, which suggest that the system is losing water over the long-term. This is intuitively correct if one

considers the fact that the climate hosts a net negative water balance with the average precipitation being about a third of the annual potential evaporation. However, what gives credit to these findings is the fact that the overall long-term trend for the Kidston tailings impoundment has shown a decrease in the pond water level, and associated phreatic levels since monitoring started in 1997. These data are presented in Appendix F.

9.5 References

GEO-SLOPE International Ltd. (1991). SEEP/W for finite element seepage analysis, Version 4 for Windows 95 and NT, Getting Started Guide, Calgary, Alberta, Canada.

Lin, H.J., Richards, D.R., Talbot, C.A., Yeh, G., Cheng, J., Cheng, H., Jones, N.L. (1997). FEMWATER: A Three-Dimensional Finite Element Computer Model for Simulating Density-Dependent Flow and Transport in Variably Saturated Media. Technical Report CHL-97-12, July.

McDonald, M.C., Harbaugh, A.W. (1988). MODFLOW, a Modular Three-Dimensional Finite Difference Groundwater Flow Model. U.S. Geological Survey, Open-File Report 91-536, Denver.

SoilCover. (1997). SoilCover User's Manual. Unsaturated Soils Group, Department of Civil Engineering, University of Saskatchewan, Saskatoon, Saskatchewan, Canada.

SoilVision Systems (2001). SVFlux™ : Saturated/Unsaturated Automated 3D Seepage Modeling. SoilVision Systems Ltd.

Staley, R.W. (1957). Effect of depth of water table on Evaporation from fine sand. Master of Science Thesis, Colorado State University, Fort Collins, Colorado, U.S.A.

Wilson, G.W., Fredlund, D.G., Barbour, S.L. (1997). Coupled soil-atmosphere modeling for soil evaporation. Canadian Geotechnical Journal, Vol. 31, pp. 151-161.

This page was intentionally left blank.

CHAPTER 10

Evaluation of Spatial Flux Boundary Functions

10.1 Introduction

This chapter documents the evaluation of the spatial flux boundary functions developed during the study. The evaluation tests conducted show that the spatial flux boundary functions are in fact a suitable method for predicting surface fluxes boundary conditions through an unsaturated tailings profile that has a spatially varying geometry, texture and phreatic surface.

10.2 Evaluation Goals and Methodology

The objective of the evaluation exercise is to show that the spatial flux boundary functions developed during this study as described in Chapter 9, is in fact a reasonable approximation of the surface fluxes through the generalized tailings impoundment cross-section. Furthermore, the evaluation exercise will determine whether the use of the flux boundary functions as direct input into multidimensional saturated/unsaturated seepage analysis models is in fact a suitable way to estimate the surface flux boundary conditions for a saturated/unsaturated system. It must be emphasized that the evaluation exercise was not a calibration exercise, and therefore minimal, if any manipulation of data is attempted. The success of the functions are judged on the outcome of the relative order of magnitude between the predicted and measured seepage rates emanating from the tailings impoundment.

One of the primary objectives of this study was to develop a spatial flux boundary function that would describe the spatial variation of surface flux boundary conditions for a tailings impoundment which has a spatially varying phreatic surface (see Chapter 1). The intention was that such a function would be required in order to allow accurate multidimensional saturated/unsaturated seepage analysis modeling. It is therefore logical that the evaluation test for the spatial flux boundary functions would be using the calculated flux boundary function as input in a multidimensional seepage analysis model of the tailings impoundment, and calculate

the seepage volume for comparison with the measured seepage volumes that was used to develop the flux boundary functions. Since 3-D numerical modeling is complicated and posses difficulties that could make interpretation of the modeling results subject to significant variation in interpretation, it was decided to carry out the evaluation for this study in a 5-step procedure. The goal of such an approach was to ensure that once full 3-D model evaluation is undertaken, the system as a whole would be completely understood. The five evaluation steps are outlined below:

Step 1: Evaluation of the surface flux boundary function for a non-vegetated tailings impoundment surface during the generic climatic year (365 days) and the generalized tailings impoundment cross-section using the 2-D seepage modeling software, SEEP/W (GEO-SLOPE, 1991) to calculate the seepage through this generalized section.

Step 2: Evaluation of the surface flux boundary function for a non-vegetated tailings impoundment surface during the generic climatic year (365 days) and the generalized tailings impoundment cross-section using a 2-D axisymmetric analysis of the seepage though the tailings impoundment with the 2-D seepage modeling software SEEP/W (GEO-SLOPE, 1991) to represent a quasi 3-D model. This test is identical to Step 1, except the analysis is axisymmetric.

Step 3: Evaluation of the surface flux boundary function for a non-vegetated tailings impoundment surface during the generic climatic year (365 days) and the generalized tailings impoundment cross-section using the 3-D seepage modeling software SVFlux™ (SoilVision, 2001) to calculate the seepage through a axisymmetric tailings impoundment. This test is identical to Step 2, except it consisted of a full 3-D analysis as opposed to a 2-D axisymmetric analysis.

Step 4: Evaluation of the surface flux boundary function for a non-vegetated tailings impoundment surface during the generic climatic year (365 days) using the actual Kidston tailings impoundment geometry within the 3-D seepage modeling software SVFlux™ (SoilVision, 2001). This test is similar to Step 3, except the actual tailings impoundment geometry is used as opposed to the generalized tailings impoundment cross-section.

Step 5: Evaluation of the surface flux boundary function for a specific time period (1 December 2000 to 31 March 2001) for which detailed field data of the Kidston tailings impoundment water balance was known together with the actual Kidston tailings impoundment geometry using the 3-D seepage modeling software SVFlux™ (SoilVision, 2001). This test is identical to Step 4, except for the fact that this test was for a specified time period as opposed to a generic period.

10.3 Evaluation Model Selection

The choice of 2-D and 3-D seepage modeling software for this study was made on the basis of using commercial software that are accepted by the industry to provide reliable results. Furthermore, the software had to be relatively user friendly, to allow the evaluation modeling to be done in a reasonable timeframe. It must be emphasized that the evaluation exercise was not intended to be a test of the 2-D and 3-D seepage modeling packages.

The 2-D seepage modeling package selected was SEEP/W, a finite element seepage analysis program developed by GEO-SLOPE International Ltd., in Calgary Alberta, Canada (GEO-SLOPE, 1991). No other packages were evaluated in making this selection, as SEEP/W has been well tested and is considered to be an industry-standard in 2-D seepage modeling. SEEP/W has the ability to perform axisymmetric analysis, which was one of the requirements. Furthermore, the University of Saskatchewan had a network version of the software available, making it immediately available for use.

The selection of a 3-D seepage-modeling package required more consideration. The first package considered was the public domain modular, three-dimensional, finite difference groundwater flow model developed by the United States Geological Survey, MODFLOW (McDonald and Harbaugh, 1988). The MODFLOW code is probably the most widely used code for 3-D seepage flow modeling and is arguably the industry standard. Although the seepage code is public domain software, MODFLOW requires a front-end to actually use the code, and there are numerous of these available, including supposedly very user-friendly Windows based versions. Kidston Gold Mine Limited had a contract with Australasian Groundwater Consultants (AGE) to develop a 3-D regional model of the tailings impoundment complex for closure purposes. AGE used MODFLOW to develop this model, with the PMWIN (Processing MODFLOW for Windows) (Chiang and Kinzelbach, 1996) interface (AGE, 2001). It was thus

decided that MODFLOW would not be used for this study, to avoid any notions of bias, and to prevent confusion of the evaluation modeling becoming a substitute or replacement for the calibrated modeling done by AGE.

The second package considered was the 3-D version of SEEP/W, Seep3D (GEO-SLOPE, 2000). The package was also developed by GEO-SLOPE International Ltd., Calgary, Alberta, Canada. This package is new to the market, and is essentially SEEP/W, but upgraded to work in three dimensions. The code consists of finite element seepage analysis, and the mesh building is by means of building blocks of specific shapes. Seep3D was not considered to be a suitable package to use, since the technique of building the actual 3-D mesh using building blocks, is not well suited to setting up real-world problems, especially not to the scale of the Kidston tailings impoundment. Furthermore, the computing requirements for Seep3D is excessive, which is somewhat limiting in a practical sense.

FEMWATER (Lin *et al*, 1997), a 3-D finite element, saturated/unsaturated, density driven, flow and transport model was the third package considered. FEMWATER is becoming a leading modeling package, however it is an extremely difficult code to use. FEMWATER runs through the graphical GMS (Groundwater Modeling System) interface which is a product of the Engineering Computer Graphics Laboratory (ECGL) of Brigham Young University, Provo, Utah (ECGL, 1998). FEMWATER is highly memory intensive and solutions can be time-consuming and convergence is more difficult than with MODFLOW. These reasons, along with the fact that the learning curve for the software is long and arduous, led to the decision not to use this code for the evaluation tests.

The final package considered was SVFlux™ (SoilVision, 2001), a 3-D saturated/unsaturated seepage modeling package developed by SoilVision Systems of Saskatoon, Saskatchewan, Canada. SVFlux™ consist of an AutoCAD style front end, and the actual seepage modeling is performed with the FlexPDE (PDE Solutions, 1999) software. FlexPDE is a partial differential equation solver that has been tested and verified to be capable of handling unsaturated seepage flow modeling problems (Pentland, 2000). Due to the AutoCAD style interface, setting up a real-world problem was easier than in any of the other packages considered. A decision was made to use SVFlux™ for the final evaluation modeling.

10.4 Generic Flux Boundary Function Evaluation

This section describes the first 4 evaluation steps as discussed in Section 10.2. The Evaluation data required for the numerical modeling is presented in terms of material properties, boundary conditions and the model geometries for each of the 4 evaluation tests. The data set for Steps 1 to 4 of the evaluation process is the same data set associated with the generic mean climatic year as discussed and documented in Chapter 8. Furthermore, the evaluation is only done for the flux boundary function developed with the composite tailings impoundment cross-section of a non-vegetated surface. The evaluation period is thus for 365 days, spanning from 1 July through to 30 June of the following year.

10.4.1 Material Properties

The material properties used in the evaluation modeling is exactly the same as that used for the SoilCover (SoilCover, 1997) modeling (see details documented in Chapter 8). There are thus 13 zones, each with a homogeneous tailings profile, consisting of coarse, intermediate or fine tailings. The first five zones (0 to 250 m) from the embankment end consist of coarse tailings, the next five zones (250 to 500 m) consist of intermediate tailings, and the final three zones (500 to 650 m) consist of fine tailings. The surface saturated hydraulic conductivity along the tailings beach (i.e. for each zone) is defined by Equation 7.4, which is repeated here for clarity:

$$k_s = 1.94 \times 10^{-5} \cdot e^{-0.00977 H_b} \qquad [7.4]$$

Where k_s = surface saturated hydraulic conductivity (m/s), and

H_b = distance down the beach from the embankment wall (m).

Each zone thus has its own unique unsaturated hydraulic conductivity curve, while the soil water characteristic curves of the zones overlap according to tailings type. The vertical to horizontal hydraulic conductivity ratio (k_s/k_h) was kept as one, which was consistent with the SoilCover modeling.

10.4.2 Boundary Conditions

The top boundary condition for the 2-D and 3-D modeling is the monthly net infiltration flux, q (broken down into equal daily increments), for each zone as defined in Chapters 8 and 9. These fluxes, broken down as daily fluxes based on monthly totals are listed in Tables 10.1 and 10.2 for each of the 13 zones. The net infiltration fluxes thus replaces the need for precipitation and evaporation inputs, and are the fluxes that need to be evaluated.

Table 10.1: Daily net infiltration fluxes, q (based on monthly totals) for zones 1-7 used in the spatial flux boundary function evaluation tests.

Month	Julian Day		Daily net infiltration flux, q (mm/d) for each zone						
	Start	End	1	2	3	4	5	6	7
July	1	31	-0.012	-0.012	-0.012	-0.012	-0.014	-0.017	-0.016
August	32	62	-0.005	-0.005	-0.005	-0.001	-0.001	-0.006	-0.006
September	63	92	-0.021	-0.018	-0.018	-0.021	-0.022	-0.024	-0.023
October	93	123	-0.027	-0.016	-0.012	-0.016	-0.021	-0.022	-0.021
November	124	153	0.004	0.003	0.003	-0.005	-0.005	0.003	-0.011
December	154	184	-0.048	-0.030	-0.036	-0.048	-0.052	-0.047	-0.055
January	185	215	0.122	0.047	-0.029	-0.053	-0.039	-0.048	-0.080
February	216	243	0.203	0.205	0.139	0.025	0.036	0.063	0.036
March	244	274	0.041	0.075	0.030	-0.050	-0.045	-0.041	-0.042
April	275	304	-0.056	-0.035	-0.014	-0.013	-0.026	-0.034	-0.035
May	305	335	-0.031	-0.018	-0.012	-0.014	-0.020	-0.021	-0.020
June	336	365	-0.006	-0.004	-0.009	-0.009	-0.002	-0.011	-0.019

Table 10.2: Daily net infiltration fluxes, q (based on monthly totals) for zones 8-13 used in the spatial flux boundary function evaluation tests.

Month	Julian Day		Daily net infiltration flux, q (mm/d) for each zone					
	Start	End	8	9	10	11	12	13
July	1	31	-0.016	-0.017	-0.055	-0.178	-0.264	-0.264
August	32	62	-0.006	-0.003	-0.131	-0.265	-0.269	-0.271
September	63	92	-0.022	-0.023	-0.231	-0.437	-0.437	-0.437
October	93	123	-0.019	-0.017	-0.219	-0.428	-0.436	-0.438
November	124	153	-0.010	0.006	-0.159	-0.328	-0.334	-0.336
December	154	184	-0.056	-0.038	-0.141	-0.269	-0.285	-0.282
January	185	215	-0.072	0.007	-0.015	-0.105	-0.122	-0.135
February	216	243	0.142	0.174	0.020	-0.066	-0.086	-0.102
March	244	274	0.001	-0.039	-0.170	-0.231	-0.242	-0.247
April	275	304	-0.086	-0.216	-0.300	-0.310	-0.318	-0.320
May	305	335	-0.083	-0.164	-0.183	-0.187	-0.191	-0.194
June	336	365	-0.087	-0.172	-0.189	-0.189	-0.190	-0.191

Further boundary conditions specific to each individual model setup will be discussed separately where relevant.

10.4.3 2-D SEEP/W Evaluation

Step 1 of the evaluation process involves modeling of the generalized tailings impoundment cross-section using the 2-D seepage modeling package SEEP/W (GEO-SLOPE, 1991). This section describes the setup and results of this evaluation exercise.

10.4.3.1 Model Setup

The basic setup of the generalized tailings impoundment cross-section to allow for analysis by SEEP/W is described in the following sections. These include the problem setup with respect to geometry, boundary conditions and convergence criteria.

10.4.3.1.1 Geometry

The generalized tailings impoundment cross-section (650 m between the embankment and the pool) was the basis for all the modeling in Steps 1 to 3 of the evaluation tests. The top surface of the tailings was thus determined using the beach shape function defined in Chapter 7, Equation 7.1 with the top corner of the tailings impoundment beach, at the embankment end at a coordinate of (10.0; 18.4). The edge of the pool was at coordinate (670.0; 15.0), and continued for 100.0 m to (770.0; 15.0). Below the pool the beach was sloped more steeply to linearly reduce in height to a final coordinate of (770.0; 14.75). The embankment wall was sloped at an angle of 35.5° (i.e. as illustrated in Chapter 2), to allow for a toe coordinate at (30.0; 5,0). The base elevation was arbitrarily set at 5.0 m. The base of the generalized tailings impoundment cross-section was fixed on a horizontal plane, and extended to 100.0 m beyond the edge of the pool (770.0; 5.0). These dimensions gave rise to the generalized section shape in Figure 10.1.

Figure 3.3 in Chapter 3 provides a schematic of the typical embankment wall cross-section through the Kidston tailings impoundment. In setting up the 2-D SEEP/W model, a decision was made to simplify the cross-section, by eliminating materials that were not relevant to the modeling at hand. Since all the seepage can be assumed to find its way to the seepage drains, and since the embankment is much more permeable than the tailings, the seepage problem was

simplified by ignoring the flow through the embankment wall and the seepage drains. All the flow can be assumed to pass through somewhere immediately above the upstream toe of the embankment.

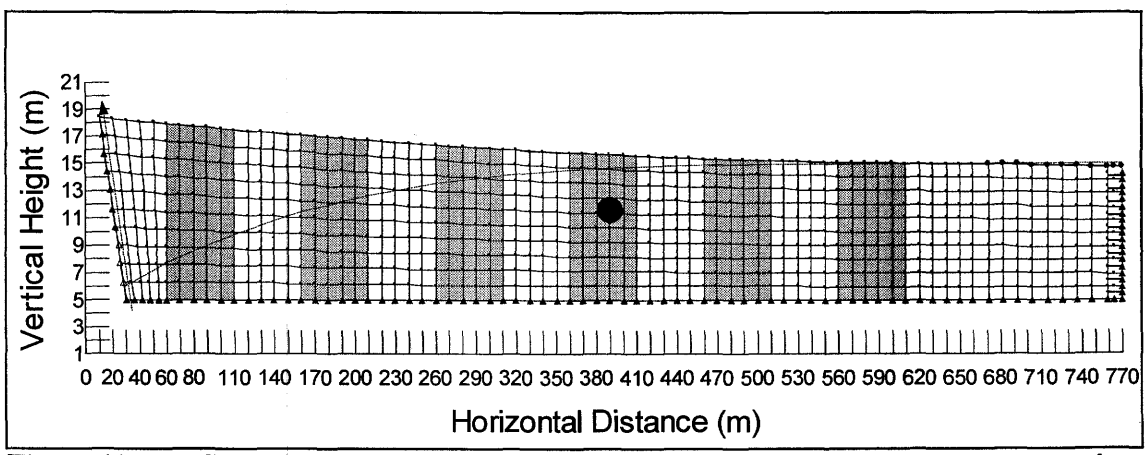

Figure 10.1: SEEP/W model of the generalized tailings impoundment cross-section. Each different shade denotes the 13 zonal interfaces.

The grid was based on five horizontal elements for each zone, and 10 vertical elements for each zone. This configuration allowed for 50 elements in each zone, with 750 elements for the overall problem. All elements were quadrilateral, which resulted in a total number of nodes of 867. Zone 13, the zone adjacent to the pool, was extended to include the area under the pool, for the purpose of assigning material properties. Since the pool in actual fact extend for quite some distance, the outer pool-edge of the problem was assigned as infinite elements. The mesh is depicted in Figure 10.1.

10.4.3.1.2 Convergence Criteria

The convergence criteria were set such that the maximum number of iterations allowed was 100. The allowable tolerance was 1% and the maximum conductivity change during a time step was one. The minimum conductivity change was set at 0.0001 and the rate of conductivity change was fixed at 1.1. These convergence criteria were kept constant for both the 2-D and the 2-D axisymmetric SEEP/W simulations.

10.4.3.1.3 Boundary Conditions

Each of the 13 material zones (each 50 m wide) had a separate surface flux boundary function assigned as described in Tables 10.1 and 10.2. From the edge of the pool to the problem outer

edge a constant head of 15 m was assigned (10 m of true head). The rest of the problem boundaries were no flow boundaries, with the exception of the upstream wall of the embankment from the toe, and up a third of the way which was set as a review boundary. This configuration meant that all seepage would exit at a zone between the embankment toe and up along the embankment wall. The assumption that there would be no seepage through the base of the problem is not entirely physically correct as had been described in Chapter 5, however the base seepage is small enough to ignore for the purpose of these calculations.

The location of the initial phreatic level is defined by the phreatic line function developed and described in Chapter 7, Equation 7.2. This line is shown on Figure 10.1.

10.4.3.2 The 2-D Simulation

As a result of the exponentially varying surface hydraulic conductivity as defined by Equation 7.4, the modeled steady state phreatic surface of the tailings impoundment will be depressed as shown in Figure 10.2. The explanation for this is quite simple: Continuity of flow requires that the flow rate of water from the pool be the same through the lower permeability material near the pool and the higher permeability material near the embankment wall. It follows from Darcy's law that the flow gradient will progressively decrease from the pool outwards, i.e. the slope of the phreatic surface must progressively flatten, thus producing the depression shown in Figure 10.2.

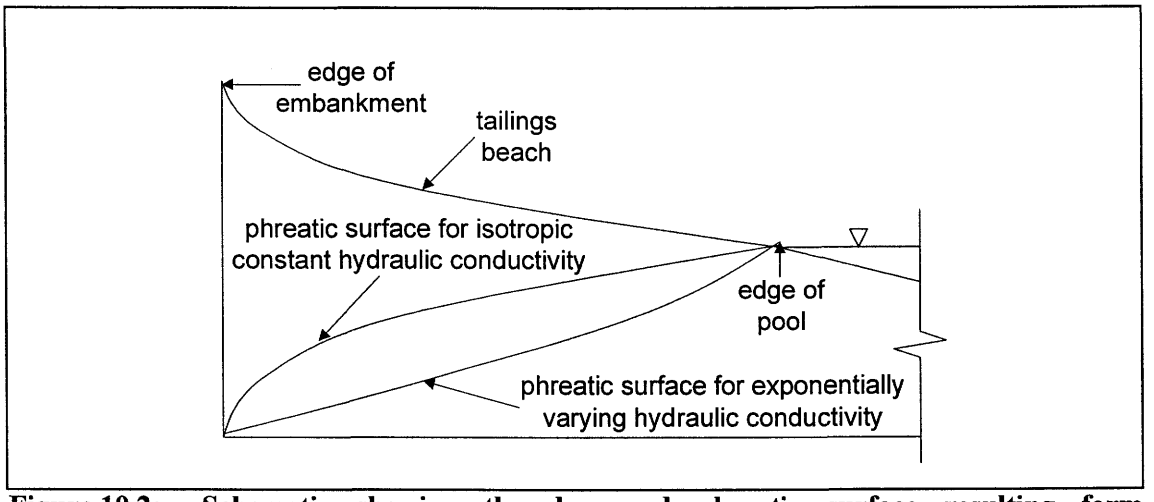

Figure 10.2: Schematic showing the depressed phreatic surface resulting form hydraulic particle sorting on a tailings beach.

The initial head profile throughout the problem is required prior to running a SEEP/W simulation. This head profile describes the position of the phreatic surface. It is standard practice to first run a steady-state simulation to generate a head profile for subsequent transient simulations. The material properties in the steady state problem can then be adjusted such that the steady state simulation produces a final phreatic level that matches an observed phreatic level. The evaluation exercise performed for this study specifically excluded such calibration modeling and the initial head profiles for the subsequent transient simulations was generated by simply using the position of the phreatic surface for the generalized tailings impoundment cross-section based on the phreatic line function described in Chapter 7 and indicated on Figure 10.1.

The results of the transient 2-D SEEP/W simulation for the generalized Kidston tailings impoundment cross-section, using 13 material zones and 13 spatial flux boundary functions, is presented in Figure 10.3. The final phreatic surface (after day 365) for the transient simulation when using the phreatic surface defined by the phreatic function described in Chapter 7 as an initial condition (i.e. as illustrated on Figure 10.1) is shown in Figure 10.3.

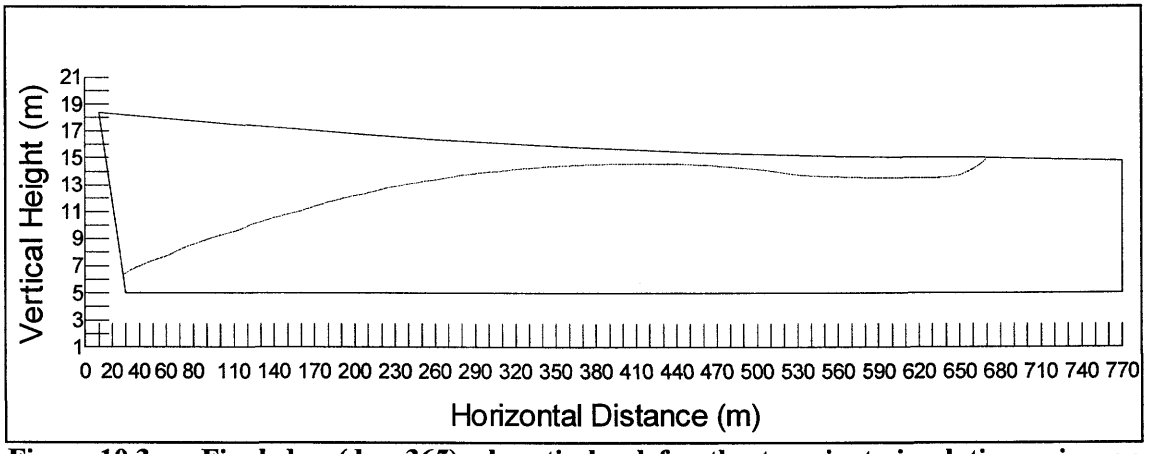

Figure 10.3: Final day (day 365) phreatic level for the transient simulation using an initial phreatic level defined by the phreatic line function (i.e. not steady state).

Close to the pool, the phreatic level is severely depressed, as a result of the intense negative net infiltration flux in this zone. This highly negative flux is driven by evaporation from the tailings surface, which is significant due to the proximity of the phreatic level as shown in Chapter 8. The overall annual seepage through the toe of the embankment (i.e. through the seepage drains) for this condition is 19.1 l/s. This assumes that the seepage is occurring from a front of 5875 m around the perimeter of the tailings impoundment as described in Chapter 5. The phreatic level

in Figure 10.3 is not depressed as the theory suggests which indicates that running the model for 365 days is not long enough to reach steady state conditions. An important observation is that the pond on the tailings impoundment is driving the seepage rate, and the flux boundary functions are not having a significant impact on the amount of seepage that reports to the drain.

The Kidston tailings impoundment water balance documented in Chapter 5, which was used to define the runoff volume for the SoilCover calibration used seepage rates between 8.1 and 10.1 l/s, with an overall average seepage rate of 9.0 l/s (including the estimated deep seepage through the impoundment foundation). It could thus be concluded that running a transient 2-D simulation with an initial phreatic surface defined by the phreatic line function and applying the calculated surface flux boundary functions as a flux boundary condition on the surface of the tailings impoundment, provides a result that agrees with the measured results both with respect to the final phreatic surface and the value of seepage calculated.

10.4.4 2-D Axisymmetric SEEP/W Evaluation

The section below describes the evaluation modeling for the generalized tailings impoundment cross-section using a 2-D axisymmetric analysis to represent a quasi 3-D model of the tailings impoundment.

10.4.4.1 Model Setup

The model geometry and mesh setup for the axisymmetric SEEP/W simulation is identical to the 2-D model described in the previous section, except that the X-axis had to be reversed, to allow the pivot axis to be at co-ordinates (0.0; 0.0) as illustrated in Figure 10.4. The time step and convergence criteria remains as described in the previous case and the boundary conditions remain the same. The model layout as described results in a circular tailings impoundment with a 1500 m diameter, to give a seepage front (circumference) of 4712 m; compared to the actual seepage path length of 5875 m.

10.4.4.2 The 2-D Axisymmetric Simulation

The initial phreatic surface as described by the phreatic line function for the generalized tailings impoundment cross-section is used as the initial head profile for the transient axisymmetric simulation. The simulation is done by applying the surface flux boundary function to the tailings impoundment surface as a flux boundary condition. The calculated overall annual seepage rate reporting to the drainage ditch totals 11.6 l/s. This number has been corrected to allow for the difference in seepage area between the 2-D and 2-D axisymmetric simulations. The phreatic surface on the last day of the simulation is presented in Figure 10.4. The calculated seepage rate of 11.6 l/s and the final phreatic surface is once again within an acceptable margin compared to field observed values.

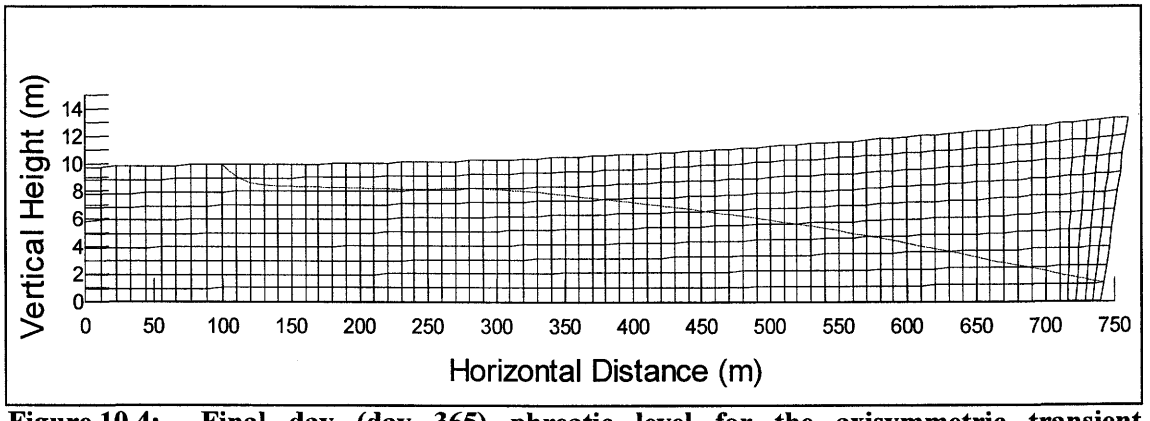

Figure 10.4: Final day (day 365) phreatic level for the axisymmetric transient simulation using the initial phreatic level defined by the phreatic line function.

The difference between the 2-D and the 2-D and the axisymmetric simulation is due to the varying flowpaths created by the "pie-effect". Close to the pool the where the fine tailings is located, the volume of material is considerably less than at the embankment where the coarser material is. In the 2-D run the volume of is constant along the length of the cross-section and thus due to continuity of flow the phreatic level is flatter for an axisymmetric simulation.

10.4.5 Circular 3-D Tailings Impoundment Evaluation

The 3rd Step in the evaluation process consists of calculating the seepage through an axisymmetric tailings impoundment using the generalized tailings impoundment cross-section as basis. The axisymmetric model will be analyzed using the 3-D modeling software SVFlux™ (SoilVision, 2001) and the following sections describe the models setup and results.

10.4.5.1 Model Setup

The setup of the axisymmetric 3-D model of the tailings impoundment is presented in the following sections with respect to the model geometry, boundary conditions as well as convergence criteria for the simulations.

10.4.5.1.1 Geometry

The purpose of this evaluation test was to set up a full 3-D model that would simulate the axisymmetric case presented in the previous section. In essence, the simulation model is a perfectly circular tailings impoundment, with beaches sloping according to a prescribed shape function as described by Equation 7.1, towards a pool in the center of the impoundment. The tailings impoundment would have a diameter of 1500 m, with the pool having a diameter of 200 m. Each of the 13 zones of the impoundment would consist of circular rings around the pool, each having a width of 50 m. Material properties for the 13 zones were identical to the 2-D and axisymmetric model simulations. For the purposes of assigning material properties, the area under the pool was assigned zone 13 material properties. Figures 10.5 and 10.6 presents a plan view and cross-section of the circular tailings impoundment, clearly showing the 13 zones.

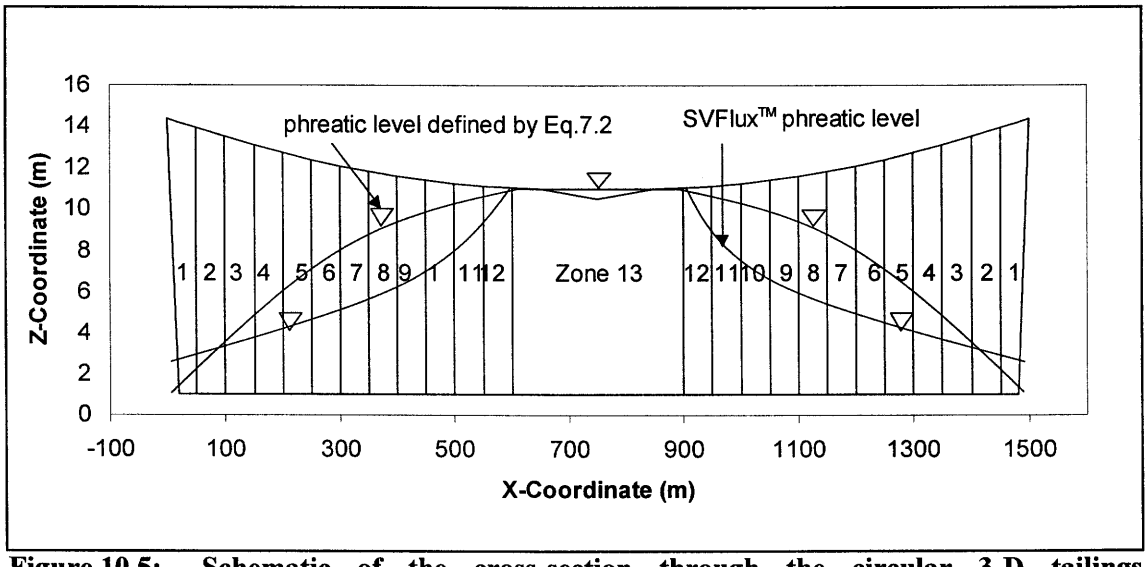

Figure 10.5: Schematic of the cross-section through the circular 3-D tailings impoundment model set up for analysis in SVFlux™ as an initial 3-D evaluation test.

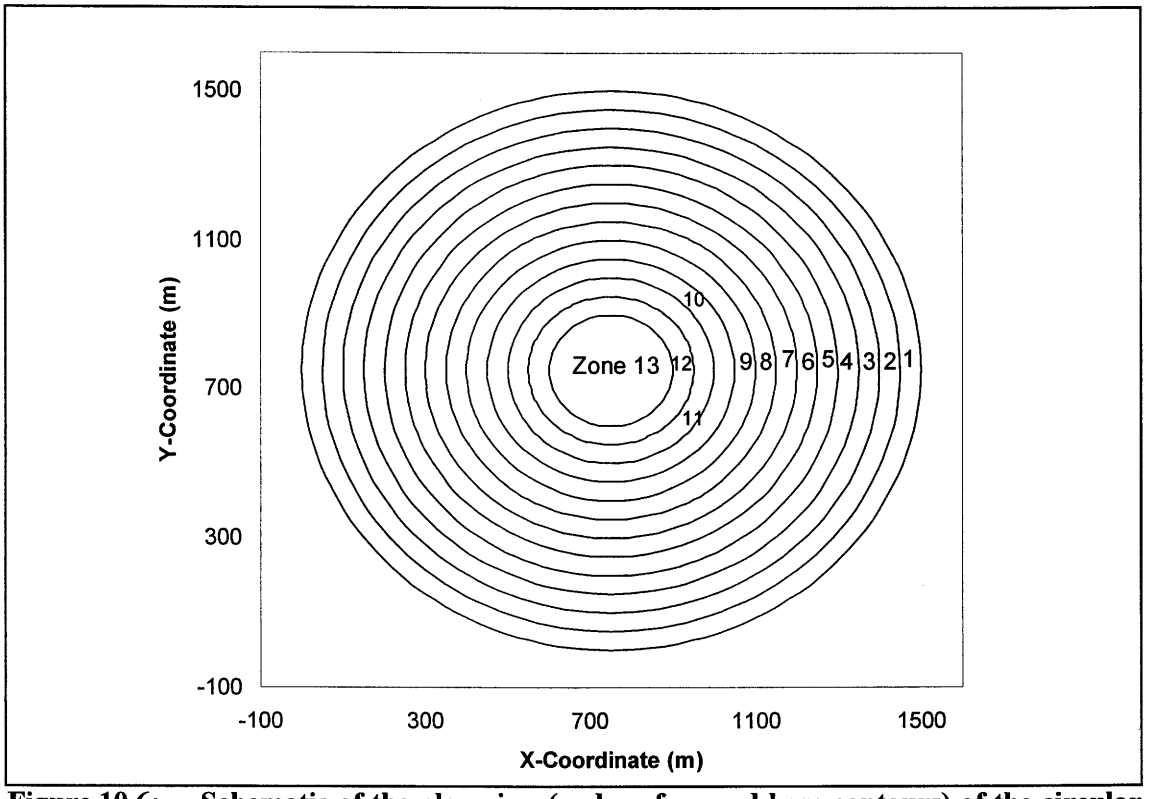

Figure 10.6: Schematic of the plan view (and surface and base contours) of the circular 3-D tailings impoundment model set up for analysis in SVFlux™.

SVFlux™ uses regions and surfaces to describe the model geometry. The circular tailings impoundment model was set up with 14 regions and three surfaces. The regions describe the different material zones to be used and the surfaces describe elevations where head boundary conditions apply. Region 1 through 13 represents each of the 13 different materials found in the problem. Region 14 contains the same material properties as region 13, but included the area under the pond. Surface 1 was the base of the problem (i.e. at elevation 1.0 m), surface 2 was the top surface of the problem (i.e. the tailings impoundment beach), and surface 3 was the pond. The base elevation of the problem was set at arbitrary at 1.0 m, and has no physical significance. The cross-section of the circular tailings impoundment in Figure 10.5 shows the upstream embankment wall slopes at the actual 35.5°, however the actual SVFlux™ model was simplified to use vertical (90°) slopes. This change has little effect on the final outcome of the model.

10.4.5.1.2 Convergence Criteria

The convergence criteria for SVFlux™ are set by selecting a maximum error. For all the simulations presented in this study the maximum error was set at 0.001. For the transient simulations the first time increment was set at 0.1 second. All other time increments were automatically set by SVFlux™, with the maximum time increment being 1 day.

10.4.5.1.3 Boundary Conditions

A SVFlux™ model must be set up such that boundary conditions can be defined on the surfaces, and on the links between surfaces. For this model, surface 1 was given a zero flux boundary (i.e. no flow). Surface 2 was assigned with the flux boundary functions developed in this study during the transient simulation only, as listed in Tables 10.1 and 10.2. For the steady state simulation this surface had no boundary conditions applied. The pond was considered to be at a constant level throughout the model simulation and was assigned a constant head of 11.0 m (10.0 m of actual head, just as in the 2-D and axisymmetric cases). The outside edges of the problem had a head boundary of 2.3 m (actual head of 1.3 m) assigned between surface 1 and 2, with the remainder of the wall having a zero flux boundary. This boundary was based upon the outcome of the 2-D SEEP/W modeling, since SVFlux™ does not have the ability to use review boundaries.

The initial phreatic level in the circular tailings impoundment, were defined by the phreatic line function as described in Chapter 7, and is schematically presented in Figure 10.5.

10.4.5.2 Steady State Simulation

Unless, the initial phreatic level required for a problem in SVFlux™ is manually input as a set of boundary conditions, the initial heads required for a transient simulation, must be obtained by first completing a steady state analysis. Since specifying the actual phreatic level as an initial head would have meant the inclusion of a number of additional surfaces, and as a result have increased the problem complexity significantly, it was decided to rather run a steady state problem to generate a head profile for input in the transient simulation. Since 13 material zones with exponentially varying hydraulic conductivity are being used the steady state phreatic surface will be depressed as illustrated in Figure 10.2. The steady state simulation was run with

no flux applied to the surface of the tailings impoundment. The overall seepage rate from the circular tailings dam at steady state was computed to be 2.46 l/s (corrected for a seepage zone of 5875 m).

10.4.5.3 Transient Simulation

The transient analysis was again run for 365 days and the calculated steady state piezometric heads was used as an initial head file. The overall average seepage rate from the tailings impoundment was computed to be 2.5 l/s (corrected for a seepage zone of 5875 m). This number can be compared to the seepage rate of 11.6 l/s calculated for the 2-D axisymmetric simulation, where the initial phreatic level was defined by the phreatic level function. The final phreatic surface location for the 2-D axisymmetric simulation illustrated in Figure 10.4 does not represent a steady state condition and the seepage rate is thus expected to be greater than for a steady state condition. The variances between these model simulation answers can be attributed to the variance in the initial phreatic levels, and although in magnitude the differences seem large, the actual relative order of magnitude is within reason. The results of the 2-D axisymmetric analysis and the 3-D circular simulations are thus within reasonable tolerances from each other.

10.4.6 Actual 3-D Kidston Tailings Impoundment Evaluation

The 4th step in the evaluation process involved a full 3-D model of the actual Kidston tailings impoundment geometry. The surface flux boundary function for this model is for a generic climatic year as described in Chapter 8. The sections below describe the details of this evaluation step.

10.4.6.1 Model Setup

The following sections describe the 3-D model setup for the actual Kidston tailings impoundment simulation. The dam geometry, boundary conditions and convergence criteria are discussed here.

10.4.6.1.1 Geometry

The next logical step in evaluation of the surface flux boundary functions was to develop a full 3-D model of the actual tailings impoundment. Figures 10.7 and 10.8 respectively show the initial base contours prior to the impoundment construction, and the final tailings impoundment surface contours. The final tailings impoundment surface contours are obtained from an actual aerial photography survey commissioned by Kidston Gold Mines in 1997. The original surface contours have been digitized using a base map used for original siting of the tailings impoundment (Gutteridge, Haskins and Davey, 1987).

The outline of the tailings impoundment on both figures demarcates the inside edge of the embankment wall (at elevation 559.0 mRL), or the line of intersection where the tailings meet Paddy's Knob. The coordinates indicated on the figures are based on a local mine coordinate system, and has no relevance to the modeling, except to denote scale. Contour intervals of 0.5 m are available for the final impoundment surface, but the 10 m contour intervals are the best resolution for Figure 10.7.

The mesh in SVFlux™ is generated by placing a node at every intersection between a surface and a region, as well as at every change in direction within a surface or region. Generating a mesh with the exact surface and base contours, as well as 13 material property zones as shown in Figure 10.9, would result in such a detailed mesh for which computing time to solve the problem would be too large for practical purposes. This meant that the actual tailings impoundment geometry had to be simplified to allow for a manageable mesh, without losing accuracy.

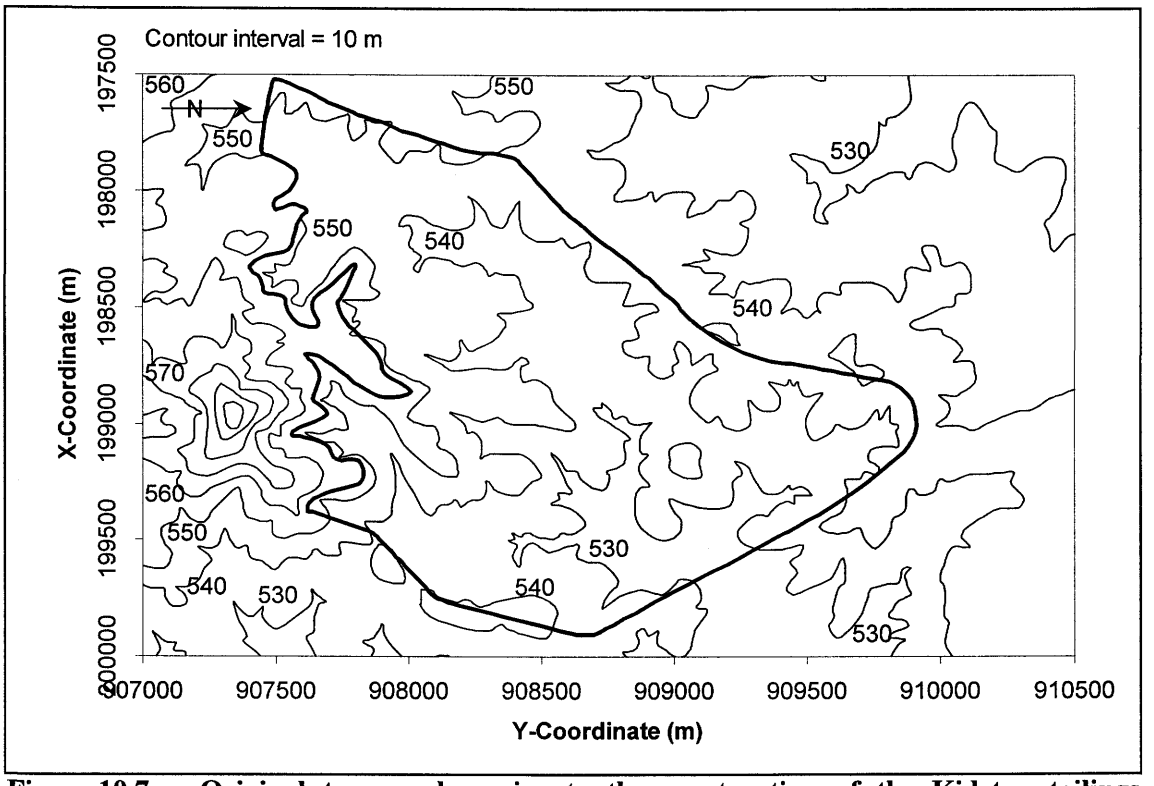

Figure 10.7: **Original topography prior to the construction of the Kidston tailings impoundment. The outline overlay demarcates where the impoundment has been constructed.**

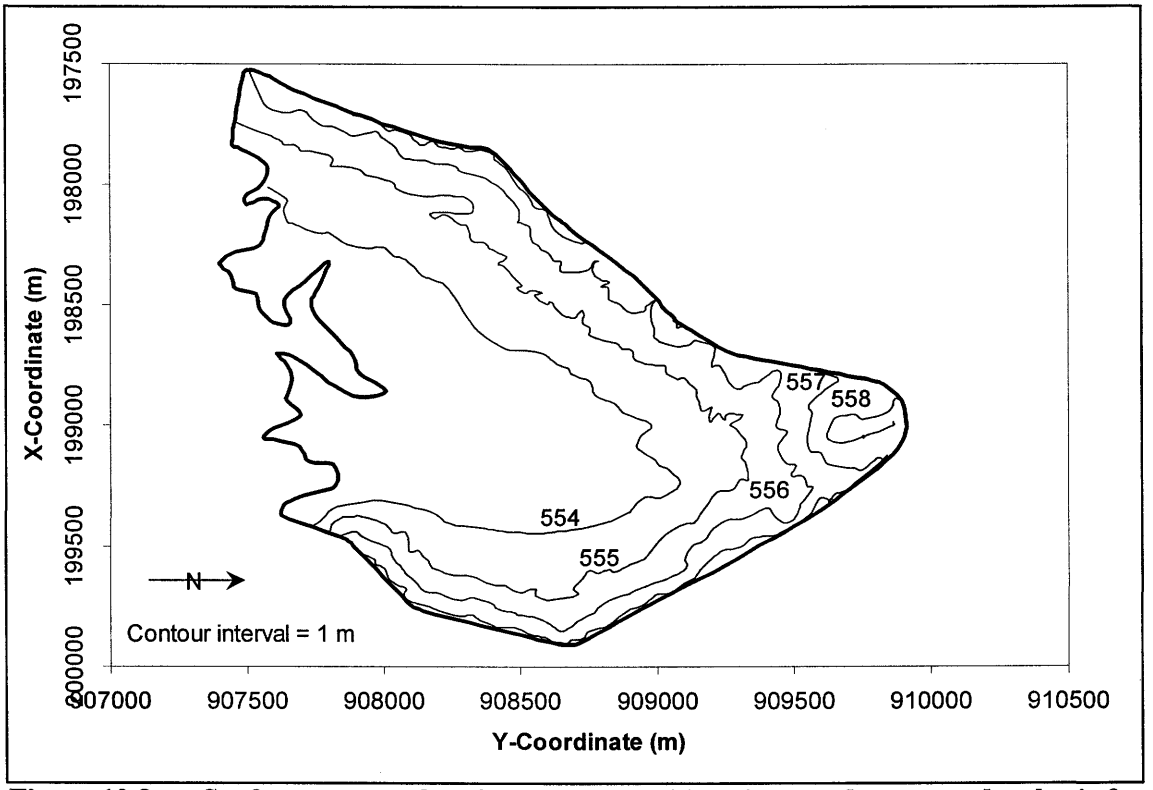

Figure 10.8: **Surface topography of the Kidston tailings impoundment, used as basis for developing a full 3-D numerical model of the impoundment.**

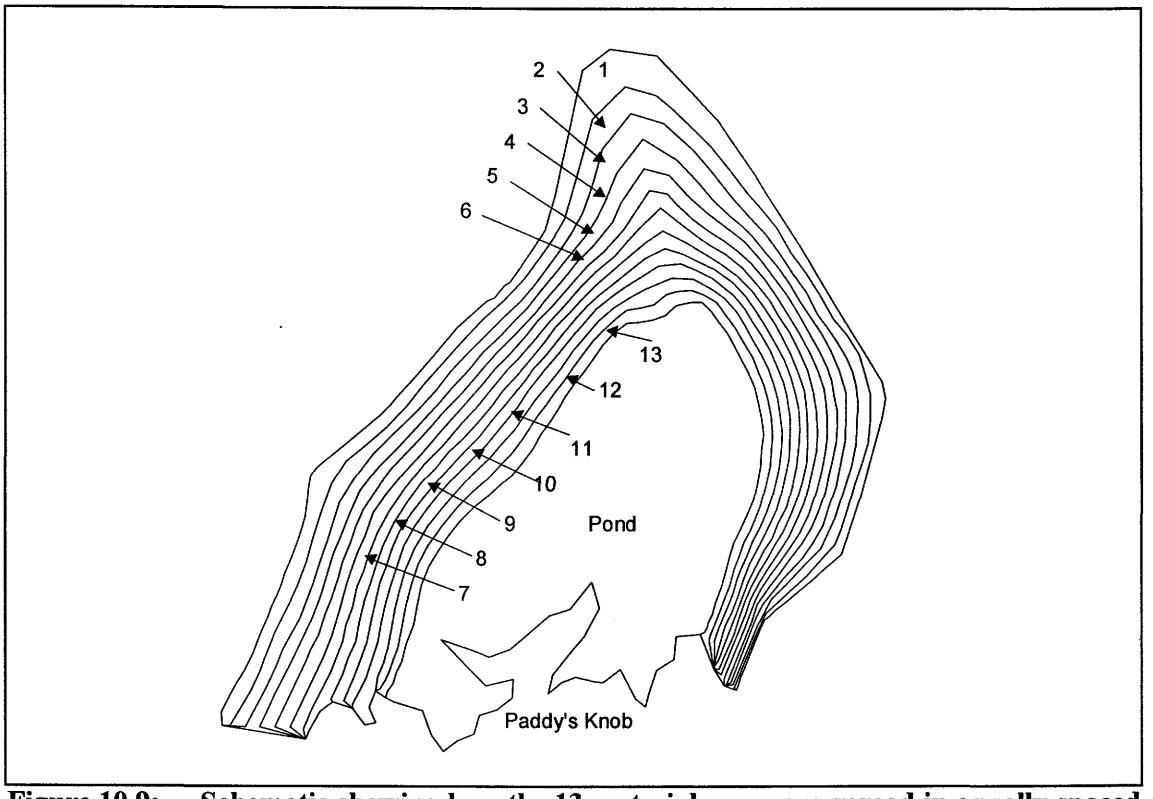

Figure 10.9: Schematic showing how the 13 material zones are spread in equally spaced rings around the pond on the Kidston tailings impoundment.

The simplified 3-D problem included three regions and two surfaces (the regions are illustrated in Figure 10.10). Region 1 was the outermost region and consisted of zones 1 through 5 lumped together. This region had the coarse tailings soil water characteristic curve assigned to it and the saturated hydraulic conductivity and unsaturated hydraulic conductivity curve of zone 5. Region 2 consisted of zones 6 through 13, had the intermediate tailings soil water characteristic curve assigned to it, and the zone 10 saturated hydraulic conductivity and unsaturated hydraulic conductivity curve was used. Region 4 comprised the area under the pond and had the material properties for zone 13 assigned to it. Surface 1 consists of the base level of the problem, i.e. the original ground surface and Surface 2 consist of the final tailings impoundment surface topography. The elevations at each of the 90 grid points were interpolated from the base and surface contours resulting in a mesh with 2889 nodes and 1368 cells. The 3-D model generated using this simplified grid was considered to be a good approximation of the actual conditions, since care was taken to select grid points at important physical intersections. Figure 10.11 shows a 3-D view of the final Kidston grid.

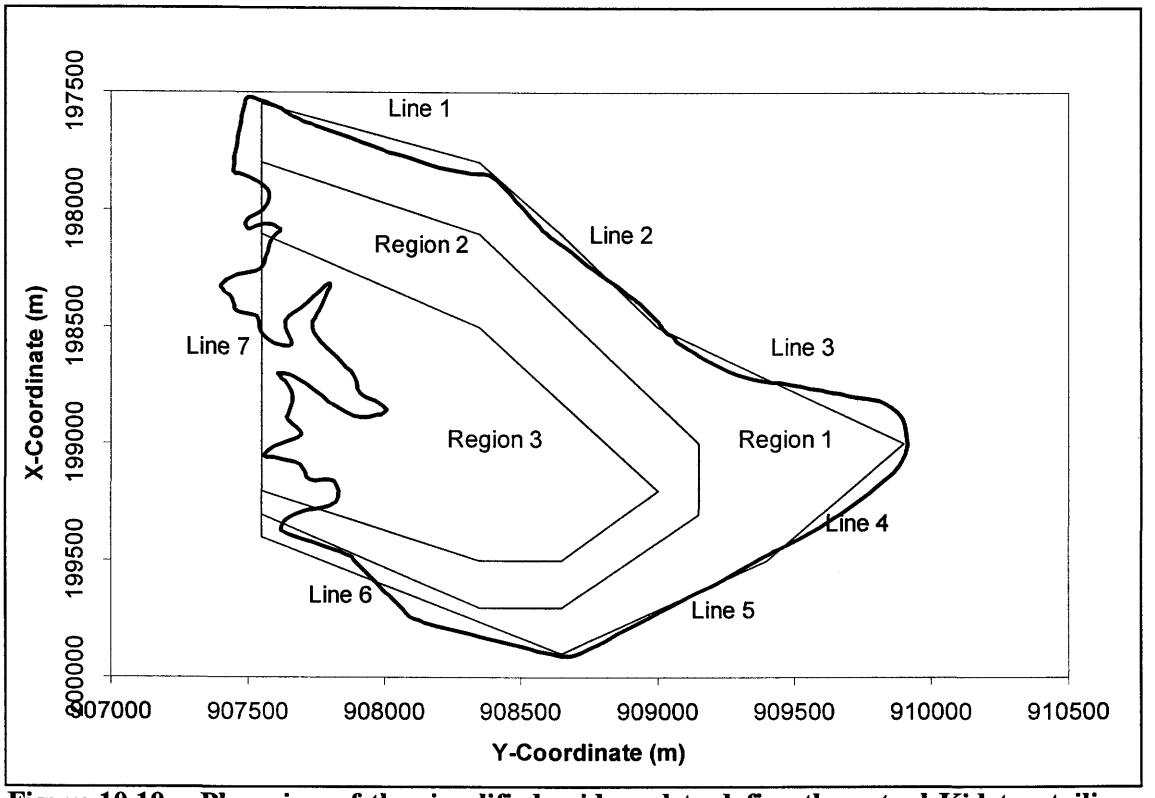

Figure 10.10: Plan view of the simplified grid used to define the actual Kidston tailings impoundment in SVFlux™.

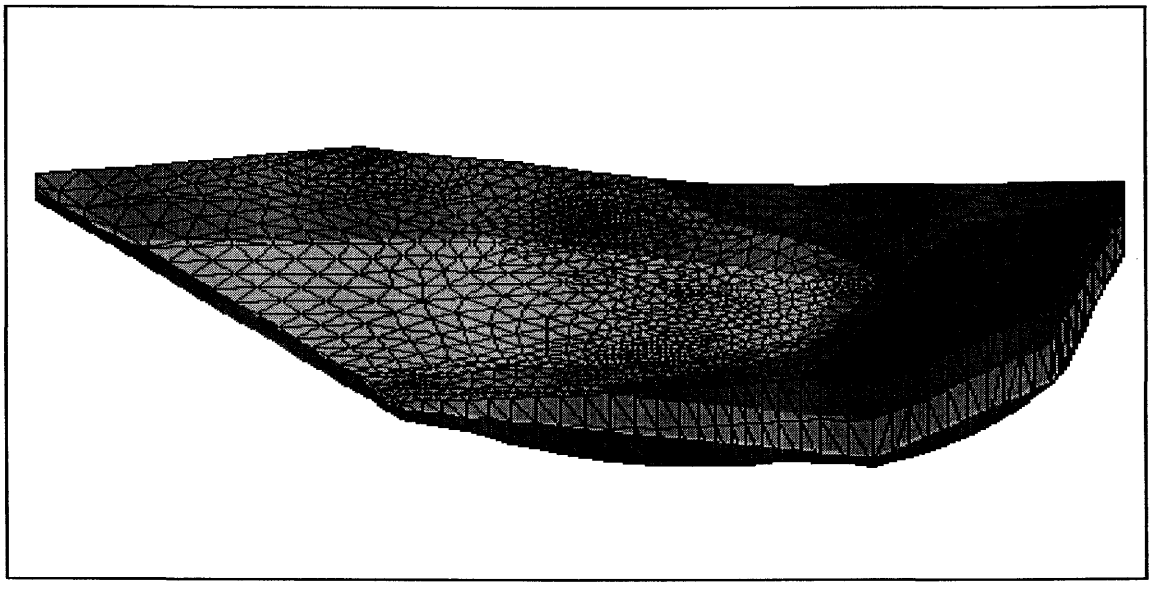

Figure 10.11: 3-D view of the mesh created for the Kidston tailings impoundment. The mesh represents the simplified grid.

The SVFlux™ model coordinate system was defined independent of the actual mine coordinate system. It does not affect the problem layout or dimensions in the x- and y-directions, however

to prevent confusion when discussing the boundary conditions it is important to note that the z-elevations have been reduced by 500 m, i.e. an elevation of 554 m on the contour plans would correspond to 54 m on the model.

10.4.6.1.2 Boundary Conditions

The boundary conditions for the transient and steady state simulations were identical, with the exception that for the steady state simulation there was no flux boundary condition applied to regions 1 and 2. Region 3 had a fixed boundary condition of 53.9 m, which represented the pond elevation. The pond elevation and the initial piezometric heads illustrated in Figure 10.12 were selected based on an analysis of the database of the piezometer reading data available for the site (these data is listed in Appendix F), and a most representative set of readings was selected to represent the phreatic level the tailings impoundment.

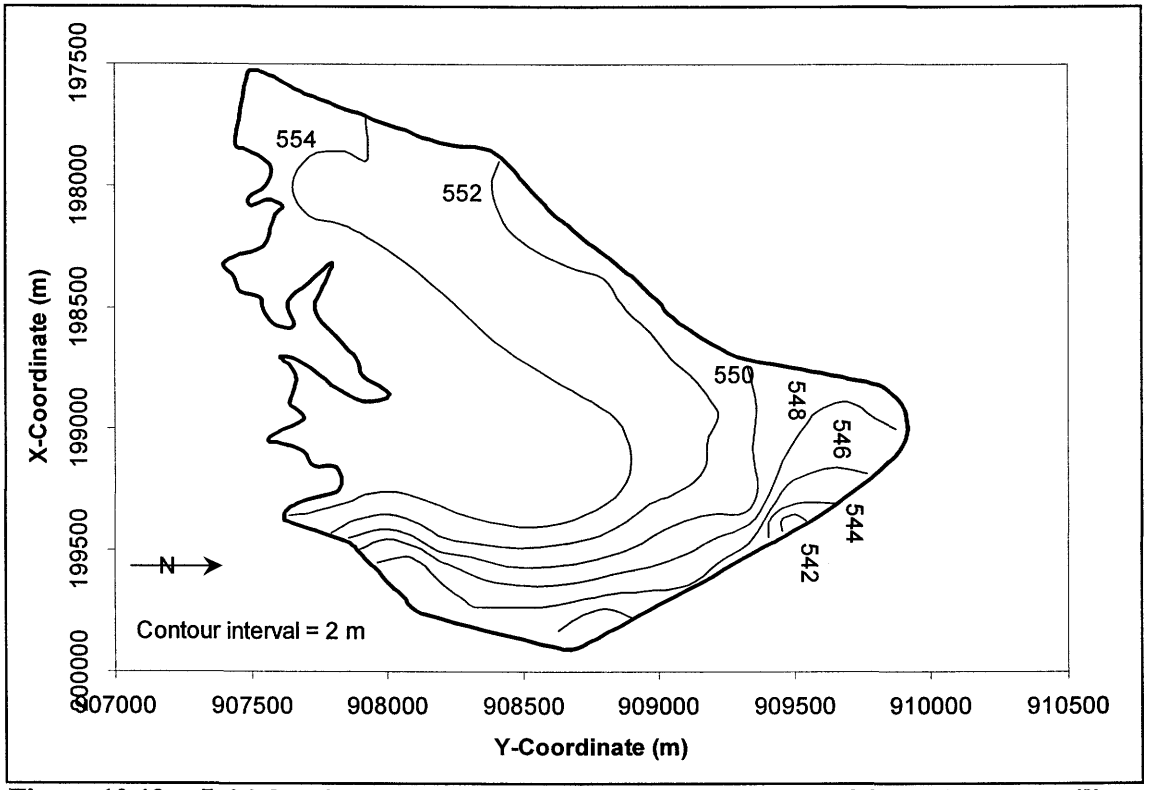

Figure 10.12: Initial piezometric head contours for the 3-D Kidston tailings impoundment simulating the generic climatic scenario.

Surface 1 (i.e. the original surface topography prior to the impoundment construction) had head boundary conditions applied to the outer boundary, which were calculated from the initial piezometric head contours illustrated in Figure 10.12. For each line segment that makes up the

outer boundary of Region 1 as depicted in Figure 10.10, an elevation of the water table at the start and end of the line was chosen from the initial piezometric head contour plot. A line or equation was then developed that would describe the sloping water table between the two points as a straight line. The equations for each line segment is given by the following general equation:

$$x = my + c \qquad [10.1]$$

Where x = x-coordinate (m),
y = y-coordinate (m),
m = slope of the function (-), and
c = intercept of the function (m).

The constants, m and c for each segment are listed in Table 10.3, with the segments starting in the southwest dam corner and moving around clockwise from gridpoint to gridpoint as illustrated in Figure 10.10.

Table 10.3: Constants for the equations that define the slope of the water table between the segments of the outer boundary of region 1, surface 1.

Segment	Slope, m (-)	Intercept, c (m)
1	-0.0090	121.85
2	-0.0027	67.07
3	-0.0027	67.07
4	-0.0120	-70.80
5	-0.0022	70.00
6	-0.0031	77.69
7	-0.0024	71.83

The remainder of surface 1 had a zero flux boundary (indicating zero foundation seepage), and the vertical link between surface 1 and 2 had a zero flux boundary, effectively forcing the seepage out at the toe of the embankment based on the initial phreatic head conditions.

10.4.6.2 Steady State Simulation

The steady state simulation was performed in order to obtain an initial head profile for the transient simulation. The model setup is identical to the transient state simulation, except for the fact that surface 2 (i.e. the final tailings impoundment topography) has no flux boundary

condition applied to it. The overall annual seepage rate from the tailings impoundment based on the steady state conditions is 4.4 l/s. The steady state phreatic level through the tailings impoundment is not as mounded as suggested by the initial piezometric head contours shown in Figure 10.12. This shape of the phreatic level is governed by the material properties. In order to model a case with a more representative water table, the material properties would have to be altered, which is not within the scope of this evaluation exercise.

10.4.6.3 Transient Simulation

The flux boundary functions listed in Tables 10.1 and 10.2 were to be used as flux boundary conditions on surface 1, however due to the fact that only two regions are being used in the simplified model to apply flux boundary conditions to, the fluxes must be combined. Region 1 contains the sum of the net infiltration fluxes for zones 1 through 5, and region 2 contains the sum total of the remainder of the net infiltration fluxes. This results in the same net flux being applied or removed from the tailings impoundment surface. Using the calculated steady state initial piezometric head profile, the overall annual seepage from the Kidston tailings impoundment was calculated to be equal to 4.3 l/s. This value is less than the steady state solution, and this difference can be ascribed to the fact that the net infiltration flux functions are net negative, which implies that water is removed from the profile. This would result in a change in the gradient of the phreatic level, which in turn would reduce the amount of seepage.

10.5 Discussion of the Generic Evaluation Tests

The 2-D, axisymmetric and 3-D modeling described in the previous sections were conducted in order to evaluate whether the net infiltration flux boundary functions developed for use as input in multidimensional seepage modeling to compensate for the lack of surface flux boundary calculations. The simulations were set up in the same way that the conceptual model for the Kidston tailings impoundment was developed, including all material properties. In general this is not the way conventional multidimensional seepage modeling is conducted, which usually involves a great deal of sensitivity analysis and calibration. As mentioned at the outset, the modeling described here is not intended to be detailed and to a level suitable for predictive purposes, but is rather intended to determine if the use of the flux boundary functions give rise to seepage numbers that are similar to field observations. The results of the measured seepage rates from the Kidston tailings impoundment, as well as al the modeled numbers have been

listed in Table 10.4. A seepage number modeled by AGE Consultants (AGE, 2001) using MODFLOW is also included. AGE used preliminary flux boundary functions provided by the author to calibrate a 3-D model of the tailings impoundment, and the reported seepage rates is the result of that modeling exercise.

Table 10.4: Summarized results of all measured and modeled seepage rates from the Kidston tailings impoundment. All the modeled results are for the transient case where the flux boundary function is applied to the tailings impoundment surface as a flux boundary condition.

Seepage value origin	Range (l/s)	Average (l/s)
General tailings impoundment water balance calculation (Chapter 5)	7.6 – 9.9	8.7
Measured data (1998/1999), includes runoff (Chapter 5)	3.2 – 18.3	9.7
Measured data (2000/2001), includes runoff (Chapter 5)	0.4 – 16.1	10.8
AGE (2001)	5.6 – 7.3	6.3
2-D SEEP/W model (actual piezometric head)	-	19.1
2-D axisymmetric SEEP/W model (actual piezometric head)	-	11.6
Circular 3-D SVFlux™ model (steady state piezometric head)	-	2.5
Actual 3-D tailings impoundment SVFlux™ model (actual piezometric head)	-	4.3

Throughout the evaluation modeling, mention has been made that the piezometric head profiles are less than the measured values. The physical reasons for this is clear, as well as the method required to overcome this problem. This problem was not rectified since the evaluation modeling program was not intended to be used as calibration. It would appear that both the 2-D and axisymmetric SEEP/W models resulted in seepage rates which are in line with the record of measured data, which suggests that in 2-D the use of the flux functions are well suited.

The 3-D circular tailings impoundment model was set up in order to gain confidence in the suitability of SVFlux™, since the results of this model should be approximately the same as the axisymmetric SEEP/W solution. Comparison of the circular dam 3-D SVFlux™ solution with the axisymmetric SEEP/W solution using similar initial piezometric heads shows that both models provide similar solutions. The absolute values do not however verify the suitability of the flux boundary functions, as the initial piezometric heads vary significantly from the known levels.

Finally a full 3-D model was set up to determine the seepage rate from the actual tailings impoundment. Again the actual steady state piezometric heads are flatter than observed in the field. However the calculated seepage rate for the impoundment as a whole remains within very

close range with the records of measured data. The evaluation exercise described here is for the generic flux functions calculated using a generic mean climatic year, and is not specific to any period of time.

10.6 Field Evaluation for the Flux Boundary Function

The final step in evaluating that the use of the spatial flux boundary functions are acceptable, was to produce a full 3-D model of the Kidston tailings impoundment, and to calculate the seepage rate from it for a specific period of time for which detailed measured climatic and seepage data exist. A specific flux boundary function corresponding to this period would be developed, and the calculated seepage rates can be compared to actual measured data. The period for which this evaluation test was done was between 1 December 2000 and 31 March 2001 as described in Chapter 5.

10.6.1 SoilCover Modeling to Develop a Flux Boundary Function

The first step in developing a net infiltration flux boundary function for the evaluation period was to perform the 13 individual SoilCover simulations that define the generalized tailings impoundment cross-section as defined in Chapter 7. The SoilCover models were run exactly as described for the vegetated case profiles in Chapter 8, with the exception that the leaf area index were for "Poor" grass as opposed to "Excellent" grass. An overall site water balance was completed for this period according to the methodology described in Chapter 5, which resulted in a runoff number from the tailings dam of 58%. The composite SoilCover analysis of the generalized tailings impoundment cross-section resulted in an overall runoff of 55%, which was considered to be excellent match. The data for these SoilCover runs are presented in Appendix M.

With the SoilCover modeling complete, the flux boundary functions could be calculated, as documented in Appendix N. The resultant daily net infiltration fluxes required for input in the 3-D numerical model is listed in Tables 10.5 and 10.6. From these flux boundary functions it can be seen that for the months of December and February the overall net infiltration to the profile is positive, reflecting the periods of high precipitation. Overall the net infiltration for the entire 4-month period is however still negative, suggesting that the overall model should reflect a lowering of the phreatic surface.

Table 10.5: Daily net infiltration fluxes, q (based on monthly totals) for zones 1-7 used in the actual evaluation data set (December 2000 to March 2001).

Month	Julian Day		Daily net infiltration flux, q (mm/d)						
	Start	End	1	2	3	4	5	6	7
December	1	31	0.266	0.144	0.054	0.032	0.117	0.117	0.028
January	32	62	-0.012	-0.032	-0.042	-0.030	-0.074	-0.077	-0.035
February	63	90	0.098	0.064	0.048	0.039	0.025	0.032	0.029
March	91	121	-0.045	-0.036	-0.023	-0.017	-0.038	-0.046	-0.023

Table 10.6: Daily net infiltration fluxes, q (based on monthly totals) for zones 8-13 used in the actual evaluation data set (December 2000 to March 2001).

Month	Julian Day		Daily net infiltration flux, q (mm/d)					
	Start	End	8	9	10	11	12	13
December	1	31	0.056	0.050	-0.013	-0.123	-0.218	-0.308
January	32	62	-0.060	-0.115	-0.311	-0.484	-0.492	-0.614
February	63	90	0.045	0.036	-0.070	-0.176	-0.224	-0.331
March	91	121	-0.033	-0.056	-0.201	-0.346	-0.360	-0.422

10.6.2 Full 3-D Evaluation

The sections that follow describe the setup and results of the full 3-D evaluation model for the Kidston tailings impoundment during the period 1 December 2000 to 31 March 2001.

10.6.2.1 Model Setup

The 3-D model setup is described in the following subsections with respect to the model geometry and boundary conditions.

10.6.2.1.1 Geometry

The 3-D model required for the 4-month evaluation data set is similar to the model for the generic data set. It was however decided to refine the regions to include a specific region for each of the three tailings types (i.e. coarse, intermediate and fine) that were not covered by the pond. The model thus had 4 regions and 2 surfaces. The revised grid illustrating the 4 regions is presented in Figure 10.13 had 1326 elements and 2811nodes.

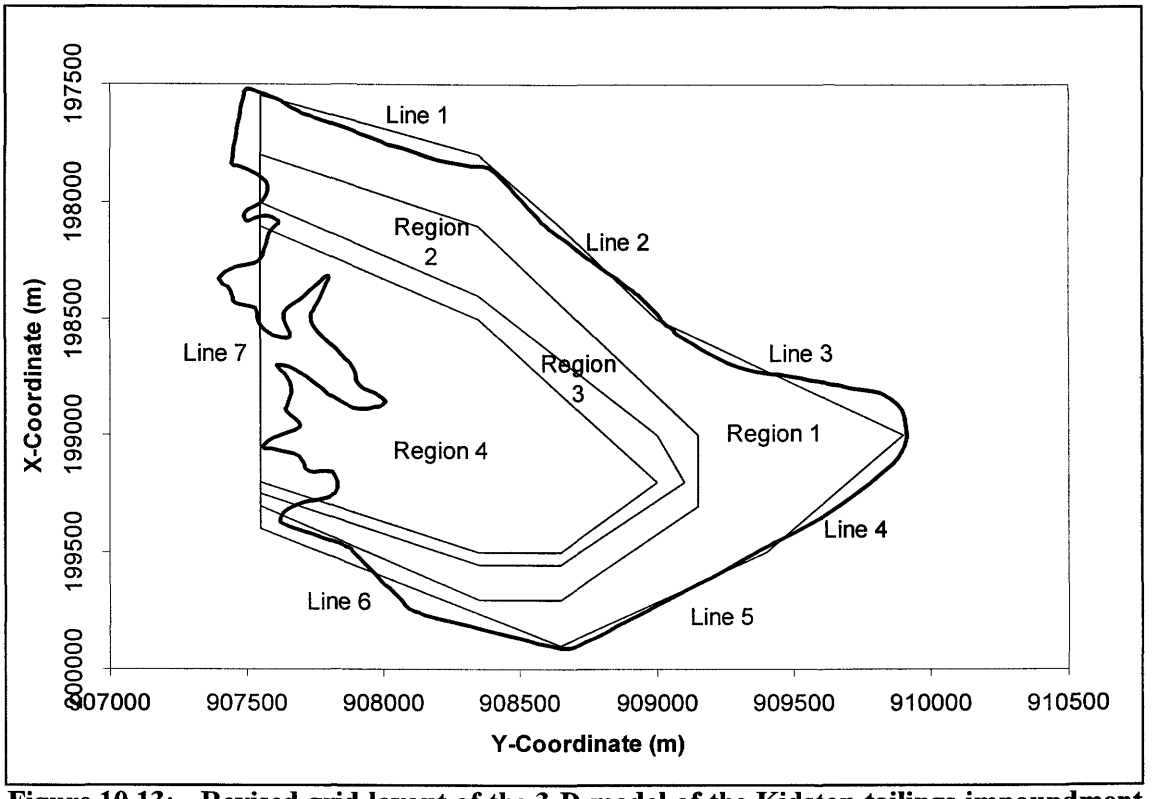

Figure 10.13: Revised grid layout of the 3-D model of the Kidston tailings impoundment for the final evaluation test.

Region 1 contains coarse tailings and the unsaturated hydraulic conductivity function assigned to the region is that of zone 5. Region 2 is the intermediate tailings, with the unsaturated hydraulic conductivity function of zone 10. Finally, region 3 consists of fine tailings and the unsaturated hydraulic conductivity function is that of zone 13. Region 4 consists of the pond, and the tailings beneath the pond comprise of the same material properties as region 3.

The model contained two surfaces with surface 1 being the original ground topography prior to the construction of the tailings impoundment, and surface 2 the final tailings impoundment surface topography (i.e. surface 1 is the base of the model and surface 2 is the top).

10.6.2.1.2 Boundary Conditions

The boundary conditions are applied in a similar fashion as before, with surface 2 having a different flux boundary function for each region. The sum of the net infiltration fluxes for zone 1 to 5 is applied to Region 1. Region 2 corresponds to the sum of the net infiltration fluxes for zone 6 to 10, and the sum of the net infiltration fluxes for zone 11 to 13 is applied to Region 3.

The initial piezometric head measured on 1 December 2000, was used as the head boundary condition for the outer boundary of surface 1, as before, by using straight-line functions between segments as illustrated in Figure 10.13. A contour plot of these piezometric heads is presented in Figure 10.14, and Table 10.7 contains the constants for these functions as described by Equation 10.1.

Table 10.7: Constants for the equations that define the slope of the water table between the segments of the outer boundary of region 1, surface 1.

Segment	Slope, m (-)	Intercept, c (m)
1	-0.0109	136.36
2	-0.0027	65.07
3	0.0120	-72.80
4	-0.0033	79.00
5	-0.0029	74.71
6	-0.0167	194.17
7	0.0013	44.56

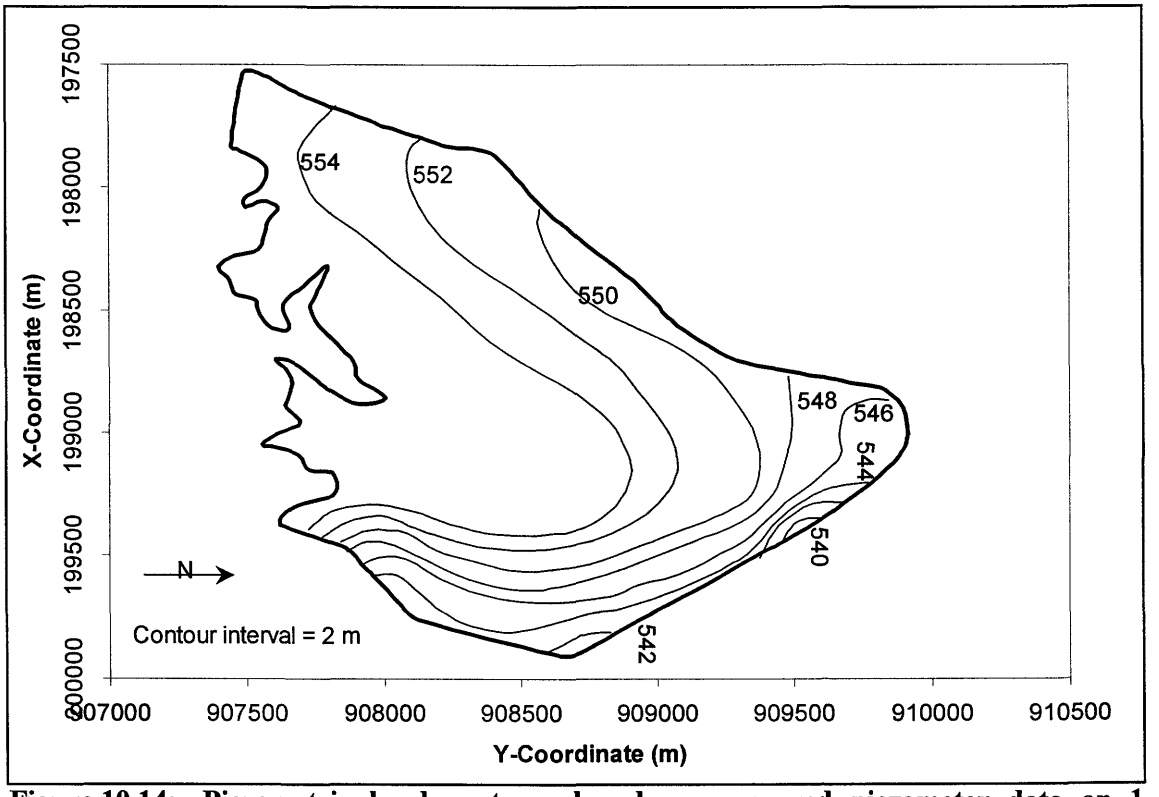

Figure 10.14: Piezometric head contours based on measured piezometer data on 1 December 2000.

The head boundary condition on region 4 represented the rise in the tailings pond over the 4-month period as described in Chapter 5, from 553.35 mRL to 554.40 mRL. This head boundary condition was defined using the following function:

$$H_{pond} = -7.00 \times 10^{-5} \cdot t^2 + 1.67 \times 10^{-2} \cdot t + 553.347 \qquad [10.2]$$

Where H_{pond} = pond level elevation (m), and
t = time period (d).

10.6.2.2 Steady State Simulation

Using the boundary conditions as described in the previous section and running the problem for steady state conditions results in an overall seepage rate from the tailings impoundment of 7.73 l/s. This seepage rate is based on the measured piezometric levels alone as surface 1 has no flux boundaries assigned to it.

10.6.2.3 Transient Simulation

The transient simulation is done using the calculated flux boundary functions as a surface flux boundary condition on surface 1. The overall seepage rate from the tailings impoundment during the 121 day transient simulation was computed to be 7.60 l/s, which is consistent with the fact that the net infiltration fluxes are net negative over the period of the run. Since more water is being removed form the profile than is being introduced, the overall seepage rate is being reduced. It is evident from these results that the principal driving force for the seepage is in fact the pond, and the impact of the surface flux boundary functions are small.

10.7 Conclusions

In section 10.5 a discussion was given to explain how the evaluation tests for the generic data set flux boundary functions performed. The conclusion was that the flux boundary functions are performing as expected. The final test was to use an actual period for which detailed measured data from the site was available, and use the calculated spatial flux boundary functions as input to the 3-D model in an attempt to calculate what the seepage from the tailings impoundment would be. To this effect a period of 4-months between December 2000 and March 2001 was

selected. Over this period detailed seepage measurements from the site was taken as described in Chapter 5, and it was calculated that an overall seepage rate of 10.8 l/s (ranging between 0.4 and 16.1 l/s) existed for this period. This seepage rate included some surface runoff that entered the seepage drains in areas between the outside embankment slope and the catchment drains. It is estimated that this runoff contributes towards 10-15% of the measured seepage rate. Alternately there are some seepage regions where seepage could not be measured, and it could be argued that between 5-10% of the actual seepage flow has not been measured. Due to these uncertainties, which are practically impossible to eliminate is could be assumed that the measured seepage rate of 10.8 l/s is probably a good estimate of the overall average seepage rate, but it could vary between 9.2 and 11.9 l/s.

The overall seepage rate of 7.6 l/s calculated by the 3-D model is considered at first glance to be a low estimate of the seepage rate. However, looking at the profiles of the head distributions through a cross section of the tailings impoundment we see that the modeled results show a depressed phreatic level, which is consistent with the exponentially varying hydraulic conductivity's between the pool and the embankment (see discussion of this earlier in chapter). Although it was not the intention of this evaluation modeling program to create a calibrated model, it can be said with confidence that if a calibration exercise were completed, the calculated and measured seepage rates would be an excellent match.

The tests performed and documented in this chapter thus supports the suggestion that the spatial infiltration fluxes do in fact provide an excellent basis for providing accurate surface flux boundaries for multidimensional seepage modeling. The calculated seepage flux boundary functions were used as a surface flux boundary input into a 3-D numerical model, and the modeled seepage rate was found to be an excellent match with physically measured seepage rates.

10.8 References

Australasian Groundwater & Environmental Consultants Pty Ltd. (2001). Kidston Tailings Dam Rehabilitation Numerical Model and Water Balance. Consultants report prepared for Kidston Gold Mines Limited, Project No. G1036/A. Edited by I.P. Callow & E.H. Briese, January, 26 pp.

Chiang W.H., Kinzelbach, W. (1996). Processing MODFLOW for WINDOWS.

Engineering Computer Graphics Laboratory (1998). The Department of Defense: Groundwater Modeling System, GMS v2.1. Brigham Young University, Provo, Utah, U.S.A.

GEO-SLOPE International Ltd. (1991). SEEP/W for finite element seepage analysis, Version 4 for Windows 95 and NT, Getting Started Guide, Calgary, Alberta, Canada.

GEO-SLOPE International Ltd. (2000). GeoStudio Seep3D for 3D finite element seepage analysis, Version 1.

Gutteridge, Haskins and Davey Pty Ltd. (1987). Kidston Project; Interim Report on Tailings Disposal. Consultants Report to Kidston Gold Mines Limited. Brisbane, Queensland, Australia. July, 9 pages.

Lin, H.J., Richards, D.R., Talbot, C.A., Yeh, G., Cheng, J., Cheng, H., Jones, N.L. (1997). FEMWATER: A Three-Dimensional Finite Element Computer Model for Simulating Density-Dependent Flow and Transport in Variably Saturated Media. Technical Report CHL-97-12, July.

McDonald, M.C., Harbaugh, A.W. (1988). MODFLOW, a Modular Three-Dimensional Finite Difference Groundwater Flow Model. U.S. Geological Survey, Open-File Report 91-536, Denver.

PDE Solutions Inc. (1999). FlexPDE Manual Version 2.11. Antioch, California, USA.

Pentland, J.S. (2000). Use of a General Partial Differential Equation Solver for Solution of Heat and Mass Transfer Problems in Soils. M.Sc. thesis, Department of Civil Engineering, University of Saskatchewan, Saskatoon, Saskatchewan, Canada, 248 pp.

Rykaart, E.M. (2000). Results of SoilCover Modeling for Kidston Tailings Dam without Vegetation – Preliminary Report. Report to Kidston Gold Mines Limited, Unsaturated Soils Group, University of Saskatchewan, Department of Civil Engineering, Saskatoon, Saskatchewan, Canada. October, 10 pp.

SoilCover. (1997). SoilCover User's Manual. Unsaturated Soils Group, Department of Civil Engineering, University of Saskatchewan, Saskatoon, Saskatchewan, Canada.

SoilVision Systems (2001). SV Flux 3D: Saturated/Unsaturated Automated 3D Seepage Modeling. SoilVision Systems Ltd.

This page was intentionally left blank.

CHAPTER 11

Summary, Conclusions and Recommendations

11.1 Introduction

This chapter summarizes the findings of the thesis in the form of a set of conclusions that can be drawn from the study. These conclusions are subdivided into a number of sections that are consistent with the layout of the thesis. The second portion of this chapter comprises of a list of future research ideas that could be done to expand and enhance the concept of a spatial flux boundary function and its application.

11.2 Summary and Conclusions

The conclusions of the study are listed in terms of the various components covered in each chapter of the thesis. A brief summary of the components of each chapter is provided and followed by a set of concise conclusions for the relevant section of the thesis. Finally, this section of the thesis is concluded with the overall conclusion for the entire study.

11.2.1 Project Goals and Spatial Flux Boundary Hypothesis

1. In Chapter 1 a spatial flux boundary hypothesis was presented that stated that surface fluxes would vary spatially along a typical tailings impoundment (low-tonnage impoundment in an arid-climate) cross-section that has a developed phreatic surface. The hypothesis states that evaporation will be at a minimum in the area farthest from the tailings impoundment pond, and will increase to a maximum value close to the pond. Inversely the infiltration should be a maximum far from the pond and decrease to a minimum close to the pond. This spatial flux boundary hypothesis is applicable to tailings impoundment closure conditions only. The shape of the spatial flux boundary functions (distributions) was not known, and the work presented in this thesis was intended to investigate the hypothesis.

2. The hypothesis was further expanded to suggest that these spatial flux boundary functions would be a method to determine more rigorous surface fluxes for use in multidimensional saturated/unsaturated flow seepage analysis models. This would effectively bridge the current gap in technology between soil/atmosphere coupled surface flux boundary models and conventional numerical modeling for multidimensional saturated/unsaturated seepage modeling.
3. The final goal of the project was to provide further insight regarding the long-term closure water balance of the tailings impoundment with respect to the impact of the vadose zone surface flux boundary conditions for a number of different cases (i.e. vegetated or non-vegetated tailings using wet, mean or dry climatic data).

11.2.2 Theoretical Framework for Surface Flux Boundary Condition Calculations

1. The basic theory describing the surface flux boundary components (i.e. precipitation, evaporation, transpiration, runoff and infiltration) was documented in Chapter 2 together with the rigorous coupled soil/atmosphere formulation to calculate these fluxes.
2. The limitations of the current numerical techniques are outlined and it is concluded that there is a need to develop a methodology to calculate rigorous flux boundary calculation methods in multi-dimensions.

Conclusion:

1. Current technology allows for rigorous flux boundary calculations to be performed in a single dimension using coupled soil/atmosphere heat and mass flow theory. Multidimensional saturated/unsaturated flow seepage analysis modeling that is most often used to simulate tailings impoundment closure water balances cannot calculate surface flux boundary conditions. There is thus a need to bridge the gap between these two modeling systems by developing a methodology to calculate spatial flux boundary conditions (i.e. multidimensional flux boundary conditions)

11.2.3 Physical and Hydraulic Characterization of Kidston Tailings Impoundment

1. Chapter 3 provided a detailed description of the Kidston Gold Mine with respect to the mining history, general climatic setting, general geology as well as the mining processes relevant to the tailings.
2. A detailed description of the tailings impoundment complex was also provided, including construction, deposition, geochemistry and rehabilitation efforts performed.
3. A detailed laboratory physical and hydraulic tailings characterization program was carried out as part of this study, and included grain size distribution tests, specific gravity tests, Atterberg limits, shrinkage tests, consolidation tests, falling head permeability tests and soil water characteristic curve testing.
4. Additional hydraulic field-testing was completed, which included double-ring infiltrometer and Guelph permeameter testing.
5. An extensive database of physical and hydraulic tailings properties was developed using all available testing performed for the Kidston tailings by all previous researchers and consultants during the life of the mine. This extensive database of information allowed for a detailed understanding of the properties.
6. The phreatic level in the tailings impoundment was completely characterized by installing 25 shallow standpipe piezometers at seven section lines on the tailings impoundment for this study. An additional 10 deep standpipe piezometers was installed by the Kidston Gold Mine and together with established standpipe piezometers on the dam, details of the phreatic regime were available since 1997.
7. The detailed physical and hydraulic testing database of the tailings impoundment made it possible to understand the system sufficiently to make defensible assumptions required for the modeling phase of the study.

Conclusion:

1. *A vital component in understanding the physical environment for which a numerical model must be developed is understanding the material properties to such an extent that confidant decisions can be made as to which properties to use where. The testing program at Kidston proved that extensive laboratory and in-situ testing of material properties are invaluable.*

11.2.4 Tailings Impoundment Closure Water Balance

1. A crucial aspect of the thesis was understanding the tailings impoundment closure water balance as a complete integrated system. To this effect, detailed seepage measurement stations were installed around the tailings impoundment perimeter to measure actual seepage rates. This monitoring included continuous tailings pond and reclaim dam water levels.
2. Detailed daily (and hourly) climatic data were obtained for the site that allowed for a detailed analysis of the climatic water balance.
3. Detailed studies were done to determine the potential evaporation rate from the tailings impoundment pond. These studies included evaporation correlation experiments using six mini-evaporation pans.
4. A detailed transient closure water balance was developed for the tailings impoundment using the available data, and from that the overall average runoff volume into the pond was estimated. This calculation suggests that the average the surface runoff from the Kidston tailings impoundment is 42%. This number does vary according to what the actual annual precipitation is, but an overall average of 42% seems reasonable for the five years of data available. The water balance calculation does not of course produce an exact result, as many assumptions had to be made along the way. It is concluded however that all assumptions were based on sound engineering judgement, and can thus be justified. This runoff number was subsequently used as a guideline towards finding optimal solutions when the numerical modeling phase of this project is undertaken.

Conclusion:

1. *It was possible to set up a detailed primary transient closure water balance for the Kidston tailings impoundment and calculate what the runoff into the pond would be over the long-term. This was done by critical analysis of all available data, as well as making specific crucial site measurements. The runoff entering the tailings pond was calculated to be 42% on average over the 5-year period for which the transient closure water balance calculations were performed.*

11.2.5 Conceptual Model

1. SoilCover was selected as the numerical model to perform the surface flux boundary calculations, as it is the only code to make use of the modified Penman formulation to calculate evaporation, and was considered the most appropriate method available. SoilCover is however a 1-D model and cannot solve complex 2-D or 3-D problems as was required for this study.
2. A conceptual model was subsequently developed that allowed SoilCover to be used to calculate spatial surface flux boundary conditions through a generalized 2-D cross-section of the Kidston tailings impoundment. The resultant spatial flux boundary function was subsequently used as a surface flux boundary input in multidimensional saturated/unsaturated seepage modeling codes.
3. The conceptual model was based on the principle of a developing a generalized tailings impoundment cross-section (for the Kidston tailings impoundments that is a low-tonnage impoundment in an arid climate). The top boundary of the conceptual model consisted of the tailings impoundment beach, defined by a beach shape function that was determined by the hydraulic deposition technique used to place the tailings. The lower boundary of the conceptual model consists of the phreatic level, and was defined by the phreatic level function. These two functions were combined delineating the vadoze zone of a generalized tailings impoundment cross-section at the Kidston Gold Mine, and since the section was non-dimensionalized it is considered representative of any location on the Kidston tailings impoundment.
4. The next step was the development of a technique to define material properties for the conceptual model in order to perform the SoilCover modeling. The surface saturated hydraulic conductivity was defined using a function that reflected particle segregation that occurs during hydraulic tailings deposition and was calibrated using the extensive database for infiltration testing. Three representative tailings types were selected; coarse, intermediate and fine, again based on the extensive testing database developed for the study. The intention was that as one moves from the embankment end of the typical tailings impoundment towards the pool the tailings would change from coarse to fine, again due to natural particle segregation. The transition of these zones was determined by the SoilCover modeling and the optimal distribution was a ratio of 5:5:3 for the three types respectively from the

embankment to the pool. Finally, an assumption was made to use homogeneous vertical profiles, and calibration modeling supported this.

5. Since SoilCover is one-dimensional it cannot solve the conceptual model, since it has a spatially varying phreatic level. A procedure was developed that involved dividing the generalized cross-section into a number of equal zones, and by performing a sequence of SoilCover simulations and integrating the results a single flux boundary function for the entire tailings impoundment cross-section could be calculated.
6. The test for checking whether the flux boundary function calculation of the composite generalized tailings impoundment cross-section was correct was by comparing the overall runoff from the cross-section with the estimated runoff of 42% calculated as part of the tailings impoundment closure water balance. If the SoilCover calculated runoff from the 2-D section matched the water balance calculated runoff the solution was deemed to be correct.

Conclusions:

1. *The Kidston tailings impoundment geometry was simplified by developing a non-dimensionalized generalized cross-section that would be representative of any location on the tailings impoundment. The top and bottom shape of this cross-section is defined by mathematical functions that are founded on the physical properties of the tailings complex. Material properties are assigned to the cross-section based on the extensive property database developed for the study that includes a mathematical function describing the surface saturated hydraulic conductivity.*
2. *A methodology is presented that allows numerical solving of the generalized cross-section for surface flux boundary conditions using rigorous coupled soil/atmosphere heat and mass flow theory.*

11.2.6 SoilCover Modeling

1. The flux boundary model had to be calibrated before actually performing the SoilCover modeling in order to ensure that it was capable of correctly calculating surface flux boundary conditions in the tailings impoundment. This was carried out

by modeling a profile of the tailings impoundment where matric suction sensors were installed and continuous matric suction readings were taken. At this site a Bowen ratio station was also installed to provide continuous evapotranspiration data to further assist in calibrating the SoilCover model.

2. The outcome of the SoilCover calibration test was that SoilCover correctly predicted surface flux boundary conditions through the tailings impoundment surface, however all precipitation events had to be distributed over 24 hours to prevent instability, and homogeneous vertical sections should be used due to the random nature of layering within the tailings impoundment.
3. The SoilCover modeling was performed for six different cases; mean-, wet- and dry climatic years, and either non-vegetated or vegetated tailings impoundment surfaces during each of these climatic years. The mean-, wet- and dry- climatic years were artificially created generic data sets based on the long-term climatic records available for the mine site. Since detailed climatic data for the site was limited, the generic approach was deemed to be more representative of long-term trends.
4. The major finding of the SoilCover modeling was that the overall closure water balance for the Kidston tailings impoundment would be negative, irrespective of what climatic condition were used. This is consistent with the climatic water balance that was also net negative. The physical meaning of this finding is that in the long term, the tailings pond will dry out, with a subsequent lowering of the phreatic level, and associated with that a reduction of the seepage rate from the impoundment will occur. Due to the rainfall pattern, it is likely that the pool would be seasonal in the long term, filling up from empty and returning to a dry state some time after the rainy season ends. The modeled results are supported by the long-term piezometric levels measured in the impoundment, that shows a continuously decreasing trend.
5. The results for the non-vegetated tailings surface appears to be a realistic prediction of what would in fact happen at Kidston Gold Mine. The results for the vegetated tailings impoundment should be considered to be conservative estimates. The actual vegetation regime on the Kidston tailings impoundment is to consist of a mixture of deep rooted trees with a grass understorey, and the root uptake algorithm in SoilCover is too simplistic to solve such a complex vegetation pattern. The results as presented does suggest that vegetating the impoundment would increase the rate at which the impoundment would dry out, however it is likely that the rate would be

higher if there is deep root water uptake. Conversely the effects of vegetation on the surface matrix, is not modeled in SoilCover, and as a result infiltration might increase as vegetation becomes well established. Although there are many theories to consider here, it can only be speculated on what the long-term performance would be.

Conclusions:

1. *The SoilCover numerical model was calibrated for the Kidston tailings impoundment conditions and were found to provide suitable results for calculating surface flux boundary conditions.*
2. *The conceptual model was solved for six cases; vegetated and non-vegetated tailings surface during a mean, wet or dry climatic year.*
3. *The major finding of the SoilCover modeling was that the overall closure water balance for the Kidston tailings impoundment would be negative, irrespective of what climatic condition or tailings surface were used. This is consistent with the climatic water balance that was also net negative. The physical meaning of this finding is that in the long term, the tailings pond will dry out, with a subsequent lowering of the phreatic level, and associated with that a reduction of the seepage rate from the impoundment will occur.*

11.2.7 Spatial Flux Boundary Functions

1. The 2-D SoilCover result (i.e. solving of the conceptual model for the generalized Kidston tailings impoundment cross-section) can be used to formulate a spatial flux boundary function, where the flux considered can be any of the individual surface flux components.
2. It was observed that the spatial flux boundary functions for evaporation and net infiltration followed the pattern suggested by the spatial flux boundary hypothesis. The exact shape of this function was found to be dependent on the climatic data used as well as whether the profile is vegetated or not.
3. The true benefit of the spatial flux boundary functions is that they can be converted to monthly, daily or even hourly fluxes, for direct input in 2-D and 3-D seepage modeling codes. These fluxes are reasonable representations of the surface fluxes

through the vadose zone based on soil/atmosphere coupled numerical surface flux boundary modeling (SoilCover). This eliminates the guesswork involved in calculating surface fluxes in the conventional manner required for these multidimensional saturated/unsaturated seepage modeling codes.

Conclusions:

1. *Solving the flux boundary conditions for the conceptual model results in spatial flux boundary functions that have a characteristic shape for each flux boundary component. This flux boundary function clearly defined how the surface flux boundary condition changes as the depth to the phreatic surface changes.*
2. *The spatial flux boundary functions supports the spatial flux hypothesis presented at the outset of the research*
3. *The spatial flux boundary functions can be used as a spatial flux boundary condition in multidimensional saturated/unsaturated flow seepage analysis modeling, effectively overcoming the current shortcoming with mutidimensional models.*

11.2.8 Spatial Flux Boundary Function Evaluation

1. The spatial flux functions were shown to exist, and a methodology has been presented to calculate them. Further is was suggested that these fluxes can be used as direct input in multidimensional seepage modeling, effectively bringing the gap between surface flux boundary and multidimensional modeling codes. In order to evaluate this statement a five-step program was undertaken to determine whether the spatial flux boundary functions could be used as suggested.
2. The evaluation tests rested on the principle that a 3-D numerical model of the Kidston tailings impoundment complex would be set up and that the flux boundary function could be used as a surface flux boundary condition. The 3-D model was then used to calculate the seepage from the tailings impoundment, and if the calculated seepage matched the measured seepage rate the functions would be considered to be effective.
3. Since 3-D modeling is complex and fraught with pitfalls, the evaluation was done by first performing 2-D SEEP/W tests. The second step was to perform an

evaluation test using a 2-D axisymmetric SEEP/W simulation, before moving into the 3-D realm and modeling the quasi 3-D axisymmetric model in the form of a circular tailings impoundment. Finally the actual dam geometry was used to set up and model the actual tailings impoundment. In the first three steps, the evaluation was done using the generalized Kidston tailings impoundment cross-section and the climatic period considered was the generic climatic year. The actual Kidston tailings impoundment was also first modeled using the generic climatic year.

4. Both the 2-D and axisymmetric SEEP/W models resulted in seepage rates which are in line with the record of measured data, suggesting that the use of the flux boundary functions are well suited for 2-D application.
5. The 3-D circular tailings impoundment model was set up in order to gain confidence with respect to the suitability of SVFlux™, since the results of this model should be close to the 2-D axisymmetric SEEP/W solution. The comparison of the circular dam 3-D solution with the axisymmetric solution using similar initial piezometric heads does in fact support the fact that SVFlux™ provides a suitable solution.
6. The final test was to use an actual period for which detailed measured data from the site was available, and use the calculated spatial flux boundary functions as input to the 3-D model in order to calculate what the seepage from the Kidston tailings impoundment would be. To this effect a period of 4-months between December 2000 and March 2001 was selected. Over this period, detailed seepage measurements from the site were taken, and the modeled results could thus be compared to actual data. The outcome of this last test was that the use of the flux boundary functions results in an excellent match for the seepage rates from the tailings impoundment.
7. The evaluation tests thus supports the suggestion that the spatial infiltration flux boundary functions do in fact provide an excellent basis for providing representative surface flux boundaries for multidimensional seepage modeling. The calculated seepage flux boundary functions were used as a surface flux boundary input into a 3-D numerical model, and the modeled seepage rate was found to be an excellent match with physically measured seepage rates.
8. The results of the 3-D model confirm that at Kidston Gold Mine the seepage is driven by the pond. The surface flux function plays a small role in defining the

magnitude of the seepage rate. Generally, with the exception of one or two months there is no recharge to the phreatic surface from the atmosphere.

Conclusion:

1. *A rigorous evaluation exercise consisting of two- and three-dimensional modeling confirmed that the spatial flux boundary functions presented in this study are in fact a good representation of the actual conditions observed at the Kidston tailings impoundment over the period of time for which measurements was made. Using the calculated spatial flux boundary function as a surface flux boundary condition in the multidimensional models resulted in calculation of seepage rates from the tailings impoundment that are in good agreement with measured seepage rates.*

11.2.9 Global Conclusion for The Study

The research documented here presents a methodology to describe the spatially varying flux boundary conditions for the Kidston tailings impoundment that allows for solving of the overall tailings impoundment closure water balance. The spatial flux boundary functions are appropriate surface flux boundary calculations based on rigorous coupled soil/atmosphere numerical modeling techniques, and can successfully be used as surface flux boundary conditions in multidimensional saturated/unsaturated seepage analysis models. This effectively bridges the gap in technology between existing coupled soil/atmosphere models and multidimensional seepage models. Furthermore, by applying the concept of the generalized Kidston tailings impoundment cross-section through to defining the multidimensional model allows for simple yet effective predictive modeling to be done.

To summarize, the research led to 4 major contributions that can be described as follows:

1. A multidimensional conceptual model was developed that describes one generalized cross-section through a tailings impoundment (i.e. for the Kidston tailings impoundment that is a low-tonnage impoundment in an arid climate). The generalized cross-section is non-dimensionalized which ensures that it is representative for any location on that tailings impoundment. The conceptual model is physically based and accounts for the actual spatial variation in the vadoze zone of the tailings impoundment.

2. A methodology was developed whereby rigorous soil/atmosphere coupled one-dimensional surface flux boundary numerical models can be used to calculate the surface flux boundary conditions for the multidimensional conceptual model of the generalized tailings impoundment cross-section.
3. A methodology was developed that allowed for the calculation of spatial surface flux boundary functions that can be used as direct input for surface flux boundary conditions in multidimensional saturated/unsaturated seepage models. This permits representative predictive modeling since the surface flux boundary conditions are based on rigorous soil/atmosphere coupled surface flux boundary theory.
4. Finally, a methodology was developed whereby a multidimensional model can be set up according to the same procedure as outlined in the conceptual model. This allows for multidimensional modeling to be physically based, which would simplify calibration modeling.

In summary, the methodology presented here to calculate spatial surface flux boundary conditions is in effect a quasi three dimensional model to calculate flux boundary conditions using rigorous coupled soil/atmosphere numerical techniques.

11.3 Recommendations for Further Research

The study presented here describes a number of new concepts and techniques, and although these techniques can be used with confidence for similar tailings impoundments (i.e. low-tonnage impoundments in arid climates), there are still numerous refinements that could be made. The following is a list of further research suggestions that would enhance the existing study, as well as some areas where there is a definite lack of understanding.

1. The methodology presented in this thesis is only applicable to tailings impoundments during closure constions. If would be worthwhile to extend this approach to account for the perational phase of the tailings impoundments as well.
2. One of the major problems that had to be dealt with during this study was overcoming the infiltration instability created by steep gradients when wetting coarse tailings form a fairly dry state. Some work has been done to using scaling techniques and similitude to overcome this problem, however none of it is developed enough for application at this stage. Further study in this area would greatly speed numerical modeling up and reduce the number of

assumptions and simplifications required in order to obtain convergence. Overcoming this problem would allow for modeling of specific storm events as opposed to spreading rainfall equally over 24 hour periods as was done for this research.

3. The spatial flux boundary functions presented here are specifically for the Kidston tailings impoundment, and although the author believes that the basic methodology is applicable to all tailings impoundments with a vadose zone, during closure conditions, the concept should be refined and tested on a number of different sites in order to get the appropriate confidence. The selection of other sites should include areas of varying climatic water balances, and different tailings types and scale of operations. For example, the mathematical formulation used for the beach shape function in this study is applicable only to the type of tailings at Kidston; however any representative mathematical function may be used to describe the beach shape for other tailings types, and the general solving methodology presented is still expected to remain valid.
4. It would be beneficial to fit a mathematical function to the spatial flux boundary function. By doing this it could be possible to determine the surface flux anywhere on the tailings impoundment by simply solving an equation.
5. There is a definite need to enhance the vegetation algorithm in the SoilCover code to overcome the shortfalls with regard to root water uptake.
6. The effect of vegetation on the infiltrability of a soil profile has been researched a fair amount, however there is still no definitive guidelines on how to predict the effect of vegetation on the vadose zone water balance specifically for engineering use. Work is required to combine the root water uptake aspects with the physical changes in the soil matrix.
7. The issue of tailings anisotropy has been mentioned, but the calculation methodology presented was simplified to account for isotropic conditions only. This simplification is justified for the Kidston tailings impoundment, however in most tailings impoundments this simplification may not be reasonable. Further refinement of the proposed methodology to deal with this aspect is required.
8. The results presented in this study was based on 5 years of detailed data. Although this might seem to be an extensive dataset, the long-term predictive capabilities of the proposed methodology should be critically judged, since it does not take aspects like changes in tailings properties into account.

This page was intentionally left blank.

APPENDIX A

Kidston Tailings Samples

A.1 Kidston Tailings Samples

Information with respect to samples that were collected for testing of the tailings are presented here. The tailings samples tested as part of this study are listed in Tables A.1, A.2 and A.3. Table A.1 list samples collected by other researchers, but tested by the author specifically for this study. The first two samples (1/7 and 2/7) were bulk samples of representative typical tailings. The last five samples (T5-T200) were taken during the installation of the tailings matric suction sensors, and are thus representative of the tailings properties immediately adjacent to these sensors. Table A.2 contains details of samples collected by the author specifically for testing in this study. These samples were selected based on visual observation of the various layers of exposed tailings after completing each double-ring infiltrometer test. The samples were excavated by hand from the sidewall of a shallow (600-800 mm deep) trench. Table A.3 in turn list samples collected by the author specifically for testing as part of this study, but by other researchers. These samples were collected during the installation of shallow piezometers on the Kidston tailings impoundment in September 1999. The hand-augured cuttings from each piezometer hole were collected at the depth intervals listed in Table A.3.

All samples were collected in plastic bags, which were sealed by tying a string to the top open end. Samples were transported from site to the University of Saskatchewan by filling 20 liter plastic containers with the plastic bags. The plastic containers were air freighted to the University. Care was taken not to expose the samples or containers to undue harsh temperatures or humid environments, but no specific storage requirements in a constant temperature and humidity room was required. None of the samples were collected undisturbed, and no attempt was made to collect any undisturbed samples.

Table A.1: Details of samples collected by other researchers, but tested as part of this study (refer to Chapter 4 for sample locations).

No.	Type*	Size (kg)	Origin	Collected by	Collection date
1/7	Fine tailings	3.70	Dam surface	Mr. Nick Currey (Senior Environmental Officer, Kidston Gold Mine)	April 1995
2/7	Coarse tailings	4.30	Dam surface		April 1995
T5	Tailings	0.32	0.05 m below surface	Mr. Andrew Durham (Graduate Student, University of Saskatchewan)	1997
T50	Tailings	0.28	0.50 m below surface		1997
T100	Tailings	0.27	1.00 m below surface		1997
T150	Tailings	0.22	1.50 m below surface		1997
T200	Tailings	0.37	2.00 m below surface		1997

* The tailings type is based on a visual observation by the author when the sample was collected.

Table A.2: Details of samples collected specifically for this study while conducting the double-ring infiltrometer field infiltration tests (all samples collected September 1999) (refer to Chapter 4 for sample locations).

Sample no.	Tailings type*	Size (g)	Origin (depth below tailings surface, in mm)
DR1-#1	Beach sand**	1120	0 – 150
DR1-#2	Slimes#	367	150 – 200
DR1-#3	Beach sand**	890	200 – 600
DR2-#1	Beach sand**	499	0 – 300
DR2-#2	Slimes#	253	300 – 420
DR3-#1	Beach sand**	731	0 – 360
DR3-#2	Slimes#	467	360 – 400
DR4-#1	Beach sand**	848	0 – 180
DR4-#2	Slimes#	526	180 – 250
DR4-#3	Beach sand**	800	250 – 600
DR5-#1	Beach sand**	363	0 – 120
DR5-#2	Slimes#	269	120 – 170
DR5-#3	Beach sand**	264	170 – 400
DR5-#4	Slimes#	509	400 – 500
DR6-#1	Beach sand**	631	0 – 400
DR6-#2	Slimes#	96	500 – 600
DR7-#1	Beach sand**	194	400 – 500
DR7-#2	Slimes#	208	320 – 400
DR7-#3	Beach sand**	299	0 – 200
DR7-#4	Slimes#	271	200 – 250
DR7-#5	Beach sand**	274	250 – 320
DR9-#1	Beach sand**	776	0 – 270
DR9-#2	Slimes#	506	270 – 320
DR9-#3	Beach sand**	579	320 – 420
DR9-#4	Slimes#	203	420 – 520
DR11-#1	Beach sand**	1030	0 – 600

* The tailings type is based on a visual observation by the author when the sample was collected; ** Beach sand = coarse tailings; # Slimes = fine tailings.

Table A.3: **Details of samples collected specifically for this study, but testing conducted by other researchers. These samples were collected in September 1999 during the installation of the shallow piezometers on the tailings impoundment (refer to Chapter 4 for sample locations).**

Piezometer hole no.	From depth (mm)	To depth (mm)	Comment
A-1	500	5500	11 Samples
A-2	500	6000	12 Samples
A-3	500	4000	8 Samples
B-1	500	4000	8 Samples
B-2	500	4500	9 Samples
B-3	500	5000	10 Samples
B-4	500	5000	10 Samples
B-5	500	6000	4 Samples only (500;1000;5500;6000)
C-1	500	3000	6 Samples
C-2	500	4000	8 Samples
C-3	500	4500	9 Samples
C-4	500	6000	12 Samples
C-5	500	6000	12 Samples
D-1	500	3000	6 Samples
D-2	500	4000	8 Samples
D-3	500	5000	10 Samples
D-4	500	6000	12 Samples
E-1	500	4000	7 Samples (no 3500 sample)
E-3	500	6000	12 Samples
E-4	500	6000	12 Samples
F	500	3500	7 Samples
F-1	500	2500	5 Samples
F-2	500	3500	7 Samples
G	500	5000	10 Samples
G-1	500	6000	12 Samples

This page was intentionally left blank.

APPENDIX B

Grain Size Distribution Data

B.1 Introduction

Data for the grain size distribution tests performed on the Kidston tailings by the author, as well as summaries of all the testing done by other researchers on the Kidston tailings, as reported in Chapter 4 are presented here.

B.2 Describing All Elements in Tables

The tables in the sections following contain similar data, and a description of the values and how they have been calculated are documented here. The grain size distribution data reported in section B.3 are from sieve and hydrometer tests conducted according to the standard testing method ASTM Designation: D 422 – 63 (ASTM, 1996).

The classification method used for the tailings is the Unified Soil Classification System (USCS) (Holtz and Kovacs, 1981). There are no tailings larger that are retained on the U.S. standard sieve no. 4 (4.75 mm), which means that there is no gravel material present. The percentage sand (% sand) is the percentage of material not passing the U.S. standard sieve no. 200 (0.075 mm) sieve. The percentage silt (% silt) is the percentage of material passing the no. 200 sieve but larger than 0.002 mm, and the percentage clay (% clay) is that percentage of material smaller than 0.002 mm.

Two shape factors, the coefficient of uniformity, C_u, and the coefficient of curvature, C_c are defined by the following expressions:

$$C_u = \frac{D_{60}}{D_{10}} \qquad [B.1]$$

$$C_c = \frac{(D_{30})^2}{(D_{10})(D_{60})} \qquad [B.2]$$

Where D_{10}, D_{30}, and D_{60} are the grain size diameters (mm) corresponding to 10%, 30% and 60% passing by weight (or mass). Similarly D_{15}, D_{50}, D_{85}, D_{90} and D_{95} are the grain diameters corresponding to 15%, 50%, 85%, 90% and 95% passing by weight.

Any tailings sample with a % sand greater than 50% was classified as sand, while all other tailings was classified as silt (ML). Any tailings classified as sands, were considered well-graded sands (SW) if the C_c was between 1 and 3 and the C_u was also greater than 6. If the C_c was between 1 and 3, but the C_u was less than 6, and the amount of fines (% silt + % clay) was less than 10%, the tailings is considered to be a poorly graded sand (SP). Tailings with a C_c between 1 and 3, and a C_u between 4 and 6, with a fines total greater than 10% is considered to be silty sands (SM). Since the tailings samples have no plasticity (see Chapter 4), there are no samples classified as clays, even though they might be clay sized.

B.3 Testing Conducted by the Author

Tables B.1 to B.3 list the grain size distribution data for the 11 samples tested by the author for this study. The grain size distribution curves for these tests are presented in Figure B.1. Summaries of the main components of each of these tests are presented in Tables B.4 and B.5. These tests were performed on samples collected in April 1995.

Table B.1: Grain size distribution data for the fine tailings sample #1/7, collected in April 1995.

Sample #1/7A		Sample #1/7B		Sample #1/7C	
Particle size (mm)	**Percent finer than**	**Particle size (mm)**	**Percent finer than**	**Particle size (mm)**	**Percent finer than**
9.5000	100.00 %	9.5000	100.00 %	9.5000	100.00 %
4.7500	100.00 %	4.7500	100.00 %	4.7500	100.00 %
2.0000	100.00 %	2.0000	100.00 %	2.0000	100.00 %
0.8500	100.00 %	0.8500	100.00 %	0.8500	100.00 %
0.4170	97.98 %	0.4170	98.42 %	0.4170	98.80 %
0.2950	84.06 %	0.2950	86.26 %	0.2950	89.08 %
0.1800	39.49 %	0.1800	46.83 %	0.1800	54.05 %
0.1500	32.41 %	0.1500	36.52 %	0.1500	45.23 %
0.0927	19.75 %	0.0916	21.46 %	0.0918	21.75 %
0.0750	14.65 %	0.0750	17.35 %	0.0750	16.43 %
0.0688	11.85 %	0.0678	14.06 %	0.0679	14.73 %

Table B.1: **Grain size distribution data for the fine tailings sample #1/7, collected in April 1995.**

Sample #1/7A		Sample #1/7B		Sample #1/7C	
Particle size (mm)	Percent finer than	Particle size (mm)	Percent finer than	Particle size (mm)	Percent finer than
0.0499	7.10 %	0.0493	9.34 %	0.0493	10.06 %
0.0355	6.31 %	0.0350	8.55 %	0.0350	9.28 %
0.0251	6.00 %	0.0249	7.76 %	0.0249	8.46 %
0.0178	5.80 %	0.0177	7.10 %	0.0177	7.68 %
0.0130	5.49 %	0.0130	6.59 %	0.0130	7.22 %
0.0092	5.14 %	0.0092	5.80 %	0.0092	6.56 %
0.0066	5.00 %	0.0065	5.45 %	0.0066	5.59 %
0.0046	4.52 %	0.0046	5.23 %	0.0046	5.24 %
0.0033	4.42 %	0.0033	5.16 %	0.0033	5.17 %
0.0023	4.35 %	0.0023	5.12 %	0.0023	5.17 %
0.0014	4.22 %	0.0014	4.54 %	0.0014	4.84 %

Table B.2: **Grain size distribution data for the coarse tailings sample #2/7, collected in April 1995.**

Sample #2/7A		Sample #2/7B		Sample #2/7C	
Particle size (mm)	Percent finer than	Particle size (mm)	Percent finer than	Particle size (mm)	Percent finer than
9.5000	100.00 %	9.5000	100.00 %	9.5000	100.00 %
4.7500	100.00 %	4.7500	100.00 %	4.7500	100.00 %
2.0000	100.00 %	2.0000	100.00 %	2.0000	100.00 %
0.8500	99.28 %	0.8500	99.13 %	0.8500	99.29 %
0.4170	79.72 %	0.4170	80.59 %	0.4170	79.70 %
0.2950	56.16 %	0.2950	61.15 %	0.2950	58.15 %
0.1800	33.50 %	0.1800	32.35 %	0.1800	31.83 %
0.1500	26.12 %	0.1500	25.56 %	0.1500	24.34 %
0.0965	15.13 %	0.0959	14.72 %	0.0964	14.83 %
0.0750	10.27 %	0.0750	9.30 %	0.0750	7.87 %
0.0709	8.47 %	0.0703	8.42 %	0.0713	6.91 %
0.0508	6.09 %	0.0505	5.74 %	0.0509	5.33 %
0.0360	5.77 %	0.0358	5.27 %	0.0360	5.01 %
0.0255	4.98 %	0.0254	4.79 %	0.0256	4.06 %
0.0181	4.50 %	0.0180	4.44 %	0.0181	4.06 %
0.0132	4.47 %	0.0132	3.94 %	0.0132	3.87 %
0.0094	3.96 %	0.0093	3.90 %	0.0094	3.67 %
0.0067	3.89 %	0.0066	3.52 %	0.0067	3.60 %
0.0047	3.89 %	0.0047	3.59 %	0.0047	3.57 %
0.0033	3.54 %	0.0033	3.17 %	0.0033	2.78 %
0.0023	3.54 %	0.0024	3.14 %	0.0024	2.64 %
0.0014	3.15 %	0.0014	2.81 %	0.0014	2.35 %

Table B.3: Grain size distribution data for the five tailings samples collected by Mr. Andrew Durham, a University of Saskatchewan graduate student, while installing the Model-229 thermal conductivity sensors in 1997.

Sample T5		Sample T50		Sample T100		Sample T150		Sample T200	
Particle size (mm)	Percent finer than (%)	Particle size (mm)	Percent finer than (%)	Particle size (mm)	Percent finer than (%)	Particle size (mm)	Percent finer than (%)	Particle size (mm)	Percent finer than (%)
9.5000	100.00	9.5000	100.00	9.5000	100.00	9.5000	100.00	9.5000	100.00
4.7500	100.00	4.7500	100.00	4.7500	100.00	4.7500	100.00	4.7500	100.00
2.0000	100.00	2.0000	100.00	2.0000	100.00	2.0000	100.00	2.0000	100.00
0.8500	100.00	0.8500	99.02	0.8500	99.93	0.8500	99.97	0.8500	99.71
0.4170	98.17	0.4170	78.48	0.4170	91.80	0.4170	97.22	0.4170	90.99
0.2950	88.68	0.2950	54.67	0.2950	71.78	0.2950	84.84	0.2950	78.99
0.1800	60.86	0.1800	31.35	0.1800	46.89	0.1800	55.25	0.1800	60.10
0.1500	52.41	0.1500	26.21	0.1500	40.57	0.1500	44.32	0.1500	52.39
0.0845	32.59	0.0940	19.17	0.0883	28.18	0.0890	27.32	0.0858	32.06
0.0750	29.51	0.0750	15.05	0.0750	24.80	0.0750	22.50	0.0750	28.20
0.0625	26.27	0.0688	13.45	0.0648	22.65	0.0660	20.21	0.0642	24.16
0.0461	19.94	0.0492	11.55	0.0466	20.27	0.0478	16.25	0.0469	19.42
0.0335	15.51	0.0351	9.96	0.0334	18.22	0.0342	14.67	0.0337	16.58
0.0240	13.26	0.0250	8.53	0.0238	16.48	0.0244	13.09	0.0241	14.68
0.0172	11.54	0.0178	7.58	0.0171	14.67	0.0174	11.47	0.0173	12.44
0.0128	9.41	0.0131	6.79	0.0126	13.05	0.0128	10.37	0.0128	10.63
0.0091	8.62	0.0093	5.57	0.0090	11.12	0.0091	9.26	0.0091	9.46
0.0065	7.13	0.0066	5.06	0.0064	9.51	0.0065	7.93	0.0065	8.16
0.0046	6.07	0.0047	3.95	0.0046	8.17	0.0046	7.03	0.0046	7.27
0.0033	5.37	0.0033	3.48	0.0033	7.10	0.0033	6.63	0.0033	6.74
0.0024	5.15	0.0024	2.36	0.0023	6.31	0.0023	5.33	0.0023	6.27
0.0014	3.93	0.0014	1.91	0.0014	5.23	0.0014	4.91	0.0014	5.06

Table B.4: Summary table of the sand, silt and clay content of the tailings, the coefficients of uniformity and curvature and the USCS classification of the tailings samples tested by the author.

Sample no.	% Sand	% Silt	% Clay	C_u	C_c	Classification
# 1/7A	85.8	9.9	4.3	3.79	1.35	SP
# 1/7B	83.1	12.0	4.9	4.21	1.37	SM
# 1/7C	83.8	11.1	5.1	4.13	1.31	SM
# 2/7A	90.2	6.4	3.4	4.23	1.17	SP
# 2/7B	90.9	6.1	3.0	3.74	1.28	SP
# 2/7C	92.4	5.1	2.5	3.75	1.20	SP
# T5	70.8	24.6	4.7	12.64	2.36	SW
# T50	85.2	12.6	2.2	9.09	2.59	SW
# T100	75.4	18.6	6.0	33.27	5.44	SM
# T150	77.8	17.1	5.2	17.13	4.23	SM
# T200	72.2	22.0	5.9	16.60	3.30	SM

Table B.5: Summary of the tailings size fractions for the tailings samples tested by the author.

Sample no.	D_{10} (mm)	D_{15} (mm)	D_{30} (mm)	D_{50} (mm)	D_{60} (mm)	D_{85} (mm)	D_{90} (mm)	D_{95} (mm)
# 1/7A	0.061	0.076	0.139	0.207	0.233	0.303	0.347	0.391
# 1/7B	0.052	0.070	0.125	0.189	0.218	0.291	0.332	0.383

Table B.5: Summary of the tailings size fractions for the tailings samples tested by the author.

Sample no.	D_{10} (mm)	D_{15} (mm)	D_{30} (mm)	D_{50} (mm)	D_{60} (mm)	D_{85} (mm)	D_{90} (mm)	D_{95} (mm)
# 1/7C	0.048	0.069	0.112	0.166	0.200	0.282	0.307	0.369
# 2/7A	0.074	0.096	0.166	0.264	0.315	0.534	0.645	0.755
# 2/7B	0.078	0.097	0.170	0.250	0.290	0.520	0.637	0.754
# 2/7C	0.082	0.097	0.173	0.259	0.305	0.534	0.645	0.755
# T5	0.014	0.031	0.077	0.142	0.177	0.280	0.312	0.376
# T50	0.035	0.075	0.172	0.272	0.322	0.554	0.660	0.765
# T100	0.007	0.018	0.097	0.194	0.241	0.376	0.406	0.587
# T150	0.012	0.037	0.099	0.166	0.198	0.297	0.346	0.395
# T200	0.011	0.026	0.080	0.142	0.180	0.356	0.407	0.616

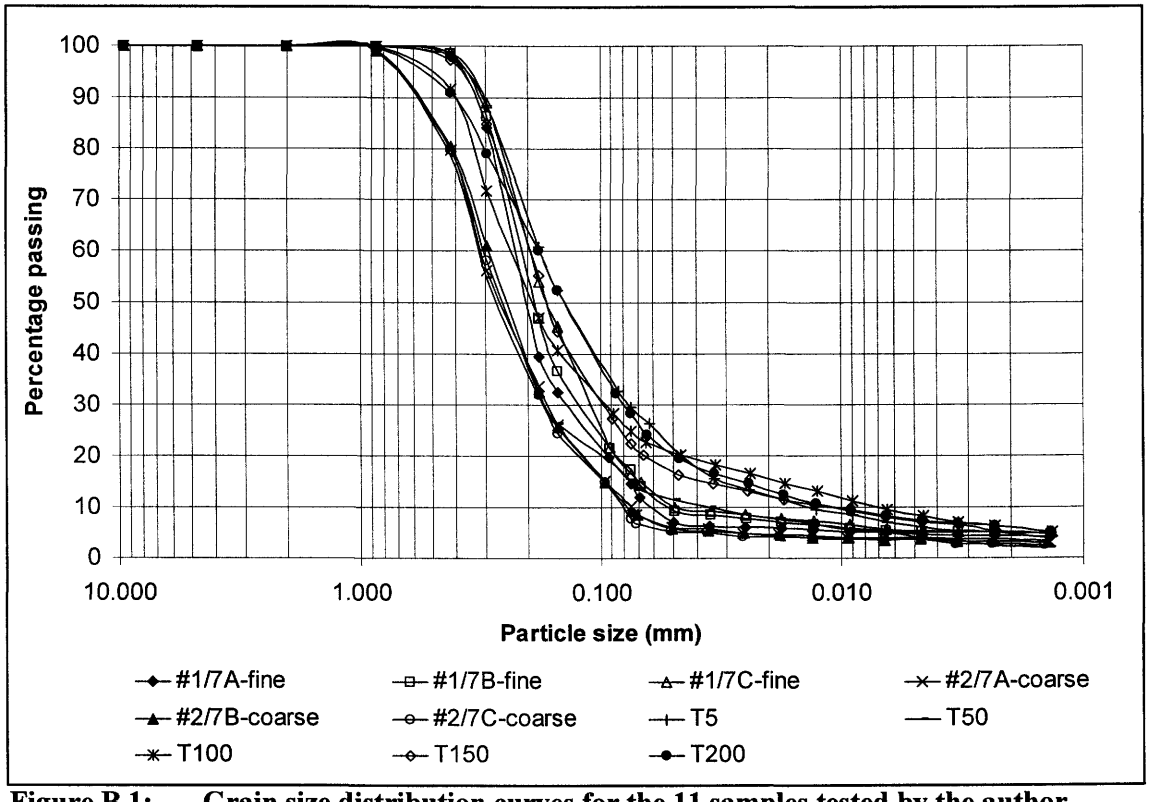

Figure B.1: Grain size distribution curves for the 11 samples tested by the author.

B.4 Testing Conducted by Gutteridge Haskins and Davey (1987)

Tables B.6 and B.7 contains the summarized grain size distribution data for the 17 tests reported by Gutteridge Haskins and Davey (1987), The grain size distribution curves for these tests are presented in Figure B.2.

Table B.6: Summary table of the sand, silt and clay content of the tailings, the coefficients of uniformity and curvature and the USCS classification of the tailings samples tested by Gutteridge Haskins and Davey (1987).

Sample no.	% Sand	% Silt	% Clay	C_u	C_c	Classification
BH2 (0.0 - 0.54 m) sieve	80.9	19.1	0.0	4.78	1.08	SM
BH2 (1.0 - 1.5 m) sieve	78.1	21.0	0.9	10.72	2.26	SW
BH3 (0.5 - 1.0 m) sieve	55.2	43.1	1.8	11.04	0.82	SM
BH3 (1.5 - 2.0 m) sieve	68.9	29.9	1.2	12.15	1.47	SW
BH3 (2.5 - 3.0 m) sieve	74.3	24.7	1.0	12.68	1.89	SW
BH4 (1.5 - 2.0 m) sieve	66.0	32.7	1.3	11.18	1.29	SW
BH5 (0.0 - 1.0 m) sieve	54.7	43.6	1.7	10.08	0.89	SM
BH5 (0.6 - 1.14 m) sieve	34.4	65.6	0.0	1.63	0.96	ML
BH5 (2.0 - 3.0 m) sieve	66.2	32.4	1.4	13.09	1.14	SW
BH6 (1.0 - 2.0 m) sieve	59.6	38.9	1.5	10.67	0.95	SM
BH6 (3.0 - 4.0 m) sieve	59.6	38.9	1.5	11.51	0.89	SM
BH7 (0.5 - 1.0 m) sieve	75.6	24.4	0.0	4.03	0.81	SM
BH8 (0.5 - 1.0 m) sieve	14.4	85.6	0.0	1.50	0.96	ML
BH8 (1.1 - 1.5 m) sieve	17.3	82.7	0.0	1.51	0.96	ML
BH1B (2.0 - 2.5 m) hydrometer	10.3	76.3	13.5	13.39	1.01	ML
BH5 (1.0 - 2.0 m) hydrometer	68.3	25.9	5.8	33.83	4.05	SM
BH8 (1.5 - 2.0 m) hydrometer	9.8	75.9	14.2	16.74	0.89	ML

Table B.7: Summary of the tailings size fractions for the tailings samples tested by Gutteridge Haskins and Davey (1987).

Sample no.	D_{10} (mm)	D_{15} (mm)	D_{30} (mm)	D_{50} (mm)	D_{60} (mm)	D_{85} (mm)	D_{90} (mm)	D_{95} (mm)
BH2 (0.0 - 0.54 m) sieve	0.057	0.066	0.129	0.225	0.272	0.496	0.548	0.600
BH2 (1.0 - 1.5 m) sieve	0.023	0.034	0.113	0.203	0.246	0.454	0.516	0.578
BH3 (0.5 - 1.0 m) sieve	0.011	0.017	0.034	0.091	0.125	0.250	0.278	0.357
BH3 (1.5 - 2.0 m) sieve	0.016	0.024	0.069	0.150	0.198	0.368	0.457	0.546
BH3 (2.5 - 3.0 m) sieve	0.020	0.030	0.097	0.200	0.251	0.472	0.528	0.584
BH4 (1.5 - 2.0 m) sieve	0.015	0.023	0.059	0.131	0.173	0.292	0.378	0.497
BH5 (0.0 - 1.0 m) sieve	0.012	0.018	0.036	0.089	0.120	0.245	0.276	0.358
BH5 (0.6 - 1.14 m) sieve	0.043	0.046	0.054	0.065	0.071	0.148	0.201	0.256
BH5 (2.0 - 3.0 m) sieve	0.015	0.022	0.056	0.142	0.191	0.363	0.447	0.532
BH6 (1.0 - 2.0 m) sieve	0.013	0.020	0.042	0.107	0.142	0.261	0.286	0.391
BH6 (3.0 - 4.0 m) sieve	0.013	0.020	0.043	0.113	0.154	0.286	0.360	0.488
BH7 (0.5 - 1.0 m) sieve	0.053	0.060	0.095	0.175	0.213	0.336	0.427	0.518
BH8 (0.5 - 1.0 m) sieve	0.042	0.044	0.051	0.059	0.063	0.074	0.090	0.128
BH8 (1.1 - 1.5 m) sieve	0.042	0.045	0.051	0.060	0.064	0.075	0.103	0.131
BH1B (2.0 - 2.5 m) hydrometer	0.001	0.002	0.005	0.012	0.018	0.057	0.075	0.119
BH5 (1.0 - 2.0 m) hydrometer	0.006	0.015	0.068	0.146	0.195	0.373	0.425	0.560
BH8 (1.5 - 2.0 m) hydrometer	0.001	0.002	0.006	0.016	0.024	0.058	0.073	0.120

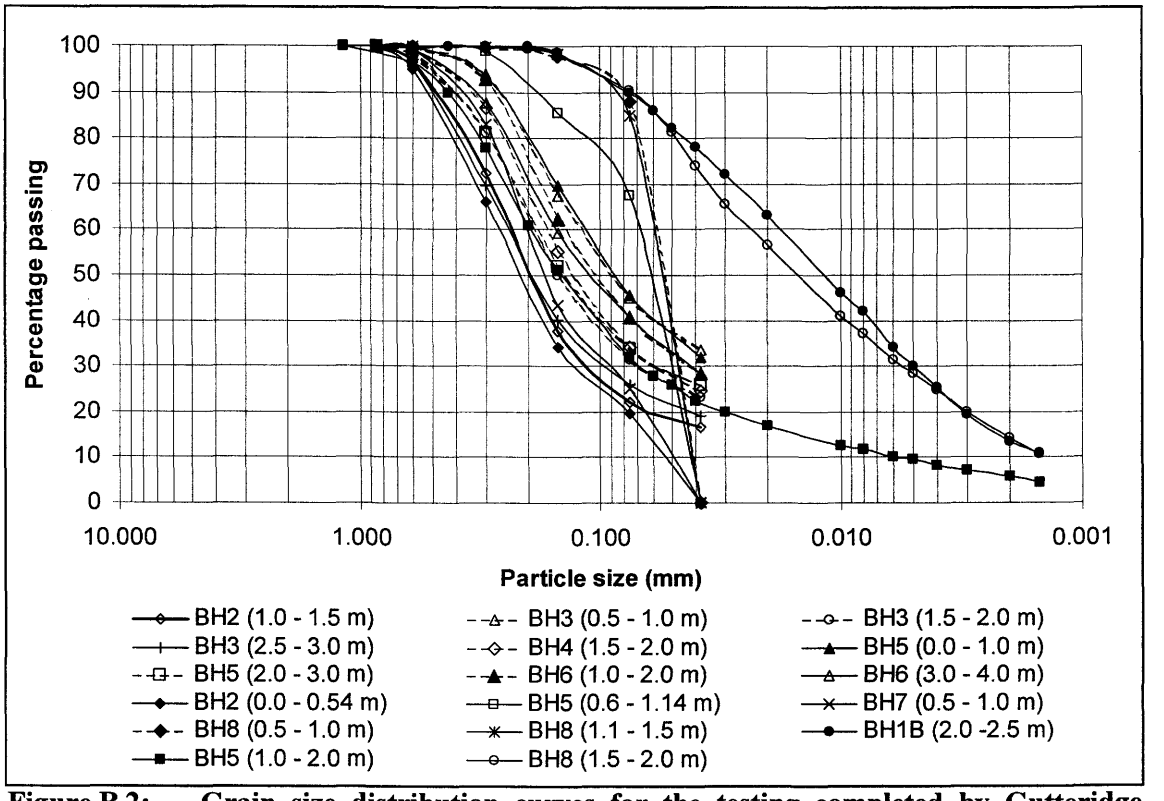

Figure B.2: Grain size distribution curves for the testing completed by Gutteridge Haskins and Davey (1987).

B.5 Testing by O'Kane (1997)

Summarized results of 2 grain size distribution tests performed by O'Kane (1997) are presented in Tables B.8 and B.9 and the grain size distribution curves are presented in Figure B.3.

Table B.8: Summary table of the sand, silt and clay content of the tailings, the coefficients of uniformity and curvature and the USCS classification of the tailings samples tested by O'Kane (1997).

Sample no.	% Sand	% Silt	% Clay	C_u	C_c	Classification
Kidston #1 Fine	91.4	8.4	0.2	2.57	1.05	SP
Kidston #2 Coarse	95.2	4.6	0.1	3.18	1.10	SP

Table B.9: Summary of the tailings size fractions for the tailings samples tested by O'Kane (1997).

Sample no.	D_{10} (mm)	D_{15} (mm)	D_{30} (mm)	D_{50} (mm)	D_{60} (mm)	D_{85} (mm)	D_{90} (mm)	D_{95} (mm)
Kidston #1 Fine	0.078	0.091	0.129	0.177	0.201	0.298	0.326	0.354
Kidston #2 Coarse	0.098	0.120	0.182	0.267	0.310	0.480	0.580	0.730

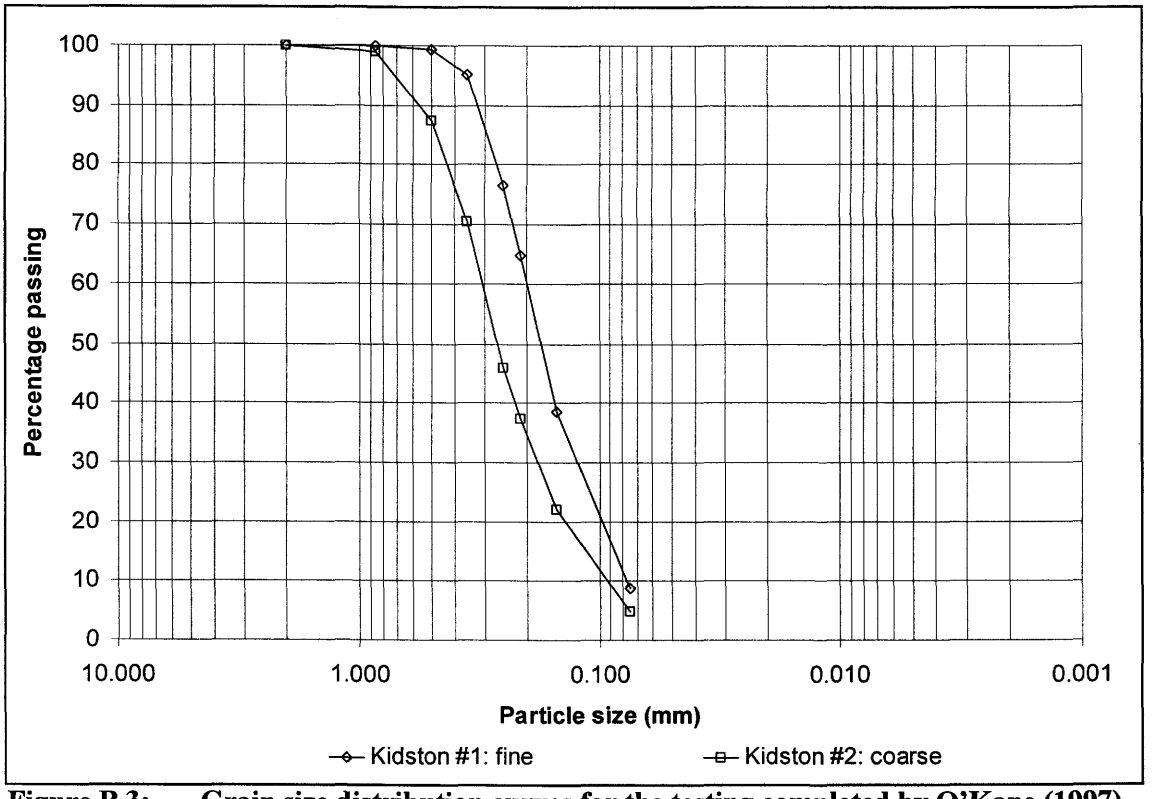

Figure B.3: Grain size distribution curves for the testing completed by O'Kane (1997).

B.6 Testing by Rassam (1998)

Rassam (1998) performed 8 grain size distribution tests on the Kidston tailings and the results of these tests are presented in Tables B.10 and B.11. The grain size distribution curves are presented in Figure B.4.

Table B.10: Summary table of the sand, silt and clay content of the tailings, the coefficients of uniformity and curvature and the USCS classification of the tailings samples tested by Rassam (1998).

Sample no.	% Sand	% Silt	% Clay	C_u	C_c	Classification
Data for 0 m	76.1	23.6	0.3	12.76	1.77	SW
Data for 50 m	89.1	10.8	0.1	5.40	1.53	SM
Data for 75 m	83.3	16.5	0.2	6.80	1.75	SW
Data for 100 m	88.4	11.4	0.2	5.58	1.68	SM
Data for 125 m	86.6	13.2	0.1	7.68	2.10	SW
Data for 150 m	71.8	27.6	0.7	9.51	1.80	SW
Data for 200 m	70.1	29.6	0.3	10.18	2.53	SW
Whole tailings	44.1	52.9	3.0	22.28	0.58	ML

Table B.11: Summary of the tailings size fractions for the tailings samples tested by Rassam (1998).

Sample no.	D_{10} (mm)	D_{15} (mm)	D_{30} (mm)	D_{50} (mm)	D_{60} (mm)	D_{85} (mm)	D_{90} (mm)	D_{95} (mm)
Data for 0 m	0.018	0.031	0.085	0.164	0.227	0.427	0.513	0.599
Data for 50 m	0.056	0.086	0.161	0.255	0.303	0.501	0.566	0.801
Data for 75 m	0.035	0.060	0.121	0.199	0.238	0.369	0.409	0.503
Data for 100 m	0.053	0.092	0.161	0.249	0.293	0.442	0.508	0.575
Data for 125 m	0.038	0.079	0.154	0.247	0.294	0.447	0.514	0.582
Data for 150 m	0.019	0.029	0.077	0.137	0.178	0.298	0.355	0.416
Data for 200 m	0.015	0.020	0.075	0.121	0.150	0.280	0.317	0.388
Whole tailings	0.004	0.006	0.014	0.044	0.090	0.210	0.245	0.280

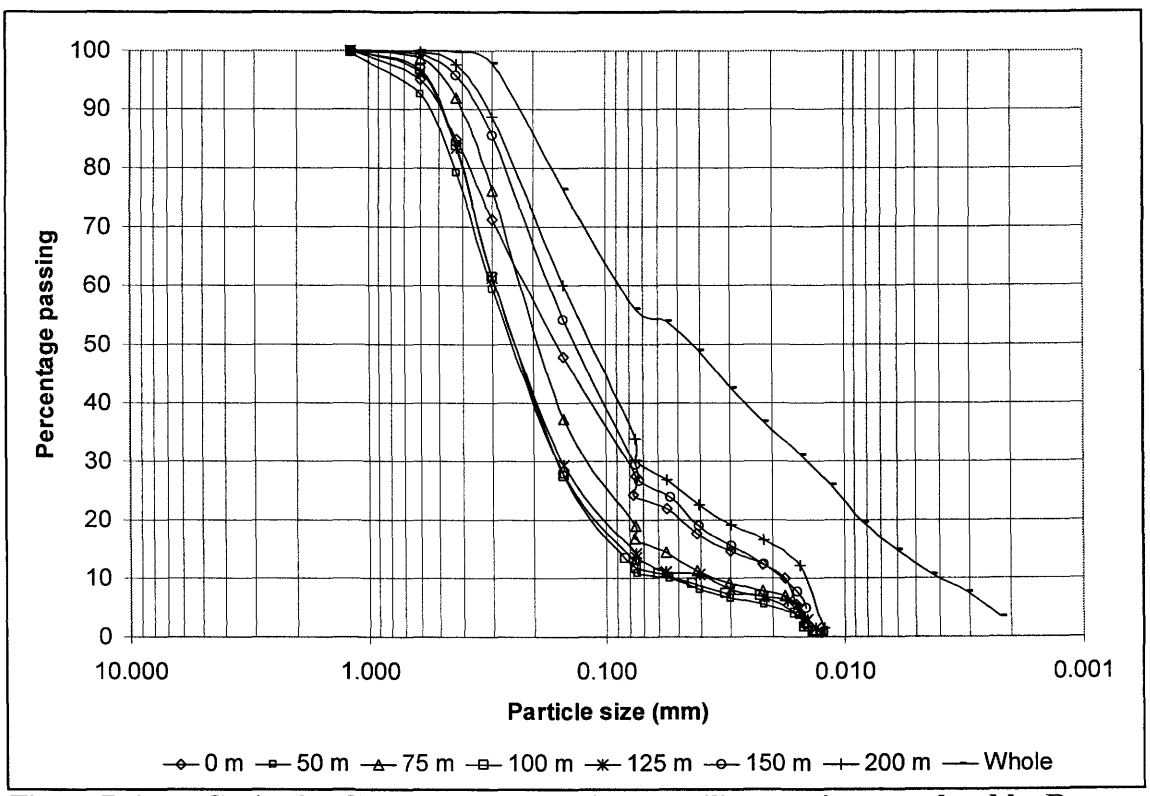

Figure B.4: Grain size distribution curves for the tailings testing completed by Rassam (1998).

B.7 Testing by Williams (2000a)

Williams (2000a) performed grain size distribution tests on 6 samples and the results are summarized in Tables B.12 and B.13. Figure B.5 presents the grain size distribution curves for these tests.

Table B.12: Summary table of the sand, silt and clay content of the tailings, the coefficients of uniformity and curvature and the USCS classification of the tailings samples tested by Williams (2000a).

Sample no.	% Sand	% Silt	% Clay	C_u	C_c	Classification
Sieve C2 : C7 (2.5 - 3.0 m)	60.4	39.3	0.3	9.69	0.72	SM
Sieve C6 : C7 (4.5 - 6.0 m)	46.7	52.7	0.6	6.35	0.34	ML
Sieve C13 : (13.5 - 14.0 m)	88.7	11.0	0.3	4.22	1.29	SM
Sieve G1 : G3 (0.0 - 1.5 m)	81.4	18.0	0.6	8.38	1.64	SW
Sieve G4 : G3 (4.5 - 5.0 m)	68.2	31.5	0.3	13.50	1.10	SW
Sieve G12 : G3 (12.5 - 13.0 m)	60.2	39.6	0.2	4.98	0.95	SM
Laser C2 : C7 (2.5 - 3.0 m)	60.6	39.2	0.2	12.61	1.94	SW
Laser C6 : C7 (4.5 - 6.0 m)	60.2	39.7	0.1	11.15	1.98	SW
Laser C13 : (13.5 - 14.0 m)	93.4	6.6	0.0	2.93	1.14	SP
Laser G1 : G3 (0.0 - 1.5 m)	77.8	22.2	0.1	6.38	1.47	SW
Laser G4 : G3 (4.5 - 5.0 m)	62.8	36.8	0.4	15.94	1.66	SW
Laser G12 : G3 (12.5 - 13.0 m)	77.7	22.1	0.2	4.23	1.25	SM

Table B.13: Summary of the tailings size fractions for the tailings samples tested by Williams (2000a).

Sample no.	D_{10} (mm)	D_{15} (mm)	D_{30} (mm)	D_{50} (mm)	D_{60} (mm)	D_{85} (mm)	D_{90} (mm)	D_{95} (mm)
Sieve C2 : C7 (2.5 - 3.0 m)	0.014	0.015	0.036	0.102	0.131	0.262	0.292	0.367
Sieve C6 : C7 (4.5 - 6.0 m)	0.014	0.014	0.020	0.055	0.087	0.162	0.215	0.267
Sieve C13 : (13.5 - 14.0 m)	0.066	0.090	0.154	0.237	0.278	0.406	0.455	0.553
Sieve G1 : G3 (0.0 - 1.5 m)	0.033	0.057	0.124	0.225	0.280	0.477	0.548	0.728
Sieve G4 : G3 (4.5 - 5.0 m)	0.013	0.015	0.051	0.134	0.179	0.319	0.374	0.436
Sieve G12 : G3 (12.5 - 13.0 m)	0.023	0.028	0.049	0.092	0.113	0.205	0.241	0.278
Laser C2 : C7 (2.5 - 3.0 m)	0.010	0.017	0.051	0.101	0.130	0.244	0.290	0.377
Laser C6 : C7 (4.5 - 6.0 m)	0.011	0.019	0.052	0.098	0.122	0.219	0.259	0.330
Laser C13 : (13.5 - 14.0 m)	0.094	0.118	0.173	0.242	0.277	0.434	0.489	0.564
Laser G1 : G3 (0.0 - 1.5 m)	0.033	0.049	0.100	0.168	0.209	0.397	0.494	0.000
Laser G4 : G3 (4.5 - 5.0 m)	0.010	0.015	0.050	0.118	0.154	0.278	0.331	0.428
Laser G12 : G3 (12.5 - 13.0 m)	0.040	0.055	0.092	0.141	0.170	0.296	0.350	0.438

B.8 Testing by Williams (2000b)

An additional 9 grain size distributions tests was performed by Williams (2000b) and the results are summarized in Tables B.14 and B.15. The grain size distribution curves for these tests are presented in Figure B.6.

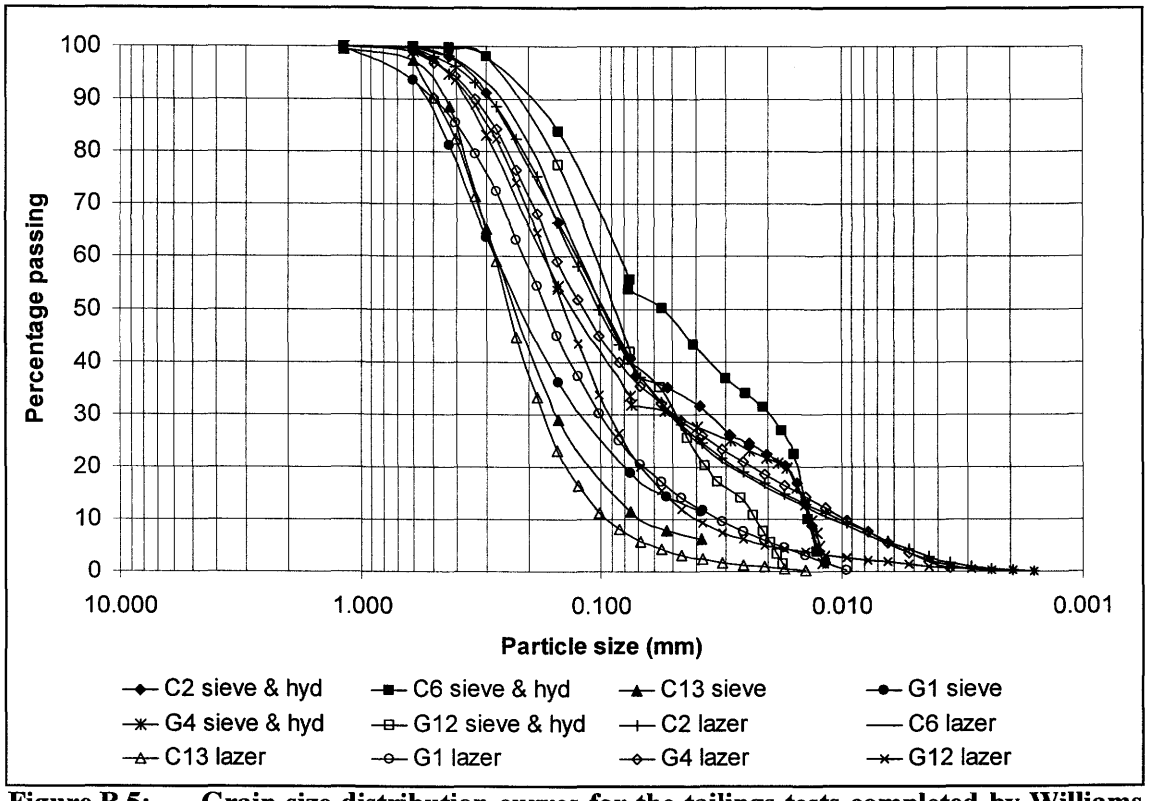

Figure B.5: **Grain size distribution curves for the tailings tests completed by Williams (2000a).**

Table B.14: **Summary table of the sand, silt and clay content of the tailings, the coefficients of uniformity and curvature and the USCS classification of the tailings samples tested by Williams (2000b).**

Sample no.	% Sand	% Silt	% Clay	C_u	C_c	Classification
Sieve C1	28.2	51.4	20.5	22.74	0.87	ML
Sieve C2	63.0	31.6	5.4	21.44	3.29	SM
Sieve C3	68.9	27.0	4.2	16.88	2.61	SW
Sieve C4	60.1	34.0	5.9	33.32	3.12	SM
Sieve C5	54.8	38.2	7.0	37.89	2.27	SW
Sieve D1	3.0	68.5	28.5	12.12	1.10	ML
Sieve D2	11.5	68.7	19.8	19.31	1.05	ML
Sieve D3	69.2	25.3	5.5	36.99	3.85	SM
Sieve D4	58.3	36.2	5.5	19.72	2.32	SW

Table B.15: **Summary of the tailings size fractions for the tailings samples tested by Williams (2000b).**

Sample no.	D_{10} (mm)	D_{15} (mm)	D_{30} (mm)	D_{50} (mm)	D_{60} (mm)	D_{85} (mm)	D_{90} (mm)	D_{95} (mm)
Sieve C1	0.001	0.001	0.004	0.010	0.019	0.140	0.188	0.253
Sieve C2	0.006	0.018	0.053	0.108	0.134	0.245	0.271	0.296
Sieve C3	0.011	0.025	0.070	0.139	0.178	0.279	0.299	0.379
Sieve C4	0.005	0.011	0.046	0.112	0.150	0.298	0.365	0.451

Table B.15: Summary of the tailings size fractions for the tailings samples tested by Williams (2000b).

Sample no.	D_{10} (mm)	D_{15} (mm)	D_{30} (mm)	D_{50} (mm)	D_{60} (mm)	D_{85} (mm)	D_{90} (mm)	D_{95} (mm)
Sieve C5	0.003	0.008	0.031	0.092	0.128	0.254	0.281	0.340
Sieve D1	0.001	0.001	0.002	0.005	0.007	0.020	0.027	0.046
Sieve D2	0.001	0.001	0.004	0.011	0.018	0.052	0.089	0.140
Sieve D3	0.006	0.014	0.070	0.165	0.217	0.390	0.450	0.531
Sieve D4	0.007	0.014	0.045	0.100	0.130	0.262	0.292	0.373

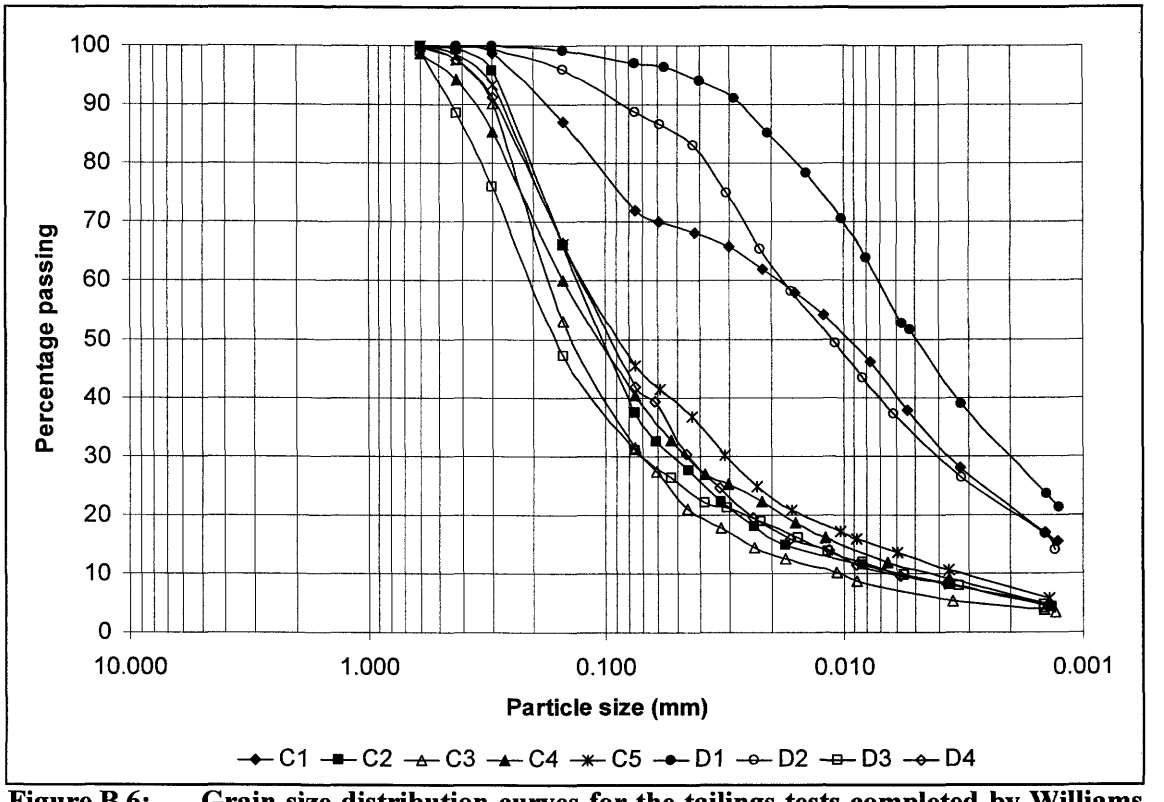

Figure B.6: Grain size distribution curves for the tailings tests completed by Williams (2000b).

B.9 Testing by Wog (2000)

The final grain size distribution testing consist of 7 tests performed by Wog (2000). The results of these tests are summarized in Tables B.16 and B.17 and the grain size distribution curves are presented in Figure B.7.

Table B.16: Summary table of the sand, silt and clay content of the tailings, the coefficients of uniformity and curvature and the USCS classification of the tailings samples tested by Wog (2000).

Sample no.	% Sand	% Silt	% Clay	C_u	C_c	Classification
DR1#1	85.8	7.9	6.3	13.41	3.33	SM
DR1#2	83.9	9.8	6.3	17.35	4.46	SM
DR1#3	87.1	8.2	4.8	13.71	4.64	SM
DR9#1	82.1	12.3	5.6	19.28	4.62	SM
DR9#2	66.2	26.8	7.0	20.88	3.55	SM
DR9#3	8.9	76.2	15.0	14.41	1.88	ML
DR9#4	3.7	75.9	20.3	17.67	1.28	ML

Table B.17: Summary of the tailings size fractions for the tailings samples tested by Wog (2000).

Sample no.	D_{10} (mm)	D_{15} (mm)	D_{30} (mm)	D_{50} (mm)	D_{60} (mm)	D_{85} (mm)	D_{90} (mm)	D_{95} (mm)
DR1#1	0.027	0.080	0.181	0.328	0.363	0.592	0.681	0.771
DR1#2	0.017	0.058	0.152	0.244	0.300	0.396	0.415	0.622
DR1#3	0.030	0.096	0.241	0.369	0.415	0.700	0.757	0.815
DR9#1	0.013	0.041	0.121	0.192	0.248	0.366	0.387	0.408
DR9#2	0.006	0.022	0.056	0.112	0.135	0.285	0.339	0.391
DR9#3	0.001	0.002	0.006	0.012	0.018	0.041	0.063	0.128
DR9#4	0.001	0.001	0.004	0.010	0.015	0.027	0.039	0.057

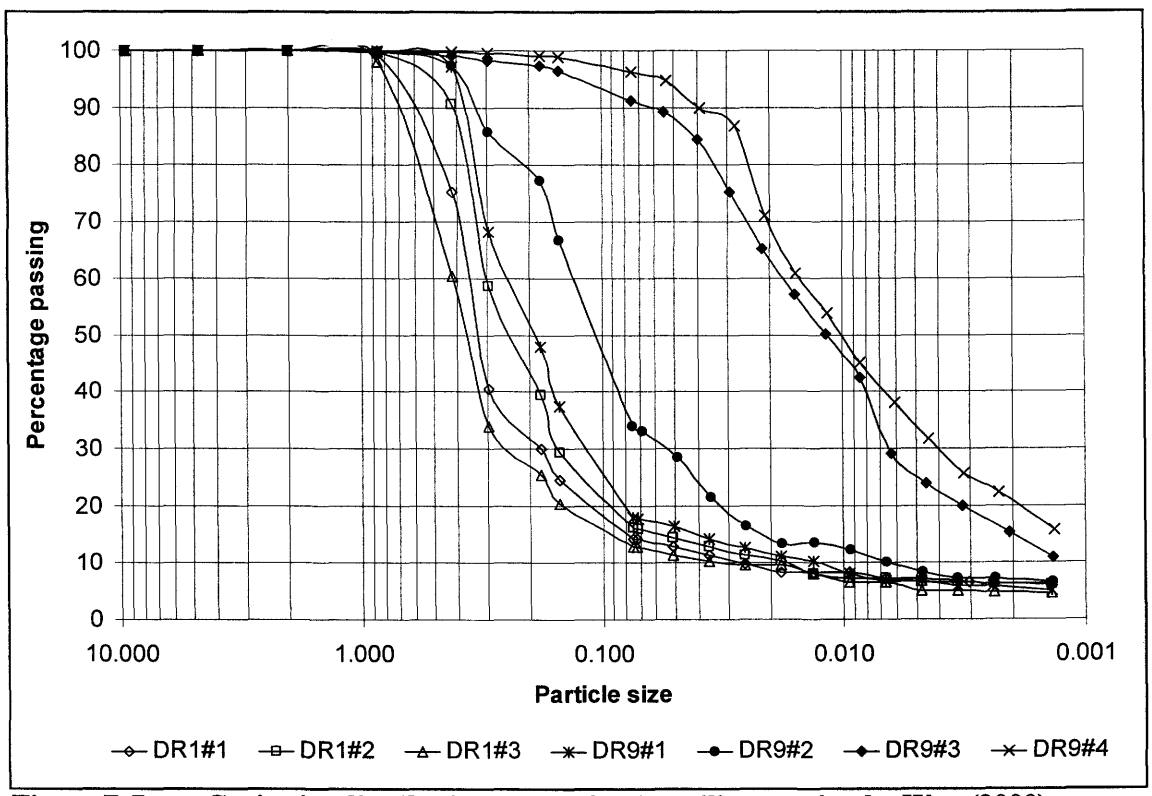

Figure B.7: Grain size distribution curves for the tailings testing by Wog (2000).

B.10 Summary Statistics of Grain Size Distribution Data

Tables B.18 through B.27 contains summary statistics on all 66 grain size distributions tests performed on the Kidston tailings as reported in this Appendix.

Table B.18: Summary statistics table of the sand, silt and clay content of the tailings, the coefficients of uniformity and curvature and the USCS classification of the combined Kidston tailings samples tested on record.

Sample no.	% Sand	% Silt	% Clay	C_u	C_c	Classification
Total number of samples	66	66	66	66	66	-
Mean value	54.6	24.3	21.1	9.53	1.59	SM
Average value	64.7	31.2	4.1	12.37	1.87	SM
Minimum value	3.0	4.6	0.01	1.50	0.34	-
Maximum value	95.2	85.6	28.5	37.89	5.44	-
Standard deviation	24.8	21.5	5.8	8.68	1.16	-

Table B.19: Summary statistics table of the sand, silt and clay content of the tailings, the coefficients of uniformity and curvature of all the combined well-graded sand (SW) tailings tested on record.

Sample no.	% Sand	% Silt	% Clay	C_u	C_c
Total number of samples	21	21	21	21	21
Mean value	70.4	26.1	0.7	11.87	1.85
Average value	71.0	27.5	1.6	12.90	1.90
Minimum value	54.8	12.6	0.1	6.38	1.10
Maximum value	86.6	39.7	7.0	37.89	2.61
Standard deviation	9.0	8.3	2.0	6.59	0.46

Table B.20: Summary statistics table of the sand, silt and clay content of the tailings, the coefficients of uniformity and curvature of all the combined poorly-graded sand (SP) tailings tested on record.

Sample no.	% Sand	% Silt	% Clay	C_u	C_c
Total number of samples	7	7	7	7	7
Mean value	91.3	6.5	0.7	3.41	1.18
Average value	91.3	6.7	1.9	3.45	1.18
Minimum value	85.8	4.6	0.0	2.57	1.05
Maximum value	95.2	9.9	4.3	4.23	1.35
Standard deviation	3.0	1.8	1.8	0.58	0.10

Table B.21: Summary statistics table of the sand, silt and clay content of the tailings, the coefficients of uniformity and curvature of all the combined silty sand (SM) tailings tested on record.

Sample no.	% Sand	% Silt	% Clay	C_u	C_c
Total number of samples	26	26	26	26	26
Mean value	72.5	20.2		11.03	1.96
Average value	73.4	23.3	3.4	14.30	2.44

Table B.21: Summary statistics table of the sand, silt and clay content of the tailings, the coefficients of uniformity and curvature of all the combined silty sand (SM) tailings tested on record.

Sample no.	% Sand	% Silt	% Clay	C_u	C_c
Minimum value	54.7	7.9	0.0	4.03	0.72
Maximum value	89.1	43.6	7.0	36.99	5.44
Standard deviation	11.5	12.0	2.6	10.35	1.55

Table B.22: Summary statistics table of the sand, silt and clay content of the tailings, the coefficients of uniformity and curvature of all the combined fine sand (ML) tailings tested on record.

Sample no.	% Sand	% Silt	% Clay	C_u	C_c
Total number of samples	12	12	12	12	12
Mean value	14.0	68.4		8.58	0.92
Average value	19.4	69.4	11.3	12.47	0.99
Minimum value	3.0	51.4	0.0	1.50	0.34
Maximum value	46.7	85.6	28.5	22.74	1.88
Standard deviation	15.2	11.7	10.1	7.94	0.37

Table B.23: Summary of the tailings size fractions for all the Kidston tailings samples tested on record.

Sample no.	D_{10} (mm)	D_{15} (mm)	D_{30} (mm)	D_{50} (mm)	D_{60} (mm)	D_{85} (mm)	D_{90} (mm)	D_{95} (mm)
Total number of samples	66	66	66	66	66	66	66	66
Mean value	0.015	0.025	0.059	0.113	0.144	0.261	0.311	
Average value	0.027	0.041	0.085	0.149	0.183	0.314	0.366	0.438
Minimum value	0.001	0.001	0.002	0.005	0.007	0.020	0.027	0.000
Maximum value	0.098	0.120	0.241	0.369	0.415	0.700	0.757	0.815
Standard deviation	0.025	0.033	0.056	0.083	0.094	0.147	0.167	0.200

Table B.24: Summary of the tailings size fractions for all the well-graded sand (SW) tailings samples tested on record.

Sample no.	D_{10} (mm)	D_{15} (mm)	D_{30} (mm)	D_{50} (mm)	D_{60} (mm)	D_{85} (mm)	D_{90} (mm)	D_{95} (mm)
Total number of samples	21	21	21	21	21	21	21	21
Mean value	0.016	0.027	0.075	0.149	0.190	0.338	0.394	
Average value	0.019	0.032	0.082	0.156	0.198	0.349	0.408	0.465
Minimum value	0.003	0.008	0.031	0.092	0.122	0.219	0.259	0.000
Maximum value	0.038	0.079	0.172	0.272	0.322	0.554	0.660	0.765
Standard deviation	0.010	0.020	0.037	0.051	0.057	0.093	0.112	0.162

Table B.25: Summary of the tailings size fractions for the poorly graded sand (SP) tailings samples tested on record.

Sample no.	D_{10} (mm)	D_{15} (mm)	D_{30} (mm)	D_{50} (mm)	D_{60} (mm)	D_{85} (mm)	D_{90} (mm)	D_{95} (mm)
Total number of samples	7	7	7	7	7	7	7	7
Mean value	0.080	0.098	0.160	0.236	0.273	0.432	0.506	0.589
Average value	0.081	0.099	0.162	0.238	0.276	0.443	0.524	0.615

Table B.25: Summary of the tailings size fractions for the poorly graded sand (SP) tailings samples tested on record.

Sample no.	D_{10} (mm)	D_{15} (mm)	D_{30} (mm)	D_{50} (mm)	D_{60} (mm)	D_{85} (mm)	D_{90} (mm)	D_{95} (mm)
Minimum value	0.061	0.076	0.129	0.177	0.201	0.298	0.326	0.354
Maximum value	0.098	0.120	0.182	0.267	0.315	0.534	0.645	0.755
Standard deviation	0.012	0.015	0.020	0.034	0.043	0.104	0.139	0.179

Table B.26: Summary of the tailings size fractions for the silty sand (SM) tailings samples tested on record.

Sample no.	D_{10} (mm)	D_{15} (mm)	D_{30} (mm)	D_{50} (mm)	D_{60} (mm)	D_{85} (mm)	D_{90} (mm)	D_{95} (mm)
Total number of samples	26	26	26	26	26	26	26	26
Mean value	0.018	0.035	0.084	0.160	0.199	0.340	0.386	0.477
Average value	0.025	0.044	0.097	0.173	0.212	0.355	0.403	0.497
Minimum value	0.005	0.011	0.034	0.089	0.113	0.205	0.241	0.278
Maximum value	0.066	0.096	0.241	0.369	0.415	0.700	0.757	0.815
Standard deviation	0.020	0.029	0.054	0.074	0.079	0.116	0.126	0.149

Table B.27: Summary of the tailings size fractions for the fine sand (ML) tailings samples tested on record.

Sample no.	D_{10} (mm)	D_{15} (mm)	D_{30} (mm)	D_{50} (mm)	D_{60} (mm)	D_{85} (mm)	D_{90} (mm)	D_{95} (mm)
Total number of samples	12	12	12	12	12	12	12	12
Mean value	0.004	0.005	0.010	0.021	0.030	0.071	0.096	0.140
Average value	0.013	0.014	0.018	0.030	0.041	0.089	0.117	0.160
Minimum value	0.001	0.001	0.002	0.005	0.007	0.020	0.027	0.046
Maximum value	0.043	0.046	0.054	0.065	0.090	0.210	0.245	0.280
Standard deviation	0.018	0.019	0.021	0.024	0.031	0.061	0.074	0.082

B.11 References

American Society for Testing and Materials (ASTM). 1996. Standard test method for particle size analysis of soils (D422-63; reapproved 1990). *In* 1996 Annual Book of ASTM Standards, Volume 4.08. ASTM, Philadelphia, PA, USA, pp. 10-16.

Gutteridge, Haskins and Davey Pty Ltd. (1987). Kidston Project; Interim Report on Tailings Disposal. Consultants Report to Kidston Gold Mines Limited. Brisbane, Queensland, Australia. July, 9 pages.

Holtz, R.D., Kovacs, W.D. (1981). An Introduction to Geotechnical Engineering. Prentice-Hall Civil Engineering and Engineering Mechanics Series, N.M. Newmark and W.J. Hall, Editors, Prentice-Hall, Englewood Cliffs, New Jersey, U.S.A.

O'Kane, M. (1997). Laboratory characterization of Kidston tailing samples #1/7 & #2/7. Unpublished data in Kidston file, Unsaturated Soils Group, Department of Civil Engineering, University of Saskatchewan, Saskatoon, Canada.

Rassam, D.W. (1998). Engineering Behavior of Metalliferous Tailings and Waste Rock Relevant to their Disposal and Rehabilitation. P.hD. dissertation, Department of Civil Engineering, University of Queensland, Brisbane, Australia.

Williams, D.J. (2000a). Tailings Dam Research Project; Report on Preliminary Testing. Report to Mr. Nick Currey, Kidston Gold Mines Limited. Department of Civil Engineering, University of Queensland, Brisbane, Australia. 20 January, 10 pages.

Williams, D.J. (2000b). Tailings Dam Research Project; Additional Grain Size Distribution Data along Section Line C and D of the Kidston Tailings Dam. Report to Mr. Maritz Rykaart, University of Saskatchewan. Department of Civil Engineering, University of Queensland, Brisbane, Australia. June.

Wog, K. (2000). Laboratory characterization of Kidston tailings samples. Unpublished data, Department of Civil Engineering, University of Saskatchewan, Saskatoon, Canada.

This page was intentionally left blank.

APPENDIX C

Falling Head Permeability Test Data

C.1 Introduction

Data with respect to falling head permeability tests performed on the Kidston tailings by the author, as well as one sample tested by O'Kane (1997) are presented here.

C.2 Falling Head Permeability Test Data Analysis

The Modified Odoemeter apparatus was used in combination with a falling head hydraulic conductivity test (O'Kane, 1995). Table C.1 contains the measured falling head permeability's at each of the loads for each of the tests performed on the Kidston tailings. Figure C.1 presents the falling head hydraulic conductivities as a function of void ratio.

Table C.1: Falling head permeability's as measured using the Modified Odoemeter apparatus (O'Kane, 1995) for the Kidston tailings.

Test no. #1A		Test no. #1B		Test no. #1C	
Load (kPa)	Permeability (m/s)	Load (kPa)	Permeability (m/s)	Load (kPa)	Permeability (m/s)
13.5	3.68E-06	13.5	5.00E-06	13.8	3.79E-06
36.2	5.45E-06	36.0	6.36E-06	36.3	3.49E-06
75.5	5.02E-06	75.6	5.50E-06	75.5	3.50E-06
155.3	6.20E-06	158.1	5.88E-06	155.4	4.60E-06
314.7	5.22E-06	318.8	5.54E-06	314.8	4.09E-06
647.7	5.27E-06	651.7	4.15E-06	647.7	3.10E-06
1250.1	5.16E-06	1251.3	4.03E-06	1250.2	2.64E-06
314.7	4.67E-06	318.8	1.58E-06	314.8	2.28E-06
75.4	4.69E-06	75.6	3.38E-06	75.5	2.08E-06
24.9	4.70E-06	24.8	3.41E-06	25.2	1.90E-06
2.4		2.2		13.8	1.63E-06
Test no. #1D		**Test no. #2A**		**Test no. #2B**	
Load (kPa)	Permeability (m/s)	Load (kPa)	Permeability (m/s)	Load (kPa)	Permeability (m/s)
13.3	5.23E-06	13.6	4.33E-06	13.3	4.73E-06
24.7	6.26E-06	36.2	3.45E-06	35.8	4.43E-06
63.8	6.18E-06	75.6	3.19E-06	75.0	4.38E-06
142.5	5.03E-06	158.0	4.30E-06	157.0	2.07E-06
304.0	5.25E-06	318.7	4.43E-06	316.5	2.07E-06
634.7	5.15E-06	651.6	4.06E-06	647.1	2.10E-06

Table C.1: Falling head permeability's as measured using the Modified Odoemeter apparatus (O'Kane, 1995) for the Kidston tailings.

1230.0	4.85E-06	1251.1	4.74E-06	1242.4	2.23E-06
304.0	4.71E-06	318.7	4.39E-06	316.5	3.11E-06
63.8	4.74E-06	75.6	5.46E-06	75.0	3.27E-06
13.5	4.56E-06	24.9	5.49E-06	24.5	2.96E-06
2.2	4.61E-06	13.6	5.50E-06	2.2	3.62E-06
Test no. #2C		**Test no. #2D**		**O'Kane (1997)**	
Load (kPa)	**Permeability (m/s)**	**Load (kPa)**	**Permeability (m/s)**	**Load (kPa)**	**Permeability (m/s)**
13.8	4.80E-06	13.6	3.82E-06	11.8	
36.3	4.76E-06	36.2	4.87E-06	38.1	3.98E-09
75.5	4.71E-06	75.7	6.45E-06	202.5	1.08E-08
155.4	4.66E-06	158.3	6.79E-06	533.0	2.29E-09
314.8	5.31E-06	318.9	7.65E-06	1029.4	2.42E-09
647.7	5.53E-06	651.9	1.18E-06	533.0	1.37E-10
1250.2	6.01E-06	1251.4	7.89E-06	202.5	1.85E-09
314.8	5.74E-06	318.9	7.89E-06	2.0	2.45E-09
75.5	5.49E-06	75.7	7.92E-06		
24.9	5.51E-06	24.9	2.13E-06		
2.5	5.53E-06	2.3	7.49E-06		

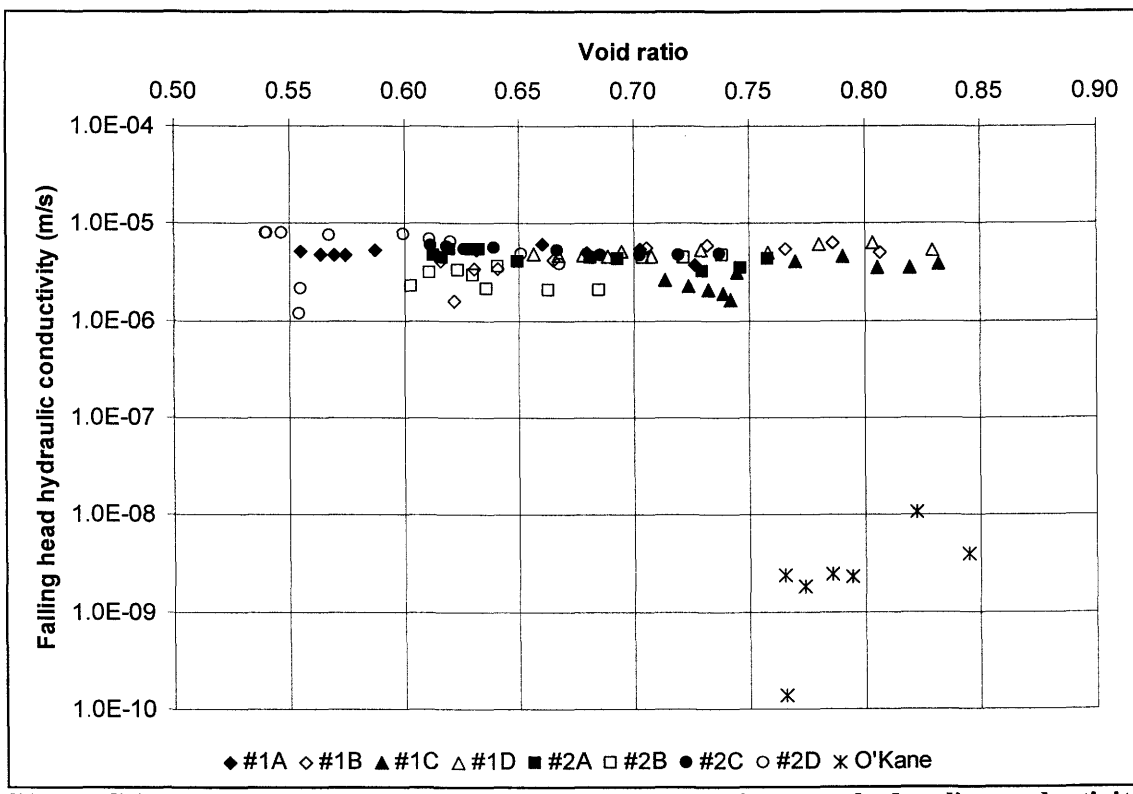

Figure C.1: Void ratio versus falling head permeability tests hydraulic conductivity plot for the 8 falling head permeability tests performed by the author and 1 by O'Kane (1997).

C.3 References

O'Kane, M. (1995). Instrumentation and Monitoring of an Engineered Soil Cover System for Acid Generating Mine Waste. M.Sc. Thesis, department of Civil Engineering, University of Saskatchewan, Saskatoon, Canada. 303 pages.

O'Kane, M. (1997). Laboratory characterization of Kidston tailing samples #1/7 & #2/7. Unpublished data in Kidston file, Unsaturated Soils Group, Department of Civil Engineering, University of Saskatchewan, Saskatoon, Canada.

This page was intentionally left blank.

APPENDIX D

Soil Water Characteristic Curve Test Data

D.1 Introduction

Data for the soil water characteristic tests performed on the Kidston tailings by the author, as well as summaries of all the testing done by other researchers on the Kidston tailings, as reported in Chapter 4 are presented here.

D.2 Testing Procedure for Soil Water Characteristic Curve Testing

The soil water characteristic curves (SWCC) were determined using the axis translation technique, using the modified pressure plate apparatus (O'Kane, 1995). The matric suction applied to the samples ranged from 0 to 300 kPa. Each sample was prepared by obtaining a representative sample split from the sample bag. A slurried sample was then placed into the testing apparatus using distilled water to mix the slurry.

Tempe cells was used for the testing and bottom porous plates with air entry values (AEV) of 100, 300 and 500 kPa was used. Table D.1 list the tested samples and the corresponding test pressure range and porous plate AEV.

Table D.1: Details of SWCC tests conducted by the author on the Kidston tailings.

Test no.	Porous disk AEV	Test pressure range	Comment
1/7A	500 kPa	0 – 40 kPa	Test stopped prematurely
1/7B	500 kPa	0 – 7 kPa	Test stopped prematurely
1/7C	100 kPa	0 – 40 kPa	Test stopped prematurely
2/7A	100 kPa	0 – 95 kPa	-
2/7B	100 kPa	0 – 4.5 kPa	Test stopped prematurely
1/7A new	100 kPa	0 – 95 kPa	-
1/7B new	500 kPa	0 – 200 kPa	-
2/7A new	500 kPa	0 – 300 kPa	-
2/7B new	500 kPa	0 – 200 kPa	-

D.3 SWCC Testing Completed by the Author

The detailed results of the soil water characteristic curve tests on the Kidston tailings by the author are listed in Tables D.2 and D.3.

Table D.2: Soil water characteristic curve data for the five fine tailings samples tested by the author.

Kidston #1A		Kidston #1B		Kidston #1C		New #1A		New #1B	
Suction (kPa)	Vol. water content	Suction (kPa)	Vol. water content	Suction (kPa)	Vol. water content	Suction (kPa)	Vol. water content	Suction (kPa)	Vol. water content
0.01	0.426	0.01	0.446	0.01	0.44	0.01	0.439	1.00	0.436
0.60	0.421	0.50	0.389	0.60	0.42	0.50	0.438	2.00	0.430
0.85	0.417	1.00	0.388	0.85	0.42	1.00	0.439	3.00	0.412
1.05	0.419	1.50	0.384	1.10	0.43	2.00	0.430	4.00	0.374
1.30	0.422	2.00	0.383	1.95	0.42	3.00	0.429	5.00	0.283
1.80	0.421	2.70	0.378	2.95	0.42	4.00	0.428	6.00	0.199
2.80	0.421	3.20	0.375	3.95	0.39	5.00	0.245	7.00	0.151
3.80	0.422	3.70	0.339	4.95	0.29	5.50	0.213	8.00	0.109
4.80	0.420	4.20	0.314	5.95	0.21	6.00	0.173	9.00	0.101
5.80	0.420	4.70	0.230	10.00	0.13	6.50	0.150	10.00	0.101
6.80	0.420	5.70	0.128	20.00	0.07	7.00	0.133	25.00	0.037
7.80	0.155			30.00	0.07	7.50	0.130	50.00	0.028
8.80	0.154			40.00	0.05	9.00	0.128	75.00	0.026
10.00	0.069					10.00	0.084	100.00	0.024
20.00	0.041					20.00	0.048	200.00	0.020
30.00	0.034					50.00	0.043		
40.00	0.030					75.00	0.036		
						95.00	0.026		

Table D.3: Soil water characteristic curve data for the five coarse tailings samples tested by the author.

Kidston #2A		Kidston #2B		New #2A		New #2B	
Suction (kPa)	Vol. water content	Suction (kPa)	Vol. water content	Suction (kPa)	Vol. water content	Suction (kPa)	Vol. water content
0.01	0.431	0.01	0.438	0.01	0.384	0.01	0.382
0.50	0.420	0.50	0.433	1.00	0.381	1.00	0.382
1.00	0.417	1.10	0.432	2.00	0.380	2.00	0.379
1.50	0.409	1.60	0.425	3.00	0.360	3.00	0.371
2.00	0.374	2.10	0.409	4.00	0.305	4.00	0.338
2.70	0.316	2.70	0.326	5.00	0.204	5.00	0.225
3.20	0.248	3.20	0.261	6.00	0.159	6.00	0.159
4.20	0.173	3.70	0.210	7.00	0.110	7.00	0.109
4.70	0.140	4.20	0.209	8.00	0.081	8.00	0.083
5.20	0.118			9.00	0.066	9.00	0.071
5.70	0.100			10.00	0.049	10.00	0.030
6.20	0.087			25.00	0.029	25.00	0.030
6.70	0.077			50.00	0.023	50.00	0.023
7.20	0.069			100.00	0.020	75.00	0.022
8.00	0.060			200.00	0.018	100.00	0.020

Table D.3: Soil water characteristic curve data for the five coarse tailings samples tested by the author.

Kidston #2A		Kidston #2B		New #2A		New #2B	
Suction (kPa)	Vol. water content	Suction (kPa)	Vol. water content	Suction (kPa)	Vol. water content	Suction (kPa)	Vol. water content
9.00	0.053			300.00	0.016	200.00	0.017
10.00	0.048						
25.00	0.033						
50.00	0.022						
75.00	0.019						
95.00	0.018						

D.4 Graphical Summary Plots For All The SWCC

This section contains graphs of all the soil water characteristic curves (Figures D.1, D.2, D.3, D.4 and D.5) discussed in this appendix. The graphs indicate the experimental data, and not any curve fitting techniques.

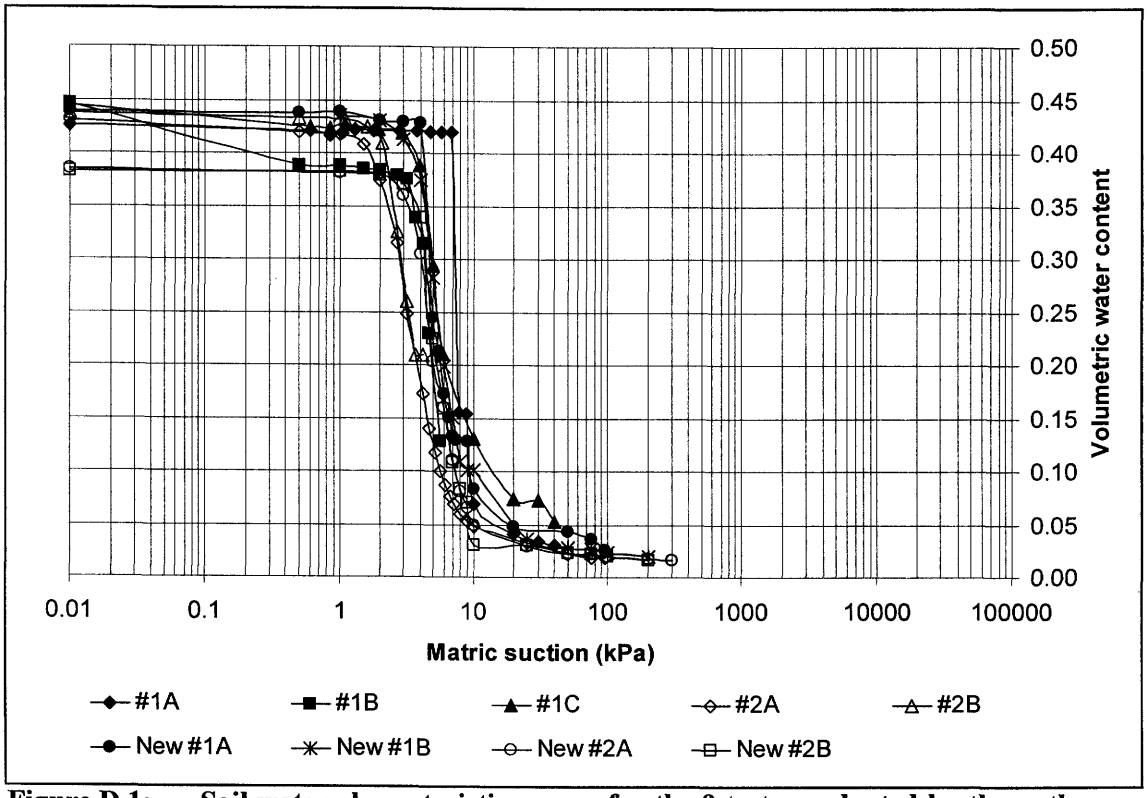

Figure D.1: Soil water characteristic curves for the 9 tests conducted by the author on the Kidston tailings.

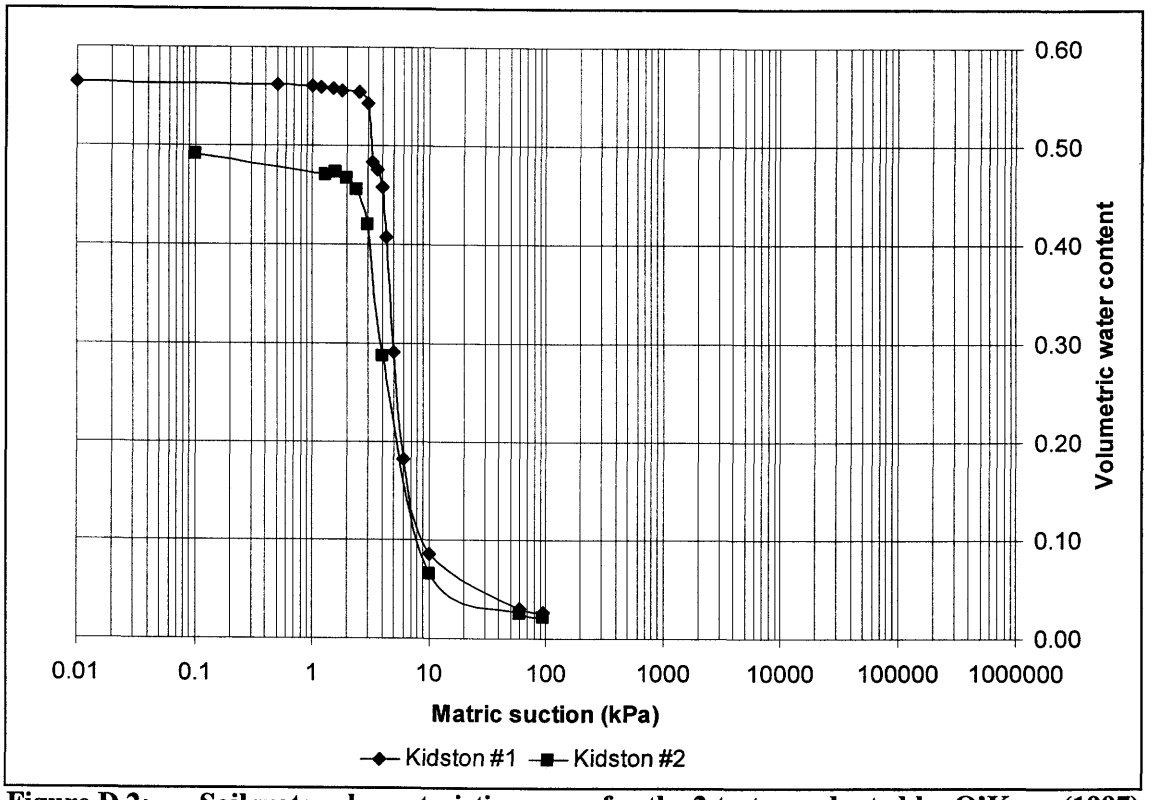

Figure D.2: **Soil water characteristic curves for the 2 tests conducted by O'Kane (1997) on the Kidston tailings.**

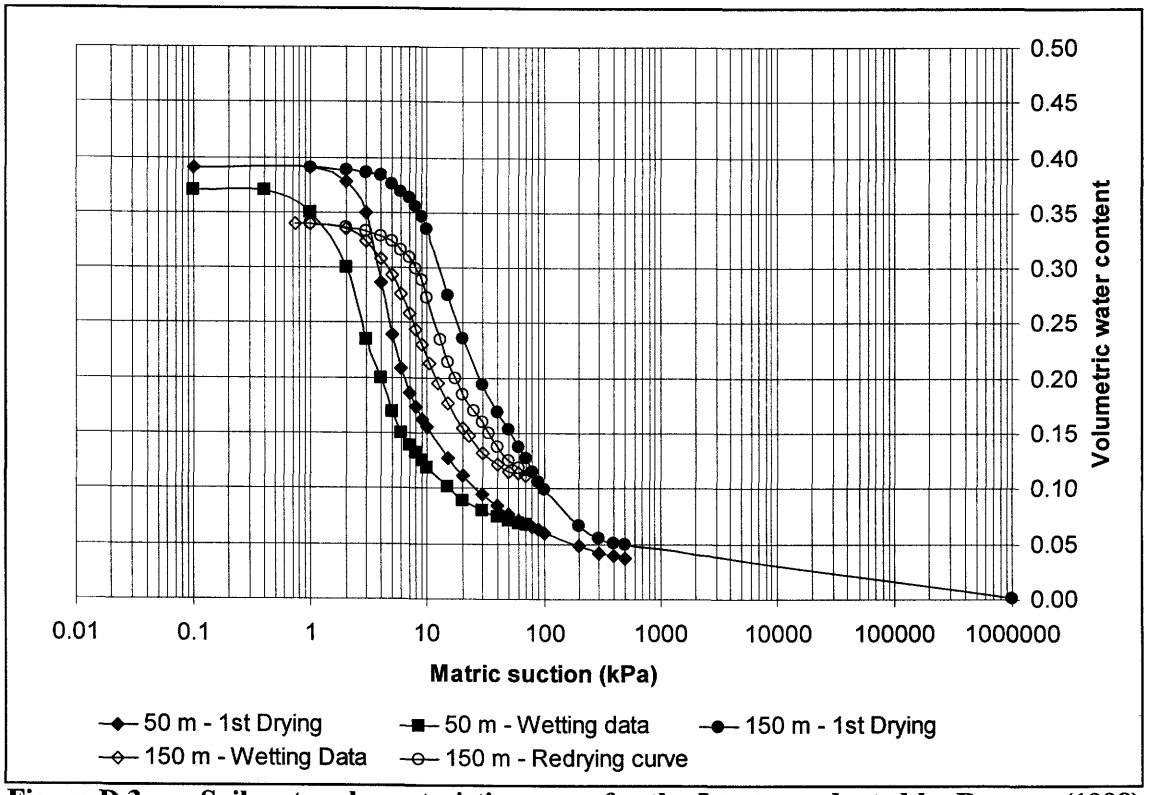

Figure D.3: **Soil water characteristic curves for the 5 tests conducted by Rassam (1998) on the Kidston tailings.**

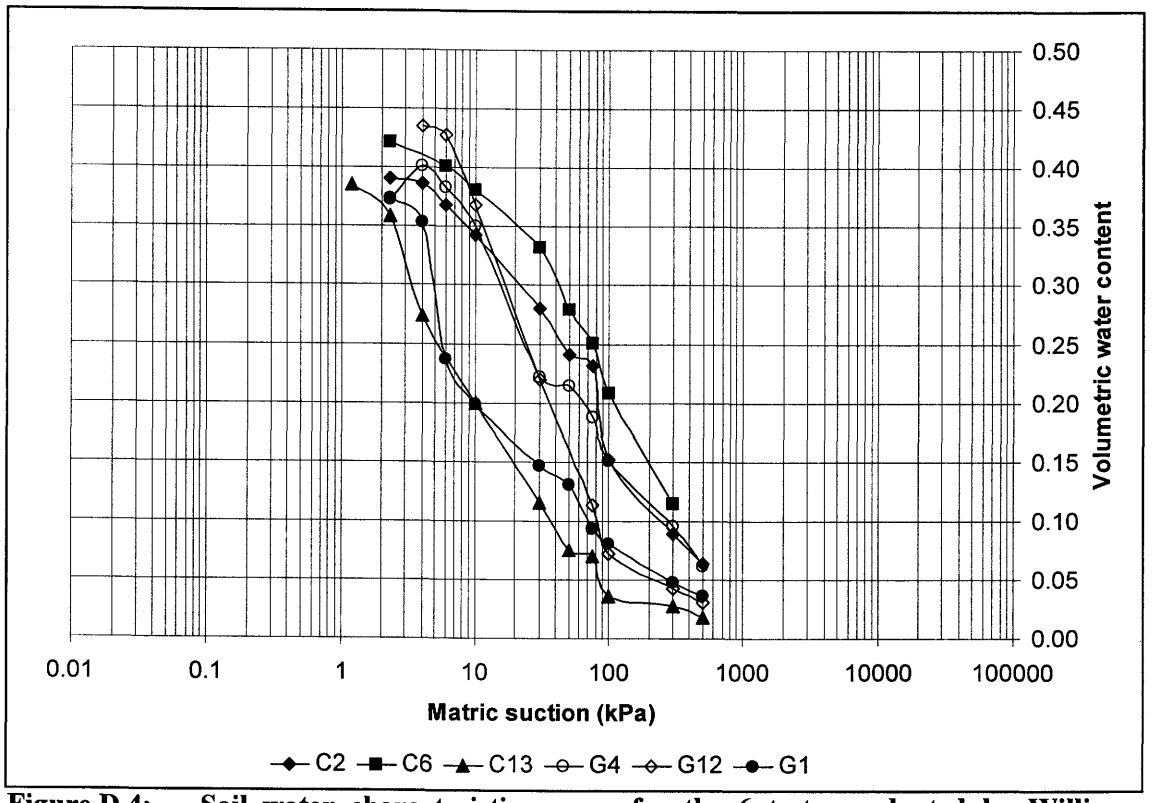

Figure D.4: **Soil water characteristic curves for the 6 tests conducted by Williams (2000) on the Kidston tailings.**

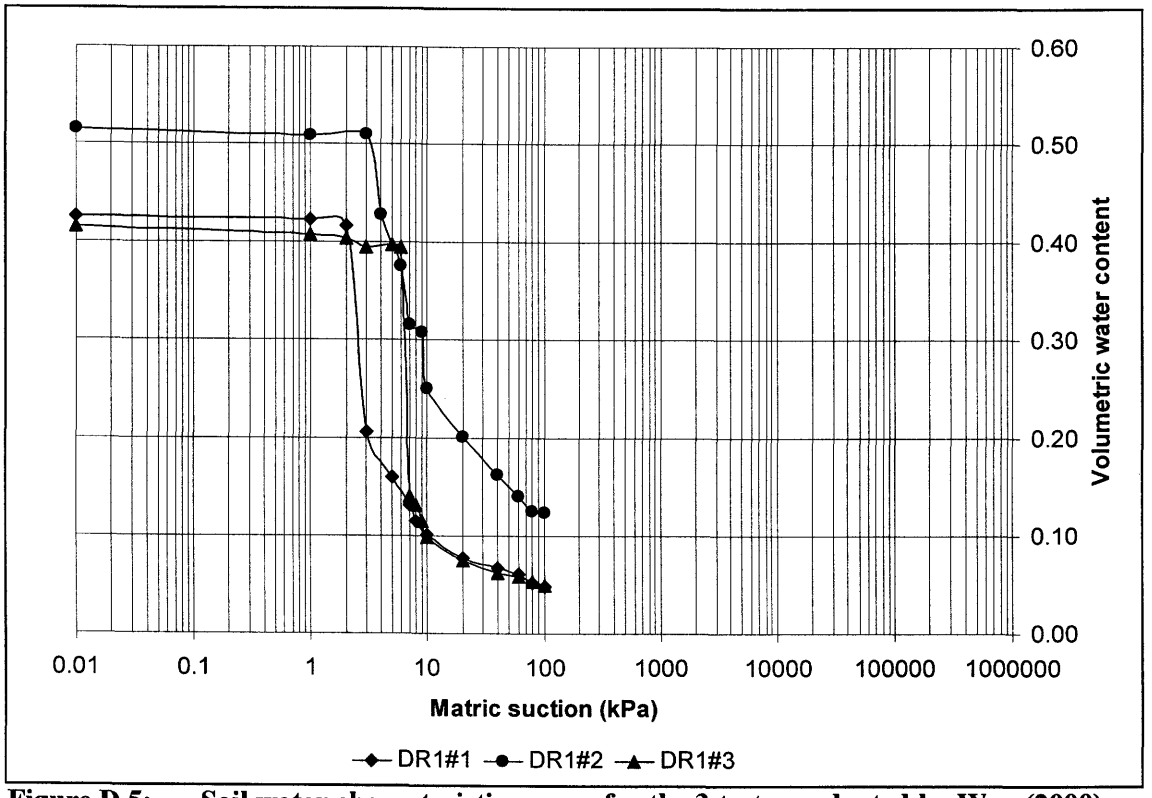

Figure D.5: **Soil water characteristic curves for the 3 tests conducted by Wog (2000) on the Kidston tailings.**

D.5 References

O'Kane, M. (1995). Instrumentation and Monitoring of an Engineered Soil Cover System for Acid Generating Mine Waste. M.Sc. Thesis, department of Civil Engineering, University of Saskatchewan, Saskatoon, Canada. 303 pages.

Rassam, D.W. (1998). Engineering Behavior of Metalliferous Tailings and Waste Rock Relevant to their Disposal and Rehabilitation. Ph.D. dissertation, Department of Civil Engineering, University of Queensland, Brisbane, Australia.

Williams, D.J. (2000). Tailings Dam Research Project; Report on Preliminary Testing. Report to Mr. Nick Currey, Kidston Gold Mines Limited. Department of Civil Engineering, University of Queensland, Brisbane, Australia. 20 January, 10 pages.

Wog, K. (2000). Laboratory characterization of Kidston tailings samples. Unpublished data, Department of Civil Engineering, University of Saskatchewan, Saskatoon, Canada.

APPENDIX E

Double-Ring Infiltrometer and Guelph Permeameter Testing Procedures

E.1 Introduction

Data analysis and test procedures for the double-ring infiltrometer and Guelph permeameter tests conducted on the Kidston tailings impoundment are presented here. The final section of this appendix contains sketches of the locations of all the Guelph permeameter tests in relation to the double-ring infiltrometer tests.

E.2 Double-Ring Infiltrometer Data Analysis Procedure

The double-ring infiltrometer test method is useful for field measurement of the infiltration rate of soils. The method consists of driving two open cylinders, one inside the other, into the ground, partially filling the rings with water, and then maintaining the water at a constant level. The volume of water added to the inner ring, to maintain the water level constant is the measure of the volume of water that infiltrates the soil. The purpose of the outer ring is to promote one-dimensional, vertical flow beneath the inner ring. The volume infiltrated during timed intervals is converted to an incremental infiltration velocity, (expressed in cm/hr) and plotted versus elapsed time. The maximum steady state or average incremental infiltration velocity, depending on the purpose of the test is equivalent to the infiltration rate (ASTM, 1996a).

The units of infiltration rate and hydraulic conductivity of soils are similar, but there is a distinct difference between these two quantities. They can only be directly related if the hydraulic boundary conditions are known, or can be reliably estimated, such as hydraulic gradient and the extent of lateral flow of water.

Many factors affect the infiltration rate, for example the soil structure, soil layering, condition of the soil surface, degree of saturation of the soil, chemical and physical nature of the soil and of the applied water, temperature of the water, and diameter and depth of imbedment of rings.

Identical results at any one site are thus unlikely. This test method is most successful on relatively uniform fine-grained soils, with an absence of plastic clays and gravel size particles and with moderate to low resistance to ring penetration. Soils with a hydraulic conductivity between 10^{-2} and 10^{-6} cm/s are best suited for this technique.

To convert the volume of liquid used during each measured time interval into an incremental infiltration rate for both the inner ring and the annular space (the difference between the inner ring and outer ring surface area), the following equations are used.

For the inner ring: $$V_{IR} = \frac{\Delta V_{IR}}{(A_{IR} \cdot \Delta t)} \quad [E.1]$$

Where, V_{IR} = inner ring incremental infiltration velocity (cm/h),
ΔV_{IR} = volume of liquid used during time interval to maintain constant head in the inner ring (cm^3),
A_{IR} = internal area of inner ring (cm^2), and
Δt = time interval (h).

For the annular space: $$V_A = \frac{\Delta V_A}{(A_A \cdot \Delta t)} \quad [E.2]$$

Where, V_A = annular space incremental infiltration velocity (cm/h),
ΔV_A = volume of liquid used during time interval to maintain constant head in the annular space (cm^3),
A_A = internal area of annular space (cm^2), and
Δt = time interval (h).

E.3 Double Ring Infiltrometer Test Procedure and Apparatus

Details specific to the field tests are documented here. The rings were driven 0.15 m into the tailing profile using a hammer and a block of wood. Around the ring edges, the tailings was not significantly disturbed, and thus not sealed using bentonite. This fact was proven when no leakage was observed during any of the tests. The head of water in the rings varied from test to

test, as the availability of test water was limited, and was governed by the infiltrability of the dry surface. The test water was from the Copperfield Dam, which supplies the mine with water. During the tests the pH was measured, giving an average value of 8.0, which was consistent with long term monitoring records of the dam water. Water and soil temperatures were taken during the tests using a standard mercury filed glass thermometer with a 0.5°C accuracy. Midway through the set of tests the thermometer was damaged, and no further temperature readings could be obtained. Outside temperatures and conditions however remained constant throughout the testing period, and thus originally measured soil and water temperatures are transferable to all data sets (all tests were done between 25 September and 9 October, 1999).

Each test was stopped when a steady state infiltration rate was reached. One test (test DR3) was continued for a period of two hours beyond the obvious point of steady state to check whether there would be any benefit to extend the tests beyond this point. The resultant infiltration rate remained at the steady state value, and from then on all tests were stopped on first observation of steady state, which appeared to be between two to three hours.

Before each test a hole was augured into the soil profile adjacent to where the test was to be conducted, and moisture content samples were collected at 0.1 m intervals. After the infiltration test, moisture content samples were again collected at 0.1 m intervals right in the center of the test site. These samples were subsequently tested for gravimetric water (moisture) content using standard test method ASTM D2216-63 (ASTM, 1996b). This testing was completed in the Kidston Gold Mine metallurgy laboratory.

After each double-ring infiltrometer test, the rings were removed and a trench was dug through the center of the wet zone up to a depth of at least 0.6 m. Samples were collected from each of the different exposed layer groups. These samples varied in size, as it was dependent on the amount of material available. The complete list of samples collected for testing at the University of Saskatchewan is listed in Appendix A. Layering was often so complex that sampling was limited to representative types (groups).

E.4 Guelph Permeameter Data Analysis Procedure

The Guelph permeameter is an in-hole constant-head permeameter, employing the Mariotte principle. The method involves measuring the steady-state rate of water recharge into

unsaturated soil from a cylindrical well hole, in which a constant depth (head) of water is maintained.

When a constant well height of water is established in a cored hole in the soil, a "bulb" of saturated soil with specific dimensions is rather quickly established. This "bulb" is very stable and its shape depends on the type of soil, the radius of the well, and the head of water in the well. The shape of the "bulb" is numerically described by the C factor used in the generalized equations below. Once the unique "bulb" shape is established the outflow of water from the well reaches a constant value which can be measured. The rate of this constant outflow of water, together with the diameter of the well, and height of water in the well can be used to accurately determine the field saturated hydraulic conductivity of the soil. This apparatus is most suited for soils in the hydraulic conductivity range of between 10^{-2} and 10^{-6} cm/s.

The Guelph permeameter comes as a complete field-ready kit, with all the equipment necessary to determine field saturated hydraulic conductivity, matric flux potential and soil sorptivity. The permeameter is broken down into four basic sections; (1) tripod assembly, (2) support tube and lower air tube fittings, (3) reservoir assembly, (4) well head scale and upper air tube fittings. In addition, auxiliary tools are included which consists of a soil auger (cutting diameter of 6.0 cm, and well height range of 2.5 to 25.0 cm) for excavating a well, sizing auger, and a collapsible water container for carrying water to the field. The soil auger, sizing auger, and well prep brush are all equipped with quick connect fitting for use on the same auger shaft (standard depth range of 15 to 75 cm).

The assembled permeameter is placed by centering the tripod over the well hole made using the soil auger. The permeameter is then slowly lowered into the well hole, and when placed on the well base, the tripod bushing is secured to stabilize the permeameter (SoilMoisture, 1986).

After the permeameter has been assembled, filled, and placed in the prepared well hole, the following procedure should be followed for making measurements. Verify that both reservoirs are connected and then establish the first well head height, H_1 (between 5 and 10 cm). Outflow of water from the permeameter into the soil is indicated by the rate of fall of water in the reservoir.

Note and record the water level in the selected reservoir and read against the scale stamped on the inner reservoir tube. Readings should be made at regular time intervals. The difference of readings at consecutive intervals, divided by the time interval, equals the rate of fall of water, R, in the reservoir. Continue monitoring the rate of fall of water in the reservoir until the rate does not significantly change, in three consecutive time intervals. This rate is called R_1 and is defined as the steady state rate of fall, of water in the reservoir at H_1.

Next, the well head height, H_2, (between 10 and 15 cm) is established. As before the rate of fall of water, R, in the reservoir is monitored until a stable value is reached. This rate is called R_2 and is defined as the steady state rate of fall, of water in the reservoir at H_2. The "Richards" analysis of steady-state discharge from a cylindrical well in unsaturated soil, as measured by the Guelph permeameter technique, accounts for all the forces that contribute to three dimensional flow of water into soils. These forces are; the hydraulic push of water into soil, the gravitational pull of liquid out through the bottom of the well, and the capillary pull of water out of the well into the surrounding soil. The Richard's analysis is the basis for the calculations used to determine field saturated hydraulic conductivity. The field saturated hydraulic conductivity, K_{fs}, can now be readily calculated using the equations in SoilMoisture (1986), based on which reservoir combination was used.

When using both reservoirs:

$$K_{fs} = (G_2)(X)(R_2) - (G_1)(X)(R_1) \qquad [E.3]$$

When using only the inner reservoir:

$$K_{fs} = (G_2)(Y)(R_2) - (G_1)(Y)(R_1) \qquad [E.4]$$

Where, X = reservoir constant used for the outer reservoir (35.69 cm^2),

Y = reservoir constant used for the inner reservoir (2.12 cm^2),

G_2 = empirical shape constant based on C-factor for the "bulb" dimension, and

G_1 = empirical shape constant based on C-factor for the "bulb" dimension.

The reservoir constants are unique to any Guelph permeameter apparatus, and the above values are only applicable to the equipment used for the tests done at Kidston Gold Mine. Due to the varying tailings properties H_1 and H_2 values were not consistent for all tests, resulting in different C-factors. Table E.1 lists the standard test parameters and the revised parameters that were used in the field.

Table E.1: Standard and revised H_1 and H_2 parameters for the Kidston Guelph permeameter testing.

Parameter	Standard	Revised
Well radius, a	3.0 cm	3.0 cm
First head of water, H_1	5.0 cm	10.0 cm
Second head of water, H_2	10.0 cm	15.0 cm

The C-factor is a numerically derived shape factor, which is dependent on the well radius and the head of water in the well. A C-factor graph in SoilMoisture (1986) is used to determine C-factors, for the cases listed in Table E.1 (see Table E.2).

Table E.2: C-factors for the Kidston Guelph permeameter test conditions (SoilMoisture, 1986).

Standard		Revised	
H/a ratio	C-factor	H/a ratio	C-factor
$H_1/a = 1.667$	0.860	$H_1/a = 3.333$	1.330
$H_2/a = 3.333$	1.330	$H_2/a = 5.000$	1.690

The empirical shape constants G_1 and G_2, from equations E.3 and E.4 is then calculated as follows:

$$G_2 = \frac{H_1 C_2}{\pi\left[2H_1H_2(H_2 - H_1) + a^2(H_1C_2 - H_2C_1)\right]} \qquad [E.5]$$

and,

$$G_1 = \frac{[H_2C_1]}{[H_1C_2]} \qquad [E.6]$$

Substitution of the values in Table E.1 and E.2 into Equations E.5 and E.6 provides the relevant G factors required for Equations E.3 and E.4 in order to calculate the field saturated hydraulic conductivity as listed in Table E.3.

Table E.3: Empirical shape constants G_1 and G_2.

Parameter	Standard	Revised
G_1	0.0055	0.0043
G_2	0.0043	0.0036

The results of measurements with the Guelph permeameter can indicate soil heterogeneity. When a negative K_{fs} value is calculated, it is indicative of the presence of a hydrologic discontinuity, typically caused by soil stratification or the presence of rodent and/or root holes. Normally additional measurements will be required to describe the nature of the heterogeneity.

E.5 Guelph Permeameter Test Procedure and Apparatus

The well depth for all tests was between 0.15 m and 0.25 m deep. The two constant head settings for each test varied according to the infiltrability, but was always between 0.05 m and 0.10 m for head #1 (H_1), and between 0.10 m and 0.15 m for head #2 (H_2).

For the 1999 set of tests, gravimetric moisture content of the soil immediately below the permeameter was measured, both before the start, and after completion of each test. The testing was done according to ASTM D2216-63 (ASTM, 1996b) in the Kidston Gold Mine metallurgy laboratorium. This moisture content was converted to a volumetric moisture content using a water density of 1 Mg/m^3, and a dry tailings density of 1.4 Mg/m^3.

Figure E.1 presents sketches of all the Guelph permeameter test locations with respect to the double ring infiltrometer tests.

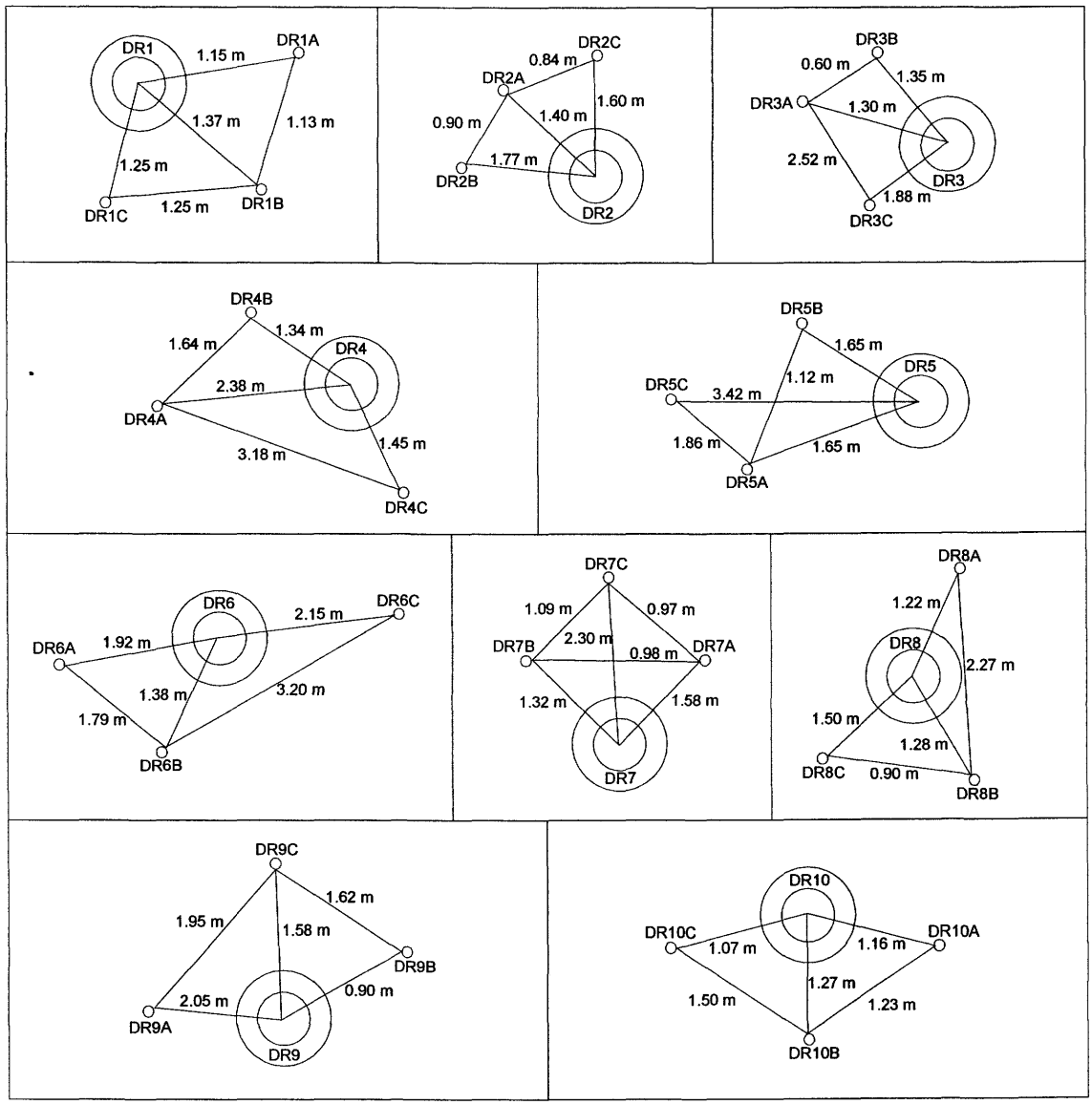

Figure E.1: Sketches of 10 of the double-ring infiltrometer tests performed on the Kidston tailings impoundment, in relation to the locations of the three Guelph permeameter tests carried out at each site.

E.6 References

American Society for Testing and Materials (ASTM). (1996a). Standard test method for infiltration rate of soil in field using double-ring infiltrometer. (D3385-94). *In* 1996 Annual Book of ASTM Standards, Volume 4.08. ASTM, Philadelphia, PA, USA, pp. 331-337.

American Society for Testing and Materials (ASTM). (1996b). Standard test method for gravimetric moisture content determination. (D2216-63). *In* 1996 Annual Book of ASTM Standards, Volume 4.08. ASTM, Philadelphia, PA, USA.

SoilMoisture Equipment Corp. (1986). Guelph Permeameter 2800KI Operating Instructions. Revision 8/86, 26 pages.

APPENDIX F

Piezometer Construction Details and Phreatic Level Data

F.1 Introduction

The details with respect to the piezometers that was installed in the Kidston tailings impoundment, both by the author and by other institutions are presented here. The appendix is concluded with graphs depicting the phreatic line elevation in each piezometer on the tailings impoundment.

F.2 Piezometer Construction Details

The sections that follow contain details regarding the construction and installation of three sets of piezometers. The first set consist of 10 piezometers installed in 1997 by the University of Queensland. The second set consist of 25 shallow piezometers installed by the author as part of this study and finally 10 deep piezometers installed by consultants for this study.

F.2.1 Piezometers by the University of Queensland

Kidston Gold Mines Limited installed 10 deep piezometers in the tailings impoundment in June 1997, and have been monitoring their phreatic levels, regularly since then. These piezometers were installed to gain clarity regarding specific seepage and stability issues on the impoundment (Williams, 1998; Douglas Partners, 1997), and were not spaced sufficiently to provide a good representation of the tailings impoundment phreatic surface. The piezometer locations are marked in Figure F.1 and the piezometer details are listed in Table F.1.

Table F.1: Details of the 10 deep piezometers installed by Douglas Partners under the direction of Prof. David Williams of the University of Queensland in 1997.

No.	Installed depth (m)	Slotted interval (m)	Top of pipe elevation (m)	Stick-up (m)	Dam surface elevation (m)	X co-ordinate	Y co-ordinate
SP1	14.80	1.0	556.600	0.440	556.160	199766.3	908768.8
SP2	15.47	1.0	556.800	0.270	556.530	199794.6	908781.7
SP4A	3.97	1.0	553.895	0.915	552.895	198407.5	908707.0
SP4B	6.03	1.0	553.720	0.860	552.860	198412.4	908699.8
SP4C	7.88	1.0	554.175	1.075	553.100	198416.8	908692.8
SP4D	10.02	1.0	554.080	1.010	553.070	198421.2	908705.8
SP5	9.80	1.0	554.740	1.400	553.340	198374.7	908771.7
SP6	9.92	1.0	555.190	1.330	553.860	198352.3	908806.7
SP7	6.73		556.390	0.130	556.260	197729.4	907762.9
SP8	4.82		553.750	0.980	552.770	197801.3	907402.9

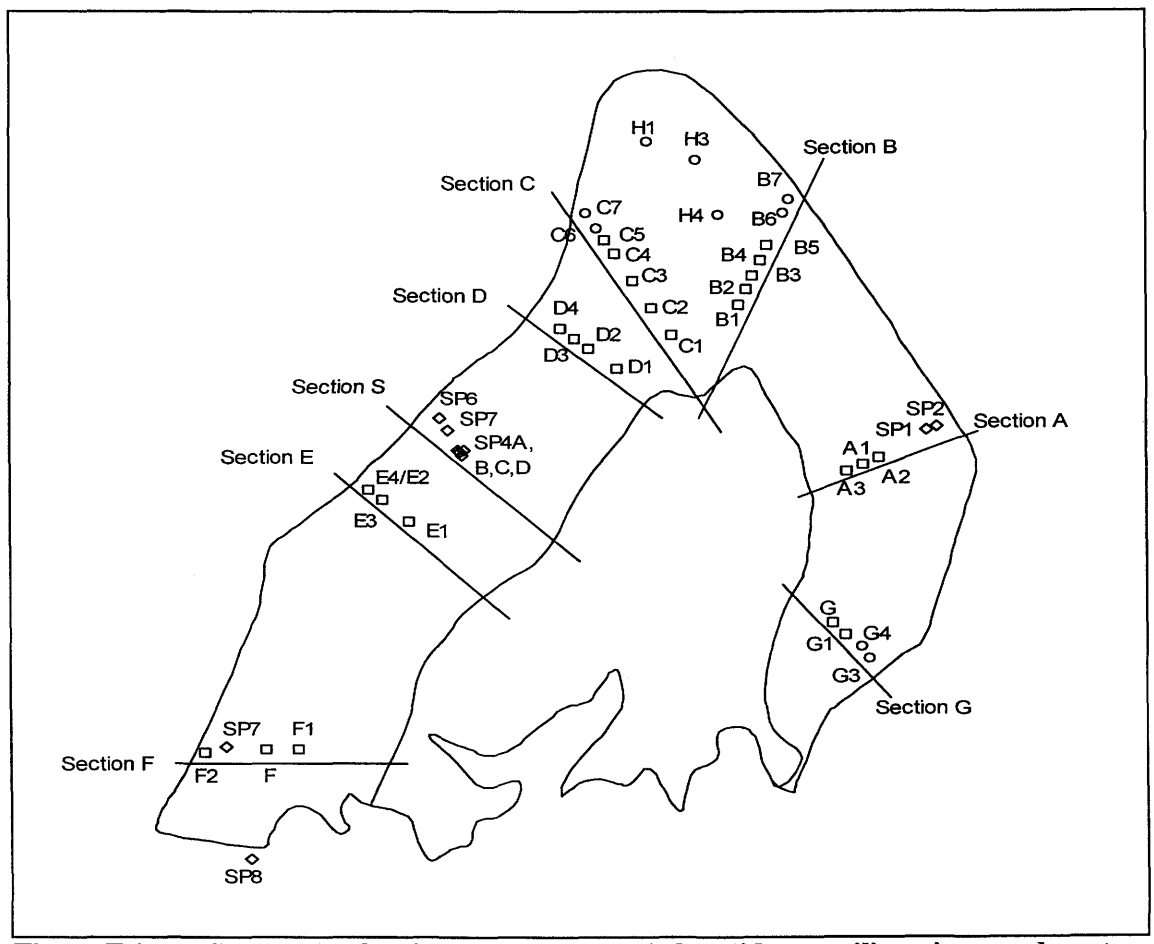

Figure F.1: Schematic showing a plan view of the Kidston tailings impoundment as well as all the piezometer locations and section lines (Diamonds = installed by University of Queensland; Squares = installed by author; Circles = installed by AGE).

The piezometer standpipes were installed during selected piezocone tests, by pushing 0.06 m diameter hollow rods to the target depth and inserting 0.025 m diameter PVC tubing down the center of the rods. The rods were then withdrawn, leaving a sacrificial steel tip and the PVC tubing in place. Prior to inserting the PVC tubing, the bottom 1.0 m was slotted and covered with a filter sock (Douglas Partners, 1997).

F.2.2 University of Saskatchewan Piezometers

The shallow piezometers installed as part of this program were designed to be simple, be assembled using basic equipment, and allow for installation by hand. Conventional piezometers are expensive and as a vast aerial coverage was required, hand augured installations proved to be the most cost efficient.

A 0.07 m diameter hole was augured into the tailings profile using a Canadian Forestry Service Hand Auger with a sand bit. The auger had a total reach of 6.5 m, which was the maximum depth that could be successfully reached. Each hole was augured to a depth of 1.0 m below water strike where possible, or if excessive sloughing occurred to whatever depth possible. Each final hole depth thus varied depending on site conditions.

Prior to auguring a hole the piezometer was made up and assembled, such that it could be installed immediately upon completion of the hole. The piezometer was constructed using 0.05 m internal diameter white PVC, Class 5, (belled) sewage pipe. The bottom 1.0 m of the pipe was slotted using a hacksaw with slots every 0.05 m, on opposite sides of the pipe at diagonal angles. The slots were at least 0.03 m long each. A 1.5 m long filter sock was then fitted around the slotted portion of the pipe. Prior to pulling the filter sock over the pipe a knot was tied at the bottom, and the other end of the filter sock was fixed to the pipe using copious amounts of duct tape. The entire assembled piezometer was pushed into the augured hole, and if some sloughing had occurred below the water strike level, the piezometer was lightly tapped down until the piezometer was installed at the determined depth (based on the hole depth). Above ground the piezometer was either extended, or cut off, such that approximately 1.0 m of the piezometer protruded above ground. A standard screw on type top cap was then fitted using PVC cement glue illustrated in Figure F.2.

Since the outside diameter of the piezometers was approximately 0.066 m it allowed for a fairly tight fit into the 0.07 m diameter auger hole. Therefore only the top collar at the surface was backfilled by hand, before being packed with some bentonite to ensure a seal which would prevent short-circuiting of rainfall down the sides of the piezometer.

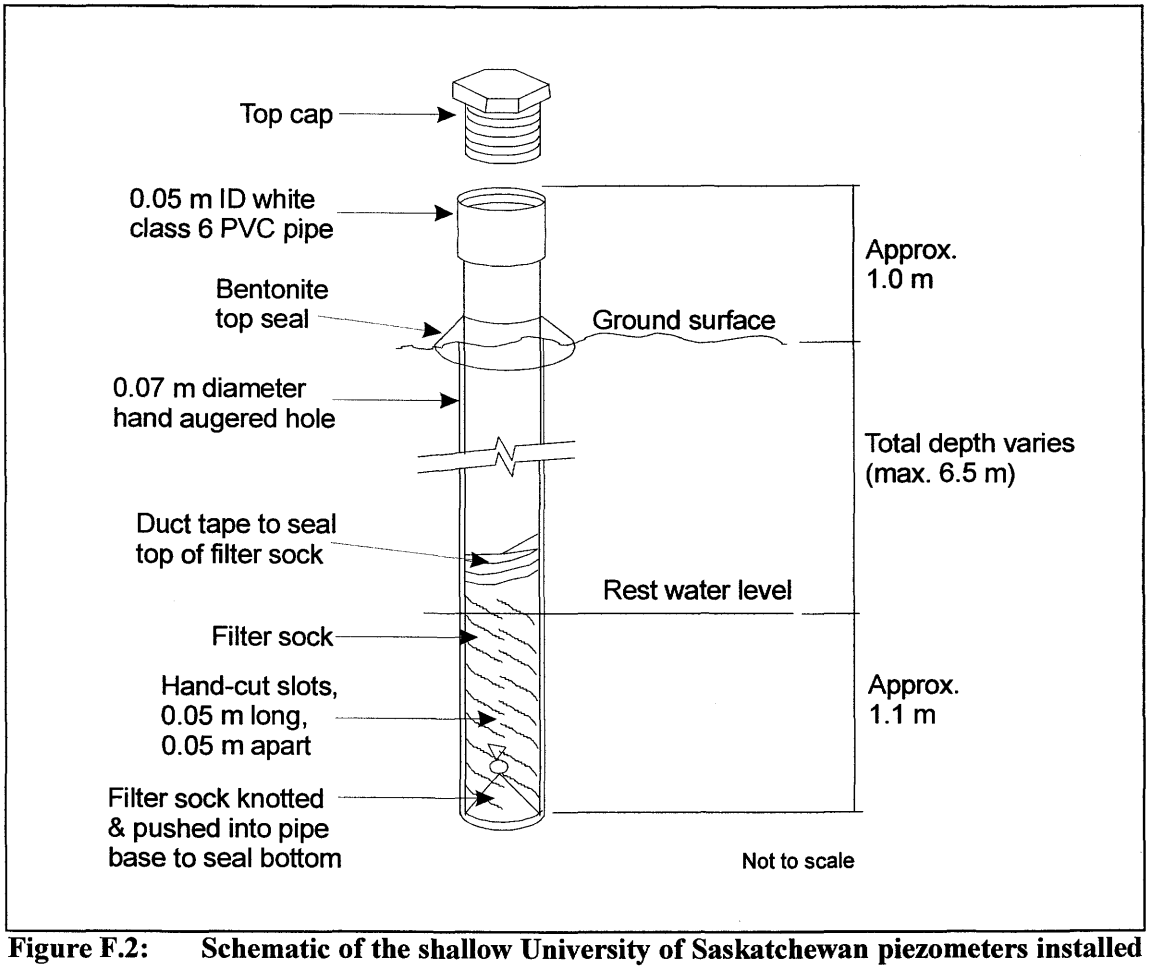

Figure F.2: Schematic of the shallow University of Saskatchewan piezometers installed on the Kidston tailings impoundment.

The exact depth of the piezometers was determined by marking the piezometers prior to installation, and thus once installation was completed it was easy to read off the exact depth. The top of each piezometer was subsequently surveyed in by the mine surveyor to provide the x, y and z co-ordinates. As the surveying was done using the top of the sealed cap of each piezometer as reference, it was necessary to apply a small correction to obtain the same reference as to where the dipmeter is read. This correction together with the other relevant information for each piezometer is listed in Table F.2.

Table F.2: Construction details of the University of Saskatchewan piezometers installed on the Kidston tailings impoundment in September 1999.

No.	Depth installed (m)	Cap height (m)	Survey level (mRL)	Cap correction (m)	Ground level (mRL)	X co-ordinate	Y co-ordinate	Water strike (mRL)	Estimated distance from wall (m)
G	5.30	0.72	555.744	0.023	554.001	908156.428	199497.0	4.22	200
G-1	6.03	1.25	555.660	0.010	554.400	908118.775	199531.6	Dry*	150
A-3	4.08	1.03	554.883	0.021	553.853	908637.3	199536.7	3.95	350
A-1	5.89	1.05	555.119	0.022	554.052	908658.0	199583.4	5.13	300
A-2	6.02	1.01	555.374	0.018	554.346	908678.8	199628.3	Dry*	250
B-1	4.26	1.04	555.333	0.024	554.269	909168.0	199224.9	3.79	400
B-2	4.15	1.04	555.665	0.019	554.606	909215.6	199245.5	4.08	350
B-3	4.93	1.09	555.915	0.020	554.805	909261.1	199265.3	4.50	300
B-4	5.88	0.92	556.037	0.014	555.103	909306.9	199285.4	4.92	250
B-5	6.07	0.97	556.356	0.019	555.367	909353.9	199306.0	5.51	200
C-1	3.42	0.78	554.785	0.024	553.981	909069.8	199027.0	2.84	500
C-2	4.58	0.91	555.487	0.025	554.552	909155.6	198972.3	3.28	400
C-3	4.62	1.02	556.154	0.020	555.114	909240.3	198918.2	4.05	300
C-4	6.20	1.03	556.616	0.019	555.567	909326.6	198863.3	5.45	200
C-5	6.33	1.00	556.721	0.021	555.700	909369.4	198835.9	6.50	150
D-1	3.52	0.99	555.018	0.021	554.007	908966.8	198868.0	2.83	250
D-2	4.55	0.92	555.497	0.025	554.552	909029.9	198788.6	3.50	150
D-3	5.15	0.87	555.761	0.023	554.868	909061.0	198749.3	3.96	100
D-4	6.16	0.95	556.191	0.020	555.221	909093.9	198707.8	4.64	50
E-1	4.23	0.84	555.618	0.015	554.763	908476.7	198262.1	3.16	200
E-3	6.29	0.92	556.340	0.023	555.397	908545.2	198186.8	4.85	100
E-4	6.20	0.99	556.893	0.026	555.877	908579.5	198148.8	6.50	50
F-1	2.75	1.03	555.575	0.010	554.535	907752.5	197943.7	2.10	300
F	3.39	0.98	555.997	0.010	555.007	907751.1	197845.8	2.25	200
F-2	3.35	1.06	557.254	0.010	556.184	907740.6	197670.8	2.01	20

**No water strike merely indicates that the water level is deeper than the maximum piezometer depth at that point.*

The purpose of installing the piezometers was to define the phreatic levels within the tailings impoundment with more accuracy. It was thus decided that installing the piezometers along a number of section lines through the tailings impoundment would render the best results. The University of Queensland piezometers already existed on the tailings impoundment, and the historic water levels in these were used to demarcate the new section lines. Where possible the existing piezometers were incorporated into section lines to maximize the data benefit.

As the piezometers that were to be installed had a maximum depth reach of 6.5 m, it was imperative to install them at locations where they would be of use. Seven section lines were subsequently selected based on available data from the 10 piezometers installed in 1997, and by visual observation of the layout. The section lines and the approximate piezometer locations are indicated in Figure F.1. Survey pegs was staked out at 100 m intervals from the wall towards

the pool along each section line. The approach along each section line was to hand auger the first piezometer hole at one of the demarcated positions where the likelihood of water strike within 6.5 m was good. If no strike was achieved, the drilling was ceased and a new hole was started at a point 50 m closer to the pool. The reverse was also true, that if a strike was achieved, a piezometer would be installed, and the next location would be at a distance of 50 or 100 m towards the wall depending on what the water strike was. By adopting this method it was possible to get the maximum benefit from the installed piezometers, and a total of 25 was thus installed.

F.2.3 Australasian Groundwater and Environmental Consultants (AGE) Piezometers

Due to the limitations of only having a 6.5 m reach in the University of Saskatchewan piezometers, a full profile of the phreatic level along each section line cannot be achieved. Kidston had however committed resources towards installing a number of deep piezometers on the tailings impoundment, and with the aid of the data gathered from this program, it was decided to drill the deep piezometers in locations along the section lines that would enhance the current data set. Details of the installed piezometers are summarized in Table F.3. The installation was done by Earthtech Consultants under the supervision of AGE (Earthtech Consultants, 1999; AGE, 2001). The author however selected the piezometer locations. The piezometers consisted of 0.06 m diameter PVC tubing pushed down machine augured holes. The bottom 3.0 m of each piezometer was slotted with a filter sock covering the slots. The standpipes above ground varied in length between 0.4 and 1.0 m.

Table F.3: Details of the 10 deep piezometers installed by Earthtech Consultants in November 1999 under supervision of Australasian Groundwater and Environmental Consultants (AGE).

No.	Installed depth (m)	Slotted interval (m)	Top of pipe elevation (m)	Stick-up (m)	Dam surface elevation (m)	X co-ordinate	Y co-ordinate
B6	21.0	3.0	555.641	0.570	555.071	199351.3	909459
B7	19.4	3.0	556.044	0.890	555.154	199368.9	909498
C6	unknown	unknown	556.100	0.750	555.350	198809.6	909407
C7	12.9	3.0	556.132	0.690	555.442	198780.3	909457
E2	14.0	3.0	557.000	0.570	556.430	198148.8	908580
G3	16.5	3.0	556.479	0.860	555.619	199601.3	908040
G4	15.0	3.0	555.696	0.880	554.816	199574.5	908079

Table F.3: Details of the 10 deep piezometers installed by Earthtech Consultants in November 1999 under supervision of Australasian Groundwater and Environmental Consultants (AGE).

No.	Installed depth (m)	Slotted interval (m)	Top of pipe elevation (m)	Stick-up (m)	Dam surface elevation (m)	X co-ordinate	Y co-ordinate
H1	16.0	3.0	558.417	0.835	557.582	198959.6	909681
H3	10.9	3.0	556.867	0.540	556.327	199101.7	909621
H4	5.4	3.0	555.437	0.420	555.017	199163.8	909453

F.3 Piezometer Phreatic Levels

The following section contains all the piezometer data collected since the installation of each piezometer. Piezometer reading frequency varied between one week and one month, depending on the season and mine personnel availability. Figure F.3 presents the pond level fluctuations at an exaggerated scale, showing clearly the seasonal fluctuations of the pond level. The results in Figures F.4 to F.13 have been grouped together in terms of the section line on which they are located (see Figure F.1), with the pond level included every time to show the relative relationship.

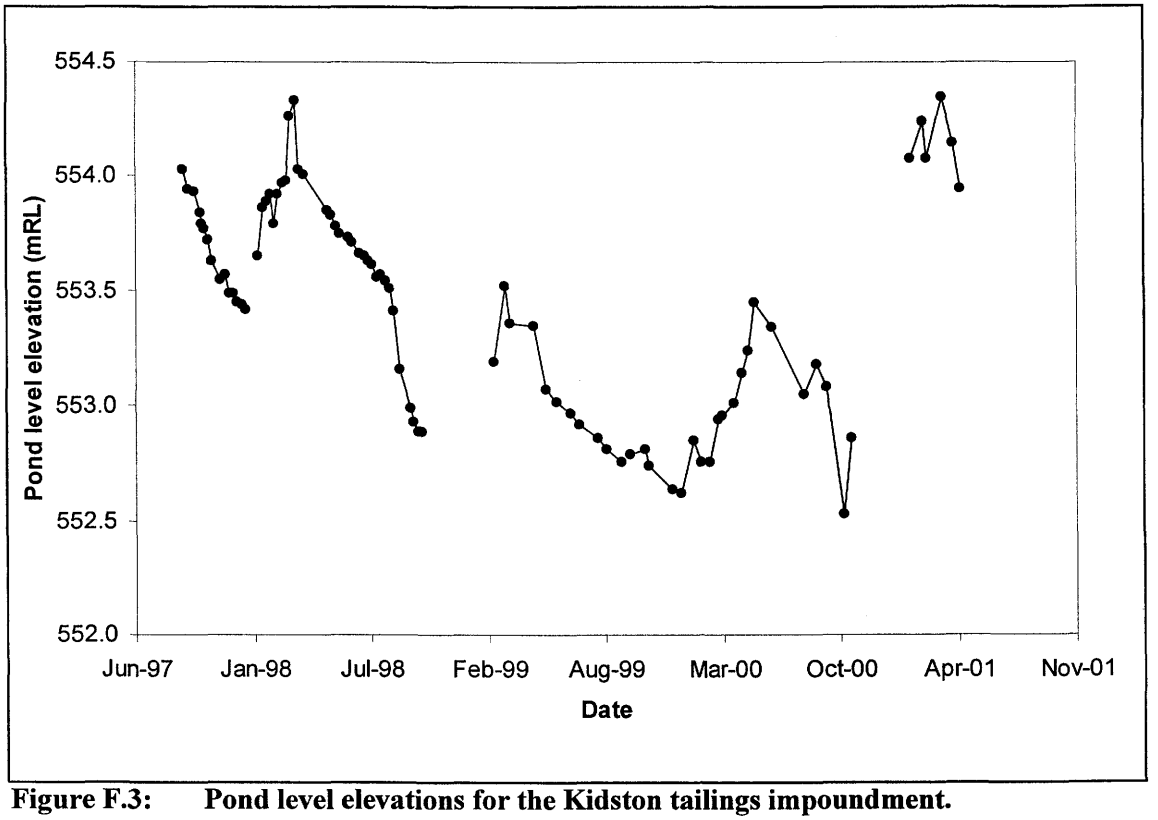

Figure F.3: Pond level elevations for the Kidston tailings impoundment.

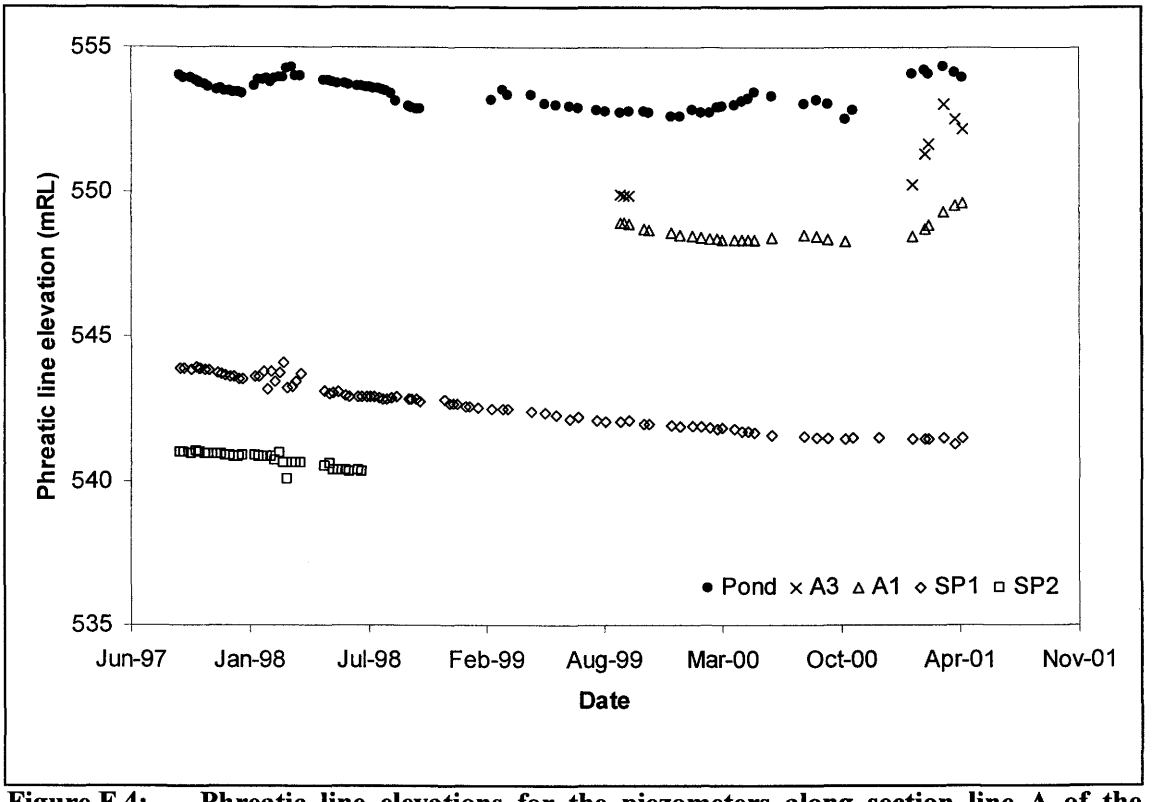

Figure F.4: **Phreatic line elevations for the piezometers along section line A of the Kidston tailings impoundment.**

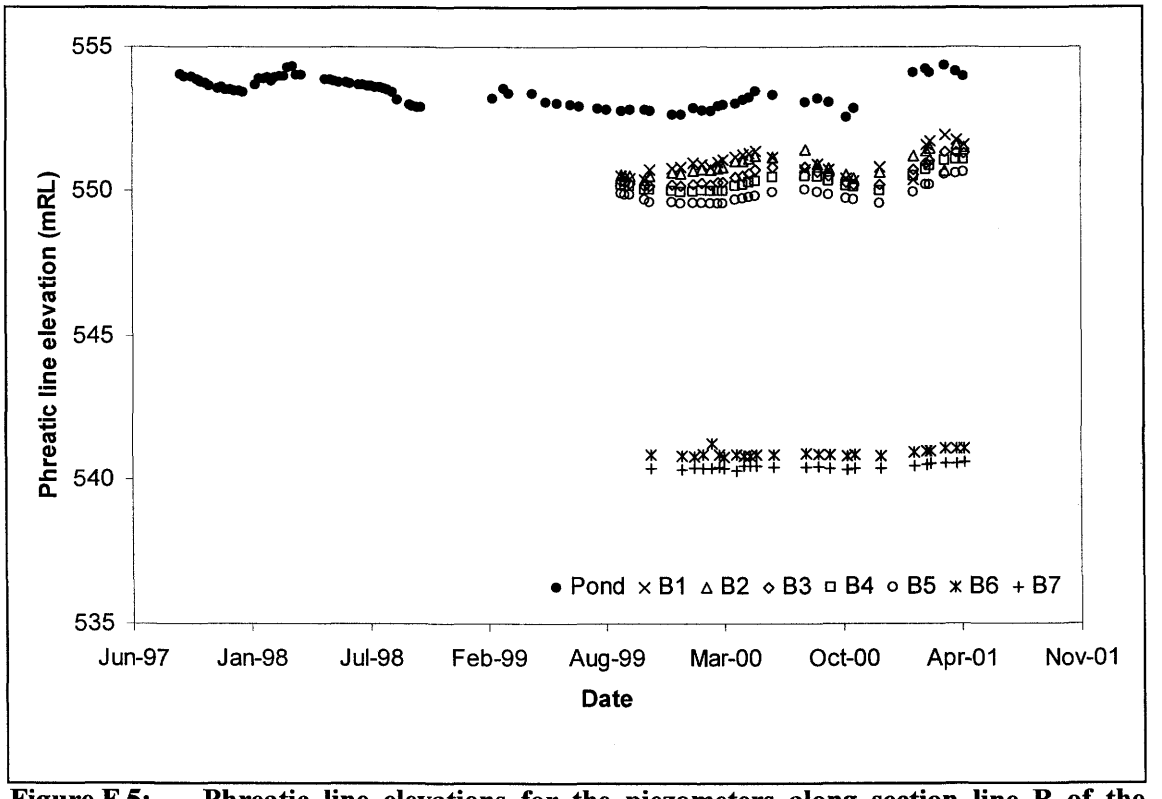

Figure F.5: **Phreatic line elevations for the piezometers along section line B of the Kidston tailings impoundment.**

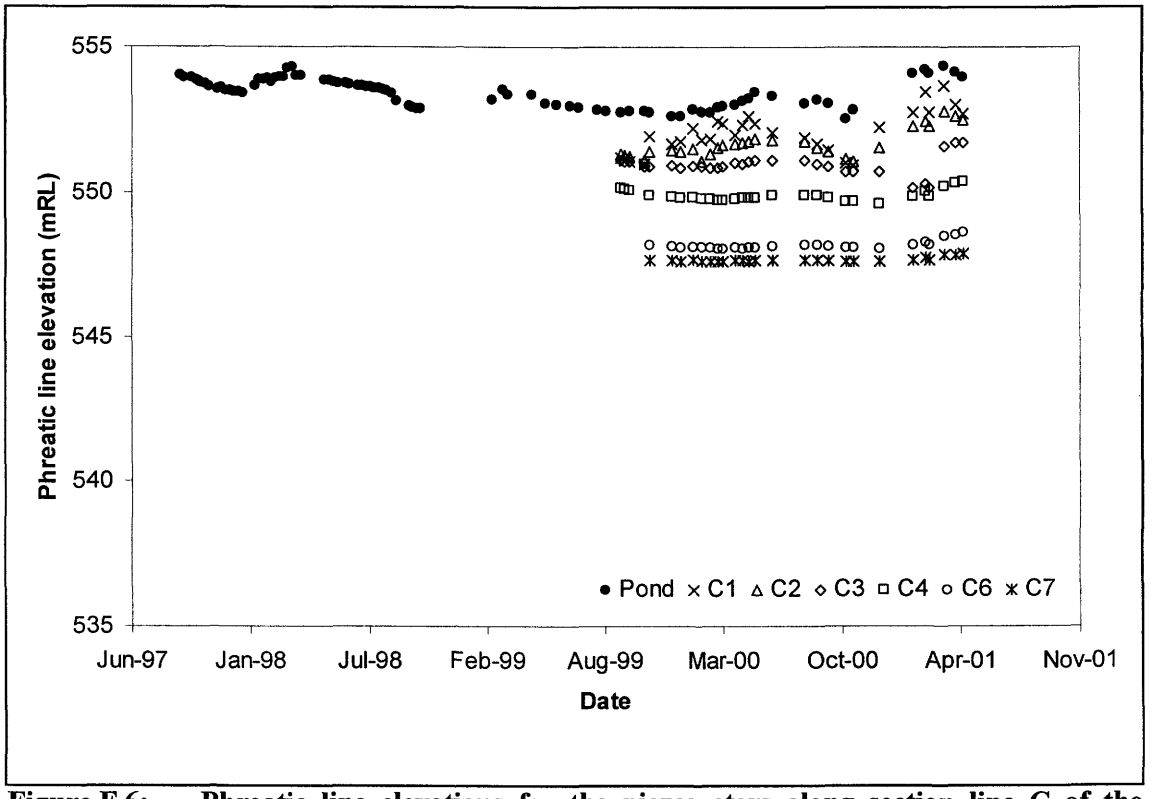

Figure F.6: Phreatic line elevations for the piezometers along section line C of the Kidston tailings impoundment.

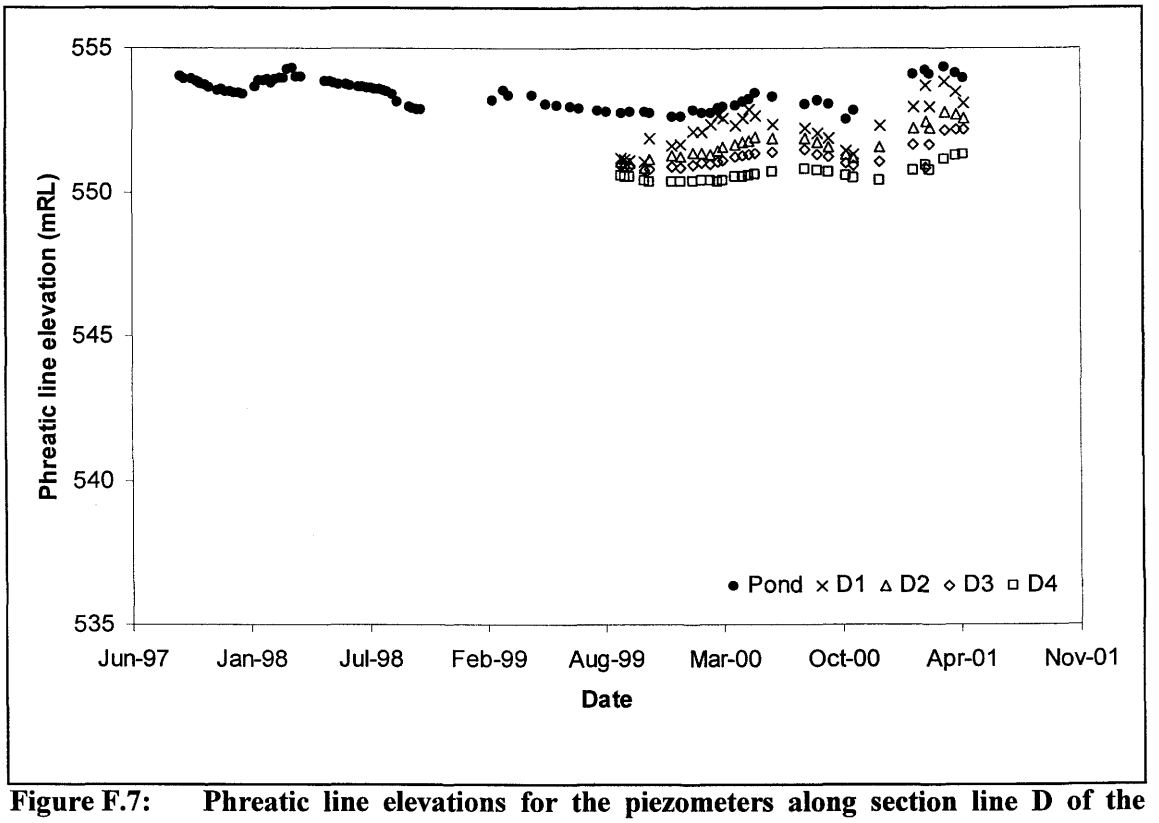

Figure F.7: Phreatic line elevations for the piezometers along section line D of the Kidston tailings impoundment.

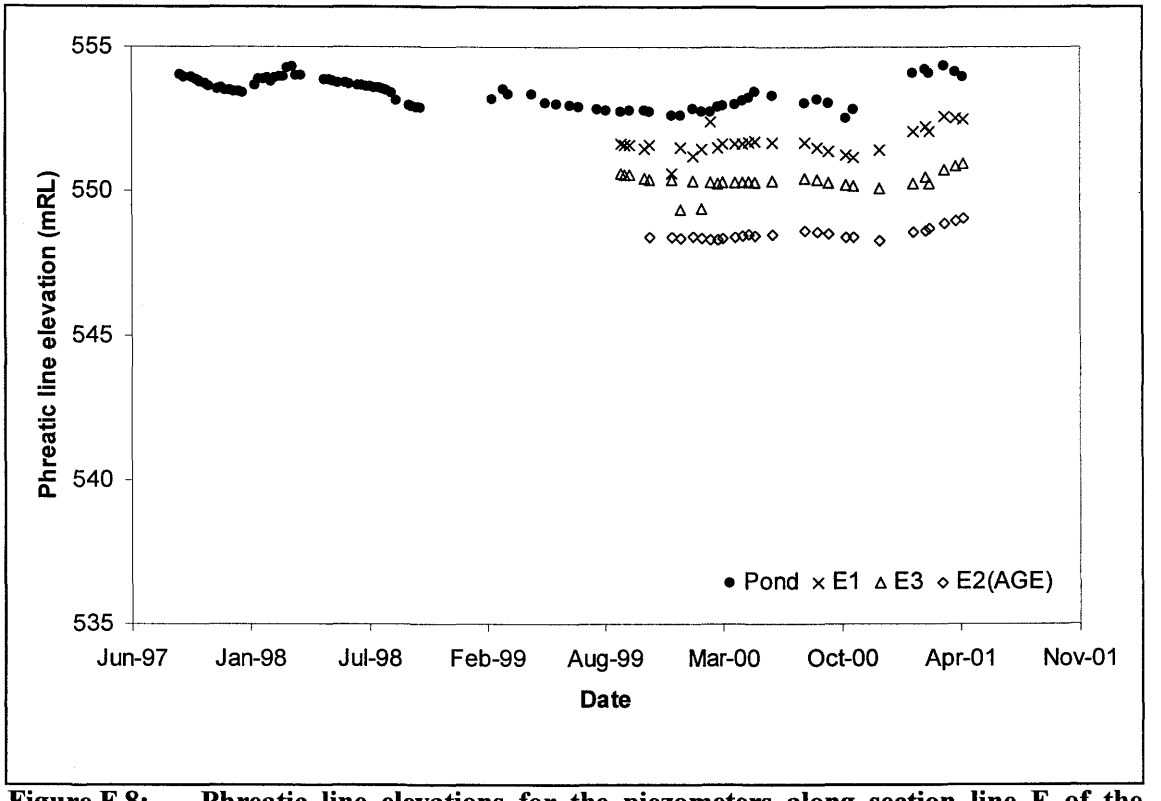

Figure F.8: **Phreatic line elevations for the piezometers along section line E of the Kidston tailings impoundment.**

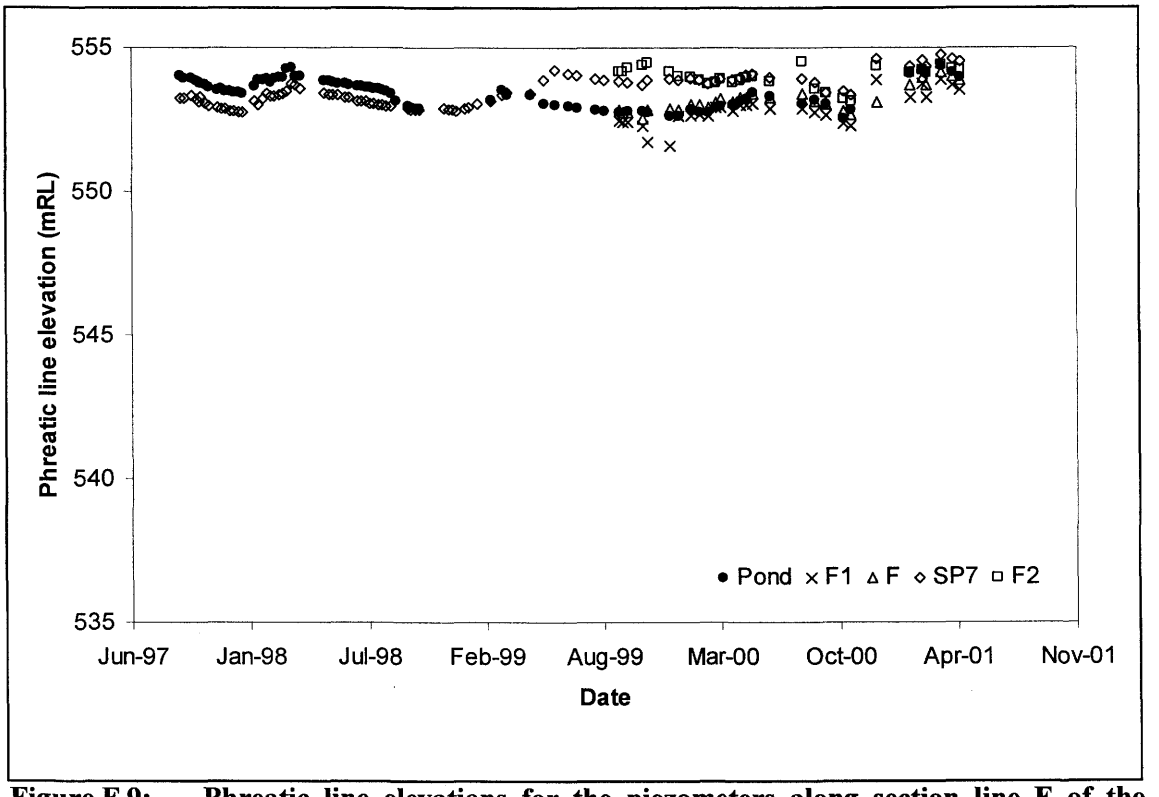

Figure F.9: **Phreatic line elevations for the piezometers along section line F of the Kidston tailings impoundment.**

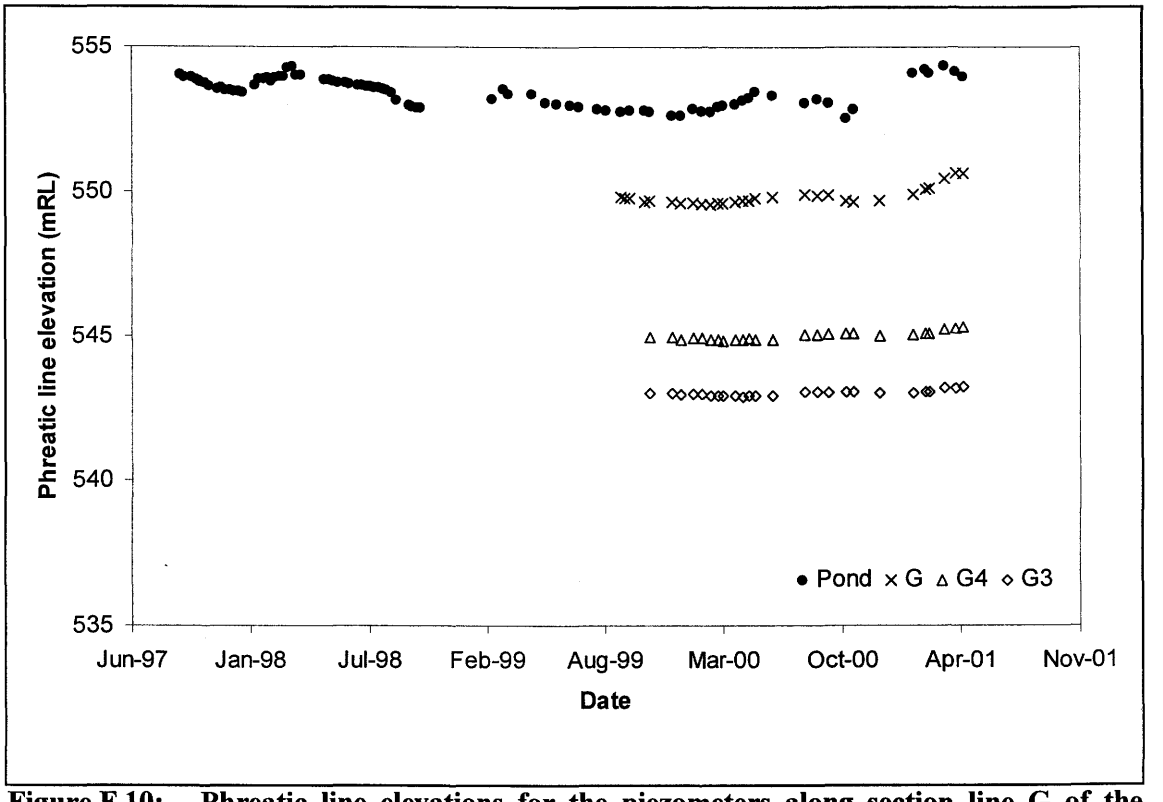

Figure F.10: Phreatic line elevations for the piezometers along section line G of the Kidston tailings impoundment.

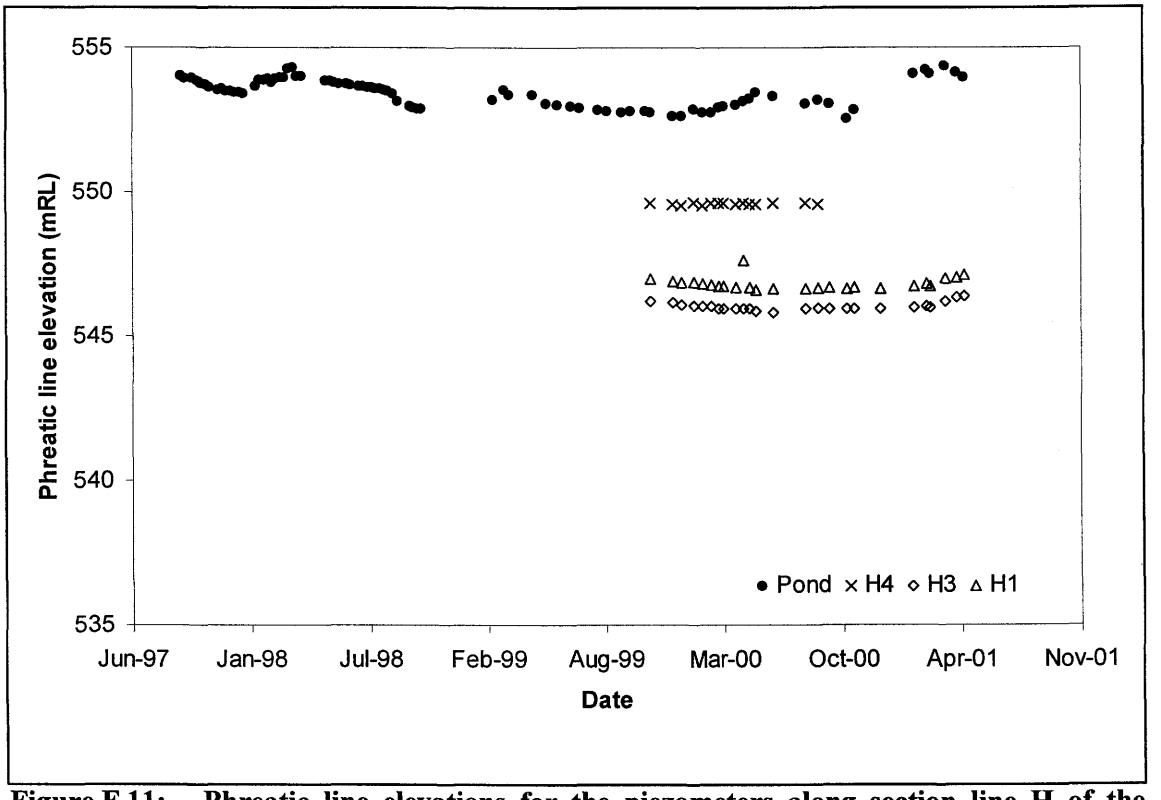

Figure F.11: Phreatic line elevations for the piezometers along section line H of the Kidston tailings impoundment.

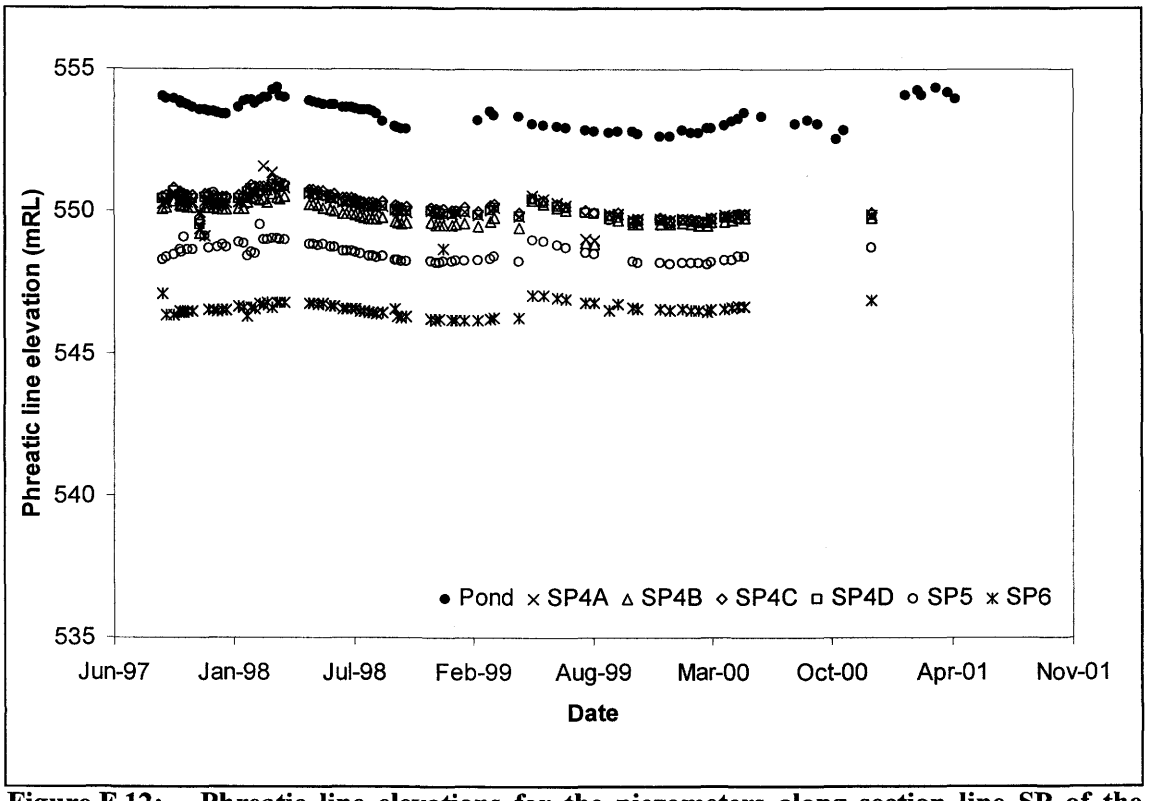

Figure F.12: Phreatic line elevations for the piezometers along section line SP of the Kidston tailings impoundment.

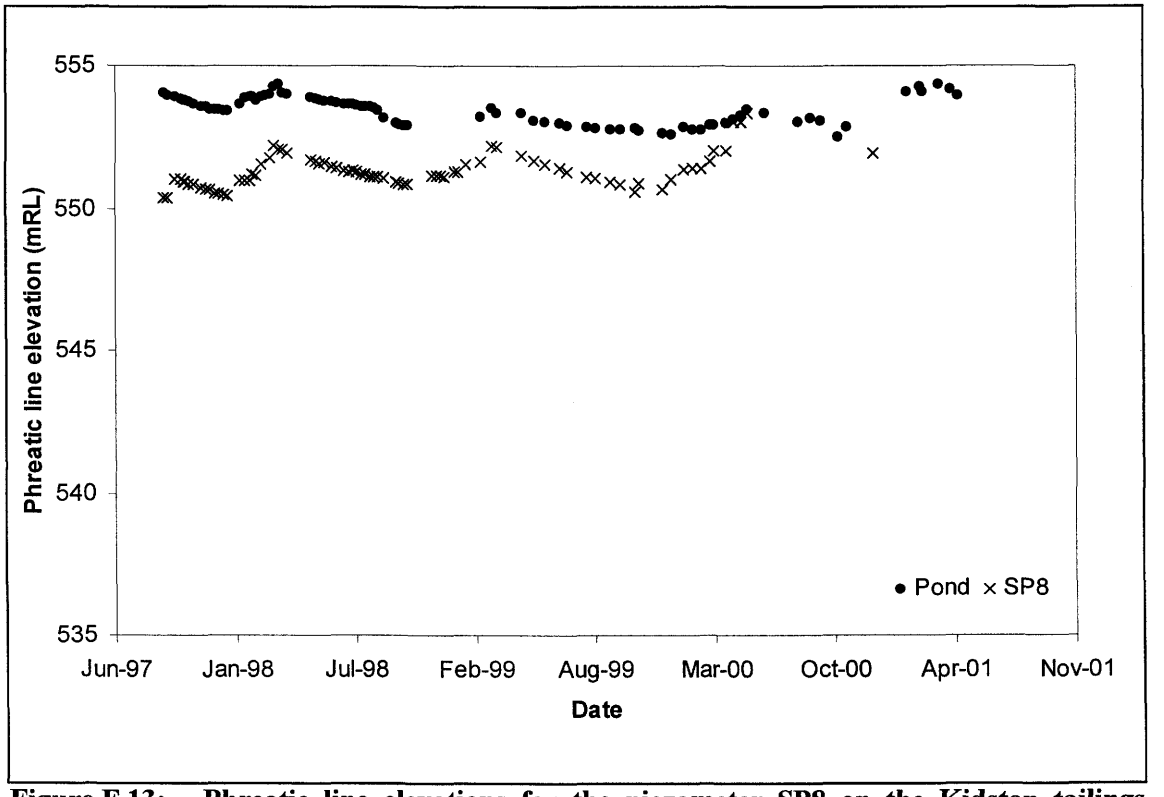

Figure F.13: Phreatic line elevations for the piezometer SP8 on the Kidston tailings impoundment.

F.4 References

Douglas Partners. (1997). Factual Report on Tailings Dam Insitu Testing at Kidston Gold Mine. Consultants report to Kidston Gold Mines, Project No. 21712, July, 5 pages.

Earthtech Consultants. (1999). Report on Piezocone Testing, Kidston Tailings Storage Facility. Consultants report to Australasian Groundwater & Environmental Consultants Pty Ltd, Project No. MF 1367, December, 3 pages.

Williams, D.J. (1998). Report on Tailings Dam Stability Audit. Report to Mr. Nick Currey, Kidston Gold Mines Limited. Department of Civil Engineering, University of Queensland, Brisbane, Australia. 10 December, 14 pages.

This page was intentionally left blank.

APPENDIX G

Manual and Automated V-Notch Weirs and Automated Level Sensor Details

G.1 Introduction

In order to measure the Kidston tailings impoundment seepage rates a number of flow measuring devices were installed. These include overflow weirs, which are both logged manually as well as one automated site. The tailings pond level and reclaim dam level was also monitored using an automated level sensor, and this appendix describes details for these installations. Table G.1 and G.2 list the measuring stations that are covered in this appendix. The locations of these stations are described in Chapter 5 of the thesis.

Table G.1: Details of the flow measuring stations on the Kidston Mine Site used to measure the tailings impoundment seepage rate.

Station name	Flow measured	Weir description	Installer (date)
Western drain	Seepage water pumped back from the western drain seepage pond	V-notch weir installed on drainage path on tailings impoundment surface; monitored manually during pumping periods.	Author (November 2000)
NW back section	Drain seepage flowing into SRB* test section	Impoundment wall in interception trench with pipe outflow; monitored manually	Kidston Gold Mine (1999)
NW mid section	Drain seepage from the SRB test section	V-notch weir installed in interception trench; monitored manually	Kidston Gold Mine (1996)
NE pipe	Drain section for the NE portion of the tailings impoundment	Pipe outflow; monitored manually	Kidston Gold Mine (1990)
N reclaim dam	Drain seepage for the tailings impoundment portion north of the reclaim dam	V-notch weir installed in interception trench; monitored manually	Author (November 2000)
Eastern drain	Drain seepage for the eastern section of the tailings impoundment	V-notch weir installed in interception trench; monitored via automated pressure transducer connected to a data acquisition system	Author (November 2000)

* SRB = sulfide reduction bed experimental site.

Table G.2: Details of the automated pond and dam level sensors on the Kidston Mine Site used to assist in seepage rate calculations.

Station location	System description	Installer (date)
Tailings pond	Automated pressure transducer connected to data acquisition system; operated from a barge	Author (December 2000)
Reclaim dam	Automated pressure transducer connected to data acquisition system; operated from a barge	Author (December 2000)

G.2 V-Notch Weir Flow Measuring Stations

The author installed two manual V-notch weirs in November 2000, and Mr. Paul Ritchie from Kidston Gold Mines installed another in 1996. The western drain seepage illustrated in Figure 5.2 flows into a pond immediately adjacent the tailings impoundment and cannot flow north towards the reclaim dam due to the natural topography preventing that. This pond was equipped with a level sensor that switches a pump to return the pond water to the surface of the tailings impoundment. No logs recording the pump volumes exist, only pump hours, and since no pump curves for the pump exist, the only way to determine the seepage rate would be to determine a stage curve for the pond. This however is not feasible due to the irregularity of the pond base, which would render an accurate survey extremely costly and difficult.

A decision was made to install a V-notch weir on the tailings impoundment surface where the pump returns the ponded water. By measuring the flow rate and volume flowing over the weir, and then logging the time the pond takes to refill before pumping is initiated, the seepage rate can be calculated. The weir was constructed from ¾" treated plywood and the notch were cut with a circular saw with a 45° angle at the nape. The weir was installed by excavating a 0.75 m deep trench in the path of the drainage channel using a backhoe. The trench width was 0.5 m, which was the size of the excavator bucket. After placing the weir into the trench and leveling it the trench was backfilled and compacted using the self-weight of the backhoe from its pneumatic tires. Fill material was imported to built dam wings at the edges of the weir to ensure that leakage does not occur when water ponds up behind the weir during pumping periods. The primary weir dimensions are presented in Table G.3.

Table G.3: Main dimensions of the V-notch weirs installed on the Kidston Mine Site.

Station	Notch angle	Overall top width (m)	Upstream height from ground level to notch base (m)	Downstream height from ground level to notch base (m)	Upstream conditions	Downstream conditions
Western drain	90°	3.0	0.20	0.15	Stilling pond 6 m back	Natural stream channel
NW mid section	90°	2.5	0.07	0.10	Stilling pond 50 m back	Natural stream channel
N reclaim dam	120°	3.0	0.12	0.12	Stilling pond 6 m back	Natural stream channel
Eastern Drain	90°	3.5	0.30	0.20	Stilling pond 10 m back	Natural stream channel

The second weir that was installed as part of this study was for the North reclaim dam seepage illustrated in Figure 5.2. The 120° V-notch weir was recovered from an unused site. The weir was constructed from ¾" plywood and the notch were cut with a circular saw with a 45° angle at the nape. The weir was installed by excavating a 0.75 m deep trench in the path of the drainage channel using a backhoe. The trench width was 0.5 m, which was the size of the excavator bucket. After placing the weir into the trench and leveling it the trench was backfilled and compacted using the self-weight of the backhoe from its pneumatic tires. Fill material was imported to built dam wings at the edges of the weir to ensure that leakage did not occur when water ponds up behind the weir. The primary weir dimensions are presented in Table G.3.

The weir that has been in place since 1996 is the one located at the Northwest mid section seepage (SRB pond outlet) illustrated in Figure 5.2. The weir was constructed from ¾" plywood and the notch were cut with a circular saw with a 45° angle at the nape. The weir was installed by excavating a 0.75 m deep trench in the path of the drainage channel using a backhoe. The trench width was 0.5 m, which was the size of the excavator bucket. After placing the weir into the trench and leveling it the trench was backfilled and compacted using the self-weight of the backhoe from its pneumatic tires. The primary weir dimensions are presented in Table G.3.

The Eastern drain weir has historically been shown to contribute towards the largest component of seepage from the tailings impoundment and as such accurate flow measurement is critical. A 90° V-notch weir has been installed in the drainage trench and an automated flow-measuring device was installed on site to record the flow continuously. The weir was constructed from ¾" plywood and the notch were cut with a circular saw with a 45° angle at the nape. Prior to installing the weir the upstream section of the stream channel where the weir was to be installed was filled and leveled with approximately 11 m^3 of dry-packed concrete. This apron was

extended 6 m back from the weir and was the entire channel width of approximately 3.5 m. The weir itself was imbedded in the dry-packed concrete mix to ensure a good seal. The primary weir dimensions are presented in Table G.3.

The automated flow measuring was done by means of a calibrated pressure transducer permanently mounted in an open-ended standpipe. The rise or fall of the water level was sensed by the pressure generated in the standpipe, and thus the water level is recorded. This water level was stored electronically via a data acquisition system directly connected to the pressure transducer and was powered by a standard 9 V Lithium battery. The interval for taking a reading and logging the flow depth was set by the user and for this installation a 15 minute interval was selected. The pressure transducer and data acquisition system was supplied to Kidston Gold Mines by a consulting engineering company in 1996 and was used at a different location on the Mine site. The equipment thus had to be salvaged, serviced and reinstalled. The pressure transducer standpipe consist of a ¾" PVC tube 1.98 m long. Since this tube would not withstand the rigors of site usage, a galvanized steel housing was concreted into the upstream apron and the pressure transducer was inside the 50 mm diameter open-ended housing. The housing has a 0.25 m x 0.25 m x 0.25 m top lockable box, which houses the data logger and the pressure transducer cable.

The flow rate over the eastern weir is calculated using the following formula:

$$Q = C_e \cdot \frac{8}{15} \cdot \sqrt{2 \cdot g} \cdot \tan\left(\frac{\theta}{2}\right) \cdot \left(h - \Delta + K_h\right) \cdot 1000 \qquad [G.1]$$

Where Q = flow rate from weir (l/s),

C_e = weir constant (0.2778),

g = gravitational acceleration (9.81 m/s^2),

θ = notch angle (90°),

h = water level measured by pressure transducer (m),

Δ = pressure transducer calibration factor (m), and

K_h = weir correction (0.00081).

Figure G.1 presents the seepage flow data recorded for the Eastern drain automated flow-measuring station. The spikes in flow rate are associated with rainfall events and constitute runoff as opposed to seepage.

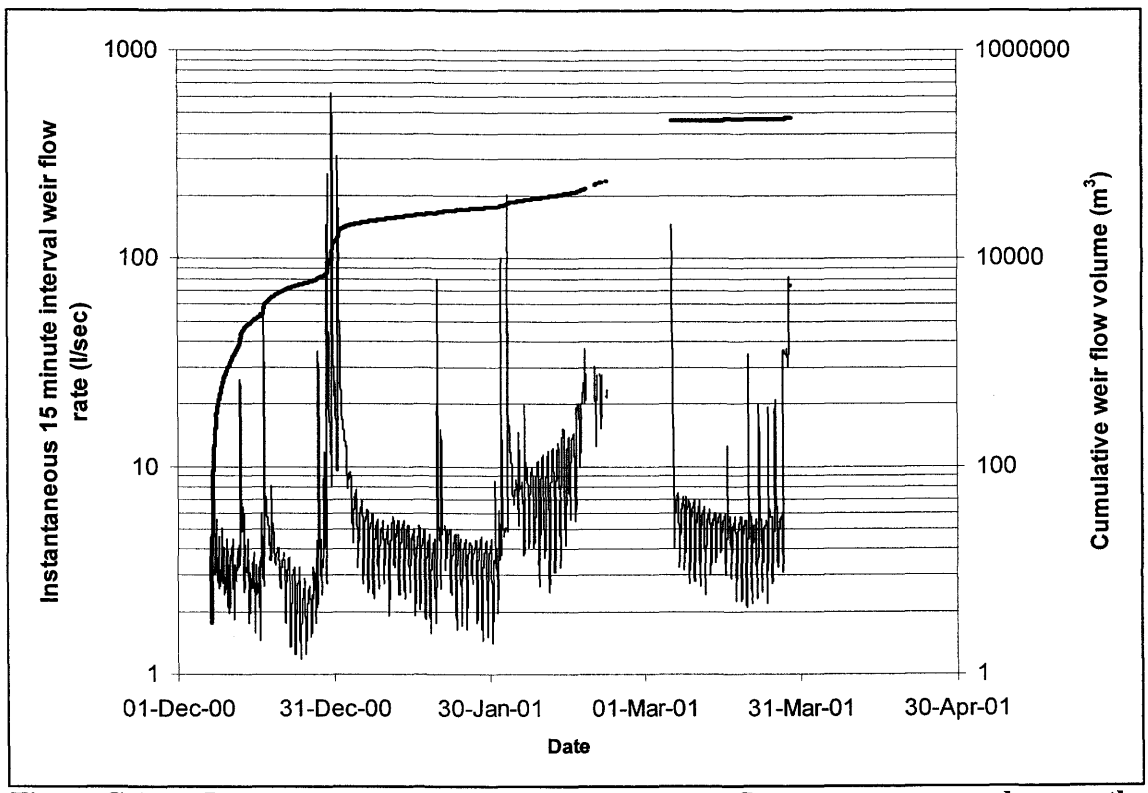

Figure G.1: Instantaneous and cumulative seepage flow rates measured over the Eastern drain V-notch weir at Kidston Gold Mine.

G.3 Pipe Flow Seepage Measurements

The flow rate is measured manually from outflow through a pipe at two locations. The pipe inlet to the SRB test site is used to determine the seepage from the Northwest back section. This pipe has an internal diameter of 65 mm. The pipe outlet for seepage from the Northeast section has an internal diameter of 310 mm. Manual measurements from these site consisted of measuring the time it takes to fill a bucket of known volume with the seepage water exiting from the pipe.

G.4 Tailings Pond and Reclaim Dam Level Sensors

Two automated dam level measuring stations were installed to gather data for the tailings impoundment water balance. The author installed the stations, measuring the tailings pond level

and reclaim dam level in November 2000. The data loggers are the same as the one used for the Eastern drain V-notch flow, consisting of a pressure transducer, which record the level of the water in a standpipe. This data was electronically stored in the memory bank of the data logger.

The tailings impoundment pond station was installed in the southeast portion of the tailings impoundment illustrated in Figure 5.2, at the same location as where the manual pond level readings were taken. Since the pressure transducer needed to be installed in the actual pond, access to the transducer had to be provided. The access was provided by constructing a raft using 210 liter steel drums and ¾" plywood. The raft components was joined together with steel wire and wood screws. The platform measured approximately 6.0 m x 1.0 m. The raft was secured in a permanent position using steel anchors driven into the ground and the required float was provided by allowing slack in the ½" polypropylene ropes joining the raft and anchors. A galvanized steel housing identical to the one used for the Eastern drain weir was secured to an 80 mm diameter steel post with u-bolts. The steel post was driven into the pond base sediments to a depth of at least 1.5 m. The logging interval was initially set to 15 minutes, but was later changed to 60 minutes.

The reclaim dam station was installed midway along the main dam wall, again having a raft access for taking the readings. The access raft was identical to the one used for the tailings impoundment pond. The securing technique differed in that only one end of the raft was secured to dry land. The opposite end was secured via two metal hoops to two 80 mm steel posts driven into the dam sediments. These posts were driven to a depth of at least 1.5 m on either side of the raft. A steel housing similar to that used in the other installations, and containing the pressure transducer and data logger were secured via u-bolts to another 80 mm steel post driven into the dam sediments. The logging interval was initially set to 15 minutes, but was later changed to 30 minutes.

The relative tailings pond and reclaim dam elevations were calibrated to the pressure transducer readings by taking a physical survey reading of the dam level elevation at a known level. The measured tailings pond and reclaim dam elevations are presented in Figures G.2 and G.3 respectively. The steady rise in the tailings pond is due to the onset of the rainy season resulting in a raising of the pond level. The rapid decrease in pond level from April 2001 is as a result of Kidston using the penstock decant to lower the pond level manually. The rapid changes observed in the reclaim dam were as a result of the water management practice of Kidston

Mine. Pond water is supplemented by rainfall but depleted by pumping to the south and north ponds for mine operational use.

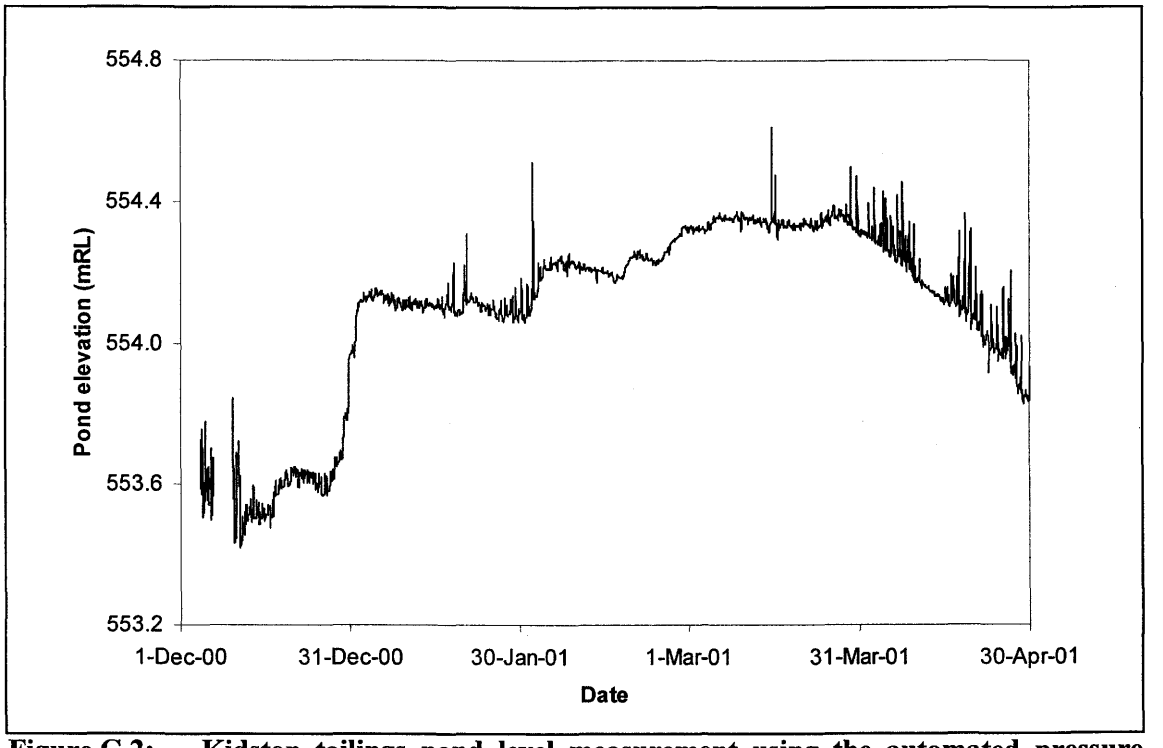

Figure G.2: Kidston tailings pond level measurement using the automated pressure transducer.

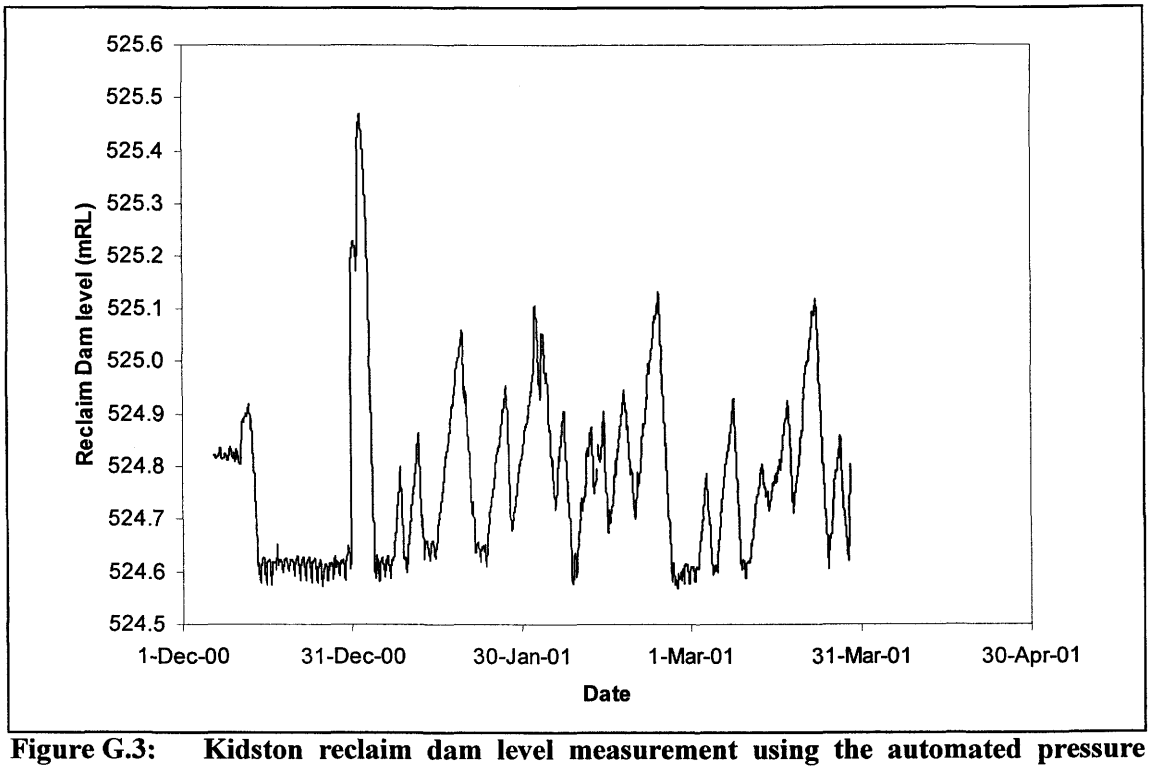

Figure G.3: Kidston reclaim dam level measurement using the automated pressure transducer.

This page was intentionally left blank.

APPENDIX H

Weather- and Bowen Ratio Station Details and Data

H.1 Introduction

The details of the equipment used for the automated weather station and Bowen ratio station installations on the Kidston Gold Mine are described here. The station locations are presented in Figure 5.2. The weather station is located on top of the Barren waste rock dump and was installed by a University of Saskatchewan research engineer, Mike O'Kane in 1996. The installation formed part of a larger study into the performance monitoring of cover systems for the waste rock dumps on the mine (Durham *et al.*, 2000). The Bowen ratio station was installed on top of the tailings impoundment and was installed specifically for the purpose of this study. The installation was by a University of Saskatchewan graduate student, Andrew Durham in 1997. Both stations were fully supplied by Campbell Scientific Corporation (Australia).

H.2 Weather Station

The sections below describe the installation of the Kidston weather station as well as the data accumulated.

H.2.1 Weather Station Components

The weather station houses sensors to monitor air temperature (°C), relative humidity (%), wind speed (m/s), wind direction (degrees), net radiation (W/m^2), and precipitation (mm). These sensors are all connected to a data logger mounted on the CM10 weather station tripod. A 20 watt solar panel/rechargeable battery system is used to supply power to the data logger and sensors. A storage module is used to reduce the frequency of trips required to download data from the weather station data logger. The storage module will retain all memory in the event of a power loss. The details of the individual components of the weather station are listed in Table H.1.

Table H.1: Details of the components of the fully automated weather station installed on the Kidston Barren waste rock dump in 1996.

Sensor	Parameter measured	Reference
HMP35CF Vaisala with Model 41004-5 multi-plate radiation shield	Air temperature & relative humidity	CSI (1994b); CSI (1990)
05103-10 RM Young Wind Monitor	Wind speed & direction	CSI (1993a)
Radiation and Energy Balance Systems, Inc. (REBS) Model Q7.1 net radiometer	Net radiation	CSI (1995)
Hydrological Services PTY LTD, TB3 W/025 Tipping Bucket	Rainfall	Hydrological Services (1995)
CM10 tripod	Tripod for mounting components	CSI (1994d)
CR10 Measurement and Control Module	Data measurement and control module	CSI (1994a)
SM716 storage module	Data storage module	CSI (1993c)
MSX-20 solar panel	20 watt solar panel	Solarex (1996)

The CR10 is a fully programmable data logger/controller in a small, rugged, sealed module (Campbell Scientific Inc., 1994a). The CR10 consists of a wiring panel, analog inputs, switched exitation outputs, pulse inputs, digital I/O ports, several analog ground terminals, 12 volt and power ground terminals, and two 5 volt outputs. The CR10 receives power from the 20 watt MSX-20 solar panel/battery system installed on the weather station tripod. The MSX-20 panel requires a voltage regulator (CH12R) to be positioned between the panel and data logger.

The wind monitor was mounted at the top of the tripod at a height of approximately 3 m above the ground surface. The air temperature and relative humidity probe was housed in a radiation shield (approximately 2.2 m above the ground surface) to minimize the effects of solar radiation. The net radiometer was installed on a metal post near the tripod at a height of approximately 1 m above the ground surface. The tipping bucket rain gauge was installed on a concrete platform near the tripod.

The supplier prior to shipping the sensors to the site calibrated the weather station sensors. The tipping bucket raingauge was the only sensor that required calibration subsequent to field installation. The gauge was calibrated in 1996 by pouring a known volume of water into the funnel and recording the number of bucket tips. The net radiometer required annual calibration checks against a calibrated sensor, however this was not performed during this study.

H.2.2 Weather Station Data Output Format

The PC208 software package (Campbell Scientific, 1994c) was used to develop and document the program for the CR10 measurement and control module used in this study. The program determined the frequency of sensor readings and the format of the data output. Precipitation data was output every minute (the length of the data logger program execution interval) only if precipitation is greater than or equal to 0.2 mm (the capacity of one-bucket tip). Data was not written to final memory of no precipitation occurs during the execution interval, thereby saving data logger storage space.

The average air temperature (°C), relative humidity (%), wind speed (m/s), and wind direction (degrees form north) are output based on the last 60 minutes of sensor readings. The execution interval of the data logger program was 60 seconds. Therefore the averages listed above are based on 60 sensor readings. Wind direction read 0° if the wind was coming from the north and 180° if the wind was coming from the south. The average net radiation (W/m^2) was output based on the last 60 minutes of sensor readings. Therefore the average was based on 60 sensor readings.

The maximum and minimum air temperature (°C), relative humidity (%), and wind speed (m/s) as well as the time of day they occurred was output at midnight. The data is based on the previous 24 hours of sensor readings. The total precipitation for the previous 24 hours was output at midnight. The average voltage supplied to the data logger was output at midnight as well and was based on the previous 24 hours of sensor readings.

H.2.3 Weather Station Data Collection and Station Maintenance

A Campbell Scientific CR10 measurement and control module was used to access and store data from the weather station sensors. Data stored in the CR10 was downloaded using a laptop computer, or by retrieving the SM716 storage module if inclement weather prevented the use of the laptop computer. The CR10 measurement and control module continued to store data from the sensors in the absence of the storage module.

Data must be downloaded from the CR10 measurement and control module every 45 days. The collection interval was estimated based on 10 days of precipitation per month with rainfall

occurring throughout the day. The collection interval may be extended or decreased based on the actual rainfall pattern. The memory on the CR10 measurement and control module and the SM716 storage module was formatted in a ring style configuration. In other word, new data continues to be stored even after the CR10 or SM716 was full since the new data replaces the oldest data.

Routine maintenance of some of the meteorological sensors was necessary to ensure the collection of accurate measurements. The responsibility for this maintenance was that of Kidston Gold Mine. The funnel of the rain gauge was cleaned out on a regular basis to ensure unrestricted movement of rainwater to the tipping bucket. The level of the tipping bucket raingauge and net radiometer was checked during each downloading session and adjusted accordingly. The plastic domes on the net radiometer were changed twice per year due to degradation of the domes by the sun.

H.2.4 General Weather Station Data

Tables H.3 to H.8 contain monthly summaries of the all the recorded weather station data, excluding precipitation data, which is reported in Appendix J. The generic year data refers to the data set generated to perform the SoilCover (SoilCover, 1997) numerical modeling. The generic data set was developed based on months of precipitation data (between March 1996 and April 2001) that most closely represented the mean monthly precipitation over the entire history of precipitation records for the Kidston Mine site. This procedure, and the months selected are documented in Appendix J. In Tables H.2 to H.7 the average, maximum and minimum monthly totals exclude the generic year and are based on the weather station data record from March 1996 to April 2001. In each table the final row labeled "Annual" represents an average value for the entire corresponding year. The complete daily weather station data is presented graphically in Figures H.1 through H.4.

Table H.2: Summary table of the average monthly maximum air temperature (°C) measured with the automated weather station.

Date	1996	1997	1998	1999	2000	2001	Generic	Average	Minimum	Maximum
Jan	nd	31.8	31.4	32.8	33.2	32.4	31.4	32.3	28.9	34.8
Feb	nd	32.0	32.6	31.2	31.1	29.9	31.1	31.4	27.6	34.0
Mar	32.2	30.0	30.6	31.1	30.8	32.3	30.6	31.1	28.2	33.5
Apr	32.1	28.5	31.7	27.5	28.4	29.6	32.1	29.7	25.6	32.7
May	27.8	26.6	27.4	27.3	26.5	29.8	26.5	27.1	24.3	29.4
June	27.5	23.4	26.2	25.8	21.5	nd	23.4	24.9	20.3	28.6

Table H.2: Summary table of the average monthly maximum air temperature (°C) measured with the automated weather station.

Date	1996	1997	1998	1999	2000	2001	Generic	Average	Minimum	Maximum
Jul	25.8	24.3	26.0	24.8	24.7	nd	25.8	25.1	22.1	28.0
Aug	27.8	26.0	27.9	26.5	26.8	nd	26.0	27.0	24.0	30.0
Sep	30.5	31.3	30.9	30.3	30.7	nd	30.5	30.7	27.4	33.6
Oct	31.0	32.9	34.1	34.2	31.2	nd	32.9	32.7	28.9	35.6
Nov	35.1	34.2	32.2	30.6	32.1	nd	34.2	32.8	29.1	36.0
Dec	34.2	32.3	33.1	31.6	29.7	nd	33.1	32.2	28.1	35.7
Annual	30.4	29.4	30.3	29.5	28.9	30.8	29.8	29.7	26.2	32.7

nd = no data available.

Table H.3: Summary table of the average monthly minimum air temperatures (°C) measured with the automated weather station.

Date	1996	1997	1998	1999	2000	2001	Generic	Average	Minimum	Maximum
Jan	nd	21.6	21.5	21.5	20.6	19.8	21.5	21.0	19.3	22.4
Feb	nd	21.7	21.7	21.4	21.3	20.4	21.3	21.3	19.7	22.6
Mar	20.9	20.1	19.2	20.8	19.4	20.5	19.2	20.1	18.0	22.0
Apr	20.2	16.5	21.1	18.2	18.9	17.7	20.2	18.8	16.0	21.5
May	16.6	14.3	16.1	14.4	15.4	17.0	15.4	15.4	12.4	18.1
June	15.0	12.7	13.1	13.1	11.6	nd	12.7	13.1	9.3	16.0
Jul	11.2	12.6	14.0	11.1	9.2	nd	11.2	11.6	8.2	15.4
Aug	13.6	12.3	14.0	12.4	11.4	nd	12.3	12.7	9.5	15.5
Sep	14.5	16.2	17.8	15.1	14.6	nd	14.5	15.6	12.7	19.0
Oct	18.9	18.1	20.0	18.6	17.9	nd	18.1	18.7	16.5	20.9
Nov	21.3	20.2	20.2	19.4	19.3	nd	20.2	20.1	18.0	22.0
Dec	22.5	22.1	21.0	20.0	19.4	nd	21.0	21.0	18.7	23.1
Annual	17.5	17.4	18.3	17.2	16.6	19.1	17.3	17.5	14.9	19.9

nd = no data available.

Table H.4: Summary table of the average monthly net radiation (W/m^2) measured with the automated weather station.

Date	1996	1997	1998	1999	2000	2001	Generic	Average	Minimum	Maximum
Jan	nd	135.9	145.2	149.4	166.4	168.7	145.2	153.1	110.7	189.1
Feb	nd	149.9	147.4	134.9	135.5	133.8	135.5	140.3	88.3	180.1
Mar	115.3	139.2	117.9	128.5	149.4	163.7	117.9	137.3	79.8	174.8
Apr	101.5	108.8	103.0	93.3	104.0	125.9	101.5	106.1	71.5	136.5
May	77.7	75.0	92.3	102.6	79.7	126.7	79.7	85.6	57.5	108.1
June	76.9	68.2	82.4	85.2	63.1	nd	68.2	75.2	49.8	92.1
Jul	77.2	82.3	90.5	86.7	88.5	nd	77.2	85.1	66.5	100.3
Aug	110.2	88.0	115.1	108.8	105.7	nd	88.0	105.6	78.6	122.4
Sep	134.8	124.3	144.5	140.6	130.9	nd	134.8	135.0	113.8	153.0
Oct	124.9	143.8	148.0	156.8	134.7	nd	143.8	141.6	100.4	169.7
Nov	119.6	151.2	153.8	125.4	153.0	nd	151.2	140.6	97.3	179.3
Dec	136.6	126.0	148.2	148.3	131.7	nd	148.2	138.2	90.0	178.8
Annual	107.5	116.1	124.0	121.7	120.2	143.8	115.9	120.3	83.7	148.7

nd = no data available.

Table H.5: Summary table of the average monthly maximum relative humidity (%) measured with the automated weather station.

Date	1996	1997	1998	1999	2000	2001	Generic	Average	Minimum	Maximum
Jan	nd	87.8	97.5	96.0	93.9	96.2	97.5	94.3	83.9	100.7
Feb	nd	91.2	94.3	97.3	98.0	99.8	98.0	96.1	87.9	101.5
Mar	84.8	86.6	92.6	96.6	97.8	101.0	92.6	94.0	81.1	101.5
Apr	80.1	84.1	95.4	93.8	99.0	96.1	80.1	91.4	73.4	100.4
May	72.8	84.3	90.6	92.9	95.1	100.6	95.1	87.2	63.8	100.0
June	79.4	83.5	83.9	86.4	92.8	nd	83.5	85.2	66.3	98.7
Jul	65.5	84.2	91.6	79.9	84.3	nd	65.5	81.1	59.7	97.8
Aug	74.3	76.0	86.1	86.2	87.0	nd	76.0	81.9	55.4	98.0
Sep	59.4	73.8	89.0	85.1	80.4	nd	59.4	77.6	49.4	96.9
Oct	81.0	72.4	88.4	86.4	92.4	nd	72.4	84.1	67.4	96.7
Nov	60.5	85.8	93.2	94.9	95.2	nd	85.8	85.9	58.2	101.3
Dec	79.9	86.9	91.1	92.2	97.3	nd	91.1	89.5	71.0	99.8
Annual	73.8	83.1	91.1	90.6	92.8	98.7	83.1	87.4	68.1	99.4

nd = no data available.

Table H.6: Summary table of the average monthly minimum relative humidity (%) measured with the automated weather station.

Date	1996	1997	1998	1999	2000	2001	Generic	Average	Minimum	Maximum
Jan	nd	38.5	47.7	41.4	35.8	38.2	47.7	40.3	27.1	57.5
Feb	nd	40.9	42.2	49.3	50.5	56.4	50.5	47.9	33.1	67.6
Mar	33.1	39.8	41.5	45.3	43.8	43.7	41.5	42.1	28.5	59.8
Apr	28.2	30.6	44.3	49.4	53.8	41.7	28.2	41.3	24.8	61.1
May	29.8	33.3	41.3	35.0	45.4	37.3	45.4	37.0	23.0	53.5
June	30.7	38.1	33.3	31.5	50.6	nd	38.1	36.8	21.9	57.5
Jul	20.1	34.0	37.9	28.1	26.7	nd	20.1	29.4	15.8	44.0
Aug	23.6	24.2	26.1	28.5	27.0	nd	24.2	25.9	13.4	39.8
Sep	13.3	21.4	30.9	22.6	21.2	nd	13.3	21.9	10.1	35.5
Oct	28.6	18.1	27.9	21.7	34.0	nd	18.1	26.1	14.7	42.5
Nov	15.5	24.0	36.5	42.5	37.2	nd	24.0	31.1	13.2	50.0
Dec	29.5	42.0	36.8	38.9	48.9	nd	36.8	39.2	23.9	57.3
Annual	25.2	32.1	37.2	36.2	39.6	43.4	32.3	34.9	20.8	52.2

nd = no data available.

Table H.7: Summary table of the average monthly wind speed (km/hr) measured with the automated weather station.

Date	1996	1997	1998	1999	2000	2001	Generic	Average	Minimum	Maximum
Jan	nd	9.2	7.0	5.8	5.4	4.6	7.0	6.4	4.4	10.0
Feb	nd	7.2	6.5	6.0	6.1	5.2	6.1	6.2	4.5	8.7
Mar	8.5	7.0	6.2	6.4	4.6	3.8	6.2	5.9	3.6	8.4
Apr	7.6	6.9	7.0	6.4	4.2	5.0	7.6	6.2	3.7	8.6
May	7.7	4.8	6.0	5.3	3.7	4.4	3.7	5.5	3.4	8.3
June	6.8	6.2	5.9	4.9	3.7	nd	6.2	5.5	3.5	7.9
Jul	6.3	6.7	6.7	5.4	3.3	nd	6.3	5.7	3.3	8.0
Aug	7.7	6.1	6.7	6.2	4.1	nd	6.1	6.1	4.0	8.8
Sep	7.7	6.1	7.8	6.6	4.5	nd	7.7	6.5	4.2	9.0
Oct	10.6	7.7	7.0	7.0	4.9	nd	7.7	7.4	4.5	10.9

Table H.7: Summary table of the average monthly wind speed (km/hr) measured with the automated weather station.

Date	1996	1997	1998	1999	2000	2001	Generic	Average	Minimum	Maximum
Nov	8.5	6.9	7.0	6.5	4.6	nd	6.9	6.7	4.4	9.4
Dec	9.3	6.9	6.8	6.5	5.2	nd	6.8	6.9	4.7	10.2
Annual	8.1	6.8	6.7	6.1	4.5	4.6	6.5	6.3	4.0	9.0

nd = no data available.

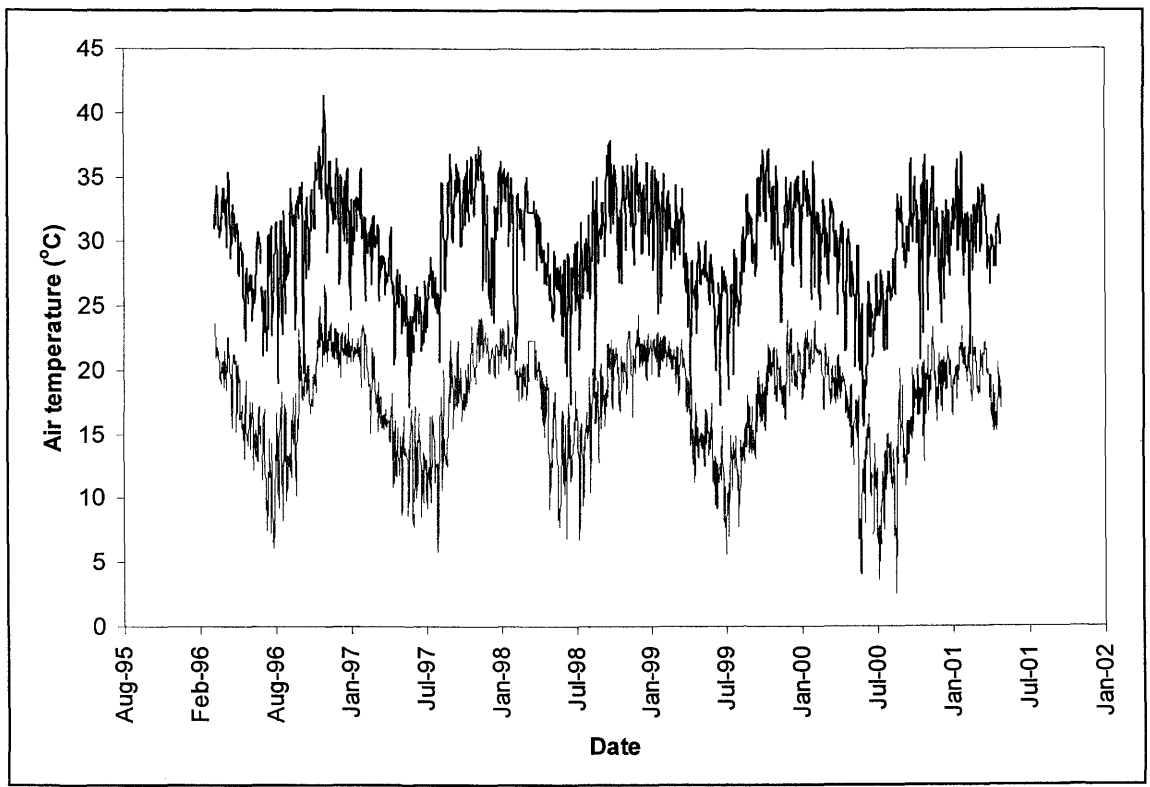

Figure H.1: Daily maximum and minimum air temperatures measured by the Kidston weather station between March 1996 and April 2001.

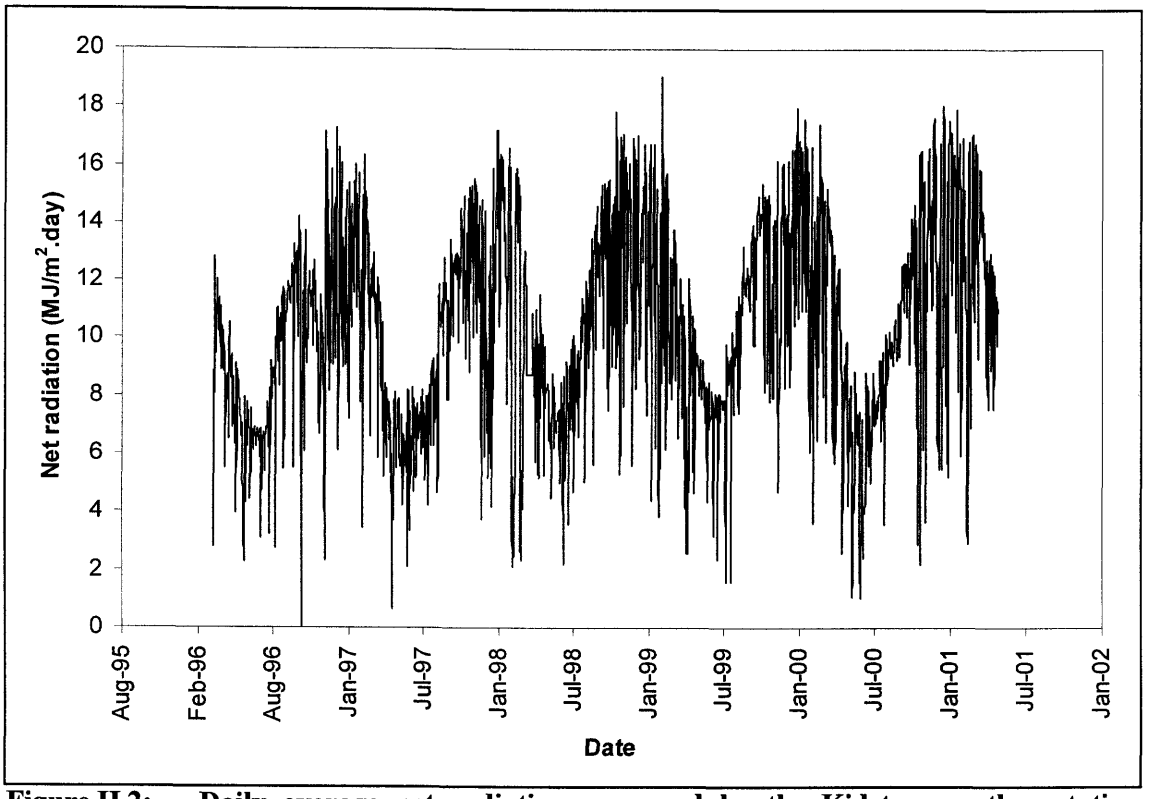

Figure H.2: **Daily average net radiation measured by the Kidston weather station between March 1996 and April 2001.**

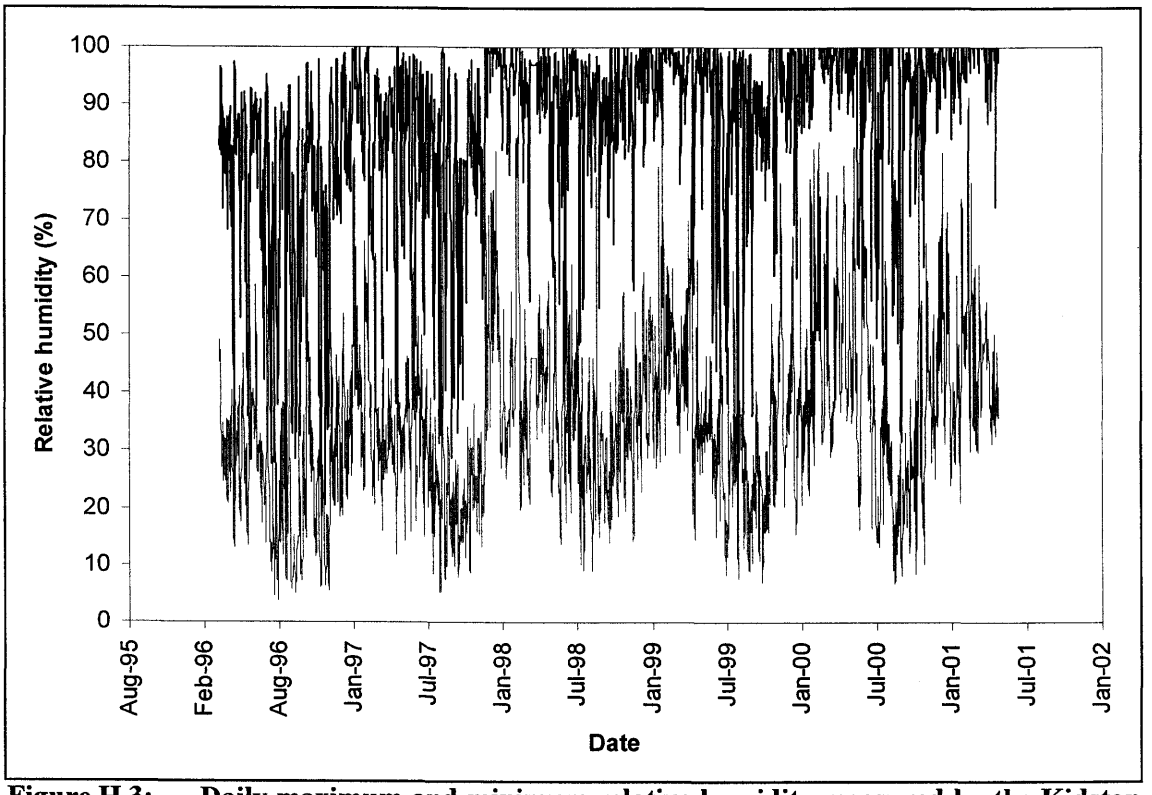

Figure H.3: **Daily maximum and minimum relative humidity measured by the Kidston weather station between March 1996 and April 2001.**

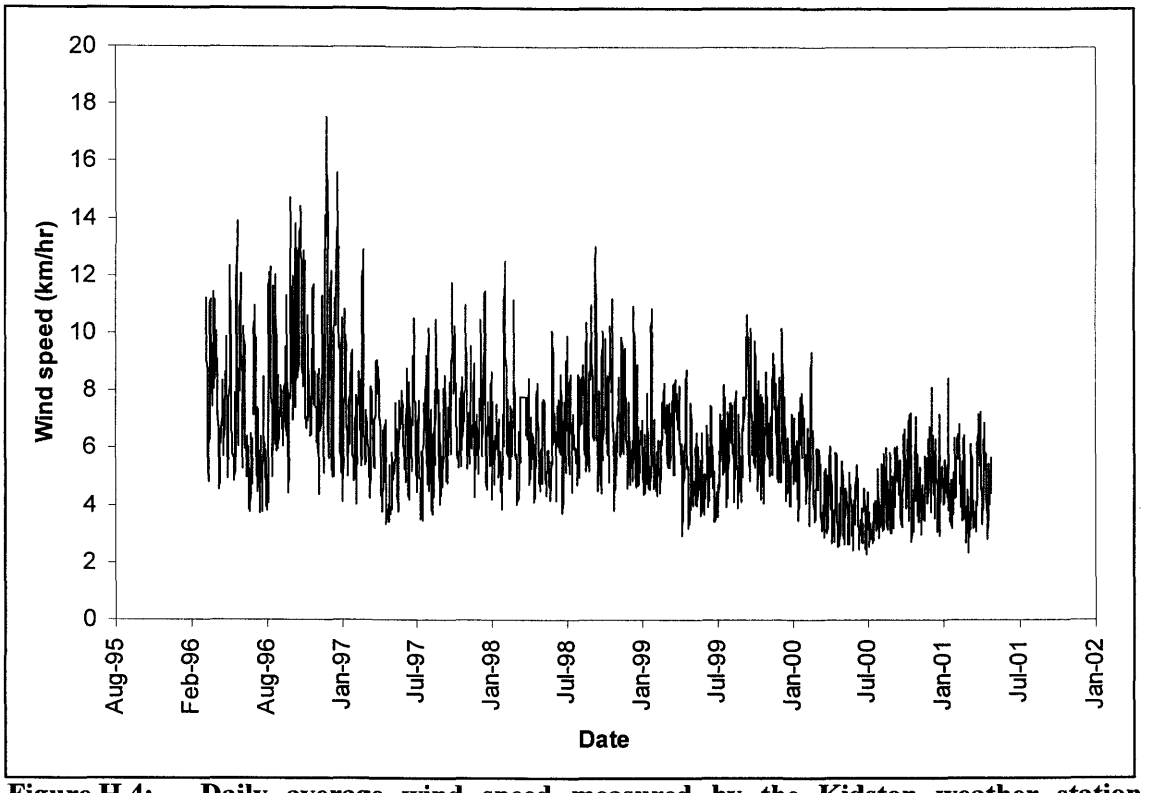

Figure H.4: Daily average wind speed measured by the Kidston weather station between March 1996 and April 2001.

H.2.5 Daily Weather Data Presented in SoilCover Format

The daily meteorological data required for the SoilCover modeling is listed in Tables H.8 and H.9. In both tables the precipitation data is excluded, as it is reported in Appendix J. Table H.8 contain the generated generic year of data, and Table H.9 contain the data for the period 1 December 2000 to 30 April 2001 used for the evaluation modeling.

Table H.8: Detailed daily meteorological data for the generated generic year.

Date	Max temp (°C)	Min temp (°C)	Net rad (MJ/ m^2.d)	Max RH (dec)	Min RH (dec)	Avg wind speed (km/hr)	Date	Max temp (°C)	Min temp (°C)	Net rad (MJ/ m^2.d)	Max RH (dec)	Min RH (dec)	Avg wind speed (km/hr)
1-Jan	27.2	20.6	10.2	0.95	0.45	7.3	3-Jul	24.7	12.8	5.9	0.85	0.39	8.9
2-Jan	24.4	21.0	6.0	1.00	0.75	5.7	4-Jul	24.5	13.9	6.8	0.95	0.49	11.0
3-Jan	30.2	21.4	10.2	1.00	0.52	6.9	5-Jul	21.2	16.2	3.1	0.95	0.62	9.4
4-Jan	30.3	21.8	12.7	1.00	0.48	7.3	6-Jul	26.2	15.4	6.3	0.92	0.48	7.4
5-Jan	26.5	21.6	5.5	0.99	0.68	7.3	7-Jul	23.0	17.0	4.8	0.88	0.47	9.8
6-Jan	30.2	21.5	13.2	0.99	0.56	10.3	8-Jul	24.7	15.7	6.0	0.79	0.35	7.7
7-Jan	29.9	21.2	9.9	1.00	0.54	7.5	9-Jul	25.1	12.7	6.7	0.66	0.21	5.2
8-Jan	26.9	21.3	10.5	0.99	0.66	11.2	10-Jul	25.6	11.2	6.5	0.50	0.14	4.9

Table H.8: Detailed daily meteorological data for the generated generic year.

Date	Max temp (°C)	Min temp (°C)	Net rad (MJ/ m².d)	Max RH (dec)	Min RH (dec)	Avg wind speed (km/hr)	Date	Max temp (°C)	Min temp (°C)	Net rad (MJ/ m².d)	Max RH (dec)	Min RH (dec)	Avg wind speed (km/hr)
9-Jan	23.8	20.2	4.2	1.00	0.82	11.5	11-Jul	26.2	9.4	6.6	0.83	0.16	4.5
10-Jan	27.6	19.4	11.1	0.96	0.63	11.1	12-Jul	25.1	9.0	6.7	0.47	0.14	7.4
11-Jan	27.3	19.6	11.8	1.00	0.63	5.2	13-Jul	21.7	9.8	5.4	0.37	0.12	7.3
12-Jan	32.7	21.4	15.9	1.00	0.47	4.5	14-Jul	22.7	7.5	6.5	0.48	0.10	4.7
13-Jan	30.3	22.1	10.0	1.00	0.65	5.3	15-Jul	23.4	9.9	6.7	0.28	0.12	5.0
14-Jan	32.3	22.1	12.0	0.97	0.51	7.6	16-Jul	23.1	8.6	6.9	0.37	0.14	5.8
15-Jan	31.9	22.1	12.9	0.97	0.48	6.4	17-Jul	27.7	8.6	6.8	0.55	0.09	3.7
16-Jan	32.6	21.9	13.3	0.97	0.45	7.2	18-Jul	30.1	12.1	6.9	0.76	0.15	3.8
17-Jan	30.9	21.2	11.6	1.00	0.50	6.1	19-Jul	30.6	11.5	7.3	0.80	0.19	5.6
18-Jan	31.8	21.3	13.4	0.98	0.48	7.1	20-Jul	29.8	14.7	7.7	0.68	0.29	6.4
19-Jan	32.3	21.6	15.8	0.98	0.32	5.4	21-Jul	27.4	14.2	6.6	0.47	0.05	6.4
20-Jan	33.5	19.7	17.2	0.96	0.29	5.4	22-Jul	27.9	10.8	6.2	0.28	0.05	4.5
21-Jan	34.8	21.4	17.2	0.95	0.27	7.4	23-Jul	28.6	7.3	7.3	0.58	0.11	4.9
22-Jan	35.7	21.1	17.2	0.99	0.27	7.6	24-Jul	30.1	10.7	7.6	0.82	0.14	3.8
23-Jan	34.4	23.3	13.8	0.83	0.35	8.7	25-Jul	31.1	12.2	8.2	0.65	0.11	7.1
24-Jan	34.6	22.1	16.2	0.90	0.36	7.2	26-Jul	22.8	14.2	3.2	0.89	0.40	8.5
25-Jan	36.2	22.2	16.2	0.92	0.29	4.2	27-Jul	23.4	9.8	9.1	0.81	0.16	7.6
26-Jan	34.1	23.0	11.3	0.99	0.44	6.9	28-Jul	25.0	7.8	8.2	0.76	0.09	5.4
27-Jan	31.2	20.6	10.4	1.00	0.54	7.6	29-Jul	25.9	6.1	8.1	0.65	0.07	5.4
28-Jan	34.5	22.4	12.1	0.98	0.42	5.9	30-Jul	25.5	6.2	8.1	0.44	0.10	6.1
29-Jan	34.0	22.1	16.3	1.00	0.37	6.3	31-Jul	26.7	6.9	7.9	0.55	0.04	4.0
30-Jan	35.3	23.3	15.9	0.95	0.29	5.8	1-Aug	24.4	9.2	6.9	0.71	0.23	6.5
31-Jan	35.1	23.0	14.8	0.97	0.31	4.7	2-Aug	23.4	10.5	5.1	0.83	0.39	7.3
1-Feb	33.6	20.2	15.8	0.96	0.28	6.6	3-Aug	24.9	11.5	7.9	0.92	0.27	7.6
2-Feb	34.0	20.7	16.5	0.95	0.23	6.2	4-Aug	25.7	12.3	8.0	0.87	0.31	5.0
3-Feb	32.1	21.4	11.5	0.92	0.41	7.8	5-Aug	26.1	12.4	7.7	0.93	0.16	4.9
4-Feb	32.4	19.8	15.3	0.86	0.32	7.7	6-Aug	25.8	12.5	8.0	0.95	0.26	4.9
5-Feb	33.6	20.1	15.8	0.92	0.37	5.7	7-Aug	27.4	10.8	7.8	0.91	0.23	3.5
6-Feb	31.7	22.4	10.7	0.96	0.49	6.5	8-Aug	26.6	11.4	4.2	0.82	0.33	3.7
7-Feb	25.7	21.6	6.1	1.00	0.77	7.9	9-Aug	27.4	16.4	8.0	0.53	0.16	5.9
8-Feb	27.2	21.1	8.9	0.99	0.67	7.2	10-Aug	27.0	9.9	7.6	0.56	0.09	4.3
9-Feb	29.6	20.8	9.9	1.00	0.51	7.4	11-Aug	28.0	11.7	8.4	0.91	0.24	3.5
10-Feb	31.6	20.5	12.6	0.88	0.36	7.1	12-Aug	28.8	10.6	8.0	0.75	0.21	5.5
11-Feb	31.5	20.7	10.4	0.92	0.46	6.4	13-Aug	27.3	13.7	7.4	0.39	0.15	5.7
12-Feb	31.4	20.7	10.4	0.96	0.51	7.0	14-Aug	26.9	12.8	6.3	0.75	0.25	6.1
13-Feb	34.2	21.4	14.4	0.97	0.40	6.4	15-Aug	25.7	16.4	7.5	0.81	0.36	7.6
14-Feb	36.2	21.9	16.6	0.96	0.27	4.4	16-Aug	25.7	15.4	8.5	0.82	0.32	7.3
15-Feb	33.9	23.8	12.6	0.96	0.42	5.8	17-Aug	27.4	14.9	9.0	0.81	0.26	6.9
16-Feb	26.5	21.9	3.6	1.00	0.83	4.1	18-Aug	27.7	15.5	9.2	0.77	0.24	7.4
17-Feb	31.5	21.9	12.3	1.00	0.50	4.9	19-Aug	26.2	14.0	8.6	0.82	0.25	6.7
18-Feb	31.3	21.7	9.4	1.00	0.57	5.2	20-Aug	26.4	11.2	8.3	0.72	0.23	9.2
19-Feb	31.4	22.1	14.0	1.00	0.52	5.8	21-Aug	25.8	12.5	9.2	0.88	0.21	8.6
20-Feb	31.9	21.9	13.2	1.00	0.53	5.2	22-Aug	24.8	12.6	6.3	0.83	0.27	6.8
21-Feb	30.7	21.3	10.0	1.00	0.56	5.6	23-Aug	26.8	12.5	8.5	0.89	0.23	4.7
22-Feb	32.3	21.7	13.4	1.00	0.51	6.7	24-Aug	27.3	12.6	8.6	0.67	0.14	7.3
23-Feb	32.1	21.6	11.8	1.00	0.51	5.7	25-Aug	25.1	12.8	7.1	0.32	0.05	10.1

Table H.8: Detailed daily meteorological data for the generated generic year.

Date	Max temp (°C)	Min temp (°C)	Net rad (MJ/ m².d)	Max RH (dec)	Min RH (dec)	Avg wind speed (km/hr)	Date	Max temp (°C)	Min temp (°C)	Net rad (MJ/ m².d)	Max RH (dec)	Min RH (dec)	Avg wind speed (km/hr)
24-Feb	30.6	21.2	11.2	1.00	0.57	4.1	26-Aug	24.8	5.9	7.4	0.42	0.05	4.8
25-Feb	28.3	21.4	7.6	1.00	0.68	3.4	27-Aug	24.5	7.8	8.4	0.34	0.07	4.5
26-Feb	24.8	21.5	6.6	1.00	0.83	5.8	28-Aug	25.7	9.6	7.6	0.88	0.22	5.1
27-Feb	31.3	21.3	14.7	1.00	0.50	6.1	29-Aug	25.9	11.6	9.4	0.87	0.19	5.6
28-Feb	30.8	21.6	12.4	0.98	0.58	7.7	30-Aug	25.0	13.6	5.9	0.92	0.39	6.1
1-Mar	23.9	19.7	5.2	1.00	0.81	5.9	31-Aug	20.6	16.5	4.7	0.98	0.76	7.3
2-Mar	23.6	20.0	4.1	1.00	0.82	6.0	1-Sep	29.0	11.7	10.5	0.39	0.07	6.0
3-Mar	22.5	19.7	4.1	1.00	0.87	5.8	2-Sep	28.4	10.8	10.5	0.40	0.06	6.4
4-Mar	20.9	18.6	2.6	1.00	0.96	7.7	3-Sep	27.3	13.4	11.1	0.34	0.08	6.6
5-Mar	24.6	18.6	7.1	1.00	0.75	6.4	4-Sep	27.7	13.0	11.2	0.57	0.08	7.7
6-Mar	30.6	20.1	15.7	1.00	0.48	6.9	5-Sep	28.5	12.5	11.6	0.78	0.09	7.1
7-Mar	33.0	19.9	14.6	0.97	0.25	5.7	6-Sep	29.2	12.9	11.6	0.66	0.10	8.1
8-Mar	33.7	17.6	15.9	0.97	0.20	5.0	7-Sep	28.7	13.5	11.8	0.68	0.15	7.9
9-Mar	33.4	18.6	15.3	0.90	0.21	4.9	8-Sep	29.6	13.1	12.0	0.77	0.14	8.0
10-Mar	32.1	20.2	15.4	0.91	0.39	6.9	9-Sep	31.4	13.1	11.7	0.53	0.06	6.7
11-Mar	31.1	20.0	13.4	0.96	0.39	7.5	10-Sep	32.6	11.7	11.5	0.32	0.05	6.6
12-Mar	31.0	19.6	15.6	0.98	0.34	7.4	11-Sep	34.1	16.1	11.5	0.29	0.06	6.7
13-Mar	31.1	19.8	13.8	0.95	0.34	6.6	12-Sep	34.0	12.9	11.2	0.44	0.07	6.1
14-Mar	31.3	17.8	15.3	0.99	0.32	5.7	13-Sep	32.2	17.8	11.4	0.33	0.11	7.7
15-Mar	32.5	18.6	14.8	0.77	0.29	5.8	14-Sep	31.4	15.7	11.5	0.35	0.10	7.5
16-Mar	32.3	17.9	14.8	0.90	0.33	6.4	15-Sep	31.4	15.3	12.0	0.68	0.15	8.2
17-Mar	32.4	19.0	14.9	0.88	0.25	6.7	16-Sep	31.2	14.2	12.3	0.74	0.13	8.3
18-Mar	30.3	19.9	2.8	0.98	0.54	6.8	17-Sep	31.4	14.6	12.6	0.83	0.15	9.5
19-Mar	29.9	20.6	4.4	0.88	0.41	11.1	18-Sep	31.7	14.5	12.4	0.79	0.15	7.7
20-Mar	30.4	20.4	2.3	0.91	0.38	9.0	19-Sep	32.0	17.1	12.1	0.84	0.22	6.5
21-Mar	30.9	18.9	5.4	0.96	0.31	7.6	20-Sep	24.3	18.2	5.5	0.94	0.38	11.0
22-Mar	28.6	18.7	4.3	0.95	0.48	6.3	21-Sep	23.2	12.9	13.2	0.47	0.11	11.3
23-Mar	29.8	18.9	4.1	0.95	0.48	5.6	22-Sep	25.8	11.0	12.6	0.32	0.08	6.0
24-Mar	31.6	20.3	7.2	0.88	0.30	5.8	23-Sep	29.7	10.3	12.4	0.42	0.15	5.0
25-Mar	32.8	17.7	9.8	0.92	0.30	4.1	24-Sep	32.8	13.7	12.4	0.66	0.07	4.4
26-Mar	33.8	17.9	11.8	0.94	0.26	4.5	25-Sep	32.7	14.6	12.2	0.73	0.09	5.3
27-Mar	33.7	17.9	12.0	0.93	0.29	4.3	26-Sep	33.1	16.2	12.8	0.49	0.09	7.9
28-Mar	35.0	18.3	13.1	0.89	0.27	4.2	27-Sep	33.0	15.0	12.9	0.84	0.12	7.7
29-Mar	35.0	20.6	12.1	0.78	0.25	4.2	28-Sep	32.3	16.0	12.0	0.86	0.25	7.7
30-Mar	34.4	20.2	12.1	0.56	0.21	5.5	29-Sep	33.5	20.9	13.0	0.67	0.24	11.2
31-Mar	33.2	19.1	11.7	0.90	0.42	6.6	30-Sep	31.8	23.3	10.0	0.71	0.36	14.7
1-Apr	34.0	20.8	10.5	0.68	0.21	9.0	1-Oct	31.3	19.2	10.1	0.90	0.28	8.1
2-Apr	32.5	18.6	10.4	0.86	0.22	11.2	2-Oct	30.0	18.4	10.2	0.95	0.27	6.6
3-Apr	32.2	19.7	9.0	0.83	0.35	9.8	3-Oct	31.2	15.5	13.4	0.95	0.17	7.9
4-Apr	33.0	20.2	9.8	0.81	0.34	9.0	4-Oct	32.9	15.7	12.3	0.89	0.17	7.6
5-Apr	34.1	21.6	10.1	0.88	0.26	10.1	5-Oct	32.0	17.9	12.5	0.94	0.17	8.5
6-Apr	31.7	19.9	8.8	0.85	0.35	9.6	6-Oct	32.1	17.0	12.4	0.77	0.23	7.3
7-Apr	32.5	18.4	10.2	0.90	0.23	8.4	7-Oct	31.9	19.7	10.1	0.56	0.28	4.8
8-Apr	33.2	19.3	9.1	0.78	0.23	7.1	8-Oct	34.1	19.4	12.6	0.80	0.17	7.0
9-Apr	29.6	20.1	7.9	0.77	0.36	9.0	9-Oct	34.7	19.0	12.3	0.33	0.08	4.8
10-Apr	30.8	22.4	5.5	0.69	0.31	5.4	10-Oct	34.3	17.6	12.3	0.59	0.12	5.3

Table H.8: Detailed daily meteorological data for the generated generic year.

Date	Max temp (°C)	Min temp (°C)	Net rad (MJ/ m^2.d)	Max RH (dec)	Min RH (dec)	Avg wind speed (km/hr)	Date	Max temp (°C)	Min temp (°C)	Net rad (MJ/ m^2.d)	Max RH (dec)	Min RH (dec)	Avg wind speed (km/hr)
11-Apr	31.6	22.2	8.6	0.81	0.41	6.5	11-Oct	33.5	17.2	12.7	0.70	0.15	6.6
12-Apr	34.0	22.6	8.5	0.83	0.28	4.6	12-Oct	35.7	17.4	12.5	0.76	0.12	5.8
13-Apr	34.5	20.9	8.6	0.83	0.26	4.9	13-Oct	36.0	19.5	12.9	0.46	0.16	6.0
14-Apr	35.3	22.6	8.6	0.76	0.19	6.5	14-Oct	35.5	22.3	12.2	0.54	0.14	7.4
15-Apr	34.4	20.3	7.9	0.69	0.17	6.7	15-Oct	33.8	17.6	12.7	0.81	0.20	6.4
16-Apr	33.5	19.9	8.7	0.27	0.13	6.7	16-Oct	34.0	18.2	12.1	0.81	0.20	6.6
17-Apr	32.4	19.9	8.7	0.40	0.16	6.1	17-Oct	33.9	18.3	12.5	0.70	0.18	8.3
18-Apr	30.5	19.7	6.5	0.97	0.27	7.4	18-Oct	35.0	18.9	13.0	0.69	0.14	7.7
19-Apr	28.7	18.3	8.8	0.95	0.39	7.4	19-Oct	35.4	18.9	12.9	0.39	0.14	5.8
20-Apr	29.6	18.6	10.5	0.89	0.22	8.4	20-Oct	34.4	19.7	9.9	0.72	0.20	8.3
21-Apr	29.8	15.5	9.5	0.84	0.25	7.1	21-Oct	31.0	20.2	12.4	0.69	0.18	9.7
22-Apr	31.1	18.2	9.5	0.81	0.29	5.9	22-Oct	29.8	18.3	12.5	0.75	0.25	11.8
23-Apr	31.9	19.7	8.6	0.87	0.33	5.7	23-Oct	29.7	17.3	12.8	0.75	0.18	11.0
24-Apr	32.4	20.9	8.9	0.86	0.33	6.8	24-Oct	30.8	16.1	11.7	0.81	0.20	8.0
25-Apr	32.8	20.6	9.1	0.88	0.30	7.3	25-Oct	30.5	16.8	12.5	0.80	0.21	8.8
26-Apr	32.0	21.2	9.4	0.84	0.29	8.5	26-Oct	31.1	17.1	13.4	0.80	0.18	9.1
27-Apr	32.2	21.2	8.8	0.88	0.32	8.7	27-Oct	32.3	18.3	14.5	0.80	0.11	10.3
28-Apr	30.4	21.3	6.9	0.85	0.41	9.9	28-Oct	32.1	17.5	13.9	0.80	0.21	9.5
29-Apr	31.3	20.5	8.6	0.88	0.35	8.0	29-Oct	33.8	16.9	13.6	0.59	0.16	8.1
30-Apr	31.3	20.8	7.0	0.88	0.24	7.7	30-Oct	34.8	18.3	13.3	0.56	0.16	8.3
1-May	27.8	17.3	7.9	0.98	0.41	3.0	31-Oct	34.0	17.2	13.2	0.85	0.18	6.9
2-May	28.5	16.9	9.1	0.96	0.41	3.4	1-Nov	35.0	18.9	13.7	0.71	0.20	7.2
3-May	29.8	16.2	8.6	1.00	0.39	2.6	2-Nov	31.3	20.1	10.5	0.94	0.34	6.4
4-May	30.4	16.3	9.4	1.00	0.35	4.0	3-Nov	33.3	19.0	14.8	0.88	0.26	5.8
5-May	30.5	15.9	9.5	1.00	0.40	3.7	4-Nov	34.1	17.6	13.6	0.96	0.15	5.6
6-May	30.9	15.9	9.9	1.00	0.38	2.6	5-Nov	35.2	17.5	11.4	0.90	0.11	5.6
7-May	29.3	17.9	8.9	0.89	0.46	3.3	6-Nov	35.4	19.0	12.3	0.92	0.09	5.3
8-May	27.7	15.5	8.6	0.94	0.49	4.6	7-Nov	36.2	20.6	11.6	0.86	0.17	6.2
9-May	26.1	18.0	4.3	0.95	0.61	3.9	8-Nov	32.5	20.6	9.3	0.82	0.32	6.6
10-May	25.7	18.9	6.6	0.98	0.53	4.8	9-Nov	33.7	18.3	12.9	0.97	0.26	7.7
11-May	26.3	16.4	6.9	0.93	0.48	5.5	10-Nov	31.6	18.4	13.6	0.98	0.31	6.5
12-May	25.9	13.9	7.1	1.00	0.44	4.7	11-Nov	32.4	18.8	11.8	0.80	0.29	5.4
13-May	27.0	14.2	7.9	1.00	0.39	3.0	12-Nov	34.7	19.4	14.8	0.89	0.24	6.9
14-May	27.1	14.7	6.1	0.97	0.46	3.0	13-Nov	35.5	20.6	14.4	0.84	0.20	8.5
15-May	28.4	15.6	8.3	1.00	0.43	2.8	14-Nov	34.0	21.3	10.6	0.84	0.31	5.9
16-May	26.7	13.8	8.0	1.00	0.35	2.6	15-Nov	36.6	21.5	15.2	0.87	0.22	5.9
17-May	26.7	12.6	6.3	0.88	0.39	3.0	16-Nov	32.9	23.4	8.8	0.80	0.38	6.7
18-May	25.9	14.7	6.7	0.99	0.44	4.0	17-Nov	35.7	21.3	14.2	0.79	0.21	6.9
19-May	25.7	16.7	3.7	1.00	0.50	4.6	18-Nov	36.4	22.2	13.0	0.75	0.26	7.5
20-May	20.3	16.5	1.1	1.00	0.82	4.6	19-Nov	33.9	21.6	11.9	0.93	0.25	8.0
21-May	22.1	17.6	2.2	1.00	0.73	4.4	20-Nov	33.8	20.8	14.7	0.88	0.23	6.9
22-May	24.6	17.4	4.9	0.96	0.62	4.0	21-Nov	33.1	20.2	15.3	0.83	0.20	7.7
23-May	24.1	17.7	3.8	0.98	0.63	4.2	22-Nov	33.4	19.5	15.1	0.71	0.16	8.2
24-May	25.0	15.9	4.4	0.98	0.59	3.9	23-Nov	31.9	20.0	11.5	0.80	0.26	8.6
25-May	26.7	15.1	8.2	1.00	0.44	2.6	24-Nov	33.2	19.7	14.6	0.74	0.21	11.0
26-May	28.2	14.7	8.9	1.00	0.39	3.1	25-Nov	32.1	18.9	10.0	0.92	0.31	7.7

Table H.8: Detailed daily meteorological data for the generated generic year.

Date	Max temp (°C)	Min temp (°C)	Net rad (MJ/ m^2.d)	Max RH (dec)	Min RH (dec)	Avg wind speed (km/hr)	Date	Max temp (°C)	Min temp (°C)	Net rad (MJ/ m^2.d)	Max RH (dec)	Min RH (dec)	Avg wind speed (km/hr)
27-May	29.5	16.5	7.0	1.00	0.47	2.6	26-Nov	34.0	20.2	15.1	0.96	0.32	6.9
28-May	29.6	17.7	8.1	0.91	0.34	3.0	27-Nov	34.2	20.2	14.7	0.96	0.32	5.3
29-May	23.1	11.4	7.1	0.73	0.31	5.1	28-Nov	36.5	21.2	15.6	0.92	0.15	6.2
30-May	20.6	6.9	6.6	0.66	0.22	4.2	29-Nov	36.8	23.0	15.3	0.80	0.18	5.8
31-May	22.2	8.4	7.4	0.62	0.20	4.4	30-Nov	35.3	22.0	11.2	0.80	0.30	7.2
1-Jun	25.5	11.2	5.6	0.63	0.14	5.2	1-Dec	33.3	21.5	14.6	0.96	0.37	6.3
2-Jun	22.9	8.6	5.6	0.70	0.24	5.4	2-Dec	33.1	20.7	14.0	0.93	0.31	9.8
3-Jun	23.9	9.6	5.7	0.93	0.45	4.9	3-Dec	31.2	19.7	16.0	0.86	0.28	9.5
4-Jun	25.4	14.7	6.0	0.97	0.42	5.3	4-Dec	32.1	19.6	15.6	0.81	0.26	8.4
5-Jun	25.9	14.5	6.3	0.96	0.36	5.3	5-Dec	34.8	16.3	15.1	0.64	0.15	6.6
6-Jun	25.7	15.2	7.3	0.96	0.43	5.4	6-Dec	35.8	18.9	14.3	0.58	0.16	5.8
7-Jun	23.9	16.4	4.2	0.89	0.46	5.7	7-Dec	35.0	19.8	14.8	0.64	0.22	6.5
8-Jun	24.5	13.8	6.6	0.86	0.35	7.6	8-Dec	33.6	20.2	14.1	0.85	0.30	9.0
9-Jun	23.8	13.4	6.0	0.88	0.39	6.6	9-Dec	30.5	21.3	9.7	0.83	0.41	9.5
10-Jun	23.4	14.0	5.1	0.93	0.46	6.7	10-Dec	28.9	20.7	5.7	0.83	0.51	8.5
11-Jun	24.1	13.7	4.8	0.94	0.45	6.4	11-Dec	28.3	20.8	7.2	0.93	0.54	8.2
12-Jun	25.9	13.3	6.6	0.95	0.34	5.1	12-Dec	30.9	20.9	9.8	0.98	0.43	7.6
13-Jun	26.6	13.5	6.2	0.98	0.33	3.8	13-Dec	31.6	19.8	12.0	0.98	0.42	7.7
14-Jun	26.5	13.7	5.8	0.86	0.33	5.0	14-Dec	33.9	20.4	16.9	0.96	0.32	6.8
15-Jun	22.8	12.6	6.1	0.65	0.24	6.8	15-Dec	34.9	21.4	16.1	0.95	0.32	5.8
16-Jun	21.3	9.5	5.4	0.60	0.16	7.7	16-Dec	35.8	22.5	12.7	0.93	0.33	5.5
17-Jun	21.2	8.6	5.6	0.60	0.27	6.8	17-Dec	36.8	21.8	14.0	0.98	0.25	4.6
18-Jun	22.5	10.2	6.9	0.72	0.38	6.7	18-Dec	34.4	23.1	8.2	0.95	0.44	5.5
19-Jun	23.7	11.1	7.1	0.80	0.38	7.1	19-Dec	36.2	21.9	16.2	0.98	0.34	6.6
20-Jun	17.2	13.8	2.1	0.94	0.70	7.4	20-Dec	33.8	24.3	11.0	0.91	0.44	7.6
21-Jun	22.3	13.0	8.2	0.89	0.48	7.4	21-Dec	33.6	22.3	13.2	1.00	0.46	5.7
22-Jun	24.2	13.2	8.1	0.91	0.37	6.9	22-Dec	34.1	22.6	14.6	1.00	0.42	4.7
23-Jun	23.4	16.7	6.9	0.99	0.56	8.0	23-Dec	32.3	22.4	12.7	1.00	0.38	4.9
24-Jun	22.1	17.0	4.3	0.98	0.63	7.3	24-Dec	34.1	20.3	16.9	0.90	0.23	5.8
25-Jun	20.5	16.2	3.7	0.91	0.64	7.6	25-Dec	34.6	20.9	16.2	1.00	0.26	5.7
26-Jun	24.3	15.7	7.5	0.79	0.36	6.8	26-Dec	34.5	21.4	14.0	0.92	0.35	5.3
27-Jun	22.1	13.1	3.4	0.90	0.43	5.6	27-Dec	33.9	22.1	10.4	0.94	0.43	6.3
28-Jun	22.1	9.1	6.6	0.49	0.24	5.3	28-Dec	33.7	22.1	11.7	0.98	0.42	5.7
29-Jun	21.5	7.8	6.4	0.66	0.18	5.3	29-Dec	31.8	21.6	9.3	1.00	0.52	4.8
30-Jun	22.7	8.7	6.6	0.76	0.27	5.2	30-Dec	29.1	20.4	10.2	1.00	0.61	6.4
1-Jul	26.4	13.2	6.6	0.59	0.16	7.3	31-Dec	29.2	20.7	9.8	1.00	0.53	10.9
2-Jul	24.8	11.4	5.9	0.75	0.14	7.1							

Table H.9: Detailed daily meteorological data for the period 1 December 2000 to 30 April 2001 measured with the Kidston automated weather station.

Date	Max temp (°C)	Min temp (°C)	Net rad (MJ/ m^2.d)	Max RH (dec)	Min RH (dec)	Avg wind speed (km/ hr)	Date	Max temp (°C)	Min temp (°C)	Net rad (MJ/ m^2.d)	Max RH (dec)	Min RH (dec)	Avg wind speed (km/ hr)
1-Dec-00	31.3	16.1	17.6	0.99	0.36	4.7	15-Feb-01	31.6	22.2	11.6	1.01	0.54	6.5
2-Dec-00	31.6	18.7	13.7	0.97	0.34	4.1	16-Feb-01	31.8	22.7	10.4	1.00	0.57	6.8
3-Dec-00	32.5	17.7	17.3	0.96	0.25	4.7	17-Feb-01	27.7	22.6	7.9	1.01	0.76	5.1
4-Dec-00	31.1	17.6	15.3	0.93	0.43	6.0	18-Feb-01	23.5	18.2	4.1	1.03	0.84	4.6
5-Dec-00	31.2	19.5	12.8	0.88	0.41	6.3	19-Feb-01	21.5	18.4	3.1	1.02	0.91	4.0
6-Dec-00	31.3	20.6	12.8	0.85	0.46	5.9	20-Feb-01	29.2	19.4	16.3	0.98	0.45	5.6
7-Dec-00	30.5	21.3	12.6	0.86	0.49	6.7	21-Feb-01	30.1	17.5	16.1	1.01	0.37	4.4
8-Dec-00	28.5	20.9	7.4	0.88	0.34	5.0	22-Feb-01	30.6	17.8	16.7	0.98	0.35	3.5
9-Dec-00	26.6	17.2	7.0	0.98	0.35	5.3	23-Feb-01	32.0	18.3	16.8	0.96	0.30	3.5
10-Dec-00	25.1	17.3	6.2	0.99	0.66	3.8	24-Feb-01	30.5	18.4	8.6	0.97	0.41	3.5
11-Dec-00	28.4	19.9	10.9	0.98	0.44	7.0	25-Feb-01	29.2	22.5	8.3	1.02	0.66	6.0
12-Dec-00	28.5	20.7	8.2	0.89	0.48	8.1	26-Feb-01	27.8	21.9	7.0	1.03	0.77	6.5
13-Dec-00	23.7	17.1	5.5	1.02	0.62	6.0	27-Feb-01	30.8	21.1	11.3	1.03	0.60	5.8
14-Dec-00	28.2	16.7	7.9	1.03	0.67	4.4	28-Feb-01	31.0	21.5	12.0	1.03	0.56	4.3
15-Dec-00	31.3	20.0	16.5	1.03	0.46	6.4	1-Mar-01	32.7	21.6	14.3	1.03	0.51	3.2
16-Dec-00	32.3	19.9	14.4	1.02	0.40	5.9	2-Mar-01	32.7	21.7	16.6	1.03	0.37	2.7
17-Dec-00	32.2	20.7	12.9	1.02	0.48	5.8	3-Mar-01	32.6	20.5	17.0	0.97	0.34	3.0
18-Dec-00	25.6	19.0	5.6	1.03	0.81	3.6	4-Mar-01	32.7	20.9	14.5	0.97	0.35	4.5
19-Dec-00	28.5	21.1	8.8	1.00	0.67	4.6	5-Mar-01	31.7	20.6	12.7	1.03	0.54	4.2
20-Dec-00	27.5	20.0	9.0	1.01	0.53	6.3	6-Mar-01	29.1	20.4	10.6	1.03	0.61	3.4
21-Dec-00	28.5	20.6	9.0	0.93	0.54	6.2	7-Mar-01	30.7	19.4	14.7	1.03	0.42	2.9
22-Dec-00	30.5	18.7	14.0	0.98	0.41	5.3	8-Mar-01	32.1	18.1	15.9	1.03	0.31	2.4
23-Dec-00	31.2	18.5	18.0	0.96	0.37	4.7	9-Mar-01	31.4	18.4	12.6	1.00	0.42	4.3
24-Dec-00	32.1	18.7	17.1	0.98	0.33	4.1	10-Mar-01	32.7	18.7	14.7	1.03	0.35	3.2
25-Dec-00	31.8	18.6	16.1	0.91	0.33	3.1	11-Mar-01	32.9	18.2	16.7	1.03	0.31	2.9
26-Dec-00	33.1	20.3	14.3	0.94	0.31	3.7	12-Mar-01	32.4	18.4	16.1	0.99	0.30	3.1
27-Dec-00	30.2	21.0	9.5	1.00	0.51	4.0	13-Mar-01	34.1	19.9	16.4	1.02	0.32	3.2
28-Dec-00	29.4	21.1	10.2	1.03	0.61	3.3	14-Mar-01	33.7	19.9	13.4	1.00	0.38	3.3
29-Dec-00	28.9	21.9	7.8	1.03	0.68	7.2	15-Mar-01	32.0	21.4	12.4	0.96	0.49	6.0
30-Dec-00	29.7	20.6	8.5	1.04	0.67	4.8	16-Mar-01	29.3	21.6	9.3	1.00	0.62	5.4
31-Dec-00	28.4	20.5	5.9	1.04	0.71	2.9	17-Mar-01	30.2	20.8	13.0	1.03	0.62	5.2
1-Jan-01	32.4	19.9	15.5	1.04	0.50	5.1	18-Mar-01	31.8	20.6	13.6	1.03	0.49	4.4
2-Jan-01	27.3	19.6	5.2	1.04	0.64	4.2	19-Mar-01	32.8	19.9	15.8	1.02	0.37	3.2
3-Jan-01	30.5	20.7	13.1	0.99	0.49	4.9	20-Mar-01	34.0	19.5	15.2	1.01	0.36	3.5
4-Jan-01	30.0	19.7	15.4	0.98	0.45	4.9	21-Mar-01	34.4	21.3	13.8	1.02	0.38	4.1
5-Jan-01	30.2	18.1	17.5	0.96	0.39	5.4	22-Mar-01	34.0	21.2	15.8	1.03	0.43	3.4
6-Jan-01	29.6	17.8	17.1	0.97	0.37	5.3	23-Mar-01	34.3	22.1	14.8	1.00	0.41	3.6
7-Jan-01	31.5	17.1	17.1	1.00	0.24	4.2	24-Mar-01	33.0	22.0	13.9	1.03	0.49	3.8
8-Jan-01	31.1	16.5	17.1	1.00	0.30	4.9	25-Mar-01	33.5	22.2	13.6	1.02	0.49	3.1
9-Jan-01	32.0	17.3	14.7	0.84	0.25	4.0	26-Mar-01	32.6	21.7	14.4	1.03	0.47	3.2
10-Jan-01	31.6	18.6	12.8	0.87	0.30	4.1	27-Mar-01	32.4	21.6	14.2	1.03	0.47	3.8
11-Jan-01	33.2	19.6	17.1	0.98	0.35	5.6	28-Mar-01	31.6	21.7	13.0	0.99	0.48	4.3
12-Jan-01	30.9	18.8	11.5	0.96	0.42	4.9	29-Mar-01	31.4	21.2	13.7	1.01	0.48	4.0
13-Jan-01	32.1	19.8	16.6	0.97	0.40	5.3	30-Mar-01	31.3	20.1	12.1	0.96	0.49	4.9

Table H.9: Detailed daily meteorological data for the period 1 December 2000 to 30 April 2001 measured with the Kidston automated weather station.

Date	Max temp (°C)	Min temp (°C)	Net rad (MJ/ m^2.d)	Max RH (dec)	Min RH (dec)	Avg wind speed (km/ hr)	Date	Max temp (°C)	Min temp (°C)	Net rad (MJ/ m^2.d)	Max RH (dec)	Min RH (dec)	Avg wind speed (km/ hr)
14-Jan-01	31.6	19.7	15.4	0.89	0.35	4.6	31-Mar-01	29.9	19.7	13.6	0.96	0.50	7.1
15-Jan-01	31.9	20.1	12.7	0.91	0.40	4.8	1-Apr-01	29.3	19.9	10.6	0.91	0.51	6.2
16-Jan-01	33.3	20.3	15.2	0.96	0.30	4.3	2-Apr-01	27.8	20.0	8.7	0.94	0.56	5.8
17-Jan-01	34.4	17.7	15.4	1.00	0.28	4.7	3-Apr-01	29.0	19.5	11.4	0.96	0.48	5.8
18-Jan-01	34.2	20.1	16.3	0.91	0.30	5.4	4-Apr-01	29.5	17.7	12.7	1.01	0.44	5.4
19-Jan-01	36.3	20.3	16.4	1.00	0.34	3.9	5-Apr-01	28.7	19.3	12.5	0.94	0.47	6.2
20-Jan-01	36.2	19.3	15.2	1.02	0.41	8.5	6-Apr-01	28.3	19.6	9.8	0.87	0.47	7.3
21-Jan-01	29.3	19.2	10.9	1.02	0.60	4.1	7-Apr-01	26.7	18.0	7.6	0.91	0.49	6.4
22-Jan-01	29.4	20.2	10.3	1.01	0.53	4.5	8-Apr-01	28.3	17.0	12.3	0.97	0.43	6.0
23-Jan-01	31.9	20.3	14.0	1.02	0.45	3.5	9-Apr-01	29.5	16.5	12.2	1.00	0.38	3.4
24-Jan-01	34.1	21.6	17.9	1.00	0.41	3.4	10-Apr-01	30.1	17.3	11.4	0.97	0.39	3.7
25-Jan-01	33.7	21.8	15.7	0.98	0.43	4.3	11-Apr-01	30.4	17.4	12.7	1.00	0.36	3.7
26-Jan-01	32.6	22.2	16.2	0.91	0.37	4.9	12-Apr-01	30.1	15.4	12.2	0.89	0.34	3.9
27-Jan-01	30.4	21.6	8.2	0.92	0.49	3.6	13-Apr-01	29.6	18.8	8.9	0.96	0.38	5.3
28-Jan-01	32.2	21.5	12.8	0.98	0.33	3.2	14-Apr-01	29.5	16.5	12.9	1.00	0.31	6.2
29-Jan-01	36.2	21.1	16.7	0.91	0.26	3.5	15-Apr-01	29.5	18.1	11.4	0.93	0.42	6.4
30-Jan-01	36.9	23.4	15.3	0.92	0.21	4.9	16-Apr-01	28.6	17.1	10.5	0.98	0.42	6.8
31-Jan-01	36.5	20.4	16.5	0.87	0.28	3.7	17-Apr-01	28.0	15.2	9.1	1.00	0.44	5.3
1-Feb-01	33.2	22.2	13.8	1.01	0.51	5.1	18-Apr-01	28.5	15.8	12.6	1.01	0.35	5.9
2-Feb-01	30.2	21.8	7.8	1.04	0.67	4.8	19-Apr-01	28.1	15.6	9.0	1.00	0.47	5.4
3-Feb-01	28.7	20.4	5.9	1.03	0.74	5.1	20-Apr-01	29.2	16.7	12.3	1.01	0.34	5.1
4-Feb-01	27.5	20.4	9.3	1.03	0.71	6.4	21-Apr-01	28.0	15.2	7.7	0.98	0.50	3.3
5-Feb-01	30.4	21.1	12.4	1.03	0.62	4.2	22-Apr-01	29.7	16.5	9.7	1.01	0.42	2.9
6-Feb-01	32.1	21.8	14.8	1.02	0.51	4.3	23-Apr-01	31.3	16.7	12.2	1.01	0.33	2.8
7-Feb-01	29.6	20.1	14.6	0.99	0.50	5.1	24-Apr-01	31.1	18.2	10.4	0.73	0.39	3.5
8-Feb-01	29.0	20.6	12.1	0.95	0.53	5.4	25-Apr-01	31.8	18.1	11.5	0.86	0.34	4.2
9-Feb-01	31.9	20.2	16.9	0.96	0.45	5.7	26-Apr-01	31.6	20.7	10.5	1.00	0.47	5.5
10-Feb-01	31.1	19.0	12.7	0.98	0.45	6.2	27-Apr-01	31.7	18.9	11.1	1.00	0.44	4.0
11-Feb-01	31.5	19.8	15.2	0.98	0.44	6.1	28-Apr-01	32.0	18.8	9.8	1.01	0.39	4.0
12-Feb-01	30.0	19.9	13.5	0.95	0.54	6.5	29-Apr-01	32.0	17.7	11.3	1.01	0.36	4.1
13-Feb-01	31.6	20.6	11.3	0.94	0.48	5.6	30-Apr-01	30.1	18.6	11.2	0.97	0.41	5.7
14-Feb-01	32.1	20.0	12.9	0.97	0.54	5.7							

H.3 Bowen Ratio Station

The following sections describe the Bowen ratio station installation as well as documents the data recorded with the equipment.

H.3.1 Bowen Ratio Station Components

The Bowen ratio station was located on the northeastern section of the tailings impoundment approximately 100 m from the wall. The Bowen ratio energy balance method of measuring evapotranspiration was selected for the field program at Kidston Gold Mine. The Bowen ratio system, supplied by Campbell Scientific (Australia) Corporation, was a fully automated monitoring system that measures net radiation, soil heat flux, and vertical gradients of air temperature and vapor pressure. Table H.10 lists all the components of the Bowen ratio station.

Table H.10: Details of the components of the fully automated Bowen ratio station installed on the Kidston tailings impoundment in 1997.

Sensor	Parameter measured	Reference
Fine-wire Thermocouples	Air temperature at two heights	CSI (1997)
Soil Heat Flux Plate	Surface soil heat flux	CSI (1993b)
Dew Point Hygrometer	Vapour pressure at two heights	CSI (1997)
Two point Averaging Thermocouple	Surface soil heat flux	CSI (1997)
05103-10 RM Young Wind Monitor	Wind speed & direction	CSI (1993a)
Radiation and Energy Balance Systems, Inc. (REBS) Model Q7.1 net radiometer	Net radiation	CSI (1995)
CM10 tripod	Tripod for mounting components	CSI (1994a)
21X Measurement and Control Module	Data Measurement and Control Module	CSI (1993d)
SM716 storage module	Data storage module	CSI (1993c)
MSX-30 solar panel	30 watt solar panel	Solarex (1996)

The various Bowen ratio parameters are measured as follows; net radiation was measured with net radiometer (CSI, 1995); soil heat flux at the surface was calculated from the sum of two measurements, 1) the soil heat flux at approximately 0.08 m below the surface, measured with a soil heat flux plate (CSI, 1993b), and 2) the heat stored above the plate, measured with a two-point averaging thermocouple (CSI, 1997); air temperature was measured at two heights with individual fine-wire thermocouples; and, vapour pressure at two heights was calculated by measuring the dew point temperature with a single cooled-mirror dew point hygrometer (CSI, 1997).

The Bowen ratio monitoring equipment and data acquisition system was installed as directed by the manufacturer. The lower and upper support arm for the fine-wire thermocouples and air intakes were mounted at heights above the ground surface of approximately 0.5 m and 2.5 m respectively. The support arms were mounted on the tripod mast as far apart as possible in order

to maximize the measuring resolution of the air temperature and vapor pressure gradients. Two soil heat flux measuring systems, each consisting of two soil thermocouples and one heat flux plate, were installed in undisturbed tailings near the station. A shovel was used the expose a vertical face in the surface soil layer in order to install the heat flux plate 0.08 m below surface and the thermocouples 0.02 m and 0.06 m below the surface. The net radiometer was mounted to a steel post at a height of approximately 0.8 m above the soil surface. The wind monitor was mounted on a steel cross arm at a height of approximately 3 m above the ground surface. The data acquisition system consisted of a 21X data logger, SM716 storage module and an MSX-30 solar panel / 12 volt deep cycle battery system.

The supplier prior to shipping the sensors to site calibrated the Bowen ratio sensors. The sensors did not require additional field calibration. The supplier recommends annual re-calibration of the net radiometer, but this was never done due to an oversight when the maintenance procedure for the study was established.

H.3.2 Bowen Ratio Station Data Output Format

The PC208 software package (Campbell Scientific, 1994c) was used to develop and document the program for the 21X measurement and control module used in this study. The program determined the frequency of sensor readings and the format of the data output.

The average lower and higher air temperature (°C), lower and higher dew point temperature (°C), net radiation (W/m^2), soil heat flux (W/m^2), wind speed (m/s), and wind direction (degrees form north) were output based on the last 20 minutes of sensor readings. The execution interval of the data logger program is 60 seconds. Therefore the averages listed above were based on 20 sensor readings. Wind direction will read 0° if the wind is coming from the north and 180° if the wind is coming from the south.

H.3.3 Bowen Ratio Station Data Collection and Station Maintenance

A Campbell Scientific 21X measurement and control module was used to access and store data from the Bowen ratio station sensors. Data stored in the 21X was downloaded using a laptop computer, or by retrieving the SM716 storage module if inclement weather prevented the use of

the laptop computer. The 21X measurement and control module continued to store data from the sensors in the absence of the storage module.

Data must be downloaded from the 21X measurement and control module every 276 days, however whenever possible data was downloaded at least once per month in order to minimize potential problems with the automated monitoring system. The memory on the 21X measurement and control module and the SM716 storage module is formatted in a ring style configuration. In other words, new data continues to be stored even after the 21X or SM716 is full since the new data replaces the oldest data.

Routine maintenance of the Bowen ratio monitoring equipment was necessary in order to ensure the collection of accurate measurements (CSI, 1997). The level of the net radiometer was checked regularly and adjusted accordingly. The filters in the upper and lower air intakes were changed and the mirror in the hygrometer cleaned at least once per month. The fine-wire thermocouples were cleaned as necessary. Kidston Gold Mines staff carried out the maintenance.

H.3.4 Bowen Ratio Energy Balance Method

The Bowen ratio energy balance (BREB) method is common method to determine actual evapotranspiration rates from various land surfaces (Blight, 1997). This technique has been reviewed and tested by many in the agricultural industry (Tanner, 1960; Fritschen, 1966; Fuchs and Tanner, 1967). Woyshner and St-Arnaud (1994) successfully used the BREB technique to evaluate evaporation from a bare tailings surface in Ontario. Bowen (1926) introduced the ratio of sensible heat flux (Q_H) to latent heat flux (Q_E), which has been subsequently termed the Bowen ratio, β. Typical values of β vary between 0.1 for oceans to as high as 10 in deserts. The Bowen ratio is determined by:

$$\beta = \frac{Q_H}{Q_E} = \gamma \frac{\Delta T}{\Delta e} \qquad [H.1]$$

Where γ = psychrometric constant, $\frac{Pc_p}{\lambda \varepsilon}$,

P = atmospheric pressure (kPa),

c_p = specific heat of air (kJ/kg°C),

λ = latent heat of vaporization (kJ/kg),

ε = ratio of the molecular weight of water to the molecular weight of dry air, and

$\Delta T, \Delta e$ = change in air temperature (°C) and vapor pressure (kPa), respectively, over the same height and interval above the ground surface.

The energy balance equation determines how the ground surface converts net radiative energy (Q^*) into heat fluxes (Oke, 1987):

$$Q^* = Q_E + Q_H + Q_G + Q_A + Q_S \qquad [H.2]$$

Where Q_E = latent heat flux (W/m^2),

Q_H = sensible heat flux (W/m^2),

Q_G = conduction of heat to or from the subsurface soil (W/m^2),

Q_A = horizontal heat advection through the atmosphere (W/m^2), and

Q_S = hear stored in the ground surface (W/m^2).

Substituting Equation H.1 into Equation H.2, and neglecting the heat storage and advection (Q_S and Q_A) in the surface energy balance, the quantity of Q_E may be computed as follows (Oke, 1987):

$$Q_E = \frac{Q^* - Q_G}{1 + \beta} \qquad [H.3]$$

Measurements of Q^*, Q_G, P, and T and e at two heights are required to estimate sensible and latent heat flux at the ground surface. Sensors for the measurement of these parameters are recorded for a specified time interval (20 minutes). Atmospheric pressure seldom varies by more than a few percent and therefore, P may be calculated from the site elevation assuming a standard atmosphere (CSI, 1997).

The accuracy of the BREB method depends on the validity of the following three assumptions (Fritschen and Simpson, 1989; Oke, 1987):

1. Steady atmospheric conditions during the observation period;
2. Constant energy and mass fluxes with height with no vertical convergence or divergence;
3. The transfer coefficients of eddy conductivity for heat and eddy difusivity for water vapor are numerically equal.

These assumptions appear to be valid when the instruments for measuring air temperature and vapor pressure are mounted close to the surface and over a large homogeneous area (Fritschen and Qian, 1990). The BREB method is subject to two main problems when applied in practice because of the resolution limits of the gradient sensors (Maidment, 1993; Ohmura, 1982). The first problem is the possibility of obtaining wrong signs for the energy fluxes (e.g. confusion between evaporation and condensation). Ohmura (1982) presents the following two conditions:

$$If\left(Q^{*}+Q_{G}\right)>0, then \Delta T>-\left(\frac{\Delta e}{\gamma}\right)$$
$$if\left(Q^{*}+Q_{G}\right)<0, then \Delta T<-\left(\frac{\Delta e}{\gamma}\right) \qquad [H.4]$$

If Bowen ratio data do not satisfy one of these conditions, then the data is not consistent with the definition of the flux / gradient relationship and should be rejected. Ohmura (1982) encountered this problem with early morning and late afternoon data and during precipitation, when gradients are small. The second practical problem with the BREB method is the possibility of obtaining an extremely inaccurate magnitude of the energy fluxes, even though the signs are correct. When β approaches –1 in Equation H.1, the value of Q_E loses its numerical meaning. Ohmura (1982) provided the following inequality:

$$-\left(\frac{\Delta e}{\gamma}\right)-2\left[\frac{R_{e}}{\gamma}+R_{T}\right]<\Delta T<-\left(\frac{\Delta e}{\gamma}\right)+2\left[\frac{R_{e}}{\gamma}+R_{T}\right] \qquad [H.5]$$

Where R_e = resolution of the vapor pressure sensor, and
R_T = resolution of the air temperature sensor.

If Bowen ratio data satisfies the above inequality, then there is a high possibility that β will be very near –1 and therefore, the data should be excluded from evaluation. Ohmura (1982)

encountered this problem during similar times he encountered the first problem. Fortunately, these problems occur during relatively uninteresting times, when heat exchange at the ground surface, and therefore evapotranspiration, is low.

H.3.5 Bowen Ratio Station Data

The Bowen ratio energy balance (BREB) method was used to measure the actual evapotranspiration (AET) on the Kidston tailings impoundment. Daily and cumulative AET data collected in from 1997 to 2000 are presented in Tables H.11 to H.14. The Bowen ratio system never performed well, and as a result the data is scarce, and often data had to be rejected due to obvious inaccuracies therein. The reason for the poor performance of the equipment is ascribed to a poor initial installation followed by subsequent frequent damage due to lightning strikes. Kidston Gold Mines had the equipment supplier out on a number of occasions, and even that had not resolved the problems. The problem with the equipment was further exasperated by the fact that virtually none of the regular maintenance required was done.

Table H.11: Daily summary of actual evapotranspiration (AET) data measured with the Bowen ratio station for 1997.

Date	AET (mm)	Cum AET (mm)	Date	AET (mm)	Cum AET (mm)	Date	AET (mm)	Cum AET (mm)
11-Dec-97	1.10	1.10	18-Dec-97	0.94	7.12	25-Dec-97	0.63	11.34
12-Dec-97	1.08	2.18	19-Dec-97	0.70	7.82	26-Dec-97	0.44	11.78
13-Dec-97	0.94	3.12	20-Dec-97	0.37	8.19	27-Dec-97	0.57	12.34
14-Dec-97	0.54	3.65	21-Dec-97	0.74	8.92	28-Dec-97	0.51	12.85
15-Dec-97	0.79	4.45	22-Dec-97	0.30	9.23	29-Dec-97	0.74	13.60
16-Dec-97	0.66	5.10	23-Dec-97	0.76	9.99	30-Dec-97	0.99	14.59
17-Dec-97	1.07	6.18	24-Dec-97	0.72	10.71	31-Dec-97	0.33	14.91

Table H.12: Daily summary of actual evapotranspiration (AET) data measured with the Bowen ratio station for 1998.

Date	AET (mm)	Cum AET (mm)	Date	AET (mm)	Cum AET (mm)	Date	AET (mm)	Cum AET (mm)
22-Oct-98	4.83	4.83	16-Nov-98	4.13	79.71	6-Dec-98	9.54	53.96
26-Oct-98	10.53	15.37	17-Nov-98	7.29	87.00	7-Dec-98	9.35	63.31
27-Oct-98	2.75	18.12	18-Nov-98	0.53	87.52	8-Dec-98	7.65	70.96
28-Oct-98	11.04	29.16	19-Nov-98	7.96	95.49	9-Dec-98	4.38	75.34
29-Oct-98	12.62	41.78	20-Nov-98	2.31	97.80	10-Dec-98	5.65	80.99
30-Oct-98	1.53	43.31	21-Nov-98	10.25	108.05	14-Dec-98	0.28	81.27
31-Oct-98	4.51	47.82	22-Nov-98	4.43	112.48	16-Dec-98	1.52	82.79
			23-Nov-98	0.22	112.70	17-Dec-98	1.37	84.16
1-Nov-98	7.93	7.93	24-Nov-98	2.17	114.87	18-Dec-98	3.15	87.31
2-Nov-98	0.55	8.48	25-Nov-98	5.44	120.31	19-Dec-98	0.43	87.73
3-Nov-98	1.94	10.42	26-Nov-98	1.56	121.87	21-Dec-98	8.76	96.49

Table H.12: Daily summary of actual evapotranspiration (AET) data measured with the Bowen ratio station for 1998.

Date	AET (mm)	Cum AET (mm)	Date	AET (mm)	Cum AET (mm)	Date	AET (mm)	Cum AET (mm)
5-Nov-98	0.15	10.57	27-Nov-98	1.60	123.47	22-Dec-98	11.55	108.04
6-Nov-98	9.71	20.28	29-Nov-98	8.05	131.51	23-Dec-98	6.03	114.07
7-Nov-98	8.16	28.44	30-Nov-98	10.42	141.94	24-Dec-98	0.04	114.11
8-Nov-98	7.67	36.11				27-Dec-98	2.05	116.16
9-Nov-98	7.60	43.71	1-Dec-98	5.90	5.90	28-Dec-98	7.58	123.74
10-Nov-98	19.75	63.45	2-Dec-98	13.68	19.58	29-Dec-98	8.79	132.53
11-Nov-98	7.93	71.39	3-Dec-98	9.21	28.79	30-Dec-98	1.11	133.64
12-Nov-98	0.60	71.99	4-Dec-98	8.40	37.18	31-Dec-98	15.34	148.98
15-Nov-98	3.60	75.59	5-Dec-98	7.24	44.42			

Table H.13: Daily summary of actual evapotranspiration (AET) data measured with the Bowen ratio station for 1999.

Date	AET (mm)	Cum AET (mm)	Date	AET (mm)	Cum AET (mm)	Date	AET (mm)	Cum AET (mm)
1-Jan-99	10.14	10.14	30-Mar-99	10.47	117.84	17-Nov-99	13.32	49.71
2-Jan-99	11.82	21.96	31-Mar-99	6.75	124.59	18-Nov-99	8.27	57.98
3-Jan-99	7.39	29.35				19-Nov-99	10.96	68.94
4-Jan-99	2.49	31.84	1-Apr-99	8.85	8.85	20-Nov-99	20.11	89.05
5-Jan-99	0.59	32.42	2-Apr-99	12.64	21.49	21-Nov-99	12.72	101.76
6-Jan-99	3.38	35.81	3-Apr-99	10.00	31.49	22-Nov-99	6.33	108.09
7-Jan-99	1.03	36.84	4-Apr-99	4.29	35.78	23-Nov-99	4.38	112.48
8-Jan-99	10.39	47.23	5-Apr-99	6.36	42.14	24-Nov-99	11.54	124.02
			6-Apr-99	2.66	44.80	25-Nov-99	6.97	130.99
7-Feb-99	0.59	0.59	7-Apr-99	2.80	47.59	26-Nov-99	9.86	140.85
8-Feb-99	6.68	7.27	16-Apr-99	0.76	48.35	27-Nov-99	7.84	148.69
9-Feb-99	12.98	20.25	17-Apr-99	0.93	49.28	28-Nov-99	1.05	149.74
10-Feb-99	9.72	29.98	18-Apr-99	0.61	49.89	29-Nov-99	2.90	152.64
11-Feb-99	22.53	52.51				30-Nov-99	7.14	159.78
12-Feb-99	0.04	52.55	28-May-99	1.84	1.84			
16-Feb-99	0.55	53.10	29-May-99	3.00	4.84	1-Dec-99	6.40	6.40
17-Feb-99	10.14	63.24	30-May-99	7.62	12.46	2-Dec-99	2.95	9.35
18-Feb-99	6.05	69.29	31-May-99	7.93	20.39	4-Dec-99	2.81	12.16
19-Feb-99	3.12	72.41				5-Dec-99	5.77	17.92
20-Feb-99	0.41	72.82	1-Jun-99	1.82	1.82	6-Dec-99	3.14	21.06
21-Feb-99	5.18	78.00				7-Dec-99	5.71	26.78
22-Feb-99	10.84	88.84	17-Oct-99	2.06	2.06	8-Dec-99	9.16	35.94
23-Feb-99	10.46	99.30	18-Oct-99	1.43	3.50	9-Dec-99	4.51	40.45
24-Feb-99	4.89	104.19	19-Oct-99	3.37	6.87	10-Dec-99	4.51	44.96
25-Feb-99	1.13	105.32	20-Oct-99	1.49	8.36	11-Dec-99	6.43	51.39
26-Feb-99	0.70	106.02	21-Oct-99	1.43	9.78	12-Dec-99	9.51	60.90
27-Feb-99	6.36	112.38	22-Oct-99	4.09	13.88	13-Dec-99	11.48	72.38
			23-Oct-99	1.64	15.52	14-Dec-99	5.20	77.58
10-Mar-99	3.01	3.01	24-Oct-99	3.60	19.13	15-Dec-99	6.31	83.88
14-Mar-99	4.34	7.35	25-Oct-99	2.00	21.13	16-Dec-99	4.02	87.90
15-Mar-99	3.37	10.72	26-Oct-99	5.54	26.67	17-Dec-99	6.91	94.81
16-Mar-99	11.24	21.96	27-Oct-99	7.76	34.43	18-Dec-99	5.99	100.81
17-Mar-99	6.74	28.70	28-Oct-99	5.03	39.46	19-Dec-99	5.97	106.78

Table H.13: Daily summary of actual evapotranspiration (AET) data measured with the Bowen ratio station for 1999.

Date	AET (mm)	Cum AET (mm)	Date	AET (mm)	Cum AET (mm)	Date	AET (mm)	Cum AET (mm)
18-Mar-99	5.40	34.10	29-Oct-99	1.76	41.23	20-Dec-99	6.62	113.39
19-Mar-99	1.63	35.73	30-Oct-99	2.12	43.34	21-Dec-99	3.92	117.31
20-Mar-99	1.07	36.80	31-Oct-99	1.18	44.52	22-Dec-99	9.00	126.31
21-Mar-99	9.63	46.44				23-Dec-99	9.43	135.74
22-Mar-99	8.04	54.47	1-Nov-99	2.14	2.14	24-Dec-99	9.46	145.21
23-Mar-99	18.18	72.65	2-Nov-99	0.69	2.84	25-Dec-99	14.05	159.25
24-Mar-99	5.20	77.85	3-Nov-99	4.12	6.95	26-Dec-99	9.42	168.67
25-Mar-99	4.24	82.09	12-Nov-99	2.37	9.32	27-Dec-99	4.48	173.15
26-Mar-99	1.41	83.51	13-Nov-99	3.48	12.80	28-Dec-99	5.67	178.82
27-Mar-99	4.94	88.45	14-Nov-99	3.70	16.50	29-Dec-99	1.76	180.58
28-Mar-99	6.64	95.08	15-Nov-99	7.09	23.59	30-Dec-99	4.42	185.00
29-Mar-99	12.29	107.37	16-Nov-99	12.80	36.39	31-Dec-99	5.13	190.13

Table H.14: Daily summary of actual evapotranspiration (AET) data measured with the Bowen ratio station for 2000.

Date	AET (mm)	Cum AET (mm)	Date	AET (mm)	Cum AET (mm)	Date	AET (mm)	Cum AET (mm)
1-Jan-00	2.28	2.28	9-Mar-00	7.46	57.98	16-May-00	2.54	48.21
2-Jan-00	1.57	3.84	10-Mar-00	9.70	67.67	17-May-00	3.73	51.95
3-Jan-00	3.91	7.76	11-Mar-00	4.86	72.54	18-May-00	5.49	57.43
4-Jan-00	5.89	13.64	12-Mar-00	8.55	81.09	19-May-00	4.08	61.52
5-Jan-00	5.52	19.16	13-Mar-00	9.02	90.11	20-May-00	3.56	65.08
6-Jan-00	13.71	32.88	14-Mar-00	6.17	96.28	21-May-00	4.71	69.79
7-Jan-00	11.02	43.89	15-Mar-00	4.83	101.10	22-May-00	3.98	73.77
8-Jan-00	6.52	50.41	16-Mar-00	9.59	110.69			
9-Jan-00	3.08	53.49	17-Mar-00	3.63	114.32	24-Jul-00	0.82	0.82
10-Jan-00	3.69	57.19	18-Mar-00	4.08	118.40	25-Jul-00	0.77	1.59
11-Jan-00	10.18	67.37	19-Mar-00	5.32	123.72	26-Jul-00	1.39	2.98
12-Jan-00	8.58	75.95	20-Mar-00	4.92	128.64	27-Jul-00	0.30	3.27
13-Jan-00	7.67	83.62	21-Mar-00	6.66	135.30	28-Jul-00	0.29	3.57
14-Jan-00	8.64	92.26	22-Mar-00	2.09	137.39	29-Jul-00	1.48	5.05
15-Jan-00	11.48	103.74	23-Mar-00	4.06	141.46	30-Jul-00	3.19	8.23
16-Jan-00	6.50	110.24	24-Mar-00	8.08	149.54	31-Jul-00	1.17	9.40
17-Jan-00	6.82	117.06	25-Mar-00	5.06	154.60			
18-Jan-00	6.03	123.09	26-Mar-00	3.04	157.64	14-Oct-00	1.72	1.72
19-Jan-00	13.40	136.49	27-Mar-00	4.83	162.47	15-Oct-00	2.67	4.39
20-Jan-00	9.45	145.94	28-Mar-00	6.23	168.70	16-Oct-00	7.45	11.84
21-Jan-00	10.33	156.26	29-Mar-00	5.20	173.89	17-Oct-00	2.25	14.09
22-Jan-00	10.00	166.26	30-Mar-00	4.82	178.72	18-Oct-00	1.35	15.44
23-Jan-00	13.42	179.68	31-Mar-00	2.44	181.16	19-Oct-00	4.56	20.00
24-Jan-00	5.95	185.63				20-Oct-00	1.70	21.70
25-Jan-00	4.22	189.85	1-Apr-00	4.44	4.44	21-Oct-00	1.33	23.03
26-Jan-00	10.50	200.35	2-Apr-00	11.41	15.85	22-Oct-00	0.83	23.86
27-Jan-00	5.80	206.15	3-Apr-00	6.48	22.33	23-Oct-00	2.05	25.91
28-Jan-00	12.46	218.61	4-Apr-00	5.58	27.91	24-Oct-00	2.11	28.02
29-Jan-00	7.17	225.78	5-Apr-00	2.37	30.27	25-Oct-00	2.07	30.10
30-Jan-00	6.06	231.84	6-Apr-00	5.78	36.06	26-Oct-00	4.02	34.12

Table H.14: Daily summary of actual evapotranspiration (AET) data measured with the Bowen ratio station for 2000.

Date	AET (mm)	Cum AET (mm)	Date	AET (mm)	Cum AET (mm)	Date	AET (mm)	Cum AET (mm)
31-Jan-00	9.18	241.02	7-Apr-00	9.07	45.13	27-Oct-00	2.71	36.83
			8-Apr-00	6.86	51.99	28-Oct-00	2.79	39.62
1-Feb-00	7.58	7.58	9-Apr-00	5.71	57.70	29-Oct-00	2.29	41.91
2-Feb-00	6.14	13.71	10-Apr-00	4.14	61.83	30-Oct-00	3.35	45.25
3-Feb-00	5.91	19.62	11-Apr-00	7.66	69.49	31-Oct-00	3.49	48.74
4-Feb-00	2.35	21.97	12-Apr-00	4.28	73.77			
5-Feb-00	3.06	25.03	13-Apr-00	2.65	76.43	1-Nov-00	4.04	4.04
6-Feb-00	6.56	31.59	14-Apr-00	2.71	79.13	2-Nov-00	4.55	8.59
7-Feb-00	2.67	34.26	15-Apr-00	5.46	84.59	3-Nov-00	4.33	12.92
8-Feb-00	5.86	40.12	16-Apr-00	3.53	88.12	4-Nov-00	2.49	15.41
9-Feb-00	2.37	42.50	17-Apr-00	3.61	91.73	28-Nov-00	1.54	16.95
10-Feb-00	3.00	45.50	18-Apr-00	3.09	94.82	29-Nov-00	9.79	26.74
11-Feb-00	4.50	50.00	19-Apr-00	5.69	100.51	30-Nov-00	7.89	34.64
12-Feb-00	8.55	58.55	20-Apr-00	2.13	102.64			
13-Feb-00	7.03	65.58	21-Apr-00	3.32	105.96	1-Dec-00	6.06	6.06
14-Feb-00	7.72	73.31	22-Apr-00	5.45	111.41	2-Dec-00	10.65	16.70
15-Feb-00	9.12	82.42	23-Apr-00	1.49	112.90	3-Dec-00	7.07	23.77
16-Feb-00	2.50	84.92	24-Apr-00	7.99	120.89	4-Dec-00	9.35	33.13
17-Feb-00	11.80	96.72	25-Apr-00	6.86	127.75	5-Dec-00	5.74	38.86
18-Feb-00	5.84	102.56	26-Apr-00	5.22	132.97	6-Dec-00	3.48	42.34
19-Feb-00	5.50	108.06	27-Apr-00	0.76	133.73	8-Dec-00	0.07	42.41
20-Feb-00	12.92	120.98	28-Apr-00	3.07	136.80	9-Dec-00	8.78	51.19
21-Feb-00	5.58	126.56	29-Apr-00	2.04	138.83	10-Dec-00	5.67	56.86
22-Feb-00	15.46	142.02	30-Apr-00	4.32	143.16	11-Dec-00	3.69	60.55
23-Feb-00	11.69	153.71				12-Dec-00	11.40	71.95
24-Feb-00	16.30	170.01	1-May-00	4.48	4.48	13-Dec-00	4.85	76.80
25-Feb-00	6.23	176.24	2-May-00	2.89	7.37	14-Dec-00	2.44	79.24
26-Feb-00	6.44	182.68	3-May-00	1.68	9.05	15-Dec-00	6.12	85.36
27-Feb-00	4.73	187.41	4-May-00	3.80	12.84	16-Dec-00	1.72	87.09
28-Feb-00	9.72	197.13	5-May-00	4.51	17.35	17-Dec-00	0.96	88.05
29-Feb-00	4.66	201.80	6-May-00	4.20	21.55	18-Dec-00	12.56	100.60
			7-May-00	2.07	23.62	19-Dec-00	5.81	106.42
1-Mar-00	9.61	9.61	8-May-00	1.50	25.13	20-Dec-00	10.46	116.87
2-Mar-00	5.04	14.66	9-May-00	2.79	27.91	23-Dec-00	7.63	124.50
3-Mar-00	4.01	18.67	10-May-00	1.28	29.20	24-Dec-00	5.00	129.50
4-Mar-00	7.86	26.53	11-May-00	2.92	32.12	25-Dec-00	3.99	133.48
5-Mar-00	5.50	32.04	12-May-00	2.21	34.33	26-Dec-00	9.07	142.55
6-Mar-00	3.07	35.11	13-May-00	2.79	37.12	27-Dec-00	4.93	147.48
7-Mar-00	7.57	42.68	14-May-00	4.39	41.52	28-Dec-00	0.50	147.98
8-Mar-00	7.84	50.52	15-May-00	4.16	45.67			

H.4 References

Blight, G.E. (1997). Interactions between the atmosphere and the Earth. Geotechnique, Vol. 47, No. 4, pp. 715-767.

Bowen, I.S. (1926). The ration of heat losses by conduction and by evaporation from any water surface. Physical Review, Vol. 27, pp. 779-787.
Campbell Scientific, Inc. (CSI) (1990). Model 41004-5 Multi-Plate Radiation Shield Instructions.
Campbell Scientific, Inc. (CSI) (1993a). 05103-10, 05305-10 and 05701-10 R.M. Young Wind Monitors Instruction Manual.
Campbell Scientific, Inc. (CSI) (1993b). HFT-3 Soil Heat Flux Plate.
Campbell Scientific, Inc. (CSI) (1993c). SM192/716 Storage Module Instruction Manual.
Campbell Scientific, Inc. (CSI) (1993d). 21X Microloggers Operator's Manual.
Campbell Scientific, Inc. (CSI) (1994a). CR10 Measurement and Control Module Operator's Manual.
Campbell Scientific, Inc. (CSI) (1994b). Model HMP35CF Temperature and Relative Humidity Probe Instruction Manual.
Campbell Scientific, Inc. (CSI) (1994c). PC208 Data logger Support Software Instruction Manual.
Campbell Scientific, Inc. (CSI) (1994d). Tripod-Based Weather Station Installation Manual.
Campbell Scientific, Inc. (CSI) (1995). Q-7 Net Radiometer.
Campbell Scientific, Inc. (CSI). (1997). Bowen Ratio Instrumentation Instruction Manual. Revision 1/97.
Durham, A.J.P., Wilson, G.W., Currey, N. (2000). Field Performance of Two Low Infiltration Cover Systems in a Semi Arid Environment. Proceedings of the Fifth international conference on Acid Rock Drainage, Denver, Colorado, USA. May, pp. 1319-1326.
Fritschen, L.J. (1966). Evapotranspiration rates of field crops determined by the Bowen ratio method. Agronomy Journal, Vol. 58, pp. 339-342.
Fritschen, L.J., Simpson, J.R. (1989). Surface energy and radiation balance systems: general description and improvements. Journal of Applied Meteorology, Vol. 28, pp. 680-689.
Fritschen, L.J., Qian, P. (1990). Net radiation, sensible and latent heat flux densities on slopes computed by the energy balance method. Boundary-Layer Meteorology, Vol. 53, pp. 163-171.
Fuchs, M, Tanner, C.B. (1967). Evaporation from a drying soil. Journal of Applied Meteorology, Vol. 6, pp. 852-857.
Hydrological Services Pty. Ltd. (1995). Instruction Manual: Tipping Bucket Rain Gauge Model T.B.3.
Maidment, D.R. (1993). Handbook of Hydrology. McGraw-Hill, Inc., New York, NY, USA.
Ohmura, A. (1982). Objective criteria for rejecting data for Bowen ratio flux calculations. Journal of Applied Meteorology, Vol. 21, pp. 595-598.
Oke, T.R. (1987). Boundary Layer Climates, Second Edition. Routledge, New York, NY, USA.
SoilCover (1997). SoilCover User's Manual. Unsaturated Soils Group, Department of Civil Engineering, University of Saskatchewan, Saskatoon, Saskatchewan, Canada.
Solarex Corporation (1996). Information Sheet: Mega Modules 39 Watts & Under.
Tanner, C.B. (1960). Energy balance approach to evapotranspiration from crops. Soil Science Society of America Proceedings, Vol. 24, pp. 1-9.
Woyshner, M.R., St-Arnaud, L.C. (1994). Hydrogeological evaluation and water balance of a thickened tailings deposit near Timmins, ON, Canada. Proceedings of the Third International Conference on the Abatement of Acidic Drainage, Pittsburgh, PA, USA. April 24-29, 1994.

This page was intentionally left blank.

APPENDIX I

Kidston Evaporation Data

I.1 Introduction

The data with regard to the evaporation data for the Kidston Mine Site is presented here. This includes historic data sets used to determine overall site evaporation averages, as well as detailed daily evaporation data. The details of an evaporation experiment to determine the actual evaporation rate from the tailings pond as well as potential evaporation calculations based on daily meteorological data are also presented here

I.2 Sources of Evaporation Data

Various evaporation data are available and have been collected at Kidston Gold Mine and surrounding areas. Table I.1 lists a summary of all the available evaporation (and other climatic data, where relevant) data available for Kidston Gold Mine and surrounds. Evaporation records are available from the Kidston Mine site since 1985. This data is from daily A-pan measurements taken by mine security personnel at the main entrance gate to the mine. No close weather stations, managed by the Australian Bureau of Meteorology maintain evaporation records. Other than the on-site readings the best historic estimation of evaporation is the rates adopted by the Water Resources Commission for the construction of the nearby Copperfield River Dam (Coffey Partners, 1992).

Table I.1: Summary of all available evaporation data for Kidston and surrounds.

Station	Components measured	Period	Source/Origin
Close to Copperfield Dam	Pan evaporation; rates adopted by Queensland Water Resources Commission (QWRC).	not stated	Overall monthly average (Coffey, 1992)
Kidston Area	Pan evaporation; after Climatic Atlas of Australia	not stated	Overall monthly average (Gutteridge Haskins and Davey, 1983)
Mount Surprise	Pan evaporation; QWRC	not stated	Annual total (Gutteridge Haskins and Davey, 1983)

Table I.1: Summary of all available evaporation data for Kidston and surrounds.

Station	Components measured	Period	Source/Origin
Georgetown	Pan evaporation; QWRC	not stated	Annual total (Gutteridge Haskins and Davey, 1983)
Kidston Mine Site	Pan evaporation	1985 – 2001	Kidston Gold Mine
Kidston Tailings Impoundment	Pan evaporation (mini-pans)	2000-2001	This study
Kidston Tailings Impoundment	Penman potential evaporation; based on daily Barren waste rock dump weather station data	1996-2001	This study

I.3 Mini-Pan Evaporation Experiment

As the pool on the tailings impoundment is of considerable size (70-100 ha), the direct evaporation from it does affect the tailings impoundment water balance significantly. The only way of determining what this value is, is to calculate the potential evaporation (PE) using the data from the automated weather station on site by means of an empirical equation. The only number available to calibrate this data with, are the daily A-pan evaporation measurements at the Kidston Gold Mine main security gate.

The A-pan at the security gate is not situated at the most suitable site as the tailings impoundment acts as a windbreak whenever winds from the south and east occurs as illustrated in Figure 4.7, and also the area immediately surrounding the pan is well vegetated. To overcome this problem it was decided to install another A-pan on the tailings impoundment and thus get direct measurements, but the capital costs of such a scheme was prohibitive. The alternate plan was to construct six mini-A-pans to conduct a correlation experiment. Four of the mini-pans would be installed at four different locations around the impoundment, and the remaining two adjacent to the existing A-pan at the main security gate. By doing readings of all six pans and the A-pan for predetermined periods, the relationship between evaporation rates on the tailings impoundment surface and those measured with the site A-pan could be determined.

The six min-pans were designed to be exact scaled down versions of the standard A-pan, using 220 liter steel drums as the basis diameter. The appropriate dimensions used, compared to that of the standard A-pan is listed in Table I.2.

Table I.2: Scaled down dimensions of the Kidston mini-evaporation pans.

Dimension	Standard A-pan	Conversion factor	Kidston mini-pans
Inside diameter	1.2065 m	None	0.5650 m
Wall height	0.2540 m	0.21053	0.1190 m
Fill height	0.2032 m	0.16842	0.0952 m
Refill height	0.1778 m	0.14737	0.0833 m

Each pan was constructed according to the dimensions in Table I.2, painted in a metallic color (similar to the standard A-pan), and placed on their selective sites as illustrated in Figure 4.7. The pans were operated manually between the operating limits of the fill height and the refill height. Single daily readings for three continuous periods ranging between 4 and 11 days, over the period December 2000 to April 2001 was taken.

Two of the mini-pans were placed at the main security gate adjacent to the standard A-pan. The remaining four mini-pans were placed on four different locations on the tailings impoundment surface adjacent to the pool. The placement of the pans was selected to obtain maximum coverage of the different evaporation extremes on the dam based on the prevailing wind direction and possible oasis effects (Oke, 1987). Table I.3 lists the details of the location of each of the pans.

Table I.3: Details on the location of the mini-pans for field measurement of evaporation from the surface of the Kidston tailings impoundment.

Pan ID	Location
A-pan	At the main mine security gate
S-1	At the main mine security gate, 3.0 m from the A-pan, 0.5 m from S-2
S-2	At the main mine security gate, 3.0 m from the A-pan, 0.5 m from S-1
D	25 m from the tailings pond edge, midway between section line D and E
C	25 m from the tailings pond edge, along section line C
A	25 m from the tailings pond edge, along section line A
G	25 m from the tailings pond edge, along section line G

The results of the three testing periods are listed in Table I.4, showing the daily evaporation rates (mm) from each of the pans. Averages for the pans on the impoundment as well as for the two pans adjacent to the A-pan, and the A-pan results for these periods are also listed. A correlation plot for the individual mini-pans on the tailings impoundment, compared to the average tailings impoundment mini-pan evaporation rates are presented in Figure I.1, indicating very little significant difference between the individual pan results. A more detailed statistical breakdown of this data was attempted to determine whether there are any significant consistent variances between the individual pans as a results of oasis effects associated with their location,

but the data set in not large enough for meaningful analysis. Similarly a correlation plot between the individual mini-pans adjacent to the A-pan and the average of the mini-pan evaporation rates illustrated in Figure I.2 show little variance between the individual pan results.

There is poor correlation between the mini-pan results on the tailings impoundment and those adjacent to the A-pan, as well as between all the mini-pans and the A-pan. Statistical analysis of this data was again attempted to find reasons for these anomalies, but again the data set was found not to be of sufficient magnitude to make conclusive findings. From an observational evaluation of the data and applying some engineering judgement it would appear reasonable that the evaporation rates in the mini-pans on the tailings impoundment surface read approximately 10% higher than the A-pan. A correction of adding 10% to the A-pan evaporation data is thus suggested, which is somewhat supported by the data in Table I.4.

Table I.4: Results of three periods of mini-evaporation pan monitoring, on top of the tailings impoundment and next to the A-pan at the Main Gate (all results are daily evaporation in mm).

Date	Mini-pans of tailings impoundment					Mini-pans next to A-pan			
	G	A	C	D	Average	S1	S2	Average	A-pan
30-Nov-00	10.6	11.4	11.2	11.1	11.1	10.6	10.6	10.6	7.8
1-Dec-00	9.2	10.2	10.1	10.1	9.9	10.1	10.1	10.1	7.6
2-Dec-00	11.4	11.6	12.8	11.9	11.9	10.6	10.6	10.6	7.8
3-Dec-00	10.0	11.1	10.9	10.8	10.7	9.9	9.9	9.9	7.4
4-Dec-00	10.4	11.5	11.6	11.6	11.3	9.6	8.7	9.2	7.2
5-Dec-00	13.3	14.2	13.3	13.4	13.6	10.5	11.4	10.9	7.4
6-Dec-00	9.6	9.6	10.8	10.7	10.2	8.5	7.5	8.0	7.0
7-Dec-00	6.8	8.7	9.6	7.7	8.2	5.8	4.9	5.4	4.6
16-Jan-01	15.3	12.8	12.3	14.7	13.8	12.6	12.1	12.3	6.9
17-Jan-01	9.1	11.1	9.4	9.9	9.9	13.5	13.6	13.5	10.0
18-Jan-01	12.0	9.3	7.3	11.3	9.9	11.0	10.0	10.5	10.0
19-Jan-01	11.0	11.8	12.5	9.0	11.1	6.5	7.0	6.8	8.0
19-Apr-01	5.0	4.0	5.0	5.0	4.8	5.4	5.4	5.4	5.3
20-Apr-01	5.0	6.0	6.0	6.0	5.8	4.8	4.8	4.8	5.6
21-Apr-01	5.0	5.0	4.0	5.0	4.8	5.0	5.0	5.0	6.5
22-Apr-01	5.0	5.0	4.0	4.0	4.5	4.8	4.8	4.8	4.6
23-Apr-01	5.0	4.0	5.0	6.0	5.0	7.1	7.1	7.1	4.6
24-Apr-01	6.0	6.0	5.0	6.0	5.8	7.0	7.0	7.0	5.7

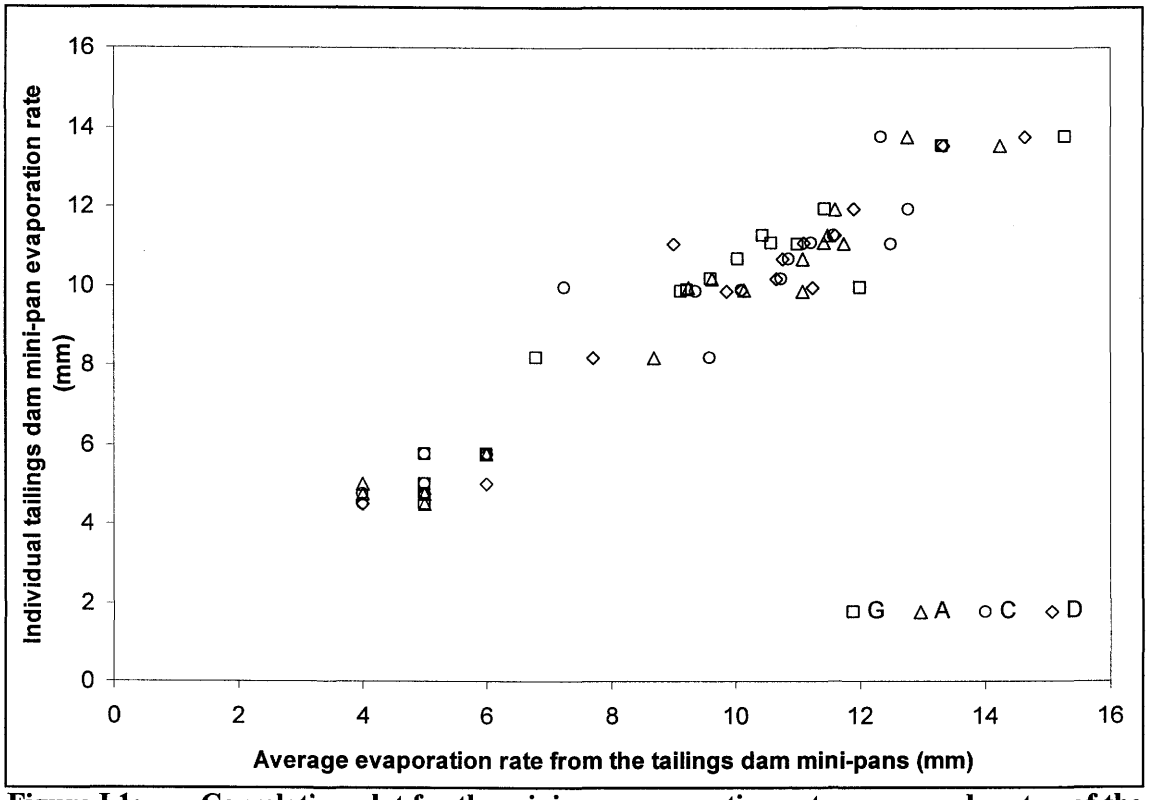

Figure I.1: **Correlation plot for the mini-pan evaporation rates measured on top of the tailings impoundment surface.**

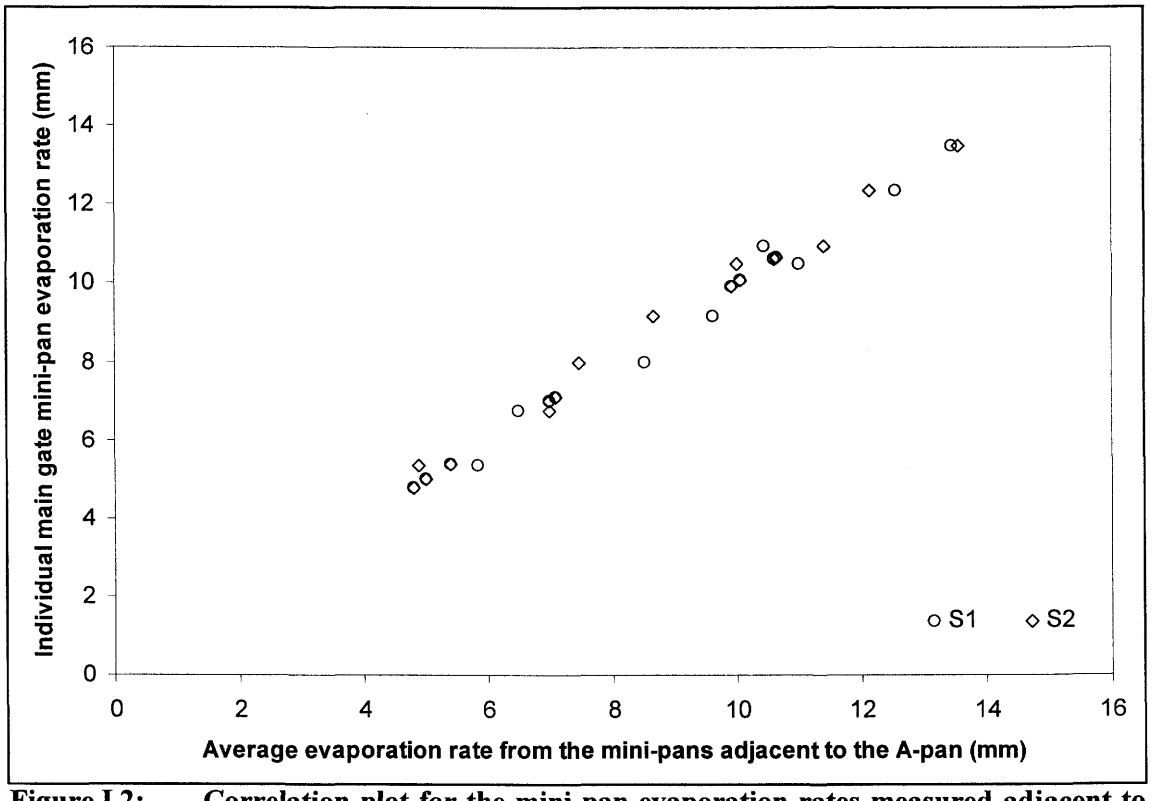

Figure I.2: **Correlation plot for the mini-pan evaporation rates measured adjacent to the A-pan.**

I.4 Complete Kidston Evaporation Data

Tables I.4 and I.5 list monthly pan evaporation totals for the Kidston Mine Site. Based on the results of the mini-pan experiment the pan evaporation rates in Table I.5 should be increased by 10% to provide an accurate estimate of the evaporation rate on the tailings impoundment surface. The resultant increased pan-evaporation rates are listed in Table I.7. None of these pan evaporation rates have been corrected by means of a pan factor, and are thus most likely an overestimation of the actual evaporation rate. There is no record of what pan factor should be adopted for the Kidston data, and as a result the potential evaporation from the Kidston Mine Site was calculated with the empirical Penman equation (Penman, 1948). This calculated potential evaporation would then be used to determine an acceptable pan factor for the Kidston site.

The hourly meteorological data for the site from the automated weather station on the Barren waste rock dump as described in Appendix H, was used for the calculations. The resultant monthly potential evaporation totals are listed in Table I.8.

Table I.5: Estimated monthly pan evaporation totals (mm) for the Kidston mine site from sources other than physical measurements on site.

Month	Coffey Partners (1992)[1]	Gutteridge Haskins and Davey (1983)[2]	Gutteridge Haskins and Davey (1983)[3]
Jan	250	299	220
Feb	200	294	217
Mar	230	267	197
Apr	220	216	159
May	190	207	152
Jun	160	193	142
Jul	180	184	136
Aug	220	211	156
Sep	280	257	189
Oct	330	321	236
Nov	320	340	250
Dec	310	333	246
Annual	2890	3122	2300

(1) Evaporation rates (assumed to be pan evaporation) adopted by the Queensland Water Resources Commission (QWRC) for the nearby Copperfield River Dam; (2) A-pan evaporation rates for Kidston area, extracted from "The Climatic Atlas of Australian Evaporation"; (3) QWRC shows annual pan evaporation rates at Mt Surprise and Georgetown (both within 100 km of Kidston) of 1700 mm and 2350 mm respectively – a value of 2300 mm for Kidston was assumed and proportioned according to the data in (2).

Table I.6: Monthly pan evaporation rates (mm) based on daily A-pan evaporation rates measured at the Kidston Main Gate.

Month	1996	1997	1998	1999	2000	2001	Average
Jan	196.7	201.8	161.8	188.5	218.1	213.6	196.7
Feb	259.8	180.2	187.6	142.8	146.8	120.2	172.9
Mar	248.9	181.1	192.4	163.9	175.9	nd	192.4
Apr	252.5	202.3	176.1	146.6	133.1	nd	182.1
May	141.8	146.6	132.1	164.7	124.0	nd	141.8
Jun	168.1	128.0	126.1	173.3	107.5	nd	140.6
Jul	132.7	134.9	123.5	140.1	132.4	nd	132.7
Aug	195.5	161.2	153.9	176.9	152.4	nd	168.0
Sep	242.3	237.6	175.2	245.9	211.5	nd	222.5
Oct	267.7	308.5	221.5	277.5	214.9	nd	258.0
Nov	309.2	219.0	211.9	170.6	192.1	nd	220.6
Dec	277.5	207.4	183.2	200.2	180.5	nd	209.8
Annual	2692.9	2308.4	2045.3	2190.9	1989.2	incom	2238.2

nd = no data is available; incom = no total is calculated due to incomplete data set.

Table I.7: Pan evaporation rates (mm) for the tailings impoundment surface (Corrected, increased by 10%, pan evaporation rates based on daily A-pan evaporation rates measured at the Kidston Main Gate).

Month	1996	1997	1998	1999	2000	2001	Average
Jan	216.4	221.9	178.0	207.4	239.9	234.9	216.4
Feb	285.8	198.2	206.4	157.1	161.5	132.3	190.2
Mar	273.8	199.2	211.7	180.3	193.5	nd	211.7
Apr	277.8	222.5	193.7	161.3	146.5	nd	200.4
May	156.0	161.3	145.3	181.1	136.4	nd	156.0
Jun	184.9	140.8	138.7	190.7	118.3	nd	154.7
Jul	146.0	148.3	135.9	154.1	145.6	nd	146.0
Aug	215.1	177.3	169.3	194.6	167.6	nd	184.8
Sep	266.5	261.4	192.7	270.5	232.7	nd	244.8
Oct	294.5	339.3	243.6	305.2	236.3	nd	283.8
Nov	340.1	240.9	233.1	187.6	211.3	nd	242.6
Dec	305.3	228.1	201.5	220.2	198.6	nd	230.8
Annual	2962.2	2539.2	2249.8	2410.0	2188.2	incom	2462.0

nd = no data is available; incom = no total is calculated due to incomplete data set.

Table I.8: Calculated potential evaporation rates (mm) (Penman method) at the Kidston Mine Site based on daily meteorological data measured with the automated weather station on the Barren waste rock dump.

Month	1996	1997	1998	1999	2000	2001	Average
Jan	154.2	160.7	141.7	147.5	166.9	165.0	156.0
Feb	134.3	142.5	150.2	123.9	120.5	109.1	130.1

Table I.8: Calculated potential evaporation rates (mm) (Penman method) at the Kidston Mine Site based on daily meteorological data measured with the automated weather station on the Barren waste rock dump.

Month	1996	1997	1998	1999	2000	2001	Average
Mar	126.7	152.5	139.1	135.7	145.6	144.9	140.8
Apr	151.5	141.8	91.6	101.0	93.9	125.0	117.5
May	124.6	103.5	112.6	120.6	85.7	nd	109.4
Jun	108.0	87.1	100.2	100.7	64.6	nd	92.1
Jul	114.4	104.4	104.5	106.1	100.3	nd	105.9
Aug	140.1	123.2	138.9	128.1	121.2	nd	130.3
Sep	184.0	161.5	155.6	163.0	154.6	nd	163.7
Oct	168.4	202.6	180.8	196.8	146.3	nd	179.0
Nov	195.5	180.8	161.9	128.7	149.7	nd	163.3
Dec	190.5	153.0	174.0	165.4	129.1	nd	162.4
Annual	1792.1	1713.7	1651.1	1617.5	1478.5	incom	1650.5

nd = no data is available; incom = no total is calculated due to incomplete data set.

Assuming that the potential evaporation numbers listed in Table I.8 are the most accurate, the 10% increased A-pan evaporation rates for the Kidston Mine Site can be reduced by multiplying with an appropriate pan factor. This factor has been calculated for each year of complete data, and is listed in Table I.9. The resultant pan factor of 0.74 can be used to calculate the appropriate evaporation rate from the Kidston tailings impoundment surface, and are listed in Table I.10. Figures I.3 to I.5 present the data reported in this section graphically.

Table I.9: Pan factor determined based on the calculated potential evaporation rate (mm) from the Kidston tailings impoundment.

Component	1996	1997	1998	1999	2000	Average
10% Increased Kidston A-pan	2962.2	2539.2	2249.8	2410.0	2188.2	2462.0
Calculated potential evaporation	1792.1	1713.7	1651.1	1617.5	1478.5	1650.5
Assumed pan factor	0.67	0.74	0.81	0.74	0.74	0.74

Table I.10: Corrected pan evaporation rates (mm) for the Kidston tailings impoundment surface based on a pan factor of 0.74.

Month	1996	1997	1998	1999	2000	2001	Average
Jan	160.2	164.2	131.7	153.5	177.5	173.8	160.2
Feb	211.5	146.7	152.7	116.2	119.5	97.9	140.7
Mar	202.6	147.4	156.6	133.4	143.2	nd	156.6
Apr	205.6	164.7	143.4	119.3	108.4	nd	148.3
May	115.5	119.3	107.5	134.0	100.9	nd	115.5
Jun	136.8	104.2	102.6	141.1	87.5	nd	114.5
Jul	108.0	109.8	100.5	114.0	107.8	nd	108.0
Aug	159.2	131.2	125.3	144.0	124.1	nd	136.7

Table I.10: Corrected pan evaporation rates (mm) for the Kidston tailings impoundment surface based on a pan factor of 0.74.

Month	1996	1997	1998	1999	2000	2001	Average
Sep	197.2	193.4	142.6	200.2	172.2	nd	181.1
Oct	217.9	251.1	180.3	225.8	174.9	nd	210.0
Nov	251.7	178.3	172.5	138.8	156.4	nd	179.5
Dec	225.9	168.8	149.1	162.9	147.0	nd	170.8
Annual	2192.0	1879.0	1664.9	1783.4	1619.2	incom	1821.9

nd = no data is available; incom = no total is calculated due to incomplete data set.

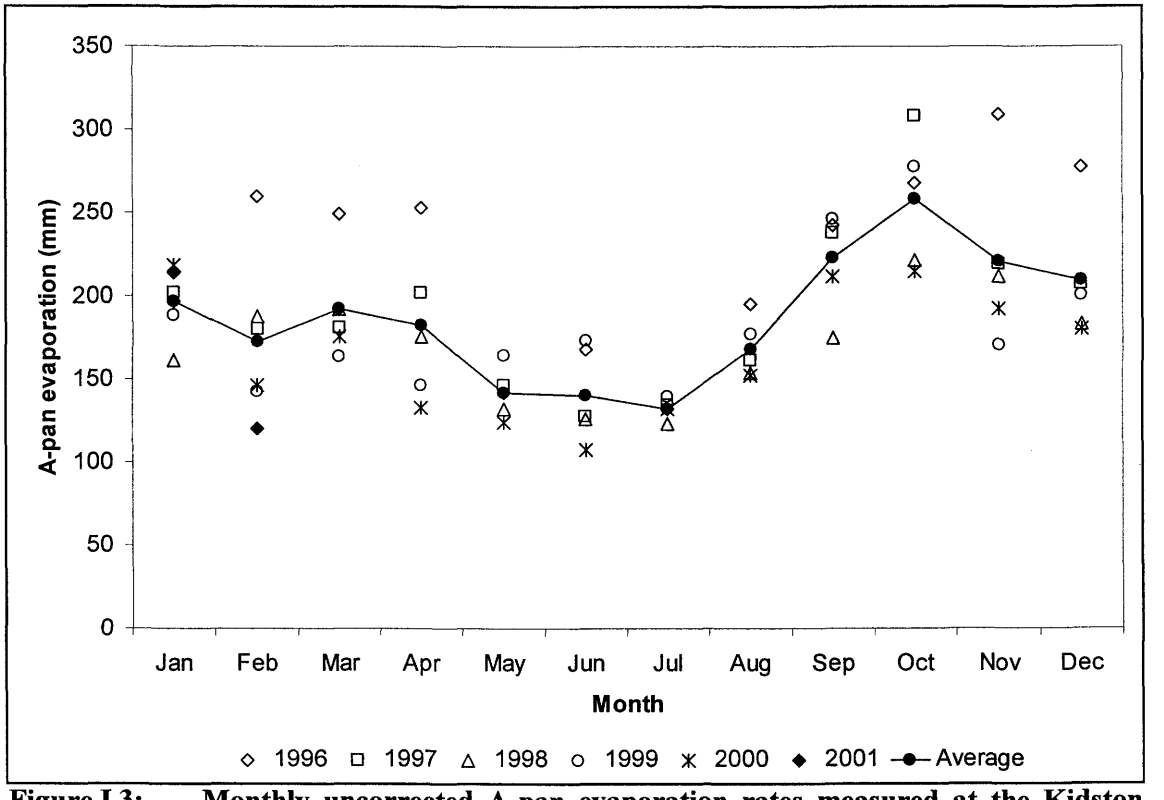

Figure I.3: Monthly uncorrected A-pan evaporation rates measured at the Kidston Main Gate.

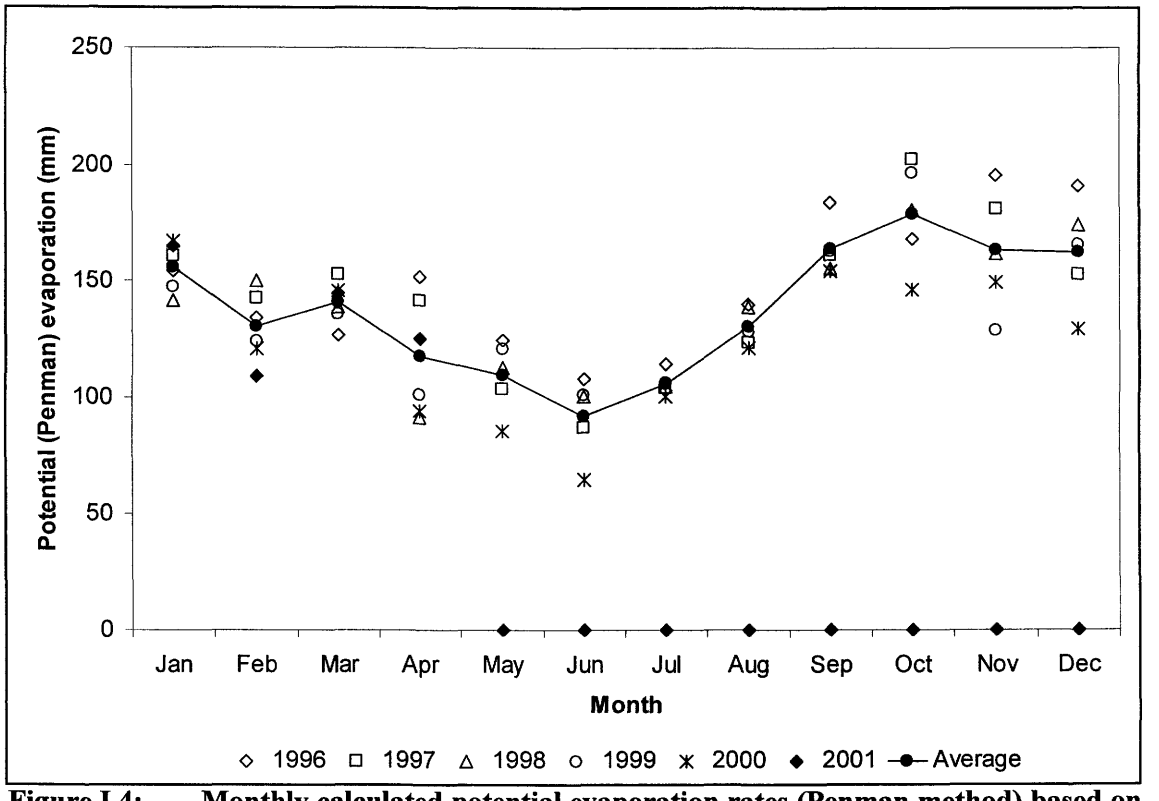

Figure I.4: **Monthly calculated potential evaporation rates (Penman method) based on hourly data from the automated weather station.**

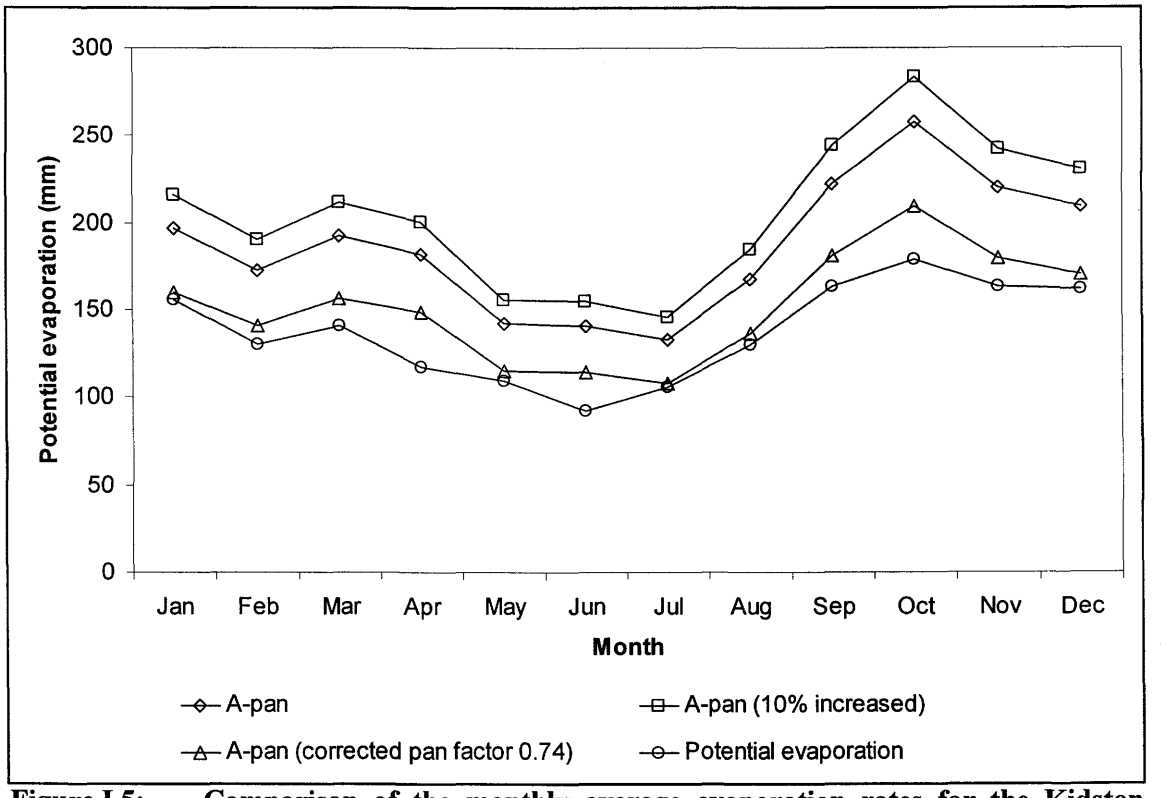

Figure I.5: **Comparison of the monthly average evaporation rates for the Kidston Mine Site.**

I.5 References

Coffey Partners (1992). Pit Hydrology Study. Consultants report to Kidston Gold Mines Limited, Report No. Z105/4-AC, 28 September.

Gutteridge Haskins & Davey Pty Ltd (1984). Kidston Project – Tailings Dam Study. Consultants Report to Kidston Gold Mines Limited, November 1983 – Amended July 1984, 19 Pages.

Oke, T.R. (1987). Boundary Layer Climates, Second Edition. Routledge, New York, NY, USA.

Penman, H.L. (1948). Natural evapotranspiration from openwater, bare soil and grass. Proc. R. Soc. London Ser. A, Vol.193, pp. 120-145.

This page was intentionally left blank.

APPENDIX J

Kidston Precipitation Data

J.1 Introduction

The data with regard to the precipitation data for the Kidston Mine Site is presented here. This includes historic data sets used to determine overall site precipitation averages, as well as detailed daily precipitation data from the continuous tipping bucket raingauge on the Barren waste rock dump as described in Appendix H.

J.2 Sources of Precipitation Data

Various precipitation data are available and have been collected at Kidston Gold Mine and surrounding areas. Table J.1 lists a summary of all the available precipitation (and other climatic data) data available for Kidston Gold Mine and surrounds.

Table J.1: Summary of precipitation data (and other meteorological data) available for Kidston Gold Mine and surrounds.

Station	Record duration	Location co-ordinates	Data format (source)
Kidston Township	1915 – 1991	18°53'S; 144°00'E	Overall total monthly rainfall (Coffey Partners, 1992)
Kidston Township	1915 – 1980	18°53'S; 144°00'E	Overall total monthly rainfall (Gutteridge Haskins and Davey, 1983)
Kidston Township	1984 – 1995	18°53'S; 144°00'E	Daily rainfall totals, maximum and minimum air temperature and relative humidity (Australian Bureau of Meteorology)
Kidston (Bagstow)	1964 – 1991	19°11'S; 143°59'E	Overall annual average rainfall (Coffey Partners, 1992)
Carpentaria Downs	1902 – 1991	18°43'S; 144°19'E	Overall annual average rainfall (Coffey Partners, 1992)
Lyndhurst	1986 – 1991	19°12'S; 144°22'E	Overall annual average rainfall (Coffey Partners, 1992)
Georgetown	1972 – 1991	18°18'S; 143°33'E	Overall annual average rainfall (Coffey Partners, 1992)
Kidston Mine Site	1984 – 2001	18°52'S; 144°09'E	Daily rainfall totals, maximum and minimum air temperature and relative humidity, maximum windspeed, average wind direction (Kidston

Table J.1: Summary of precipitation data (and other meteorological data) available for Kidston Gold Mine and surrounds.

Station	Record duration	Location co-ordinates	Data format (source)
			Gold Mine Weather Station)
Kidston Barren waste rock dump	1996 – 2001	Not available	Actual instantaneous rainfall intensity, continuous maximum, minimum and average air temperature, relative humidity, windspeed, average wind direction

In 1996 a fully automated weather station, supplied by Campbell Scientific (Australia) Corporation (Campbell Scientific, 1994) was selected for the continuous monitoring of meteorology on the Barren waste rock dump at Kidston Gold Mine. The weather station was installed by Mike O'Kane, a research engineer at the University of Saskatchewan, as part of a research project into the performance of soil covers for the Kidston waste rock dumps (Durham *et al.*, 2000). The details of the weather station are supplied in Appendix H.

J.3 Monthly Precipitation Data for Kidston

The historic and continuous weather station monthly precipitation totals for the Kidston Mine Site are listed in Tables J.2 to J.9.

Table J.2: Monthly precipitation totals (mm) measured at the Kidston Townsite obtained from the Australian Bureau of Meteorology (Data record starts in 1984 and ends June 1995).

Month	1984	1985	1986	1987	1988	1989	1990	1991	1992	1993	1994	1995
Jan	186.0	114.6	0.0	124.3	53.5	56.5	15.0	944.5	100.1	97.1	99.6	139.4
Feb	190.0	100	197.0	47.0	180.5	244.8	30.3	317.3	307.1	277.9	63.5	309.8
Mar	107.0	107	1.5	0.0	4.0	110.0	176.5	4.6	28.6	26.1	71.4	219.8
Apr	9.8	48.5	10.0	0.0	3.0	24.0	22.2	0.4	0.0	1.0	0.0	3.4
May	0.0	27	40.0	12.0	0.0	0.0	44.4	0.0	19.0	0.0	0.0	4.0
Jun	0.7	15	8.0	8.0	6.5	30.0	67.0	0.0	0.0	0.0	9.5	5.5
Jul	69.6	50	0.0	0.0	7.5	17.5	3.5	0.0	0.0	66.4	0.0	nd
Aug	1.5	0	0.0	0.0	73.0	0.0	0.0	0.0	0.0	0.0	0.0	nd
Sep	1.4	0	8.5	0.0	0.0	0.0	0.0	0.0	5.4	4.8	0.0	nd
Oct	0.0	11	56.0	6.5	2.0	7.0	6.6	0.0	1.0	0.0	4.2	nd
Nov	33.3	239	37.0	47.5	14.0	206.0	28.6	40.5	0.0	0.0	37.2	nd
Dec	194.4	116	116.0	106.5	383.0	102.3	43.6	68.8	67.0	0.0	24.4	nd
Total	793.7	828.1	474.0	351.8	727.0	798.0	437.7	1376.1	528.2	473.3	309.8	incom

nd = no data is available; incom = totals cannot be calculated due to incomplete data records.

Table J.3: Summarized precipitation totals (mm) measured at the Kidston Townsite obtained from the Australian Bureau of Meteorology, reduced from Table J.2 (Data record starts in 1984 and ends June 1995).

Month	Average	Minimum	Maximum	1915-1980*	1915-1991**
Jan	160.9	0.0	944.5	186	197
Feb	188.8	30.3	317.3	190	181
Mar	71.4	0.0	219.8	107	99
Apr	10.2	0.0	48.5	21	21
May	12.2	0.0	44.4	12	14
Jun	12.5	0.0	67.0	11	10
Jul	19.5	0.0	69.6	6	7
Aug	6.8	0.0	73.0	9	9
Sep	1.8	0.0	8.5	8	7
Oct	8.6	0.0	56.0	18	16
Nov	62.1	0.0	239.0	45	49
Dec	111.1	0.0	383.0	106	102
Totals	665.8	30.3	2470.6	719	712
Annual totals#	645.2	309.8	1376.1	-	-

* Average monthly precipitation at the Kidston town site from 1915 to 1980 as reported by Gutteridge Haskins and Davey (1983); ** Average monthly precipitation at the Kidston town site from 1915 to 1991 as reported by Coffee Partners (1992); # Average, maximum and minimum of the annual precipitation totals listed in Table J.2.

Table J.4: Monthly precipitation totals (mm) measured at the Kidston Main Gate weather station obtained from Kidston Gold Mines Limited (Data record starts in 1985, continued in following table).

Month	1985	1986	1987	1988	1989	1990	1991	1992
Jan	64	222	132	50	0	24	944	100
Feb	59	162	33	140	164	37	317	307
Mar	64	0	154	3	105	177	5	29
Apr	6	8	0	0	15	70	0	0
May	9	36	17	0	12	45	12	19
Jun	3	11	7	0	29	0	0	0
Jul	51	4	0	0	19	4	0	0
Aug	0	0	0	82	0	0	0	0
Sep	0	6	0	0	0	0	0	0
Oct	3	39	4	0	0	1	1	1
Nov	147	30	58	0	132	23	41	41
Dec	110	13	85	310	66	44	69	69
Total	516	531	490	585	542	425	1389	566

Table J.5: Monthly precipitation totals (mm) measured at the Kidston Main Gate weather station obtained from Kidston Gold Mines Limited (Data record starts in 1985, continued from preceding table).

Month	1993	1994	1995	1996	1997	1998	1999	2000	2001
Jan	97.0	69.0	148.8	141.2	39.0	190.8	169.6	145.4	107.1
Feb	278.0	63.0	285.8	36.0	109.2	85.9	152.0	167.1	164.2
Mar	26.0	71.0	219.8	41.2	170.8	105.4	114.9	86.7	nd
Apr	1.0	0.0	3.4	12.8	0.0	9.8	66.2	221.2	nd
May	0.0	0.0	4.0	4.1	45.8	33.0	13.2	16.4	nd

Table J.5: Monthly precipitation totals (mm) measured at the Kidston Main Gate weather station obtained from Kidston Gold Mines Limited (Data record starts in 1985, continued from preceding table).

Month	1993	1994	1995	1996	1997	1998	1999	2000	2001
Jun	0.0	9.5	0.0	0.0	0.0	4.8	0.0	89.0	nd
Jul	66.0	0.0	0.0	0.0	0.0	1.6	0.5	0.0	nd
Aug	0.0	0.0	14.0	3.0	0.0	0.0	0.0	0.0	nd
Sep	4.8	0.0	0.0	7.8	20.6	13.8	15.1	0.0	nd
Oct	0.0	4.2	25.8	43.1	0.0	60.4	1.6	103.6	nd
Nov	48.0	37.2	42.4	6.6	41.2	159.5	215.3	149.8	nd
Dec	69.0	24.4	62.4	69.3	174.5	148.3	65.1	297.9	nd
Total	589.8	278.3	806.4	365.1	601.1	813.3	813.5	1277.1	nd

nd = no data is available.

Table J.6: Summarized precipitation totals (mm) measured at the Kidston Main Gate weather station obtained from Kidston Gold Mines Limited, reduced from the previous two tables (Data record starts in 1985).

Month	Average	Minimum	Maximum
Jan	155.5	0.0	944.0
Feb	150.4	33.0	317.0
Mar	85.8	0.0	219.8
Apr	25.8	0.0	221.2
May	16.7	0.0	45.8
Jun	9.6	0.0	89.0
Jul	9.1	0.0	66.0
Aug	6.2	0.0	82.0
Sep	4.3	0.0	20.6
Oct	18.0	0.0	103.6
Nov	73.2	0.0	215.3
Dec	104.8	13.0	310.0
Totals	659.4	46.0	2634.3
Annual totals[#]	661.8	278.3	1389.0

[#] Average, maximum and minimum of the annual precipitation totals listed in Table J.4 and J.5.

Table J.7: Monthly precipitation totals (mm) measured on the Kidston Mine Site with the continuos tipping bucket raingauge (data start in March 1996 and end April 2001).

Month	1996	1997	1998	1999	2000	2001	Average	Min	Max
Jan	nd	90.4	173.8	72.4	12.0	53.0	80.3	12.0	173.8
Feb	nd	80.0	88.4	69.4	165.0	164.2	113.4	69.4	165.0
Mar	11.4	161.6	86.6	21.2	38.6	45.2	60.8	11.4	161.6
Apr	11.8	0.0	6.4	6.0	197.4	0.0	36.9	0.0	197.4
May	2.2	48.2	28.2	9.6	13.4	nd	20.3	2.2	48.2
Jun	0.4	6.6	3.6	0.0	79.2	nd	18.0	0.0	79.2
Jul	2.0	0.0	1.4	0.2	0.0	nd	0.7	0.0	2.0
Aug	2.6	3.6	0.0	0.0	0.0	nd	1.2	0.0	3.6
Sep	4.2	15.0	9.4	0.2	0.0	nd	5.8	0.0	15.0
Oct	49.4	2.6	69.6	0.0	83.4	nd	41.0	0.0	83.4

Table J.7: Monthly precipitation totals (mm) measured on the Kidston Mine Site with the continuos tipping bucket raingauge (data start in March 1996 and end April 2001).

Month	1996	1997	1998	1999	2000	2001	Average	Min	Max
Nov	5.0	46.8	119.0	56.8	81.0	nd	61.7	5.0	119.0
Dec	79.8	164.4	93.4	34.2	206.6	nd	115.7	34.2	206.6
Totals	incom	619.2	679.8	270.0	876.6	incom	555.8	134.2	1254.8
Annual totals[#]	-	-	-	-	-	-	611.4	270.0	876.6

nd = no data is available; incom = totals cannot be calculated due to incomplete data records; [#] Average, maximum and minimum of the annual precipitation totals.

Table J.8: Summary of all the available Kidston Mine Site and surrounding areas annual average precipitation data (mm) sets.

Station	Data record	Precipitation	Source
Kidston township	1915 to 1991	712.0	Coffey Partners (1992)
Kidston township	1915 to 1980	719.0	Gutteridge Haskins and Davey (1983)
Kidston township	1984 to 1995	645.2	Australian Bureau of Meteorology
Kidston Main Gate	1985 to 2001	661.8	Kidston Gold Mine
Kidston Tailings Impoundment	1996 to 2000	611.4	This study
Kidston (Bagstow)	1964 to 1991	785.0	Coffey Partners (1992)
Carpentaria Downs	1902 to 1991	659.0	Coffey Partners (1992)
Lyndhurst	1886 to 1991	737.0	Coffey Partners (1992)
Georgetown	1972 to 1991	830.0	Coffey Partners (1992)
Mine Site	1984 to 1991	801.0	Coffey Partners (1992)
Overall Summary	1915 to 2000	702.2	This study

Table J.9: Summary of the monthly average, maximum and minimum precipitation totals (mm) calculated based on all the available monthly records.

Month	Average	Minimum	Maximum
Jan	184.9	0.0	944.0
Feb	181.8	33.0	317.0
Mar	102.7	0.0	293.0
Apr	20.6	0.0	197.4
May	12.6	0.0	48.2
Jun	10.4	0.0	79.2
Jul	7.3	0.0	69.6
Aug	8.8	0.0	82.0
Sep	6.8	0.0	15.0
Oct	17.5	0.0	83.4
Nov	45.6	0.0	147.0
Dec	103.0	13.0	310.0
Totals	702.2	46.0	2585.8
Annual totals[#]	702.2	270.0	1535.0

[#] Average, maximum and minimum of the annual precipitation totals.

Figure J.1 presents a graphical comparison between all the annual precipitation totals, while Figure J.2 presents a graphical comparison between all the monthly precipitation totals. These figures have been produced from the data contained in Tables J.2 to J.9.

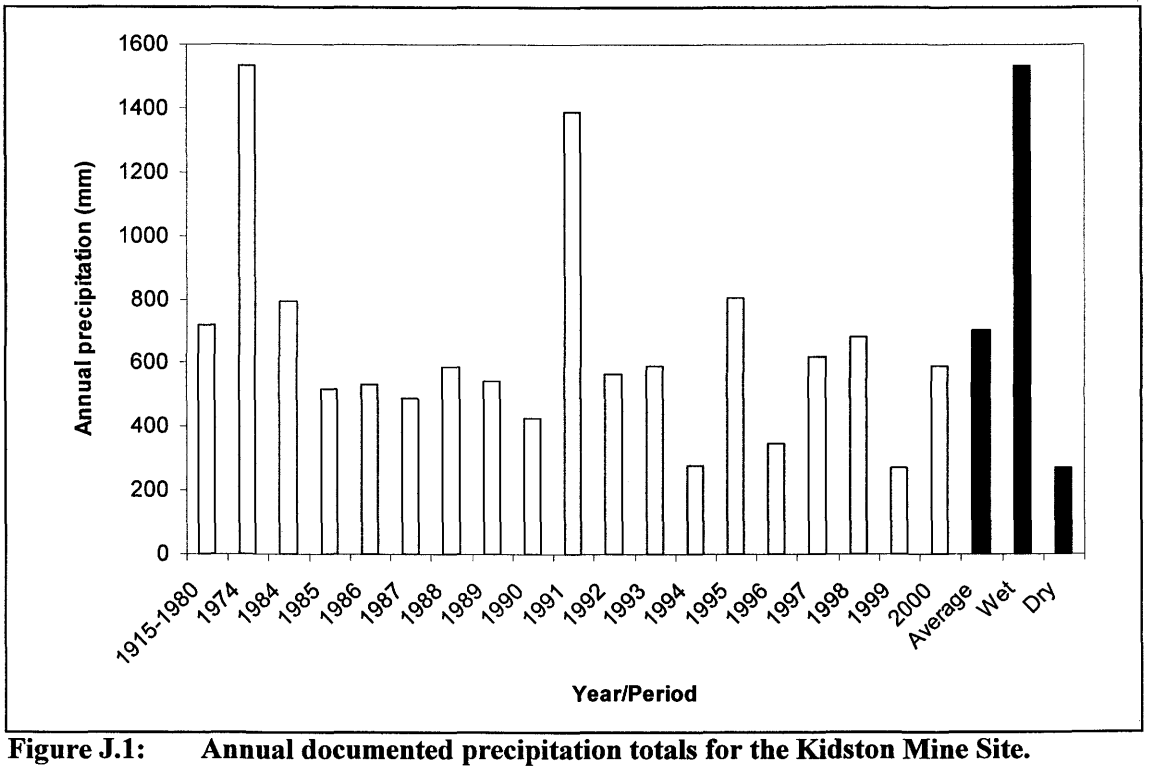

Figure J.1: Annual documented precipitation totals for the Kidston Mine Site.

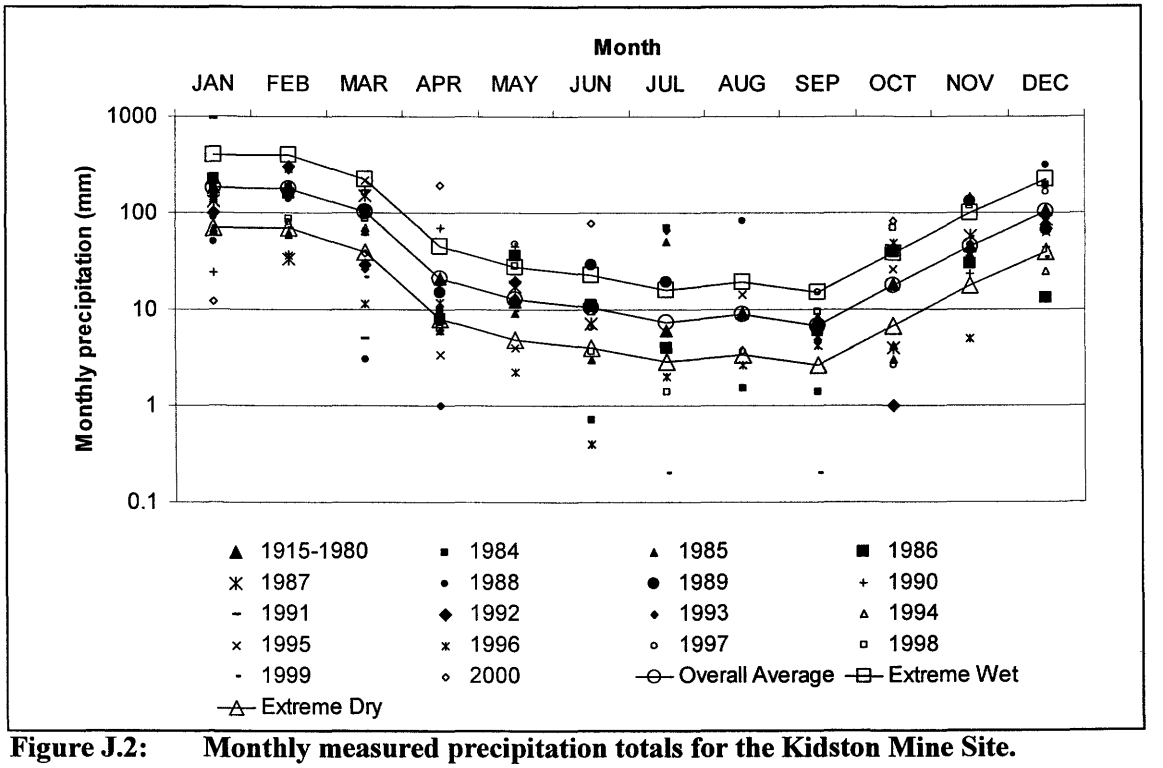

Figure J.2: Monthly measured precipitation totals for the Kidston Mine Site.

J.4 Extreme Precipitation Events

For the purpose of extreme climatic event numerical modeling it was necessary to calculate an extreme wet and extreme dry year of data. Since records of extreme daily precipitation data required for the numerical modeling were not available, generic wet and dry years were created. Firstly a multiplication factor was used to convert the overall average monthly precipitation data to wet and dry year totals. The multiplication factor was calculated by dividing the extreme event annual precipitation by the average annual precipitation (see Table J.10). To then calculate the corresponding monthly precipitation totals for the wet and dry years, the average monthly totals was multiplied by the multiplication factor to give hypothetical wet and dry year monthly precipitation totals (see Table J.11).

The second requirement was to break the monthly totals down to daily precipitation events. This was done by selecting months where detailed daily precipitation data (from the automated tipping bucket raingauge) was available, and most closely resembled the average monthly precipitation totals (see Table J.11). A multiplication factor was subsequently calculated for each month by dividing the average monthly total by the closest actual month total. The generic daily average, wet and dry year precipitation data was then calculated by multiplying the daily precipitation value for the chosen months by the monthly and extreme event multiplication factors. Table J.12 contain the data for the generic average, wet and dry year as used in the SoilCover (SoilCover, 1997) modeling program, and Figure J.3 presents the average year data graphically.

Table J.10: Summary of the wettest and driest precipitation years on record, together with the multiplication factor to calculate corresponding monthly totals based on the average year data.

Description	Rainfall (mm)	Mult. Factor
Overall average rainfall	702.2	-
Wettest year on record is 1974 (Coffee Partners, 1992)	1535.0	2.19
Driest Year on record is 1999	270.0	0.38

Table J.11: Summary table showing hypothetical wettest and driest precipitation monthly totals based on the average monthly totals together with the corresponding closest actual monthly precipitation totals on record.

Month	Average year (mm)	Wettest year (mm)	Driest year (mm)	Mth/yr	Value (mm)	Mult. factor
Jan	184.9	404.2	71.1	Jan-98	173.8	1.06
Feb	181.8	397.4	69.9	Feb-00	165.0	1.10

Table J.11: Summary table showing hypothetical wettest and driest precipitation monthly totals based on the average monthly totals together with the corresponding closest actual monthly precipitation totals on record.

Month	Average year (mm)	Wettest year (mm)	Driest year (mm)	Mth/yr	Value (mm)	Mult. factor
Mar	102.7	224.6	39.5	Mar-98	86.6	1.19
Apr	20.6	45.1	7.9	Apr-96	11.8	1.75
May	12.6	27.6	4.9	May-99	13.4	0.94
Jun	10.4	22.8	4.0	Jun-97	6.6	1.58
Jul	7.3	16.0	2.8	Jul-96	2.0	3.66
Aug	8.8	19.3	3.4	Aug-97	3.6	2.45
Sep	6.8	14.8	2.6	Sep-96	4.2	1.61
Oct	17.5	38.3	6.7	Oct-97	2.6	6.74
Nov	45.6	99.7	17.5	Nov-97	46.8	0.97
Dec	103.0	225.2	39.6	Dec-98	93.4	1.10
Total	702.2	1535.0	270.0	-	609.8	-

Table J.12: Daily precipitation data (mm) used for SoilCover modeling for the three climatic scenarios considered; mean year, wet year and dry year.

Date	Generic year	Average year	Wet year	Dry year	Date	Generic year	Mean year	Wet year	Dry year
2-Jan	4.8	5.1	11.2	2.0	5-Mar	15.2	18.0	39.4	6.9
3-Jan	3.0	3.2	7.0	1.2	6-Mar	0.2	0.2	0.5	0.1
4-Jan	0.4	0.4	0.9	0.2	18-Mar	1.6	1.9	4.1	0.7
5-Jan	6.0	6.4	14.0	2.5	12-Apr	1.4	2.4	5.3	0.9
6-Jan	0.2	0.2	0.5	0.1	19-Apr	10.0	17.5	38.2	6.7
7-Jan	14.8	15.7	34.4	6.1	21-Apr	0.2	0.3	0.8	0.1
8-Jan	3.0	3.2	7.0	1.2	30-Apr	0.2	0.3	0.8	0.1
9-Jan	20.0	21.3	46.5	8.2	18-May	13.00	12.3	26.8	4.7
10-Jan	3.2	3.4	7.4	1.3	19-May	0.40	0.4	0.8	0.1
11-Jan	8.2	8.7	19.1	3.4	7-Jun	0.4	0.6	1.4	0.2
12-Jan	6.8	7.2	15.8	2.8	20-Jun	3.6	5.7	12.4	2.2
13-Jan	36.6	38.9	85.1	15.0	21-Jun	0.2	0.3	0.7	0.1
16-Jan	1.2	1.3	2.8	0.5	23-Jun	2.2	3.5	7.6	1.3
17-Jan	12.4	13.2	28.8	5.1	24-Jun	0.2	0.3	0.7	0.1
18-Jan	0.2	0.2	0.5	0.1	27-Jul	2.0	7.3	16.0	2.8
19-Jan	0.4	0.4	0.9	0.2	31-Aug	3.6	8.8	19.3	3.4
26-Jan	21.0	22.3	48.8	8.6	21-Sep	4.0	6.4	14.1	2.5
27-Jan	19.8	21.1	46.1	8.1	29-Sep	0.2	0.3	0.7	0.1
28-Jan	11.6	12.3	27.0	4.7	1-Oct	2.6	17.5	38.3	6.7
29-Jan	0.2	0.2	0.5	0.1	2-Nov	8.4	8.2	17.9	3.1
5-Feb	0.2	0.2	0.5	0.1	3-Nov	0.2	0.2	0.4	0.1
6-Feb	2.6	2.9	6.3	1.1	4-Nov	0.2	0.2	0.4	0.1
7-Feb	1.0	1.1	2.4	0.4	9-Nov	10.0	9.7	21.3	3.7
8-Feb	2.0	2.2	4.8	0.8	10-Nov	0.4	0.4	0.9	0.1
13-Feb	4.2	4.6	10.1	1.8	19-Nov	6.0	5.8	12.8	2.2
14-Feb	0.0	0.0	0.0	0.0	25-Nov	4.2	4.1	8.9	1.6
15-Feb	20.6	22.7	49.6	8.7	26-Nov	9.6	9.4	20.4	3.6
16-Feb	8.2	9.0	19.7	3.5	27-Nov	1.6	1.6	3.4	0.6

Table J.12: Daily precipitation data (mm) used for SoilCover modeling for the three climatic scenarios considered; mean year, wet year and dry year.

Date	Generic year	Average year	Wet year	Dry year	Date	Generic year	Mean year	Wet year	Dry year
17-Feb	11.6	12.8	27.9	4.9	30-Nov	6.2	6.0	13.2	2.3
18-Feb	2.4	2.6	5.8	1.0	12-Dec	21.0	23.2	50.6	8.9
19-Feb	0.6	0.7	1.4	0.3	13-Dec	0.0	0.0	0.0	0.0
20-Feb	8.4	9.3	20.2	3.6	16-Dec	0.6	0.7	1.4	0.3
21-Feb	0.2	0.2	0.5	0.1	18-Dec	8.6	9.5	20.7	3.6
22-Feb	8.2	9.0	19.7	3.5	19-Dec	2.2	2.4	5.3	0.9
23-Feb	13.2	14.5	31.8	5.6	21-Dec	36.0	39.7	86.8	15.3
24-Feb	32.4	35.7	78.0	13.7	22-Dec	6.0	6.6	14.5	2.5
25-Feb	15.2	16.7	36.6	6.4	27-Dec	0.2	0.2	0.5	0.1
27-Feb	0.4	0.4	1.0	0.2	28-Dec	0.2	0.2	0.5	0.1
28-Feb	33.6	37.0	80.9	14.2	29-Dec	12.0	13.2	28.9	5.1
1-Mar	20.4	24.2	52.9	9.3	30-Dec	6.0	6.6	14.5	2.5
2-Mar	7.6	9.0	19.7	3.5	31-Dec	0.6	0.7	1.4	0.3
3-Mar	11.0	13.1	28.5	5.0	-	-	-	-	-
4-Mar	30.6	36.3	79.4	14.0	Total	609.8	702.2	1535.0	270.0

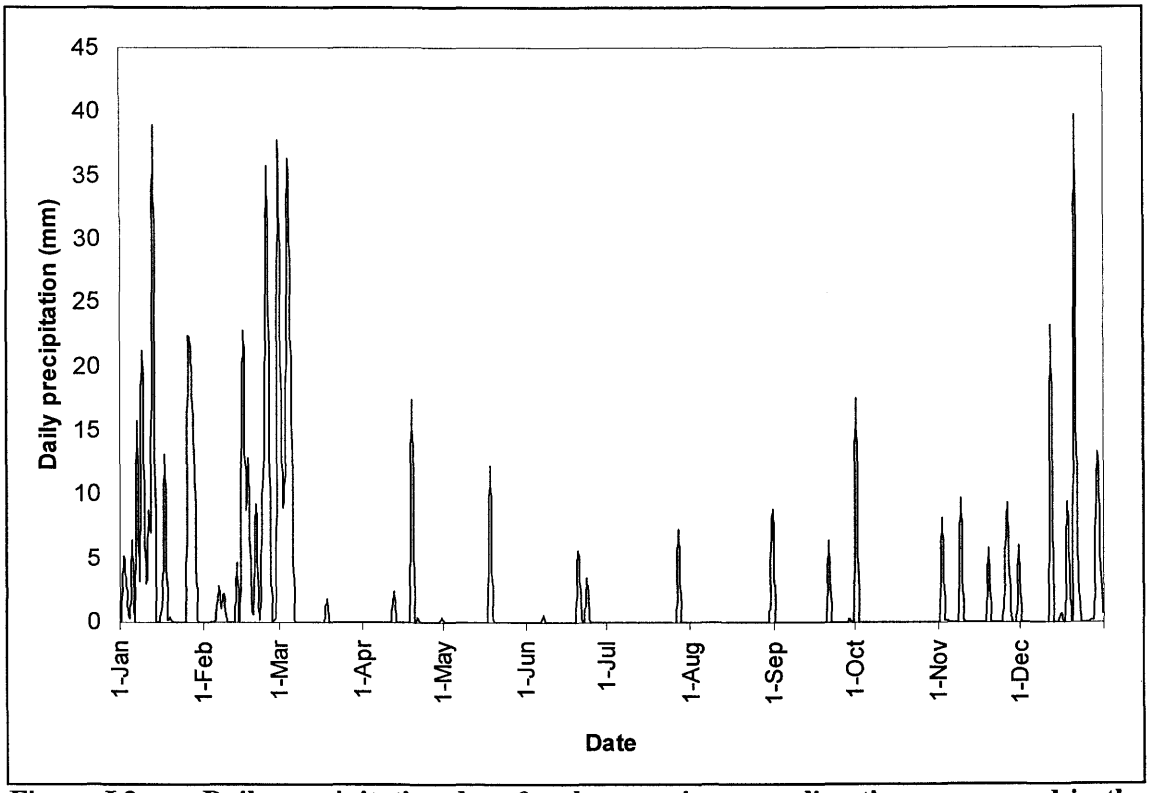

Figure J.3: Daily precipitation data for the generic mean climatic year as used in the SoilCover modeling.

J.5 Precipitation Frequency, Storm Intensities and Durations

The automated tipping bucket raingauge measured actual rainfall events in real time, and thus it is possible to determine exactly the magnitude, duration and intensity of each precipitation event. Table J.13 provides a summary of these parameters and Tables J.14 and J.15 list the number of days that precipitation events occurred for every year of measured data, both with the automated tipping bucket and the manual station at the Kidston Main Gate. The reason for the lower count measured by the manual precipitation recording by the Kidston Mine personnel, is the large number of small events that the automated system are more sensitive towards picking up. Figures J.4 to J.7 presents the frequency graphs of all the parameters listed in Table J.13.

The average storm intensity is calculated by dividing the total precipitation received for an event by the total event duration. The maximum storm intensity is based on the actual maximum intensity of precipitation recorded by the automated tipping bucket during a precipitation event. This intensity may only be for a short portion of the total event duration.

Table J.13: Summary of the storm duration, intensity and magnitude frequencies for 50%, 75% and 95% of the time as determined from the automated tipping bucket raingauge on Kidston Gold Mine (data from March 1996 to April 2001).

Parameter	50% of time	75% of time	95% of time
Total daily precipitation (mm)	< 2	< 10	<35
Storm duration (min)	< 45	< 90	< 240
Average storm intensity (mm/hr)	< 4	< 12	< 24
Maximum storm intensity (mm/hr)	< 8	< 24	< 84

Table J.14: Number of days for which rainfall was recorded with the automated tipping bucket raingauge on the Kidston Barren waste rock dump.

Year	1996**	1997	1998	1999	2000	2001#	Average*	Generic year
No. of rain days	35	79	83	70	79	28	78	84

* average is calculated for complete years only; ** data starts in March 1996; # data stops after April 2001.

Table J.15: Number of days for which rainfall was recorded at the Kidston Main Gate weather station.

Year	1995	1996	1997	1998	1999	2000	2001#	Average*
No. of rain days	42	45	58	72	72	71	15	60

* average is calculated for complete years only; # data stops in February 2001.

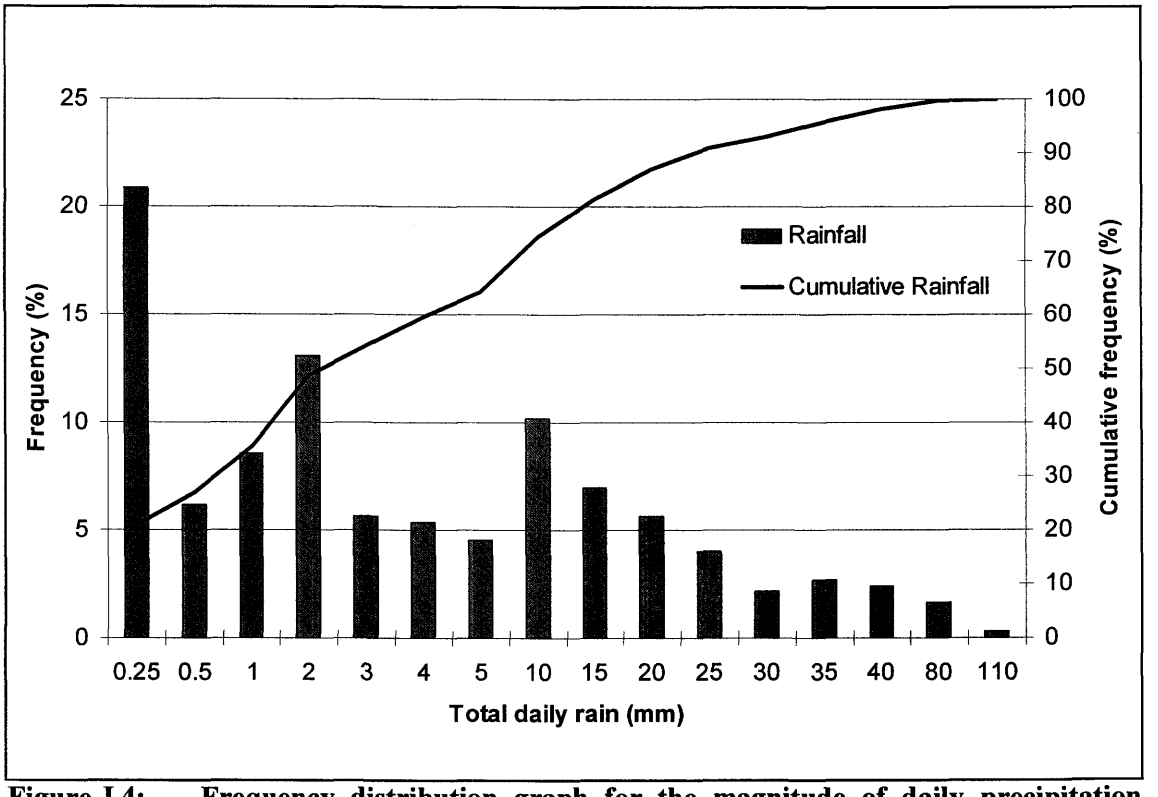

Figure J.4: **Frequency distribution graph for the magnitude of daily precipitation events measured at Kidston Gold Mine.**

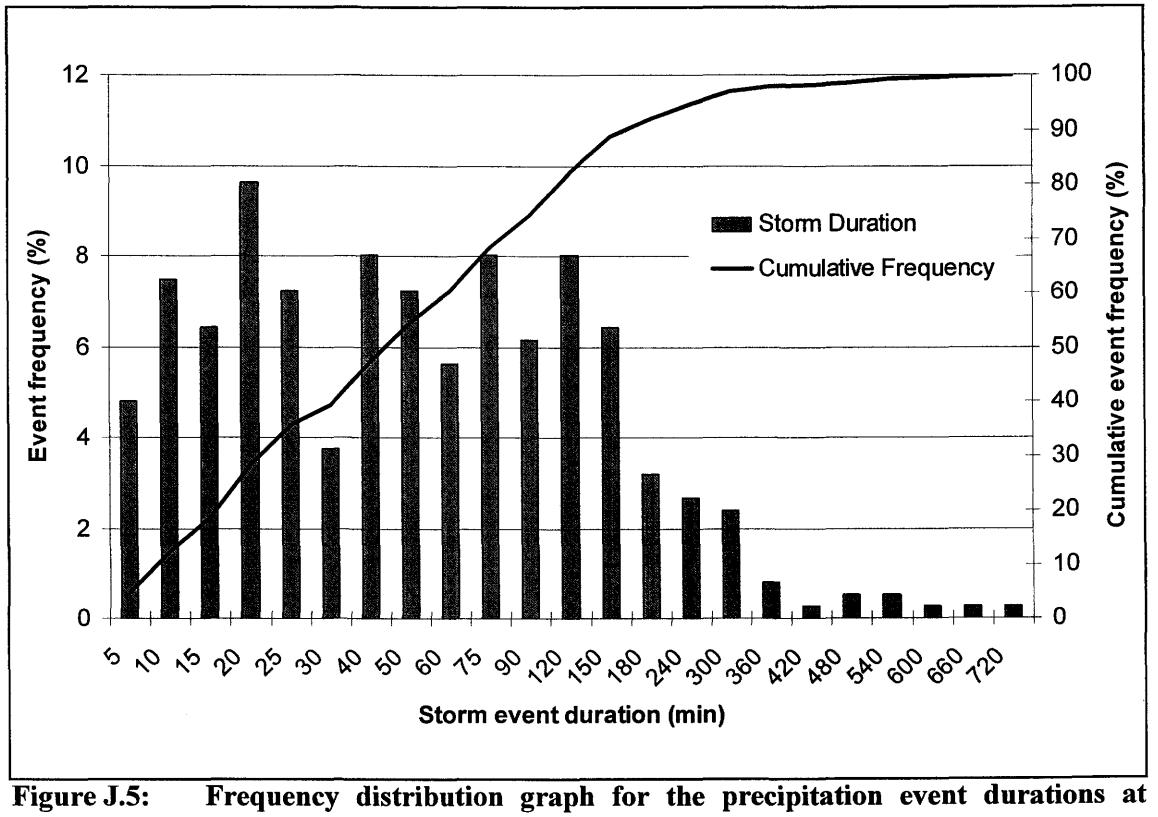

Figure J.5: **Frequency distribution graph for the precipitation event durations at Kidston Gold Mine.**

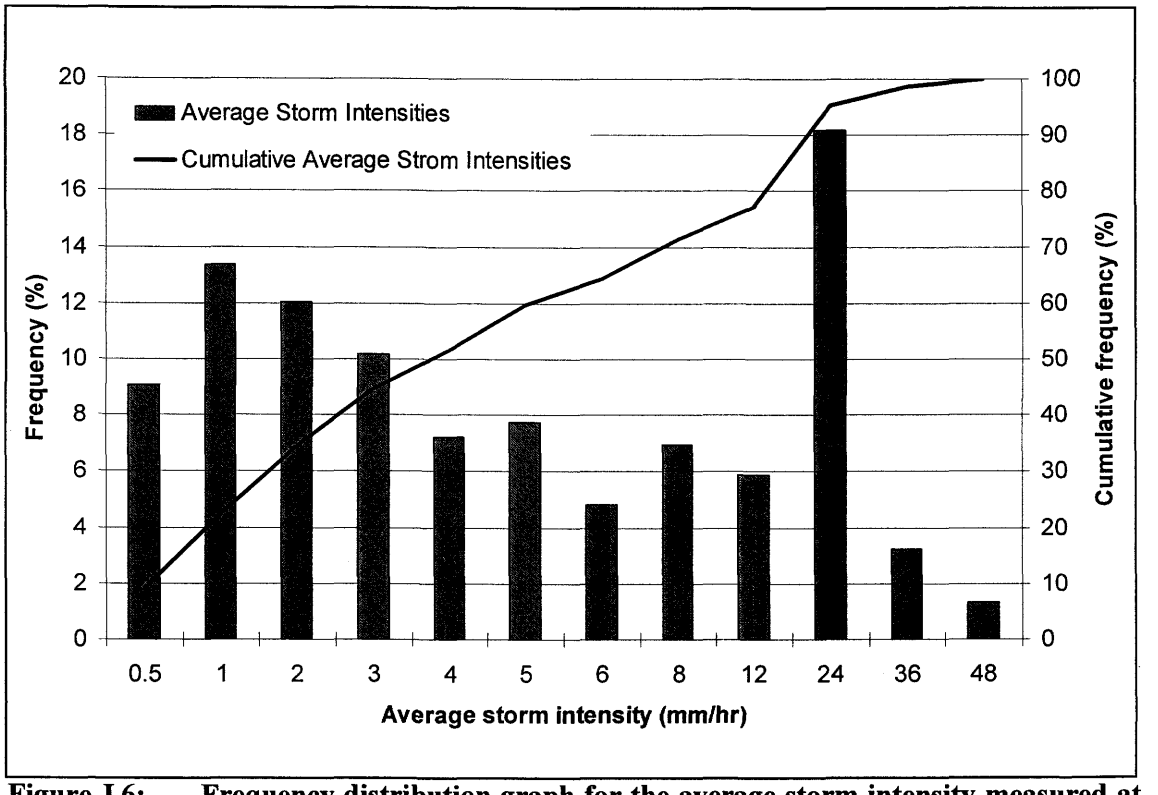

Figure J.6: **Frequency distribution graph for the average storm intensity measured at Kidston Gold Mine.**

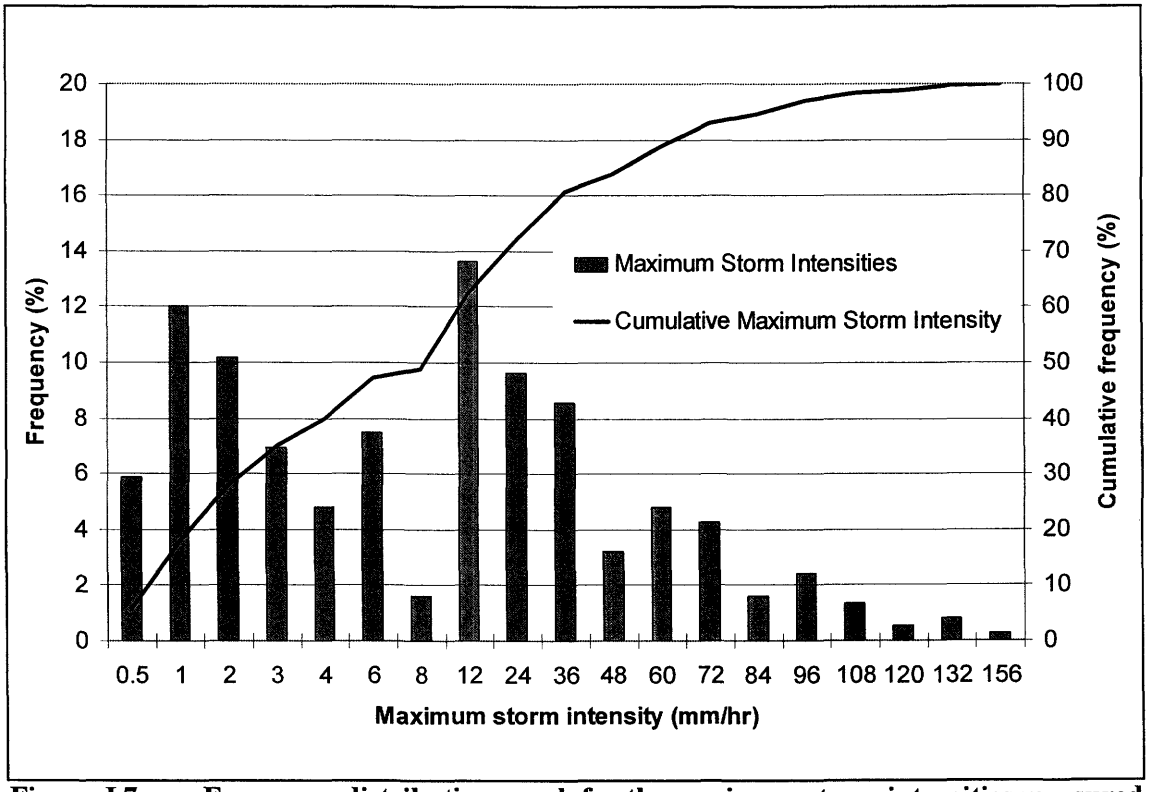

Figure J.7: **Frequency distribution graph for the maximum storm intensities measured at Kidston Gold Mine.**

J.6 Evaluation Set Precipitation Data

The period between 1 December 2000 and 30 April 2001 was selected to perform a detailed evaluation check for the spatial flux boundary functions, and the tailings impoundment water balance. The daily precipitation data measured with the automated tipping bucket raingauge is listed in Table J.16, and Figure J.8 presents the data graphically.

Table J.16: Daily precipitation data as measured with the automated tipping bucket raingauge for the period 1 December 2000 to 30 April 2001.

Date	Daily rain (mm)	Average intensity (mm/hr)	Maximum intensity (mm/hr)	Rain start time (hr:min)	Rain stop time (hr:min)	Event duration (hr:min)
08-Dec-00	1.00	0.97	1.50	20:00	21:01	1:01
09-Dec-00	1.20	0.73	4.00	0:00	1:38	1:38
12-Dec-00	20.00	6.48	24.00	18:50	21:55	3:05
13-Dec-00	16.40	6.48	24.00	0:00	2:31	2:31
14-Dec-00	0.40	1.61	1.71	22:30	22:44	0:14
15-Dec-00	1.80	2.46	6.00	0:00	0:43	0:43
16-Dec-00	1.20	2.59	4.00	21:12	21:39	0:27
17-Dec-00	32.80	17.65	96.00	0:00	1:51	1:51
18-Dec-00	3.00	1.28	3.00	12:20	14:40	2:20
19-Dec-00	2.00	1.23	4.00	0:12	1:49	1:37
27-Dec-00	5.20	4.49	24.00	0:35	1:44	1:09
28-Dec-00	24.40	15.77	60.00	0:00	1:32	1:32
29-Dec-00	53.00	17.15	108.00	0:00	3:05	3:05
30-Dec-00	44.20	39.23	96.00	10:00	11:07	1:07
01-Jan-01	51.20	12.28	60.00	2:00	6:10	4:10
20-Jan-01	1.00	0.96	2.40	6:00	7:02	1:02
21-Jan-01	0.20	0.75	0.75	15:00	15:16	0:16
23-Jan-01	0.20	0.71	0.71	22:30	22:47	0:17
31-Jan-01	0.40	0.26	0.50	2:30	4:03	1:33
01-Feb-01	37.60	22.69	96.00	5:00	6:39	1:39
02-Feb-01	38.60	18.81	96.00	8:35	10:38	2:03
04-Feb-01	1.20	5.67	12.00	0:18	0:30	0:12
05-Feb-01	1.60	4.78	12.00	17:45	18:05	0:20
15-Feb-01	2.20	1.86	4.00	17:00	18:10	1:10
16-Feb-01	0.20	0.20	0.20	21:00	21:59	0:59
17-Feb-01	26.60	6.26	24.00	10:26	14:41	4:15
18-Feb-01	15.00	1.68	12.00	0:00	8:56	8:56
24-Feb-01	5.40	17.17	72.00	15:00	15:18	0:18
25-Feb-01	28.00	14.03	60.00	0:30	2:29	1:59
26-Feb-01	5.60	2.86	12.00	8:00	9:57	1:57
27-Feb-01	0.60	0.12	0.21	3:00	8:06	5:06
28-Feb-01	1.60	5.42	12.00	5:00	5:17	0:17
03-Mar-01	16.00	7.45	48.00	3:25	5:33	2:08
04-Mar-01	1.80	3.47	12.00	1:00	1:31	0:31

Table J.16: Daily precipitation data as measured with the automated tipping bucket raingauge for the period 1 December 2000 to 30 April 2001.

Date	Daily rain (mm)	Average intensity (mm/hr)	Maximum intensity (mm/hr)	Rain start time (hr:min)	Rain stop time (hr:min)	Event duration (hr:min)
09-Mar-01	0.20	0.92	0.92	7:30	7:43	0:13
14-Mar-01	0.20	2.00	2.00	17:00	17:06	0:06
15-Mar-01	14.80	25.49	72.00	18:00	18:34	0:34
19-Mar-01	0.80	0.70	1.50	22:00	23:08	1:08
22-Mar-01	0.40	2.40	2.40	0:00	0:10	0:10
23-Mar-01	1.40	8.75	24.00	18:50	18:59	0:09
24-Mar-01	0.60	0.62	1.50	21:00	21:57	0:57
25-Mar-01	9.00	29.18	84.00	1:10	1:28	0:18
Total	469.0	-	-	-	-	-

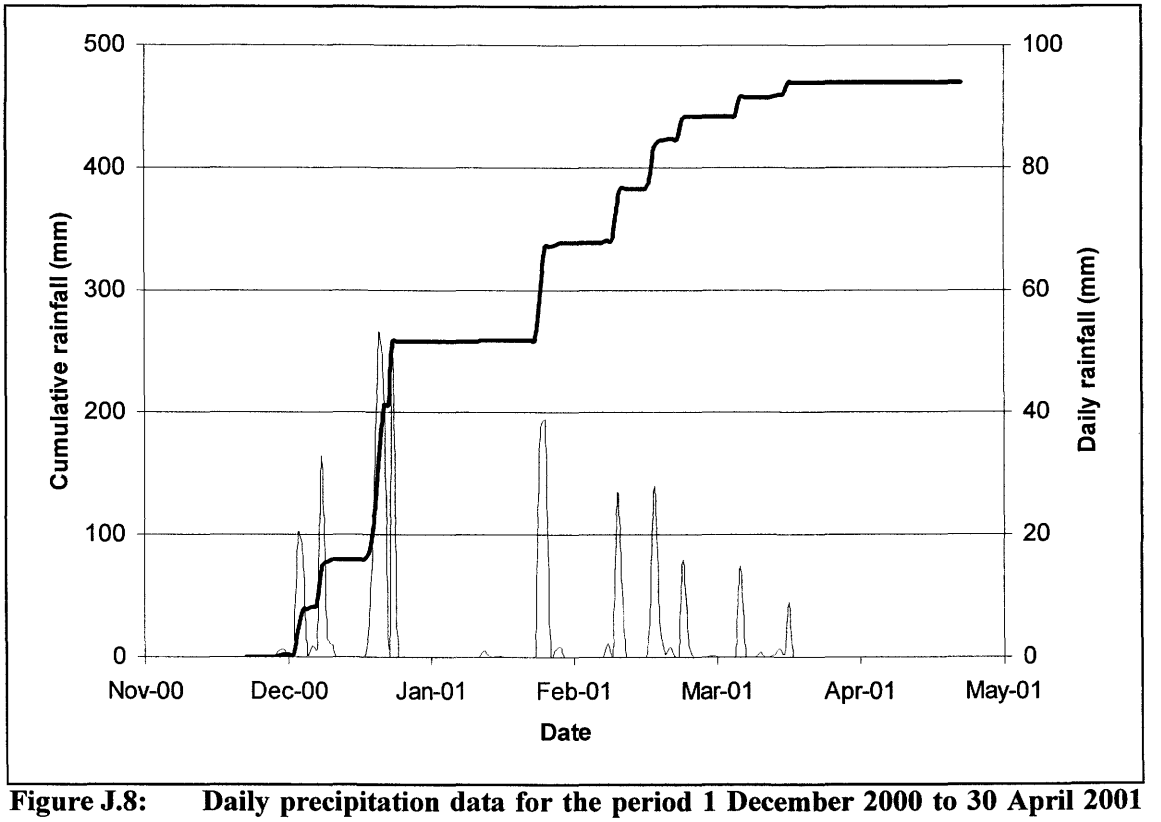

Figure J.8: Daily precipitation data for the period 1 December 2000 to 30 April 2001 at the Kidston Mine Site.

J.7 Complete Daily Precipitation Data for Kidston

Detailed daily precipitation data for the Kidston Mine Site is available from March 1996 through to April 2001. This data is presented graphically in Figure J.9.

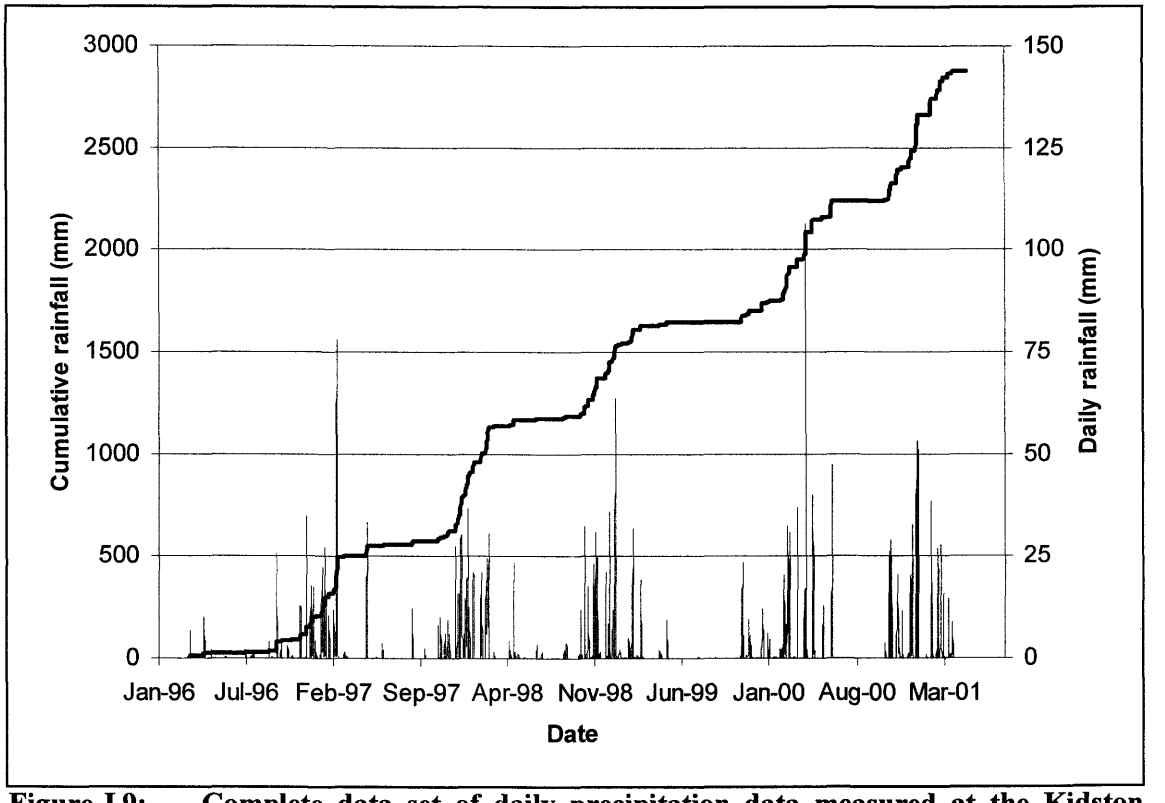

Figure J.9: Complete data set of daily precipitation data measured at the Kidston Mine Site for period March 1996 through April 2001.

J.8 References

Campbell Scientific, Inc. (CSI) (1994). Tripod-Based Weather Station Installation Manual.

Coffey Partners (1992). Pit Hydrology Study. Consultants report to Kidston Gold Mines Limited, Report No. Z105/4-AC, 28 September.

Durham, A.J.P., Wilson, G.W., Currey, N. (2000). Field Performance of Two Low Infiltration Cover Systems in a Semi Arid Environment. Proceedings of the Fifth international conference on Acid Rock Drainage, Denver, Colorado, USA. May, pp. 1319-1326.

Gutteridge Haskins & Davey Pty Ltd (1984). Kidston Project – Tailings Dam Study. Consultants Report to Kidston Gold Mines Limited, November 1983 – Amended July 1984, 19 Pages.

SoilCover. (1997). SoilCover User's Manual. Unsaturated Soils Group, Department of Civil Engineering, University of Saskatchewan, Saskatoon, Saskatchewan, Canada.

This page was intentionally left blank.

APPENDIX K

Tailings Response Monitoring

K.1 Introduction

Details of the Campbell Scientific Model-229 matric suction sensors installed on the Kidston tailings impoundment to measure the tailings response to real-time moisture change are presented here. The sensor calibration, installation procedure and a summary of the measured data is included in this appendix. Tailings response monitoring involves monitoring the hydraulic and thermal response of the soil profile to the atmospheric supply and demand of moisture and energy. Soil response monitoring in this study consisted of in-situ measurements of matric suction and soil temperature. The continuous monitoring of soil responses is essential for proper calibration of the SoilCover (SoilCover, 1997) numerical modeling (see Chapter 6). In situ measurements of matric suction are important for a number of reasons.

K.2 Campbell Scientific Modell-229 Matric Suction Sensors

The Campbell Scientific Model-229 Matrix Water Potential Sensor (CSI, 1993), a thermal conductivity sensor, was used for measurements of matric suction and soil temperature in the tailings profile. At the time of the installation these sensors were considered to be the most reliable and were compatible with the data acquisition systems in use on the mine site. The Model-229 sensor consists of a probe inserted axially in a porous cylinder (length of 0.03 m and diameter of 0.015 m) (CSI, 1993). The probe consists of a stainless steel tube (length of 0.025 m and diameter of 0.9 mm) in which a heating element and a thermocouple (copper-Constantine) are embedded (CSI, 1993). The heating element and thermocouple are connected to extension wires; this connection is embedded in an electrical insulating resin (length of 0.02 m and diameter of 0.015 m) (CSI, 1993). The Model-229 sensor has a reported suction measuring range of approximately 0 to 400 kPa (CSI, 1993). The measuring accuracy depends on the field installation and laboratory calibration of the sensors. The thermal conductivity sensors were connected to a data acquisition system for the automated monitoring of the matric suction.

K.3 Calibration of the Model-229 Matric Suction Sensors

The Model-229 thermal conductivity sensors were calibrated at the factory and in the laboratory. The supplier of the Model-229 thermal conductivity sensor provides a single point factory calibration (CSI, 1993) for each sensor. However, it was determined that the factory calibration curve, which relates relative temperature rise to matric suction, was unacceptable for the purpose of this study. This was primarily due to the variability in the range of responses of each sensor.

The Model-229 sensors used in this study were thus re-calibrated in the University of Saskatchewan Soils Laboratory using the procedure described by Durham and Fredlund (1996). A single sensor calibration pod was used to calibrate each sensor. The calibration pod consisted of a high air entry disk and employed the axis translation technique to apply matric suction. An automated data acquisition system was used to record changes in sensor output. The resultant calibration curves produced for each sensor by Mr. Andrew Durham, were composite straight-line functions for the suction range between 15 and 350 kPa.

It was however believed that these calibration curves were not sufficient and as part of this study the calibration data was re-analyzed and the curve fitting technique suggested by Fredlund *et al.*, (2000) for calibrating the Beta-97 matric suction sensors (Fredlund *et al*, 1998) was used. The analysis method and the resulting calibration parameters and functions are presented below. Based on the calibration data as well as previous experience with the Model-229 sensors, they are believed to be truly accurate in the 50-200 kPa matric suction range only. The measured voltage change (voltage differential) are related to the soil matric suction based on the following equation:

$$\psi = \left[\frac{b(\Delta V - a)}{c - \Delta V}\right]^{d} \qquad [K.1]$$

Where ψ = matric suction (kPa),

ΔV = voltage change measured by the matric suction sensor (mV),

a = calibration coefficient representing the output voltage at saturated condition,

b = calibration coefficient representing the output voltage under a total dry condition,

c = calibration coefficient representing the slope of the calibration curve, and

d = calibration coefficient representing the inflection point on the calibration curve.

By applying Equation K.1 to the laboratory calibration data as listed in Table K.1 and Figures K.1 to K.9), the calibration coefficients listed in Table K.2 for each sensor used on the tailings impoundment were selected. The use of Equation K.1 and the coefficients of Table K.2 made it possible to estimate the matric suction for any voltage differential measured by the individual sensors on site. Even though the calibration curve covers the entire suction rage between 0 and 1000000 kPa the accurate range of the sensor still only remain between 50 to 200 kPa.

Table K.1: Laboratory calibration data for the Campbell Scientific Model-229 matric suction sensors installed on the Kidston tailings impoundment.

Test matric suction (kPa)	Model-229 sensor number (installed depth) – voltage change readings, ΔV (mV)								
	# 16 (50 mm)	# 20 (150 mm)	# 15 (300 mm)	# 21 (500 mm)	# 17 (750 mm)	# 19 (1000 mm)	# 18 (1250 mm)	NC150 (1500 mm)	NC200 (2000 mm)
0.1	0.03067	0.03001	0.02434	0.03001	0.03001	0.03067	0.03001	0.0270	0.0262
15	0.03401	0.03835	0.03035	0.03701	0.03501	0.04035	0.03601	0.0311	0.0300
50	0.05202	0.05602	0.05202	0.05469	0.05269	0.05502	0.05469	0.0385	0.0375
100	0.06069	0.06503	0.06567	0.06136	0.06269	0.06469	0.06203	0.0500	0.0480
200	0.07202	0.07769	0.07602	0.07402	0.07402	0.07269	0.07436	0.0744	0.0725
350	0.07770	0.08470	0.08770	0.08136	0.08036	0.08036	0.08036	0.0925	0.0820
150000	0.11871	0.12471	0.12802	0.11470	0.11971	0.10704	0.11604	0.1184	0.1184

Table K.2: Calibration coefficients for the Campbell Scientific Model-229 matric suction sensors installed on the Kidston tailings impoundment.

Calibration coefficients	Model-229 sensor number (installed depth)								
	# 16 (50 mm)	# 20 (150 mm)	# 15 (300 mm)	# 21 (500 mm)	# 17 (750 mm)	# 19 (1000 mm)	# 18 (1250 mm)	NC150 (1500 mm)	NC200 (2000 mm)
a	0.03067	0.03001	0.02434	0.03001	0.03001	0.03067	0.03001	0.02700	0.02620
b	80.00	60.00	230.00	70.00	60.00	40.00	70.00	500.00	400.00
c	0.11871	0.12471	0.12802	0.11470	0.11971	0.10704	0.11604	0.11842	0.11842
d	1.28	1.30	0.94	1.22	1.35	1.35	1.24	0.86	0.93

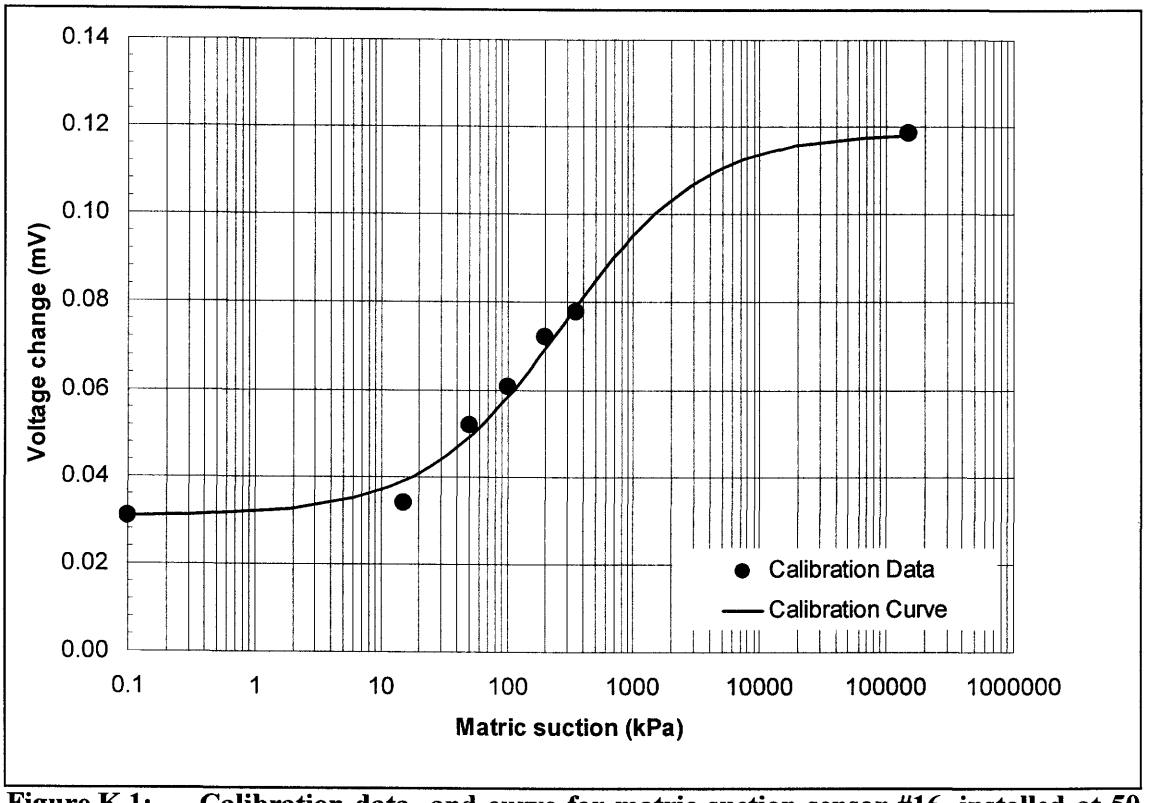

Figure K.1: **Calibration data- and curve for matric suction sensor #16, installed at 50 mm depth in the Kidston tailings impoundment.**

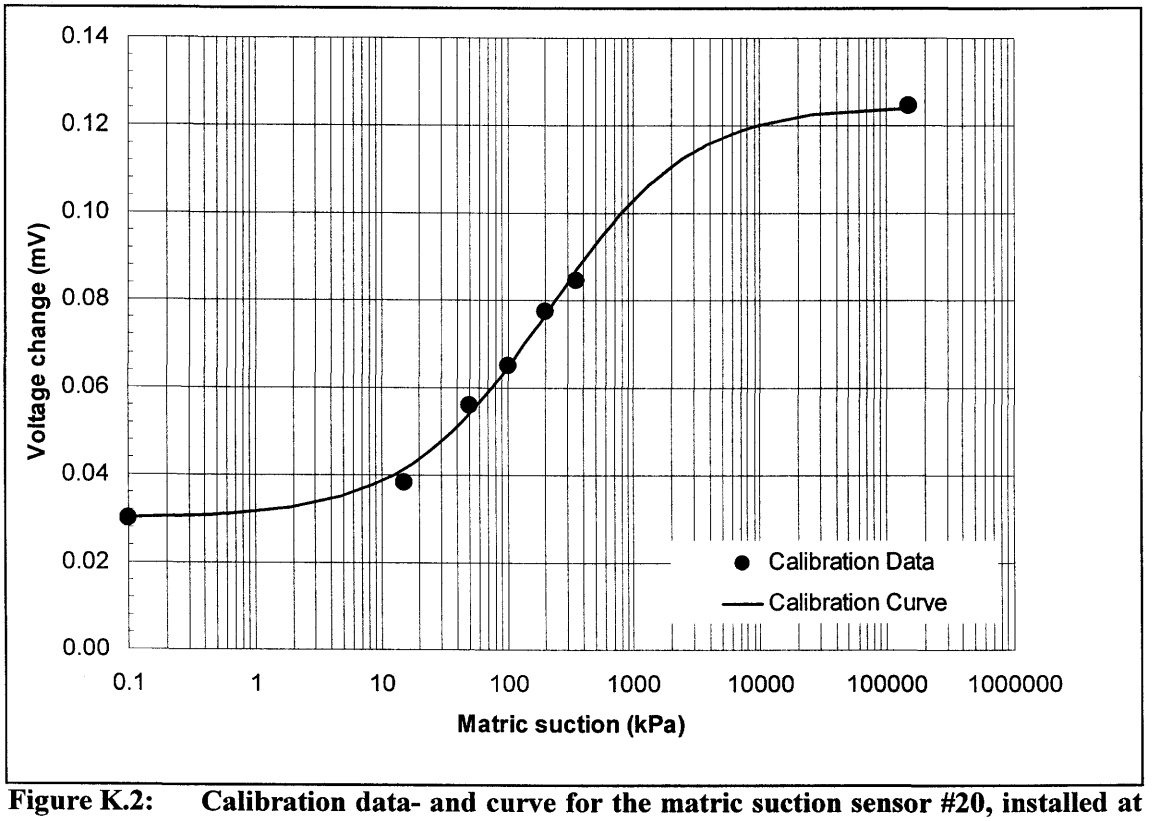

Figure K.2: **Calibration data- and curve for the matric suction sensor #20, installed at 150 mm depth in the Kidston tailings impoundment.**

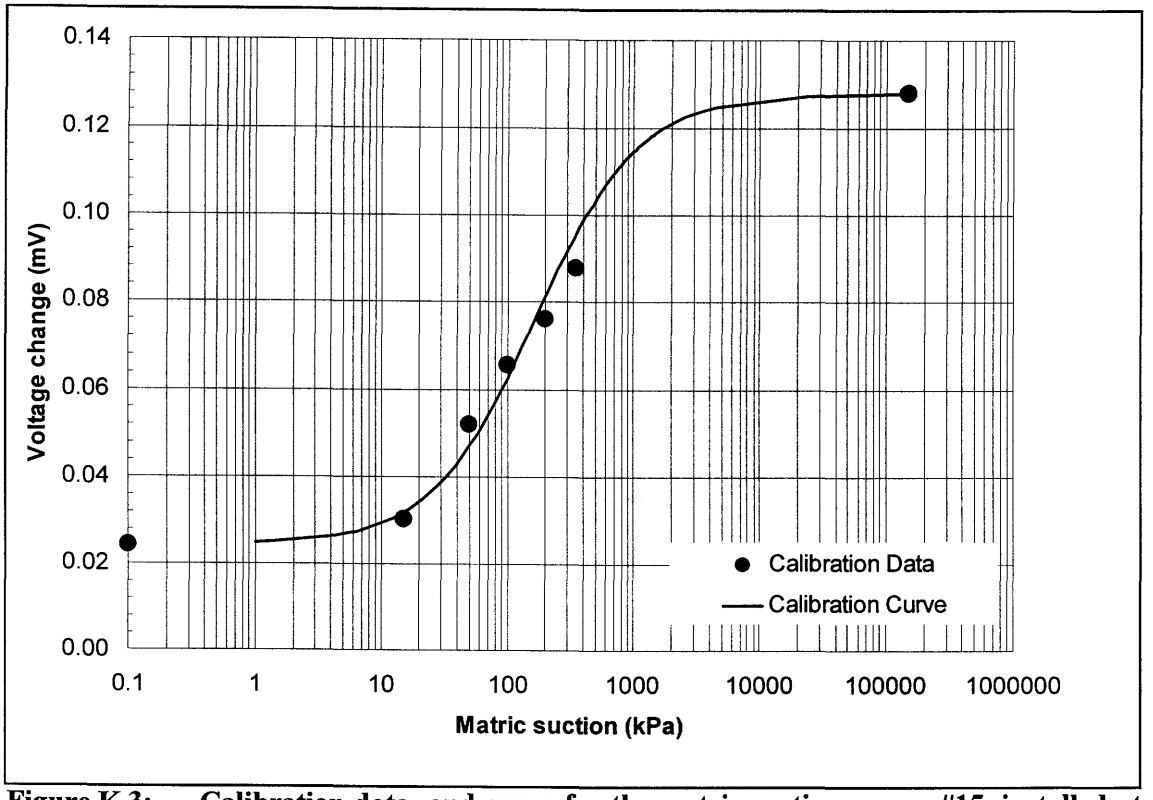

Figure K.3: **Calibration data- and curve for the matric suction sensor #15, installed at 300 mm depth in the Kidston tailings impoundment.**

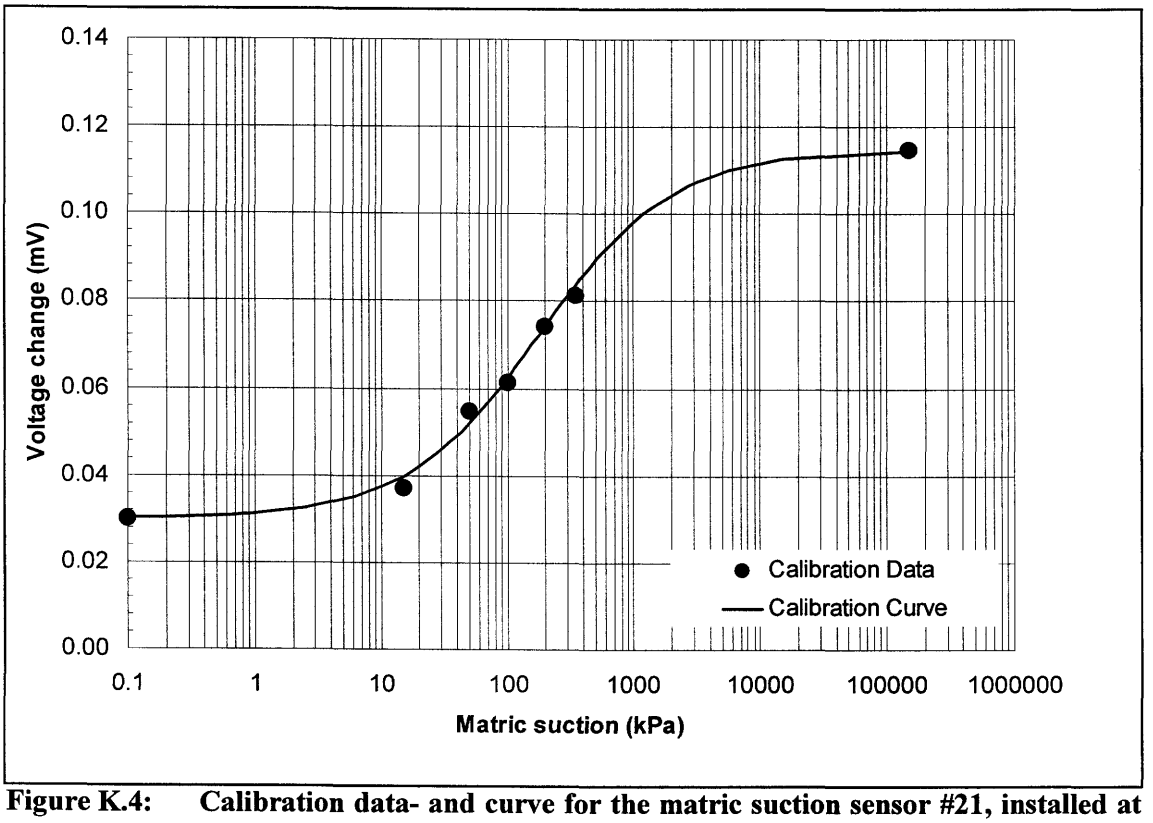

Figure K.4: **Calibration data- and curve for the matric suction sensor #21, installed at 500 mm depth in the Kidston tailings impoundment.**

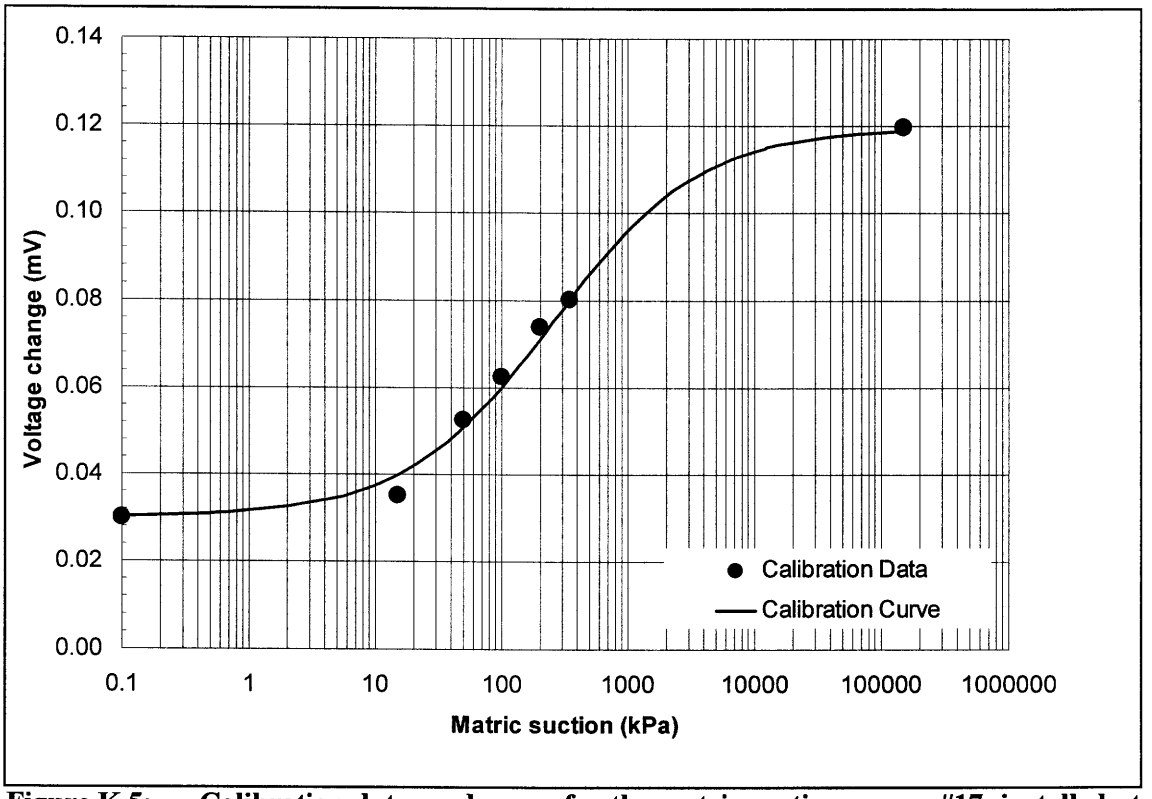

Figure K.5: **Calibration data- and curve for the matric suction sensor #17, installed at 750 mm depth in the Kidston tailings impoundment.**

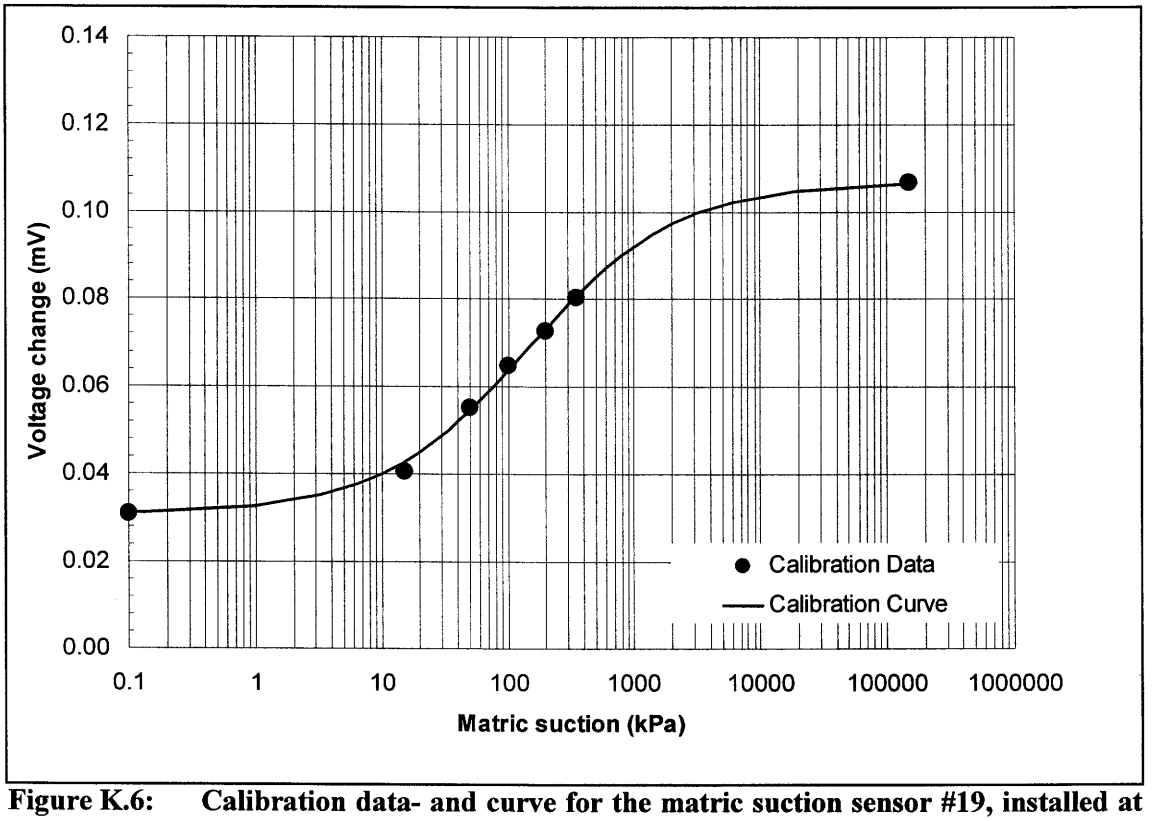

Figure K.6: **Calibration data- and curve for the matric suction sensor #19, installed at 1000 mm depth in the Kidston tailings impoundment.**

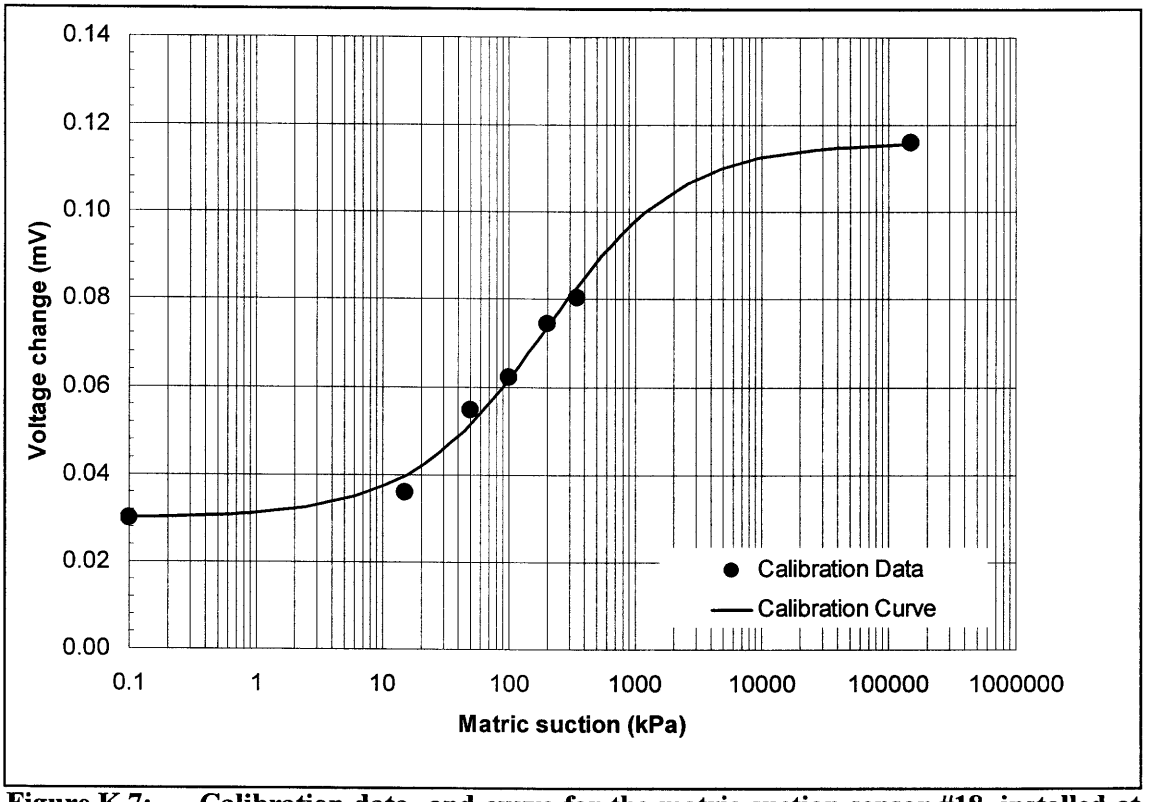

Figure K.7: **Calibration data- and curve for the matric suction sensor #18, installed at 1250 mm depth in the Kidston tailings impoundment.**

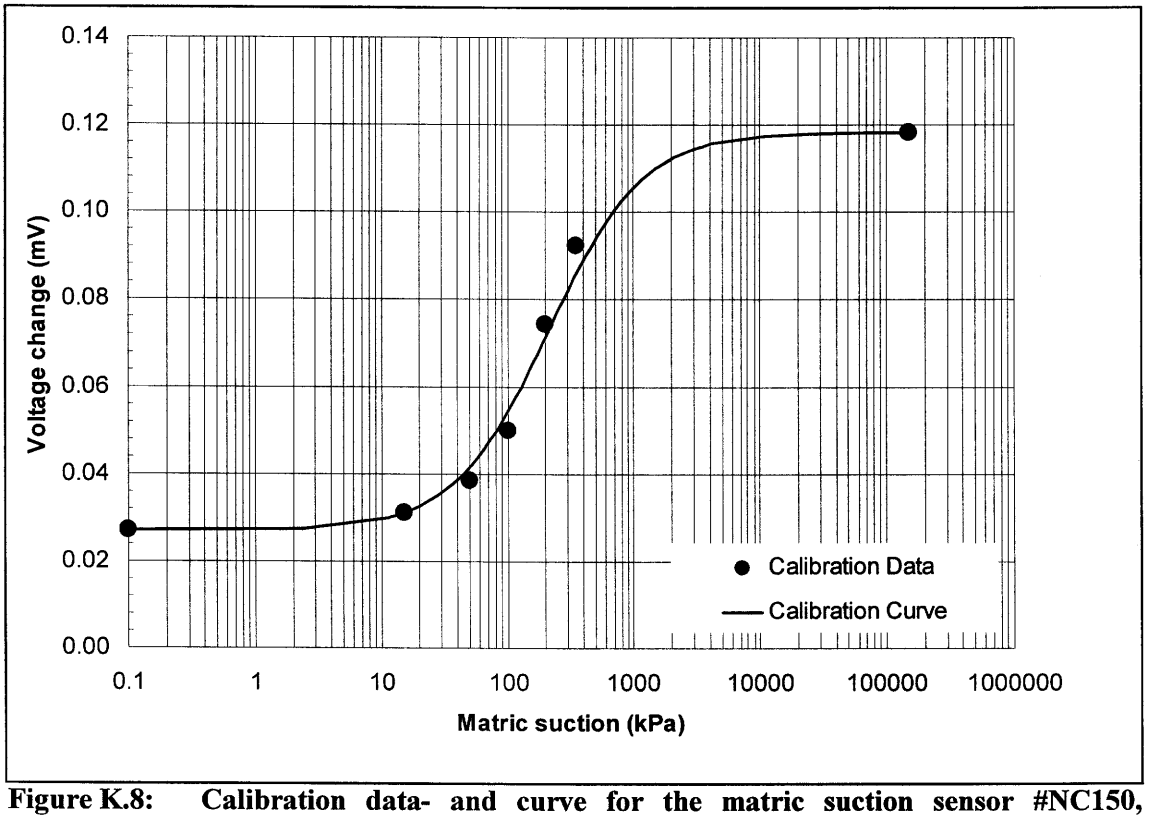

Figure K.8: **Calibration data- and curve for the matric suction sensor #NC150, installed at 1500 mm depth in the Kidston tailings impoundment.**

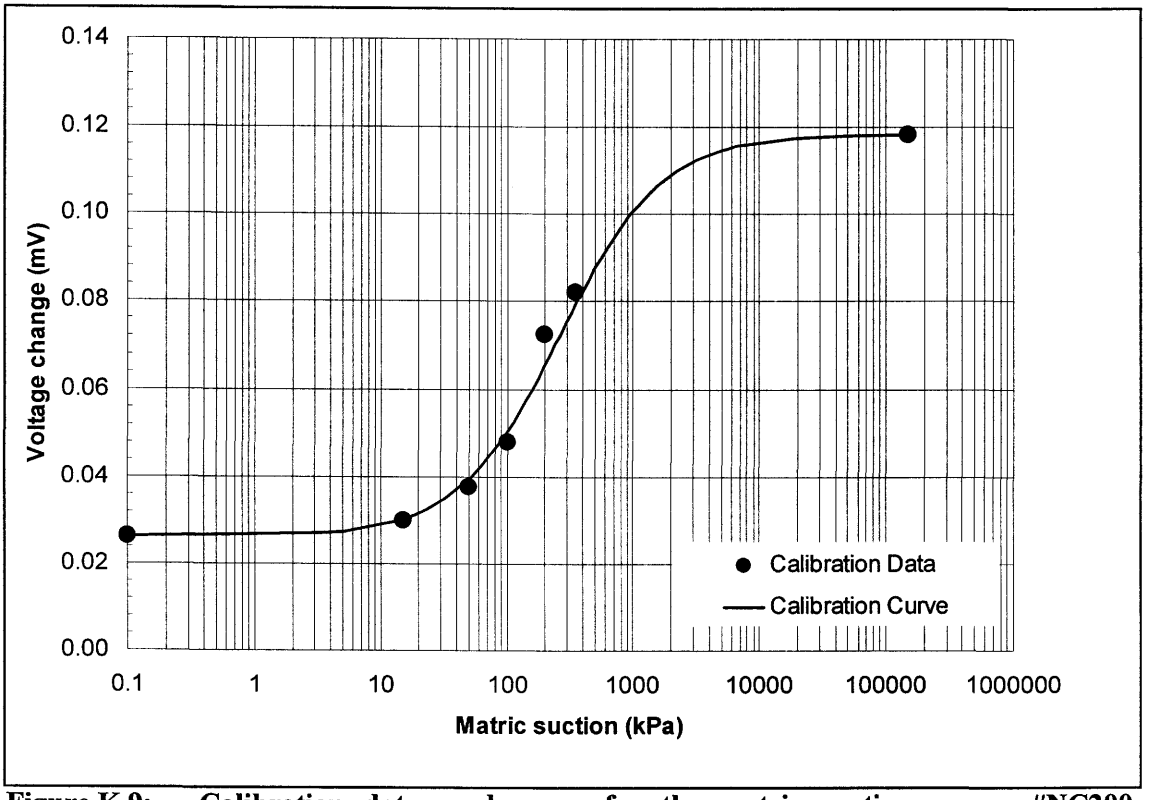

Figure K.9: Calibration data- and curve for the matric suction sensor #NC200, installed at 2000 mm depth in the Kidston tailings impoundment.

K.4 Installation of the Model-229 Matric Suction Sensors

Model-229 thermal conductivity sensors were installed at the same site as the Bowen ratio station on the tailings impoundment (see Appendix H). These sensors were connected to the Bowen ratio station data acquisition system, for the measurement of matric suction and tailings temperature every 12 hours (at noon and at midnight). A University of Saskatchewan graduate student, Mr. Andrew Durham, completed the sensor installation at the same time as the Bowen ration station installation in 1997.

Model-229 thermal conductivity sensors were installed laterally into the tailings profile at depths of 0.05, 0.15, 0.30, 0.50, 0.75, 1.00, 1.25, 1.50 and 2.00 m. A pit was excavated into the tailings profile using an excavator. From the least disturbed wall of the pit the sensors was installed laterally into the tailings profile at the required depths by drilling a 0.016 m horizontal hole 0.5 m deep into the side of the excavation wall, using a hand auger. A small sample of the excavated tailings was collected for laboratory testing (see Appendix A). The sensors were then

inserted into the drilled holes using a special tool, and the remainder of the hole was backfilled ensuring a secure fit. All the lead wires from the sensors were clustered together and brought to surface immediately adjacent the wall against which the sensors was installed. The remainder of the excavation was then backfilled using the excavator taking due care not to damage the sensors.

The data acquisition system has been described in Appendix H, and only additional components will be described here. Since the 21X data logger does not have enough available excitation channels, the wiring was relayed through an AM416 multiplexer prior to connection with the datalogger (CSI, 1992). All the sensors are connected to the AM416 and the AM416 in turn is connected to the 21X.

K.5 Summary of the Model-229 Matric Suction Sensor Data

The same operational problems experienced with the Bowen ratio station, were experienced in the tailings response data (see Appendix H). The equipment was thus off-line for long periods of time resulting in a non-continuous data set. Table K.3 lists the details of the available data sets. The 3rd data set in Table K.3 is thus clearly contains too many gaps to be of any real use and will not be reported any further.

Table K.3: Details of the available tailings response data sets for the Kidston tailings impoundment installation.

Data set no.	Dates	No. of days	No. of missing days
1	24 October 1997 to 31 December 1998	69	7
2	22 October 1998 to 8 January 1999	79	6
3	7 February 1999 to 1 June 1999	73	57
4	17 October 1999 to 22 May 2000	218	16

Tables K.5 and K.6 contain the measured tailings temperature and matric suction data at noon (PM) and midnight (AM) for periods 1, 2 and 4 in Table K.3. The volumetric moisture content listed in Table K.7 was calculated using the matric suction listed in Table K.6 and applying the Fredlund and Xing (1994) curve fit equation. The parameters for the Fredlund and Xing (1994) curve fit equation was based on the soil water characteristic curve data of sample G3 (12.0-15.5m) tested by Williams (2000) and reported in Appendix D. The parameters are listed in Table K.4.

Table K.4: Fredlund and Xing (1994) curve fit parameters for calculating the volumetric moisture content corresponding to in-situ matric suction readings.

Symbol	Meaning	Value
θ_s	saturated volumetric water content	0.435
a	suction related to the air-entry value of the soil	19.0
n	a soil parameter related to the slope at the inflection point on the soil water characteristic curve	1.95
m	a soil parameter related to the residual water content	1.38
ψ_r	residual water content	1500 kPa

Table K.5: Tailings temperatures (at noon and midnight) measured with the Model-229 Campbell Scientific matric suction sensors installed on the Kidston tailings impoundment.

Date	Tailings temperature (°C)																	
	NC200 (2000 mm)		NC150 (1500 mm)		#18 (1250 mm)		#19 (1000 mm)		#17 (750 mm)		#21 (500 mm)		#15 (300 mm)		#20 (150 mm)		16 (50 mm)	
	PM	AM	PM	AM	PM	AM	PM	AM	PM	AM	PM	AM	PM	AM	PM	AM	PM	AM
24-Oct-97	25.9	25.7	25.5	25.1	25.3	24.9	25.5	25.3	26.0	25.4	25.9	25.7	25.1	26.3	25.4	25.8	28.7	24.8
25-Oct-97	25.9	25.8	25.8	25.6	25.7	25.5	26.0	25.9	26.2	25.9	26.1	26.1	25.4	26.9	25.9	26.5	29.0	25.5
26-Oct-97	26.1	25.9	26.2	25.9	26.1	25.9	26.3	26.2	26.6	26.2	26.5	26.4	25.6	27.0	26.0	26.5	29.2	25.6
27-Oct-97	26.1	26.0	26.4	26.2	26.3	26.2	26.6	26.5	26.9	26.5	26.8	26.7	26.2	27.4	26.8	27.0	30.1	26.0
28-Oct-97	26.2	26.1	26.5	26.3	26.5	26.4	26.8	26.8	27.1	26.7	27.1	27.1	26.4	27.9	26.9	27.6	30.0	26.5
29-Oct-97	26.3	26.1	26.7	26.5	26.7	26.6	27.0	27.0	27.4	26.9	27.4	27.4	26.5	28.2	27.0	27.8	30.6	26.6
30-Oct-97	26.4	26.2	26.8	26.6	26.9	26.7	27.2	27.2	27.5	27.2	27.6	27.6	27.0	28.4	27.7	28.2	31.8	27.0
31-Oct-97	26.4	26.2	26.9	26.6	27.0	26.8	27.3	27.3	27.7	27.3	28.0	27.9	27.4	28.9	28.1	29.1	31.9	28.2
1-Nov-97	26.5	26.3	27.0	26.8	27.2	26.9	27.6	27.4	28.1	27.5	28.5	28.2	28.0	29.4	28.8	29.5	32.7	28.6
2-Nov-97	26.7	26.4	27.2	26.9	27.3	27.1	27.8	27.7	28.4	27.9	28.9	28.7	28.6	29.9	29.2	30.2	32.5	29.5
5-Nov-97	26.6	26.5	27.3	27.2	27.5	27.5	28.1	28.1	28.5	28.2	28.8	29.1	28.2	30.1	29.2	29.7	33.4	27.7
6-Nov-97	26.9	26.6	27.6	27.3	27.8	27.6	28.3	28.3	28.9	28.5	29.2	29.2	28.6	30.2	29.4	29.8	33.3	28.3
7-Nov-97	26.7	26.7	27.4	27.3	27.6	27.7	28.2	28.3	29.2	28.5	29.5	29.3	29.1	30.6	30.1	30.7	34.4	29.7
8-Nov-97	27.1	26.8	27.8	27.5	28.0	27.9	28.6	28.5	29.3	28.9	29.9	29.8	29.6	31.0	30.5	30.9	34.8	29.7
9-Nov-97	27.1	27.0	27.9	27.8	28.1	28.1	28.7	28.8	29.5	29.3	29.7	30.1	28.8	30.7	28.9	29.7	32.5	27.7
10-Nov-97	27.1	27.0	27.9	27.8	28.2	28.2	28.7	28.9	29.3	29.2	29.0	29.8	27.5	30.4	26.7	28.7	28.9	25.6
11-Nov-97	27.3	26.9	28.0	27.7	28.2	28.1	28.6	28.8	29.0	28.8	28.1	28.6	26.2	28.0	25.8	25.9	30.4	23.5
12-Nov-97	27.3	27.1	28.0	27.9	28.2	28.2	28.4	28.7	28.5	28.4	27.9	28.2	26.9	28.3	28.8	27.2	34.7	25.5
13-Nov-97	27.4	27.0	28.0	27.8	28.2	28.1	28.4	28.4	28.7	28.2	28.7	28.5	28.0	29.6	29.5	29.5	35.3	28.1
14-Nov-97	27.4	27.0	28.1	27.8	28.2	28.0	28.5	28.4	29.0	28.3	29.5	29.2	29.1	30.8	30.0	30.9	33.5	29.5
15-Nov-97	27.4	27.1	28.0	27.8	28.2	28.0	28.5	28.5	29.2	28.7	29.7	29.6	29.5	31.0	31.9	30.9	38.7	29.5
16-Nov-97	27.4	27.2	28.0	27.9	28.2	28.1	28.7	28.7	29.7	29.0	30.7	30.5	31.0	32.8	33.4	33.3	40.1	31.9
17-Nov-97	27.5	27.2	28.1	27.9	28.4	28.2	29.0	28.9	30.0	29.6	30.7	31.0	30.2	32.0	31.7	31.3	37.7	29.7
18-Nov-97	27.5	27.1	28.2	27.9	28.6	28.3	29.2	29.1	30.3	29.6	31.2	31.0	31.1	32.8	33.4	33.0	39.9	31.6
19-Nov-97	27.5	27.3	28.3	28.1	28.6	28.5	29.4	29.4	30.6	30.1	31.6	31.7	31.3	33.6	31.9	33.6	37.3	31.9
20-Nov-97	27.6	27.4	28.4	28.3	28.8	28.7	29.7	29.6	30.7	30.5	31.2	31.8	30.1	33.0	30.2	31.4	34.7	28.0
21-Nov-97	27.6	27.3	28.5	28.3	28.9	28.8	29.8	29.7	30.6	30.3	31.0	31.2	30.4	32.3	31.8	31.8	37.5	30.0
22-Nov-97	27.7	27.4	28.6	28.3	29.1	28.9	29.8	29.8	30.7	30.3	31.3	31.4	30.7	32.8	31.9	32.3	37.2	30.2
23-Nov-97	27.8	27.4	28.7	28.5	29.2	29.0	29.9	29.9	30.8	30.4	31.3	31.5	30.7	32.9	31.6	32.4	36.6	30.3
24-Nov-97	27.7	27.6	28.7	28.6	29.2	29.1	30.0	30.1	30.7	30.5	31.0	31.4	30.2	32.4	31.4	31.5	36.6	29.2
25-Nov-97	28.0	27.7	29.0	28.8	29.4	29.3	30.1	30.2	30.9	30.6	31.2	31.4	30.4	32.5	31.0	31.7	36.0	29.4

Table K.5: Tailings temperatures (at noon and midnight) measured with the Model-229 Campbell Scientific matric suction sensors installed on the Kidston tailings impoundment.

Date	Tailings temperature (°C)																	
	NC200 (2000 mm)		NC150 (1500 mm)		#18 (1250 mm)		#19 (1000 mm)		#17 (750 mm)		#21 (500 mm)		#15 (300 mm)		#20 (150 mm)		16 (50 mm)	
	PM	AM	PM	AM	PM	AM	PM	AM	PM	AM	PM	AM	PM	AM	PM	AM	PM	AM
26-Nov-97	28.1	27.9	29.0	28.9	29.4	29.5	30.1	30.3	30.7	30.7	30.6	31.3	29.2	31.4	29.7	29.1	34.7	25.9
27-Nov-97	28.0	27.9	29.0	29.0	29.3	29.5	29.8	30.2	30.5	30.3	30.3	30.8	29.0	31.6	29.2	29.8	32.9	26.5
28-Nov-97	28.3	27.9	29.2	28.9	29.5	29.4	29.9	30.1	30.4	30.1	30.0	30.3	28.9	30.3	31.2	28.7	38.1	26.8
29-Nov-97	28.2	27.8	29.1	28.8	29.4	29.2	29.8	29.8	30.4	29.8	30.6	30.4	30.3	31.7	32.7	31.7	39.4	30.3
30-Nov-97	28.4	27.8	29.2	28.8	29.4	29.2	29.9	29.8	30.8	30.0	31.4	31.1	31.3	32.8	33.4	33.1	39.0	31.7
1-Dec-97	28.2	28.1	29.1	29.0	29.3	29.4	29.9	30.1	30.7	30.6	30.6	31.5	29.4	31.4	30.6	28.9	36.1	26.2
2-Dec-97	28.3	28.2	29.1	29.0	29.4	29.4	29.9	30.1	30.4	30.4	30.3	30.8	29.3	31.0	31.0	29.3	37.2	26.8
3-Dec-97	28.3	28.0	29.2	28.9	29.5	29.3	30.0	30.0	30.6	30.1	31.1	30.9	30.8	32.4	31.2	32.5	34.5	30.9
4-Dec-97	28.3	28.0	29.2	28.9	29.5	29.3	30.0	30.0	30.7	30.2	31.2	31.1	30.9	32.3	33.4	32.3	39.5	30.8
5-Dec-97	28.3	28.0	29.2	28.9	29.5	29.4	30.2	30.1	31.0	30.4	31.7	31.8	31.2	33.5	32.4	33.3	36.8	31.1
12-Dec-97	29.2	29.0	30.4	30.2	31.0	30.9	31.8	31.8	33.1	32.7	33.7	34.2	33.3	35.4	33.4	34.8	37.1	32.9
13-Dec-97	29.6	29.1	30.8	30.3	31.6	31.0	32.5	31.9	33.4	32.8	33.9	33.8	33.5	34.7	33.8	34.1	36.0	32.2
14-Dec-97	28.7	29.2	29.9	30.4	30.6	31.2	31.4	32.0	32.1	32.7	32.2	33.4	31.3	33.7	29.0	32.5	27.2	30.3
15-Dec-97	29.4	29.1	30.7	30.4	31.4	31.1	32.0	31.8	32.1	32.2	31.0	31.7	29.3	30.2	28.8	27.7	29.6	25.6
16-Dec-97	29.1	29.3	30.3	30.5	30.8	31.2	31.0	31.7	30.9	31.5	29.8	30.6	28.4	29.6	29.6	27.7	32.5	25.6
17-Dec-97	28.9	29.3	29.9	30.5	30.4	31.0	30.5	31.2	30.3	30.9	29.5	30.4	28.6	30.2	31.1	28.8	36.5	27.0
18-Dec-97	28.8	29.2	29.7	30.2	30.0	30.7	30.0	30.8	30.1	30.5	29.7	30.5	29.2	31.1	32.9	30.1	39.3	28.2
19-Dec-97	28.6	29.4	29.5	30.3	29.8	30.7	30.0	30.8	30.2	30.7	30.3	31.3	30.2	32.5	32.4	31.8	34.8	29.8
20-Dec-97	29.2	29.3	30.0	30.2	30.3	30.6	30.5	30.8	30.6	30.9	30.1	31.0	29.2	30.6	30.6	28.7	34.1	26.5
21-Dec-97	29.9	29.3	30.7	30.1	30.9	30.5	31.0	30.7	31.1	30.6	30.4	30.4	29.5	29.9	30.8	28.4	34.6	26.6
22-Dec-97	29.1	29.2	29.8	30.0	30.1	30.3	30.1	30.5	30.0	30.3	29.4	30.1	28.1	29.9	27.4	28.1	28.2	25.9
23-Dec-97	29.1	29.2	29.7	30.0	30.0	30.3	29.9	30.3	29.5	30.0	28.3	29.2	26.9	27.9	27.1	25.9	28.6	24.3
24-Dec-97	28.9	29.2	29.5	29.9	29.6	30.1	29.4	30.0	29.1	29.4	28.0	28.5	26.9	27.9	27.5	26.6	31.2	25.2
25-Dec-97	28.9	29.3	29.4	29.9	29.5	30.1	29.3	29.9	29.0	29.2	28.3	28.8	27.7	28.8	29.5	27.9	33.6	26.1
26-Dec-97	29.0	29.3	29.5	29.8	29.5	29.9	29.3	29.7	29.1	29.3	28.7	29.3	27.9	29.6	27.6	28.8	29.3	27.1
27-Dec-97	28.7	29.0	29.2	29.5	29.2	29.6	29.1	29.4	28.8	29.1	28.2	28.8	27.3	28.5	27.6	27.4	29.4	26.1
28-Dec-97	29.3	29.2	29.7	29.6	29.7	29.6	29.5	29.5	29.2	29.1	28.3	28.6	27.0	28.2	26.2	26.5	26.3	24.5
29-Dec-97	27.9	29.0	28.2	29.4	28.2	29.4	28.0	29.2	27.4	28.7	26.3	27.7	25.0	26.7	24.6	25.2	25.3	23.8
30-Dec-97	28.0	29.1	28.4	29.5	28.4	29.4	28.0	29.1	27.2	28.4	25.8	27.4	24.3	26.4	23.3	24.4	23.3	22.6
31-Dec-97		28.9		29.2		29.1		28.7		27.8		26.4		25.2		23.5		22.2
22-Oct-98	27.8	27.5	28.2	27.9	28.5	28.2	29.0	28.6	29.7	29.2	30.6	30.5	30.7	32.2	32.9	32.2	39.1	30.3
23-Oct-98	27.5	27.6	28.0	28.0	28.3	28.4	28.8	28.9	29.6	29.6	29.8	30.9	28.5	31.6	27.4	28.8	28.8	25.8
24-Oct-98	27.7	27.5	28.2	28.0	28.5	28.4	28.8	29.0	29.2	29.4	28.7	29.5	27.4	29.2	27.6	27.5	33.6	25.5
25-Oct-98	28.3	27.6	28.7	28.2	29.0	28.5	29.2	28.9	29.4	29.0	29.0	29.0	27.9	29.4	29.9	28.2	37.7	25.8
26-Oct-98	28.4	27.9	28.9	28.4	29.1	28.8	29.2	29.0	29.5	29.0	29.4	29.4	28.7	30.3	31.2	29.4	38.1	27.2
27-Oct-98	28.2	27.5	28.6	28.0	28.7	28.3	28.8	28.5	29.4	28.6	29.9	29.5	29.4	31.3	30.0	31.2	36.7	29.6
28-Oct-98	28.1	27.8	28.6	28.3	28.8	28.6	29.1	28.9	29.7	29.2	30.1	30.2	29.7	31.5	31.2	31.0	36.0	29.0
29-Oct-98	28.6	28.0	29.0	28.4	29.3	28.7	29.5	29.1	30.2	29.5	30.6	30.5	30.2	31.9	33.1	31.3	41.1	28.7
30-Oct-98	27.8	27.9	28.2	28.4	28.6	28.7	29.0	29.1	29.8	29.7	30.7	31.1	30.6	33.2	31.5	33.1	37.6	30.7
31-Oct-98	28.3	27.7	28.8	28.2	29.1	28.6	29.6	29.1	30.5	29.8	30.9	31.1	30.0	32.1	31.0	30.4	38.1	27.2
1-Nov-98	27.8	27.8	28.3	28.3	28.7	28.8	29.2	29.3	29.8	29.9	29.6	30.5	28.4	30.3	28.1	28.1	30.0	25.7
2-Nov-98	28.2	28.2	28.8	28.8	29.1	29.2	29.3	29.7	29.5	29.9	28.6	29.6	27.0	28.7	27.0	26.4	31.1	24.1
3-Nov-98	28.1	27.9	28.7	28.5	28.9	28.9	29.0	29.2	29.0	29.0	28.1	28.6	26.7	28.3	27.0	26.6	32.0	24.6

Table K.5: Tailings temperatures (at noon and midnight) measured with the Model-229 Campbell Scientific matric suction sensors installed on the Kidston tailings impoundment.

Date	Tailings temperature (°C)																	
	NC200 (2000 mm)		NC150 (1500 mm)		#18 (1250 mm)		#19 (1000 mm)		#17 (750 mm)		#21 (500 mm)		#15 (300 mm)		#20 (150 mm)		16 (50 mm)	
	PM	AM	PM	AM	PM	AM	PM	AM	PM	AM	PM	AM	PM	AM	PM	AM	PM	AM
4-Nov-98	27.8	28.1	28.2	28.6	28.4	28.9	28.4	29.0	28.3	28.8	27.5	28.4	26.0	28.5	26.1	27.0	31.2	24.5
5-Nov-98	27.9	28.0	28.4	28.5	28.5	28.7	28.4	28.8	28.2	28.4	27.5	28.1	26.1	28.5	26.2	27.1	29.2	24.0
6-Nov-98	28.4	28.0	28.7	28.4	28.7	28.5	28.5	28.5	28.3	28.1	27.5	27.6	26.1	27.5	27.2	26.1	31.8	23.9
7-Nov-98	28.3	28.1	28.6	28.5	28.5	28.5	28.3	28.4	28.1	28.0	27.6	27.8	26.5	28.3	28.3	27.3	34.8	25.0
8-Nov-98	28.7	28.1	28.9	28.3	28.7	28.4	28.5	28.2	28.6	27.9	28.5	28.3	27.9	29.6	30.1	29.3	35.6	27.0
9-Nov-98	28.1	27.9	28.2	28.1	28.2	28.1	28.1	28.1	28.4	28.1	28.3	28.6	27.6	29.3	29.9	27.9	35.8	25.2
10-Nov-98	27.9	28.0	28.1	28.2	28.1	28.3	28.2	28.3	28.5	28.4	28.9	29.2	28.6	30.8	29.1	30.4	31.1	28.0
11-Nov-98	27.7	28.0	27.9	28.1	28.0	28.2	28.1	28.4	28.4	28.6	28.5	29.2	27.7	29.9	27.3	28.9	29.2	26.6
12-Nov-98		28.0		28.2		28.3		28.5		28.6		28.6		28.3		26.7		24.1
15-Nov-98	28.2		28.3		28.3		28.2		28.3		28.1		27.4		30.5		39.0	
16-Nov-98	28.6	27.9	28.8	28.1	28.8	28.2	28.7	28.1	29.1	28.1	29.5	28.9	29.4	30.7	32.9	30.6	40.3	28.6
17-Nov-98	28.9	27.9	29.1	28.1	29.1	28.2	29.1	28.3	29.8	28.5	30.4	29.7	30.2	31.7	33.7	31.5	41.5	29.0
18-Nov-98	28.2	28.0	28.3	28.2	28.4	28.3	28.6	28.6	29.3	29.0	29.5	30.2	28.6	31.2	29.2	29.1	34.8	26.0
19-Nov-98	28.0	27.8	28.2	28.0	28.3	28.2	28.5	28.5	29.0	28.8	28.9	29.3	28.1	29.8	29.9	29.0	36.2	27.4
20-Nov-98	27.4	28.1	27.6	28.4	27.7	28.6	27.8	28.9	28.2	29.0	28.1	29.4	27.3	30.1	28.1	29.3	34.5	27.5
21-Nov-98	27.8	27.9	28.0	28.2	28.1	28.4	28.2	28.6	28.4	28.8	27.8	28.8	26.5	28.5	28.3	26.3	35.3	23.6
22-Nov-98	28.0	28.0	28.2	28.3	28.3	28.5	28.3	28.6	28.3	28.4	27.4	28.2	26.2	27.8	27.8	25.6	33.9	23.3
23-Nov-98	28.3	28.0	28.6	28.3	28.5	28.4	28.4	28.4	28.3	28.1	27.5	27.9	26.2	27.8	27.3	25.7	31.7	23.1
24-Nov-98	27.9	27.6	28.2	27.8	28.1	27.9	27.9	27.9	27.8	27.5	27.3	27.2	26.5	27.4	28.5	26.7	35.6	25.1
25-Nov-98	28.1	28.0	28.3	28.2	28.2	28.2	28.0	28.1	28.1	27.8	28.1	28.1	27.7	29.2	30.0	28.9	36.7	27.4
26-Nov-98	28.5	27.9	28.6	28.0	28.5	28.0	28.3	28.0	28.6	27.9	28.9	28.6	28.8	30.1	30.3	30.0	36.2	28.4
27-Nov-98		28.2		28.3		28.3		28.4		28.6		29.5		30.9		30.7		28.8
29-Nov-98	27.5		27.6		27.8		28.1		28.9		29.6		29.5		30.7		37.6	
30-Nov-98	27.5	28.0	27.8	28.2	28.1	28.4	28.6	28.9	29.3	29.5	29.9	30.6	29.7	31.8	32.4	31.1	40.2	29.1
1-Dec-98	28.1	28.0	28.4	28.3	28.7	28.6	29.2	29.1	30.0	29.7	30.5	30.9	30.2	32.2	32.5	30.8	37.5	27.9
2-Dec-98	27.8	28.1	28.2	28.4	28.5	28.8	29.0	29.3	29.7	29.9	30.1	30.9	29.5	31.9	30.8	30.7	36.0	28.1
3-Dec-98	28.1	28.1	28.6	28.6	28.9	28.9	29.3	29.5	30.0	29.9	30.3	30.9	29.6	32.1	31.2	31.3	37.0	28.4
4-Dec-98	28.2	28.2	28.7	28.7	29.0	29.1	29.5	29.5	30.2	30.0	30.5	30.9	29.8	32.2	31.3	31.1	37.3	28.3
5-Dec-98	28.2	28.2	28.7	28.7	29.0	29.1	29.4	29.6	30.1	30.0	30.4	31.0	29.5	32.3	31.9	31.4	39.4	28.3
6-Dec-98	28.4	28.4	28.9	29.0	29.3	29.3	29.7	29.9	30.4	30.3	30.7	31.2	30.1	32.7	32.7	31.9	40.5	28.8
7-Dec-98	28.6	28.3	29.2	28.8	29.5	29.3	29.9	29.8	30.7	30.3	31.2	31.3	30.8	33.0	33.5	32.6	42.1	30.3
8-Dec-98	28.1	28.2	28.6	28.8	29.1	29.2	29.6	29.7	30.4	30.3	31.2	31.6	30.9	33.5	32.7	33.3	39.6	30.9
9-Dec-98	28.1	28.2	28.7	28.8	29.1	29.3	29.7	29.8	30.4	30.5	31.0	31.7	30.4	33.0	30.2	32.5	33.9	30.1
10-Dec-98	28.3	28.4	28.9	29.1	29.4	29.5	29.9	30.2	30.5	30.7	30.6	31.4	29.7	32.0	29.3	30.9	30.9	28.4
11-Dec-98		28.5		29.1		29.6		30.2		30.5		30.6		30.5		29.2		27.1
12-Dec-98	28.5		29.2		29.6		29.9		30.1		29.8		28.9		30.3		35.5	
13-Dec-98	28.2	28.8	28.8	29.4	29.1	29.8	29.3	30.1	29.5	30.1	28.9	30.2	27.4	30.1	26.5	27.8	28.7	24.9
14-Dec-98	28.5	28.8	29.1	29.4	29.3	29.7	29.3	29.9	29.4	29.8	28.6	29.4	27.5	29.1	29.8	27.8	36.4	26.2
15-Dec-98	29.2	28.7	29.7	29.2	29.9	29.5	29.9	29.6	30.2	29.4	30.3	29.7	30.0	31.0	33.1	30.9	40.2	29.1
16-Dec-98	28.4	28.9	28.9	29.4	29.1	29.7	29.2	29.8	29.7	29.9	30.3	30.9	30.4	32.9	34.0	33.0	42.2	31.0
17-Dec-98	28.6	28.7	29.1	29.2	29.3	29.4	29.5	29.7	30.2	30.1	30.6	31.3	30.1	32.6	32.2	31.3	40.4	28.5
18-Dec-98	30.0	29.0	30.5	29.4	30.8	29.7	31.2	30.2	31.9	30.6	32.5	31.7	32.4	33.1	34.7	32.8	36.5	31.0
19-Dec-98	29.0	28.5	29.5	29.0	29.8	29.3	30.2	29.8	30.7	30.2	30.4	30.7	29.4	30.4	31.0	28.2	37.7	25.8

Table K.5: Tailings temperatures (at noon and midnight) measured with the Model-229 Campbell Scientific matric suction sensors installed on the Kidston tailings impoundment.

Date	Tailings temperature (°C)																	
	NC200 (2000 mm)		NC150 (1500 mm)		#18 (1250 mm)		#19 (1000 mm)		#17 (750 mm)		#21 (500 mm)		#15 (300 mm)		#20 (150 mm)		16 (50 mm)	
	PM	AM	PM	AM	PM	AM	PM	AM	PM	AM	PM	AM	PM	AM	PM	AM	PM	AM
20-Dec-98	28.9	28.7	29.5	29.2	29.8	29.6	30.1	29.9	30.5	30.1	30.5	30.5	30.0	31.5	30.3	30.6	31.7	28.3
21-Dec-98	28.8	28.7	29.3	29.3	29.5	29.6	29.8	29.9	30.1	30.1	29.8	30.3	28.8	30.3	29.6	29.2	34.7	27.9
22-Dec-98	28.4	28.7	28.9	29.2	29.1	29.5	29.2	29.8	29.5	29.8	29.0	29.8	28.0	29.7	29.0	28.1	34.1	26.3
23-Dec-98	28.3	28.9	28.8	29.4	29.0	29.7	29.0	29.8	29.2	29.8	28.9	29.8	27.8	29.9	27.3	28.8	29.8	27.1
24-Dec-98		29.0		29.5		29.8		29.9		29.8		29.6		29.5		28.1		26.2
27-Dec-98	29.4		29.7		29.9		30.0		30.3		30.6		30.6		33.2		38.5	
28-Dec-98	29.6	28.7	29.9	29.1	30.0	29.3	30.1	29.5	30.5	29.7	30.3	30.3	29.5	30.4	31.7	28.6	40.6	26.3
29-Dec-98	28.5	28.9	28.9	29.3	28.9	29.5	29.0	29.7	29.5	29.8	29.4	30.2	28.5	31.0	28.2	30.2	31.4	27.8
30-Dec-98	28.4	28.8	28.8	29.1	28.9	29.4	29.0	29.6	29.1	29.6	28.5	29.6	27.0	29.1	26.5	27.4	29.5	25.4
31-Dec-98	28.4	28.9	28.7	29.2	28.8	29.4	28.8	29.5	28.6	29.4	27.8	28.9	26.3	28.3	25.3	26.6	26.2	24.6
1-Jan-99	28.6	28.7	29.0	29.1	29.0	29.2	28.8	29.2	28.5	28.8	27.3	28.0	25.8	27.0	25.9	25.2	30.5	23.6
2-Jan-99	28.6	28.7	28.9	29.0	28.9	29.0	28.6	28.9	28.3	28.3	27.6	27.7	26.8	27.7	28.6	27.1	35.0	26.3
3-Jan-99	28.9	29.1	29.1	29.4	29.0	29.4	28.7	29.2	28.7	28.8	28.7	28.9	28.4	30.1	30.8	30.2	39.3	28.6
4-Jan-99	28.0	28.6	28.2	28.8	28.1	28.8	28.0	28.6	28.3	28.5	28.6	29.4	27.8	31.2	27.7	30.7	31.2	28.4
5-Jan-99	29.2	28.8	29.3	29.0	29.3	29.0	29.3	29.1	29.6	29.1	29.5	29.4	28.9	29.9	30.0	29.2	34.7	27.5
6-Jan-99	28.5	28.8	28.6	29.0	28.6	29.0	28.6	29.1	28.8	29.2	28.7	29.5	27.9	30.0	27.4	29.1	29.5	27.3
7-Jan-99	28.2	28.8	28.4	29.0	28.4	29.1	28.5	29.2	28.4	29.1	27.9	29.0	26.6	28.7	26.1	27.1	28.1	24.9
8-Jan-99		28.8		29.0		29.1		29.1		28.9		28.6		28.8		27.9		25.9
17-Oct-99	26.8		27.3		27.7		28.3		29.1		30.0		29.8		31.0		37.5	
18-Oct-99	27.0	27.6	27.6	28.2	28.0	28.7	28.5	29.4	29.4	30.0	30.0	31.1	29.5	32.6	30.6	32.3	38.2	29.6
19-Oct-99	27.0	28.0	27.5	28.6	27.9	29.2	28.4	29.8	29.3	30.4	29.8	31.4	29.1	32.8	30.1	32.7	37.9	29.8
20-Oct-99	27.4	27.9	28.1	28.5	28.4	29.0	28.9	29.6	29.7	30.2	30.2	31.1	29.6	32.5	30.6	32.4	38.3	29.8
21-Oct-99	27.3	27.7	27.9	28.3	28.3	28.8	28.7	29.4	29.5	29.9	30.1	30.8	29.8	32.4	30.7	32.8	38.1	31.0
22-Oct-99	27.2	27.6	27.9	28.3	28.2	28.8	28.6	29.3	29.5	29.9	30.1	30.8	30.0	32.2	31.4	32.4	38.5	30.6
23-Oct-99	26.9	27.6	27.5	28.2	27.9	28.7	28.3	29.3	29.1	29.9	29.5	30.8	29.0	31.8	28.6	31.2	32.2	28.9
24-Oct-99	27.9	28.1	28.5	28.8	28.9	29.3	29.3	29.8	30.0	30.4	30.2	30.9	29.6	31.6	31.0	31.3	38.8	29.3
25-Oct-99	27.7	27.8	28.3	28.5	28.7	29.0	29.0	29.5	29.8	29.9	30.2	30.6	29.8	32.0	31.3	32.2	39.5	29.9
26-Oct-99	27.5	27.9	28.1	28.6	28.5	29.0	28.8	29.5	29.7	30.0	30.4	31.0	30.6	32.7	32.5	33.6	40.4	32.1
27-Oct-99	26.8	27.8	27.4	28.5	27.7	28.9	28.1	29.5	29.1	30.1	30.0	31.3	30.0	33.2	31.0	33.9	39.1	32.4
28-Oct-99	27.8	28.1	28.4	28.8	28.8	29.3	29.3	29.9	30.3	30.6	31.2	31.9	31.2	33.8	32.9	34.3	41.0	32.3
29-Oct-99	27.9	28.0	28.6	28.6	29.0	29.1	29.5	29.8	30.6	30.5	31.5	31.8	31.6	33.6	33.4	34.2	41.6	32.5
30-Oct-99	27.6	28.0	28.3	28.7	28.7	29.3	29.3	30.0	30.4	30.8	31.4	32.2	31.5	34.1	33.0	34.6	40.8	32.5
31-Oct-99	27.2	28.1	27.9	28.8	28.5	29.4	29.2	30.2	30.2	31.0	31.1	32.4	31.2	34.2	31.5	34.5	35.6	32.5
1-Nov-99	27.4	28.0	28.1	28.8	28.7	29.4	29.3	30.2	30.2	30.9	30.3	31.8	29.3	32.1	30.1	30.0	34.4	27.4
2-Nov-99	27.6	28.4	28.4	29.2	28.8	29.8	29.3	30.5	30.0	30.9	29.7	31.3	28.6	31.4	29.8	29.9	36.2	27.6
3-Nov-99		28.3		29.1		29.7		30.2		30.5		30.8		31.4		30.4		28.3
12-Nov-99	26.6		26.9		26.9		26.6		26.6		26.1		25.0		24.5		28.0	
13-Nov-99	27.3	28.5	27.6	28.8	27.5	28.9	27.4	28.8	27.2	28.5	26.5	28.1	25.2	28.2	25.8	26.8	30.5	24.9
14-Nov-99	27.7	28.5	27.9	28.8	27.8	28.8	27.5	28.7	27.3	28.2	26.6	27.8	25.5	27.9	27.3	26.8	33.4	25.0
15-Nov-99	27.9	28.6	28.0	28.8	27.9	28.8	27.5	28.6	27.4	28.2	27.1	28.1	26.3	29.0	28.8	28.5	35.1	26.7
16-Nov-99	28.2	28.5	28.3	28.7	28.1	28.6	27.8	28.5	27.9	28.2	28.0	28.5	27.5	29.9	29.4	30.0	34.7	28.3
17-Nov-99	28.3	28.1	28.4	28.2	28.2	28.1	28.0	28.1	28.3	27.9	28.6	28.5	28.4	29.7	31.5	29.7	38.1	28.2

Table K.5: Tailings temperatures (at noon and midnight) measured with the Model-229 Campbell Scientific matric suction sensors installed on the Kidston tailings impoundment.

Date	Tailings temperature (°C)																	
	NC200 (2000 mm)		NC150 (1500 mm)		#18 (1250 mm)		#19 (1000 mm)		#17 (750 mm)		#21 (500 mm)		#15 (300 mm)		#20 (150 mm)		16 (50 mm)	
	PM	AM	PM	AM	PM	AM	PM	AM	PM	AM	PM	AM	PM	AM	PM	AM	PM	AM
18-Nov-99	28.0	28.0	28.0	28.1	27.9	28.1	27.8	28.1	28.3	28.2	28.7	29.0	28.3	30.4	30.5	30.0	36.3	27.7
19-Nov-99	27.6	28.1	27.6	28.2	27.5	28.2	27.5	28.3	28.1	28.5	28.2	29.3	27.4	29.9	28.4	28.7	31.9	26.9
20-Nov-99	27.8	27.8	27.9	28.0	28.0	28.1	28.1	28.2	28.3	28.4	28.2	28.7	27.5	29.0	28.3	27.7	30.4	26.2
21-Nov-99	27.4	27.9	27.6	28.1	27.6	28.2	27.7	28.3	27.8	28.3	27.4	28.3	26.7	28.3	28.2	27.1	31.5	25.8
22-Nov-99	27.4	27.9	27.5	28.1	27.5	28.2	27.4	28.2	27.6	28.1	27.2	28.1	26.3	28.2	27.2	27.1	31.1	25.7
23-Nov-99	27.0	27.9	27.1	28.1	27.0	28.2	26.9	28.2	27.0	28.1	26.5	28.0	25.6	28.1	26.5	26.8	30.2	25.2
24-Nov-99	27.3	27.8	27.4	28.0	27.4	28.0	27.3	28.0	27.2	27.8	26.9	27.7	26.3	28.1	27.0	27.4	29.4	26.1
25-Nov-99	27.4	27.9	27.5	28.0	27.5	28.1	27.4	28.0	27.3	27.8	26.9	27.7	26.1	27.6	26.0	26.6	26.9	25.4
26-Nov-99	27.3	27.9	27.4	28.0	27.3	28.0	27.0	27.9	26.8	27.6	26.0	27.2	24.9	26.6	24.3	25.4	25.0	24.1
27-Nov-99	27.4	27.9	27.5	28.0	27.4	28.0	27.1	27.8	26.7	27.3	25.8	26.6	24.8	26.0	24.6	24.8	25.3	23.7
28-Nov-99	27.3	28.2	27.3	28.2	27.1	28.2	26.8	27.9	26.3	27.3	25.3	26.5	24.2	26.0	24.7	25.0	26.1	23.7
29-Nov-99	26.8	28.0	26.8	28.0	26.6	27.8	26.3	27.5	25.6	26.8	24.8	26.1	24.0	25.9	24.4	25.2	25.3	24.1
30-Nov-99	27.3	28.1	27.2	28.0	27.0	27.9	26.5	27.5	26.0	26.8	25.3	26.2	24.4	26.2	24.6	25.5	25.8	24.1
1-Dec-99	27.0	28.2	26.8	28.1	26.5	27.9	26.0	27.5	25.6	26.9	24.8	26.3	23.8	26.3	24.0	25.5	26.1	24.2
2-Dec-99		27.9		27.8		27.5		27.1		26.5		26.0		26.2		25.8		24.9
4-Dec-99	27.4		27.1		26.7		26.2		26.0		25.8		25.2		26.4		30.8	
5-Dec-99	27.2	28.0	26.9	27.8	26.6	27.5	26.2	27.2	26.1	26.8	26.0	27.0	25.5	28.0	26.5	27.8	30.7	26.3
6-Dec-99	27.2	28.2	27.0	27.9	26.6	27.7	26.3	27.4	26.4	27.2	26.3	27.5	25.8	28.5	26.8	28.4	31.5	26.7
7-Dec-99	27.4	28.3	27.1	28.1	26.9	27.9	26.6	27.7	26.8	27.6	26.9	28.0	26.6	29.2	27.9	29.4	33.0	27.7
8-Dec-99	27.3	27.9	27.0	27.7	26.8	27.6	26.6	27.5	26.9	27.4	27.3	28.0	27.1	29.4	28.4	29.9	33.3	28.5
9-Dec-99	27.2	28.0	27.0	27.8	26.8	27.7	26.6	27.7	27.1	27.8	27.6	28.5	27.6	29.9	28.9	30.3	34.1	29.2
10-Dec-99	27.0	27.7	26.9	27.6	26.7	27.6	26.6	27.7	27.3	27.8	27.9	28.7	27.9	30.1	28.7	30.6	33.2	29.5
11-Dec-99	27.5	27.7	27.4	27.6	27.4	27.6	27.6	27.8	28.2	28.0	28.8	28.9	28.9	30.3	29.8	30.8	33.4	29.6
12-Dec-99	27.1	28.2	27.1	28.2	27.1	28.3	27.2	28.5	28.0	28.9	28.6	29.8	28.7	31.1	29.2	31.8	31.2	30.6
13-Dec-99	27.3	27.6	27.3	27.6	27.4	27.7	27.7	28.1	28.2	28.5	28.6	29.2	28.4	29.8	29.5	29.5	33.8	28.3
14-Dec-99	26.5	27.3	26.6	27.4	26.8	27.6	27.0	27.9	27.5	28.3	27.8	28.9	27.4	29.6	27.2	29.0	28.4	27.4
15-Dec-99	26.9	27.5	27.1	27.6	27.2	27.8	27.4	28.1	27.8	28.4	27.8	28.7	27.2	29.0	27.1	28.2	29.4	26.8
16-Dec-99	27.3	28.0	27.4	28.2	27.5	28.5	27.6	28.8	28.0	28.8	28.1	29.1	27.6	29.8	28.3	29.8	33.2	28.6
17-Dec-99	27.8	27.7	28.0	28.0	28.1	28.2	28.2	28.4	28.6	28.5	28.9	29.0	28.7	30.0	29.2	30.1	32.5	29.0
18-Dec-99	27.6	27.6	27.8	27.8	27.9	28.0	28.0	28.3	28.5	28.5	28.7	28.9	28.4	29.4	28.9	29.2	31.2	28.1
19-Dec-99	27.8	27.5	28.0	27.8	28.1	28.0	28.2	28.2	28.7	28.4	28.8	28.8	28.2	29.3	28.6	29.1	31.4	28.3
20-Dec-99	27.4	27.8	27.6	28.0	27.8	28.3	28.0	28.5	28.3	28.7	28.4	29.1	28.1	29.7	28.5	29.3	30.3	28.1
21-Dec-99	27.2	27.8	27.5	28.1	27.7	28.3	27.8	28.5	28.2	28.7	28.3	29.1	27.8	29.7	27.6	29.5	28.9	28.6
22-Dec-99	27.6	27.9	27.9	28.2	28.0	28.4	28.1	28.7	28.4	28.8	28.2	28.9	27.4	29.0	27.5	28.2	30.1	26.9
23-Dec-99		28.2		28.5		28.7		28.9		28.9		29.0		29.4		29.3		28.1
24-Dec-99	26.6	27.8	26.9	28.1	27.0	28.3	27.1	28.4	27.3	28.4	27.2	28.6	26.7	29.0	26.1	28.5	26.4	27.3
25-Dec-99	27.0	27.8	27.3	28.1	27.3	28.3	27.3	28.4	27.5	28.4	27.2	28.3	26.3	28.2	25.8	27.4	26.4	26.1
26-Dec-99	26.9	27.9	27.2	28.1	27.2	28.3	27.2	28.4	27.3	28.3	27.0	28.1	26.4	28.1	26.3	27.6	27.6	26.5
27-Dec-99	27.6	27.7	27.8	27.9	27.9	28.1	27.8	28.1	27.8	28.0	27.5	27.8	26.9	27.7	26.6	27.2	27.5	26.4
28-Dec-99	28.3	27.6	28.4	27.9	28.4	28.0	28.3	28.0	28.4	27.8	28.0	27.7	27.1	27.7	26.9	27.2	29.4	25.9
29-Dec-99	28.4	28.5	28.5	28.7	28.5	28.8	28.3	28.8	28.4	28.6	28.0	28.4	27.1	28.7	26.9	28.0	29.9	26.5
30-Dec-99	27.7	28.5	27.9	28.7	27.8	28.8	27.7	28.8	27.8	28.6	27.6	28.6	26.8	29.0	26.9	28.6	30.4	27.3
31-Dec-99	28.2	28.4	28.3	28.6	28.2	28.7	28.1	28.7	28.3	28.5	28.0	28.5	27.3	28.9	27.5	28.5	31.6	27.2
1-Jan-00	28.1	28.2	28.2	28.3	28.2	28.4	28.0	28.4	28.2	28.2	28.1	28.3	27.4	29.0	27.1	28.9	29.0	27.8

Table K.5: Tailings temperatures (at noon and midnight) measured with the Model-229 Campbell Scientific matric suction sensors installed on the Kidston tailings impoundment.

Date	Tailings temperature (°C)																	
	NC200 (2000 mm)		NC150 (1500 mm)		#18 (1250 mm)		#19 (1000 mm)		#17 (750 mm)		#21 (500 mm)		#15 (300 mm)		#20 (150 mm)		16 (50 mm)	
	PM	AM	PM	AM	PM	AM	PM	AM	PM	AM	PM	AM	PM	AM	PM	AM	PM	AM
2-Jan-00	27.8	27.6	27.9	27.7	27.9	27.8	27.8	27.8	27.9	27.7	27.6	27.7	26.6	28.0	26.5	27.3	30.7	25.7
3-Jan-00	27.8	28.6	27.9	28.7	27.9	28.8	27.8	28.8	27.9	28.6	27.9	28.7	27.5	29.6	28.1	29.9	31.2	28.5
4-Jan-00	27.0	28.3	27.1	28.4	27.1	28.5	27.1	28.5	27.3	28.4	27.6	28.8	27.5	29.6	27.9	30.0	30.6	29.2
5-Jan-00	27.8	28.0	27.9	28.2	27.9	28.2	27.9	28.3	28.3	28.4	28.6	28.8	28.4	29.6	29.1	29.9	33.1	29.0
6-Jan-00	28.0	28.1	28.1	28.2	28.1	28.3	28.1	28.5	28.7	28.6	29.2	29.2	29.3	30.5	30.0	31.2	34.0	30.4
7-Jan-00	27.6	28.1	27.7	28.3	27.8	28.4	28.0	28.6	28.5	28.9	28.7	29.5	28.2	30.0	28.4	29.1	31.1	27.6
8-Jan-00	28.0	27.8	28.2	28.0	28.2	28.2	28.3	28.5	28.8	28.7	28.7	29.0	28.0	29.0	28.1	28.0	30.4	26.8
9-Jan-00	28.0	28.1	28.3	28.3	28.4	28.5	28.5	28.8	28.9	28.8	29.0	29.1	28.7	29.6	29.0	29.5	31.0	28.5
10-Jan-00	28.2	28.2	28.5	28.5	28.5	28.7	28.5	28.9	29.0	29.0	29.1	29.4	28.5	30.0	28.3	29.5	30.4	28.3
11-Jan-00	27.3	28.2	27.6	28.5	27.6	28.7	27.6	29.0	28.2	29.1	28.2	29.3	27.4	29.8	26.7	29.7	27.9	28.9
12-Jan-00		27.8		28.1		28.3		28.5		28.6		28.7		29.1		28.0		26.0
13-Jan-00	28.3	28.1	28.5	28.4	28.6	28.6	28.7	28.7	28.7	28.7	28.2	28.4	27.2	28.1	26.6	27.1	27.9	25.5
14-Jan-00	28.1	28.5	28.4	28.9	28.5	29.0	28.4	29.1	28.3	28.9	27.8	28.6	26.8	28.4	26.3	27.4	27.7	25.9
15-Jan-00	28.3	28.7	28.5	29.0	28.5	29.1	28.4	29.1	28.3	28.8	27.8	28.5	26.7	28.5	26.4	27.6	28.5	26.0
16-Jan-00	28.3	28.5	28.5	28.8	28.5	28.9	28.4	28.9	28.3	28.5	27.8	28.3	26.9	28.4	26.8	27.8	29.4	26.3
17-Jan-00	28.3	28.5	28.4	28.7	28.4	28.8	28.2	28.7	28.1	28.4	27.9	28.2	27.3	28.5	27.4	28.3	30.2	27.4
18-Jan-00	28.1	28.7	28.3	28.9	28.2	28.9	28.1	28.9	28.1	28.6	28.0	28.7	27.4	29.3	27.4	29.3	29.9	28.3
19-Jan-00	28.3	28.6	28.4	28.7	28.3	28.8	28.2	28.7	28.3	28.6	28.3	28.7	27.9	29.3	28.3	29.4	31.3	28.4
20-Jan-00	28.9	28.4	29.0	28.6	28.9	28.6	28.8	28.6	29.1	28.5	29.4	28.9	29.1	29.9	29.3	30.2	32.3	29.1
21-Jan-00	27.9	28.3	28.1	28.4	28.1	28.5	28.1	28.5	28.4	28.6	28.7	29.1	28.7	29.9	28.7	30.2	30.0	29.4
22-Jan-00	28.6	28.6	28.7	28.7	28.8	28.8	28.8	28.9	29.2	29.1	29.3	29.6	28.7	30.2	28.5	30.1	30.2	28.8
23-Jan-00	28.9	28.1	29.0	28.3	29.1	28.4	29.2	28.6	29.5	28.7	29.5	28.9	29.0	29.3	29.0	28.7	31.0	27.4
24-Jan-00	28.6	28.0	28.7	28.2	28.7	28.4	28.8	28.6	29.1	28.6	29.2	28.9	28.8	29.4	29.1	29.0	31.7	28.1
25-Jan-00	28.4	28.1	28.6	28.4	28.7	28.5	28.9	28.7	29.2	28.8	29.2	29.1	28.8	29.5	28.8	29.0	30.4	27.9
26-Jan-00	27.9	28.5	28.1	28.7	28.2	28.9	28.4	29.1	28.6	29.2	28.8	29.5	28.4	30.1	28.5	30.0	30.3	29.0
27-Jan-00	28.3	28.3	28.6	28.6	28.6	28.8	28.7	29.0	29.1	29.1	29.2	29.4	28.8	30.0	28.9	29.8	31.5	28.8
28-Jan-00	28.1	28.1	28.4	28.4	28.5	28.6	28.6	28.8	28.9	28.9	29.0	29.2	28.7	29.7	28.6	29.4	30.3	28.6
29-Jan-00	28.5	28.0	28.8	28.3	28.9	28.5	29.1	28.7	29.3	28.8	29.4	29.0	28.8	29.3	28.6	28.9	30.5	28.0
30-Jan-00	28.1	28.6	28.4	28.9	28.5	29.1	28.7	29.3	28.9	29.4	29.2	29.7	29.0	30.4	29.1	30.6	30.9	29.8
31-Jan-00	28.6	28.5	28.9	28.8	29.1	29.0	29.2	29.2	29.5	29.4	29.7	29.7	29.4	30.3	29.4	30.2	32.0	29.2
1-Feb-00	28.9	28.5	29.2	28.9	29.4	29.1	29.5	29.4	29.9	29.5	30.2	29.9	29.9	30.7	29.9	30.7	32.6	29.4
2-Feb-00	27.9	28.7	28.3	29.0	28.4	29.3	28.6	29.5	29.0	29.8	29.4	30.2	29.2	31.2	29.0	31.4	30.5	30.3
3-Feb-00	28.5	28.8	28.9	29.2	29.1	29.4	29.3	29.7	29.7	30.0	29.9	30.4	29.6	30.9	29.3	30.8	31.5	29.5
4-Feb-00	28.6	28.9	29.0	29.3	29.2	29.6	29.4	29.9	29.8	30.1	30.1	30.5	29.9	31.3	29.8	31.5	32.2	30.2
5-Feb-00	28.3	28.3	28.7	28.8	28.9	29.1	29.1	29.4	29.6	29.6	30.0	30.1	30.0	31.0	29.8	31.5	30.7	30.6
6-Feb-00	28.3	28.3	28.7	28.8	29.0	29.1	29.3	29.4	29.7	29.7	29.9	30.2	29.5	30.6	28.4	30.1	27.3	28.6
7-Feb-00	27.6	28.4	28.1	28.8	28.3	29.1	28.5	29.4	28.8	29.7	28.4	29.7	27.4	29.1	26.2	27.8	26.1	26.2
8-Feb-00	27.7	28.5	28.1	29.0	28.4	29.3	28.5	29.6	28.5	29.5	28.0	29.2	27.1	28.7	25.9	27.7	25.5	26.5
9-Feb-00	28.2	28.9	28.6	29.4	28.8	29.6	28.9	29.8	28.7	29.6	28.2	29.2	27.1	28.6	26.3	27.6	27.1	26.2
10-Feb-00	27.8	28.9	28.2	29.3	28.3	29.6	28.3	29.6	28.2	29.4	27.8	29.0	27.1	29.0	26.6	28.8	27.9	27.9
11-Feb-00	28.2	28.8	28.6	29.2	28.7	29.4	28.6	29.5	28.6	29.2	28.3	29.0	27.8	29.2	27.7	29.1	29.8	28.1
12-Feb-00	28.7	28.6	29.1	29.0	29.1	29.1	29.1	29.1	29.2	29.0	29.1	29.0	28.7	29.3	28.9	29.2	31.3	28.3
13-Feb-00	29.4	28.7	29.7	29.1	29.8	29.2	29.8	29.3	30.0	29.3	30.3	29.5	30.1	30.4	30.2	31.1	32.5	30.5
14-Feb-00	28.5	29.0	28.8	29.3	28.9	29.5	28.9	29.6	29.3	29.7	29.7	30.2	29.8	31.1	29.8	31.7	31.9	31.1
15-Feb-00	28.6	28.6	28.9	28.9	29.1	29.1	29.3	29.3	29.6	29.5	29.9	30.0	29.5	30.5	28.3	30.0	27.7	28.9

Table K.5: Tailings temperatures (at noon and midnight) measured with the Model-229 Campbell Scientific matric suction sensors installed on the Kidston tailings impoundment.

Date	Tailings temperature (°C)																	
	NC200 (2000 mm)		NC150 (1500 mm)		#18 (1250 mm)		#19 (1000 mm)		#17 (750 mm)		#21 (500 mm)		#15 (300 mm)		#20 (150 mm)		16 (50 mm)	
	PM	AM	PM	AM	PM	AM	PM	AM	PM	AM	PM	AM	PM	AM	PM	AM	PM	AM
16-Feb-00	28.5	28.8	28.8	29.2	29.0	29.4	29.1	29.6	29.4	29.8	29.0	29.8	28.2	29.4	27.9	28.4	29.0	27.4
17-Feb-00	27.8	28.6	28.2	29.0	28.2	29.2	28.3	29.4	28.5	29.4	28.2	29.3	27.4	29.4	26.7	28.6	27.2	27.4
18-Feb-00	28.5	28.6	28.8	29.0	28.9	29.2	28.9	29.3	29.0	29.3	28.6	29.1	27.8	28.9	27.4	28.0	28.5	27.0
19-Feb-00	29.1	28.7	29.4	29.1	29.6	29.3	29.7	29.4	29.6	29.2	29.4	29.1	28.8	29.1	28.8	28.5	30.1	27.4
20-Feb-00	28.5	28.9	28.8	29.2	28.9	29.4	28.9	29.4	29.0	29.3	28.8	29.3	28.3	29.5	28.1	29.1	29.2	28.1
21-Feb-00	29.1	28.7	29.3	29.0	29.4	29.2	29.5	29.2	29.5	29.2	29.2	29.1	28.5	28.9	28.3	28.0	29.3	26.9
22-Feb-00	28.6	28.7	28.8	29.1	28.9	29.2	28.8	29.2	28.9	29.1	28.6	29.0	28.0	29.0	27.5	28.4	28.2	27.3
23-Feb-00	28.8	28.7	29.0	29.0	29.1	29.1	29.0	29.1	29.0	29.0	28.7	28.9	28.0	28.8	27.5	28.0	28.3	26.9
24-Feb-00	27.8	28.7	28.0	28.9	28.0	29.0	27.9	29.0	27.9	28.9	27.4	28.6	26.7	28.3	26.0	27.5	26.0	26.6
25-Feb-00	28.7	28.7	29.0	28.9	29.0	29.0	28.8	29.0	28.7	28.7	28.0	28.3	27.2	27.8	26.4	26.9	26.3	26.1
26-Feb-00	28.2	28.7	28.4	29.0	28.4	29.0	28.2	28.9	27.9	28.6	27.1	27.9	26.1	27.2	25.3	26.2	25.4	25.4
27-Feb-00	28.5	29.0	28.7	29.2	28.6	29.2	28.3	29.0	28.0	28.5	27.4	27.9	26.8	27.7	26.3	27.4	26.5	26.6
28-Feb-00	28.4	28.7	28.5	28.8	28.4	28.8	28.2	28.5	27.8	28.1	27.3	27.7	26.6	27.4	25.7	26.8	25.2	25.9
29-Feb-00	27.9	28.9	28.0	29.0	27.8	28.9	27.5	28.7	27.3	28.3	26.6	27.7	25.6	27.2	24.6	26.3	24.5	25.4
1-Mar-00	27.9	29.0	28.0	29.1	27.8	29.0	27.4	28.8	27.0	28.3	26.2	27.6	25.2	27.0	24.1	26.0	23.9	25.0
2-Mar-00	29.1	29.0	29.0	29.0	28.8	28.9	28.4	28.6	27.9	28.0	27.0	27.2	26.1	26.5	25.2	25.8	25.3	25.1
3-Mar-00	28.6	29.3	28.6	29.2	28.3	29.1	27.8	28.8	27.3	28.1	26.5	27.4	25.4	26.9	24.2	26.2	24.3	25.1
4-Mar-00	29.0	28.8	28.9	28.7	28.6	28.5	28.1	28.2	27.6	27.5	26.7	26.8	25.5	26.2	24.4	25.0	24.9	23.8
5-Mar-00	29.1	28.6	28.9	28.5	28.6	28.3	28.1	27.9	27.6	27.2	26.6	26.4	25.3	25.8	24.3	24.8	25.0	23.8
6-Mar-00	29.2	28.4	28.9	28.3	28.6	28.0	28.0	27.6	27.5	26.9	26.6	26.1	25.6	25.5	24.8	24.5	25.8	23.6
7-Mar-00	28.9	28.1	28.6	27.9	28.2	27.6	27.7	27.2	27.2	26.5	26.4	25.8	25.4	25.4	24.6	24.6	25.5	23.8
8-Mar-00	29.0	28.4	28.7	28.1	28.3	27.8	27.7	27.4	27.3	26.8	26.7	26.1	25.9	25.8	25.4	25.6	26.3	25.2
9-Mar-00	27.6	28.5	27.4	28.2	27.0	27.9	26.5	27.5	26.1	26.9	25.6	26.5	24.9	26.3	24.2	25.9	24.5	25.4
10-Mar-00	28.4	28.3	28.1	28.0	27.7	27.7	27.2	27.3	26.9	26.8	26.4	26.3	25.7	26.0	25.2	25.6	25.6	25.2
11-Mar-00	27.8	28.3	27.5	28.0	27.2	27.7	26.8	27.3	26.4	26.9	25.9	26.4	25.3	26.1	24.8	25.6	24.9	25.0
12-Mar-00	27.9	28.7	27.6	28.5	27.3	28.2	27.0	27.9	26.6	27.4	26.0	27.0	25.3	26.6	24.7	26.0	25.1	25.0
13-Mar-00	28.2	28.6	27.9	28.4	27.5	28.1	27.1	27.8	26.7	27.3	26.2	26.8	25.4	26.5	24.8	26.0	25.4	25.3
14-Mar-00	28.2	28.6	27.8	28.3	27.5	28.0	27.0	27.7	26.8	27.2	26.1	26.7	25.4	26.4	24.7	25.7	25.5	24.8
15-Mar-00	28.0	28.6	27.7	28.3	27.3	28.0	26.9	27.7	26.6	27.2	26.0	26.7	25.3	26.5	24.7	26.1	25.5	25.6
16-Mar-00	27.7	28.5	27.3	28.2	27.0	28.0	26.7	27.7	26.3	27.2	25.8	26.8	25.1	26.5	24.4	25.9	25.0	25.2
17-Mar-00	26.8	28.3	26.5	28.0	26.1	27.7	25.7	27.4	25.5	27.0	24.9	26.5	24.2	26.1	23.6	25.7	24.0	25.2
18-Mar-00	27.3	28.2	27.0	27.9	26.7	27.7	26.4	27.4	26.0	26.9	25.4	26.4	24.7	26.0	24.1	25.3	24.2	24.8
19-Mar-00	27.7	28.4	27.3	28.1	27.0	27.9	26.7	27.6	26.3	27.1	25.6	26.6	24.8	26.1	24.0	25.5	24.3	24.8
20-Mar-00	27.4	28.6	27.1	28.3	26.7	28.0	26.3	27.7	26.0	27.2	25.2	26.6	24.2	26.2	23.2	25.5	23.3	24.8
21-Mar-00	27.8	28.5	27.5	28.2	27.1	28.0	26.6	27.6	26.2	27.0	25.4	26.3	24.3	25.8	23.4	25.1	24.1	24.3
22-Mar-00	27.8	28.4	27.5	28.1	27.0	27.8	26.4	27.5	26.1	26.9	25.3	26.1	24.1	25.7	22.9	24.9	23.7	24.0
23-Mar-00	27.9	28.2	27.5	27.9	27.1	27.6	26.5	27.2	26.1	26.6	25.2	25.8	24.1	25.2	23.1	24.5	24.0	23.8
24-Mar-00	27.8	28.0	27.4	27.7	27.0	27.4	26.4	26.9	26.0	26.3	25.3	25.5	24.4	25.1	23.8	24.6	24.7	24.2
25-Mar-00	27.6	28.3	27.2	28.0	26.7	27.7	26.1	27.2	25.8	26.7	25.1	26.0	24.2	25.8	23.2	25.4	24.2	25.0
26-Mar-00	27.5	27.8	27.1	27.4	26.6	27.1	26.1	26.7	25.8	26.1	25.2	25.5	24.4	25.2	23.8	24.7	24.8	24.3
27-Mar-00	27.6	28.2	27.1	27.9	26.7	27.6	26.1	27.2	25.9	26.6	25.4	26.1	24.7	25.9	24.1	25.7	25.1	25.4
28-Mar-00	27.5	28.3	27.1	27.8	26.6	27.6	26.0	27.2	25.9	26.8	25.4	26.4	24.5	26.2	23.4	25.8	24.4	25.2
29-Mar-00	27.2	27.6	26.8	27.2	26.4	26.9	25.9	26.6	25.7	26.2	25.1	25.7	24.2	25.4	23.3	24.8	24.4	23.7
30-Mar-00	27.2	28.0	26.8	27.7	26.4	27.4	25.9	27.1	25.7	26.6	25.1	26.2	24.3	25.9	23.5	25.4	24.4	24.6
31-Mar-00	27.1	28.5	26.7	28.2	26.3	27.9	25.8	27.6	25.6	27.2	25.1	26.7	24.4	26.5	23.6	26.2	24.5	25.6

Table K.5: Tailings temperatures (at noon and midnight) measured with the Model-229 Campbell Scientific matric suction sensors installed on the Kidston tailings impoundment.

Date	Tailings temperature (°C)																	
	NC200 (2000 mm)		NC150 (1500 mm)		#18 (1250 mm)		#19 (1000 mm)		#17 (750 mm)		#21 (500 mm)		#15 (300 mm)		#20 (150 mm)		16 (50 mm)	
	PM	AM	PM	AM	PM	AM	PM	AM	PM	AM	PM	AM	PM	AM	PM	AM	PM	AM
1-Apr-00	27.0	28.9	26.6	28.5	26.2	28.3	25.8	28.0	25.6	27.6	25.1	27.2	24.1	27.0	23.0	26.6	23.7	25.6
2-Apr-00	26.9	28.0	26.6	27.7	26.3	27.4	26.0	27.1	25.6	26.8	25.0	26.2	24.2	25.8	23.4	25.0	23.7	24.0
3-Apr-00	26.8	27.6	26.4	27.3	26.1	27.0	25.7	26.7	25.4	26.3	24.8	25.7	24.0	25.3	23.4	24.7	23.5	24.0
4-Apr-00	26.5	27.7	26.2	27.4	25.8	27.2	25.4	26.9	25.2	26.4	24.5	25.8	23.8	25.5	23.1	25.1	23.3	24.6
5-Apr-00	27.4	27.9	27.0	27.6	26.6	27.4	26.0	27.0	25.9	26.6	25.1	26.0	24.2	25.6	23.2	25.1	23.5	24.4
6-Apr-00	27.0	27.8	26.7	27.5	26.3	27.3	25.8	26.9	25.5	26.4	24.6	25.8	23.3	25.2	22.1	24.3	22.5	23.1
7-Apr-00	26.7	28.2	26.3	27.9	25.8	27.6	25.3	27.3	24.9	26.7	24.1	25.9	23.1	25.3	22.4	24.8	22.9	24.3
8-Apr-00	26.5	27.7	26.1	27.4	25.6	27.1	24.9	26.7	24.5	26.1	23.2	25.3	22.1	24.5	21.1	23.3	21.3	22.5
9-Apr-00	26.4	27.6	25.9	27.2	25.4	26.8	24.7	26.2	24.1	25.4	23.2	24.4	22.4	23.8	21.9	23.3	22.1	23.0
10-Apr-00	26.8	27.7	26.3	27.2	25.8	26.8	25.1	26.2	24.5	25.4	23.8	24.6	23.3	24.2	23.0	24.0	23.4	23.8
11-Apr-00	26.6	28.0	26.0	27.5	25.4	27.1	24.7	26.5	24.3	25.8	23.7	25.3	23.2	25.1	22.7	25.0	23.0	24.6
12-Apr-00	26.0	27.7	25.4	27.2	24.8	26.8	24.2	26.3	23.9	25.7	23.3	25.2	22.7	25.0	22.2	24.7	22.7	24.2
13-Apr-00	26.3	27.8	25.7	27.2	25.2	26.8	24.6	26.4	24.3	25.8	23.7	25.4	22.8	25.1	21.9	24.5	22.1	23.8
14-Apr-00	25.4	27.6	24.8	27.0	24.2	26.6	23.6	26.2	23.3	25.6	22.6	25.1	21.9	24.6	21.3	24.0	21.8	23.5
15-Apr-00	26.2	27.9	25.5	27.4	25.0	27.0	24.3	26.6	24.1	26.0	23.4	25.5	22.7	25.2	22.0	24.8	22.6	24.1
16-Apr-00	25.5	27.7	24.9	27.1	24.3	26.8	23.6	26.4	23.4	25.8	22.7	25.3	21.9	24.9	21.0	24.3	21.6	23.5
17-Apr-00	25.4	27.5	24.8	26.9	24.2	26.6	23.6	26.1	23.4	25.6	22.7	25.0	21.8	24.7	21.1	24.0	21.8	23.2
18-Apr-00	25.8	27.3	25.2	26.8	24.7	26.4	24.0	26.0	23.8	25.4	23.2	24.9	22.4	24.6	21.6	24.2	22.3	23.6
19-Apr-00	25.8	27.4	25.2	26.9	24.6	26.5	24.0	26.1	23.8	25.6	23.2	25.1	22.4	24.8	21.6	24.3	22.3	23.6
20-Apr-00	25.7	27.3	25.1	26.7	24.5	26.4	23.9	26.0	23.8	25.5	23.2	25.0	22.5	24.8	21.9	24.6	22.5	24.2
21-Apr-00	25.6	27.3	25.0	26.7	24.5	26.4	24.0	26.0	23.8	25.5	23.3	25.1	22.8	24.9	22.3	24.8	22.9	24.6
22-Apr-00	26.3	27.4	25.8	26.9	25.3	26.5	24.9	26.1	24.7	25.7	24.3	25.4	23.7	25.2	23.1	24.9	23.6	24.4
23-Apr-00	25.9	27.1	25.3	26.6	24.9	26.3	24.5	25.9	24.3	25.5	23.8	25.2	23.3	25.0	22.9	24.7	23.3	24.4
24-Apr-00	25.9	27.0	25.3	26.5	24.8	26.1	24.3	25.8	24.2	25.4	23.5	25.1	22.7	24.7	22.0	24.0	22.3	23.4
25-Apr-00	26.3	27.0	25.8	26.6	25.5	26.2	25.1	25.9	24.7	25.4	24.1	24.9	23.4	24.6	22.6	24.1	22.5	23.6
26-Apr-00	26.4	27.0	25.9	26.6	25.5	26.3	25.0	25.9	24.6	25.4	23.9	24.7	23.1	24.2	22.3	23.6	22.0	23.1
27-Apr-00	25.8	26.9	25.3	26.5	24.8	26.2	24.2	25.7	23.8	25.2	23.0	24.4	22.1	23.8	21.2	23.0	21.2	22.5
28-Apr-00	26.0	27.0	25.5	26.6	25.0	26.2	24.5	25.7	24.0	25.1	23.1	24.3	22.3	23.6	21.6	23.0	21.5	22.6
29-Apr-00	26.0	27.0	25.4	26.6	25.0	26.2	24.3	25.6	23.8	25.0	23.0	24.2	22.3	23.6	21.6	23.1	21.7	22.8
30-Apr-00	25.6	27.1	25.0	26.5	24.4	26.2	23.6	25.7	23.4	24.9	22.4	24.2	21.4	23.7	20.2	22.9	20.6	22.0
1-May-00	25.9	26.9	25.3	26.4	24.7	26.0	23.9	25.4	23.5	24.7	22.5	24.0	21.4	23.4	20.2	22.4	20.6	21.5
2-May-00	25.8	27.2	25.1	26.6	24.5	26.2	23.7	25.7	23.3	24.9	22.4	24.1	21.1	23.5	19.7	22.7	20.2	21.9
10-May-00	25.2		24.4		23.7		23.0		22.7		22.0		21.0		20.0		20.3	
11-May-00	25.0	27.2	24.2	26.5	23.6	26.1	22.9	25.6	22.5	24.9	21.7	24.3	20.6	23.8	19.1	22.9	19.3	22.0
12-May-00	24.8	27.3	24.0	26.6	23.3	26.2	22.6	25.7	22.2	24.9	21.2	24.1	19.9	23.5	18.3	22.5	18.6	21.5
13-May-00	24.5	27.0	23.7	26.4	23.1	25.9	22.4	25.4	21.8	24.6	20.7	23.7	19.3	22.9	17.8	21.8	18.0	20.8
14-May-00	24.3	26.6	23.5	25.9	22.8	25.4	22.0	24.8	21.5	24.0	20.3	22.9	19.0	22.1	17.7	21.1	18.2	20.1
15-May-00	25.1	26.8	24.3	26.1	23.6	25.6	22.8	25.0	22.2	24.1	21.1	23.1	19.6	22.5	17.9	21.6	18.1	20.6
16-May-00	24.6	27.0	23.8	26.3	23.1	25.8	22.1	25.2	21.6	24.3	20.3	23.2	18.7	22.4	16.9	21.2	17.3	20.3
17-May-00	25.1	26.9	24.3	26.1	23.6	25.6	22.8	24.9	22.0	24.0	20.7	22.8	19.4	21.8	18.1	20.8	18.4	19.8
18-May-00	25.5	26.2	24.7	25.5	24.0	24.9	23.2	24.2	22.4	23.2	21.4	22.1	20.4	21.3	19.7	20.6	20.0	20.2
19-May-00	25.7	26.3	24.9	25.6	24.2	25.0	23.5	24.2	22.7	23.4	21.7	22.4	20.8	21.8	20.0	21.1	20.0	20.5
20-May-00	25.3	26.2	24.5	25.4	23.8	24.8	23.0	24.1	22.3	23.2	21.4	22.3	20.5	21.5	19.8	20.9	19.9	20.6
21-May-00	25.2	26.3	24.4	25.6	23.7	24.9	22.9	24.2	22.3	23.4	21.4	22.5	20.6	21.9	20.0	21.5	20.1	21.2

Table K.5: Tailings temperatures (at noon and midnight) measured with the Model-229 Campbell Scientific matric suction sensors installed on the Kidston tailings impoundment.

Date	Tailings temperature (°C)																	
	NC200 (2000 mm)		NC150 (1500 mm)		#18 (1250 mm)		#19 (1000 mm)		#17 (750 mm)		#21 (500 mm)		#15 (300 mm)		#20 (150 mm)		16 (50 mm)	
	PM	AM	PM	AM	PM	AM	PM	AM	PM	AM	PM	AM	PM	AM	PM	AM	PM	AM
22-May-00	25.4	26.2	24.6	25.4	23.9	24.8	23.2	24.1	22.5	23.3	21.7	22.5	21.1	22.0	20.6	21.6	20.7	21.3

Table K.6: Tailings matric suctions (at noon and midnight) measured with the Model-229 Campbell Scientific matric suction sensors installed on the Kidston tailings impoundment.

Date	Tailings matric suction (kPa)																	
	NC200 (2000 mm)		NC150 (1500 mm)		#18 (1250 mm)		#19 (1000 mm)		#17 (750 mm)		#21 (500 mm)		#15 (300 mm)		#20 (150 mm)		16 (50 mm)	
	PM	AM	PM	AM	PM	AM	PM	AM	PM	AM	PM	AM	PM	AM	PM	AM	PM	AM
24-Oct-97	2.0	7.0	25.8	30.3	5.6	8.5	17.2	21.1	18.6	21.2	53.6	60.5	55.7	54.8	35.0	36.1	67.0	80.0
25-Oct-97	3.3	2.1	25.8	28.1	7.3	6.7	21.0	21.0	21.2	22.1	54.9	57.7	55.7	53.9	37.0	36.1	62.0	74.3
26-Oct-97	0.0	4.6	23.6	28.0	7.3	7.9	18.7	20.2	20.3	22.1	56.2	56.3	54.7	53.0	37.0	36.1	67.0	72.5
27-Oct-97	2.0	3.3	26.9	28.0	7.8	6.7	19.4	20.2	20.2	22.0	56.2	55.0	55.6	53.0	36.0	37.1	61.9	74.3
28-Oct-97	2.0	4.6	26.9	28.0	6.7	7.9	19.4	20.2	19.4	21.2	53.6	56.3	54.7	53.9	37.0	34.1	65.2	78.0
29-Oct-97	0.0	4.6	24.7	28.0	6.7	7.9	17.9	21.0	18.5	21.2	52.3	55.0	54.7	53.9	38.0	35.1	63.6	78.0
30-Oct-97	3.2	2.1	24.7	25.8	6.2	7.3	17.9	20.2	19.4	22.1	53.6	55.0	54.7	53.9	36.0	36.1	55.5	74.3
31-Oct-97	0.7	2.0	24.7	26.9	7.3	9.0	21.0	19.4	20.2	20.3	53.6	55.0	53.8	54.8	37.0	37.1	67.0	76.1
1-Nov-97	0.0	0.7	24.7	29.1	7.3	6.7	18.7	21.0	19.4	23.0	52.3	56.3	55.6	54.8	36.0	36.1	61.9	72.4
2-Nov-97	0.7	3.3	25.8	25.8	6.7	7.8	18.7	19.4	20.2	20.3	53.6	56.3	52.8	53.8	35.0	35.1	61.9	74.2
5-Nov-97	0.6	3.3	26.8	30.2	8.4	9.7	20.9	20.3	22.0	21.2	52.3	56.3	55.6	53.0	39.1	38.1	60.2	72.5
6-Nov-97	0.0	2.0	24.7	26.9	5.6	9.0	17.9	21.0	18.5	21.2	52.3	52.4	55.6	53.8	36.0	37.1	61.9	76.0
7-Nov-97	0.6	0.7	23.5	28.0	7.2	7.8	17.9	21.0	16.8	21.2	51.0	54.9	52.8	53.8	35.0	36.0	53.9	74.2
8-Nov-97	0.0	0.0	25.7	29.1	7.2	9.0	18.6	19.4	20.2	22.1	53.5	54.9	53.7	52.0	37.0	37.1	61.8	74.2
9-Nov-97	0.0	3.3	23.6	25.8	6.7	7.9	16.5	18.7	20.2	20.3	51.0	53.7	53.8	53.9	37.0	39.1	65.2	79.9
10-Nov-97	0.7	2.1	28.0	27.0	7.8	8.5	18.7	20.3	20.3	22.1	49.8	52.4	46.7	53.0	16.7	37.1	12.7	52.6
11-Nov-97	0.7	2.0	24.7	29.1	5.6	8.4	14.4	19.4	16.1	20.3	40.4	49.8	36.7	39.2	14.0	13.4	20.7	21.7
12-Nov-97	0.0	0.0	25.8	25.8	6.7	7.3	17.2	18.0	16.1	17.7	38.2	42.7	38.3	36.7	18.1	16.0	24.7	28.0
13-Nov-97	0.0	0.7	24.7	25.8	6.2	7.8	16.5	17.9	16.9	19.4	38.2	41.6	40.8	38.4	19.6	18.1	31.3	34.9
14-Nov-97	0.0	0.0	21.4	26.9	6.2	7.8	15.1	17.9	16.9	18.6	38.2	41.6	40.0	40.0	21.1	20.3	37.3	42.6
15-Nov-97	0.0	0.7	23.5	28.0	6.7	7.3	16.4	17.9	16.8	17.7	42.6	42.7	44.9	43.3	25.0	25.1	37.2	49.6
16-Nov-97	0.6	2.0	24.6	24.7	6.7	7.3	16.4	18.7	18.5	18.6	43.7	45.0	45.8	42.5	26.7	25.9	41.1	52.6
17-Nov-97	0.0	0.7	24.6	26.9	6.1	8.4	18.6	19.4	17.7	20.3	42.6	45.0	47.5	46.7	32.1	32.1	49.4	63.6
18-Nov-97	0.0	3.3	25.7	28.0	7.2	9.0	16.4	20.2	19.3	18.5	44.9	48.5	48.4	47.6	31.1	30.3	45.2	65.3
19-Nov-97	0.6	0.7	25.8	30.2	7.8	8.4	18.6	19.4	20.2	21.2	44.9	46.2	48.4	46.7	35.0	33.1	55.4	72.4
20-Nov-97	0.0	2.0	28.0	28.0	7.8	9.7	19.4	20.2	16.9	20.3	44.9	48.6	51.1	51.1	34.0	36.1	55.5	74.3
21-Nov-97	0.7	0.0	26.9	28.0	7.8	9.6	17.2	19.4	19.4	20.3	46.1	48.5	47.5	49.3	31.2	32.1	52.4	63.6
22-Nov-97	0.7	2.0	25.8	29.1	8.4	9.6	17.2	20.2	19.4	20.3	47.3	49.8	51.1	49.3	33.1	33.1	57.1	72.4
23-Nov-97	0.0	2.0	28.0	29.1	7.8	9.7	17.9	19.4	16.9	23.0	49.8	49.8	52.0	51.1	38.0	37.1	60.2	78.0
24-Nov-97	0.0	0.0	28.0	29.1	9.0	8.4	17.2	19.4	22.0	22.1	51.0	49.8	51.1	52.0	36.0	37.1	58.6	79.9
25-Nov-97	0.0	2.0	26.8	28.0	7.8	8.4	17.9	21.0	18.5	22.1	44.9	51.1	52.8	52.0	35.0	38.1	57.0	81.9
26-Nov-97	0.0	0.0	27.9	28.0	8.4	9.7	17.9	18.7	19.3	23.0	42.6	51.1	52.0	52.0	36.0	42.4	55.4	79.9
27-Nov-97	0.0	2.0	29.0	28.0	9.6	9.0	20.2	20.2	17.7	22.1	43.7	49.8	50.2	51.1	32.1	36.1	30.1	74.2

Table K.6: Tailings matric suctions (at noon and midnight) measured with the Model-229 Campbell Scientific matric suction sensors installed on the Kidston tailings impoundment.

Date	Tailings matric suction (kPa)																	
	NC200 (2000 mm)		NC150 (1500 mm)		#18 (1250 mm)		#19 (1000 mm)		#17 (750 mm)		#21 (500 mm)		#15 (300 mm)		#20 (150 mm)		16 (50 mm)	
	PM	AM	PM	AM	PM	AM	PM	AM	PM	AM	PM	AM	PM	AM	PM	AM	PM	AM
28-Nov-97	0.0	0.0	25.7	28.0	7.2	10.3	16.4	20.2	19.3	21.2	43.7	48.6	45.8	47.6	25.0	27.6	31.2	41.2
29-Nov-97	0.0	0.0	27.9	32.4	8.4	9.0	17.9	20.2	19.3	20.3	43.7	44.9	46.6	45.0	25.8	26.7	36.0	46.6
30-Nov-97	0.0	0.0	25.7	30.2	9.0	9.0	17.2	18.7	18.5	22.0	42.6	46.1	46.6	46.7	30.2	27.6	41.1	50.9
1-Dec-97	0.0	0.0	26.8	29.1	9.6	9.7	19.4	19.4	20.2	21.2	46.0	46.2	49.3	48.5	29.3	33.1	39.8	55.6
2-Dec-97	0.0	0.0	30.1	29.1	8.4	9.0	18.6	19.4	20.2	20.3	43.7	45.0	48.4	46.7	28.4	30.3	39.8	55.6
3-Dec-97	0.0	0.0	26.8	28.0	8.4	9.6	18.6	20.2	17.7	19.4	43.8	47.3	45.8	46.7	27.6	29.4	49.4	55.5
4-Dec-97	0.0	0.7	26.8	29.1	8.4	9.6	18.6	21.0	18.5	22.0	46.0	48.5	49.2	46.6	30.2	31.2	42.4	61.9
5-Dec-97	0.0	0.0	27.9	30.2	7.8	9.6	18.6	19.4	18.5	22.0	47.3	47.4	49.3	49.3	33.1	32.1	57.0	67.0
12-Dec-97	0.0	0.0	14.1	20.9	2.5	3.9	8.3	10.0	8.6	10.7	27.9	30.0	36.3	37.3	19.9	23.2	38.0	46.4
13-Dec-97	0.0	0.0	20.8	18.8	4.8	3.9	11.7	10.1	12.0	11.4	31.7	29.0	40.4	38.1	23.1	22.5	40.7	45.0
14-Dec-97	0.0	0.0	16.7	16.7	3.1	3.5	9.5	10.1	10.8	10.8	31.2	30.0	40.7	39.9	39.1	36.0	0.8	74.4
15-Dec-97	0.0	0.0	17.6	18.9	3.4	4.0	8.9	9.6	10.0	10.8	22.0	29.3	11.7	30.5	0.0	3.1	0.0	0.8
16-Dec-97	0.0	0.0	16.3	17.7	2.9	4.0	7.3	8.4	6.9	9.4	12.9	17.4	11.0	13.1	0.0	2.7	0.0	3.6
17-Dec-97	0.0	0.0	15.2	16.6	2.0	3.0	7.8	7.9	6.8	7.6	14.3	13.2	15.7	13.8	1.9	1.6	3.4	10.2
18-Dec-97	0.0	0.0	14.1	16.6	1.6	2.1	6.8	7.0	5.8	6.5	13.6	13.2	15.0	15.2	2.2	7.6	2.4	16.8
19-Dec-97	0.0	0.0	18.6	14.5	2.9	2.2	8.3	6.5	7.5	5.9	17.2	13.1	22.0	18.7	6.0	9.1	10.0	22.5
20-Dec-97	0.0	0.0	16.3	14.5	2.1	1.8	7.8	7.0	8.7	5.9	17.9	15.2	23.5	22.2	6.9	13.3	8.5	26.7
21-Dec-97	0.0	0.0	14.2	14.5	2.1	1.8	5.5	6.5	5.2	6.5	15.7	17.4	19.9	30.4	5.5	12.7	8.5	26.7
22-Dec-97	0.0	0.0	15.5	15.7	2.1	2.2	6.9	7.0	7.0	7.1	15.8	16.0	18.6	22.9	1.6	12.1	0.7	6.7
23-Dec-97	0.0	0.0	14.3	14.6	1.7	2.2	6.9	7.0	6.4	7.7	10.5	25.6	6.4	13.9	0.0	0.5	0.0	0.1
24-Dec-97	0.0	0.0	14.2	14.4	1.7	1.8	6.4	6.9	4.3	5.4	5.3	6.0	5.1	7.1	0.0	1.9	0.0	0.8
25-Dec-97	0.0	0.0	14.2	14.4	1.7	1.4	5.9	6.1	4.2	4.9	6.3	6.0	9.0	8.5	0.0	2.3	0.0	5.4
26-Dec-97	0.0	0.0	12.0	13.2	0.6	1.4	4.7	6.1	3.4	3.5	6.4	6.0	10.4	10.5	0.7	3.8	2.5	10.2
27-Dec-97	0.0	0.0	14.3	13.3	1.3	1.0	5.5	5.6	3.8	4.4	8.7	8.2	14.5	20.1	2.6	7.0	5.9	15.9
28-Dec-97	0.0	0.0	9.9	13.3	0.0	1.0	3.9	5.2	3.4	3.5	6.0	8.8	6.5	15.9	0.1	6.6	0.0	0.8
29-Dec-97	0.0	0.0	8.7	9.9	0.0	0.4	5.1	4.8	1.4	3.0	1.4	6.5	11.1	11.2	0.1	0.3	0.4	0.0
30-Dec-97	0.0	0.0	14.4	10.0	0.7	1.1	5.2	11.3	8.2	8.3	6.5	7.6	11.1	9.9	0.2	0.0	0.0	0.0
		0.0		12.3		0.7		9.6		7.1		4.5		9.9		0.0		0.0
22-Oct-98	0.0	0.0	4.9	6.3	7.5	7.7	15.4	15.7	12.6	13.6	27.0	24.6	38.7	35.0	19.9	19.4	28.5	37.2
23-Oct-98	0.0	0.0	5.1	5.4	7.1	6.6	14.3	15.1	10.7	12.3	23.7	25.8	26.5	35.9	4.2	12.7	7.3	6.7
24-Oct-98	0.0	0.0	0.9	5.3	5.4	7.1	11.7	15.1	8.1	10.8	18.8	23.1	23.5	25.2	6.5	6.1	10.8	11.0
25-Oct-98	0.0	0.0	0.8	5.3	5.9	6.5	12.3	14.4	7.5	10.2	19.5	22.2	25.7	25.8	8.5	8.1	11.6	16.9
26-Oct-98	0.0	0.0	0.6	4.0	4.8	6.6	11.1	14.5	6.3	9.5	18.7	21.4	27.9	27.4	10.7	11.4	16.5	21.6
27-Oct-98	0.0	0.0	2.3	3.9	5.4	6.0	12.9	13.7	10.0	8.8	21.1	20.5	30.9	28.8	13.8	12.0	18.3	25.6
28-Oct-98	0.0	0.0	3.6	3.9	6.4	7.7	12.9	14.3	9.3	10.7	20.3	23.0	31.7	31.1	14.4	14.6	26.3	30.0
29-Oct-98	0.0	0.0	0.8	5.2	4.8	7.7	11.6	14.4	8.0	10.1	21.0	24.6	33.9	34.2	15.6	16.7	21.1	34.8
30-Oct-98	0.0	0.0	6.1	5.1	7.0	7.1	14.8	14.3	11.3	10.8	26.2	24.7	38.0	35.0	20.0	17.9	28.6	38.6
31-Oct-98	0.0	0.0	3.6	4.0	5.9	7.7	13.5	14.5	11.3	13.7	25.3	25.7	38.8	39.0	20.7	25.1	26.4	46.7
1-Nov-98	0.0	0.0	6.2	5.1	7.6	7.7	15.6	15.7	14.3	14.4	26.3	26.7	28.7	37.4	4.6	10.3	7.2	8.1
2-Nov-98	0.0	0.0	3.8	4.1	6.0	7.8	13.0	14.5	11.4	12.9	18.8	23.1	15.2	21.6	1.0	1.0	2.5	2.1
3-Nov-98	0.0	0.0	3.8	4.0	6.0	7.7	13.7	14.4	10.1	12.9	15.9	19.8	18.6	18.7	3.0	3.5	8.0	6.7
4-Nov-98	0.0	0.0	3.8	4.1	6.5	6.6	13.7	14.5	10.7	11.6	18.9	18.3	22.9	20.9	7.5	6.1	13.3	13.5
5-Nov-98	0.0	0.0	5.2	6.6	6.5	6.7	13.7	13.9	10.1	11.0	18.9	18.3	26.6	23.7	10.3	9.8	19.6	20.7

Table K.6: Tailings matric suctions (at noon and midnight) measured with the Model-229 Campbell Scientific matric suction sensors installed on the Kidston tailings impoundment.

Date	Tailings matric suction (kPa)																	
	NC200 (2000 mm)		NC150 (1500 mm)		#18 (1250 mm)		#19 (1000 mm)		#17 (750 mm)		#21 (500 mm)		#15 (300 mm)		#20 (150 mm)		16 (50 mm)	
	PM	AM	PM	AM	PM	AM	PM	AM	PM	AM	PM	AM	PM	AM	PM	AM	PM	AM
6-Nov-98	0.0	0.0	3.8	4.0	5.4	6.7	12.4	13.8	8.8	9.6	18.1	19.1	28.0	26.7	11.4	12.8	21.3	25.8
7-Nov-98	0.0	0.0	0.9	6.4	4.9	6.7	11.7	13.8	7.5	9.6	18.8	22.3	30.2	29.6	13.8	14.7	21.3	31.4
8-Nov-98	0.0	0.0	0.0	6.4	3.4	6.6	11.1	14.4	7.5	9.5	18.0	22.3	31.8	31.9	15.1	15.9	24.4	31.4
9-Nov-98	0.0	0.0	2.3	3.9	6.4	6.6	14.9	13.8	12.0	13.7	23.6	22.3	35.6	33.5	17.1	18.1	26.4	37.4
10-Nov-98	0.0	0.0	3.8	3.9	6.5	7.8	14.3	13.8	12.8	13.0	23.7	24.7	37.3	35.2	19.4	18.8	37.1	39.9
11-Nov-98	0.0	0.0	3.9	5.2	7.1	7.2	15.0	15.1	12.9	13.7	27.3	25.7	42.3	38.2	25.8	22.7	45.2	45.4
12-Nov-98		0.0		4.0		7.1		14.5		13.0		27.5		40.7		27.7		54.3
15-Nov-98	0.0		4.9		7.5		14.1		11.3		20.2		25.7		7.9		10.0	
16-Nov-98	0.0	0.0	6.1	5.2	7.5	8.3	13.5	15.0	11.9	12.9	20.2	19.8	25.6	25.1	8.4	8.6	12.3	17.7
17-Nov-98	0.0	0.0	7.3	7.6	6.9	7.1	13.4	15.0	10.5	11.5	19.4	20.5	30.0	28.9	11.8	11.5	16.4	23.6
18-Nov-98	0.0	0.0	2.3	3.9	5.9	6.6	12.9	13.2	9.3	10.2	19.5	19.8	25.0	28.2	4.6	9.2	8.6	9.6
19-Nov-98	0.0	0.0	2.3	6.3	6.4	6.6	12.9	13.7	8.7	10.1	18.0	19.8	22.0	23.6	3.7	7.1	5.9	15.0
20-Nov-98	0.0	0.0	0.0	4.0	4.9	7.1	11.7	13.1	6.9	9.5	15.8	19.0	22.1	21.5	6.0	5.6	10.1	12.6
21-Nov-98	0.0	0.0	2.4	4.0	5.4	6.6	11.7	13.8	7.5	8.3	18.0	18.3	24.3	25.2	8.0	8.2	13.2	17.9
22-Nov-98	0.0	0.0	2.3	4.2	5.4	6.1	13.0	12.6	6.9	7.7	18.8	19.9	24.3	25.2	6.0	8.2	7.2	16.1
23-Nov-98	0.0	0.0	2.4	4.0	4.4	6.6	11.1	13.2	6.9	8.4	16.6	20.0	18.6	23.0	1.9	3.9	1.6	2.1
24-Nov-98	0.0	0.0	2.3	6.4	5.3	6.6	12.3	13.7	5.8	8.2	18.7	19.7	20.6	20.8	4.2	4.7	8.6	8.1
25-Nov-98	0.0	0.0	2.3	8.7	5.9	7.7	12.3	14.4	5.8	7.0	16.5	17.4	24.3	21.5	7.4	6.6	12.3	14.2
26-Nov-98	0.0	0.0	0.0	3.9	3.8	5.5	10.5	13.1	5.8	5.9	13.6	16.6	21.3	22.9	7.4	8.1	10.8	18.6
27-Nov-98		0.0		3.9		6.0		12.5		8.9		18.2		26.7		10.3		21.5
29-Nov-98	0.0		0.0		4.8		12.2		9.3		17.9		30.9		14.4		20.2	
30-Nov-98	0.0	0.0	8.3	5.2	8.7	6.0	14.8	12.5	11.9	10.1	24.3	21.3	36.3	32.7	19.2	17.4	22.1	33.5
1-Dec-98	0.0	0.0	4.9	2.7	5.8	6.0	14.1	13.1	12.0	11.5	26.2	23.0	40.4	35.8	20.7	18.7	29.7	38.5
2-Dec-98	0.0	0.0	4.9	3.9	5.9	6.1	12.9	12.6	12.7	10.8	25.3	23.8	39.7	35.2	21.5	20.2	32.0	42.7
3-Dec-98	0.0	0.0	5.0	6.5	6.4	7.2	11.7	14.4	11.3	12.2	23.6	26.5	39.7	37.6	24.0	23.3	35.7	46.8
4-Dec-98	0.0	0.0	5.0	4.0	6.5	6.6	13.6	14.4	12.1	12.3	27.1	25.6	42.2	40.0	24.8	25.0	39.5	52.8
5-Dec-98	0.0	0.0	3.6	6.6	7.5	7.2	15.5	14.4	14.9	14.5	29.8	27.4	45.4	41.5	29.0	28.5	35.5	58.9
6-Dec-98	0.0	0.0	3.5	2.6	6.9	7.2	14.8	15.8	15.6	15.2	31.6	28.4	47.1	42.5	29.0	29.6	40.4	60.4
7-Dec-98	0.0	0.0	4.9	7.6	7.0	8.3	14.8	17.1	14.1	16.7	30.6	32.1	47.1	45.8	30.7	32.1	37.9	63.7
8-Dec-98	0.0	0.0	7.3	6.4	9.9	8.3	17.6	17.2	15.7	15.1	31.8	30.2	49.0	44.9	32.7	32.0	43.5	67.0
9-Dec-98	0.0	0.0	0.9	6.4	7.0	9.5	16.3	16.4	16.6	16.7	32.9	32.1	49.1	47.4	35.8	33.1	58.4	70.7
10-Dec-98	0.0	0.0	5.1	7.6	8.8	8.3	17.8	16.5	16.7	16.8	36.0	34.0	51.0	49.3	37.9	37.1	68.5	72.6
11-Dec-98		0.0		6.4		9.5		17.2		16.7		36.2		51.1		40.3		80.1
12-Dec-98	0.0		9.7		10.0		18.4		19.9		39.0		53.5		38.8		56.7	
13-Dec-98	0.0	0.0	5.1	6.5	8.2	10.8	18.5	17.2	17.5	17.7	32.9	36.3	43.1	48.7	17.9	28.7	19.5	21.6
14-Dec-98	0.0	0.0	5.0	6.4	8.7	9.6	16.9	17.1	15.7	18.5	29.9	32.1	39.6	40.7	15.7	16.6	20.3	29.0
15-Dec-98	0.0	0.0	10.8	7.5	10.5	9.5	18.4	17.1	18.1	16.7	30.7	31.1	40.4	37.4	17.1	18.7	20.2	31.2
16-Dec-98	0.0	0.0	3.5	5.1	6.9	8.9	13.4	16.4	12.6	15.9	27.9	29.1	37.9	38.2	19.1	18.7	22.0	35.9
17-Dec-98	0.0	0.0	4.8	6.4	6.9	8.9	14.8	16.4	14.8	16.0	30.6	28.3	41.2	40.0	21.4	23.4	25.2	43.8
18-Dec-98	0.0	0.0	10.8	9.9	11.2	10.1	18.4	17.1	19.0	16.7	33.7	32.1	46.4	39.8	28.2	25.0	36.9	45.0
19-Dec-98	0.0	0.0	7.3	4.0	9.9	8.9	17.6	16.5	16.5	15.2	30.8	31.2	40.4	41.6	17.8	22.7	22.2	32.4
20-Dec-98	0.0	0.0	7.4	6.4	8.8	8.3	16.3	16.4	15.8	16.7	29.9	28.3	38.1	37.5	14.4	17.3	19.4	22.5
21-Dec-98	0.0	0.0	6.1	6.3	7.6	8.3	15.5	15.7	14.2	15.9	26.2	28.3	34.0	34.2	10.7	13.9	10.8	23.5

Table K.6: Tailings matric suctions (at noon and midnight) measured with the Model-229 Campbell Scientific matric suction sensors installed on the Kidston tailings impoundment.

Date	Tailings matric suction (kPa)																	
	NC200 (2000 mm)		NC150 (1500 mm)		#18 (1250 mm)		#19 (1000 mm)		#17 (750 mm)		#21 (500 mm)		#15 (300 mm)		#20 (150 mm)		16 (50 mm)	
	PM	AM	PM	AM	PM	AM	PM	AM	PM	AM	PM	AM	PM	AM	PM	AM	PM	AM
22-Dec-98	0.0	0.0	2.3	7.5	5.9	8.3	14.8	16.4	13.5	16.0	22.8	27.3	24.2	28.9	3.7	6.1	5.9	6.7
23-Dec-98	0.0	0.0	5.0	5.2	7.6	8.3	14.9	15.7	14.3	14.4	20.4	23.1	18.6	22.3	1.9	2.3	5.3	3.7
24-Dec-98		0.0		5.1		8.3		15.1		14.4		21.3		20.1		3.9		9.5
27-Dec-98	0.0		6.1		6.9		14.7		12.0		20.2		29.3		11.9		21.2	
28-Dec-98	0.0	0.0	0.0	5.2	4.8	6.5	12.2	13.1	9.3	11.6	19.4	20.6	28.6	30.4	11.8	14.0	13.9	27.9
29-Dec-98	0.0	0.0	2.4	3.9	5.4	6.1	12.3	13.7	11.4	12.2	21.2	19.8	29.5	30.4	9.1	14.6	10.8	29.0
30-Dec-98	0.0	0.0	0.9	5.1	4.9	7.1	13.0	13.8	10.0	13.0	19.6	21.5	24.3	27.3	5.5	6.6	9.4	9.5
31-Dec-98	0.0	0.0	2.5	4.0	5.4	6.6	13.0	14.4	11.4	12.3	18.1	19.8	18.6	24.5	1.6	4.7	3.6	5.5
1-Jan-99	0.0	0.0	0.9	3.9	4.9	6.6	11.7	13.7	10.7	12.2	16.6	18.2	18.6	18.7	3.8	3.1	6.6	7.4
2-Jan-99	0.0	0.0	4.9	5.2	7.0	6.6	12.9	13.7	12.7	12.2	18.0	18.2	21.3	20.1	6.0	4.7	9.3	11.8
3-Jan-99	0.0	0.0	3.5	5.2	6.4	6.0	12.9	14.3	11.3	12.2	18.0	19.8	24.2	23.7	9.0	8.6	11.5	18.7
4-Jan-99	0.0	0.0	3.7	3.9	6.5	6.5	13.6	13.1	10.7	10.1	18.8	18.2	11.1	25.1	0.1	9.7	0.0	20.6
5-Jan-99	0.0	0.0	4.9	6.4	5.9	7.1	12.3	13.7	8.7	11.4	11.0	13.8	10.4	10.5	0.0	0.0	0.1	0.0
6-Jan-99	0.0	0.0	0.0	4.0	3.4	5.5	10.6	11.9	5.9	8.2	7.5	9.4	7.8	10.5	0.0	0.5	0.7	2.6
7-Jan-99	0.0	0.0	2.5	4.0	4.4	4.5	10.1	10.8	5.9	7.0	8.7	8.8	12.5	11.2	1.3	1.0	4.7	3.7
8-Jan-99		0.0		5.1		5.0		10.7		7.1		10.0		12.6		2.7		8.8
17-Oct-99	0.0		10.9		13.3		24.1		26.5		53.4		67.1		63.4		114.9	
18-Oct-99	0.0	0.0	7.4	11.1	12.6	14.3	23.2	25.3	25.5	29.9	50.8	58.0	68.2	69.7	63.4	68.3	107.6	191.2
19-Oct-99	0.0	0.0	9.7	11.3	12.6	15.0	23.2	25.4	26.5	31.1	53.3	56.9	69.1	69.5	63.3	67.1	107.0	192.1
20-Oct-99	0.0	0.0	9.6	12.3	12.6	15.0	22.3	25.3	26.4	30.0	52.0	55.4	69.0	69.9	63.3	68.5	112.2	190.9
21-Oct-99	0.0	0.0	8.6	13.4	12.6	14.9	22.4	26.1	26.5	32.1	53.4	55.0	67.1	69.6	63.4	66.7	114.9	179.3
22-Oct-99	0.0	0.0	8.6	11.0	13.3	14.2	22.4	26.2	25.5	29.9	52.1	57.8	68.1	68.5	63.4	67.0	117.6	179.9
23-Oct-99	0.0	0.0	7.5	12.1	11.4	14.9	21.7	24.4	24.7	28.9	51.0	55.3	67.2	69.5	66.5	68.3	145.6	183.8
24-Oct-99	0.0	0.0	8.5	13.3	13.2	14.9	24.8	26.2	28.4	29.9	55.8	57.8	68.0	70.8	61.8	67.0	107.2	172.3
25-Oct-99	0.0	0.0	8.5	12.2	12.6	15.7	25.7	24.4	28.4	30.0	54.4	56.4	69.0	68.6	61.7	64.0	109.5	175.8
26-Oct-99	0.0	0.0	9.8	11.0	13.2	14.8	24.8	26.9	27.4	29.8	53.1	57.7	66.9	67.4	60.4	62.4	104.9	175.6
27-Oct-99	0.0	0.0	10.9	11.0	13.2	15.6	23.1	26.9	27.4	30.8	51.9	54.9	67.0	67.2	60.3	65.0	107.2	175.1
28-Oct-99	0.0	0.0	9.6	15.6	13.1	15.6	23.9	26.0	27.4	30.9	53.0	56.3	68.0	69.5	61.7	65.1	109.5	186.0
29-Oct-99	0.0	0.0	10.7	13.3	13.9	16.3	23.9	26.9	28.4	30.8	53.1	56.3	67.9	68.4	60.3	64.9	104.4	182.2
30-Oct-99	0.0	0.0	10.8	13.3	14.0	14.9	24.0	27.1	26.4	30.0	53.2	56.4	68.0	67.4	60.5	65.3	112.2	186.9
31-Oct-99	0.0	0.0	13.1	14.4	14.7	15.6	25.8	27.1	29.6	29.9	54.6	56.3	68.1	66.5	69.2	64.1	145.2	190.7
1-Nov-99	0.0	0.0	11.9	12.2	14.7	15.0	24.0	25.3	29.5	28.9	54.6	56.5	65.0	69.6	40.9	66.8	28.6	48.4
2-Nov-99	0.0	0.0	12.0	14.4	11.9	15.0	21.5	24.4	24.5	27.9	46.9	52.6	56.3	60.6	29.1	33.3	30.8	41.3
3-Nov-99		0.0		13.3		13.5		24.4		28.9		51.3		53.9		30.4		48.4
12-Nov-99	0.0		7.6		5.5		9.6		4.9		4.4		8.5		2.0		7.4	
13-Nov-99	0.0	0.0	8.7	10.1	6.0	5.5	9.5	10.8	5.9	6.6	7.0	7.7	15.2	13.2	4.2	4.0	9.4	10.4
14-Nov-99	0.0	0.0	8.6	11.2	3.9	6.7	8.9	10.8	5.3	7.1	6.4	8.3	16.5	16.6	5.6	5.7	10.1	15.2
15-Nov-99	0.0	0.0	7.4	8.9	4.9	6.1	9.4	11.5	5.8	7.1	8.6	10.7	20.0	20.1	8.5	9.3	14.9	20.7
16-Nov-99	0.0	0.0	7.4	10.0	4.9	5.6	10.0	11.3	5.8	7.1	10.4	11.3	23.5	21.5	10.7	10.4	19.3	23.7
17-Nov-99	0.0	0.0	7.2	9.9	4.3	5.5	9.8	10.7	6.8	7.7	12.3	13.2	27.9	25.9	13.0	14.0	22.1	31.2
18-Nov-99	0.0	0.0	6.2	9.0	3.8	5.5	10.0	11.3	5.8	7.7	13.7	13.2	30.9	29.7	17.8	17.4	35.6	42.8
19-Nov-99	0.0	0.0	5.0	9.0	3.9	5.0	9.4	11.3	6.4	7.7	14.4	16.7	15.8	24.5	0.7	0.7	0.1	0.0

Table K.6: Tailings matric suctions (at noon and midnight) measured with the Model-229 Campbell Scientific matric suction sensors installed on the Kidston tailings impoundment.

Date	Tailings matric suction (kPa)																	
	NC200 (2000 mm)		NC150 (1500 mm)		#18 (1250 mm)		#19 (1000 mm)		#17 (750 mm)		#21 (500 mm)		#15 (300 mm)		#20 (150 mm)		16 (50 mm)	
	PM	AM	PM	AM	PM	AM	PM	AM	PM	AM	PM	AM	PM	AM	PM	AM	PM	AM
20-Nov-99	0.0	0.0	7.5	7.7	4.9	5.0	10.6	11.3	6.4	7.1	13.1	15.3	13.1	16.7	0.1	0.5	1.1	0.2
21-Nov-99	0.0	0.0	8.6	8.9	5.4	5.6	11.7	10.8	6.9	7.1	11.1	11.3	13.7	13.3	1.3	0.8	3.6	1.7
22-Nov-99	0.0	0.0	6.3	9.0	4.4	5.5	10.6	10.7	6.4	7.1	8.7	10.7	9.1	11.9	0.0	0.0	0.0	0.0
23-Nov-99	0.0	0.0	5.1	10.1	3.9	4.5	10.1	10.8	5.4	7.1	6.4	8.2	6.5	9.2	0.0	0.0	0.0	0.0
24-Nov-99	0.0	0.0	7.4	8.8	4.9	5.0	9.5	9.6	5.3	6.5	5.4	7.1	8.5	8.6	0.1	0.0	1.6	1.6
25-Nov-99	0.0	0.0	9.9	7.7	4.4	5.5	10.1	10.7	5.9	6.6	6.5	6.6	9.8	9.2	0.3	0.0	1.2	0.5
26-Nov-99	0.0	0.0	2.7	8.8	2.6	4.5	7.5	9.6	3.9	5.4	5.5	6.6	8.5	9.2	0.0	0.3	1.6	2.1
27-Nov-99	0.0	0.0	9.9	7.7	4.0	3.6	9.0	9.1	5.4	5.0	6.5	7.1	10.5	10.0	0.5	0.3	2.1	1.7
28-Nov-99	0.0	0.0	5.1	6.6	3.5	4.2	8.5	8.5	4.9	5.0	6.5	6.6	9.8	10.6	0.3	0.5	2.1	2.2
29-Nov-99	0.0	0.0	8.8	8.8	4.0	3.6	9.6	8.1	4.9	4.0	8.2	6.6	11.8	10.6	1.3	0.5	4.8	3.7
30-Nov-99	0.0	0.0	5.1	6.5	3.0	2.7	8.0	8.0	4.4	4.4	7.0	6.6	11.8	11.2	1.6	1.3	5.4	5.5
1-Dec-99	0.0	0.0	6.3	7.7	2.2	3.6	7.9	8.1	4.4	4.0	7.6	7.7	13.8	13.2	3.0	3.1	8.7	8.9
2-Dec-99		0.0		6.5		2.6		8.0		4.4		8.2		16.0		5.2		13.5
4-Dec-99	0.0		3.8		1.7		7.4		3.9		10.5		23.6		11.4		22.4	
5-Dec-99	0.0	0.0	3.8	6.5	2.5	2.7	7.9	9.2	4.8	5.0	13.1	10.7	29.5	27.5	17.2	16.0	34.6	40.1
6-Dec-99	0.0	0.0	5.1	7.6	2.6	3.1	8.4	9.2	4.3	5.5	15.2	14.7	34.1	31.3	24.9	23.5	58.5	62.5
7-Dec-99	0.0	0.0	5.0	7.7	2.5	3.1	9.5	10.3	4.8	5.5	19.6	18.3	40.6	39.2	37.9	35.3	98.4	106.5
8-Dec-99	0.0	0.0	6.2	8.9	3.4	4.0	10.0	11.4	5.8	6.5	23.6	24.1	49.1	48.5	49.0	49.4	151.1	166.0
9-Dec-99	0.0	0.0	3.7	8.8	2.9	4.0	10.0	11.9	6.4	7.7	30.9	32.2	56.4	53.9	59.2	59.8	204.5	236.9
10-Dec-99	0.0	0.0	5.0	8.7	3.9	5.0	11.1	12.5	8.1	8.3	34.8	37.3	60.1	60.5	70.7	69.8	278.8	317.3
11-Dec-99	0.0	0.0	8.5	7.6	4.8	5.0	14.1	13.7	11.3	10.1	44.6	41.6	69.0	65.4	85.3	82.7	429.8	472.5
12-Dec-99	0.0	0.0	6.2	8.7	4.3	5.5	14.2	15.7	12.1	11.5	44.6	49.9	69.1	68.6	92.7	91.7	599.4	648.4
13-Dec-99	0.0	0.0	6.2	9.9	5.9	6.6	16.9	17.1	19.9	14.4	50.7	48.6	73.3	72.6	100.4	99.2	551.0	740.7
14-Dec-99	0.0	0.0	7.5	6.5	6.5	6.6	15.7	16.4	20.1	20.3	52.3	49.9	73.5	71.7	99.0	105.7	408.2	853.1
15-Dec-99	0.0	0.0	8.7	7.7	6.5	7.2	17.0	17.3	20.0	21.0	50.9	51.2	71.4	71.7	93.1	95.5	303.2	343.5
16-Dec-99	0.0	0.0	6.2	8.8	5.9	7.8	17.0	19.4	21.7	22.9	52.1	52.5	74.4	73.9	98.6	97.7	367.4	403.1
17-Dec-99	0.0	0.0	7.4	10.0	7.0	8.3	17.7	19.4	23.6	23.8	54.7	57.8	76.6	76.0	106.6	107.6	528.8	570.4
18-Dec-99	0.0	0.0	5.1	9.9	8.2	8.3	18.4	20.2	23.6	24.8	53.3	56.4	73.3	77.0	104.6	109.6	574.8	693.7
19-Dec-99	0.0	0.0	7.4	8.8	8.1	8.9	19.2	20.1	24.5	26.8	53.3	56.4	74.4	77.0	69.2	107.4	20.3	740.7
20-Dec-99	0.0	0.0	9.7	11.1	9.3	10.1	19.2	21.8	23.6	25.8	49.5	55.0	56.4	62.5	28.2	31.2	30.9	30.0
21-Dec-99	0.0	0.0	8.7	9.9	7.6	9.5	18.5	21.0	21.8	23.8	44.9	47.5	53.7	53.8	31.1	29.4	47.9	45.2
22-Dec-99	0.0	0.0	8.6	10.0	7.6	8.3	18.5	18.7	22.7	22.0	42.5	44.0	56.4	53.9	37.9	36.2	72.1	67.4
23-Dec-99		0.0		10.0		9.0		18.6		22.0		46.4		55.8		44.8		101.3
24-Dec-99	0.0	0.0	7.6	10.0	8.3	8.3	17.9	19.5	21.0	22.0	46.2	45.2	59.4	59.7	51.8	53.2	86.1	129.3
25-Dec-99	0.0	0.0	7.6	10.0	7.1	8.3	17.1	18.6	21.0	22.0	43.8	47.5	57.5	59.6	36.0	45.9	27.8	69.1
26-Dec-99	0.0	0.0	7.5	8.8	8.2	8.3	17.8	17.9	20.1	23.0	42.6	45.2	49.2	54.9	14.5	25.1	11.7	26.8
27-Dec-99	0.0	0.0	7.5	8.8	7.7	7.7	17.8	18.7	20.0	22.0	38.1	42.8	14.5	39.2	0.0	3.1	0.0	3.1
28-Dec-99	0.0	0.0	8.6	8.8	7.0	7.7	16.3	17.9	18.3	21.1	19.6	28.4	11.1	11.8	0.1	0.1	1.1	1.2
29-Dec-99	0.0	0.0	6.2	9.9	6.5	8.4	14.9	17.3	15.0	18.6	13.7	17.6	13.7	14.6	1.9	1.1	5.3	5.4
30-Dec-99	0.0	0.0	8.5	10.2	7.0	7.8	16.2	15.9	15.0	16.9	17.3	16.2	17.8	17.4	5.5	4.3	12.3	11.9
31-Dec-99	0.0	0.0	7.4	10.1	6.4	6.7	14.8	15.1	14.2	14.5	16.5	16.8	22.0	21.0	9.6	8.7	18.4	19.8
1-Jan-00	0.0	0.0	6.2	8.9	5.4	7.1	13.0	15.7	13.5	15.2	17.3	18.3	25.7	26.7	13.8	13.4	32.2	30.1
2-Jan-00	0.0	0.0	7.3	9.0	5.8	5.5	14.2	14.4	13.5	15.3	21.1	20.7	33.3	30.5	20.8	18.9	47.6	48.4
3-Jan-00	0.0	0.0	6.2	8.8	5.4	6.1	13.5	15.1	13.5	14.5	22.7	22.3	39.6	37.5	32.8	29.3	79.4	84.4

Table K.6: Tailings matric suctions (at noon and midnight) measured with the Model-229 Campbell Scientific matric suction sensors installed on the Kidston tailings impoundment.

Date	Tailings matric suction (kPa)																	
	NC200 (2000 mm)		NC150 (1500 mm)		#18 (1250 mm)		#19 (1000 mm)		#17 (750 mm)		#21 (500 mm)		#15 (300 mm)		#20 (150 mm)		16 (50 mm)	
	PM	AM	PM	AM	PM	AM	PM	AM	PM	AM	PM	AM	PM	AM	PM	AM	PM	AM
4-Jan-00	0.0	0.0	6.1	9.9	6.4	7.1	14.9	15.0	16.6	15.9	29.0	26.5	48.2	43.2	46.5	41.3	122.3	123.4
5-Jan-00	0.0	0.0	7.3	8.7	6.4	7.1	14.2	15.1	15.7	16.0	30.8	30.2	53.5	50.1	53.8	51.9	153.9	162.0
6-Jan-00	0.0	0.0	6.1	8.7	4.8	6.5	15.4	15.7	14.8	19.2	35.7	38.2	57.1	58.4	63.1	62.3	203.2	240.8
7-Jan-00	0.0	0.0	7.3	8.9	7.6	7.7	17.7	16.4	19.0	19.4	42.4	40.6	63.0	62.5	64.7	74.6	93.7	237.2
8-Jan-00	0.0	0.0	7.4	7.7	7.0	7.2	16.3	16.5	19.0	20.2	31.8	40.6	15.1	40.8	0.1	0.1	0.0	0.0
9-Jan-00	0.0	0.0	8.6	10.0	7.0	7.7	16.9	17.1	17.4	19.2	22.0	26.5	17.1	16.6	2.2	1.6	5.9	4.2
10-Jan-00	0.0	0.0	6.2	7.6	5.9	7.8	13.0	15.8	13.5	16.0	18.0	20.6	17.9	18.7	4.2	4.3	10.8	11.0
11-Jan-00	0.0	0.0	5.1	8.8	5.4	7.7	12.4	15.8	12.8	16.7	18.9	21.4	15.2	23.7	0.5	8.6	1.1	18.7
12-Jan-00		0.0		7.6		6.6		14.5		15.3		18.3		8.6		0.0		0.0
13-Jan-00	0.0	0.0	7.5	6.4	5.4	6.6	12.4	13.8	8.8	11.6	3.0	4.0	7.8	8.0	0.0	0.0	0.1	0.0
14-Jan-00	0.0	0.0	6.3	9.0	5.4	6.1	10.6	12.5	7.6	8.3	4.4	4.5	8.4	9.2	0.0	0.0	3.0	1.2
15-Jan-00	0.0	0.0	5.0	6.5	3.9	5.6	9.4	10.8	6.4	8.3	4.4	4.6	10.4	9.8	1.6	1.4	6.6	5.4
16-Jan-00	0.0	0.0	8.6	8.8	4.4	5.0	8.9	10.2	6.4	7.8	6.4	6.6	15.1	12.6	4.2	4.4	11.6	11.8
17-Jan-00	0.0	0.0	5.0	6.5	3.4	4.5	8.9	9.6	6.4	7.1	6.9	7.6	18.5	18.0	8.0	7.1	15.7	18.8
18-Jan-00	0.0	0.0	6.2	8.8	3.0	4.5	8.9	9.6	6.9	7.7	9.2	8.8	23.5	22.9	12.5	12.1	25.4	24.7
19-Jan-00	0.0	0.0	7.4	8.8	3.0	4.0	9.4	10.1	6.4	7.1	10.4	9.9	27.9	27.4	16.4	16.0	34.4	37.4
20-Jan-00	0.0	0.0	4.9	6.4	2.5	4.0	8.9	10.1	5.8	6.5	12.9	12.5	33.2	31.2	23.8	21.8	56.4	54.1
21-Jan-00	0.0	0.0	6.2	8.8	3.4	4.5	10.0	10.7	7.5	8.9	17.2	17.4	39.7	37.5	34.7	33.1	87.3	86.1
22-Jan-00	0.0	0.0	4.9	6.4	3.4	4.0	10.5	10.7	8.7	8.2	22.7	22.3	41.3	42.3	9.6	42.5	4.6	121.2
23-Jan-00	0.0	0.0	6.1	7.7	4.3	4.0	10.5	11.3	8.7	8.9	20.3	21.4	28.6	31.2	8.0	7.1	10.0	8.8
24-Jan-00	0.0	0.0	3.5	6.4	3.3	4.0	9.4	11.9	5.7	8.3	17.9	20.5	26.3	28.1	9.6	10.3	16.5	16.9
25-Jan-00	0.0	0.0	7.4	7.7	3.9	4.5	11.7	11.9	8.1	8.3	19.6	20.7	25.7	28.2	7.0	7.1	12.4	10.3
26-Jan-00	0.0	0.0	7.4	7.6	4.3	4.5	11.7	11.8	8.1	9.5	18.8	20.5	28.6	28.1	11.9	10.9	21.3	19.6
27-Jan-00	0.0	0.0	4.9	8.8	3.8	5.5	11.1	11.9	8.7	10.1	19.5	21.3	33.2	32.0	18.5	15.3	30.8	31.2
28-Jan-00	0.0	0.0	6.2	6.4	4.3	4.5	10.5	12.5	8.7	9.5	20.3	21.3	36.4	35.1	24.8	21.8	49.1	46.8
29-Jan-00	0.0	0.0	6.2	7.6	4.8	5.0	11.7	11.8	8.7	10.1	23.6	23.0	41.3	39.1	31.8	29.3	66.5	62.1
30-Jan-00	0.0	0.0	6.2	7.6	4.4	5.5	12.9	13.1	10.0	10.1	28.9	25.6	49.0	45.0	43.1	40.1	107.3	101.3
31-Jan-00	0.0	0.0	6.2	6.4	4.4	5.5	13.5	11.9	10.0	11.5	32.8	30.2	54.4	52.1	55.2	50.6	157.3	152.3
1-Feb-00	0.0	0.0	7.4	7.6	4.9	5.0	13.5	13.8	11.3	11.5	36.9	37.3	60.1	58.6	69.1	66.8	238.7	245.7
2-Feb-00	0.0	0.0	6.2	8.8	4.9	5.5	13.6	15.1	11.3	13.7	41.3	43.8	65.1	64.3	83.8	82.6	406.3	417.8
3-Feb-00	0.0	0.0	5.0	8.8	6.5	6.6	14.9	15.8	14.3	14.5	47.1	48.8	69.2	69.7	100.7	97.4	519.1	571.1
4-Feb-00	0.0	0.0	6.2	10.0	7.6	7.7	17.7	16.5	19.1	20.2	52.0	54.0	75.5	72.7	113.0	107.7	697.9	726.4
5-Feb-00	0.0	0.0	7.4	7.7	8.2	8.3	18.5	19.4	23.6	23.8	56.1	59.2	77.8	78.1	120.1	125.5	1050	984.1
6-Feb-00	0.0	0.0	9.9	8.7	8.3	9.0	18.7	18.7	22.9	24.8	55.2	59.2	77.1	78.2	120.8	128.1	1316	1320
7-Feb-00	0.0	0.0	8.7	7.7	8.9	8.9	17.8	19.4	21.8	23.9	53.6	56.5	75.8	76.0	111.5	121.0	979.8	1284
8-Feb-00	0.0	0.0	7.6	9.9	8.3	9.5	19.3	19.4	22.8	22.9	55.0	56.6	76.9	77.1	111.5	118.8	809.0	990.7
9-Feb-00	0.0	0.0	9.8	9.9	10.1	9.6	19.3	19.5	24.6	24.9	54.9	58.0	79.0	77.1	115.7	116.4	673.0	816.3
10-Feb-00	0.0	0.0	9.8	11.1	10.1	10.1	20.8	21.1	25.6	26.8	57.6	60.7	79.0	80.4	117.9	123.3	735.2	853.1
11-Feb-00	0.0	0.0	8.6	11.0	10.6	10.2	20.7	21.8	25.5	27.8	57.3	60.7	81.1	80.4	124.5	125.6	764.1	918.1
12-Feb-00	0.0	0.0	8.5	8.7	10.0	10.8	20.7	22.6	26.5	26.9	61.4	63.5	79.8	80.4	124.1	125.7	817.4	1012
13-Feb-00	0.0	0.0	7.2	13.3	11.8	12.8	23.1	26.0	27.4	30.9	61.3	67.9	82.0	84.8	133.5	143.4	1119	1245
14-Feb-00	0.0	0.0	10.8	14.5	11.9	13.5	22.3	26.0	27.5	32.0	62.8	69.4	81.0	86.0	134.1	145.3	1323	1559
15-Feb-00	0.0	0.0	11.1	9.9	12.1	12.8	24.4	24.3	28.9	29.9	63.4	64.9	85.0	83.7	140.5	146.0	126.4	1518
16-Feb-00	0.0	0.0	8.6	12.3	10.6	12.8	22.4	24.4	25.5	28.9	57.4	62.1	75.5	81.5	73.9	114.1	64.9	78.3
17-Feb-00	0.0	0.0	9.8	9.9	9.4	12.2	20.8	22.7	24.6	27.0	53.5	59.2	67.2	75.0	45.6	55.9	37.1	69.2

Table K.6: Tailings matric suctions (at noon and midnight) measured with the Model-229 Campbell Scientific matric suction sensors installed on the Kidston tailings impoundment.

Date	Tailings matric suction (kPa)																	
	NC200 (2000 mm)		NC150 (1500 mm)		#18 (1250 mm)		#19 (1000 mm)		#17 (750 mm)		#21 (500 mm)		#15 (300 mm)		#20 (150 mm)		16 (50 mm)	
	PM	AM	PM	AM	PM	AM	PM	AM	PM	AM	PM	AM	PM	AM	PM	AM	PM	AM
18-Feb-00	0.0	0.0	8.6	11.2	10.6	12.2	20.8	20.9	25.6	27.0	52.1	53.8	57.3	64.5	17.2	34.1	14.0	20.7
19-Feb-00	0.0	0.0	12.0	11.0	11.3	12.2	23.2	21.9	27.5	25.9	48.3	48.8	41.3	47.6	11.3	11.5	17.5	13.4
20-Feb-00	0.0	0.0	9.7	11.1	10.7	10.9	20.0	21.8	22.7	24.7	36.9	42.8	35.7	37.5	11.3	12.1	22.3	19.6
21-Feb-00	0.0	0.0	10.9	11.1	11.3	10.2	20.7	21.1	24.5	24.9	39.0	37.2	35.7	35.9	8.5	12.2	14.0	16.1
22-Feb-00	0.0	0.0	8.6	10.0	10.0	10.2	18.5	21.0	20.9	23.0	32.9	37.3	30.3	32.8	8.0	9.2	14.1	15.1
23-Feb-00	0.0	0.0	9.7	11.2	9.4	9.6	18.4	18.7	20.8	21.2	31.9	32.2	27.2	30.5	5.5	8.7	10.1	8.1
24-Feb-00	0.0	0.0	9.8	9.8	8.3	9.5	17.8	19.5	20.1	20.3	25.5	28.3	11.8	21.5	0.1	0.5	1.2	0.8
25-Feb-00	0.0	0.0	7.6	11.1	8.9	8.9	17.1	17.1	17.6	19.4	6.0	21.4	7.2	7.9	0.0	0.0	0.0	0.0
26-Feb-00	0.0	0.0	7.5	10.1	8.2	8.9	14.3	15.8	6.4	13.7	1.0	1.8	7.2	7.9	0.0	0.0	0.0	0.0
27-Feb-00	0.0	0.0	8.7	11.1	6.5	7.7	9.5	12.5	1.8	3.5	1.0	1.4	7.8	7.2	0.0	0.0	0.0	0.0
28-Feb-00	0.0	0.0	9.9	10.0	5.5	5.5	7.0	7.5	2.1	1.8	2.2	2.2	7.8	7.9	0.0	0.0	2.6	2.1
29-Feb-00	0.0	0.0	7.5	7.6	3.5	4.1	6.0	7.5	1.1	1.8	1.8	2.7	7.8	9.2	0.0	0.5	1.2	4.3
1-Mar-00	0.0	0.0	5.1	7.7	1.8	3.1	4.3	6.1	0.0	1.1	0.1	1.0	6.5	6.6	0.0	0.0	0.0	0.0
2-Mar-00	0.0	0.0	5.1	7.7	0.4	1.8	1.8	3.3	0.0	0.0	0.0	0.7	5.1	7.9	0.0	0.0	0.0	0.0
3-Mar-00	0.0	0.0	1.0	8.9	0.0	0.7	0.8	2.2	0.0	0.0	0.0	1.1	5.8	8.6	0.0	0.0	0.4	0.8
4-Mar-00	0.0	0.0	3.8	5.4	0.0	0.0	1.3	1.6	0.0	0.0	1.4	1.5	7.1	7.3	0.7	1.1	5.4	4.3
5-Mar-00	0.0	0.0	2.4	5.5	0.0	0.0	1.3	2.2	0.0	0.0	1.7	1.9	9.7	10.6	3.0	2.7	10.9	8.9
6-Mar-00	0.0	0.0	2.4	4.1	0.0	0.0	1.8	1.9	0.0	0.0	3.0	2.3	15.1	13.3	5.1	5.2	16.6	14.4
7-Mar-00	0.0	0.0	2.3	2.6	0.0	0.0	1.8	1.9	0.0	0.0	4.3	3.6	19.9	18.1	10.8	9.3	23.3	21.7
8-Mar-00	0.0	0.0	0.0	3.9	0.0	0.0	1.8	2.8	0.0	0.0	4.8	5.4	25.0	23.7	14.5	13.9	32.1	31.2
9-Mar-00	0.0	0.0	2.5	3.9	0.0	0.0	2.8	3.6	0.1	0.1	7.5	8.7	30.3	28.9	21.7	21.0	49.4	48.2
10-Mar-00	0.0	0.0	0.0	5.2	0.0	0.0	2.8	3.6	0.0	0.1	9.9	10.0	31.9	34.3	23.3	27.7	45.1	60.5
11-Mar-00	0.0	0.0	2.5	2.6	0.1	0.0	3.9	4.4	0.5	0.1	13.8	12.5	35.8	35.9	23.3	25.1	50.9	49.7
12-Mar-00	0.0	0.0	5.1	3.9	0.1	0.0	4.7	4.8	1.1	0.8	16.6	14.7	39.0	37.6	30.1	27.8	61.7	57.4
13-Mar-00	0.0	0.0	1.0	5.2	0.0	0.4	5.5	5.2	1.7	1.4	18.8	18.2	42.3	40.0	36.8	35.1	85.6	76.6
14-Mar-00	0.0	0.0	2.4	4.0	0.1	0.2	5.5	5.7	2.9	2.2	21.2	21.5	49.0	46.7	50.2	46.1	125	109
15-Mar-00	0.0	0.0	2.4	6.4	0.6	0.7	6.9	6.5	6.4	3.9	26.3	25.7	55.5	53.9	59.3	58.4	168	153
16-Mar-00	0.0	0.0	3.8	4.0	0.6	1.1	8.4	8.0	9.4	9.5	33.9	31.3	64.2	62.4	77.2	74.6	264	252
17-Mar-00	0.0	0.0	1.0	3.9	0.4	1.8	7.9	9.1	8.8	11.6	35.0	37.3	62.3	68.6	80.9	90.0	276	338
18-Mar-00	0.0	0.0	5.1	5.3	2.2	1.4	10.6	10.2	12.9	11.6	37.1	40.6	40.7	65.5	5.1	18.2	6.6	3.7
19-Mar-00	0.0	0.0	5.1	6.5	2.1	1.8	11.2	11.3	12.1	12.3	28.2	31.2	25.8	28.2	6.0	5.7	10.9	7.4
20-Mar-00	0.0	0.0	5.1	5.2	2.2	2.2	11.2	11.4	11.5	13.1	23.8	26.6	27.3	28.2	8.0	7.7	15.0	14.3
21-Mar-00	0.0	0.0	3.8	5.4	2.1	2.2	10.0	10.7	10.7	12.3	23.7	24.8	31.0	29.6	12.0	10.9	24.4	22.7
22-Mar-00	0.0	0.0	3.8	6.6	1.7	2.7	9.5	10.8	10.7	11.6	22.9	24.9	34.2	34.4	17.9	17.5	34.6	32.5
23-Mar-00	0.0	0.0	3.7	6.5	2.1	2.3	10.6	11.4	12.8	13.0	28.1	26.6	39.7	37.6	24.8	23.5	50.6	47.0
24-Mar-00	0.0	0.0	6.2	6.6	2.5	2.2	10.5	11.9	12.8	12.3	27.9	28.4	46.4	43.3	36.8	33.3	83.3	70.9
25-Mar-00	0.0	0.0	6.2	7.7	2.9	3.5	11.1	13.1	12.8	15.2	31.8	35.2	55.4	53.9	55.2	54.5	145	135
26-Mar-00	0.0	0.0	7.3	6.5	3.4	3.5	13.0	13.8	15.0	17.7	41.2	39.5	68.1	64.5	75.4	74.6	243	232
27-Mar-00	0.0	0.0	5.0	7.7	3.4	4.0	14.2	15.1	19.0	18.5	48.4	46.4	76.6	75.9	104	101	390	387
28-Mar-00	0.0	0.0	4.9	7.8	4.3	5.5	15.6	17.2	20.0	21.2	55.9	58.0	86.8	85.2	137	133	610	609
29-Mar-00	0.0	0.0	7.4	9.0	5.4	6.1	19.2	18.7	24.5	25.0	64.5	63.8	96.8	93.8	178	174	923	860
30-Mar-00	0.0	0.0	6.2	7.8	7.6	7.2	20.8	21.1	29.5	29.0	73.7	70.0	103	102	210	212	1333	1160
31-Mar-00	0.0	0.0	6.2	10.0	8.2	9.6	23.3	24.4	32.9	34.3	75.4	77.8	112	110	253	246	1742	1527
1-Apr-00	0.0	0.0	7.4	11.2	10.1	11.6	26.8	27.2	36.3	38.1	80.5	83.1	119	116	272	293	2124	2199
2-Apr-00	0.0	0.0	9.8	7.7	11.4	10.9	25.9	26.3	37.7	35.7	84.3	83.1	119	114	300	298	2484	2377

Table K.6: Tailings matric suctions (at noon and midnight) measured with the Model-229 Campbell Scientific matric suction sensors installed on the Kidston tailings impoundment.

Date	Tailings matric suction (kPa)																	
	NC200 (2000 mm)		NC150 (1500 mm)		#18 (1250 mm)		#19 (1000 mm)		#17 (750 mm)		#21 (500 mm)		#15 (300 mm)		#20 (150 mm)		16 (50 mm)	
	PM	AM	PM	AM	PM	AM	PM	AM	PM	AM	PM	AM	PM	AM	PM	AM	PM	AM
3-Apr-00	0.0	0.0	8.7	11.1	12.1	12.8	26.0	28.0	36.6	39.2	77.5	83.0	109	115	196	320	36.0	40.0
4-Apr-00	0.0	0.0	9.9	9.0	12.1	12.9	24.3	27.1	33.1	36.7	71.0	78.1	83.7	103	13.9	65.7	6.7	37.4
5-Apr-00	0.0	0.0	6.3	10.0	10.1	12.1	23.3	26.2	29.7	33.3	54.9	66.7	36.5	53.0	7.1	7.6	9.4	9.6
6-Apr-00	0.0	0.0	9.7	13.7	11.3	12.3	24.1	26.3	32.9	33.5	48.4	52.9	36.5	37.7	9.6	9.8	17.6	16.1
7-Apr-00	0.0	0.0	6.3	12.3	8.8	12.8	20.8	24.4	26.6	32.2	40.3	48.8	37.3	37.5	13.2	14.7	22.4	24.7
8-Apr-00	0.0	0.0	6.5	11.2	6.0	11.6	11.9	22.7	0.0	30.1	0.1	1.5	6.5	8.6	0.0	0.0	0.0	0.0
9-Apr-00	0.0	0.0	8.7	10.0	2.6	5.5	1.6	4.8	0.0	0.0	0.7	1.4	8.5	9.2	0.0	0.0	0.0	0.0
10-Apr-00	0.0	0.0	8.7	8.8	0.4	2.2	1.3	1.6	0.0	0.0	1.0	1.1	9.8	8.5	0.0	0.0	0.4	0.2
11-Apr-00	0.0	0.0	2.5	7.6	0.0	0.1	0.8	1.6	0.0	0.0	0.1	1.4	7.2	9.9	0.0	0.3	2.1	3.2
12-Apr-00	0.0	0.0	2.5	6.4	0.0	0.0	1.3	1.3	0.0	0.0	1.8	1.1	10.4	9.9	1.9	1.3	5.4	4.2
13-Apr-00	0.0	0.0	1.1	5.3	0.0	0.0	1.0	1.3	0.0	0.0	1.8	1.8	9.8	9.9	2.0	2.3	6.7	6.8
14-Apr-00	0.0	0.0	0.0	5.4	0.0	0.0	1.3	2.2	0.0	0.0	2.6	3.1	13.8	14.6	3.0	3.9	8.0	8.8
15-Apr-00	0.0	0.0	0.9	3.9	0.0	0.0	1.8	1.9	0.0	0.0	3.0	4.5	15.8	16.7	5.1	5.7	10.9	12.7
16-Apr-00	0.0	0.0	1.0	4.0	0.0	0.0	1.9	2.6	0.0	0.0	4.4	4.5	19.3	19.5	7.5	7.7	16.7	16.9
17-Apr-00	0.0	0.0	3.7	5.2	0.0	0.0	2.1	2.2	0.0	0.0	5.9	5.5	22.1	22.3	10.2	10.4	20.3	22.7
18-Apr-00	0.0	0.0	2.4	2.8	0.0	0.0	2.5	2.9	0.0	0.0	8.1	7.7	25.0	27.4	13.2	14.0	26.6	26.9
19-Apr-00	0.0	0.0	2.3	4.0	0.0	0.0	3.1	3.3	0.0	0.0	9.8	9.5	31.0	29.7	17.2	17.5	34.5	33.8
20-Apr-00	0.0	0.0	2.5	3.9	0.0	0.0	3.5	3.6	1.0	0.5	12.4	11.3	32.6	33.6	20.9	21.9	42.3	41.3
21-Apr-00	0.0	0.0	6.3	5.2	0.0	0.1	3.9	4.3	3.4	2.2	15.1	15.3	35.7	36.7	25.7	25.9	50.7	52.6
22-Apr-00	0.0	0.0	5.0	2.7	0.0	0.0	5.1	4.4	4.3	3.5	18.8	16.8	42.2	40.0	34.8	32.3	66.7	64.1
23-Apr-00	0.0	0.0	3.8	4.0	0.1	0.0	5.6	5.2	5.3	5.5	21.2	20.6	46.5	44.2	40.0	39.3	77.9	74.7
24-Apr-00	0.0	0.0	1.0	5.3	0.0	0.1	5.1	5.7	4.9	6.0	15.9	23.1	10.5	39.2	0.0	0.0	0.0	0.0
25-Apr-00	0.0	0.0	6.5	5.3	0.7	0.1	7.0	6.6	6.5	6.0	2.6	12.6	8.5	9.9	0.0	0.0	0.0	0.0
26-Apr-00	0.0	0.0	1.3	5.3	0.0	0.8	4.8	6.1	1.9	3.5	1.1	1.5	6.6	8.6	0.0	0.0	0.0	0.0
27-Apr-00	0.0	0.0	1.2	2.7	0.0	0.2	4.0	5.3	0.3	1.5	1.4	2.3	7.9	7.2	0.0	0.0	0.2	0.5
28-Apr-00	0.0	0.0	2.7	4.2	0.0	0.1	3.6	3.6	0.5	0.8	2.2	2.7	7.2	8.6	0.0	0.0	1.7	1.7
29-Apr-00	0.0	0.0	3.9	4.0	0.0	0.0	3.2	3.6	0.8	0.6	2.6	2.3	8.5	9.2	0.3	0.5	3.7	3.7
30-Apr-00	0.0	0.0	0.0	2.8	0.0	0.0	2.8	3.6	0.3	0.8	2.2	3.1	9.2	10.0	1.0	1.7	3.6	5.6
1-May-00	0.0	0.0	1.0	1.4	0.0	0.0	3.2	4.0	1.1	1.1	3.9	3.6	11.1	11.3	3.1	3.1	9.4	7.5
2-May-00	0.0	0.0	2.4	4.1	0.0	0.2	3.5	4.4	1.4	1.5	3.9	4.6	14.4	15.3	4.3	4.8	10.9	12.8
10-May-00	0.0		0.0		0.0		5.6		5.4		18.2		40.7		30.3		57.1	
11-May-00	0.0	0.0	2.6	5.4	0.1	0.2	6.1	7.1	7.0	7.3	22.2	23.4	44.1	43.4	35.0	34.5	70.7	71.3
12-May-00	0.0	0.0	2.6	4.0	0.0	0.4	6.5	7.6	7.6	9.0	24.7	24.2	51.1	47.8	42.4	40.9	84.0	87.3
13-May-00	0.0	0.0	0.0	2.7	0.0	1.1	8.0	9.2	8.9	9.7	27.4	27.8	53.7	52.3	49.3	48.7	99.0	105
14-May-00	0.0	0.0	1.0	4.3	0.4	0.4	8.4	8.1	10.1	9.7	30.1	30.4	54.6	57.1	52.9	53.5	113	117
15-May-00	0.0	0.0	2.6	4.2	0.4	0.8	9.0	9.7	11.5	11.8	34.0	32.5	61.3	60.0	59.6	60.5	131	133
16-May-00	0.0	0.0	1.0	4.2	0.4	1.9	9.5	11.5	12.9	14.0	38.3	36.6	65.4	62.8	66.7	70.5	155	160
17-May-00	0.0	0.0	1.1	5.3	1.0	1.2	10.7	10.9	14.4	14.7	40.4	39.9	70.5	67.7	75.8	78.6	175	177
18-May-00	0.0	0.0	3.9	4.0	1.8	1.1	11.3	12.0	16.8	16.1	45.1	44.1	71.5	70.8	82.8	83.2	194	192
19-May-00	0.0	0.0	5.3	5.4	1.8	1.5	12.6	12.6	16.9	16.2	45.3	45.4	66.6	74.0	25.2	83.2	12.7	15.2
20-May-00	0.0	0.0	4.0	4.1	1.8	2.3	11.9	13.3	16.8	16.9	38.4	42.0	43.3	54.0	10.9	14.1	15.2	15.3
21-May-00	0.0	0.0	5.2	4.1	2.2	2.2	11.9	13.3	16.8	16.9	33.2	38.6	37.5	40.9	12.7	13.5	19.7	18.9
22-May-00	0.0	0.0	3.9	4.3	2.2	2.2	12.5	12.0	16.0	16.1	30.2	34.3	37.5	37.6	13.3	12.8	21.6	21.7

Table K.7: Tailings volumetric water contents (at noon and midnight) calculated from the matric suctions measured with the Model-229 Campbell Scientific matric suction sensors installed on the Kidston tailings impoundment.

Date	Tailings volumetric water content (fraction)																	
	NC200 (2000 mm)		NC150 (1500 mm)		#18 (1250 mm)		#19 (1000 mm)		#17 (750 mm)		#21 (500 mm)		#15 (300 mm)		#20 (150 mm)		16 (50 mm)	
	PM	AM	PM	AM	PM	AM	PM	AM	PM	AM	PM	AM	AM	PM	PM	AM	PM	AM
24-Oct-97	0.43	0.41	0.25	0.22	0.42	0.39	0.31	0.28	0.30	0.28	0.13	0.12	0.13	0.13	0.19	0.19	0.11	0.10
25-Oct-97	0.43	0.43	0.25	0.23	0.40	0.41	0.28	0.28	0.28	0.27	0.13	0.13	0.13	0.13	0.18	0.19	0.12	0.10
26-Oct-97	0.44	0.42	0.26	0.23	0.40	0.40	0.30	0.29	0.29	0.27	0.13	0.13	0.14	0.13	0.18	0.19	0.11	0.10
27-Oct-97	0.43	0.43	0.24	0.23	0.40	0.41	0.29	0.29	0.29	0.27	0.13	0.13	0.14	0.13	0.19	0.18	0.12	0.10
28-Oct-97	0.43	0.42	0.24	0.23	0.41	0.40	0.29	0.29	0.29	0.28	0.13	0.13	0.13	0.13	0.18	0.20	0.11	0.10
29-Oct-97	0.44	0.42	0.25	0.23	0.41	0.40	0.31	0.28	0.30	0.28	0.14	0.13	0.13	0.13	0.18	0.19	0.12	0.10
30-Oct-97	0.43	0.43	0.25	0.25	0.41	0.40	0.31	0.29	0.29	0.27	0.13	0.13	0.13	0.13	0.19	0.19	0.13	0.10
31-Oct-97	0.43	0.43	0.25	0.24	0.40	0.39	0.28	0.29	0.29	0.29	0.13	0.13	0.13	0.13	0.18	0.18	0.11	0.10
1-Nov-97	0.44	0.43	0.25	0.22	0.40	0.41	0.30	0.28	0.29	0.27	0.14	0.13	0.13	0.13	0.19	0.19	0.12	0.10
2-Nov-97	0.43	0.43	0.25	0.25	0.41	0.40	0.30	0.29	0.29	0.29	0.13	0.13	0.13	0.14	0.19	0.19	0.12	0.10
5-Nov-97	0.43	0.43	0.24	0.22	0.39	0.38	0.28	0.29	0.27	0.28	0.14	0.13	0.14	0.13	0.18	0.18	0.12	0.10
6-Nov-97	0.44	0.43	0.25	0.24	0.42	0.39	0.31	0.28	0.30	0.28	0.14	0.14	0.13	0.13	0.19	0.18	0.12	0.10
7-Nov-97	0.43	0.43	0.26	0.23	0.40	0.40	0.31	0.28	0.32	0.28	0.14	0.13	0.13	0.14	0.19	0.19	0.13	0.10
8-Nov-97	0.44	0.44	0.25	0.22	0.40	0.39	0.30	0.29	0.29	0.27	0.13	0.13	0.14	0.13	0.19	0.18	0.12	0.10
9-Nov-97	0.44	0.43	0.26	0.25	0.41	0.40	0.32	0.30	0.29	0.29	0.14	0.13	0.13	0.13	0.18	0.18	0.11	0.10
10-Nov-97	0.43	0.43	0.23	0.24	0.40	0.39	0.30	0.29	0.29	0.27	0.14	0.14	0.14	0.15	0.32	0.18	0.36	0.14
11-Nov-97	0.43	0.43	0.25	0.22	0.42	0.39	0.34	0.29	0.32	0.29	0.17	0.14	0.18	0.19	0.34	0.35	0.28	0.28
12-Nov-97	0.44	0.44	0.25	0.25	0.41	0.40	0.31	0.31	0.32	0.31	0.18	0.16	0.19	0.18	0.31	0.32	0.25	0.23
13-Nov-97	0.44	0.43	0.25	0.25	0.41	0.40	0.32	0.31	0.32	0.29	0.18	0.17	0.18	0.17	0.29	0.31	0.21	0.19
14-Nov-97	0.44	0.44	0.28	0.24	0.41	0.40	0.33	0.31	0.32	0.30	0.18	0.17	0.17	0.17	0.28	0.29	0.18	0.16
15-Nov-97	0.44	0.43	0.26	0.23	0.41	0.40	0.32	0.31	0.32	0.31	0.16	0.16	0.16	0.16	0.25	0.25	0.18	0.14
16-Nov-97	0.43	0.43	0.25	0.25	0.41	0.40	0.32	0.30	0.30	0.30	0.16	0.16	0.16	0.15	0.24	0.24	0.17	0.14
17-Nov-97	0.44	0.43	0.25	0.24	0.41	0.39	0.30	0.29	0.31	0.29	0.16	0.16	0.15	0.15	0.21	0.21	0.14	0.12
18-Nov-97	0.44	0.43	0.25	0.23	0.40	0.39	0.32	0.29	0.30	0.30	0.16	0.15	0.15	0.15	0.21	0.22	0.16	0.11
19-Nov-97	0.43	0.43	0.25	0.22	0.40	0.39	0.30	0.29	0.29	0.28	0.16	0.15	0.15	0.15	0.19	0.20	0.13	0.10
20-Nov-97	0.44	0.43	0.23	0.23	0.40	0.38	0.29	0.29	0.32	0.29	0.16	0.15	0.14	0.14	0.20	0.19	0.13	0.10
21-Nov-97	0.43	0.44	0.24	0.23	0.40	0.38	0.31	0.29	0.29	0.29	0.15	0.15	0.14	0.15	0.21	0.21	0.14	0.12
22-Nov-97	0.43	0.43	0.25	0.22	0.39	0.38	0.31	0.29	0.29	0.29	0.15	0.14	0.14	0.14	0.20	0.20	0.13	0.10
23-Nov-97	0.44	0.43	0.23	0.22	0.40	0.38	0.31	0.29	0.32	0.27	0.14	0.14	0.14	0.14	0.18	0.18	0.12	0.10
24-Nov-97	0.44	0.44	0.23	0.22	0.39	0.39	0.31	0.29	0.27	0.27	0.14	0.14	0.14	0.14	0.19	0.18	0.12	0.10
25-Nov-97	0.44	0.43	0.24	0.23	0.40	0.39	0.31	0.28	0.30	0.27	0.16	0.14	0.14	0.14	0.19	0.18	0.13	0.09
26-Nov-97	0.44	0.44	0.23	0.23	0.39	0.38	0.31	0.30	0.30	0.27	0.16	0.14	0.14	0.14	0.19	0.16	0.13	0.10
27-Nov-97	0.44	0.43	0.22	0.23	0.38	0.39	0.29	0.29	0.31	0.27	0.16	0.14	0.14	0.14	0.21	0.19	0.22	0.10
28-Nov-97	0.44	0.44	0.25	0.23	0.40	0.38	0.32	0.29	0.30	0.28	0.16	0.15	0.15	0.15	0.25	0.23	0.21	0.17
29-Nov-97	0.44	0.44	0.23	0.21	0.39	0.39	0.31	0.29	0.30	0.29	0.16	0.16	0.16	0.15	0.25	0.24	0.19	0.15
30-Nov-97	0.44	0.44	0.25	0.22	0.39	0.39	0.31	0.30	0.30	0.27	0.16	0.15	0.15	0.15	0.22	0.23	0.17	0.14
1-Dec-97	0.44	0.44	0.24	0.22	0.38	0.38	0.29	0.29	0.29	0.28	0.15	0.15	0.15	0.14	0.22	0.20	0.17	0.13
2-Dec-97	0.44	0.44	0.22	0.22	0.39	0.39	0.30	0.29	0.29	0.29	0.16	0.16	0.15	0.15	0.23	0.22	0.17	0.13
3-Dec-97	0.44	0.44	0.24	0.23	0.39	0.38	0.30	0.29	0.31	0.29	0.16	0.15	0.15	0.15	0.23	0.22	0.14	0.13
4-Dec-97	0.44	0.43	0.24	0.22	0.39	0.38	0.30	0.28	0.30	0.27	0.15	0.15	0.15	0.14	0.22	0.21	0.16	0.12
5-Dec-97	0.44	0.44	0.23	0.22	0.40	0.38	0.30	0.29	0.30	0.27	0.15	0.15	0.14	0.14	0.20	0.21	0.13	0.11
12-Dec-97	0.44	0.44	0.34	0.28	0.43	0.43	0.40	0.38	0.39	0.37	0.23	0.22	0.18	0.19	0.29	0.26	0.18	0.15
13-Dec-97	0.44	0.44	0.28	0.30	0.42	0.42	0.37	0.38	0.36	0.37	0.21	0.22	0.18	0.17	0.26	0.27	0.17	0.16

Table K.7: Tailings volumetric water contents (at noon and midnight) calculated from the matric suctions measured with the Model-229 Campbell Scientific matric suction sensors installed on the Kidston tailings impoundment.

Date	Tailings volumetric water content (fraction)																	
	NC200 (2000 mm)		NC150 (1500 mm)		#18 (1250 mm)		#19 (1000 mm)		#17 (750 mm)		#21 (500 mm)		#15 (300 mm)		#20 (150 mm)		16 (50 mm)	
	PM	AM	PM	AM	PM	AM	PM	AM	PM	AM	PM	AM	AM	PM	PM	AM	PM	AM
14-Dec-97	0.44	0.44	0.32	0.32	0.43	0.43	0.39	0.38	0.37	0.37	0.21	0.22	0.17	0.17	0.18	0.19	0.43	0.10
15-Dec-97	0.44	0.44	0.31	0.30	0.43	0.42	0.39	0.38	0.38	0.37	0.27	0.22	0.22	0.37	0.44	0.43	0.44	0.43
16-Dec-97	0.44	0.44	0.32	0.31	0.43	0.42	0.40	0.39	0.41	0.39	0.35	0.31	0.35	0.37	0.44	0.43	0.44	0.43
17-Dec-97	0.44	0.44	0.33	0.32	0.43	0.43	0.40	0.40	0.41	0.40	0.34	0.35	0.35	0.33	0.43	0.43	0.43	0.38
18-Dec-97	0.44	0.44	0.34	0.32	0.43	0.43	0.41	0.41	0.41	0.41	0.35	0.35	0.33	0.33	0.43	0.40	0.43	0.32
19-Dec-97	0.44	0.44	0.30	0.34	0.43	0.43	0.40	0.41	0.40	0.41	0.31	0.35	0.30	0.27	0.41	0.39	0.38	0.27
20-Dec-97	0.44	0.44	0.32	0.34	0.43	0.43	0.40	0.41	0.39	0.41	0.31	0.33	0.27	0.26	0.41	0.35	0.39	0.24
21-Dec-97	0.44	0.44	0.34	0.34	0.43	0.43	0.42	0.41	0.42	0.41	0.33	0.31	0.22	0.29	0.42	0.36	0.39	0.24
22-Dec-97	0.44	0.44	0.33	0.33	0.43	0.43	0.41	0.41	0.41	0.41	0.33	0.33	0.27	0.30	0.43	0.36	0.43	0.41
23-Dec-97	0.44	0.44	0.34	0.34	0.43	0.43	0.41	0.41	0.41	0.40	0.38	0.25	0.34	0.41	0.44	0.43	0.44	0.43
24-Dec-97	0.44	0.44	0.34	0.34	0.43	0.43	0.41	0.41	0.42	0.42	0.42	0.41	0.40	0.42	0.44	0.43	0.44	0.43
25-Dec-97	0.44	0.44	0.34	0.34	0.43	0.43	0.41	0.41	0.42	0.42	0.41	0.41	0.39	0.39	0.44	0.43	0.44	0.42
26-Dec-97	0.44	0.44	0.36	0.35	0.43	0.43	0.42	0.41	0.43	0.43	0.41	0.41	0.38	0.38	0.43	0.43	0.43	0.38
27-Dec-97	0.44	0.44	0.34	0.35	0.43	0.43	0.42	0.42	0.43	0.42	0.39	0.40	0.29	0.34	0.43	0.41	0.41	0.33
28-Dec-97	0.44	0.44	0.38	0.35	0.44	0.43	0.42	0.42	0.43	0.43	0.41	0.39	0.33	0.41	0.43	0.41	0.44	0.43
29-Dec-97	0.44	0.44	0.39	0.38	0.44	0.43	0.42	0.42	0.43	0.43	0.43	0.41	0.37	0.37	0.43	0.43	0.43	0.44
30-Dec-97	0.44	0.44	0.34	0.38	0.43	0.43	0.42	0.37	0.40	0.40	0.41	0.40	0.38	0.37	0.43	0.44	0.44	0.44
31-Dec-97		0.44		0.36		0.43		0.38		0.40		0.42	0.38			0.44		0.44
22-Oct-98	0.44	0.44	0.42	0.41	0.40	0.40	0.33	0.33	0.36	0.35	0.24	0.25	0.19	0.18	0.29	0.29	0.23	0.18
23-Oct-98	0.44	0.44	0.42	0.42	0.41	0.41	0.34	0.33	0.37	0.36	0.26	0.25	0.19	0.24	0.42	0.36	0.40	0.41
24-Oct-98	0.44	0.44	0.43	0.42	0.42	0.40	0.37	0.33	0.40	0.37	0.30	0.26	0.25	0.26	0.41	0.41	0.37	0.37
25-Oct-98	0.44	0.44	0.43	0.42	0.41	0.41	0.36	0.34	0.40	0.38	0.29	0.27	0.25	0.25	0.39	0.40	0.37	0.32
26-Oct-98	0.44	0.44	0.43	0.42	0.42	0.41	0.37	0.34	0.41	0.39	0.30	0.28	0.23	0.23	0.37	0.37	0.32	0.28
27-Oct-98	0.44	0.44	0.43	0.43	0.42	0.41	0.35	0.35	0.38	0.39	0.28	0.29	0.23	0.21	0.35	0.36	0.30	0.25
28-Oct-98	0.44	0.44	0.43	0.43	0.41	0.40	0.35	0.34	0.39	0.37	0.29	0.27	0.21	0.21	0.34	0.34	0.24	0.22
29-Oct-98	0.44	0.44	0.43	0.42	0.42	0.40	0.37	0.34	0.40	0.38	0.28	0.25	0.20	0.20	0.33	0.32	0.28	0.19
30-Oct-98	0.44	0.44	0.41	0.42	0.41	0.40	0.34	0.34	0.37	0.37	0.24	0.25	0.19	0.18	0.29	0.31	0.23	0.18
31-Oct-98	0.44	0.44	0.43	0.42	0.41	0.40	0.35	0.34	0.37	0.35	0.25	0.25	0.18	0.18	0.28	0.25	0.24	0.15
1-Nov-98	0.44	0.44	0.41	0.42	0.40	0.40	0.33	0.33	0.34	0.34	0.24	0.24	0.18	0.23	0.42	0.38	0.40	0.40
2-Nov-98	0.44	0.44	0.43	0.42	0.41	0.40	0.35	0.34	0.37	0.35	0.30	0.26	0.28	0.33	0.43	0.43	0.43	0.43
3-Nov-98	0.44	0.44	0.43	0.42	0.41	0.40	0.35	0.34	0.38	0.35	0.33	0.29	0.30	0.30	0.43	0.43	0.40	0.41
4-Nov-98	0.44	0.44	0.43	0.42	0.41	0.41	0.35	0.34	0.37	0.37	0.30	0.30	0.28	0.27	0.40	0.41	0.35	0.35
5-Nov-98	0.44	0.44	0.42	0.41	0.41	0.41	0.35	0.35	0.38	0.37	0.30	0.30	0.26	0.24	0.38	0.38	0.29	0.28
6-Nov-98	0.44	0.44	0.43	0.42	0.42	0.41	0.36	0.35	0.39	0.38	0.31	0.30	0.24	0.23	0.37	0.35	0.28	0.25
7-Nov-98	0.44	0.44	0.43	0.41	0.42	0.41	0.37	0.35	0.40	0.38	0.30	0.27	0.22	0.22	0.35	0.34	0.28	0.21
8-Nov-98	0.44	0.44	0.44	0.41	0.43	0.41	0.37	0.34	0.40	0.39	0.31	0.27	0.21	0.21	0.33	0.33	0.26	0.21
9-Nov-98	0.44	0.44	0.43	0.43	0.41	0.41	0.34	0.35	0.36	0.35	0.26	0.27	0.20	0.19	0.31	0.31	0.24	0.18
10-Nov-98	0.44	0.44	0.43	0.42	0.41	0.40	0.34	0.35	0.35	0.35	0.26	0.25	0.19	0.18	0.29	0.30	0.18	0.17
11-Nov-98	0.44	0.44	0.43	0.42	0.41	0.40	0.33	0.33	0.35	0.35	0.24	0.25	0.18	0.16	0.25	0.27	0.16	0.16
12-Nov-98		0.44		0.42		0.40		0.34		0.35		0.23	0.17			0.23		0.13
15-Nov-98	0.44		0.42		0.40		0.34		0.37		0.29			0.25	0.40		0.38	
16-Nov-98	0.44	0.44	0.41	0.42	0.40	0.40	0.35	0.33	0.36	0.35	0.29	0.29	0.25	0.25	0.39	0.39	0.36	0.31
17-Nov-98	0.44	0.44	0.40	0.40	0.41	0.40	0.35	0.33	0.38	0.37	0.29	0.29	0.23	0.22	0.36	0.37	0.32	0.26

Table K.7: Tailings volumetric water contents (at noon and midnight) calculated from the matric suctions measured with the Model-229 Campbell Scientific matric suction sensors installed on the Kidston tailings impoundment.

Date	Tailings volumetric water content (fraction)																	
	NC200 (2000 mm)		NC150 (1500 mm)		#18 (1250 mm)		#19 (1000 mm)		#17 (750 mm)		#21 (500 mm)		#15 (300 mm)		#20 (150 mm)		16 (50 mm)	
	PM	AM	PM	AM	PM	AM	PM	AM	PM	AM	PM	AM	AM	PM	PM	AM	PM	AM
18-Nov-98	0.44	0.44	0.43	0.43	0.41	0.41	0.35	0.35	0.39	0.38	0.29	0.29	0.23	0.25	0.42	0.39	0.39	0.38
19-Nov-98	0.44	0.44	0.43	0.41	0.41	0.41	0.35	0.35	0.39	0.38	0.31	0.29	0.26	0.27	0.43	0.41	0.41	0.33
20-Nov-98	0.44	0.44	0.44	0.42	0.42	0.40	0.37	0.35	0.41	0.39	0.33	0.30	0.28	0.27	0.41	0.42	0.38	0.36
21-Nov-98	0.44	0.44	0.43	0.42	0.42	0.41	0.37	0.35	0.40	0.40	0.31	0.30	0.25	0.26	0.40	0.40	0.35	0.31
22-Nov-98	0.44	0.44	0.43	0.42	0.42	0.41	0.35	0.36	0.41	0.40	0.30	0.29	0.25	0.26	0.41	0.40	0.40	0.32
23-Nov-98	0.44	0.44	0.43	0.42	0.42	0.41	0.37	0.35	0.41	0.39	0.32	0.29	0.27	0.30	0.43	0.43	0.43	0.43
24-Nov-98	0.44	0.44	0.43	0.41	0.42	0.41	0.36	0.35	0.41	0.40	0.30	0.29	0.28	0.28	0.42	0.42	0.39	0.40
25-Nov-98	0.44	0.44	0.43	0.39	0.41	0.40	0.36	0.34	0.41	0.41	0.32	0.31	0.28	0.26	0.40	0.41	0.36	0.34
26-Nov-98	0.44	0.44	0.44	0.42	0.43	0.42	0.38	0.35	0.41	0.41	0.35	0.32	0.27	0.28	0.40	0.40	0.37	0.30
27-Nov-98		0.44		0.43		0.41		0.36		0.39		0.31	0.24			0.38		0.28
29-Nov-98	0.44		0.44		0.42		0.36		0.39		0.31			0.21	0.34		0.29	
30-Nov-98	0.44	0.44	0.40	0.42	0.39	0.41	0.34	0.36	0.36	0.38	0.26	0.28	0.20	0.19	0.30	0.31	0.27	0.20
1-Dec-98	0.44	0.44	0.42	0.43	0.41	0.41	0.34	0.35	0.36	0.37	0.24	0.27	0.19	0.17	0.28	0.30	0.22	0.18
2-Dec-98	0.44	0.44	0.42	0.43	0.41	0.41	0.35	0.36	0.36	0.37	0.25	0.26	0.19	0.17	0.28	0.29	0.21	0.16
3-Dec-98	0.44	0.44	0.42	0.41	0.41	0.40	0.37	0.34	0.37	0.36	0.26	0.24	0.18	0.17	0.26	0.26	0.19	0.15
4-Dec-98	0.44	0.44	0.42	0.42	0.41	0.41	0.35	0.34	0.36	0.36	0.24	0.25	0.17	0.17	0.25	0.25	0.17	0.14
5-Dec-98	0.44	0.44	0.43	0.41	0.40	0.40	0.33	0.34	0.34	0.34	0.22	0.23	0.17	0.16	0.22	0.23	0.19	0.12
6-Dec-98	0.44	0.44	0.43	0.43	0.41	0.40	0.34	0.33	0.33	0.33	0.21	0.23	0.16	0.15	0.23	0.22	0.17	0.12
7-Dec-98	0.44	0.44	0.42	0.40	0.41	0.40	0.34	0.31	0.34	0.32	0.22	0.21	0.15	0.15	0.21	0.21	0.18	0.12
8-Dec-98	0.44	0.44	0.40	0.41	0.38	0.40	0.31	0.31	0.33	0.33	0.21	0.22	0.16	0.15	0.20	0.21	0.16	0.11
9-Dec-98	0.44	0.44	0.43	0.41	0.41	0.39	0.32	0.32	0.32	0.32	0.20	0.21	0.15	0.15	0.19	0.20	0.13	0.11
10-Dec-98	0.44	0.44	0.42	0.40	0.39	0.40	0.31	0.32	0.32	0.32	0.19	0.20	0.14	0.14	0.18	0.18	0.11	0.10
11-Dec-98		0.44		0.41		0.39		0.31		0.32		0.19	0.14			0.17		0.10
12-Dec-98	0.44		0.38		0.38		0.30		0.29		0.18			0.13	0.18		0.13	0.44
13-Dec-98	0.44	0.44	0.42	0.41	0.40	0.37	0.30	0.31	0.31	0.31	0.20	0.19	0.15	0.16	0.31	0.23	0.29	0.28
14-Dec-98	0.44	0.44	0.42	0.41	0.39	0.38	0.32	0.31	0.33	0.30	0.22	0.21	0.17	0.17	0.33	0.32	0.29	0.23
15-Dec-98	0.44	0.44	0.37	0.40	0.38	0.39	0.30	0.31	0.31	0.32	0.22	0.21	0.18	0.17	0.32	0.30	0.29	0.21
16-Dec-98	0.44	0.44	0.43	0.42	0.41	0.39	0.35	0.32	0.36	0.33	0.23	0.22	0.18	0.18	0.30	0.30	0.27	0.19
17-Dec-98	0.44	0.44	0.42	0.41	0.41	0.39	0.34	0.32	0.34	0.33	0.22	0.23	0.17	0.17	0.28	0.26	0.25	0.16
18-Dec-98	0.44	0.44	0.37	0.38	0.37	0.38	0.30	0.32	0.30	0.32	0.20	0.21	0.17	0.15	0.23	0.25	0.19	0.16
19-Dec-98	0.44	0.44	0.40	0.42	0.38	0.39	0.31	0.32	0.32	0.33	0.21	0.21	0.17	0.17	0.31	0.27	0.27	0.21
20-Dec-98	0.44	0.44	0.40	0.41	0.39	0.40	0.32	0.32	0.33	0.32	0.22	0.23	0.18	0.18	0.34	0.31	0.29	0.27
21-Dec-98	0.44	0.44	0.41	0.41	0.40	0.40	0.33	0.33	0.34	0.33	0.24	0.23	0.20	0.20	0.37	0.34	0.37	0.26
22-Dec-98	0.44	0.44	0.43	0.40	0.41	0.40	0.34	0.32	0.35	0.33	0.27	0.24	0.23	0.26	0.43	0.41	0.41	0.41
23-Dec-98	0.44	0.44	0.42	0.42	0.40	0.40	0.34	0.33	0.34	0.34	0.29	0.26	0.27	0.30	0.43	0.43	0.42	0.43
24-Dec-98		0.44		0.42		0.40		0.33		0.34		0.28	0.29			0.43		0.39
27-Dec-98	0.44		0.41		0.41		0.34		0.36		0.29			0.22	0.36		0.28	
28-Dec-98	0.44	0.44	0.44	0.42	0.42	0.41	0.36	0.35	0.39	0.37	0.29	0.28	0.22	0.23	0.36	0.34	0.34	0.23
29-Dec-98	0.44	0.44	0.43	0.43	0.42	0.41	0.36	0.35	0.37	0.36	0.28	0.29	0.22	0.22	0.39	0.34	0.37	0.23
30-Dec-98	0.44	0.44	0.43	0.42	0.42	0.40	0.35	0.35	0.38	0.35	0.29	0.28	0.24	0.26	0.42	0.41	0.39	0.39
31-Dec-98	0.44	0.44	0.43	0.42	0.42	0.41	0.35	0.34	0.37	0.36	0.31	0.29	0.25	0.30	0.43	0.42	0.43	0.42
1-Jan-99	0.44	0.44	0.43	0.42	0.42	0.41	0.37	0.35	0.37	0.36	0.32	0.30	0.30	0.30	0.43	0.43	0.41	0.40
2-Jan-99	0.44	0.44	0.42	0.42	0.41	0.41	0.35	0.35	0.36	0.36	0.31	0.31	0.29	0.28	0.41	0.42	0.39	0.36

Table K.7: Tailings volumetric water contents (at noon and midnight) calculated from the matric suctions measured with the Model-229 Campbell Scientific matric suction sensors installed on the Kidston tailings impoundment.

Date	Tailings volumetric water content (fraction)																	
	NC200 (2000 mm)		NC150 (1500 mm)		#18 (1250 mm)		#19 (1000 mm)		#17 (750 mm)		#21 (500 mm)		#15 (300 mm)		#20 (150 mm)		16 (50 mm)	
	PM	AM	PM	AM	PM	AM	PM	AM	PM	AM	PM	AM	AM	PM	PM	AM	PM	AM
3-Jan-99	0.44	0.44	0.43	0.42	0.41	0.41	0.35	0.34	0.37	0.36	0.31	0.29	0.26	0.26	0.39	0.39	0.37	0.30
4-Jan-99	0.44	0.44	0.43	0.43	0.41	0.41	0.35	0.35	0.37	0.38	0.30	0.31	0.25	0.37	0.43	0.38	0.44	0.28
5-Jan-99	0.44	0.44	0.42	0.41	0.41	0.41	0.36	0.35	0.39	0.37	0.37	0.35	0.38	0.38	0.44	0.44	0.43	0.44
6-Jan-99	0.44	0.44	0.44	0.42	0.43	0.42	0.38	0.36	0.41	0.40	0.40	0.39	0.38	0.40	0.44	0.43	0.43	0.43
7-Jan-99	0.44	0.44	0.43	0.42	0.42	0.42	0.38	0.37	0.41	0.41	0.39	0.39	0.37	0.36	0.43	0.43	0.42	0.43
8-Jan-98		0.44		0.42		0.42		0.38		0.41		0.38	0.36			0.43		0.39
17-Oct-99	0.44		0.37		0.35		0.26		0.24		0.14			0.11	0.12		0.07	
18-Oct-99	0.44	0.44	0.40	0.37	0.36	0.34	0.26	0.25	0.25	0.22	0.14	0.13	0.11	0.11	0.12	0.11	0.08	0.05
19-Oct-99	0.44	0.44	0.38	0.37	0.36	0.33	0.26	0.25	0.24	0.21	0.14	0.13	0.11	0.11	0.12	0.11	0.08	0.05
20-Oct-99	0.44	0.44	0.38	0.36	0.36	0.33	0.27	0.25	0.24	0.22	0.14	0.13	0.11	0.11	0.12	0.11	0.08	0.05
21-Oct-99	0.44	0.44	0.39	0.35	0.36	0.34	0.27	0.24	0.24	0.21	0.14	0.13	0.11	0.11	0.12	0.11	0.07	0.06
22-Oct-99	0.44	0.44	0.39	0.37	0.35	0.34	0.27	0.24	0.25	0.22	0.14	0.13	0.11	0.11	0.12	0.11	0.07	0.06
23-Oct-99	0.44	0.44	0.40	0.36	0.37	0.33	0.28	0.26	0.25	0.23	0.14	0.13	0.11	0.11	0.11	0.11	0.06	0.05
24-Oct-99	0.44	0.44	0.39	0.35	0.35	0.34	0.25	0.24	0.23	0.22	0.13	0.13	0.11	0.11	0.12	0.11	0.08	0.06
25-Oct-99	0.44	0.44	0.39	0.36	0.36	0.33	0.25	0.26	0.23	0.22	0.13	0.13	0.11	0.11	0.12	0.12	0.08	0.06
26-Oct-99	0.44	0.44	0.38	0.37	0.35	0.34	0.25	0.24	0.23	0.22	0.14	0.13	0.11	0.11	0.12	0.12	0.08	0.06
27-Oct-99	0.44	0.44	0.37	0.37	0.35	0.33	0.26	0.24	0.23	0.21	0.14	0.13	0.11	0.11	0.12	0.11	0.08	0.06
28-Oct-99	0.44	0.44	0.38	0.33	0.35	0.33	0.26	0.24	0.23	0.21	0.14	0.13	0.11	0.11	0.12	0.11	0.08	0.05
29-Oct-99	0.44	0.44	0.37	0.35	0.34	0.32	0.26	0.24	0.23	0.21	0.14	0.13	0.11	0.11	0.12	0.11	0.08	0.05
30-Oct-99	0.44	0.44	0.37	0.35	0.34	0.34	0.26	0.24	0.24	0.22	0.14	0.13	0.11	0.11	0.12	0.11	0.08	0.05
31-Oct-99	0.44	0.44	0.35	0.34	0.34	0.33	0.25	0.24	0.22	0.22	0.13	0.13	0.11	0.11	0.11	0.12	0.06	0.05
1-Nov-99	0.44	0.44	0.36	0.36	0.34	0.33	0.26	0.25	0.22	0.23	0.13	0.13	0.11	0.11	0.17	0.11	0.23	0.15
2-Nov-99	0.44	0.44	0.36	0.34	0.36	0.33	0.28	0.26	0.25	0.23	0.15	0.14	0.12	0.13	0.22	0.20	0.21	0.17
3-Nov-99		0.44		0.35		0.35		0.26		0.23		0.14	0.13			0.22		0.15
12-Nov-99	0.44		0.40		0.42		0.38		0.42		0.42			0.39	0.43		0.40	
13-Nov-99	0.44	0.44	0.39	0.38	0.41	0.42	0.39	0.37	0.41	0.41	0.41	0.40	0.35	0.33	0.42	0.42	0.39	0.38
14-Nov-99	0.44	0.44	0.39	0.37	0.42	0.41	0.39	0.37	0.42	0.41	0.41	0.40	0.32	0.32	0.42	0.41	0.38	0.33
15-Nov-99	0.44	0.44	0.40	0.39	0.42	0.41	0.39	0.37	0.41	0.40	0.39	0.37	0.29	0.29	0.39	0.39	0.34	0.28
16-Nov-99	0.44	0.44	0.40	0.38	0.42	0.42	0.38	0.37	0.41	0.41	0.38	0.37	0.28	0.26	0.37	0.38	0.30	0.26
17-Nov-99	0.44	0.44	0.40	0.38	0.42	0.42	0.38	0.37	0.41	0.40	0.36	0.35	0.24	0.23	0.35	0.34	0.27	0.21
18-Nov-99	0.44	0.44	0.41	0.39	0.43	0.42	0.38	0.37	0.41	0.40	0.35	0.35	0.22	0.21	0.31	0.31	0.19	0.16
19-Nov-99	0.44	0.44	0.42	0.39	0.43	0.42	0.39	0.37	0.41	0.40	0.34	0.32	0.25	0.33	0.43	0.43	0.43	0.44
20-Nov-99	0.44	0.44	0.40	0.40	0.42	0.42	0.38	0.37	0.41	0.40	0.35	0.33	0.32	0.35	0.43	0.43	0.43	0.43
21-Nov-99	0.44	0.44	0.39	0.39	0.42	0.42	0.37	0.37	0.41	0.40	0.37	0.37	0.35	0.35	0.43	0.43	0.43	0.43
22-Nov-99	0.44	0.44	0.41	0.39	0.42	0.42	0.38	0.37	0.41	0.40	0.39	0.37	0.36	0.39	0.44	0.44	0.44	0.44
23-Nov-99	0.44	0.44	0.42	0.38	0.42	0.42	0.38	0.37	0.42	0.41	0.41	0.40	0.39	0.41	0.44	0.44	0.44	0.44
24-Nov-99	0.44	0.44	0.40	0.39	0.42	0.42	0.39	0.38	0.42	0.41	0.42	0.41	0.39	0.39	0.43	0.44	0.43	0.43
25-Nov-99	0.44	0.44	0.38	0.40	0.42	0.42	0.38	0.37	0.41	0.41	0.41	0.41	0.39	0.38	0.43	0.44	0.43	0.43
26-Nov-99	0.44	0.44	0.43	0.39	0.43	0.42	0.40	0.38	0.42	0.42	0.42	0.41	0.39	0.39	0.44	0.43	0.43	0.43
27-Nov-99	0.44	0.44	0.38	0.40	0.42	0.43	0.39	0.39	0.42	0.42	0.41	0.40	0.38	0.38	0.43	0.43	0.43	0.43
28-Nov-99	0.44	0.44	0.42	0.41	0.43	0.42	0.39	0.39	0.42	0.42	0.41	0.41	0.38	0.38	0.43	0.43	0.43	0.43
29-Nov-99	0.44	0.44	0.39	0.39	0.42	0.43	0.38	0.40	0.42	0.42	0.40	0.41	0.38	0.36	0.43	0.43	0.42	0.43
30-Nov-99	0.44	0.44	0.42	0.41	0.43	0.43	0.40	0.40	0.42	0.42	0.41	0.41	0.37	0.36	0.43	0.43	0.42	0.42

Table K.7: Tailings volumetric water contents (at noon and midnight) calculated from the matric suctions measured with the Model-229 Campbell Scientific matric suction sensors installed on the Kidston tailings impoundment.

Date	Tailings volumetric water content (fraction)																	
	NC200 (2000 mm)		NC150 (1500 mm)		#18 (1250 mm)		#19 (1000 mm)		#17 (750 mm)		#21 (500 mm)		#15 (300 mm)		#20 (150 mm)		16 (50 mm)	
	PM	AM	PM	AM	PM	AM	PM	AM	PM	AM	PM	AM	AM	PM	PM	AM	PM	AM
1-Dec-99	0.44	0.44	0.41	0.40	0.43	0.43	0.40	0.40	0.42	0.42	0.40	0.40	0.35	0.35	0.43	0.43	0.39	0.39
2-Dec-99		0.44		0.41		0.43		0.40		0.42		0.40	0.32			0.42		0.35
4-Dec-99	0.44		0.43		0.43		0.40		0.43		0.38			0.26	0.37		0.27	
5-Dec-99	0.44	0.44	0.43	0.41	0.43	0.43	0.40	0.39	0.42	0.42	0.35	0.37	0.23	0.22	0.31	0.32	0.20	0.17
6-Dec-99	0.44	0.44	0.42	0.40	0.43	0.43	0.39	0.39	0.42	0.42	0.33	0.34	0.21	0.20	0.25	0.26	0.12	0.12
7-Dec-99	0.44	0.44	0.42	0.40	0.43	0.43	0.39	0.38	0.42	0.42	0.29	0.30	0.18	0.17	0.18	0.19	0.08	0.08
8-Dec-99	0.44	0.44	0.41	0.39	0.43	0.42	0.38	0.37	0.41	0.41	0.26	0.26	0.15	0.15	0.15	0.14	0.06	0.06
9-Dec-99	0.44	0.44	0.43	0.39	0.43	0.42	0.38	0.36	0.41	0.40	0.21	0.21	0.13	0.13	0.12	0.12	0.05	0.05
10-Dec-99	0.44	0.44	0.42	0.39	0.43	0.42	0.37	0.36	0.40	0.40	0.19	0.18	0.12	0.12	0.11	0.11	0.04	0.04
11-Dec-99	0.44	0.44	0.39	0.40	0.42	0.42	0.34	0.35	0.37	0.38	0.16	0.17	0.11	0.11	0.09	0.09	0.03	0.03
12-Dec-99	0.44	0.44	0.41	0.39	0.42	0.42	0.34	0.33	0.36	0.37	0.16	0.14	0.11	0.11	0.09	0.09	0.03	0.03
13-Dec-99	0.44	0.44	0.41	0.38	0.41	0.41	0.32	0.31	0.29	0.34	0.14	0.15	0.10	0.10	0.08	0.08	0.03	0.03
14-Dec-99	0.44	0.44	0.40	0.41	0.41	0.41	0.33	0.32	0.29	0.29	0.14	0.14	0.11	0.10	0.08	0.08	0.04	0.03
15-Dec-99	0.44	0.44	0.39	0.40	0.41	0.40	0.32	0.31	0.29	0.28	0.14	0.14	0.11	0.11	0.09	0.08	0.04	0.04
16-Dec-99	0.44	0.44	0.41	0.39	0.41	0.40	0.32	0.29	0.28	0.27	0.14	0.14	0.10	0.10	0.08	0.08	0.04	0.04
17-Dec-99	0.44	0.44	0.40	0.38	0.41	0.40	0.31	0.29	0.26	0.26	0.13	0.13	0.10	0.10	0.08	0.08	0.03	0.03
18-Dec-99	0.44	0.44	0.42	0.38	0.40	0.40	0.30	0.29	0.26	0.25	0.14	0.13	0.10	0.10	0.08	0.08	0.03	0.03
19-Dec-99	0.44	0.44	0.40	0.39	0.40	0.39	0.30	0.29	0.25	0.24	0.14	0.13	0.10	0.10	0.11	0.08	0.29	0.03
20-Dec-99	0.44	0.44	0.38	0.37	0.39	0.38	0.30	0.27	0.26	0.25	0.14	0.13	0.12	0.13	0.23	0.21	0.21	0.22
21-Dec-99	0.44	0.44	0.39	0.38	0.40	0.39	0.30	0.28	0.27	0.26	0.16	0.15	0.13	0.13	0.21	0.22	0.15	0.16
22-Dec-99	0.44	0.44	0.39	0.38	0.40	0.40	0.30	0.30	0.27	0.27	0.16	0.16	0.13	0.13	0.18	0.19	0.11	0.11
23-Dec-99		0.44		0.38		0.39		0.30		0.27		0.15	0.13			0.16		0.08
24-Dec-99	0.44	0.44	0.40	0.38	0.40	0.40	0.31	0.29	0.28	0.27	0.15	0.16	0.12	0.12	0.14	0.14	0.09	0.07
25-Dec-99	0.44	0.44	0.40	0.38	0.40	0.40	0.31	0.30	0.28	0.27	0.16	0.15	0.12	0.13	0.19	0.15	0.23	0.11
26-Dec-99	0.44	0.44	0.40	0.39	0.40	0.40	0.31	0.31	0.29	0.27	0.16	0.16	0.13	0.14	0.34	0.25	0.37	0.24
27-Dec-99	0.44	0.44	0.40	0.39	0.40	0.40	0.31	0.30	0.29	0.27	0.18	0.16	0.18	0.34	0.44	0.43	0.44	0.43
28-Dec-99	0.44	0.44	0.39	0.39	0.41	0.40	0.32	0.31	0.30	0.28	0.29	0.23	0.36	0.37	0.43	0.43	0.43	0.43
29-Dec-99	0.44	0.44	0.41	0.38	0.41	0.39	0.34	0.31	0.33	0.30	0.35	0.31	0.34	0.35	0.43	0.43	0.42	0.42
30-Dec-99	0.44	0.44	0.39	0.38	0.41	0.40	0.32	0.33	0.33	0.32	0.31	0.32	0.31	0.31	0.42	0.42	0.36	0.36
31-Dec-99	0.44	0.44	0.40	0.38	0.41	0.41	0.34	0.33	0.34	0.34	0.32	0.32	0.28	0.27	0.38	0.39	0.30	0.29
1-Jan-00	0.44	0.44	0.41	0.39	0.42	0.40	0.35	0.33	0.35	0.33	0.31	0.30	0.24	0.25	0.35	0.35	0.21	0.22
2-Jan-00	0.44	0.44	0.40	0.39	0.41	0.42	0.34	0.34	0.35	0.33	0.28	0.28	0.22	0.20	0.28	0.30	0.15	0.15
3-Jan-00	0.44	0.44	0.41	0.39	0.42	0.41	0.35	0.33	0.35	0.34	0.27	0.27	0.18	0.17	0.20	0.22	0.10	0.09
4-Jan-00	0.44	0.44	0.41	0.38	0.41	0.40	0.34	0.33	0.32	0.33	0.23	0.24	0.16	0.15	0.15	0.17	0.07	0.07
5-Jan-00	0.44	0.44	0.40	0.39	0.41	0.40	0.34	0.33	0.33	0.33	0.21	0.22	0.14	0.13	0.13	0.14	0.06	0.06
6-Jan-00	0.44	0.44	0.41	0.39	0.42	0.41	0.33	0.33	0.34	0.30	0.19	0.18	0.13	0.13	0.12	0.12	0.05	0.05
7-Jan-00	0.44	0.44	0.40	0.39	0.40	0.40	0.31	0.32	0.30	0.29	0.16	0.17	0.12	0.12	0.11	0.10	0.09	0.05
8-Jan-00	0.44	0.44	0.40	0.40	0.41	0.40	0.32	0.32	0.30	0.29	0.21	0.17	0.17	0.33	0.43	0.43	0.44	0.44
9-Jan-00	0.44	0.44	0.39	0.38	0.41	0.40	0.32	0.31	0.31	0.30	0.27	0.24	0.32	0.31	0.43	0.43	0.41	0.42
10-Jan-00	0.44	0.44	0.41	0.40	0.41	0.40	0.35	0.33	0.35	0.32	0.31	0.28	0.30	0.31	0.42	0.42	0.37	0.37
11-Jan-00	0.44	0.44	0.42	0.39	0.42	0.40	0.36	0.33	0.35	0.32	0.30	0.28	0.26	0.33	0.43	0.39	0.43	0.30
12-Jan-00		0.44		0.40		0.41		0.34		0.33		0.30	0.39			0.44		0.44
13-Jan-00	0.44	0.44	0.40	0.41	0.42	0.41	0.36	0.35	0.39	0.37	0.43	0.42	0.40	0.40	0.44	0.44	0.43	0.44
14-Jan-00	0.44	0.44	0.41	0.39	0.42	0.41	0.38	0.36	0.40	0.40	0.42	0.42	0.39	0.39	0.44	0.44	0.43	0.43

Table K.7: Tailings volumetric water contents (at noon and midnight) calculated from the matric suctions measured with the Model-229 Campbell Scientific matric suction sensors installed on the Kidston tailings impoundment.

Date	Tailings volumetric water content (fraction)																	
	NC200 (2000 mm)		NC150 (1500 mm)		#18 (1250 mm)		#19 (1000 mm)		#17 (750 mm)		#21 (500 mm)		#15 (300 mm)		#20 (150 mm)		16 (50 mm)	
	PM	AM	PM	AM	PM	AM	PM	AM	PM	AM	PM	AM	AM	PM	PM	AM	PM	AM
15-Jan-00	0.44	0.44	0.42	0.41	0.43	0.42	0.39	0.37	0.41	0.40	0.42	0.42	0.38	0.38	0.43	0.43	0.41	0.42
16-Jan-00	0.44	0.44	0.39	0.39	0.42	0.42	0.39	0.38	0.41	0.40	0.41	0.41	0.36	0.33	0.42	0.42	0.37	0.36
17-Jan-00	0.44	0.44	0.42	0.41	0.43	0.42	0.39	0.38	0.41	0.41	0.41	0.40	0.31	0.30	0.40	0.41	0.33	0.30
18-Jan-00	0.44	0.44	0.41	0.39	0.43	0.42	0.39	0.38	0.41	0.40	0.39	0.39	0.27	0.26	0.36	0.36	0.25	0.25
19-Jan-00	0.44	0.44	0.40	0.39	0.43	0.42	0.39	0.38	0.41	0.41	0.38	0.38	0.23	0.23	0.32	0.33	0.20	0.18
20-Jan-00	0.44	0.44	0.42	0.41	0.43	0.42	0.39	0.38	0.41	0.41	0.35	0.36	0.21	0.20	0.26	0.28	0.13	0.13
21-Jan-00	0.44	0.44	0.41	0.39	0.43	0.42	0.38	0.37	0.40	0.39	0.31	0.31	0.18	0.17	0.19	0.20	0.09	0.09
22-Jan-00	0.44	0.44	0.42	0.41	0.43	0.42	0.38	0.37	0.39	0.40	0.27	0.27	0.16	0.17	0.38	0.16	0.42	0.07
23-Jan-00	0.44	0.44	0.41	0.40	0.42	0.42	0.38	0.37	0.39	0.39	0.29	0.28	0.21	0.23	0.40	0.41	0.38	0.39
24-Jan-00	0.44	0.44	0.43	0.41	0.43	0.42	0.39	0.36	0.41	0.40	0.31	0.29	0.23	0.24	0.38	0.38	0.32	0.32
25-Jan-00	0.44	0.44	0.40	0.40	0.43	0.42	0.37	0.36	0.40	0.40	0.29	0.28	0.23	0.25	0.41	0.41	0.36	0.38
26-Jan-00	0.44	0.44	0.40	0.40	0.42	0.42	0.37	0.36	0.40	0.39	0.30	0.29	0.23	0.23	0.36	0.37	0.28	0.29
27-Jan-00	0.44	0.44	0.42	0.39	0.43	0.42	0.37	0.36	0.39	0.38	0.29	0.28	0.21	0.20	0.30	0.33	0.21	0.21
28-Jan-00	0.44	0.44	0.41	0.41	0.42	0.42	0.38	0.36	0.39	0.39	0.29	0.28	0.19	0.19	0.25	0.28	0.15	0.15
29-Jan-00	0.44	0.44	0.41	0.40	0.42	0.42	0.37	0.36	0.39	0.38	0.26	0.27	0.18	0.17	0.21	0.22	0.11	0.12
30-Jan-00	0.44	0.44	0.41	0.40	0.42	0.42	0.35	0.35	0.38	0.38	0.23	0.25	0.16	0.15	0.16	0.17	0.08	0.08
31-Jan-00	0.44	0.44	0.41	0.41	0.42	0.42	0.35	0.36	0.38	0.37	0.20	0.22	0.14	0.13	0.13	0.14	0.06	0.06
1-Feb-00	0.44	0.44	0.40	0.40	0.42	0.42	0.35	0.35	0.37	0.37	0.19	0.18	0.12	0.12	0.11	0.11	0.05	0.05
2-Feb-00	0.44	0.44	0.41	0.39	0.42	0.42	0.35	0.33	0.37	0.35	0.17	0.16	0.12	0.11	0.09	0.09	0.04	0.04
3-Feb-00	0.44	0.44	0.42	0.39	0.41	0.41	0.34	0.33	0.34	0.34	0.15	0.15	0.11	0.11	0.08	0.08	0.03	0.03
4-Feb-00	0.44	0.44	0.41	0.38	0.40	0.40	0.31	0.32	0.30	0.29	0.14	0.13	0.10	0.10	0.07	0.08	0.03	0.03
5-Feb-00	0.44	0.44	0.40	0.40	0.40	0.40	0.30	0.29	0.26	0.26	0.13	0.12	0.10	0.10	0.07	0.07	0.02	0.02
6-Feb-00	0.44	0.44	0.38	0.39	0.40	0.39	0.30	0.30	0.27	0.25	0.13	0.12	0.10	0.10	0.07	0.07	0.02	0.02
7-Feb-00	0.44	0.44	0.39	0.40	0.39	0.39	0.31	0.29	0.27	0.26	0.13	0.13	0.10	0.10	0.08	0.07	0.02	0.02
8-Feb-00	0.44	0.44	0.40	0.38	0.40	0.39	0.30	0.29	0.27	0.27	0.13	0.13	0.10	0.10	0.08	0.07	0.03	0.02
9-Feb-00	0.44	0.44	0.38	0.38	0.38	0.38	0.30	0.29	0.25	0.25	0.13	0.13	0.10	0.10	0.07	0.07	0.03	0.03
10-Feb-00	0.44	0.44	0.38	0.37	0.38	0.38	0.28	0.28	0.25	0.24	0.13	0.12	0.10	0.10	0.07	0.07	0.03	0.03
11-Feb-00	0.44	0.44	0.39	0.37	0.38	0.38	0.28	0.27	0.25	0.23	0.13	0.12	0.10	0.10	0.07	0.07	0.03	0.02
12-Feb-00	0.44	0.44	0.39	0.39	0.38	0.37	0.28	0.27	0.24	0.24	0.12	0.12	0.10	0.10	0.07	0.07	0.03	0.02
13-Feb-00	0.44	0.44	0.40	0.35	0.36	0.36	0.26	0.24	0.23	0.21	0.12	0.11	0.09	0.09	0.07	0.06	0.02	0.02
14-Feb-00	0.44	0.44	0.37	0.34	0.36	0.35	0.27	0.24	0.23	0.21	0.12	0.11	0.09	0.10	0.07	0.06	0.02	0.02
15-Feb-00	0.44	0.44	0.37	0.38	0.36	0.36	0.26	0.26	0.23	0.22	0.12	0.11	0.09	0.09	0.06	0.06	0.07	0.02
16-Feb-00	0.44	0.44	0.39	0.36	0.38	0.36	0.27	0.26	0.25	0.23	0.13	0.12	0.10	0.10	0.10	0.07	0.11	0.10
17-Feb-00	0.44	0.44	0.38	0.38	0.39	0.36	0.28	0.27	0.25	0.24	0.13	0.12	0.10	0.11	0.15	0.13	0.18	0.11
18-Feb-00	0.44	0.44	0.39	0.37	0.38	0.36	0.28	0.28	0.25	0.24	0.14	0.13	0.12	0.13	0.31	0.20	0.34	0.28
19-Feb-00	0.44	0.44	0.36	0.37	0.37	0.36	0.26	0.27	0.23	0.24	0.15	0.15	0.15	0.17	0.37	0.37	0.31	0.35
20-Feb-00	0.44	0.44	0.38	0.37	0.38	0.37	0.29	0.27	0.27	0.25	0.19	0.16	0.18	0.19	0.37	0.36	0.27	0.29
21-Feb-00	0.44	0.44	0.37	0.37	0.37	0.38	0.28	0.28	0.25	0.25	0.18	0.18	0.19	0.19	0.39	0.36	0.34	0.32
22-Feb-00	0.44	0.44	0.39	0.38	0.38	0.38	0.30	0.28	0.28	0.27	0.20	0.18	0.20	0.22	0.40	0.39	0.34	0.33
23-Feb-00	0.44	0.44	0.38	0.37	0.39	0.38	0.30	0.30	0.28	0.28	0.21	0.21	0.22	0.24	0.42	0.39	0.38	0.40
24-Feb-00	0.44	0.44	0.38	0.38	0.40	0.39	0.31	0.29	0.29	0.29	0.25	0.23	0.28	0.36	0.43	0.43	0.43	0.43
25-Feb-00	0.44	0.44	0.40	0.37	0.39	0.39	0.31	0.31	0.31	0.29	0.41	0.28	0.40	0.40	0.44	0.44	0.44	0.44
26-Feb-00	0.44	0.44	0.40	0.38	0.40	0.39	0.34	0.33	0.41	0.35	0.43	0.43	0.40	0.40	0.44	0.44	0.44	0.44
27-Feb-00	0.44	0.44	0.39	0.37	0.41	0.40	0.39	0.36	0.43	0.43	0.43	0.43	0.40	0.40	0.44	0.44	0.44	0.44
28-Feb-00	0.44	0.44	0.38	0.38	0.42	0.42	0.41	0.40	0.43	0.43	0.43	0.43	0.40	0.40	0.44	0.44	0.43	0.43

Table K.7: Tailings volumetric water contents (at noon and midnight) calculated from the matric suctions measured with the Model-229 Campbell Scientific matric suction sensors installed on the Kidston tailings impoundment.

Date	Tailings volumetric water content (fraction)																	
	NC200 (2000 mm)		NC150 (1500 mm)		#18 (1250 mm)		#19 (1000 mm)		#17 (750 mm)		#21 (500 mm)		#15 (300 mm)		#20 (150 mm)		16 (50 mm)	
	PM	AM	PM	AM	PM	AM	PM	AM	PM	AM	PM	AM	AM	PM	PM	AM	PM	AM
29-Feb-00	0.44	0.44	0.40	0.40	0.43	0.42	0.41	0.40	0.43	0.43	0.43	0.43	0.39	0.40	0.44	0.43	0.43	0.42
1-Mar-00	0.44	0.44	0.42	0.40	0.43	0.43	0.42	0.41	0.44	0.43	0.43	0.43	0.41	0.41	0.44	0.44	0.44	0.44
2-Mar-00	0.44	0.44	0.42	0.40	0.43	0.43	0.43	0.43	0.44	0.44	0.44	0.43	0.40	0.42	0.44	0.44	0.44	0.44
3-Mar-00	0.44	0.44	0.43	0.39	0.44	0.43	0.43	0.43	0.44	0.44	0.44	0.43	0.39	0.41	0.44	0.44	0.43	0.43
4-Mar-00	0.44	0.44	0.43	0.42	0.44	0.44	0.43	0.43	0.44	0.44	0.43	0.43	0.40	0.40	0.43	0.43	0.42	0.42
5-Mar-00	0.44	0.44	0.43	0.42	0.44	0.44	0.43	0.43	0.44	0.44	0.43	0.43	0.38	0.38	0.43	0.43	0.37	0.39
6-Mar-00	0.44	0.44	0.43	0.42	0.44	0.44	0.43	0.43	0.44	0.44	0.43	0.43	0.35	0.33	0.42	0.42	0.32	0.34
7-Mar-00	0.44	0.44	0.43	0.43	0.44	0.44	0.43	0.43	0.44	0.44	0.42	0.43	0.31	0.29	0.37	0.39	0.26	0.28
8-Mar-00	0.44	0.44	0.44	0.43	0.44	0.44	0.43	0.43	0.44	0.44	0.42	0.42	0.26	0.25	0.34	0.34	0.21	0.21
9-Mar-00	0.44	0.44	0.43	0.42	0.44	0.44	0.43	0.43	0.43	0.43	0.40	0.39	0.23	0.22	0.28	0.28	0.14	0.15
10-Mar-00	0.44	0.44	0.44	0.42	0.44	0.44	0.43	0.43	0.44	0.43	0.38	0.38	0.20	0.21	0.26	0.23	0.16	0.12
11-Mar-00	0.44	0.44	0.43	0.43	0.43	0.44	0.42	0.42	0.43	0.43	0.35	0.36	0.19	0.19	0.26	0.25	0.14	0.14
12-Mar-00	0.44	0.44	0.42	0.42	0.43	0.44	0.42	0.42	0.43	0.43	0.32	0.34	0.18	0.18	0.22	0.23	0.12	0.13
13-Mar-00	0.44	0.44	0.43	0.42	0.44	0.43	0.42	0.42	0.43	0.43	0.30	0.30	0.17	0.17	0.19	0.19	0.09	0.10
14-Mar-00	0.44	0.44	0.43	0.42	0.43	0.43	0.42	0.41	0.43	0.43	0.28	0.28	0.15	0.15	0.14	0.15	0.07	0.08
15-Mar-00	0.44	0.44	0.43	0.41	0.43	0.43	0.41	0.41	0.41	0.43	0.24	0.25	0.13	0.13	0.12	0.13	0.06	0.06
16-Mar-00	0.44	0.44	0.43	0.42	0.43	0.43	0.39	0.40	0.39	0.39	0.20	0.21	0.12	0.12	0.10	0.10	0.04	0.05
17-Mar-00	0.44	0.44	0.43	0.43	0.43	0.43	0.40	0.39	0.39	0.37	0.19	0.18	0.11	0.12	0.10	0.09	0.04	0.04
18-Mar-00	0.44	0.44	0.42	0.42	0.43	0.43	0.38	0.38	0.35	0.37	0.18	0.17	0.11	0.17	0.42	0.31	0.41	0.43
19-Mar-00	0.44	0.44	0.42	0.41	0.43	0.43	0.37	0.37	0.36	0.36	0.23	0.21	0.23	0.25	0.41	0.42	0.37	0.40
20-Mar-00	0.44	0.44	0.42	0.42	0.43	0.43	0.37	0.37	0.37	0.35	0.26	0.24	0.23	0.24	0.40	0.40	0.33	0.34
21-Mar-00	0.44	0.44	0.43	0.42	0.43	0.43	0.38	0.37	0.37	0.36	0.26	0.25	0.22	0.21	0.36	0.37	0.25	0.27
22-Mar-00	0.44	0.44	0.43	0.41	0.43	0.43	0.39	0.37	0.37	0.37	0.27	0.25	0.20	0.20	0.31	0.31	0.20	0.21
23-Mar-00	0.44	0.44	0.43	0.41	0.43	0.43	0.38	0.37	0.36	0.35	0.23	0.24	0.18	0.17	0.25	0.26	0.14	0.15
24-Mar-00	0.44	0.44	0.41	0.41	0.43	0.43	0.38	0.36	0.36	0.36	0.23	0.23	0.16	0.15	0.19	0.20	0.09	0.11
25-Mar-00	0.44	0.44	0.41	0.40	0.43	0.43	0.37	0.35	0.36	0.33	0.21	0.19	0.13	0.13	0.13	0.13	0.06	0.07
26-Mar-00	0.44	0.44	0.40	0.41	0.43	0.43	0.35	0.35	0.33	0.31	0.17	0.18	0.12	0.11	0.10	0.10	0.05	0.05
27-Mar-00	0.44	0.44	0.42	0.40	0.43	0.42	0.34	0.33	0.30	0.30	0.15	0.15	0.10	0.10	0.08	0.08	0.04	0.04
28-Mar-00	0.44	0.44	0.42	0.40	0.42	0.42	0.33	0.31	0.29	0.28	0.13	0.13	0.09	0.09	0.07	0.07	0.03	0.03
29-Mar-00	0.44	0.44	0.40	0.39	0.42	0.41	0.30	0.30	0.25	0.25	0.12	0.12	0.09	0.08	0.06	0.06	0.02	0.03
30-Mar-00	0.44	0.44	0.41	0.40	0.40	0.40	0.28	0.28	0.22	0.23	0.10	0.11	0.08	0.08	0.05	0.05	0.02	0.02
31-Mar-00	0.44	0.44	0.41	0.38	0.40	0.38	0.26	0.26	0.20	0.20	0.10	0.10	0.08	0.08	0.05	0.05	0.02	0.02
1-Apr-00	0.44	0.44	0.40	0.37	0.38	0.37	0.24	0.24	0.19	0.18	0.10	0.09	0.07	0.07	0.04	0.04	0.02	0.02
2-Apr-00	0.44	0.44	0.38	0.40	0.37	0.37	0.24	0.24	0.18	0.19	0.09	0.09	0.07	0.07	0.04	0.04	0.02	0.02
3-Apr-00	0.44	0.44	0.39	0.37	0.36	0.35	0.24	0.23	0.19	0.18	0.10	0.09	0.07	0.08	0.05	0.04	0.19	0.17
4-Apr-00	0.44	0.44	0.38	0.39	0.36	0.35	0.26	0.24	0.20	0.19	0.11	0.10	0.08	0.09	0.34	0.11	0.41	0.18
5-Apr-00	0.44	0.44	0.41	0.38	0.38	0.36	0.26	0.24	0.22	0.20	0.13	0.11	0.14	0.19	0.41	0.40	0.39	0.38
6-Apr-00	0.44	0.44	0.38	0.35	0.37	0.36	0.26	0.24	0.20	0.20	0.15	0.14	0.18	0.19	0.38	0.38	0.31	0.32
7-Apr-00	0.44	0.44	0.41	0.36	0.39	0.36	0.28	0.26	0.24	0.21	0.17	0.15	0.18	0.18	0.35	0.34	0.27	0.25
8-Apr-00	0.44	0.44	0.41	0.37	0.41	0.37	0.36	0.27	0.44	0.22	0.43	0.43	0.39	0.41	0.44	0.44	0.44	0.44
9-Apr-00	0.44	0.44	0.39	0.38	0.43	0.42	0.43	0.42	0.44	0.44	0.43	0.43	0.39	0.39	0.44	0.44	0.44	0.44
10-Apr-00	0.44	0.44	0.39	0.39	0.43	0.43	0.43	0.43	0.44	0.44	0.43	0.43	0.39	0.38	0.44	0.44	0.43	0.43
11-Apr-00	0.44	0.44	0.43	0.40	0.44	0.43	0.43	0.43	0.44	0.44	0.43	0.43	0.38	0.40	0.44	0.43	0.43	0.43
12-Apr-00	0.44	0.44	0.43	0.41	0.44	0.44	0.43	0.43	0.44	0.44	0.43	0.43	0.38	0.38	0.43	0.43	0.42	0.42
13-Apr-00	0.44	0.44	0.43	0.42	0.44	0.44	0.43	0.43	0.44	0.44	0.43	0.43	0.38	0.38	0.43	0.43	0.41	0.41

Table K.7: Tailings volumetric water contents (at noon and midnight) calculated from the matric suctions measured with the Model-229 Campbell Scientific matric suction sensors installed on the Kidston tailings impoundment.

Date	Tailings volumetric water content (fraction)																	
	NC200 (2000 mm)		NC150 (1500 mm)		#18 (1250 mm)		#19 (1000 mm)		#17 (750 mm)		#21 (500 mm)		#15 (300 mm)		#20 (150 mm)		16 (50 mm)	
	PM	AM	PM	AM	PM	AM	PM	AM	PM	AM	PM	AM	AM	PM	PM	AM	PM	AM
14-Apr-00	0.44	0.44	0.44	0.42	0.44	0.44	0.43	0.43	0.44	0.44	0.43	0.43	0.34	0.35	0.43	0.43	0.40	0.39
15-Apr-00	0.44	0.44	0.43	0.42	0.44	0.44	0.43	0.43	0.44	0.44	0.43	0.42	0.32	0.33	0.42	0.41	0.37	0.36
16-Apr-00	0.44	0.44	0.43	0.42	0.44	0.44	0.43	0.43	0.44	0.44	0.42	0.42	0.29	0.30	0.40	0.40	0.32	0.32
17-Apr-00	0.44	0.44	0.43	0.42	0.44	0.44	0.43	0.43	0.44	0.44	0.41	0.42	0.27	0.27	0.38	0.38	0.29	0.27
18-Apr-00	0.44	0.44	0.43	0.43	0.44	0.44	0.43	0.43	0.44	0.44	0.40	0.40	0.23	0.25	0.35	0.34	0.24	0.24
19-Apr-00	0.44	0.44	0.43	0.42	0.44	0.44	0.43	0.43	0.43	0.44	0.38	0.39	0.22	0.21	0.31	0.31	0.20	0.20
20-Apr-00	0.44	0.44	0.43	0.42	0.44	0.44	0.43	0.43	0.43	0.43	0.36	0.37	0.20	0.21	0.28	0.27	0.16	0.17
21-Apr-00	0.44	0.44	0.41	0.42	0.44	0.43	0.43	0.42	0.43	0.43	0.33	0.33	0.19	0.19	0.25	0.24	0.14	0.14
22-Apr-00	0.44	0.44	0.42	0.43	0.44	0.44	0.42	0.42	0.42	0.43	0.30	0.32	0.17	0.17	0.19	0.21	0.11	0.12
23-Apr-00	0.44	0.44	0.43	0.42	0.43	0.44	0.42	0.42	0.42	0.42	0.28	0.28	0.16	0.15	0.17	0.18	0.10	0.10
24-Apr-00	0.44	0.44	0.43	0.42	0.44	0.43	0.42	0.42	0.42	0.41	0.33	0.26	0.18	0.38	0.44	0.44	0.44	0.44
25-Apr-00	0.44	0.44	0.41	0.42	0.43	0.43	0.41	0.41	0.41	0.41	0.43	0.36	0.38	0.39	0.44	0.44	0.44	0.44
26-Apr-00	0.44	0.44	0.43	0.42	0.44	0.43	0.42	0.41	0.43	0.43	0.43	0.43	0.39	0.41	0.44	0.44	0.44	0.44
27-Apr-00	0.44	0.44	0.43	0.43	0.44	0.43	0.42	0.42	0.43	0.43	0.43	0.43	0.40	0.40	0.44	0.44	0.43	0.43
28-Apr-00	0.44	0.44	0.43	0.42	0.44	0.43	0.43	0.43	0.43	0.43	0.43	0.43	0.39	0.40	0.44	0.44	0.43	0.43
29-Apr-00	0.44	0.44	0.42	0.42	0.44	0.44	0.43	0.43	0.43	0.43	0.43	0.43	0.39	0.39	0.43	0.43	0.43	0.43
30-Apr-00	0.44	0.44	0.44	0.43	0.44	0.44	0.43	0.43	0.43	0.43	0.43	0.43	0.38	0.39	0.43	0.43	0.43	0.42
1-May-00	0.44	0.44	0.43	0.43	0.44	0.44	0.43	0.42	0.43	0.43	0.42	0.43	0.37	0.37	0.43	0.43	0.39	0.40
2-May-00	0.44	0.44	0.43	0.42	0.44	0.43	0.43	0.42	0.43	0.43	0.43	0.42	0.33	0.34	0.42	0.42	0.37	0.36
10-May-00	0.44		0.44		0.44		0.42		0.42		0.31			0.17	0.22		0.13	
11-May-00	0.44	0.44	0.43	0.42	0.43	0.43	0.41	0.40	0.41	0.40	0.27	0.26	0.16	0.16	0.19	0.20	0.11	0.11
12-May-00	0.44	0.44	0.43	0.42	0.44	0.43	0.41	0.40	0.40	0.39	0.25	0.26	0.15	0.14	0.16	0.17	0.09	0.09
13-May-00	0.44	0.44	0.44	0.43	0.44	0.43	0.40	0.39	0.39	0.38	0.23	0.23	0.14	0.13	0.14	0.15	0.08	0.08
14-May-00	0.44	0.44	0.43	0.42	0.43	0.43	0.39	0.40	0.38	0.38	0.22	0.22	0.13	0.13	0.14	0.13	0.07	0.07
15-May-00	0.44	0.44	0.43	0.42	0.43	0.43	0.39	0.38	0.37	0.36	0.20	0.21	0.12	0.12	0.12	0.12	0.07	0.07
16-May-00	0.44	0.44	0.43	0.42	0.43	0.43	0.39	0.37	0.35	0.34	0.18	0.19	0.12	0.11	0.11	0.11	0.06	0.06
17-May-00	0.44	0.44	0.43	0.42	0.43	0.43	0.38	0.37	0.34	0.34	0.17	0.17	0.11	0.11	0.10	0.10	0.06	0.06
18-May-00	0.44	0.44	0.42	0.42	0.43	0.43	0.37	0.36	0.32	0.32	0.16	0.16	0.11	0.11	0.09	0.09	0.05	0.05
19-May-00	0.44	0.44	0.42	0.42	0.43	0.43	0.36	0.36	0.32	0.32	0.16	0.16	0.10	0.11	0.25	0.09	0.36	0.33
20-May-00	0.44	0.44	0.42	0.42	0.43	0.43	0.36	0.35	0.32	0.32	0.18	0.17	0.13	0.16	0.37	0.34	0.33	0.33
21-May-00	0.44	0.44	0.42	0.42	0.43	0.43	0.36	0.35	0.32	0.32	0.20	0.18	0.17	0.18	0.36	0.35	0.29	0.30
22-May-00	0.44	0.44	0.42	0.42	0.43	0.43	0.36	0.36	0.32	0.32	0.22	0.20	0.18	0.18	0.35	0.36	0.28	0.28

K.6 References

Campbell Scientific, Inc. (CSI) (1992). AM416 Relay Multiplexer Instruction Manual.

Campbell Scientific, Inc. (CSI) (1993). 229 Matrix Water Potential Sensor Operator's Manual.

Durham, A, Fredlund, D.G. (1996). Laboratory Calibration Procedure for the Campbell Scientific 229 Suction Sensors. Unpublished Internal Unsaturated Soils Group Procedure. Department of Civil Engineering, University of Saskatchewan, Saskatoon, Canada. 28 November, 3 pages.

Fredlund, D.G., Shuai, F, Feng, M. (2000). Increase in accuracy in suction measurements using an improved thermal conductivity sensor. In Proceedings of Tailings and Mine Waste '00, Colorado.

Fredlund, D.G., Shuai, F, Yazdani, J, Feng, M. (1998). Recent Developments on a Sensor for the Insitu Measurement of Matric Suction. In Proceedings of the 51st Canadian Regional Conference, Edmonton, Alberta, Canada, October 4-7. Vol. 1, pp. 81-86, ISBN 0-920505-13-9.

Fredlund, D.G., Xing, A. (1994). Equations for the soil-water characteristic curve. Canadian Geotechnical Journal, Vol. 31, No. 3, pp. 521-532.

SoilCover. (1997). SoilCover User's Manual. Unsaturated Soils Group, Department of Civil Engineering, University of Saskatchewan, Saskatoon, Saskatchewan, Canada.

Williams, D.J. (2000). Tailings Dam Research Project; Report on Preliminary Testing. Report to Mr. Nick Currey, Kidston Gold Mines Limited. Department of Civil Engineering, University of Queensland, Brisbane, Australia. 20 January, 10 pages.

APPENDIX L

Tailings Impoundment Water Balance Calculations

L.1 Introduction

The water balance calculations data as discussed in Chapter 5 of the thesis are presented here. The stage curves for the dams and ponds as well as other relevant supporting data are documented in this appendix.

L.2 Stage Curves

Stage curves describing the relationships between water level and pond/dam volume and area were constructed for four of the containment structures. These were (1) tailings impoundment, (2) reclaim dam, (3) seepage dam and (4) south dam. Data for the tailings impoundment stage curve illustrated in Figure L.1 was obtained from survey data and maps produced by Kidston Gold Mine from annual aerial photography.

A storage/elevation curve was developed for the reclaim dam by the Kidston Environmental Officer (Ritchie, 1988) in 1988. However, with the final raising of the tailings impoundment embankment wall, the storage volume of the reclaim dam was reduced invalidating the curve by Ritchie (1988). Evaluation of mine survey data of the reduced reclaim dam, suggested that the original storage curve could be used with a 25% volume reduction. In order to determine an area/elevation relationship for the reclaim dam the crest (528.0 mRL) area of the dam was simplified to measure 275 m at the dam wall, and reach 200 m back towards the toe of the tailings impoundment embankment. This provided for a surface area of 55000 m^2, assuming a square surface. The rate at which the area was reduced with lowering of the water level was calculated using a constant wedge shape based on a dam base slope of 1:22.22 and a reclaim dam wall upstream slope of 1:1.5. The two slopes intersected at the lowest dam elevation of 519.0 mRL. The resultant stage curve for the reclaim dam is presented in Figure L.2.

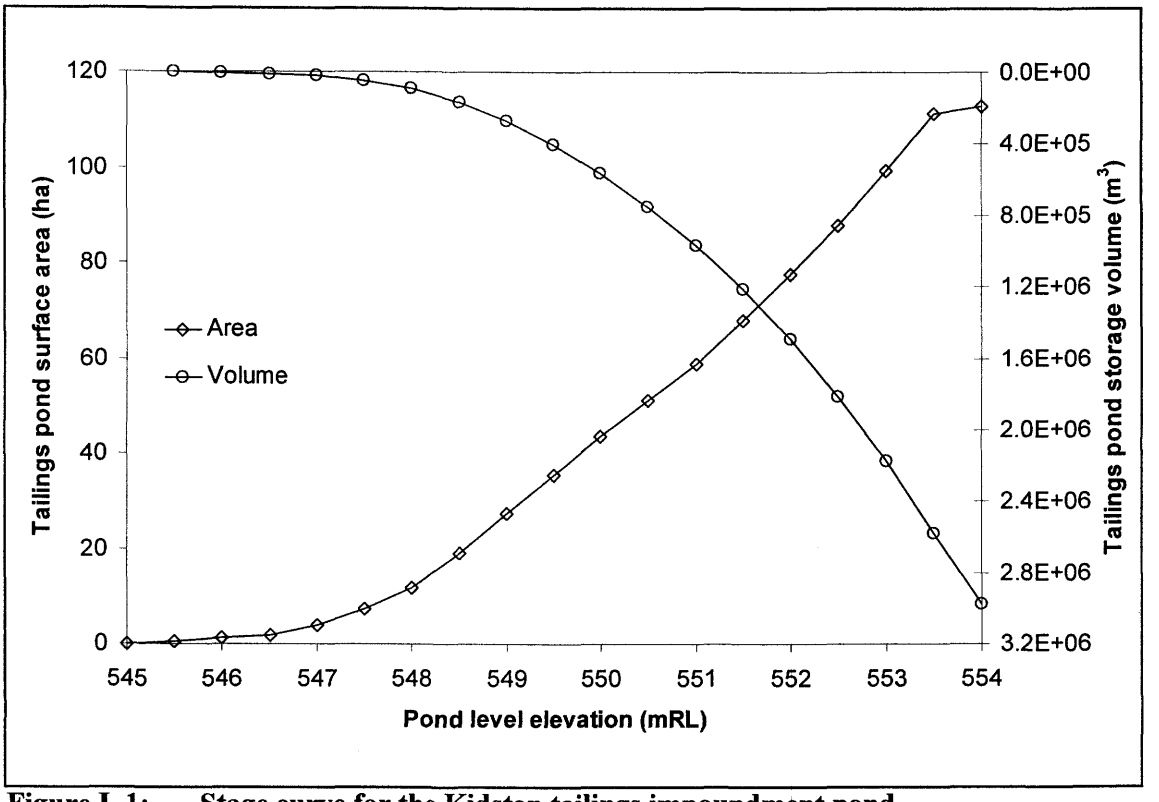

Figure L.1: Stage curve for the Kidston tailings impoundment pond.

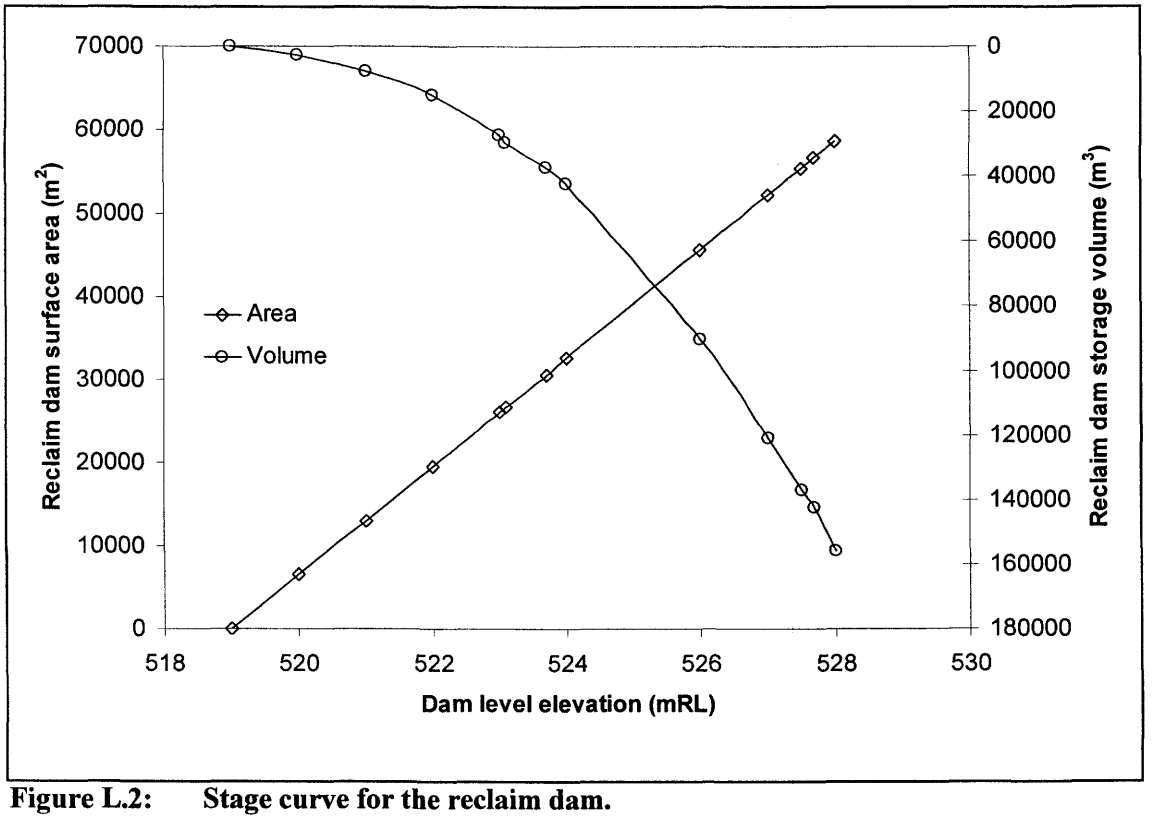

Figure L.2: Stage curve for the reclaim dam.

Ritchie (1988) also produced a storage curve for the south pond in 1988. Unfortunately this curve was invalidated by the fact that siltation of the pond had reduced the volume dramatically (Gutteridge, Haskins and Davey, 1987). A correction for the reduced pond volume was made by factoring the original full supply volume with the new full supply volume and applying the correction over the entire storage range. The area/elevation relationship was based on evaluation of mine survey data that suggested a surface area of 135 x 135 m when the pond is full (537.1 mRL), reducing in size to 0 m^2 at an elevation of 533.0 mRL, via an inverse pyramid shape. The stage curve is presented in Figure L.3.

The final stage curve is for the reclaim dam seepage dam, and it was developed from survey and contour data made available by Kidston Gold Mine. The stage curve is presented in Figure L.4.

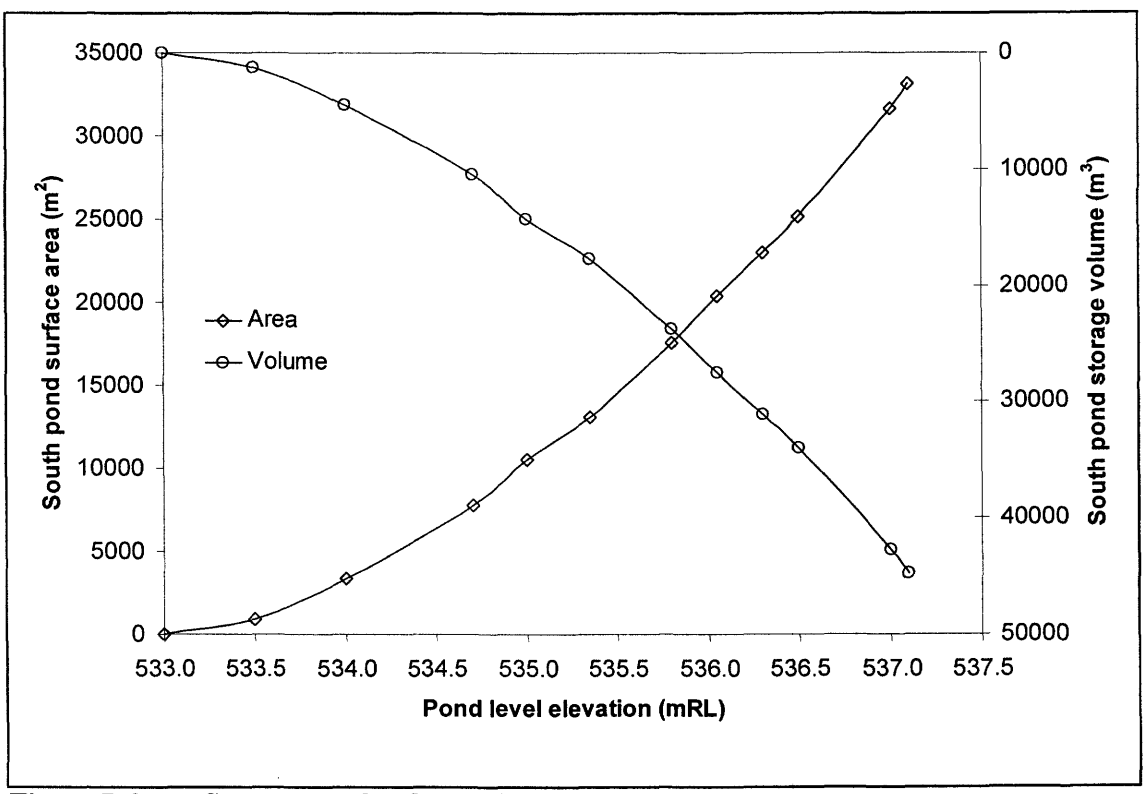

Figure L.3: Stage curve for the south pond.

L.3 Water Balance Calculation Data

The formulas and conditions for calculating the Kidston tailings impoundment water balance are discussed in Chapter 5. The subsequent calculated results for each individual period are listed in the tables below. Any constants relevant to the calculations in the tables are presented

in Chapter 5. Table L.1 to L.4 contains the data for the tailings impoundment water balance. Table L.5 contains the north pond water balance data and the south pond data is listed in Table L.6. The reclaim dam seepage dam data is listed in Table L.7 and finally the reclaim dam water balance data is contained in Tables L.8 and L.9.

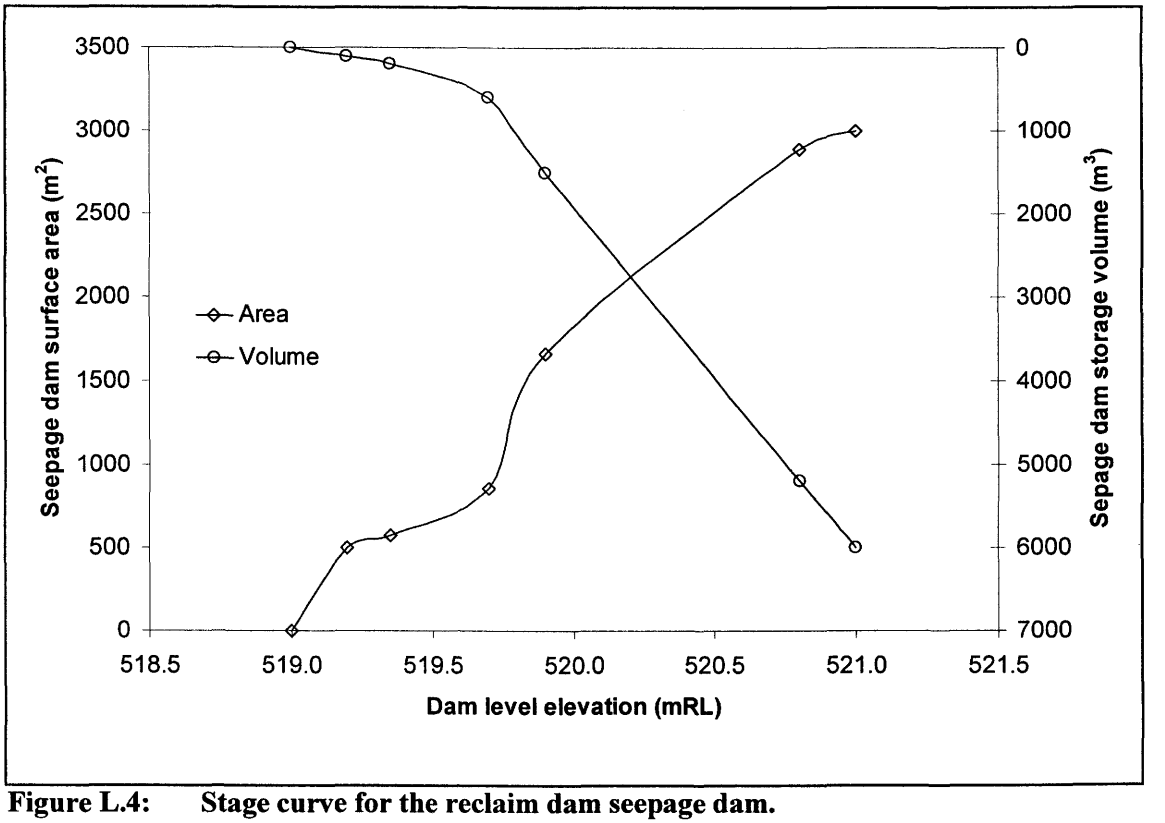

Figure L.4: Stage curve for the reclaim dam seepage dam.

Table L.1: Kidston tailings impoundment water balance calculations: Section 1, pond level details.

Date	True level (mRL)	Pond drop (m)	Pond volume (m^3)	Pond area (ha)	Tailings area (ha)	# days between	Cum # days
8-Sep-97	554.03	0.66	2748622	108	202	0	0
15-Sep-97	553.94	0.75	2675039	106	204	7	7
27-Sep-97	553.93	0.76	2666919	105	205	12	19
6-Oct-97	553.84	0.85	2594358	103	207	9	28
10-Oct-97	553.79	0.90	2554443	102	208	4	32
13-Oct-97	553.77	0.92	2538557	101	209	3	35
20-Oct-97	553.72	0.97	2499039	100	210	7	42
27-Oct-97	553.63	1.06	2428623	98	212	7	49
10-Nov-97	553.55	1.14	2366803	96	214	14	63
18-Nov-97	553.57	1.12	2382190	97	213	8	71
24-Nov-97	553.49	1.20	2320915	95	215	6	77
1-Dec-97	553.49	1.20	2320915	95	215	7	84
8-Dec-97	553.45	1.24	2290550	94	216	7	91

Table L.1: Kidston tailings impoundment water balance calculations: Section 1, pond level details.

Date	True level (mRL)	Pond drop (m)	Pond volume (m^3)	Pond area (ha)	Tailings area (ha)	# days between	Cum # days
16-Dec-97	553.44	1.25	2282987	94	216	8	99
22-Dec-97	553.42	1.27	2267895	93	217	6	105
12-Jan-98	553.65	1.04	2444192	99	211	21	126
20-Jan-98	553.86	0.83	2610403	104	206	8	134
28-Jan-98	553.89	0.80	2634556	104	206	8	142
2-Feb-98	553.92	0.77	2658812	105	205	5	147
9-Feb-98	553.79	0.90	2554443	102	208	7	154
16-Feb-98	553.92	0.77	2658812	105	205	7	161
23-Feb-98	553.97	0.72	2699464	106	204	7	168
2-Mar-98	553.98	0.71	2707629	107	203	7	175
9-Mar-98	554.26	0.43	2940846	114	196	7	182
17-Mar-98	554.33	0.36	3000541	115	195	8	190
23-Mar-98	554.03	0.66	2748622	108	202	6	196
31-Mar-98	554.01	0.68	2732191	107	203	8	204
11-May-98	553.85	0.84	2602375	103	207	41	245
18-May-98	553.83	0.86	2586352	103	207	7	252
25-May-98	553.78	0.91	2546494	102	208	7	259
2-Jun-98	553.75	0.94	2522716	101	209	8	267
15-Jun-98	553.73	0.96	2506920	100	210	13	280
22-Jun-98	553.71	0.98	2491170	100	210	7	287
6-Jul-98	553.66	1.03	2451993	99	211	14	301
13-Jul-98	553.65	1.04	2444192	99	211	7	308
20-Jul-98	553.63	1.06	2428623	98	212	7	315
27-Jul-98	553.61	1.08	2413100	98	212	7	322
3-Aug-98	553.56	1.13	2374491	96	214	7	329
10-Aug-98	553.57	1.12	2382190	97	213	7	336
18-Aug-98	553.54	1.15	2359127	96	214	8	344
24-Aug-98	553.51	1.18	2336166	95	215	6	350
31-Aug-98	553.41	1.28	2260366	93	217	7	357
10-Sep-98	553.16	1.53	2075835	87	223	10	367
30-Sep-98	552.99	1.70	1954406	83	227	20	387
5-Oct-98	552.93	1.76	1912332	82	228	5	392
12-Oct-98	552.89	1.80	1884510	81	229	7	399
19-Oct-98	552.89	1.80	1884510	81	229	7	406
18-Feb-99	553.19	1.50	2097604	88	222	122	528
9-Mar-99	553.52	1.17	2343808	95	215	19	547
17-Mar-99	553.36	1.33	2222892	92	218	8	555
27-Apr-99	553.35	1.34	2215432	91	219	41	596
19-May-99	553.07	1.62	2011140	85	225	22	618
7-Jun-99	553.02	1.67	1975596	84	226	19	637
30-Jun-99	552.97	1.72	1940336	83	227	23	660
14-Jul-99	552.92	1.77	1905360	82	228	14	674
16-Aug-99	552.86	1.83	1863762	80	230	33	707
31-Aug-99	552.81	1.88	1829410	79	231	15	722
24-Sep-99	552.76	1.93	1795342	78	232	24	746
10-Oct-99	552.79	1.90	1815749	79	231	16	762

Table L.1: Kidston tailings impoundment water balance calculations: Section 1, pond level details.

Date	True level (mRL)	Pond drop (m)	Pond volume (m^3)	Pond area (ha)	Tailings area (ha)	# days between	Cum # days
4-Nov-99	552.81	1.88	1829410	79	231	25	787
11-Nov-99	552.74	1.95	1781794	78	232	7	794
20-Dec-99	552.64	2.05	1714736	76	234	39	833
4-Jan-00	552.62	2.07	1701461	75	235	15	848
25-Jan-00	552.85	1.84	1856869	80	230	21	869
8-Feb-00	552.76	1.93	1795342	78	232	14	883
22-Feb-00	552.76	1.93	1795342	78	232	14	897
7-Mar-00	552.94	1.75	1919316	82	228	14	911
14-Mar-00	552.96	1.73	1933318	83	227	7	918
4-Apr-00	553.01	1.68	1968521	84	226	21	939
17-Apr-00	553.14	1.55	2061379	87	223	13	952
28-Apr-00	553.24	1.45	2134113	89	221	11	963
9-May-00	553.45	1.24	2290550	94	216	11	974
6-Jun-00	553.34	1.35	2207982	91	219	28	1002
1-Aug-00	553.05	1.64	1996889	85	225	56	1058
22-Aug-00	553.18	1.51	2090336	88	222	21	1079
8-Sep-00	553.08	1.61	2018283	85	225	17	1096
8-Oct-00	552.53	2.16	1642284	73	237	30	1126
21-Oct-00	552.86	1.83	1863762	80	230	13	1139
30-Jan-01	554.08	0.61	2789899	109	201	101	1240
20-Feb-01	554.24	0.45	2923893	113	197	21	1261
26-Feb-01	554.08	0.61	2789899	109	201	6	1267
24-Mar-01	554.35	0.34	3017699	116	194	26	1293
12-Apr-01	554.15	0.54	2848164	111	199	19	1312
24-Apr-01	553.95	0.74	2683169	106	204	12	1324

Table L.2: Kidston tailings impoundment water balance calculations: Section 2, seepage drain details.

Date	SW sect., W_1 (l/s)	West. drain, W_2 (l/s)	NW back, W_3 (l/s)	NW mid, W_4 (l/s)	NW front, W_5 (l/s)	All W seep, W (l/s)	NE pipe, E_1 (l/s)	RD north E_2 (l/s)	TD direct E_3 (l/s)	East drain, E_4 (l/s)	All E seep, E (l/s)	Deep seep, D (l/s)	All seep, Q_6 (l/s)
15-Sep-97	-0.23	2.30	0.78	0.08	0.22	3.14	0.49	1.07	0.93	2.70	5.20	1.01	9.35
27-Sep-97	-0.23	2.30	0.78	0.08	0.22	3.14	0.49	1.07	0.92	2.70	5.19	1.01	9.33
6-Oct-97	-0.25	2.28	0.77	0.07	0.22	3.08	0.49	1.07	0.92	2.67	5.15	0.99	9.21
10-Oct-97	-0.26	2.27	0.76	0.07	0.21	3.05	0.48	1.06	0.91	2.66	5.12	0.97	9.15
13-Oct-97	-0.27	2.26	0.76	0.07	0.21	3.04	0.48	1.06	0.91	2.65	5.11	0.97	9.12
20-Oct-97	-0.28	2.25	0.75	0.07	0.21	3.01	0.48	1.06	0.91	2.64	5.09	0.96	9.06
27-Oct-97	-0.29	2.23	0.74	0.07	0.21	2.96	0.47	1.05	0.90	2.61	5.04	0.94	8.94
10-Nov-97	-0.31	2.21	0.73	0.07	0.21	2.91	0.47	1.05	0.90	2.59	5.00	0.92	8.83
18-Nov-97	-0.31	2.22	0.73	0.07	0.21	2.92	0.47	1.05	0.90	2.59	5.01	0.92	8.86
24-Nov-97	-0.32	2.20	0.72	0.07	0.21	2.88	0.46	1.04	0.89	2.57	4.97	0.91	8.76
1-Dec-97	-0.32	2.20	0.72	0.07	0.21	2.88	0.46	1.04	0.89	2.57	4.97	0.91	8.76
8-Dec-97	-0.33	2.19	0.71	0.07	0.21	2.85	0.46	1.04	0.89	2.56	4.95	0.90	8.71
16-Dec-97	-0.33	2.19	0.71	0.07	0.21	2.85	0.46	1.04	0.89	2.56	4.95	0.89	8.69
22-Dec-97	-0.33	2.18	0.71	0.07	0.21	2.84	0.46	1.04	0.89	2.55	4.94	0.89	8.67

Table L.2: Kidston tailings impoundment water balance calculations: Section 2, seepage drain details.

Date	SW sect., W_1 (l/s)	West. drain, W_2 (l/s)	NW back, W_3 (l/s)	NW mid, W_4 (l/s)	NW front, W_5 (l/s)	All W seep, W (l/s)	NE pipe, E_1 (l/s)	RD north E_2 (l/s)	TD direct E_3 (l/s)	East drain, E_4 (l/s)	All E seep, E (l/s)	Deep seep, D (l/s)	All seep, Q_6 (l/s)
12-Jan-98	-0.29	2.23	0.74	0.07	0.21	2.97	0.47	1.06	0.90	2.62	5.05	0.94	8.96
20-Jan-98	-0.25	2.28	0.77	0.07	0.22	3.09	0.49	1.07	0.92	2.68	5.16	0.99	9.24
28-Jan-98	-0.24	2.29	0.77	0.07	0.22	3.11	0.49	1.07	0.92	2.69	5.17	1.00	9.28
2-Feb-98	-0.24	2.30	0.78	0.08	0.22	3.13	0.49	1.07	0.92	2.70	5.19	1.00	9.32
9-Feb-98	-0.26	2.27	0.76	0.07	0.21	3.05	0.48	1.06	0.91	2.66	5.12	0.97	9.15
16-Feb-98	-0.24	2.30	0.78	0.08	0.22	3.13	0.49	1.07	0.92	2.70	5.19	1.00	9.32
23-Feb-98	-0.23	2.31	0.78	0.08	0.22	3.16	0.50	1.08	0.93	2.71	5.21	1.02	9.39
2-Mar-98	-0.22	2.31	0.78	0.08	0.22	3.17	0.50	1.08	0.93	2.71	5.22	1.02	9.40
9-Mar-98	-0.17	2.38	0.82	0.08	0.23	3.34	0.52	1.10	0.95	2.80	5.36	1.09	9.78
17-Mar-98	-0.15	2.39	0.83	0.08	0.23	3.38	0.52	1.10	0.95	2.82	5.39	1.10	9.88
23-Mar-98	-0.21	2.32	0.79	0.08	0.22	3.20	0.50	1.08	0.93	2.73	5.24	1.03	9.47
31-Mar-98	-0.22	2.32	0.79	0.08	0.22	3.18	0.50	1.08	0.93	2.72	5.23	1.03	9.44
11-May-98	-0.25	2.28	0.77	0.07	0.22	3.09	0.49	1.07	0.92	2.68	5.15	0.99	9.23
18-May-98	-0.25	2.28	0.76	0.07	0.22	3.08	0.49	1.07	0.92	2.67	5.14	0.98	9.20
25-May-98	-0.26	2.26	0.76	0.07	0.21	3.05	0.48	1.06	0.91	2.66	5.12	0.97	9.13
2-Jun-98	-0.27	2.26	0.75	0.07	0.21	3.03	0.48	1.06	0.91	2.65	5.10	0.96	9.09
15-Jun-98	-0.27	2.25	0.75	0.07	0.21	3.02	0.48	1.06	0.91	2.64	5.09	0.96	9.07
22-Jun-98	-0.28	2.25	0.75	0.07	0.21	3.01	0.48	1.06	0.91	2.64	5.08	0.96	9.04
6-Jul-98	-0.29	2.24	0.74	0.07	0.21	2.98	0.48	1.06	0.91	2.62	5.06	0.94	8.98
13-Jul-98	-0.29	2.23	0.74	0.07	0.21	2.97	0.47	1.06	0.90	2.62	5.05	0.94	8.96
20-Jul-98	-0.29	2.23	0.74	0.07	0.21	2.96	0.47	1.05	0.90	2.61	5.04	0.94	8.94
27-Jul-98	-0.30	2.23	0.74	0.07	0.21	2.95	0.47	1.05	0.90	2.61	5.03	0.93	8.91
3-Aug-98	-0.31	2.21	0.73	0.07	0.21	2.92	0.47	1.05	0.90	2.59	5.01	0.92	8.85
10-Aug-98	-0.31	2.22	0.73	0.07	0.21	2.92	0.47	1.05	0.90	2.59	5.01	0.92	8.86
18-Aug-98	-0.31	2.21	0.73	0.07	0.21	2.91	0.47	1.05	0.90	2.59	5.00	0.92	8.82
24-Aug-98	-0.32	2.20	0.72	0.07	0.21	2.89	0.47	1.05	0.89	2.58	4.98	0.91	8.78
31-Aug-98	-0.34	2.18	0.71	0.07	0.21	2.83	0.46	1.04	0.89	2.55	4.94	0.89	8.65
10-Sep-98	-0.38	2.13	0.68	0.07	0.20	2.69	0.44	1.02	0.87	2.48	4.82	0.83	8.34
30-Sep-98	-0.41	2.09	0.66	0.07	0.20	2.60	0.43	1.01	0.86	2.43	4.74	0.80	8.13
5-Oct-98	-0.42	2.08	0.65	0.07	0.20	2.56	0.43	1.01	0.86	2.42	4.71	0.78	8.05
12-Oct-98	-0.43	2.07	0.64	0.07	0.20	2.54	0.42	1.01	0.85	2.41	4.69	0.78	8.00
19-Oct-98	-0.43	2.07	0.64	0.07	0.20	2.54	0.42	1.01	0.85	2.41	4.69	0.78	8.00
18-Feb-99	-0.38	2.13	0.68	0.07	0.20	2.71	0.44	1.02	0.87	2.49	4.83	0.84	8.38
9-Mar-99	-0.31	2.21	0.72	0.07	0.21	2.89	0.47	1.05	0.90	2.58	4.99	0.91	8.80
17-Mar-99	-0.34	2.17	0.70	0.07	0.21	2.80	0.46	1.04	0.88	2.54	4.91	0.88	8.59
27-Apr-99	-0.35	2.17	0.70	0.07	0.21	2.80	0.45	1.04	0.88	2.53	4.91	0.87	8.58
19-May-99	-0.40	2.11	0.67	0.07	0.20	2.64	0.44	1.02	0.86	2.46	4.77	0.81	8.23
7-Jun-99	-0.41	2.09	0.66	0.07	0.20	2.61	0.43	1.01	0.86	2.44	4.75	0.80	8.16
30-Jun-99	-0.42	2.08	0.65	0.07	0.20	2.58	0.43	1.01	0.86	2.43	4.73	0.79	8.10
14-Jul-99	-0.43	2.07	0.65	0.07	0.20	2.56	0.43	1.01	0.85	2.41	4.70	0.78	8.04
16-Aug-99	-0.44	2.06	0.64	0.07	0.19	2.52	0.42	1.00	0.85	2.40	4.67	0.77	7.97
31-Aug-99	-0.44	2.05	0.63	0.06	0.19	2.50	0.42	1.00	0.85	2.38	4.65	0.76	7.91
24-Sep-99	-0.45	2.04	0.63	0.06	0.19	2.47	0.42	1.00	0.84	2.37	4.63	0.75	7.85
10-Oct-99	-0.45	2.05	0.63	0.06	0.19	2.49	0.42	1.00	0.85	2.38	4.64	0.75	7.88

Table L.2: Kidston tailings impoundment water balance calculations: Section 2, seepage drain details.

Date	SW sect., W_1 (l/s)	West. drain, W_2 (l/s)	NW back, W_3 (l/s)	NW mid, W_4 (l/s)	NW front, W_5 (l/s)	All W seep, W (l/s)	NE pipe, E_1 (l/s)	RD north E_2 (l/s)	TD direct E_3 (l/s)	East drain, E_4 (l/s)	All E seep, E (l/s)	Deep seep, D (l/s)	All seep, Q_6 (l/s)
4-Nov-99	-0.44	2.05	0.63	0.06	0.19	2.50	0.42	1.00	0.85	2.38	4.65	0.76	7.91
11-Nov-99	-0.46	2.03	0.63	0.06	0.19	2.46	0.42	1.00	0.84	2.37	4.62	0.74	7.82
20-Dec-99	-0.47	2.01	0.61	0.06	0.19	2.41	0.41	0.99	0.84	2.34	4.57	0.72	7.70
4-Jan-00	-0.48	2.01	0.61	0.06	0.19	2.40	0.41	0.99	0.83	2.33	4.56	0.72	7.68
25-Jan-00	-0.44	2.06	0.64	0.07	0.19	2.52	0.42	1.00	0.85	2.39	4.67	0.77	7.96
8-Feb-00	-0.45	2.04	0.63	0.06	0.19	2.47	0.42	1.00	0.84	2.37	4.63	0.75	7.85
22-Feb-00	-0.45	2.04	0.63	0.06	0.19	2.47	0.42	1.00	0.84	2.37	4.63	0.75	7.85
7-Mar-00	-0.42	2.08	0.65	0.07	0.20	2.57	0.43	1.01	0.86	2.42	4.71	0.79	8.07
14-Mar-00	-0.42	2.08	0.65	0.07	0.20	2.58	0.43	1.01	0.86	2.42	4.72	0.79	8.09
4-Apr-00	-0.41	2.09	0.66	0.07	0.20	2.61	0.43	1.01	0.86	2.44	4.74	0.80	8.15
17-Apr-00	-0.39	2.12	0.68	0.07	0.20	2.68	0.44	1.02	0.87	2.47	4.81	0.83	8.31
28-Apr-00	-0.37	2.14	0.69	0.07	0.20	2.73	0.45	1.03	0.88	2.50	4.85	0.85	8.44
9-May-00	-0.33	2.19	0.71	0.07	0.21	2.85	0.46	1.04	0.89	2.56	4.95	0.90	8.71
6-Jun-00	-0.35	2.16	0.70	0.07	0.20	2.79	0.45	1.03	0.88	2.53	4.90	0.87	8.57
1-Aug-00	-0.40	2.10	0.66	0.07	0.20	2.63	0.44	1.02	0.86	2.45	4.76	0.81	8.20
22-Aug-00	-0.38	2.13	0.68	0.07	0.20	2.70	0.44	1.02	0.87	2.49	4.83	0.84	8.36
8-Sep-00	-0.40	2.11	0.67	0.07	0.20	2.65	0.44	1.02	0.87	2.46	4.78	0.82	8.24
8-Oct-00	-0.49	1.99	0.60	0.06	0.19	2.35	0.40	0.98	0.83	2.31	4.52	0.70	7.57
21-Oct-00	-0.44	2.06	0.64	0.07	0.19	2.52	0.42	1.00	0.85	2.40	4.67	0.77	7.97
30-Jan-01	-0.20	2.33	0.80	0.08	0.22	3.23	0.50	1.08	0.94	2.74	5.27	1.04	9.53
20-Feb-01	-0.17	2.37	0.82	0.08	0.22	3.32	0.52	1.09	0.95	2.79	5.35	1.08	9.75
26-Feb-01	-0.20	2.33	0.80	0.08	0.22	3.23	0.50	1.08	0.94	2.74	5.27	1.04	9.53
24-Mar-01	-0.15	2.40	0.84	0.08	0.23	3.39	0.52	1.10	0.95	2.82	5.40	1.11	9.90
12-Apr-01	-0.19	2.35	0.81	0.08	0.22	3.27	0.51	1.09	0.94	2.76	5.30	1.06	9.63
24-Apr-01	-0.23	2.30	0.78	0.08	0.22	3.15	0.50	1.08	0.93	2.70	5.20	1.01	9.36

Table L.3: Kidston tailings impoundment water balance calculations: Section 3, pump back, rainfall and evaporation details.

Date	SW sect. pump, P_1 (l/s)	West drain pump, P_2 (l/s)	RD pump, P_3 (l/s)	SP pump, P_4 (l/s)	All pump, Q_{10} (l/s)	Rain, P (mm)	Rain on pond, Q_1 (m^3)	Rain on tails, Q_2 (m^3)	Evap., PE (mm)	Evap. from pond, Q_3 (m^3)	Evap. from tails, Q_4 (m^3)
15-Sep-97	0	2.301			2	0.0	0	0	46.4	49026	18993
27-Sep-97	0	2.298	30	59	92	0.0	0	0	70.4	74161	28832
6-Oct-97	0	2.278			2	2.6	2681	5379	53.5	55171	22142
10-Oct-97	0	2.266			2	0.0	0	0	24.4	24888	10166
13-Oct-97	0	2.262	17	31	50	0.0	0	0	20.2	20443	8410
20-Oct-97	0	2.250	17	29	48	0.0	0	0	48.4	48514	20315
27-Oct-97	0	2.230			2	0.0	0	0	44.0	43187	18671
10-Nov-97	0	2.212		2	4	19.2	18462	41058	88.9	85455	38010
18-Nov-97	0	2.216	40	83	125	0.0	0	0	46.7	45138	19935
24-Nov-97	0	2.198			2	6.0	5685	12915	38.4	36412	16546
1-Dec-97	0	2.198			2	21.8	20654	46926	42.5	40226	18279
8-Dec-97	0	2.189		60	62	0.2	188	432	46.1	43280	19950

Table L.3: Kidston tailings impoundment water balance calculations: Section 3, pump back, rainfall and evaporation details.

Date	SW sect. pump, P_1 (l/s)	West drain pump, P_2 (l/s)	RD pump, P_3 (l/s)	SP pump, P_4 (l/s)	All pump, Q_{10} (l/s)	Rain, P (mm)	Rain on pond, Q_1 (m^3)	Rain on tails, Q_2 (m^3)	Evap., PE (mm)	Evap. from pond, Q_3 (m^3)	Evap. from tails, Q_4 (m^3)
16-Dec-97	0	2.187			2	29.4	27510	63630	41.7	39051	18065
22-Dec-97	0	2.183			2	36.8	34263	79817	28.9	26950	12556
12-Jan-98	0	2.234			2	168.2	165724	355696	66.9	65888	28283
20-Jan-98	0	2.282		66	68	50.8	52625	104855	36.5	37848	15082
28-Jan-98	0	2.289			2	52.4	54666	107774	52.1	54323	21420
2-Feb-98	0	2.296	62	100	164	0.2	210	410	29.7	31183	12166
9-Feb-98	0	2.266			2	0.0	0	0	47.2	48136	19663
16-Feb-98	0	2.296	10	26	39	37.8	39712	77468	31.6	33249	12972
23-Feb-98	0	2.308	45	100	147	5.2	5527	10593	41.3	43942	16844
2-Mar-98	0	2.310			2	73.4	78195	149345	20.5	21869	8353
9-Mar-98	0	2.375	21	100	123	57.0	64714	111986	23.3	26504	9173
17-Mar-98	0	2.392	65	140	208	0.0	0	0	49.9	57539	19429
23-Mar-98	0	2.322			2	1.6	1724	3236	21.9	23560	8842
31-Mar-98	0	2.317	25	46	73	0.0	0	0	41.0	43967	16618
11-May-98	0	2.280		22	24	31.4	32451	64889	202.3	209105	83624
18-May-98	0	2.275		17	19	2.6	2674	5386	21.6	22203	8942
25-May-98	0	2.264	3	5	10	0.0	0	0	28.3	28768	11793
2-Jun-98	0	2.257		21	23	0.6	606	1254	25.0	25256	10464
15-Jun-98	0	2.253	20	35	57	0.0	0	0	48.7	48954	20426
22-Jun-98	0	2.248	10	21	34	0.0	0	0	21.5	21532	9048
6-Jul-98	0	2.237		14	16	3.6	3556	7604	43.1	42570	18209
13-Jul-98	0	2.234		41	43	1.4	1379	2961	23.6	23285	9995
20-Jul-98	0	2.230	12	23	37	0.0	0	0	23.3	22890	9896
27-Jul-98	0	2.225	12	25	39	0.0	0	0	24.0	23385	10182
3-Aug-98	0	2.214			2	0.0	0	0	28.7	27657	12258
10-Aug-98	0	2.216	25	50	77	0.0	0	0	28.2	27269	12043
18-Aug-98	0	2.210	15	21	39	0.0	0	0	36.0	34570	15431
24-Aug-98	0	2.203	8	15	25	0.0	0	0	26.2	24943	11254
31-Aug-98	0	2.181			2	0.0	0	0	35.8	33291	15566
10-Sep-98	0	2.125			2	9.4	8190	20950	42.7	37244	19053
30-Sep-98	0	2.088	3	8	13	0.0	0	0	112.8	94008	51158
5-Oct-98	0	2.075			2	0.0	0	0	29.5	24164	13441
12-Oct-98	0	2.067		42	44	1.2	973	2747	46.7	37865	21375
19-Oct-98	0	2.067		0	2	12.8	10381	29299	37.1	30087	16984
18-Feb-99	0	2.132			2	407.6	357918	905642	629.5	552780	279740
9-Mar-99	0	2.205	77	100	179	23.0	21953	49347	82.5	78712	35387
17-Mar-99	0	2.169			2	0.4	367	873	31.7	29046	13827
27-Apr-99	0	2.167		57	60	6.0	5489	13111	154.8	141613	67654
19-May-99	0	2.106			2	9.6	8170	21590	88.0	74886	39582
7-Jun-99	0	2.095	15	25	42	0.0	0	0	70.5	59241	31887
30-Jun-99	0	2.084	12	25	39	0.0	0	0	75.9	62925	34494
14-Jul-99	0	2.073	10	13	25	0.0	0	0	43.6	35607	19880
16-Aug-99	0	2.060		37	39	0.2	161	459	123.4	99258	56653
31-Aug-99	0	2.049	10	25	37	0.0	0	0	67.2	53298	30987

Table L.3: Kidston tailings impoundment water balance calculations: Section 3, pump back, rainfall and evaporation details.

Date	SW sect. pump, P_1 (l/s)	West drain pump, P_2 (l/s)	RD pump, P_3 (l/s)	SP pump, P_4 (l/s)	All pump, Q_{10} (l/s)	Rain, P (mm)	Rain on pond, Q_1 (m^3)	Rain on tails, Q_2 (m^3)	Evap., PE (mm)	Evap. from pond, Q_3 (m^3)	Evap. from tails, Q_4 (m^3)
24-Sep-99	0	2.039		57	59	0.2	157	463	128.9	100886	59750
10-Oct-99	0	2.045	30	67	99	0.0	0	0	94.4	74530	43653
4-Nov-99	0	2.049		91	93	1.4	1111	3229	155.9	123704	71921
11-Nov-99	0	2.034			2	32.2	25060	74760	31.9	24845	14824
20-Dec-99	0	2.013		29	31	23.8	18010	55770	187.0	141482	87623
4-Jan-00	0	2.009			2	33.6	25282	78878	77.3	58192	36311
25-Jan-00	0	2.058	48	100	150	11.8	9466	27114	114.5	91884	52638
8-Feb-00	0	2.039		14	16	6.0	4695	13905	74.0	57904	34294
22-Feb-00	0	2.039			2	64.4	50398	149242	57.8	45241	26794
7-Mar-00	0	2.077			2	95.8	78750	218230	57.2	47039	26071
14-Mar-00	0	2.082	9	80	91	0.4	331	909	29.5	24407	13428
4-Apr-00	0	2.093			2	59.6	49919	134841	95.9	80332	43398
17-Apr-00	0	2.121			2	114.2	98985	255035	43.3	37519	19333
28-Apr-00	0	2.143			2	60.8	54082	134398	31.6	28110	13971
9-May-00	0	2.189	70	149	221	0.0	0	0	33.1	31047	14311
6-Jun-00	0	2.165			2	13.4	12227	29313	74.4	67915	32562
1-Aug-00	0	2.101			2	79.2	67044	178476	150.3	127206	67726
22-Aug-00	0	2.130	40	62	104	0.0	0	0	73.5	64341	32678
8-Sep-00	0	2.108	4	19	25	0.0	0	0	84.2	71865	37847
8-Oct-00	0	1.990			2	0.0	0	0	157.7	115611	74623
21-Oct-00	0	2.060	97	160	259	3.6	2896	8264	66.1	53163	30344
30-Jan-01	0	2.333		25	28	420.0	457846	844154	474.6	517372	190781
20-Feb-01	0	2.371			2	123.4	139474	243066	83.1	93976	32755
26-Feb-01	0	2.333			2	39.0	42514	78386	25.4	27705	10216
24-Mar-01	0	2.397	31	100	134	38.4	44476	74564	119.8	138751	46523
12-Apr-01	0	2.349			2	0.0	0	0	82.7	91544	32935
24-Apr-01	0	2.303			2	0.0	0	0	49.6	52498	20266

Table L.4: Kidston tailings impoundment water balance calculations: Section 4, Paddy's Knob runoff, irrigation, penstock decant and runoff details.

Date	Paddy's runoff, Q_5 (m^3)	Irrigation, Q_9 (m^3)	Penstock decant, Q_8 (l/s)	Pond storage change, ΔS (m^3)	Infiltration, Q_{11} (m_3)	Runoff to pond, Q_7 (m^3)	Runoff to pond, Q_7 (%)
15-Sep-97	0	5544	11	-73583			
27-Sep-97	0	9504		-8119			
6-Oct-97	1082	7128	8	-72562	4949	430	8%
10-Oct-97	0	3168	16	-39915			
13-Oct-97	0	2376		-15886			
20-Oct-97	0	5544		-39517			
27-Oct-97	0	5544	17	-70416			
10-Nov-97	7987			-61820	29562	11496	28%
18-Nov-97	0			15387			
24-Nov-97	2496		50	-61275	10074	2841	22%
1-Dec-97	9069		23	0	29563	17363	37%

Table L.4: Kidston tailings impoundment water balance calculations: Section 4, Paddy's Knob runoff, irrigation, penstock decant and runoff details.

Date	Paddy's runoff, Q_5 (m^3)	Irrigation, Q_9 (m^3)	Penstock decant, Q_8 (l/s)	Pond storage change, ΔS (m^3)	Infiltration, Q_{11} (m_3)	Runoff to pond, Q_7 (m^3)	Runoff to pond, Q_7 (%)
8-Dec-97	83			-30365	424	9	2%
16-Dec-97	12230		71	-7563	39450	24179	38%
22-Dec-97	15309		196	-15092	39111	40707	51%
12-Jan-98	69971		170	176297	149392	206304	58%
20-Jan-98	21133			166211	49282	55573	53%
28-Jan-98	21798		115	24153	51732	56043	52%
2-Feb-98	83			24255	398	12	3%
9-Feb-98	0		54	-104369			
16-Feb-98	15725			104369	41058	36410	47%
23-Feb-98	2163			40653	8686	1907	18%
2-Mar-98	30534		356	8165	56751	92594	62%
9-Mar-98	23712			233217	48154	63832	57%
17-Mar-98	0			59695			
23-Mar-98	666		427	-251919	2944	291	9%
31-Mar-98	0			-16431			
11-May-98	13062			-129816	53857	11031	17%
18-May-98	1082			-16023	4739	646	12%
25-May-98	0			-39858			
2-Jun-98	250			-23779	1217	38	3%
15-Jun-98	0			-15796			
22-Jun-98	0			-15750			
6-Jul-98	1498			-39177	6996	608	8%
13-Jul-98	582			-7801	2872	89	3%
20-Jul-98	0			-15569			
27-Jul-98	0			-15523			
3-Aug-98	0	5544	0	-38609			
10-Aug-98	0	5544		7699			
18-Aug-98	0	6336		-23063			
24-Aug-98	0	4752		-22961			
31-Aug-98	0	5544	47	-75799			
10-Sep-98	3910	7920	190	-184532	15084	5866	28%
30-Sep-98	0	15841		-121429			
5-Oct-98	0	3960	14	-42074			
12-Oct-98	499	5544		-27822	2637	110	4%
19-Oct-98	5325	5544		0	21388	7911	27%
18-Feb-99	169562		31	213094	570554	335087	37%
9-Mar-99	9568			246204	36023	13324	27%
17-Mar-99	166		109	-120916	856	17	2%
27-Apr-99	2496			-7461	12718	393	3%
19-May-99	3994		59	-204291	18784	2807	13%
7-Jun-99	0			-35544			
30-Jun-99	0			-35260			
14-Jul-99	0			-34976			
16-Aug-99	83	26137		-41597	445	14	3%
31-Aug-99	0	11880		-34352			

Table L.4: Kidston tailings impoundment water balance calculations: Section 4, Paddy's Knob runoff, irrigation, penstock decant and runoff details.

Date	Paddy's runoff, Q_5 (m^3)	Irrigation, Q_9 (m^3)	Penstock decant, Q_8 (l/s)	Pond storage change, ΔS (m^3)	Infiltration, Q_{11} (m_3)	Runoff to pond, Q_7 (m^3)	Runoff to pond, Q_7 (%)
24-Sep-99	83	19009		-34068	454	9	2%
10-Oct-99	0	12672		20407			
4-Nov-99	582	19801		13661	3132	97	3%
11-Nov-99	13395		195	-47616	43361	31399	42%
20-Dec-99	9901			-67058	45174	10596	19%
4-Jan-00	13978		23	-13275	53637	25241	32%
25-Jan-00	4909			155408	21962	5152	19%
8-Feb-00	2496			-61527	10706	3198	23%
22-Feb-00	26790		122	0	88053	61189	41%
7-Mar-00	39853		110	123974	106933	111297	51%
14-Mar-00	166			14002	891	18	2%
4-Apr-00	24794		22	35203	90343	44497	33%
17-Apr-00	47507		218	92857	109665	145370	57%
28-Apr-00	25293		98	72734	71231	63167	47%
9-May-00	0			156437			
6-Jun-00	5574		6	-82568	25795	3518	12%
1-Aug-00	32947	44354	64	-211094	130287	48189	27%
22-Aug-00	0	16633		93448			
8-Sep-00	0	13464		-72053			
8-Oct-00	0	23761	75	-375999			
21-Oct-00	1498	10296		221479	7603	661	8%
30-Jan-01	174720			926137	481168	362986	43%
20-Feb-01	51334		88	133994	128825	114241	47%
26-Feb-01	16224		443	-133994	38409	39977	51%
24-Mar-01	15974			227800	55177	19387	26%
12-Apr-01	0		20	-169535			
24-Apr-01	0		82	-164994			

Table L.5: Kidston tailings impoundment water balance calculations: North pond water balance.

Date	Rain, Q_P (m^3)	Evap., Q_E (m^3)	Runoff, Q_R (m^3)	Q_P-Q_E+Q_R (m^3)	NP Pump, P_{NP} (m^3)	NP volume, V_{NP} (m^3)	NP level, h_{NP} (m)
8-Sep-97	0	0	0	0	0	3613	0.5
15-Sep-97	0	336	0	3277	0	3277	0.5
27-Sep-97	0	509	0	2768	0	2768	0.4
6-Oct-97	19	387	85	2486	0	2486	0.3
10-Oct-97	0	176	0	2309	0	2309	0.3
13-Oct-97	0	146	0	2163	0	2163	0.3
20-Oct-97	0	350	0	1814	0	1814	0.3
27-Oct-97	0	318	0	1495	0	1495	0.2
10-Nov-97	139	642	630	1622	0	1622	0.2
18-Nov-97	0	338	0	1284	0	1284	0.2
24-Nov-97	43	278	197	1247	0	1247	0.2
1-Dec-97	158	307	715	1813	0	1813	0.3
8-Dec-97	1	333	7	1487	0	1487	0.2

Table L.5: Kidston tailings impoundment water balance calculations: North pond water balance.

Date	Rain, Q_P (m^3)	Evap., Q_E (m^3)	Runoff, Q_R (m^3)	$Q_P-Q_E+Q_R$ (m^3)	NP Pump, P_{NP} (m^3)	NP volume, V_{NP} (m^3)	NP level, h_{NP} (m)
16-Dec-97	212	302	964	2362	0	2362	0.3
22-Dec-97	266	209	1207	3626	3626	0	0.0
12-Jan-98	1215	0	5517	6732	6732	0	0.0
20-Jan-98	367	0	1666	2033	0	2033	0.3
28-Jan-98	379	376	1719	3754	3754	0	0.0
2-Feb-98	1	0	7	8	0	8	0.0
9-Feb-98	0	341	0	0	0	0	0.0
16-Feb-98	273	0	1240	1513	0	1513	0.2
23-Feb-98	38	299	171	1422	0	1422	0.2
2-Mar-98	530	148	2408	4212	4212	0	0.0
9-Mar-98	412	0	1870	2281	0	2281	0.3
17-Mar-98	0	361	0	1921	0	1921	0.3
23-Mar-98	12	158	52	1827	0	1827	0.3
31-Mar-98	0	296	0	1531	0	1531	0.2
11-May-98	227	1462	1030	1326	0	1326	0.2
18-May-98	19	156	85	1274	0	1274	0.2
25-May-98	0	204	0	1069	0	1069	0.1
2-Jun-98	4	181	20	913	0	913	0.1
15-Jun-98	0	352	0	561	0	561	0.1
22-Jun-98	0	156	0	405	0	405	0.1
6-Jul-98	26	311	118	238	0	238	0.0
13-Jul-98	10	171	46	123	0	123	0.0
20-Jul-98	0	169	0	0	0	0	0.0
27-Jul-98	0	0	0	0	0	0	0.0
3-Aug-98	0	0	0	0	0	0	0.0
10-Aug-98	0	0	0	0	0	0	0.0
18-Aug-98	0	0	0	0	0	0	0.0
24-Aug-98	0	0	0	0	0	0	0.0
31-Aug-98	0	0	0	0	0	0	0.0
10-Sep-98	68	0	308	376	0	376	0.1
30-Sep-98	0	815	0	0	0	0	0.0
5-Oct-98	0	0	0	0	0	0	0.0
12-Oct-98	9	0	39	48	0	48	0.0
19-Oct-98	92	268	420	292	0	292	0.0
18-Feb-99	2945	4548	13369	12058	12058	0	0.0
9-Mar-99	166	0	754	921	0	921	0.1
17-Mar-99	3	229	13	708	0	708	0.1
27-Apr-99	43	1118	197	0	0	0	0.0
19-May-99	69	0	315	384	0	384	0.1
7-Jun-99	0	510	0	0	0	0	0.0
30-Jun-99	0	0	0	0	0	0	0.0
14-Jul-99	0	0	0	0	0	0	0.0
16-Aug-99	1	0	7	8	0	8	0.0
31-Aug-99	0	485	0	0	0	0	0.0
24-Sep-99	1	0	7	8	0	8	0.0
10-Oct-99	0	682	0	0	0	0	0.0

Table L.5: Kidston tailings impoundment water balance calculations: North pond water balance.

Date	Rain, Q_P (m^3)	Evap., Q_E (m^3)	Runoff, Q_R (m^3)	Q_P-Q_E+Q_R (m^3)	NP Pump, P_{NP} (m^3)	NP volume, V_{NP} (m^3)	NP level, h_{NP} (m)
4-Nov-99	10	0	46	56	0	56	0.0
11-Nov-99	233	231	1056	1114	0	1114	0.2
20-Dec-99	172	1351	781	716	0	716	0.1
4-Jan-00	243	559	1102	1502	0	1502	0.2
25-Jan-00	85	828	387	1147	0	1147	0.2
8-Feb-00	43	535	197	852	0	852	0.1
22-Feb-00	465	418	2112	3012	0	3012	0.4
7-Mar-00	692	413	3142	6433	6433	0	0.0
14-Mar-00	3	0	13	16	0	16	0.0
4-Apr-00	431	693	1955	1709	0	1709	0.2
17-Apr-00	825	313	3746	5967	5967	0	0.0
28-Apr-00	439	0	1994	2434	0	2434	0.3
9-May-00	0	239	0	2194	0	2194	0.3
6-Jun-00	97	538	440	2193	0	2193	0.3
1-Aug-00	572	1086	2598	4277	4277	0	0.0
22-Aug-00	0	0	0	0	0	0	0.0
8-Sep-00	0	0	0	0	0	0	0.0
8-Oct-00	0	0	0	0	0	0	0.0
21-Oct-00	26	0	118	144	0	144	0.0
30-Jan-01	3035	3429	13776	13526	13526	0	0.0
20-Feb-01	892	0	4048	4939	4939	0	0.0
26-Feb-01	282	0	1279	1561	0	1561	0.2
24-Mar-01	277	866	1260	2232	0	2232	0.3
12-Apr-01	0	597	0	1635	0	1635	0.2
24-Apr-01	0	359	0	1277	0	1277	0.2

Table L.6: Kidston tailings impoundment water balance calculations: South pond water balance.

Date	Area, A_{SP} (m^2)	Rain, Q_P, (m^3)	Evap., Q_E (m^3)	Run., Q_R (m^3)	Ditch, S_{DD} (m^3)	Pump, P_{NP} (m^3)	Plant use, Q_{plant} (m^3)	Pump, P_4 (m^3)	Vol., V_{SP} (m^3)	Vol. req. by RD (m^3)	Pump, P_{SP} (m^3)	Vol. ret. V_{SP} (m^3)
8-Sep-97	15057	0	0	0	0	0	0	0	20341	0	0	20341
15-Sep-97	15024	0	-698	0	9072	0	-13306	0	15410	4931	4931	20341
27-Sep-97	15024	0	-1058	0	15552	0	-22810	-61559	-49534	69875	69875	20341
6-Oct-97	15024	39	-804	228	11664	0	-17107	0	14361	5980	5980	20341
10-Oct-97	15024	0	-367	0	5184	0	-7603	0	17555	2786	2786	20341
13-Oct-97	15024	0	-303	0	3888	0	-5702	-7963	10261	10080	10080	20341
20-Oct-97	15024	0	-727	0	9072	0	-13306	-17601	-2221	22562	22562	20341
27-Oct-97	15024	0	-662	0	9072	0	-13306	0	15446	4895	4895	20341
10-Nov-97	15024	288	-1335	1682	18144	0	-26611	-2148	10361	9980	9980	20341
18-Nov-97	15024	0	-702	0	10368	0	-15206	-57403	-42603	62944	62944	20341
24-Nov-97	15024	90	-577	526	7776	0	-11405	0	16751	3590	3590	20341
1-Dec-97	15024	328	-638	1910	9072	0	-13306	0	17707	0	0	17707
8-Dec-97	14280	3	-659	18	9072	0	-13306	-36102	-23268	43609	43609	20341
16-Dec-97	15024	442	-627	2575	10368	0	-15206	0	17893	0	0	17893
22-Dec-97	14341	528	-415	3224	7776	3626	-11405	0	21226	0	0	21226

Table L.6: Kidston tailings impoundment water balance calculations: South pond water balance.

Date	Area, A_{SP} (m^2)	Rain, Q_P, (m^3)	Evap., Q_E (m^3)	Run., Q_R (m^3)	Ditch, S_{DD} (m^3)	Pump, P_{NP} (m^3)	Plant use, Q_{plant} (m^3)	Pump, P_4 (m^3)	Vol., V_{SP} (m^3)	Vol. req. by RD (m^3)	Pump, P_{SP} (m^3)	Vol. ret. V_{SP} (m^3)
12-Jan-98	15225	2561	-1018	14734	27216	6732	-39917	0	31535	0	0	31535
20-Jan-98	18431	936	-673	4450	10368	0	-15206	-45338	-13928	34269	34269	20341
28-Jan-98	15024	787	-782	4590	10368	3754	-15206	0	23852	0	0	23852
2-Feb-98	15767	3	-468	18	6480	0	-9504	-43200	-22819	43160	43160	20341
9-Feb-98	15024	0	-710	0	9072	0	-13306	0	15398	4943	4943	20341
16-Feb-98	15024	568	-475	3311	9072	0	-13306	-15884	3627	16714	16714	20341
23-Feb-98	15024	78	-621	456	9072	0	-13306	-60480	-44460	64801	64801	20341
2-Mar-98	15024	1103	-308	6430	9072	4212	-13306	0	27544	0	0	27544
9-Mar-98	16774	956	-392	4993	9072	0	-13306	-60480	-31612	51953	51953	20341
17-Mar-98	15024	0	-750	0	10368	0	-15206	-96908	-82155	102496	102496	20341
23-Mar-98	15024	24	-328	140	7776	0	-11405	0	16548	3793	3793	20341
31-Mar-98	15024	0	-616	0	10368	0	-15206	-31797	-16910	37251	37251	20341
11-May-98	15024	472	-3040	2751	53136	0	-77933	-77118	-81391	101732	101732	20341
18-May-98	15024	39	-324	228	9072	0	-13306	-10170	5880	14461	14461	20341
25-May-98	15024	0	-425	0	9072	0	-13306	-3045	12638	7703	7703	20341
2-Jun-98	15024	9	-376	53	10368	0	-15206	-14557	631	19710	19710	20341
15-Jun-98	15024	0	-732	0	16848	0	-24710	-38776	-27030	47371	47371	20341
22-Jun-98	15024	0	-324	0	9072	0	-13306	-12891	2893	17448	17448	20341
6-Jul-98	15024	54	-648	315	18144	0	-26611	-17099	-5503	25844	25844	20341
13-Jul-98	15024	21	-355	123	9072	0	-13306	-24626	-8730	29071	29071	20341
20-Jul-98	15024	0	-351	0	9072	0	-13306	-14017	1740	18601	18601	20341
27-Jul-98	15024	0	-360	0	9072	0	-13306	-14830	917	19424	19424	20341
3-Aug-98	15024	0	-431	0	9072	0	-13306	0	15676	4665	4665	20341
10-Aug-98	15024	0	-424	0	9072	0	-13306	-30366	-14682	35023	35023	20341
18-Aug-98	15024	0	-541	0	10368	0	-15206	-14804	157	20184	20184	20341
24-Aug-98	15024	0	-394	0	7776	0	-11405	-7747	8572	11769	11769	20341
31-Aug-98	15024	0	-539	0	9072	0	-13306	0	15569	4772	4772	20341
10-Sep-98	15024	141	-642	823	12960	0	-19008	0	14615	5726	5726	20341
30-Sep-98	15024	0	-1695	0	25920	0	-38016	-13148	-6599	26940	26940	20341
5-Oct-98	15024	0	-443	0	6480	0	-9504	0	16874	3467	3467	20341
12-Oct-98	15024	18	-701	105	9072	0	-13306	-25246	-9716	30057	30057	20341
19-Oct-98	15024	192	-557	1121	9072	0	-13306	-113	16751	3590	3590	20341
18-Feb-99	15024	6124	-9458	35706	158112	12058	-231898	0	-9015	29356	29356	20341
9-Mar-99	15024	346	-1239	2015	24624	0	-36115	-164160	-154189	174530	174530	20341
17-Mar-99	15024	6	-476	35	10368	0	-15206	0	15068	5273	5273	20341
27-Apr-99	15024	90	-2326	526	53136	0	-77933	-203421	-209586	229927	229927	20341
19-May-99	15024	144	-1322	841	28512	0	-41818	0	6699	13642	13642	20341
7-Jun-99	15024	0	-1060	0	24624	0	-36115	-40924	-33134	53475	53475	20341
30-Jun-99	15024	0	-1141	0	29808	0	-43718	-50274	-44984	65325	65325	20341
14-Jul-99	15024	0	-654	0	18144	0	-26611	-15634	-4415	24756	24756	20341
16-Aug-99	15024	3	-1854	18	42768	0	-62726	-104320	-105770	126111	126111	20341
31-Aug-99	15024	0	-1009	0	19440	0	-28512	-32684	-22424	42765	42765	20341
24-Sep-99	15024	3	-1937	18	31104	0	-45619	-118900	-114991	135332	135332	20341
10-Oct-99	15024	0	-1419	0	20736	0	-30413	-92516	-83271	103612	103612	20341
4-Nov-99	15024	21	-2342	123	32400	0	-47520	-197217	-194194	214535	214535	20341
11-Nov-99	15024	484	-480	2821	9072	0	-13306	0	18932	0	0	18932
20-Dec-99	14657	349	-2740	2085	50544	0	-74131	-97536	-102498	122839	122839	20341

Table L.6: Kidston tailings impoundment water balance calculations: South pond water balance.

Date	Area, A_{SP} (m^2)	Rain, Q_P, (m^3)	Evap., Q_E (m^3)	Run., Q_R (m^3)	Ditch, S_{DD} (m^3)	Pump, P_{NP} (m^3)	Plant use, Q_{plant} (m^3)	Pump, P_4 (m^3)	Vol., V_{SP} (m^3)	Vol. req. by RD (m^3)	Pump, P_{SP} (m^3)	Vol. ret. V_{SP} (m^3)
4-Jan-00	15024	505	-1162	2943	19440	0	-28512	0	13555	6786	6786	20341
25-Jan-00	15024	177	-1721	1034	27216	0	-39917	-181440	-174310	194651	194651	20341
8-Feb-00	15024	90	-1112	526	18144	0	-26611	-16599	-5222	25563	25563	20341
22-Feb-00	15024	968	-869	5641	18144	0	-26611	0	17614	0	0	17614
7-Mar-00	14250	1365	-815	8392	18144	6433	-26611	0	24522	0	0	24522
14-Mar-00	15914	6	-470	35	9072	0	-13306	-48384	-28524	48865	48865	20341
4-Apr-00	15024	895	-1441	5221	27216	0	-39917	0	12316	8025	8025	20341
17-Apr-00	15024	1716	-650	10004	16848	5967	-24710	0	29515	0	0	29515
28-Apr-00	17563	1068	-555	5326	14256	0	-20909	0	28701	0	0	28701
9-May-00	17218	0	-570	0	14256	0	-20909	-141459	-119981	140322	140322	20341
6-Jun-00	15024	201	-1118	1174	36288	0	-53222	0	3664	16677	16677	20341
1-Aug-00	15024	1190	-2258	6938	72576	4277	-106445	0	-3380	23721	23721	20341
22-Aug-00	15024	0	-1104	0	27216	0	-39917	-112569	-106033	126374	126374	20341
8-Sep-00	15024	0	-1265	0	22032	0	-32314	-27326	-18532	38873	38873	20341
8-Oct-00	15024	0	-2369	0	38880	0	-57024	0	-172	20513	20513	20341
21-Oct-00	15024	54	-993	315	16848	0	-24710	-179712	-167857	188198	188198	20341
30-Jan-01	15024	6310	-7131	36792	130896	13526	-191981	-220411	-211658	231999	231999	20341
20-Feb-01	15024	1854	-1249	10810	27216	4939	-39917	0	23994	0	0	23994
26-Feb-01	15797	616	-401	3416	7776	0	-11405	0	23996	0	0	23996
24-Mar-01	15798	607	-1893	3364	33696	0	-49421	-224640	-214291	234632	234632	20341
12-Apr-01	15024	0	-1242	0	24624	0	-36115	0	7608	12733	12733	20341
24-Apr-01	15024	0	-746	0	15552	0	-22810	0	12338	8003	8003	20341

Table L.7: Kidston tailings impoundment water balance calculations: Seepage dam water balance.

Date	Area, A_{RDSD} (m^2)	Rain, Q_P (m^3)	Evap., Q_E (m^3)	Runoff, Q_R (m^3)	North dump seep, S_{ND} (m^3)	Volume, V_{RDSD} (m^3)	Pumped to RD, P_{RDSD} (m_3)	Ret. volume, V_{RDSD} (m^3)	New level, h_{RDSD} (m)
8-Sep-97	1667	0	0	0	0	1500	1400	100	519
15-Sep-97	1706	0	-79	0	1210	1230	0	1230	520
27-Sep-97	1887	0	-133	0	2074	3171	3071	100	519
6-Oct-97	1706	4	-91	26	1555	1594	1494	100	519
10-Oct-97	1706	0	-42	0	691	750	0	750	519
13-Oct-97	1806	0	-36	0	518	1232	0	1232	520
20-Oct-97	1887	0	-91	0	1210	2350	2250	100	519
27-Oct-97	1706	0	-75	0	1210	1234	0	1234	520
10-Nov-97	1888	36	-168	192	2419	3714	3614	100	519
18-Nov-97	1706	0	-80	0	1382	1403	0	1403	520
24-Nov-97	1918	12	-74	60	1037	2437	2337	100	519
1-Dec-97	1706	37	-72	218	1210	1492	0	1492	520
8-Dec-97	1934	0	-89	2	1210	2615	2515	100	519
16-Dec-97	1706	50	-71	294	1382	1755	1655	100	519
22-Dec-97	1706	63	-49	368	1037	1518	1418	100	519
12-Jan-98	1706	287	-114	1682	3629	5584	5484	100	519
20-Jan-98	1706	87	-62	508	1382	2015	1915	100	519

Table L.7: Kidston tailings impoundment water balance calculations: Seepage dam water balance.

Date	Area, A_{RDSD} (m^2)	Rain, Q_P (m^3)	Evap., Q_E (m^3)	Runoff, Q_R (m^3)	North dump seep, S_{ND} (m^3)	Volume, V_{RDSD} (m^3)	Pumped to RD, P_{RDSD} (m_3)	Ret. volume, V_{RDSD} (m^3)	New level, h_{RDSD} (m)
28-Jan-98	1706	89	-89	524	1382	2007	1907	100	519
2-Feb-98	1706	0	-51	2	864	916	0	916	519
9-Feb-98	1833	0	-87	0	1210	2039	1939	100	519
16-Feb-98	1706	65	-54	378	1210	1698	1598	100	519
23-Feb-98	1706	9	-71	52	1210	1300	0	1300	520
2-Mar-98	1899	139	-39	734	1210	3344	3244	100	519
9-Mar-98	1706	97	-40	570	1210	1937	1837	100	519
17-Mar-98	1706	0	-85	0	1382	1397	0	1397	520
23-Mar-98	1917	3	-42	16	1037	2411	2311	100	519
31-Mar-98	1706	0	-70	0	1382	1412	0	1412	520
11-May-98	1920	60	-388	314	7085	8483	8383	100	519
18-May-98	1706	4	-37	26	1210	1303	0	1303	520
25-May-98	1900	0	-54	0	1210	2459	2359	100	519
2-Jun-98	1706	1	-43	6	1382	1447	0	1447	520
15-Jun-98	1926	0	-94	0	2246	3599	3499	100	519
22-Jun-98	1706	0	-37	0	1210	1273	0	1273	520
6-Jul-98	1894	7	-82	36	2419	3653	3553	100	519
13-Jul-98	1706	2	-40	14	1210	1286	0	1286	520
20-Jul-98	1897	0	-44	0	1210	2451	2351	100	519
27-Jul-98	1706	0	-41	0	1210	1269	0	1269	520
3-Aug-98	1894	0	-54	0	1210	2424	2324	100	519
10-Aug-98	1706	0	-48	0	1210	1261	0	1261	520
18-Aug-98	1892	0	-68	0	1382	2576	2476	100	519
24-Aug-98	1706	0	-45	0	1037	1092	0	1092	520
31-Aug-98	1863	0	-67	0	1210	2235	2135	100	519
10-Sep-98	1706	16	-73	94	1728	1865	1765	100	519
30-Sep-98	1706	0	-193	0	3456	3363	3263	100	519
5-Oct-98	1706	0	-50	0	864	914	0	914	519
12-Oct-98	1833	2	-86	12	1210	2052	1952	100	519
19-Oct-98	1706	22	-63	128	1210	1396	0	1396	520
18-Feb-99	1917	781	-1207	4076	21082	26128	26028	100	519
9-Mar-99	1706	39	-141	230	3283	3512	3412	100	519
17-Mar-99	1706	1	-54	4	1382	1433	0	1433	520
27-Apr-99	1923	12	-298	60	7085	8292	8192	100	519
19-May-99	1706	16	-150	96	3802	3864	3764	100	519
7-Jun-99	1706	0	-120	0	3283	3263	3163	100	519
30-Jun-99	1706	0	-130	0	3974	3945	3845	100	519
14-Jul-99	1706	0	-74	0	2419	2445	2345	100	519
16-Aug-99	1706	0	-211	2	5702	5594	5494	100	519
31-Aug-99	1706	0	-115	0	2592	2577	2477	100	519
24-Sep-99	1706	0	-220	2	4147	4030	3930	100	519
10-Oct-99	1706	0	-161	0	2765	2704	2604	100	519
4-Nov-99	1706	2	-266	14	4320	4170	4070	100	519
11-Nov-99	1706	55	-54	322	1210	1632	1532	100	519

Table L.7: Kidston tailings impoundment water balance calculations: Seepage dam water balance.

Date	Area, A_{RDSD} (m^2)	Rain, Q_P (m^3)	Evap., Q_E (m^3)	Runoff, Q_R (m^3)	North dump seep, S_{ND} (m^3)	Volume, V_{RDSD} (m^3)	Pumped to RD, P_{RDSD} (m_3)	Ret. volume, V_{RDSD} (m^3)	New level, h_{RDSD} (m)
20-Dec-99	1706	41	-319	238	6739	6799	6699	100	519
4-Jan-00	1706	57	-132	336	2592	2953	2853	100	519
25-Jan-00	1706	20	-195	118	3629	3671	3571	100	519
8-Feb-00	1706	10	-126	60	2419	2463	2363	100	519
22-Feb-00	1706	110	-99	644	2419	3174	3074	100	519
7-Mar-00	1706	163	-98	958	2419	3543	3443	100	519
14-Mar-00	1706	1	-50	4	1210	1264	0	1264	520
4-Apr-00	1893	113	-182	596	3629	5420	5320	100	519
17-Apr-00	1706	195	-74	1142	2246	3609	3509	100	519
28-Apr-00	1706	104	-54	608	1901	2659	2559	100	519
9-May-00	1706	0	-56	0	1901	1944	1844	100	519
6-Jun-00	1706	23	-127	134	4838	4968	4868	100	519
1-Aug-00	1706	135	-256	792	9677	10448	10348	100	519
22-Aug-00	1706	0	-125	0	3629	3603	3503	100	519
8-Sep-00	1706	0	-144	0	2938	2894	2794	100	519
8-Oct-00	1706	0	-269	0	5184	5015	4915	100	519
21-Oct-00	1706	6	-113	36	2246	2276	2176	100	519
30-Jan-01	1706	717	-810	4200	17453	21660	21560	100	519
20-Feb-01	1706	211	-142	1234	3629	5031	4931	100	519
26-Feb-01	1706	67	-43	390	1037	1550	1450	100	519
24-Mar-01	1706	66	-204	384	4493	4838	4738	100	519
12-Apr-01	1706	0	-141	0	3283	3242	3142	100	519
24-Apr-01	1706	0	-85	0	2074	2089	1989	100	519

Table L.8: Kidston tailings impoundment water balance calculations: Reclaim dam water balance, section 1.

Date	Rain, Q_P (m^3)	Evap., Q_E (m^3)	Runoff, Q_R (m^3)	RD wall seep, S_W (m^3)	RD base, S_B (m^3)	N RD seep, E_2 (m^3)	Direct RD seep, E_3 (m^3)	East drain seep, E_4 (m^3)
8-Sep-97	0	0	0	0.0000	0.00	0	0	0
15-Sep-97	0	-1658	0	-0.0003	-0.22	650	559	1634
27-Sep-97	0	-2514	0	-0.0005	-0.37	1113	958	2798
6-Oct-97	93	-1911	177	-0.0004	-0.28	830	714	2078
10-Oct-97	0	-872	0	-0.0002	-0.12	368	316	919
13-Oct-97	0	-720	0	-0.0001	-0.09	276	237	687
20-Oct-97	0	-1730	0	-0.0003	-0.22	641	550	1595
27-Oct-97	0	-1574	0	-0.0003	-0.22	637	546	1580
10-Nov-97	686	-3177	1306	-0.0006	-0.43	1268	1086	3132
18-Nov-97	0	-1670	0	-0.0003	-0.25	726	621	1794
24-Nov-97	215	-1374	408	-0.0002	-0.19	541	463	1333
1-Dec-97	780	-1519	1482	-0.0003	-0.22	632	540	1556
8-Dec-97	7	-1650	14	-0.0003	-0.22	630	539	1549
16-Dec-97	1052	-1493	1999	-0.0003	-0.25	720	615	1768
22-Dec-97	1317	-1036	2502	-0.0002	-0.19	539	461	1323
12-Jan-98	6023	-2395	11438	-0.0008	-0.65	1914	1641	4750

Table L.8: Kidston tailings impoundment water balance calculations: Reclaim dam water balance, section 1.

Date	Rain, Q_P (m^3)	Evap., Q_E (m^3)	Runoff, Q_R (m^3)	RD wall seep, S_W (m^3)	RD base, S_B (m^3)	N RD seep, E_2 (m^3)	Direct RD seep, E_3 (m^3)	East drain seep, E_4 (m^3)
20-Jan-98	1819	-1309	3454	-0.0003	-0.25	739	635	1851
28-Jan-98	1877	-1865	3563	-0.0003	-0.25	740	637	1857
2-Feb-98	7	-1063	14	-0.0002	-0.15	464	399	1165
9-Feb-98	0	-1693	0	-0.0003	-0.22	644	553	1608
16-Feb-98	1355	-1134	2570	-0.0003	-0.22	649	559	1630
23-Feb-98	186	-1482	354	-0.0003	-0.22	651	561	1639
2-Mar-98	2632	-736	4991	-0.0003	-0.22	651	561	1641
9-Mar-98	2044	-837	3876	-0.0003	-0.22	663	573	1691
17-Mar-98	0	-1790	0	-0.0003	-0.25	761	659	1947
23-Mar-98	57	-784	109	-0.0002	-0.19	560	483	1414
31-Mar-98	0	-1471	0	-0.0003	-0.25	746	643	1882
11-May-98	1128	-7269	2135	-0.0016	-1.27	3785	3254	9477
18-May-98	93	-776	177	-0.0003	-0.22	645	555	1615
25-May-98	0	-1017	0	-0.0003	-0.22	643	553	1606
2-Jun-98	22	-900	41	-0.0003	-0.25	734	630	1829
15-Jun-98	0	-1753	0	-0.0005	-0.40	1191	1022	2966
22-Jun-98	0	-775	0	-0.0003	-0.22	640	550	1594
6-Jul-98	130	-1551	245	-0.0006	-0.44	1277	1095	3170
13-Jul-98	50	-851	95	-0.0003	-0.22	638	547	1583
20-Jul-98	0	-840	0	-0.0003	-0.22	637	546	1580
27-Jul-98	0	-863	0	-0.0003	-0.22	636	545	1576
3-Aug-98	0	-1033	0	-0.0003	-0.22	634	543	1568
10-Aug-98	0	-1016	0	-0.0003	-0.22	635	544	1569
18-Aug-98	0	-1298	0	-0.0003	-0.25	724	620	1788
24-Aug-98	0	-944	0	-0.0002	-0.19	542	464	1336
31-Aug-98	0	-1292	0	-0.0003	-0.22	628	537	1542
10-Sep-98	339	-1541	639	-0.0004	-0.31	884	752	2143
30-Sep-98	0	-4070	0	-0.0008	-0.62	1748	1485	4204
5-Oct-98	0	-1063	0	-0.0002	-0.16	435	369	1044
12-Oct-98	43	-1685	82	-0.0003	-0.22	608	516	1455
19-Oct-98	462	-1339	870	-0.0003	-0.22	608	516	1455
18-Feb-99	14759	-22794	27717	-0.0048	-3.82	10801	9200	26228
9-Mar-99	833	-2988	1564	-0.0008	-0.59	1718	1470	4237
17-Mar-99	14	-1148	27	-0.0003	-0.25	716	611	1753
27-Apr-99	218	-5616	408	-0.0016	-1.29	3667	3131	8972
19-May-99	348	-3194	653	-0.0009	-0.69	1933	1644	4667
7-Jun-99	0	-2562	0	-0.0008	-0.60	1664	1414	4008
30-Jun-99	0	-2760	0	-0.0009	-0.72	2008	1705	4824
14-Jul-99	0	-1583	0	-0.0006	-0.44	1218	1034	2920
16-Aug-99	7	-4490	14	-0.0013	-1.04	2861	2425	6836
31-Aug-99	0	-2445	0	-0.0006	-0.47	1296	1098	3090
24-Sep-99	7	-4696	14	-0.0010	-0.76	2067	1750	4916
10-Oct-99	0	-3442	0	-0.0006	-0.50	1381	1169	3288
4-Nov-99	51	-5686	95	-0.0010	-0.79	2160	1830	5150
11-Nov-99	1174	-1164	2190	-0.0003	-0.22	602	510	1430
20-Dec-99	869	-6827	1618	-0.0015	-1.23	3334	2816	7879
4-Jan-00	1227	-2825	2285	-0.0006	-0.47	1280	1082	3024
25-Jan-00	431	-4186	802	-0.0008	-0.66	1819	1542	4345

Table L.8: Kidston tailings impoundment water balance calculations: Reclaim dam water balance, section 1.

Date	Rain, Q_P (m^3)	Evap., Q_E (m^3)	Runoff, Q_R (m^3)	RD wall seep, S_W (m^3)	RD base, S_B (m^3)	N RD seep, E_2 (m^3)	Direct RD seep, E_3 (m^3)	East drain seep, E_4 (m^3)
8-Feb-00	219	-2705	408	-0.0006	-0.44	1206	1021	2867
22-Feb-00	2356	-2115	4379	-0.0006	-0.44	1206	1021	2867
7-Mar-00	3506	-2094	6514	-0.0006	-0.44	1220	1035	2927
14-Mar-00	15	-1081	27	-0.0003	-0.22	611	518	1467
4-Apr-00	2183	-3512	4053	-0.0008	-0.66	1838	1561	4425
17-Apr-00	4183	-1586	7766	-0.0005	-0.41	1147	977	2779
28-Apr-00	2228	-1158	4134	-0.0004	-0.35	977	833	2378
9-May-00	0	-1213	0	-0.0004	-0.35	990	847	2434
6-Jun-00	492	-2730	911	-0.0011	-0.89	2503	2136	6121
1-Aug-00	2910	-5521	5386	-0.0022	-1.78	4914	4177	11852
22-Aug-00	0	-2700	0	-0.0008	-0.67	1858	1582	4510
8-Sep-00	0	-3098	0	-0.0007	-0.54	1495	1271	3610
8-Oct-00	0	-5803	0	-0.0012	-0.95	2546	2148	5985
21-Oct-00	133	-2433	245	-0.0005	-0.41	1127	955	2693
30-Jan-01	15507	-17523	28560	-0.0040	-3.22	9459	8160	23934
20-Feb-01	4559	-3072	8391	-0.0008	-0.67	1987	1718	5062
26-Feb-01	1441	-939	2652	-0.0002	-0.19	562	485	1422
24-Mar-01	1420	-4429	2611	-0.0010	-0.83	2477	2144	6342
12-Apr-01	0	-3057	0	-0.0008	-0.61	1787	1543	4536
24-Apr-01	0	-1836	0	-0.0005	-0.38	1115	960	2804

Table L.9: Kidston tailings impoundment water balance calculations: Reclaim dam water balance, section 2.

Date	Pumped to SD, P_{RD} (m^3)	Pump to TD, P_3 (m^3)	volume, V_{RD} (m^3)	Volume req. by SP (m^3)	Pumped to SP, P_{RD} (m^3)	Revised volume, V_{RD} (m^3)	TD decant, Q_8 (m^3)	Ret. volume, V_{RD} (m^3)
	(m3)		(m3)	(m3)	(m3)	(m3)	(m3)	(m3)
8-Sep-97	1400	0	38635	0	0	38635	0	38635
15-Sep-97	0	0	41264	4931	4931	36332	0	36332
27-Sep-97	3071	-31104	16427	69875	69875	-53448	90683	37235
6-Oct-97	1494	0	44332	5980	5980	38352	0	38352
10-Oct-97	0	0	39568	2786	2786	36781	0	36781
13-Oct-97	0	-4406	34508	10080	10080	24428	12807	37235
20-Oct-97	2250	-10282	33046	22562	22562	10484	26751	37235
27-Oct-97	0	0	41188	4895	4895	36292	0	36292
10-Nov-97	3614	0	50636	9980	9980	40656	0	40656
18-Nov-97	0	-27648	14198	62944	62944	-48746	85981	37235
24-Nov-97	2337	0	43496	3590	3590	39906	0	39906
1-Dec-97	0	0	43434	0	0	43434	0	43434
8-Dec-97	2515	0	43555	43609	43609	-53	37288	37235
16-Dec-97	1655	0	46654	0	0	46654	0	46654
22-Dec-97	1418	0	46082	0	0	46082	0	46082
12-Jan-98	5484	0	74395	0	0	74395	0	74395
20-Jan-98	1915	0	49566	34269	34269	15297	21938	37235
28-Jan-98	1907	0	49186	0	0	49186	0	49186
2-Feb-98	0	-26735	13511	43160	43160	-29649	66884	37235
9-Feb-98	1939	0	43089	4943	4943	38146	0	38146
16-Feb-98	1598	-6048	41252	16714	16714	24538	12697	37235

Table L.9: Kidston tailings impoundment water balance calculations: Reclaim dam water balance, section 2.

Date	Pumped to SD, P_{RD} (m^3)	Pump to TD, P_3 (m^3)	volume, V_{RD} (m^3)	Volume req. by SP (m^3)	Pumped to SP, P_{RD} (m^3)	Revised volume, V_{RD} (m^3)	TD decant, Q_8 (m^3)	Ret. volume, V_{RD} (m^3)
23-Feb-98	0	-26957	15038	64801	64801	-49763	86998	37235
2-Mar-98	3244	0	53073	0	0	53073	0	53073
9-Mar-98	1837	-12481	37529	51953	51953	-14424	51659	37235
17-Mar-98	0	-44928	-2749	102496	102496	-105246	142481	37235
23-Mar-98	2311	0	43842	3793	3793	40049	0	40049
31-Mar-98	0	-17280	25025	37251	37251	-12227	49462	37235
11-May-98	8383	0	74644	101732	101732	-27088	64323	37235
18-May-98	0	0	42359	14461	14461	27898	9337	37235
25-May-98	2359	-1814	42366	7703	7703	34663	0	34663
2-Jun-98	0	0	42784	19710	19710	23074	14161	37235
15-Jun-98	3499	-22464	26876	47371	47371	-20495	57730	37235
22-Jun-98	0	-6048	35980	17448	17448	18532	18703	37235
6-Jul-98	3553	0	50695	25844	25844	24851	12384	37235
13-Jul-98	0	0	42067	29071	29071	12996	24239	37235
20-Jul-98	2351	-7258	37015	18601	18601	18413	18822	37235
27-Jul-98	0	-7258	34631	19424	19424	15207	22028	37235
3-Aug-98	2324	0	44017	4665	4665	39352	0	39352
10-Aug-98	0	-15120	26594	35023	35023	-8429	45664	37235
18-Aug-98	2476	-10368	34308	20184	20184	14124	23111	37235
24-Aug-98	0	-4147	36829	11769	11769	25059	12176	37235
31-Aug-98	2135	0	43493	4772	4772	38721	0	38721
10-Sep-98	1765	0	45994	5726	5726	40269	0	40269
30-Sep-98	3263	-5184	46119	26940	26940	19179	18056	37235
5-Oct-98	0	0	39869	3467	3467	36402	0	36402
12-Oct-98	1952	0	42784	30057	30057	12727	24508	37235
19-Oct-98	0	0	42386	3590	3590	38795	0	38795
18-Feb-99	26028	0	175399	29356	29356	146044	0	146044
9-Mar-99	3412	-126094	-71189	174530	174530	-245719	282954	37235
17-Mar-99	0	0	42289	5273	5273	37016	0	37016
27-Apr-99	8192	0	71975	229927	229927	-157952	195187	37235
19-May-99	3764	0	55291	13642	13642	41649	0	41649
7-Jun-99	3163	-24624	27382	53475	53475	-26093	63328	37235
30-Jun-99	3845	-23846	31547	65325	65325	-33779	71014	37235
14-Jul-99	2345	-12096	36244	24756	24756	11488	25747	37235
16-Aug-99	5494	0	62503	126111	126111	-63609	100844	37235
31-Aug-99	2477	-12960	35274	42765	42765	-7491	44726	37235
24-Sep-99	3930	0	53954	135332	135332	-81378	118613	37235
10-Oct-99	2604	-41472	6601	103612	103612	-97011	134246	37235
4-Nov-99	4070	0	54045	214535	214535	-160490	197725	37235
11-Nov-99	1532	0	46051	0	0	46051	0	46051
20-Dec-99	6699	0	67652	122839	122839	-55187	92422	37235
4-Jan-00	2853	0	51546	6786	6786	44760	0	44760
25-Jan-00	3571	-87703	-34437	194651	194651	-229087	266322	37235
8-Feb-00	2363	0	47708	25563	25563	22145	15090	37235
22-Feb-00	3074	0	55117	0	0	55117	0	55117
7-Mar-00	3443	0	58967	0	0	58967	0	58967
14-Mar-00	0	-5681	35706	48865	48865	-13159	50394	37235
4-Apr-00	5320	0	60925	8025	8025	52900	0	52900

Table L.9: Kidston tailings impoundment water balance calculations: Reclaim dam water balance, section 2.

Date	Pumped to SD, P_{RD} (m^3)	Pump to TD, P_3 (m^3)	volume, V_{RD} (m^3)	Volume req. by SP (m^3)	Pumped to SP, P_{RD} (m^3)	Revised volume, V_{RD} (m^3)	TD decant, Q_8 (m^3)	Ret. volume, V_{RD} (m^3)
17-Apr-00	3509	0	60913	0	0	60913	0	60913
28-Apr-00	2559	0	53373	0	0	53373	0	53373
9-May-00	1844	-66528	-20121	140322	140322	-160444	197679	37235
6-Jun-00	4868	0	62294	16677	16677	45617	0	45617
1-Aug-00	10348	0	92241	23721	23721	68519	0	68519
22-Aug-00	3503	-72576	-18639	126374	126374	-145012	182247	37235
8-Sep-00	2794	-5875	43807	38873	38873	4934	32301	37235
8-Oct-00	4915	0	57704	20513	20513	37191	0	37191
21-Oct-00	2176	-108955	-62050	188198	188198	-250248	287483	37235
30-Jan-01	21560	0	168441	231999	231999	-63558	100793	37235
20-Feb-01	4931	0	69577	0	0	69577	0	69577
26-Feb-01	1450	0	46776	0	0	46776	0	46776
24-Mar-01	4738	-70283	-6784	234632	234632	-241416	278651	37235
12-Apr-01	3142	0	53053	12733	12733	40320	0	40320
24-Apr-01	1989	0	47145	8003	8003	39141	0	39141

L.4 References

Gutteridge, Haskins and Davey Pty Ltd. (1987). Kidston Project; Interim Report on Tailings Disposal. Consultants Report to Kidston Gold Mines Limited. Brisbane, Queensland, Australia. July, 9 pages.

Ritchie, P. (1988). Survey of Kidston's Water Management System. Kidston Gold Mines Limited Memorandum (Unpublished), 12 October 1988.

APPENDIX M

SoilCover Modeling Results

M.1 Introduction

The main SoilCover modeling results as reported on in Chapters 8, 9 and 10 of the thesis are presented here. The appendix begins with a description of the numbering protocol, before listing the modeling result data, including supporting graphs where necessary.

M.2 Numbering Protocol for Model Simulations

Throughout this appendix individual SoilCover model simulations will be referred to by means of a unique model number. A complete summary of all the model simulation numbers is listed in Tables M.1 to M.4. All the numbers are based on a 6 or 7 digit system, which allows for identification of the model simulation by looking at the number only. In all instances the first digit is a "K", which denotes that the model simulation is for the Kidston tailings impoundment. The second digit is either an "U" or a "V", which stand for non-vegetated and vegetated respectively. Unvegetated means the model simulation is for a non-vegetated tailings surface, and vegetated logically implies the model simulation is for a vegetated tailings surface. The third digit denotes the climatic data used in the model simulation, and consist of an "A" (mean climatic year), "W" (wet climatic year), "D" (dry climatic year) or a "V" (evaluation data set).

The fourth digit identifies the tailings type used in the model run. "C" denotes coarse tailings, "I" denotes intermediate tailings, and "F" denotes fine tailings. The fifth digit, "r" are most often omitted and a dash is inserted in its place. The presence of the "r" denotes that the model run had to be rerun due to numerical instability. The last two digits work together to denote a number between 1 and 13. Each number indicates the location of the model simulation along the generalized tailings impoundment cross-section, as well as the associated saturated hydraulic conductivity (see Tables M.1 to M.4).

Table M.1: Numbering protocol for SoilCover simulations with a mean climatic year.

k_s (m/sec)	Depth (m)	Non-vegetated			Vegetated		
		Coarse	Interm	Fine	Coarse	Interm	Fine
1.94E-05	1.3400	K-UAC-01	K-UAI-01	K-UAF-01	K-VAC-01	K-VAI-01	K-VAF-01
1.19E-05	1.0192	K-UAC-02	K-UAI-02	K-UAF-02	K-VAC-02	K-VAI-02	K-VAF-02
7.30E-06	0.7622	K-UAC-03	K-UAI-03	K-UAF-03	K-VAC-03	K-VAI-03	K-VAF-03
4.48E-06	0.5594	K-UAC-04	K-UAI-04	K-UAF-04	K-VAC-04	K-VAI-04	K-VAF-04
2.75E-06	0.4019	K-UAC-05	K-UAI-05	K-UAF-05	K-VAC-05	K-VAI-05	K-VAF-05
1.69E-06	0.2819	K-UAC-06	K-UAI-06	K-UAF-06	K-VAC-06	K-VAI-06	K-VAF-06
1.03E-06	0.1922	K-UAC-07	K-UAI-07	K-UAF-07	K-VAC-07	K-VAI-07	K-VAF-07
6.35E-07	0.1267	K-UAC-08	K-UAI-08	K-UAF-08	K-VAC-08	K-VAI-08	K-VAF-08
3.90E-07	0.0799	K-UAC-09	K-UAI-09	K-UAF-09	K-VAC-09	K-VAI-09	K-VAF-09
2.39E-07	0.0474	K-UAC-10	K-UAI-10	K-UAF-10	K-VAC-10	K-VAI-10	K-VAF-10
1.47E-07	0.0254	K-UAC-11	K-UAI-11	K-UAF-11	K-VACr11	K-VAIr11	K-VAFr11
9.00E-08	0.0112	K-UAC-12	K-UAI-12	K-UAF-12	K-VACr12	K-VAIr12	K-VAFr12
5.52E-08	0.0030	K-UAC-13	K-UAI-13	K-UAF-13	K-VAC-13	K-VAI-13	K-VAF-13

Table M.2: Numbering protocol for SoilCover simulations with a wet climatic year.

k_s (m/sec)	Depth (m)	Non-vegetated			Vegetated		
		Coarse	Interm	Fine	Coarse	Interm	Fine
1.94E-05	1.3400	K-UWC-01	K-UWI-01	K-UWF-01	K-VWC-01	K-VWI-01	K-VWF-01
1.19E-05	1.0192	K-UWC-02	K-UWI-02	K-UWF-02	K-VWC-02	K-VWI-02	K-VWF-02
7.30E-06	0.7622	K-UWC-03	K-UWI-03	K-UWF-03	K-VWC-03	K-VWI-03	K-VWF-03
4.48E-06	0.5594	K-UWC-04	K-UWI-04	K-UWF-04	K-VWC-04	K-VWI-04	K-VWF-04
2.75E-06	0.4019	K-UWC-05	K-UWI-05	K-UWF-05	K-VWC-05	K-VWI-05	K-VWF-05
1.69E-06	0.2819	K-UWC-06	K-UWI-06	K-UWF-06	K-VWC-06	K-VWI-06	K-VWF-06
1.03E-06	0.1922	K-UWC-07	K-UWI-07	K-UWF-07	K-VWC-07	K-VWI-07	K-VWF-07
6.35E-07	0.1267	K-UWC-08	K-UWI-08	K-UWF-08	K-VWC-08	K-VWI-08	K-VWF-08
3.90E-07	0.0799	K-UWC-09	K-UWI-09	K-UWF-09	K-VWC-09	K-VWI-09	K-VWF-09
2.39E-07	0.0474	K-UWC-10	K-UWI-10	K-UWF-10	K-VWC-10	K-VWI-10	K-VWF-10
1.47E-07	0.0254	K-UWC-11	K-UWI-11	K-UWF-11	K-VWCr11	K-VWIr11	K-VWFr11
9.00E-08	0.0112	K-UWC-12	K-UWI-12	K-UWF-12	K-VWCr12	K-VWIr12	K-VWFr12
5.52E-08	0.0030	K-UWC-13	K-UWI-13	K-UWF-13	K-VWC-13	K-VWI-13	K-VWF-13

Table M.3: Numbering protocol for SoilCover simulations with a dry climatic year.

k_s (m/sec)	Depth (m)	Non-vegetated			Vegetated		
		Coarse	Interm	Fine	Coarse	Interm	Fine
1.94E-05	1.3400	K-UDC-01	K-UDI-01	K-UDF-01	K-VDC-01	K-VDI-01	K-VDF-01
1.19E-05	1.0192	K-UDC-02	K-UDI-02	K-UDF-02	K-VDC-02	K-VDI-02	K-VDF-02
7.30E-06	0.7622	K-UDC-03	K-UDI-03	K-UDF-03	K-VDC-03	K-VDI-03	K-VDF-03
4.48E-06	0.5594	K-UDC-04	K-UDI-04	K-UDF-04	K-VDC-04	K-VDI-04	K-VDF-04
2.75E-06	0.4019	K-UDC-05	K-UDI-05	K-UDF-05	K-VDC-05	K-VDI-05	K-VDF-05
1.69E-06	0.2819	K-UDC-06	K-UDI-06	K-UDF-06	K-VDC-06	K-VDI-06	K-VDF-06

Table M.3: Numbering protocol for SoilCover simulations with a dry climatic year.

k_s (m/sec)	Depth (m)	Non-vegetated			Vegetated		
		Coarse	Interm	Fine	Coarse	Interm	Fine
1.03E-06	0.1922	K-UDC-07	K-UDI-07	K-UDF-07	K-VDC-07	K-VDI-07	K-VDF-07
6.35E-07	0.1267	K-UDC-08	K-UDI-08	K-UDF-08	K-VDC-08	K-VDI-08	K-VDF-08
3.90E-07	0.0799	K-UDC-09	K-UDI-09	K-UDF-09	K-VDC-09	K-VDI-09	K-VDF-09
2.39E-07	0.0474	K-UDC-10	K-UDI-10	K-UDF-10	K-VDC-10	K-VDI-10	K-VDF-10
1.47E-07	0.0254	K-UDC-11	K-UDI-11	K-UDF-11	K-VDCr11	K-VDIr11	K-VDFr11
9.00E-08	0.0112	K-UDC-12	K-UDI-12	K-UDF-12	K-VDCr12	K-VDIr12	K-VDFr12
5.52E-08	0.0030	K-UDC-13	K-UDI-13	K-UDF-13	K-VDC-13	K-VDI-13	K-VDF-13

Table M.4: Numbering protocol for SoilCover simulations for the evaluation data set.

k_s (m/sec)	Depth (m)	Coarse	k_s (m/sec)	Depth (m)	Interm	k_s (m/sec)	Depth (m)	Fine
1.94E-05	1.3400	K-VVC-01	1.69E-06	0.2819	K-VVI-06	1.47E-07	0.0254	K-VVF-r11
1.19E-05	1.0192	K-VVC-02	1.03E-06	0.1922	K-VVI-07	9.00E-08	0.0112	K-VVF-r12
7.30E-06	0.7622	K-VVC-03	6.35E-07	0.1267	K-VVI-08	5.52E-08	0.0030	K-VVF-13
4.48E-06	0.5594	K-VVC-04	3.90E-07	0.0799	K-VVI-09			
2.75E-06	0.4019	K-VVC-05	2.39E-07	0.0474	K-VVI-10			

M.3 Annual SoilCover Simulation Results

Tables M.5 to M.10 below list the individual SoilCover results for all 234 model runs (includes all cases). The results listed in the tables are the cumulative annual totals for the water balance components calculated by SoilCover. These components are; net infiltration (NI); bottom flux (BF); runoff (R); potential- and actual evaporation (PE and AE); potential- and actual transpiration (PT and AT); and potential- and actual evapotranspiration (PET and AET).

Table M.5: Annualized results of individual SoilCover simulations for a mean year, with no vegetation on the tailings surface (702.2 mm precipitation).

Model no.	Tailings type	NI (mm)	BF (mm)	R (mm)	PE (mm)	AE (mm)	PT (mm)	AT (mm)	PET (mm)	AET (mm)
K-UAC-01	Coarse	53.9	222.2	120.8	1639.0	527.5	0.0	0.0	1639.0	527.5
K-UAC-02	Coarse	65.1	160.5	137.5	1639.4	499.7	0.0	0.0	1639.4	499.7
K-UAC-03	Coarse	74.4	146.0	192.4	1639.3	435.5	0.0	0.0	1639.3	435.5
K-UAC-04	Coarse	-64.8	145.8	376.9	1639.4	390.2	0.0	0.0	1639.4	390.2
K-UAC-05	Coarse	-112.3	81.7	435.9	1639.2	378.6	0.0	0.0	1639.2	378.6
K-UAC-06	Coarse	-95.7	160.5	448.1	1639.8	349.8	0.0	0.0	1639.8	349.8
K-UAC-07	Coarse	-84.8	127.7	450.3	1639.7	336.7	0.0	0.0	1639.7	336.7
K-UAC-08	Coarse	-64.8	128.5	448.7	1639.4	318.3	0.0	0.0	1639.4	318.3
K-UAC-09	Coarse	-106.8	118.9	464.3	1639.5	344.8	0.0	0.0	1639.5	344.8
K-UAC-10	Coarse	-100.2	78.7	474.9	1639.7	327.5	0.0	0.0	1639.7	327.5

Table M.5: Annualized results of individual SoilCover simulations for a mean year, with no vegetation on the tailings surface (702.2 mm precipitation).

Model no.	Tailings type	NI (mm)	BF (mm)	R (mm)	PE (mm)	AE (mm)	PT (mm)	AT (mm)	PET (mm)	AET (mm)
K-UAC-11	Coarse	-449.8	366.8	335.1	1639.9	817.0	0.0	0.0	1639.9	817.0
K-UAC-12	Coarse	-555.7	527.7	309.6	1639.8	948.3	0.0	0.0	1639.8	948.3
K-UAC-13	Coarse	-1272.5	1276.4	340.5	1636.6	1634.3	0.0	0.0	1636.6	1634.3
K-UAI-01	Interm	21.5	325.0	56.7	1638.7	624.1	0.0	0.0	1638.7	624.1
K-UAI-02	Interm	57.6	301.4	67.4	1638.6	577.3	0.0	0.0	1638.6	577.3
K-UAI-03	Interm	27.6	301.6	81.6	1639.5	593.0	0.0	0.0	1639.5	593.0
K-UAI-04	Interm	8.9	175.9	90.7	1639.2	602.7	0.0	0.0	1639.2	602.7
K-UAI-05	Interm	52.9	171.8	140.8	1639.6	508.5	0.0	0.0	1639.6	508.5
K-UAI-06	Interm	-59.8	286.1	311.9	1639.7	450.4	0.0	0.0	1639.7	450.4
K-UAI-07	Interm	-108.6	253.6	375.5	1639.5	435.3	0.0	0.0	1639.5	435.3
K-UAI-08	Interm	-128.1	215.0	401.4	1639.3	429.0	0.0	0.0	1639.3	429.0
K-UAI-09	Interm	-130.6	202.6	180.7	1639.0	652.1	0.0	0.0	1639.0	652.1
K-UAI-10	Interm	-276.1	367.1	138.8	1639.6	839.5	0.0	0.0	1639.6	839.5
K-UAI-11	Interm	-443.2	458.7	195.2	1641.8	950.2	0.0	0.0	1641.8	950.2
K-UAI-12	Interm	-1234.4	1140.0	360.2	1639.0	1576.4	0.0	0.0	1639.0	1576.4
K-UAI-13	Interm	-1274.3	1276.4	340.4	1636.2	1636.2	0.0	0.0	1636.2	1636.2
K-UAF-01	Fine	163.2	830.9	0.0	1639.5	539.0	0.0	0.0	1639.5	539.0
K-UAF-02	Fine	76.6	625.0	19.2	1639.5	606.5	0.0	0.0	1639.5	606.5
K-UAF-03	Fine	59.4	375.2	53.9	1639.0	589.0	0.0	0.0	1639.0	589.0
K-UAF-04	Fine	70.0	349.9	55.0	1638.9	577.3	0.0	0.0	1638.9	577.3
K-UAF-05	Fine	-11.6	181.6	93.3	1638.9	620.6	0.0	0.0	1638.9	620.6
K-UAF-06	Fine	-91.3	616.6	117.8	1639.3	675.8	0.0	0.0	1639.3	675.8
K-UAF-07	Fine	-206.7	692.2	103.4	1638.4	805.6	0.0	0.0	1638.4	805.6
K-UAF-08	Fine	-216.0	567.5	102.9	1638.8	815.3	0.0	0.0	1638.8	815.3
K-UAF-09	Fine	-260.3	421.7	66.4	1640.0	896.1	0.0	0.0	1640.0	896.1
K-UAF-10	Fine	-869.3	962.1	106.2	1640.8	1465.3	0.0	0.0	1640.8	1465.3
K-UAF-11	Fine	-1131.9	1072.3	262.5	1640.4	1571.6	0.0	0.0	1640.4	1571.6
K-UAF-12	Fine	-1244.1	1198.5	307.1	1639.3	1639.3	0.0	0.0	1639.3	1639.3
K-UAF-13	Fine	-1274.3	1274.6	340.5	1636.0	1636.0	0.0	0.0	1636.0	1636.0

Table M.6: Annualized results of individual SoilCover simulations for a wet year, with no vegetation on the tailings surface (1535.0 mm precipitation).

Model no.	Tailings type	NI (mm)	BF (mm)	R (mm)	PE (mm)	AE (mm)	PT (mm)	AT (mm)	PET (mm)	AET (mm)
K-UWC-01	Coarse	587.0	222.2	333.1	1638.8	614.9	0.0	0.0	1638.8	614.9
K-UWC-02	Coarse	513.6	160.4	427.5	1638.6	593.9	0.0	0.0	1638.6	593.9
K-UWC-03	Coarse	199.9	146.0	827.6	1639.5	507.5	0.0	0.0	1639.5	507.5
K-UWC-04	Coarse	-157.4	145.9	1230.2	1639.6	462.2	0.0	0.0	1639.6	462.2
K-UWC-05	Coarse	-193.0	82.7	1279.4	1639.6	448.6	0.0	0.0	1639.6	448.6
K-UWC-06	Coarse	-162.8	159.5	1279.1	1639.5	418.7	0.0	0.0	1639.5	418.7
K-UWC-07	Coarse	-142.0	127.7	1293.7	1639.7	383.3	0.0	0.0	1639.7	383.3
K-UWC-08	Coarse	-100.8	128.6	1275.4	1639.3	360.4	0.0	0.0	1639.3	360.4
K-UWC-09	Coarse	-164.7	118.8	1292.6	1639.6	407.1	0.0	0.0	1639.6	407.1
K-UWC-10	Coarse	-133.3	95.0	1282.7	1639.8	385.6	0.0	0.0	1639.8	385.6
K-UWC-11	Coarse	-386.0	249.1	1080.6	1639.9	840.4	0.0	0.0	1639.9	840.4
K-UWC-12	Coarse	-562.9	488.4	1070.0	1640.3	1027.9	0.0	0.0	1640.3	1027.9

Table M.6: Annualized results of individual SoilCover simulations for a wet year, with no vegetation on the tailings surface (1535.0 mm precipitation).

Model no.	Tailings type	NI (mm)	BF (mm)	R (mm)	PE (mm)	AE (mm)	PT (mm)	AT (mm)	PET (mm)	AET (mm)
K-UWC-13	Coarse	-1181.5	1186.9	1082.0	1636.9	1634.6	0.0	0.0	1636.9	1634.6
K-UWI-01	Interm	452.7	325.0	221.8	1637.8	860.4	0.0	0.0	1637.8	860.4
K-UWI-02	Interm	503.0	301.3	261.8	1638.3	770.2	0.0	0.0	1638.3	770.2
K-UWI-03	Interm	350.7	301.8	373.4	1638.7	810.9	0.0	0.0	1638.7	810.9
K-UWI-04	Interm	308.0	177.2	520.2	1639.1	706.8	0.0	0.0	1639.1	706.8
K-UWI-05	Interm	117.5	173.5	822.9	1639.5	594.6	0.0	0.0	1639.5	594.6
K-UWI-06	Interm	-104.8	286.0	1102.5	1639.7	537.3	0.0	0.0	1639.7	537.3
K-UWI-07	Interm	-128.3	253.5	1139.7	1639.6	523.6	0.0	0.0	1639.6	523.6
K-UWI-08	Interm	-174.3	239.5	1187.0	1639.7	522.3	0.0	0.0	1639.7	522.3
K-UWI-09	Interm	92.6	1.2	721.7	1639.2	720.8	0.0	0.0	1639.2	720.8
K-UWI-10	Interm	-79.9	108.3	724.7	1640.3	890.2	0.0	0.0	1640.3	890.2
K-UWI-11	Interm	-399.7	402.7	826.0	1641.5	1108.7	0.0	0.0	1641.5	1108.7
K-UWI-12	Interm	-1187.2	1003.4	1144.7	1640.0	1577.5	0.0	0.0	1640.0	1577.5
K-UWI-13	Interm	-1183.7	1187.7	1081.9	1636.8	1636.8	0.0	0.0	1636.8	1636.8
K-UWF-01	Fine	676.6	830.9	33.6	1638.8	824.8	0.0	0.0	1638.8	824.8
K-UWF-02	Fine	692.3	624.9	29.2	1638.6	813.5	0.0	0.0	1638.6	813.5
K-UWF-03	Fine	653.1	727.6	58.0	1638.7	823.9	0.0	0.0	1638.7	823.9
K-UWF-04	Fine	499.6	621.7	251.5	1638.4	783.9	0.0	0.0	1638.4	783.9
K-UWF-05	Fine	349.6	547.6	413.3	1639.2	772.2	0.0	0.0	1639.2	772.2
K-UWF-06	Fine	345.4	63.1	356.4	1638.4	833.2	0.0	0.0	1638.4	833.2
K-UWF-07	Fine	100.9	259.6	521.6	1638.3	912.5	0.0	0.0	1638.3	912.5
K-UWF-08	Fine	122.5	31.5	493.3	1639.5	919.2	0.0	0.0	1639.5	919.2
K-UWF-09	Fine	104.7	38.9	399.2	1641.3	1031.0	0.0	0.0	1641.3	1031.0
K-UWF-10	Fine	-617.2	679.1	592.0	1641.1	1560.2	0.0	0.0	1641.1	1560.2
K-UWF-11	Fine	-930.1	839.4	893.2	1640.7	1572.0	0.0	0.0	1640.7	1572.0
K-UWF-12	Fine	-1204.5	1065.4	1099.3	1640.2	1640.2	0.0	0.0	1640.2	1640.2
K-UWF-13	Fine	-1184.3	1186.5	1082.1	1637.2	1637.2	0.0	0.0	1637.2	1637.2

Table M.7: Annualized results of individual SoilCover simulations for a dry year, with no vegetation on the tailings surface (270.0 mm precipitation).

Model no.	Tailings type	NI (mm)	BF (mm)	R (mm)	PE (mm)	AE (mm)	PT (mm)	AT (mm)	PET (mm)	AET (mm)
K-UDC-01	Coarse	-24.7	222.3	12.4	1639.8	282.3	0.0	0.0	1639.8	282.3
K-UDC-02	Coarse	-25.0	160.5	27.3	1639.4	267.7	0.0	0.0	1639.4	267.7
K-UDC-03	Coarse	-17.9	146.0	32.2	1639.8	255.7	0.0	0.0	1639.8	255.7
K-UDC-04	Coarse	-47.2	145.8	60.3	1639.5	256.9	0.0	0.0	1639.5	256.9
K-UDC-05	Coarse	-65.6	82.7	86.4	1639.7	249.1	0.0	0.0	1639.7	249.1
K-UDC-06	Coarse	-59.4	162.8	91.5	1639.8	237.9	0.0	0.0	1639.8	237.9
K-UDC-07	Coarse	-52.4	127.7	94.2	1639.5	228.1	0.0	0.0	1639.5	228.1
K-UDC-08	Coarse	-42.4	128.5	103.1	1639.5	209.4	0.0	0.0	1639.5	209.4
K-UDC-09	Coarse	-52.6	120.1	93.4	1639.8	229.2	0.0	0.0	1639.8	229.2
K-UDC-10	Coarse	-60.0	80.9	105.9	1639.6	224.1	0.0	0.0	1639.6	224.1
K-UDC-11	Coarse	-544.5	552.0	56.4	1639.9	758.1	0.0	0.0	1639.9	758.1
K-UDC-12	Coarse	-612.6	625.6	33.6	1640.3	849.0	0.0	0.0	1640.3	849.0
K-UDC-13	Coarse	-1410.8	1416.0	46.7	1636.4	1634.1	0.0	0.0	1636.4	1634.1
K-UDI-01	Interm	-8.1	325.0	0.0	1639.6	278.1	0.0	0.0	1639.6	278.1

Table M.7: Annualized results of individual SoilCover simulations for a dry year, with no vegetation on the tailings surface (270.0 mm precipitation).

Model no.	Tailings type	NI (mm)	BF (mm)	R (mm)	PE (mm)	AE (mm)	PT (mm)	AT (mm)	PET (mm)	AET (mm)
K-UDI-02	Interm	-7.7	301.4	0.0	1639.7	277.7	0.0	0.0	1639.7	277.7
K-UDI-03	Interm	-12.1	301.8	0.0	1639.6	282.1	0.0	0.0	1639.6	282.1
K-UDI-04	Interm	-26.9	177.1	12.2	1639.7	284.7	0.0	0.0	1639.7	284.7
K-UDI-05	Interm	-34.5	173.4	23.8	1639.5	280.7	0.0	0.0	1639.5	280.7
K-UDI-06	Interm	-26.9	286.3	36.1	1639.6	260.8	0.0	0.0	1639.6	260.8
K-UDI-07	Interm	-34.8	253.6	47.6	1639.5	257.2	0.0	0.0	1639.5	257.2
K-UDI-08	Interm	-71.7	210.6	88.9	1639.5	252.8	0.0	0.0	1639.5	252.8
K-UDI-09	Interm	-12.9	154.5	28.5	1639.9	254.5	0.0	0.0	1639.9	254.5
K-UDI-10	Interm	-367.9	495.5	9.7	1639.2	628.2	0.0	0.0	1639.2	628.2
K-UDI-11	Interm	-619.7	670.3	21.0	1640.9	868.7	0.0	0.0	1640.9	868.7
K-UDI-12	Interm	-1249.3	1257.7	31.4	1640.4	1487.9	0.0	0.0	1640.4	1487.9
K-UDI-13	Interm	-1412.2	1415.4	46.6	1635.6	1635.6	0.0	0.0	1635.6	1635.6
K-UDF-01	Fine	9.6	830.9	0.0	1639.7	260.4	0.0	0.0	1639.7	260.4
K-UDF-02	Fine	-4.9	625.0	0.0	1639.7	274.9	0.0	0.0	1639.7	274.9
K-UDF-03	Fine	-7.3	554.3	0.0	1639.8	277.3	0.0	0.0	1639.8	277.3
K-UDF-04	Fine	-6.8	524.4	0.0	1639.7	276.8	0.0	0.0	1639.7	276.8
K-UDF-05	Fine	-5.3	441.9	0.0	1639.8	275.3	0.0	0.0	1639.8	275.3
K-UDF-06	Fine	-13.3	628.6	0.0	1639.9	283.3	0.0	0.0	1639.9	283.3
K-UDF-07	Fine	-14.8	298.0	10.3	1639.8	274.6	0.0	0.0	1639.8	274.6
K-UDF-08	Fine	-24.4	443.2	10.7	1639.8	283.7	0.0	0.0	1639.8	283.7
K-UDF-09	Fine	-459.2	708.6	0.0	1639.4	729.2	0.0	0.0	1639.4	729.2
K-UDF-10	Fine	-652.6	790.7	0.0	1639.7	922.6	0.0	0.0	1639.7	922.6
K-UDF-11	Fine	-1276.9	1261.8	73.8	1640.5	1473.1	0.0	0.0	1640.5	1473.1
K-UDF-12	Fine	-1393.2	1402.6	22.4	1640.8	1640.8	0.0	0.0	1640.8	1640.8
K-UDF-13	Fine	-1413.0	1414.4	46.7	1636.3	1636.3	0.0	0.0	1636.3	1636.3

Table M.8: Annualized results of individual SoilCover simulations for a mean year, with vegetation on the tailings surface (702.2 mm precipitation).

Model no.	Tailings type	NI (mm)	BF (mm)	R (mm)	PE (mm)	AE (mm)	PT (mm)	AT (mm)	PET (mm)	AET (mm)
K-VAC-01	Coarse	138.5	222.2	65.7	1638.9	146.7	695.4	351.3	2334.3	498.0
K-VAC-02	Coarse	162.1	160.5	75.3	1638.6	131.2	695.1	333.6	2333.8	464.8
K-VAC-03	Coarse	124.2	146.1	170.0	1638.9	129.7	695.8	278.3	2334.7	408.0
K-VAC-04	Coarse	9.9	146.0	297.6	1639.1	130.6	695.8	264.1	2334.9	394.7
K-VAC-05	Coarse	-24.7	82.8	395.3	1639.4	128.3	696.0	203.4	2335.4	331.6
K-VAC-06	Coarse	-94.0	154.4	494.7	1639.4	116.6	695.8	184.9	2335.2	301.5
K-VAC-07	Coarse	-36.3	127.9	491.6	1639.4	108.8	695.9	138.1	2335.3	246.9
K-VAC-08	Coarse	-33.2	129.0	515.7	1639.1	103.3	695.8	116.5	2334.9	219.7
K-VAC-09	Coarse	-56.6	100.9	534.3	1639.8	117.9	696.3	106.7	2336.2	224.6
K-VAC-10	Coarse	-377.6	435.5	563.0	1640.0	106.8	696.5	410.0	2336.5	516.8
K-VACr11	Coarse	-575.8	589.9	232.1	1639.2	349.8	695.7	695.7	2334.9	1045.5
K-VACr12	Coarse	-705.3	703.9	301.9	1639.4	410.2	695.4	695.4	2334.8	1105.7
K-VAC-13	Coarse	-1377.6	1380.3	370.9	1636.8	1014.1	694.8	694.8	2331.6	1708.9
K-VAI-01	Interm	31.0	325.0	9.8	1638.4	162.2	694.8	499.2	2333.2	661.4
K-VAI-02	Interm	22.9	301.4	28.1	1638.6	160.0	695.1	491.3	2333.6	651.3
K-VAI-03	Interm	79.4	301.8	84.8	1638.9	152.0	695.5	386.0	2334.4	538.0

Table M.8: Annualized results of individual SoilCover simulations for a mean year, with vegetation on the tailings surface (702.2 mm precipitation).

Model no.	Tailings type	NI (mm)	BF (mm)	R (mm)	PE (mm)	AE (mm)	PT (mm)	AT (mm)	PET (mm)	AET (mm)
K-VAI-04	Interm	98.6	177.2	82.5	1639.1	152.8	695.6	368.3	2334.6	521.1
K-VAI-05	Interm	73.8	173.6	142.5	1639.8	134.8	695.2	351.1	2335.1	486.0
K-VAI-06	Interm	-31.9	285.8	304.4	1639.0	136.6	695.5	293.1	2334.4	429.8
K-VAI-07	Interm	-28.7	253.7	315.3	1638.4	137.1	694.9	278.6	2333.4	415.7
K-VAI-08	Interm	-46.3	213.1	391.4	1639.1	138.4	695.6	218.9	2334.7	357.2
K-VAI-09	Interm	-228.4	383.7	175.6	1638.8	271.1	695.4	483.9	2334.2	755.0
K-VAI-10	Interm	-443.8	547.1	148.4	1638.7	348.0	695.3	649.6	2334.0	997.6
K-VAIr11	Interm	-598.6	641.2	199.2	1639.6	405.8	695.9	695.9	2335.5	1101.7
K-VAIr12	Interm	-1235.8	1237.0	287.6	1638.6	955.3	695.2	695.2	2333.8	1650.5
K-VAI-13	Interm	-1377.9	1379.9	370.2	1635.7	1016.0	693.9	693.9	2329.6	1709.9
K-VAF-01	Fine	80.7	831.1	0.0	1639.2	153.9	695.6	467.6	2334.7	621.6
K-VAF-02	Fine	64.8	625.0	6.6	1638.1	153.4	694.6	477.4	2332.7	630.8
K-VAF-03	Fine	70.9	554.3	7.9	1639.0	152.6	695.4	470.9	2334.4	623.4
K-VAF-04	Fine	80.7	524.6	15.1	1638.8	147.6	695.3	458.8	2334.2	606.4
K-VAF-05	Fine	34.8	442.2	48.5	1639.0	152.0	695.4	466.9	2334.4	618.9
K-VAF-06	Fine	-18.8	677.7	106.6	1638.5	163.8	695.0	450.6	2333.5	614.4
K-VAF-07	Fine	-206.3	738.3	87.9	1638.3	332.3	695.1	488.4	2333.4	820.7
K-VAF-08	Fine	-280.1	669.6	108.4	1638.8	347.3	695.4	526.7	2334.1	874.0
K-VAF-09	Fine	-344.8	573.1	33.6	1638.8	355.9	695.4	657.5	2334.2	1013.4
K-VAF-10	Fine	-935.2	1046.7	99.8	1639.0	841.9	695.8	695.8	2334.7	1537.7
K-VAFr11	Fine	-1134.8	1174.6	193.2	1638.2	948.8	695.0	695.0	2333.2	1643.8
K-VAFr12	Fine	-1298.9	1294.4	288.5	1638.3	1017.8	694.8	694.8	2333.1	1712.7
K-VAF-13	Fine	-1378.2	1378.2	370.3	1635.8	1016.1	694.0	694.0	2329.8	1710.1

Table M.9: Annualized results of individual SoilCover simulations for a wet year, with vegetation on the tailings surface (1535.0 mm precipitation).

Model no.	Tailings type	NI (mm)	BF (mm)	R (mm)	PE (mm)	AE (mm)	PT (mm)	AT (mm)	PET (mm)	AET (mm)
K-VWC-01	Coarse	656.4	222.2	303.8	1638.9	195.3	695.5	379.5	2334.4	574.8
K-VWC-02	Coarse	606.7	160.4	391.2	1638.6	178.1	695.5	359.0	2334.0	537.1
K-VWC-03	Coarse	233.4	146.0	831.3	1639.3	169.1	696.2	301.3	2335.5	470.4
K-VWC-04	Coarse	7.7	146.0	1078.1	1639.4	163.3	696.2	286.0	2335.6	449.2
K-VWC-05	Coarse	6.7	82.5	1169.0	1638.8	150.4	695.4	209.0	2334.2	359.4
K-VWC-06	Coarse	-57.9	154.1	1254.0	1639.3	134.2	695.8	204.8	2335.1	338.9
K-VWC-07	Coarse	-61.4	127.9	1288.7	1639.4	127.7	695.9	180.1	2335.4	307.7
K-VWC-08	Coarse	-32.8	129.0	1328.0	1638.9	118.9	695.5	120.8	2334.4	239.8
K-VWC-09	Coarse	-59.5	101.0	1349.5	1639.6	137.1	696.1	107.9	2335.7	244.9
K-VWC-10	Coarse	-398.3	435.0	1397.8	1639.7	123.1	696.3	412.3	2336.0	535.4
K-VWCr11	Coarse	-444.1	473.7	927.3	1638.5	356.8	695.0	695.0	2333.6	1051.8
K-VWCr12	Coarse	-625.4	618.3	1046.5	1639.1	418.7	695.1	695.1	2334.3	1113.9
K-VWC-13	Coarse	-1297.6	1301.6	1124.0	1636.5	1014.5	694.1	694.1	2330.6	1708.6
K-VWI-01	Interm	464.5	325.1	85.1	1637.8	394.3	694.7	591.1	2332.5	985.3
K-VWI-02	Interm	668.9	301.3	161.4	1638.9	225.2	695.4	479.6	2334.3	704.7
K-VWI-03	Interm	553.6	301.8	313.8	1638.6	221.7	695.4	445.9	2333.9	667.6
K-VWI-04	Interm	334.1	177.2	579.9	1639.2	206.6	695.8	414.5	2335.0	621.1
K-VWI-05	Interm	145.4	173.6	829.5	1639.3	180.7	695.7	379.5	2335.0	560.2

Table M.9: Annualized results of individual SoilCover simulations for a wet year, with vegetation on the tailings surface (1535.0 mm precipitation).

Model no.	Tailings type	NI (mm)	BF (mm)	R (mm)	PE (mm)	AE (mm)	PT (mm)	AT (mm)	PET (mm)	AET (mm)
K-VWI-06	Interm	-103.6	285.8	1142.7	1639.5	182.4	695.8	313.5	2335.2	495.9
K-VWI-07	Interm	-107.2	253.6	1161.9	1639.5	180.4	696.0	300.0	2335.4	480.3
K-VWI-08	Interm	-70.0	214.3	1187.1	1639.1	172.6	695.7	245.4	2334.8	418.0
K-VWI-09	Interm	-17.0	114.4	701.2	1639.2	313.5	695.9	537.6	2335.1	851.0
K-VWI-10	Interm	-225.7	253.0	722.5	1638.7	381.8	695.1	656.4	2333.8	1038.2
K-VWIr11	Interm	-504.6	521.5	859.0	1639.2	485.5	695.2	695.2	2334.3	1180.6
K-VWIr12	Interm	-1113.8	1118.0	997.9	1639.1	955.8	695.1	695.1	2334.1	1650.9
K-VWI-13	Interm	-1298.8	1302.9	1123.6	1636.0	1016.5	693.8	693.8	2329.8	1710.2
K-VWF-01	Fine	612.1	831.1	55.2	1638.7	277.5	695.2	590.2	2333.9	867.7
K-VWF-02	Fine	624.5	625.0	50.6	1638.3	280.0	694.9	579.9	2333.2	859.9
K-VWF-03	Fine	603.7	592.5	69.4	1638.8	272.3	695.3	589.6	2334.1	861.9
K-VWF-04	Fine	576.6	631.6	185.7	1639.0	238.8	695.5	534.0	2334.5	772.7
K-VWF-05	Fine	427.4	531.3	343.4	1638.6	240.2	695.1	524.0	2333.7	764.2
K-VWF-06	Fine	417.5	-22.1	349.7	1638.9	246.9	695.4	521.0	2334.3	767.8
K-VWF-07	Fine	171.0	314.5	438.0	1639.0	388.0	695.6	537.9	2334.6	925.9
K-VWF-08	Fine	236.7	25.2	372.0	1638.8	380.6	695.4	545.7	2334.2	926.3
K-VWF-09	Fine	34.6	118.3	388.7	1638.7	424.3	695.3	687.3	2334.0	1111.6
K-VWF-10	Fine	-702.0	783.7	604.3	1639.3	937.1	695.6	695.6	2334.9	1632.7
K-VWFr11	Fine	-935.1	959.8	826.3	1638.3	949.0	694.9	694.9	2333.2	1643.9
K-VWFr12	Fine	-1178.9	1177.6	1000.0	1639.5	1018.7	695.2	695.2	2334.7	1713.9
K-VWF-13	Fine	-1299.4	1301.5	1123.9	1636.3	1016.5	694.0	694.0	2330.3	1710.5

Table M.10: Annualized results of individual SoilCover simulations for a dry year, with vegetation on the tailings surface (270.0 mm precipitation).

Model no.	Tailings type	NI (mm)	BF (mm)	R (mm)	PE (mm)	AE (mm)	PT (mm)	AT (mm)	PET (mm)	AET (mm)
K-VDC-01	Coarse	-16.7	222.2	0.9	1639.2	72.3	695.6	213.5	2334.8	285.8
K-VDC-02	Coarse	1.1	160.6	1.2	1638.6	72.1	695.7	195.5	2334.3	267.7
K-VDC-03	Coarse	-12.0	146.0	12.1	1639.1	71.6	695.6	198.3	2334.8	269.9
K-VDC-04	Coarse	0.8	145.9	19.6	1639.3	71.3	695.8	178.4	2335.0	249.6
K-VDC-05	Coarse	3.5	82.8	24.1	1638.9	72.3	695.4	169.6	2334.3	241.9
K-VDC-06	Coarse	-13.6	154.8	53.7	1639.3	73.6	695.8	156.3	2335.2	229.9
K-VDC-07	Coarse	-25.7	127.8	96.3	1639.4	72.2	695.9	127.1	2335.2	199.3
K-VDC-08	Coarse	-56.5	128.9	148.0	1639.2	68.4	695.8	110.1	2334.9	178.5
K-VDC-09	Coarse	-37.7	100.7	133.6	1639.5	71.5	696.0	102.7	2335.5	174.1
K-VDC-10	Coarse	-369.7	436.0	160.9	1639.5	70.1	696.0	408.7	2335.6	478.8
K-VDCr11	Coarse	-759.4	818.7	14.4	1639.5	318.8	696.2	696.2	2335.7	1015.0
K-VDCr12	Coarse	-817.9	834.0	36.8	1640.6	354.5	696.6	696.6	2337.2	1051.1
K-VDC-13	Coarse	-1496.1	1500.3	57.5	1636.6	1014.2	694.5	694.5	2331.0	1708.6
K-VDI-01	Interm	-10.4	325.0	0.0	1639.4	72.8	695.8	207.5	2335.2	280.4
K-VDI-02	Interm	-10.9	301.4	0.0	1639.5	72.6	696.0	208.3	2335.5	280.9
K-VDI-03	Interm	-11.2	301.6	0.0	1639.4	72.4	695.9	208.8	2335.3	281.2
K-VDI-04	Interm	-17.0	177.2	0.3	1639.3	72.1	695.7	214.5	2335.0	286.7
K-VDI-05	Interm	-1.1	173.6	0.6	1639.1	71.5	695.6	199.1	2334.7	270.5
K-VDI-06	Interm	-10.5	285.9	7.0	1639.2	75.9	695.6	197.6	2334.8	273.5
K-VDI-07	Interm	-28.8	253.7	25.2	1639.4	74.1	695.8	199.5	2335.2	273.6

Table M.10: Annualized results of individual SoilCover simulations for a dry year, with vegetation on the tailings surface (270.0 mm precipitation).

Model no.	Tailings type	NI (mm)	BF (mm)	R (mm)	PE (mm)	AE (mm)	PT (mm)	AT (mm)	PET (mm)	AET (mm)
K-VDI-08	Interm	-11.7	212.0	42.7	1639.2	74.3	695.7	164.8	2334.9	239.1
K-VDI-09	Interm	-326.5	549.6	6.1	1638.7	155.0	695.1	435.4	2333.9	590.4
K-VDI-10	Interm	-688.4	824.7	6.4	1638.4	303.4	695.0	648.6	2333.4	951.9
K-VDIr11	Interm	-784.2	846.7	11.4	1640.0	346.3	696.5	696.5	2336.5	1042.8
K-VDIr12	Interm	-1323.0	1338.6	30.7	1640.4	865.8	696.5	696.5	2336.8	1562.3
K-VDI-13	Interm	-1497.9	1500.5	57.4	1636.2	1016.3	694.3	694.3	2330.5	1710.5
K-VDF-01	Fine	1.7	831.1	0.0	1638.9	75.1	695.3	193.2	2334.1	268.3
K-VDF-02	Fine	-0.9	625.1	0.0	1638.8	75.0	695.3	195.8	2334.1	270.9
K-VDF-03	Fine	-9.1	375.2	0.0	1639.4	74.1	695.8	205.0	2335.2	279.1
K-VDF-04	Fine	-10.1	524.6	0.0	1639.3	73.6	695.7	206.5	2335.0	280.1
K-VDF-05	Fine	-10.0	442.2	0.0	1639.2	73.0	695.6	207.0	2334.7	280.0
K-VDF-06	Fine	-31.0	704.0	3.0	1639.1	79.0	695.5	219.0	2334.6	298.0
K-VDF-07	Fine	-16.7	445.8	6.7	1639.3	75.7	695.8	204.3	2335.1	280.0
K-VDF-08	Fine	-423.5	822.6	0.3	1638.8	301.6	695.4	391.6	2334.1	693.2
K-VDF-09	Fine	-691.7	941.4	0.0	1638.0	308.6	694.6	653.1	2332.6	961.7
K-VDF-10	Fine	-788.7	926.9	0.0	1638.6	363.4	695.4	695.4	2334.0	1058.7
K-VDFr11	Fine	-1285.4	1342.8	9.3	1639.3	850.0	696.1	696.1	2335.4	1546.1
K-VDFr12	Fine	-1475.5	1485.4	30.9	1640.2	1018.8	695.8	695.8	2336.0	1714.6
K-VDF-13	Fine	-1497.7	1498.5	57.4	1636.0	1016.2	694.1	694.1	2330.1	1710.3

M.4 Monthly SoilCover Simulation Results (Single Tailings Type)

Each of the 234 model runs listed in Tables M.5 to M.10 were further broken down into monthly time increments, giving rise to an additional 2808 monthly data sets. Since, documenting this data would be too voluminous for this thesis, only the summarized results of the composite cross-section integrated solution for the 13 individual SoilCover simulations for each homogeneous tailings type set are documented here. These results are listed in Tables M.11 to M28. The results are all presented in terms of percentages of the annual precipitation. Runoff (R), is always expressed as a positive value and cannot be greater than 100%. The net infiltration (NI) can be both positive and negative, with a negative number indicating a loss of water from the profile. The evaporation (E), transpiration (T) and evapotranspiration (ET) are always expressed as positive values although they are in fact indicative of a system water loss. These values can also be greater than 100%, as the volume of water lost through evapotranspiration can exceed the amount of precipitation (in fact this causes a negative NI).

Table M.11: Monthly results of the composite cross-section SoilCover simulations using only coarse tailings, a mean year, and non-vegetated tailings.

Month	P (mm)	R	NI	E	T	ET
July	7.3	0.3%	-2.8%	3.6%	0.0%	3.6%
August	8.8	0.9%	-2.1%	2.5%	0.0%	2.5%
September	6.8	0.0%	-3.7%	4.7%	0.0%	4.7%
October	11.5	1.7%	-3.7%	4.6%	0.0%	4.6%
November	45.6	1.0%	-2.8%	8.3%	0.0%	8.3%
December	103.0	9.3%	-4.2%	9.5%	0.0%	9.5%
January	184.9	12.6%	-2.3%	16.0%	0.0%	16.0%
February	181.8	12.5%	1.1%	12.3%	0.0%	12.3%
March	102.8	9.7%	-4.5%	9.4%	0.0%	9.4%
April	20.6	1.6%	-5.4%	6.8%	0.0%	6.8%
May	12.7	1.0%	-3.4%	4.2%	0.0%	4.2%
June	10.4	0.3%	-3.1%	4.3%	0.0%	4.3%
YEAR	702.2	50.9%	-37.0%	86.1%	0.0%	86.1%

Table M.12: Monthly results of the composite cross-section SoilCover simulations using only intermediate tailings, a mean year, and non-vegetated tailings.

Month	P (mm)	R	NI	E	T	ET
July	7.3	0.0%	-3.0%	4.0%	0.0%	4.0%
August	8.8	0.6%	-3.1%	3.7%	0.0%	3.7%
September	6.8	0.0%	-5.8%	6.8%	0.0%	6.8%
October	11.5	1.6%	-6.0%	6.9%	0.0%	6.9%
November	45.6	0.2%	-3.5%	9.8%	0.0%	9.8%
December	103.0	8.4%	-5.9%	12.2%	0.0%	12.2%
January	184.9	7.7%	0.0%	18.6%	0.0%	18.6%
February	181.8	6.3%	5.3%	14.3%	0.0%	14.3%
March	102.8	5.0%	-4.2%	13.9%	0.0%	13.9%
April	20.6	1.2%	-8.7%	10.5%	0.0%	10.5%
May	12.7	0.5%	-5.7%	6.9%	0.0%	6.9%
June	10.4	0.1%	-4.8%	6.1%	0.0%	6.1%
YEAR	702.2	31.6%	-45.3%	113.7%	0.0%	113.7%

Table M.13: Monthly results of the composite cross-section SoilCover simulations using only fine tailings, a mean year, and non-vegetated tailings.

Month	P (mm)	R	NI	E	T	ET
July	7.3	0.0%	-4.0%	5.1%	0.0%	5.1%
August	8.8	0.1%	-4.0%	5.2%	0.0%	5.2%
September	6.8	0.0%	-9.3%	10.2%	0.0%	10.2%
October	11.5	0.9%	-9.4%	10.9%	0.0%	10.9%
November	45.6	0.1%	-6.2%	12.6%	0.0%	12.6%
December	103.0	6.4%	-6.9%	15.2%	0.0%	15.2%

Table M.13: Monthly results of the composite cross-section SoilCover simulations using only fine tailings, a mean year, and non-vegetated tailings.

Month	P (mm)	R	NI	E	T	ET
January	184.9	4.6%	2.3%	19.4%	0.0%	19.4%
February	181.8	4.2%	6.6%	15.1%	0.0%	15.1%
March	102.8	2.9%	-5.4%	17.1%	0.0%	17.1%
April	20.6	0.3%	-11.3%	14.0%	0.0%	14.0%
May	12.7	0.1%	-7.2%	8.9%	0.0%	8.9%
June	10.4	0.0%	-7.1%	8.6%	0.0%	8.6%
YEAR	702.2	19.7%	-62.0%	142.3%	0.0%	142.3%

Table M.14: Monthly results of the composite cross-section SoilCover simulations using only coarse tailings, a mean year, and vegetated tailings.

Month	P (mm)	R	NI	E	T	ET
July	7.3	0.1%	-2.6%	3.6%	0.0%	3.6%
August	8.8	0.6%	-1.9%	2.5%	0.0%	2.5%
September	6.8	0.0%	-3.8%	4.7%	0.0%	4.7%
October	11.5	1.4%	-3.5%	4.6%	0.0%	4.6%
November	45.6	0.7%	-3.6%	7.5%	1.9%	9.4%
December	103.0	9.8%	-5.4%	2.1%	8.2%	10.3%
January	184.9	14.3%	-2.7%	0.8%	13.9%	14.7%
February	181.8	12.7%	1.0%	0.7%	11.6%	12.2%
March	102.8	8.9%	-6.9%	1.8%	10.8%	12.6%
April	20.6	1.6%	-7.0%	4.5%	3.8%	8.4%
May	12.7	0.9%	-3.6%	3.9%	0.7%	4.5%
June	10.4	0.2%	-3.0%	4.3%	0.0%	4.3%
YEAR	702.2	51.1%	-42.9%	41.0%	50.9%	91.9%

Table M.15: Monthly results of the composite cross-section SoilCover simulations using only intermediate tailings, a mean year, and vegetated tailings.

Month	P (mm)	R	NI	E	T	ET
July	7.3	0.0%	-3.0%	4.0%	0.0%	4.0%
August	8.8	0.3%	-2.7%	3.7%	0.0%	3.7%
September	6.8	0.0%	-5.8%	6.8%	0.0%	6.8%
October	11.5	1.1%	-5.5%	6.9%	0.0%	6.9%
November	45.6	0.1%	-4.5%	8.8%	2.1%	10.9%
December	103.0	6.9%	-5.2%	2.4%	10.6%	13.0%
January	184.9	7.6%	-0.5%	0.8%	18.4%	19.3%
February	181.8	6.7%	3.5%	0.7%	15.1%	15.7%
March	102.8	5.7%	-8.2%	2.3%	14.9%	17.2%
April	20.6	1.1%	-10.0%	6.0%	5.9%	11.9%
May	12.7	0.4%	-5.0%	5.5%	0.9%	6.4%
June	10.4	0.0%	-4.5%	5.9%	0.0%	5.9%

Table M.15: Monthly results of the composite cross-section SoilCover simulations using only intermediate tailings, a mean year, and vegetated tailings.

Month	P (mm)	R	NI	E	T	ET
YEAR	702.2	29.8%	-51.5%	53.8%	67.9%	121.7%

Table M.16: Monthly results of the composite cross-section SoilCover simulations using only fine tailings, a mean year, and vegetated tailings.

Month	P (mm)	R	NI	E	T	ET
July	7.3	0.0%	-4.0%	5.1%	0.0%	5.1%
August	8.8	0.1%	-4.0%	5.2%	0.0%	5.2%
September	6.8	0.0%	-9.3%	10.2%	0.0%	10.2%
October	11.5	0.5%	-8.9%	10.9%	0.0%	10.9%
November	45.6	0.1%	-7.1%	10.9%	2.6%	13.5%
December	103.0	4.2%	-5.8%	2.6%	13.6%	16.3%
January	184.9	5.1%	0.1%	0.8%	20.3%	21.1%
February	181.8	3.7%	5.4%	0.7%	16.2%	16.8%
March	102.8	2.7%	-8.1%	2.7%	17.4%	20.1%
April	20.6	0.5%	-14.1%	7.5%	9.1%	16.6%
May	12.7	0.1%	-6.9%	7.1%	1.5%	8.6%
June	10.4	0.0%	-6.3%	7.7%	0.0%	7.7%
YEAR	702.2	17.0%	-69.1%	71.5%	80.6%	152.1%

Table M.17: Monthly results of the composite cross-section SoilCover simulations using only coarse tailings, a wet year, and non-vegetated tailings.

Month	P (mm)	R	NI	E	T	ET
July	16.0	0.7%	-1.4%	1.7%	0.0%	1.7%
August	19.3	1.1%	-1.0%	1.2%	0.0%	1.2%
September	14.8	0.4%	-1.9%	2.4%	0.0%	2.4%
October	38.3	2.1%	-1.7%	2.1%	0.0%	2.1%
November	99.7	3.9%	-1.9%	4.5%	0.0%	4.5%
December	225.3	11.8%	-2.4%	5.2%	0.0%	5.2%
January	404.2	18.7%	-0.3%	7.9%	0.0%	7.9%
February	397.4	17.1%	2.6%	6.2%	0.0%	6.2%
March	224.6	10.8%	-0.6%	4.4%	0.0%	4.4%
April	45.1	2.1%	-2.4%	3.3%	0.0%	3.3%
May	27.6	1.4%	-1.6%	2.0%	0.0%	2.0%
June	22.7	0.8%	-1.5%	2.2%	0.0%	2.2%
YEAR	1535.0	70.8%	-13.9%	43.1%	0.0%	43.1%

Table M.18: Monthly results of the composite cross-section SoilCover simulations using only intermediate tailings, a wet year, and non-vegetated tailings.

Month	P (mm)	R	NI	E	T	ET
July	16.0	0.7%	-1.7%	2.1%	0.0%	2.1%
August	19.3	1.1%	-1.5%	1.7%	0.0%	1.7%
September	14.8	0.3%	-2.9%	3.6%	0.0%	3.6%
October	38.3	2.2%	-2.9%	3.2%	0.0%	3.2%
November	99.7	3.1%	-2.8%	6.3%	0.0%	6.3%
December	225.3	11.2%	-3.2%	6.6%	0.0%	6.6%
January	404.2	14.0%	3.3%	9.0%	0.0%	9.0%
February	397.4	10.7%	7.9%	7.3%	0.0%	7.3%
March	224.6	6.8%	1.2%	6.6%	0.0%	6.6%
April	45.1	1.6%	-3.9%	5.2%	0.0%	5.2%
May	27.6	0.8%	-2.6%	3.6%	0.0%	3.6%
June	22.7	0.3%	-2.1%	3.3%	0.0%	3.3%
YEAR	1535.0	52.9%	-11.3%	58.4%	0.0%	58.4%

Table M.19: Monthly results of the composite cross-section SoilCover simulations using only fine tailings, a wet year, and non-vegetated tailings.

Month	P (mm)	R	NI	E	T	ET
July	16.0	0.4%	-2.1%	2.7%	0.0%	2.7%
August	19.3	0.9%	-2.5%	2.8%	0.0%	2.8%
September	14.8	0.1%	-4.5%	5.3%	0.0%	5.3%
October	38.3	1.8%	-4.5%	5.1%	0.0%	5.1%
November	99.7	1.8%	-2.6%	7.3%	0.0%	7.3%
December	225.3	7.7%	-1.2%	8.2%	0.0%	8.2%
January	404.2	9.2%	7.6%	9.5%	0.0%	9.5%
February	397.4	6.4%	11.5%	7.9%	0.0%	7.9%
March	224.6	4.4%	2.4%	7.9%	0.0%	7.9%
April	45.1	0.6%	-4.7%	7.1%	0.0%	7.1%
May	27.6	0.3%	-3.0%	4.5%	0.0%	4.5%
June	22.7	0.1%	-3.1%	4.5%	0.0%	4.5%
YEAR	1535.0	33.8%	-6.6%	72.8%	0.0%	72.8%

Table M.20: Monthly results of the composite cross-section SoilCover simulations using only coarse tailings, a wet year, and vegetated tailings.

Month	P (mm)	R	NI	E	T	ET
July	16.0	0.6%	-1.2%	1.7%	0.0%	1.7%
August	19.3	1.0%	-0.9%	1.2%	0.0%	1.2%
September	14.8	0.3%	-1.8%	2.4%	0.0%	2.4%
October	38.3	2.0%	-1.6%	2.1%	0.0%	2.1%
November	99.7	3.5%	-1.7%	3.8%	0.9%	4.7%
December	225.3	12.2%	-2.4%	1.1%	3.8%	4.9%

Table M.20: Monthly results of the composite cross-section SoilCover simulations using only coarse tailings, a wet year, and vegetated tailings.

Month	P (mm)	R	NI	E	T	ET
January	404.2	18.2%	1.2%	0.4%	6.5%	6.9%
February	397.4	17.1%	2.7%	0.3%	5.7%	6.0%
March	224.6	10.7%	-2.0%	0.9%	5.1%	6.0%
April	45.1	2.1%	-3.1%	2.2%	1.8%	4.0%
May	27.6	1.3%	-1.7%	1.8%	0.3%	2.1%
June	22.7	0.6%	-1.3%	2.2%	0.0%	2.2%
YEAR	1535.0	69.7%	-13.8%	20.1%	24.1%	44.2%

Table M.21: Monthly results of the composite cross-section SoilCover simulations using only intermediate tailings, a wet year, and vegetated tailings.

Month	P (mm)	R	NI	E	T	ET
July	16.0	0.4%	-1.5%	2.1%	0.0%	2.1%
August	19.3	0.8%	-1.3%	1.7%	0.0%	1.7%
September	14.8	0.2%	-2.8%	3.6%	0.0%	3.6%
October	38.3	1.9%	-2.6%	3.2%	0.0%	3.2%
November	99.7	2.3%	-2.2%	5.3%	1.1%	6.4%
December	225.3	9.8%	-1.7%	1.4%	5.2%	6.6%
January	404.2	14.1%	3.1%	0.4%	8.8%	9.1%
February	397.4	11.9%	6.1%	0.3%	7.6%	7.9%
March	224.6	7.6%	-0.8%	1.0%	6.7%	7.8%
April	45.1	1.7%	-4.4%	2.9%	2.8%	5.7%
May	27.6	1.0%	-2.4%	2.7%	0.5%	3.2%
June	22.7	0.3%	-2.0%	3.2%	0.0%	3.2%
YEAR	1535.0	52.0%	-12.4%	27.8%	32.6%	60.3%

Table M.22: Monthly results of the composite cross-section SoilCover simulations using only fine tailings, a wet year, and vegetated tailings.

Month	P (mm)	R	NI	E	T	ET
July	16.0	0.2%	-1.9%	2.7%	0.0%	2.7%
August	19.3	0.6%	-2.1%	2.8%	0.0%	2.8%
September	14.8	0.0%	-4.4%	5.3%	0.0%	5.3%
October	38.3	1.6%	-4.3%	5.1%	0.0%	5.1%
November	99.7	1.2%	-2.4%	6.2%	1.5%	7.7%
December	225.3	7.1%	-0.9%	1.5%	7.0%	8.5%
January	404.2	8.6%	7.8%	0.4%	9.5%	9.9%
February	397.4	6.4%	11.0%	0.3%	8.2%	8.5%
March	224.6	4.3%	0.9%	1.3%	8.1%	9.4%
April	45.1	1.0%	-6.4%	3.7%	4.7%	8.3%
May	27.6	0.6%	-3.1%	3.5%	0.8%	4.3%
June	22.7	0.1%	-2.7%	4.0%	0.0%	4.0%

Table M.22: Monthly results of the composite cross-section SoilCover simulations using only fine tailings, a wet year, and vegetated tailings.

Month	P (mm)	R	NI	E	T	ET
YEAR	1535.0	31.8%	-8.4%	36.8%	39.8%	76.6%

Table M.23: Monthly results of the composite cross-section SoilCover simulations using only coarse tailings, a dry year, and non-vegetated tailings.

Month	P (mm)	R	NI	E	T	ET
July	2.8	0.0%	-6.9%	7.9%	0.0%	7.9%
August	3.4	0.0%	-5.3%	6.5%	0.0%	6.5%
September	2.6	0.0%	-9.2%	10.2%	0.0%	10.2%
October	6.7	0.3%	-8.9%	11.1%	0.0%	11.1%
November	17.5	0.0%	-6.9%	13.4%	0.0%	13.4%
December	39.6	4.8%	-8.3%	18.2%	0.0%	18.2%
January	71.1	5.8%	-11.0%	31.5%	0.0%	31.5%
February	69.9	5.6%	-5.6%	25.9%	0.0%	25.9%
March	39.5	8.0%	-14.2%	20.8%	0.0%	20.8%
April	7.9	0.1%	-13.2%	16.0%	0.0%	16.0%
May	4.9	0.0%	-8.2%	10.0%	0.0%	10.0%
June	4.0	0.0%	-8.1%	9.6%	0.0%	9.6%
YEAR	270.0	24.5%	-105.7%	181.2%	0.0%	181.2%

Table M.24: Monthly results of the composite cross-section SoilCover simulations using only intermediate tailings, a dry year, and non-vegetated tailings.

Month	P (mm)	R	NI	E	T	ET
July	2.8	0.0%	-7.8%	8.8%	0.0%	8.8%
August	3.4	0.0%	-6.1%	7.3%	0.0%	7.3%
September	2.6	0.0%	-13.9%	14.9%	0.0%	14.9%
October	6.7	0.0%	-13.5%	16.0%	0.0%	16.0%
November	17.5	0.0%	-11.2%	17.7%	0.0%	17.7%
December	39.6	2.9%	-11.8%	23.5%	0.0%	23.5%
January	71.1	1.8%	-8.5%	33.0%	0.0%	33.0%
February	69.9	2.2%	-2.6%	26.3%	0.0%	26.3%
March	39.5	3.6%	-16.8%	27.8%	0.0%	27.8%
April	7.9	0.0%	-17.4%	20.3%	0.0%	20.3%
May	4.9	0.0%	-10.7%	12.5%	0.0%	12.5%
June	4.0	0.0%	-10.5%	12.0%	0.0%	12.0%
YEAR	270.0	10.5%	-130.7%	220.2%	0.0%	220.2%

Table M.25: Monthly results of the composite cross-section SoilCover simulations using only fine tailings, a dry year, and non-vegetated tailings.

Month	P (mm)	R	NI	E	T	ET
July	2.8	0.0%	-10.7%	11.7%	0.0%	11.7%
August	3.4	0.0%	-9.2%	10.4%	0.0%	10.4%
September	2.6	0.0%	-18.9%	19.9%	0.0%	19.9%
October	6.7	0.0%	-18.8%	21.3%	0.0%	21.3%
November	17.5	0.0%	-15.9%	22.3%	0.0%	22.3%
December	39.6	1.9%	-15.8%	28.6%	0.0%	28.6%
January	71.1	1.0%	-9.9%	35.2%	0.0%	35.2%
February	69.9	1.3%	-5.8%	30.4%	0.0%	30.4%
March	39.5	1.1%	-17.6%	31.1%	0.0%	31.1%
April	7.9	0.0%	-21.5%	24.4%	0.0%	24.4%
May	4.9	0.0%	-13.2%	15.0%	0.0%	15.0%
June	4.0	0.0%	-12.9%	14.4%	0.0%	14.4%
YEAR	270.0	5.3%	-170.2%	264.9%	0.0%	264.9%

Table M.26: Monthly results of the composite cross-section SoilCover simulations using only coarse tailings, a dry year, and vegetated tailings.

Month	P (mm)	R	NI	E	T	ET
July	2.8	0.0%	-6.9%	7.9%	0.0%	7.9%
August	3.4	0.0%	-5.3%	6.5%	0.0%	6.5%
September	2.6	0.0%	-9.2%	10.2%	0.0%	10.2%
October	6.7	0.0%	-8.7%	11.1%	0.0%	11.1%
November	17.5	0.0%	-10.9%	12.5%	4.9%	17.4%
December	39.6	5.7%	-15.7%	3.9%	20.8%	24.7%
January	71.1	6.0%	-13.3%	2.1%	31.5%	33.6%
February	69.9	5.5%	-6.0%	1.8%	24.5%	26.3%
March	39.5	4.8%	-20.8%	4.6%	26.0%	30.6%
April	7.9	0.4%	-18.4%	11.0%	9.9%	21.0%
May	4.9	0.0%	-9.2%	9.3%	1.7%	11.0%
June	4.0	0.0%	-8.2%	9.7%	0.0%	9.7%
YEAR	270.0	22.4%	-132.5%	90.8%	119.3%	210.1%

Table M.27: Monthly results of the composite cross-section SoilCover simulations using only intermediate tailings, a dry year, and vegetated tailings.

Month	P (mm)	R	NI	E	T	ET
July	2.8	0.0%	-7.8%	8.8%	0.0%	8.8%
August	3.4	0.0%	-6.1%	7.3%	0.0%	7.3%
September	2.6	0.0%	-13.9%	14.9%	0.0%	14.9%
October	6.7	0.0%	-13.5%	16.0%	0.0%	16.0%
November	17.5	0.0%	-14.9%	16.1%	5.3%	21.4%
December	39.6	1.9%	-17.1%	4.6%	25.2%	29.9%

Table M.27: Monthly results of the composite cross-section SoilCover simulations using only intermediate tailings, a dry year, and vegetated tailings.

Month	P (mm)	R	NI	E	T	ET
January	71.1	1.3%	-14.1%	2.1%	37.0%	39.2%
February	69.9	1.0%	-4.0%	1.8%	27.1%	28.9%
March	39.5	1.9%	-24.7%	5.2%	32.2%	37.4%
April	7.9	0.0%	-24.3%	13.5%	13.7%	27.2%
May	4.9	0.0%	-12.5%	12.0%	2.3%	14.3%
June	4.0	0.0%	-11.7%	13.2%	0.0%	13.2%
YEAR	270.0	6.2%	-164.6%	115.5%	142.9%	258.4%

Table M.28: Monthly results of the composite cross-section SoilCover simulations using only fine tailings, a dry year, and vegetated tailings.

Month	P (mm)	R	NI	E	T	ET
July	2.8	0.0%	-10.7%	11.7%	0.0%	11.7%
August	3.4	0.0%	-9.2%	10.4%	0.0%	10.4%
September	2.6	0.0%	-18.9%	19.9%	0.0%	19.9%
October	6.7	0.0%	-18.8%	21.3%	0.0%	21.3%
November	17.5	0.0%	-19.7%	19.8%	6.3%	26.2%
December	39.6	0.6%	-20.6%	5.4%	29.2%	34.7%
January	71.1	0.9%	-15.2%	2.1%	38.5%	40.6%
February	69.9	1.0%	-6.2%	1.8%	29.2%	31.0%
March	39.5	1.2%	-26.5%	5.7%	34.2%	39.9%
April	7.9	0.0%	-30.5%	16.9%	16.6%	33.5%
May	4.9	0.0%	-16.5%	15.5%	2.8%	18.3%
June	4.0	0.0%	-15.1%	16.6%	0.0%	16.6%
YEAR	270.0	3.9%	-208.0%	147.2%	156.9%	304.1%

M.5 Monthly SoilCover Simulation Results (Composite Tailings Type)

Tables M.29 to M.34 list the composite cross-section results for combining the three tailings types for all the monthly SoilCover simulations. This data is reported in a similar fashion as described in the previous section, with the added component of a monthly averaged daily net infiltration flux, q. The step functions describing these fluxes are presented in Figures M.14 and M.15. Figure M.1 to M.13 presents the data of Tables M.29 to M.34 in a graphical form, which allows for easy comparison of the cases. Care must be taken when comparing the results of the various climatic scenarios, especially when using the values expressed as percentages of the annual precipitation. Since the precipitation numbers differ, the relative magnitude of the flux changes may not be accurate.

Table M.29: Summarized results of the integrated cross-section SoilCover simulations using the combined coarse, intermediate and fine tailings profile, for a mean year, and non-vegetated tailings (702.2 mm precipitation).

Month	R	NI	E	T	ET	Days	NI (mm)	q (mm/d)
July	0.0%	-3.9%	5.0%	0.0%	5.0%	31	-27.57	-0.889
August	0.7%	-4.3%	4.8%	0.0%	4.8%	62	-30.21	-0.974
September	0.0%	-7.4%	8.4%	0.0%	8.4%	92	-51.99	-1.733
October	1.5%	-7.5%	8.5%	0.0%	8.5%	123	-52.45	-1.692
November	0.3%	-5.0%	11.2%	0.0%	11.2%	153	-35.04	-1.168
December	8.7%	-6.1%	12.1%	0.0%	12.1%	184	-43.03	-1.388
January	10.9%	-2.3%	17.8%	0.0%	17.8%	215	-16.19	-0.522
February	9.1%	3.1%	13.7%	0.0%	13.7%	243	22.05	0.787
March	6.9%	-4.2%	11.9%	0.0%	11.9%	274	-29.81	-0.961
April	1.3%	-7.5%	9.1%	0.0%	9.1%	304	-52.87	-1.762
May	0.9%	-5.0%	6.0%	0.0%	6.0%	335	-35.34	-1.140
June	0.2%	-4.6%	5.9%	0.0%	5.9%	365	-32.39	-1.080
YEAR	40.4%	-54.8%	114.4%	0.0%	114.4%	365	-384.83	-12.523

Table M.30: Summarized results of the integrated cross-section SoilCover simulations using the combined coarse, intermediate and fine tailings profile, for a mean year, and vegetated tailings (702.2 mm precipitation).

Month	R	NI	E	T	ET	Days	NI (mm)	q (mm/d)
July	0.0%	-3.9%	5.0%	0.0%	5.0%	31	-27.57	-0.889
August	0.4%	-3.9%	4.8%	0.0%	4.8%	62	-27.65	-0.892
September	0.0%	-7.4%	8.4%	0.0%	8.4%	92	-52.19	-1.740
October	1.2%	-7.2%	8.5%	0.0%	8.5%	123	-50.50	-1.629
November	0.2%	-5.7%	9.9%	2.1%	12.0%	153	-40.03	-1.334
December	8.2%	-5.5%	2.4%	9.5%	11.9%	184	-38.30	-1.236
January	9.7%	-1.2%	0.8%	17.0%	17.8%	215	-8.51	-0.275
February	7.8%	3.3%	0.7%	14.0%	14.7%	243	23.50	0.839
March	7.1%	-7.3%	2.1%	12.7%	14.8%	274	-51.00	-1.645
April	1.2%	-9.3%	5.7%	5.2%	11.0%	304	-65.22	-2.174
May	0.6%	-5.0%	5.3%	0.9%	6.2%	335	-35.08	-1.132
June	0.1%	-4.5%	5.9%	0.0%	5.9%	365	-31.38	-1.046
YEAR	36.6%	-57.5%	59.4%	61.5%	120.9%	365	-403.94	-13.152

Table M.31: Summarized results of the integrated cross-section SoilCover simulations using the combined coarse, intermediate and fine tailings profile, for a wet year, and non-vegetated tailings (1535.0 mm precipitation).

Month	R	NI	E	T	ET	Days	NI (mm)	q (mm/d)
July	0.7%	-2.1%	2.4%	0.0%	2.4%	31	-31.78	-1.025
August	1.0%	-1.9%	2.2%	0.0%	2.2%	62	-29.53	-0.953
September	0.4%	-3.6%	4.2%	0.0%	4.2%	92	-55.18	-1.839

Table M.31: Summarized results of the integrated cross-section SoilCover simulations using the combined coarse, intermediate and fine tailings profile, for a wet year, and non-vegetated tailings (1535.0 mm precipitation).

Month	R	NI	E	T	ET	Days	NI (mm)	q (mm/d)
October	2.0%	-3.4%	3.9%	0.0%	3.9%	123	-52.75	-1.702
November	3.3%	-2.9%	6.1%	0.0%	6.1%	153	-44.16	-1.472
December	11.5%	-3.1%	6.2%	0.0%	6.2%	184	-46.82	-1.510
January	17.0%	0.8%	8.5%	0.0%	8.5%	215	12.76	0.412
February	13.9%	5.3%	6.8%	0.0%	6.8%	243	80.70	2.882
March	8.9%	0.1%	5.6%	0.0%	5.6%	274	0.90	0.029
April	1.8%	-3.3%	4.4%	0.0%	4.4%	304	-49.99	-1.666
May	1.2%	-2.2%	2.8%	0.0%	2.8%	335	-33.85	-1.092
June	0.6%	-2.0%	3.0%	0.0%	3.0%	365	-31.09	-1.036
YEAR	62.3%	-18.3%	56.0%	0.0%	56.0%	365	-280.79	-8.973

Table M.32: Summarized results of the integrated cross-section SoilCover simulations using the combined coarse, intermediate and fine tailings profile, for a wet year, and vegetated tailings (1535.0 mm precipitation).

Month	R	NI	E	T	ET	Days	NI (mm)	q (mm/d)
July	0.5%	-1.9%	2.4%	0.0%	2.4%	31	-28.61	-0.923
August	0.9%	-1.8%	2.2%	0.0%	2.2%	62	-27.82	-0.897
September	0.2%	-3.4%	4.2%	0.0%	4.2%	92	-52.52	-1.751
October	1.9%	-3.3%	3.9%	0.0%	3.9%	123	-50.72	-1.636
November	2.8%	-2.4%	5.2%	1.0%	6.1%	153	-37.05	-1.235
December	11.3%	-2.6%	1.4%	4.5%	5.9%	184	-39.36	-1.270
January	15.7%	2.2%	0.4%	8.1%	8.5%	215	33.71	1.087
February	14.2%	4.4%	0.3%	6.9%	7.2%	243	67.99	2.428
March	9.6%	-1.8%	1.0%	5.9%	6.8%	274	-27.53	-0.888
April	1.8%	-4.0%	2.8%	2.4%	5.2%	304	-61.88	-2.063
May	1.1%	-2.2%	2.5%	0.4%	2.9%	335	-33.63	-1.085
June	0.4%	-1.9%	2.9%	0.0%	2.9%	365	-28.45	-0.948
YEAR	60.4%	-18.6%	29.0%	29.2%	58.2%	365	-285.87	-9.180

Table M.33: Summarized results of the integrated cross-section SoilCover simulations using the combined coarse, intermediate and fine tailings profile, for a dry year, and non-vegetated tailings (270.0 mm precipitation).

Month	R	NI	E	T	ET	Days	NI (mm)	q (mm/d)
July	0.0%	-10.3%	11.4%	0.0%	11.4%	31	-27.93	-0.901
August	0.0%	-8.8%	10.1%	0.0%	10.1%	62	-23.80	-0.768
September	0.0%	-18.5%	19.4%	0.0%	19.4%	92	-49.89	-1.663
October	0.0%	-18.3%	20.8%	0.0%	20.8%	123	-49.46	-1.596
November	0.0%	-15.5%	22.0%	0.0%	22.0%	153	-41.77	-1.392
December	4.0%	-15.4%	26.1%	0.0%	26.1%	184	-41.64	-1.343

Table M.33: Summarized results of the integrated cross-section SoilCover simulations using the combined coarse, intermediate and fine tailings profile, for a dry year, and non-vegetated tailings (270.0 mm precipitation).

Month	R	NI	E	T	ET	Days	NI (mm)	q (mm/d)
January	3.2%	-10.2%	33.3%	0.0%	33.3%	215	-27.43	-0.885
February	3.5%	-4.0%	26.4%	0.0%	26.4%	243	-10.75	-0.384
March	6.1%	-17.0%	25.6%	0.0%	25.6%	274	-45.99	-1.484
April	0.0%	-16.9%	19.8%	0.0%	19.8%	304	-45.70	-1.523
May	0.0%	-10.6%	12.4%	0.0%	12.4%	335	-28.50	-0.919
June	0.0%	-10.4%	11.9%	0.0%	11.9%	365	-28.16	-0.939
YEAR	16.8%	-155.9%	239.1%	0.0%	239.1%	365	-421.03	-13.797

Table M.34: Summarized results of the integrated cross-section SoilCover simulations using the combined coarse, intermediate and fine tailings profile, for a dry year, and vegetated tailings (270.0 mm precipitation).

Month	R	NI	E	T	ET	Days	NI (mm)	q (mm/d)
July	0.0%	-10.3%	11.4%	0.0%	11.4%	31	-27.93	-0.901
August	0.0%	-8.8%	10.1%	0.0%	10.1%	62	-23.80	-0.768
September	0.0%	-18.5%	19.4%	0.0%	19.4%	92	-49.89	-1.663
October	0.0%	-18.3%	20.8%	0.0%	20.8%	123	-49.46	-1.596
November	0.0%	-18.3%	19.5%	5.3%	24.8%	153	-49.37	-1.646
December	3.0%	-17.9%	5.3%	24.2%	29.5%	184	-48.20	-1.555
January	1.6%	-14.3%	2.1%	36.9%	39.0%	215	-38.63	-1.246
February	1.0%	-4.0%	1.8%	27.1%	28.9%	243	-10.80	-0.386
March	1.9%	-23.5%	5.2%	31.0%	36.2%	274	-63.44	-2.047
April	0.1%	-24.3%	13.5%	13.6%	27.2%	304	-65.57	-2.186
May	0.0%	-12.5%	11.9%	2.3%	14.3%	335	-33.63	-1.085
June	0.0%	-11.7%	13.2%	0.0%	13.2%	365	-31.57	-1.052
YEAR	7.7%	-182.3%	134.2%	140.4%	274.6%	365	-492.31	-16.129

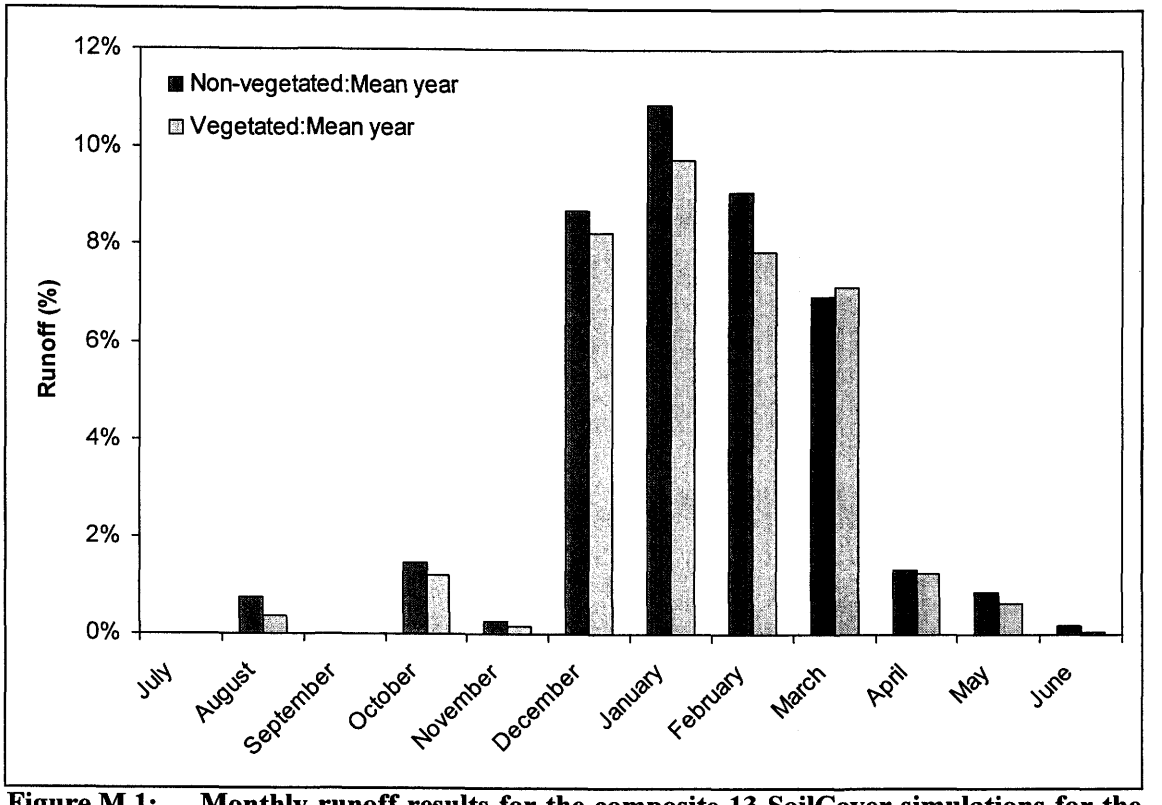

Figure M.1: Monthly runoff results for the composite 13 SoilCover simulations for the mean climatic year.

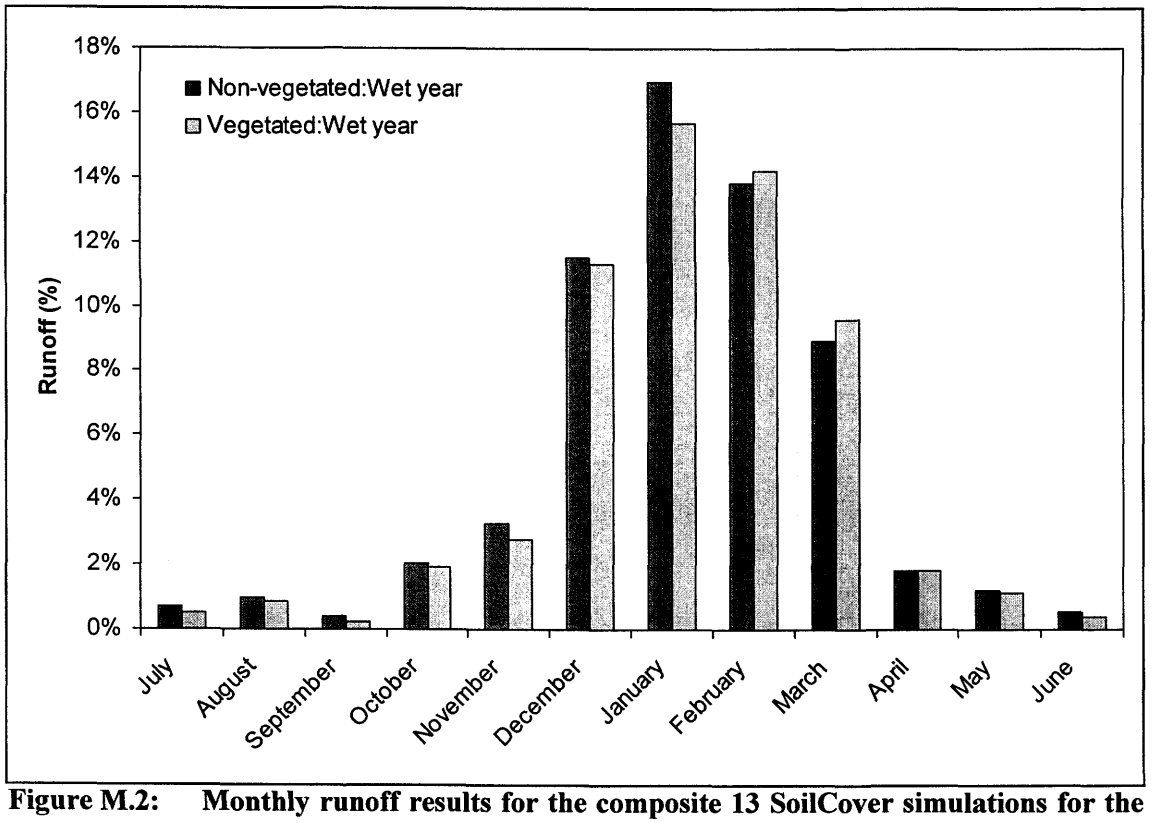

Figure M.2: Monthly runoff results for the composite 13 SoilCover simulations for the wet climatic year.

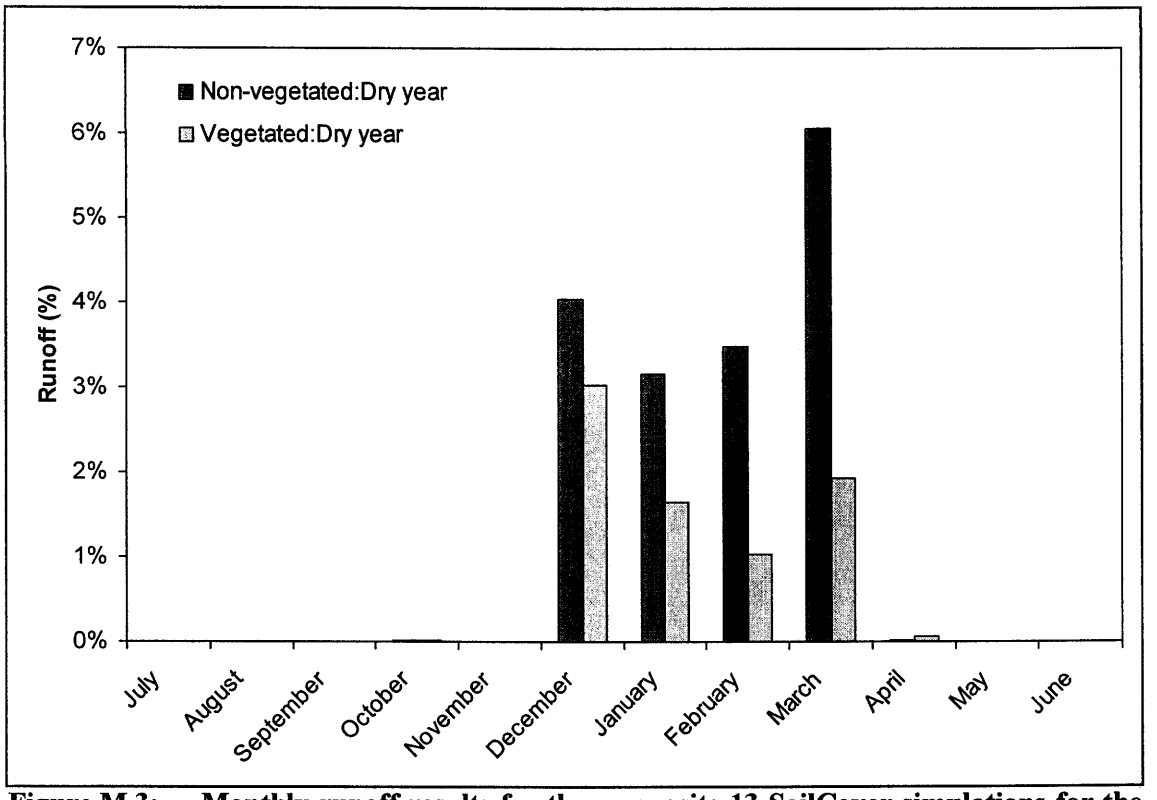

Figure M.3: Monthly runoff results for the composite 13 SoilCover simulations for the dry climatic year.

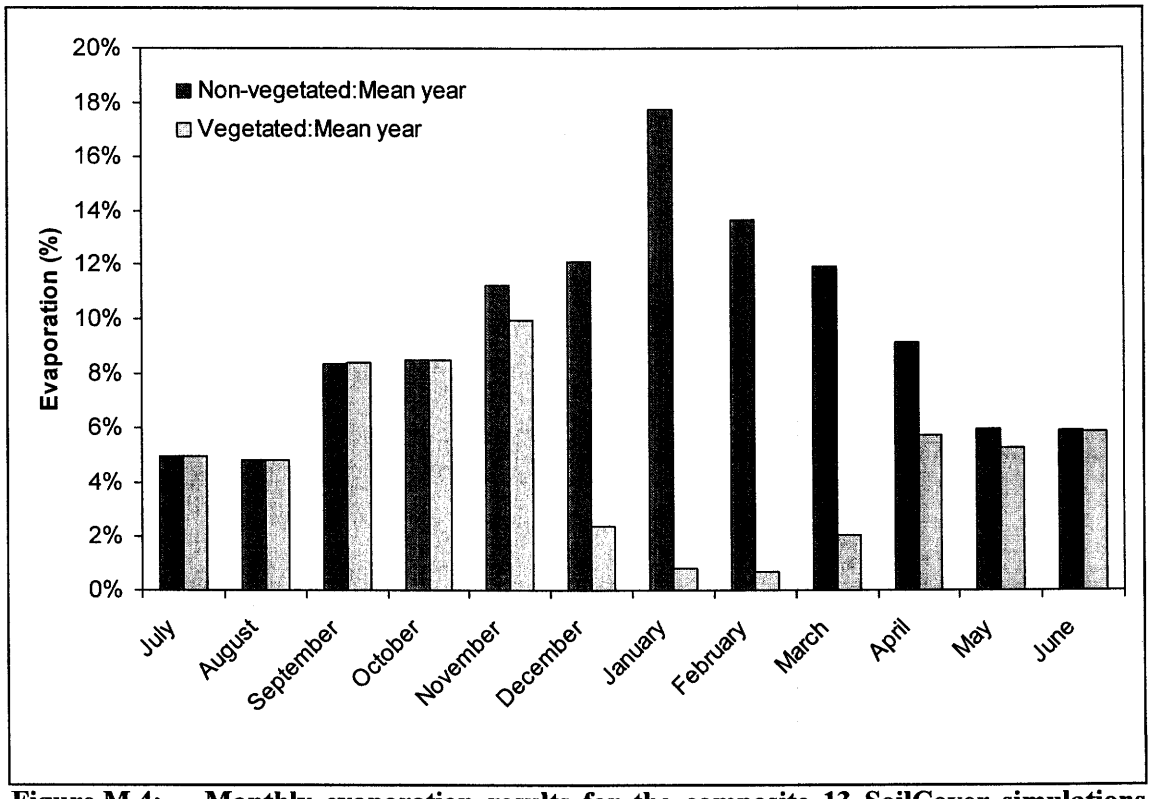

Figure M.4: Monthly evaporation results for the composite 13 SoilCover simulations for the mean climatic year.

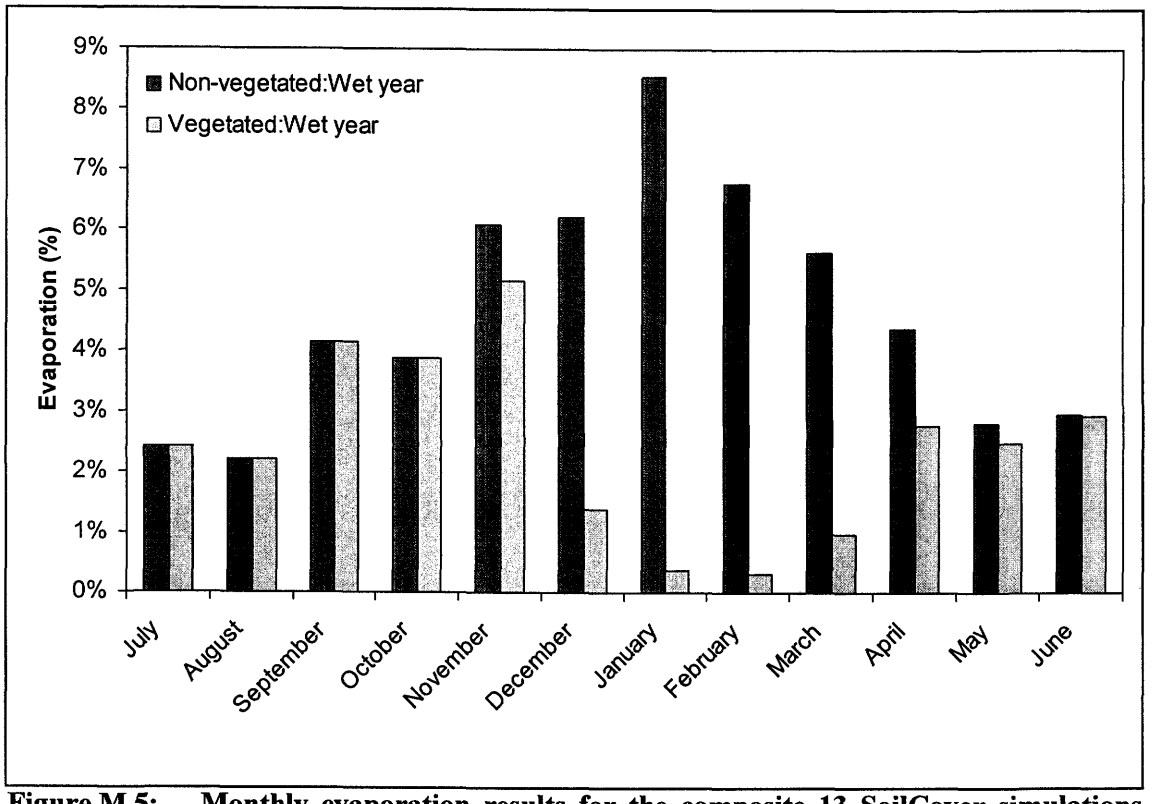

Figure M.5: Monthly evaporation results for the composite 13 SoilCover simulations for the wet climatic year.

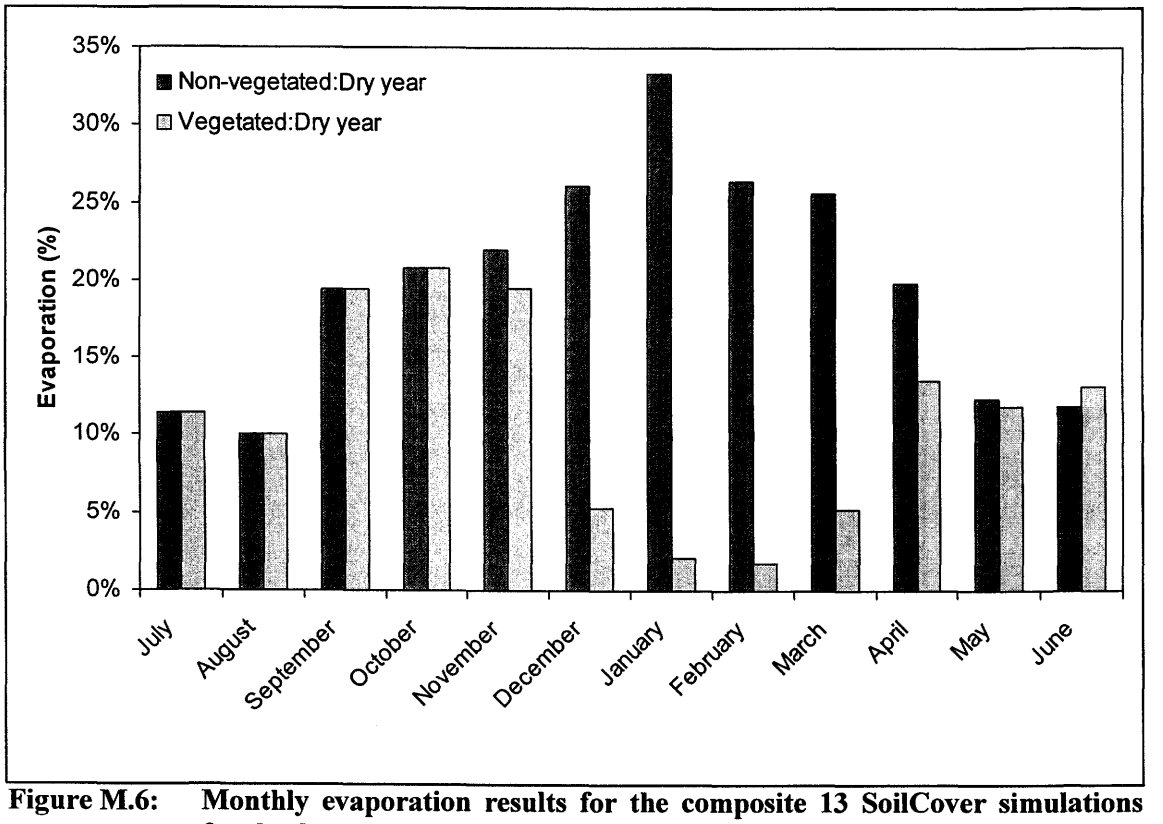

Figure M.6: Monthly evaporation results for the composite 13 SoilCover simulations for the dry climatic year.

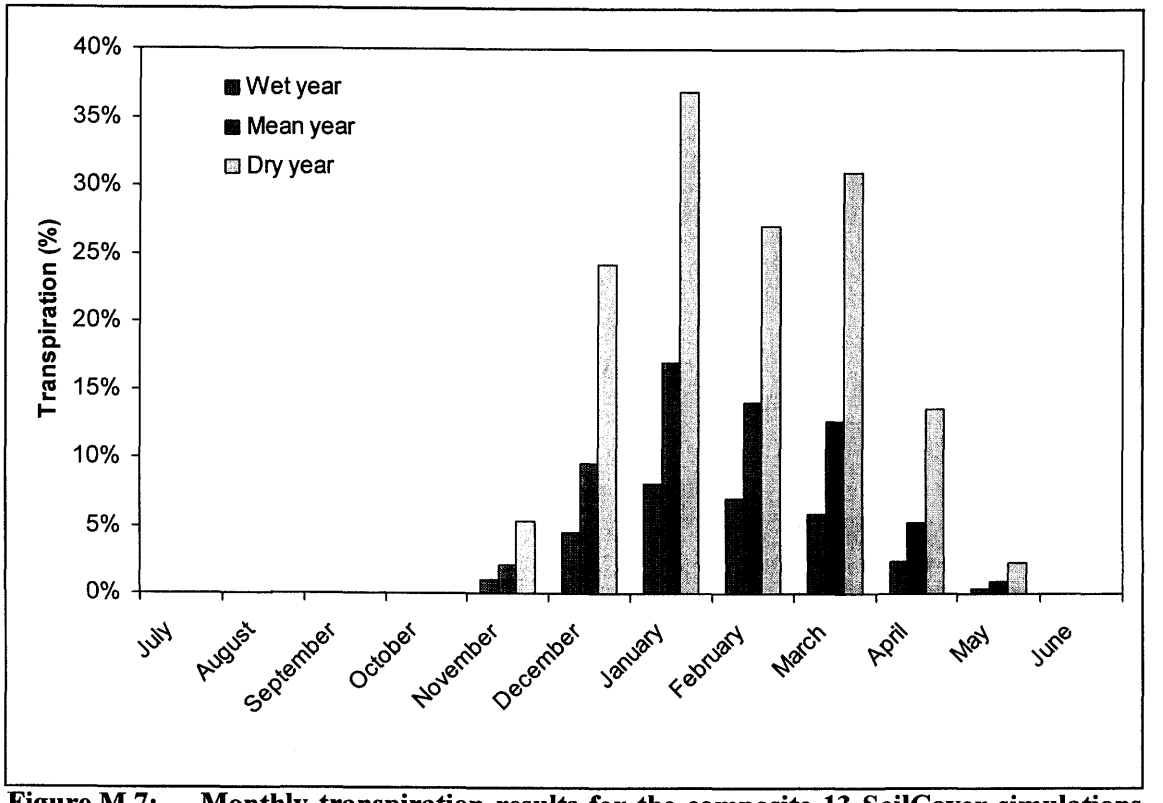

Figure M.7: Monthly transpiration results for the composite 13 SoilCover simulations for all climatic years.

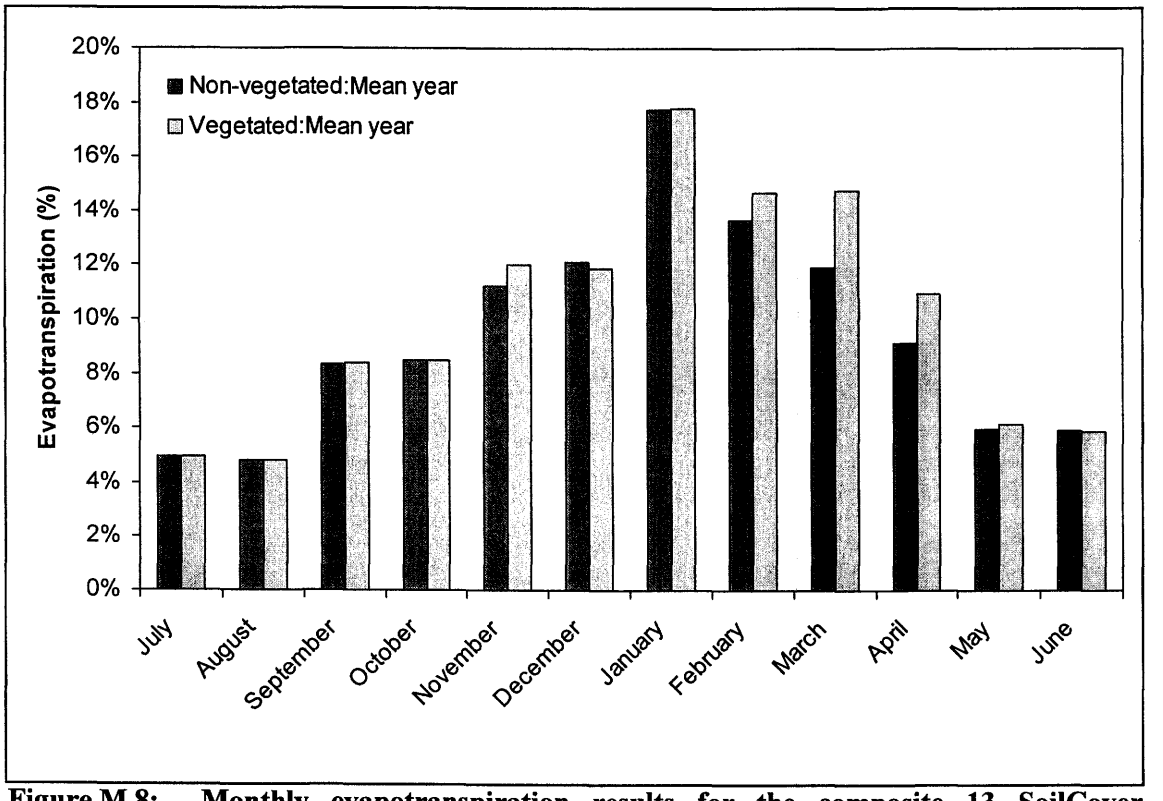

Figure M.8: Monthly evapotranspiration results for the composite 13 SoilCover simulations for mean climatic year.

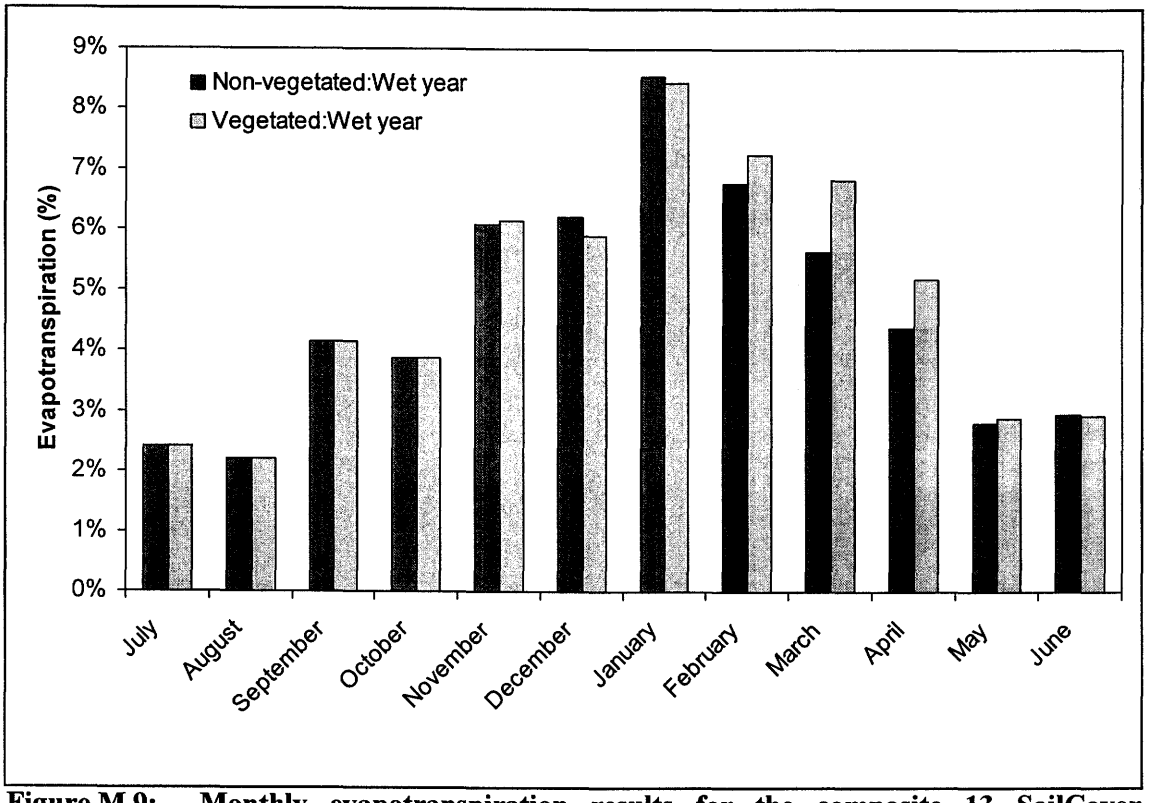

Figure M.9: Monthly evapotranspiration results for the composite 13 SoilCover simulations for wet climatic year.

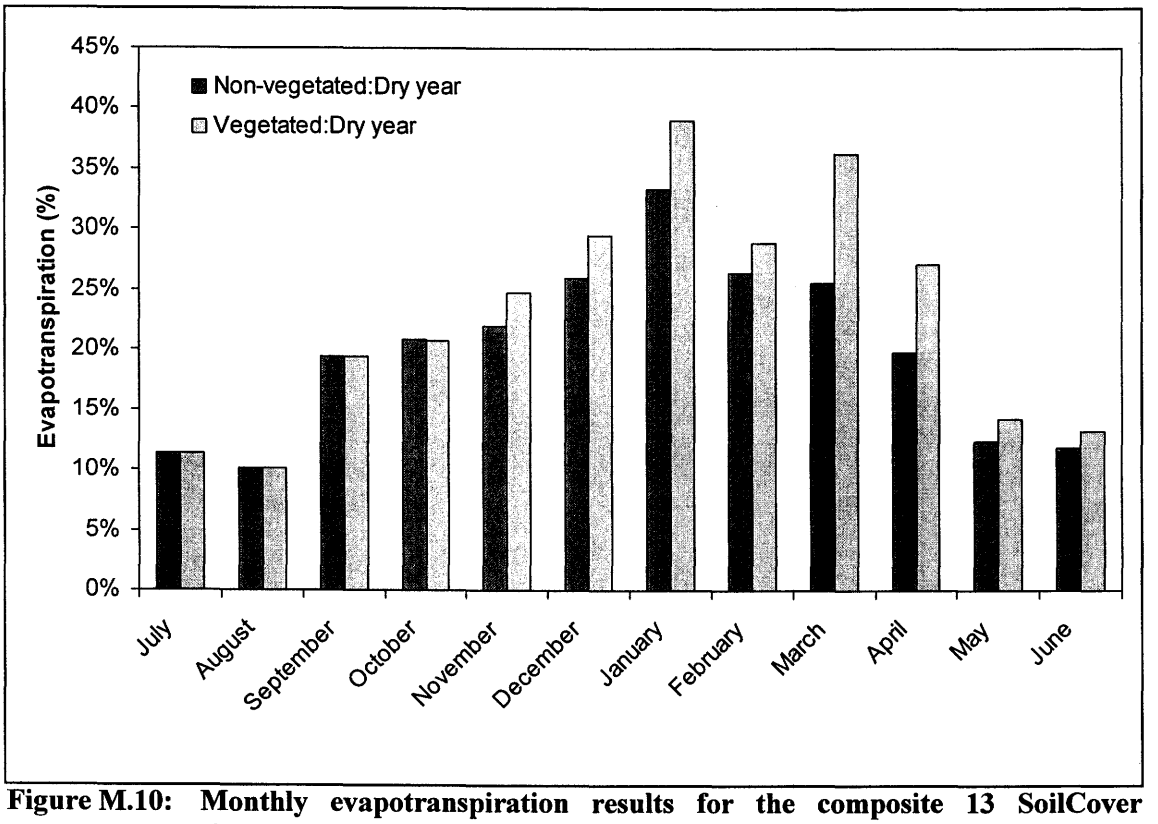

Figure M.10: Monthly evapotranspiration results for the composite 13 SoilCover simulations for dry climatic year.

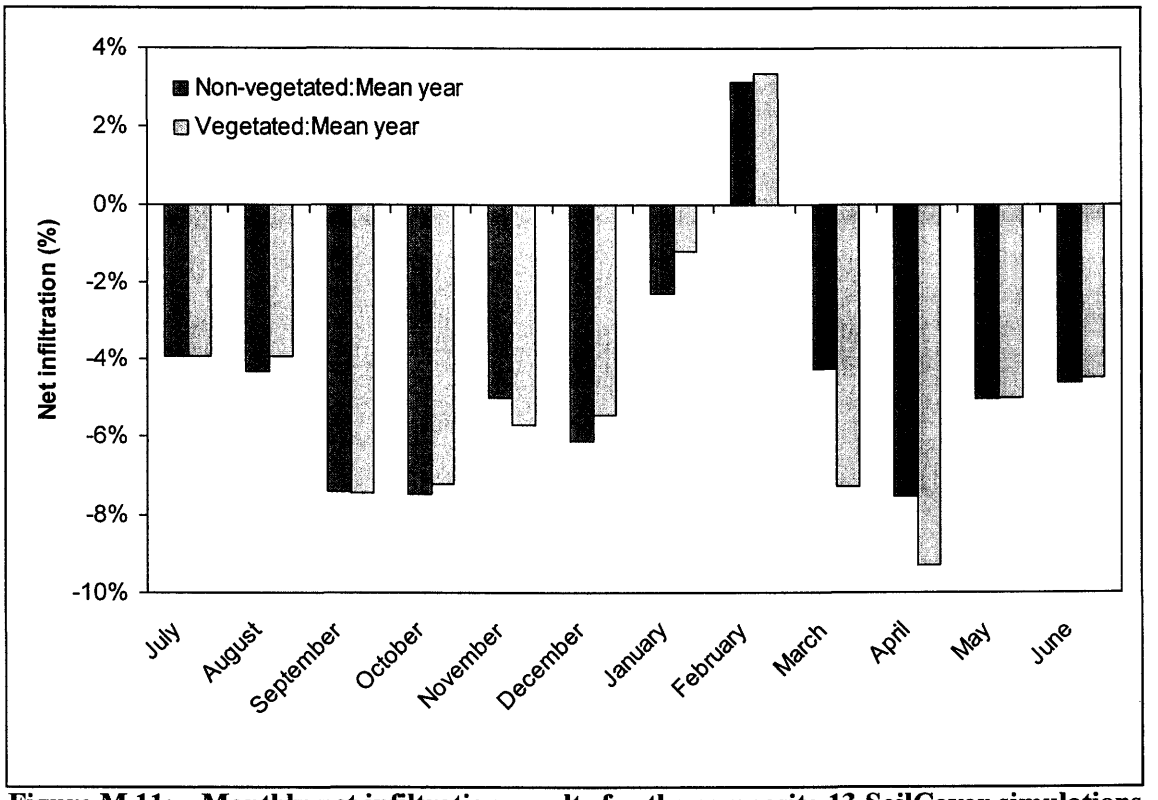

Figure M.11: Monthly net infiltration results for the composite 13 SoilCover simulations for the mean climatic year.

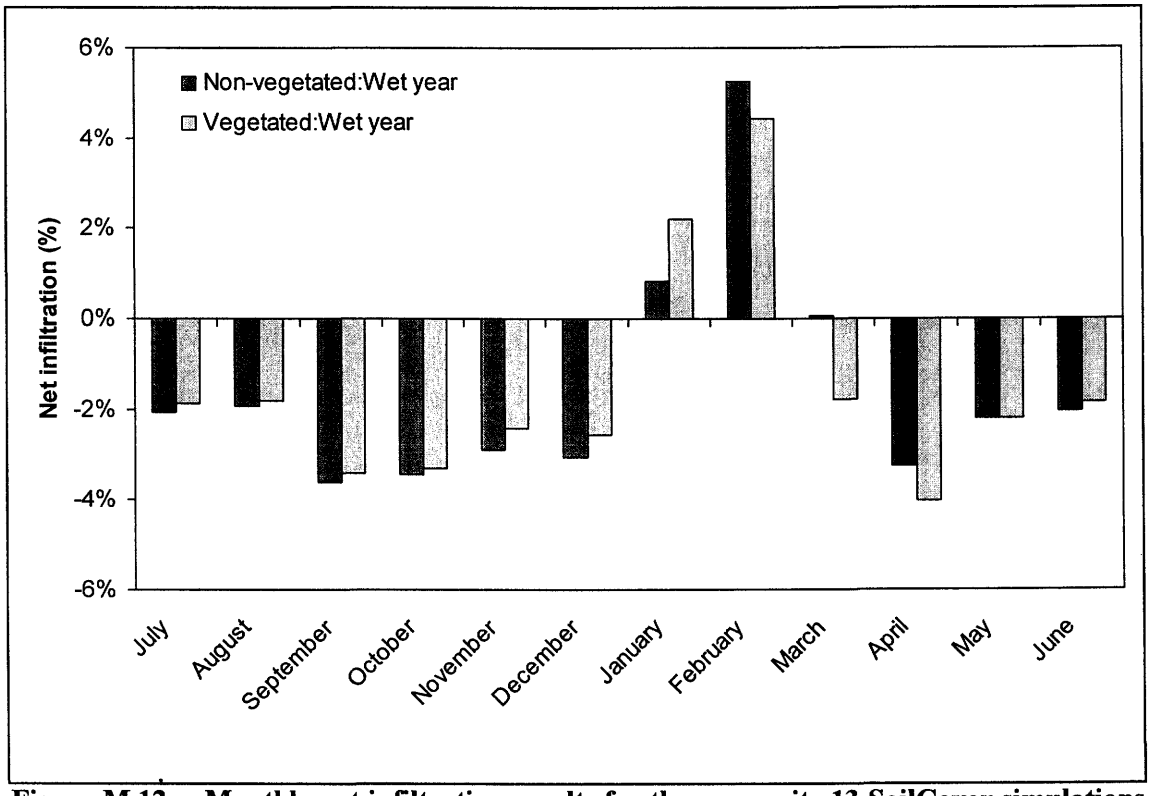

Figure M.12: Monthly net infiltration results for the composite 13 SoilCover simulations for the wet climatic year.

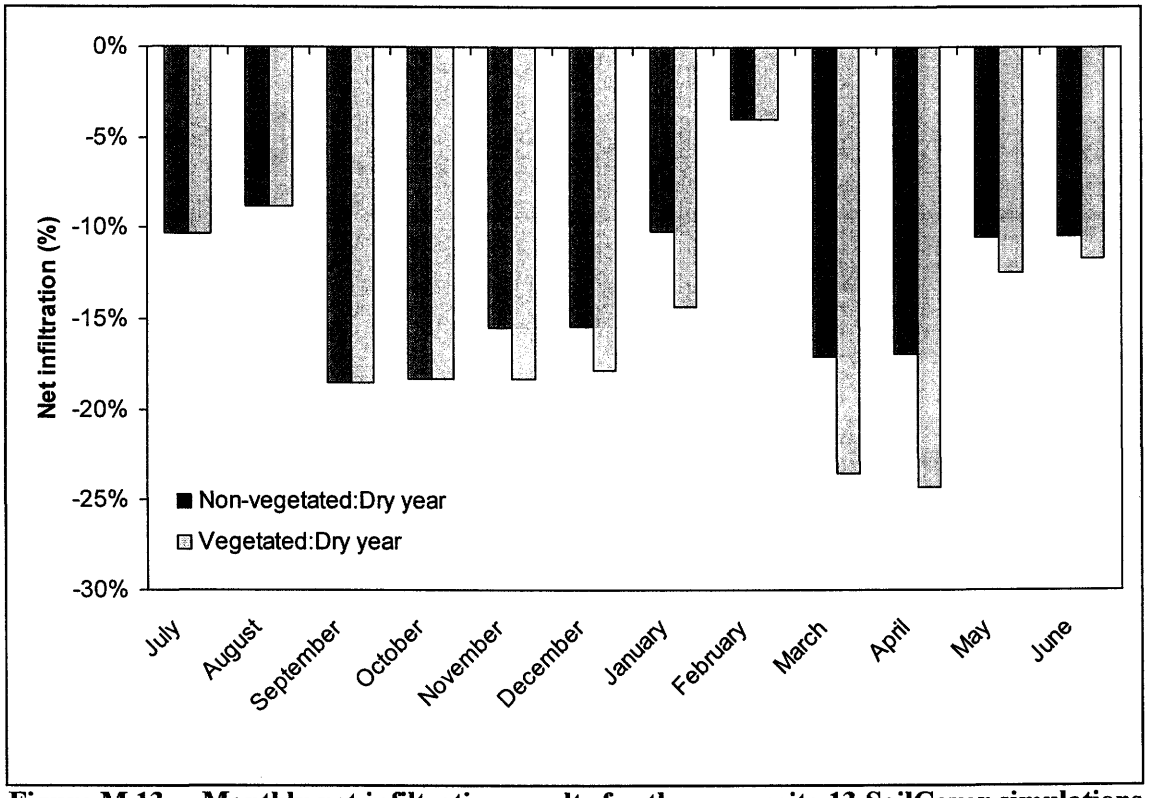

Figure M.13: Monthly net infiltration results for the composite 13 SoilCover simulations for the dry climatic year.

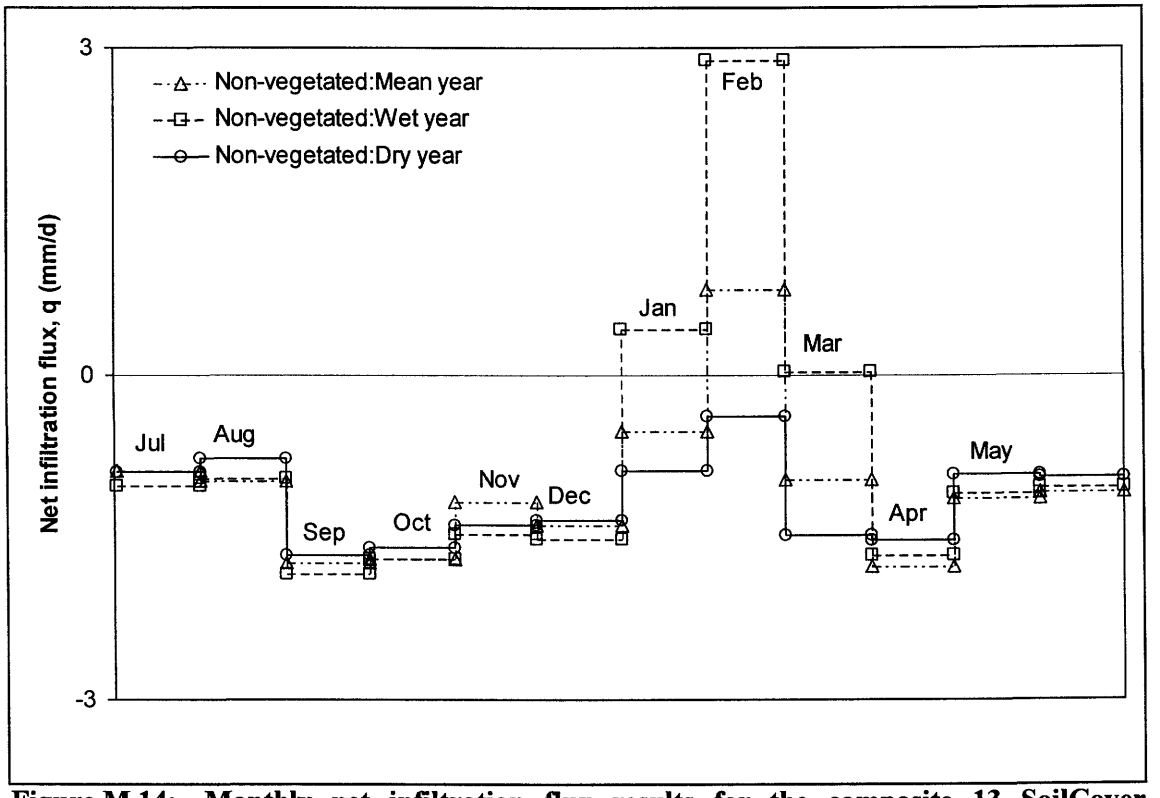

Figure M.14: Monthly net infiltration flux results for the composite 13 SoilCover simulations for all climatic years when no vegetation is present.

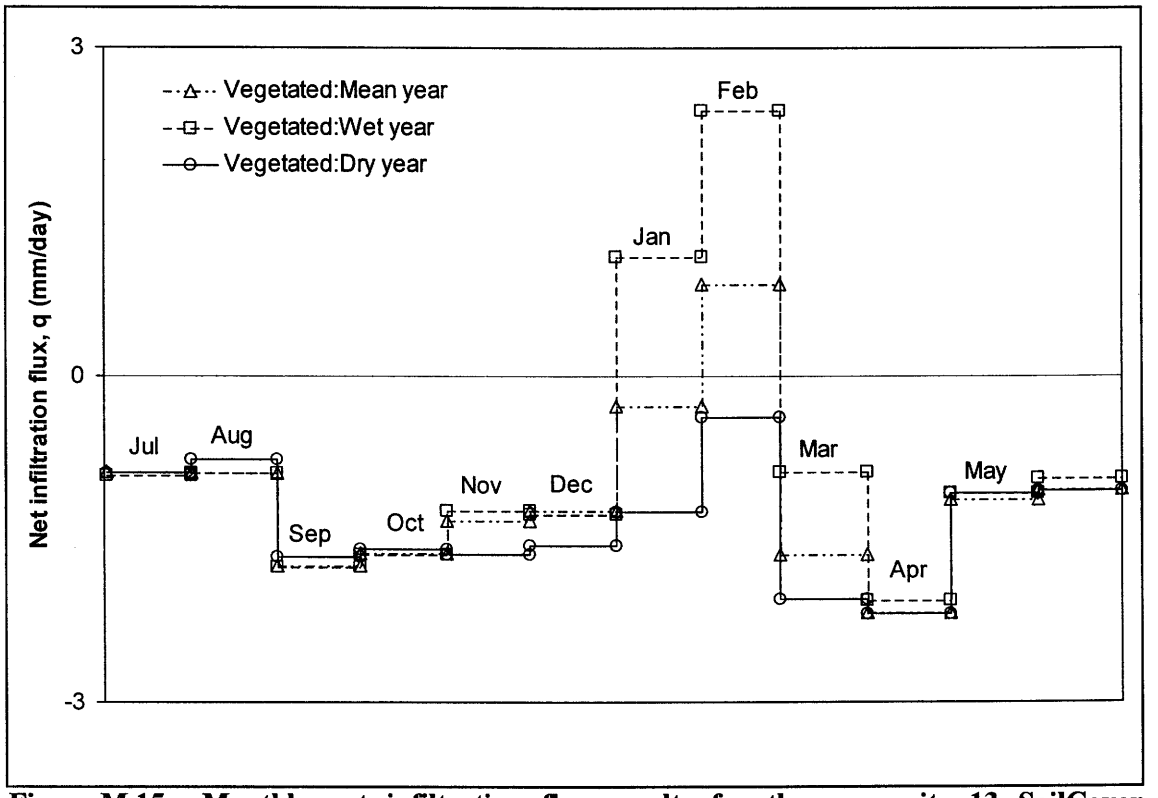

Figure M.15: Monthly net infiltration flux results for the composite 13 SoilCover simulations for all climatic years when vegetation is present.

M.6 Evaluation Data Set SoilCover Model Simulations

The SoilCover modeling results for the 4-month (December 2000 to March 2001) evaluation period are presented in the following tables. The complete overall 4-month period results are presented in Table M.35 and the monthly composite results are presented in Table M.36.

Table M.35: Results of the 4-month evaluation data set SoilCover modeling (469.0 mm precipitation).

Model no	NI (mm)	BF (mm)	R (mm)	PE (mm)	AE (mm)	PT (mm)	AT (mm)	PET (mm)	AET (mm)
K-VVC-01	141.3	143.9	94.5	583.4	144.5	368.3	88.7	951.7	233.3
K-VVC-02	98.8	142.6	144.6	583.2	149.6	368.2	76.1	951.4	225.7
K-VVC-03	9.0	143.8	272.2	583.1	140.1	368.2	47.8	951.3	187.8
K-VVC-04	17.2	79.0	303.5	583.3	125.6	368.3	22.7	951.6	148.3
K-VVC-05	-0.5	79.1	337.4	583.3	120.7	368.3	11.3	951.6	132.1
K-VVI-06	23.6	217.1	150.0	583.3	153.8	368.2	141.7	951.5	295.4
K-VVI-07	-5.2	144.0	308.5	583.2	128.9	368.2	36.8	951.4	165.7
K-VVI-08	2.4	145.5	317.8	583.2	131.4	368.2	17.4	951.4	148.8

Table M.35: Results of the 4-month evaluation data set SoilCover modeling (469.0 mm precipitation).

Model no	NI (mm)	BF (mm)	R (mm)	PE (mm)	AE (mm)	PT (mm)	AT (mm)	PET (mm)	AET (mm)
K-VVI-09	0.2	109.1	251.9	583.4	157.3	368.3	59.5	951.7	216.8
K-VVI-10	-70.6	115.0	265.8	583.3	152.9	368.3	120.9	951.6	273.8
K-VVFr11	-403.5	462.0	209.3	583.1	295.0	368.3	368.3	951.4	663.3
K-VVFr12	-492.7	513.2	266.7	583.4	326.5	368.5	368.5	951.9	695.0
K-VVF-13	-533.2	535.4	308.7	582.1	325.9	367.6	367.6	949.7	693.5

Table M.36: Results of the monthly SoilCover results for the 4-month evaluation data set (469.0 mm precipitation).

Month	R		NI		E		T		ET		Days	q
	(mm)	(%)	(mm)	(%)	(mm)	(%)	(mm)	(%)	(mm)	(%)		(mm/d)
Dec	117.7	25.1	6.3	1.3	49.6	10.6	33.1	7.1	82.7	17.6	31	0.202
Jan	31.2	6.7	-73.8	-15.7	40.8	8.7	54.8	11.7	95.6	20.4	62	-2.379
Feb	102.0	21.8	-10.8	-2.3	42.9	9.2	30.0	6.4	72.9	15.6	90	-0.385
Mar	5.9	1.2	-50.9	-10.9	64.5	13.8	25.7	5.5	90.3	19.2	121	-1.643
SUM	256.8	54.7	-129.2	-27.5	197.8	42.2	143.6	30.6	341.4	72.8	121	-4.205

This page was intentionally left blank.

APPENDIX N

Additional Flux Boundary Functions

N.1 Introduction

The flux boundary functions for all the cases modeled for this thesis, and not documented in Chapter 9 and 10 are presented here. These data were too voluminous to include in the main body of the thesis, but had to be documented for reference purposes.

N.2 Annual Flux Boundary Functions

Tables N.1 to N.20 contain the annualized flux boundary functions for runoff, evapotranspiration and net infiltration, for the five cases not documented in Chapter 9. These are; (1) vegetated, mean climatic year, (2) non-vegetated, wet climatic year, (3) vegetated, wet climatic year, (4) non-vegetated, dry climatic year, and (5) vegetated, dry climatic year. For each case, a composite graph depicting the evapotranspiration and net infiltration flux is presented, which allows for direct comparison with the spatial flux hypothesis illustrated in Chapter 1.

N.3 Monthly Flux Boundary Functions

Tables N.21 to N.45 contain the monthly flux boundary functions for runoff, evapotranspiration and net infiltration, for the five cases not documented in Chapter 9. These are; (1) vegetated, mean climatic year, (2) non-vegetated, wet climatic year, (3) vegetated, wet climatic year, (4) non-vegetated, dry climatic year, and (5) vegetated, dry climatic year. For each case the net infiltration fluxes for each zone is also illustrated. These monthly zonal net infiltration fluxes can be used as a direct input in multidimensional saturated/unsaturated seepage and flow modeling packages. For all the monthly data presented in this appendix only the composite tailings cross-section results have been used, since presenting the data for each individual tailings type as well would mean and additional 75 graphs.

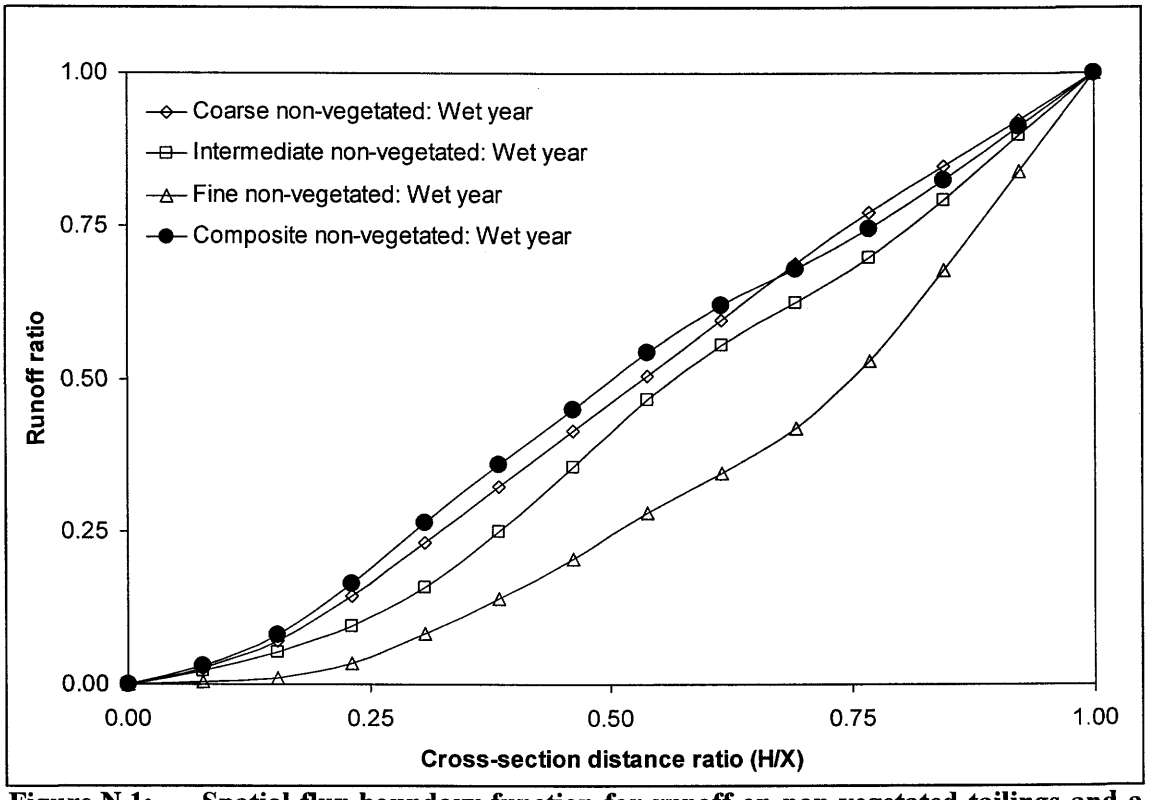

Figure N.1: Spatial flux boundary function for runoff on non-vegetated tailings and a wet climatic year.

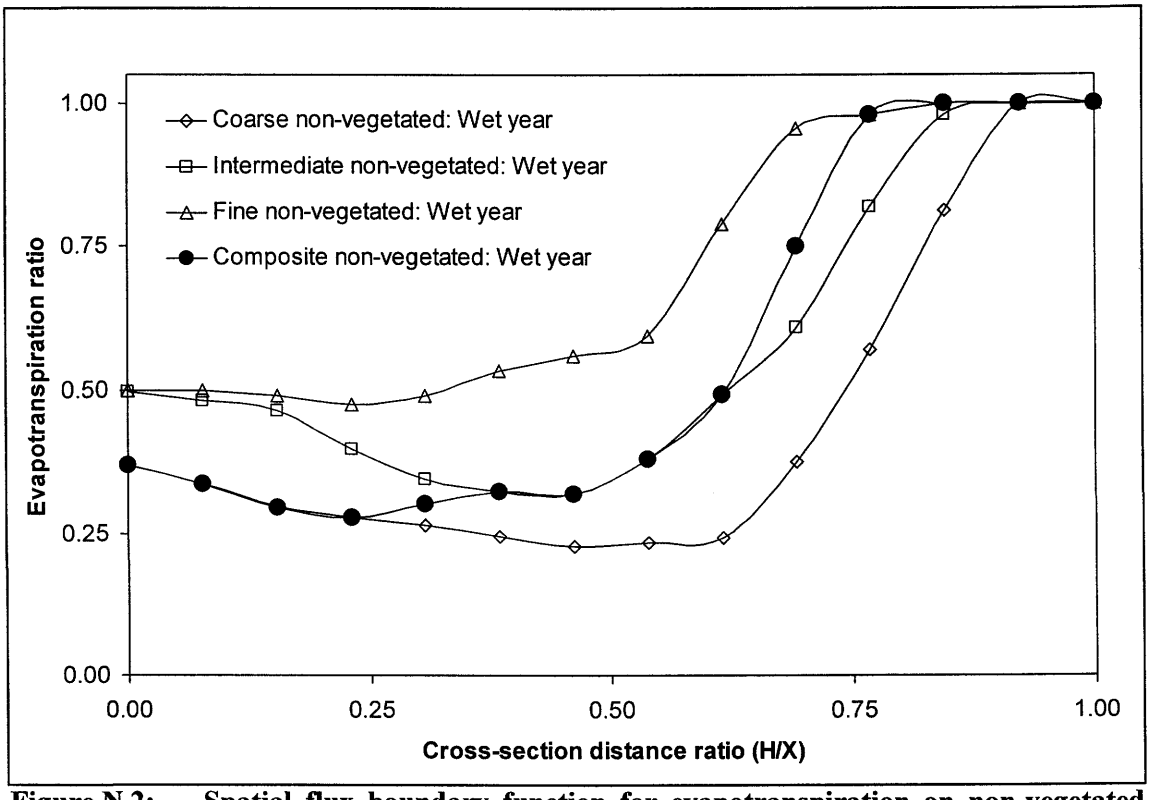

Figure N.2: Spatial flux boundary function for evapotranspiration on non-vegetated tailings for a wet year.

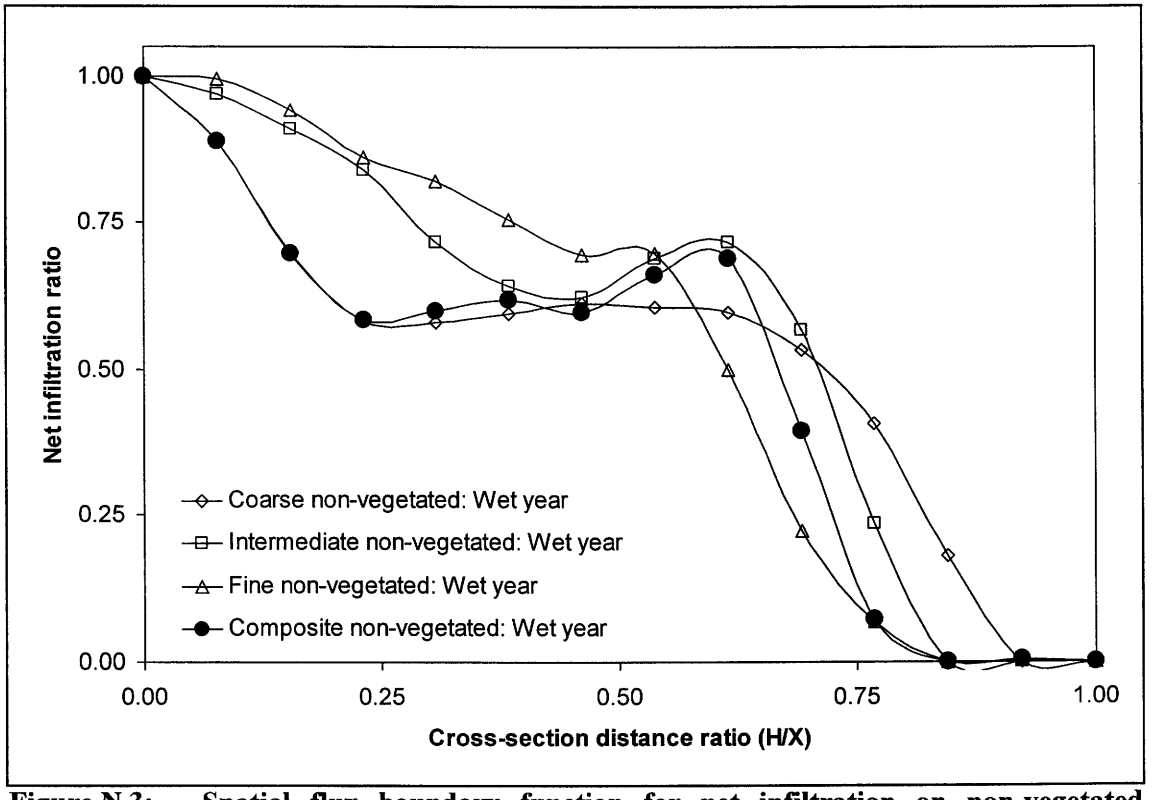

Figure N.3: **Spatial flux boundary function for net infiltration on non-vegetated tailings for a wet climatic year.**

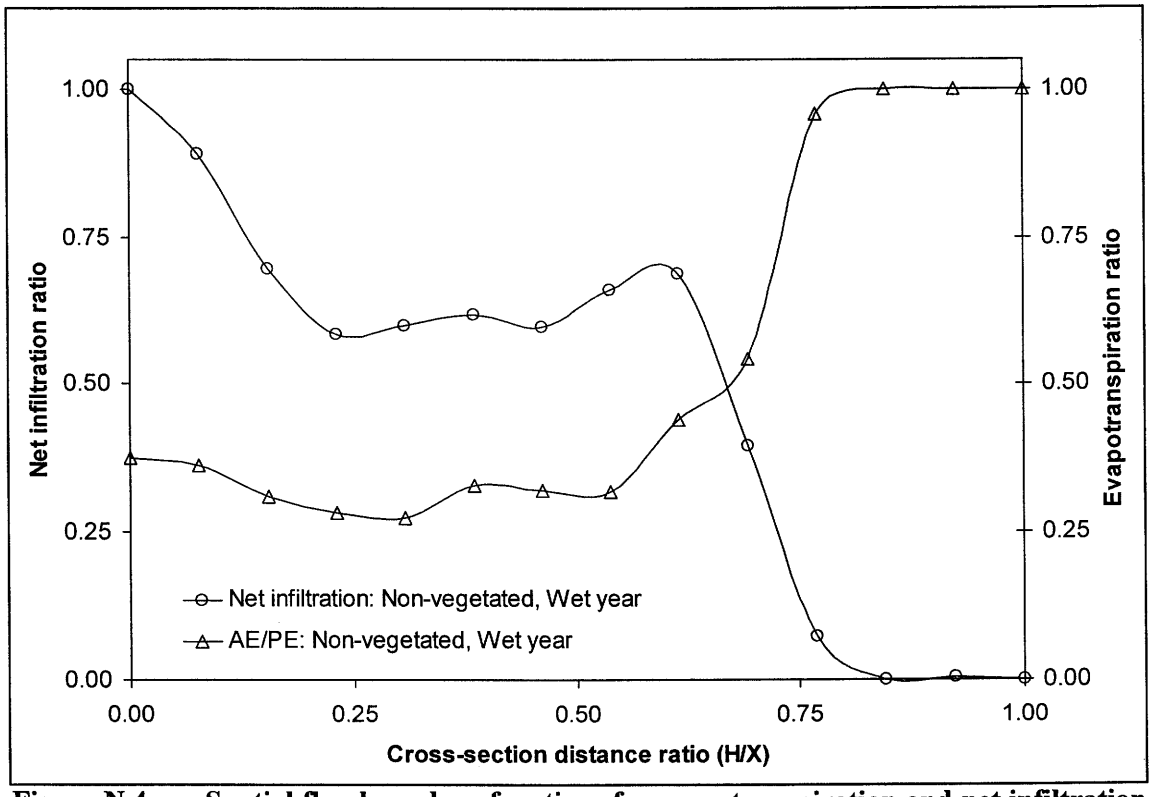

Figure N.4: **Spatial flux boundary functions for evapotranspiration and net infiltration on non-vegetated tailings during a wet climatic year.**

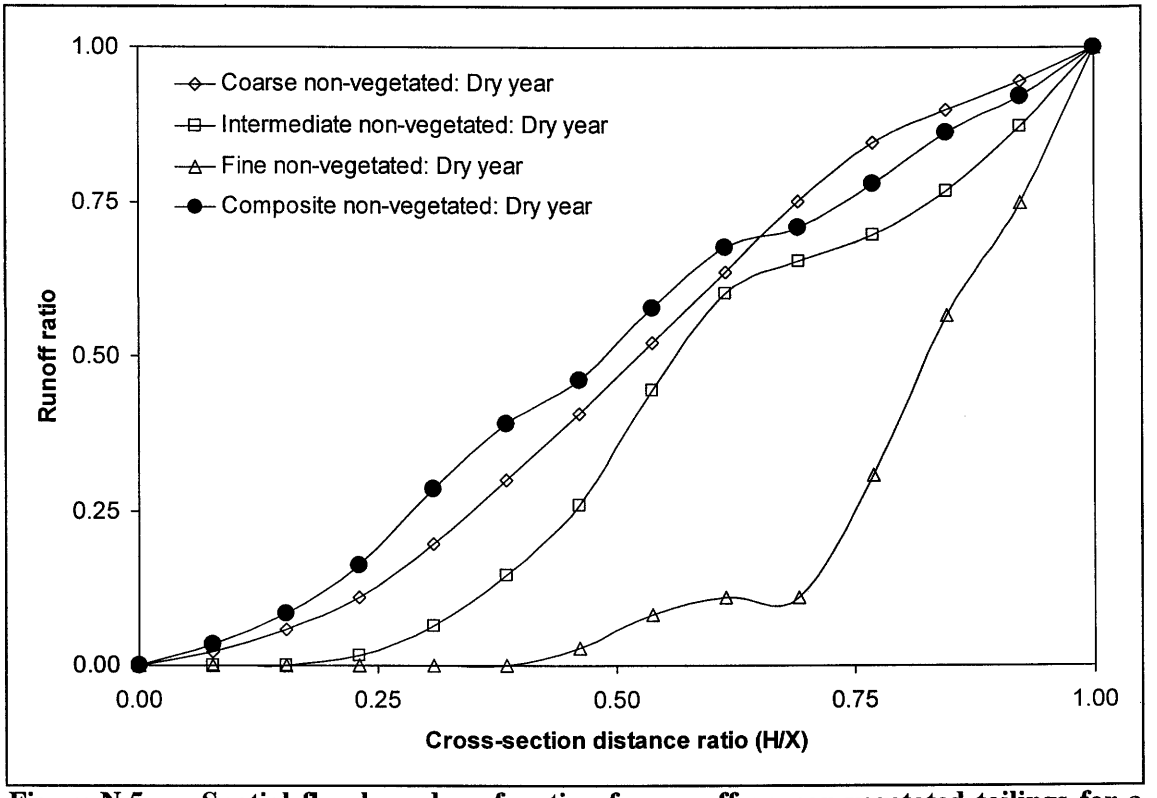

Figure N.5: **Spatial flux boundary function for runoff on non-vegetated tailings for a dry climatic year.**

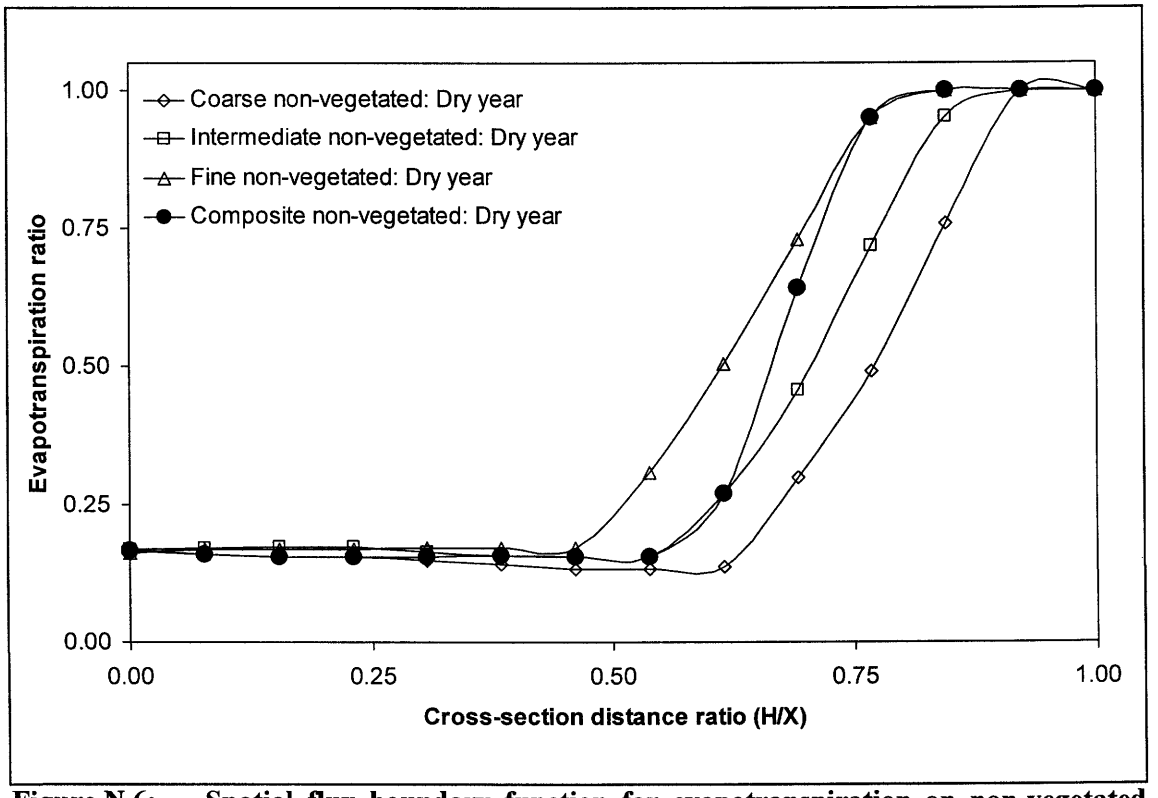

Figure N.6: **Spatial flux boundary function for evapotranspiration on non-vegetated tailings for a dry climatic year.**

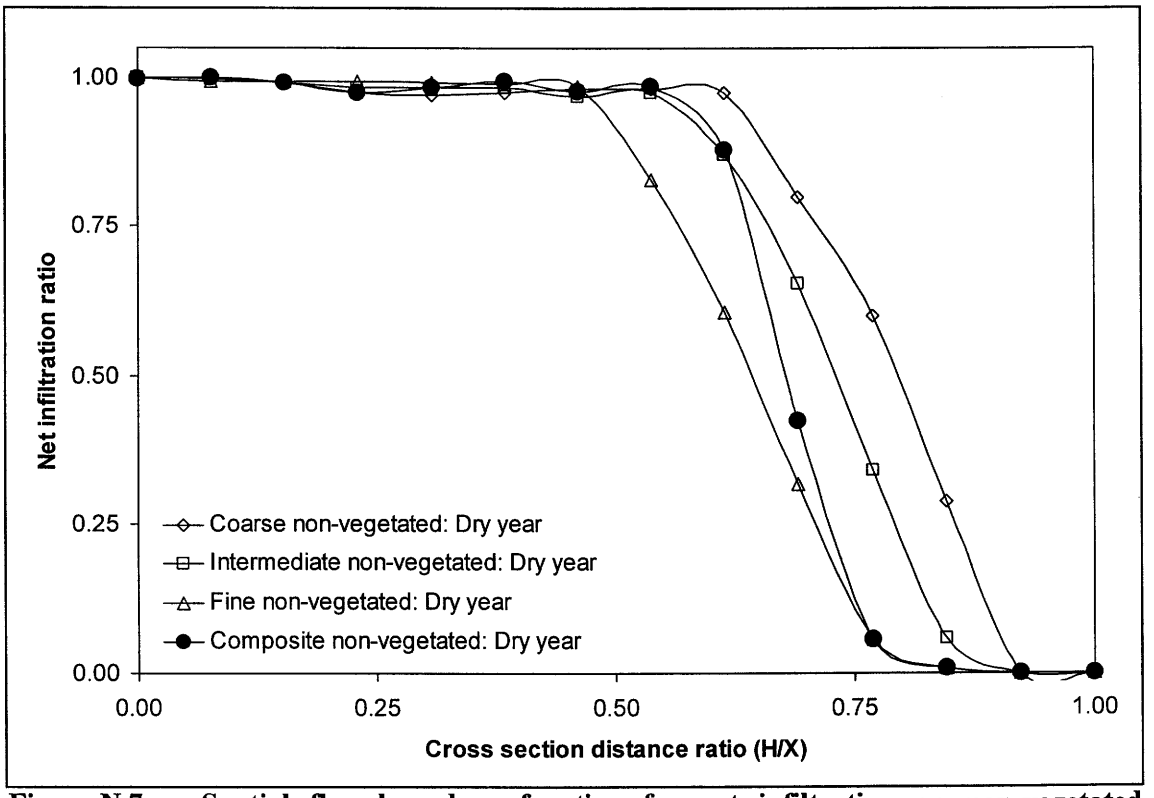

Figure N.7: **Spatial flux boundary function for net infiltration on non-vegetated tailings for a dry climatic year.**

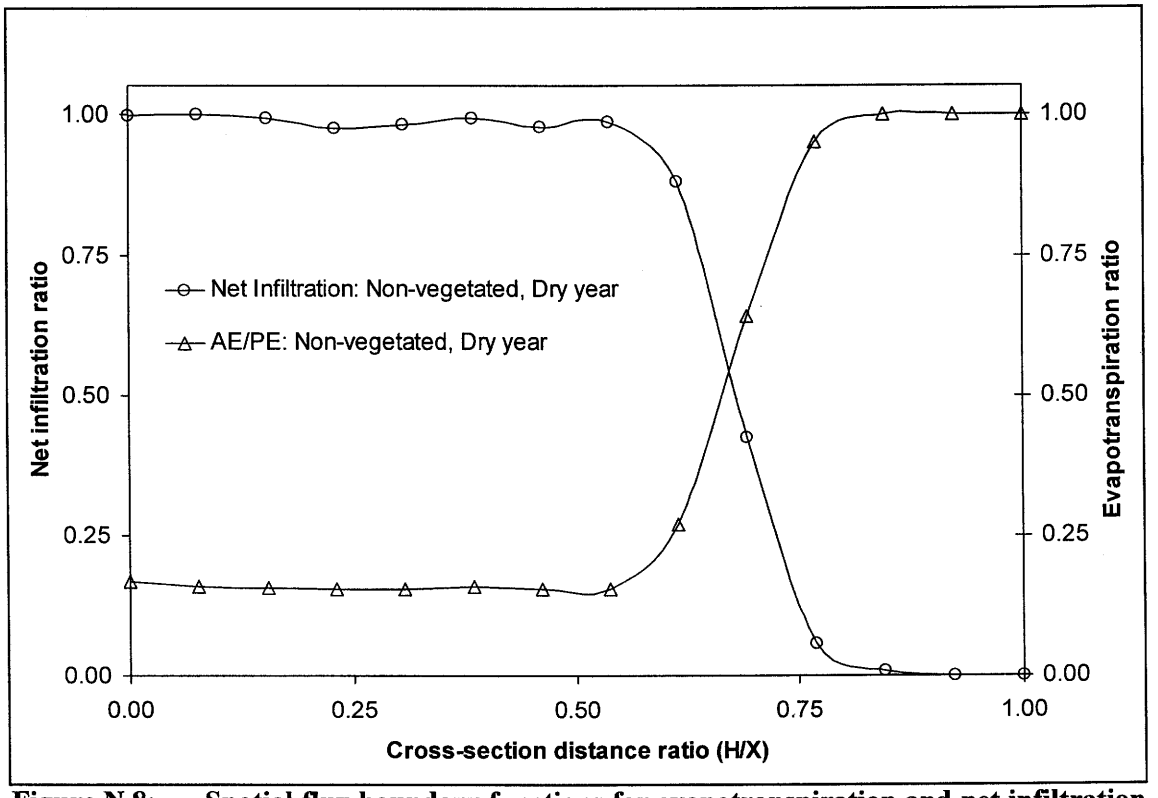

Figure N.8: **Spatial flux boundary functions for evapotranspiration and net infiltration on non-vegetated tailings for a dry climatic year.**

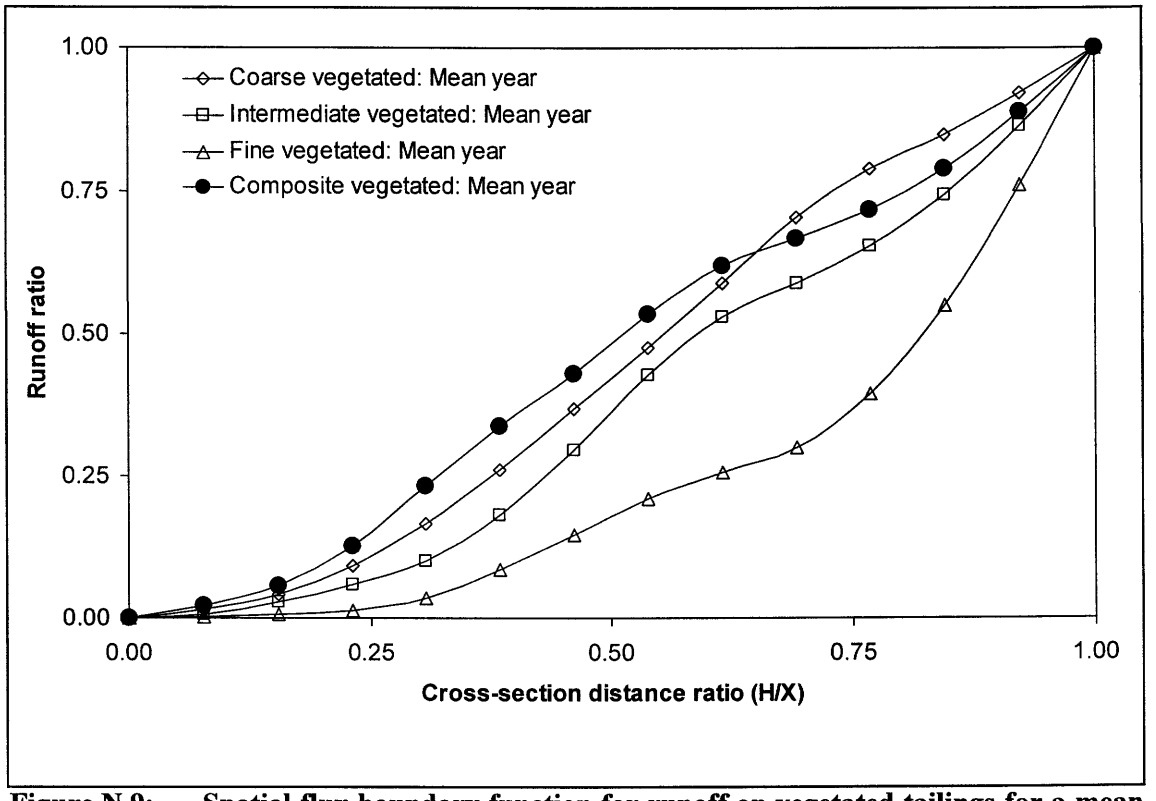

Figure N.9: **Spatial flux boundary function for runoff on vegetated tailings for a mean climatic year.**

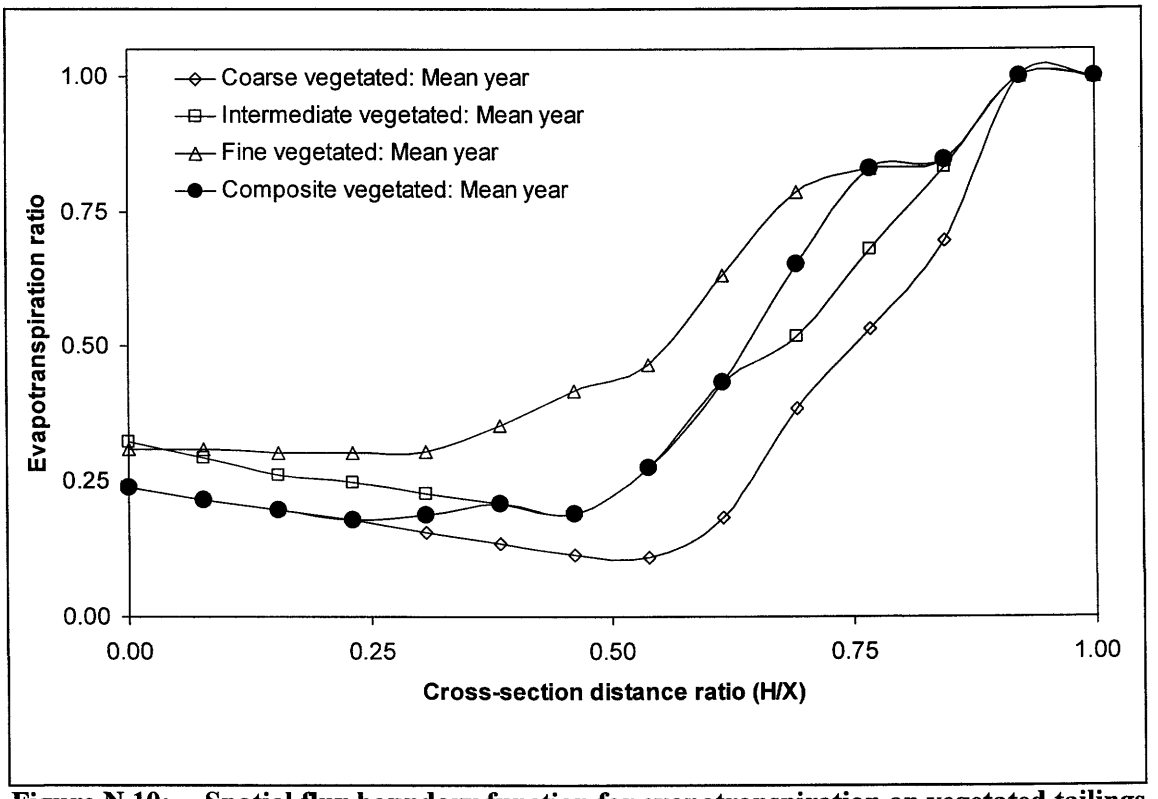

Figure N.10: **Spatial flux boundary function for evapotranspiration on vegetated tailings for a mean climatic year.**

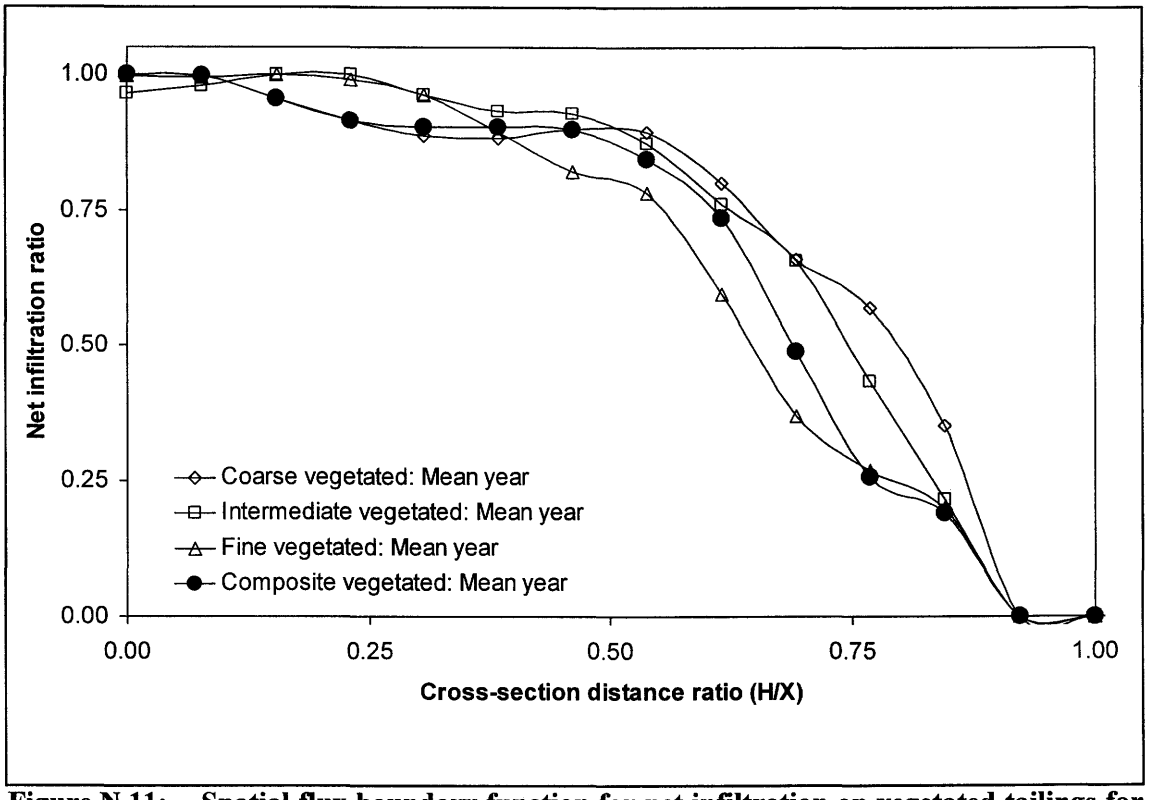

Figure N.11: Spatial flux boundary function for net infiltration on vegetated tailings for a mean climatic year.

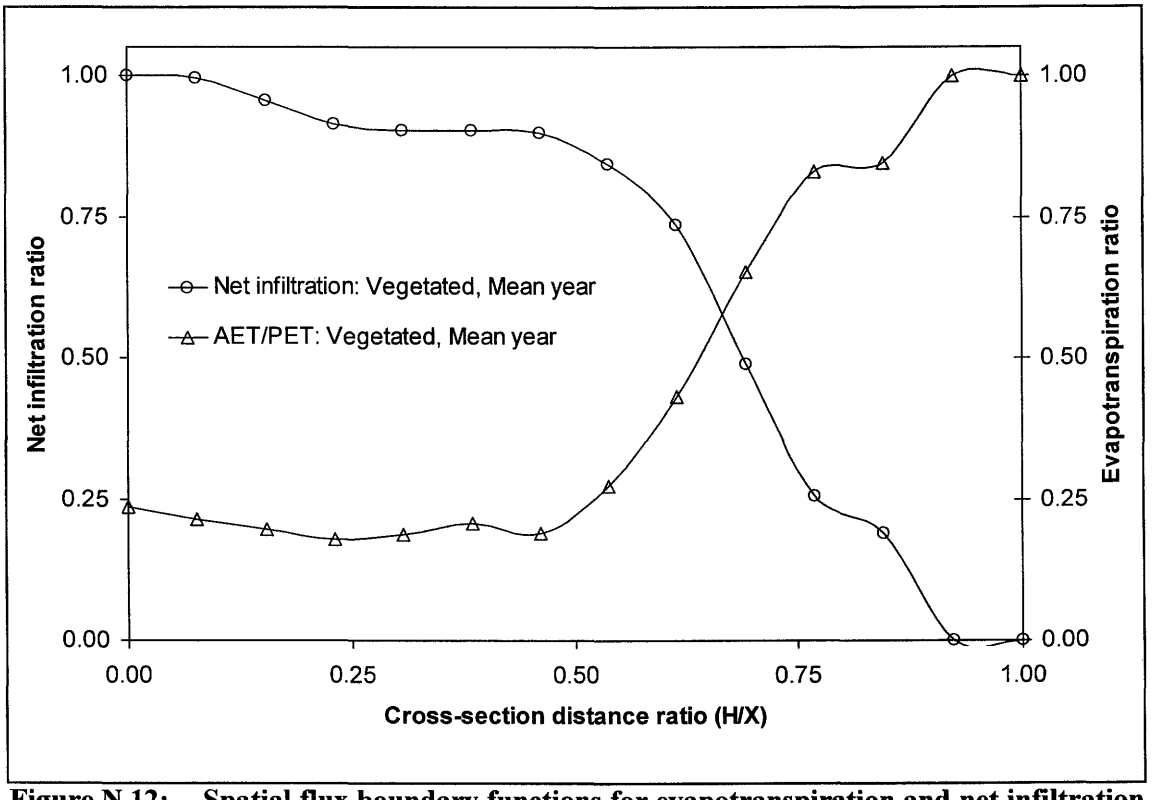

Figure N.12: Spatial flux boundary functions for evapotranspiration and net infiltration on vegetated tailings for a mean climatic year.

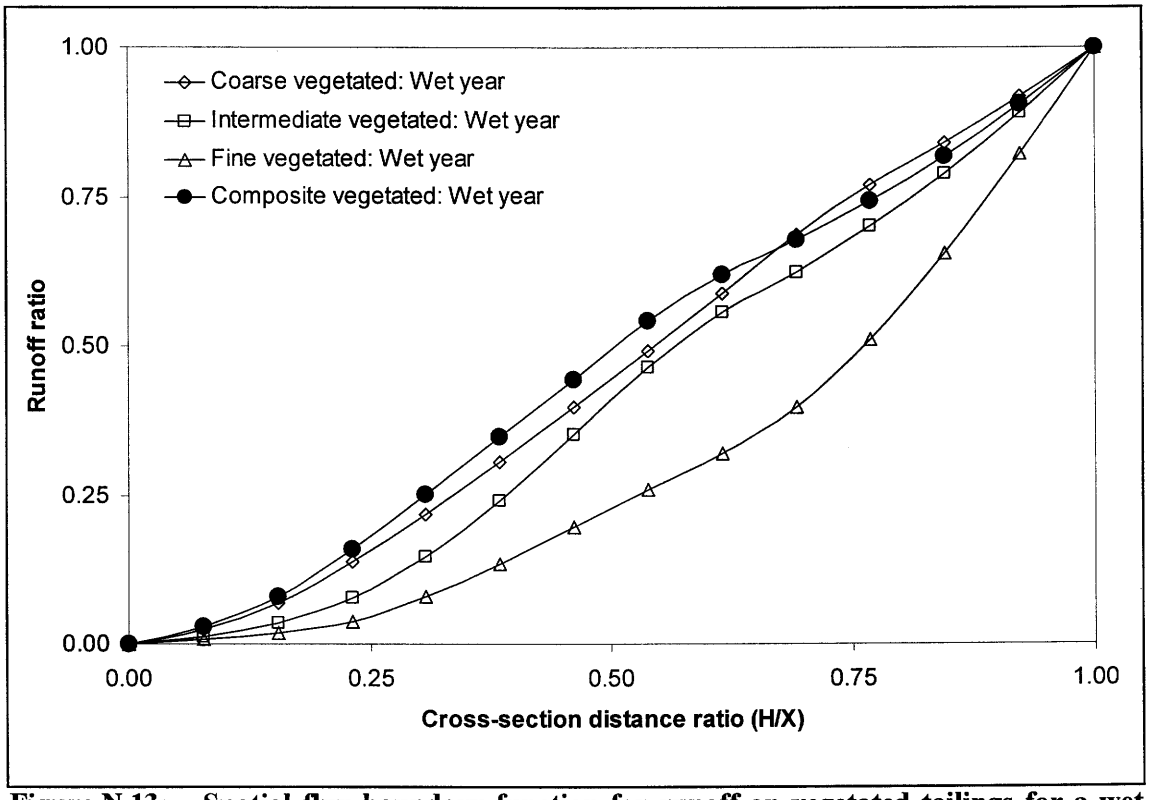

Figure N.13: Spatial flux boundary function for runoff on vegetated tailings for a wet climatic year.

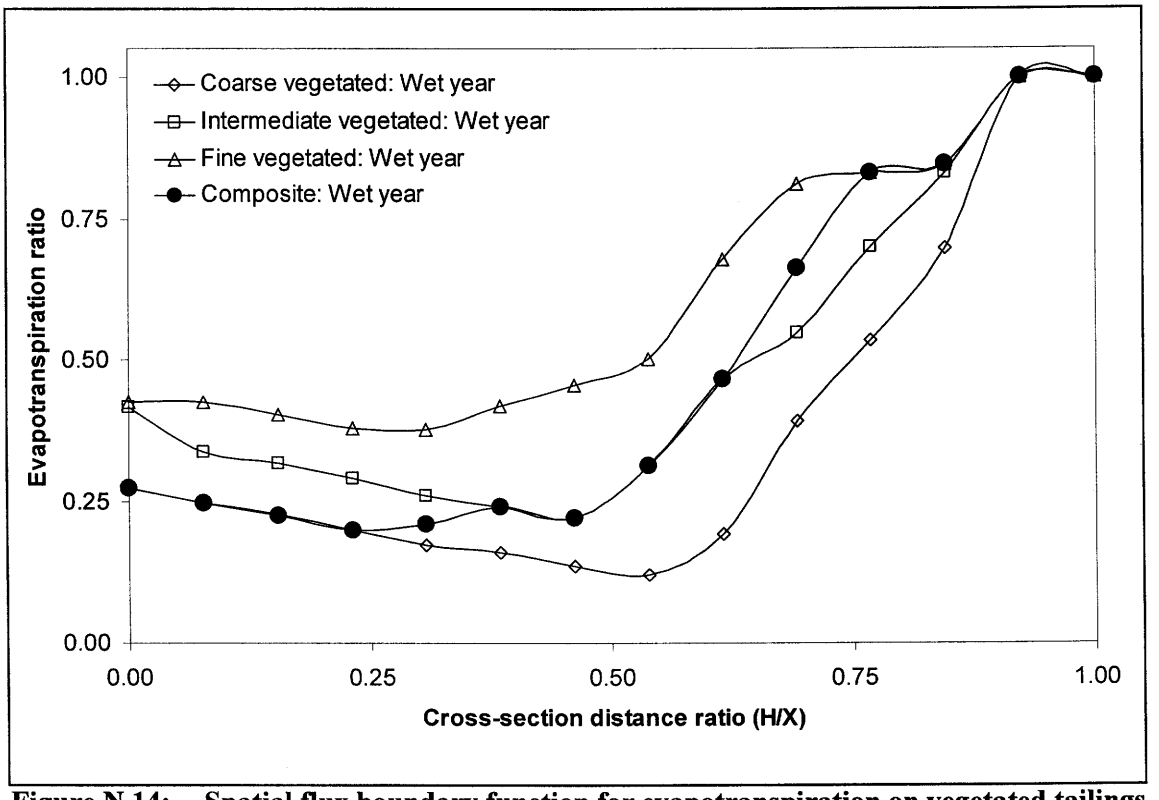

Figure N.14: Spatial flux boundary function for evapotranspiration on vegetated tailings for a wet climatic year.

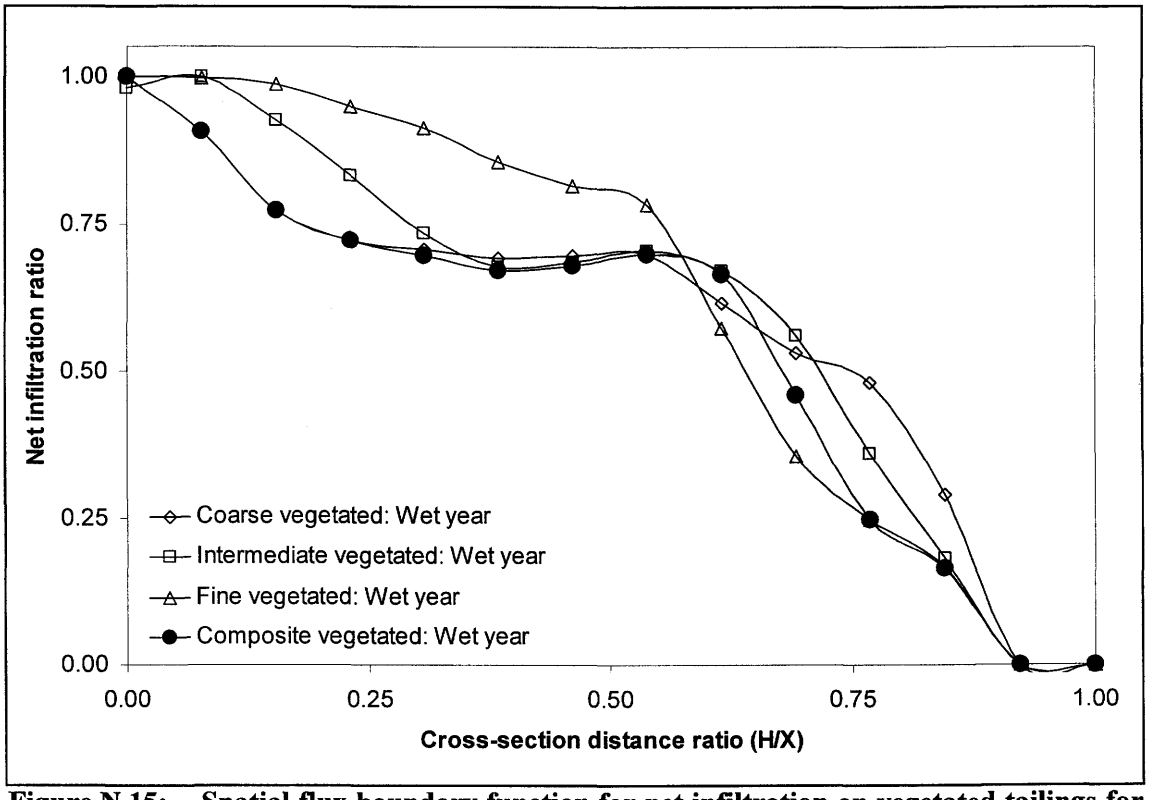

Figure N.15: Spatial flux boundary function for net infiltration on vegetated tailings for a wet climatic year.

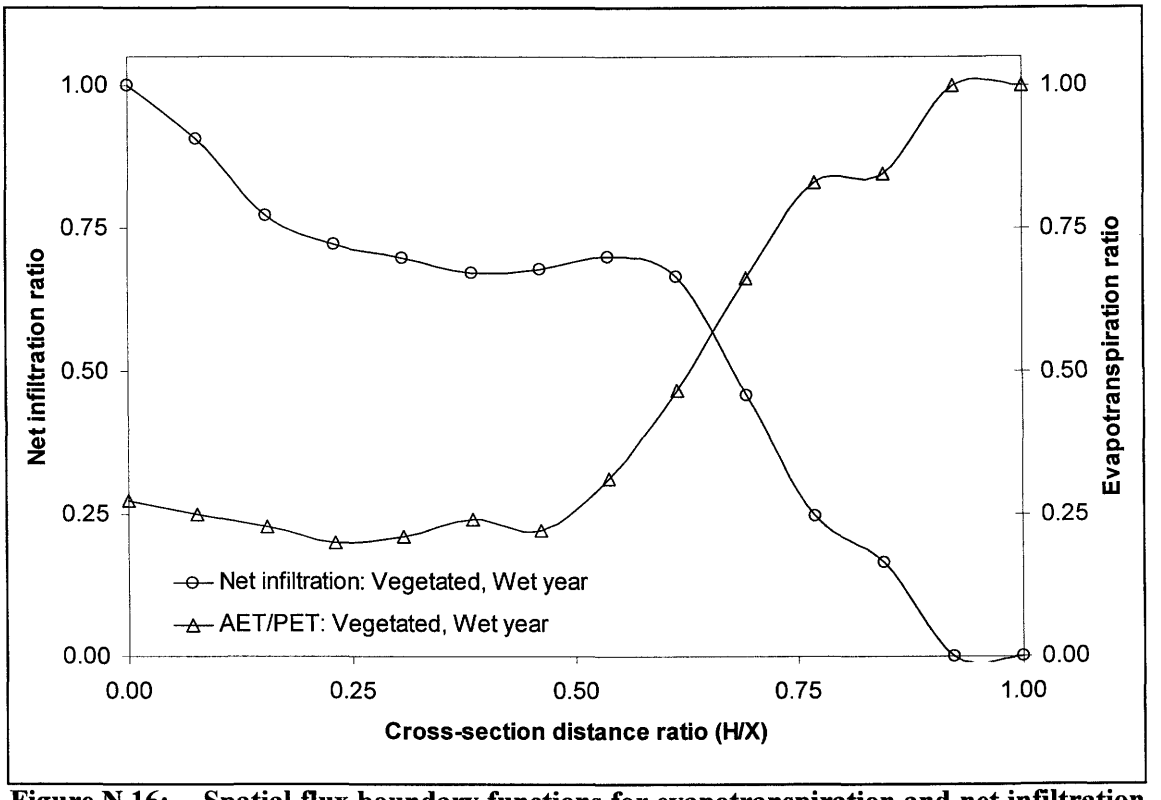

Figure N.16: Spatial flux boundary functions for evapotranspiration and net infiltration on vegetated tailings for a wet climatic year.

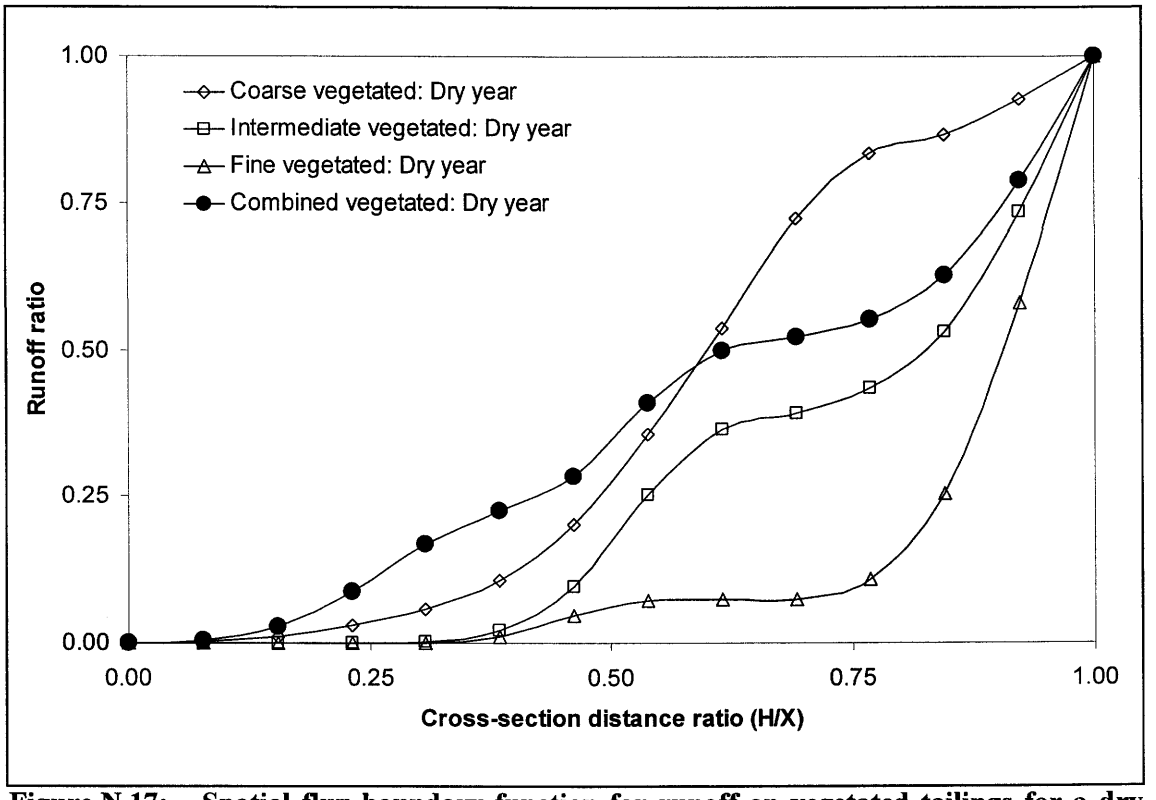

Figure N.17: Spatial flux boundary function for runoff on vegetated tailings for a dry climatic year.

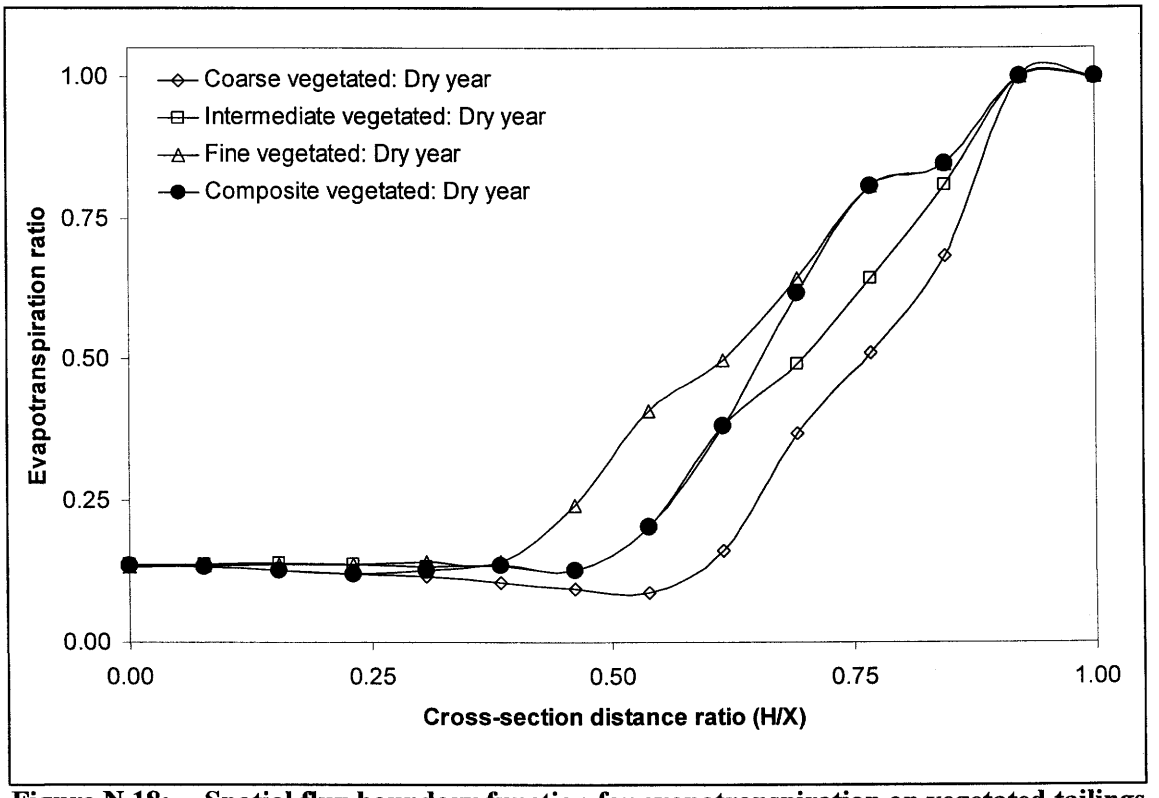

Figure N.18: Spatial flux boundary function for evapotranspiration on vegetated tailings for a dry climatic year.

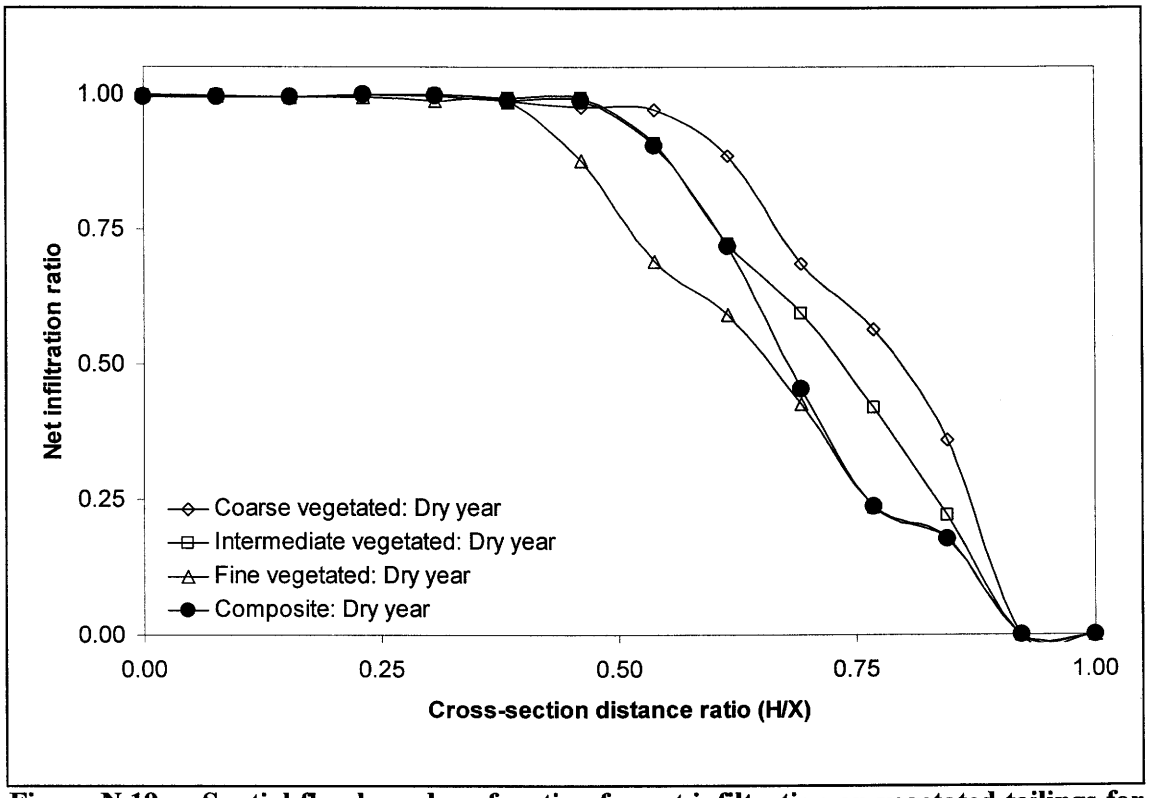

Figure N.19: Spatial flux boundary function for net infiltration on vegetated tailings for a dry climatic year.

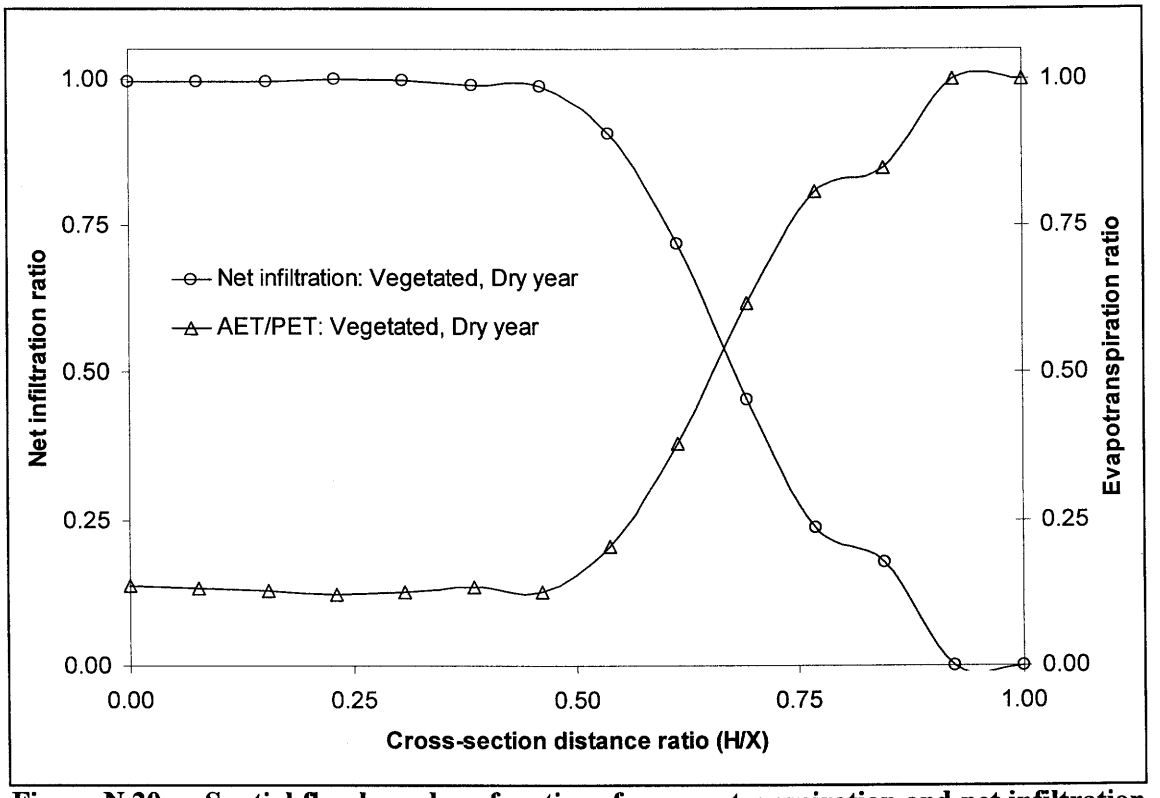

Figure N.20: Spatial flux boundary functions for evapotranspiration and net infiltration on vegetated tailings for a dry climatic year.

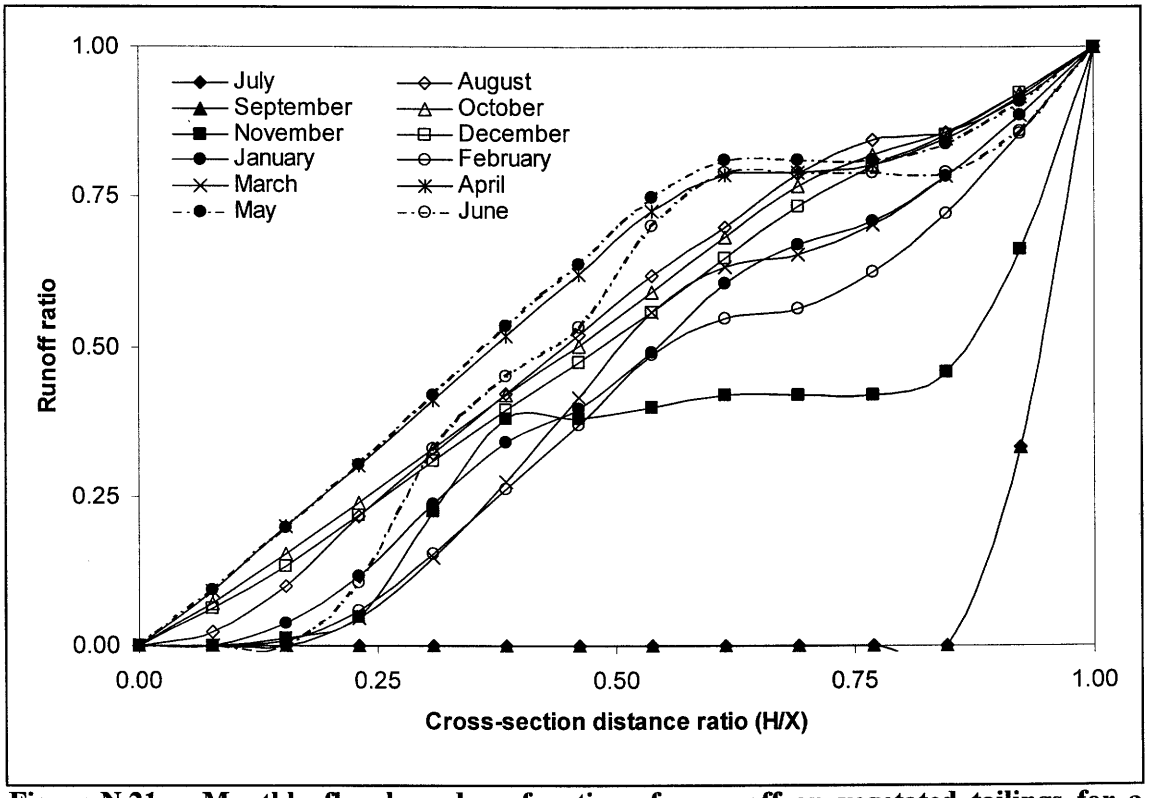

Figure N.21: Monthly flux boundary functions for runoff on vegetated tailings for a mean climatic year.

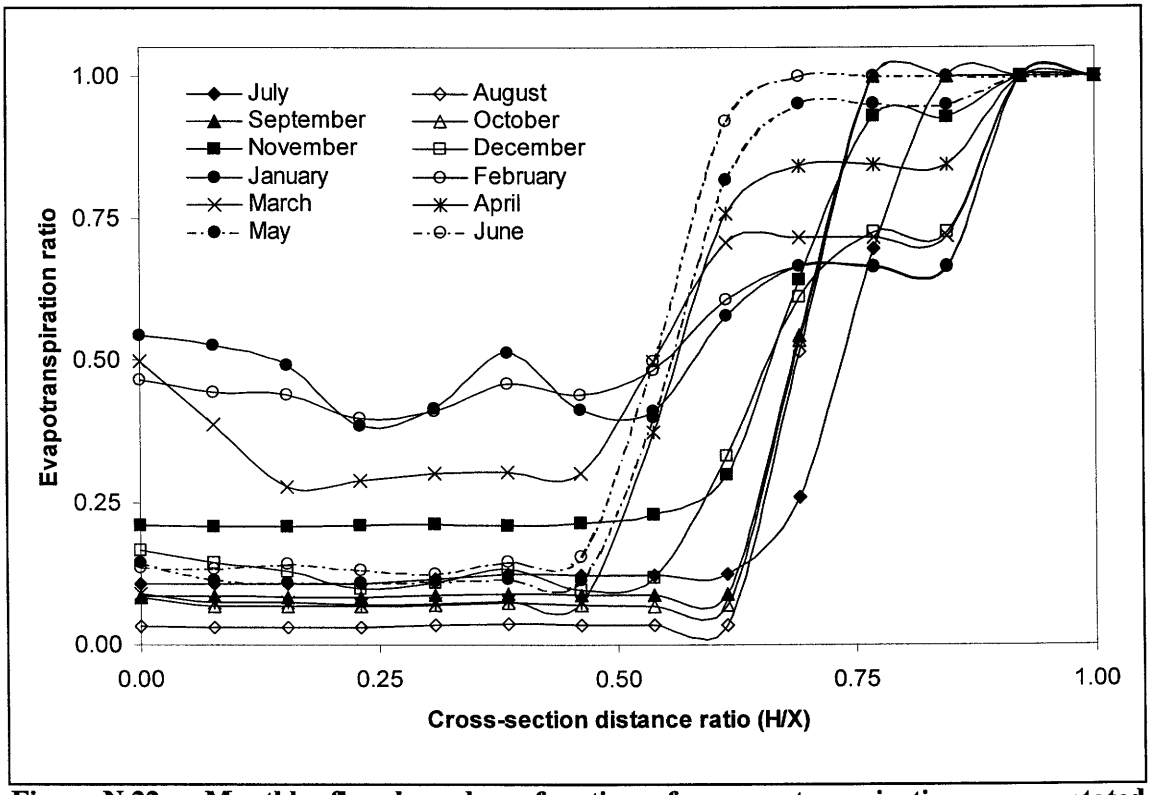

Figure N.22: Monthly flux boundary functions for evapotranspiration on vegetated tailings for a mean climatic year.

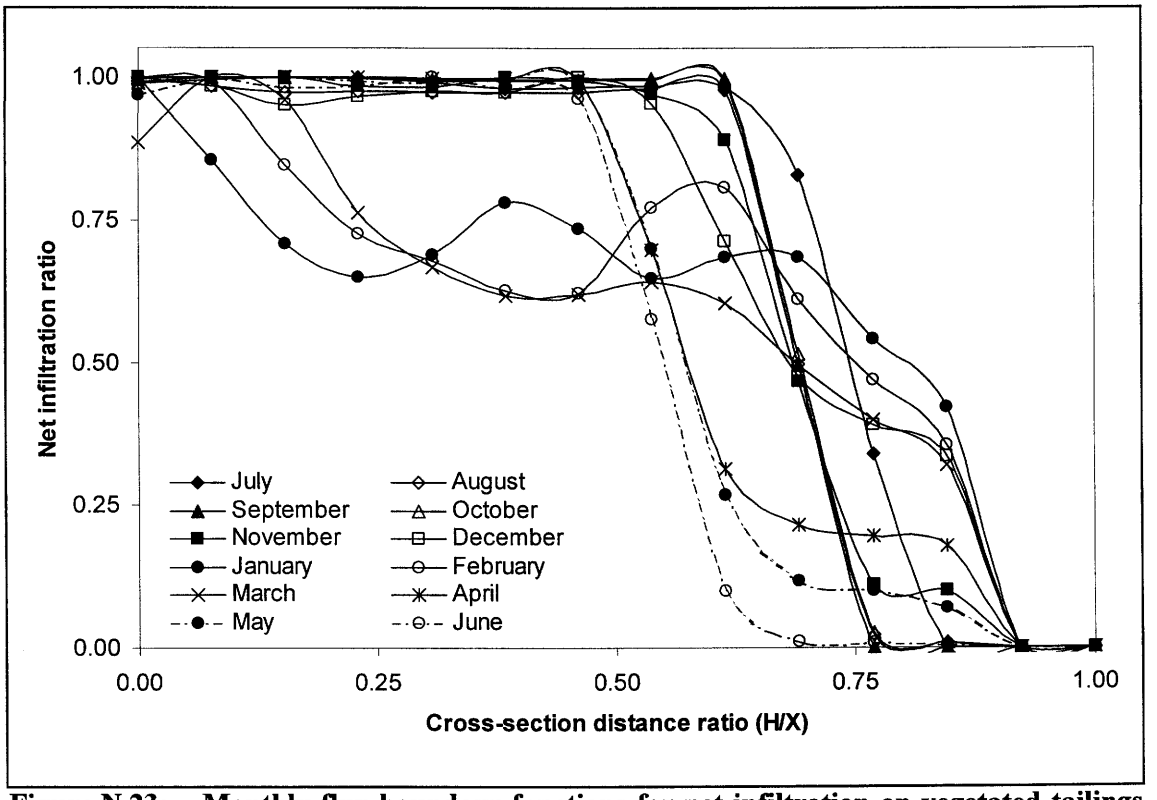

Figure N.23: Monthly flux boundary functions for net infiltration on vegetated tailings for a mean climatic year.

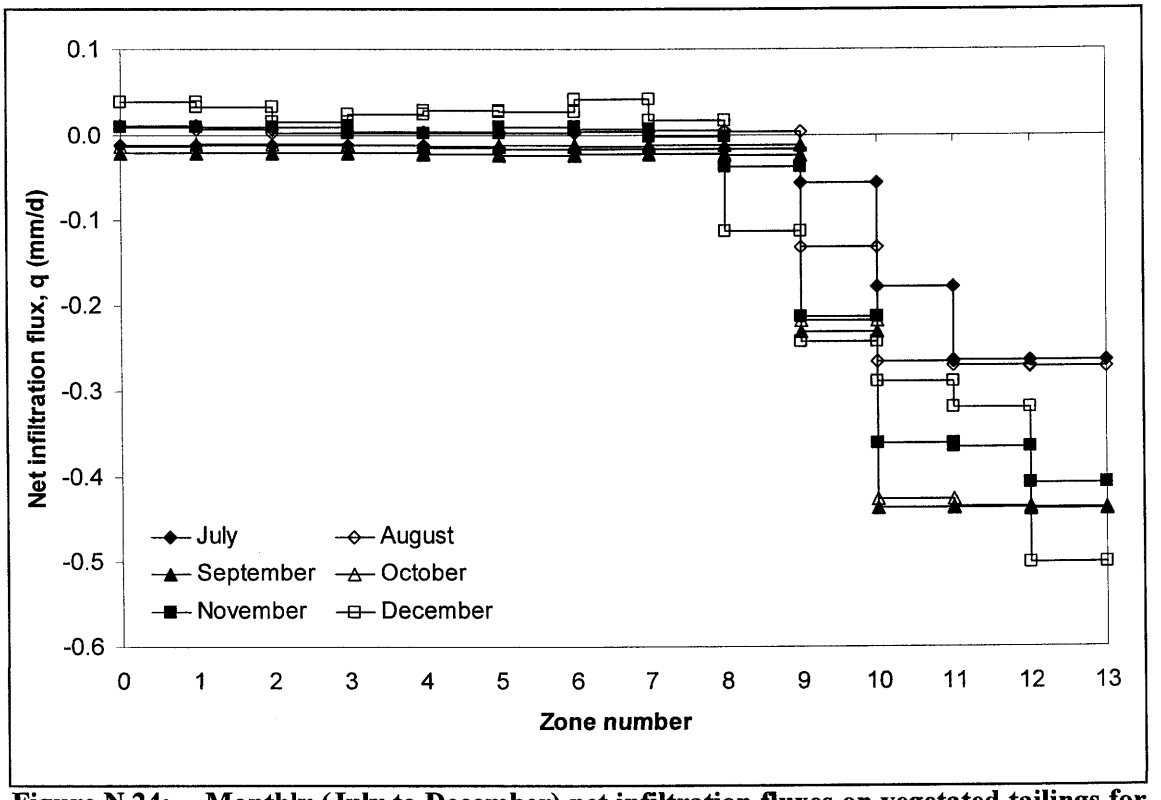

Figure N.24: Monthly (July to December) net infiltration fluxes on vegetated tailings for a mean climatic year.

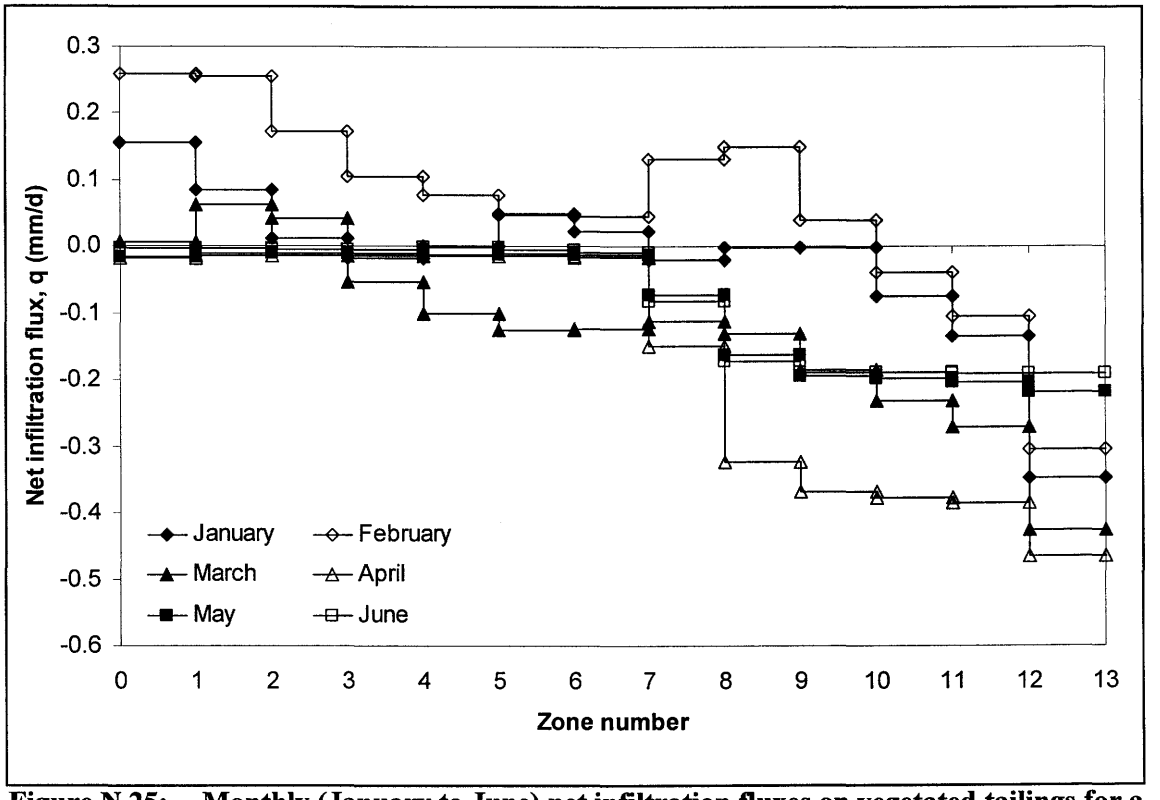

Figure N.25: Monthly (January to June) net infiltration fluxes on vegetated tailings for a mean climatic year.

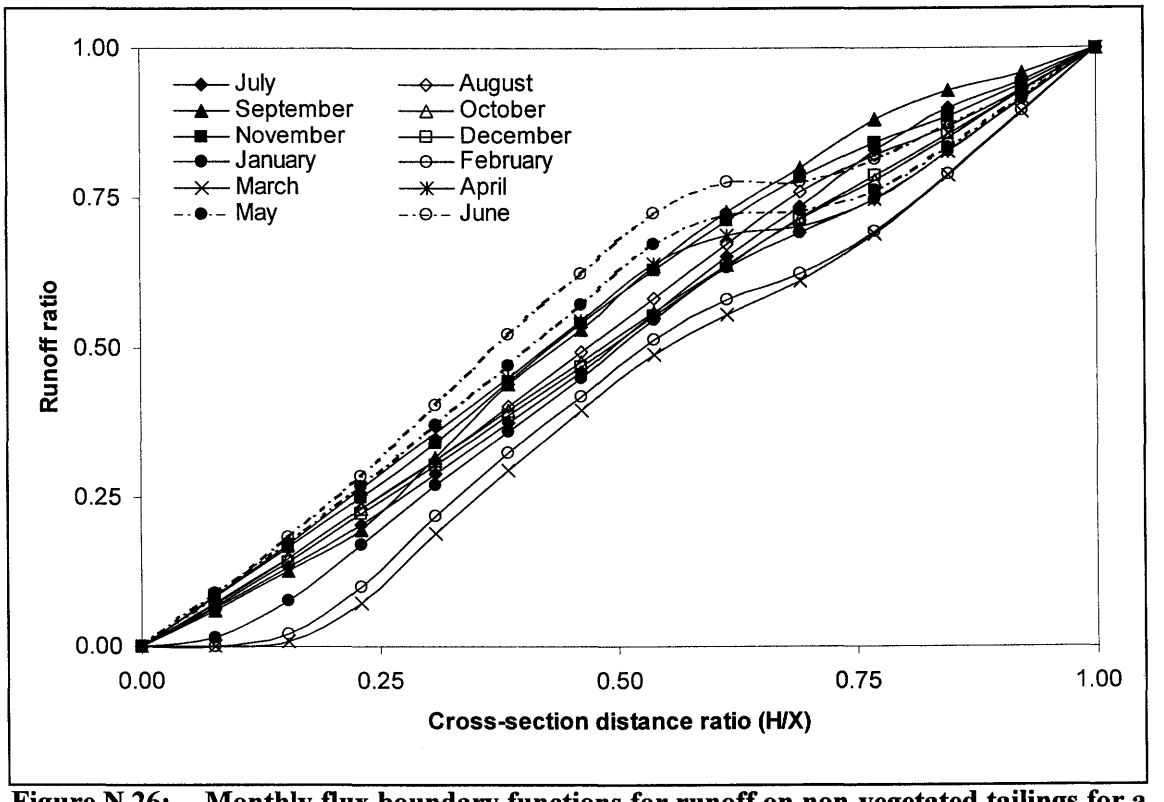

Figure N.26: Monthly flux boundary functions for runoff on non-vegetated tailings for a wet climatic year.

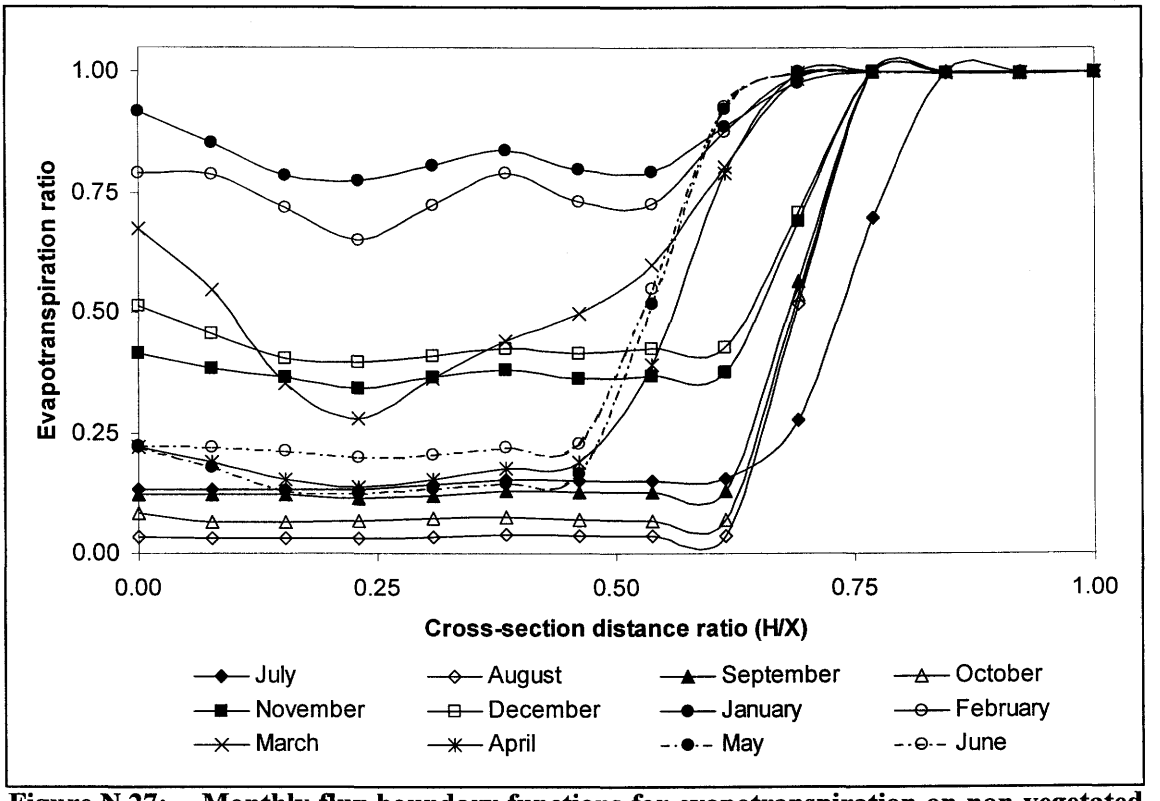

Figure N.27: Monthly flux boundary functions for evapotranspiration on non-vegetated tailings for a wet climatic year.

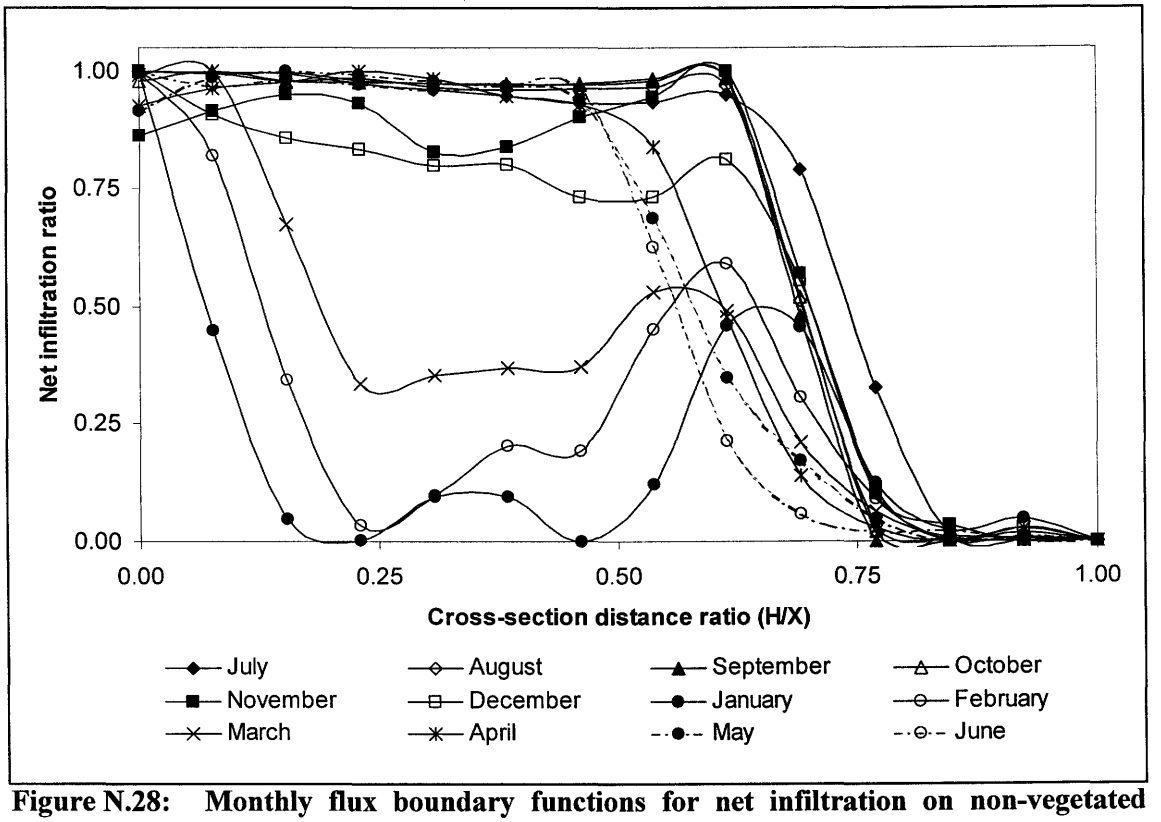

Figure N.28: Monthly flux boundary functions for net infiltration on non-vegetated tailings for a wet climatic year.

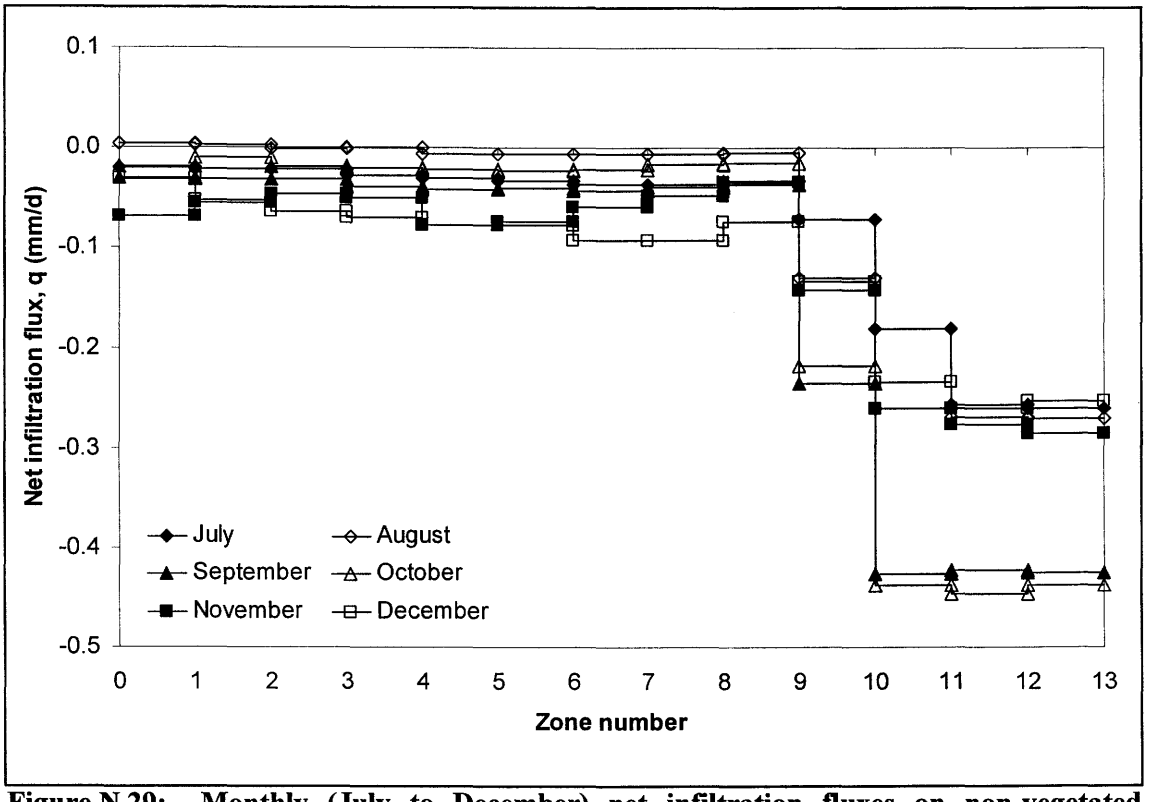

Figure N.29: Monthly (July to December) net infiltration fluxes on non-vegetated tailings for a wet climatic year.

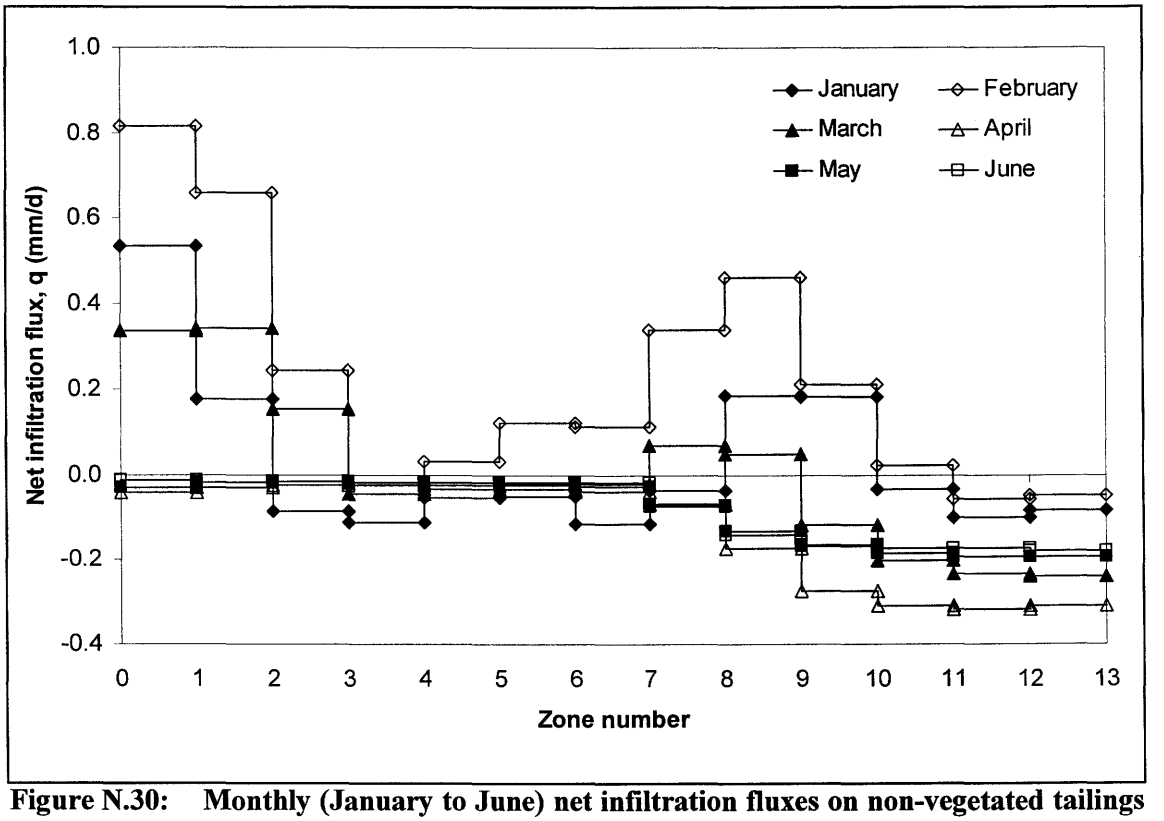

Figure N.30: Monthly (January to June) net infiltration fluxes on non-vegetated tailings for a wet climatic year.

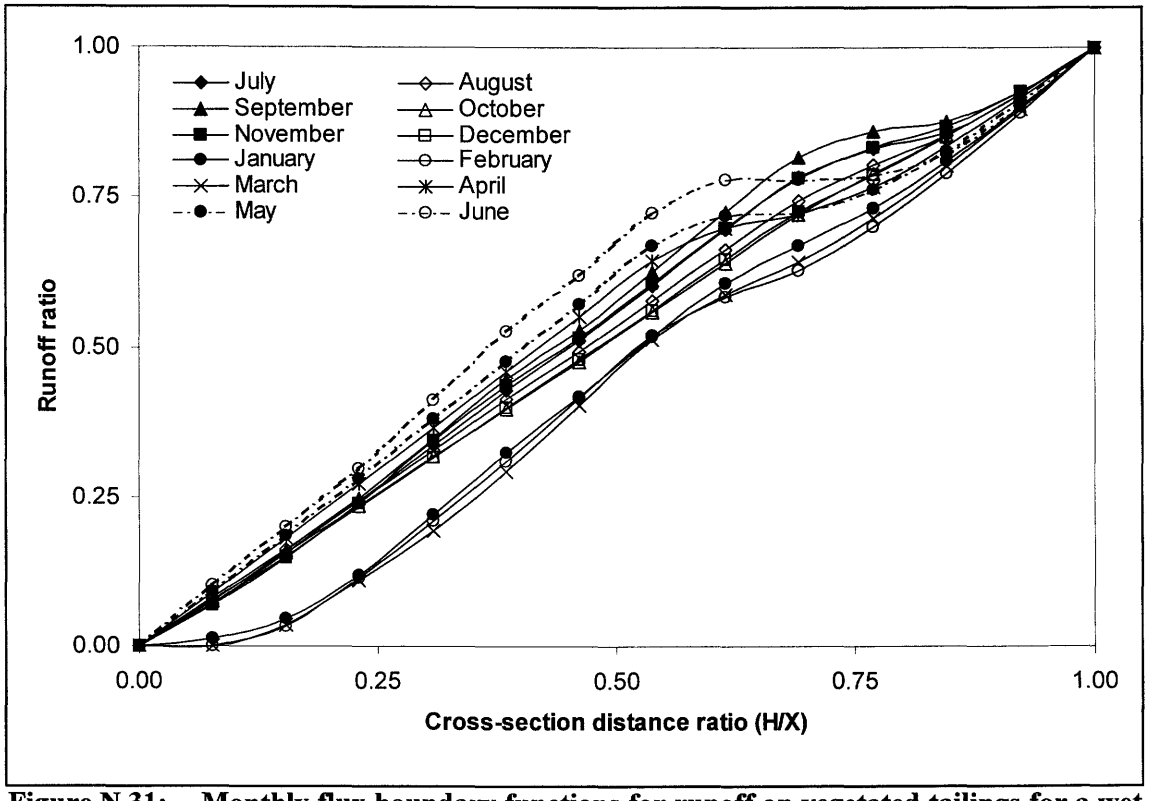

Figure N.31: Monthly flux boundary functions for runoff on vegetated tailings for a wet climatic year.

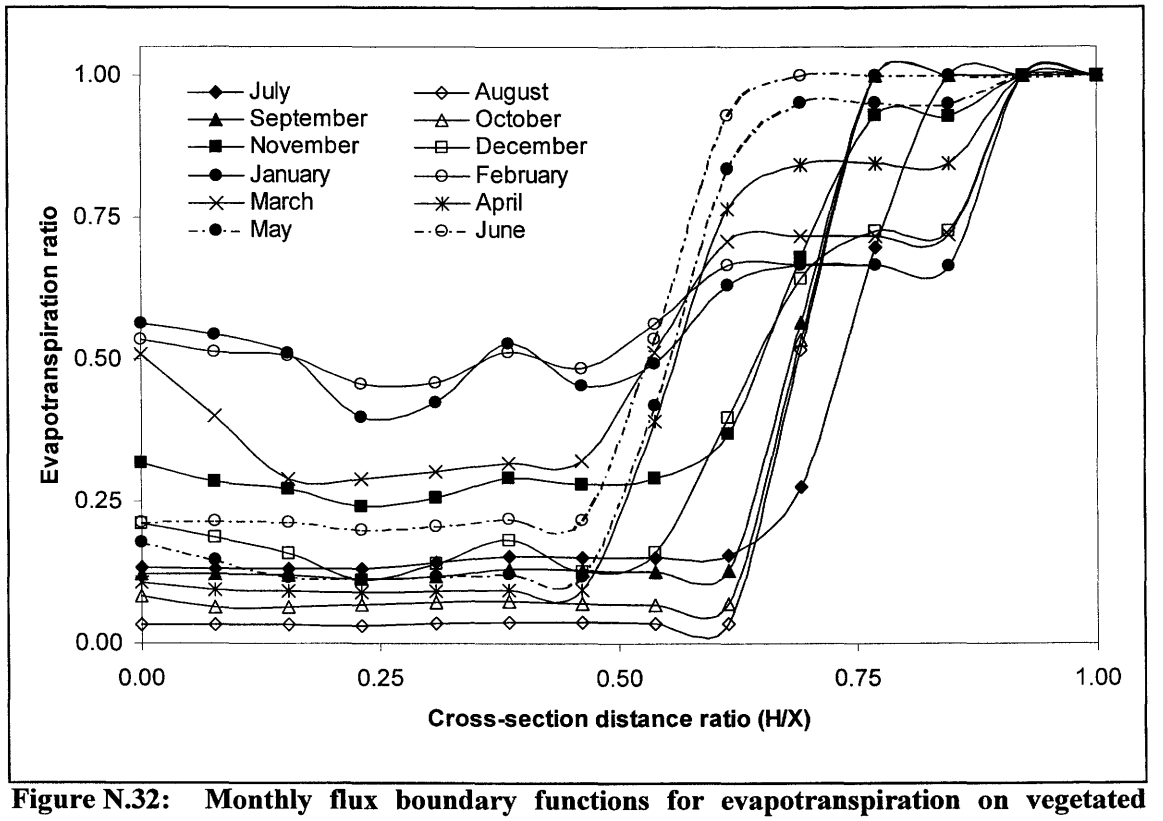

Figure N.32: Monthly flux boundary functions for evapotranspiration on vegetated tailings for a wet climatic year.

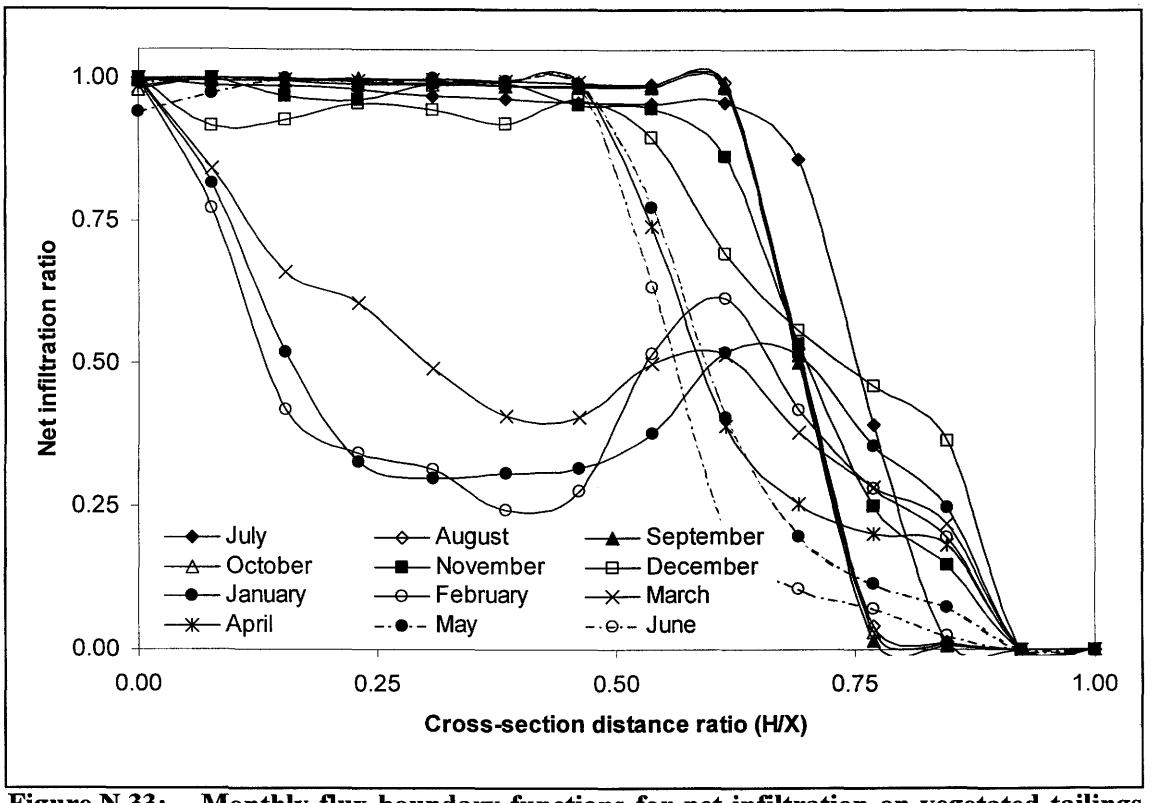

Figure N.33: Monthly flux boundary functions for net infiltration on vegetated tailings for a wet climatic year.

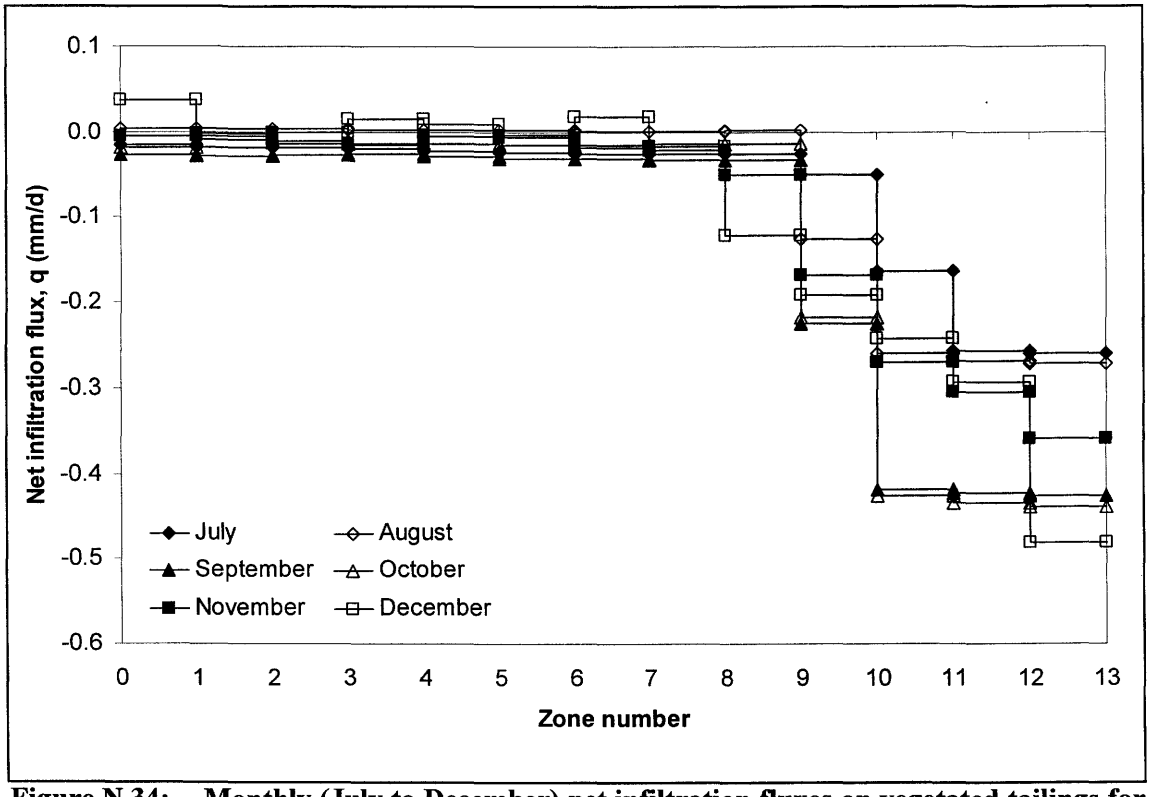

Figure N.34: Monthly (July to December) net infiltration fluxes on vegetated tailings for a wet climatic year.

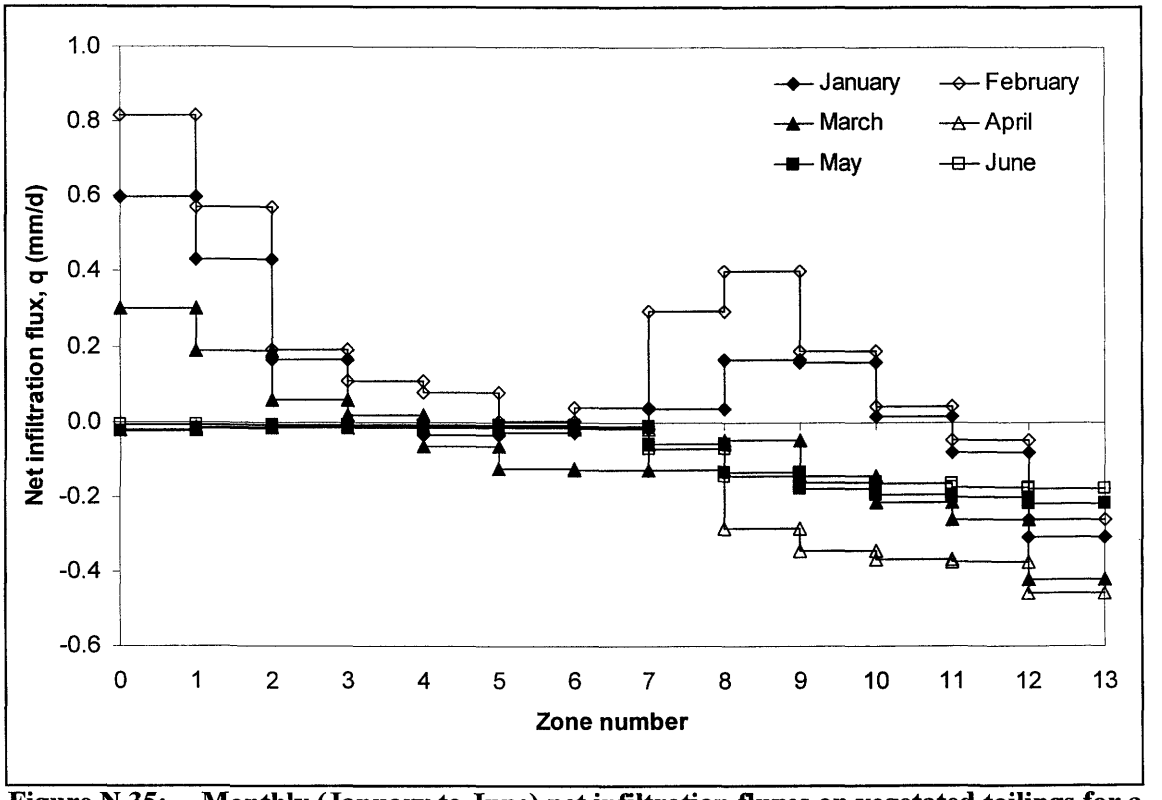

Figure N.35: Monthly (January to June) net infiltration fluxes on vegetated tailings for a wet climatic year.

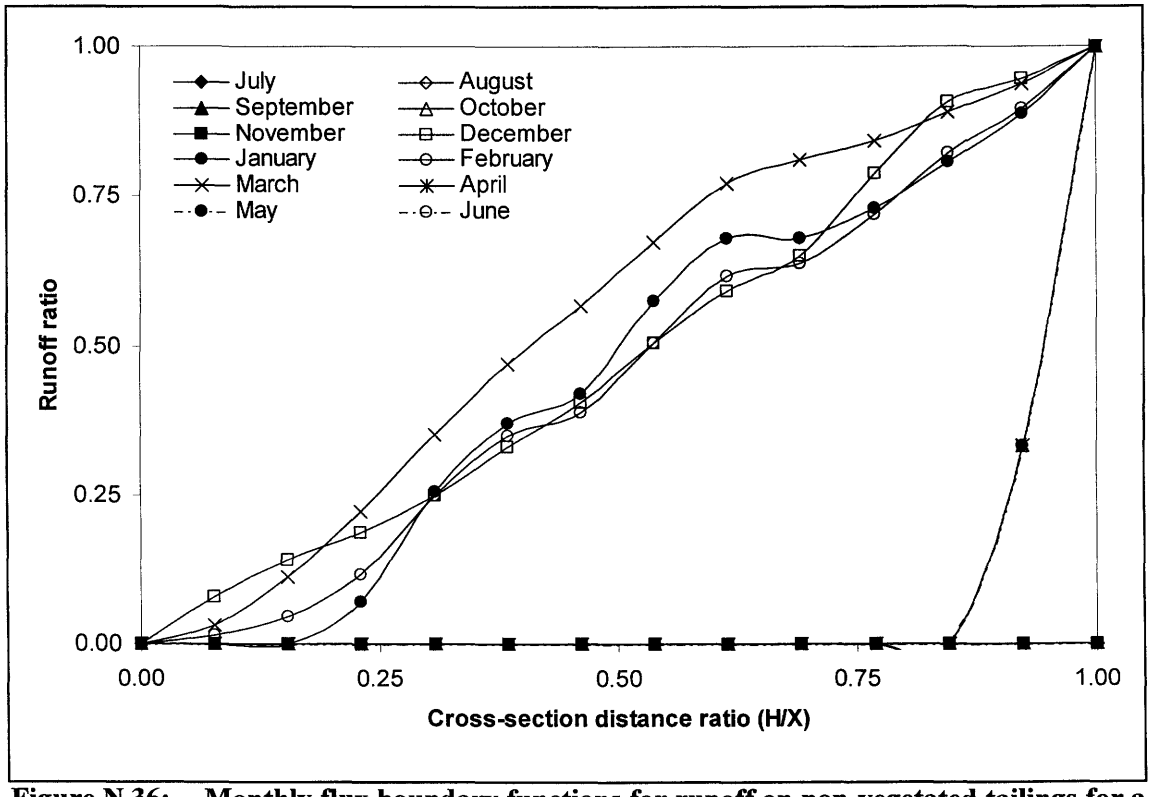

Figure N.36: Monthly flux boundary functions for runoff on non-vegetated tailings for a dry climatic year.

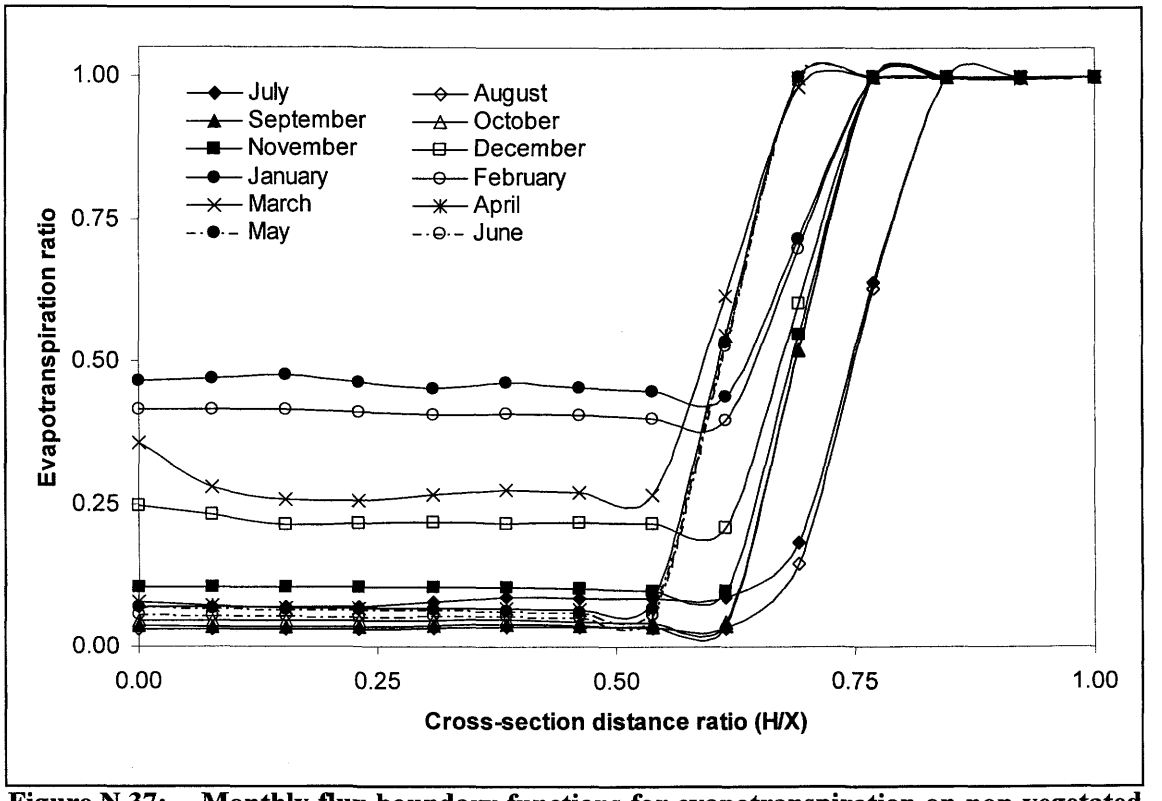

Figure N.37: Monthly flux boundary functions for evapotranspiration on non-vegetated tailings for a dry climatic year.

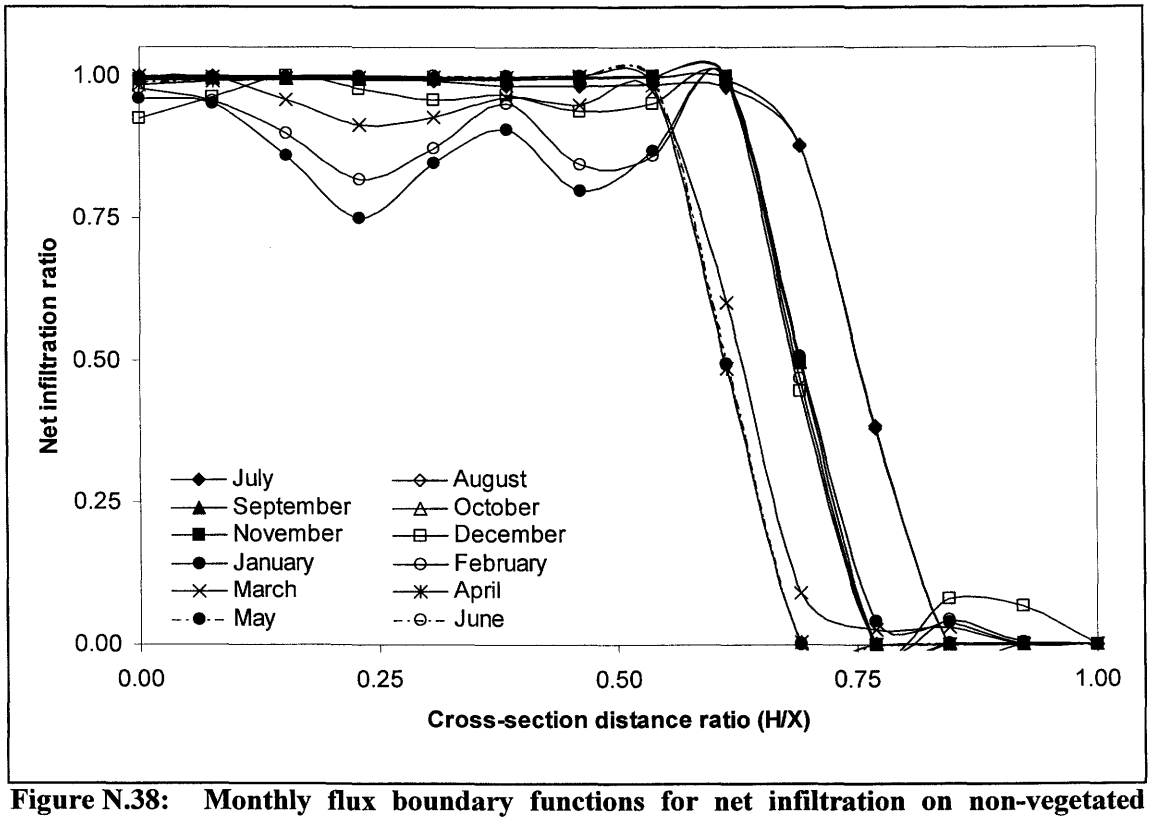

Figure N.38: Monthly flux boundary functions for net infiltration on non-vegetated tailings for a dry climatic year.

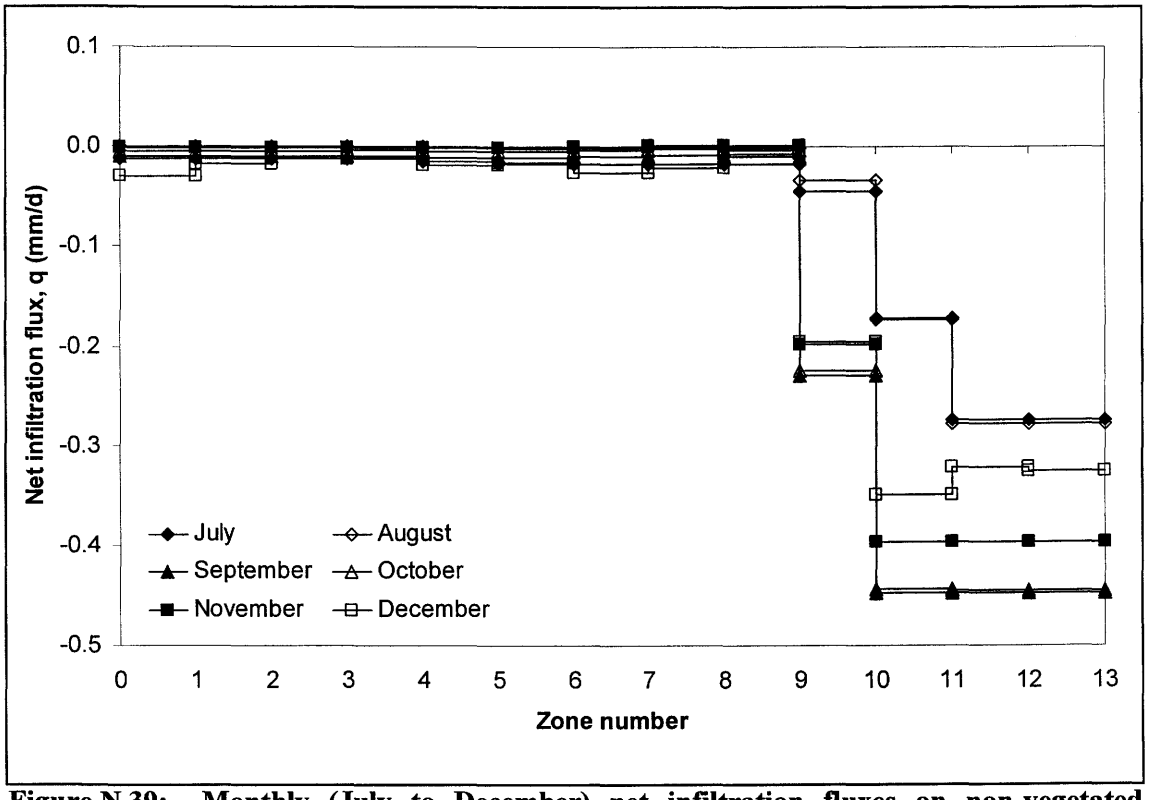

Figure N.39: Monthly (July to December) net infiltration fluxes on non-vegetated tailings for a dry climatic year.

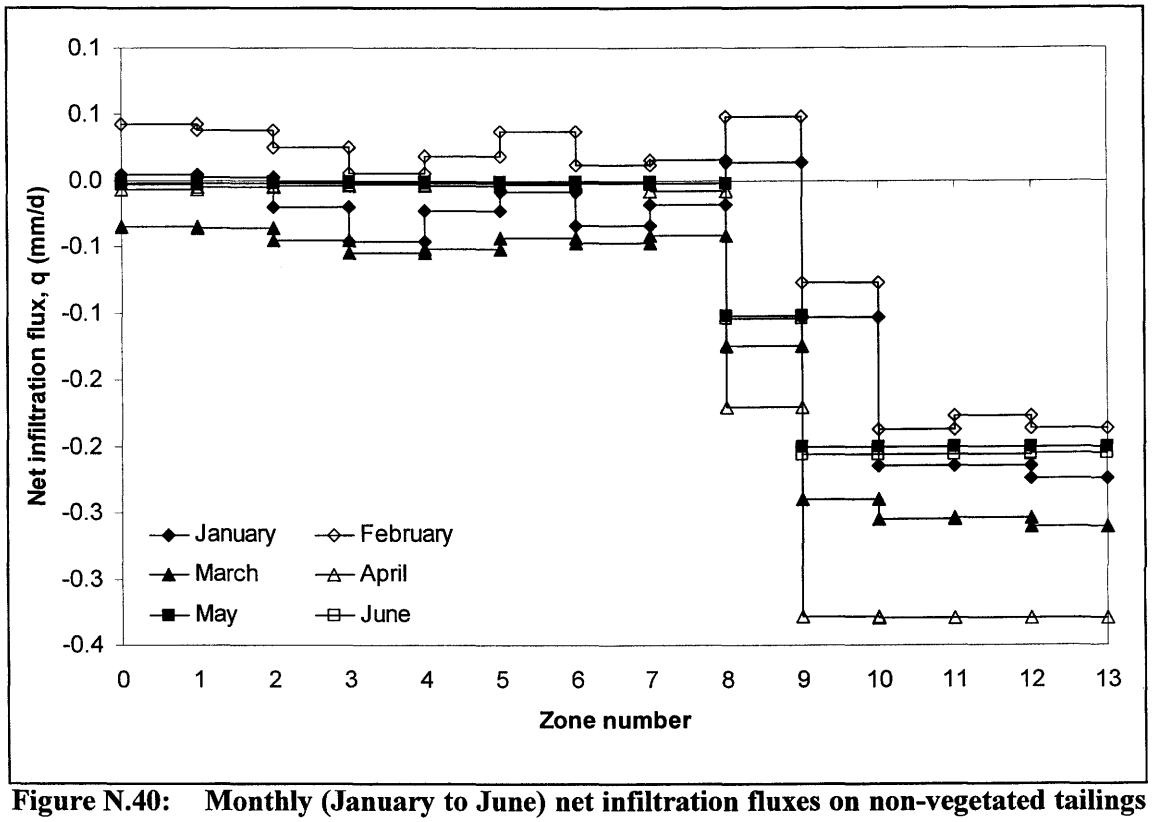

Figure N.40: Monthly (January to June) net infiltration fluxes on non-vegetated tailings for a dry climatic year.

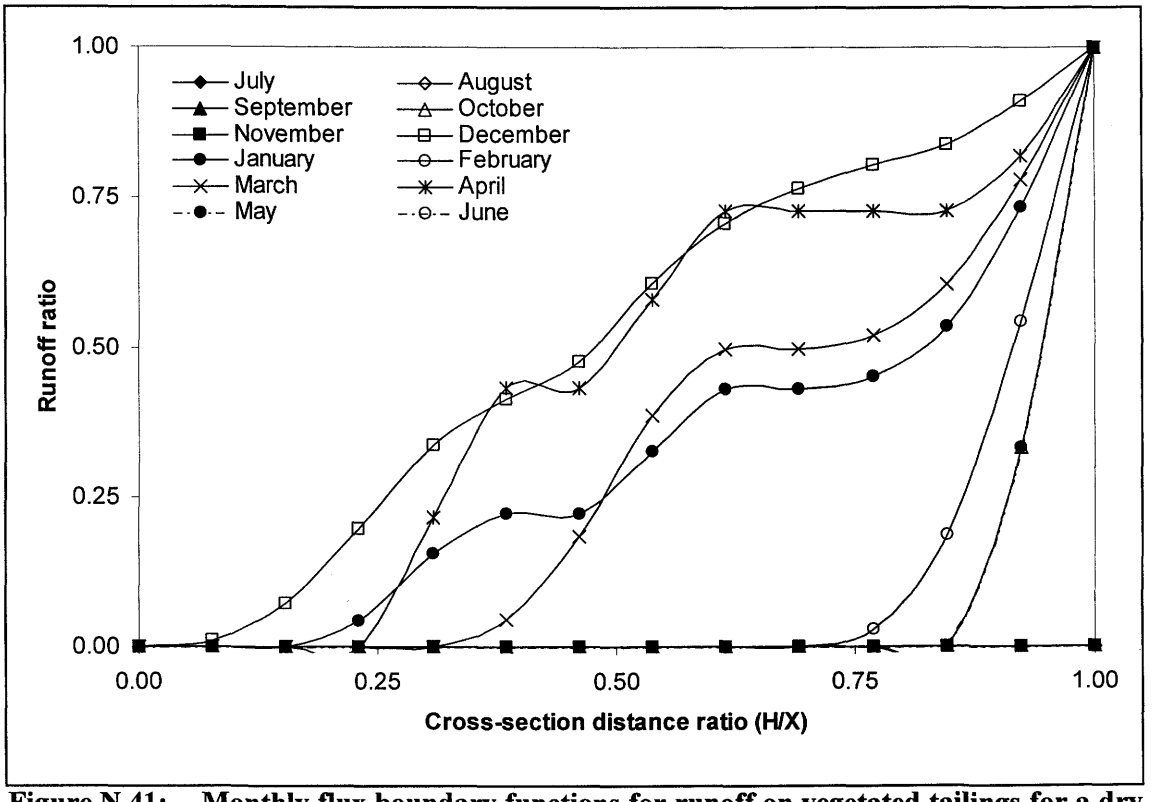

Figure N.41: Monthly flux boundary functions for runoff on vegetated tailings for a dry climatic year.

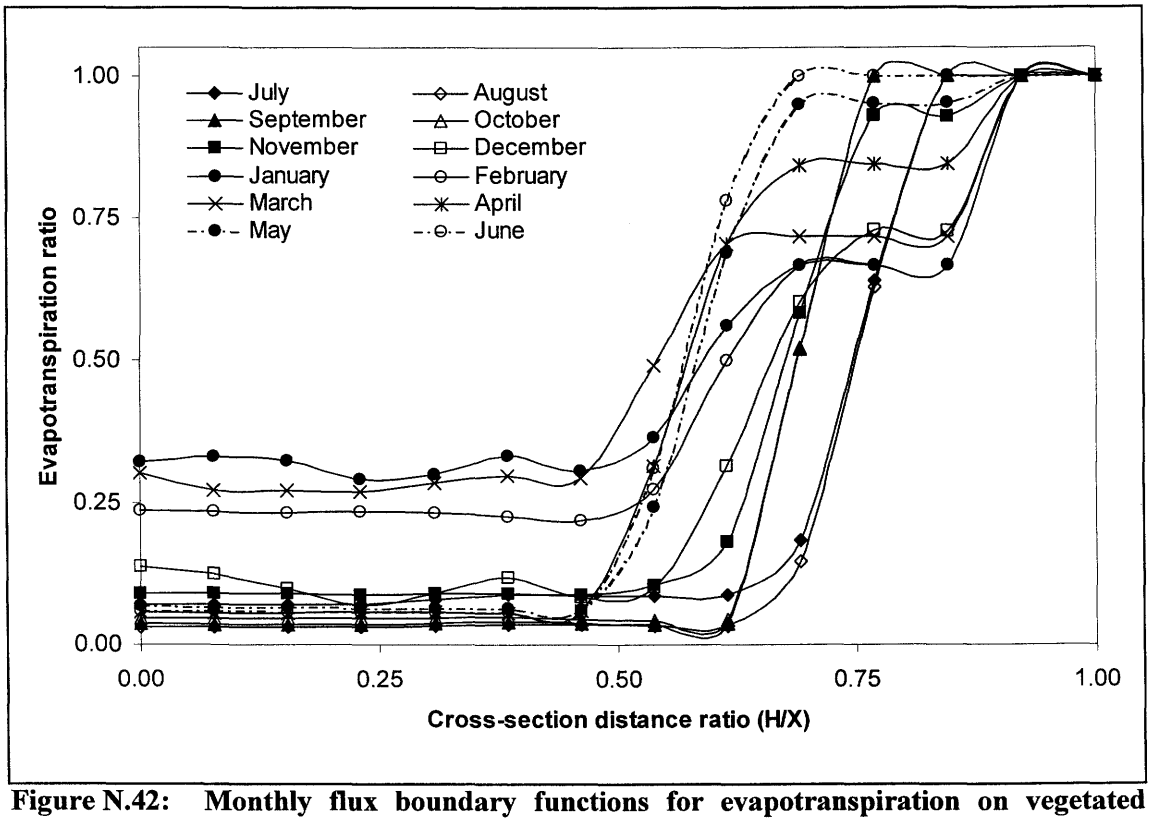

Figure N.42: Monthly flux boundary functions for evapotranspiration on vegetated tailings for a dry climatic year.

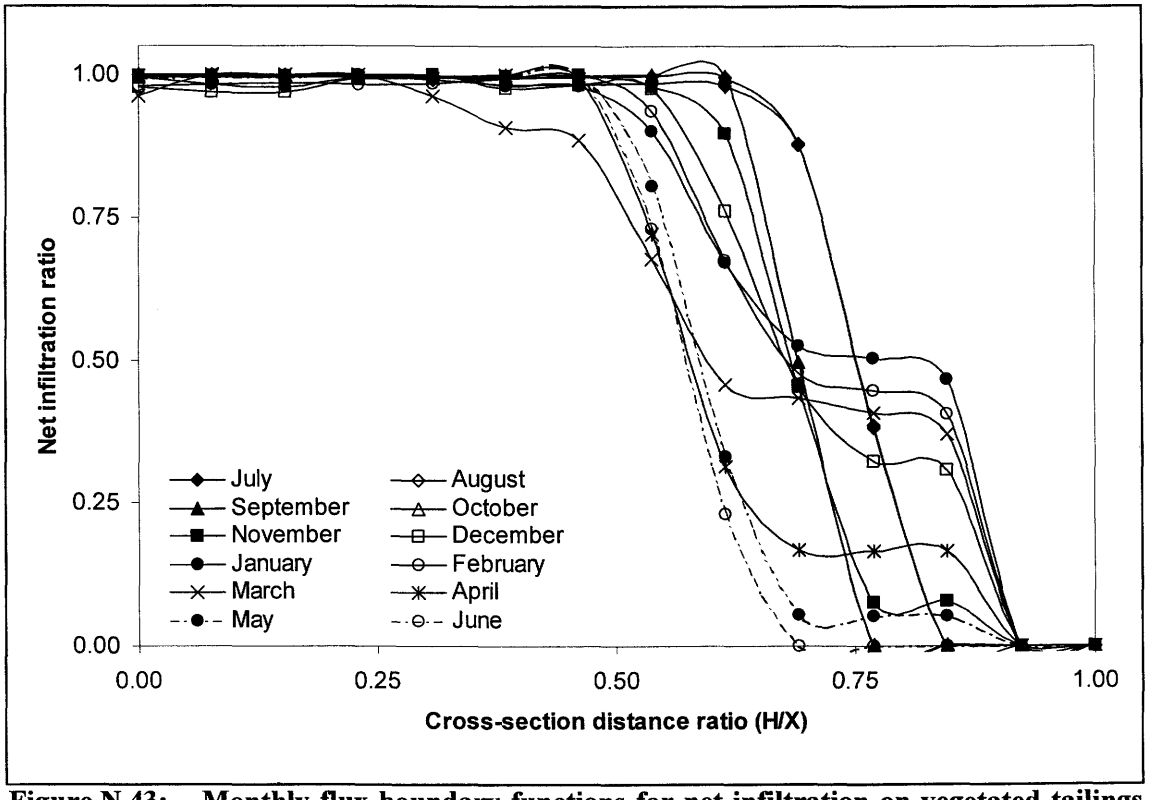

Figure N.43: Monthly flux boundary functions for net infiltration on vegetated tailings for a dry climatic year.

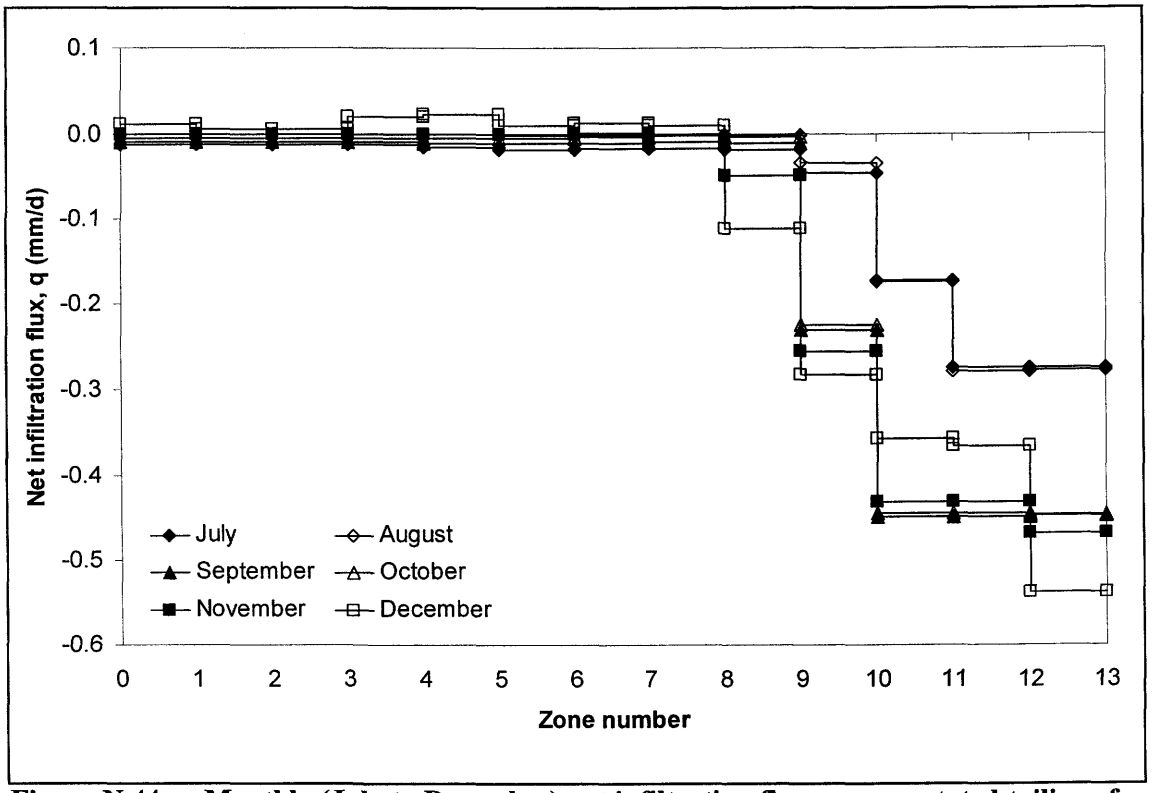

Figure N.44: Monthly (July to December) net infiltration fluxes on vegetated tailings for a dry climatic year.

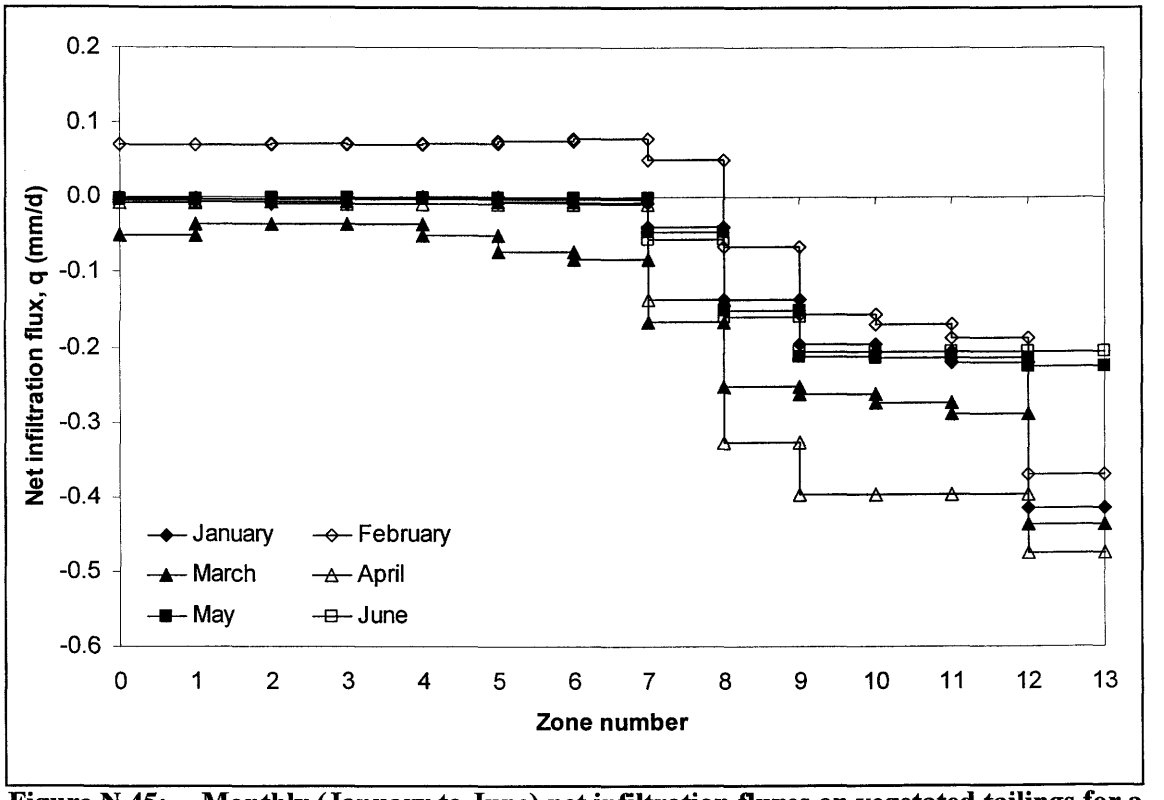

Figure N.45: Monthly (January to June) net infiltration fluxes on vegetated tailings for a dry climatic year.

N.4 Evaluation Data Set Flux Boundary Functions

The flux boundary functions for the evaluation data set are presented in the following section. Figures N.46 and N.47 present the results of the composite cross-cross section for the overall 4-month (December 2000 to March 2001) data set. Figures N.48 to N.51 presents the monthly flux boundary functions for this time period for the composite Kidston tailings impoundment cross-section.

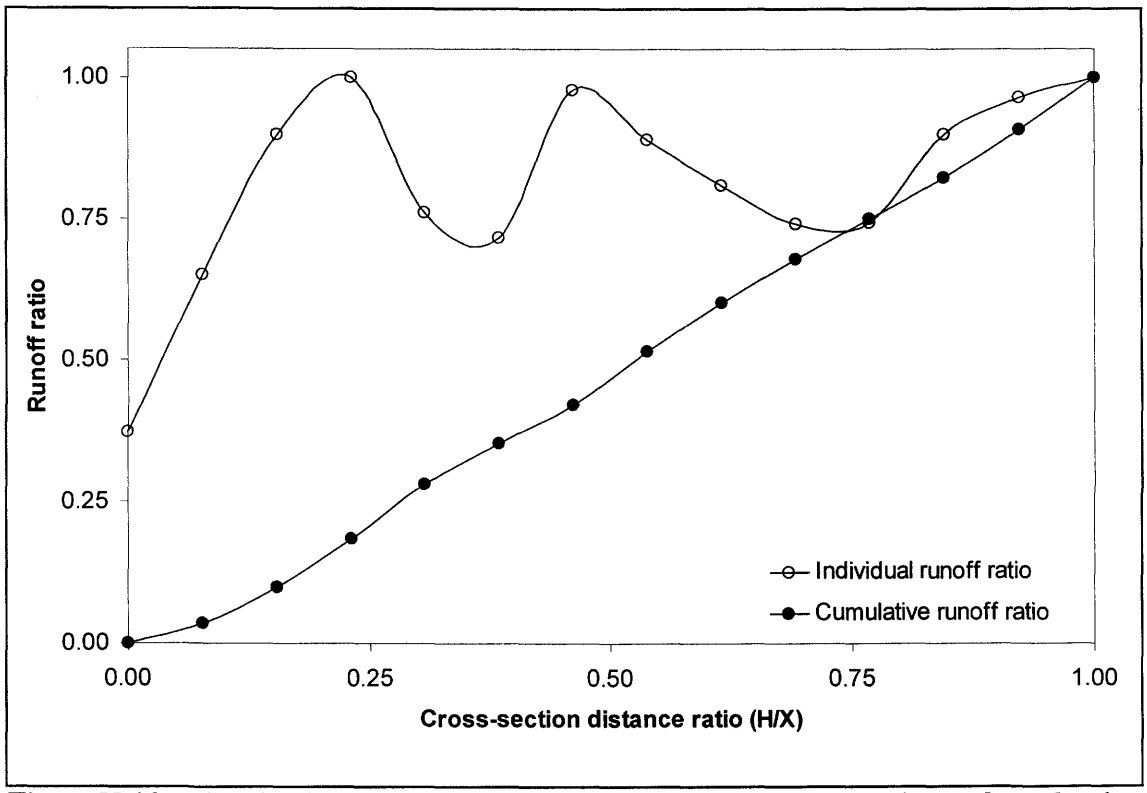

Figure N.46: Spatial flux boundary function for runoff during the 4-month evaluation data set period.

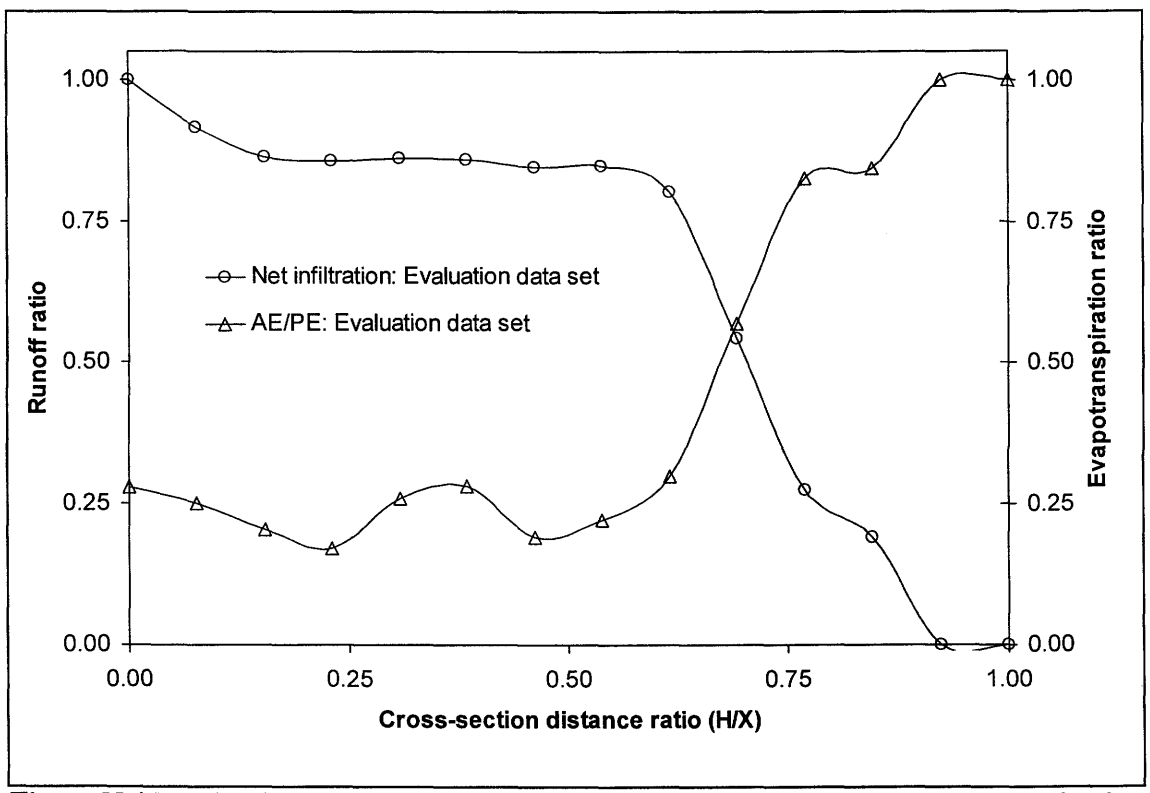

Figure N.47: Spatial flux boundary functions for net infiltration and evapotranspiration during the 4-month evaluation data set period.

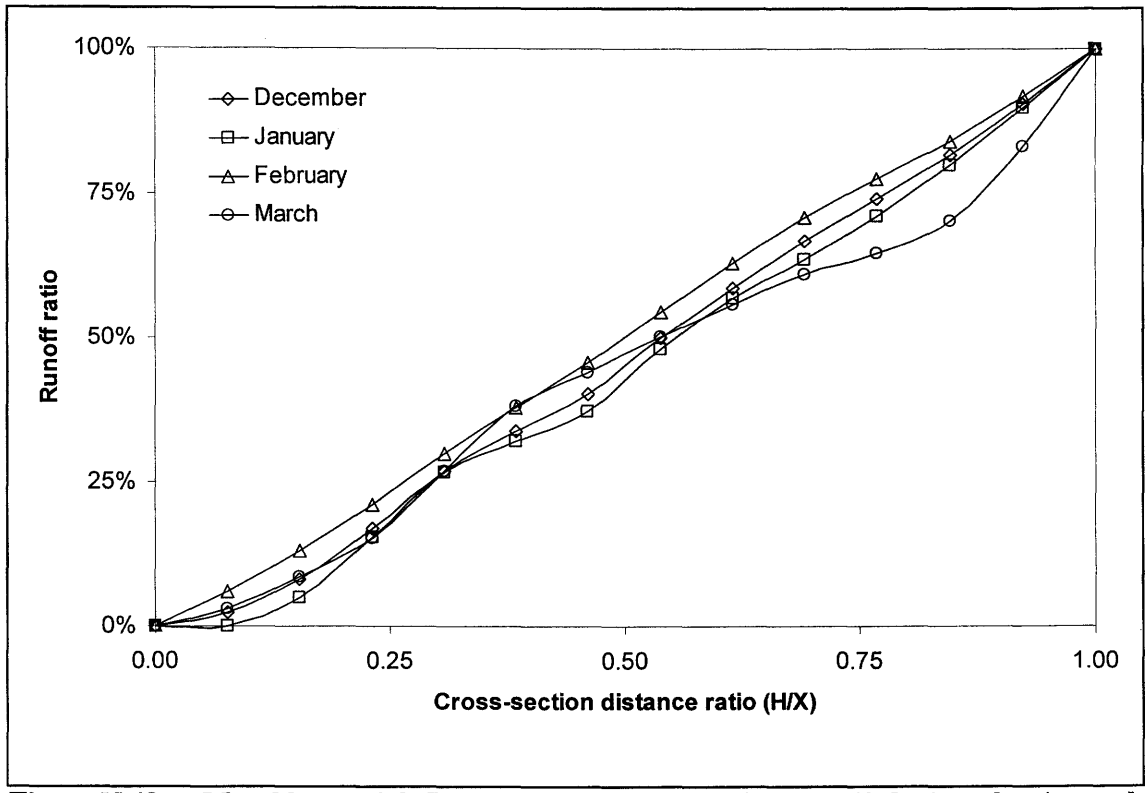

Figure N.48: Monthly spatial flux boundary function for runoff during the 4-month evaluation data set period.

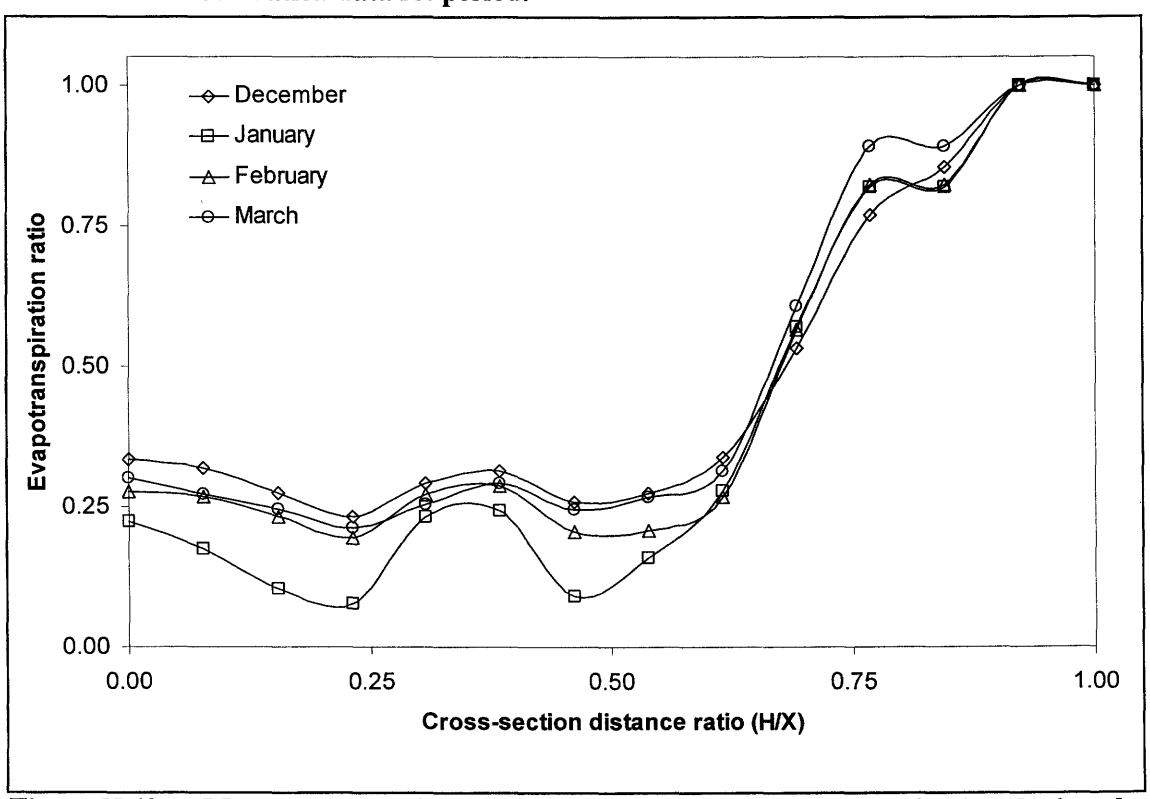

Figure N.49: Monthly spatial flux boundary function for evapotranspiration during the 4-month evaluation data set period.

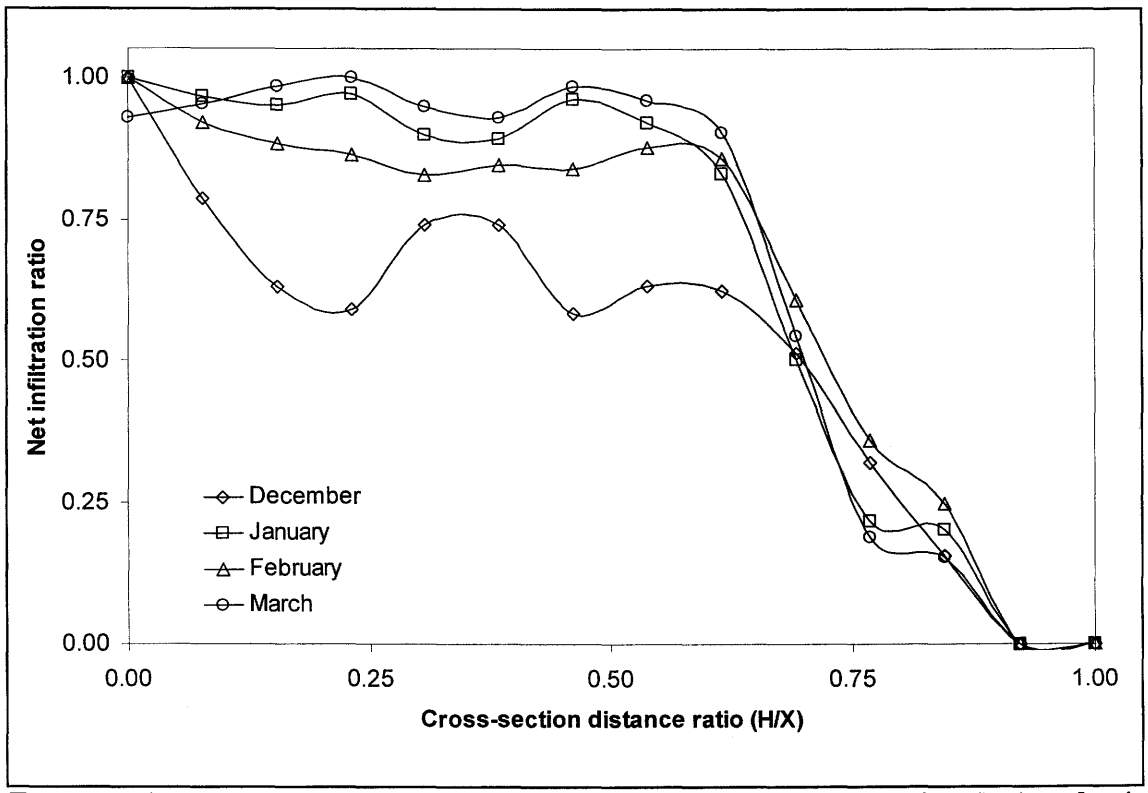

Figure N.50: Monthly spatial flux boundary function for net infiltration during the 4-month evaluation data set period.

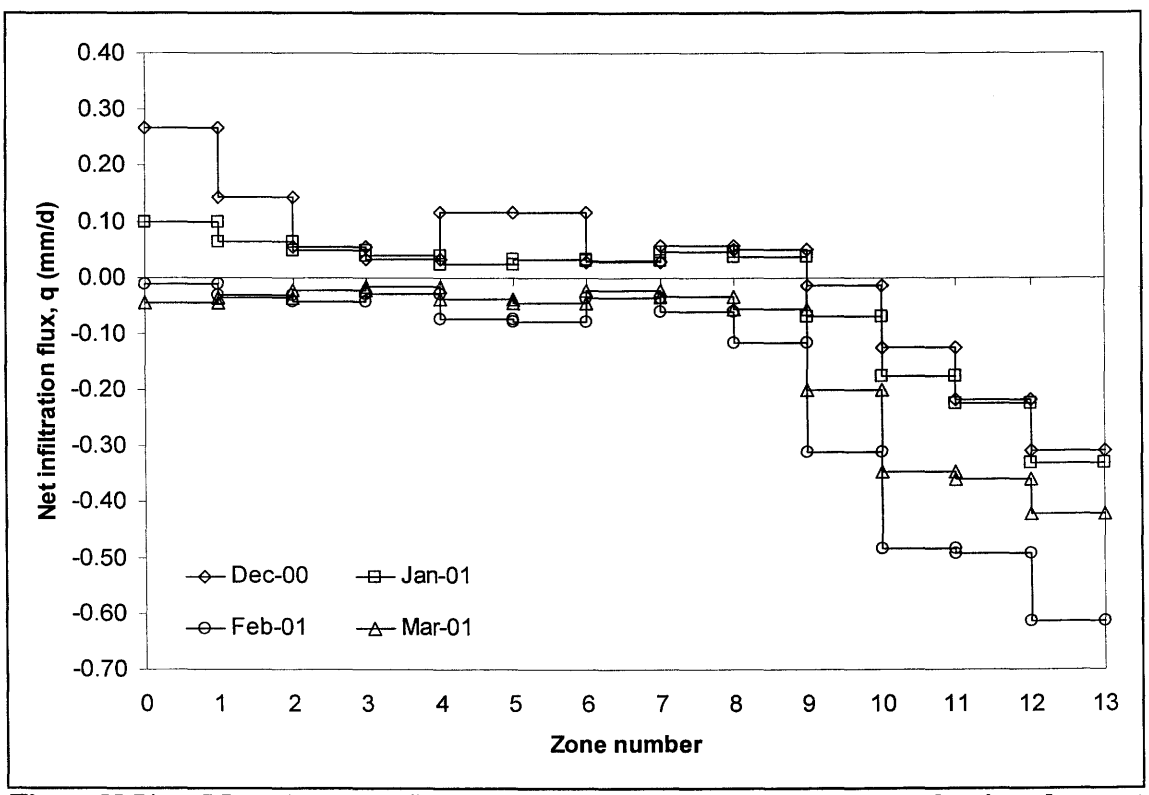

Figure N.51: Monthly net infiltration fluxes during the 4-month evaluation data set period.

This page was intentionally left blank.